

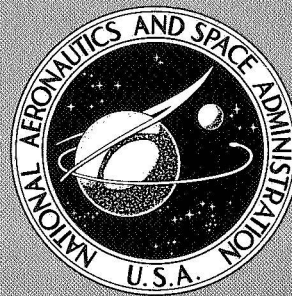
NASA SP-308

N73-10760 - N73-10816

# SOLAR WIND

## CASE FILE COPY

A conference held at  
PACIFIC GROVE, CALIFORNIA  
March 21-26, 1971



NATIONAL AERONAUTICS AND SPACE ADMINISTRATION

# SOLAR WIND

The proceedings of a conference sponsored by the National Aeronautics and Space Administration and held March 21-26, 1971, at the Asilomar Conference Grounds, Pacific Grove, California

*Edited by*

C. P. SONETT, P. J. COLEMAN, JR., AND J. M. WILCOX

*Prepared at Ames Research Center*



*Scientific and Technical Information Office*

NATIONAL AERONAUTICS AND SPACE ADMINISTRATION

Washington, D.C.

1972



---

For sale by the Superintendent of Documents  
U.S. Government Printing Office, Washington, D.C. 20402  
Price \$6.00    Stock Number 3300-00464  
*Library of Congress Catalog Card Number 72-600187*

## ORGANIZING COMMITTEE

*P. J. Coleman*  
University of Calif.  
Los Angeles, Calif.

*C. P. Sonett*  
NASA Ames Research Center  
Moffett Field, Calif.

*J. M. Wilcox*  
University of Calif.  
Berkeley, Calif.

## ADVISORY COMMITTEE

*W. I. Axford*  
University of Calif.  
San Diego, Calif.

*L. Davis, Jr.*  
Calif. Institute of Technology  
Pasadena, Calif.

*John W. Firor*  
Natl. Center for Atmospheric Research  
Boulder, Colo.

*A. J. Hundhausen*  
Los Alamos Scientific Laboratory  
Los Alamos, New Mexico

*Robert P. Kraft*  
University of Calif.  
Santa Cruz, Calif.

*N. F. Ness*  
NASA Goddard Space Flight Center  
Greenbelt, Md.

*E. N. Parker*  
University of Chicago  
Chicago, Ill.

*P. A. Sturrock*  
Stanford University  
Stanford, Calif.



## PREFACE

Some seven years have elapsed since the first solar wind conference held at the California Institute of Technology in Pasadena in 1964. Although the existence of a solar wind had hitherto been provocatively discussed, it was not till 1962 with the flight of Mariner II that the solar wind could be certified as a continuous corpuscular emission from the Sun. The first conference called attention to the fundamental importance of this subject in solar system physics, and in the years which ensued till the 1971 conference the subject has grown enormously in scope.

The breadth of solar system astronomy, influenced by the solar wind, is so large today that a working conference such as that at Asilomar could not hope to cover the entire scope. From discussions which the organizers had with the advisory committee, it soon became apparent that a conference would be most beneficial, if limited to specific topics of high current interest. It seemed especially important to emphasize the solar wind as an astrophysical entity, since it does constitute a convecting stellar envelope, indeed the only one available to direct examination.

Although many of the tools used in solar wind research are borrowed from laboratory physics, the integration of the techniques into large spacecraft systems, and their completely remote operation places novel burdens upon experimenters and scientists involved in interpretive efforts. Thus, we thought it also important to try to assess plasma experiments; the thread of this carries through the various chapters.

The conference began with discussions centered on the Sun. Chapter 2 connects the magnetic structure of the solar atmosphere with interplanetary space, while Chapter 3 is devoted to the solar wind plasma. Both theoretical and experimental topics are included. Chapter 4 reports a round table discussion on solar and stellar angular momentum and its relation to the solar wind. Later chapters are devoted to the detailed structure of the solar wind using both spacecraft and ground observational techniques, and the last chapter is an examination of the outer boundary of the solar wind and its confluence with the local arm of the galaxy. We have deliberately suppressed such topics as cosmic rays and modulation mechanisms, and the interaction of the solar wind with the planets. Although equally important they have been covered in other conferences and their inclusion would have extended the conference length well beyond one week.

Our thanks are extended to the many scientists, some from distant countries, who attended and made the conference a stimulating experience; to Darlyne Moen and Bob Cooper for their expert handling of the conference business; and to Miss Moen, Carol Tinling, Bonnie Simrell, and Harry DeVoto for their aid in compiling transcripts and papers and transforming them into these volumes.





# TABLE OF CONTENTS

Page

## CHAPTER 1 — PHOTOSPHERIC AND CORONAL MAGNETIC FIELDS

### Invited Reviews

Photospheric Magnetic Fields <i>Robert Howard</i> . . . . .	3
Discussion . . . . .	10
Coronal Magnetic Fields and the Solar Wind <i>Gordon Newkirk, Jr.</i> . . . .	11
Discussion . . . . .	29

### Contributed Papers

Large-Scale Negative Polarity Magnetic Fields on the Sun and Particle-Emitting Flares <i>V. Bumba</i> . . . . .	31
Discussion . . . . .	38
Comments <i>P. H. Scherrer, Robert Howard, and John Wilcox</i> . . . . .	39
Discussion . . . . .	43
Current Sheet Magnetic Model for the Solar Corona <i>Kenneth H. Schatten</i> . . . . .	44
Discussion . . . . .	54
Structure of Coronal Neutral Sheets <i>G. W. Pneuman</i> . . . . .	55
Discussion . . . . .	62

## CHAPTER 2 — THE INTERPLANETARY MAGNETIC FIELD

### Invited Reviews

Large-Scale Properties of the Interplanetary Magnetic Field <i>Kenneth H. Schatten</i> . . . . .	65
Discussion . . . . .	92
The Interplanetary Magnetic Field <i>Leverett Davis, Jr.</i> . . . .	93
Discussion . . . . .	103

### Contributed Papers

The Electromagnetic Structure of Interplanetary Space <i>J. O. Stenflo</i> . . . . .	115
Helmet and Active Streamers From Radio Observations <i>Y. Avignon, F. Axisa, M. J. Martres, M. Pick, and P. Simon</i> . . . . .	119
The Interplanetary and Solar Magnetic Field Sector Structures, 1962–1968 <i>Douglas E. Jones</i> . . . . .	122
Discussion . . . . .	132
Comments <i>E. J. Smith</i> . . . . .	132
Discussion . . . . .	134
Large-Scale Solar Magnetic Fields and H-Alpha Patterns <i>Patrick S. McIntosh</i> . . . . .	136
Comments <i>E. C. Roelof</i> . . . . .	140
Discussion . . . . .	142
Comments <i>F. C. Michel</i> . . . . .	142
Discussion . . . . .	149
Solar Large-Scale Positive Polarity Magnetic Fields and Geomagnetic Disturbances <i>V. Bumba</i> . . . . .	151
Discussion . . . . .	157

## CHAPTER 3 — LARGE-SCALE FEATURES OF THE SOLAR WIND PLASMA

### Invited Reviews

Present Developments in Theory of the Solar Wind <i>E. N. Parker</i> . . . . .	161
Discussion . . . . .	168
The Large-Scale Structure of the Solar Wind <i>John H. Wolfe</i> . . . . .	170
Discussion . . . . .	196
Comments <i>D. S. Intriligator</i> . . . . .	199
Discussion . . . . .	201

## TABLE OF CONTENTS — Continued

	Page
<b>CHAPTER 3 — LARGE-SCALE FEATURES OF THE SOLAR WIND PLASMA — Concluded</b>	
<b>Contributed Papers</b>	
Temporal Evolution of Velocity Structures in the Solar Wind <i>J. T. Gosling</i> . . . . .	202
Discussion . . . . .	206
Average Thermal Characteristics of Solar Wind Electrons <i>Michael D. Montgomery</i> . . . . .	208
Comments <i>J. D. Scudder</i> . . . . .	211
Comments <i>F. W. Perkins</i> . . . . .	215
Discussion . . . . .	216
Model for Energy Transfer in the Solar Wind: Model Results <i>Aaron Barnes and</i>	
<i>R. E. Hartle</i> . . . . .	219
Comments <i>J. V. Hollweg</i> . . . . .	223
Discussion . . . . .	226
Magnetic Latitude Effects in the Solar Wind <i>C. Richard Winge, Jr., and</i>	
<i>Paul J. Coleman, Jr.</i> . . . . .	227
Transition From a Supersonic to a Subsonic Solar Wind <i>B. Durney</i> . . . . .	232
Conversion of Magnetic Field Energy Into Kinetic Energy in the Solar Wind <i>Y. C. Whang</i> . . . . .	236
Some Physical Implications of Recent Solar Wind Measurements <i>S. Cuperman and</i>	
<i>A. Harten</i> . . . . .	244
Model for Energy Transfer in the Solar Wind: Formulation of Model <i>R. E. Hartle</i>	
<i>and Aaron Barnes</i> . . . . .	248
A Gas-Dynamic Calculation of Type II Shock Propagation Through the Corona	
<i>Roger A. Kopp</i> . . . . .	252
<b>CHAPTER 4 — SOLAR AND STELLAR SPIN DOWN; ANGULAR MOMENTUM OF THE SOLAR</b>	
<b>WIND — Round Table Discussion</b>	
Evidence for an Angular Momentum Flux in the Solar Wind	
Opening Remarks <i>R. P. Kraft</i> . . . . .	261
Introduction <i>A. J. Hundhausen</i> . . . . .	261
Comments <i>A. J. Lazarus</i> . . . . .	265
Discussion . . . . .	266
Comments <i>E. J. Weber</i> . . . . .	268
Discussion . . . . .	271
Comments <i>L. Davis and I. Strong</i> . . . . .	275
Evidence for Changes in the Angular Velocity of the Surface Regions of the Sun and Stars	
Introduction <i>R. P. Kraft</i> . . . . .	276
Discussion . . . . .	281
Comments <i>B. Durney</i> . . . . .	282
Evidence for the Distribution of Angular Velocity Inside the Sun and Stars	
Introduction <i>L. Mestel</i> . . . . .	287
Comments <i>R. Kraft and R. H. Dicke</i> . . . . .	290
Comments <i>E. Schatzman</i> . . . . .	297
Comments <i>A. Ingersoll</i> . . . . .	298
Discussion . . . . .	300
Comments <i>C. P. Sonett</i> . . . . .	301
Comments <i>W. C. Livingston</i> . . . . .	304

## TABLE OF CONTENTS — Continued

	Page
<b>CHAPTER 5 — MICROSTRUCTURE, "TURBULENCE," AND HYDROMAGNETIC WAVES IN THE SOLAR WIND</b>	
<b>Invited Reviews</b>	
Microstructure of the Interplanetary Medium <i>L. F. Burlaga</i> . . . . .	309
Discussion . . . . .	331
Microscale Fluctuations in the Solar Wind <i>Aaron Barnes</i> . . . . .	333
Discussion . . . . .	343
Comments <i>D. W. Forslund</i> . . . . .	346
Comments <i>H. J. Volk</i> . . . . .	351
<b>Contributed Papers</b>	
Electron Plasma Oscillations in the Near-Earth Solar Wind: Preliminary Observations and Interpretations <i>R. W. Fredricks, F. L. Scarf, and I. M. Green</i> . . . . .	353
Discussion . . . . .	358
Magnetic Field Merging in the Solar Wind <i>Karl Schindler</i> . . . . .	360
Discussion . . . . .	364
Comments on the Measurement of Power Spectra of the Interplanetary Magnetic Field <i>Christopher T. Russell</i> . . . . .	365
Power Spectra of the Interplanetary Magnetic Field Near the Earth <i>D. D. Childers and C. T. Russell</i> . . . . .	375
Coronal Alfvén Waves and the Solar Wind <i>J. W. Belcher</i> . . . . .	382
Discussion . . . . .	386
<b>CHAPTER 6 — SHOCK WAVES AND THE STRUCTURE OF LARGE SCALE DISTURBANCES</b>	
<b>Invited Reviews</b>	
Interplanetary Shock Waves and the Structure of Solar Wind Disturbances <i>A. J. Hundhausen</i> . . . . .	393
Discussion . . . . .	417
Comparison of Deep Space and Near-Earth Observations of Plasma Turbulence at Solar Wind Discontinuities <i>F. L. Scarf, R. W. Fredricks, and I. M. Green</i> . . . . .	421
Discussion . . . . .	429
<b>Contributed Papers</b>	
Corotating Shock Structures <i>K. W. Ogilvie</i> . . . . .	430
Shock Pair Observation <i>J. K. Chao, V. Formisano, and P. C. Hedgecock</i> . . . . .	435
A Two-Spacecraft Test of a Single Spacecraft Method of Estimating Shock Normals <i>R. P. Lepping</i> . . . . .	444
Comments <i>T. A. Croft</i> . . . . .	448
Discussion . . . . .	450
Interplanetary Double-Shock Ensembles With Anomalous Electrical Conductivity <i>Murray Dryer</i> . . . . .	453
Discussion . . . . .	466
Comments <i>D. S. DeYoung</i> . . . . .	466
Discussion . . . . .	468
Comments <i>E. J. Smith</i> . . . . .	469
The Nature of Stream-Stream Interaction in the Large-Scale Structure of the Solar Wind <i>T. S. Lee</i> . . . . .	472

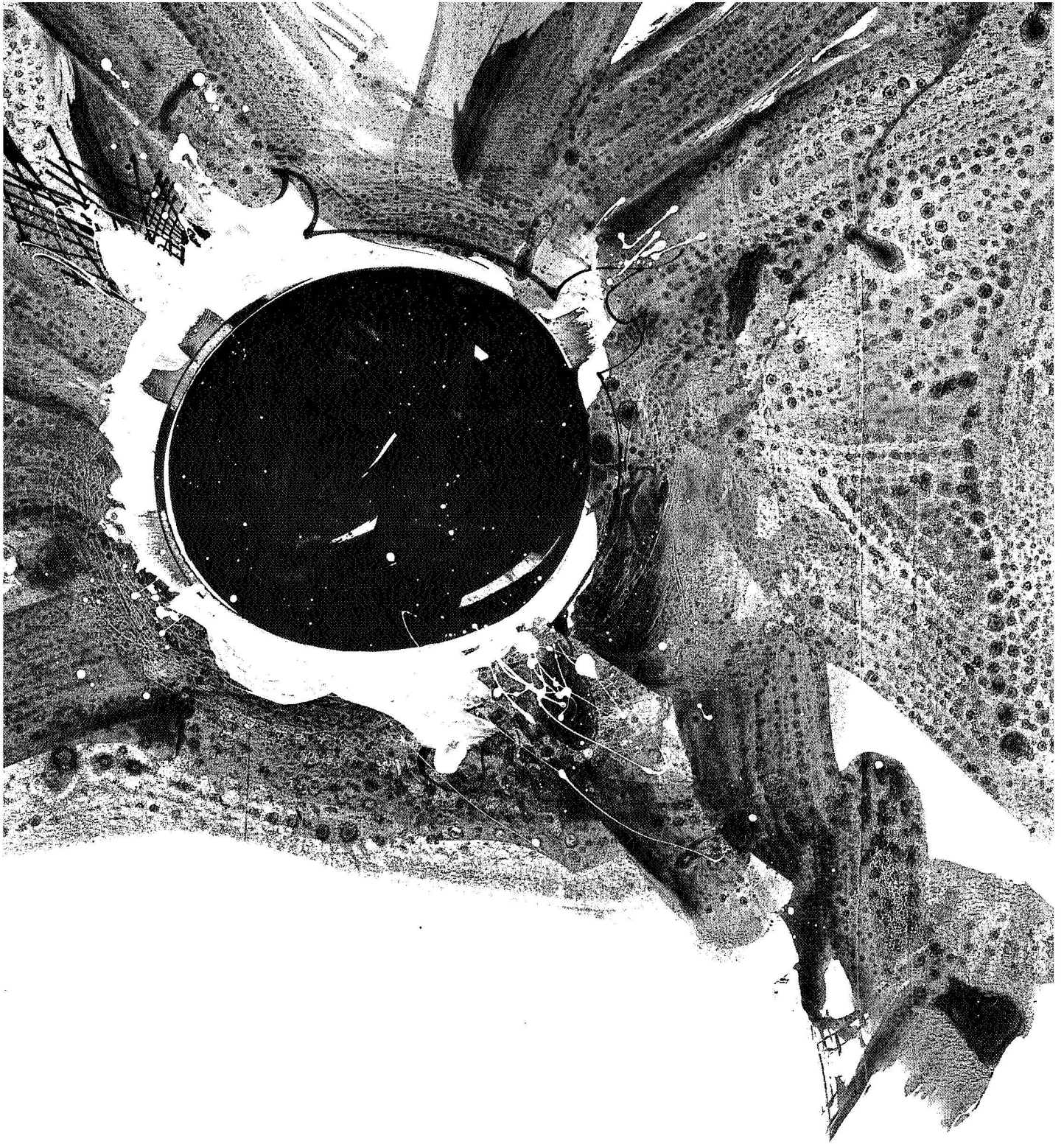


## TABLE OF CONTENTS — Continued

	Page
<b>CHAPTER 7 — RADIO OBSERVATIONS OF THE SOLAR WIND</b>	
<b>Invited Review</b>	
Observations of the Solar Plasma Using Radio Scattering and Scintillation Methods	
<i>A. Hewish</i> . . . . .	477
Discussion . . . . .	485
Comments <i>W. A. Coles</i> . . . . .	488
Discussion . . . . .	493
<b>Contributed Papers</b>	
Wavelength Dependence of the Interplanetary Scintillation Index <i>J. V. Hollweg and</i>	
<i>J. R. Jokipii</i> . . . . .	494
Discussion . . . . .	497
Comments <i>D. S. Intriligator</i> . . . . .	497
Discussion . . . . .	502
Comments <i>J. V. Hollweg</i> . . . . .	503
Discussion . . . . .	504
Spectra and Cross Spectra of Solar Wind Parameters From Mariner 5 <i>B. Goldstein and</i>	
<i>G. L. Siscoe</i> . . . . .	506
Discussion . . . . .	515
Evidence for a Continuous, Power Law, Electron Density Irregularity Spectrum	
<i>Willard M. Cromyn</i> . . . . .	517
Discussion . . . . .	520
Corotation of an Intermittent Solar Wind Source <i>Thomas A. Croft</i> . . . . .	521
Discussion . . . . .	529
Comments <i>N. F. Ness</i> . . . . .	529
<b>CHAPTER 8 — OBSERVATIONAL EVIDENCE AND THEORY OF THE IONIC COMPOSITION OF THE SOLAR WIND AND FRACTIONATION EFFECTS AT THE CORONAL BASE AND IN THE SOLAR WIND</b>	
<b>Invited Reviews</b>	
Spacecraft Observations of the Solar Wind Composition <i>S. J. Bame</i> . . . . .	535
Discussion . . . . .	558
Elemental and Isotopic Abundances in the Solar Wind <i>Johannes Geiss</i> . . . . .	559
Discussion . . . . .	579
<b>Contributed Papers</b>	
Solar Wind Helium Enhancements Following Major Solar Flares <i>J. Hirshberg</i> . . . . .	582
Discussion . . . . .	587
HEOS 1 Helium Observations in the Solar Wind <i>D. Bollea, V. Formisano, P. C. Hedgecock,</i>	
<i>G. Moreno, and F. Palmiotto</i> . . . . .	588
Discussion . . . . .	596
Radio Detection of Solar-Wind Discontinuities <i>Jeremy A. Landt</i> . . . . .	598
Discussion . . . . .	605

## TABLE OF CONTENTS — Concluded

	Page
<b>CHAPTER 9 — INTERACTION OF THE HELIOSPHERE AND THE GALACTIC MEDIUM: THE DISTANT SOLAR WIND</b>	
<b>Invited Review</b>	
The Interaction of the Solar Wind With the Interstellar Medium <i>W. I. Axford</i> . . . . .	609
Discussion . . . . .	658
<b>Contributed Papers</b>	
Observation of Lyman- $\alpha$ Emission in Interplanetary Space <i>J. L. Bertaux and J. E. Blamont</i> . . . . .	661
Properties of Nearby Interstellar Hydrogen Deduced From Lyman $\alpha$ Sky Background Measurements <i>G. E. Thomas</i> . . . . .	668
Discussion . . . . .	681
Interstellar Helium in Interplanetary Space <i>William C. Feldman, J. J. Lange, and F. Scherb</i> . . . . .	684
Effects of Interstellar Particles Upon the Interplanetary Magnetic Field <i>Paul J. Coleman, Jr., and Edwin M. Winter</i> . . . . .	698
Discussion . . . . .	702
New Evidence for Solar Cycle Variations at Great Distances <i>D. Venkatesan and V. K. Balasubrahmanyam</i> . . . . .	704
<b>CONFERENCE ATTENDEES</b> . . . . .	709



# CHAPTER I

Photospheric and Coronal Magnetic Fields

The present state of understanding and outstanding problems of the solar and coronal magnetic fields.



## PHOTOSPHERIC MAGNETIC FIELDS

Robert Howard

An invited review

Our knowledge of the nature of magnetic fields on the solar surface is reviewed. At least a large part of the magnetic flux in the solar surface is confined to small bundles of lines of force within which the field strength is of the order of 500 gauss. Magnetic fields are closely associated with all types of solar activity. Magnetic flux appears at the surface at the clearly defined birth or regeneration of activity of an active region. As the region ages, the magnetic flux migrates to form large-scale patterns and the polar fields. Some manifestations of the large-scale distribution are discussed.

### ABSTRACT

### INTRODUCTION

Soon after the invention of the spectroheliograph, astronomers observed the beautiful swirling patterns of chromospheric fibrils, and noted their similarity to patterns of iron filings around magnets. *George Ellery Hale* in 1908 was the first person to observe magnetic fields in any astronomical object when he showed that sunspots contain strong fields. Soon after this discovery *Hale* and his co-workers set out to detect a general dipole magnetic field of the sun. After many years of hard work and uncertain results, a value of about 20 gauss for a dipole field was published [*Hale et al.*, 1918]. More years of work were devoted to the problem by the Mount Wilson group without improving the precision of this number. Recent examination of the older plates by *Stenflo* [1971] has shown that the earlier measurements were in error.

Following World War II, improved photoelectric techniques became available, and several attempts were made at photoelectric measurements of solar magnetic fields. Difficulties still remained, however, and it was not until the development of the magnetograph by *H. W. Babcock* [1953] that reliable measurements of weak magnetic fields in the photosphere could be made. Except perhaps for a few scattered observations, the polar fields of the sun were not measured until the 1950 s.

The first *Babcock* magnetograph measured line splitting in the longitudinal Zeeman effect. *Stepanov and Severny* [1962] at the Crimean Astrophysical Observatory were the first to build a magnetograph that uses the transverse Zeeman effect to measure magnetic fields perpendicular to the line of sight. Observatories throughout the world now have magnetographs of one sort or another. By far most measurements of magnetic fields on the sun use only the longitudinal Zeeman effect because of the relatively great difficulties in the measurement of the polarized signal in the transverse effect and in the physical interpretation of the measurements once they are made. Compared with the longitudinal measurements, the transverse measurements depend to a greater extent on an accurate model atmosphere and knowledge of the mechanisms important in the formation of the absorption line [*Beckers*, 1971].

This paper covers several aspects of solar magnetism that are of interest in the study of the interplanetary medium. It is generally believed that magnetic field lines encountered by interplanetary probes originate in the photosphere of the sun or lower. The extent to which the small-scale structural characteristics of the solar magnetic fields extend into interplanetary space is not clear, but certainly the nature of the small-scale photospheric field bears on such problems as possible wave motions in the interplanetary field. On the large scale, the relationship of the distribution of photospheric fields to the interplanetary field sector structure has been the subject of considerable study, results of which are reviewed.

---

*The author is with Hale Observatories, California Institute of Technology and Carnegie Institution of Washington.*

Finally, some aspects of the rotation rates of various features on the solar surface are of great interest with respect to the possibility of spindown and momentum transfer through the interplanetary field. Recent results in this area are reviewed.

#### SMALL-SCALE MAGNETIC FIELDS ON THE SUN

Solar physicists are seriously hampered in their observations by the distorting effects of the earth's atmosphere. The smallest area measurements of magnetic field strength that are currently practical cover about  $10^6$  km<sup>2</sup> on the sun, and such measurements are possible only under the most favorable conditions of the terrestrial atmosphere. Thus "small-scale" measurements are not small in scale compared with those made in a physics laboratory or in interplanetary space.

It was not until some years after the first magnetograph measurements that it was realized that the magnetic fields in the solar photosphere, when viewed on a small scale, show the same intricate patterns as one sees in the chromospheric emission of the calcium K-line [Leighton, 1959; Howard, 1959]. More recently, attention has been given to the very finest scale features observable. In these studies magnetic fields measured in the photosphere are seen to be clumped into small areas called "gaps" or "knots" [Sheeley, 1967; Beckers and Schröter, 1968]. Figure 1 is a view of solar magnetic fields on a small scale, and figure 2 is a spectrum of some small magnetic features. These small features have areas

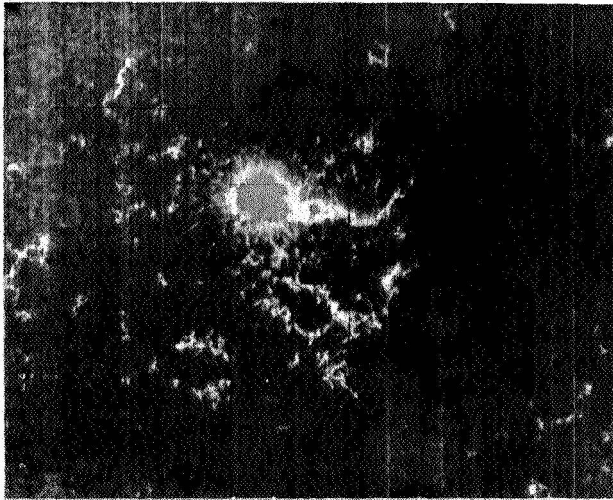


**Figure 1.** A videomagnetogram of a portion of the solar disk. Polarities are distinguished by either a brighter or darker shade than the background. [Courtesy D. Vrabec, Aerospace Corporation.]

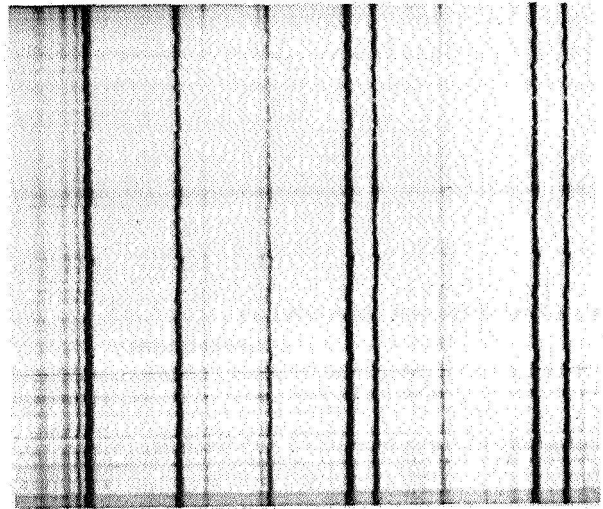


**Figure 2.** A spectrum of the photosphere in the region of  $\lambda 5250$ . Note the weakening (gaps) in several places of the absorption lines. [Courtesy N. R. Sheeley, Kitt Peak National Observatory.]

of perhaps slightly less than  $10^6$  and km<sup>2</sup> and contain magnetic fields of many hundreds of gauss.

The gaps correspond to long-lived dark intergranular regions in the photosphere, and to bright points in H $\alpha$  or the calcium K<sub>2,3,2</sub> network in the chromosphere [Sheeley, 1967; Beckers and Schröter, 1968; Abdussamatov and Krat, 1969; Vrabec, 1971]. It has been established that the gaps occur at boundaries of supergranular cells where there is also downward motion [Tanenbaum et al., 1969; Frazier, 1971; Grigorev and Kuklin, 1971]. However, there is some disagreement among observers as to whether there is downward motion associated with magnetic fields [Gopasyuk and Tsap, 1971; Bhatnagar, 1971; Sheeley, 1971]. There are roughly 10 gaps per 100 granules near spots and about one gap per 100 granules far away from spots. The high density of gaps around sunspots suggests that they are an important part of the structure of an active region. The magnetic flux from the gaps of an active region is comparable with that of the sunspots. Sawyer [1971] suggests a higher concentration of field elements.

In recent interesting work that deserves confirmation, Livingston and Harvey [1969] present evidence for the quantization of magnetic flux measured in gaps, which could be explained if all gaps have the same magnetic flux.

Evidence exists for high horizontal gradients in the chromosphere of the order of 17 gauss/km [Title and Andelin, 1971], although vertical gradients, even in

spots, are probably smaller—of the order of 0.5 to 0.8 gauss/km [Abdussamatov, 1971]. In general, fields at different levels in the solar atmosphere have different strengths; sometimes even increasing with height [Tsap, 1971; Harvey and Hall, 1971].

Field concentrations have been observed to move outward from large spots [Sheeley, 1971; Vrabec, 1971]. This may be associated with the well-known Evershed motion. The velocities (1 to 2 km/sec) are about the same as the Evershed velocities, but the features themselves are outside the region generally considered to contain the Evershed motions.

Theoretical considerations [Zwaan, 1967; Weart, 1970] show that the magnetic gaps may be stable features. Musman [1971] has shown by analysis of magnetic and velocity observations that the accumulation of magnetic flux at the boundaries of supergranular cells does not proceed as rapidly as one might expect.

The important question of how much of the solar flux may be concentrated in small bundles of lines of force and how much is spread more or less evenly over large areas of the solar surface has not yet been answered. Certainly at least a large fraction even of the polar magnetic fields is contained in small regions with high field strength.

The measurements of these small gaps are on the borderline of the impossible at all observatories during almost all the available observing time. In the future, satellite telescopes hopefully will clear up many of the problems that face us now. Not only is the earth's atmosphere a problem in small-scale observations, but the sun's atmosphere also presents difficulties. Practically all the spectrum lines commonly used in magnetographs present problems of one sort or another in the measurement of magnetic fields in gaps, even when using only the longitudinal component of the field. Harvey and Livingston [1969] have shown that due to the higher temperature in gaps, the commonly used absorption lines change their profiles—for example,  $\lambda_{5250}$  of FeI weakens considerably (fig. 2) — and since most measurements are made with resolution much lower than the size of the gaps, the measured field does not represent a good average over the magnetograph aperture. This problem has not been resolved, and no one has yet found the ideal line to be used for solar magnetic field measurements.

Several observatories are concentrating their efforts on observations of magnetic fields on the smallest possible scale, using various video techniques to obtain good resolution in time. It is hoped that observations such as that shown in figure 1 will help us to understand the complex processes that make up solar activity on the small scale.

## LARGE-SCALE SOLAR MAGNETIC FIELDS

The great bulk of the observational data available for the study of the large-scale magnetic field of the sun comes from the Mount Wilson Observatory. Full-disk magnetic scans of the sun have been obtained there daily starting with the original magnetograph [Babcock, 1953] in Pasadena. In recent years the data have been recorded in digital form, and through the years various technical refinements have been made so that although the principle of operation remains the same, the present instrument is a considerable improvement over the original magnetograph. The angular resolution used in the daily scans is 17 arc sec. The isogauss magnetograms, which are now computer-drawn (fig 3), are published monthly in the bulletin *Solar-Geophysical Data* by the National Oceanic and Atmospheric Administration of the Department of Commerce.

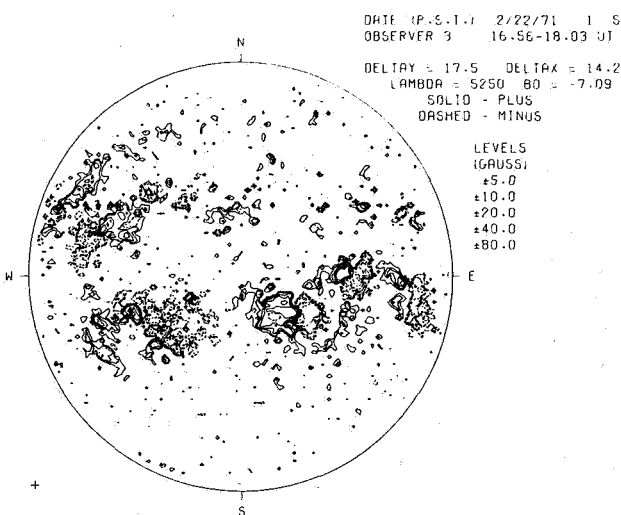
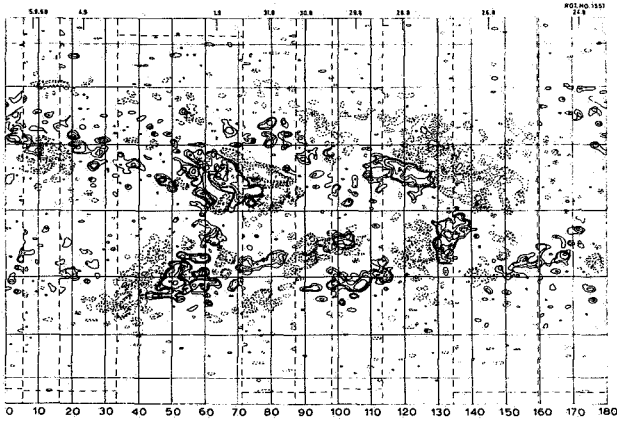


Figure 3. A solar magnetogram from Mt. Wilson. The gauss levels are listed. Solid lines are positive isogauss levels, and dashed lines are negative levels. The angular resolution is 17.5 arc sec.

To examine the magnetic fields of the sun on a large scale, it is convenient to plot them on a global scale. Such a plot is called a synoptic chart (fig 4) and covers the entire surface area of the sun during one rotation in an equal-area projection. Synoptic charts of the sun from the Mount Wilson magnetic data are now published in the International Astronomical Union publication *Quarterly Bulletin on Solar Activity*. The interval from the summer of 1959 to the summer of 1966 was covered in an atlas of synoptic charts published a few years ago [Howard et al., 1967].

On the magnetograms and synoptic charts we see a



**Figure 4.** A portion of a synoptic chart of solar magnetic fields from Mt. Wilson data. The levels and resolution are the same as for Figure 3.

number of easily distinguishable features. In general, although sunspots always contain strong magnetic fields, they are not obvious features on the Mount Wilson isogauss maps because they are small compared with the angular resolution of the instrument and because there are obvious large patterns of nonspot fields which dominate the maps. The obvious strong-field features which one sees on the isogauss maps are all active regions. A 20-gauss contour line delineates a calcium plage [Leighton, 1959; Howard, 1959]. The plage fields, seen with the low resolution of the full-disk scan, reach 40 or 50 gauss. The appearance of solar magnetic features on a large scale varies with the level of solar activity. During an active period the most prominent features on solar maps comprise what is known as the "background field pattern" [Bumba and Howard, 1965]. In 1959 this pattern and the active regions, within 4-gauss contour lines, occupied nearly half the surface area of the sun. The pattern is one of the features of alternating polarity inclined to the meridian by the shearing effects of differential rotation. During periods of low solar activity, the background field pattern is extremely weak and generally is lost in noise around 1 or 2 gauss. In the polar regions, the fields measured during the last five years or so are very weak, generally less than 1 gauss. At the time of the last solar maximum the polar fields were somewhat stronger. This weakening of the polar fields is probably due to the lowering of the level of solar activity, as will be discussed below.

In view of the existence of a regular pattern of magnetic fields on the large scale, it seems worthwhile to examine more exactly the flux distribution on the solar surface. In such a study Altschuler *et al.* [1971] analyzed Mount Wilson magnetic field data in terms of surface harmonics. Between 1959 and 1962 the dominant

harmonic corresponded to a dipole lying in the plane of the equator. There was also a significant harmonic in which both solar poles had the same magnetic polarity, opposite to that at the equator. From the end of 1962 through 1964, the harmonic corresponding to four sectors grew dominant as the dipole faded. In 1965 and 1966 the north-south dipole became significant. It is hoped that the analysis can be extended soon to more recent data, which are of better quality than the older data.

The correlation between photospheric and interplanetary magnetic fields is well known [Ness and Wilcox, 1966]. The clear existence of a sector pattern in the interplanetary field [Wilcox and Ness, 1965] implies the existence of some sort of sector pattern in the photospheric magnetic field. Such a pattern has been observed [Wilcox and Howard, 1968]. In the case of the 1964 data, the solar sector boundaries, determined from a cross-correlation analysis with the interplanetary field data, showed a more or less symmetric pattern, stretched by differential rotation, centered on a latitude of  $N 15^\circ$ . Analyses of subsequent data have shown to a lesser extent the effects of differential rotation [Wilcox *et al.*, 1969; Wilcox, 1971]. However, all these studies seem to show that the equator plays little or no role in the appearance of the pattern; that is, the pattern stretches unchanged across the solar equator. This tendency for the background magnetic field pattern to ignore the equator has been noted by Bumba and Howard [1969] from an inspection of synoptic charts. Wilcox and Ness [1967] have shown that active regions tend to cluster in the preceding portions of solar sectors. Unfortunately, we do not yet know enough about solar activity or solar magnetism (which is, perhaps, the same thing) to be able to answer the important question: Which is the fundamental quantity: the sector or the activity? That is, is the sector there because of the chance clustering of active regions, or are the active regions forced to cluster in the preceding portion of a fundamental, deep rooted structure — the solar sector? It does not now seem likely that a definitive answer to this question will appear within the next few years.

New magnetic flux arrives at the surface of the sun from below at the birth of an active region, or at a rather sharply defined resurgence of activity in an old active region. There is no evidence that magnetic fields come to the surface of the sun in any other manner. The large weak-field features of the background field pattern develop over many weeks or months from the expansion and weakening of remnants of old active region fields [Bumba and Howard, 1965]. Individual features of the background field pattern may persist for many months,

although individual field features are not in general distinguishable for more than a few rotations. The distinction between the *pattern* and the individual field elements is made clear by a study of the rotation of each. The pattern rotates with a period of 27 days at latitudes below about  $20^\circ$ , whereas the individual field elements, when they can be followed, rotate with the rates appropriate for their latitudes [Bumba and Howard, 1969; Wilcox *et al.*, 1970]. In general, the following polarity in each solar hemisphere predominates in a poleward drift of magnetic flux. In each hemisphere a large poleward-moving unipolar region may form at high latitude from the following polarity flux of many active regions. Such unipolar magnetic regions (UMR) may cover more than  $180^\circ$  in longitude at a latitude greater than  $60^\circ$ . It is assumed that this effect during a sunspot cycle builds up the following polarity in the polar regions as the polar field.

The field in the polar regions is weak and variable, and at least largely confined to small bundles of lines of force originating in the polar faculae [Howard, 1965]. A clear reversal of the polar fields was observed at the maximum of cycle 19 by H. D. Babcock [1959]. No such well-defined reversal has been observed yet in cycle 20. It is possible that because of the lower level of activity in the last cycle, the buildup of polar fields is proceeding more slowly than it did in the last cycle. However, the work of Sheeley [1964] in examining old polar faculae data and the well-known periodic migration and disappearance of the polar prominence ring indicate a regular cyclic behavior of the polar magnetic fields at least during this century.

Recent comparisons of the magnetic field of integrated sunlight measured at the Crimean Astrophysical Observatory with the interplanetary magnetic field indicate a very good correlation [Severny *et al.*, 1970] for a period of several months in the spring of 1968. This suggests a very large-scale coherent pattern. More recent results from Mount Wilson measurements (see p.39) indicate that this correlation is not as straightforward as had been believed. It seems possible that the correlation may be a consequence of the large, slowly evolving solar sector pattern.

### THE SOLAR ROTATION

In the last few years, interest in the rotation of the sun has increased. The classic work on the differential rotation of sunspots is that of Newton and Nunn [1951]. This is still the standard reference on the subject, although, as Newton and Nunn point out, the observational difficulties in establishing the rotation rate of sunspots are considerable [Ward, 1966]. Attempts early in

this century to establish the rotational velocity of the sun from Doppler shifts of spectral lines gave rather disparate results. [See Howard and Harvey, 1970, for complete references.] One observer [Plaskett, 1916] concluded that the rotational velocity of the sun must vary. The observations were so difficult and the results so varied that very little was done in this field from the early 1930's until a few years ago when accurate line shift measurements became possible with solar magnetographs. Livingston [1969a; 1969b] and Howard and Harvey [1970] have found, using different observing techniques, a rotation rate for the photospheric material that is slower by about 4 percent than that for sunspots. This is a difference of roughly one day per rotation. Fig 5,

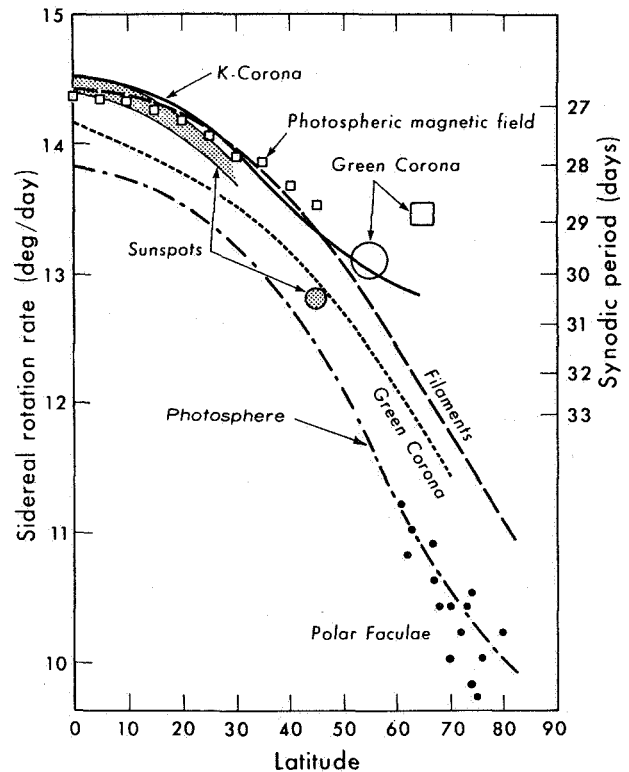


**Figure 5.** Comparison of various rotation results. K-corona at  $1.125 R_\odot$  (solid curve) [Hansen *et al.*, 1969]; photospheric magnetic field (squares) [Wilcox and Howard, 1970]; all sunspots (top of shaded area) [Ward, 1966] recurrent sunspots (bottom of shaded area) [Newton and Nunn, 1951]; high-latitude spots at  $45^\circ$  (shaded circle) [Waldmeier, 1957; Kopecky *et al.*, 1957]; polar faculae (dots) [Muller, 1954; Waldmeier, 1957]; filaments (dashed line) [d'Azambuja and d'Azambuja, 1948; Bruzek, 1961]; green corona (dotted curve) [Trellis, 1957], (circle) [Waldmeier, 1950], (square) [Cooper and Billings, 1962]; photosphere (dot-dashed line) [Howard and Harvey, 1970].

redrawn from *Hansen et al.* [1969], shows a comparison of rotation rates of various solar features. It appears that the spots, the photospheric magnetic fields (outside sunspots), the K-corona, and the filaments maintain roughly the same rotation rates for latitudes below about  $15^\circ$  or  $20^\circ$ . At latitudes higher than this the photospheric magnetic fields, the filaments, and the K-corona maintain a significantly faster rate of rotation than do the spots, while the photospheric material rotates much slower.

Variations in the rotation rates are well-established for the K-corona [*Hansen et al.*, 1969], the photospheric magnetic fields [*Wilcox and Howard*, 1970], and the photospheric material [*Howard and Harvey*, 1970; *Howard*, 1971]. The reason for these variations is not now understood, and as yet no correlation analyses between the various rates have been attempted.

The magnetic fields extending into the interplanetary medium cannot be slowing the photospheric material at the photospheric level because the fields there are rotating about 80 m/sec faster than the gas. The more rapidly rotating magnetic field lines may be connected with more rapidly rotating inner layers of the sun. Note that the filaments and the corona are closely related to the magnetic field structure. It would be puzzling if these features maintained significantly different rotation rates than do the magnetic fields.

## REFERENCES

- Abdussamatov, H. I.: Observations of the Two-Level Structure of Sunspot Magnetic Fields. *IAU Symposium No. 43*. R. Howard and D. Reidel, eds., 1971. (in press)
- Abdussamatov, H. I.; and V. A. Krat: Magnetic "Knots" in the Solar Photosphere. *Solar Phys.*, Vol. 2, 1969, pp. 420-422.
- Altschuler, Martin D.; Newkirk, G.; and Trotter, D.: Time Evolution of the Large Scale Solar Magnetic Field. *IAU Symposium No. 43*. R. Howard and D. Reidel, eds., 1971. (in press)
- Babcock, H. D.: The Sun's Polar Magnetic Field. *Astrophys. J.*, Vol. 130, 1959, pp. 364-365.
- Babcock, H. W.: The Solar Magnetograph. *Astrophys. J.*, Vol. 118, 1953, pp. 387-396.
- Beckers, J. M.: The Measurement of Solar Magnetic Fields. *IAU Symposium No. 43*. R. Howard and D. Reidel, eds., 1971. (in press)
- Beckers, J. M.; and Schröeter, E.H.: The Intensity, Velocity and Magnetic Structure of a Sunspot Region. *Solar Phys.*, Vol. 4, 1968, pp. 142-164.
- Bhatnagar, A.: Fine-scan Velocity and Magnetic-Field Measurements in Solar Regions. *Solar Phys.*, Vol. 16, 1971. pp. 40-50.
- Bumba, V.; and Howard, R.: Large-Scale Distribution of Solar Magnetic Fields. *Astrophys. J.*, Vol. 141, 1965, pp. 1502-1512.
- Bumba, V.; and Howard, R.: Solar Activity and Recurrences in Magnetic Field Distribution. *Solar Phys.*, Vol. 7, 1969, pp. 28-38.
- Frazier, E. N.: Supergranulation at the Center of the Disk. *IAU Symposium No. 43*. R. Howard and D. Reidel, eds., 1971. (in press)
- Gopasyuk, S. I.; and Tsap, T.: The Magnetic and Velocity Fields and Brightness in the Solar Atmosphere. *IAU Symposium No. 43*. R. Howard and D. Reidel, eds., 1971. (in press)
- Grigorev, V. M.; and Kuklin, G.V.: On the Fine Structure of the Magnetic Field in the Undisturbed Photosphere. *IAU Symposium No. 43*. R. Howard and D. Reidel, eds., 1971. (in press)
- Hale, G. E.: On the Probable Existence of a Magnetic Field in Sunspots. *Astrophys. J.*, Vol. 28, 1908, pp. 315-343.
- Hale, G. E.; Seares, F. H.; Van Maanen, A.; and Ellerman, F.: The General Magnetic Field of the Sun. *Astrophys. J.*, Vol. 47, 1918, pp. 206-254.
- Hansen, R. T.; Hansen, S. F.; and Loomis, H. G.: Differential Rotation of the Solar Electron Corona. *Solar Phys.*, Vol. 10, 1969, pp. 135-149.
- Harvey, J.; and Hall, D.: Magnetic Fields Measured with the 10830Å HeI Line. *IAU Symposium No. 43*. R. Howard and D. Reidel, eds., 1971. (in press)
- Harvey, J.; and Livingston, W. C.: Magnetograph Measurements with Temperature-Sensitive Lines. *Solar Phys.*, Vol. 10, 1969, pp. 283-293.
- Howard, R.: Observations of Solar Magnetic Fields. *Astrophys. J.*, Vol. 130, 1959, pp. 193-201.
- Howard, R.: Large Scale Solar Magnetic Fields. *IAU Symposium No. 22*, edited by R. Lüft, North Holland, 1965, pp. 129-143.
- Howard, R.: The Large-Scale Velocity Fields of the Solar Atmosphere. *Solar Phys.*, Vol. 16, 1971, pp. 21-36.
- Howard, R.; Bumba, V.; and Smith, S.: *Atlas of Solar Magnetic Fields*. Carnegie Institution of Washington Publication 626, 1967.
- Howard, R.; and Harvey, J.: Spectroscopic Determinations of Solar Rotation. *Solar Phys.*, Vol. 12, 1970, pp. 23-51.
- Leighton, R. B.: Observations of Solar Magnetic Fields in Plage Regions. *Astrophys. J.*, Vol. 130, 1959, pp. 366-380.
- Livingston, W. C.: Solar Rotation, 1966-68. *Solar Phys.*, Vol. 7, 1969a, pp. 144-146.

- Livingston, W. C.: On the Differential Rotation with Height in the Solar Atmosphere. *Solar Phys.*, Vol. 9, 1969b, pp. 448-451.
- Livingston, W. C.; and Harvey, J.: Observational Evidence for Quantization in Photospheric Magnetic Flux. *Solar Phys.*, Vol. 10, 1969, pp. 294-296.
- Musman, S.: Observations and Interpretations of Supergranule Velocity and Magnetic Fields. *IAU Symposium No. 43*. R. Howard and D. Reidel, eds., 1971. (in press)
- Ness, N. F.; and Wilcox, J. M.: Extension of the Photospheric Magnetic Field Into Interplanetary Space. *Astrophys. J.*, Vol. 143, 1966, pp. 23-31.
- Newton, H. W.; and Nunn, M. L.: The Sun's Rotations Derived from Sunspots 1934-1944 and Additional Results. *Monthly Notices Roy. Astron. Soc.*, Vol. 111, 1951, pp. 413-421.
- Plaskett, H. H.: A Variation in the Solar Rotation. *Astrophys. J.*, Vol. 43, 1916, pp. 145-160.
- Sawyer, C.: On the Reality of Magnetic Fine Structure. *IAU Symposium No. 43*. R. Howard and D. Reidel, eds., 1971. (in press)
- Severny, A.; Wilcox, J. M.; Scherrer, P.H.; and Colburn, D. S.: Comparison of the Mean Photospheric Magnetic Field and the Interplanetary Magnetic Field. *Solar Phys.*, Vol. 15, 1970, pp. 3-14.
- Sheeley, N. R., Jr.: Polar Faculae During the Sunspot Cycle. *Astrophys. J.*, Vol. 140, 1964, pp. 731-735.
- Sheeley, N. R., Jr.: Observations of Small-Scale Solar Magnetic Fields. *Solar Phys.*, Vol. 1, 1967, pp. 171-179.
- Sheeley, N. R., Jr.: The Time Dependence of Magnetic, Velocity and Intensity Fields in the Solar Atmosphere. *Proc. IAU Symposium No. 43*, 1971. (in press)
- Stenflo, J.O.: Observation of the Polar Magnetic Fields. *IAU Symposium No. 43*. R. Howard and D. Reidel, eds., 1971. (in press)
- Stepanov, V. E.: and Severny, A. B.: A Photoelectric Method for Measurements of the Magnitude and Direction of the Solar Magnetic Field. *Izv. Crimean Astrophys. Obs.*, Vol. 28, 1962, pp. 166-193.
- Tanenbaum, A. S.; Wilcox, J. M.; Frazier, E. N.; and Howard R.: Solar Velocity Fields: 5-min. Oscillations and Supergranulation. *Solar Phys.*, Vol. 9, 1969, pp. 328-342.
- Title, A. M.; and Andelin, J. P., Jr.: Spectra-spectroheliograph Measurements. *IAU Symposium No. 43*. R. Howard and D. Reidel, eds., 1971. (in press)
- Tsap, T. T.: The Magnetic Fields at Different Levels in the Active Regions of the Solar Atmosphere. *IAU Symposium No. 43*. R. Howard and D. Reidel, eds., 1971. (in press)
- Vrabec, D.: Magnetic Field Spectroheliograms From the San Fernando Observatory. *IAU Symposium No. 43*. R. Howard and D. Reidel, eds., 1971. (in press)
- Ward, F.: Determination of the Solar-Rotation Rate From the Motion of Identifiable Features. *Astrophys. J.*, Vol. 145, 1966, pp. 416-425.
- Weart, S. R.: Production of the Solar Magnetic Fine-Structure by Convection. *Solar Phys.*, Vol. 10, 1970, pp. 274-279.
- Wilcox, J. M.: Sector Structure of the Solar Magnetic Field. *Comments on Astrophysics and Space Physics*, 1971. (in press)
- Wilcox, J. M.; and Howard, R.: A Large-Scale Pattern in the Solar Magnetic Field. *Solar Phys.*, Vol. 5, 1968, pp. 564-574.
- Wilcox, J. M.; and Howard, R.: Differential Rotation of the Photospheric Magnetic Field. *Solar Phys.*, Vol. 13, 1970, pp. 251-260.
- Wilcox, J. M.; and Ness, N. F.: Quasi-stationary Corotating Structure in the Interplanetary Medium. *J. Geophys. Res.*, Vol. 70, 1965, pp. 5793-5805.
- Wilcox, J.M.; and Ness, N.F.: Solar Source of the Interplanetary Sector Structure. *Solar Phys.*, Vol. 1, 1967, pp. 437-445.
- Wilcox, J. M.; Schatten, K. H.; Tanenbaum, A. S.; and Howard R.: Photospheric Magnetic Field Rotation: Rigid and Differential. *Solar Phys.*, Vol. 14, 1970, pp. 255-262.
- Wilcox, J. M.; Severny, A.; and Colburn, D. S.: Solar Source of Interplanetary Magnetic Fields. *Nature*, Vol. 224, 1969, pp. 353-354.
- Zwaan, C.: Small-scale Solar Magnetic Fields and "Invisible Sunspots." *Solar Phys.*, Vol. 1, 1967, pp. 478-480.

## DISCUSSION

*E. N. Parker* The polar fields of the sun reversed, as I remember, in late 1958. As a consequence there has been a strong psychological feeling that since they are tied to the sunspot cycle, if you add eleven years to late 1958 you get roughly 1969 or 1970—am I correct that the fields have not yet reversed again?

*R. Howard* I can't answer that with a yes or no. There has not been a clear reversal of magnetic field polarity at the solar poles; at the moment, at least, within the last year or two, the fields at both poles have been slightly negative. However, about a year or a year and a half ago the south pole became somewhat more negative than the north pole. If you define that as a reversal, then there has been a reversal.



## CORONAL MAGNETIC FIELDS AND THE SOLAR WIND

An invited review

Gordon Newkirk, Jr.

This paper reviews current information on coronal magnetic fields as they bear on problems of the solar wind. Both steady-state fields and coronal transient events are considered. We begin with a brief critique of the methods of calculating coronal magnetic fields including the potential (current free) models, exact solutions for the solar wind and field interaction, and the source surface models. These solutions are compared with the meager quantitative observations which are available at this time. Qualitative comparisons between the shapes of calculated magnetic field lines and the forms visible in the solar corona at several recent eclipses are displayed. These suggest that: (1) coronal streamers develop above extended magnetic arcades which connect unipolar regions of opposite polarity; and (2) loops, arches, and rays in the corona correspond to preferentially filled magnetic tubes in the approximately potential field.

### ABSTRACT

Current information regarding the connection of visual coronal forms and such interplanetary features as sector boundaries is still too fragmentary for a definitive analysis. However, it appears that every system of high magnetic arches in the corona can be expected to have a current sheet in the outer corona and to produce a helmet streamer and a sector boundary in the interplanetary field. The accident of perspective has apparently prevented the detection of this relationship between streamers and such geomagnetically significant features of the solar wind as sector boundaries in the past.

Recent observations have partly explained why particular tubes in the approximately potential field present in the corona are preferentially filled with material. Intense knots of field at photospheric levels give rise to elevated densities in the overlying corona, presumably as a result of increased mechanical energy transport into the chromosphere and corona above such regions. Such a mechanism would be expected to produce a mapping of small-scale fluctuations of the magnetic field at photospheric levels well out into the interplanetary medium although their identification in space remains uncertain.

Because of the paucity of information, the evolution of coronal magnetic fields can be discussed only briefly. Magnetic fields and transient events are examined in terms of three categories of phenomena:

1. Events channeled by the ambient field (surges, loop prominences, type III radio bursts, stationary type IV radio bursts, and cosmic ray events)
2. Events in which the ambient field is perturbed significantly (*Disparition Brusque*, Moreton waves, and type II bursts)
3. Mass ejections such as accompany the most violent flares.

Future problems involving magnetic fields in the corona are suggested.

---

*The author is at the High Altitude Observatory, National Center for Atmospheric Research, Boulder, Colorado. The National Center for Atmospheric Research is sponsored by the National Science Foundation.*

## INTRODUCTION

In the solar corona, we find organized magnetic fields of great variety—from the extended, weak fields of the sector structure to the active region and sunspot fields and the intense but small magnetic pores. These fields play a crucial role in determining the structure of the corona and the solar wind: at a low level they influence the flux of mechanical energy into the corona, and thus determine the distribution of temperature and density. The configuration of the fields in the corona further influences the density distribution and the flow of the inner solar wind and partially accounts for the forms we observe there. Changes wrought in the inner corona are finally reflected in the state of the interplanetary plasma and field, as well as in the rotation of the solar wind.

Coronal fields are also central in the various coronal transient phenomena observed. Several current theories of flares require that the energy of the event be derived from the fields. The shock waves and high energy particles responsible for radio bursts appear to be channeled by the fields. These same fields guide and may be responsible for the storage of solar cosmic rays.

In discussing magnetic fields in the corona we should keep two facts in mind. First, the photospheric fields can be regarded as a boundary condition of our problem—the coronal fields can have only a negligible influence at the photospheric level. Second, it is the large-scale and, unfortunately for our ability to observe them, the weak fields that are most influential in the corona.

## MAGNETIC FIELDS IN THE QUIET CORONA

### Computations

Since the study of coronal magnetic fields depends almost exclusively on their computation from observed photospheric fields, a brief review of the calculations involved is in order. These all begin with measurements of Zeeman splitting due to the line-of-sight photospheric field  $B_L$ . The potential field or modified potential field in the corona is then calculated either in rectangular coordinates [Schmidt, 1964] over a volume small with respect to the sun or in spherical coordinates over a large volume [Newkirk *et al.*, 1968; Schatten *et al.*, 1969; Altschuler and Newkirk, 1969]. The Schmidt technique employs a distribution of monopoles of surface density

$$\sigma(x, y) = kB_n(x, y)$$

where  $B_n = B_L$ , and arrives at the potential field according to ordinary magnetostatic theory. Techniques for analyzing global fields are identical to those used in

geomagnetism [Chapman and Bartels, 1940] and fit a series of spherical harmonics, which are solutions of the Laplace equation, to the distribution of the line-of-sight field over the entire sun and express the potential field in terms of harmonic coefficients.

The Schmidt program can be used only for heights small with respect to the dimensions of the photospheric area scanned and at points well removed from the borders of that area. On the other hand, the simplicity of the mathematics allows a large number of data points to be processed for detailed analysis of the field above this restricted area. The harmonic expansion, while applicable to larger coronal distances, is limited in the total number of coefficients that can be fitted to the data; with current computers we can incorporate only a rather coarse pattern of the surface fields. Thus, this technique cannot be used to calculate the fine details of the field above an active region. The Schmidt program requires observations near the center of the disk for  $B_n(x, y)$ , while the harmonic expansion demands the field over the entire sun—a distribution that is frequently a rather uncertain average of the temporally varying fields at the surface.

Neither technique includes the influence of electric currents that may be present in active regions and flow in the corona as a result of the solar wind. Since the latter currents are known to be significant, they must be accounted for in any complete theory. Ideally, we should be able to specify the magnetic field, density, temperature, and velocity at any level in the corona once the spatial distribution of these conditions is known at the top of the chromosphere. Since such a complete solution for a realistic sun is still beyond our resources, we must consider two partial solutions. One, pioneered by Pneuman [1968, 1969] and Pneuman and Kopp [1970, 1971], solves the dynamic, thermal, and magnetic equations for a simple initial field such as that of a dipole. The success of this method is judged by the fact that realistic profiles of coronal streamers result. The model also affords quantitative predictions of such still inaccessible parameters as the temperature and velocity structure within streamers.

A second technique, which can be applied to fields of greater complexity, simulates the effect of the solar wind on the potential field by the introduction of a zero-potential on the sphere  $R_w \cong 1.6R_\odot - 2.5R_\odot$ , where the wind becomes super-Alfvénic in the physical models. This surface, first introduced by Schatten *et al.*, [1969], forces the higher field lines to become radial at that radius. They are presumed to remain radial above  $R_w$  except for the “garden hose” spiraling. (Actually, in

such a model the field closes above  $R_w$ , and any comparison of field lines and the corona should be restricted to  $R \leq R_w$ .) Note that this technique is equivalent to replacing the volume currents, which flow in the corona as a result of the interaction of the solar wind and the field, by a set of surface currents on  $R = R_w$ .<sup>1</sup> The exact value of  $R_w$  is chosen empirically either to match the shape of the calculated field lines to the shape of the corona [ $R_w \sim 2.5R_\odot$ , Altschuler and Newkirk, 1969], or to bring correspondence between the average magnitude of the field and its frequency spectrum at 1 AU and that projected from  $R_w \sim 1.6R_\odot$  [Schatten *et al.*, 1969].

We naturally ask how well the physical solution,

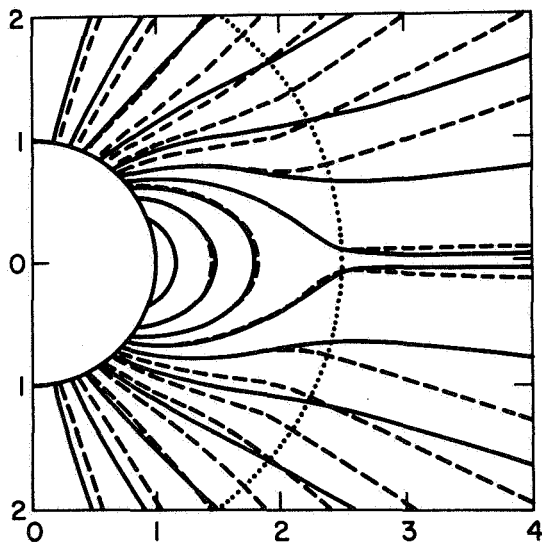


**Figure 1.** Comparison of the shapes of coronal magnetic field lines calculated for a dipole surface field according to Pneuman and Kopp [1971] (solid lines) and for a potential field (dashed lines) with a zero-potential surface at  $R_w$ . The zero-potential solution is not valid above  $R_w$  (dotted arc). Foot points for high-latitude field lines are separated for clarity. The super-Alfvénic point in the exact solution occurs at  $2.56 R_\odot$  in the streamer.

<sup>1</sup>Later in this chapter (p. 44) Schatten describes an algorithm for drawing the field lines that is the equivalent of introducing a current sheet above each magnetic arch that osculates  $R_w$  in the pure potential solution. This method gives an improved approximation to the fields beyond  $R_w$ . It requires  $R_w$  to be set well within the super-Alfvénic point to achieve a match of the field line shapes and the flux transported to 1 AU with those of the physical models.

which can handle only a simple field configuration, compares with the empirical solutions, which can handle complex fields. Figure 1 displays such a comparison for the simple case of a dipole surface field. Within the region of validity of the zero-potential solution, the agreement in the shapes of the field lines appears to be good. Moreover, the flux carried out by the solar wind is the same in the two models. Of course, the value  $R_w = 2.49R_\odot$  was chosen to produce good coincidence in the shapes although this value is close to the height of the super-Alfvénic point in the streamer. Thus, we conclude that the zero-potential surface model for more complex photospheric field distributions can also give a good approximation to fields in the corona.

The discrepancy between the value of  $R_w = 1.6R_\odot$  chosen by Schatten *et al.* and the  $R_w = 2.5R_\odot$  found by Altschuler and Newkirk remains unexplained. This might be due to (1) a difference in the level of solar activity between the two periods examined; (2) the underestimation of the field strength at the source surface by the Green's function method; or (3) an underestimation of the strength of the photospheric fields by the Mt. Wilson magnetograph.<sup>2</sup>

#### Observations

True validation of such calculations by a comparison of computed and measured coronal fields is not yet possible. We must rely on statistical information or fields measured in prominences. Figure 2 displays a statistical comparison of the absolute magnitude of the field vs. height. Since the original figure was drawn, the analyses of the Razin effect in a single radio burst [Boischot and Clavelier, 1967; Ramaty and Lingenfelter, 1968; Bohlin and Simon, 1969] and of the weak polarization in some correlated bursts [Kai, 1969a] have added a few more measures of the absolute magnitude of the field at coronal heights. In the absence of any event-by-event comparison between observed and calculated coronal fields, we compare the observations with three simple models: (1) an  $R^2$  extrapolation from interplanetary space; (2) the Legendre polynomial field above a plane for the surface fields of November 1966; and (3) a

<sup>2</sup>Note added to proof: J. O. Stenflo has pointed out that the filamentary nature of the photospheric field results in an error in field strengths measured by the 5250 Å line of Fe I and that the apparent fields must be multiplied by a factor of about 2.5 [Livingston and Harvey, 1969; Stenflo, 1971a]. When this factor is applied, the field strength at 1 AU is best predicted with  $R_w = 2.5R_\odot$  [Stenflo, 1971b].

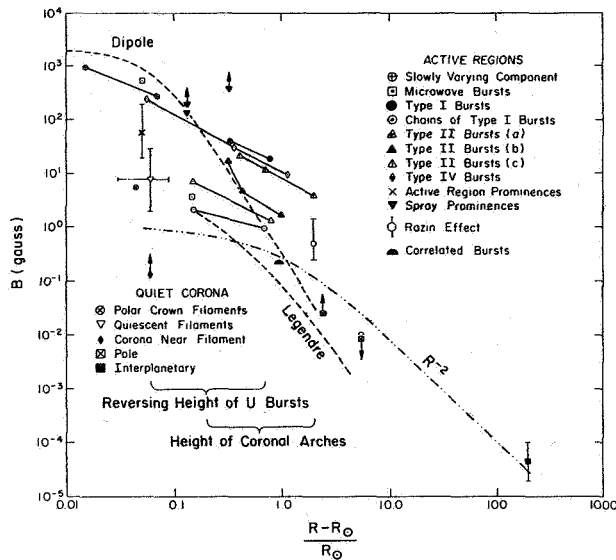


**Figure 2.** Summary of measurements of magnetic fields in the solar corona compared with (1)  $R^{-2}$  extrapolation from interplanetary space, (2) the field above a typical active region using the harmonic expansion method with  $N = 9$ , and (3) a simple dipole potential model for an active region. Except for the Razin effect and the correlated burst measurements, all references are to be found in Newkirk [1967].

potential dipole model of a plage region. This comparison suggests two conclusions: (1) The Legendre approximation will *not* yield accurate results near active regions (a fact well known); and (2) radio bursts at about  $2R_{\odot}$  appear to represent events in which a transient field disturbance is injected into the corona and may be unsuitable as a measure of the ambient magnetic field.

The only comparisons between observed and calculated magnetic fields in coronal space now at our disposal are those for prominence fields [Harvey, 1969; Rust, 1966]. In general, these comparisons show an agreement between the shapes of the fields and currently accepted ideas about the occurrence of prominences within the fields. A discrepancy between the magnitudes of the fields as measured and as calculated appears to be attributable to inaccurate measurement of the surface fields [Rust and Roy, 1971]. Comparison of the shapes of bright coronal emission regions with calculated magnetic fields gives some confidence that the potential field is at least a good first approximation and that the loops, arches, and similar coronal structures constitute magnetic tubes of abnormally high density (fig. 3).

#### Large-Scale Coronal Density Structures

In comparing the shapes of the calculated field lines with

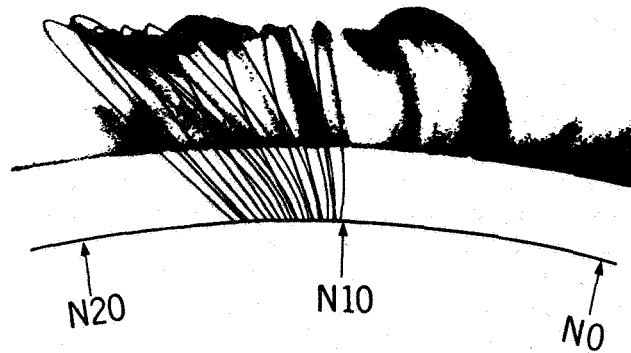


**Figure 3.** Computed potential field lines for the coronal loops observed in the 5303 Å line on 2 November 1969. The loops are seen here on an overocculted negative photograph of the corona. The lower arc indicates the level of the chromosphere. Such coronal loops are often nearly identical to the  $H\alpha$  loops observed in the same region [Courtesy Rust and Roy, 1971].

larger coronal structures such as streamers we should examine only the general morphology of both features. Our approximate models for the field and the geometrical choice of foot points precludes comparison of the shapes of individual magnetic lines with particular outlines in the corona. Let us examine the pattern of calculated fields present during November 1966 as seen against an  $H\alpha$  spectroheliogram and a photograph of the corona (fig. 4). The magnetic fields may be conveniently divided into diverging fields, which are found in close association with plages, low magnetic arcades (LMA), and high magnetic arcades (HMA). A most striking feature of the field is the existence of magnetic arches connecting widely separated active regions. Such arches may well be the lines of communication that give rise to nearly simultaneous radio bursts in separated active regions [Wild, 1969a].

We can conclude from this type of comparison, in which the three-dimensional structure of the corona and the field are known, that coronal streamers form over high magnetic arcades. This conclusion substantiates the concept long used in theoretical models [Kuperus and Tandberg-Hanssen, 1967; Pneuman, 1968; 1969] that streamers develop above the neutral lines separating large-scale adjacent regions of opposite polarity.

#### Coronal Structure, Sector Boundaries, and Geomagnetic Activity

Hypotheses concerning the correlation between large coronal streamers, interplanetary sector structure, and recurrent geomagnetic storms [Mustel, 1961; 1962a, b;

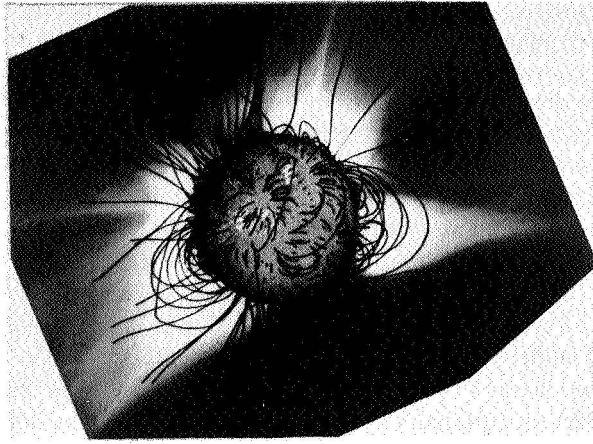


**Figure 4.** Calculated coronal magnetic field lines (least-mean-square fit to  $B_L$ ,  $R_w = 2.5R_\odot$ , corrected for magnetograph saturation), superimposed on the appropriate  $H\alpha$  spectroheliogram [courtesy Sacramento Peak Observatory] and a photograph of the corona of 12 November 1966. [Unless otherwise noted, the coronal field maps are based on photosphere magnetic data furnished by R. Howard (Hale Observatories) and obtained in a program supported in part by the Office of Naval Research under contract NR 013-023, N00014-66-C-0239.]

1964] have long lacked conclusive proof. However, several factors suggest that they must be related: (1) current sheets are thought to be required to produce coronal streamers [Pneuman and Kopp, 1971]; (2) each

sector boundary must contain a current sheet; and (3) geomagnetic activity is known to be connected with the passage of a sector boundary at 1 AU. Recent studies suggest that an accident of perspective may have obscured the true connection. One study of this correlation [Bohlin, 1968; 1970a, b] analyzed streamers that had been located both in latitude and longitude and showed that of 12 streamers observed during two periods in 1964 and 1965 only two could be held responsible for recurrent magnetic storms. Both were located so that they might reasonably be expected to intersect the earth. More recently Couturier and Leblanc [1970] deduced from radio and emission-line coronal observations that solar wind velocity peaks originate in coronal enhancements. Using similar coronal data Martres et al. [1970] determined that the sector boundary originates approximately  $14^\circ$  west of a coronal condensation, a finding in agreement with the conclusion of Wilcox [1968] that the sector boundary falls statistically one day west of a stable plage region. Because statistical samples involved in these studies are sparse and because not every enhancement in the low corona appears as a streamer in the outer corona, we should use caution in drawing conclusions regarding the connection of streamers and the interplanetary sector structure.

To examine the problem further let us compare the sector structure boundaries, coronal streamers, and coronal magnetic fields observed in November, 1966. Table 1 gives data on the sector boundaries, which are compared in figure 5 with the coronal structure of the same period. Newkirk and Altschuler, [1970] identify

**Table 1.** Sector boundaries and coronal structure.

Sector Boundary	Date of Sector Boundary Crossing at 1 AU* (1966)	Character of Sector Boundary	CMP at the Sun†	Longitude at the Sun†	Associated Coronal Magnetic Structure	Position of Sector Boundary Compared to Associated Coronal Density Structure
A	Nov. 15.5	field very mixed between these dates	11	$280^\circ$	LMA	West of enhancement $\alpha$
B	Nov. 20		15.5	$225^\circ$		East of enhancement $\alpha$
C	Nov. 23.5 - 25 (data gaps)	stable	19 - 20.5	$180^\circ - 160^\circ$	LMA & HMA	coincident or west of streamer $\beta - \beta'$
D	Dec. 4.5	stable	30	$35^\circ$	LMA & HMA	North of streamer $\delta$ West of streamer $\gamma$

\*From Wilcox and Colburn [1970]

†Assuming a 4.5 day transit time

such distinctive forms in the calculated coronal magnetic fields as low magnetic arcades, high magnetic arcades, and the various coronal enhancements and streamers.

From our general ideas about the nature of the interplanetary sector structure, we should expect that sector boundaries would coincide with HMAs in the calculated coronal magnetic field. This expectation is well borne out in two of the four cases examined; the only sector boundary for which this coincidence fails completely (B) was developing during the observing period; sector boundary A, which is associated only with an LMA, was also in a state of evolution. Boundaries C and D are of special interest; they were located near the solar limbs of 12 November 1966, and showed exceptional stability.

The position of boundary C is somewhat uncertain because of gaps in the Pioneer 7 magnetic data. It appears associated either with a system of HMAs having its axis approximately parallel to the equator or, if the

earlier CMP date is used, with a similar system having its axis approximately north-south. Identification with the east-west system would require that this sector boundary be definitely associated with streamer  $\beta'$ . Such an identification is suspect, however, because the narrow streamer spike leaves the sun some  $20^\circ$  south of the equator and could hardly be expected to intersect the earth's orbit at 1 AU. Placement of sector boundary C at the western limit suggested by table 1 would associate it with the north-south HMA system and place it in a position consistent with the result of *Martres et al.* [1970]. Boundary D appears to satisfy our hypothesis ideally. It lies along the axis of an HMA system and is some  $20^\circ$  west of coronal enhancement  $\gamma$ . Its connection with coronal streamer  $\delta$  appears to be largely coincidental. Again, with a southward axial inclination of about  $25^\circ$ , streamer  $\delta$  could not be expected to intersect the earth's orbit.

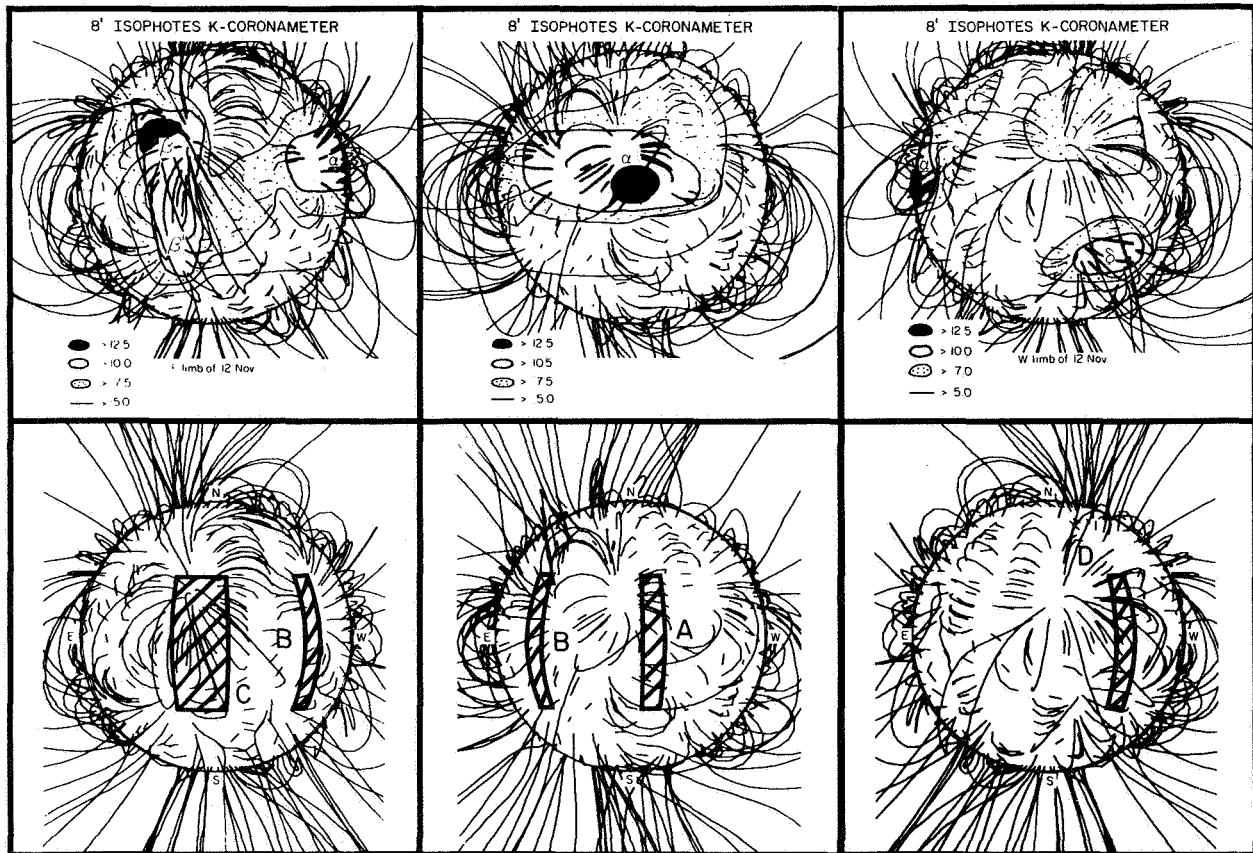


**Figure 5.** Upper Row: Isopleths of K-coronameter signal (proportional to electron density integrated along the line of sight) for a height of  $1.5 R_\odot$  for November 1966, compared with calculated coronal magnetic field lines. At the time of the eclipse of 12 November the east limb was at approximately  $180^\circ$  (central meridian of left figures) and the west limb at  $0^\circ$  (central meridian of right figures). Thus, streamer  $\beta'$  and the low enhancement  $\beta$  were just over the east limb while streamer  $\delta$  was just over the west limb. Feature  $\alpha$  was also an enhancement. Lower Row: Location of the sector boundaries from table 1 compared with calculated coronal magnetic fields.



Taken together these data suggest the overall model schematically represented in figure 6. Here we see an HMA system winding sinuously across the solar surface. A current sheet and a helmet streamer exist above the entire length of the HMA system, while the postulated current sheet contains the axis of the HMA. Clearly, such a sheet will be conspicuous only when viewed edge-on, when it will appear as the spike of a helmet streamer containing a system of concentric arches at its base. In a view normal to the HMA axis the current sheet, which will lie nearly in the plane of the sky, will evade detection. Instead, we shall see the nearly edge-on magnetic arches as divergent rays or a coronal "bush" [Bugoslavskaya, 1949] in the enhancement. However, such a current sheet, since it extends approximately north-south, will probably intersect the earth's orbit and be detected as an interplanetary sector boundary.

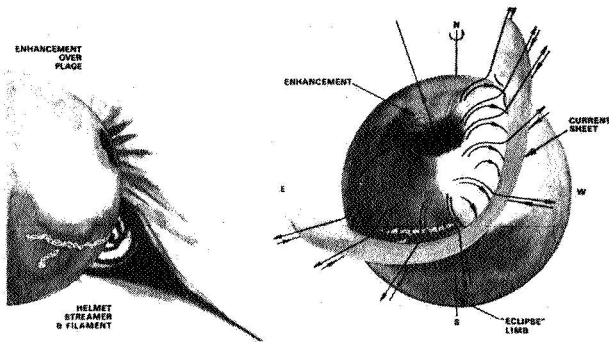


**Figure 6.** A schematic drawing of the relationship between coronal magnetic fields, the sector boundary, and the coronal density structure. The central meridian of the right drawing corresponds to the limb of the left drawing showing the appearance of the corona. Magnetic arcades in the right drawing are surmounted by a current sheet (sector boundary). A coronal enhancement overlies a plage (not shown). The southern portion of the HMA has its axis along the line of sight so that the current sheet is visible as a typical helmet streamer with coronal arches at its base. The northern portion of the HMA system has its axis in the plane of the sky and appears as a typical coronal bush, or active-region enhancement lying above a plage.

In summary, we suggest that every HMA system can potentially form a coronal streamer with its accompanying current sheet. Only those with axes and current sheets lying approximately along the line-of-sight appear as coronal streamers. Such orientation usually precludes detection of the current sheet as an interplanetary sector boundary at the earth. Streamers with HMA axes lying in a meridian and crossing the equator, on the other hand, are inconspicuous in the optical corona but generally produce sector boundaries at 1 AU.

### Fields and Coronal Rotation

In addition to influencing the distribution of material and the expansion velocity of the solar corona, large-scale magnetic fields clearly determine the rotation and transfer of angular momentum into the interplanetary medium. Here we must distinguish the corotation of such features as coronal streamers or sector boundaries in the field from the angular velocity of the ions comprising the features. Observational evidence for the tangential velocity of the corona at 1 AU derives from the orientation of comet tails [Brandt, 1967] and direct detection from space probes [Hundhausen, 1968]. Both techniques yield a tangential velocity of 4 to 10 km/sec, which would require rotation of the corona out to about  $15R_{\odot}$  if simple conservation of angular momentum occurred in the remainder of interplanetary space. Theoretical analyses [Pneuman, 1966; Weber and Davis, 1967; Modisette, 1967; Brandt et al., 1969] show this concept to be vastly oversimplified. Coronal ions actually lag behind the solar surface at all heights; however, they receive significant angular momentum from the solar magnetic field far out into the interplanetary medium. Except for measurements in interplanetary space, we have no data on the rotation of coronal ions for comparison with these calculations.

The rotation of structures in the corona can be largely independent of the motions of the individual ions. Present information [Hansen et al., 1969] shows that the low coronal enhancements rotate with the large-scale magnetic structures on the surface [Wilcox and Howard, 1970] rather than with active regions. Moreover, these data suggest that the rate of rotation at a given latitude may increase with height as it does in the photosphere [Livingston, 1969]. This apparently anomalous behavior can be explained by the confinement of coronal gas to loops in the magnetic field having their foot points anchored at different latitudes and having different rates of rotation [Pneuman, 1971].

### Small-Scale Coronal Density Structures

A comparison of the congruence of the shapes of small-scale features in the corona with the magnetic field lines is almost inevitably restricted to an evaluation of their projected positions and appearances. Considering both figures 4 and 7, we find the agreement to be quite good: open rays, polar plumes, arches, loops, and other structures appear in the corona where they are indicated in the field. However, lest we become too hypnotized by these successes, let us compare some findings from the most recent eclipse (fig. 8). Although there are many coincidences between the shapes of the coronal forms

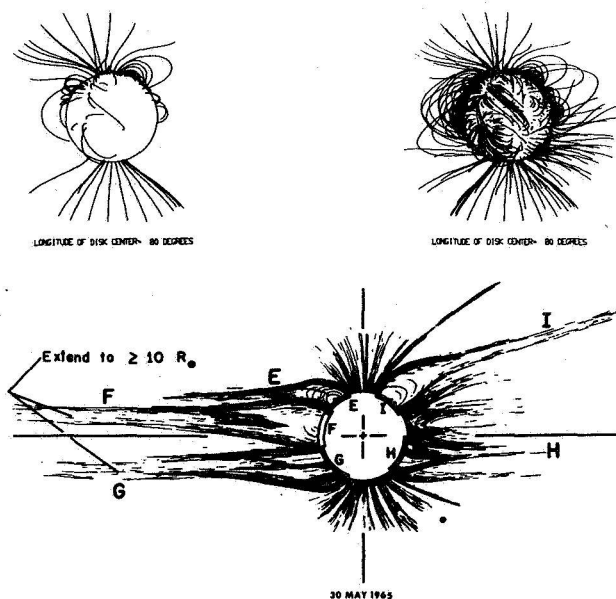


**Figure 7.** Comparison of the solar corona of 30 May 1965 (drawing from Bohlin, 1968) with the corresponding magnetic maps. Note particularly the similarity between (1) the magnetic and coronal arches in streamer I and (2) the polar magnetic field and polar plumes. The left figure shows strong fields in which are displayed only those field lines originating where  $B_L \geq 10\%$  of the maximum line of sight field present at the surface are displayed; the right figure shows weak fields with field lines originating at foot points where  $B_L \geq 0.16$  gauss.

and the shapes of the field lines, there are many discrepancies as well. These are particularly sobering when we recall that the surface magnetic data from Mt. Wilson (corrected for magnetograph saturation) and Kitt Peak were compared and found to be in good agreement. Apparently, the surface data for this relatively active period were inadequate because of temporal changes. Of course, undetected large-scale coronal electric current systems may also be modifying the fields. Nevertheless, we conclude that much of the fine-scale density structure visible in the corona corresponds to preferentially filled magnetic tubes that approximately follow the zero-potential model.

#### The Mapping Hypothesis

Recent work [Schatten *et al.*, 1969] has demonstrated a good correspondence between the interplanetary field and the large-scale pattern of fields present at the solar photosphere or, more correctly, at the source surface  $R_w \approx 1.6-2.5R_\odot$ . Thus, we conclude that the solar wind originates from a large fraction of the corona and

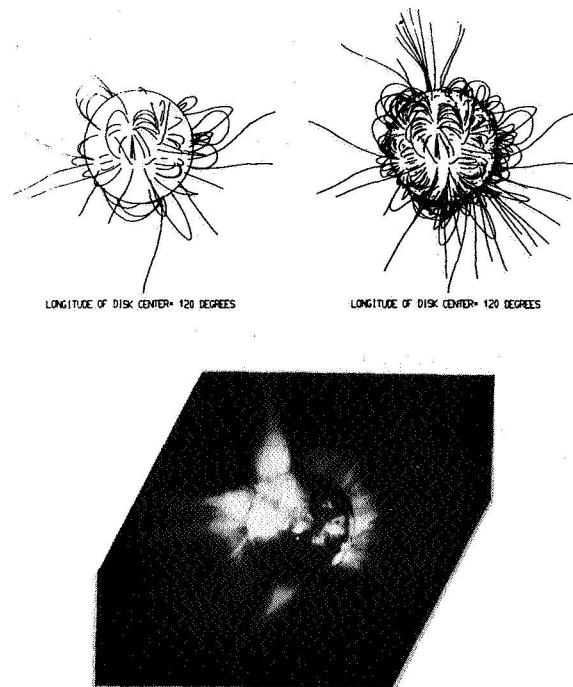


**Figure 8.** Comparison of the solar corona of 7 March 1970 [outer corona HAO; x-ray corona seen on the disk courtesy Vaiana *et al.*, 1970. American Science and Engineering] with the corresponding coronal magnetic maps. The left figure shows strong fields in which are displayed only those field lines originating where  $B_L \geq 10\%$  of the maximum line of sight field present at the surface are displayed; the right figure shows weak fields with field lines originating at foot points where  $B_L \geq 0.16$  gauss.

that conditions in the interplanetary field reflect or "map" photospheric conditions. We naturally ask if smaller scale structures are mapped in a similar way [Michel, 1967]. The filamentary structure of the corona, which appears to correspond to preferentially filled magnetic tubes, suggests that this is so. Two questions arise: (1) What mechanism singles out particular tubes? (2) How does the presence of such filled tubes influence the outer corona and the solar wind?

To answer the first question, we must examine conditions in the photosphere and chromosphere at the base of such preferred tubes. In a general way we know that elevated coronal density, modified chromospheric structure (plages and supergranulation boundary) and strong magnetic fields appear together on the sun [Billings, 1966; Hansen *et al.*, 1971]. Recently, Noyes *et al.*, [1970] have found that the energy flux in the chromosphere-corona transition above a plage is about five times



as great as that above quiet regions. Data from *Withbroe and Noyes* [1971], figure 9, show that the pressure at the base of the corona varies approximately as  $B^{1/2}$  once  $B$  exceeds about 4 gauss. These observations are consistent with theoretical conclusions that the presence of strong magnetic fields in the photosphere increases the flux of mechanical energy into the chromosphere and corona and consequently increases the density of the overlying corona [Kulsrud, 1955; Kuperus, 1965, 1969; Kopp and Kuperus, 1968; Kopp, 1968]. Although the exact chromospheric origin of the filled magnetic tubes is now known, indirect inferences [Harvey, 1965; Newkirk and Harvey, 1968] indicate that tubes that appear as polar plumes *do* originate in bright calcium faculae where the chromospheric field is stronger than average.

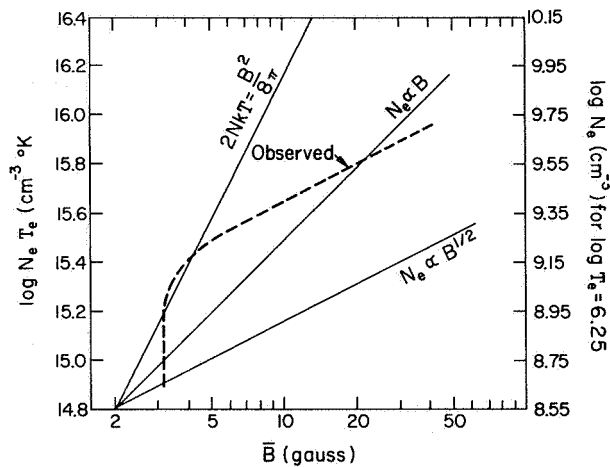


**Figure 9.** Variation of the pressure at the base of the corona with the strength of the underlying magnetic field as determined from OSO-VI measurements of the  $MgX(625A)$  line in active and quiet regions. [Courtesy Withbroe and Noyes, 1971]. The field and coronal data are averaged over an element of approximately one min of arc diameter.

Taken together, these data suggest that the bright coronal rays, plumes, and arches are magnetic tubes containing more material than the average because of high field *strength* at their foot points. The surface fields are generally organized into large patterns each containing a dominant magnetic polarity with a few intense knots of field along the supergranulation boundary. Thus, we should expect the filled tubes to originate at these intense knots and the shapes of the tubes in the corona below  $2.5R_{\odot}$  to correspond to the zero-potential field. A simple consideration indicates that the apparently characteristic width of 30,000 km found in many of

these features [Saito, 1958; Ivanchuk, 1968; Newkirk and Harvey, 1968] is probably a reflection of the scale of the supergranulation cells. This is because, in an extended region of uniform polarity, the field lines from a concentrated knot of field in the photosphere expand in the corona to a diameter approximately equal to that of the circulation cell presumed to have concentrated the field (fig. 10). In a region with mixed polarity, diameters equal to the circulation cells cannot be expected, although a type of mapping of the surface conditions by the corona may still occur.

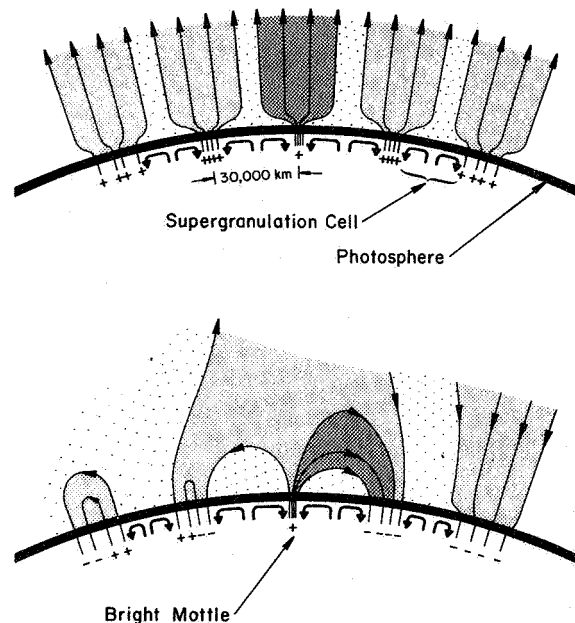


**Figure 10.** The magnetic field in the corona above the pattern of supergranulation cells, for a region of uniform polarity (top) and for a region of mixed polarity (bottom). The cell circulation is the same in both cases. Intense concentration of the field at the supergranulation border causes an increased density at the base of the overlying corona.

Let us accept, for the moment, the above explanation of why particular magnetic tubes “light up” and examine the consequences of this model for the outer corona and interplanetary medium. Judging from the appearance of rays and polar plumes, one should conclude that such tubes maintain their identity as they are swept up in the general coronal expansion into interplanetary space. Thus, a mapping of relatively small-scale (about 30,000 km) structures in the chromosphere out to the source surface and beyond should occur. Have we any evidence for this other than the examination of eclipse photographs? Discrete radio source occultations [Cohen

and Gunderman, 1969; Hewish and Symonds, 1969; Jokipii and Hollweg, 1970; Lovelace et al. 1970; Hewish, 1971] solar radio burst fine structure [Warwick and Dulk, 1969; Fainberg and Stone, 1970], and spacecraft observations [Jokipii and Coleman, 1968; Hundhausen, 1968] indicate that an intricate filamentary structure exists in both the density and the magnetic field of the outer corona and of interplanetary space. Although much of this filamentary structure doubtless originates in the plasma as waves, shocks, and streaming instabilities, the foregoing discussion suggests that some fraction originates at chromospheric levels. Such density fluctuations in interplanetary space could be expected to be recognized by the condition  $(B^2/8\pi) + NkT = \text{const.}$

Identification of such fluctuations in interplanetary space has been somewhat ambiguous. Although tangential discontinuities appear to be conducted past a spacecraft with an average time of about 1 hour or with a size of about  $1.3 \times 10^6$  km or at any other wavelength [Jokipii and Coleman, 1968; Siscoe et al., 1968]. Presumably, any such characteristic scale has become washed out by the turbulent nature of the interplanetary plasma. However, a search during periods of extremely stable sector structure might be rewarding.

### THE EVOLUTION OF CORONAL FIELDS

At the present time little is known regarding the evolution of coronal magnetic fields except through indirect inference. Judging from the evolution of the surface fields, we should expect the coronal and the interplanetary magnetic pattern to reflect the following characteristic times:

1. The characteristic lifetime of about 1 day for the supergranulation network.
2. The development of an active region over about one month.
3. The growth and spreading of unipolar magnetic field regions over one to three months.
4. The lifetime of the photospheric magnetic sector structure of several months to one-half year.

Such patterns of evolution in the corona do appear, although their direct connection with the field has not been conclusively established. For example, the lifetime of polar plumes is estimated to be about one-half day [Waldmeier, 1955]. The evolution of coronal enhancements in concert with the underlying plage is well known [Kiepenheuer, 1953; Hansen et al., 1971]. While the lifetime of coronal streamers [Bohlin, 1970a,b] compares well with that of the unipolar regions, which are believed to be largely responsible, some particularly long-lived streamers appear to be connected to the sector structure fields.

Concerning the field itself, we have only the suggestion [Schatten et al., 1969] that the fields of an active region require about one month to evolve sufficiently to reach the source surface from which they are connected into interplanetary space, and the observation of Valdez and Altschuler [1970] of the opening of coronal field loops near active regions following this occurrence of proton flares. The modulation of the interplanetary field by the large-scale photospheric sector fields is well known [Wilcox et al., 1969].

### MAGNETIC FIELDS AND TRANSIENT PHENOMENA

We have examined coronal magnetic fields as if both the fields and the ambient medium were constant in time. This is often not the case. We discuss magnetic fields and transient phenomena in three groups: (1) those in which the coronal fields remain stable and channel the disturbance, (2) those in which a perturbation of the coronal field occurs, and (3) those in which a major disruption of the field occurs. These distinctions are somewhat arbitrary: a given disturbance may be completely channeled at one level and may disrupt the field at another, and practically all transient phenomena in the corona may have ramifications in interplanetary space. Although most of these transient phenomena are associated with solar flares, we shall not discuss the role of magnetic fields in producing flares but simply consider the flare as an accomplished fact and examine several of the accompanying phenomena that occur in the corona and appear to have a direct consequence on the solar wind.

#### Field-Channeled Phenomena

*Surge Prominences* These objects represent an organized ejection of material from active regions, usually following flares with an average upward velocity of about 300 km/sec followed by an apparently gravity-induced return to the photosphere along the same trajectory [Tandberg-Hanssen, 1967]. They present a general appearance of being channeled and contained by the field, and the fact that the highest surges contain the weakest fields [Harvey, 1969] emphasizes that they are under magnetic control. The energy density associated with their motion (about 750 ergs/cm<sup>3</sup>) when compared to that of the field (table 2) suggests that the most violent surges may disrupt the field. Except for the surge-sprays, to be discussed later, it is questionable whether surges ever permanently escape the sun.

*Loop Prominences* These post-flare prominences appear in both  $H\alpha$  and the 5303 line of the corona (fig. 3) and contain densities of  $10^9$  to  $10^{10}$  with

temperatures from  $4 \times 10^4$  to  $3 \times 10^7$  °K. Their appearance and the data in table 2 suggest that they are under strict magnetic control and have no obvious contact with the interplanetary medium. However, *Jefferies and Orrall* [1965a,b] found it necessary to postulate the presence of 10-keV protons in loop prominences to account for their  $H\alpha$  profiles and their duration. They conclude that some of the 10-keV particles produced by flares are stored high in the corona, while others of the same energy are rapidly thermalized [*Culhane et al.*, 1970] and impact on the chromosphere, or are lost to interplanetary space.

**Type III Radio Bursts** These events are ascribed to the passage through the corona of about  $10^{35}$  electrons per burst in the 10- to 200-keV energy range [*Kundu*, 1965] or about  $10^{30}$  protons per burst in the 50 MeV energy range [*Smith*, 1970a,b]. They have been observed down to 0.6 MHz (at about  $40 R_{\odot}$ ) [*Hartz*, 1969; *Haddock and Graedel*, 1970] and are considered to propagate out along a streamer of abnormally high density. The burst of particles postulated in these mechanisms carry sufficient momentum to distort the magnetic field in the corona above about  $2 R_{\odot}$ . In fact, *Warwick* [1967] reasons that a typical sequence of bursts may heat the outer corona and thus have an influence on the solar wind. The burst particles required by the second mechanism would be guided by the field out to at least  $5 R_{\odot}$ . At present the relationship between the trajectories of type III bursts, coronal magnetic fields, and density structures in the corona is largely unknown [*Kai*, 1970]. *Pneuman and Kopp* [1971] have suggested that these bursts are channeled along narrow current sheets and that the conditions inferred from their frequency and duration do not represent the ambient corona at large.

**Stationary Type IV Bursts** These events are believed to be due to the synchrotron radiation of semirelativistic particles trapped in closed magnetic arches high in the corona [*Kundu*, 1965]. Tentative comparisons [*Smerd and Dulk*, 1971; *Newkirk*, 1971] between the calculated and inferred magnetic arches indicate that this is so. The direct influence of these trapped particles on the solar wind is negligible, although they may provide useful diagnostic information.

**High-Energy Particle Events** There is ample evidence for the presence of high-energy particles accompanying solar flares. Although such particles cannot be expected to influence coronal magnetic fields or the solar wind directly, they may provide us with useful diagnostic information on outer coronal fields. A current problem is that of the storage of such particles near the sun and their dispersion over longitudes widely separated from the parent flare [*Bryant et al.*, 1965]. This problem has not yet been analyzed using realistic coronal magnetic fields.

#### Field-Perturbing Phenomena

**Disarption Brusque** Some of the characteristics of the several phenomena that have been ascribed to waves propagating through the corona appear in table 3. One of the earliest of these to be described was the *disarption brusque* [*d'Azambuja and d'Azambuja* 1948], in which a quiescent prominence far distant from the flare suddenly becomes agitated and erupts. Frequently, the prominence reforms at its original location. On other occasions, the activation of the prominence may show only as a change in its form. Two facts suggest that the disturbance may well be a slow-mode MHD wave guided by the magnetic field: the activation often occurs only in a preferred direction from the flare, and the velocity of propagation

Table 2. Energy density comparison.

High Energy Particles								Thermalized Plasma					
R ( $R_{\odot}$ )	B (gauss)	$B^2/8\pi$	Type of Event	$\epsilon$ (particle $^{-1}$ )	N(cm $^{-3}$ )	E (ergs)	E V (ergs/cm $^3$ )	References	Location	$T_e$	$N_e$ (obs)	$2N_e k T$	Reference
1.03	$10^3$	$4 \times 10^4$	Microwave X-ray bursts	100 keV	$10^5$	$10^{12}$	$10^{-2}$	Wild [1963]	Immediately above active region (flare)	$3 \times 10^7$ $4 \times 10^6$	$< 3 \times 10^{11}$ $10^{11} - 10^{12}$	$2.5 \times 10^3$ $10^3 - 10^2$	Culhane et al. [1970] Zirin [1970]
1.15	$10^2$	$4 \times 10^2$	Loop prominence	10 keV	$2 \times 10^7$	$5 \times 10^{11}$	$2 \times 10^{-3}$	Jefferies & Orrall [1965a,b]	Loops above active region (sporadic coronal condensation)	$4 \times 10^6$ $1.8 \times 10^6$	$10^{11} - 10^{12}$ $7 \times 10^9$	$10^3 - 10^2$ 1.5	Zirin [1970] Reidy et al. [1968]
2.0	$2 \times 10^3$	$1.6 \times 10^4$	Type III burst	10-200 keV 50 MeV protons	$10^6$ $10^2$	$2 \times 10^{12}$ $8 \times 10^{12}$	$2 \times 10^{-1}$ $8 \times 10^{-3}$	Kundu [1965] Smith [1970a,b]	Coronal enhancement above active region	$1.5 \times 10^6$	$10^7$	$4.1 \times 10^{-3}$	Newkirk et al. [1969]
4.0	$4 \times 10^2$	$6.4 \times 10^3$	Type IV burst	0.4 MeV	$10^3$	$2.5 \times 10^{12}$	$10^{-4}$	Kundu [1965]	Corona above active region	$1.3 \times 10^6$	$6 \times 10^6$	$2.2 \times 10^{-3}$	Newkirk [1967]

ranges from 100 to 250 km/sec [Dodson and Hedeman, 1964] as would be expected for sonic waves in the corona.

However, this explanation may well be oversimplified. Bruzek [1952] has found evidence for the triggering of the *disparition brusque* by an activity wave that migrates outward from developing sunspot regions at a very slow speed (about 1 km/sec). Perhaps both mechanisms are at work.

**Moreton Waves and Type II Bursts** Further inspection of table 3 shows several wave-like phenomena with a characteristic propagation speed of the order of 1000 km/sec. In the Moreton wave the disturbance causes short-term oscillations in the chromosphere [Moreton, 1960; Smith and Harvey, 1971], which spread out from the flare over a restricted sector. This disturbance appears directly related to that of "winking filaments," in which a distant filament is caused to oscillate vertically by the disturbance. Three explanations have been offered to account for these observations. In one [Anderson, 1966; Uchida, 1968] a weak Alfvénic shock wave travels from the flare through the corona along magnetic field lines; in the second [Athay and Moreton, 1961] a spray of magnetically guided particles is responsible; in the third [Meyer, 1968] fast-mode MHD waves channeled by refraction remain in the chromosphere and cause the activation. Recently, Uchida [1970] has calculated the coronal propagation of fast-mode MHD waves for several models of an active region.

Before discussing the merits of these mechanisms, let us turn to another phenomenon long associated with coronal waves. Type II radio bursts are interpreted as a shock disturbance moving out through the corona at speeds of about 1000 km/sec. The shock is believed to set off oscillations that emit radio radiation at the local plasma frequency. That such MHD shocks *are* directed by the ambient magnetic field is demonstrated by a comparison (fig. 11) of the field lines calculated from the surface magnetic fields with the wave front of the Type II burst [Kai, 1969b]. In this particular event we see not only the channeling of the shock by the field but also the activation of a distant filament and the generation of a moving Type IV radio burst. The latter is presumed to be caused by the synchrotron radiation of relativistic particles accelerated in the shock front as it moves through the corona.

Have we any visual evidence for these events in the corona? The answer appears to be yes. Movies of the corona in the 5303 Å line [Dunn, 1970] occasionally display a moving "whip" in a previously existing magnetic arch in the corona [Evans, 1957]. Examination of several of these whips [Kleczek, 1963; Bruzek and Demastus, 1970] shows that:

1. The motion begins gradually and rapidly accelerates to velocities in excess of several hundred km/sec.
2. Some motion of the coronal forms can be detected

Table 3. Wave phenomena in the corona.

Phenomenon	Velocity	Type of Wave Inferred	E	Reference
Prominence activation and <i>disparition brusque</i>	~100-250 km/sec (flare-induced)	Magnetically guided sound (slow-mode MHD)	?	Tandberg-Hanssen [1967]
	~1 km/sec (sunspot-induced)	Activity wave		Bruzek [1952]
Winking filaments	500-1500 km/sec	Weak Alfvén shock (along magnetic field lines in Corona)	$4 \times 10^{29}$ ergs	Anderson [1966]
Moreton wave	~1000 km/sec	Fast-mode MHD through chromosphere	$\lesssim 10^{29}$ ergs	Meyer [1968]
Coronal whip	accelerating to several 100 km/sec	Alfvén growing to MHD shock	?	Bruzek and Demastus [1970]
Spray prominences	150-1300 km/sec		$10^{31}$ ergs	Bruzek [1969a,b]
Types II and IV Bursts	~1000 km/sec	MHD shock	$10^{29}$ ergs	D. F. Smith, private communication
Interplanetary shock	700 km/sec at 1 AU but transit time yields 950 km/sec	MHD shock	$10^{32}$ ergs	Ness and Taylor [1969]
			$5 \times 10^{31}$ ergs	Hundhausen et al. [1970]

before the flash phase of the associated flare, although the most rapid acceleration appears to be coincident with the flash phase.

In addition to the characteristics noted by Bruzek and Demastus, we note that there is no evidence for any increase in the density or temperature of the material enveloped by the loops. We conclude that the arch is not being driven out by an explosion from below but that a dramatic disruption of the magnetic field has occurred; the coronal material is simply carried along by the field, which is readjusting to the new configuration with the Alfvén speed.

The rapid acceleration and final disruption with velocities of about 1000 km/sec of a previously stable configuration is reminiscent of the behavior of spray prominences [Smith, 1968]. Although there is evidence that such sprays originate in the flare itself, the ejection of previously existing quiescent prominences also occurs [Dodson and Hedeman, 1968]. Some of the material is observed to return to the surface along the legs of the

arch. However, knots are frequently observed that have greater than escape velocity and unquestionably leave the sun.

Apparently, the coronal whips, spray prominences, and type II and type IV bursts [Smerd and Dulk, 1971] are various aspects of the same phenomenon—a developing MHD shock causing rapid readjustment of the coronal magnetic field which may or may not result in significant mass motion.<sup>3</sup> Wild [1969b] and Stewart and Sheridan [1970] proposed earlier that the Moreton wave and type II burst were two ramifications of the same disturbance. The sequence of events might well be visualized as follows:<sup>4</sup>

1. The preflare storage of energy in the field, caused by a gradual relocation of the surface magnetic fields, produces a slow motion of the arches visible in 5303 Å and in overlying filaments if any exist.
2. The occurrence of a triggering instability causes a sudden release of magnetic energy at chromospheric levels (the flare), MHD shock, and the subsequent readjustment of the field at Alfvén speeds in the corona (the whip or spray prominence).
3. The shock wave grows as it expands into the corona (production of type II and type IV bursts, high energy particles, postflare X-ray emission).
4. Some of the shock energy returns to the chromosphere far from the flare, given an appropriate field configuration (activation of distant filaments, *disparition brusque*, Moreton wave, triggering of sympathetic flares).
5. The shock escapes into interplanetary space at  $v \cong 1000$  km/sec and gradually decelerates to about 700 km/sec at 1 AU.

That such a sequence of events is at least plausible is shown in figures 11 and 12, in which a spray prominence [McCabe and Fisher, 1970] preceded a rapidly moving type IV burst [Riddle, 1970], which could be followed to several solar radii. The disturbance appears to have propagated out along the ambient field lines. Dulk and Altschuler [1971] have examined a similar event and

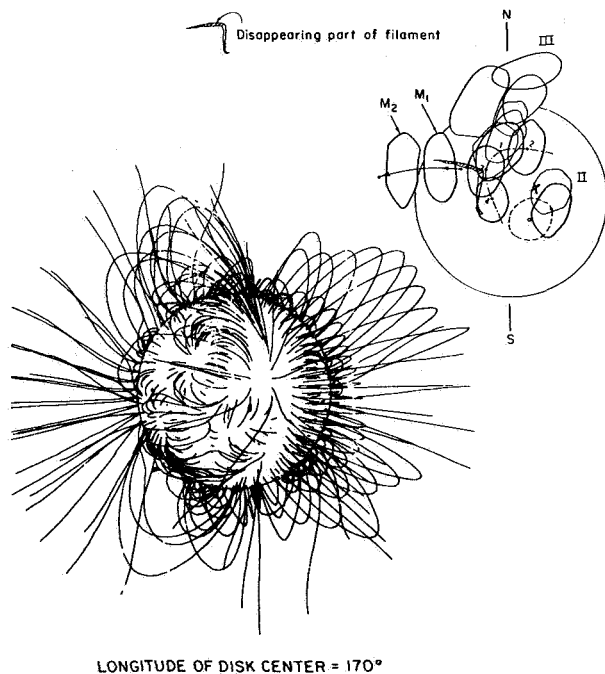
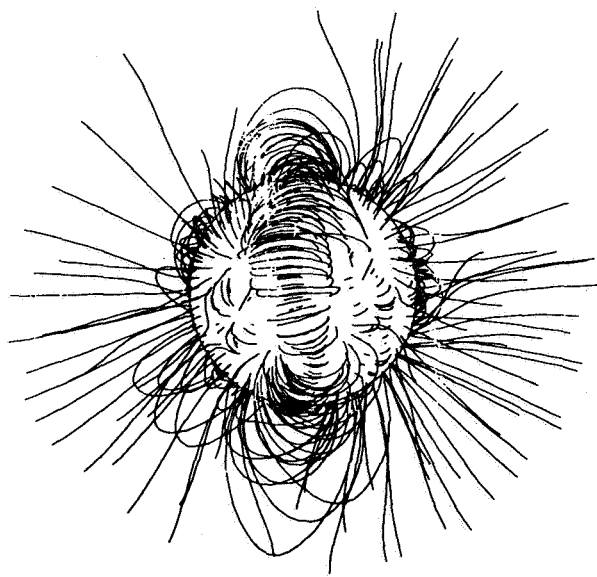


**Figure 11.** Channeling of a directed shock, which gave rise to a complex of type II (line connecting points 2, 1, 3, 4), moving type IV ( $M_1$  and  $M_2$ ), and type III (light enclosed regions in north) radio events and a disappearing prominence [Kai, 1969a] by the coronal magnetic field. The flare was at x. Field lines originating at foot points where  $B_L \geq 0.16$  gauss are displayed.

<sup>3</sup>The observation of Orrall and Smith [1961] suggests that the connection may be more complex. On one occasion a spray traversed the corona with no visible influence on the overlying coronal arches.

<sup>4</sup>Recently Kopp [1971] has proposed that the entire phenomenon is caused by a single large shock originating at the photosphere. The ejected spray material is interpreted as part of the chromosphere blown off and acting as the driver gas in the corona.



LONGITUDE OF DISK CENTER = 340 DEGREES

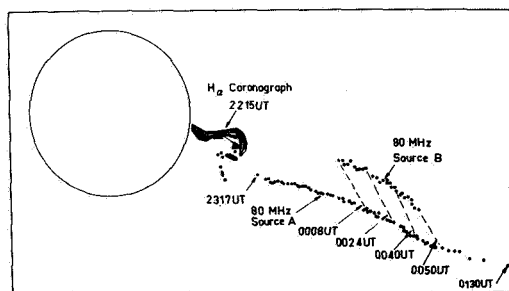


**Figure 12.** An ejected spray prominence [McCabe and Fisher, 1970] and an associated moving type IV burst [Riddle, 1970] move out along the coronal magnetic field lines. Field lines originating at foot points where  $B_L \geq 0.16$  gauss are displayed.

concluded that the ejected plasmoid was, in their case, a ring-current vortex whose poloidal magnetic field contained the mildly relativistic electrons. Similar vortices have been observed optically [Hagen and Neidig, 1970].

**Mass Ejections** In the previous section we emphasized those phenomena in which waves in the corona were believed to be the principal cause of the disturbance. In other instances the gradual or explosive transport of material may occur. The magnetic fields may channel the flow or, in the most violent cases, be completely disrupted by the material (see table 2). Early observers of the corona ascribed the changes observed in loops and arches either to the motion of an excitation phenomenon or to the gradual filling and emptying of adjacent

magnetic tubes of force. Although spectral measurements [Newkirk, 1957] show that true, macroscopic motions do occur, they are relatively rare. Most of the changes observed appear to be due to the filling mechanism.

The gradual expansion of regions of high density such as coronal enhancements also occurs, although their causal connection with flares is uncertain. Associated with the proton flares of 7 July and 2 September 1966 [Newkirk *et al.*, 1969] the electron density in the corona above the active regions increased by a factor of about two. However, it is impossible to say unambiguously that the flares were the source of the material. On one hand, radio observations [Tanaka *et al.*, 1969] show that a gradual increase in the density began before the proton flare of 7 July 1966. On the other hand, in a few days following each of these flares, the electron density distribution showed a concentration of material below  $1.5 R_\odot$  from the center of the sun — a concentration that was not observed in this active region at any other time during its two-month lifetime. The fact that the density bubble appeared to expand at almost the same speed as that reported for the late expansion stages of  $H\alpha$  loop prominence systems in general [Bruzek, 1964] and for the loops observed two days following the flare of 7 July [Valnicek *et al.*, 1969], suggests that we may be seeing two aspects of the same phenomenon: a gradual filling of successively higher magnetic loops in the corona. That this material is actually pushing out the loops seems questionable from a comparison of the energy density of the material with that of the field (table 2).

Observations of genuine ejections of coronal material from flares are rather scarce. One such event has been analyzed by Zirin [1966], who determines the following parameters for the coronal cloud:

$$\text{Diameter} \cong 2 \times 10^9 \text{ cm}$$

$$N_e \cong 10^{11} \text{ cm}^{-3}$$

$$T_e \cong 4 \times 10^6 \text{ }^\circ\text{K}$$

$$\text{Total } N \cong 10^{39} \text{ electrons}$$

$$\text{Total mass} \cong 2 \times 10^{15} \text{ gm}$$

Although Zirin states that the material left the flare site "explosively," he does not make clear whether the material was in fact ejected from the corona. The actual expulsion of a considerable mass of material together with the magnetic field to form a temporary magnetic bottle extending out to about  $10 R_\odot$  has recently been inferred from satellite occultation observations [Schatten, 1970].

Shock waves observed in interplanetary space afford the most unambiguous evidence for the true ejection of flare material. As summarized by *Hundhausen et al.*, [1970] such shocks have a mean energy of  $6.8 \times 10^{31}$  ergs and a mean mass of flare ejecta of  $5 \times 10^{16}$  gm. A linear relation obtains between the ejected mass (from  $3 \times 10^{15}$  to  $3 \times 10^{17}$  gm) and the shock energy at the sun (from  $10^{31}$  ergs to  $3 \times 10^{32}$  ergs). Flares accompanied by shock events in the corona (type II and IV radio bursts) are most likely to produce interplanetary shocks.

The present picture is anything but clear. We must conclude that the flare injects into its local environment some  $10^{41}$  particles. Of these, some  $3 \times 10^{40}$  may escape into interplanetary space to be observed ultimately at 1 AU as the driver of a shock wave. How this is channeled by the ambient coronal fields is unknown. Another  $3 \times 10^{40}$  particles take up fairly permanent residence in the coronal condensation while the remaining  $3 \times 10^{40}$  particles may ultimately return to the photosphere by the formation and maintenance of the loop prominences [*Jefferies and Orrall*, 1965a,b].

#### FUTURE PROBLEMS

As mentioned in the first part of the discussion, practically all our conclusions regarding coronal magnetic fields and their relation to optical, radio, and solar wind phenomena are based on the computation of these fields from data at photospheric levels. We desperately need actual measurements of both the magnitude and direction of fields in coronal space to compare with these calculations. Such data will come from several sources. Observations of the degree and orientation of linear polarization of coronal emission lines can yield information on the direction of the field in the inner corona. The Zeeman splitting of the circularly polarized components of these lines is proportional to the line-of-sight field in the same region. Although such measurements are difficult, they are feasible with present-day techniques. At radio wavelengths, the polarization of the slowly varying (thermal) component, the polarization of microwave, type I, and type II bursts, and the frequency distribution of type IV bursts give partial information on both the magnitude and direction of the field at various heights in the corona. The present ambiguity in the interpretation of some of these observations apparent in figure 2 is largely due to a lack of angular resolution in our radio telescopes, the use of unrealistically simple models of the coronal field, and uncertainty as to the exact mechanisms responsible for some of the bursts.

All these factors can be expected to improve rapidly in the next few years as we examine data from the new

radioheliographs, use actually measured surface fields in our calculations, and, generally learn more about radio bursts. It is likely that a combination of several of these types of observations rather than a single technique will be required.

The continued study of the Faraday rotation of the signals which transverse the corona from satellite-borne radio transmitters and natural pulsars hopefully will give a more complete picture of the fields in the outer corona than we have currently.

Also on the observational side, we require detailed information on the chromospheric conditions existing at the feet of the more densely filled magnetic tubes in the corona. Such observations should indicate how the mass and energy flux into the corona is modulated by the presence of magnetic fields at photospheric levels. Given this information, an extension of the exact solutions for the interaction between the field and the solar wind to more complex and realistic field configurations should be attempted. Such an investigation would not only improve our understanding of the density structure of the solar corona as we see it, but also illuminate the role played by the corona in the mapping of chromospheric conditions into the interplanetary medium.

The intriguing question of the connection of visible structures in the corona to conditions in interplanetary space requires additional study. The data currently available are fragmentary. However, with the launching of orbital coronagraphs in the next few years, we should obtain the necessary data to replace conjecture with knowledge.

Although the synoptic development of magnetic field patterns in the photosphere is well known, the consequences of this development on the coronal fields have yet to be investigated. Similarly, the role played by the evolution of these fields on that of the solar corona is unknown.

Earlier we mentioned coronal transient events, particularly those observed at radio wavelengths, as useful diagnostic tools for measuring coronal fields. Such events bear study in their own right. At present we know little about the general relation of the various radio bursts to the ambient magnetic field. Such fundamental questions as whether the disturbances propagate along or normal to the field and the detailed mechanism responsible for some bursts remain uncertain. The magnetic channeling of the shock disturbances responsible for the Moreton waves, winking filaments, and coronal whips has not been conclusively demonstrated. Equally unknown are the roles played by coronal fields in directing shock waves escaping into interplanetary space and in channeling and storing high energy particles.

## REFERENCES

- Altschuler, M.A.; and Newkirk, G., Jr.: Magnetic Fields and Structure of the Solar Corona. *Solar Phys.* Vol. 9, 1969, p. 131.
- Anderson, G. F.: Transient Flare Associated Phenomena in the Solar Atmosphere. Ph.D. Thesis, University of Colorado, 1966.
- Athay, R. G.; and Moreton, G. E.: Impulsive Phenomena in the Solar Atmosphere. *Astrophys. J.*, Vol. 133, 1961, p. 935.
- Billings, D.E.: *Guide to the Solar Corona*. Academic Press Inc., New York, 1966.
- Bohlin, J.D.: The Structure, Dynamics, and Evolution of Solar Coronal Streamers. Ph.D. Thesis, University of Colorado, 1968.
- Bohlin, J. D.: Solar Coronal Streamers. I: Observed Locations, General Evolution, and Classification. *Solar Phys.* Vol. 12, 1970a, p. 240.
- Bohlin, J. D.: Solar Coronal Streamers. II: Evolution of Discrete Features From the Sun to 1 AU. *Solar Phys.* Vol. 13, 1970b, p. 153.
- Bohlin, J. D., and Simon, M.: Coronal Densities and Magnetic Fields. *Solar Phys.*, Vol. 9, 1969, p. 183.
- Boischot, A.; and Clavelier, B.: Razin Effect in Solar Corona and Determination of the Magnetic Field at One Solar Radius. *Astrophys. Lett.*, Vol. 1, 1967, p. 7.
- Brandt, J. C., Interplanetary gas XIII. Gross Plasma Velocities From Orientation of Ionic Comet Tails. *Astrophys J.*, Vol. 147, 1967, p. 201.
- Brandt, J. C.; Wolff, C.; and Cassinelle, C.: A Calculation of the Angular Momentum of the Solar Wind. *Astrophys J.*, Vol. 156, 1969, p. 1117.
- Bruzek, A.; and Demastus, H.: Flare Associated Coronal Expansion Phenomena. *Solar Phys.*, Vol. 12, 1970, p. 447.
- Bruzek, A.: Über die ursache der 'plotzlichen' filament-auflosungen. *Z. Astrophys.*, Vol. 31, 1952, p. 99.
- Bruzek, A., On the Association Between Loop Prominences and Flares. *Astrophys. J.*, Vol. 140, 1964, p. 746.
- Bruzek, A.: Solar Flares. *Plasma Instabilities in Astrophysics*. D. G. Wentzel and D. A. Tidman, eds., Gordon and Breach, 1969, p. 71.
- Bruzek, Z.: *Symposium on Solar Flares and Space Research, 1968*. C. de Jager and Z. Svestka, eds., North Holland, Amsterdam, 1969, p. 61.
- Bryant, D. A.; Cline, T. L.; Desai, U. D.; and McDonald, F. B.: Studies of Solar Protons with Explorer XII and XIV. *Astrophys. J.*, Vol. 141, 1965, p. 478.
- Bugoslavskoya, E.Y.: Structure of the Solar Corona. *Publ. Sternberg Inst.*, 1949, p. 19.
- Chapman, S.; and Bartels, J.: *Geomagnetism*. Oxford University Press, London, 1940.
- Cohen, M. H., and Gunderman, E. J.: Interplanetary Scintillations. *Astrophys. J.*, Vol. 155, 1969, p. 645.
- Couturier, P.; and Leblanc, Y.: On Origin of Solar Wind Velocity Variations. *Astron. Astrophys.*, Vol. 7, 1970, p. 254.
- Culhane, J. L., Vesecky, J. F.; and Phillips K. J. H.: Cooling of Flare Produced Plasmas in the Solar Corona. *Solar Phys.*, Vol. 15, 1970, p. 394.
- d'Azambuja, L.; and d'Azambuja, M.: Etude d'ensemble des Proturberances Solaire et de Leurs Evolution. *Ann. Obs. Meudon Paris*, Vol. 6, 1948, no. 7.
- Dodson, H. W.; and Hedeman, E. R.: Moving Material Accompanying the Flare of 1959 July 16. *NASA Symposium on Physics of Solar Flares*, NASA SP-50, 1964, p. 15.
- Dodson, H.W.; Hedeman, E. R.: Increasing Optical Evidence for Mass Motions in Solar Flares 1937-1967. *Proc. Ninth Nobel Symposium*. Y. Öhman, ed., Wiley Interscience Div., J. Wiley & Sons, 1968, p. 37.
- Dulk, G. A.: and Altschuler, M. D.: Moving Type IV Radio Burst of 1970 April 29 and Its Relation to Coronal Magnetic Field. *Solar Phys.* 1971 (in press)
- Dunn, R.: Optical Performance of Vacuum Solar Telescope. *AIAA Bull.*, Vol. 7, 1970, p. 564.
- Evans, J.W.: Observations of the Solar Emission Corona Outside Eclipse. *Publ. Astron. Soc. Pac.*, Vol. 69, 1957, p. 421.
- Fainberg, J.; and Stone, R. G.: Type III Solar Radio Burst Storms Observed at Low Frequencies. *Solar Phys.*, Vol. 13, 1970, p. 433.
- Haddock, F. T.; and Graedel, T. E.: Dynamic Spectra of Type III Solar Bursts From 4 to 2 MHz Observed by OGO-III. *Astrophys. J.*, Vol. 160, 1970, p. 293.
- Hagen, J. P.; and Neidig, D. F.: Observation of a Vortex Ring in the Solar Atmosphere. *Astrophys. J.*, Vol. 161, 1970, p. 751.
- Hansen, R.; Hansen, S.; Garcia, C. and Trotter, D.: K-Coronal Enhancement and Chromospheric Plage. *Solar Phys.*, 1971. (in press)
- Hansen, R. T.; Hansen, S. and Loomis, H.G.: Differential Rotation of the Solar Electron Corona. *Solar Phys.*, Vol. 10, 1969, p. 135.
- Hartz, T. R.: Type III Solar Radio Noise Bursts at Hectometer Wavelengths. *Planet Space Sci.*, Vol. 17, 1969, p. 267.
- Harvey, J. W.: Coronal Polar Rays and Polar Magnetic Fields. *Astrophys. J.*, Vol. 141, 1965, p. 832.



- Harvey, J. W.: Magnetic Fields Associated in Solar Active Region Prominences. Ph.D. Thesis, University of Colorado, 1969.
- Hewish, A.: Spectrum of Plasma-Density Irregularities in the Solar Wind. *Astrophys. J.*, Vol. 163, 1971, p. 645.
- Hewish, A.; and Symonds, M. D.: Radio Investigation of the Solar Plasma. *Planet. Space Sci.*, Vol. 17, 1969, p. 313.
- Hundhausen, A. J.: Direct Observations of Solar Wind Particles. *Space Sci. Rev.*, Vol. 8, 1968, p. 690.
- Hundhausen, A. J.; Bame, S. J.; and Montgomery M. D.: Large Scale Characteristics of Flare Associated Solar Wind Disturbances. *J. Geophys. Res.*, Vol. 75, 1970, p. 4631.
- Ivanchuk, V. I.: Fine Structure of Solar Corona and Association with Calcium Network. *Solnechnye Dannye*, Vol. 4, 1968, p. 63.
- Jefferies, J. T.; and Orrall, F. Q.: Loop Prominences and Coronal Condensations. I: Non-thermal Velocities Within Loop Prominences. *Astrophys. J.*, Vol. 141, 1965a., p. 505.
- Jefferies, J. T.; and Orrall, F. Q.: Loop Prominences and Coronal Condensations. II: The Source of Mass and Energy and a Model of the Loop Prominence Mechanism. *Astrophys. J.*, Vol. 141, 1965b, p. 519.
- Jokipii, J. R.; and Coleman, P. J.: Cosmic-Ray Diffusion Tensor and Its Variation Observed with Mariner IV. *J. Geophys. Res.*, Vol. 73, 1968, p. 5495.
- Jokipii, J. R.; and Hollweg, J. V.: Interplanetary Scintillations and the Structure of Solar Wind Fluctuations, *Astrophys. J.*, Vol. 160, 1970, p. 745.
- Kai, K.: Correlated Bursts Between Distant Forces on the Sun. *Proc. Astron. Soc. Australia*, Vol. 1, 1969a., p. 186.
- Kai, K., Radio Evidence of Directive Shock-Wave Propagation in the Solar Corona. *Solar Phys.*, Vol. 10, 1969b., p. 460.
- Kai, K.: The Structure, Polarization, and Spatial Relationship of Solar Radio Sources of Spectral Types I and II. *Solar Phys.*, Vol. 11, 1970, p. 456.
- Kiepenheuer, K. O.: *Solar Activity in the Sun*, G. Kuiper, ed., 1953, p. 332.
- Kleczek, J., Regular Structures in the Green Solar Corona. *Publ. Astron. Soc. Pac.*, Vol. 75, 1963, p. 9.
- Kopp, R. A.: The Equilibrium Structure of a Shock-Heated Corona. Ph.D. Thesis, Harvard University, 1968.
- Kopp, R. A.: A Gas Dynamic Calculation of Type II Shock-Propagation Through the Corona, submitted to *Solar Phys.*, 1971.
- Kopp, R. A.; and Kuperus, M.: Magnetic Fields and the Temperature Structure of the Chromosphere-Corona Interface. *Solar Phys.*, Vol. 4, 1968, p. 212.
- Kulsrud, R. M.: Effect of Magnetic Fields on Generation of Noise by Isotropic Turbulence. *Astrophys. J.*, Vol. 121, 1955, p. 461.
- Kundu, M. R.: *Solar Radio Astronomy*. Interscience, 1965.
- Kuperus, M.: The Transfer of Mechanical Energy in the Sun and the Heating of the Corona. *Rech. Ast. Obs. Utrecht*, 1965, p. 17.
- Kuperus, M.: The Heating of the Solar Corona. *Space Sci. Rev.*, Vol. 9, 1969, p. 713.
- Kuperus, M.; and Tandberg-Hanssen, E.: The Nature of Quiescent Solar Prominences. *Solar Phys.*, Vol. 2, 1967, p. 39.
- Livingston, W. C.: On the Differential Rotation with Height in the Solar Atmosphere. *Solar Phys.*, Vol. 9, 1969, p. 448.
- Livingston, W. C.; and Harvey, J. W.: Observational Evidence for the Quantization in Photospheric Magnetic Flux. *Solar Phys.*, Vol. 10, 1969, p. 294.
- Lovelace, R. V. E.; Salpeter, E. E.; and Sharp, L. E.: Analysis of Observations of Interplanetary Scintillations. *Astrophys. J.*, Vol. 159, 1970, p. 1047.
- Martres, M.; Pick, M.; and Parks, G. K.: Origin of Interplanetary Sectors From Radio Observations. *Solar Phys.*, Vol. 15, 1970, p. 48.
- McCabe, M. K.; and Fisher, R. R.: H $\alpha$  Coronagraph Observations of a Flare Spray March 1, 1965. *Solar Phys.*, Vol. 14, 1970, p. 212.
- Meyer, F.: Flare Produced Coronal Waves. *Proc. IAU Symposium, No. 35*, Reidel-Dordrecht, 1968, p. 485.
- Michel, F. C.: Model of Solar Wind Structure. *J. Geophys. Res.*, Vol. 72, 1967, p. 1917.
- Modisette, J. L.: Solar Wind Induced Torque on the Sun. *J. Geophys. Res.*, Vol. 72, 1967, p. 1521.
- Moreton, G. E.: H $\alpha$  Observations of Flare-Initiated Disturbances with Velocities About 1000 km/sec. *Astron. J.*, Vol. 65, 1960, p. 494.
- Mustel, E.: On the General Structure of the Solar Corona. *Proc. IAU Symposium No. 16*, J. W. Evans, Ed., Academic Press, 1961.
- Mustel, E.: The Spatial Structure of the Solar Corona, I. *Soviet Astronomy*, Vol. 6, No. 3, 1962a., p. 333.
- Mustel, E.: On the Spatial Structure of the Solar Corona. *Soviet Astronomy*, Vol. 6, No. 4, 1962b, p. 488.
- Mustel, E.: Quasi-Stationary Emission of Gases From the Sun. *Space Sci. Rev.*, Vol. 3, 1964, p. 139.

- Ness, N. F.; and Taylor, H. E.: Observations of Interplanetary Magnetic Field, 4-12 July 1966. *Annals of the IQSY*, Vol. 3, MIT Press, Cambridge, 1969, p. 366.
- Newkirk, G., Jr.: Doppler Motions in the Corona. *Ann. d'Astrophys.*, Vol. 20, 1957, p. 127.
- Newkirk, G., Jr.: Structure of the Solar Corona. *Ann. Rev. Astron. Astrophys.*, Vol. 5, 1967, p. 213.
- Newkirk, G. Jr.: Coronal Magnetic Fields. *Proc. 1970 NATO Advanced Study Inst. on Physics of the Solar Corona*, Macris, Ed. Reidel-Dordrecht, 1971. (in press)
- Newkirk, G., Jr.; and Altschuler, M. D.: Magnetic Fields and the Solar Corona, III: The Observed Connection Between Magnetic Fields and the Density Structure of the Corona. *Solar Phys.*, Vol. 13, 1970, p. 131.
- Newkirk, G., Jr.; Altschuler, M. D.; and Harvey, J. W.: Influence of Magnetic Fields on the Structure of the Solar Corona. *Proc. IAU Symposium, No. 35*, 1968, p. 379.
- Newkirk, G., Jr.; and Harvey, J. W.: Coronal Polar Plumes. *Solar Phys.*, Vol. 3, 1968, p. 321.
- Newkirk, G., Jr.; Hansen, R. T.; and Hansen, S.: Coronal Electron Densities During Period of July 1966 Proton Flares. *Ann. IQSY*, Vol. 3, MIT Press, Cambridge, 1969, p. 10.
- Noyes, R. W.; Withbroe, G. L.; and Kirshner, R. P.: Extreme Ultraviolet Observations of Active Regions in Chromosphere and Corona. *Solar Phys.*, Vol. 11, 1970, p. 388.
- Orrall, F. Q.; and Smith, H. J.: Passage of a Flare Spray Through the Solar Corona. *Sky and Tel.*, Vol. 22, 1961, p. 330.
- Pneuman, G. W.: Rotation of the Solar Corona. *Astrophys. J.*, Vol. 145, 1966, p. 800.
- Pneuman, G. W.: The Rotation of Magnetic Loop Systems in the Solar Atmosphere. *Solar Phys.*, 1971. (in press)
- Pneuman, G. W.: Some General Properties of Helmeted Coronal Structures. *Solar Phys.*, Vol. 3, 1968, p. 578.
- Pneuman, G. W.: Coronal Streamers II: Open Streamer Configurations. *Solar Phys.*, Vol. 6, 1969, p. 255.
- Pneuman, G. W.; and Kopp, R. A.: Coronal Streamers III: Energy Transport in Streamers and Interstreamer Regions. *Solar Phys.*, Vol. 13, 1970, p. 176.
- Pneuman, G. W.; and Kopp, R. A.: Gas-Magnetic Field Interactions in the Solar Corona. *Solar Phys.*, 1971. (in press)
- Ramaty, R.; and Lingenfelter, R. E.: Determination of the Coronal Magnetic Field and the Radio-Emitting Electron Energy From Type IV Solar Radio Burst. *Solar Phys.*, Vol. 5, 1968, p. 531.
- Reidy, W. P.; Vaiana, G. S.; Zehnpfenning, T.; and Giacconi, R.: Study of X-Ray Images of Sun at Solar Minimum. *Astrophys. J.*, Vol. 151, Pt. I, Univ. Chicago Press, 1968.
- Riddle, A. C.: 80 MHz Observations of a Moving IV Solar Burst, March 1, 1970. *Solar Physics*, Vol. 13, 1970, p. 448.
- Rust, D.: Measurement of the Magnetic Fields in Quiescent Solar Prominences. Ph.D. Thesis, University of Colorado, 1966.
- Rust, D.; and Roy, J-R: Coronal Magnetic Fields Above Active Regions. *Proc. IAU Symposium No. 43* 1971. (in press)
- Saito, K: Polar Rays of the Solar Corona I. *Publ. Astron. Soc. Japan*, Vol. 10, 1958, p. 49.
- Schatten, K. H.: Evidence for a Coronal Magnetic Bottle at  $10 R_{\odot}$ . *Solar Phys.*, Vol. 12, 1970, p. 484.
- Schatten, K. H.; Wilcox, J. M; and Ness, N. F.: Model of Interplanetary and Coronal Magnetic Fields. *Solar Phys.*, Vol. 6, 1969, p. 442.
- Schmidt, H. U.: On the Observable Effects of Magnetic Energy Storage and Release Connected with Solar Flares, *NASA Symposium on Physics of Solar Flares*, NASA SP-50, 1964, p. 107.
- Siscoe, G. L.; Davis, L., Jr.; Coleman, P. J., Jr.; Smith, E. J.; and Jones, D. E.: Power Spectra and Discontinuities of the Interplanetary Magnetic Field: Mariner 4. *J. Geophys. Res.*, Vol. 73, 1968, p. 61.
- Smerd, S. F.; and Dulk, G. A.: 80 MHz Radioheliograph Evidence on Moving Type IV Bursts and Coronal Magnetic Fields. *IAU Symposium No. 43: Solar Magnetic Fields*, R. Howard and D. Reidel, eds., 1971. (in press)
- Smith, D. F.: Type III Solar Radio Bursts. *Advan. Astron. Astrophys.*, Vol. 7, 1970a, p. 147.
- Smith, D. F.: Towards a Theory for Type III Solar Radio Bursts. *Solar Phys.*, Vol. 15, 1970b, p. 202.
- Smith, E.V.P.: Mass Motions in Solar Flares and Related Phenomena. *Proc. Ninth Nobel Symposium*, Y. Öhman, ed., Wiley Interscience Div., N.Y., 1968, p. 137.
- Smith, S. F.; and Harvey, K. L.: Observational Effects of Flare-Associated Waves. *Proc. 1970 NATO Advanced Study Inst. on Physics of the Solar Corona*, Macris, ed. Reidel-Dordrecht, 1971. (in press)

- Stenflo, J. O.: The Formation of Absorption Lines in a Magnetic Field. *Proc. IAU Symposium No. 43*, R. Howard, ed. Reidel-Dordrecht, 1971a.
- Stenflo, J. O.: Interplanetary Magnetic Field at the Time of the Solar Eclipse of 7 March 1970. *Proc. COSPAR Symposium on the Total Solar Eclipse of 7 March 1970*, Seattle, 1971b.
- Stewart, R. T.; and Sheridan, K. V.: Evidence of Type II and IV Radio Emission From a Common Flare Induced Shocks. *Solar Phys.*, Vol. 12, 1970, p. 229.
- Tanaka, H.; Kakinuma, T.; and Enome, S.: The Slowly Varying Component of the Radio Emission During the Period of the July 1966 Proton Flare. *Ann. IQSY*, Vol. 3, MIT Press, Cambridge, 1969, p. 63.
- Tandberg-Hanssen, E.: *Solar Activity*. Blaisdell Pub. Co., Waltham, Mass., 1967.
- Uchida, Y.: Propagation of Hydromagnetic Disturbances in the Solar Corona and Moreton's Wave Phenomenon. *Solar Physics*, Vol. 4, 1968, p. 30.
- Uchida, Y.: Diagnosis of Coronal Magnetic Structure by Flare-Associated Hydromagnetic Disturbances. *Publ. Astron. Soc. Japan*, Vol. 22, 1970, p. 341.
- Vaiana, G. S.; Krieger, A. S.; and Van Speybroeck, L. P.: Photospheric Magnetic Fields and X-Ray Corona. *Proc. of IAU Symposium No. 43*, 1971, Paris.
- Valdez, J.; and Altschuler, M. D.: Preliminary Observations of Coronal Magnetic Fields Before and After Solar Proton Events. *Solar Phys.*, Vol. 15, 1970, p. 446.
- Valnicek, B.; Godoli, G.; and Mazzucconi, F.: The West Limb Activity on 9, 10, and 11 July 1966, as Observed in the H $\alpha$  Line. *Ann. IQSY*, Vol. 3, MIT Press, Cambridge, 1969, p. 113.
- Waldmeier, M.: Die Minimumsstruktur der Sonnenkorona. *Z. Astrophys.*, Vol. 37, 1955, p. 233.
- Warwick J. W.: Solar Radio Bursts of Type V Interpreted as Type IIIs in Superheated Coronal Streamers. *Astrophys. J.*, Vol. 150, 1967, p. 1081.
- Warwick, J. W.; and Dulk, G. A.: Spectrum and Polarization of Solar Radio Bursts on a 10 Millisecond Time Scale. *Astrophys. J.*, Vol. 158, 1969, p. 123.
- Weber, E. J.; and Davis, L., Jr.: The Angular Momentum of the Solar Wind. *Astrophys. J.*, Vol. 148, 1967, p. 217.
- Wilcox, J. M.: Interplanetary Magnetic Field: Solar Origin and Terrestrial Effects. *Space Sci. Rev.*, Vol. 8, 1968, p. 258.
- Wilcox, J. M.; and Colburn, D. S.: Interplanetary Sector Structure Near Maximum of Sunspot Cycle. *J. Geophys. Res.*, Vol. 75, 1970, p. 6366.
- Wilcox, J. M.; and Howard, R.: Differential Rotation of the Photosphere Magnetic Field. *Solar Phys.*, Vol. 13, 1970, p. 251.
- Wilcox, J. M.; Severny, A.; and Colburn, D. S.: Solar Source of Interplanetary Magnetic Fields. *Nature*, Vol. 224, 1969, p. 353.
- Wild, J. P.: Radio Observations of Solar Flares. *AAS-NASA Symposium on Physics of Solar Flares*, 1963, p. 161.
- Wild, J. P.: Interaction Between Distant Centres Around the Sun. *Proc. Astron. Soc. Australia*, Vol. 1, 1969a, p. 181.
- Wild, J. P.: Radio Evidence of Instabilities and Shock Waves in the Solar Corona. *Plasma Instabilities in Astrophys.*, ed. by D. G. Wentzel and D. A. Tidman, Gordon and Breach, Pub., 1969b, p. 119.
- Withbroe, G. L.; and Noyes, R. W.: Solar EUV Observations: Lines of Lithium-Like Ions. *Solar Phys.*, 1971. (in press)
- Zirin, H.: Coronagraph Observations of Coronal Condensation of 4 February 1962. *Solar Phys.*, Vol. 11, 1970, p. 497.
- Zirin, H.: *The Solar Atmosphere*. Blaisdell Pub. Co., Waltham, Mass., 1966.

*P. McIntosh* In comparing these sector boundary locations with the computed magnetic fields you mentioned that some of these boundaries were steady, some were unsteady. Could you clarify what you meant by this difference?

*G. Newkirk* Simply that if you look in the presentation of the interplanetary magnetic field polarities, rotation by rotation that from one rotation to the next the sector boundary may appear, disappear, change sign and be very unsteady. On the other hand, a steady sector boundary will be seen month after month after month in approximately the same position. Now, I admit it is rather daring, on the basis of four events, of which two fit your conception, to draw a whole picture of what the sector boundary and the connection between the magnetic field is, but this is all the data we have.

*E. J. Smith* I notice that one of the assumptions made in these analyses is that there is no displacement of the corona relative to the photosphere.

## DISCUSSION

*G. Newkirk* Yes, this is rather tacitly assumed. The evidence we have for that is simply the fairly good connection between high density enhancements in the corona and the high magnetic field concentrations which we see in plages, and this is a very well established sort of thing. Now, as to whether or not the angular velocity of the corona and the photosphere match well enough to prevent distortion, the observations suggest that in general the coronal rotation rate is the same as that of the magnetic fields in the underlying photosphere, with one suggestion of a slight acceleration with altitude. That acceleration is apparently due to the fact that the field is anchored at lower latitudes and tends to drag the material along. We are then looking at a place where the characteristic velocity isn't that of the underlying latitude point.

*M. Dryer* Gordon, in the one sequence in the movie when we saw the material flowing back toward the sun, does that material cause the kind of flare that Hyder has talked about? Do flares result from that material?

*G. Newkirk* Well, these -- you're trying to get me in trouble, aren't you? These loop prominences follow flares. Now, Hyder talks about the impact infall flares and flare-like brightenings. Now, I don't believe he would assume that a loop prominence causes this sort of thing. He is talking more about events which characteristically look a little different than this.

*J. M. Wilcox* Could you comment on the ejection of material from the lower layers of the solar atmosphere out into the interplanetary medium?

*G. Newkirk* The general impression you get from seeing these field distribution coronal maps, as well as from seeing coronal events, is that the material is generally collimated rather strongly by the magnetic field. Now, whether or not, for example, one of these type IV moving bursts is the radio evidence of such an ejection we really don't know; but if it is we then have pretty good reason to see how the collimation occurs. That sort of event is collimated by the nearly radial magnetic field. The composition of the polarization of those radio events suggests at least some of them are toroidal magnetic field ejections. So what we have is a sort of smoke ring in the field with actually a current going around and the field containing all these type IV relativistic or mildly relativistic particles. This thing drifts out essentially with the Alfvén speed, and it is apparently associated with the shock wave which eventually arrives out into the interplanetary space.

*R. Howard* While we're talking about velocities I just want to say that although we see pictures of the upward motion of surges and so on, those who observe velocities on the solar surface in general agree that if there is anything at all characterizes the residual velocity fields over the solar surface, it is that where there are strong magnetic fields the velocities in the photosphere are toward the surface of the sun.

*C. P. Sonett* I assume that when you are looking with a white light coronagraph you're looking at the Thompson-scattered light from electrons, that in effect measures your plasma density. But there are also observations in H-alpha, which is recombination radiation. Could you clarify the plasma temperature and density structures?

*G. Newkirk* When you look at the white light coronagraph you are indeed seeing Thompson-scattering from free electrons; that's just the straight electron density. You look in the 5303 line of the corona and you're looking at a material which for you to see has to be of the order of one or two million degrees. And where it's bright, it's high electron density. A feature such as loop prominence which I showed has a very intricate temperature structure, because approximately in the same region you also see H-alpha, which is representative of an electron density that is approximately a factor of a hundred over the ambient corona, and where the temperatures may be only 20, 30, 40 thousand degrees. So you may have a very intricate temperature structure, and just asking what is the plasma density in that thing is something that we can't give you a straight answer to. You've got to ask what the plasma density is at what temperature.

## LARGE-SCALE NEGATIVE POLARITY MAGNETIC FIELDS ON THE SUN AND PARTICLE-EMITTING FLARES.

V. Bumba

Some observational facts about the large-scale patterns formed by solar negative polarity magnetic fields during the 19th and 20th cycles of solar activity are presented. The close relation of the position of occurrence of very large flares accompanied by cosmic ray and PCA events as well as other phenomena of solar activity during the declining part of the 19th cycle of the regularities in the internal structure of large-scale negative polarity features are demonstrated. **ABSTRACT**

### INTRODUCTION

During recent years a great interest of space physicists and geophysicists was evoked by the large-scale sector structure of the interplanetary magnetic field, which is closely related to the large-scale organization of photospheric magnetic field patterns. Many studies demonstrating this correlation were published [Wilcox, 1968; Wilcox and Colburn, 1969; Wilcox and Ness, 1965; and others].

In several papers we tried to study the regularities and recurrences in this large-scale distribution of solar magnetic fields [Bumba and Howard, 1965a; Bumba and Howard, 1969] and the dynamics of the development of such regular background field patterns [Bumba and Howard, 1965b; Bumba, 1970a,b]. In a recent paper [Ambrož et al., 1970] we tried to demonstrate the tendency of certain giant regular structures to develop in streams of individual polarities, the morphology of which reminds one of very large cellular features. We call them "supergiant" structures and they are related to "active longitudes." They are best seen in the negative polarity magnetic fields. They have their own internal structure in which during the periods of best visibility we may recognize subordinate structures ( $30^\circ$  to  $35^\circ$ ;  $60^\circ$ ) [Bumba et al., 1969]. The length of the whole best-developed feature may sometimes reach nearly  $180^\circ$  not counting the tail.

Here we present some more facts about these "supergiant" structures and show the close relation of the position of very large flares (flares with cosmic ray and PCA events) to the regularities in the internal structure of such huge features formed in negative polarity streams. This observational fact we think speaks in favor of the physical meaning of these formations. The close relationship of positive polarity streams to the geomagnetic disturbances is demonstrated in Chapter 2 (p. 151).

### THE OBSERVATIONAL DATA

The basic observational data are those of the Atlas of Solar Magnetic Fields 1959-1966 [Howard et al., 1967], supplemented by draft copies of magnetic synoptic charts of subsequent rotations also constructed from the daily magnetograms of the Mount Wilson Observatory. The data used extend through the first half of 1970. Because of the inhomogeneity of some of the magnetic charts the maps were integrated through the use of two or three sequential overlays. For some periods of time we studied only the equatorial strips ( $\pm 20^\circ$ ) of maps as well as the whole maps, drawn separately for each polarity.

As a catalog of great flares the List of type IV bursts connected with the cosmic ray increases or PCA events, published by Švestka and Olm [1966], for the time periods for which good quality synoptic charts were available, was used.

---

The author is at the Astronomical Institute of the Czechoslovak Academy of Sciences, Observatory Ondřejov, Czechoslovakia.

### MINUS POLARITY DISTRIBUTION

In previous papers [Bumba and Howard, 1969; Ambrož *et al.*, 1970] concerning the preceding cycle of solar activity (no. 19), the better visibility and definition of negative polarity rows and streams in equatorial parts of synoptic charts was mentioned. During this 19th cycle the negative polarity was the following one on the northern, more active solar hemisphere. Studying the first half of the present cycle (no. 20) in which the negative polarity is the leading one on the northern hemisphere, we may see the same narrow and concentrated rows of minus polarity fields and the same tendency of positive polarity rows and streams to grow broader and more diffuse (fig. 1). And again we may observe not only the 27-day period of rotation in the inclination of these rows and streams (drawn in Carrington's coordinate system), but the successive rows and streams of negative polarity may be again seen to be intensified in succession, giving the appearance on the large-scale of a different rotation period (28 to 29 days).

In the first half of the present cycle as well as in the previous cycle, the formation of "supergiant" features during the greatest part of the time interval covered by our synoptic charts is observable in the minus polarity magnetic fields, although such clear separation of both polarities in two opposite longitudinal zones such as during the rotations 1437 through 1442 was not so often observed (fig. 2). The rules of the "supergiant" regular structures development in the opposite polarities separated in the individual active longitudes seem to be not very simple, and more systematic and exact methods of investigation will be needed to find them. In any case, it may be seen that the growth and the decay of these objects [which for the most long lasting one during the present cycle takes about 15 rotations (fig. 3) (1541 - 1555)] occur somewhat differently in comparison with the preceding cycle, and this difference seems to be related to the mutual relation of individual polarities and active longitudes in the formation of structures. Although only the morphological changes of these features have been studied, the consistency of the rules and recurrences during their development seems to speak against their explanation by pure chance.

Again in the present cycle as in the previous one the concentrations of solar activity inevitably coincide with concentrations of negative polarity fields on the large-scale, and the daily geomagnetic disturbances, shifted four days to account for the travel time of the solar wind plasma from the sun to the earth, show a fairly close correlation with positive polarity magnetic features, as will be demonstrated in Chapter 2 (p. 151).

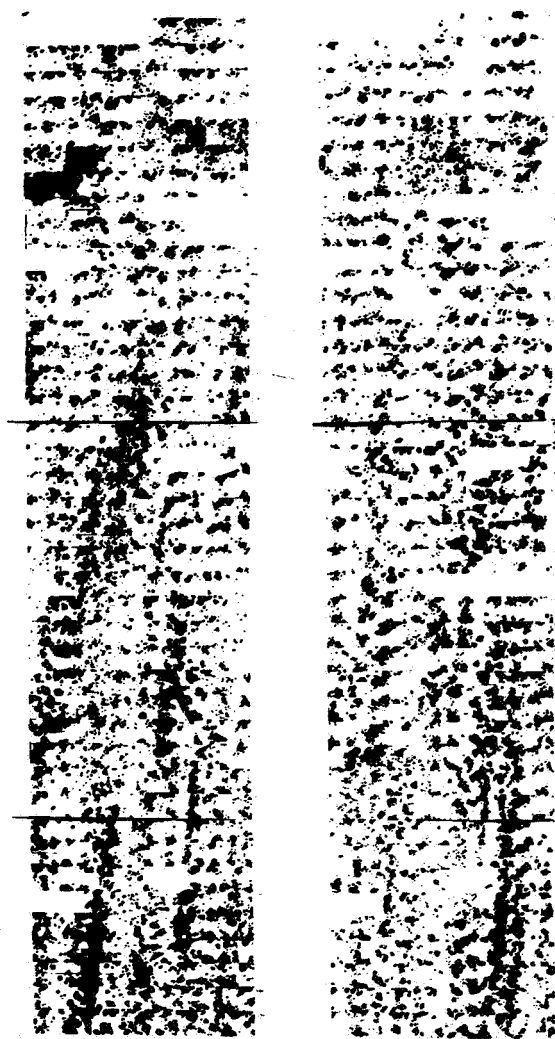
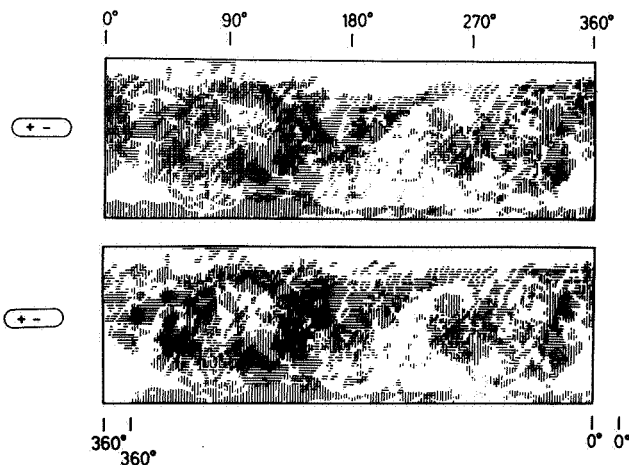


Figure 1. Photospheric synoptic charts cut into equatorial strips ( $\pm 20^\circ$ ) and mounted in chronological order for rotations 1522 through 1562 (1967 - 1970). Both polarities are drawn separately. Minus polarity is on the left, plus on the right of the figure. The main inclination of 27 days can be clearly seen especially in the left picture. On the minus polarity drawing may be found the intensification of subsequent individual magnetic rows, starting in the upper left-hand corner and going in a regular succession toward the lower right-hand corner, forming the 28-day active longitude.

### CORRELATION OF PARTICLE-EMITTING FLARES WITH "SUPERGIANT" NEGATIVE FEATURES

We may find one more argument in favor of the physical meaning of these large-scale formations if we correlate



**Figure 2.** Synoptic charts demonstrating the degree of symmetry of both polarities "supergiant" structures, developed during the rotations 1434 through 1444. The maximum stage of development of two "supergiant" regular structures is shown, each of them occupying practically one half of the Sun in both main active longitudes, formed from opposite polarities. The regularity and repeated internal structure of "supergiant" bodies of both active longitudes may be seen.

the position of large flares followed by particle emission measured as cosmic ray, or PCA events, with the internal structure of these features. For this discussion we have used only part of our maps that concerns the 19th cycle of activity, because the lists of large flares for the 20th cycle are still incomplete. Table 1 gives the list of correlated flares taken from *Svestka and Olm* [1966]. Altogether there are 46 flares in 22 active regions observed from August 1959 till September 1963. From this number about 32, or possibly 40 flares in 11, or possibly 17 active regions lie in a very specific minus polarity magnetic field configuration. (Four flares in three active regions cannot be correlated because of poor quality maps.) Figure 4 shows some examples of this very complex magnetic situation. On the left side of each part of the figure the large body of the "supergiant" negative polarity structure, drop shaped having its head to the west, is presented. This structure is about  $90^\circ$  to  $100^\circ$  in length and is a result of a long-lasting evolution (several rotations). The center of gravity of the largest solar activity is located at the eastern part of the structure, below its tail, in the center of each figure. This is the location of greatest probability occurrence of particle emitting flares. The right side of each figure is not so regular as its left part because of greater activity changes.



**Figure 3.** Magnetic synoptic charts of the negative polarity fields for rotations 1544 through 1556. For integration two consecutive maps, one of which is repeated, are overlapped. The development of negative "supergiant" regular structures is shown. The positive large-scale features are formed between them.

More specific and detailed characteristics of the development of such a situation are not possible here, but certainly this complicated process will be demonstrated in a more extended paper.

Another point of view on this close relation of large flares to the negative polarity formations on the sun may be obtained from one other observational fact. From Supplement II to the list of particle emitting flares published by Krivský (1969), concerning the first half of the

Table 1. Flares followed by particle emission occurring in solar cycle 19 [taken from Švestka and Olmr, 1966].

No	Date		Start of flare SID		Flare position imp.		Magn. storm delay		C.R. Start	PCA Delay	A.R. No	Correlation with MF
092	1959	Aug. 18	1014	1025	12N,	33W	3	42ms	—	0.5–1.5	49	+
095		Sep. 1	1923	1928	12N,	60E	2+	51ms	—	8.5	52	?(+)
100	1960	Jan. 11	<2040	2100	22N,	02E	3	46ms	—	1.0–10.0	55	+
101		Jan. 15	1336	1340	20S,	69W	2	31ms	—	13.5	56	+
103		Mar. 28	2042	2048	14N,	37E	2	62S	—	11.0–14.0	58	+
104		Mar. 29	<0640	0652	12N,	30E	2+	52S	—	1.0–4.0	58	+
105		Mar. 30	0216	0220	09N,	15E	1+	34S	—	7.0–17.5	58	+
106		Mar. 30	1455	1520	12N,	12E	2	28si	—	11.5–22.5	58	+
107		Apr. 1	0843	0850	12N,	12W	3	38ms	—	1.0–1.5	58	+
108		Apr. 5	<0215	0140	12N,	62W	2+	39m	—	2.5–8.5	58	+
109		Apr. 28	<0130	0120	05S,	35E	3	48S	—	0.5–8.5	59	+
110		Apr. 29	<0107	0205	14N,	21W	2+	24S	—	0.5–5.5	58	+
111		May 4	1000	1015	13N,	90W	2	54ms	1030	0.3–1.0	58	+
112		May 6	1404	1427	08S,	08E	3	38ms	—	0.0–11.5	60	?(+)
113		May 13	0519	0512	29N,	68W	3	53si	—	1.0–2.5	61	?(+)
114		May 26	0818	0914	14N,	15W	2	59ms	—	1.0	58	+
115		Jun 1	0824	0837	29N,	47E	3+	66m	—	5.5–59.5	62	?(+)
116		Jun 25	<1131	1530	20N,	06E	3	32W	—	5.0	63	?(+)
117		Jun 25	1659	1659	19N,	01W	1	27W	—	0.0	63	?(+)
121		Jun 27	2140	2345	21N,	25W	2+	33si	—	1.5	63	?(+)
124		Aug. 11	1916	1925	22N,	27E	3	68m	—	4.5–66.0	64	+
125		Sep. 3	0037	0045	19N,	88E	2+	26ms	0200	4.5–22.5	64	+
127		Sep. 26	0525	0534	19S,	64W	2	75m	—	–8.5–7.5	65	+
131		Oct. 29	1026	1029	22N,	26E	3	no	—	1.5	67	(+)?
132		Nov. 10	1009	1022	28N,	25E	3	51S	—	8.0	68	+
133		Nov. 11	0305	0311	29N,	12E	2+	35S	—	0.5	68	+
134		Nov. 12	1315	1325	26N,	04W	3+	21m	1340	0.5–1.5	68	+
135		Nov. 14	0246	0300	27N,	19W	2+	72ms 34ms	—	19.0	68	+
136		Nov. 15	0207	0217	26N,	33W	3	43m 20m	0227	2.0–9.5	68	+



Table 1. Flares followed by particle emission occurring in solar cycle 19 [taken from Švestka and Olm, 1966]. (Concluded)

No	Date	Start of flare SID	Flare position imp.	Magn. storm delay	C.R. Start	PCA Delay	A.R. No	Correlation with MF
137	Nov. 20	1955	1938 2023	25N, 90W	2+ 26si	2055	3.5-16.5	68 +
138	Dec. 5	1825	1830	27N, 70E	3+ 47m	—	10.5	68 +
143	1961 Jul. 11	1615	1648	07S, 31E	2+ 42ms	—	3.0-7.0	73 +
144	Jul. 12	0950	1023	07S, 22E	3 46m	—	1.0-20.5	73 +
145	Jul. 15	1433	1435	13N, 15E	3 52ms	—	1.2	74 +
146	Jul. 18	0920	0943	08S, 59W	3+ 41m	1020	2.0-2.5	73 +
147	Jul. 20	1524	1530	06S, 90W	2+ no	1610	6.0-11.0	73 +
151	Sep. 10	1950	1942	16N, 90W	1 68m	—	0.5-3.5	76 bad qual. maps
152	Sep. 28	2202	2216	13N, 29E	3 47S	—	1.0-1.5	76 —"
153	Nov. 10	1434	1436	19N, 90W	1+ no	—	0.5	78 —"
163	Oct. 23	1642	no	03N, 70W	2 47si	—	0.5	87 —"
166	1963 Aug. 6	0855	0859	13N, 12W	2 no	—	2.3	88 ? -
167	Aug. 9	2234	2234	07N, 80W	1 no	—	0.7	89 ? -
169	Sep. 16	1300	1303	11N, 49E	2 65m	—	6.3	90 +
170	Sep. 20	0713	0714	14N, 04E	2 31ms	—	3.0	90 +
171	Sep. 20	2314	2351	10N, 09W	2 14ms	—	0.0	90 +
172	Sep. 26	<0638	0709	13N, 78W	3 37ms	—	0.5	90 +

+ means good correlation  
 ?(+) possibly may be a correlation  
 ? - probably no correlation

**Table 2.** *Flares followed by particle emission occurring in solar cycle 20 [taken from Křivský, 1969].*

No	Date	Flare Class	Position	Start	C.R. Start	PCA Delay min.	Polarity of Interplanetary magnetic field	
							0 d	+ 4d
1965	Feb. 5	2	8° N, 25° W	1750	—	>40	—	(0)/+
	Jun. 15	1+	22° N, 30° W	0735	—	?	+/(—)	
	Jul. 10	1+	19° N, 17° W	0940	—	?	—	0
	Jul. 13	1	20° N, 55° W	1046	—	?	—	—
	Oct. 4	2	23° S, 30° W	0935	—	(~125)	—	—
1966	Jul. 7	2B	35° N, 48° W	0022	0055–0100	~87	0	—
	Aug. 28	2B	21° N, 4° E	1522	1550	~64	—	—
	Sep. 2	2B	22° N, 57° W	0541	?	65	—	+
1968	Apr. 25	1N	15° N, 30° W	0035	—	+	—	—
	Jul. 9	2B	14° S, 9° W	0831	—	?	0	0
	Jul. 12	2N	12° N, 10° E	0000	—	+	—	—
	Sep. 29	2B	17° N, 50° W	~1616	+	?	+/(—)	0
	Nov. 18	2N	22° N, 87° W	<1030	1045		—	—

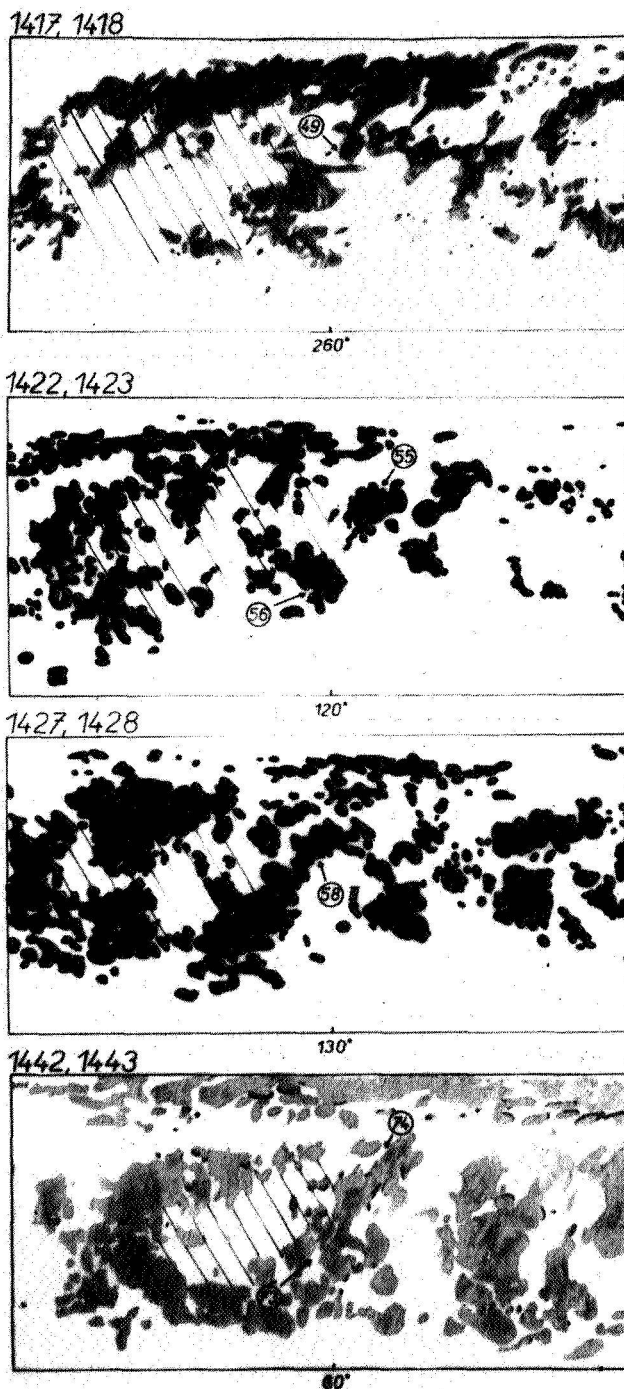


Figure 4. Four examples of very complex magnetic situations in the negative polarity large-scale distribution within six active regions in which large particle-emitting flares developed. On the left side of each picture the large body of the "supergiant" negative polarity structure may be seen. In the center of each picture the position of the active region producing the large flares is indicated by an arrow and number of A.R. Again for integration two consecutive maps are overlapped.

present cycle (no. 20) of solar activity we can correlate the occurrence of these flares with the already published [Wilcox and Colburn, 1969; Severny *et al.*, 1970] interplanetary magnetic field polarity data. Table 2 presents the very preliminary results showing again that in the present cycle the greatest flares are more often related to the negative polarity on the sun as well as in the interplanetary space.

## CONCLUSIONS

The results presented here provide some new observational evidence for the existence of some difference in the behavior of negative and positive polarity of the photospheric magnetic fields, not only in the mode of their large-scale (and possibly also small-scale) distribution, organization, and development but also in their relation to solar activity and interplanetary magnetic fields. The development of large-scale features of both polarities takes place over a wide range of heliographic longitudes as well as latitudes and does not seem to be influenced by the differential rotation. It is still not possible to give the reason for the formation of "supergiant" structures, but the same forces responsible for the occurrence of active longitudes with different periods of rotation seem to play an important role in this process.

As was demonstrated, large-scale solar regions with predominant negative polarity are closely related to the regions with the more developed and progressive activity and greater frequency of large flares. This can also mean that during the period when the integrated magnetic field has the negative sign, the sun observed as a star will have more pronounced emission in some ionized calcium and hydrogen lines and greater absorption in helium D<sub>3</sub> line, and so forth. Greater radio emission can be expected during this period of time.

The present results are very preliminary. Still more systematic work is needed to find more physical relations between the individual polarities of solar magnetic fields and other solar and interplanetary phenomena, and the exact rules of the development of their various morphological features.

## REFERENCES

- Ambrož, P.; Bumba, V.; Howard, R.; and Šýkora, J.: Opposite Polarities in the Development of Some Irregularities in the Distribution of Large Scale Magnetic Fields. *Proc. IAU Symposium No. 43 on Solar Magnetic Fields*, Paris, 1970. (in press)
- Bumba, V.: Concerning The Formation of Giant Regular Structures in the Solar Atmospheres. *Solar Phys.*, Vol. 14, 1970a, p. 80.

- Bumba V.: Large-Scale Magnetic Field and Activity Patterns on the Sun. *The Proc. Leningrad Symposium on Solar Terrestrial Phys.*, 1970b. (in press)
- Bumba, V.; and Howard, R.: Large-Scale Distribution of Solar Magnetic Fields. *Astrophys. J.* Vol. 141, 1965a., p. 1502.
- Bumba, V.; and Howard, R.: A Study of the Development of Active Regions on the Sun. *Astrophys. J.* Vol. 141, 1965b, p. 1492.
- Bumba, V.; and Howard, R.: Solar Activity and Recurrences in Magnetic Field Distribution. *Solar Phys.*, Vol. 7, 1969, p. 28.
- Bumba, V.; Howard, R.; Kopecky, M.; and Kuklin, G. V.: Some Regularities in the Distribution of Large-Scale Magnetic Fields on the Sun. *Bull. Astron. Inst. Czech.* Vol. 20, 1969, p. 18.
- Howard, R.; Bumba, V.; and Smith, S. F.: Atlas of Solar Magnetic Fields, August 1959-June 1966. *Carnegie Inst. of Washing., D.C. Publ. 626*, Washington, D.C., 1967.
- Křivský, L.: Flight Time of Solar Fast Particles From Flares to the Earth. *Bull. Astron. Inst. Czech.* Vol. 20, 1969, p. 293.
- Severny, A.; Wilcox, J. M.; Scherrer, P. H.; and Colburn, D. S.: Comparison of the Mean Photospheric Magnetic Field and the Interplanetary Magnetic Field. *Solar Phys.*, Vol. 15, 1970, p. 3.
- Švestka, Z.; and Olmr, J.: Type IV Bursts — 1. List of Events. *Bull. Astron. Inst. Czech.* Vol. 17, 1966, p. 4.
- Wilcox, J. M.: The Interplanetary Magnetic Field, Solar Origin and Terrestrial Effects. *Space Sci. Revs.* Vol. 8, 1968, p. 258.
- Wilcox, J. M.; and Colburn, D.S.: Interplanetary Sector Structure in the Rising Portion of the Sunspot Cycle. *J. Geophys. Res.*, Vol. 74, 1969, p. 2388.
- Wilcox, J. M.; and Ness, N. F.: Quasi-Stationary Corotating Structure in the Interplanetary Medium. *J. Geophys. Res.* Vol. 70, 1965, p. 5793.

## DISCUSSION

*J. M. Wilcox* I would just make a brief comment. Some of the aspects of what Dr. Bumba presents seem similar to the proposed solar sector pattern. For example, he finds a preferred polarity over both northern and southern hemispheres, and he finds the same kind of structure over long periods of time, maybe even over several solar cycles, and he finds that it seems to be in a rigid rotation system similar to the solar sector pattern. So that perhaps when we understand these matters we will see more detailed connections.

*P. McIntosh* I would like to suggest that the persistence of the large-scale patterns is due to a preference for more frequent active region formation in some longitudes than in others. Since the same sources apparently produce the sector pattern, perhaps we will have to go into the interior of the sun to look for why we get more regions coming up in some places than others. We know from other studies in the literature that proton flares come from the combination of two or more active regions coalescing, so that this would of course be the case if you had more frequent regions in one longitude than another.

*L. Carovillano* In any attempt to make a hydromagnetic description of the solar wind flow, one must say something about the magnetic field. At the source is it dipole or quadrupole or some kind of multipole field? If you do anything that makes the field very complicated, your equations which are already non-linear, become extremely difficult. I understood from a couple of comments this morning that the general feeling is that the multipole analysis indicated that the macrostructure of the field at the photosphere is quite predominantly dipolar or perhaps quadrupolar. It might change from one to the other but that basically the dominant component is that.

It seems to me when I look at the synoptic charts of the photospheric magnetic field I see the field direction changing many times once around the sun. Sometimes I counted eight times, twelve times. And anyone who knows the simplest things about multipole fields realizes the number of times the field changes directly implies a multipolarity, and all of these charts imply very high multipolarity. I couldn't imagine how a dipole field could be a dominant component in any picture where a field changes direction twelve times going around the sun. Could you comment on just the general macrostructure with regard to the simple field configuration?

*G. Newkirk* I'm afraid that the configurations are not simple. The dominant term in the spherical analysis in 1959 and 1960 was dipolar in the plane of the equator, more or less. That came about at a time in the activity cycle when there was quite a bit of activity. A little later this activity trailed off a bit and the solar disk began to look a little bit more simple because you didn't see the regular alternations every  $20^\circ$  or  $30^\circ$  of longitude. In fact, the solution got somewhat more complicated and it became a quadripole.

*J. M. Wilcox* Just briefly, it seems to me the question touches on what has been a truly surprising result of the work of the last few years, particularly for the sector structure first seen in the interplanetary field. Namely, as you look at these synoptic charts of the photospheric field you see a situation in which the field appears to be changing very frequently. Yet, if you defocus this, or smear out the high frequency terms, you don't tend to go to zero, as we would have thought a few years ago, but you tend to go into the solar sector structure, which has predominantly either two or four sectors per rotation. And I think it is a surprising result. It's not what you see if you just look casually at the synoptic chart.

*R. L. Carovillano* Maybe I can add to my question, then. Let's put it this way, over what spatial scale on the surface of the sun do we have to perform an average in order to get a polarity which resembles what we see in the solar wind at larger distances? This correlation is the important one which must be relevant in the full structure.

*J. M. Wilcox* I would just like to thank Dr. Carovillano for asking this question. It is precisely what we are trying to answer in a future observational program. We'll have a little rectangular mask whose area can be varied and we'll run it across the solar disk and measure the mean photospheric magnetic field.

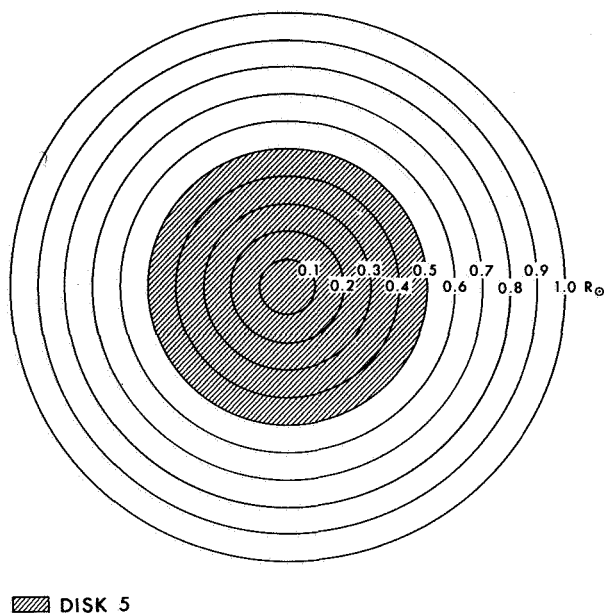
## COMMENTS

*P. H. Scherrer, Robert Howard, and John Wilcox* The mean photospheric field has been compared with the interplanetary field polarity by crosscorrelating averages of Mount Wilson daily magnetograms obtained over a  $2\frac{1}{2}$ -year period with the interplanetary sector polarity determined from the Ames Research Center magnetometers on Explorer 33 and Explorer 35. Agreement was found between the two measurements with a lag of about four and one half days.

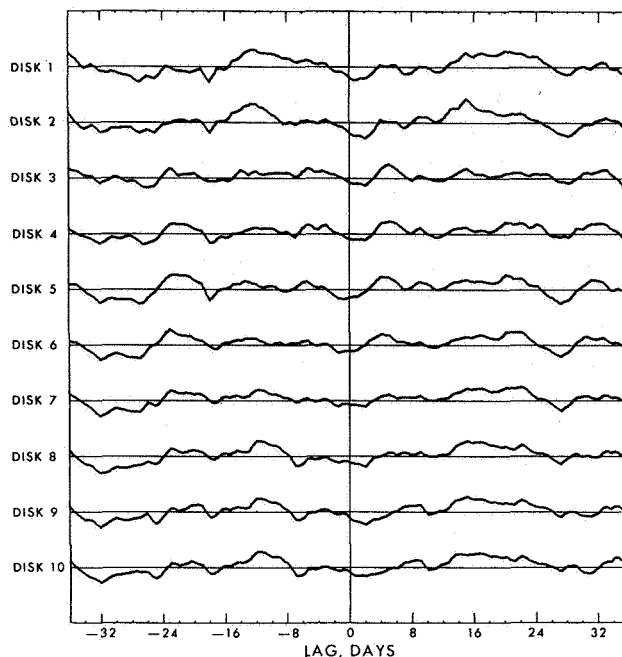
The most interesting results were found when averages over different large areas of the disk were compared to the interplanetary field. These averages, referred to as "bull's eye" averages of daily magnetograms, were available as a result of another investigation for July 1967 through June 1970.

Figure 1 shows that the bull's eye averages consist of ten averages over disks of radii stepping from one-tenth the full solar disk radius to the whole disk in steps of one-tenth the full radius. We labeled the disks and the averages "disk 1" through "disk 10." Disk five, for example, shown shaded in the figure, has a radius one-half the full disk.

The cross correlation between these disks and the interplanetary field polarity was determined as a function of lag for various time periods. Figures 2 through 6 show the results of these calculations for the disks for the five 6-month intervals from July of 1967 through December of 1969; the 1970 interplanetary data are not yet available. Figure 2 shows that there is a correlation at a lag of about  $4\frac{1}{2}$  days for disk 3 through disk 6 for the last half of 1967, but no correlation for the larger disks. Note that the  $4\frac{1}{2}$ -day lag corresponds to the transit time of solar wind plasma from sun to earth. Figure 3 shows quite different results for the first 6 months in 1968. In this period there are similar peaks for all the disks. Measurements by *Severny et al.* [1970] of the mean field in 1968 were made during about half of this period. The bull's eye correlations showed a similar pattern when the exact time interval was used during which *Severny et al.* had found good agreement with the interplanetary field.



**Figure 1.** Schematic drawing shown areas of disk averages of the photospheric magnetic field.



**Figure 2.** Cross correlation of disk averages of the photospheric magnetic field with interplanetary magnetic field polarity for the six months, July through December 1967. The curve near the line labeled "disk 5" represents the cross correlation of the disk 5 data for lags -36 to +36 days. The line labeled "disk 5" represents a correlation coefficient of zero. The line labeled "disk 4" represents a correlation coefficient of 1.0 for disk 5, and similarly the line labeled "disk 6" represents a correlation coefficient of -1.0. All the other disk and ring correlations are in the same format.

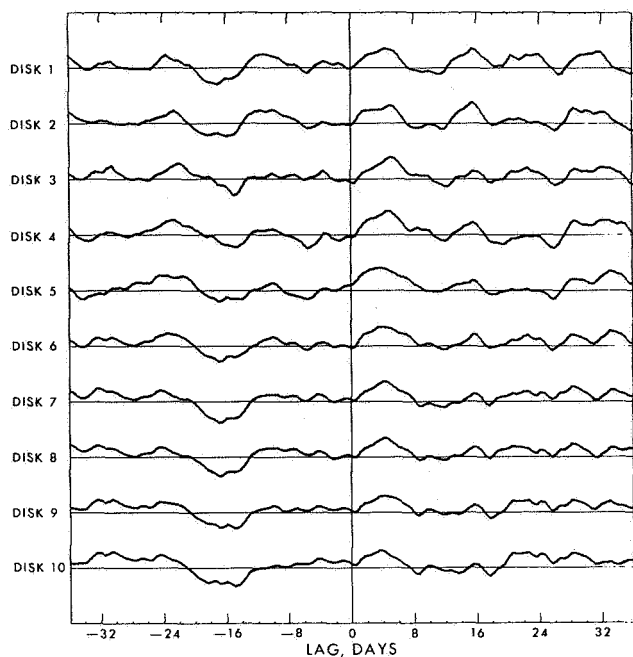


**Figure 3.** Cross correlation of disk averages of the photospheric magnetic field with interplanetary magnetic field polarity for the six months, January through June 1968. The curve near the line labeled "disk 5" represents the cross correlation of the disk 5 data for lags -36 to +36 days. The line labeled "disk 5" represents a correlation coefficient of zero. The line labeled "disk 4" represents a correlation coefficient of 1.0 for disk 5, and similarly the line labeled "disk 6" represents a correlation coefficient of -1.0. All the other disk and ring correlations are in the same format.

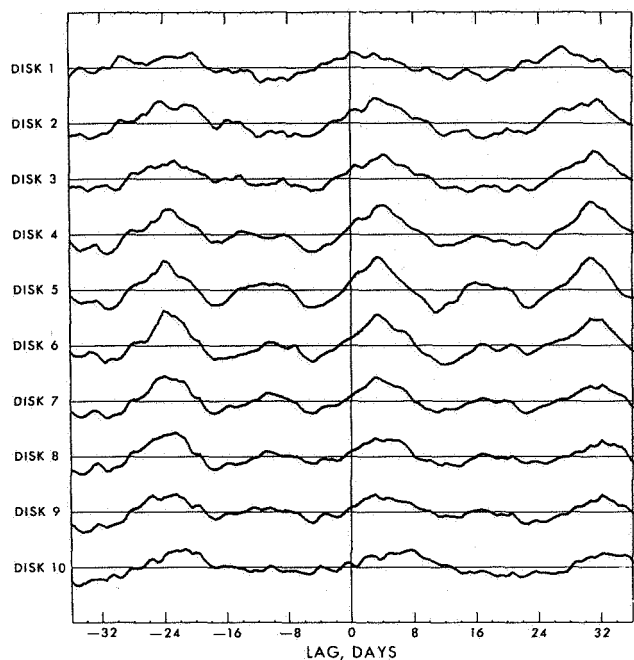


**Figure 4.** Cross correlation of disk averages of the photospheric magnetic field with interplanetary magnetic field polarity for the six months, July through December 1968. The curve near the line labeled "disk 5" represents the cross correlation of the disk 5 data for lags -36 to +36 days. The line labeled "disk 5" represents a correlation coefficient of zero. The line labeled "disk 4" represents a correlation coefficient of 1.0 for disk 5, and similarly the line labeled "disk 6" represents a correlation coefficient of -1.0. All the other disk and ring correlations are in the same format.

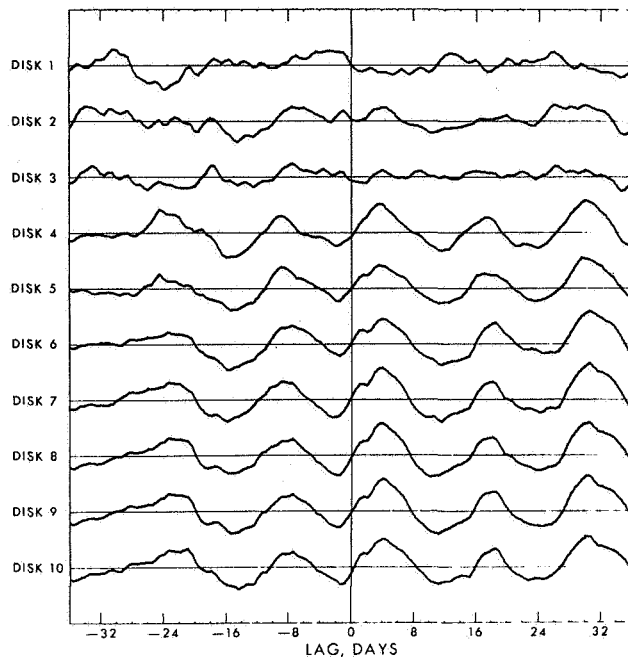


**Figure 5.** Cross correlation of disk averages of the photospheric magnetic field with interplanetary magnetic field polarity for the six months, January through June 1969. The curve near the line labeled "disk 5" represents the cross correlation of the disk 5 data for lags -36 to +36 days. The line labeled "disk 5" represents a correlation coefficient of zero. The line labeled "disk 4" represents a correlation coefficient of 1.0 for disk 5, and similarly the line labeled "disk 6" represents a correlation coefficient of -1.0. All the other disk and ring correlations are in the same format.

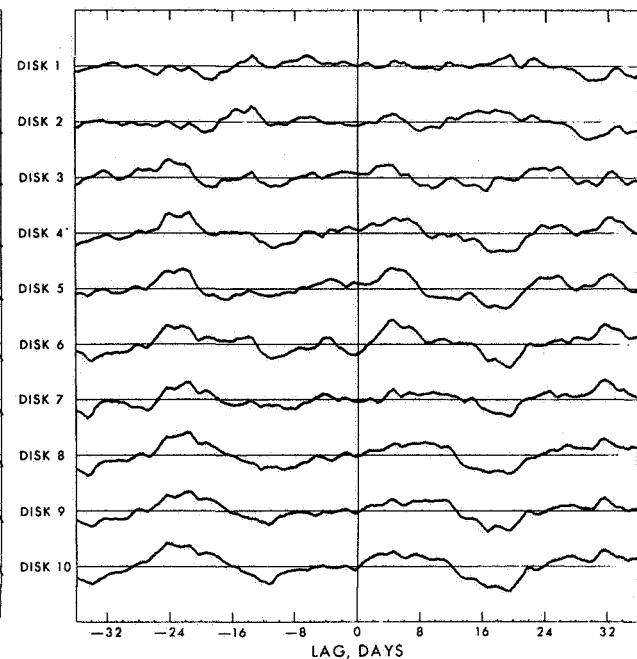


**Figure 6.** Cross correlation of disk averages of the photospheric magnetic field with interplanetary magnetic field polarity for the six months, July through December 1969. The curve near the line labeled "disk 5" represents the cross correlation of the disk 5 data for lags -36 to +36 days. The line labeled "disk 5" represents a correlation coefficient of zero. The line labeled "disk 4" represents a correlation coefficient of 1.0 for disk 5, and similarly the line labeled "disk 6" represents a correlation coefficient of -1.0. All the other disk and ring correlations are in the same format.



The next three 6-month intervals also show that the amount of correlation at different disks fluctuates in time. In the last half of 1968 (fig. 4) there is some correlation for all disks, but the peak at disk five is the largest. In the first half of 1969 (fig. 5) the seven larger disks have similar peaks. Finally, the last half of 1969 (fig. 6) shows good correlation only for the middle disks, and is similar to pattern for the last half of 1967.

The main conclusion from these results is that the most consistent comparison between daily magnetograms and the interplanetary field is found when one averages the magnetogram over an area about equal to disk five. We interpret this to mean that the smaller disks do not show large scale features and are influenced by small scale active regions more than the larger disks. The large disks include contributions from more than one sector boundary and thus show smaller correlations, therefore, if too small an area is used, no correlation results; and if the whole disk is used, sometimes lower correlation results.

## REFERENCE

Severny, A.; Wilcox, J. M.; Scherrer, P. H.; and Colburn, D.S.: Comparison of the Mean Photospheric Magnetic Field and the Interplanetary Magnetic Field. *Solar Phys.*, Vol. 15, 1970, p. 3.

*H. Schmidt* What was the size of those disks, angular size?

## DISCUSSION

*P. H. Scherrer* They range from one-tenth the diameter of the disk to the full disk; so that, for instance, disk five then would be  $30^\circ$  from the center of the sun.

*R. H. Dicke* Has the same thing been done, changing latitudes on the disks, seeking correlation?

*P. H. Scherrer* We are working on it.

*R. B. Leighton* I take it your disks were not from any *a priori* feeling that that's what it should be, but that your data came in such a form that that was an easy thing to do.

*P. H. Scherrer* Yes, this was an easy way to start the analysis.

*R. Howard* Just to add to that, because the activities are spread in active latitudes across the sun, the upper latitude portion of the rings, in fact, doesn't contribute very much to the results of the rings. This is really like taking sectors along the equator, and easier to get in the computer.

*D. E. Jones* I was just wondering if there are any plans to perhaps weight the readings, that is, the averaging, by the brightness in H-alpha, or something such as this, to give more weight?

*P. H. Scherrer* Not right now.

## CURRENT SHEET MAGNETIC MODEL FOR THE SOLAR CORONA *Kenneth H. Schatten*

**ABSTRACT** A new magnetic model is developed and compared with previous models and the observed solar corona. An attempt is made to more accurately compute the three-dimensional currents flowing in the solar corona. Physical reasons are given that require most of the large-scale currents flowing in the solar corona to lie near thin sheets. The current sheets are not constrained into any particular geometry or symmetry as in the previous models of *Altschuler and Newkirk* [1969] and *Schatten et al.* [1969]. A comparison with the axisymmetric, isothermal MHD solution of *Pneuman and Kopp* [1970] suggests that the model is able to simulate to high accuracy an isothermal corona. A comparison of the model with the May 30, 1965, solar eclipse and the November 12, 1966, solar eclipse shows the model is capable of computing many features including the polar plume orientations as well as radial and nonradial streamers in the solar corona.

### INTRODUCTION

The advent of large digital computers and detailed magnetograms has permitted sophisticated analyses of magnetic field configurations in the vicinity of the sun as suggested by *Gold* [1956]. Computations of the coronal magnetic field utilizing potential theory began with the *Schmidt* [1964] program to plot current-free magnetic fields above active regions. *Rust* [1966] has compared the field configuration of the Schmidt program with direct observations of prominent material. *Newkirk et al.* [1968] utilized potential theory over the entire sun to calculate field patterns for a comparison with the projected appearance of the November 12, 1966 solar eclipse. *Schatten* [1968a,b] and *Schatten et al.* [1969] developed a "source surface" technique to calculate the effect of coronal currents upon the field. The currents were chosen to draw the field into a radial direction (fig. 1). This model allowed comparisons of fields calculated with the interplanetary field, a Faraday rotation eclipse [*Schatten*, 1968a,b 1969, 1970; *Stelzried et al.*, 1970; and *Smith and Schatten*, 1970]. The technique has received favorable review by *Cowling* [1969].

*Schatten et al.* [1969] utilized a "source surface"

located at 0.6 solar radii above the photosphere. This distance was chosen from a parametric fit of this quantity based on comparisons of the model with the observed interplanetary field. This would be the location in the model where the highest coronal loops would form. *Bugoslavskaya* [1950] observed the solar corona from 1887 to 1945, and *Newkirk* [1967] found the highest closed arches have a mean height of 0.6 solar radii above the limb.

Further evidence for the highest closed magnetic loops lying near 0.6 solar radii above the limb is provided by the observations of *Takakura* [1966] that U bursts have a maximum height near this value. U bursts are thought to be essentially type III radio bursts caused by the motion of high speed particles through the solar atmosphere, in which an increase in radio frequency emitted follows the usual decrease. The inversion in radio frequency emitted is interpreted as a decrease in altitude of these particles as they move through the corona on the magnetic field lines which govern their motion.

Although the magnetic models of the corona of *Altschuler and Newkirk* [1969] and *Schatten et al.* [1969] appear to be capable of calculating the large-scale structure of the coronal and interplanetary magnetic fields moderately well, there are two areas

---

*The author is at the Laboratory for Extraterrestrial Physics NASA-Goddard Space Flight Center, Greenbelt, Maryland.*

where notable deviations may be found that relate to the magnetic models:

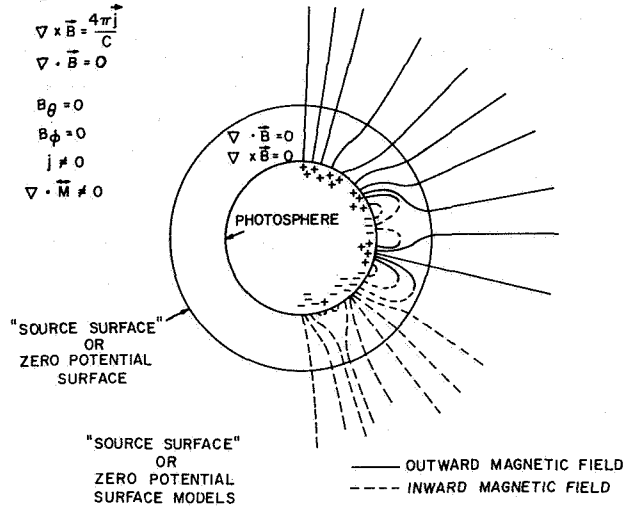


**Figure 1.** Magnetic field geometry in the "source surface" or "zero-potential surface" models. The fields are constrained to the radial direction by the solar wind in these models. The equations obeyed in the different regions are shown.

1. Solar flares appear to affect the large-scale magnetic field of the corona. The influence may appear in a solar eclipse photograph as the formation of series of fine rays directed radially away from the source of the flare [Smith and Schatten, 1970].
2. Although much of the open field structures and closed field structures have the correct topology, the structures are not always directed properly. A notable example is the polar plumes, which appear to bend continually equatorward, whereas the magnetic models orient them in the radial direction at the "source surface" or "zero potential surface". Another example are streamers, whose axes show a preferential lean to the equator near solar minimum and toward the poles at solar maximum [Waldmeier, 1970]. Figure 2 illustrates the nonradial aspects or coronal features.

The first area of disagreement is expected due to the large amount of hot plasma emitted by a flare. The current-free assumption in the inner corona is violated by this hot plasma and thus the potential solution is no longer valid. The second area of disagreement may relate to the latitudinal and azimuthal magnetic pressure terms that are important in coronal structure but have been neglected beyond the zero potential surface in prior work for mathematical simplicity. The purpose of this work will be to improve the model by including this effect. The energy density of the radial magnetic field

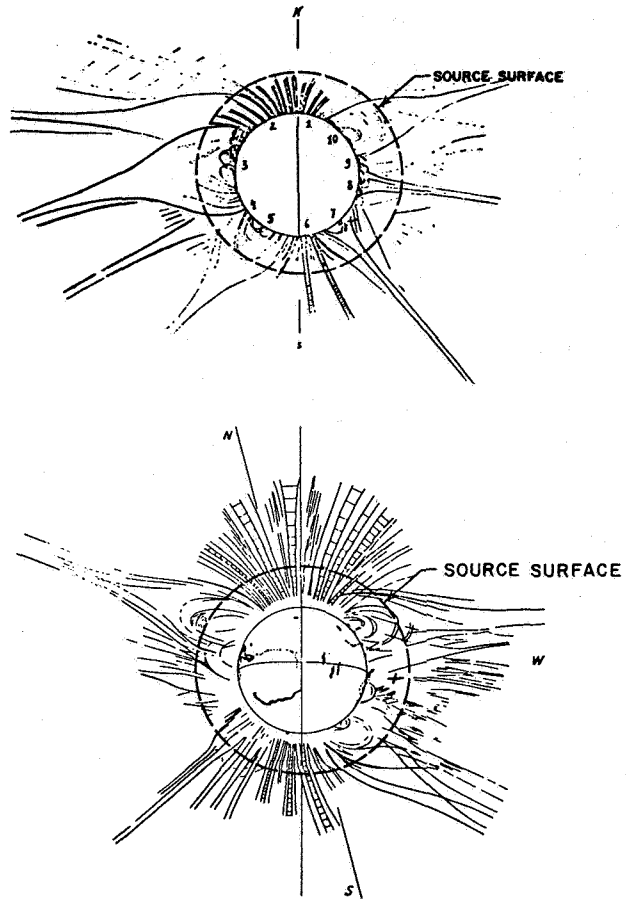


**Figure 2.** Drawing of the February 15, 1961 solar eclipse (top) and the February 25, 1952 solar eclipse (bottom) superposed with a "source surface" at 1.6 solar radii. Note that most closed arches fall below this surface. Beyond this distance most structures are "open" but not strictly radially oriented.

(providing transverse pressure stresses) falls off much less rapidly than that of the transverse field [Schatten *et al.* 1969]. The energy density of the transverse field approximately equals that of the plasma at about 0.6 solar radii (above the photosphere). Thus the plasma extends the magnetic field outward near this point. In the case of the radial field, equality with the plasma energy density is only reached at the Alfvén point near 25 solar radii. Thus transverse magnetic pressure is expected to be an important effect long after the coronal plasma has become supersonic. The magnetic field behaves like open rigid wires along which the plasma is constrained to flow. The magnetic field thus may still guide the plasma motion from 0.6 to 25 solar radii. This paper suggests a method to mathematically calculate the magnetic structure in this region.

### CURRENT SHEET MODEL

Out to the Alfvén point, the value of  $\beta$  (ratio of plasma to field energy density) for the coronal plasma is significantly less than one. Thus currents flowing in the coronal plasma cannot apply a significant pressure on the magnetic field except where the field is weak (near regions of opposite polarity fields). Currents are necessary to open the magnetic field into sector-like structures. If any significant transverse currents were located in regions of moderate field strength, a strong  $\mathbf{j} \times \mathbf{B}$  force would occur which the plasma could not resist. Thus, the currents tend to be present in high  $\beta$  regions, where the field reverses, and the  $\mathbf{j} \times \mathbf{B}$  forces are small. For these reasons, the transverse currents flowing in the coronal plasma in this model are constrained to flow only where the field is weak (near zero), hence on sheets near oppositely directed field regions.

The magnetic model can be used for computing the location and strength of these current sheets as follows. The magnetic field is first calculated directly from potential theory by means of Legendre polynomial techniques to a particular surface — for example, a sphere of radius 1.6 solar radii. Although not utilized in exactly the same way, this sphere will again be referred to as the “source surface.” The magnetic field then is reoriented

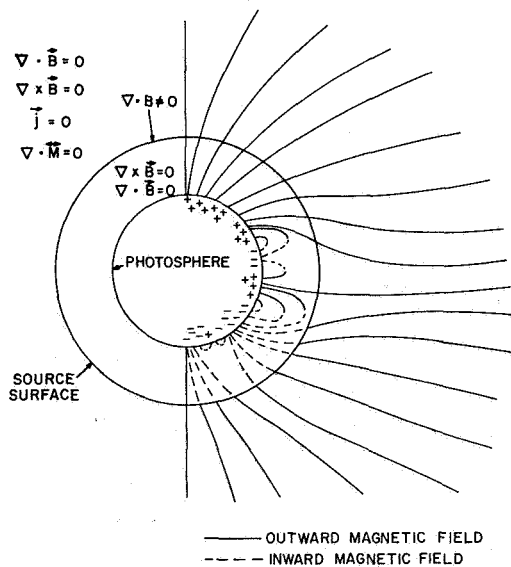


**Figure 3.** First step in the current sheet magnetic model. A potential solution is derived for the field between the “source surface” and the photosphere. The field computed on the source surface is then reoriented so that it points outward everywhere. The field is then computed beyond the “source surface” from potential theory. The sense of the magnetic field is opposite half the time to what it should be. This “error” is corrected in the next step.

such that it points outward everywhere; however, it is still along the same direction and possesses the same field magnitude. Thus if  $B_r \geq 0$  on this “source surface” the field is unchanged, but if  $B_r < 0$  then  $B_r$ ,  $B_\theta$ , and  $B_\phi$  are replaced by  $-B_r$ ,  $-B_\theta$ , and  $-B_\phi$ . The field is then calculated beyond the “source surface” from potential theory, again using a Legendre polynomial expansion of the field (see appendix). Now the monopole term is non-zero and rather large; thus it appears as if the sun has a high magnetic monopole moment and all the Legendre polynomial coefficients bear little or no relationship to their previous values (fig. 3). The physical effect is that beyond the “source surface” the magnetic fields cannot now form closed arches as they are all directed outward. This temporarily violates  $\nabla \cdot \mathbf{B} = 0$  on the source surface but this error will be corrected in a later step. This change of field direction does not affect the magnetic stresses: They will remain the same across the “source surface” and the field will still form a minimum energy configuration (with the condition that the field lines remain open). The last step (fig. 4) is to return the

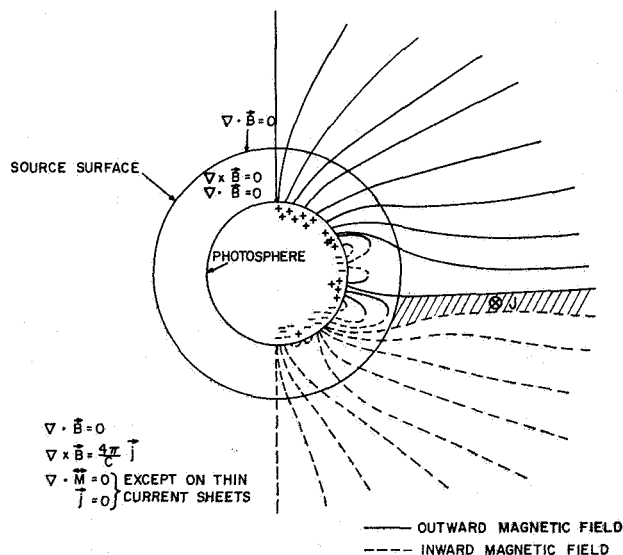


**Figure 4.** Second step in the current sheet magnetic model. The field that was disoriented is reoriented by reversing the sense of the magnetic field components. This requires a current sheet to be employed in the corona to separate regions of oppositely directed field to obey Maxwell’s equations. Allow the magnetic field to “open” by thin current sheets is consistent with the physical model of this region of the corona possessing a low  $\beta$ . If significant transverse currents flowed elsewhere a strong  $\mathbf{j} \times \mathbf{B}$  force would develop which the plasma could not maintain. This model may be used to calculate the magnetic oriented structures in the corona with less simplified solar wind currents.

magnetic field to its former sense of direction with the calculated strength and orientation. This violates  $\nabla \times \mathbf{B} = 4\pi\mathbf{j}/C = 0$  unless appropriate current sheets are introduced as shown. Physically, current sheets are introduced between areas of oppositely directed fields and thus prevent the field from forming arches beyond the "source surface." Note that the polar fields and streamer fields possess similar shapes to those in the corona (fig. 2) and not the radial orientation seen in figure 1.

The invariance of the Maxwell stress tensor under this field reversal scheme is important to ensure against unequal stresses across the "source surface." The Maxwell stress tensor is defined such that  $\mathbf{j} \times \mathbf{B} = \nabla \cdot \mathbf{M}$ . The stress tensor is shown in figure 5. As can be seen, changing the sign of the three components leaves  $\mathbf{M}$  unchanged; thus, the magnetic stresses in the corona are balanced.

$$\mathbf{j} \times \mathbf{B} = \nabla \cdot \mathbf{M}$$

$$\mathbf{M} = \frac{1}{\mu_0} \begin{bmatrix} \frac{1}{2}(B_x^2 - B_y^2 - B_z^2) & B_x B_y & B_x B_z \\ B_x B_y & \frac{1}{2}(B_y^2 - B_x^2 - B_z^2) & B_y B_z \\ B_x B_z & B_y B_z & \frac{1}{2}(B_z^2 - B_x^2 - B_y^2) \end{bmatrix}$$

Figure 5. The Maxwell stress tensor. Note that it is identical if all three components are reversed. This allows the stresses to be balanced after the field reversal processes.

#### COMPARISONS OF THE CURRENT SHEET MODEL WITH OTHER MODELS AND THE SOLAR CORONA

The current sheet model is first compared with the "source surface" and the "zero potential surface" models as well as an exact MHD solution for an axisymmetric isothermal corona. This latter solution has been computed after the formalism of *Pneuman and Kopp* [1970] for the corona with a temperature of  $1.56 \times 10^6$  °K and a dipole field. Figure 6 shows this comparison with an assumed dipolar solar field. The field lines labeled with crosses represent the present study with the "source surface" located at 1.6 solar radii. Solid lines indicate field directed away from the sun, and dashed lines indicate field toward the sun. The heavy solid lines indicate the MHD isothermal coronal solution of *Pneuman and Kopp*. The dashed and dotted lines indicate the field lines calculated by the *Altschuler and Newkirk* model with a zero potential surface located at 2.5 solar radii. The "source surface" solution of *Schatten et al.* [1969] is similar to this solution except the field lines would be oriented radially somewhat closer to the sun. As can be seen, the field lines computed from the isothermal MHD solution and the current sheet solution are nearly identical. The foot points

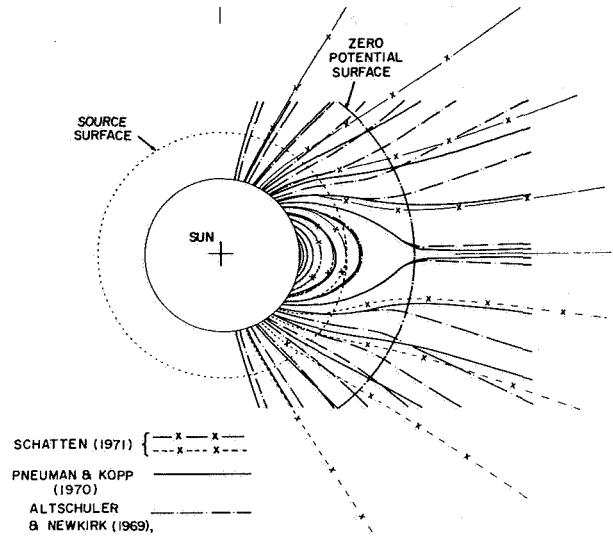


Figure 6. A comparison of solutions for a dipole solar field with the zero potential surface model [*Altschuler and Newkirk*, 1969] the present model and the exact isothermal MHD coronal solution [*Pneuman and Kopp*, 1970]. Note that the present solution is quite similar to the isothermal coronal solution supporting the suggestion that the coronal currents are confined to thin sheets.

of the field lines indicate the quality of their agreement. The magnetic potential solution begins to diverge from the other solutions near the zero potential surface. The rather close agreement between the current sheet solution and the MHD solution suggests that much of the current flowing in an isothermal corona does so near current sheets as suggested earlier. *Altschuler and Newkirk* [1969] chose the location of the zero potential sphere to be 2.5 solar radii based on a comparison of field geometry with coronal forms, whereas *Schatten et al.* [1969] chose the 1.6 solar radii value for the "source surface" based upon the observed highest closed arches and agreement with comparisons of their model with the interplanetary magnetic field. In the present model, if the "source surface" is set at 1.6 solar radii, the shapes of features are similar (out to 2+ solar radii) to the *Altschuler and Newkirk* result, and the coronal magnetic field extends out from 1.6 solar radii, similar to the result of *Schatten et al.* [1969]. Thus the disagreement between these two values where the coronal magnetic fields extends outward may be ended by utilizing this new model. The agreement with the axisymmetric MHD solution suggests that the current sheet model may now be used with more confidence in calculating fields in three dimensional nonsymmetric situations as well.

First, however, let us examine whether the current

sheet model can calculate nonradial streamers and compare them with observed nonradial streamers. Figure 7 is a drawing from Bohlin of the May 30, 1965, solar eclipse from photographs by Smith (top). This eclipse shows several nonradial streamers in addition to the nonradial

polar plumes. The field pattern beneath shows calculations from the current sheet model using an axisymmetric magnetic condition. As can be seen, rather nonradial field lines may be computed in the model quite similar in appearance to the structures observed. The

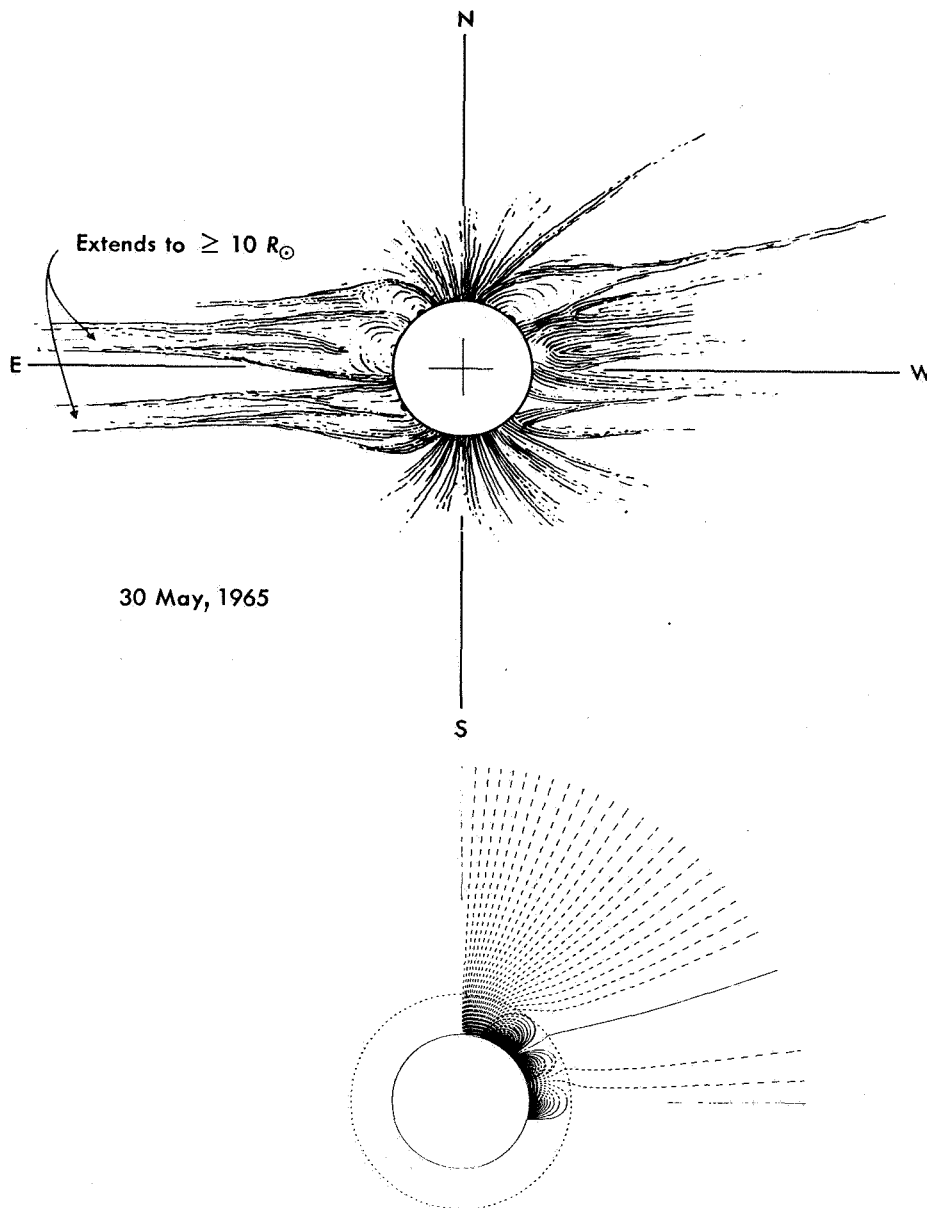


**Figure 7.** A comparison of the structure of the solar corona during the May 30, 1965 solar eclipse (top) with computations from an assumed axisymmetric photospheric field pattern (bottom). The shape of the polar plumes is calculated quite well in this model as well as a nonradial helmet streamer.

polar field lines appear similar to the polar plumes. The computed field configuration in the equatorial regions are also oriented toward the equator as in the eclipse drawing.

A computation of the magnetic field projected into the plane of the sky from this model for the November 12, 1966, solar eclipse is shown in figure 8 superimposed with a drawing of the coronal forms by *Newkirk et al.* [1970]. The solid lines indicate away-from-the-sun magnetic field, and dashed lines indicate toward-the-sun field. Many of the features line up surprisingly well with

the field lines calculated as can be seen. Large-scale magnetic loops are calculated near streamers  $\beta'$  and  $\zeta$  and closed arches are observed underlying these streamers. Many of the "open" magnetic field lines near regions  $\beta$ ,  $\zeta$ , and  $\gamma$  are closely aligned with coronal features in the same areas. The general agreement of the magnetic field calculations with the observed features for this solar eclipse is rather good.

## CONCLUSIONS

A new current sheet magnetic model for the solar corona

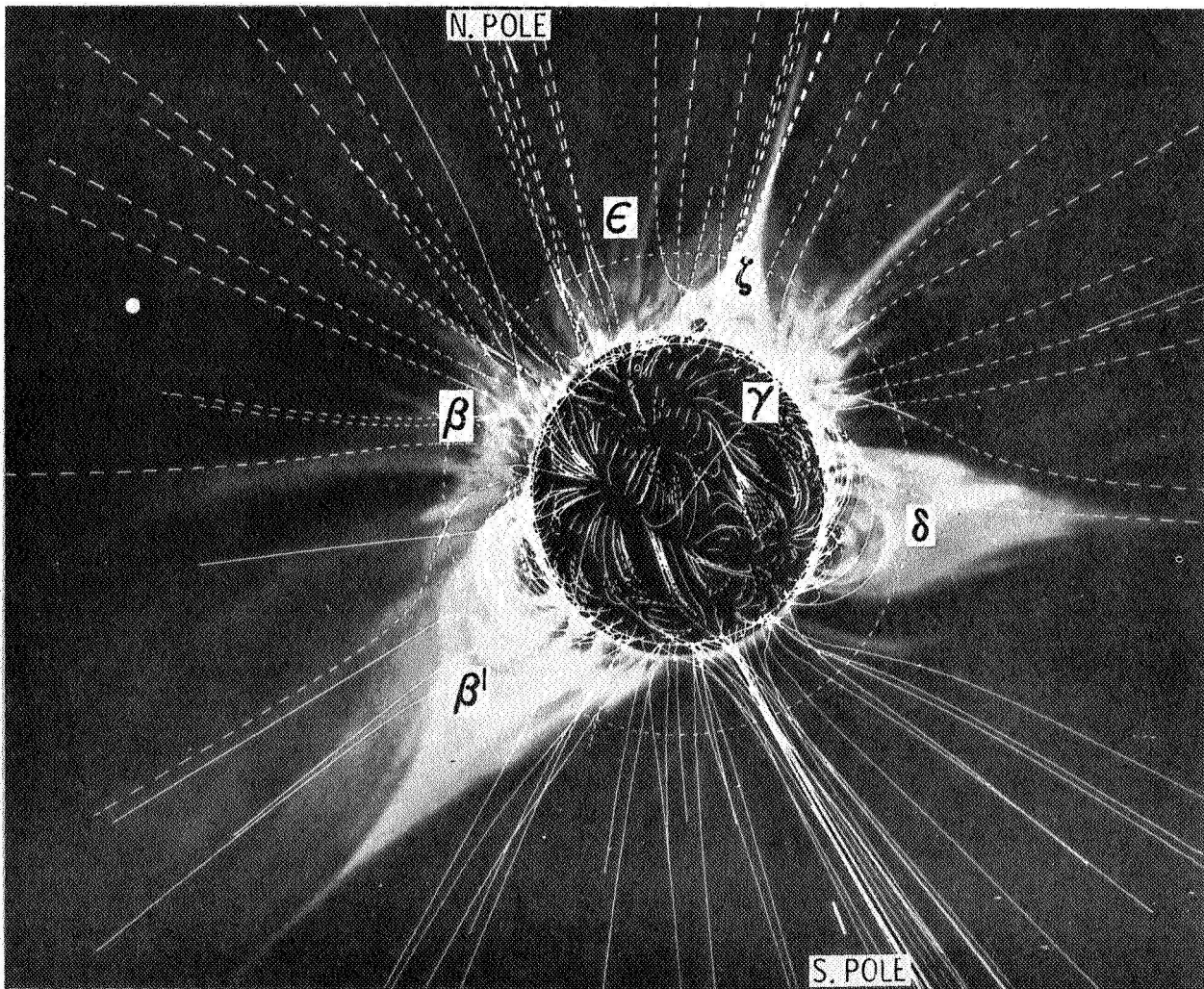


**Figure 8.** A comparison of the computed coronal magnetic field with a drawing of the solar eclipse features from Newkirk and Altschuler [1970] for the November 12, 1966 solar eclipse. The solid lines represent magnetic field directed away from the sun and the dashed lines field toward the sun. The field lines originate on the photosphere in the center of each of the 648 grid points. Many of the observed features line up with the computed field lines. The computed field lines terminate at five solar radii and are projected into the plane of the sky.

has been developed. It is capable of calculating the quiet large-scale magnetic field structure in the corona. As suggested by physical arguments, thin current sheets are utilized to separate regions of oppositely directed fields. This approximation appears to be a rather good one in that the dipole solution is nearly identical with the isothermal MHD coronal solution of *Pneuman and Kopp* [1970].

A comparison of field computations with the observed structure for the May 30, 1965, solar eclipse reveals that the model appears to be capable of calculating the orientation of the polar plumes fairly well, as well as nonradial streamer configurations. A comparison between the computed magnetic field and the observed solar corona for the November 12, 1966, solar eclipse is shown. Many of the observed features are also seen in the computed magnetic field.

## APPENDIX

This appendix discusses the solution of the field beyond the "source surface" method of fitting the vector Legendre polynomial coefficients to the three dimensional vector field on the "source surface." The vector field up to and including the "source surface" is computed in accord with the techniques of *Altschuler and Newkirk* [1969] without using any currents in the solar corona. The present model may be improved in the future by an iterative process using the currents computed in the present model to calculate the solution below the "source surface" as well and then recomputing the field beyond the "source surface." This may represent a minimum improvement, however.

The solution for the Laplacian equation in spherical coordinates for  $r \geq R$  is

$$\psi(r, \theta, \phi) = R \sum_{n=0}^{\infty} \sum_{m=0}^n \left\{ \left( \frac{R}{r} \right)^{n+1} \left[ g_n^m \cos(m\phi) + h_n^m \sin(m\phi) \right] P_n^m(\theta) \right\} \quad (1)$$

The components of the magnetic field are:

$$B_r = -\frac{\partial \psi}{\partial r} = f_1(g_n^m, h_n^m) \quad (2)$$

$$B_\theta = -\frac{1}{r} \frac{\partial \psi}{\partial \theta} = f_2(g_n^m, h_n^m) \quad (3)$$

$$B_\phi = -\frac{1}{r \sin \theta} \frac{\partial \psi}{\partial \phi} = f_3(g_n^m, h_n^m) \quad (4)$$

The associated Legendre polynomials utilizing the Schmidt normalization have been used [*Chapman and Bartels*, 1940]. Thus to determine the magnetic field beyond the "source surface" it is necessary to compute  $g_n^m$  and  $h_n^m$  from the vector field on the "source surface" as a boundary condition.



The components of the magnetic field on the "source surface" are first oriented away-from-the sun so that if  $B_r < 0$  on the "source surface," the signs of  $B_r$ ,  $B_\theta$ , and  $B_\phi$  are reversed.

In this analysis we have utilized a photospheric grid of 27 longitudes and 24 latitudes in equal steps of sine (latitude). We have also chosen  $N=9$  as the maximum principal Legendre index to consider for practical considerations. A least-mean-square fit to an overdetermined linear system of 1944 ( $27 \times 24 \times 3$ ) equations involving 100 unknowns is then utilized to best fit the vector field on the "source surface," we let

$$F = \sum_{i=1}^{24} \sum_{j=1}^{27} \sum_{k=1}^3 \left[ B(i, j, k) - f_k(g_n^m, h_n^m) \right]^2 \quad (5)$$

where  $B(i, j, k)$  equal the vector field components, and  $k = 1, 2$ , or  $3$  refers to the radial, latitudinal, or azimuthal field component at  $\theta_i$  and  $\phi_j$ .

It is necessary now to obtain the  $g_n^m$  and  $h_n^m$  that minimize  $F$ ; the sums of squares of the differences between the known components of the field on the "source surface"  $B_r(i, j)$ ,  $B_\theta(i, j)$  and  $B_\phi(i, j)$ ; and the component values computed from  $g_n^m$  and  $h_n^m$  at  $\theta_i$  and  $\phi_j$ .

Let us choose

$$\left. \begin{aligned} \alpha_{nm1} &= (n+1) \cos m\phi P_n^m(\theta) \\ \beta_{nm1} &= (n+1) \sin m\phi P_n^m(\theta) \\ \alpha_{nm2} &= -\cos m\phi \frac{d}{d\theta} P_n^m(\theta) \\ \beta_{nm2} &= -\sin m\phi \frac{d}{d\theta} P_n^m(\theta) \\ \alpha_{nm3} &= \frac{m}{\sin \theta} \sin m\phi P_n^m(\theta) \\ \beta_{nm3} &= \frac{m}{\sin \theta} \cos m\phi P_n^m(\theta) \end{aligned} \right\} \quad (6)$$

Thus equation (5) becomes

$$F = \sum_i \sum_j \sum_k \left[ B(i, j, k) - \sum_n \sum_m (g_n^m \alpha_{nmk} + h_n^m \beta_{nmk}) \right]^2 \quad (7)$$

The equations to minimize  $F$  are:

$$\frac{\partial F}{\partial g_n^m} = 0 \quad \frac{\partial F}{\partial h_n^m} = 0 \quad (8)$$

For each  $(n, m)$  may be rewritten:

$$\sum_i \sum_j \sum_k \left\{ B(i, j, k) \alpha_{nmk}(ij) - \alpha_{nmk}(ij) \sum_{t=0}^N \sum_{s=0}^t \left[ g_t^s \alpha_{tsk}(ij) + h_t^s \beta_{tsk}(ij) \right] \right\} = 0 \quad (9)$$

$$\sum_i \sum_j \sum_k \left\{ B(i, j, k) \beta_{nmk}(ij) - \beta_{nmk}(ij) \sum_{t=0}^N \sum_{s=0}^t \left[ g_t^s \alpha_{tsk}(ij) + h_t^s \beta_{tsk}(ij) \right] \right\} = 0 \quad (10)$$

where  $t$  and  $s$  are dummy indices used for  $n$  and  $m$ . The unknowns are  $g_n^m$  and  $h_n^m$ , and  $B(i, j, k)$  is the known vector field;  $\alpha$  and  $\beta$  are known from equation (6).

The column vectors

$$\left. \begin{aligned} \alpha_{NM} &= \begin{bmatrix} \alpha_{\theta_1 \phi_1 1} \\ \alpha_{\theta_1 \phi_2 1} \\ \cdot \\ \cdot \\ \cdot \\ \alpha_{\theta \phi 1} \\ \alpha_{\theta_1 \phi_1 2} \\ \cdot \\ \cdot \\ \cdot \\ \alpha_{\theta \phi 3} \end{bmatrix} & \beta_{NM} &= \begin{bmatrix} \beta_{\theta_1 \phi_1 1} \\ \beta_{\theta_1 \phi_2 1} \\ \cdot \\ \cdot \\ \cdot \\ \beta_{\theta \phi 1} \\ \beta_{\theta_1 \phi_1 2} \\ \cdot \\ \cdot \\ \cdot \\ \beta_{\theta \phi 3} \end{bmatrix} \end{aligned} \right\} \quad (11)$$

are of length  $24 \times 27 \times 3$  for each  $NM$  and

$$\mathbf{B} = \begin{bmatrix} B(\theta_1, \phi_1, 1) \\ B(\theta_1, \phi_2, 1) \\ \cdot \\ \cdot \\ \cdot \\ B(\theta, \phi, 1) \\ B(\theta_1, \phi_1, 2) \\ \cdot \\ \cdot \\ \cdot \\ B(\theta, \phi, 3) \end{bmatrix} \quad \mathbf{GH} = \begin{bmatrix} g_0^0 \\ g_1^0 \\ g_1^1 \\ \cdot \\ \cdot \\ \cdot \\ g_N^N \\ h_1^1 \\ h_2^1 \\ \cdot \\ \cdot \\ h_N^N \end{bmatrix}$$

Now defining the matrix  $\alpha\beta$  such that the rows of  $\alpha\beta$  are as follows:

$$\begin{aligned}\alpha\beta(1) &= \alpha_{00} \\ \alpha\beta(2) &= \alpha_{10} \\ \alpha\beta(3) &= \alpha_{11} \\ &\dots \\ \alpha\beta(55) &= \alpha_{99} \\ \alpha\beta(56) &= \beta_{11} \\ &\dots \\ \alpha\beta(100) &= \beta_{99}\end{aligned}$$

with all  $m = 0$  elements missing from  $h_n^m$  and from  $\beta$ ;  $\mathbf{GH}$  is a  $100 \times 1$  matrix and  $\alpha\beta$  is a  $100 \times 1944$  matrix. Equations (9) and (10) may be rewritten as

$$A\beta \cdot \mathbf{B} = AB \cdot \mathbf{GH} \quad (12)$$

choosing  $AB(i,j) = \alpha\beta(i) \cdot \alpha\beta(j)$  so that  $\alpha\beta$  is a  $100 \times 1944$  matrix,  $\mathbf{B}$  is a  $1944 \times 1$  matrix,  $AB_{ij}$  is a  $100 \times 100$  matrix and  $\mathbf{GH}$  is a  $100 \times 1$  matrix.

By an inversion of the symmetric matrix  $AB$ ,  $\mathbf{GH}$  may be solved as follows:

$$\mathbf{GH} = AB^{-1} \cdot \alpha\beta \cdot \mathbf{B}$$

This requires inverting a square matrix each of whose sides equals  $(N+1)^2$  which for  $N=9$  is 100, yielding estimates for  $g_n^m$  and  $h_n^m$  that arise from a least mean square fit to the three vector components of the magnetic field on the source surface. Equations (2), (3), and (4) allow a computation of the magnetic field everywhere above the "source surface." It is necessary, however, to reverse the sense of the three components of the magnetic field depending on whether the footpoint of the field line has had its sense reversed (if  $B_r < 0$ ). Those field lines are shown as dashed lines in the figures.

#### ACKNOWLEDGMENTS

The author wishes to thank David Howell for help with the computer programming necessary to develop this model. The author also wishes to thank Judith Schatten for encouragement and discussions related to this model. I am also appreciative of Gordon Newkirk, Jr. and Gerry Pneuman of the High Altitude Observatory for discussions and for the use of Newkirk's data for the November 12, 1966 solar eclipse.

#### REFERENCES

- Altschuler, M. D.; and Newkirk, G., Jr.: Magnetic Fields and the Structure of the Solar Corona. *Solar Physics*, Vol. 9, 1969, p. 131.
- Bugoslavaskaya, E. Ya.; Trud. Gos. Astronom. Inst. in Shternberga, Vol. 19, 1950, p. 3.
- Chapman, S.; and Bartels, J.: *Geomagnetism*. Oxford University Press, London, 1940.
- Cowling, T. G.; The Solar Wind. *The Observatory*, Vol. 89, 1969, p. 217.
- Gold, T., The Magnetic Field in the Corona. *IAU Symposium No. 6*, 1956, p. 275.
- Newkirk, G.A., Jr.: *Ann. Rev. Astron. and Astrophys.* Vol. 5, 1967, p. 213.
- Newkirk, G. A., Jr.; Altschuler, M. D.; and Harvey, J. W.: Influence of Magnetic Fields on the Structure of the Solar Corona. *Structure and Development of Solar Active Regions* (ed. by K. O. Kiepenheuer) *IAU Symposium No. 35*, D. Reidel Publ. Co., Dordrecht, 1968, p. 379.
- Newkirk, G. A., Jr.; Schmahl, E.; and Deupree, R.: Magnetic Fields and the Structure of the Solar Corona II: Observations of the 12 November 1966 Solar Eclipse. *Solar Physics*, Vol. 15, 1970, p. 15.

- Pneuman, G. W.; and Kopp, R. A.: Coronal Streamers III: Energy Transport in Streamer and Interstreamer Regions. *Solar Physics*, Vol. 13, 1970, p. 176.
- Rust, D. M.: Measurements of the Magnetic Fields in Quiescent Solar Prominences. Ph.D. thesis, University of Colorado, 1966.
- Schatten, K. H.: Large-Scale Configuration of the Coronal and Interplanetary Magnetic Field. *Thesis*, University of California, Berkeley, 1968a.
- Schatten, K. H.: Prediction of the Coronal Structure for the Solar Eclipse of September 22, 1968. *Nature*, Vol. 220, 1968b, p. 1211.
- Schatten, K. H.: Coronal Structure at the Solar Eclipse of September 22, 1968. *Nature*, Vol. 223, 1969, p. 652.
- Schatten, K. H.: Prediction of the Coronal Structure for the Solar Eclipse of March 7, 1970. *Nature*, Vol. 226, 1970, p. 251.
- Schatten, K. H.; Wilcox, J. M.; and Ness, N. F.: A Model of Coronal and Interplanetary Magnetic Fields. *Solar Physics*, Vol. 9, 1969, pp. 442-455.
- Schmidt, H. U.: On the Observable Effects of Magnetic Energy Storage and Release Connected with Solar Flares. *AAS-NASA Symposium Phys. Solar Flares*, ed. W. N. Hess, NASA-SP-50, 1964, p. 107.
- Smith, S. M., and Schatten, K. H. *Nature*, Vol. 226, 1970, p. 1130.
- Stelzried, C. T.; Levy, G. S.; Sato, T.; Rusch, W. V. T.; Ohlson, J. E.; Schatten, K. H.; and Wilcox, J. M.: *Solar Physics*, Vol. 14, 1970, p. 440.
- Takakura, T.: *Space Science Reviews*. Vol. 5, 1966, p. 80.
- Waldmeier, M.: *Nature*, Vol. 226, 1970, p. 1131.

#### DISCUSSION

*R. A. Kopp* I just wanted to know how you got the field lines to go through the source surface radially. You said you did that calculation first with the ordinary source surface. Don't the field lines have to go perpendicular as they pass through the source surface?

*K. H. Schatten* No, they weren't taken to be radial in this case. It was strictly a potential theory using the Legendre polynomial coefficients, and we did not constrain them to be radial – they just occur in whatever direction they happen to be there. Then we did a least-mean-square solution so that the three vectors,  $B_r$ ,  $B_\theta$ ,  $B_\phi$ , are at the source surface, so that there was no necessary restriction into the radial direction there.

*R. B. Leighton* It's a kind of heuristic way of recognizing you're going from a case where there is essentially a potential magnetic field problem to a fluid problem but in which the magnetic field still plays a role in terms of its stress, in guiding the flow. This is why you get away with reversing the field there and keeping on going and damn the torpedoes – right?

*K. H. Schatten* Right.

*F. C. Michel* I don't know if it's directed to Ken Schatten or to Gordon Newkirk. But the eclipse of 1970 looked quantitatively as if it had been drawn by a student who hadn't learned his lessons very well, and if he had drawn it in the form it appeared he would be criticized for having a rather poor representation of how the lines should go. There are great regions where the striations are essentially parallel; and not only that but they didn't appear at all radially from the sun, and there were about five such regions. I just wondered, what's your attitude towards this? Do you think this is a significant deviation from the theory or do you think that's easy to account for?

*K. H. Schatten* Yes, I think it is a significant deviation. As Gordon Newkirk mentioned, there was a lot of solar activity at the time. These models essentially assume quasistationary conditions with no sort of solar activity to mess things up. When you have activity you get a lot of plasma ejected into the corona, and currents can form which will twist the field to almost any configuration, and you can't just compute it from the photospheric field. You can imagine a very strong flare occurring in a particular location where you have, say, a stream or something like that, and it blows all the field lines out into radially away from that point, or into some other configuration. That probably is why the solar eclipse calculations for 1970 were not as good as some of the others.

## STRUCTURE OF CORONAL NEUTRAL SHEETS *G. W. Pneuman*

A qualitative model for the structure of the neutral sheet lying along the axis of coronal streamers is developed. The internal topology of the sheet is that of extremely thin magnetic tongues greatly distended outward by the solar wind expansion inside the sheet. Due to finite conductivity effects, expansion is taking place across the field lines but is retarded relative to the external flow by the reverse  $\mathbf{j} \times \mathbf{B}$  force. The sheet thickness is determined by three considerations: the electrical conductivity that specifies the magnitude of the gradients in field strength, the expansion velocity that stretches the field lines outward decreasing the sheet thickness, and finally, the lateral pressure balance that limits the approach of the oppositely directed external field toward the neutral plane.

If  $\sigma$  is the electrical conductivity, the sheet thickness is shown to be proportional to  $\sigma^{-1/3}$ . For an electron conductivity evaluated perpendicular to the internal field in the sheet, the thickness is of the order of 100 km in the inner corona and 10,000 km at 1 AU. Microturbulence and instabilities are expected to yield dimensions greater than these theoretical values since these effects tend to reduce the "effective" conductivity.

### INTRODUCTION

It is clear that a great number of neutral sheets should exist in the solar corona, considering the numerous polarity reversals in the observed photospheric magnetic field. The intersection of these sheets with the ecliptic at 1 AU can be observed with satellites and are normally referred to as "sector boundaries." However, the detection of structures as thin as these in the inner corona would be difficult through normal photographic techniques. Since an eclipse photograph of the inner corona reflects an integration of electron density over the line of sight, these sheets, even though denser than their surroundings, would be essentially transparent unless they were not only planar but also had their plane coinciding exactly with the line of sight direction.

There seems to be an increasing amount of indirect observational evidence that such sheets may be the tracks along which high energy particles released during flares travel from the sun to the earth. For example, the

most favored theory of type III radio bursts proposes that this emission is produced by a cloud of outward traveling electrons exciting plasma oscillations at successively higher levels in the corona. It has been proposed [Wild, 1964] that these electrons move out along the neutral sheets situated along coronal streamers. In addition, Bumba and Obridko [1969] have suggested that proton flare activity associated with Bartels' active longitudes occurs in the neighborhood of the sector boundaries of the interplanetary magnetic field.

In this paper, we describe a physical model of the expected structure of such coronal neutral sheets. Though the approximations are crude, it is hoped that the model will provide physical insight as to the grossest features that would be expected to be associated with these structures.

### DESCRIPTION OF THE MODEL

Since the structure of a neutral sheet essentially is produced by finite conductivity effects, the simplest way to visualize it is to first consider a coronal streamer for the case  $\sigma = \infty$ , introduce a small amount of resistivity to the plasma, and examine the consequences. A typical helmet

---

*The author is at the High Altitude Observatory, National Center for Atmospheric Research, Boulder, Colorado. The National Center for Atmospheric Research is sponsored by the National Science Foundation.*

streamer (fig. 1) consists of a region of closed magnetic loops in the corona with open field lines adjacent to and above the loops, and is commonly observed during solar eclipses. For  $\sigma = \infty$ , a neutral point exists at the top of the closed loops, and true sheet currents of zero

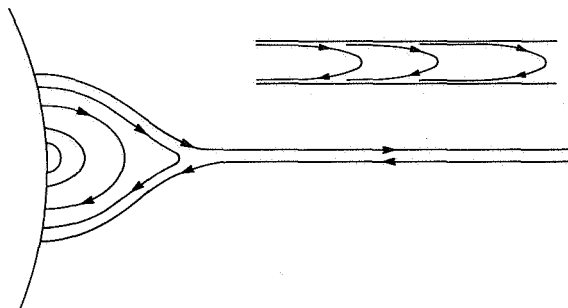


**Figure 1.** Schematic of typical helmet streamers. The insert shows a blown up section of the neutral sheet along the streamer axis.

dimension exist both above the neutral point and below it between the open and closed regions [Pneuman and Kopp, 1971]. These lower sheet currents exist because expansion occurs along the open field lines but not along the closed ones, resulting in a pressure discontinuity between the two regions that must be balanced by a jump in magnetic field strength. The location of the neutral point is determined by the condition that the pressure differential between the closed and open regions at that point is exactly balanced by the magnetic pressure in the open region; that is,

$$p_{cl} - p_{st} = \frac{B_{st}^2}{8\pi} \quad (1)$$

where *cl* refers to the closed region and *st* to the streaming region.

We now investigate the consequences of introducing a small resistivity into this model. Obviously, the first will be reconnection of open field lines at the neutral point. The outward part of the reconnected field will just be expelled outward along the sheet, whereas the inward part will become a new closed loop attached to the solar surface. Consequently, a hydrostatic pressure distribution will be set up along this loop. However, the new loop will lie outside that for which equation (1) is satisfied, and the pressure differential will be larger than the external magnetic pressure. As a result, the loop will expand outward along the sheet and, were the conductivity infinite, it would continue expanding to infinity (since the field and material are frozen). Hence, this loop would eventually become a new *open* field line and the configuration would revert to that which existed before reconnection took place. If, on the other hand,  $\sigma$  is

finite, a small amount of relative motion between the field and gas is permitted and the loop will not be expelled to infinity but will only be pulled outward to some location where the diffusion of field backward through the material is just balanced by the outward convection of the field lines. When a steady state is achieved, the neutral sheet will have a finite thickness and will contain loops of weak magnetic field attached to the solar surface with the plasma expanding outward across the loops. The resulting configuration might look something like that shown at the top of figure 1. Since the relative diffusion of the field through the gas is expected to be very small for coronal conditions, these internal loops would be extremely distended and, consequently, the transverse field there should be very small.

If this physical picture of the neutral sheet is adopted, the sheet thickness will depend on three factors:

1. The magnitude of the electrical conductivity. This determines how large the gradients in magnetic field strength can be within the sheet. As one would expect, the sheet dimension should vary inversely with the conductivity.
2. The expansion velocity within the sheet. Large velocities will stretch the field lines more and decrease the sheet thickness.
3. The lateral pressure balance between the sheet and its surroundings. This consideration will limit the approach of the external field towards the neutral plane.

In the next section, we employ these concepts to develop a first-order model of coronal neutral sheets. We employ the MHD approach throughout. Since these structures are expected to be thin, one must ascertain whether collisions will be frequent enough to make this approximation valid. However, since the sheet dimensions are not known *a priori*, it seems most fruitful to investigate this question in the light of the properties of the resulting solution.

### MAGNETIC FIELD CONFIGURATION

Consider a coronal streamer, situated at the solar equator, which is axisymmetric with respect to the rotational axis. If  $\theta$  is the polar angle; then, the neutral sheet will lie along the plane  $\theta = \pi/2$ . As a first approximation, the sheet is assumed radial in cross section and the fluid velocity inside is also taken to be radial.<sup>1</sup> In line with the arguments of the previous section, the magnetic field

<sup>1</sup>Throughout this work we omit the effects of solar rotation.

will have both radial and transverse components. Hence, the velocity and magnetic field vectors are given respectively by

$$\mathbf{V} = V_r \hat{e}_r \quad \text{and} \quad \mathbf{B} = B_r \hat{e}_r + B_\theta \hat{e}_\theta$$

where  $\hat{e}_r$  and  $\hat{e}_\theta$  are unit vectors in the radial and polar directions.

For steady state conditions, the expression for conservation of magnetic flux and the induction equation are

$$\nabla \cdot \mathbf{B} = 0 \quad (2)$$

$$\nabla \times \left[ \mathbf{V} \times \mathbf{B} \cdot \left( \frac{1}{4\pi\sigma} \right) \nabla \times \mathbf{B} \right] = 0 \quad (3)$$

where  $\sigma$  is the electrical conductivity. In deriving equation (3), we have taken  $\sigma$  to be a scalar. This would not be the case in the presence of a strong magnetic field, but the field inside the sheet is expected to be weak and the reduction in conductivity due to the field may not be great. This question will be considered again later so that actual conditions may be more realistically assessed. We merely consider here that the conductivity is a function of temperature only; we also assume isothermal conditions such that  $\sigma$  is a constant.

Subject to the above conditions, equations (2) and (3) can be solved in the limit  $Rem \gg 1$  to yield expressions for both the radial and transverse components of the magnetic field. We merely tabulate the results here.

$$B_r = \frac{B_0}{x^2} \exp \left[ -\frac{n(n+1)}{Rem} \int_1^x \frac{dx}{x^2 u} \right] \frac{P_n(\cos \theta)}{P_n(\cos \theta_b)} \quad (4)$$

$$B_\theta = \frac{-B_0}{Rem x^3 u} \exp \left[ -\frac{n(n+1)}{Rem} \int_1^x \frac{dx}{x^2 u} \right] \frac{P'_n(\cos \theta)}{P_n(\cos \theta_b)} \quad (5)$$

Here,  $x = r/r_0$ , where  $r_0$  is the radial distance to the top of the helmet in the streamer. This is where the sheet is assumed to originate and is where the neutral point would be located if the conductivity were infinite.  $B_0$  is the magnetic field strength at  $r_0$  just outside the sheet:  $u = V_r/V_s$  ( $V_s$  being the sound speed);  $Rem$  is a magnetic Reynolds number given by  $Rem = 4\pi\sigma r_0 V_s$ ;  $P_n(\cos \theta)$  is

a Legendre polynomial of order  $n$ ; and  $\theta_b$  is the angle representing the sheet boundary. The prime denotes differentiation with respect to  $\theta$ . (Note that for a coronal temperature of  $1.0 \times 10^6$  °K and  $r_0 = 2R_\odot$ ,  $Rem = 4.5 \times 10^{14}$ . This is an enormous number and shows just how effectively the field and material are frozen in the corona.) To satisfy the two conditions that  $B_r = 0$  for  $\theta = \pi/2$  and  $B_\theta = 0$  for  $\theta = \theta_b$ , we require that  $n$  be odd and also a root of the equation

$$P'_n(\cos \theta_b) = 0 \quad (6)$$

Since  $n$  characterizes the variation of quantities across the sheet, it will be a large number inversely proportional to the sheet thickness. For example, if  $n \gg 1$ , we can write

$$P_n(\cos \theta) \approx \left( \frac{2}{n\pi \sin \theta} \right)^{1/2} \sin \left[ \left( n + \frac{1}{2} \right) \theta + \frac{\pi}{4} \right]$$

Condition (6) then reduces to

$$\cos \left[ \left( n + \frac{1}{2} \right) \theta_b + \frac{\pi}{4} \right] = 0 \quad \text{or} \quad n = \frac{\theta_b + (\pi/2)}{\pi - 2\theta_b}$$

and since  $\pi/2 - \theta_b = \delta/r$  where  $\delta$  is the sheet thickness, we have

$$\delta \approx \frac{\pi r}{2n} \quad (7)$$

#### CURRENT DENSITY, PRESSURE DISTRIBUTION, EXPANSION VELOCITY, AND SHEET THICKNESS

Having derived the magnetic field configuration, we can now derive the current density  $\mathbf{J}$  from Ampere's law.

$$\mathbf{J} = \frac{-B_0}{4\pi r_0 x^3} \left\{ 1 - \frac{1}{Rem x^2 u^2} \left[ \frac{d}{dx} (x^2 u) + \frac{n(n+1)}{Rem} \right] \right\} \exp \left[ -\frac{n(n+1)}{Rem} \int_1^x \frac{dx}{x^2 u} \right] \frac{P'_n(\cos \theta)}{P_n(\cos \theta_b)} \quad (8)$$

Considering the lateral balance of forces across the sheet, we require that

$$\frac{1}{r} \frac{\partial p}{\partial \theta} = (\mathbf{J} \times \mathbf{B})_\theta \quad (9)$$

where  $p$  is the gas pressure. Integration of equation (9) then yields an expression for the gas pressure in the sheet.

$$p = p_e(x) + \frac{B_0^2}{8\pi x^4} \exp \left[ \frac{2n(n+1)}{R_{em}} \int_1^x \frac{dx}{x^2 u} \right] \left\{ 1 - \frac{1}{R_{em} x^2 u^2} \left[ \frac{d}{dx} (x^2 u) + \frac{n(n+1)}{R_{em}} \right] \right\} \left\{ 1 - \left[ \frac{P_n(\cos \theta)}{P_n(\cos \theta_b)} \right]^2 \right\} \quad (10)$$

Note that if  $\sigma = \infty$ , we have

$$p(x) = p_e(x) + \frac{B_0^2}{8\pi x^4} = p_e(x) + \frac{[B_e(x)]^2}{8\pi}$$

where  $B_e(x)$  is the external magnetic field strength. This is the condition one would expect were there no magnetic field inside the sheet. We now see that the departure from this condition is entirely due to finite resistivity effects since these effects introduce an internal magnetic field.

Evaluating equation (10) at  $x = 1$ , we can solve for  $n$  as a function of the pressure difference across the sheet.

$$n = \sqrt{R_{em}^2 u_1^2 (1 - \alpha) - R_{em} \frac{d}{dx} (x^2 u) \Big|_{x=1}} \quad (11)$$

where  $u_1 = u(x=1)$  and  $\alpha = (E-1)/\phi \cdot E = P_s(1)/P_e(1)$ , with  $P_s(1)$  being the pressure in the sheet at  $x=1$  and  $P_e(1)$  the pressure just outside, and  $\phi = B_0^2/8\pi P_e(1)$  represents the ratio of magnetic to gas pressure outside the sheet at the reference level. A cursory examination of equation (11) might suggest that  $\delta \propto 1/R_{em}$  (since  $\delta \propto 1/n$ ), yielding an extremely small value for the sheet thickness. However, the velocity terms  $u_1$  and  $d/dx(x^2 u)|_{x=1}$  are expected to be very small. Also, if  $\sigma = \infty$ ,  $P_s(1) = P_e(1) + B_0^2/8\pi$  [Pneuman and Kopp, 1971] so that  $\alpha = 1$ . In our case  $\alpha$  will not be exactly one but extremely close to one since  $R_{em} \gg 1$ . Hence, the right-hand side of equation (11) will be significantly reduced by these considerations, resulting in an increased sheet thickness.

To evaluate  $\alpha$ ,  $u_1$ ,  $d/dx(x^2 u)|_{x=1}$ , it is necessary to calculate the flow along the sheet. To do this, we must take into account the radial  $\mathbf{j} \times \mathbf{B}$  force, which because of the high current density is *not* small. (It will be shown that the radial  $\mathbf{j} \times \mathbf{B}$  force is actually independent of the electrical conductivity close to the sun.) The radial

momentum equation, once the density is eliminated via the continuity equation, then becomes approximately

$$\left( u - \frac{1}{u} \right) \frac{du}{dx} = \frac{2}{x} - \frac{\psi}{x^2} - \frac{2n^2 \phi}{(1 + \alpha \phi) u_1 R_{em} x^4} \quad (12)$$

where  $\psi = GM_\odot/r_0 V_s^2$ . In deriving equation (12), we have assumed that

$$\exp \left[ -\frac{n(n+1)}{R_{em}} \int_1^x \frac{dx}{x^2 u} \right] \approx 1$$

Equation (12) without the last term is the solar wind equation used by Parker [1958] for an isothermal corona. The critical point in that case is seen to be at  $x_c = \psi/2$  where  $u = 1$ . The last term here is the radial component of the magnetic force, which is negative and hence acts to retard the expansion. As a result, the critical point is moved outward and occurs where the left-hand side of equation (12) vanishes, yielding

$$x_c^2 \left( x_c - \frac{\psi}{2} \right) = \frac{n^2 \phi}{R_{em} u_1 (1 + \alpha \phi)} \quad (13)$$

For no field,  $\phi = 0$  and equation (13) reduces to  $x_c = \psi/2$  [Parker, 1958].

We now integrate equation (12) to obtain

$$\frac{u^2}{2} - \ln u - 2 \ln x - \frac{\psi}{x} - \frac{2n^2 \phi}{3 R_{em} u_1 (1 + \alpha \phi) x^3} = \text{const}$$

which, evaluated both at the critical point and at  $x = 1$ , yields

$$\begin{aligned} \frac{1}{2} - 2 \ln x_c - \frac{\psi}{x_c} - \frac{2n^2 \phi}{3 u_1 R_{em} (1 + \alpha \phi) x_c^3} \\ = \frac{u_1^2}{2} - \ln u_1 - \psi - \frac{2n^2 \phi}{3 u_1 R_{em} (1 + \alpha \phi)} \end{aligned} \quad (14)$$

Equations (13) and (14) represent two coupled equations for  $x_c$  and  $u_1$ . However, the quantities  $n$  and  $\alpha$  are also functions of  $u_1$  and must be evaluated.

To do this, consider the portion of the streamer below  $r_0$  which leads up into the sheet. Here the flow is along the field and no magnetic force exists along field lines.



Conservation of momentum along the field then shows that

$$P_s(I) = p_o \exp \left[ - \left( 1 - \frac{R_o}{r_o} \right) + \frac{1}{2} (u_o^2 - u_1^2) \right] \quad (15)$$

where  $p_o$  is the pressure at the solar surface ( $r = R_o$ ) and  $u_o$  is the velocity there. Noting that  $u_o \ll u_1$ , we can write equation (15) in the form

$$p_s(I) = p_c^* \exp \left( - \frac{u_1^2}{2} \right)$$

where  $p_c^*$  is the pressure at the neutral point that would be obtained for  $\sigma = \infty$  (the hydrostatic value). Now we have

$$\alpha = \frac{E-1}{\phi} = \frac{[P_s(I)/p_e(I)] - 1}{\phi} \\ = \frac{[p_c^*/p_e(I)] \exp(-u_1^2/2) - 1}{\phi}$$

But  $p_c^*/p_e(1) = 1 + \phi$  [Pneuman and Kopp, 1971]. Hence

$$\alpha = \frac{(1 + \phi) \exp(-u_1^2/2) - 1}{\phi}$$

and, since  $u_1 \ll 1$ , we can expand the exponential in the numerator and obtain

$$\alpha \approx 1 - \left( \frac{1 + \phi}{2\phi} \right) u_1^2$$

Using equation (12), we also can evaluate  $d/dx(x^2 u)|_{x=1}$  and find

$$\frac{d}{dx} (x^2 u) \Big|_{x=1} = \psi u_1 + \frac{2n^2 \phi}{R_{em}(1 + \phi)}$$

Equation (11) now reduces to

$$n = \sqrt{R_{em} \left( \frac{1 + \phi}{1 + 3\phi} \right) u_1 \left[ R_{em} u_1^3 \left( \frac{1 + \phi}{\phi} \right) - \psi \right]} \quad (16)$$

and, after some manipulation, equations (13) and (14) become

$$\left( \frac{1 + \phi}{2\phi} \right) R_{em} u_1^3 = \psi + \left( \frac{1 + 3\phi}{\phi} \right) x_c^2 \left( x_c - \frac{\psi}{2} \right) \quad (17)$$

$$\frac{u_1^2}{2} - \ln u_1 = \frac{2}{3} x_c^2 \left( x_c - \frac{\psi}{2} \right) - 2 \ln x_c + \psi - \frac{1}{6} \quad (18)$$

Noting that  $u_1^2/2 \ll |\ln u_1|$  we finally obtain a single transcendental equation for  $x_c$ .

$$\ln \left[ \frac{2\psi\phi + (1 + 3\phi)x_c^2(2x_c - \psi)}{R_{em}(1 + \phi)x_c^6} \right] + x_c^2(2x_c - \psi)$$

$$- \frac{2\psi}{x_c} + 3\psi - \frac{1}{2} = 0 \quad (19)$$

The numerical procedure is to solve equation (19) for  $x_c$ ; then  $u_1$  can be found from equation (17) or (18). The sheet thickness  $\delta$  ( $\sim \pi r/4n$ ) can then be evaluated from equation (16). Figure 2 shows a plot of  $\delta$  at the coronal base as a function of temperature for various values of  $\phi$ . For reasons to be discussed later, these values should properly be considered lower limits to the actual sheet dimensions.

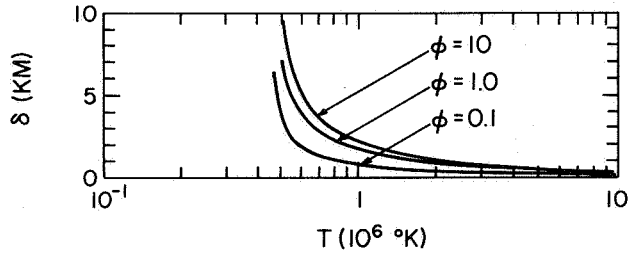


**Figure 2.** Sheet thickness at the coronal base as a function of coronal temperature. These values are based upon an electrical conductivity unaffected by the magnetic field and should be considered lower limits.

We now summarize the solutions (approximate) for the pertinent properties inside the sheet using the approximations  $R_{em} \gg 1$  and

$$\exp \left[ - \frac{n(n+1)}{R_{em}} \int_1^x \frac{dx}{x^2 u} \right] \approx 1$$

$$B_r = \frac{B_0}{x^2} \sin \left[ \left( n + \frac{1}{2} \right) \theta + \frac{\pi}{4} \right] \quad (20)$$

$$B_\theta = \frac{-B_0 n}{R_{em} x^3 u} \cos \left[ \left( n + \frac{1}{2} \right) \theta + \frac{\pi}{4} \right] \quad (21)$$

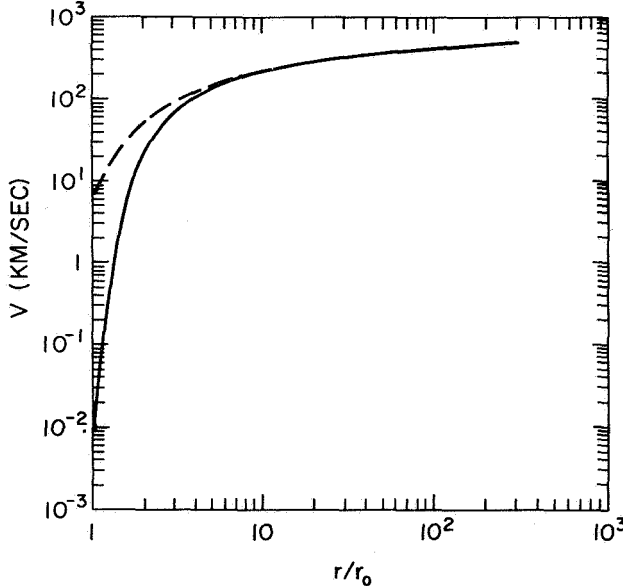
$$J = \frac{-B_0 n}{4\pi r_0 x^3} \cos \left[ \left( n + \frac{1}{2} \right) \theta + \frac{\pi}{4} \right] \quad (22)$$

$$p = p_e(x) + \frac{B_0^2}{8\pi x^4} \cos^2 \left[ \left( n + \frac{1}{2} \right) \theta + \frac{\pi}{4} \right] \quad (23)$$

The velocity  $u$  is given by the equation

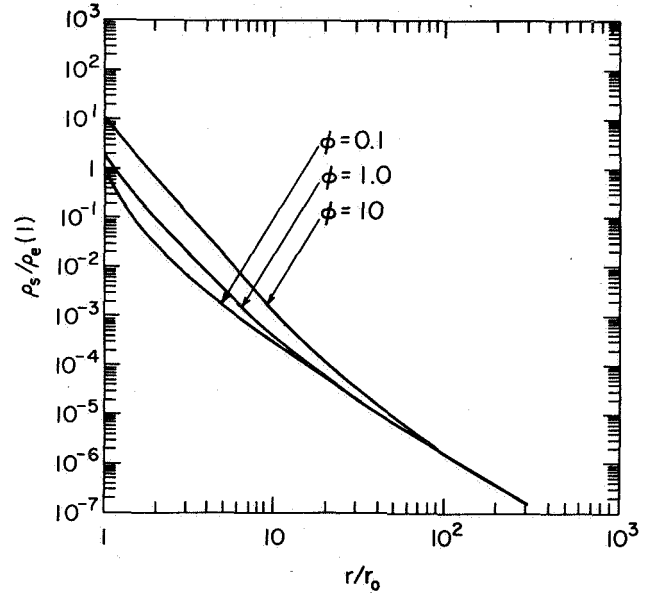
$$\begin{aligned} \frac{u^2}{2} - \ln u = \frac{u_1^2}{2} - \ln u_1 + 2 \ln x - \psi \left( 1 - \frac{1}{x} \right) \\ - \frac{2n^2 \phi}{3u_1 R_{em}(1 + \phi)} \left( 1 - \frac{1}{x^3} \right) \end{aligned} \quad (24)$$

Figure 3 shows the expansion velocity both inside and outside the sheet as a function of radial distance. The



**Figure 3.** Variation of expansion velocity with radial distance for  $\phi = 1$ ,  $r_0 = 2 R_\odot$ , and  $T = 1.0 \times 10^6$  K. The solid curve represents the velocity inside the sheet whereas the dashed curve is the velocity just outside. Note that the flow in the sheet near the base is extremely small due to the inhibiting effect of the magnetic field.

small velocities in the sheet near the coronal base reflect the retarding force of the internal magnetic field. The density enhancement for various field strengths is shown in figure 4. As expected, the enhancement close to the sun increases with increasing field strength (increasing  $\phi$ ). In this model, the enhancement falls to zero at large distances; however, this behavior may be due to the omission of thermal conduction effects in the model. It is expected that thermal conduction will be inhibited in the sheet by the transverse magnetic field, whereas conduction is essentially unimpeded outside. As shown by *Pneuman and Kopp* [1970], the inclusion of this effect could tend to maintain significant density enhancements at large distances.



**Figure 4.** Density enhancement (ratio of density in the sheet to that outside) as a function of radial distance for the cases  $\phi = 0.1, 1$ , and  $10$ .

It is of special interest to note the dependence of the various physical quantities on the electrical conductivity  $R_{em}$ . Solutions of equation (19) over a wide range of magnetic Reynolds numbers reveals that the location of the critical point ( $x_c$ ) is not a very sensitive function of  $R_{em}$ . For example, for coronal temperatures in excess of  $10^6$  K,  $x_c$  only varies from 1 to about 4 for  $1 < R_{em} < 10^{14}$ . Equation (17) then shows that  $u_1 \propto R_{em}^{1/3}$ , and from equation (16) we have  $n \propto R_{em}^{1/3}$ . This means that the sheet thickness  $\delta$  varies as

$$\delta \propto R_{em}^{-1/3}$$

We can now use equations (21) and (22) to evaluate the transverse field in the sheet ( $B_\theta$ ) and the electric current density  $J$ . Close to the sun,  $u \approx u_1 \propto R^{-1/3}$ . Hence, near  $x = 1$ , we have (since  $n \propto R_{em}^{1/3}$ ).

$$B_\theta \propto R_{em}^{-1/3} \quad x \approx 1$$

At larger distances,  $u$  is of order 1 and

$$B_\theta \propto \frac{R_{em}^{-2/3}}{x^3} \quad x \gg 1$$

The current  $J$  has the dependence

$$J \propto \frac{R_{em}^{1/3}}{x^3}$$

Consequently, the radial JXB force ( $\propto JB_\theta$ ) is independent if  $R_{em}$  close to the sun but varies as  $R_{em}^{-1/3}$  at large  $x$ , signifying that the magnetic stresses are important at lower levels but do not significantly affect the expansion at large distances.

## DISCUSSION

Since the neutral sheet model presented in the previous sections is based upon the MHD approximation, it is appropriate now to examine its validity in structures whose lateral dimensions may be of the order of a mean free path. For example, a coronal temperature of  $10^6$  °K and an electron density of  $10^8/\text{cm}^3$  corresponds to a mean free path of 100 km, which is larger than the dimensions shown in figure 2. However, the Larmor radius, probably the more appropriate dimension in this case, is only 20 cm for a field strength of 1 gauss. This dimension is small relative to the thickness so that electrons are very effectively tied to the field lines. For this reason, ion-electron collisions will be frequent making the MHD approximation a reasonable initial approach to the problem.

The dimensions shown in figure 2 should also properly be considered as lower limits since they are based on an electrical conductivity unaffected by the

magnetic field. From equation (21) the transverse field  $B_\theta$  at the center of the sheet at  $x = 1$  for  $B_0 = 1$  gauss,  $r_0 = 2R_\theta$ , and a temperature of  $10^6$  °K ( $R_{em} = 4.5 \times 10^{14}$ ) is found to be only  $3 \times 10^{-5}$  gauss and decreases outward rapidly. The product of the cyclotron frequency and collision time for electrons in this field is about 70. Hence,  $R_{em}$  could be reduced by a factor as great as  $2 \times 10^{-4}$ . This consideration would increase the sheet dimension by the factor 17 yielding widths in the inner corona in the order of 100 km. This figure corresponds to a thickness of 10,000 km at 1 AU. Another important consideration may be various forms of micro-turbulence and instabilities in the plasma, which would tend to increase the "effective" collision frequency, resulting in a further reduction in electrical conductivity.

With regard to the generating mechanism for type III radio emission, we should note that the neutral sheet described here contains a weak but finite transverse magnetic field. This field would have a retarding effect on electrons traveling outward along the sheet. One might well ask whether the concept of electrons moving outward at velocities of the order  $0.3c$  across a magnetic field of  $10^{-5}$  gauss is realistic. On the other hand, stabilization of the beam in such a configuration seems more possible here than in the ambient corona since the rapid increase in field strength outward from the center of the sheet should have a confining effect on the electrons.

## REFERENCES

- Bumba, V.; and Obridko, V. N.: 'Bartels' Active Longitudes'. Sector Boundaries and Flare Activity. *Solar Physics*, Vol. 6, 1969, pp. 104-110.
- Parker, E. N.: Dynamics of the Interplanetary Gas and Magnetic Fields. *Astrophys. J.*, Vol. 128, 1958, pp. 664-676.
- Pneuman, G. W.; and Kopp, R. A.: Coronal Streamers III: Energy Transport in Streamer and Interstreamer Regions. *Solar Physics*, Vol. 13, 1970, pp. 176-193.
- Pneuman, G. W.; and Kopp, R. A.: Gas-Magnetic Field Interactions in the Solar Corona. *Solar Physics*, 1971. (in press)
- Wild, J. P.: Radio Observations of Solar Flares. *AAS-NASA Symposium on the Physics of Solar Flares*, ed. W. N. Hess, 1964, pp. 161-177.

## DISCUSSION

*R. A. Kopp* It's always nice to not worry about the convergence problem by iterating just once, but it seems like your thickness is varying by three orders of magnitude from the assumption of radial. Are you sure this is conclusive? Shouldn't you work it out?

*G. W. Pneuman* I would say it is not a conclusive result, no.

*F. W. Perkins* As far as I can see, the reason why we require finite conductivity is because you assume that there was flow out. I suspect there is a possibility of having a static solution, too, with infinite conductivity. Is the flow really observed or necessary?

*G. W. Pneuman* I believe it is necessary to satisfy the condition of almost zero pressure at infinity.

*T. G. Cowling* I would like to ask, in view of the background to these latest contributions, whether in fact we are approaching the idea that the layer that you get at the boundary between two sectors is to be regarded as a shear layer, the equivalent of the earthquake boundary we've heard so much about? Is it a thing where the field virtually becomes detached, field from the one side is to be regarded as detached from the field on the other side? Is that a picture we have come to? And is there a genuine reason for that?

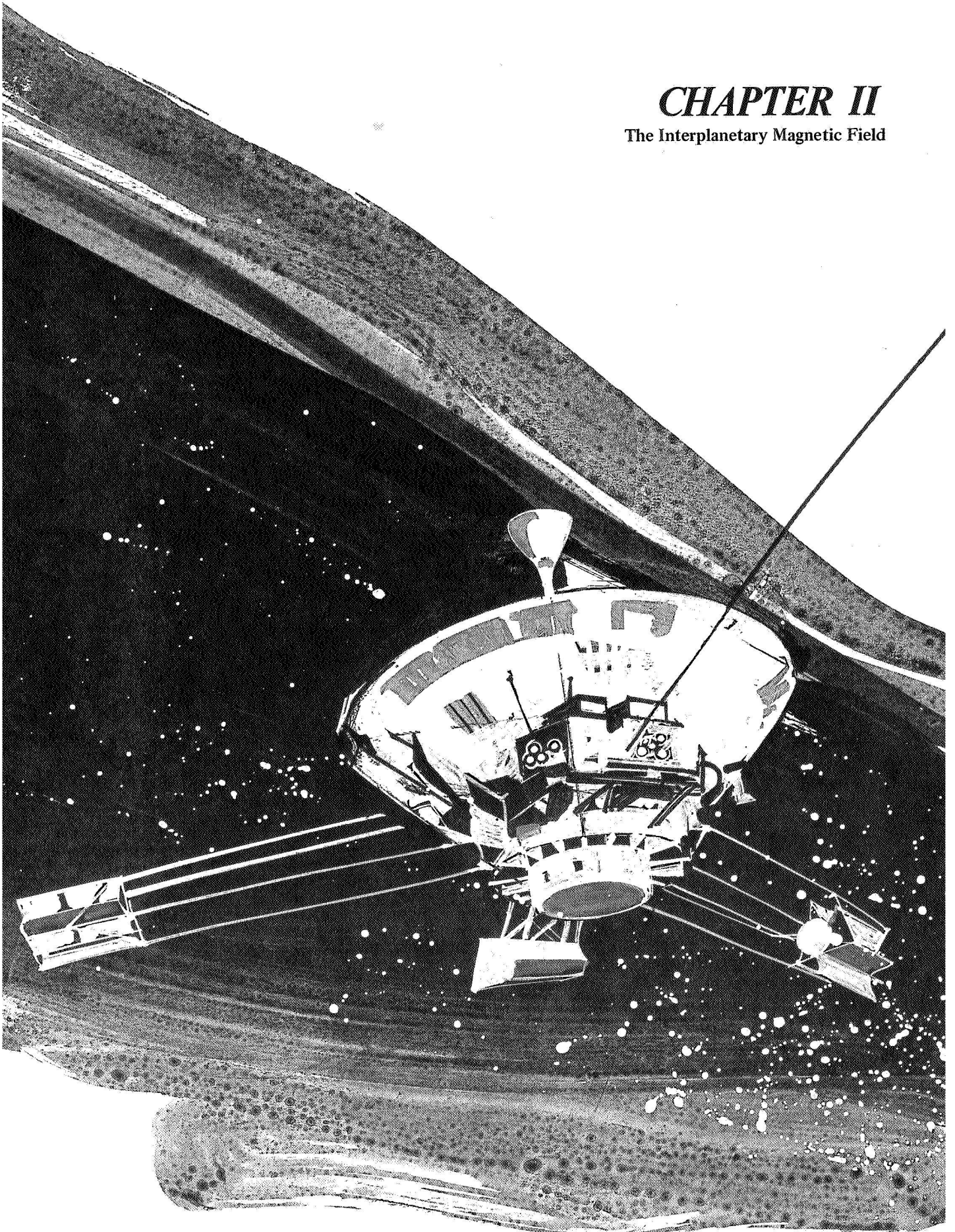
*G. W. Pneuman* I'm not sure. In this particular model I would consider it that way. I would like to look at it as the loops, the low down loops, actually being drawn up inside the sheet so that actually there are never really any open field lines inside the sheet; sort of an extension of the lower part of the streamer.

*Unidentified.* You'd still have a discontinuity involved above and below?

*G. W. Pneuman.* No, there is no discontinuity.

## *CHAPTER II*

The Interplanetary Magnetic Field



Relation of the solar field to the interplanetary magnetic field; the large scale interplanetary magnetic field including sector structure and the evolution of sectors and the field through the solar cycle; filamentary structure in the solar wind.

# LARGE-SCALE PROPERTIES OF THE INTERPLANETARY MAGNETIC FIELD

Kenneth H. Schatten

An invited review

Our knowledge of the large-scale properties of the interplanetary magnetic field is reviewed. The early theoretical work of Parker is presented along with the observational evidence supporting his Archimedes spiral model. The variations present in the interplanetary magnetic field from the spiral angle are related to structures in the solar wind. The causes of these structures are found to be either nonuniform radial solar wind flow or the time evolution of the photospheric field. The coronal magnetic models are related to the connection between the solar magnetic field and the interplanetary magnetic field. The direct extension of the solar field-magnetic nozzle controversy is discussed along with the coronal magnetic models. The effect of active regions on the interplanetary magnetic field is discussed with particular reference to the evolution of interplanetary sectors. The variation of the interplanetary magnetic field magnitude is shown throughout the solar cycle. The percentage of time the field magnitude is greater than  $10 \gamma$  is shown to closely parallel sunspot number. The suggested influence of the sun's polar field on the interplanetary field and alternative views of the magnetic field structure out of the ecliptic plane are presented. In addition, a variety of significantly different interplanetary field structures are discussed.

## ABSTRACT

## INTRODUCTION

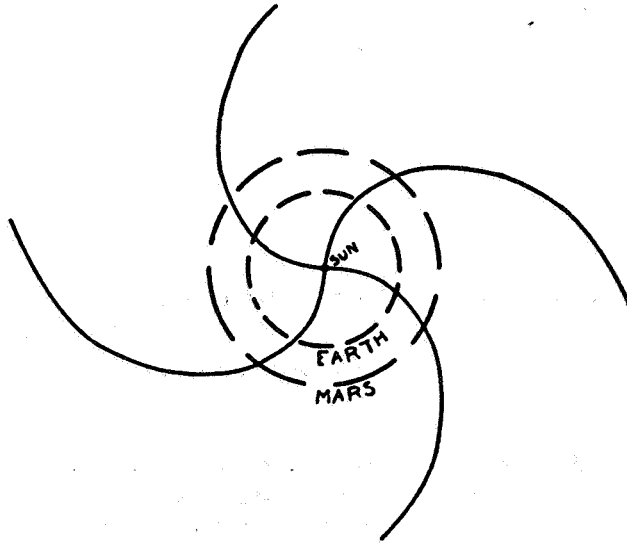
Our knowledge of the large-scale properties of the interplanetary magnetic field began with Parker's work in 1958. Parker reasoned that the kinetic energy of the solar wind plasma as it left the sun should decrease as  $r^{-2}$ , whereas the magnetic energy density would decrease as  $r^{-4}$ . It followed, therefore, that the general solar dipole field would not significantly influence the motion of the outflowing gas once the gas left the solar corona. Parker then considered the "frozen-in" magnetic field configuration of interplanetary space. "Frozen-in" field lines generally are those that obey the equation  $\mathbf{E} + \mathbf{v}/c \times \mathbf{B} = 0$ ; in terms of a simple physical picture, the field lines are constrained to move with the plasma flow. The field lines thus follow the stream lines of the plasma, which, for a rotating sun and radially flowing solar wind, is the Archimedean spiral configuration.

Figure 1 from *Parker* [1958] shows such an Archimedean spiral field for a solar wind flowing at 1000 km/sec. *Parker* [1963] later revised the solar wind speed to 300 km/sec to correspond to quiet periods; this figure led to the near  $45^\circ$  average interplanetary magnetic field direction from the sun-earth line. Whether the solar active region fields contributed to the general streaming of gas from the sun as proposed by *Biermann* [1951] was an open question. The magnetic energy density associated with the active region fields was very much larger than that associated with the background solar field. Much more energy would be required to extend these fields into interplanetary space; thus, only the background solar field was thought to extend into interplanetary space.

Other than Parker's theoretical treatment of the interplanetary magnetic field, our knowledge of its properties has developed mostly on theories and observations based directly on the results of space

---

*The author is at the Laboratory for Extraterrestrial Physics, NASA-Goddard Space Flight Center, Greenbelt, Maryland.*



**Figure 1.** Projection onto the solar equatorial plane of the lines of force of any solar field which is carried away from the sun by outward-streaming gas with a velocity of  $10^3$  km/sec [Parker, 1958].

experiments. A variety of magnetometers have been employed in the study of the interplanetary magnetic field. The measurement of the interplanetary magnetic field is difficult owing to the low field strength. The field is typically  $5 \gamma$  ( $1 \gamma = 10^{-5}$  gauss). Ness [1970a] has recently completed an extensive review of the use of various magnetometers for space research, the most common of which is the fluxgate magnetometer.

Although first evidence showed disagreement with Parker's interplanetary field model, later evidence supported it. Figure 2 from Davis *et al.* [1964] supporting Parker's model, shows a scatterplot of the observed interplanetary magnetic field from Mariner 2. Each point represents a "smoothed" hourly average of five successive hourly averages. The dashed line shows the expected result for the Parker spiral field model. Davis also noted that despite the averaging, one must surely be "impressed by the disorder and irregularity shown in these measurements." This point was dramatically illustrated in the movie of the interplanetary magnetic field by Wilcox *et al.* [1966] where a great deal of variability was seen on a short time scale. This variability, of course, relates to structural properties of the field.

In addition to the unexplained structural variations, our knowledge of the origin of the interplanetary magnetic field was also rather limited at the 1964 solar wind conference. Since then, much knowledge has been acquired concerning both the structural variability and the origin of the interplanetary magnetic field. This

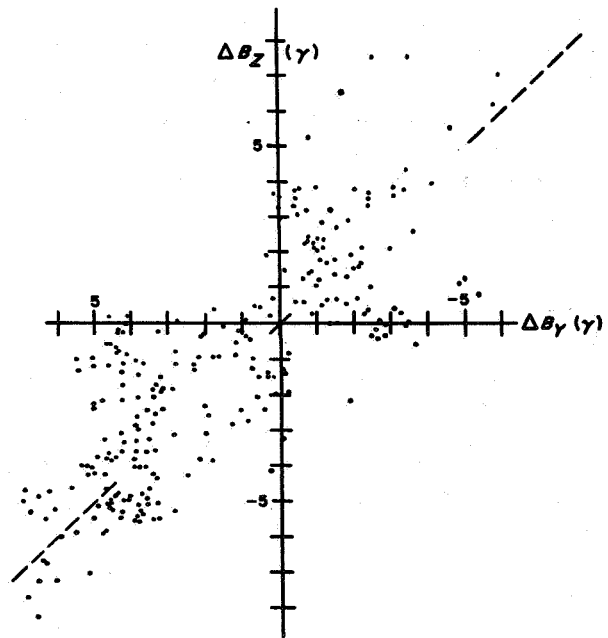


**Figure 2.** Scatterplot of the radial and azimuthal interplanetary magnetic field component changes from Mariner 2. The dashed line shows the expected average for theoretical spiral field lines from the sun.  $\Delta B_z$  corresponds to field pointed away from the sun and  $\Delta B_y$  to field in the direction opposite to the spacecraft motion about the sun [Davis *et al.*, 1964].



paper outlines much of this work and discusses remaining gaps in our understanding of some of these points. An earlier review by Dessler [1967] gives a more detailed historical summary of the development of our knowledge concerning the interplanetary magnetic field.

## LARGE-SCALE SPATIAL STRUCTURE

### Quasi-stationary Structure

The early work of Ness and Wilcox [1964] showed that the interplanetary magnetic field had a 27-day periodicity and that it correlated with the average direction of the photospheric magnetic field during three successive solar rotations near the minimum of the last sunspot cycle. The 27-day periodicity was related to the 27-day rotation period of the sun as seen from the earth. This supports Parker's hypothesis that the sun was the origin of the interplanetary magnetic field. A 4-1/2 day time lag was found for their highest correlations, representing the time necessary for a radially flowing solar wind to transport the solar magnetic field to a position near the earth.

It was found that the interplanetary magnetic field as observed near the earth tended to point predominantly away from the sun or toward the sun (along Parker's theoretical spiral angle) for a duration of several days. This repeated every 27 days, forming a pattern referred to as *sector structure*. This early sector structure pattern is shown in figure 3. As can be seen, a definite pattern emerges. There were four sectors, three approximately equal in size and one sector half as large as the other three. In a reference frame rotating with the sun this pattern was quasi-stationary in time and persisted possibly for longer than a year [Fairfield and Ness, 1967].

### Interplanetary Magnetic Field Mapping

One approach to mapping the interplanetary magnetic field is shown in figure 4 from McCracken and Ness [1966]. The 7.5-min average magnetic field was projected into the ecliptic plane and the vectors were placed end to end. The scale of this figure is such that it extends a distance of  $5 \times 10^6$  km or about 0.03 AU. Localized "kinks" or "regressions" were observed in the magnetic field. The "kinks" in the magnetic field are significant in that high energy particles are affected by them as they travel through space. Figure 4 shows the magnetic field structure as well as the cosmic ray anisotropy on December 30, 1965. During this period, the solar-generated cosmic radiation arriving at the earth was markedly anisotropic and varied considerably in

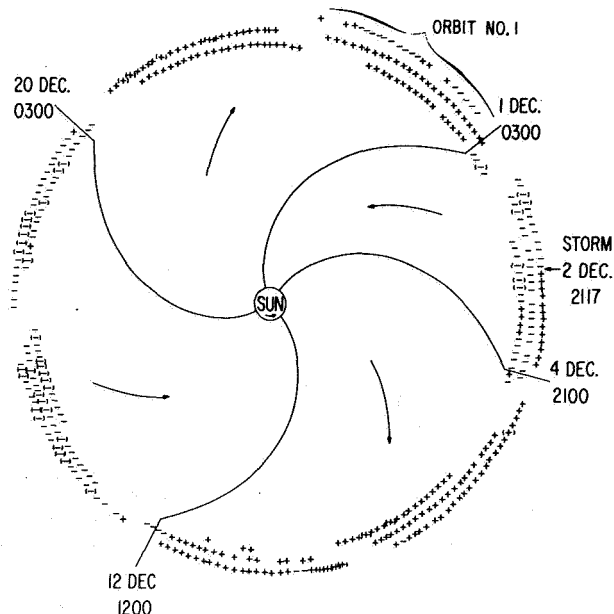


**Figure 3.** Schematic representation of the sector structure of the interplanetary magnetic field suggested from the IMP-1 observations [Wilcox and Ness, 1965]. The + and - signs along the circumference of this figure indicate the direction of the measured interplanetary magnetic field during successive 3-hr intervals. Parentheses indicate times when the field direction is substantially displaced from the spiral angle.

direction. As shown, despite major changes in the interplanetary magnetic field direction, the cosmic ray anisotropy remained well aligned with the field. Thus, the cosmic ray anisotropy can be considered a measurement of the average field direction over the scale of a cyclotron radius of the particles. The observations by McCracken and Ness of occasional abrupt changes in cosmic ray anisotropy suggested to them that the interplanetary magnetic field was filamentary in nature. This model of interplanetary field filaments has sometimes been referred to as the "spaghetti" model. (Its geometry shown in panel figure 30(h).)

Although the McCracken and Ness method of mapping the interplanetary magnetic field works well on a small scale, it is also necessary to consider the effects of solar rotation and field transport due to the solar wind flow.

At first glance, a time sequence of local magnetic measurements from a single spacecraft at 1 AU would seem inadequate to determine the large-scale geometry of the interplanetary magnetic field. This is not necessarily the case, however, if the feature under

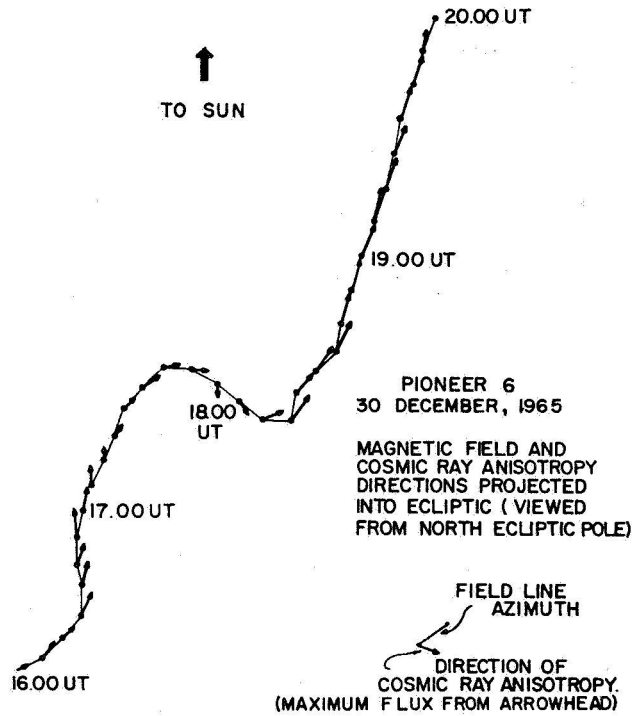


**Figure 4.** Interplanetary magnetic field and cosmic ray anisotropy on December 30, 1965, from Pioneer 6 observations. The interplanetary magnetic field shows a "kink" structure which is also seen in the cosmic ray anisotropy directions [McCracken and Ness, 1966].

investigation exhibits certain properties that allow extrapolations of the structure of the field. These basic properties are the rapid convection of the field away from the sun; the high conductivity of the solar wind plasma, which apparently inhibits the field from diffusing a substantial distance; the relatively constant nature of the source of the field; and the relatively steady direction and slowly varying magnitude of the solar wind velocity. These last two conditions are at times invalid, resulting in magnetic field extrapolations that are not meaningful. Field patterns that incorrectly show a nonzero field divergence usually indicate that one of the conditions has been violated.

Utilizing a steady radial solar wind velocity, one obtains the following relationships concerning the behavior of the interplanetary magnetic field with distance from the sun:

$$B_r(R_1) = B_r(R_0)(R_0/R_1)^2 \quad (1)$$

$$B_\phi(R_1) = B_\phi(R_0)(R_0/R_1) \quad (2)$$

$$B_\perp(R_1) = B_\perp(R_0)(R_0/R_1) \quad (3)$$

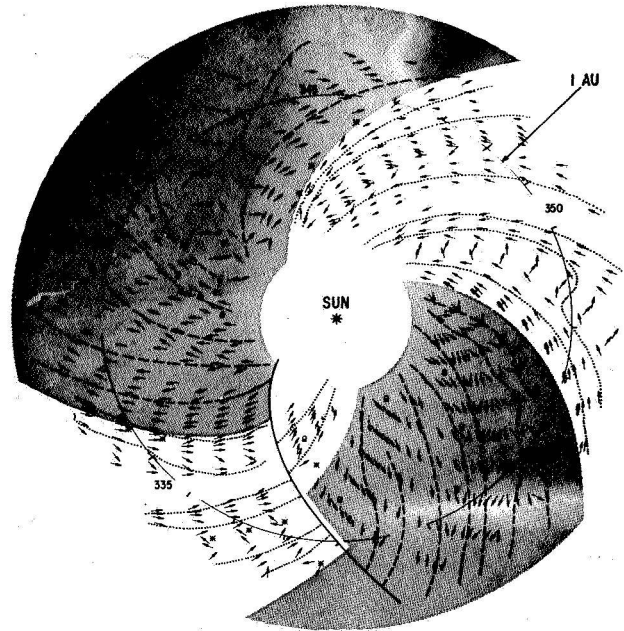


**Figure 5.** Extrapolated ecliptic magnetic field pattern during Bartels' solar rotation number 1784, prepared from IMP-1 magnetic field measurements. The gaps in the circle at 1 AU and in the data represent times when the satellite is near perigee and unable to sample the interplanetary medium. The tick marks at 1 AU indicate the amount of solar rotation during one day. The interval between the tick marks is labeled with the date of observation. The line drawn at the bottom of the figure separates observations 27 days apart. The observations extend from November 28, 1963 through December 25, 1963 [Schatten et al., 1968].

where  $B_r$ ,  $B_\phi$  and  $B_\perp$  are the three solar ecliptic components of the magnetic field, and  $R_0$  and  $R_1$  are two radial distances from the sun. An extrapolation of the field is then made, taking into account corotation of the field and the radially flowing plasma. Figure 5 from Schatten et al. [1968] shows this extrapolated magnetic field in the plane of the ecliptic for December 1963, prepared from the IMP-1 magnetic field measurements of Ness et al. [1964]. The gaps in the circle at 1 AU represent times when the IMP-1 satellite was near perigee (and therefore within the region influenced by the geomagnetic field) and interplanetary field observations could not be obtained. The data progress clockwise in time since the sun rotates counterclockwise, as seen from the north ecliptic pole. The solid curved line at the bottom separates observations taken 27 days apart. This is the time period necessary for a position on the sun

facing earth to return to the same location. A 400 km/sec solar wind speed and a synodic period near 27 days was employed in this and all the figures of its kind.

As can be seen, the magnetic field calculated is generally well represented by an Archimedean spiral. The sector boundary on day 336 is well defined. Some of the field lines are more radially oriented and others more curved than the average Archimedes spiral. The main point, though, is that the field lines have the same topology as the Archimedean spiral geometry. The field lines can be "tied" to the sun and directed into interplanetary space past the orbit of the earth. The whole system may corotate with little change for many solar rotations.

#### Magnetic "Kinks" and Velocity Gradient Variations

The field lines in figure 5 are occasionally distorted from a uniform spiral configuration; it is important to understand how such "distorted" structures arise. Schatten [1968] analyzed to first order the effect of radial (or temporal), azimuthal, and poloidal solar wind velocity gradients on the magnetic field structure. The structures analyzed were the large scale kinks, similar to those shown in figure 5 on days 343 and 352.

If one considers the magnetic field embedded within an element of plasma flowing radially away from the sun with an assumed azimuthal velocity gradient, one obtains the following equations governing the components of the field variation with radial distance:

$$B_r R_1 = B_r R_o \left( \frac{R_o}{R_1} \right)^2 + B_\phi R_o \left( \frac{R_o}{R_1} \right)^2 \frac{1-R_1}{R_o} \frac{1}{v(dv/d\phi)} \quad (4)$$

$$B_\phi R_1 = B_\phi R_o \frac{R_o}{R_1} \quad (5)$$

$$B_\perp R_1 = B_\perp R_o \frac{R_o}{R_1} \quad (6)$$

Computations in table 1 are based on values of  $R_o$  chosen to correspond to a position close to the sun where the velocity gradient has not caused substantial changes in the magnetic field pattern, and a value of  $R_1$  at 1 AU where the field is observed. The table shows that if one assumes azimuthal velocity gradients were responsible for the change in field direction, the directions computed using the ratio of equations (4) and (5) and the solar wind velocity measurements of the MIT plasma probe (next to last column) agree quite well with the observed field directions (last column). The interplanetary magnetic field spiral angle computed from the average (for each time period in table 1) solar wind velocity is in considerable disagreement for these time periods. This indicates that there were regions near the sun at this time emanating plasma at different velocities rather than a single source for each sector with a smooth temporal velocity variation.

Let us now consider in a more general way the causes of these substantial alterations of the magnetic field from the Archimedean spiral geometry. Close to the sun, the plasma is partially constrained by the strong magnetic field to rotate with the sun. Beyond a few solar radii the plasma velocity becomes more radial than azimuthal. At these distances the corotation speed is substantially less than the solar wind velocity. The magnetic field has on the average an almost radial direction with a small, but important, azimuthal component that depends on the rotation rate of the sun.

Table 1. Regions with azimuthal velocity gradients in the solar wind speed

Starting time UT			End time UT			V <sub>start</sub> km/sec	V <sub>end</sub> km/sec	φ spiral angle	$1 - \frac{\Delta V}{V} \frac{27.5}{\Delta t + (2\pi)}$	φ azimuthal velocity gradient	φ observed
0300	343	63	0300	344	63	435	283	130°	-0.85	50°	48°
2100	351	63	2100	352	63	305	215	301°	-1.08	223°	227°
0000	011	64	0000	015	64	493	210	310°	0.11	276°	273°
1500	033	64	1500	034	64	378	307	129°	0.07	94°	53°
2100	037	64	2100	038	64	460	350	314°	-0.2	259°	244°
2100	001	64	2100	002	64	310	490	133°	3.0	162°	145°

Beyond this distance the magnetic field is altered continually by the flow of the solar wind according to the equation

$$\frac{d\mathbf{B}}{dt} = (\mathbf{V} \cdot \nabla) \mathbf{B} + \frac{\partial \mathbf{B}}{\partial t} = -\mathbf{B}(\nabla \cdot \mathbf{V}) + (\mathbf{B} \cdot \nabla) \mathbf{V} \quad (7)$$

which is obtained by using Faraday's law, assuming infinite conductivity, and using the definition of a convective derivative. Thus the initial field after a 5-day transit from sun to earth may be computed from

$$\mathbf{B}(R_1) = \int_0^T [-\mathbf{B}(\nabla \cdot \mathbf{V}) + (\mathbf{B} \cdot \nabla) \mathbf{V}] dt \quad (8)$$

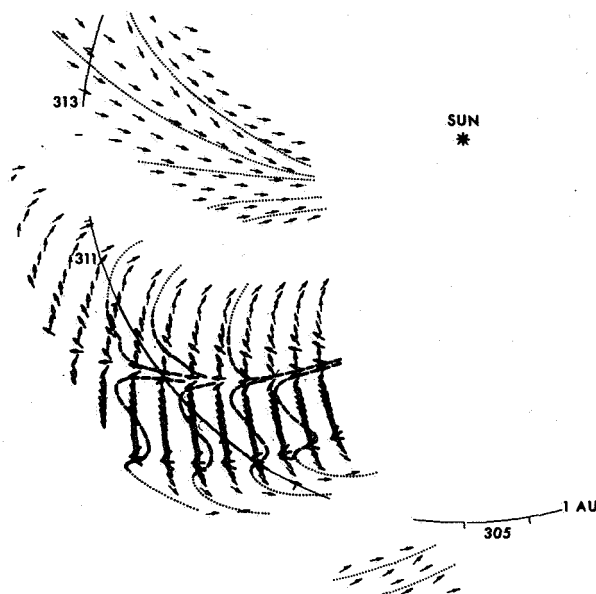
where  $T$  equals 5 days and  $R_1$  is 1 AU. Under steady-state conditions, with a constant radial solar wind velocity this condition implies a spiral magnetic field. The first term in the integrand of equation (8) can serve to increase or decrease the field magnitude but not alter its direction. The second term is responsible for the changing direction of the magnetic field. The magnetic field can "know" at what angle to point only by gaining knowledge of the rotation rate of the sun. The velocity field, being essentially radial, carries no such information. Thus the small, initial azimuthal magnetic field serves to inform the interplanetary field of this rotation. The information is transmitted and *amplified* by the solar wind through the dyadic term involving the velocity. Any additional gradients in the velocity field as a result of temporal or spatial variations in the solar wind velocity would tend to significantly alter the interplanetary field direction from the Archimedean spiral angle due to the integration and differentiation of the solar wind velocity in equation (8). Such alteration is exemplified by the kinks in figure 5, where modest longitudinal velocity gradients resulted in significant alterations in the field geometry. Velocity gradients may become more important at greater radial distances from the sun as will be seen in a later section.

#### Dynamic Effects on Magnetic Field Structure

In addition to the possibility of solar wind velocity variations causing a non-Archimedean spiral interplanetary magnetic field, a variable source of magnetic field near the sun may also produce a nonspiral field

geometry. In this case, the magnetic field near the sun no longer is oriented radially with a slight azimuthal component but rather has some other field geometry, which is then frozen into the plasma and transported to 1 AU. If no large-scale velocity perturbations exist to disrupt the pattern it may then be observed.

Figure 6 shows the interplanetary magnetic field in the ecliptic plane for November 1-9, 1965, from Schatten *et al.* [1968]. A new feature is suggested: Magnetic loops



IMP-3 ECLIPTIC MAGNETIC FIELD  
305/65-313/65  
NOV. 1, 1965-NOV. 9, 1965

**Figure 6.** Enlargement of the magnetic flux loops observed near day 310, 1965. The dip in the field pattern on day 308 has associated with it a strong northward field [Schatten *et al.*, 1968].

are observed that consist of field lines that appear to leave the sun, reach into interplanetary space, and then connect back to the sun. This magnetic loop configuration represents a dynamic process, in so far as these field lines cannot remain in this shape in a quasi-stationary configuration. This configuration is convected out by the solar wind to form new spiral field lines. The looped field pattern is an enlargement of a structure that presumably existed in the corona 5 days before it was observed a 1 AU. It is thus necessary to examine the

relationship between the interplanetary magnetic field and source of the field near the sun. This particular feature is discussed in greater detail in a later section.

### Magnetic Field Diffusion

Coleman and Rosenberg [1970] using Mariner 2, 4, and 5 data have observed an effect in the interplanetary magnetic field, the physical cause of which is not quite clear. It may, however, relate to magnetic field diffusion in interplanetary space. They have investigated in detail the north-south component of the interplanetary magnetic field. They observe a skewing of the magnetic field away from the solar equatorial plane. A particularly good example of their result is shown in figure 7 using the Mariner 4 observations. Twenty-seven day running average values of  $B_\theta$  are computed separately for toward and away sectors. As can be seen  $B_{\theta s}$  which represents the field skewing, closely follows heliographic latitude. Note that Mariner 4 was below the solar equatorial plane from day 347 of 1964 until day 230 of 1965. The effect is equivalent to a skewing of the magnetic field away from the solar equatorial plane.

If the field were "frozen-into" the solar wind, the velocity would follow the same pattern. Coleman and Rosenberg estimate such skewing would require a 30 km/sec north-south directed solar wind velocity component. The magnitude of  $V_\theta$  for the same overlapping 27-day averages, using the MIT group's plasma velocity, was typically one-third that required for the alignment of  $B$  and  $V$ ,<sup>1</sup> and the sign of the velocity was opposite to that required for alignment—that is, the observations indicated the solar wind velocity was directed towards the plane of the solar equator. The meaning of their observations is not quite clear; as yet there is no physical explanation for their observations.

### Radial Variation of the Interplanetary Magnetic Field

Figure 8 from Burlaga and Ness [1968] shows the interplanetary magnetic field variation from 0.8 to 1.0 AU as observed by Pioneer 6 in 1966. The figure shows the transverse and radial components of the field as well as the magnitude as a function of radial distance. The dashed line (except for  $B_{total}$ ) corresponds to Parker's

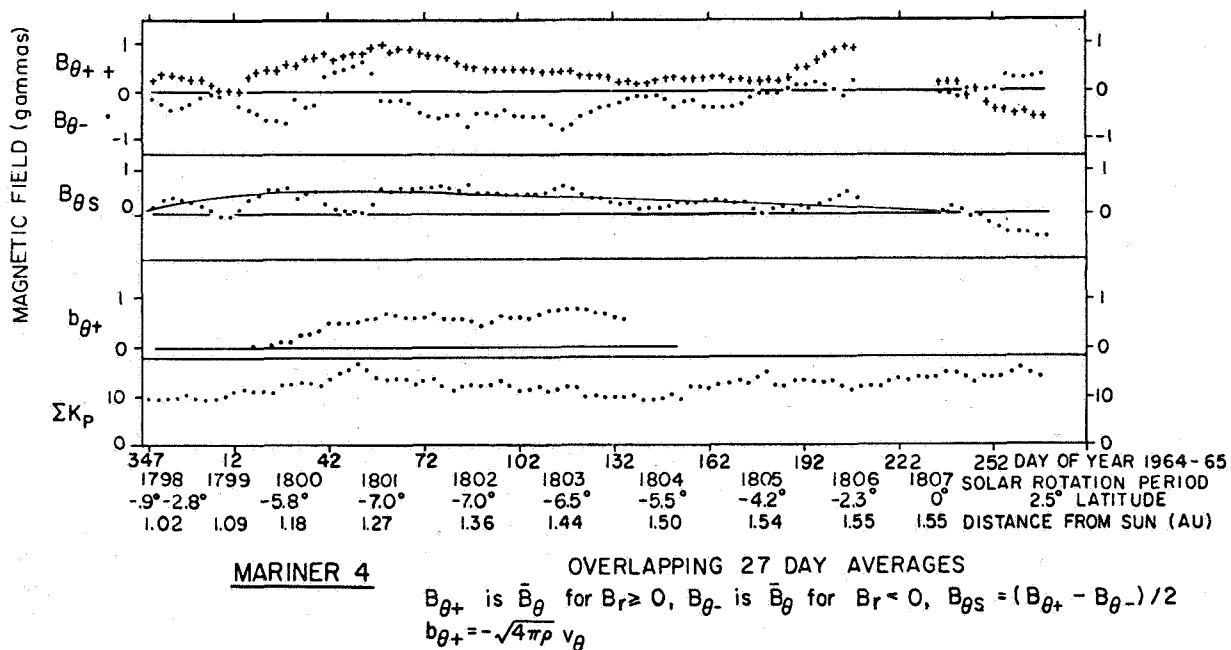


**Figure 7.** Averages over 27 days of  $B_{\theta+}$ ,  $B_{\theta-}$ ,  $B_{\theta s}$ ,  $b_{\theta+}$  and  $K_p$  for the interval covered by the Mariner 4 data. The solid curve drawn in the  $B_{\theta s}$  panel represents a best fit to  $B_{\theta s}$  with a function proportional to heliographic latitude [Coleman and Rosenberg, 1970].

<sup>1</sup>Rosenberg in a recent private communication has noted that his calculations of  $b_{\theta+}$ , related to solar wind velocity, are uncertain for this time period.

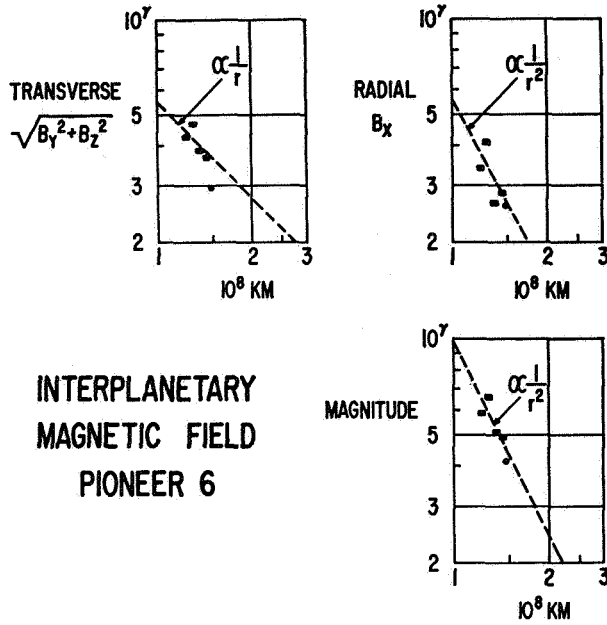


Figure 8. Average interplanetary magnetic field components as a function of radial distance from the sun. The dashed line is that magnitude expected for an Archimedes spiral field geometry. Each point is a 29-day average [Burlaga and Ness, 1968].

theoretical model. Burlaga and Ness observe that the measurements are consistent with Parker's model. Coleman and Rosenberg [1968] analyzed the radial variation of the interplanetary magnetic field between 0.7 and 1.0 AU with similar results.

Coleman *et al.* [1969] utilized the observations of Mariner 4 to ascertain the radial dependence of the field from 1.0 to 1.5 AU. Figure 9 from Coleman *et al.* shows the joint distribution of pairs of components at a radial distance of 1.5 AU and colatitude  $95.2^\circ$ . The distribution of field components appears to be rather similar to the distribution at 1.0 AU. Figure 10 shows the mean values they obtain for various field component magnitudes as a function of radial distance. The quantities  $B$ ,  $B_L$ ,  $B_p$ , and  $|B_r|$  compare well with the theoretical values from Parker's model. Coleman *et al.* also calculated the variation of many quantities according to the best fit to a function of the form  $C_0 r^k$ . Of interest are the exponents of the radial, azimuthal, and north-south components of the magnetic field. In accordance with a "frozen-in" field and a uniform radial velocity flow these values should be  $-2.$ ,  $-1.$ , and  $-1.$ , respectively. Coleman *et al.* calculate values of  $-1.46$ ,  $-1.27$ , and  $-1.29$  with RMS deviations near 0.02. Thus the exponent values for the three field components are

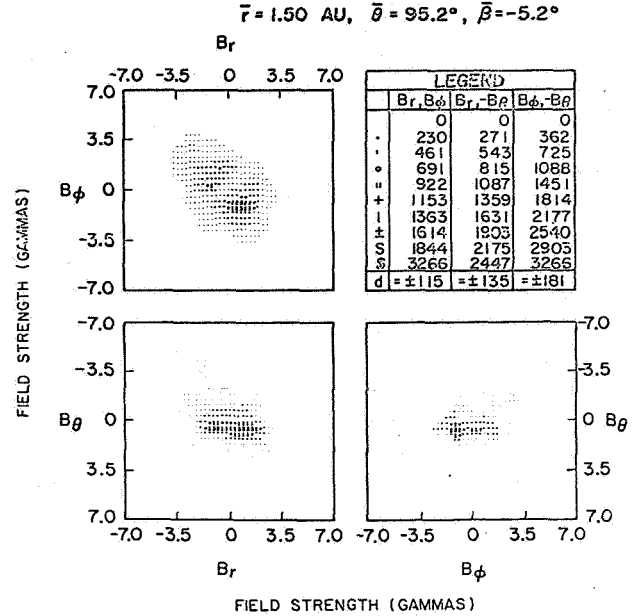
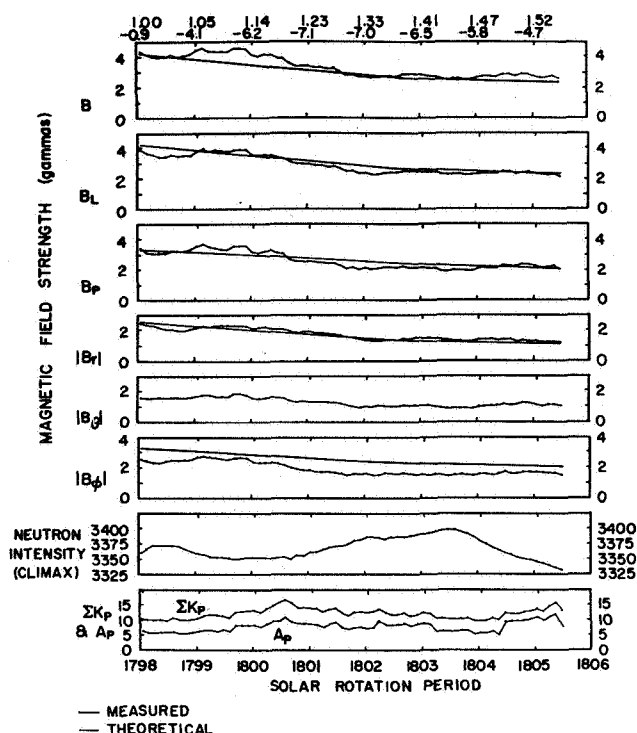


Figure 9. Joint distributions of pairs of component variables from measurements taken near 1.5 AU, Bartels' solar rotation 1804, May 22-June 17, 1965 by Mariner 4 [Coleman *et al.*, 1969]

nearly equal and are decreasing in a more isotropic fashion than would be expected for Parker's model. As was suggested by equations (4) through (8), the dyadic term  $\nabla \mathbf{V}$  can serve to alter the configuration of the magnetic field in the solar wind. If the velocity variations become sufficiently large, the magnetic field direction is altered according to equation (8) and the field does not point along the appropriate Archimedean spiral angle. This results in a randomizing effect on the field direction and thus a more isotropic behavior than Parker's model suggests.

This aspect of magnetic field behavior is apparent in the calculations of Coleman *et al.* concerning the field direction. They fit the tangent of the spiral angle with a function of the form  $C_0 r^k$  and obtain a value of  $k$  equal to 0.16 rather than 1.0. Thus, although the solar wind appears capable of orienting the interplanetary magnetic field in accordance with the spiral model out to 1 AU; beyond this point it becomes increasingly ineffective.

In these analyses of the variation of the interplanetary magnetic field with radial distance, temporal variations due to changing solar activity could cause effects which would apparently be related to radial distance. Coleman *et al.* attempted to remove this aspect of the problem by analyzing a data set with a low geomagnetic activity



**Figure 10.** Mean values of the magnitudes of various components used to describe the interplanetary magnetic field versus time, heliocentric range (AU) and solar latitude (degrees).  $B$  is field magnitude;  $B_L$  is the projection of the field on the  $r\phi$  plane and  $B_P$  is the projection of the field on the  $\theta\phi$  plane. Averages were taken over periods of one rotation of the sun. The time assigned to each solar rotation is the time of the middle of the rotation period. The smooth curves are values expected for an ideal spiral field. Averages of  $A_p$ , the daily sum of  $K_p$ , and the mean neutron intensity at climax are also plotted [Coleman *et al.*, 1969].

index, thus removing temporal variations by ensuring a somewhat uniform amount of solar activity. The results were nearly equal to those obtained with the entire data set, suggesting that the interplanetary field variations observed were indeed mainly due to radial influences.

It thus appears that the magnetic field components obey the Parker spiral model quite well from 0.7 to 1.0 AU. The magnitude of the field also decreases in accordance with the Parker spiral model from 1.0 to 1.5 AU. The directional aspects of Parker's spiral model appear not to be obeyed as well by the interplanetary magnetic field out to 1.5 AU. The field appears to become more irregular and chaotic. Processes occur that alter the direction of the magnetic field as it is convected outwards, and the random nature (and increasing strength as a function of radial distance) of these

processes may be responsible for the disagreements between the observations of Coleman *et al.* and Parker's idealized model. These processes may be waves, shocks, or high speed streams. Figure 30(h) showing "chaotic" fields may describe the behavior of the interplanetary magnetic field at a few AU.

In discussing the directional aspects of Parker's spiral model, it is worthwhile to note that Dessler [1967] reviewed the theoretical problems associated with any net southward or northward interplanetary magnetic field component. This has been a serious problem in that experimental observations suggest a net southward oriented interplanetary magnetic field of about  $1 \gamma$ .

## RELATIONSHIP TO SOLAR FEATURES

### Early Thoughts Concerning the Source of the Interplanetary Magnetic Fields

Parker's [1958, 1963] analysis appears to imply that the source of the interplanetary field is the general solar field. For mathematical simplicity, Parker assumed the solar field to be a dipole. Ahluwalia and Dessler [1962] suggested that the polarity of the interplanetary magnetic field might be related to the observations of the photospheric magnetic field. Inspection of solar magnetograms taken by Babcock and Babcock [1955] suggested to Ahluwalia and Dessler that the spiral field be divided into tubes of flux whose diameters range in size from 0.1 AU to 1 AU at the orbit of the earth. Each tube would contain only field lines of a single sense (toward or away from the sun).

### Direct Extension of Solar Fields: The Solar Magnetic Nozzle Controversy

The first evidence for a solar origin of the interplanetary magnetic field was obtained by Ness and Wilcox [1964]. They showed that the direction of the interplanetary magnetic field had a 27-day periodicity and that it correlated well with the average direction of the photospheric magnetic field during three solar rotations near the minimum of the last sunspot cycle. Although high correlations were found for many latitudes, the recurrence period of the interplanetary magnetic field suggested a source on the photosphere  $10^\circ$  to  $15^\circ$  from the equator. The large-scale "sector" property of the interplanetary magnetic field discussed earlier was also noted.

The large-scale sector ordering of the interplanetary magnetic field led Davis [1965] to suggest that the interplanetary sectors originated from small regions on the sun, essentially "nozzles," in which the field was essentially unidirectional. Wilcox [1968] supports a contrary position in which a "mapping" hypothesis

allows the sector to originate from large, well-ordered magnetic structures on the sun in which there is a tendency for each longitude near the sun to be connected to a longitude at the orbit of the earth by magnetic field lines.

The amount of "nozzling" or nonradial flow is an important concern. The maximum one might expect would occur if all the field lines from a sector originated in a single sunspot. This would be about a 1:3000 area expansion above that which would occur from direct radial flow. Thus the source of the undirected sectors was debated. Did they arise from a small-scale, large magnitude, undirected field on the sun or a large scale, weak field? The "source surface" model sheds some light on this question.

#### "Source Surface" and "Zero-Potential" Magnetic Models

Magnetic models have been developed by *Altschuler and Newkirk* [1969] and *Schatten et al.* [1969] that allow calculations of the coronal magnetic field from the observed photospheric magnetic field. Figure 11 from *Schatten et al.* [1969] is a schematic representation of these two similar models. The topology of the magnetic

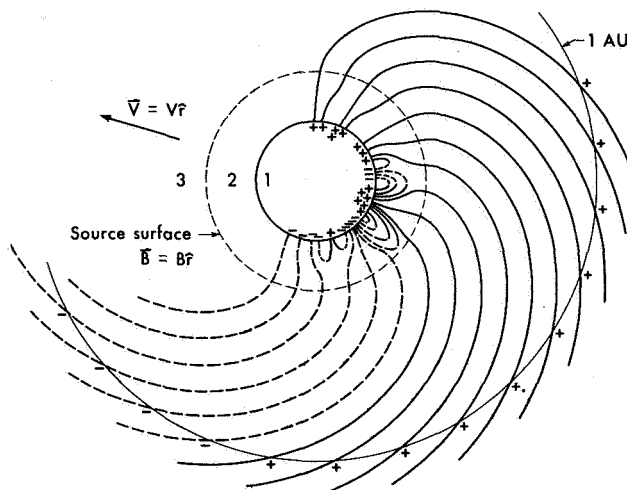


**Figure 11.** Schematic representation of the source surface model. The photospheric magnetic field is measured in region 1 at the Mt. Wilson Observatory. Closed field lines (loops) exist in region 2. The field in this region is calculated from potential theory. Currents flowing near the source surface eliminate the transverse components of the magnetic field and the solar wind extends the source surface magnetic field into interplanetary space. The magnetic field is then observed by spacecraft near 1 AU [*Schatten et al.*, 1969].

field in the solar corona as suggested by the magnetic models may be examined in figure 11. There are three distinct regions in these models where different physical phenomena occur. Region 1 represents the photosphere, where the magnetic field motion is governed by the detailed motions of the plasma near the photosphere. Above the photosphere the plasma density diminishes very rapidly with only moderate decreases in the magnetic energy density. This results in region 2, where the magnetic energy density is greater than the plasma energy density and hence controls the configuration. One may then utilize the force-free condition,  $\mathbf{j} \times \mathbf{B} = 0$ , and in fact make the more restrictive assumption that region 2 is current free. The magnetic field in region 2 may then be derived from a potential that obeys the Laplace equation  $\nabla^2 \phi = 0$ . The scalar potential may then be employed in this region. Substantially farther out in the corona the total magnetic energy density diminishes to a value less than the plasma energy density, and the magnetic field can no longer structure the solar wind flow. The magnetic field has, however, become oriented very much in the radial direction, as suggested by *Davis* [1965]. Thus, before the total magnetic energy density falls below the plasma energy density, a region is reached where the transverse magnetic energy density does so. It is the transverse magnetic field that interacts with the coronal plasma; a radial magnetic field would neither affect nor be affected by a radially flowing plasma. Regions 2 and 3 are separated by the surface where the transverse magnetic energy density falls below the plasma energy density. In region 3 transverse magnetic fields are transported away from the sun by the radially flowing plasma. Thus, fields transverse to the average Archimedean spiral geometry cannot exist in a quasistationary fashion, and the magnetic field passing through the surface boundary between regions 2 and 3 is oriented in approximately the radial direction, serving as a source for the interplanetary magnetic field.

Figure 12 is a synoptic chart of the photospheric magnetic field obtained by the Mt. Wilson Observatory for Carrington solar rotation 1496. The dark grey regions represent magnetic field into the sun and the light gray regions represent magnetic field out of the sun. The contours of the magnetic field calculated on the source surface are shown superimposed. At the bottom of the figure is a strip representing the sector pattern of the interplanetary magnetic field displaced by 5 days, the approximate transit time of the solar wind from the sun to the earth, and a graph of the interplanetary field magnitude.

The smoothing of the photospheric field to a more



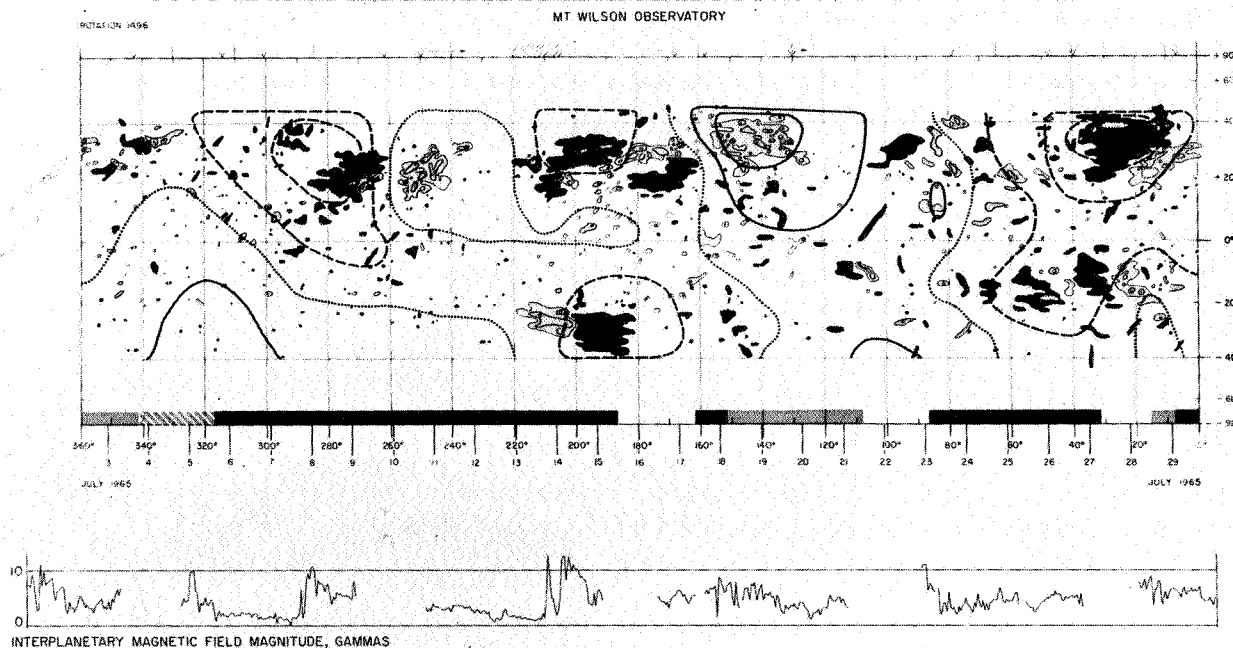


**Figure 12.** A synoptic chart of the photospheric magnetic field obtained by the Hale Observatory on Mount Wilson for Carrington solar rotation 1496. The dark gray regions represent magnetic field into the sun, the light gray regions magnetic field out of the sun. The contour levels are 6, 12, 20 and 30 gauss. Contours of the magnetic field on the source surface are shown. Dashed contours represent field directed toward the sun and solid contours, field directed away from the sun. Dotted contours represent regions of zero field. Contour levels are 0.25 and 0.75 gauss. Also shown at the bottom of the figure are the interplanetary sector structure and magnetic field magnitude displaced by 5 days. Toward sectors are represented by heavy shading, away sectors by light shading, and mixed polarity fields by diagonal shading.

sectorlike pattern on the source surface is evident. In the regions of the source surface where the field magnitude has reached the first contour level, the agreement with the direction of the interplanetary field is very good. The low magnitude of the interplanetary magnetic field from July 10 through July 14 may be related to the low field magnitude on the source surface at these times. On either side of this interval both the interplanetary and the source surface fields have larger magnitudes. Note that the photospheric field has scattered positive and negative fields over most ranges of longitudes, but the field computed on the source surface has a smoothly varying field quite similar in many aspects to the interplanetary sector pattern field. The large-scale features of the photospheric field appear to persist to the source surface and to be extended out by the solar wind. Correlations between the source surface field and the interplanetary magnetic field show definite peaks near 5 days time lag at all latitudes, whereas the

photospheric interplanetary field correlated poorly at this time. Comparisons of eclipse observations with computed magnetic field structures by Altschuler and Newkirk and by Schatten suggest that the magnetic models, although not perfect, do provide a first-order representation of the coronal and interplanetary magnetic field during quiet times. It has been recognized that flares can seriously disrupt the field patterns calculated.

The calculations of the coronal magnetic field allow the amount of nozzling to be estimated. Schatten [1968] estimated a 1:6 area expansion beyond that expected for radial flow as that typical of sectors during the 1965–66 period studied. The number calculated is not very accurate and probably varies significantly with time. However, the amount of nozzling calculated is not very large compared with the sunspot extension possibility, although it is certainly significantly different from a direct extension of the large scale field of the sun.

### "Mean" Solar Field Observations and Suggested Interpretation

Recently observations of a "mean" solar field (the sun seen as a star) have been made using the Crimean solar telescope [Severny, 1969]. The term "disk" field might have been a better notation for the observation as only the visible hemisphere of the sun contributes to the mean solar field. Severny *et al.* [1970] compared this observation with the interplanetary magnetic field (fig. 13). As can be seen, there is good agreement both in sign and magnitude. It is important to note that the interplanetary magnetic field is measured 4-1/2 days after the mean solar field to account for transport of the field from the sun to earth.

An interesting effect is that a cross correlation between the two fields provides high peak at a lag of 4-1/2 days, as expected, but also a larger peak at 27 + 4-1/2 days. Schatten *et al.* [1969] found this same effect earlier in other work and attributed it to a delay of approximately one solar rotation between the appearance of a new magnetic feature in the photosphere and the resulting change in the interplanetary sector pattern.

Severny *et al.* [1970] note that their work implies that large areas on the sun (mostly outside of active regions) have a field whose predominant polarity agrees with the interplanetary magnetic field polarity. This result is important in that it suggests that sunspots and most flares do not affect the interplanetary field structure substantially. In fact, they find an inverse correlation of sign of the sunspot flux with the sign of the mean solar field.

The high correlation that Severny *et al.* [1970] have found suggests that the interplanetary field at the earth in gammas can be predicted either 4-1/2 days or 31-1/2 days in advance from mean solar field measurements simply by multiplying the value of the mean solar field in gauss by 8.

Schatten [1970] has recently shown that the mean solar field-interplanetary field correlation may be explained from the coronal magnetic models. Figure 14 illustrates the manner in which the source surface model suggests the mean solar field-interplanetary field correlation. The observed mean solar field is an average of the photospheric field over the solar disk with an appropriate weighting factor. This factor is a function of the angle from a position on the photosphere to the subsolar point. The main contribution to this factor is a result of the difference between the magnetograph measuring the line-of-sight magnetic field and the angular distribution of the photospheric field (perhaps radial on the average). Limb darkening and effects of

sunspots (not seen by the magnetograph) are also contributing factors.

The source surface model implies that the interplanetary field near the earth results from the source surface field convected by the solar wind outward in about 4-1/2 days. Thus, the field at the earth is the extended field from position A in figure 14. The field at position A may be computed in this model as an integral of the photospheric field as follows:

$$\begin{aligned} B_{INT} &= B_n \sqrt{2} \frac{R_s^2}{(215 R_\odot)^2} \\ &= \frac{\sqrt{2}}{(215)^2} \frac{\int_{\text{sol surf}} B_n (R_s/R_\odot)^2 M d\Omega}{\int_{\text{sol surf}} d\Omega} \\ &= \frac{\sqrt{2}}{4\pi(215)^2} \int_0^\pi B_n \left(\frac{R_s}{R_\odot}\right)^2 M 2\pi \sin \gamma d\gamma \\ &= \frac{\sqrt{2}}{2(215)^2} \int_0^\pi B_{sf} (\text{weighting factor}) d\gamma \quad (9) \end{aligned}$$

where (weighting factor) =

$$-\sin \gamma \left(\frac{R_s}{R_\odot}\right) \left[ \frac{1 - (R_s/R_\odot)^2}{1 + (R_s^2/R_\odot^2) - (2R_s/R_\odot) \cos \gamma} \right]^{3/2}$$

The quantity  $B_{INT}$  is the interplanetary magnetic field,  $B_n$  is the magnetic field at position A in figure 14,  $B_{SF}$  is the solar field,  $R_s$  is the source surface radius, and  $\gamma$  is the angle from any point in the photosphere to the subsolar point. This integral also has a weighting factor as a function of angle from the subsolar point and was shown to be quite similar to the mean solar field integral. Thus, the agreement between interplanetary field and the mean photospheric field is partly due to the fortunate coincidence between the source surface weighting factor and the integrated line-of-sight disk factor.

### Effects of Active Regions.

Active regions can influence the interplanetary magnetic field in one of two ways. The first way is through a rapid dynamic process whereby a flare occurring within an active region ejects a plasma outburst with resulting shock effects. The second is through the gradual

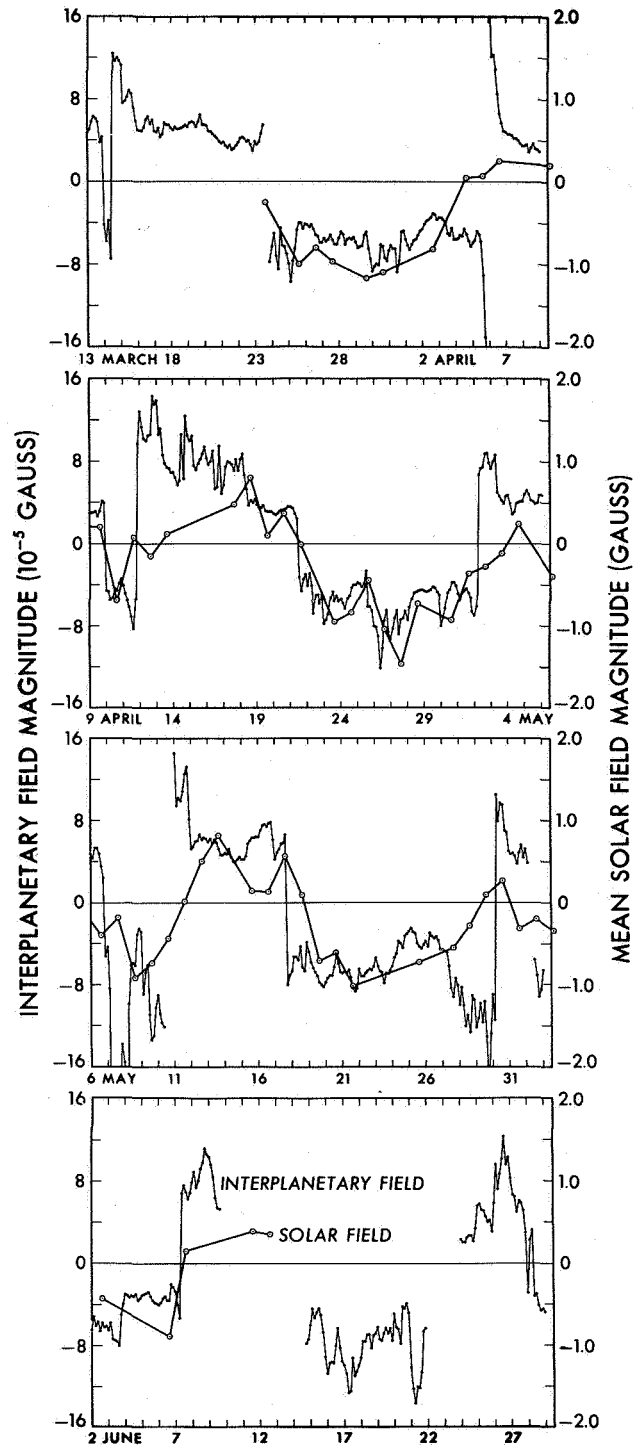


**Figure 13.** Comparison of the magnitude of the "mean" solar field and of the interplanetary field. The open circles are the daily observations of the mean solar field, and the dots are 3-hr average values of the interplanetary field magnitude observed near the earth. The solar observations are displaced by 4½ days to allow for the average sun-earth transit time. The abscissa is at the time of the interplanetary observations [Severny et al., 1970].

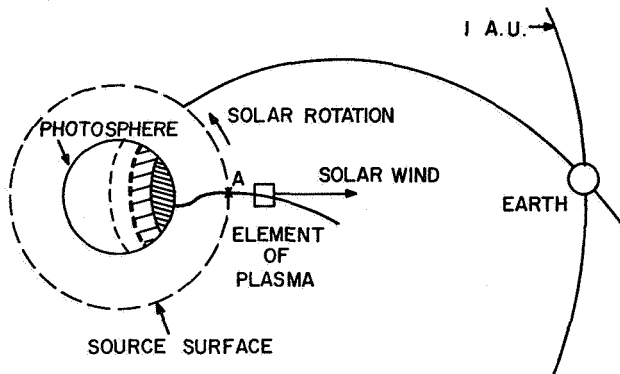


**Figure 14.** Relationship between the mean solar field, the source surface field, and the interplanetary field. The mean solar field is a weighted average of the disk field (indicated by the shading). The source surface field is the magnetic field on the source surface, position A. This is computed from a weighted average of the photospheric field, quite similar to the mean solar field. The solar wind convects this field to the earth in about 4½ days while solar rotation twists the field to approximate an Archimedes spiral as shown [Schatten, 1970].

evolutionary effect of the active region field upon the large-scale solar field accompanied by an evolving sector pattern.

**Influence of Flares** This first aspect suggested to Gold [1959] the possibility of magnetic tongues being ejected by active regions. Parker [1963] considered a blast wave model resulting in "kinked" azimuthally oriented fields due to the faster flare plasma. Taylor [1969] made a statistical study of shock surfaces and their relationship to solar flares. Figure 15 from Taylor shows the orientation of 8 probable shock surfaces relative to the flare position on the sun causing them. The dashed circle is a simplified picture of Hirshberg's [1968] large-scale shock structure. This line is an arc of a circle of radius 0.75 AU centered on the 0° line, 0.5 AU from the center of the sun. Many of the shock surfaces appear to be tangentially oriented to circles concentric with the one drawn. The shock surfaces imply that the radius of curvature of the shock front is less than, but of the order of 1 AU. All but shock surface 101a and 101b are consistent with the shock circle drawn. One of these, Taylor points out, is consistent with Gold's model and the other with Parker's. Needless to say, it would be beneficial to have several spacecraft widely separated in heliographic longitude to determine accurately the structure for individual events rather than relying on the statistical approach. Although shocks from flares appear to distort the plasma and magnetic field in a large region

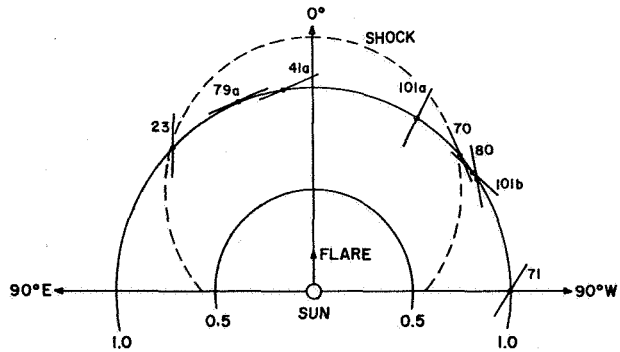


**Figure 15.** A plot of the orientation of eight probable shock surfaces at the eight appropriate heliocentric longitude relative to the flare. The dashed line is an arc of a circle of radius 0.75 AU centered on the 0° line 0.5 AU from the sun [Taylor, 1969].

of space, they generally do so only for a relatively short period of time.

**Evolutionary Influence** Figure 16 from Wilcox and Colburn [1970] illustrates the evolutionary changes of the interplanetary magnetic sectors over six years. The observed sector structure is superimposed on the daily geomagnetic character index C9. Near solar minimum, with few active regions present, the sector structure was quasistationary. With the rise of solar activity, the sector patterns began to evolve more rapidly, changing with periods of a few months. New sectors are occasionally born and others decay away. Near the maximum of the solar cycle, there appear to be two large sectors per rotation. Wilcox and Colburn note that even approaching the maximum of the solar cycle, the interplanetary magnetic field retains the property of almost always having the same polarity for several consecutive days. Changes in the sector pattern are often related to the birth or decay of a sector. A classic example of the process will now be reviewed.

The birth of a sector was recorded in November 1965 and traced to the later stages in the evolutionary development of an active region. Figure 6 showing the magnetic loops, represents the birth of these new field lines in space. Figure 17 shows the history of this region as ascertained by Schatten *et al.* [1968].

In the first solar rotation 1498 (fig. 17) one sees old background activity on the sun and toward-the-sun magnetic field present in the interplanetary medium and on the sun. In solar rotation 1499, the new activity is already present by the time the region appears at the east limb. At the central meridian passage of the region, sunspots, major flares, type III radio bursts, and strong coronal Fe XIV emission have developed, together with

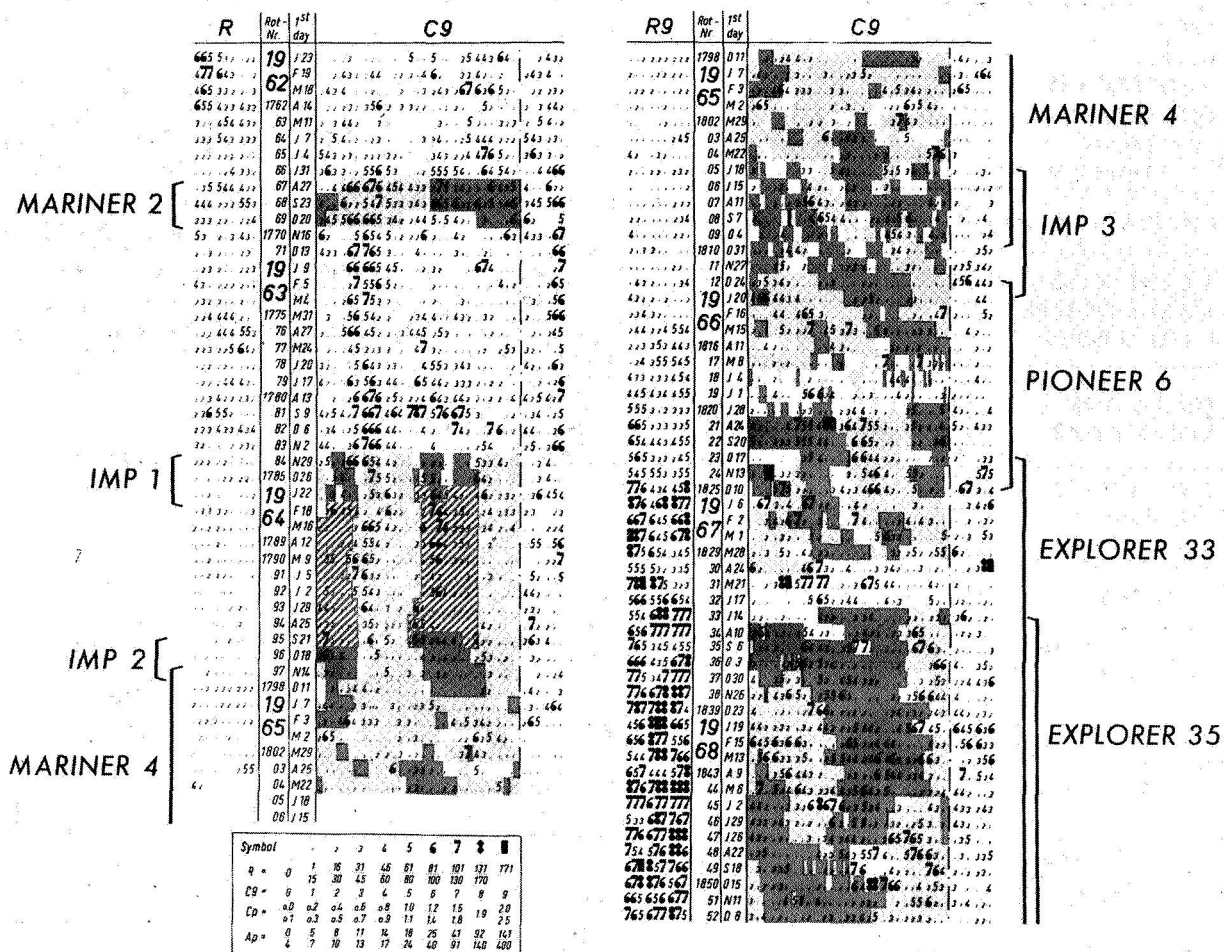


Figure 16. Observed sector structure of the interplanetary magnetic field, superimposed on the daily geomagnetic character index C9, prepared by the Geophysikalisches Institut in Göttingen. Light shading indicates sectors with field predominantly away from the sun. Diagonal bars indicate an interpolated quasi-stationary structure during 1964 [Wilcox and Colburn, 1970].

an extensive plage and bipolar magnetic region. The interplanetary magnetic sector pattern has not been altered appreciably. In solar rotation 1500 magnetic loops appear in the interplanetary medium while strong 5303 emission and a bright plage remain. The bipolar magnetic feature on the sun appears to have grown larger and there is evidence of a north-south filament running through the plage.

During the next solar rotation, 1501, a quasi-static, away-from-the-sun sector has developed in the interplanetary medium, accompanied by an elongation of the plage by differential rotation and a dispersal of the bipolar magnetic fields. It is interesting that the breakup of the bipolar group on the sun is associated with the formation of the away sector. The background magnetic

field on the sun now appears to be oriented away from the sun.

The away sector is seen in the interplanetary medium in solar rotation 1502 as well. The first contour level on the magnetogram has been omitted in this rotation due to increased noise in the instrument, and thus the solar magnetic observations are less accurate here. Other forms of solar activity have subsided.

Calculations of the flux in the magnetic loops show that in the few days in which the loops were seen in interplanetary space, they transported all the flux in the solar bipolar region. Thus the probability of seeing such an event for each occurrence is about 10 percent. Thus it is fortunate that this event was observed during the birth process. Other similar events would not be expected to

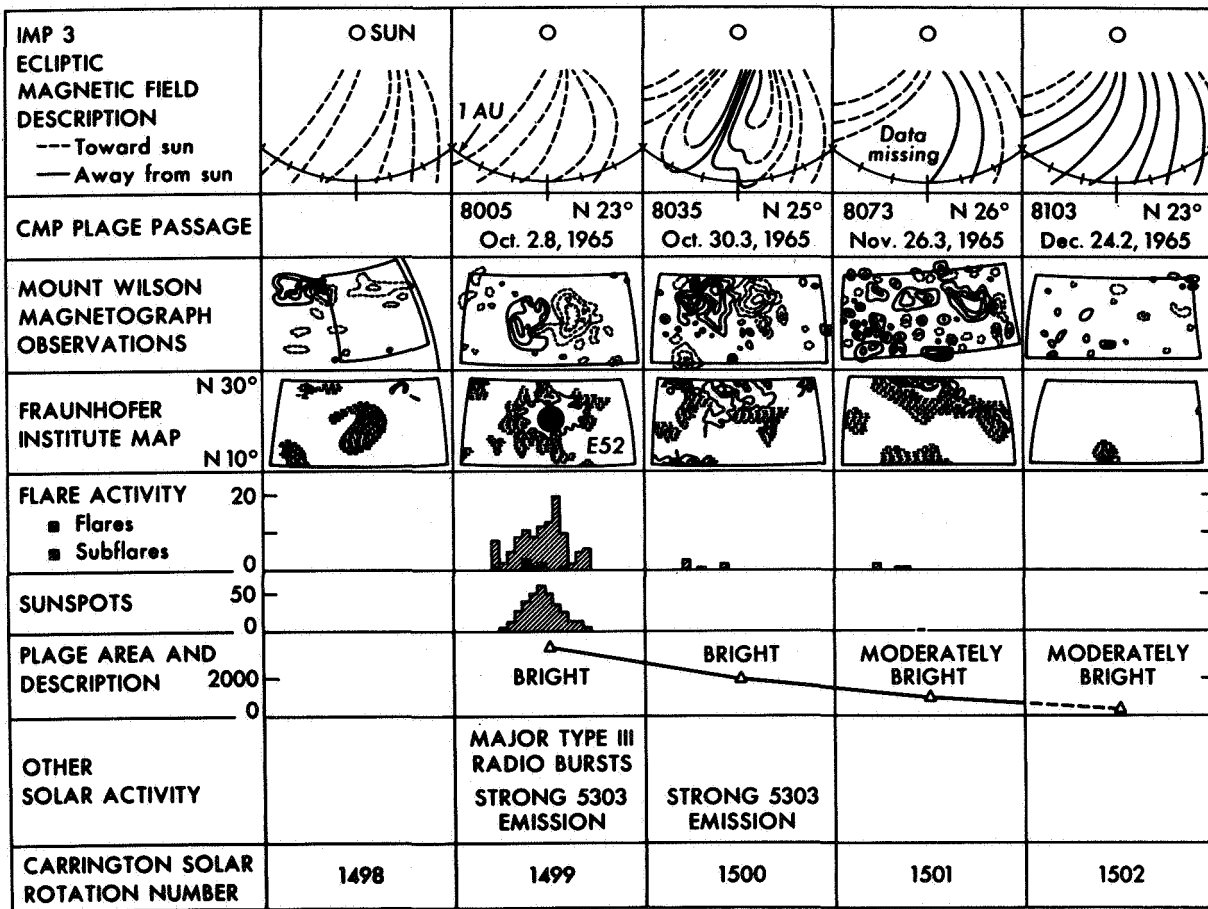


Figure 17. Chart showing the history of the active region associated with the interplanetary magnetic loop event. Each column shows the development of the feature during successive solar rotations. Each row describes different observations of the region. The figures are centered on the central meridian plage passage with the Mount Wilson magnetograph observations and the Fraunhofer Institute maps extending over a scale of  $40^\circ$  in longitude and  $20^\circ$  in latitude. The first contour level on the Mount Wilson magnetogram for solar rotation 1502 has been omitted due to an increase in noise during that time period. The plage area is graphed on a scale of millionths of the solar disk [Schatten et al., 1968].

be so well documented. The solar bipolar region was unusual in that the background flux changed sign from toward-the-sun to away-from-the-sun following the breakup of the active region. Bumba and Howard [1965] have shown that most bipolar magnetic regions do not affect the photospheric background field. The amount of flux transported from the bipolar region agrees with the flux observed in the new sector formed. Thus the birth of a sector appears to be the aftermath of the magnetic loop formation process in the interplanetary medium and is related to a change in the background field polarity on the photosphere.

#### Interplanetary Field near Solar Maximum

In this section several interplanetary magnetic field maps obtained near solar maximum are shown to illustrate the structural properties of the field due to solar activity.

The first solar rotation under discussion is Bartels' rotation 1843 (April 1968) shown in figure 18. This rotation is one of those discussed by Severny et al. [1970] where the "mean" solar field correlated well with the interplanetary magnetic field. As is typical of many of the rotations under consideration by Severny et al., the field patterns shown are relatively smooth and obey the Archimedean spiral configuration quite well.

The smooth field pattern is not related to any reduced amount of geomagnetic activity as shown by the indices C9 in figure 16. This period appears relatively placid in terms of sector fields. Thus solar activity at times does not appear to influence the large-scale interplanetary magnetic field structure near 1 AU.

One region of interest in figure 18 is the small 1-1/2 day wide sector of polarity toward-the-sun near day 101 (April 10) as shown in figure 13; it correlates with a negative field pattern on the sun and hence may be classified as a "filament" of solar origin, although it may be rather large for some definitions of "filament." It would be the smallest observed sector related to a solar feature, however. The distorted fields on days 112 and 113, probably represent some unknown field structures in space.

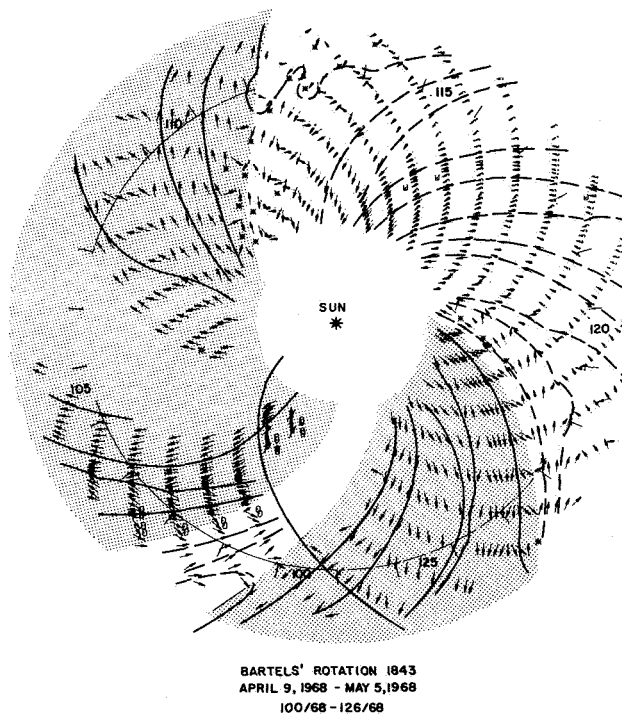


Figure 18. Interplanetary magnetic field map for Bartels' rotation 1843. The field patterns are similar to those observed by IMP-1 although the period is close to solar maximum [Severny *et al.*, 1970].

Figure 19 shows Bartels' rotation 1845 (June 1968). The first eight days of this rotation, still showing relatively placid field patterns, ended the studies of Severny *et al.* [1970]. Of greater interest here are the field patterns near days 180 and 174. These are similar to those one might expect for decaying sector fields. They are not, however, related to the disappearance of

any of the sectors in which they occur. In fact, the positive sector near day 160, showing no such field patterns, disappeared a few rotations later.

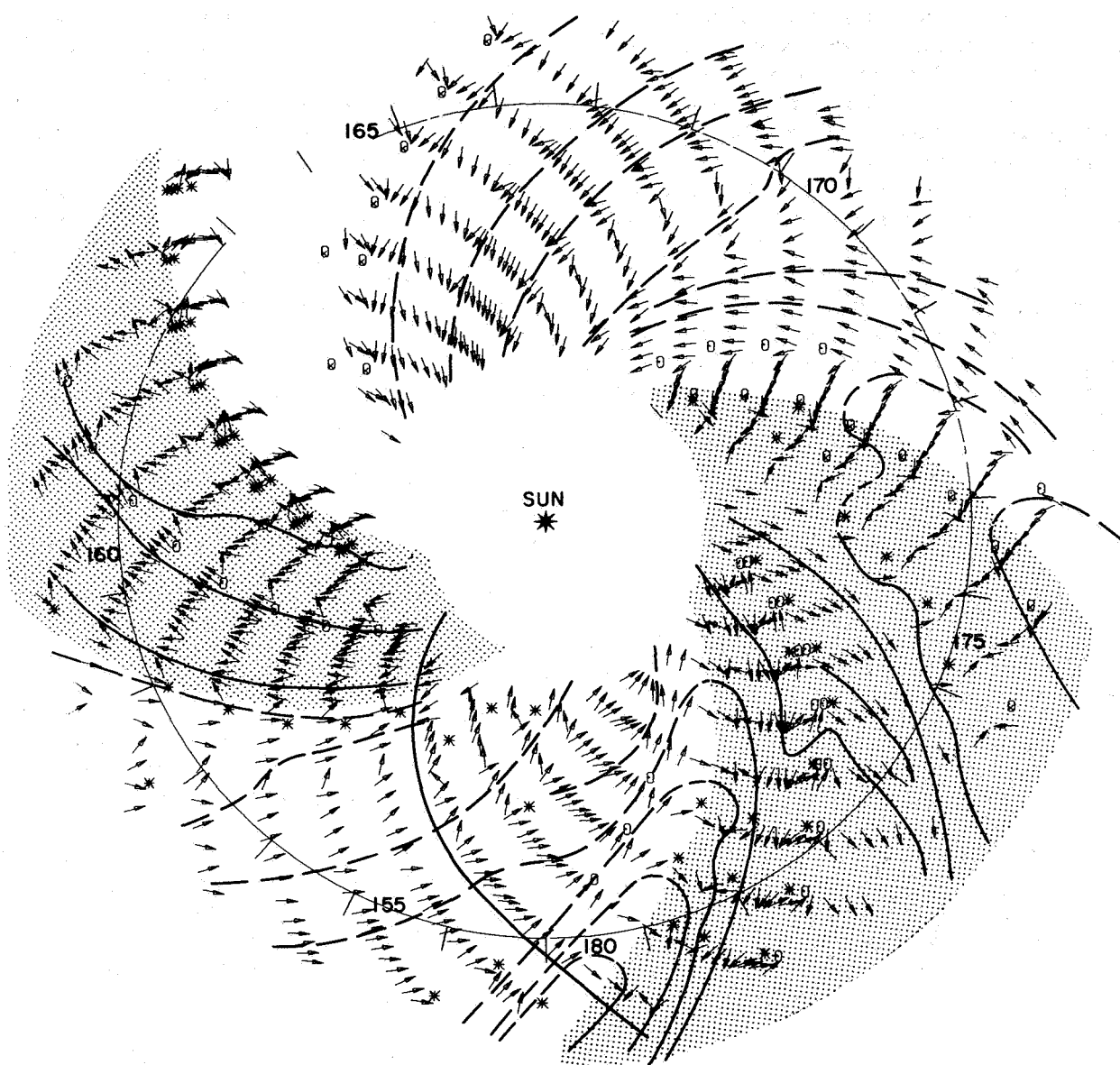
There is an unusual kink in the field on day 178 that probably is not well represented in this map, and on day 175 there are fields directly opposed to each other. These are probably dynamic events of one sort or another with a rather complex structure. The high field strength, chaotic structure beginning near the end of day 162 occurs simultaneously with a geomagnetic storm. It is thus clear that at times the field is non-Archimedean.

Figure 20 shows Bartels' rotation 1849 (September-October 1968); note the completely chaotic fields in one large portion. On days 270 through 276, the field can by no means be represented by a simplified model. It would probably require at least several spacecraft separated in solar longitude, latitude, and radial distance to attempt to unravel the field structures embedded in the solar wind on these days. Surprisingly, in the same rotation, near day 263, there is a perfectly smooth sector boundary repeated 27 days later.

Figure 21 shows details of the sector structure for 1968 from Fairfield *et al.* [1969]. During the times when the field is twisted in a non-Archimedean structure or is of a filamentary nature, it often appears on this diagram as small opposite polarity regions. As can be seen there are many such polarity filaments, but they are rather limited in time, and although few sectors can be found without them, they do not confuse the sector pattern. This illustrates what may be the major effect of solar activity upon the interplanetary magnetic field: occasional disruptions in the smooth Archimedean field pattern. Farther out in interplanetary space, the effects of these disturbances may be more pronounced with perhaps a significant influence on cosmic ray modulation. It is thus important to analyze the structure and evolution of these twisted field patterns. It will probably be necessary to utilize at least two spacecraft to disentangle the field structure.

### Solar Cycle Variations

In addition to the changing sector patterns throughout the solar cycle, other properties of the interplanetary magnetic field are somewhat altered. Figure 22 from Wilcox and Colburn [1970] shows the synodic rotation rate of the interplanetary magnetic field as well as the sunspot number as a function of time. These authors point out that near sunspot minimum the rotation period was close to 27.0 days and that with the rise of new high-latitude solar activity in 1965 the interplanetary field recurrence period increased to about 28.0 days. The period then declined to 27.0 days near solar



BARTELS' ROTATION 1845  
JUNE 2, 1968 - JUNE 28, 1968  
154/68- 180/68

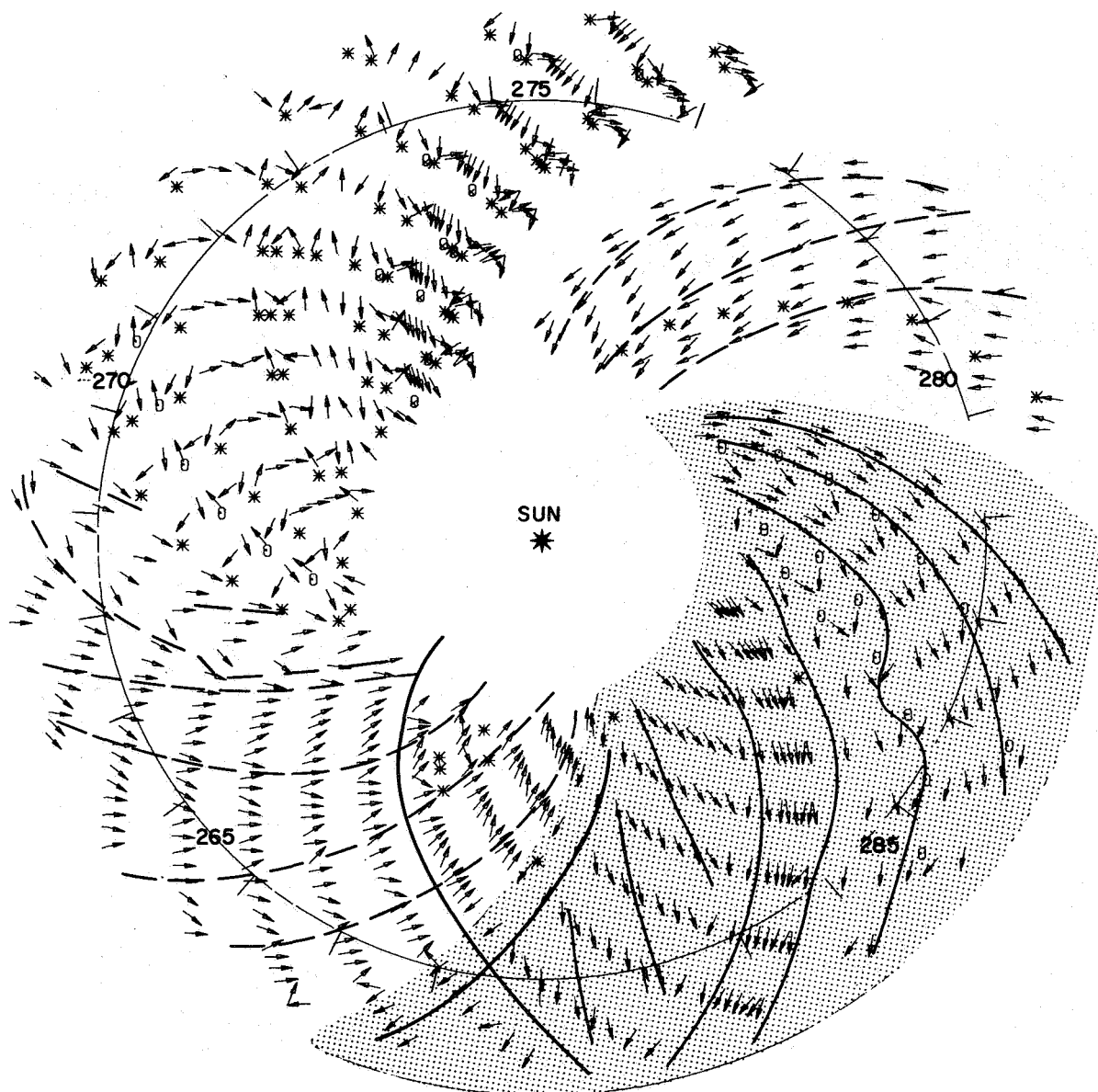
**Figure 19.** *Interplanetary magnetic field map for Bartels' rotation 1845. This figure shows looped field lines (near days 180 and 174) which appear to be in the process of being transported out of the interplanetary medium by the solar wind. This process may be related to sector decay [Severny et al., 1970].*

maximum. The authors suggest that the period will remain near 27.0 days until the increase of new sunspot activity near 1975. The data may be correlated not only with the period of the interplanetary field but perhaps also with the average latitude of the source of the field on the sun. This suggests the possibility that the source

of the interplanetary field in the ecliptic is a low-latitude source except when new activity is present and then the latitude is nearer  $25^{\circ}$ – $30^{\circ}$  heliographic latitude.

Hirshberg [1969] studied the average interplanetary magnetic field strength for a limited period and found no significant change. Figure 23 shows a more extensive





BARTELS' ROTATION 1849  
SEPT 18, 1968-OCT 14, 1968  
262/68 - 288/68

**Figure 20.** *Interplanetary magnetic field for Bartels' rotation 1849. Note the completely chaotic field structure at the top of the figure [Severny et al., 1970].*

analysis of the magnetic field magnitude distribution as a function of time. The top panel shows the field magnitude using hourly average IMP-1 data. The other panels utilize hourly average interplanetary magnetic field data from the Goddard Space Flight Center magnetometer experiments on Explorers 33, 34, and 35, which provided fairly complete coverage of the interplanetary field. There is a small shift in the distribution

towards higher field strengths as solar maximum is approached, but variability is not as large as the sunspot number. The average field strength changes from about  $4.5 \gamma$  in 1963-64 and 1965 to about  $6.2 \gamma$  for 1967-68, an increase of 38 percent. Part of this increase may be due to the use of field component averages to compare field magnitudes in the IMP-1 and Explorer 33 analyses whereas later results were based on direct field

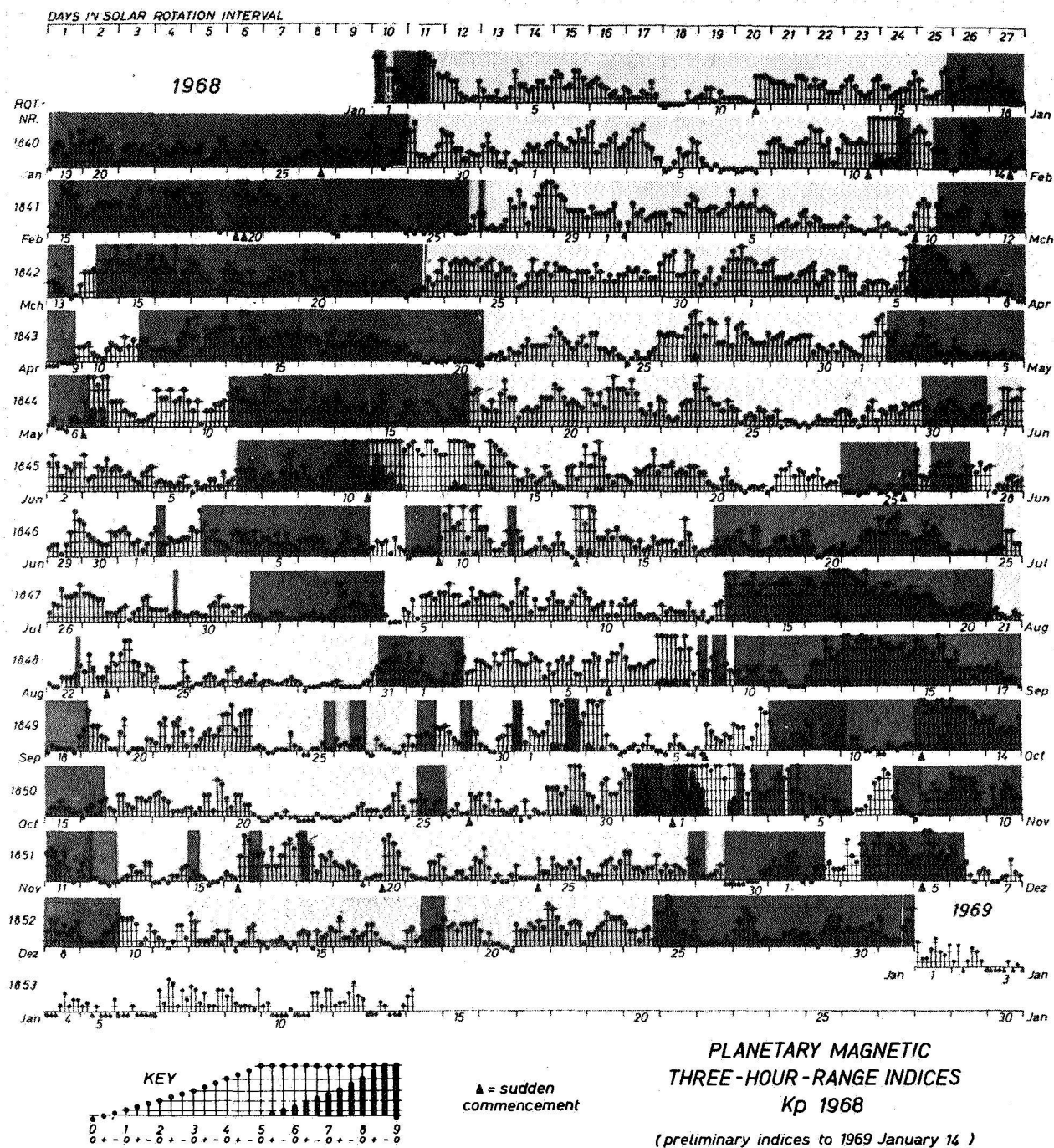


**Figure 21.** Interplanetary magnetic sector structure for 1968 overlayed on chart of planetary magnetic 3-hr-indices Kp [after Bartels]. The heavy shading represents magnetic field away from the sun, and the light shading, field toward the sun [Fairfield et al., 1969].

magnitude averages. Fairfield [1971] using IMP 3 obtained field magnitude averages of  $4.6 \gamma$  and  $5.7 \gamma$  for observations and employing only component averages 1965 and 1966, respectively. These results imply that

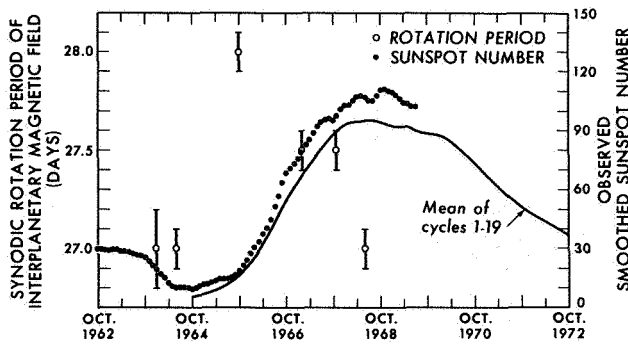


**Figure 22.** Synodic rotation period of the interplanetary magnetic field and sunspot number as a function of time [Wilcox and Colburn, 1970].

the observed variations in figure 23 are real. The dashed line distribution for the IMP 1 time period from Ness *et al.* [1965] corresponds to the 3-hr field magnitude average computed from 5.46-min field magnitudes rather than field components. The average is shown by the  $\langle F_{3H} \rangle$  symbol. The  $\langle F_I \rangle$  symbol represents the average instantaneous magnetic field from Ness [1970b] obtained at 20.5-sec intervals.

It is interesting to compare these changes in the interplanetary field magnitude with the changes in the solar field magnitude. Figure 24 shows the large-scale solar magnetic field [Howard *et al.*, 1967] near sunspot minimum (top) and near sunspot maximum (bottom). The top panel contour levels are 4, 8, 16, 24, and 50 gauss, and the bottom panels levels are 5, 10, 20, 40, and 80 gauss. Including the approximate 25 percent field magnitude increase in contour levels, and accounting for the data gap near September 16, 1968, there is approximately twice as much photospheric flux at solar maximum as at solar minimum. This number is very uncertain due to the month-to-month variation in the solar field. Thus the 38 percent increase in interplanetary field magnitude, although by no means insignificant, is small compared with the crude estimate of a 100 percent increase in average photospheric field strength for the same period and the change in sunspot number from 10 to 110 throughout this solar cycle.

An examination of figure 23 shows that the high field strength tail of the distribution is significantly enhanced. It appears that increased solar activity does not influence the field magnitude distribution very much but is associated with occasional enhancements in field strengths greater than 10  $\gamma$ . Figure 25 shows the percentage of the time that the field magnitude was greater than 10  $\gamma$  for each of the time periods in figure 23 along with sunspot number. The vertical error bars

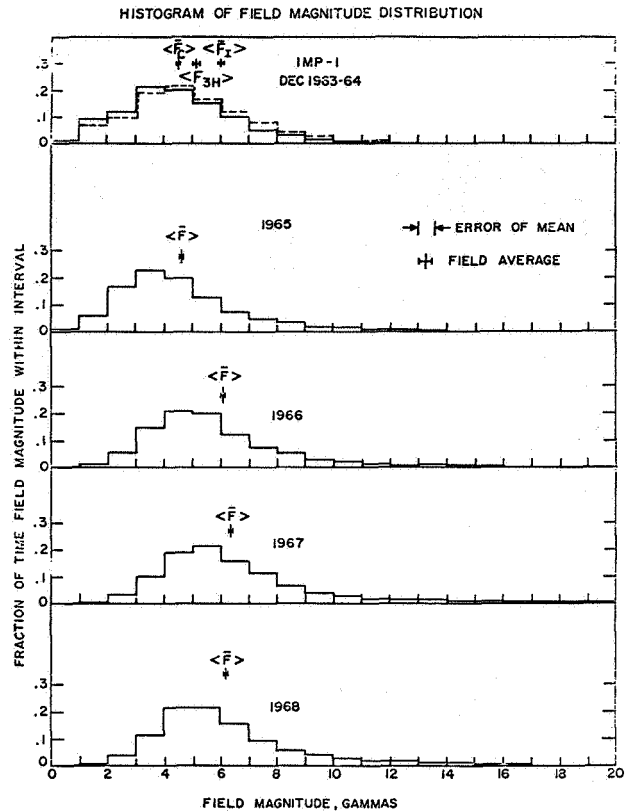


**Figure 23.** Interplanetary magnetic field magnitude distribution as a function of time. Average field magnitude is shown by the symbols. Somewhat different data processing has occurred throughout the years discussed in the text. Note the change from 1965 to 1966.

along the 1963–64 result suggest variability due to different averaging methods. The  $I$  shows the effect of using instantaneous field magnitudes. The increase in this value is due to not averaging high field strengths with low ones. Surprisingly, the high field magnitudes show variability similar to sunspot number. Although the spacecraft used and the data processing are not identical throughout the years shown, the results suggest that the magnitude enhancements are directly related to solar activity rather than differing data analyses. Many of the enhanced magnetic field magnitudes undoubtedly are also related to high speed streams and shocks, occurrences in the solar wind that may be related to solar “events.”

## RECENT DEVELOPMENTS, PROBLEM AREAS, AND FUTURE WORK

### Influence of Sun's Polar Fields on the Interplanetary Magnetic Field

Parker [1958] discussed the interplanetary magnetic

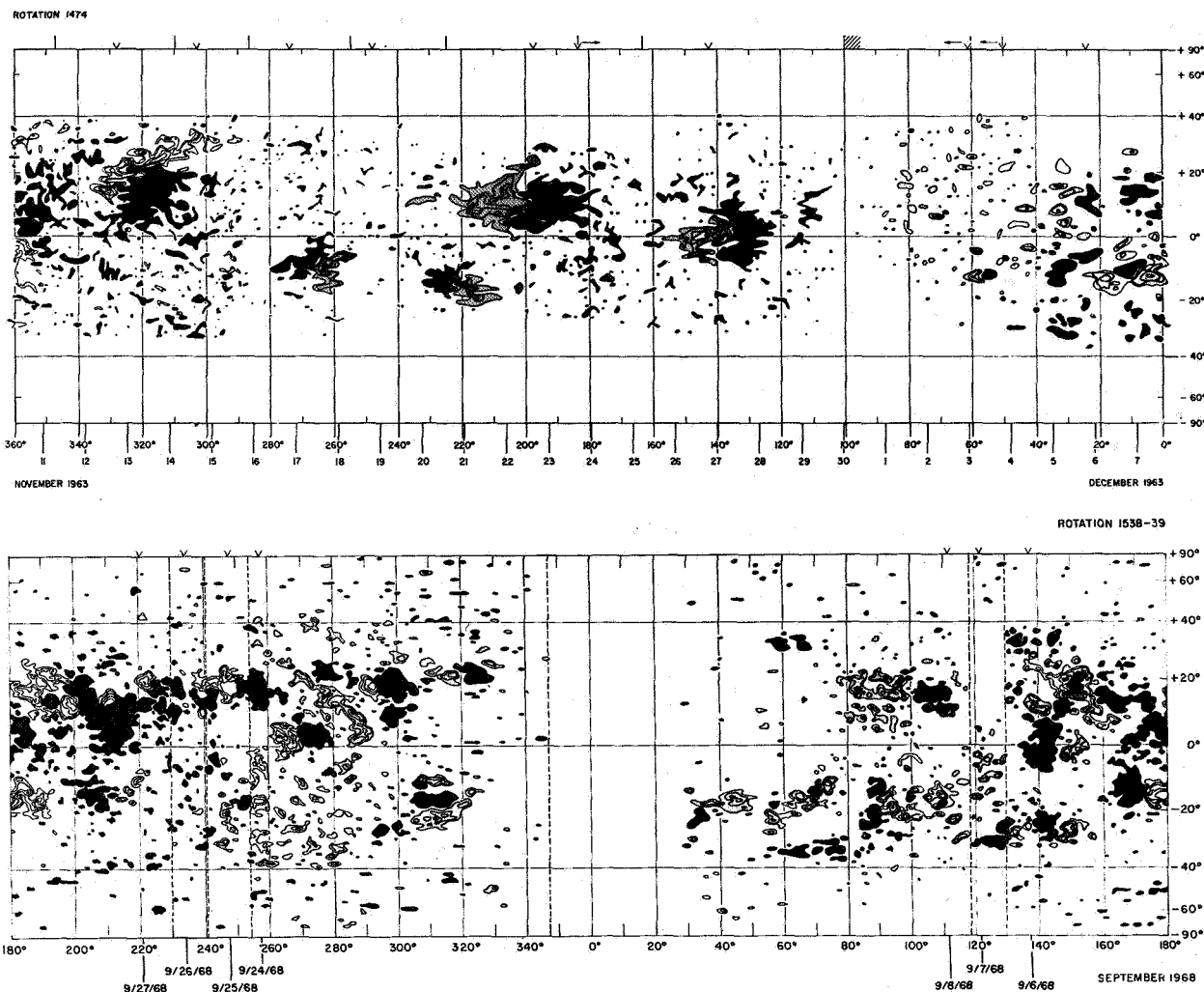


**Figure 24.** Two synoptic charts of the photospheric magnetic field obtained by the Hale Observatory on Mt. Wilson. One rotation is obtained near sunspot minimum (top) and one near solar maximum (bottom). There is a data gap near the center in the lower panel. The heavy shading indicates into-the-sun magnetic field and the light shading, out-of-the-sun field. The contour levels on the top panel are 4, 8, 16, 24 and 50 gauss and on the bottom, they are 5, 10, 20, 40 and 80 gauss [Howard et al., 1967].

field as an extension of the general solar field, which he assumed to be a dipole for mathematical simplicity. The analyses of Wilcox and Ness [1965] and Schatten et al. [1969] related the interplanetary magnetic field polarities to the predominant polarity areas of the sun's background field. The experimental results showed that the predominant polarity areas of the sun were exerting a greater influence on the interplanetary field polarities in the ecliptic than were the polar fields of the sun.

Recently, however, Rosenberg and Coleman [1969] have looked for an influence of the sun's dipole field

upon the interplanetary magnetic field in the ecliptic. Figure 26 shows Wilcox's [1970a] extension of their analysis. The percentage of time of negative (directed-toward-the-sun) interplanetary field polarity is plotted against time. A sine curve is fitted with a period of one year (shown). The resulting curve indicates a tendency for the interplanetary field to have negative polarity near the earth when the earth is at a positive heliographic latitude. This correlates with the sense of the sun's dipole field. Rosenberg [1970] suggests that this is not the influence of the observed high-latitude polar field

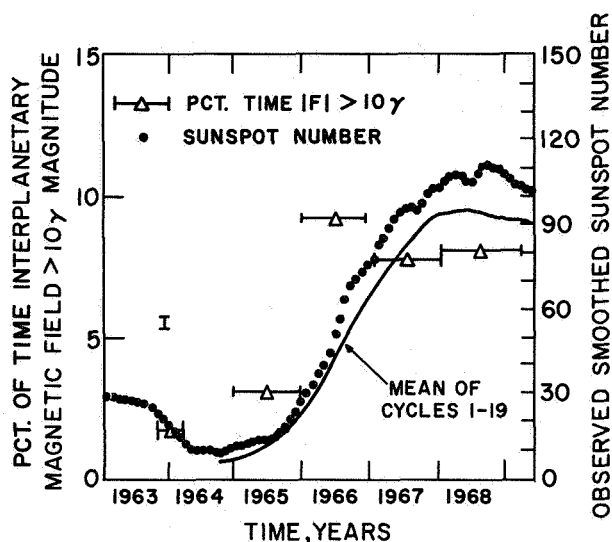


**Figure 25.** Percentage time the hourly average interplanetary magnetic field magnitude exceeds  $10\gamma$  and sunspot number as a function of time in years. The enhanced field magnitudes appear to be related to enhanced sunspot number and thus possibly to solar activity. The *I* refers to the instantaneous field exceeding  $10\gamma$ .

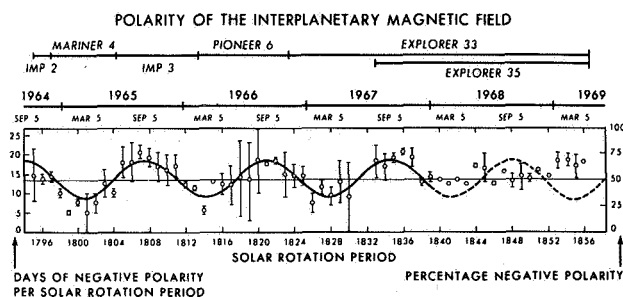


**Figure 26.** Interplanetary field polarity observed by spacecraft having nearly the earth's heliographic latitude. For each solar rotation period the lower bar is the actual number of days of negative polarity. The upper bar is 27 minus the number of days of positive polarity. The distance between the bars is the number of days of missing data. The sine function is the least-squares, best-fit function to the data (9.1 percent rms deviation) with a 1-yr period. The data for solar rotation periods 1795 through 1840 were used. This function is  $50.9 - 17.6 \sin(\omega t - 0.171)$ , where  $t$  is measured in terms of Bartels' solar rotations. This function leads by only  $5^\circ$  the heliographic latitude of the earth,  $\beta(t) = -0.73^\circ \sin(\omega t - 0.085)$ . Some of the Mariner 4 and Pioneer 6 data were taken at latitudes differing somewhat from that of the earth [Wilcox, 1970a].

but rather an unobserved extension of the polar field to lower latitudes on the sun (ecliptic latitudes). Wilcox [1970a] has questioned the statistical significance of Rosenberg and Coleman's [1969] result and provided additional data points (1968 and 1969 data) to their curve which fail to support their proposal. Two or three more years of data with a clear sense of the sun's polar field should provide a definite confirmation or rejection of the proposed effect.

### Structure out of the Ecliptic Plane

Perhaps the most important aspect of the field out of the ecliptic plane is the three-dimensional average field structure. In accordance with Parker's [1963] model, the magnetic field would be directed along Archimedean spirals wound on cones with a half-angle corresponding to the heliographic co-latitude. This would result in away-from-the-sun sectors possessing an average northward directed field component (if represented in solar ecliptic coordinates) above the solar equator. The sign would reverse for toward-the-sun sectors in the opposite hemisphere.

Another aspect of the field out of the ecliptic plane is the percentage of time spent in away-from-the-sun or toward-the-sun sectors. In the ecliptic plane they occur nearly equally. A consequence of Rosenberg and Coleman's [1969] proposal, should it be correct, relates to the polarity of the interplanetary magnetic field out of the ecliptic plane. They fit the percentage negative polarity to a sine wave as a function of time, implying a direct relationship with heliocentric latitude. The relationship they obtain is such that approximately 70 percent of the time a negative polarity should occur when the earth is at  $7.25^\circ$  north heliographic latitude. Considering a 50 percent probability occurs at zero latitude, this implies that the field is directed toward the sun 100 percent of the time at only  $18^\circ$  north heliographic latitude. Beyond this point, the extrapolation of their result obviously must end and in fact probably does so somewhat earlier.

The unidirected polar fields on the sun begin at higher latitudes near the locations of the polar prominence zones (located at  $+70^\circ$  and  $-55^\circ$  latitude during 1968). These higher latitude fields still show occasional regions of opposite polarity [Kotov and Stenflo, 1970]. Thus the explanation of the extended sun's polar fields to low latitudes would seem implausible. Independent of the origin of these magnetic fields close to the sun, an extrapolation of Rosenberg and Coleman's analysis, if valid, implies nearly unidirected fields at  $20^\circ$  heliographic latitude at 1 AU.

Wilcox [1970b] suggests a different view in which the

solar sector pattern of approximately equal and opposite fields occurs over a wide range of latitudes. Figure 27 shows a schematic of his model. A boundary exists

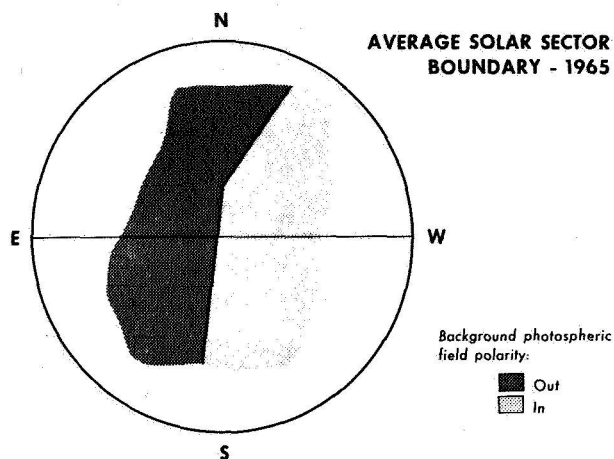


**Figure 27.** A schematic of Wilcox's average position of a solar sector boundary during 1965. On each side of the boundary the weak background photospheric magnetic field is predominantly of a single polarity in equatorial latitudes on both sides of the equator. This solar sector extends to latitudes near  $40^\circ$  or  $50^\circ$  [Wilcox, 1970b].

approximately in the north-south direction. The pattern exists over a wide range of latitudes on both sides of the equator. The boundary rotates in an approximately rigidly rotating coordinate system. The solar sector pattern is the source of a corresponding interplanetary sector pattern. It has nearly equal amounts of positive and negative field over a wide range of latitude. Thus if the Wilcox model is correct, one would not expect to find much change in the polarity pattern of the interplanetary magnetic field out of the ecliptic until at least  $40^\circ$  or  $50^\circ$  heliographic latitude, in contrast to the Rosenberg and Coleman [1969] analysis.

A compromise between the two proposals appears reasonable. Perhaps a gradually increasing percentage polarity change would occur, resulting in a nearly 100 percent unidirectional field not at  $20^\circ$  but more typically at  $30^\circ$ , subject to fluctuations with time. The unidirectional fields would occur at a lower latitude at times when the sun's polar fields were large (near solar minimum) and at higher latitudes when they were small (near solar maximum).

The coronal magnetic models might be related to this work. It is not necessary to require the sun's low-latitude polar field to extend to ecliptic latitudes in order to

explain Rosenberg and Coleman's observations. Figure 28 shows how polar fields, in accordance with the coronal models presented earlier, would provide a statistical influence on the field near the ecliptic. Some

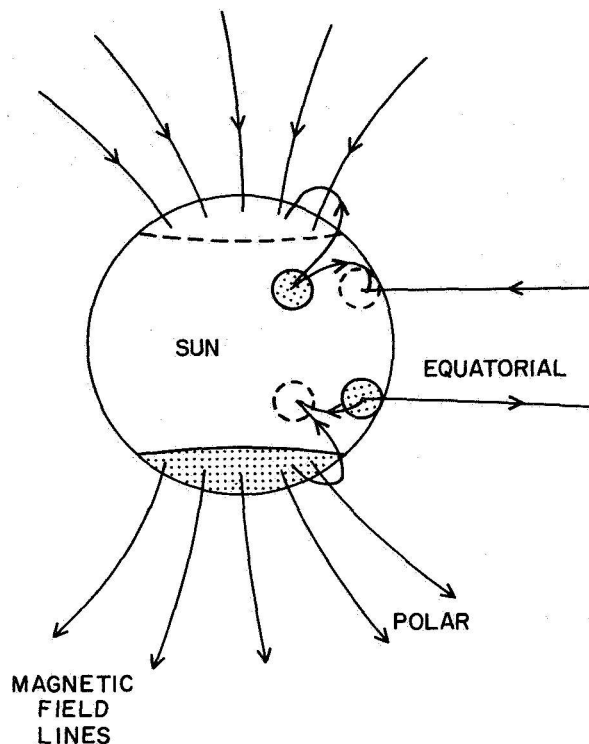


**Figure 28.** Schematic showing how polar fields can cause coronal magnetic loops to form which will influence the statistical distribution of toward-and-away-from-the-sun sectors at 1 AU with respect to heliographic latitude. Shaded areas represent out-of-the-sun magnetic field. In the northern hemisphere, coronal loops form allowing some magnetic flux to leave the positive (out-of-the-sun) magnetic regions and be directed into the negative polar field. This allows some negative flux to extend to 1 AU north of the solar equatorial plane. The situation is reversed in the southern hemisphere. This process allows Rosenberg and Coleman's hypothesis to be extended to higher latitudes and yet be consistent with the polar field being confined to the sun's polar regions as observed.

field lines in the northern hemisphere from the positive background field pattern would loop back to the northern polar fields, thus freeing additional toward-the-sun magnetic flux and allowing it the possibility of extending to 1 AU at positive heliographic latitudes.

The other possibility is that the high-latitude polar

fields occasionally do extend to low latitudes at 1 AU. Figure 29 from Schatten [1968] shows the structure of the solar eclipse of June 30, 1954, near the minimum of the solar cycle. The drawing was prepared by Kiev astronomers from photographs taken at Kozeletsk, USSR. Note the long equatorial streamers and polar

plumes. The bottom panel shows the field structure that would result from the source surface model with no equatorial magnetic field. Thus, with high polar field values and low equatorial field strengths, the polar fields appear able to reach to very low heliographic latitudes in the corona and presumably near 1 AU.

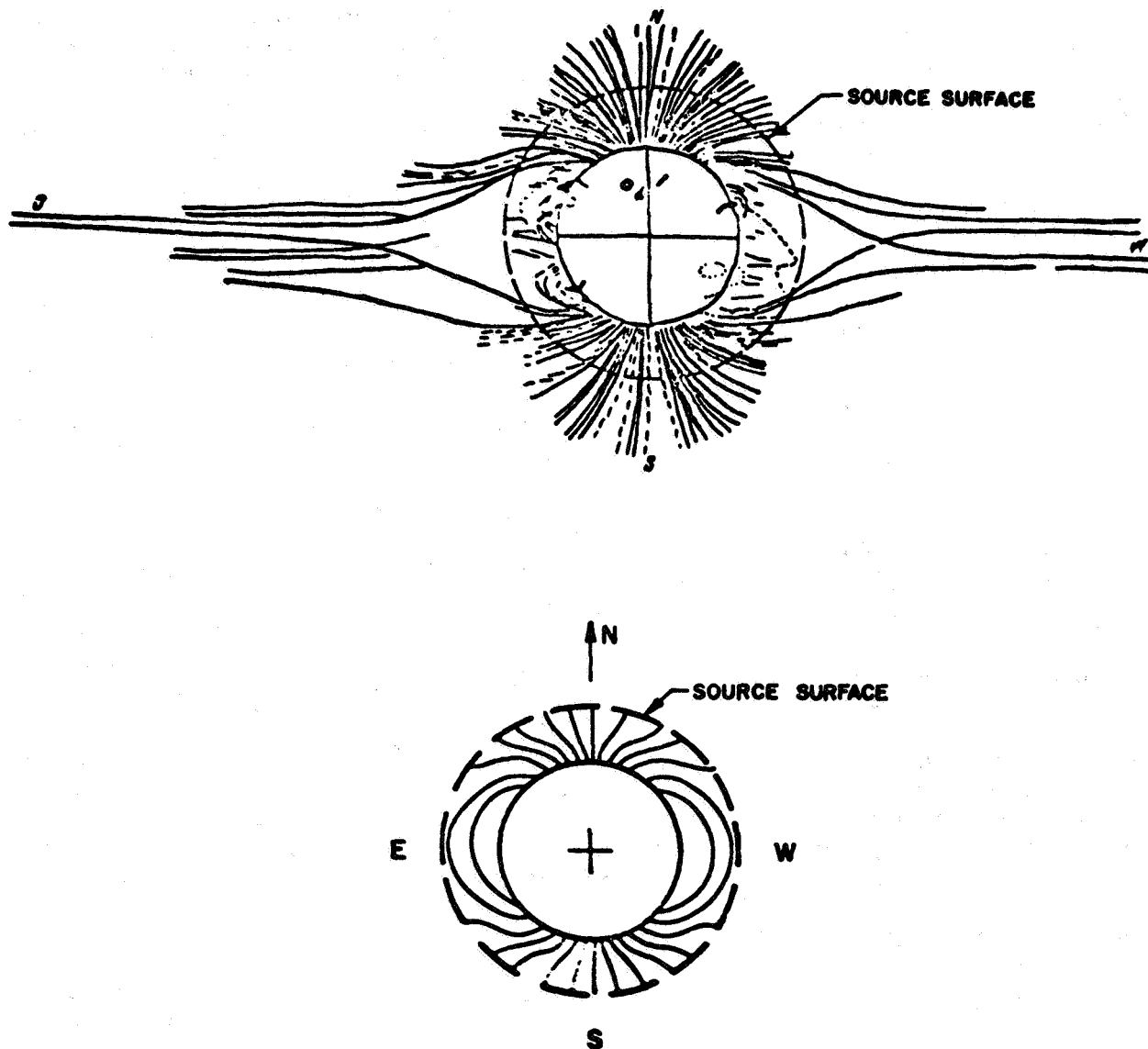


**Figure 29.** Drawing of the corona at the June 30, 1965 eclipse near solar minimum [Vseskhsvjatsky, 1963] (top). Appearance of the field line configuration in the corona using the "source surface" model with only polar fields present in the photosphere (bottom). These drawings show how the sun's polar field may extend to lower heliographic latitudes with increasing radial distance in the corona and the solar wind [Schatten, 1968].



### Hypothetical Interplanetary Field Structures

The interplanetary magnetic field may form rather unusual structures. Figure 30 shows several possibilities of interest. The first three are structures previously

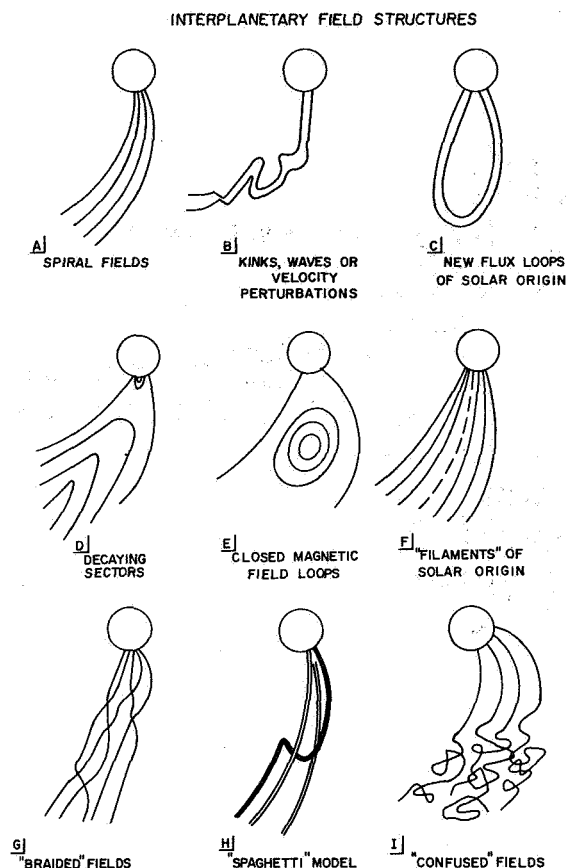


**Figure 30.** Schematic showing nine types of interplanetary magnetic field structures. The three in the first row have rather strong observational support. The remaining six are suggested field patterns that may occur but probably require several spacecraft or detailed observations to identify. Future work should be devoted to examining and classifying the observed interplanetary magnetic field according to these structures.

discussed. Structure (D) is the inverse process of structure (C) whereby field lines near sector boundaries can decay away through a magnetic reconnection process close to the sun (inside of the Alfvén point). Additional closed field lines in the corona result, along with a U-shaped interplanetary field pattern.

Structure (E) is similar to structure (D) in that magnetic

fields are decaying. However, in structure (E), the sector boundary itself may decay in many such closed magnetic field loops. This process may occur at 1 AU but may be more important farther out in the interplanetary medium where it could result in the dissolution of the sectors. Structure (F) shows a small negative field polarity embedded within a positive sector. Such a filament may represent a "kink" convected past the spacecraft or may be of solar origin as shown here.

Structure (G) is a schematic resulting from the work of Jokipii and Parker [1969]. Solar cosmic ray diffusion suggested that interplanetary magnetic field lines could be "braided" due to the granular and super-granular motions on the sun, causing the footpoints of the field lines to undergo a random-walk process. It might be possible to detect this "braiding" of field lines at 1 AU.

Structure (H) is the "spaghetti" model proposed by McCracken and Ness [1966] [see also Michel, 1967]. The main properties that distinguish this model from some of the previous ones are that "kinks" occur along a particular field line, which is braided with other non-kinked fields, and that the structures are discrete rather than continuous. If velocity perturbations in the solar wind are responsible for the kinks, one might expect all field lines in a particular region of space to be similarly distorted.

Structure (I) represents the ultimate effect of a nonuniform, radially flowing solar wind. The dyadic velocity term  $\nabla \mathbf{V}$ , which under a uniform flow results in the Archimedes spiral structure, now results in a "chaotic" field structure with the Archimedes spiral being obeyed weakly. The magnetic field becomes oriented in an almost isotropic distribution.

### Future Work

The important physical processes occurring in the solar wind plasma need to be tabulated and quantitatively treated. Their range of validity requires further study and they need to be brought together into a coherent entity. This concerns not only the large-scale field structure but the solar wind plasma as a whole: large-scale, small-scale, individual particle motions, waves, shocks, high speed streams, and so forth.

Many of the models discussed in this paper have received a certain amount of support, but by no means has any of them been shown to be completely valid 100 percent of the time. Many of the interplanetary magnetic field structures discussed earlier need to be sought, and much imaginative work, often with multiple satellite observations, will be required to uniquely identify some of the field structures proposed (and to separate temporal effects properly).

Classifying the interplanetary field in terms of



identified field structures rather than only "toward" or "away" sectors may aid our understanding of the relationship between the field and other phenomena. The relationship of these field structures to the sun needs further study, as does the propagation of both galactic and solar cosmic rays within them. The geophysical effects of various structures may also be important. The variation of the interplanetary magnetic field needs to be more closely related to solar wind plasma parameters and to changing solar conditions. The relationship between microstructure and mesostructure within the solar wind also needs study.

The magnetic field out of the ecliptic plane obviously requires observational work. Observations closer to the sun and farther from the sun than the earth, with a spacecraft located near earth as a monitor would provide useful results. In the near future, Pioneers F and G will explore interplanetary space farther from the sun and Mariner-Venus-Mercury and Helios will explore closer to the sun than has any previous spacecraft.

#### ACKNOWLEDGEMENTS

The author wishes to thank N. F. Ness, K. W. Ogilvie, D. H. Fairfield, R. P. Lepping, K. W. Behannon, and J. E. Schatten from the Goddard Space Flight Center, and J. M. Wilcox of the University of California Space Sciences Laboratory for discussions concerning the material and scientific aspects of this paper.

This work was performed under the auspices of the National Aeronautics and Space Administration.

#### REFERENCES

- Ahluwalia, H. S.; and Dessler, A. J.: Diurnal Variations of Cosmic Radiation Intensity Produced by a Solar Wind. *Planet. Space Sci.*, Vol. 9, 1962, p. 195.
- Altschuler, M.D.; and Newkirk, G. Jr.: Magnetic Fields and the Structure of the Solar Corona. *Solar Phys.*, Vol. 9, 1969, p. 131.
- Babcock, H. W.; and Babcock, H. D.: The Sun's Magnetic Field, 1952-1954. *Astrophys. J.*, Vol. 121, 1955, p. 349.
- Biermann, L. Z.: Kometenschweif und solare korpuscular strahlung. *Z. Astrophys.*, Vol. 29, 1951, p. 274.
- Bumba, V.; and Howard, R.: Large-Scale Distribution of Photospheric Magnetic Fields. *Astrophys. J.*, Vol. 141, 1965, p. 1502.
- Burlaga, L. F.; and Ness, N. F.: Macro- and Micro-Structure of the Interplanetary Magnetic Fields. *Can. J. Phys.*, Vol. 46, 1968, p. 5962.
- Coleman, P. J., Jr.; and Rosenberg, R. L.: The North-South Component of the Interplanetary Magnetic Field. *Inst. Geophys. and Planet. Phys., Univ. of California at Los Angeles*, Pub. 818, 1970.
- Coleman P. J., Jr.; and Rosenberg, R. L.: The Radial Dependence of the Interplanetary Magnetic Field: 1.0-0.7 AU. *Trans. Amer. Geophys. Union*, Vol. 49, 1968, p. 727.
- Coleman, P. J., Jr.; Smith, E. J.; Davis, L. Jr.; and Jones, D. E.: The Radial Dependence of the Interplanetary Magnetic Field: 1.0-1.5 AU. *J. Geophys. Res.*, Vol. 74, 1969, p. 2826.
- Davis, L., Jr.: Mariner II Observations Relevant to Solar Fields. *Stellar and Solar Magnetic Fields*, R. Lüst, ed., North-Holland, Amsterdam, 1965, p. 202.
- Davis, L., Jr.; Smith, E. J.; Coleman, P. J., Jr.; and Sonett, C. P.: Interplanetary Magnetic Measurements. *The Solar Wind*, Mackin and Neugebauer, eds., Pergamon Press, London, 1964, p. 35.
- Dessler, A. J.: Solar Wind and Interplanetary Magnetic Field. *Rev. Geophys.*, Vol. 5, 1967, p. 1.
- Fairfield, D. H.: private communication, 1971.
- Fairfield, D. H.; and Ness, N. F.: Magnetic Field Measurements with the IMP 2 Satellite. *J. Geophys. Res.*, Vol. 72, 1967, p. 2379.
- Fairfield, D. H.; Behannon, K. W.; and Ness, N. F.: Interplanetary Magnetic Field Polarity: 1966-1968. *Trans. Amer. Geophys. Union*, 1969, p. 300.
- Gold, T.: Plasma and Magnetic Fields in the Solar System. *J. Geophys. Res.*, Vol. 64, 1959, p. 1665.
- Hirshberg, J.: The Transport of Flare Plasma From the Sun to the Earth, *Planet. Space Sci.*, Vol. 16, 1968, p. 309.
- Hirshberg, J.: Interplanetary Magnetic Field During the Rising Part of the Solar Cycle. *J. Geophys. Res.*, Vol. 74, 1969, p. 5814.
- Howard, R.; Bumba, V.; and Smith, S. F.: Atlas of Solar Magnetic Fields. *Publ. 626, Carnegie Inst. Washington*, 1967.
- Jokipii, G.; and Parker, E. N.: Stochastic Aspects of Magnetic Lines of Force with Application to Cosmic Ray Propagation. *Astrophys. J.*, Vol. 155, 777, 1969.
- Kotov, V. A.; and Stenflo, J. O.: A Comparison of Simultaneous Measurements of the Polar Magnetic Fields Made at Crimea and Mount Wilson. *Solar Phys.*, Vol. 15, 1970, p. 265-272.
- McCracken, K. G.; and Ness, N. F.: The Collimation of Cosmic Rays by the Interplanetary Magnetic Field. *J. Geophys. Res.* Vol. 71, 1966, p. 3315.
- Michel, F. C.: Model of Solar Wind Structure. *J. Geophys. Res.*, Vol. 72, 1967, p. 1917.

- Ness, N. F.: Magnetometers for Space Research. *Space Sci. Rev.*, Vol. 11, 1970a, pp. 459-554.
- Ness, N. F.: *The Magnetic structure of interplanetary space*. Proc. XI International Conf. Cosmic Rays (invited papers and rapporteur talks). Publ. by Central Research Institute of Physics of the Hungarian Academy of Sciences, Budapest, 1970b p. 41.
- Ness, N. F.; Searce, C. S.; and Seek, J. B.: Initial Results of the IMP 1 Magnetic Field Experiment. *J. Geophys. Res.* Vol. 69, 1964, p. 3531.
- Ness, N. F.; Searce, C. S.; Seek, J. B.; and Wilcox, J. M.: A summary of Results from the IMP-1 Magnetic Field Experiment. GSFC preprint X-612-65-180, 1965.
- Ness, N. F.; and Wilcox, J. M.: Solar Origin of the Interplanetary Magnetic Field. *Phys. Rev. Let.*, Vol. 13, 1964, p. 461.
- Parker, E. N.: Dynamics of the Interplanetary and Magnetic Fields. *Astrophys. J.*, Vol. 128, 1958, p. 664.
- Parker, E. N.: *Interplanetary Dynamical Processes*. Interscience, N.Y., 1963.
- Rosenberg, R. L.: Unified theory of the interplanetary magnetic field. *Solar Phys.*, Vol. 15, 1970, p. 72.
- Rosenberg, R. L.; and Coleman, P. J., Jr.: Heliographic Latitude Dependence of the Dominant Polarity of the Interplanetary Magnetic Field. *J. Geophys. Res.*, Vol. 74, 1969, p. 5611.
- Schatten, K. H.: A "Source Surface Theory" Corollary: The Mean Solar Field-Interplanetary Field Correlation. *Solar Phys.*, Vol. 15, 1970, p. 499-503.
- Schatten, K. H.: Large-Scale Configuration of the Coronal and Interplanetary Magnetic Field. *Thesis*, Univ. California, Berkeley, 1968.
- Schatten, K. H.; Ness, N. F.; and Wilcox, J. M.: Influence of a Solar Active Region on the Interplanetary Magnetic Fields. *Solar Phys.*, Vol. 5, 1968, pp. 240-256.
- Schatten, K. H.; Wilcox, J. M.; and Ness, N. F.: A Model of Coronal and Interplanetary Magnetic Fields. *Solar Phys.*, Vol. 9, 1969, pp. 442-455.
- Severny, A.: *Nature*. Vol. 224, 1969, p. 53.
- Severny, A.; Wilcox, J. M.; Scherrer, P. H.; and Colburn, D. S.: Comparison of the Mean Photospheric Magnetic Field and the Interplanetary Magnetic Field. *Solar Phys.*, Vol. 15, 1970, p. 3.
- Taylor, H. E.: Sudden Commencement Associated Discontinuities in the Interplanetary Magnetic Field Observed by IMP 3. *Solar Phys.*, Vol. 6, 1969, p. 320.
- Vseskhsjatsky, S. K.: *The Solar Corona* edited by J. W. Evans, Academic Press, London, 1963.
- Wilcox, J. M.: The Interplanetary Magnetic Field: Solar Origin and Terrestrial Effects. *Space Sci. Rev.*, Vol. 8, 1968, p. 258.
- Wilcox, J. M.: Statistical Significance of the Proposed Heliographic Latitude Dependence of the Dominant Polarity of the Interplanetary Magnetic Field. *J. Geophys. Res.*, Vol. 75, 1970a, pp. 2587-2590.
- Wilcox, J. M.: The Extended Coronal Magnetic Field, to be published in the *Proc. NATO Advanced Study Inst.*, Athens, 1970b.
- Wilcox, J. M.; and Colburn, D. S.: Interplanetary Sector Structure in the Rising Portion of the Sunspot Cycle. *J. Geophys. Res.*, Vol. 75, 1970, p. 6366.
- Wilcox, J. M.; and Ness, N. F.: Quasi-Stationary Corotating Structure in the Interplanetary Medium. *J. Geophys. Res.*, Vol. 70, 1965, p. 5793.
- Wilcox, J. M.; Ritchie, A. D.; and Ness, N. F.: Movie of the Interplanetary Magnetic Field. *Space Sciences Lab*. Univ. California at Berkeley, Series 7, issue 53, 1966.

**DISCUSSION** J. M. Wilcox The question often comes up of how necessary it is to have continuing observations of the interplanetary medium. The error bars on figure 26 really represent missing days in each solar rotation. If one observes the entire 27-day rotation, then the error bar decreases to zero. If we had continuous coverage, then when these error bars dip down to zero, one would be in much better position to evaluate the proposed effect.

## THE INTERPLANETARY MAGNETIC FIELD *Leverett Davis, Jr.* An invited review

This paper examines the large-scale properties of the interplanetary magnetic field as determined by the solar wind velocity structure. The various ways in which magnetic fields affect phenomena in the solar wind are summarized. The dominant role of high and low velocity solar wind streams that persist, with fluctuations and evolution, for weeks or months is emphasized. High velocity streams are almost invariably identified with a single magnetic polarity, and most patterns of large scale, regularly recurring phenomena in interplanetary space are best organized by relating them to the high velocity streams. It is suggested that for most purposes the sector structure is better identified with the stream structure than with the magnetic polarity and that the polarity does not necessarily change from one velocity sector to the next. Several mechanisms that might produce the stream structure are considered. The interaction of the high and low velocity streams is analyzed in a model that is steady state when viewed in a frame that corotates with the sun. A number of observed features are well explained, but typically the regions of high plasma density appear to occur too soon. Long-term average deviations from the expected spiral structure have been reported. Those in the azimuthal direction should be explainable in terms of the mechanisms that transport angular momentum in the interplanetary medium. The meridional deviations identified by *Ness and Wilcox* [1964] and *Coleman and Rosenberg* [1970] raise serious difficulties that seem to require that we either modify the usual theoretical treatments significantly or question the data.

### ABSTRACT

### INTRODUCTION

The source of the interplanetary magnetic field is the solar magnetic field, in particular the photospheric field that is swept out by the solar wind. In the absence of the solar wind, the interplanetary magnetic field near 1 AU from the sun would be weaker by several orders of magnitude and would have a completely different configuration. Thus the field we observe owes its existence to the solar wind. Nonetheless, the interplanetary magnetic field plays a significant role in many of the phenomena associated with the solar wind. Therefore, let us first review briefly some of the situations in which the magnetic field is important.

1. The magnetic field organizes the plasma into a fluid in regions where collisions become unimportant, roughly beyond  $10 R_{\odot}$ . Thus, solar wind streams of different velocities cannot interpenetrate.
2. At distances larger than about  $20 R_{\odot}$  from the sun, the radial bulk velocity is greater than the Alfvén velocity and hence the energy density in bulk motion is greater than the magnetic field energy density. Thus signals cannot be propagated upwind toward the sun and the field structure near the sun is not affected directly by anything that happens farther out. The flow pattern determines the magnetic field structure and field lines near 1 AU are like paper streamers in a gale that mark the flow lines but do not determine them. Similarly, in and below the

---

*The author is at the California Institute of Technology, Pasadena, California.*

photosphere the energy density in bulk motion is usually greater than the magnetic field energy density, although here the determining factor is the independent photospheric velocity patterns, rather than the velocity with which the gas is rising up to supply the solar wind. Thus (except in sunspots) the magnetic field patterns observed in the photosphere may be regarded as produced by fluid motions that convect frozen-in field in response to mainly non-magnetic forces. But in the corona out to about  $20 R_{\odot}$  the magnetic field dominates the flow. Alfvén waves carry signals both inward and outward. The magnetic field pattern tends to require a rough balance of magnetic stresses (i.e., a force-free field), and the fluid flow tends to follow the magnetic field lines. Even in this region the plasma can have a significant indirect effect. Suppose small local pressure gradients stretch out an arched structure to the point where it is swept outward into a bipolar radial pattern leading out to the normal spiral pattern at large distances. This pattern will then be maintained right through the region where the magnetic field dominates because the upper and lower ends of the field lines are anchored in regions where the plasma dominates, and in the intermediate region the only effective magnetic forces merely compress the plasma in the interface between the field lines running in opposite directions. Thus a reliable calculation of the magnetic field at a distance  $1/2 R_{\odot}$  above the surface requires as boundary conditions a knowledge not only of the radial component of the field at the photosphere but also of which tubes of force extend to infinity and which return to the photosphere.

3. The magnetic field makes Alfvénic and magneto-acoustic waves possible. The energy in these waves is mainly convected, but to a smaller extent it is propagated. It can be converted to other forms of energy. Ways in which this wave energy and momentum can significantly affect the motion and other properties of the solar wind are discussed in chapter 5, p. 309).
4. The magnetic field profoundly influences the thermal conductivity and hence the energy flow in the solar wind.
5. The magnetic stresses are essentially as important as bulk motion in any discussion of the angular momentum transport of the solar wind.
6. Any anisotropy of the thermal gas or of the cosmic ray gas will have a high degree of axial symmetry about the direction of the local  $\mathbf{B}$ .
7. The irregular magnetic field, nonstatic in a frame

moving with the wind, is embedded in outwardly flowing plasma and partially screens galactic cosmic rays from the inner solar system. This can be described in terms of cosmic ray diffusion and energy change, processes that are important for both galactic and solar cosmic rays.

8. The interplanetary magnetic field is more easily observed than most other properties of the solar wind and provides valuable clues to other phenomena of interest.

### HIGH VELOCITY WIND STREAMS

For the purposes of this conference, the most important feature of the interplanetary region, at least between the orbit of Mercury and the asteroid belt, is the alternation between high and low velocity solar wind streams. Almost all other features except the basic average spiral pattern seem best organized by reference to the wind streams, and most are either dominated by or are greatly modified by the wind structure. The kinetic energy density in the solar wind is the largest energy density in interplanetary space, and the energy available from fluctuations in velocity is considerably larger than any other energy density.

Let us consider the evidence for the existence and nature of the solar wind streams. The Mariner 2 data on wind velocity in 1962 as observed by *Neugebauer and Snyder* [1966a] were presented at the first Solar Wind Conference in 1964. Mariner 2 was the first spacecraft to make such measurements completely removed from the influence of the magnetosphere, and it was clear at once that during the part of the solar cycle when these observations were made high velocity streams tended to recur at approximately the solar rotation period (figure 1). Hence it was argued persuasively that many such streams flow continuously, each from its own source on the sun, for periods of several months. The obvious changes in character of a stream from one appearance at a spacecraft to the next made it clear from the beginning that they were fluctuating and presumably evolving features. Half a solar cycle later, the Mariner 5 plasma data of Lazarus and Bridge shown in figure 2 reveal a somewhat different situation. In any single solar rotation the alternation between high and low velocity regimes is very similar to that observed 5 years earlier, but it is much more difficult to find any features that clearly repeat for several rotations. The streams clearly last a few days and presumably longer, perhaps a few weeks, but the whole stream pattern evolves substantially in a month or less.

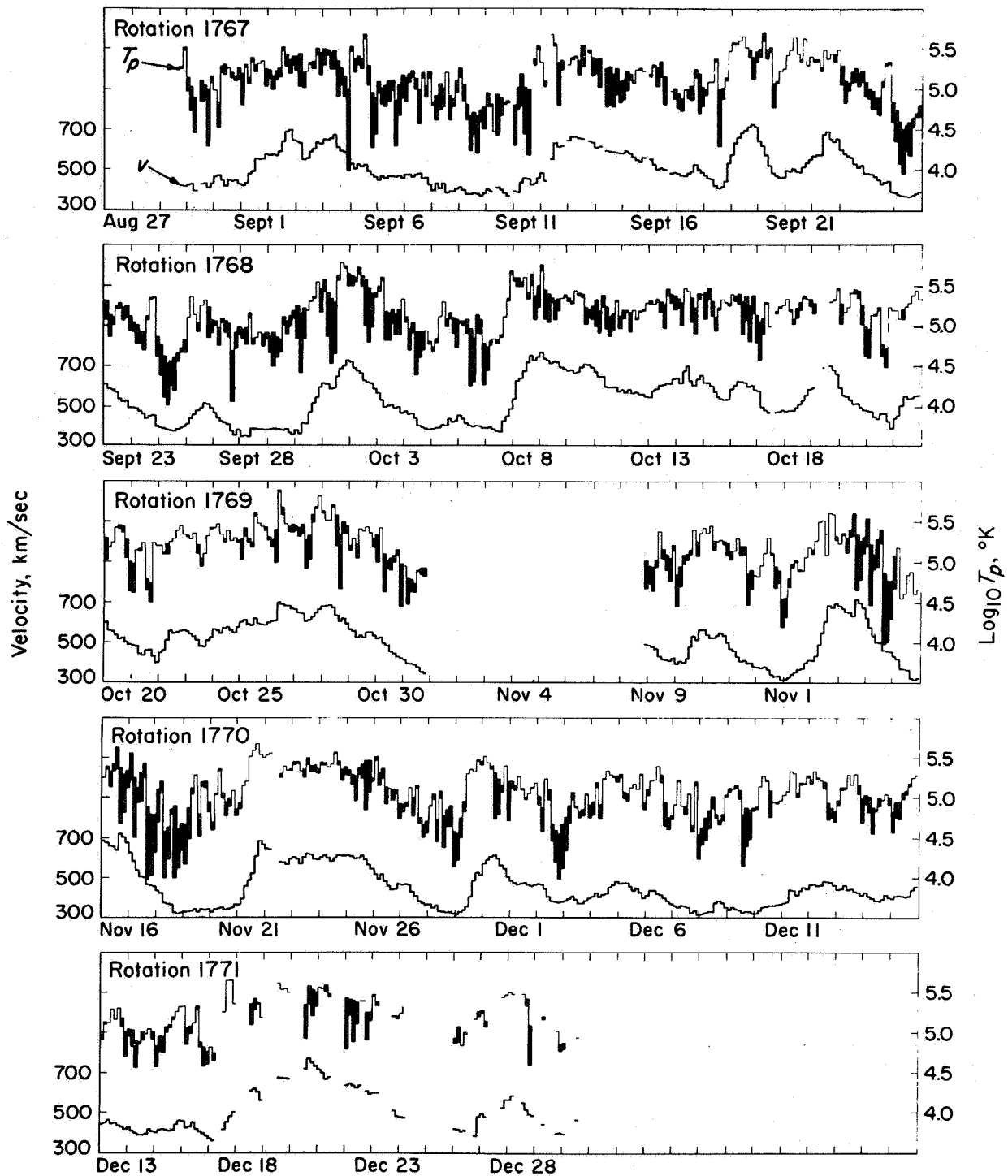


**Figure 1.** Three-hour average values of plasma velocity (lower curve) and proton temperature (upper curve, logarithmic scale) versus time from the Mariner 2 data for September through December 1962. Features on the same vertical line in the different panels are separated by multiples of 27 days [Neugebauer and Snyder, 1966b].

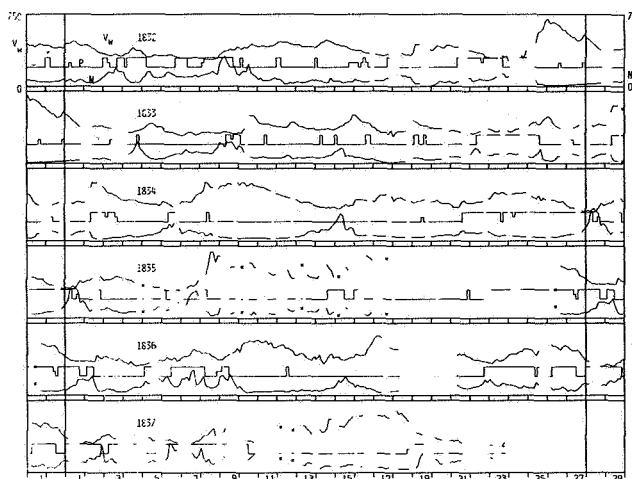


**Figure 2.** Three-hour averages of Mariner 5 data on plasma velocity,  $V_w$  (upper curve), proton number density,  $N$  (lower curve), and magnetic polarity,  $P$  (middle curve), where the upper level corresponds to positive (outward) polarity, the lower level to negative (inward) polarity, and the intermediate level to intervals when the polarity is not well defined. Each panel shows the data for one solar rotation plus two days overlap at each end. The abscissas are day number of the solar rotation; the time covered is June 15 through November 21, 1967 (solar rotations 1832–1837).

Summarizing these and other observations, one concludes that high velocity streams often persist for several months but also often change substantially from one solar rotation to the next. The low velocity is almost always somewhere near 300 km/sec while the high velocities typically range from 450 to 750 km/sec if we characterize them by 3-hr averages to suppress shorter period fluctuations. Because the low velocity regions seem more uniform in velocity than the high, and because any changes in the magnetic polarity usually occur in low velocity regions, we can think of the sun as having a more or less uniform low velocity steady state on which are superposed a number of high velocity streams. But it could well be the other way around, or the velocity distribution could just be irregular with no background and no isolated streams.

Our direct observations give information only on the streams coming from equatorial regions on the sun. Observations of comet tails demonstrates that the solar wind extends to high latitudes with apparently much the same properties as at low. Since it typically takes a particular velocity regime from 1 to 4 days to sweep past a spacecraft, we must think of streams as extending from  $15^\circ$  to  $60^\circ$  or more in solar longitude. We have no good

idea of how far they extend in solar latitude; the differential rotation of the sun might lead to the conjecture that the width in this direction is somewhat less, at least for long-lasting streams.

Let us now consider the relation of magnetic fields to these solar wind streams. The basic pattern of these fields in interplanetary space is the well-known spiral on which irregular fluctuations are superposed. The polarity of the field is said to be positive when the vector field is, on the average, directed outward along the spiral and to be negative when the field direction is inward. The polarity can fluctuate back and forth in a few hours but typically it stays the same for extended periods, for periods of four days, a week, or even two weeks (fig. 2). As demonstrated so beautifully by *Wilcox and Ness* [1965], this polarity of the interplanetary magnetic field correlates well with the observed polarity of the average radial field in the photosphere and hence shows that the spiral structure extends into the photosphere. From the observations near 1 AU or from the photospheric observations, we conclude that the polarity in the photosphere is patchy but that the regions of one polarity tend to be larger than individual high velocity streams. It was pointed out at the first Solar Wind Conference that at least one such stream always had the same polarity, and subsequent observations have confirmed that changes in polarity usually occur between high velocity streams and only rarely, if ever, in them.

Thus a model that seems very attractive is one in which there is an irregular distribution of high velocity streams over the surface of the sun, each stream situated in a larger region of one dominant polarity from the outer parts of which come low velocity solar wind. The polarity changes in an irregular way from one high velocity stream to the next, sometimes alternating, as in the IMP 1 data [*Wilcox and Ness*, 1965], and sometimes not, as in the Mariner 5 data shown in figure 2. Perhaps the polarities of the streams are distributed at random. It makes little difference to most phenomena whether or not the polarity changes between streams. The only obvious effect is on the nature of the presumably thin interface layer, which will consist of a current sheet when the polarity reverses and be very inconspicuous when it does not. Until we know more about non-equatorial regions, the assumption that the high velocity streams have the same distribution at high latitudes as at low is as plausible as any other. However, the magnetic polarity of polar streams seems unlikely to be as random as that of equatorial streams.

Like the origin of the solar wind, the origin of the stream structure will be found in conditions near the

surface of the sun. One suggestion is that the magnetic field patterns in the corona may act like nozzles of different degrees of divergence that produce streams of different characters. One can consider either an exaggerated or a mild form of this model. In the exaggerated form, all the wind might come from a small fraction of the surface area with small nozzles directed along the axes of the high velocity streams and the low velocity flow between them originating from the fringing field of the central part of the nozzle. This model has never seemed attractive since it does not easily explain the observed tendency for low velocity streams to have high densities and low proton temperatures. Also it is inconsistent with the observed relations between interplanetary and photospheric fields. In the mild version of the nozzle hypothesis there would be only a small variation in the ratio of the cross-sectional area of a tube of force at 1 AU to that at the photosphere. As Parker pointed out, this would introduce an extra degree of freedom into his equations for the solar wind, and would give a greater variety of solutions, facilitating the fit to the great variety of observations. In particular, it would make it easier to explain why high velocity regions do not have the highest densities as in simple models.

Alternatively, since the material in high velocity streams has greater kinetic energy and higher temperatures, one can argue that these streams arise where the energy supply to the corona is greater than normal. The source of coronal energy is believed to be waves that transmit mechanical energy from the photosphere to the corona, where dissipation converts the ordered motion into thermal motion. If the waves are stronger over active regions, then such regions should be the ultimate source of the high velocity wind streams. In considering which coronal regions get the maximum net energy supply, one must allow for the redistribution of energy by thermal conductivity. This is strongly modified by the magnetic field, whose structure will therefore modify the possible correlation between active regions and sources of the solar wind.

Recently, *Belcher* [1971] has demonstrated that high velocity wind streams near 1 AU are usually associated with Alfvén waves propagating outward from the sun. This association is evident in the Mariner 5 plasma and magnetometer data of figure 3, which shows the main features of 5 high velocity wind streams occurring in a 35-day period in 1967. Note from the bars between the  $N$  and  $V_w$  curves that each stream is associated with an enhancement of Alfvénic wave activity. It is possible that these waves are generated in the high velocity streams far from the sun, but then, as *Belcher* has pointed out, they should propagate both inward and

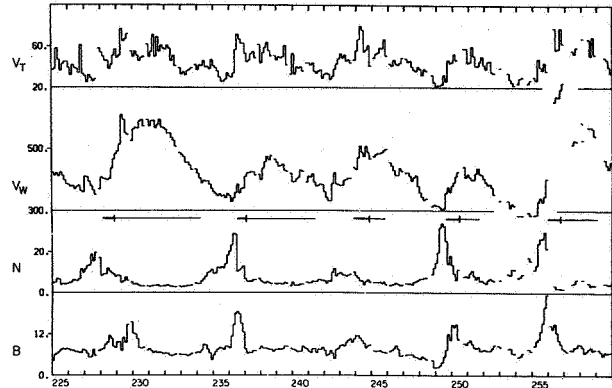


**Figure 3.** *Mariner 5 data for 35 days plotted using 3-hr averages and showing the large scale stream structure of the solar wind.  $B$  is the magnetic field strength in gamma,  $N$  is the proton number density in  $\text{cm}^{-3}$ ,  $V_w$  is the proton bulk radial velocity, and  $V_T$  is the most probable proton thermal speed, both in km/sec. The horizontal bars between the  $N$  and  $V_w$  curves show the times when Alfvén waves were prominent, the heavier bars to the left of the short vertical strokes identifying periods of the highest amplitude waves [Belcher, 1971].*

outward. Since the outward component is all that has been identified, he concludes that they are the remnants of waves that were present in the lower corona. He suggests that they may be the Alfvénic component of the waves that heat the corona and that it is to be expected that such remnants would preferentially be found in gas coming from the coronal regions receiving the greatest energy supply—i.e., the bases of the high velocity wind streams.

## SECTOR STRUCTURE

It is of interest to note how all the data in figure 3—the magnetic field strength, the plasma density, and the proton temperature—may be organized by correlation with the high velocity solar wind streams. This emphasis on the wind streams as the key to the organization of the data is very natural since they must provide the basis for the physical understanding of the phenomena shown. Historically this organization was first discovered and expressed as a correlation with the polarity of the magnetic field. After the initial work of *Neugebauer and Snyder* [1966a,b], the development of these ideas was dominated for several years by the beautiful work of *Wilcox and Ness* [1965] and their collaborators on the sector structure. They showed the connection between the magnetic fields observed in space and those observed in the photosphere. They showed how a great variety of phenomena could be organized on the basis of the sector

structure. They showed how, at times, the sector structure persisted for a number of solar rotations and how, at other times, as also emphasized by Coleman and his collaborators, there was substantial evolution of the polarity patterns from one solar rotation to the next. Much of this was discussed in the preceding paper.

Sectors were originally identified [Ness and Wilcox, 1964] by the polarity of the magnetic field. At that time, each sector contained one high velocity solar wind stream, i.e., the polarity changed from each stream to the next. A good deal of the time, perhaps the majority of the time, this is not the case. It seems clear that the basic physical structure is the high velocity wind stream, not the magnetic polarity. It is thus natural to question whether we should continue to identify a sector as a region of uniform magnetic polarity or as a region containing a single high velocity stream plus the appropriate surrounding low velocity boundary region. Identification by polarity is more useful if one's main interest is the correlation of interplanetary and photospheric fields or if it is the current layers and, perhaps, neutral sheets that separate regions of different polarity. For most other purposes, identification in terms of the velocity structure seems more useful. If it is decided not to use the term *sector* with this modified sense, and a term similar to *polarity region* for the original sense, then new terms should be devised. Perhaps *velocity sector* and *magnetic sector* would be appropriate. In any case, it seems safe to predict that the term identifying the high velocity streams will be more basic than that identifying magnetic polarity.

### COROTATING STREAM STRUCTURES

Now consider the interaction of these streams emitted with different velocities from different regions of the sun. Assume a steady state in which there are no changes with time. If the sun did not rotate, each stream would flow purely radially in a cone and, except for the shear between adjacent streams and possible pressure inequalities, there would be no interaction. But the sun does rotate and a nonrotating, slender radial cone that at one time starts from a low velocity source will, at a later time, be fed from a high velocity source. As time goes on, the high velocity plasma will overtake the slow, compressing the adjacent parts of both. Even if the sources on the sun do not vary with time, the flow pattern in an inertial coordinate system will. The velocity will be nearly radial everywhere, and the field lines will spiral.

It is instructive to consider all of this in a reference frame that corotates with the sun. In this frame, nothing appears to change with time, the velocity is truly steady state but nonradial. The stream lines coincide with the

magnetic field lines, which have the same spiral pattern as the inertial frame. Near the sun, all spirals are nearly radial; but far out the spirals of slow streams become flatter than those of fast streams. If there were no modification of the spiral patterns they would intersect. Since this is impossible, there is an interaction region where both spirals are deflected (fig. 4). The flow is still

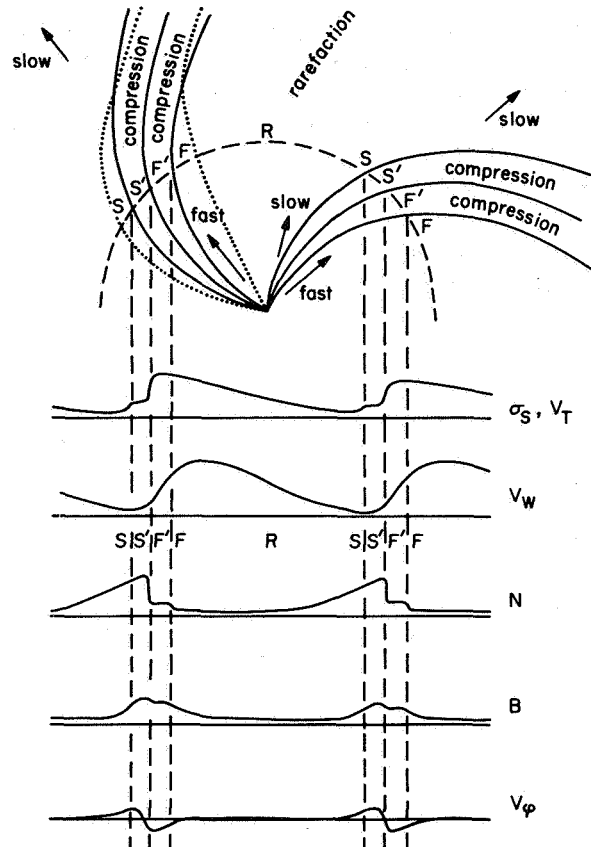


**Figure 4.** Top: two compression regions and one rarefaction region produced by the interaction of high and low velocity wind streams. Arrows indicate wind velocities in an inertial coordinate system; solid lines bound the various regions; dotted lines are field and stream lines in a system that corotates with the sun and in which the patterns shown are stationary. The circular dashed line at approximately 1 AU is the trajectory of an observing spacecraft in this corotating frame. Bottom: typical schematic curves showing, as functions of time, the changes in solar wind parameters as observed by the spacecraft.  $V_\phi$  and  $V_W$  are azimuthal and radial solar wind velocity components, respectively.  $B$  is the magnetic field strength,  $N$  the proton density,  $V_T$  the most probable proton thermal speed, and  $\sigma_S$  the square root of the sum of the variances over 5.04 min of the three orthogonal components of the field [Belcher, 1971].



steady state out along the magnetic tubes of force but as the gas passes a point where a tube is deflected, the gas is compressed and its velocity changes, becoming slightly nonradial. This happens both to the gas in the slow stream as it passes from region  $S$  to region  $S'$  in figure 4 and to the gas in the fast stream as it goes from  $F$  to  $F'$ . The farther out one goes from the sun, the larger is the fraction of the gas, and of the field lines, that have entered the interaction or compression region. Alfvén waves propagating outward from the sun will follow the field lines and go from  $S$  to  $S'$  as well as from  $F$  to  $F'$ , just as the gas does. Any waves generated at the interface will be swept into the compressed region by the supersonic flow (supersonic in the tangential if not in the normal direction) whether the direction of propagation is inward or outward along the field lines.

In constructing such a model [Dessler and Fejer, 1963] or drawing a figure, it is natural to introduce surfaces of discontinuity where the stream lines are deflected and at the interface between the fast and slow gas. The former should be shocks and the latter a contact surface through which neither plasma nor field lines penetrate and which has different tangential velocities on the two sides. However, such shocks are rarely, if ever, observed; instead, the transitions are gradual. In a way, this is not surprising since the transitions from low to high velocity on the sun must be gradual. It is not clear whether the velocity gradients are sufficiently small that they would not be expected to evolve into shocks by the time they reach 1 AU or whether various dissipative processes must be invoked to prevent the generation of a discontinuity. Even though the shock is replaced by a gradual but still short-scale transition, the integrations of the equations that yield the usual jump conditions across a shock should yield similar jump conditions across the transition region, and moderately large scale phenomena should be essentially the same as though there were a shock.

In the regions such as  $R$  of figure 4 where fast wind is radially outside slow wind, a gap would tend to form between the simple spirals. Actually, the magnetic and thermal pressures normal to the tubes of force cause them to expand and fill the region. Since the flow tubes will thus have larger than normal cross sections, the plasma density should be lowered.

Belcher [1971] and Belcher and Davis [1971] have used this corotating, steady-state model to analyze the magnetometer and plasma data from Mariner 5. This model turns out to be very helpful in understanding what can be understood and in showing clearly what some of the puzzles are. If the top half of figure 4 is regarded as corotating with the sun, then an observing

spacecraft will appear to move along the circular dashed trajectory with a period of about 27 days. If its observations are plotted as functions of time, one obtains the curves shown in the lower half of figure 4, correspondence with the model being indicated by the vertical dashed lines. The data plots shown are not those for any particular 10-day period but instead are schematic, smoothed curves showing features that Belcher finds to be typical for the entire 160-day period.

One of the interesting features is that the density ( $N$ ) starts to rise while the spacecraft is still in the slow region and before the velocity indicates that compression should start. It appears that the region of the sun near the source of a high velocity stream is influenced in such a way that it emits streams of higher density than normal. This might be expected if its temperature were higher than that in the center of the low velocity region. However, there is no evidence for similar phenomena on the other side of the fast stream; perhaps a better explanation should be sought. Note, however, that the region where the magnetic field strength is high fits much better the compression region defined by the velocity structure than does the density, which drops rapidly shortly after the velocity increase starts.

The thermal velocity of the plasma and the magnetic fluctuations with periods less than 10 min show approximately the same pattern and hence are represented by a single curve in figure 4. Both are much greater in the compressed high velocity gas than in the compressed low velocity gas, perhaps because the compression ratio should be higher in the high velocity gas than in the low because its original density tends to be lower. This partial summary should make it clear why so much attention is given to the influence of the high velocity solar wind streams in a discussion whose primary aim is an understanding of the interplanetary magnetic field.

Figure 5 shows 1 week of reasonably typical Mariner 5 data. Essentially all the phenomena seen more clearly in the schematic curves of the previous figure can be found here and in numerous other simple plots.

#### DEVIATIONS FROM EXPECTED SPIRALS

Parker's [1963] original discussion of the solar wind pointed out that a radially flowing, highly conducting solar wind ejected from a rotating sun would comb out any solar magnetic fields into spirals wound on circular cones whose vertices are the center of the sun, whose axes are the sun's rotation axis, and whose half angles are the polar angle of the source on the sun. Typical interplanetary magnetometer data for periods of a few hours show many fluctuations but little evidence for the

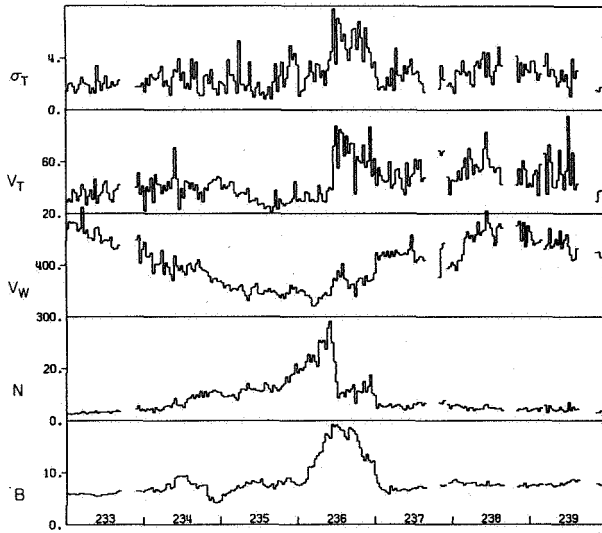


**Figure 5.** An example of detailed stream structure from 7 days of Mariner 5 data, using 40.4-min averages. The quantities plotted are as defined in figures 3 and 4.

expected spiral pattern. If the data are suitably averaged over longer periods, it becomes evident that the basic spiral pattern is present but that superposed on it are large amplitude fluctuations due to waves and convected magnetic structures. In addition to these fluctuations, the averages suggest the presence of systematic deviations from the spirals computed from the observed radial velocity of the solar wind. It is these systematic deviations, not the superposed shorter period fluctuations, that are discussed here.

If the pitch of a spiral field line does not have quite the average value expected on the basis of the radial velocity, it must be explained in terms of  $V_\phi$ , the azimuthal velocity component of the solar wind. This is associated with the angular momentum transport from the sun and will be discussed in a later session. First, with the usual mathematical treatment, substantial deviations in average pitch of the spiral, and hence substantial average azimuthal velocity, implies a substantial torque applied as a boundary condition at infinity. This could be torque exerted by the galactic magnetic field, but it is more likely associated with transverse momentum imparted to solar gas as it reaches the outer boundary of the heliosphere Davis [1971]. The deviations of the magnetic spirals on entering the compression regions shown in figure 4 lead us to expect azimuthal velocity components which seem to be consistent with those observed by Lazarus [1970] and by Wolfe [1970].

There are also observations that indicate the presence of a long-term average component of the interplanetary

magnetic field that is normal to the cone on which the spiral should be wound; there is a  $B_\theta$  component. We shall now see that this has much more puzzling consequences than an unexpected  $B_\phi$  component. Since most observations are made near the ecliptic, which is inclined at only  $7^\circ.25$  to the solar equatorial plane, the cone is very flat.

The best known observations of this kind were made by IMP 1, where Ness and Wilcox [1964] found a southward component that averaged a substantial part of a gamma over a 3-month period. The field lines had a modal angle with the equatorial plane of the order of  $20^\circ$ , and whether they were inward or outward along the spiral they also pointed a bit southward more often than a bit northward. That this raises difficulties of a very basic character can be seen in a number of ways. For example, consider a circle in the ecliptic whose radius is 1 AU and which bounds a hemispherical cap whose center is the sun, as indicated in meridional cross section in figure 6. Magnetic tubes of force are shown to the left in an outward pointing sector. As they are swept

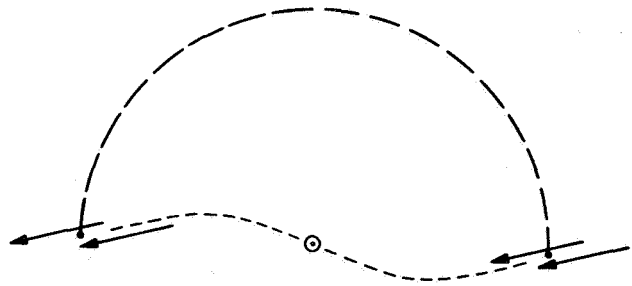


**Figure 6.** Schematic meridional projection of the average interplanetary magnetic field, as based on IMP 1 data, and of a northern hemisphere bounded by the earth's orbit. With this model, the outward flux through this hemisphere tends to increase rapidly.

outward radially by the solar wind, they are carried across the circle and increase the outward flux through the hemisphere. On the right are tubes of force in an inward pointing sector. As they are swept radially outward across the circle, they remove inward flux through the hemisphere and hence increase the net outward flux. Hypothetical connections of these tubes to the sun are shown, but they are irrelevant to the argument. However they are arranged, the flux through the hemisphere must increase steadily.

An approximate estimate of the time constant of this increase is easily made, the result being that it takes

about 40 days for the total flux through the hemisphere to increase by the equivalent of a uniform  $5\gamma$  radial component of  $\mathbf{B}$  over the entire hemisphere. It is literally incredible that this can continue for long and it seems likely that a rather unpalatable modification either of the data or of our theoretical understanding of the solar wind will have to be accepted. Among the modifications that might be contemplated are (1) the IMP 1 data grossly misrepresent the true situation because of statistical fluctuations; (2) the magnetometer zero level is in error; (3) the wind does not flow radially but has a southward velocity component that matches the observed inclination of the magnetic field; (4) the conductivity of the solar wind is so much lower than is usually believed that the plasma need not slide along the lines of force; or if all the preceding are rejected because each is very unpalatable to someone, (5) Maxwell's equations are invalid.

A different and to this author more intriguing proposal for nonspiral mean fields is that made by *Rosenberg and Coleman* [1969] and *Coleman and Rosenberg* [1970]. Figure 7 summarizes in schematic fashion their deductions from an extensive body of observations made between  $7^\circ S$  and  $7^\circ N$  solar latitude. In the equatorial

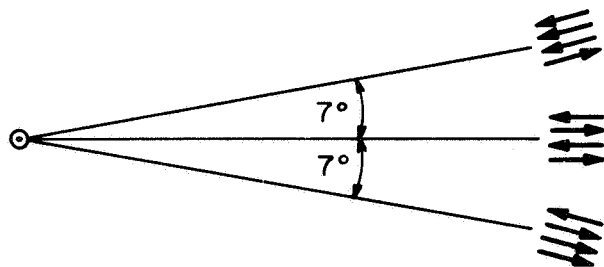


**Figure 7.** Schematic meridional projection of the average interplanetary magnetic field based on the analysis by *Coleman and Rosenberg* [1970]. The multiple arrows at  $7^\circ S$ ,  $0^\circ$ , and  $7^\circ N$  solar latitude indicate roughly the fraction of the time that the meridional projection of the average field in these locations is directed as shown. The median line is the solar equatorial plane. Note that the upper and lower sets of arrows are inclined at a greater angle than the corresponding radial vectors.

plane, positive and negative polarities are of essentially equal frequency. Rosenberg and Coleman find that the spacecraft goes to north solar latitudes, the fraction of the time spent in negative polarity sectors increases until at  $7^\circ N$  latitude it is roughly three-fourths. As the spacecraft goes to  $7^\circ S$  latitude, the fraction of the time spent in positive polarity regions increases to roughly three-fourths.

There is no basic difficulty in accepting these observations. If we were to map on the surface of the sun the patches of positive and of negative polarity, we could find them equally frequent along the equator but with a substantial preponderance of patches of negative polarity to the north and of positive polarity to the south. This would probably require that the patches be smaller in latitude than was suggested earlier, but there were no strong grounds for that suggestion. There is probably no good reason to extrapolate these observations to conclude that twice as far from the equator there will be only patches of a single polarity. However, if one wishes, one could easily reproduce the observations using a model in which at middle latitudes the northern hemisphere is exclusively of negative polarity and the southern hemisphere exclusively of positive polarity with a single wavy boundary between, although this is not at all the model that is usually deduced from photospheric observations.

A second, more puzzling deduction made by Coleman and Rosenberg is that on the average the field lines, when projected on the meridional plane, are not precisely radial; on the average they make a larger angle (very roughly by a factor of  $3/2$ ) with the solar equatorial plane than does the radius from the center of the sun to the point of observation. It is apparent from figure 7 that the latitude dependence of polarity then implies an average southward net flux, although not as large as that implied by the IMP 1 data. (The point under consideration is not the clearly apparent preponderance of lines that are directed southward with respect to the solar equatorial plane; it is that they are directed southward with respect to the local radius from the sun.) If the solar wind is radial, this excess tilt of the field lines means that tubes of force that at one time emerged through portions of a sphere at 1 AU lying either north of  $7^\circ N$  latitude or south of  $7^\circ S$  latitude are being swept into a belt  $14^\circ$  wide around the equator. The total net flux through this belt need not change since as much negative flux is convected inward over its northern boundary as positive flux is convected inward over its southern boundary. However, the only way to keep the flux of each sign from growing and thus rapidly increasing the field strength is to have some kind of field merging by which tubes of opposite polarity "eat each other up." The time constant for this must be of the order of 10 days, which seems unacceptably short.

Another way of looking at the difficulty is that the negative flux in the cap north of  $7^\circ N$  latitude is being convected into the equatorial belt at a rate that would reduce the flux through the cap to zero in approximately 100 days. This flux cannot be regenerated by the

drawing out of loops from the lower corona unless the positive leg of each loop comes from south of  $7^\circ\text{N}$  and the negative leg comes out from the north of  $7^\circ\text{N}$ . But if this happens, a corresponding amount of north-pointing flux should be observed passing a spacecraft at  $7^\circ\text{N}$  solar latitude.

If the observations are accepted at face value, we seem driven to one of three conclusions: (1) The solar wind, by chance, behaves consistently in one way on the side of the sun where the spacecraft happens to be and on the other side behaves consistently in the reverse way; with the large number of solar rotations involved, this is highly implausible. (2) The effective conductivity of the solar wind is low enough, or our knowledge of plasma physics is so incomplete, that the field lines can remain fixed in space and the wind blows partially across them. (3) The wind velocity is not radial, rather being directed parallel to the field lines.

If we attempt to follow this escape route, we are at once confronted with two further difficulties. First, as pointed out by Schatten in the preceding paper, Rosenberg and Coleman's interpretation disagrees with the perhaps still tentative plasma observations. Further, all the magnetic flux and all the plasma that pass through the  $14^\circ$  belt over which observations have been made at 1 AU would have to come through a narrower belt nearer the sun and follow a path curved away from the equatorial plane. The dynamics of this curved flow requires that forces act on the plasma. It would be very surprising if the gradients in plasma pressure were large enough to produce this deflection. Let us therefore consider electromagnetic forces. Parker's ideal spiral in the solar equatorial plane is a force-free configuration. But out of the equatorial plane it produces a small force normal to the cone on which it is wound and away from the equatorial plane. If the force is computed for the ideal spiral, it appears from a crude calculation to be too small by a factor of roughly 3 to 10. This discrepancy may not be important since, in a more complete model in which the  $\theta$  component of the magnetic field is not zero, the force in the  $\theta$  direction may be larger. A similar process occurs for the azimuthal motion, where if the ends of the field lines as  $r$  approaches  $\infty$  are assumed to be pulled in the  $\varphi$  direction, the curvature of the field lines for intermediate values of  $r$  produces forces that deflect the wind in the  $\varphi$  direction. A necessary feature of a model having the desired forces in the  $\theta$  direction is likely to be some process that draws the lines of force toward the axis of rotation when they are very far from the sun and from the equatorial plane. This will require curvature toward the poles all along the field line and might produce the forces necessary to deflect the wind along the curving field lines.

In summary, there appears to be no theoretically acceptable model that is in agreement with all the observations of long-term average components of the magnetic field and of wind velocity in the  $\theta$  direction. If the data are accepted, one must accept very uncomfortable theoretical consequences. If one makes himself comfortable theoretically, he must suffer the unpleasant consequences of disagreeing with those who have worked very hard and skillfully in carrying out difficult experiments to get badly needed data. For the moment it seems best to suspend judgement.

Although it was argued above that there could be no significant rapid cancellation of oppositely directed flux tubes near 1 AU in the solar wind in the equatorial belt, there must be some such phenomena somewhere in the solar system, although with a much longer time scale. From time to time magnetic arches push up through the photosphere with the birth of spot groups. Some of these may later be pulled back down inconspicuously along the border between regions of positive and negative polarity. But many such arches extend high into the corona and their apexes are occasionally swept outward by the solar wind, increasing the number of tubes of force that extend from below the photosphere to the outermost reaches of the solar system. Once the vertex of such an arch passes the Alfvénic critical point, it can never be simply pulled back. Some process must be found to keep the number of tubes of force from increasing indefinitely. The surface currents that flow between regions of opposite polarity will produce some cancellation because of the finite conductivity, but in and above the corona the rate at which this happens is very small. The conductivity, or at least the decay time of surface currents of the significant scale, is smallest in the photosphere. And in the photosphere there are fluid motions driven by mechanical forces that are large compared to the magnetic forces. Thus, from time to time flux tubes of opposite polarity must be driven together, producing very thin current sheets. One result will be a very local cancellation of oppositely directed flux tubes and a reconnection of the parts of the tubes that do not mutually "eat each other up." Below the region of cancellation there will be an arch whose legs go deep down into the sun. This can be submerged below the photosphere by magnetic tension in the legs or by random fluid motions. Above the region of cancellation there will be a field loop that is suspended from above. When enough of the gas in it has risen up and flowed off in the solar wind, the entire loop will rise and blow away. By this somewhat complicated process, two entire oppositely directed tubes of force are removed from interplanetary space. It is necessary only that this process operate rapidly enough to keep up with the new

flux that is added when the tops of arches rise in the solar wind.

As a final comment, it is urged that a Copernican viewpoint be adopted for the interplanetary medium. The earth's orbit has much less influence than the sun's axis of rotation on the phenomena we have been considering. Thus it is better to use solar polar coordinates than ecliptic coordinates. The radial components of field and velocity vectors are the same in the two systems, even when the spacecraft is in neither equatorial plane, but the true  $\theta$  component can be mixed with as much as 12 percent of the  $\varphi$  component if the wrong coordinate system is used. Angles can be shifted by  $7^\circ$ . For example, this may account for a small part of the southward excess found by IMP 1. Unfortunately, there has been a strong, although currently dying, tradition of using ecliptic coordinates even where they are inappropriate. It is to be hoped that this tradition will not long survive.

#### ACKNOWLEDGEMENTS

I am greatly indebted to the generosity of the Mariner 5 plasma experimenters, H. S. Bridge, A. J. Lazarus, and C. W. Snyder, and to the other Mariner 5 magnetometer experimenters for the use of large quantities of carefully reduced data before publication, and for helpful discussions and comments. I am particularly indebted to J. W. Belcher for many discussions and for the use of the results of his analysis. Financial support from NASA under research grant NGR-05-002-160 is gratefully acknowledged.

#### REFERENCES

- Belcher, J. W.: Alfvén Waves in the Interplanetary Medium. Ph.D. Thesis, California Institute of Technology, 1971.
- Belcher, J. W.; and Davis, L., Jr.: Large-Amplitude Alfvén Waves in the Interplanetary Medium, 2. *J. Geophys. Res.*, Vol. 76, 1971, p. 3534.
- Coleman, P. J., Jr.; and Rosenberg, R. L.: The North-South Component of the Interplanetary Magnetic Field. *Inst. Geophys. Planet. Phys., Univ. California at Los Angeles*, Pub. 818, 1970.
- Davis, L., Jr.: The Configuration of the Interplanetary Magnetic Field, in *The Interplanetary Medium*, edited by Roederer and Hundhausen, p. 19, Reidel, Dordrecht-Holland, in press, 1971.
- Dessler, A. J.; and Fejer, J. A.: Interpretation of  $K_p$  Index and M-Region Geomagnetic Storms. *Planet. Space Sci.*, Vol. 11, 1963, p. 505.
- Lazarus, A. J.: Pioneer 6 and 7 Observations of Average Solar Wind Properties. *Trans. Amer. Geophys. Union*, Vol. 51, 1970, p. 413.
- Ness, N. F.; and Wilcox, J. M.: Solar Origin of the Interplanetary Magnetic Field, *Phys. Rev. Lett.*, Vol. 13, 1964, p. 461.
- Neugebauer, M.; and Snyder, C. W.: Mariner 2 Observations of the Solar Wind. *The Solar Wind*, edited by R. J. Mackin, Jr., and M. Neugebauer, Pergamon Press, New York, 1966a, p. 3.
- Neugebauer, M.; and Snyder, C. W.: Mariner 2 Observations of the Solar Wind, 1, Average Properties, *J. Geophys. Res.*, Vol. 71, 1966b, p. 4469.
- Parker, E. N.: *Interplanetary Dynamical Processes*. Interscience, New York, 1963.
- Rosenberg, R. L.; and Coleman, P. J., Jr.: Heliographic Latitude Dependence of the Dominant Polarity of the Interplanetary Magnetic Field. *J. Geophys. Res.*, Vol. 74, 1969, p. 5611.
- Wilcox, J. M.; and Ness, N. F.: Quasi-stationary Corotating Structure in the Interplanetary Medium. *J. Geophys. Res.*, Vol. 70, 1965, p. 5793.
- Wolfe, J. M.: Solar Wind Characteristics Associated with Interplanetary Field Sector Structure. *Trans. Amer. Geophys. Union*, Vol. 51, 1970, p. 412.

*M. Dryer* I have a question about the Alfvén waves [fig. 4]. I'm a little puzzled by looking at the description of the data here or looking at the data and seeing that the deviations of the magnetic field and density and so forth are quite large. When I think of Alfvén waves I think of linear waves where, let's say,  $\delta b$  divided by  $b$ ,  $\delta n$  divided by  $n$ , and so forth, are all much less than one. Is there some explanation for that?

*L. Davis* The Alfvén waves are part of the small-scale structures. The things that I was showing are very large-scale structures, those changes in density which last during periods of the order of a day, where there were substantial changes in density and field strength. Variations on a scale which you couldn't see on this diagram at all would be the Alfvén wave fluctuations.

*C. P. Sonett* On one of the earlier slides, you show the plot with the velocity decreasing in the slow stream. The field changing, the density changing—it all looks sort

#### DISCUSSION

of like a snowplow. The temperature showed a very distinct very large jump very suddenly. Now, it seems this wasn't a velocity jump at that time. Would you attribute that to something like an electric field in a shear layer?

*L. Davis* I wouldn't want to tie myself down now completely on any explanation. What you would like to argue is that at that place where the temperature jumped one had gone from gas on the low temperature side, one was in gas which originally originated in the low velocity stream. When one went to the high temperature one was in a gas which had originally come in the high velocity stream. And I think these gases were different all the way out from the sun, and that it is a remnant of this past history that accounts for the high temperatures. I wouldn't want to say there weren't electric fields involved.

*J. M. Wilcox* With regard to the planning of future spacecraft observations, I would like to point out specifically that in the paper by Schatten there was shown very clearly a difference in what one might expect for observations at a heliographic latitude of  $40^\circ$  and at 1 AU distance from the sun, namely, that on one viewpoint one would expect to find a sector structure very similar to that observed near the earth or in the solar equatorial plane, but on another picture one would expect to find essentially a continuous polarity either always away from the sun or toward the sun. I think this is the kind of specific physical question one likes to have available when thinking about where one might look for new observations.

*B. McCormac* On those velocity jumps, the field plots, wouldn't it be useful to put on there the momentum and energy? It seems like they don't vary nearly as much as the velocity, in some cases might even stay relatively constant.

*L. Davis* Then I would really be getting into talking about the plasma, giving a plasma paper, and I think I should leave that for the people who will talk tomorrow.

*E. J. Weber* I would think, Leverett, you would just have to think about the plasma if you want to talk about your magnetic field at 1 AU. The reason for that is I think of a magnetic field in the plasma flow which is perpendicular to the ecliptic plane, which we seem to have, despite the fact that you tried to average it away a couple of years ago, if I remember, because it couldn't be possible. I think this really is one of the possibilities which might exist, as follows: Suppose you have on the sun temperature gradients along the polar direction and further down these are basically shielded from each other because of strong magnetic fields and you can't conduct the heat perpendicular to them. Further out, though, they act on it and in a sense can give an acceleration to the plasma, and therefore can produce a velocity perpendicular to the ecliptic plane.

*L. Davis* You're going to have to produce something on the general order of 40 km/sec. This gets in the range of acoustical velocities. I think this gets a little large to produce. That is the transverse velocity you will have to have there.

*M. Dryer* You were speaking about trying to get a mechanism for dissipating magnetic flux. Would it be possible if we accepted Alfvén's admonition and ruled out infinite conductivity, and tried to get rid of some of it that way? Would that be sufficient?

*L. Davis* Well, I did rule out infinite conductivity in the photosphere. I think when we say the solar wind is infinitely conducting we don't really mean that, we mean that it has a very high conductivity. I think we have some idea of what it should be, and it is large enough so that it is hard in the interfaces between the positive and negative polarity regions to eat up very much flux there. I think you will have to make some mechanism which reduces the conductivity very greatly before you can manage that way.

*A. J. Hundhausen* In the slide in which you showed some idealized structures for the high speed streams, which I believe was from one of John Belcher's papers, you showed beneath this some structures for various parameters as a function of time. Were those theoretical structures, observed structures, or idealizations of one or the other?

*L. Davis* They were basically an idealization of observed structures.

*A. J. Hundhausen* Well, in your interpretation of that density rise preceding the

velocity rise are you certain that that is really a property of the steady wind that might exist in front of the high speed stream, or is that just the back end of the rarefaction from the previous high speed stream? Can you really distinguish between the two?

*L. Davis* It is hard to distinguish between them. I perhaps should ask John Belcher to give a comment on this if he wishes. I might say that I think the argument I gave, that this high density reflected some different condition in the low velocity stream near the sun, near the high velocity stream—I'll be responsible for that and John may or may not want to partake in it, I don't know. But the observation that many times just before the velocity increases, sometimes when the velocity has been coming down and is about to start right back up, or when the velocity has come down and gone more or less constant for a while and then goes up, each time it is just before the velocity goes up that one gets this high density spike.

*C. P. Sonett* I'm a bit hesitant to bring this particular subject up, but I think in view of the importance of the field measurements in terms of what Leverett has had to say this question at least ought to be aired once more, even though cosmic plasmas are neutral. What I am referring to in particular is that there have been a number of field measurements showing in some cases components out of the ecliptic and in other cases fields in which as far as experimental accuracy permitted the component out of the ecliptic was essentially zero. In the first case, in the case of the IMP 1, if I remember correctly, it was about  $1 \gamma$ . There's another case taken from our data on Explorer 33 and possibly 35 which was carried out by Joan Hirshberg some years ago, in which she constructed histograms of the type that Ness and his group employed in the IMP reduction. In the case that she carried out, which was published in a letter in JGR\*, the residuals were below the error levels, and that means something like two-tenths of a gamma or perhaps less. Joan is here. Would you like to say something about it?

*J. Hirshberg* Perhaps only to add that the results were the same for the equatorial plane or the ecliptic plane.

*A. J. Dessler* This might be an appropriate place to take a short poll among the experimenters. Is there complete agreement between all the experimenters that there is a southward field of 1 to 2  $\gamma$ ? Dr. Ness, can you say something?

*N. F. Ness* It is not unpleasant to hear old data brought back to life, and it certainly has had a good ride since 1963 or '64. I think if you read the papers, if you are interested in this problem, one would specify the quantitative value to the component transverse to the ecliptic plane. I think we should realize, however, that if one studies this problem from a variety of satellite data you would first of all have different intervals of time, in a sense different polarities. You also have different time intervals over which they can be averaged. That is, in some of the work one is averaging over a solar rotation only and then doing this on successive solar rotations. In other cases one is averaging over a period of 3 months or 6 months or perhaps 18 months with gaps interspersed for various reasons. So that in all of this, in attempting to reconstruct what the net view is on the field component transverse to the ecliptic, one is faced with the problem of essentially incomplete data. I think we still believe that for the IMP 1 time interval the perpendicular component of about  $1 \gamma$  was valid within the accuracies quoted in the paper. And since that time I must say it's been interesting to see the turnaround as to how the southward component in the interplanetary field has resurrected itself in the framework of the recent studies of the interplanetary field topology related to the solar field. It is obviously a difficult measurement to make but I caution those of you who simply take scrawls from abstracts or from review papers to be certain that when you are looking for the magnitude of the component transverse to the ecliptic you understand it is over a solar rotation and which solar rotation, because it is clear that it changes.

---

\*Hirshberg, J., Interplanetary Magnetic Field during the Rising Part of the Solar Cycle, J. Geophys. Res., 74, 5814–5818, 1969.

*A. J. Lazarus* Just one comment on the interaction between high and low speed streams. I think you can tell where the interaction has occurred by looking at the transverse component of velocity and seeing how it changes as you move from a slow to a high speed. You can therefore talk about an interaction region where perhaps there is some compression; but I think it is important to look at some of these regions in detail, as we will do later in this Conference.

*P. J. Coleman, Jr.* From our data from the Mariners and Explorers and so on, if one averages the north-south flux at the solar equatorial plane, it seems as far as we can tell within our statistical accuracy that it's zero.

*J. M. Wilcox* I should like to mention a matter of terminology. Of course, physics gets involved in it. I would like to propose that the name *sector*, as used in the interplanetary medium, could be saved for an interval in which you have several days of continuous dominant magnetic field polarity in one direction. If a feature lasts for only half a day, then that is a filament or something but it is not a sector. Now, it is certainly true that there is this other kind of structure where you may have two peaks in solar wind velocity, each a few days wide, but all within the same polarity of the magnetic field. One possibility is to call each of these peaks of solar wind velocity a *subsector* or a *stream*. Now, in my opinion it is not clear which is the dominant physical structure, this subsector as I just described it or a sector. In fact, I think the answer to that question depends upon the specific problem that you are thinking about. But if we could have a standard terminology it might help the discussion. I wonder if Leverett Davis could comment.

*L. Davis* I wouldn't object to that. All I was trying to emphasize was that if you looked at, say, the sector pattern based on the IMP data, where everything was nice and repetitive, and you find that within a sector the polarity reverses from one sector to the next, the field strength has the characteristic pattern across the polarity, velocity has the characteristic pattern across the polarity, you get cosmic rays in one, not the other—all these things—suppose you look at some later period of time and you find that—I'm not claiming that you do but I suspect there will be times when you do—that in one of these subsectors all of these things will go through the characteristic changes but the polarity will happen to be the same for two adjacent subsectors. Then, of course, for these things which fit this pattern the subsector is the dominant thing and it may be convenient to call it a subsector rather than a sector. I think it depends a lot on whether you're thinking about the sector as being traced back to the sun and are worrying very much about what's happening on the sun to make this thing. Then John's use of the word *sector* is clearly the right one.

*J. M. Wilcox* It seems to me that if we could agree to call these things subsectors without in any way judging the physical significance of that term it might help to clarify the discussion.

*A. J. Dessler* Is it correct that the sectors have a particular dominant polarity when you are above the solar equatorial plane?

*L. Davis* That is what you will find in the papers by Coleman and Rosenberg. I should perhaps make it quite clear, I'm somewhat neutral in my own mind as to whether all of these observations mean what they appear to mean. When they don't satisfy the theorist sometimes it's rather awkward to explain the consequences. As a friend of the people who do the experimental work it is difficult to argue with them. It's even difficult to argue with the somewhat convincing data if I weren't a friend of theirs. Like all experimental data there are some bits of it that fit together and some that don't. It depends on what you want to believe, what you finally accept. But I do think that there is enough indication that there are funny things going on here, funny in terms of the simple model, that one should forget for the moment whether he's trying to decide whether you agree with the data or not but just say if it's right what are the



consequences? That's what I was doing.

*A. J. Dessler* I guess one might summarize, then, by saying the existence of a perpendicular component on the average would be a matter of taste.

*K. H. Schatten* I just wanted to make one comment that might be relevant to this discussion. In the Babcock picture of solar magnetic fields, the bipolar magnetic regions separate, one pole drifts to the north and becomes part of the polar field or tries to minimize the polar field and make it change sign; the other pole goes towards the equator and supposedly connects back with the opposite polarity from the opposite hemisphere. This may then be convected out, flux lines merging, this may be convected out through the solar wind and possibly cause some north-south asymmetries. I don't know, I haven't looked into the magnitudes. This has just crossed my mind, and it might relate to this type of analysis.

*P. J. Coleman* I would like to make two points concerning the north-south component of the interplanetary magnetic field. First, the average *magnitude* apparently depends upon heliographic latitude and, second, the mean value of this component in the equatorial plane is probably zero.

Figure 1 shows the effect that we are dealing with. It's a skewing of the distribution of the field in the  $r\theta$  plane of the spherical polar coordinate system. Here the solar equatorial plane is the plane of reference. For the particular distribution, the outward field ( $B_r > 0$ ) is more northward than the inward field.

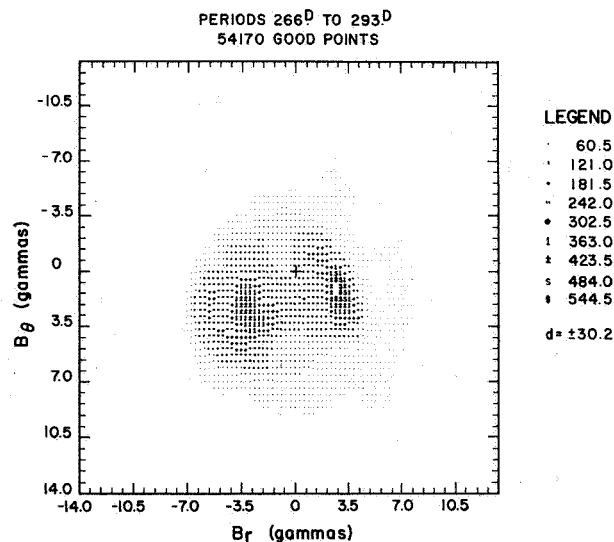


**Figure 1.** Joint distribution of  $B_r$  and  $B_\theta$  for a 27-day interval of the Mariner 2 flight. The zero level of  $B_\theta$  is arbitrary [after Coleman and Rosenberg, *J. Geophys. Res.*, Vol. 76, 1971, p. 2917].

As a measure of the skewing we use the quantity  $B_{\theta S} = (\langle B_{\theta+} \rangle - \langle B_{\theta-} \rangle) / 2$  where, for a 27-day distribution,  $\langle B_{\theta+} \rangle$  is the mean value of  $B_\theta$  for the outward field and  $\langle B_{\theta-} \rangle$  is the mean value of  $B_\theta$  for the inward field. Figure 2 shows  $B_{\theta+}$ ,  $B_{\theta-}$ , and  $B_{\theta S}$  versus time, heliocentric range, and heliographic latitude from Mariner 5. Here  $B_{\theta S}$  is

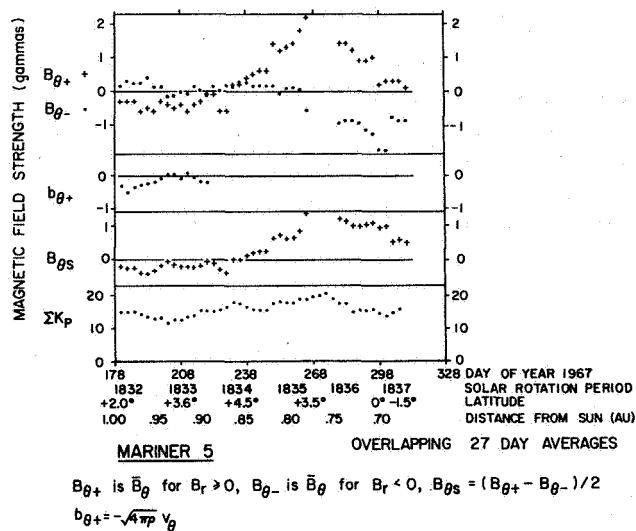


Figure 2. Plots of  $\langle B_{\theta+} \rangle$ ,  $\langle B_{\theta-} \rangle$ , and  $B_{\theta S}$  versus time, heliocentric range, and heliographic latitude for the Mariner 5 flight. These three quantities are defined in the text. The others shown are not pertinent here [after Coleman and Rosenberg, *J. Geophys. Res.*, Vol. 76, 1971, p. 2917].

from 27-day distributions taken at 3-day intervals. We see that  $B_{\theta S}$  changes sign sometime before Mariner 5 crossed the equator. This is an active period, but there is still a clear reversal despite the activity.

Figure 3 shows  $B_{\theta S}$  from Mariner 4 data. We had a longer stretch of data at a quieter time. The spacecraft was below the equatorial plane for most of the interval. But as Mariner 4 crossed the equatorial plane  $B_{\theta+}$ ,  $B_{\theta-}$ , and  $B_{\theta S}$  reverse polarities. The problem

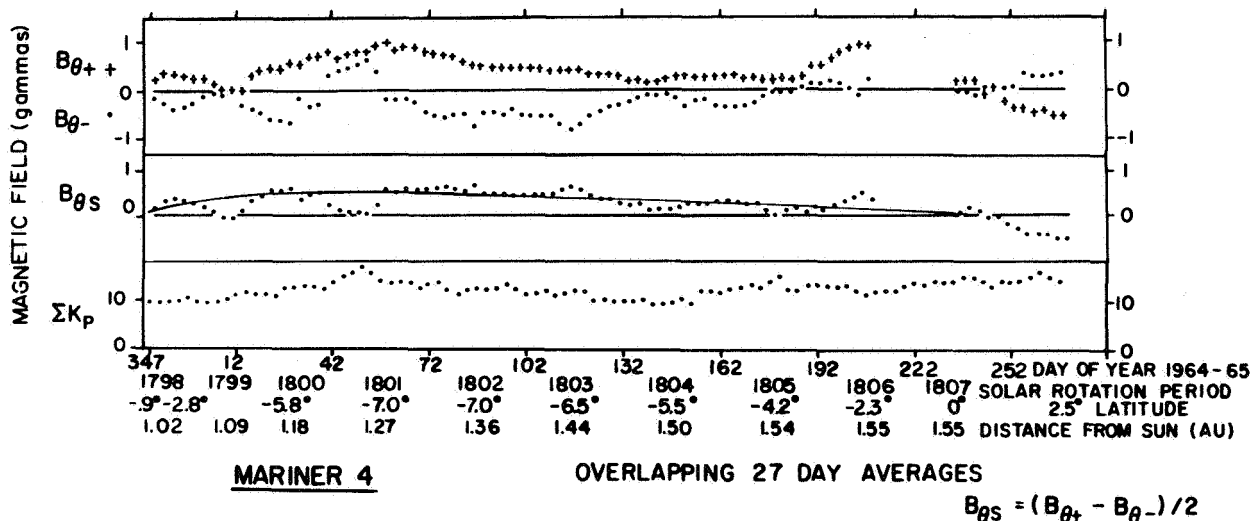


Figure 3. Plots of  $\langle B_{\theta+} \rangle$ ,  $\langle B_{\theta-} \rangle$ , and  $B_{\theta S}$  versus time, heliocentric range and heliographic latitude for the Mariner 4 flight [after Coleman and Rosenberg, *J. Geophys. Res.*, Vol. 76, 1971, p. 2917].

with the Mariners is that they simultaneously move in heliocentric range and heliographic latitude. So, with the cooperation of Dave Colburn and his colleagues at Ames, Ron Rosenberg and I used the Explorer 33 and 35 data to test for the dependence on heliographic latitude. The results are shown in figures 4 and 5. We found the least-squares

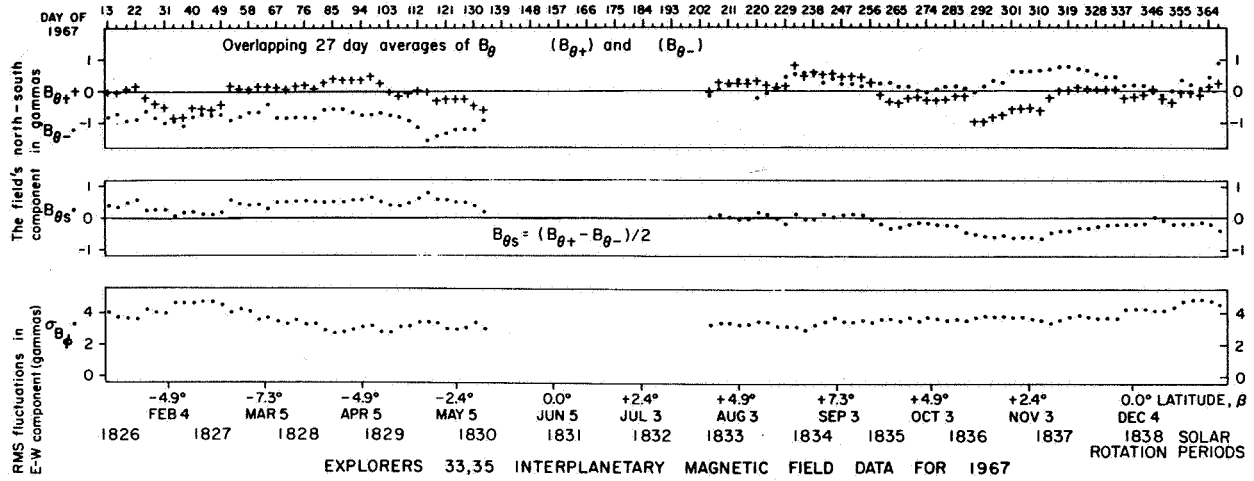


Figure 4. Plots of  $\langle B_{\theta+} \rangle$ ,  $\langle B_{\theta-} \rangle$ , and  $B_{\theta S}$  versus time, heliocentric range, and heliographic latitude for the Explorers 33 and 35, 1967 [after Rosenberg, Coleman, and Colburn, *J. Geophys. Res.*, Vol. 76, 1971, p. 6661].

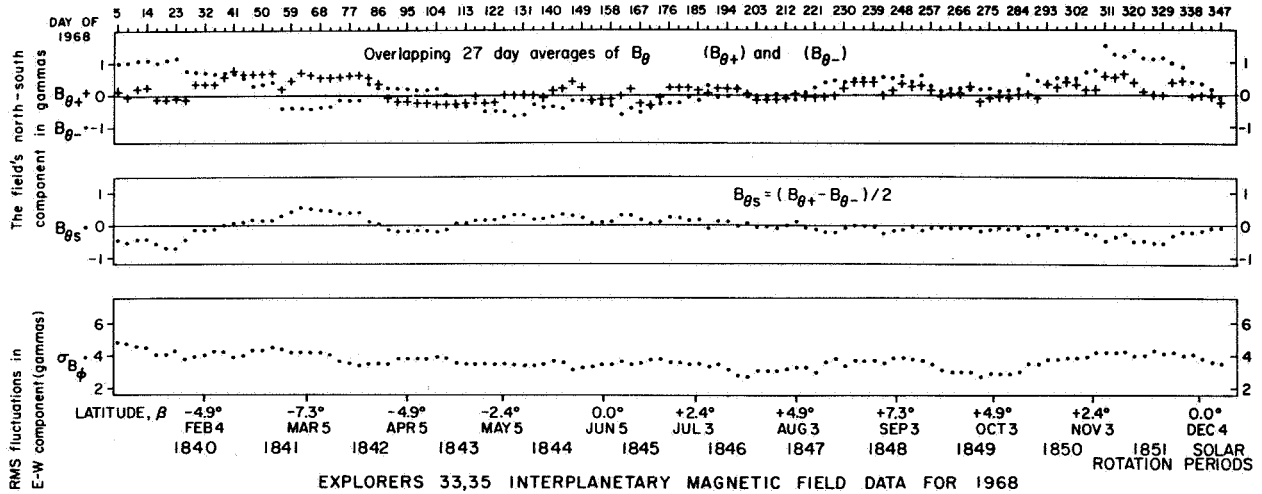


Figure 5. Plots of  $\langle B_{\theta+} \rangle$ ,  $\langle B_{\theta-} \rangle$ , and  $B_{\theta S}$  versus time, heliocentric range, and heliographic latitude for the Explorers 33 and 35, 1968 [after Rosenberg, Coleman, and Colburn, *J. Geophys. Res.*, Vol. 76, 1971, p. 6661].

best-fit sinusoid to be one with a period in the range  $1.0 \pm 0.1$  years. For 1967 the amplitude of the sine wave is about  $0.4 \gamma$ . For 1968 it is about  $0.2 \gamma$ . For Mariner 4, which is complicated by radial effects, we estimated the amplitude to be  $0.6 \gamma$  using another model. So it's conceivable that during more active periods such as 1962, when Mariner 2 was launched the amplitude could have been as high as  $1 \gamma$  or something close to that.

Finally, I want to stress once again that these results indicate that the observations of a nonzero north-south component can be accounted for without requiring that the sun lose flux transverse to the equatorial plane. In other words, they indicate that  $\langle B_\theta \rangle$  would be zero everywhere in the equatorial plane if the sun were axially symmetrical.

*A. J. Hundhausen* I must confess to feeling somewhat out of place speaking in this session, but as the plasma observations I will describe are relevant to the present discussion, Alex Dessler has convinced me that I should get up here despite the risk of getting caught in a magnetic crossfire. I will briefly describe a search for heliographic latitude dependence in plasma flow properties, based primarily on Vela 3 data obtained between July 1965, and mid-1967, but also using earlier Vela 2 data and Vela 4 data obtained between May 1967 and mid-1968. A more complete discussion of this study will be published in the *Journal of Geophysical Research*.

Figure 1 shows 27-day averages of the solar wind proton density (uppermost frame) and

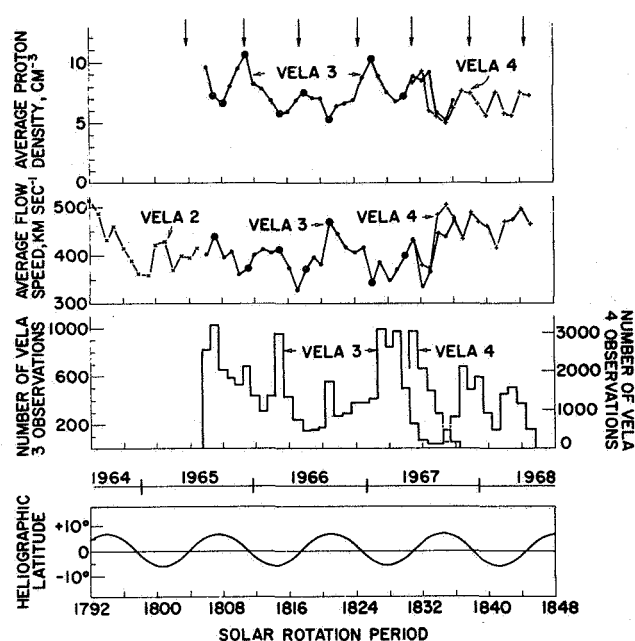


**Figure 1.** Solar wind observations made by Vela satellites between July 1964 and mid-1968. Twenty-seven day averages of the proton density observed by Vela 3 and 4 and of the solar wind speed observed by Vela 2, 3, and 4 are shown in the top two frames. The third frame gives the number of Vela 3 and 4 observations made within each 27-day solar rotation interval. The heliographic latitude of observation is shown in the fourth frame; the times of crossings of the solar equator are also indicated in the top frame by arrows.

flow speed (second frame) obtained by these various satellites. By averaging over 27 days we have presumably taken out longitude effects and can look for seasonal or latitude variations. The third frame of figure 1 shows the number of observations made by Vela 3 or Vela 4 during each 27-day averaging period. The lowest frame of the figure shows a familiar plot of the heliographic latitude of the earth as a function of time during this

4-year period. In the uppermost frame crossings of the solar equatorial plane are indicated by arrows.

The average density curve of figure 1 clearly hints at a seasonal variation. Maxima in the solar wind density occur near the crossings of the solar equatorial plane; minima occur near the extremes of the latitude excursion. The pattern is less evident in the flow speed averages but the flow speed is generally high when the density is low (away from the solar equatorial plane) and conversely low when the density is high (near the equatorial plane).

Before interpreting these variations as a latitude dependence in the plasma flow, one should consider several other possibilities. For example, could this be an instrumental effect? Fortunately, we are limited to *very* short contributions at this meeting, so no thorough discussion of such effects can be given. In fact, careful consideration must be given to this possibility, as the spin axes of Vela 3 spacecraft are not normal to the ecliptic plane and thus undergo annual precessions that could lead to an apparent annual variation in an observed quantity. The density variation could result from the spin axis precession if the Vela 3 analyzer systems were to transmit incoming particles at  $\sim 30^\circ$  from the entrance aperture normal with an efficiency 30 to 40 percent higher than particles at normal incidence. Such transmission characteristics are not expected and have not been encountered in laboratory calibrations of these instruments. Further, the Vela 4 spacecraft, earth-oriented and thus subject to a different spin axis variation, measures the same density variation as Vela 3 in mid-1967.

The statistical significance of the variations must also be considered. Figure 2 shows distributions of the observed proton densities from the solar rotations at the maxima and minima of figure 1 (indicated on fig. 1 by circles). Now, the difference between the averages (indicated by the arrows along the abscissae) for these differential solar rotations are about equal to the *standard deviations* of the individual distributions. The *standard error* in the determination of the average density in a given rotation is some fraction of the standard deviations. Therefore, the density variations under discussion are probably statistically significant. The possibility that these variations are random but accidentally resemble a periodic variation for the  $\sim 4$  cycles of figure 1 can be examined using standard statistical tests on runs. The probability of this accident is somewhere between one in a hundred and one in a thousand. Thus both of these possible statistical sources of the density variations are improbable. Figure 3 shows the flow speed distributions observed for the same solar rotations. Again, the variation in the average flow speeds results from large changes in the distributions. Note that high solar wind speeds, say above  $400 \text{ km sec}^{-1}$ , are much rarer near the solar equator.

Having thus dismissed instrumental and statistical sources for the observed variations, can we find a plausible physical explanation? The simplest such interpretation would envision a steady solar wind with high density and low velocity near the solar equatorial plane, and low density and high velocity at higher latitudes, produced by a coronal expansion that is not spherically symmetric. In fact, the Vela observations appear to show that such an interpretation is incomplete. Figure 4 shows 3-hr averages of the proton density and flow speed as a function of time from a solar rotation in 1965 when the satellite is approaching the maximum northern excursion from the solar equatorial plane. Note the presence of pronounced high velocity streams, each of which produced a very pronounced but short-lived density compression followed by a longer period of low densities that very much suggests a rarefaction. In averaging over such a solar rotation, the longer periods of low density dominate and lead to a low average density. Figure 5 shows the same observed quantities from a solar rotation three months later, that includes the crossing of the solar equator. The high velocity stream structure is not nearly so well defined as in figure 4, nor does the most prominent high velocity feature involve as large a velocity excursion. The pattern of density compressions and rarefactions is present but

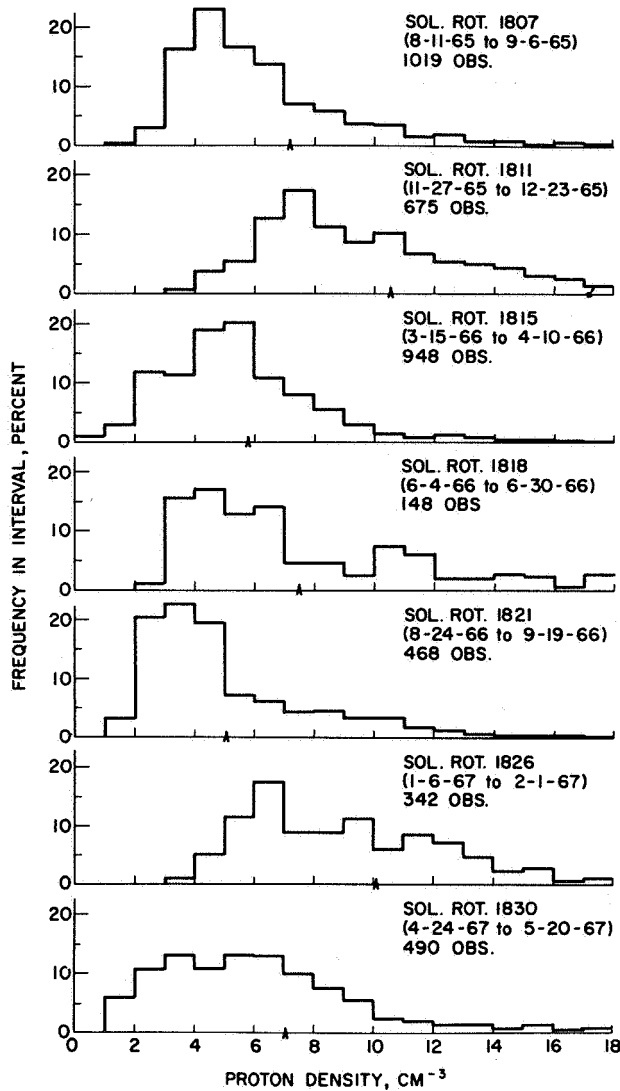


**Figure 2.** Histograms of the Vela 3 proton density observations made during the 27-day solar rotations indicated by circles around the density averages on figure 1. The arrows along the abscissae indicate the averages derived from each distribution.

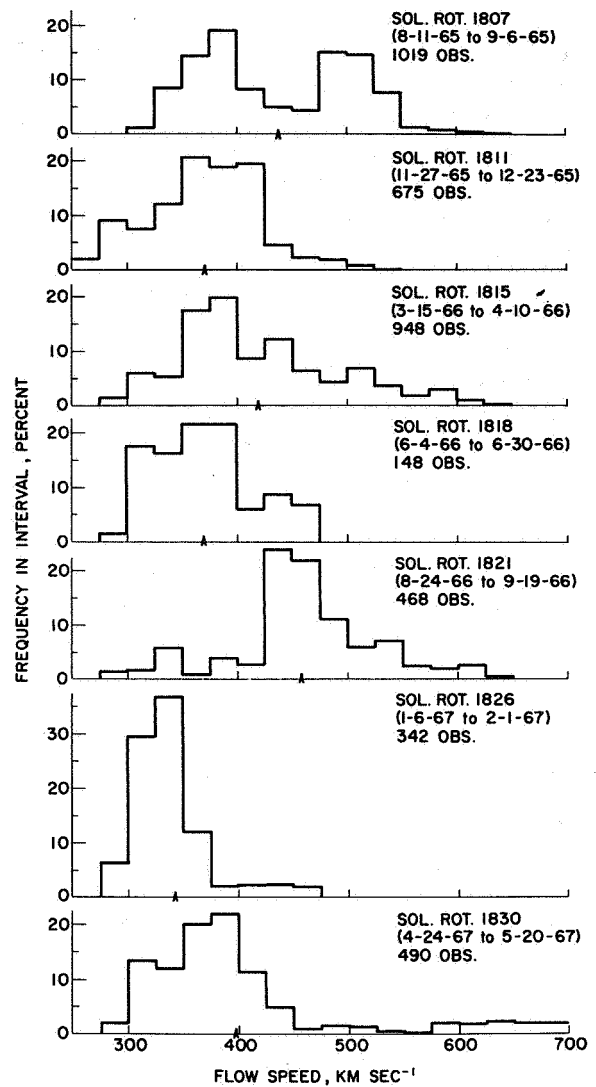


**Figure 3.** Histograms of the Vela 3 solar wind flow speed observations made during the same set of solar rotations as in figure 2.

less pronounced. In averaging over this rotation one naturally obtains a higher average density. The difference between these two solar rotations might well reflect a latitude dependence in the *solar activity* that presumably produces the high speed stream structure. For the early portion of a solar cycle (when these observations were made), it is well known that solar activity occurs at solar latitudes near 30 to 40°, not near the equator. One might interpret our observations as showing that the high speed streams observed at 1 AU are also confined to latitudes away from the solar equator.

These observations were made during the same period in which Rosenberg and Coleman observed a latitude structure in the magnetic field polarity. Wilcox has pointed out that the structure described by Coleman seemed to disappear sometime in late 1967. Note from figure 1 that our apparent latitude variation in the plasma flow also seemed to

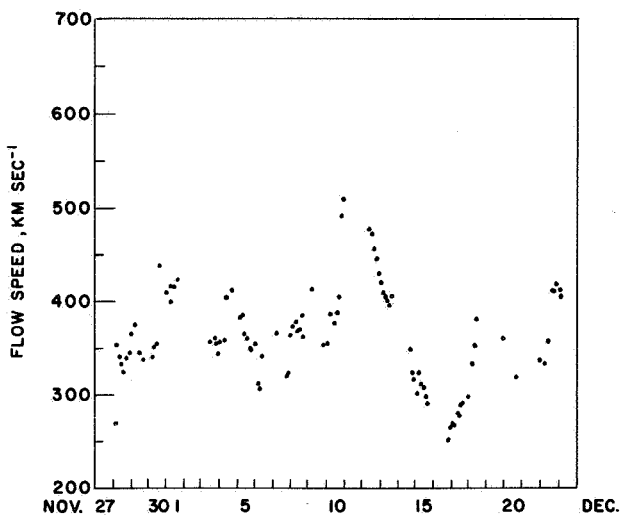
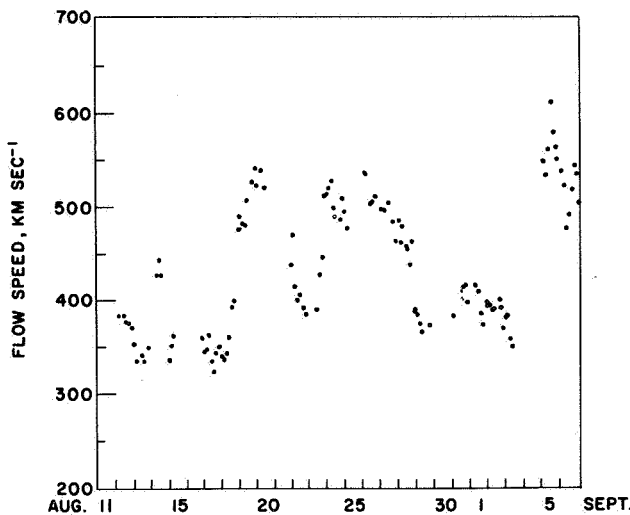
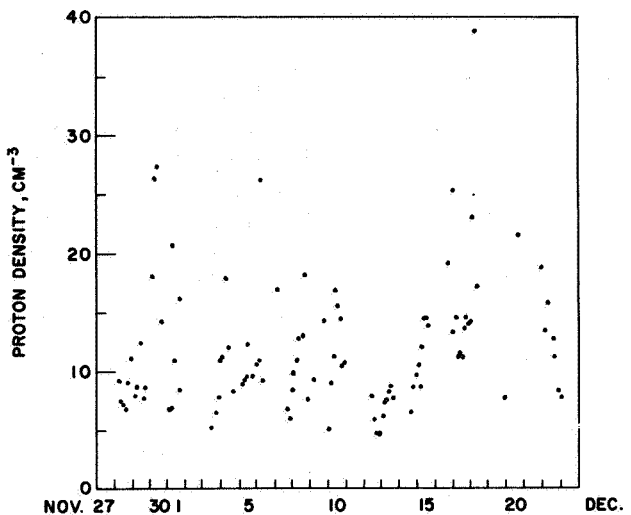
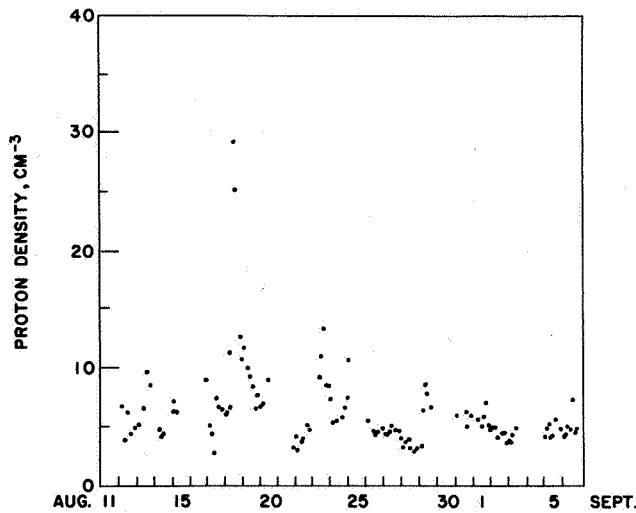


**Figure 4.** Three-hour averages of the proton density and flow speed observed during a solar rotation in Aug.-Sept., 1965—that is, near  $+7^\circ$  heliographic latitude.

**Figure 5.** Three-hour averages of the proton density and flow speed observed during a solar rotation in Nov.-Dec., 1965—that is, near the solar equator.

disappear near this same time. A simple and plausible explanation of this change can be proposed on the basis of the above discussion. As the solar cycle progresses, the centers of solar activity move toward the equator. That very motion of the sources of the streams might lead to their penetration into the equatorial region.

I should also mention that part of Rosenberg's interpretation of the magnetic field observations has been that the dividing surface between the north and south "regions" might at times be depressed because of the greater solar activity in the northern solar hemisphere. If the Vela 3 observations are used to compare the regions north and south of the solar equator, one finds the flow speeds are about 10 percent higher in the northern solar hemisphere than in the southern solar hemisphere. This may lend some plausibility to Rosenberg's speculation.

In conclusion, the presence of the structures I have described in the plasma flow may add to the plausibility of magnetic fields organized in solar latitude. The next task should

be to search for direct relationships between the plasma flow and magnetic field structures.

*J. M. Wilcox* In Rosenberg's analysis the change from positive to negative dominant polarity occurs sometimes when the earth is at zero heliographic latitude. At other times the change occurs when the earth is several degrees away from this. It is at these latter times when they would like to invoke a southward flow of the solar wind. Do you have the ability to check that from your data?

*A. J. Hundhausen* For this particular period, yes. That is the kind of detailed thing we haven't done yet. But you will note that many of our density maxima were not directly lined up with those equatorial crossings, either. If in fact this variation does depend on solar activity, then since solar activity does not vary smoothly you would expect such offsets.

*E. J. Smith* Did you make any comments at all about flow direction, or would you like to comment on what you see or whether you are able to say anything about flow direction?

*A. J. Hundhausen* As far as the latitude density is concerned, I don't think we see anything. But, remember, we only measure the flow roughly in the ecliptic.



# THE ELECTROMAGNETIC STRUCTURE OF INTERPLANETARY SPACE

J. O. Stenflo

A method to calculate the three-dimensional structure of the interplanetary magnetic field is presented. The integrations are based on magnetograph recordings of longitudinal magnetic fields in the solar photosphere. The program by *Altschuler and Newkirk* [1969] is used to calculate the radial component of the magnetic field on the "source surface," situated at  $r = 2.6r_{\odot}$ . This determines the inner boundary conditions for the integration outwards of the interplanetary field equations by means of the method that is described.

Computer-drawn plots of the interplanetary field lines out to the earth's orbit are presented for the periods around the total solar eclipses of November 12, 1966, and March 7, 1970. During the former period the interplanetary field exhibited a clean, dipole-type structure, while during the latter period the field was more complicated and had four sectors in the equatorial plane. A movie has been presented, showing how the interplanetary field structure rotates as seen by a magnetometer in the sun's equatorial plane.

## METHOD OF CALCULATING INTERPLANETARY MAGNETIC FIELDS

The two principal assumptions made are:

1. The magnetic-field structure is stationary in a frame rotating with the sun.
2. The solar wind velocity has no component in the  $\theta$  direction ( $\theta$  is the colatitude), but only in the radial and azimuthal ( $\phi$ ) directions. If we neglect the effect of space charges, assumption (1) implies, that the magnetic field vector and the flow velocity are parallel in the rotating frame. From this and assumption (2) it follows that the magnetic field has no component in the  $\theta$  direction. Hence the interplanetary field lines will lie on conical surfaces of constant  $\theta$ . This simplifies the problem considerably.

As  $\mathbf{v} \times \mathbf{B} = 0$  in the rotating frame, the relation between the  $\phi$  and  $r$  components of the field is

$$B_{\phi} = \frac{(\omega - \Omega) r \sin \theta}{v_r} B_r \quad (1)$$

where  $\omega$  is the angular velocity of the solar wind,  $\Omega$  the angular velocity of the footpoints of the field lines (the angular velocity of the rotating frame), and  $v_r$  the radial component of the solar wind velocity.

The condition  $\text{div } \mathbf{B} = 0$  can be written

$$\frac{1}{r^2} \frac{\partial}{\partial r} (r^2 B_r) + \frac{1}{r \sin \theta} \frac{\partial B_{\phi}}{\partial \phi} = 0 \quad (2)$$

Equations (1) and (2) together with some boundary conditions are sufficient to determine the field structure if  $v_r$  and  $\omega$  have first been determined or specified throughout space. If  $v_r$  and  $\omega$  are assumed to be known, the procedure adopted for calculating the field is the following:

As boundary conditions we assume that the radial component of the field is given on an inner spherical surface. Using equation (1) we can calculate the  $B_{\phi}$  component. Thus knowing the  $B_{\phi}$  distribution on the boundary surface, we can determine  $\partial B_{\phi} / \partial \phi$ . According to equation (2), this determines how  $B_r$  changes with  $r$ . Hence we can calculate the value of  $B_r$  on a spherical surface that lies a step  $\Delta r$  farther out and, using (1),

*The author is at the High Altitude Observatory, National Center for Atmospheric Research (sponsored by the National Science Foundation), Boulder, Colorado. He is currently at the Astronomical Observatory at Lund, Sweden.*

calculate the  $B_\phi$  component on that surface, and so forth. In this way we can proceed from the outer corona to beyond the orbit of earth.

Turning to the determination of the angular velocity  $\omega$  of the solar wind, we can proceed in a manner similar to that of *Weber and Davis* [1967], except that our calculations have to allow for any variation of  $B_r$  and  $B_\phi$  with  $\theta$  and  $\phi$ , and we want to determine what happens outside the sun's equatorial plane. It can be shown [Stenflo, 1971] that

$$\omega = \Omega \frac{(r_A/r)^2 - M_A^{-2}}{1 - M_A^{-2}} \quad (3)$$

where

$$M_A = v_r \sqrt{\frac{\mu_0 \rho}{B_r}} \quad (4)$$

is the Alfvénic Mach number,  $\mu_0$  the permeability of vacuum,  $\rho$  the mass density, and  $r_A$  the distance at which  $M_A = 1$ . A line above a symbol means that it is averaged over all  $\phi$ .

It has been assumed above that all physical quantities except the magnetic field are independent of  $\phi$ . This assumption is not physically consistent, since fluctuations in the magnetic field will lead to fluctuations in the other physical parameters as well. It is only used, however, to derive an approximate expression for  $\omega$ . As it turns out,  $\omega$  according to equation (3) drops off very rapidly with distance and thus will be small compared to  $\Omega$ . Hence, errors in the determination of  $\omega$  will not affect the field structure seriously.

With our assumptions above, it can further be shown [Stenflo, 1971] that the mass flux and  $(r^2 B_r)^2$  averaged over all  $\phi$  are independent of distance. Hence

$$r^2 \rho v_r = F \quad (5)$$

and

$$\overline{(r^2 B_r)^2} = C \quad (6)$$

where  $F$  and  $C$  are constants. These constants can be fixed by the conditions at 1 AU. Since we can write

$$\overline{M_A^{-2}} = \frac{C}{\mu_0} F r^2 v_r \quad (7)$$

both the Alfvénic Mach number and  $\omega$  can be calculated if we know the wind velocity  $v_r$ .

Our remaining task is therefore to specify  $v_r$ . As indicated by the work of *Weber and Davis* [1967], the magnetic field and solar rotation do not greatly influence the solution for  $v_r$ . Their  $v_r$  curve was almost identical to that of *Parker* [1958], which was derived neglecting magnetic fields and rotation. Accordingly, we have assumed that Parker's solution is a reasonably good

approximation also for the case when the field varies with  $\theta$  and  $\phi$ .

## THE BOUNDARY VALUES AND THE SELECTION OF FIELD LINES

In the method by *Altschuler and Newkirk* [1969] of calculating coronal magnetic fields it is assumed that the magnetic field is pulled out radially by the solar wind at a distance  $r = r_s$ . The surface at which this occurs represents a kind of "source surface" for the interplanetary field, a concept that has been introduced and used by *Schatten et al.* [1969]. According to *Altschuler and Newkirk* [1969], the best agreement between the calculated field lines and coronal structures seen on eclipse photographs is obtained for  $r_s = 2.6 r_\odot$ . The inner boundary surface for integrating equations (1) and (2) outwards has therefore been placed at  $r = 2.6 r_\odot$ . The program by *Altschuler and Newkirk* has been used to calculate from the recorded line-of-sight component of the photospheric magnetic field the  $B_r$  component of the field on our "source surface." This determines our inner boundary conditions.

The constants  $F$  and  $C$  in equations (5) and (6) have been fixed by assuming a mass density corresponding to 6 protons per  $\text{cm}^3$  at 1 AU and an rms value of  $B_r$  of 4  $\gamma$  at the same distance. For  $v_r$  we have assumed *Parker's* [1958] solution for an isothermal corona of  $1 \times 10^6$  °K, with  $v_r$  normalized to 400 km/sec at 1 AU. The influence of the field structure of the choice of these parameters has been discussed elsewhere [Stenflo, 1971].

Two alternative methods of selecting the field lines have been used [Altschuler and Newkirk, 1969]. One is the "geometric" selection, for which the footpoints of the field lines are evenly distributed over the sphere independent of fluxes or field strengths. According to the other method, all weaker fields are suppressed and the number of field lines assigned to a region is proportional to the flux carried by the stronger fields through that region. Further details are given by *Stenflo* [1971].

## RESULTS OF NUMERICAL INTEGRATIONS

Figure 1 is a computer-drawn plot of the interplanetary field as seen from the direction of the heliographic north pole. The footpoints of the field lines are selected on the "source surface" according to the "strong-field" method. The calculations are based on Mt. Wilson recordings of photospheric magnetic fields during the period February 17–March 16, 1970. All field lines are traced out to a distance of about 250  $r_\odot$  (1 AU = 215

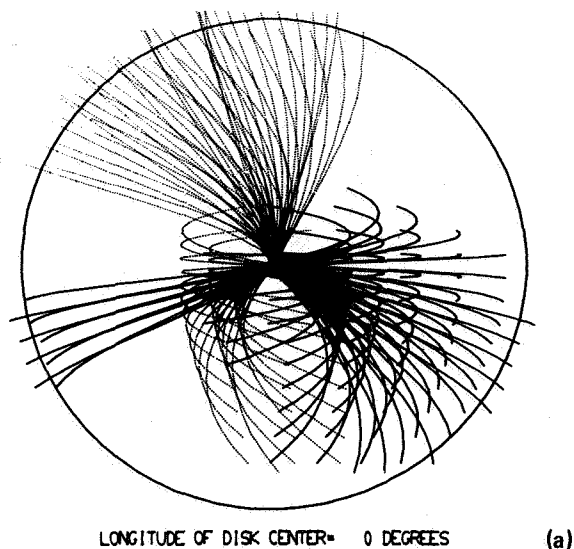
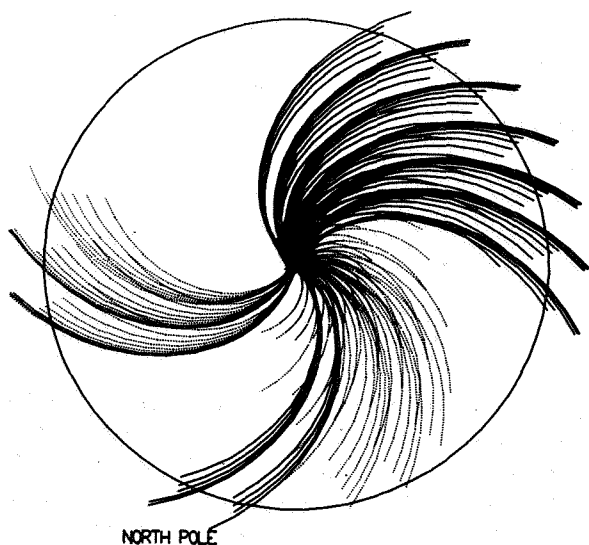


**Figure 1.** The interplanetary magnetic field calculated out to a distance of  $250 r_{\odot}$ . The calculations are based on Mt. Wilson recordings of photospheric magnetic fields during the period February 17-March 16, 1970. Solid lines: positive polarity. Dashed lines: negative polarity. View from the direction of the heliographic north pole. Zero longitude is toward the right.

$r_{\odot}$ ). Some field lines appear to be shorter due to projection effects. They originate at higher latitudes. The field in the equatorial plane exhibits four sectors.

When viewed from a position far out in the equatorial plane, the structure appears to be much more complicated (fig. 2(a)). To obtain a stereoscopic impression of the structure, a movie has been produced (presented at the Solar Wind Conference at Asilomar), showing the whole field structure rotate as seen by an observer in the equatorial plane.

A considerable contribution to the interplanetary field comes from old, diffused active regions. Accordingly, we should expect a simpler structure to occur before the solar activity maximum. Such a case is shown in figure 2b, which is based on Mt. Wilson recordings from the period October 29–November 26, 1966. The interplanetary field shows a clean dipole-type structure with negative polarity in the north hemisphere and positive polarity in the south.

Figure 3 shows maps of the coronal field out to a distance of  $17 r_{\odot}$ . The “geometric” procedure for selecting the footpoints of the field lines on the solar surface has been used. The circumstance that the field lines in figure 3 are almost straight has nothing to do

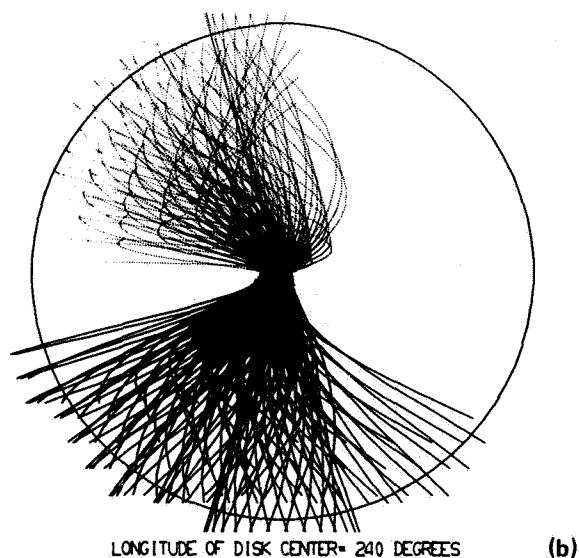
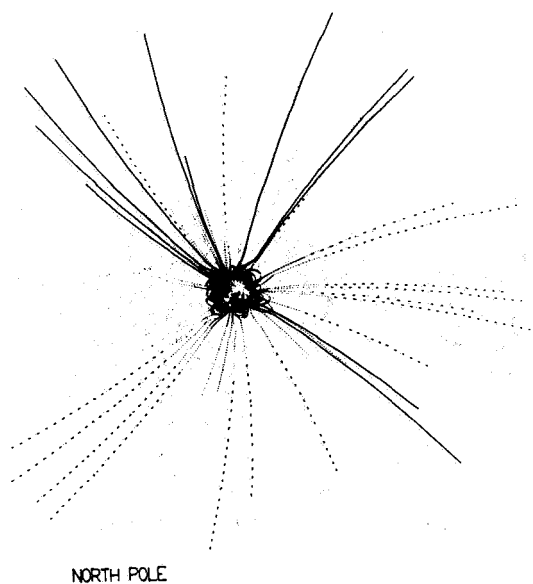
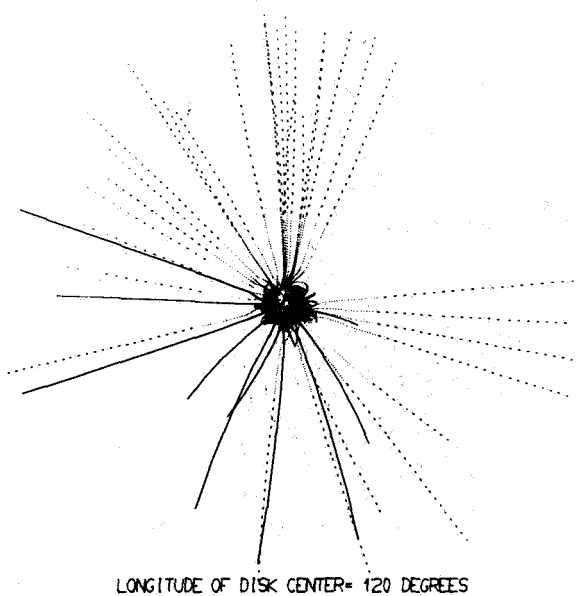


**Figure 2.** (a) The same structure as shown in figure 1 viewed from the equatorial plane. North is upwards, east to the left. Longitude of central meridian  $0^{\circ}$ . (b) The same structure as in (a), except that the calculations are based on Mt. Wilson recordings from the period October 29–November 26, 1966, and that the longitude of the central meridian on the sun is  $240^{\circ}$ .



(a)



(b)

**Figure 3.** Coronal magnetic fields calculated out to a distance of  $17 r_{\odot}$ . The calculations are based on the same material as figure 1. (a) View from the direction of the heliographic north pole. Zero longitude is towards the right. (b) View from the equatorial plane. North is upward, east to the left. Longitude  $120^{\circ}$  of the central meridian corresponds to the time of the March 7, 1970, total solar eclipse.

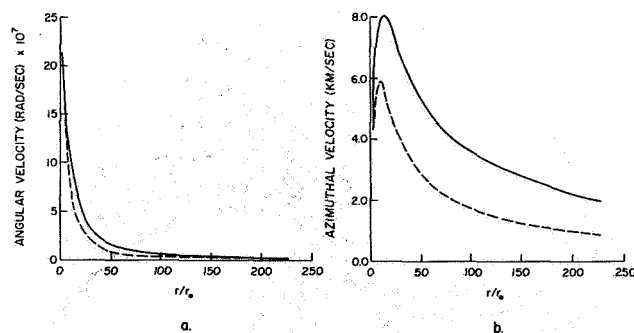


**Figure 4.** (a) Angular velocity and (b) azimuthal velocity of the solar wind. The solid curves are determined from the numerical values given in the text. For comparison the dashed curves have been derived assuming that the rms value of the  $B_r$  component of the field at 1 AU is  $2\gamma$  (instead of  $4\gamma$  for the solid curves).

with corotation of the coronal plasma. The angular velocity decreases very rapidly with distance, as shown by figure 4a, which has been calculated from equation (3). The curvature of the field lines is so small because  $v_r$  is much larger than  $r\Omega$  in most of the region.

The magnetic field at 1 AU calculated by the present method has been compared with actual spacecraft observations during the period around the March 7, 1970, solar eclipse (Ames Research Center magnetometer experiment on Explorer 35, C. P. Sonett, D. S. Colburn, and J. M. Wilcox). The correlations between the computed and observed field are 0.73 for  $B_r$ , 0.72 for  $B_{\phi}$ , and 0.90 for the sign of  $B_r$ .

## REFERENCES

- Altschuler, M. D.; and Newkirk, G., Jr.: Magnetic Fields and the Structure of the Solar Corona. *Solar Phys.*, Vol. 9, 1969, p. 131.
- Parker, E. N.: Dynamics of the Interplanetary Gas and Magnetic Fields. *Astrophys. J.*, Vol. 128, 1958, p. 664.
- Schatten, K. H.; Wilcox, J. M.; and Ness, N. F.: A Model of Interplanetary and Coronal Magnetic Fields. *Solar Phys.*, Vol. 6, 1969, p. 442.
- Stenflo, J. O.: Structure of the Interplanetary Magnetic Field. *Cosmic Electrodyn.*, Vol. 2, 1971, p. 309.
- Weber, E. J.; and Davis, L., Jr.: The Angular Momentum of the Solar Wind. *Astrophys. J.*, Vol. 148, 1967, p. 217.

## HELMET AND ACTIVE STREAMERS FROM RADIO OBSERVATIONS

Y. Avignon, F. Axisa,  
M. J. Martres, M. Pick,  
and P. Simon

Large coronal regions disconnected from any calcium plages and identified by their thermal emission at 169 mHz play a basic role in the sector structure of the interplanetary medium. We now conclude that these coronal regions are to be interpreted as streamers.

### ABSTRACT

We have shown that the basic structure of helmet and active streamers would be traced by the presence, length, and orientation of filaments, the structure of both types of objects being determined by magnetic fields. Here we present some properties of active and helmet streamers based on radio observations, in particular some consequences concerning the medium corona and the interplanetary medium [Axisa *et al.*, 1971].

At 169 mHz, the slowly varying component of thermal origin is best explained in terms of emission by streamers at a typical altitude of  $0.4 R_{\odot}$  (fig. 1). A plasma frequency of 169 mHz corresponds to an electron density of  $3.5 \times 10^8 \text{ e/cm}^3$ . Therefore, at an altitude of  $0.4 R_{\odot}$ , the quiet sun can be considered practically transparent for such a frequency. So a value of  $3.5 \times 10^8 \text{ e/cm}^3$  may be considered as an upper limit for the actual density in streamers at  $0.4 R_{\odot}$ . In any case, it is seen that the electron density as deduced from our radio data will be higher than proposed in Newkirk's model. It is in agreement with the electron density deduced from radio burst observations. At the same frequency, similar altitudes have been found for the sources of type III emission [Mercier, 1971].

As seen at 169 mHz, streamers schematically may be considered as dense plates extending from the filaments, with roughly the same length. The actual width of such

plates cannot be estimated because of the limited resolving power of our instrument. But a recent study relative to type III bursts obtained with the Nancay radioheliograph leads to an estimation of 20,000 km [Mercier, 1971]. Koutchmy deduced similar results from the March 1970 eclipse [Koutchmy, 1971].

We would like to discuss some implications concerning the coronal expansion. Independently, Schatten and Newkirk pointed out that through the medium corona, a very important filtering effect occurs and therefore the knowledge of coronal structure at a typical altitude of  $0.6 R_{\odot}$  is of great importance [Schatten, 1968; Newkirk *et al.*, 1968]. The coronal structures observed in radioastronomy at this level after the filtering effect have the same stability and longitudinal extent as the underlying filaments. Because large filaments reflect large regular magnetic field structures, it may help to understand physically why a relatively good correlation between interplanetary and photospheric large scale patterns has been found [Wilcox and Ness, 1965].

In connection with this problem, Martres *et al.* [1970] have emphasized that large coronal regions disconnected from any calcium plages and identified by their thermal emission at 169 mHz play a basic role in the sector structure of the interplanetary medium (fig. 2). In the light of our present results, we now conclude that these coronal regions are to be interpreted as streamers. This result is in full agreement with Bohlin's [1970] paper showing the connection between an asymmetrical helmet streamer and the interplanetary magnetic field.

---

Drs. Avignon, Martres, Pick, and Simon are at the Meudon Observatory, France; Dr. Axisa is at the Service d'Electronique Physique, Centre d'Etudes Nucléaires de Saclay, France.

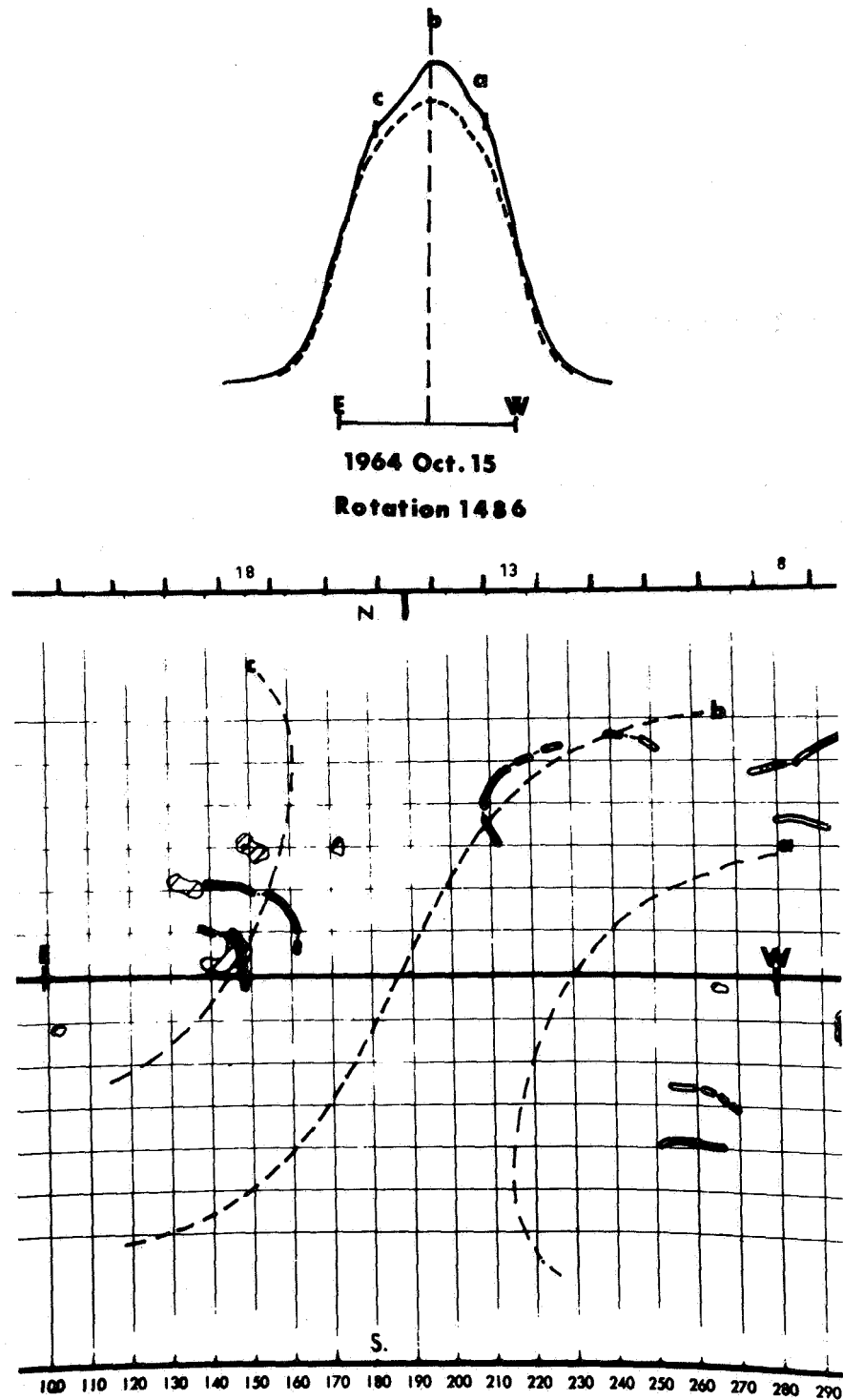


**Figure 1.** Correlation between RFIs and optical features. The upper part of the figure shows an RFI (b) which crossed the meridian on October 15, 1964. Other RFIs (a) and (c) are distinguishable on the flanks. In the lower part, the synoptic map of Meudon is reproduced. The dashed line (b) is the plot of the meridian trace which crosses a high latitude filament. Dashed lines (a) and (c) represent the traces of the scans corresponding to RFIs (a) and (c) [Axisa et al., 1971].

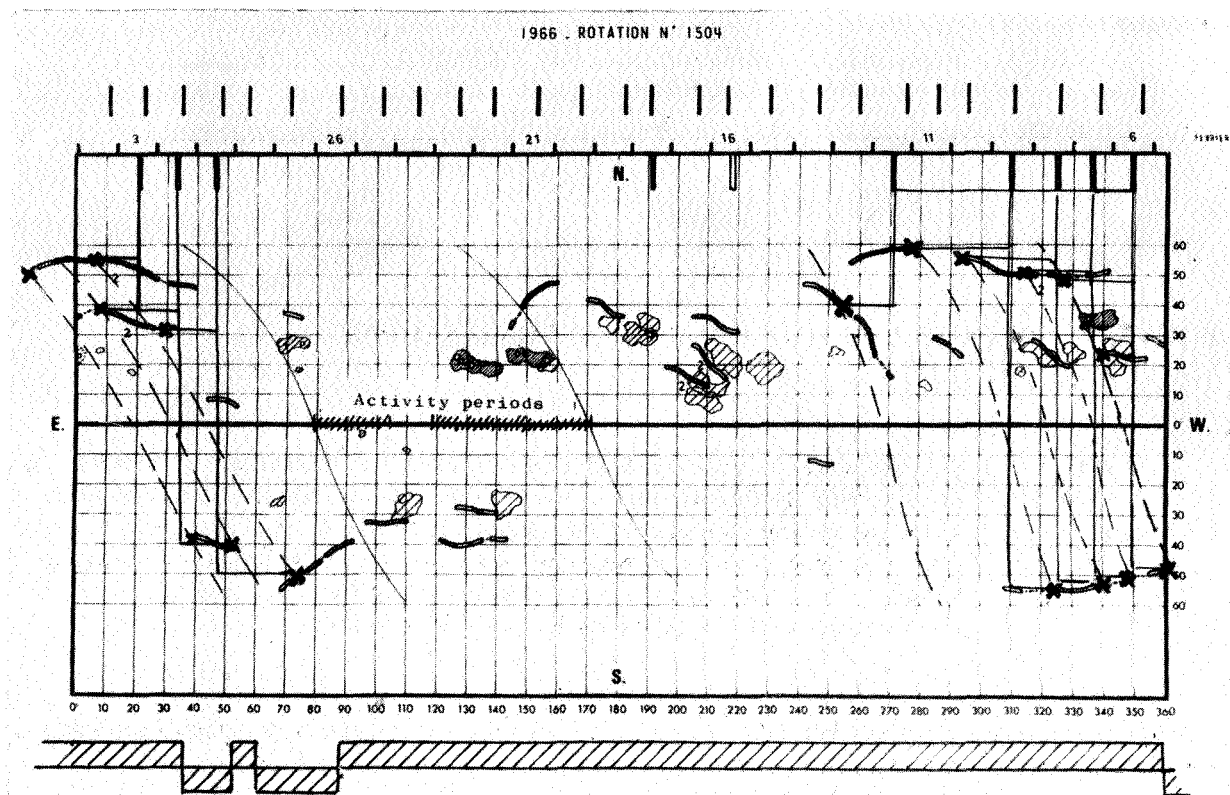


Figure 2. Comparison between the streamers positions and the inversion of interplanetary magnetic field (taking into account the velocity of solar wind).

Finally, we would like to emphasize that as the slowly varying component observed near 169 mHz, contrasting with higher frequencies, is not at all representative of the solar activity (eruptive centers, calcium plages, coronal condensations, coronal enhancements), the pattern of the interplanetary sectors would not be simply linked to calcium plages.

We now come to the solar wind expansion. Referring to the theoretical work of *Pneuman* [1969], we think that it is not so much the streamer itself that is of crucial importance, but the surrounding region. It is quite clear that solar activity will have a basic role to play by supplying energy. For the transfer of that energy throughout the medium corona, active streamers and helmet streamers will play an important role.

#### REFERENCES

- Axsa, F.; Avignon, Y.; Martres, M. J.; Pick, M.; and Simon, P.: Streamers and Active Streamers from Radio Observations. *Solar Phys.*, 1971 (in press).
- Bohlin, J. D.: Evolution of Discrete Features from the Sun to 1 AU. *Solar Phys.*, Vol. 13, 1970, pp. 153–175.
- Koutchmy, S.: Un modèle de grant jet coronal avec renforcement de région active. *Astron. Astrophys.*, 1971 (in press).
- Martres, M. J.; Parks, G. K.; and Pick, M.: The Origin of Interplanetary Sectors from Radio-Observations. *Solar Phys.*, Vol. 15, 1970, pp. 49–59.
- Mercier, C.: Altitude of Type III Bursts Observed at 169 mHz, and Coronal Structure. *Solar Phys.*, 1971, to be submitted.
- Newkirk, G.; Altschuler, M. D.; and Harvey, J.: Influence of Magnetic Fields on the Structure of the Solar Corona. I.A.U. Symposium No. 35, 1968.
- Pneuman, G. W.: Coronal Streamers. *Solar Physics*, Vol. 6, 1969, pp. 255–275.
- Schatten, K. H.: Large Scale Configuration of the Coronal Interplanetary Magnetic Field. Thesis, University of California, Berkeley, 1968.
- Wilcox, J. M.; and Ness, N. F.: Quasi-Stationary Corotating Structure in the Interplanetary Medium. *J. Geophys. Res.*, Vol. 70, 1965, pp. 5793–5805.

## THE INTERPLANETARY AND SOLAR MAGNETIC FIELD SECTOR STRUCTURES, 1962–1968

Douglas E. Jones

**ABSTRACT** The interplanetary magnetic field sector structure has been observed from late 1962 through 1968. During this time it has been possible to study the manner in which the sector pattern and its relation to the photospheric magnetic field configuration changes from solar minimum to solar maximum. Observations have also been made relating sector boundaries to specific regions on the solar disk. These and other observations related to the solar origin of the interplanetary field are briefly reviewed.

The interplanetary sector structure has been studied throughout a major portion of the period from August 1962 through December 1968, which corresponds to Bartel's solar rotation numbers 1967 through 1852. There are, however, two major data gaps in the interplanetary data. The first occurs during the interval between Mariner 2 and IMP 1 and amounts to 14 solar rotations. The second is for 9 solar rotations during the interval between IMPs 1 and 2. No large data gaps exist during the remainder of this period.

In constructing the sector pattern, the assignment of polarity was first made on a 3-hr basis, and then on a daily basis or longer. The polarity assigned was that which occurred most frequently during the particular data interval. If no single polarity dominated, the data interval was designated as "mixed." However, it is not clear what percentage was required before a data block was assigned either a positive or negative polarity. During the relatively stable period just prior to solar minimum there was little difficulty in assigning the polarity as there occurred data blocks of several days in which the ratio of occurrence of one polarity to the opposite was as high as 100 to 1 [Fairfield and Ness, 1967]. However, beginning with the new solar cycle, long intervals consisting of one dominant polarity occurred less frequently and hence the assignment of polarity was done with less certainty. For example, one

interval designated by one group as mixed was assigned a definite polarity by another [Coleman *et al.*, 1967; Ness and Wilcox, 1967].

Figure 1 illustrates the interplanetary sector structure

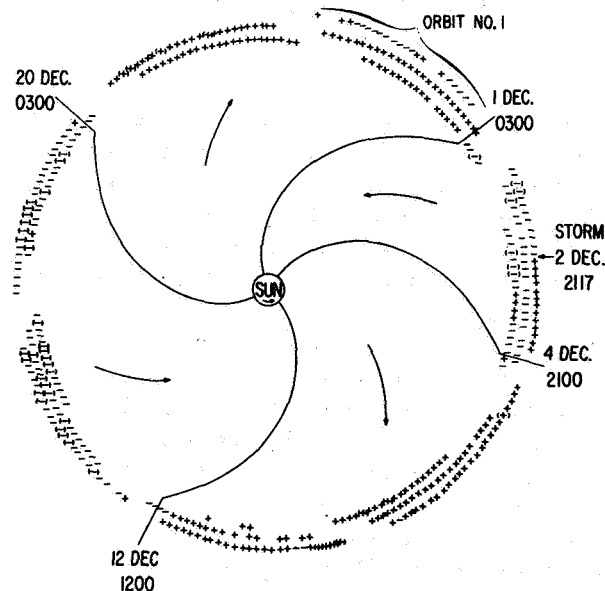


**Figure 1.** The interplanetary sector structure observed by IMP-1. The + signs (away from the sun) and - signs (toward the sun) at the circumference of the figure indicate the direction of the measured interplanetary magnetic field during successive 3-hr intervals [after Wilcox and Ness, 1965].

The author is at the Department of Physics and Astronomy, Brigham Young University, Provo, Utah.



and shows the well-known 2/7, 2/7, 2/7, 1/7 alternating polarity pattern obtained from IMP 1 data that was reported by Wilcox and Ness [1965]. Each polarity symbol (+ or -) represents the dominant polarity observed in each 3-hr interval of the data. The sectors are clearly delineated by the spiral lines separating regions of differing polarity.

Figure 2, which is a sector polarity overlay on the daily C9 character figure for the years 1962 through 1968, portrays the manner in which the sector structure was seen to vary during this period. Each row shows the polarity pattern for one Bartel's solar rotation [Wilcox and Colburn, 1970]. The sector configuration is indicated by the shading—the dark intervals referring to

away sectors and the lighter gray intervals to toward sectors. Intervals that are white refer to times of mixed polarity or missing data. Diagonal bars indicate interpolated sector structure.

Referring to figure 2, note that the polarity pattern observed during the declining portion of the solar cycle prior to 1965 is characterized by the slow evolution of the sectors. During the interval between November and December of 1962 the data from Mariner 2 exhibited a 2-sector pattern [Coleman et al., 1966]. The data from IMP 1, obtained between November 1963 and February 1964, showed a 4-sector pattern. A similar 4-sector pattern persisted from September through December 1964, as evidenced by the combined data from IMP 2

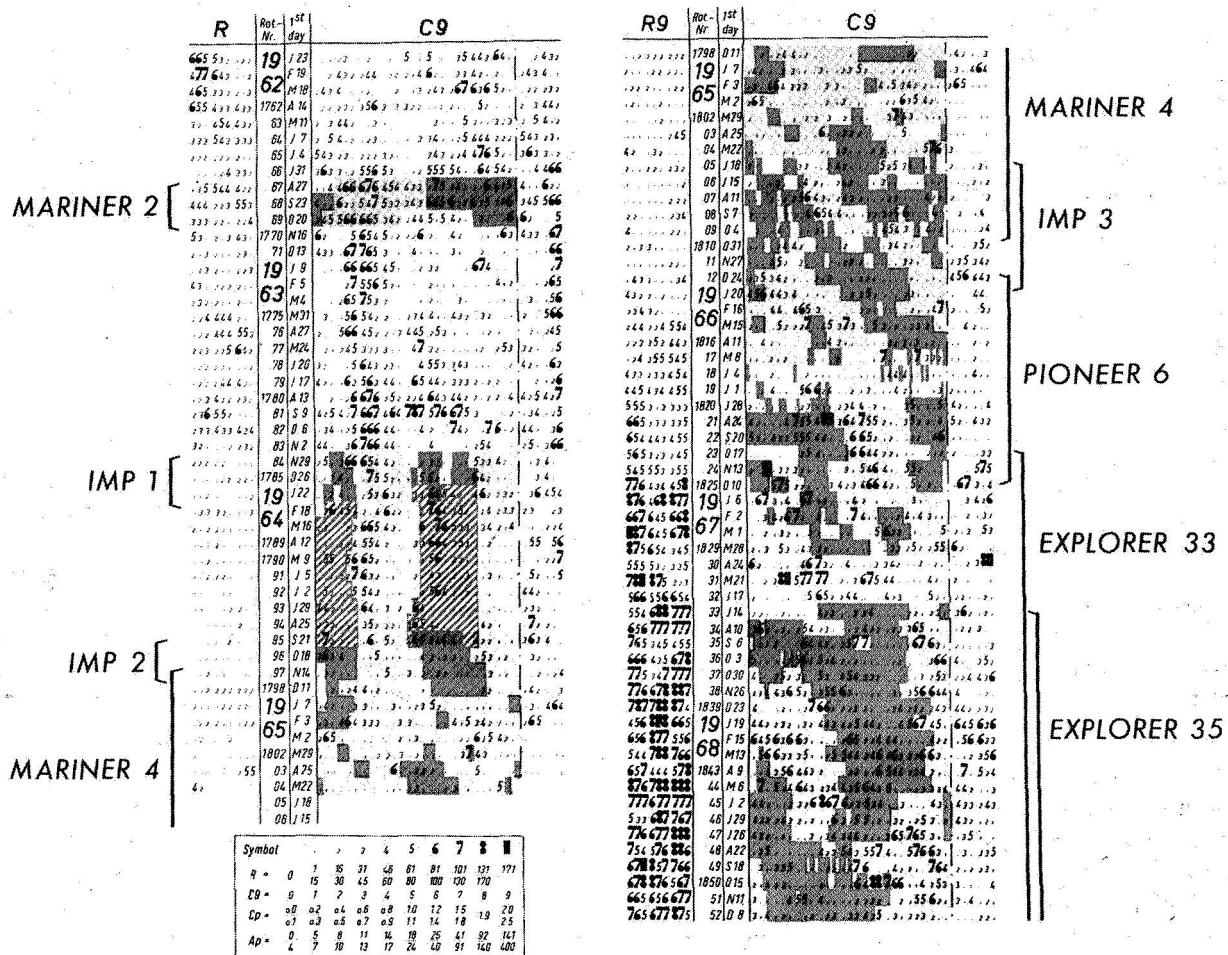


**Figure 2.** Observed sector structure of the interplanetary magnetic field, overlying the daily geomagnetic character index C9, as prepared by the Geophysikalisches Institut in Göttingen. Light shading indicates sectors with field predominantly away from the sun, and dark shading indicates sectors with field predominantly toward the sun. Diagonal bars indicate an interpolated quasi-stationary structure during 1964 [after Wilcox and Colburn, 1970].

and Mariner 4. However, in January 1965, one of the positive sectors disappeared.

The most stable sector configuration to date appears to be that which may have occurred between IMPs 1 and 2. Since this has been inferred by interpolation, we consider this point in some detail. The method of interpolating used was based on the manner in which the geomagnetic index sum  $K_p$  varied within the sectors observed by IMPs 1 and 2, and the variation of sum  $K_p$  during the interval in question [Wilcox and Ness, 1965; Ness and Wilcox, 1967]. Figure 3 displays the manner in which sum  $K_p$  was observed as a function of position in the 2/7 sectors seen by IMP [Wilcox and Ness, 1965].

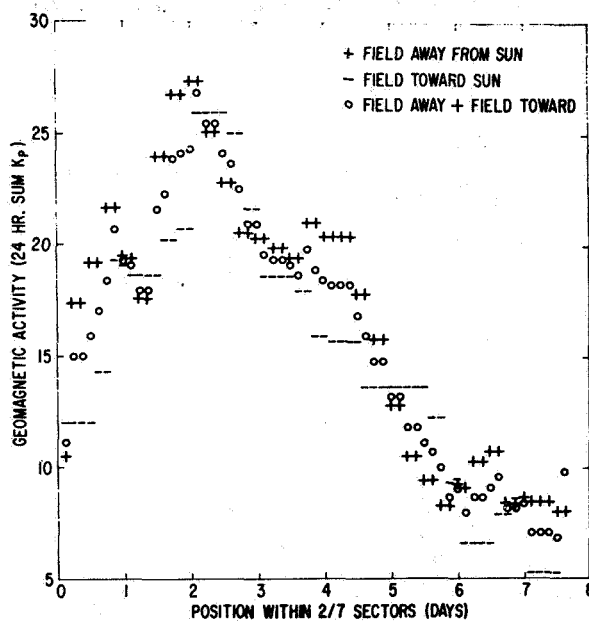


**Figure 3.** Superposed epoch analysis of the geomagnetic activity index 24-hr sum  $K_p$  as a function of position within the 2/7 sectors [after Wilcox and Ness, 1965].

The observed variation in the Deep River neutron monitor counting rate with position in the 2/7 sectors observed by IMP 1 [Wilcox and Ness, 1965] has also been used in support of this interpolated pattern [Wilcox and Howard, 1968]. Also, Asbridge *et al.* [1967] reported that the galactic cosmic ray intensity measured by the Vela satellites at times exhibited an approximate 7-day periodicity for a number of solar rotations and suggested that this variation may be related to the sector structure observed by IMP 1.

However, neither the variation in geomagnetic activity nor cosmic ray intensity has been shown to be uniquely related to the sector pattern. For example, excellent

correlation between  $K_p$  and fluctuations in the transverse component of the interplanetary field have been reported by Ballif *et al.* [1967, 1969]. Also, the Mariner 2 magnetic field and plasma data showed that whereas it is likely that high velocity streams in the solar wind originate in regions of the solar atmosphere throughout which the magnetic field has a single polarity, adjacent streams having the same polarity produce distinct geomagnetic events and no sector boundary is seen [Snyder *et al.*, 1963; Coleman *et al.*, 1966]. Coleman *et al.* [1966] have specifically investigated the possible persistence of a sector structure over the interval between Mariners 2 and 4 using observed correlations between geomagnetic effects and the solar wind velocity, and between polarity transitions of the field and minima in the solar wind velocity. They concluded that interpolation of the pattern between one observation and the next may be unreliable.

Figure 2 clearly portrays the rapid evolution of the sector pattern that began in 1965. In many cases the sectors are difficult to identify and the number and widths of intervals of constant polarity show considerable variability. Clearly the original concept of a magnetic sector, so evident in the earlier data, breaks down. Beginning with the latter half of 1966, there is a trend toward fewer sectors, and by 1968 it appears that the number of sectors has again reduced to 2. The evolution of the pattern near solar maximum is quite interesting as 2-sector patterns, differing in phase by about  $180^\circ$ , are separated by a period of about 4 solar rotations in which a 4-sector pattern persisted. During this time, however, it is difficult to see a direct relationship between dominant polarity intervals and the manner in which the  $K_p$  index varies (fig. 4). Recalling the Mariner 2 polarity pattern, it is tempting to infer that the gross magnetic polarity pattern of the field may exhibit only 2 sectors during the remainder of the present solar cycle [Wilcox and Colburn, 1970].

A well-defined 27-day periodicity of the interplanetary field was seen in the Mariner 2 data and interpreted as evidence for a connection between the field at 1 AU and large persistent magnetic field patterns on the sun [Davis *et al.*, 1964, 1965; Davis, 1965a, b]. The manner in which the sector pattern tends to move down and to the right suggests that the rotation period of the field may have increased between 1964 and 1966, and then returned to approximately 27 days in 1968. To obtain a quantitative estimate of the manner in which the rotation period of the field may have varied, autocorrelations of the interplanetary field were performed approximately each year from 1963 through 1968 [Ness and Wilcox, 1967; Wilcox and Ness, 1967; Wilcox and

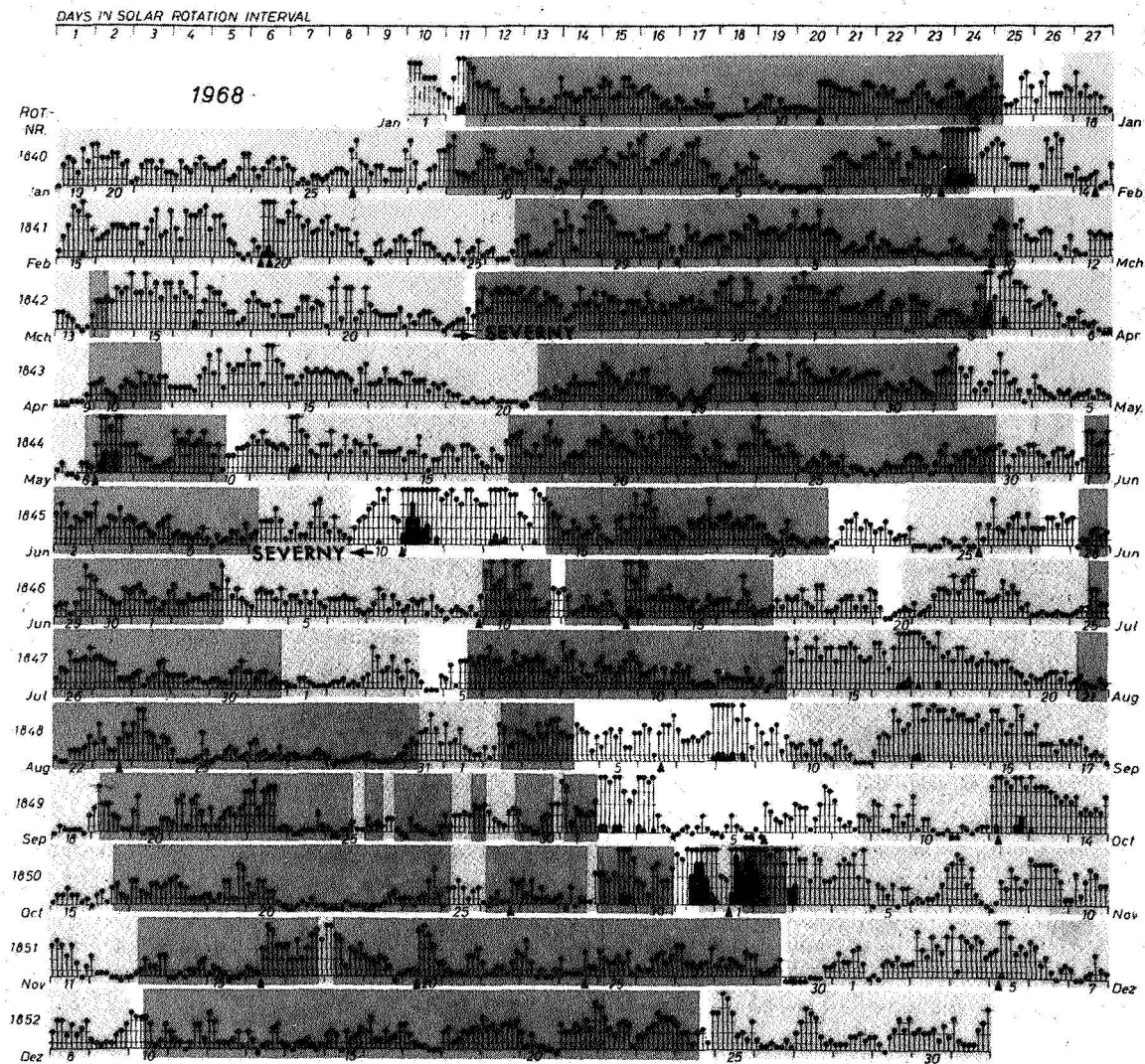


**Figure 4.** Interplanetary sector structure observed with Explorers 33 and 35 overlying a chart of planetary magnetic 3-hr range indices  $K_p$  [after Bartels]. Dark shading is field polarity toward the sun, and light shading is field polarity away from the sun [after Wilcox et al., 1969].

Howard, 1968; Wilcox and Colburn, 1969; and Wilcox and Colburn, 1970]. Figure 5 summarizes these results and also shows the mean and present variation in sunspot number. The marked increase in the rotation

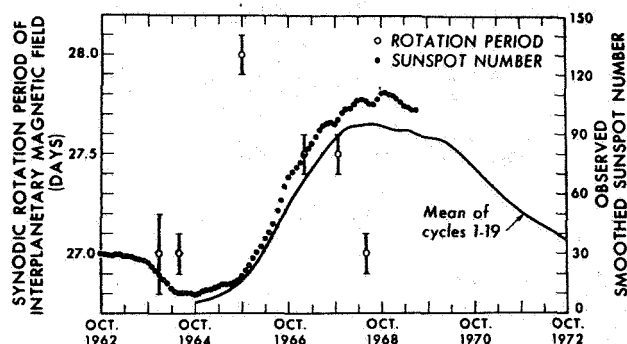


**Figure 5.** The synodic rotation period of the interplanetary magnetic field and the observed sunspot numbers during the last several years [after Wilcox and Colburn, 1970].

period that occurred near the beginning of the new cycle is quite evident and suggests that the interplanetary field source could have shifted to higher latitudes at this time much like the sunspots [Wilcox and Colburn, 1969], although other possibilities may exist. Wilcox and Colburn [1970] suggest that the period will likely remain at 27 days until solar minimum occurs again in 1975.

Some information regarding the variation in general latitude of the solar source of the interplanetary field can be inferred from the observed rotation period of the latter. Figure 6, derived by performing an autocorrelation on latitude strips of the photospheric field data [Wilcox et al., 1970], displays the manner in which the rotation period of the photospheric field varies with heliographic latitude. We see that the variation in period noted previously can be interpreted in terms of a variation in the heliographic latitude of the source. It appears that the average latitude of the source of the observed interplanetary field may have changed from about  $15^{\circ}$  N during solar minimum to a latitude higher than  $25^{\circ}$  N near the start of the new sunspot cycle, and then gradually declined as the cycle progressed [Ness and Wilcox, 1967; Wilcox and Colburn, 1969].

Cross and autocorrelations of the photospheric and interplanetary fields have also been computed by Ness and Wilcox [1964], Winters et al. [1969] and Schatten et al. [1969] to determine the solar origin of the interplanetary sector structure and the manner in which

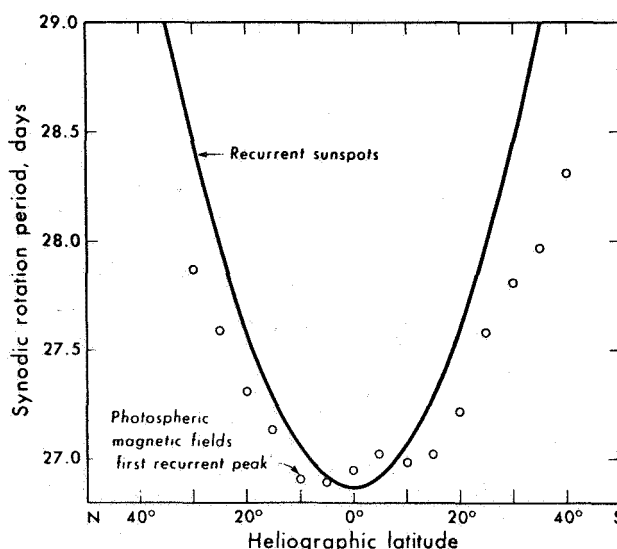


**Figure 6.** Solar differential rotation. The solid curve represents the results for long-lived sunspots. The circles are at the period associated with the first recurrence peak at each latitude in autocorrelations of photospheric magnetic field direction [after Wilcox et al., 1970].

any relationship might change as the solar cycle progresses. Using synoptic charts of the photospheric field supplied by R. Howard, Ness and Wilcox [1967] obtained cross-correlation coefficients of about 0.8 at a lag consistent with the plasma data when the IMP 1 data were compared to  $5^{\circ}$  wide latitude strips of the photospheric field data between  $15^{\circ}$  S and  $15^{\circ}$  N (fig. 7). It was also found that autocorrelations of the photospheric data between  $10^{\circ}$  and  $20^{\circ}$  N displayed the same sector-like character seen in the interplanetary field, in spite of the fact that IMP 1 was  $3.5^{\circ}$  south. These results suggested a "mapping" relation between the interplanetary and photospheric fields. On the other hand, Winters et al. [1969] were unable to duplicate these results using Mariner 4 data. Although poor correlations might be expected as a result of the evolving character of the sector structure noted earlier, one would have expected better correlations if the mapping hypothesis were indeed the case. Schatten et al. [1969] found that the IMP 3 data also correlated poorly with the photospheric field data, but they were able to obtain cross-correlation coefficients as high as 0.3 at the proper lag when the interplanetary field was compared instead with a "source surface" field derived from the photospheric field data and corresponding to about  $0.5 R_{\odot}$  above the photosphere (fig. 8). Thus, it would appear that the relationship seen earlier that led to the mapping hypothesis

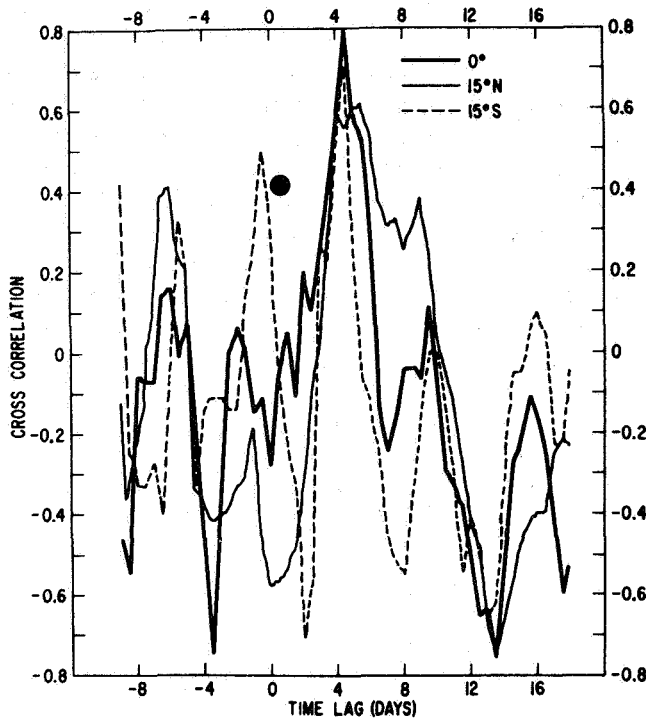


**Figure 7.** Cross correlation between IMP magnetic field direction (toward or away from the sun) and the photospheric field direction (into or out of the sun) for three latitudes on the sun [after Ness and Wilcox, 1964].

relating the interplanetary and solar fields may have been unique to that particular data interval.

By performing a cross correlation between latitudinal strips of the solar field and interplanetary sector configuration (40% observed, 60% interpolated) spanning the interval from December 1963 through December 1964, Wilcox and Howard [1968] found that a similar photospheric sector configuration may have existed over a range of latitudes of at least  $40^\circ$  N to  $35^\circ$  S (fig. 9). During this period, the pattern was found to change at all latitudes investigated within an interval of a few solar rotations. Because the shapes of the IMP 3 source surface correlations were different in the northern and southern solar hemispheres (fig. 8), Wilcox [1970a] has suggested that during the interval from June 1965 to February 1966 the persistent solar magnetic pattern may have been significantly different in the north and south. However, one should note that the correlation peaks obtained in this latter study were only 0.3 to 0.4.

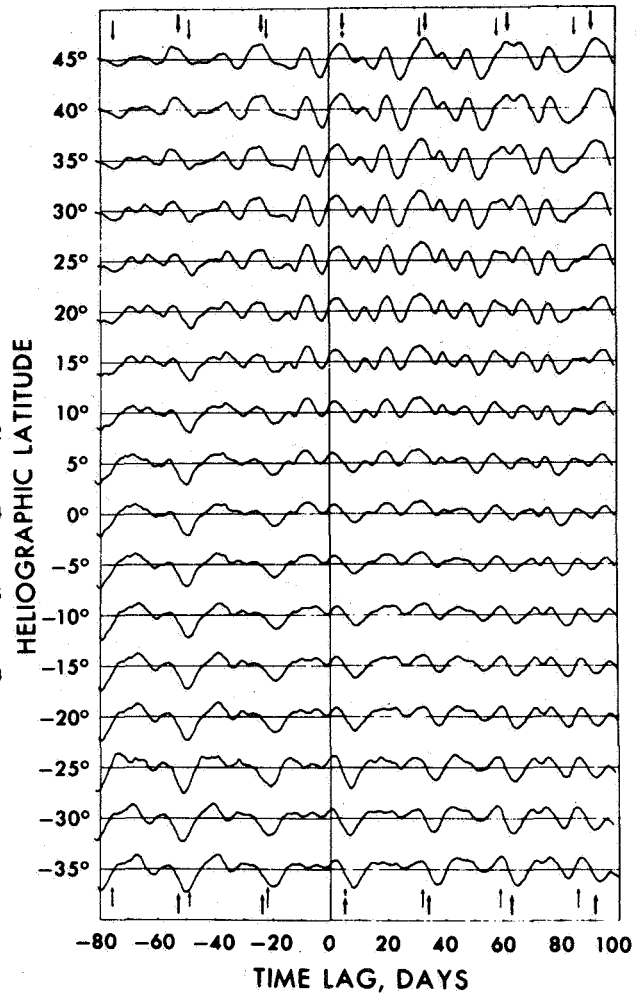


**Figure 8.** Cross correlation of the magnetic field calculated on a source surface  $0.5 R_\odot$  above the photosphere with the radial component of the interplanetary magnetic field as a function of time lag. Nine solar rotations of data are utilized, with correlations extending from  $35^\circ$  S to  $45^\circ$  N in intervals of  $5^\circ$ . Arrows at the bottom of the graph indicate time lags of 5 days plus an integral number of solar rotations [after Schatten et al., 1969].

The weighted mean solar field and the interplanetary field near earth for a period of several solar rotations in 1968 have been compared by Wilcox et al. [1969] and Severny et al. [1970] (fig. 10). They found a peak in the cross-correlation coefficient of nearly 0.7 at a lag of about 4-1/2 days. This significant result has been considered by Schatten [1970] who has shown that a high correlation is to be expected because of the similar dependence on subsolar angle of the mean solar field

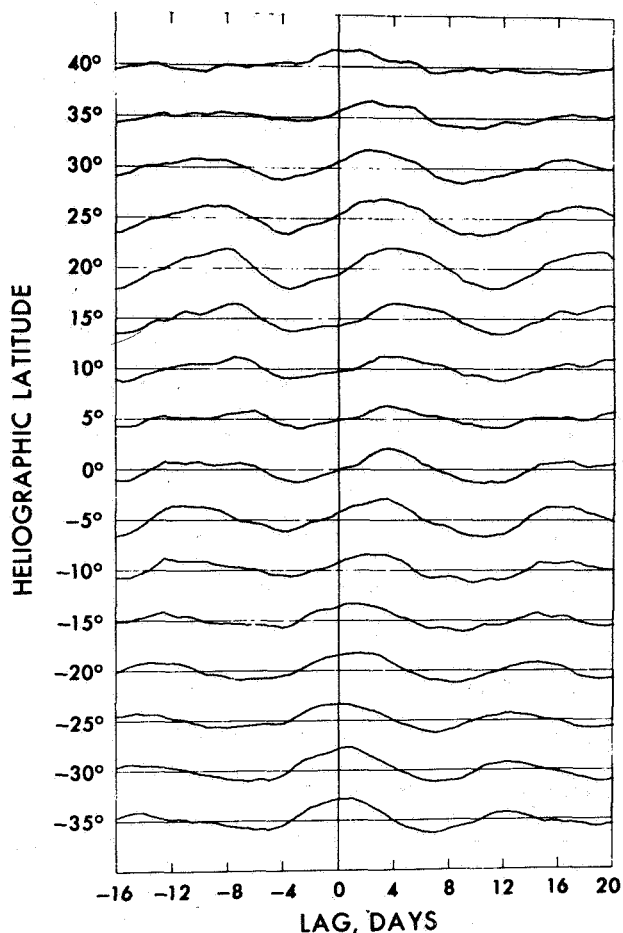


Figure 9. Cross correlation of the direction of the photospheric magnetic field and an interpolated pattern of the direction of the interplanetary magnetic field during a 1-year interval, from December 1963 to December 1964 [after Wilcox and Howard, 1968].

weighting factor and the weighting factor present in his source surface model. Assuming a symmetric brightness distribution, the weighting factors for the mean solar field integral and source surface integral for a  $2.0 R_{\odot}$  surface peak at subsolar angles between  $30^{\circ}$  and  $35^{\circ}$ . This apparent outward shift of the source surface to  $\sim 2.0 R_{\odot}$  appears consistent with the trend suggested by a comparison of the cross-correlation studies in 1963 and 1965 if one interprets the 1963 results in terms of a source surface at the photospheric level. One might conclude, therefore, that near solar minimum, the source surface lies essentially at the photospheric level, and as solar activity increases it moves outward, reaching a peak height above the photosphere of roughly  $2 R_{\odot}$  near solar maximum.

The mean field results offer an alternate interpretation, however. If one considers the presence of active centers and the attendant biasing effect on the brightness distribution across the solar disk, it would appear that perhaps all we are seeing is an excellent correlation between the magnetic polarity of an interplanetary plasma stream and the smoothed field of the solar active center that is its source. This could be checked by constructing ring averages of the photospheric field that incorporate brightness weighting factors derived from H-alpha and similar photographs of the sun, and comparing these with the mean field data.

Another important result seen in the cross-correlation studies of Schatten *et al.* [1969] and later by Severny *et al.* [1970] is that the magnitude of the correlation peak at a lag of  $4\frac{1}{2} + 27$  days was greater than that corresponding to a lag of  $4\frac{1}{2}$  days. Schatten *et al.* [1969] have interpreted this as suggesting that there may be a delay of approximately one solar rotation between the appearance of a new magnetic feature in the photosphere and a change in the interplanetary sector pattern that may result. It will be of great interest to follow changes in the lag over a major portion of a solar cycle. One might ask, for example, whether or not the additional lag always occurs or whether it is necessary that the field configuration in the vicinity of an active region change after it is at least  $\sim 45^{\circ}$  west of CMP.

On an even larger scale, Rosenberg and Coleman [1969] have found evidence suggesting that the dominant polarity of the interplanetary magnetic field follows the direction of the sun's dipolar field except perhaps just before solar minimum, near solar maximum, and at other times of high geomagnetic activity [Rosenberg, 1970]. They found, for example, that between 1965 and 1967 the dominant polarity of the interplanetary field was inward at heliographic latitudes above the solar equatorial plane and outward at latitudes below this plane. They also suggest that different polarity sectors can originate from different solar latitudes. However, Wilcox [1970b] extended this type of analysis to include the 1968 and 1969 data from Explorers 33 and 35 and found a disagreement between the observed polarity and the predicted curve. Wilcox has proposed that the 1965 result reported by Rosenberg and Coleman [1969] could be easily explained in terms of the dominant polarity exhibited by the synoptic charts of the photospheric magnetic fields at this time. On the other hand, Rosenberg [1970] attributes the negative results obtained with the 1968 and 1969 data to a southward shift of the dipolar field

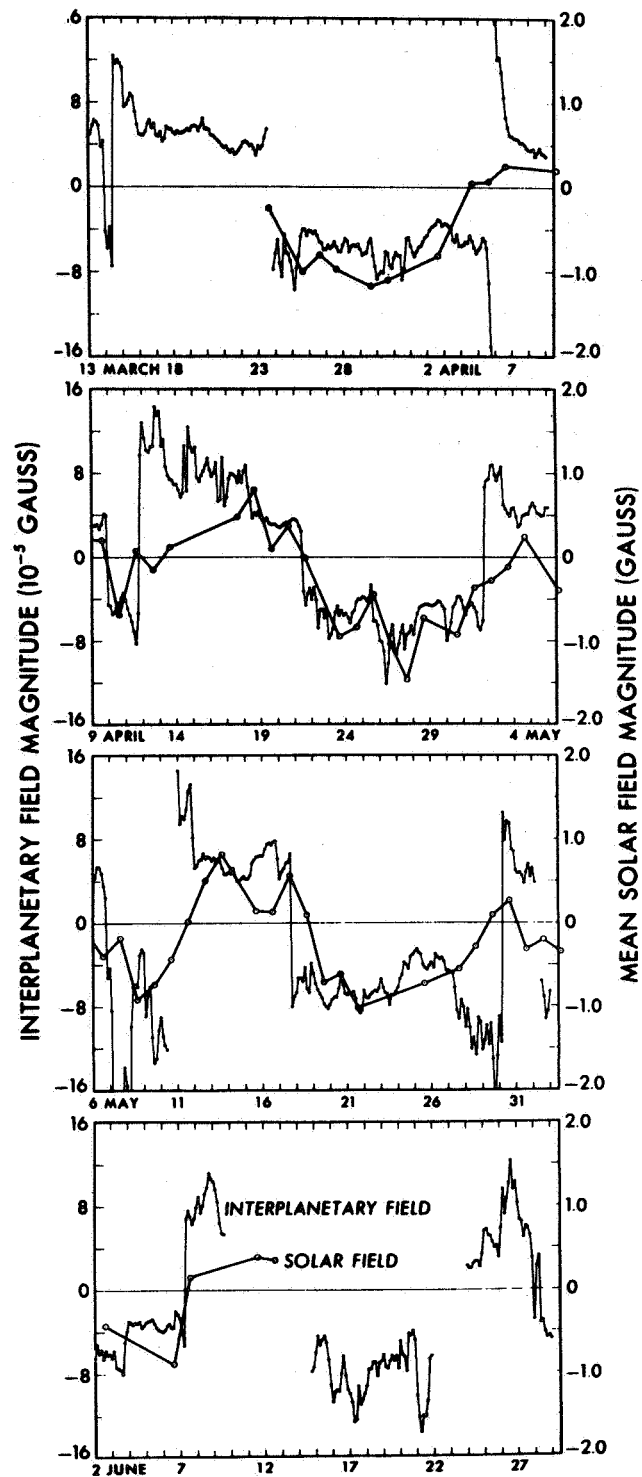


**Figure 10.** Comparison of the magnitude of the mean solar field and of the interplanetary field. The open circles are the daily observations of the mean solar field, and the dots are 3-hr average values of the interplanetary field magnitude observed near the earth. The solar observations are displaced by 4½ days to allow for the average sun-earth transit time. The abscissa is the time of the interplanetary observations [after Severny et al., 1970].



boundary in space that was caused by dominating activity in the northern hemisphere at this time. Data obtained during the new solar cycle should offer critical tests for the models that have been proposed.

There has also been much attention given to the solar source of the sector boundary and its effect on geomagnetic activity. Results of several radio interferometric studies of the sun have recently been reported which offer crucial information regarding the possible solar origin of sector boundaries. *Couturier and Leblanc* [1970], operating at 169 mHz, have recently found that coronal enhancements occur just eastward of solar sector boundaries although figure 11 shows that the converse is not necessarily true. *Wilcox* [1970a] has postulated the existence of subsectors.

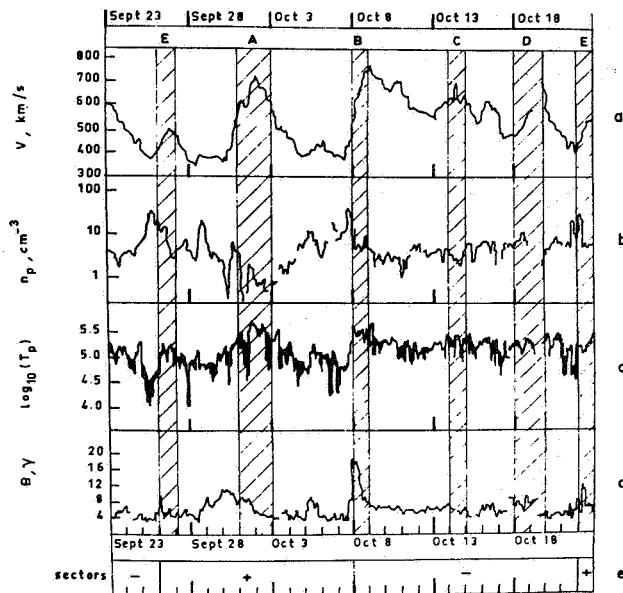


**Figure 11.** Solar wind activity during solar rotation 1968. The vertical hatched regions represent CMP of coronal enhancements. a, solar wind velocity, b, proton density, c, temperature (upper and lower limits) d, interplanetary magnetic field magnitude, and e, sector polarity pattern [after *Couturier and Leblanc*, 1970].

Using interferometer data obtained at 169, 408, and 9300 mHz, *Martres et al.* [1970] found further that coronal condensations associated with eruptive active centers are never found coincident with sector boundaries, but are related to the size of the sectors. They also found that when sector boundaries do follow coronal condensations, the meridian passage of a sector boundary always occurs within one day of the observed

crossing of the coronal condensation. In addition, the effect of active centers is to systematically displace the boundary toward the east.

The manner in which the 3-hr geomagnetic index  $K_p$  varies with time relative to the passage of a sector boundary may also have important implications in this regard. Using IMP 1 data, *Wilcox and Ness* [1965] found that when a superposed epoch analysis of  $K_p$  as a function of position within the 2/7 sectors was performed, the geomagnetic index exhibited a rapid increase after the passage of a sector boundary, reached a peak about 2 days later, and then slowly declined. This type of relationship was also noted then a comparison was made using the IMP 2 data [*Ness and Wilcox*, 1967]. A similar type of study has been performed using data related to the rising and maximum portions of the solar cycle by *Wilcox and Colburn* [1969, 1970]. The results for these three periods are shown in figure 12.

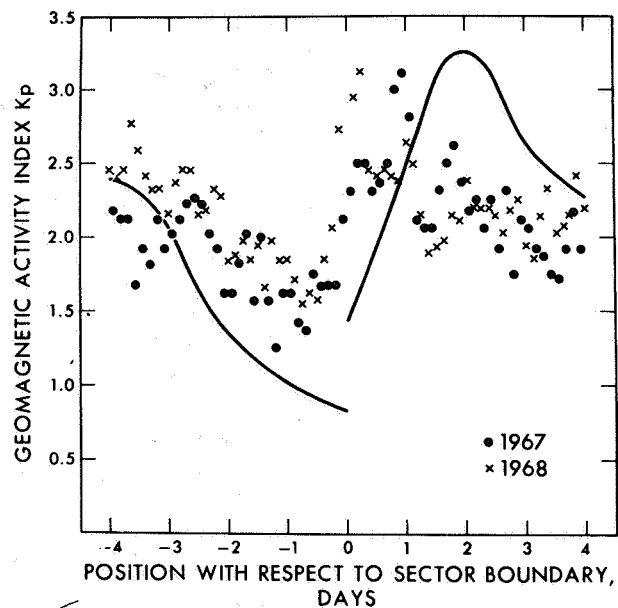


**Figure 12.** Superposed epoch analysis of the magnitude of the planetary magnetic 3-hr range indices  $K_p$  as a function of position with respect to a sector boundary. The abscissa represents position with respect to a sector boundary, measured in days, as the sector pattern sweeps past the earth. The solid line represents similar results obtained near solar minimum by *Wilcox and Ness* [1965], and the dots and crosses represent results obtained during the rising portion and near solar maximum, respectively [after *Wilcox and Colburn*, 1970].



The same general relationship noted in the earlier data appears to be present although some differences are seen, perhaps resulting from the different level of activity. During the later periods,  $K_p$  appears to increase more rapidly, and the peak appears to have moved closer to the time of the boundary crossing. One also notes that for 1967 and 1968 the minimum in  $K_p$  occurs as much as 18 hr before the sector boundary crossing. If real, this effect could be interpreted as an eastward shift in the position of the sector boundary with respect to the plasma stream causing geomagnetic activity that results from the increased level of activity at the sun in a manner consistent with the radio data. Evidence has also been given by Ballif and Jones [1969a,b] and Ballif et al. [1971] suggesting a direct relationship between localized flare producing regions on the sun and the geomagnetic and cosmic ray variability measured at earth. Certainly, regions of localized activity on the sun must play an important role in solar-terrestrial relations.

#### ACKNOWLEDGEMENTS

The author wishes to acknowledge many stimulating discussions on this and related subjects with his colleague, Jae R. Ballif.

This work was supported by the National Aeronautics and Space Administration under grant NMR 45-001-011.

#### REFERENCES

- Asbridge, J. R.; Bame, S. J.; Feltheuser, H. E.; and Gosling, J. T.: *Trans. Amer. Geophys. Union*, Vol. 48, 1967, p. 172.
- Ballif, J. R.; Jones, D. E.; Coleman, P. J., Jr.; Davis, L., Jr.; and Smith, E. J.: Transverse Fluctuations in the Interplanetary Magnetic Field: a Requisite for Geomagnetic Variability. *J. Geophys. Res.* Vol. 72, 1967, p. 4357.
- Ballif, J. R.; Jones, D. E.; and Coleman, P. J., Jr.: Further Evidence on the Correlation Between Transverse Fluctuations in the Interplanetary Magnetic Field and  $K_p$ . *J. Geophys. Res.* Vol. 74, 1969, p. 2289.
- Ballif, J. R.; and Jones, D. E.: Flares, Forbush Decreases, and Geomagnetic Storms. *J. Geophys. Res.* Vol. 74, 1969a, p. 3499.
- Ballif, J. R.; and Jones, D. E.: Morphology of a Solar-Terrestrial Event in March 1966. *J. Geophys. Res.*, Vol. 74, 1969b, p. 3512.
- Ballif, J. R.; Jones, D. E.; Skousen, E. N.; and Smith, D. T.: Cosmic Ray Decreases and the Occurrence of Solar Flares. Submitted to *J. Geophys. Res.*, 1971.
- Coleman, P. J., Jr.; Davis, L., Jr.; Smith, E. J.; and Jones, D. E.: Variations in the Polarity Distribution of the Interplanetary Magnetic Field. *J. Geophys. Res.*, Vol. 71, 1966, p. 2831.
- Coleman, P. J., Jr.; Davis, L., Jr.; Smith, E. J.; and Jones, D. E.: The Polarity Pattern of the Interplanetary Magnetic Field During Solar Rotations 1798-1808. *J. Geophys. Res.*, Vol. 72, 1967, p. 1637.
- Couturier, P.; and Leblanc, Y.: On the Origin of the Solar Wind Velocity Variations. *Astron. Astrophys.*, Vol. 7, 1970, p. 254.
- Davis, L., Jr.; Smith, E. J.; Coleman, P. J., Jr.; and Sonett, C. P.: The Interplanetary Magnetic Field Measurements of Mariner 2 (Abstract). *Trans. Amer. Geophys. Union*, Vol. 45, 1964, p. 79.
- Davis, L., Jr.; Smith, E. J.; Coleman, P. J., Jr.; and Sonett, C. P.: Interplanetary Magnetic Measurements, in *The Solar Wind*, (Proc. Conf. Solar Wind, Pasadena, 1964), edited by R. J. Mackin and M. M. Neugebauer, Pergamon Press, New York, 1965, p. 35.
- Davis, L., Jr.: Mariner 2 Observations Relevant to Solar Fields, in *Stellar and Solar Magnetic Fields*, (Proc. Intern. Astron. Union Symp., 22nd, 1963), edited by R. Lust, North-Holland Publishing Co., Amsterdam, 1965a, p. 202.
- Davis, L., Jr.: Models of the Interplanetary Fields and Plasma Flow, in *The Solar Wind*, (Proc. Conf. Solar Wind, Pasadena, 1964), edited by R. J. Mackin and M. M. Neugebauer, Pergamon Press, New York, 1965b, p. 147.
- Fairfield, D. H.; and Ness, N. F.: Magnetic Field Measurements with the IMP 2 Satellite. *J. Geophys. Res.*, Vol. 72, 1967, p. 2379.
- Ness, N. F.; and Wilcox, J. M.: Solar Origin of the Interplanetary Magnetic Field. *Phys. Rev. Letters*, Vol. 13, 1964, p. 461.
- Ness, N. F.; and Wilcox, J. M.: Interplanetary Sector Structure, 1962-1966. *Solar Phys.*, Vol. 2, 1967, p. 351.
- Martres, M.; Pick, M.; and Parks, G. K.: The Origin of Interplanetary Sectors from Radio Observations. *Solar Phys.*, Vol. 15, 1970, p. 48.
- Rosenberg, R. L.; and Coleman, P. J., Jr.: Heliographic Latitude Dependence of the Dominant Polarity of the Interplanetary Magnetic Field. *J. Geophys. Res.*, Vol. 74, 1969, p. 5611.
- Rosenberg, R. L.: Unified Theory of the Interplanetary Magnetic Field. *Solar Phys.*, Vol. 15, 1970, p. 72.
- Schatten, K. H.; Wilcox, J. M.; and Ness, N. F.: A Model of Interplanetary and Coronal Magnetic Fields. *Solar Phys.*, Vol. 6, 1969, p. 442.

- Schatten, K. H.: A "Source Surface Theory" Corollary: the Mean Solar Field-Interplanetary Field Correlation. *Solar Phys.*, Vol. 15, 1970, p. 499.
- Severny, A.; Wilcox, J. M.; Scherrer, P. H.; and Colburn, D. S.: Comparison of the Mean Photospheric Magnetic Field and the Interplanetary Magnetic Field. *Solar Phys.*, Vol. 15, 1970, p. 3.
- Snyder, C. W.; Neugebauer, M.; and Rao, U. R.: The Solar Wind Velocity and Its Correlation with Cosmic-Ray Variations and With Solar and Geomagnetic Activity. *J. Geophys. Res.*, Vol. 68, 1963, p. 6361.
- Wilcox, J. M.: Sector Structure of the Solar Magnetic Field, to be published in *Solar Magnetic Fields*, (Proc. I.A.U. Symp. No. 43, Paris), 1970a.
- Wilcox, J. M.: Statistical Significance of the Proposed Heliographic Latitude Dependence of the Dominant Polarity of the Interplanetary Magnetic Field. *J. Geophys. Res.*, Vol. 75, 1970b p. 2587.
- Wilcox, J. M.; and Ness, N. F.: Quasi-Stationary Corotating Structure in the Interplanetary Medium. *J. Geophys. Res.*, Vol. 70, 1965, p. 5793.
- Wilcox, J. M.; and Ness, N. F.: Solar Source of the Interplanetary Sector Structure. *Solar Phys.*, Vol. 1, 1967, p. 437.
- Wilcox, J. M.; and Howard, R.: A Large-Scale Pattern in the Solar Magnetic Field. *Solar Phys.*, Vol. 5, 1968, p. 564.
- Wilcox, J. M.; and Colburn, D. S.: Interplanetary Sector Structure in the Rising Portion of the Sunspot Cycle. *J. Geophys. Res.*, Vol. 74, 1969, p. 2388.
- Wilcox, J. M.; Severny, A.; and Colburn, D. S.: Solar Source of Interplanetary Magnetic Fields. *Nature*, Vol. 224, 1969, p. 353.
- Wilcox, J. M.; and Colburn, D. S.: Interplanetary Sector Structure Near the Maximum of the Sunspot Cycle. *J. Geophys. Res.*, Vol. 75, 1970, p. 6366.
- Wilcox, J. M.; Schatten, K. H.; and Tanenbaum, A. S.: Photospheric Magnetic Field Rotation. *Solar Phys.*, Vol. 14, 1970, p. 255.
- Winters, J. B.; Ballif, J. R.; and Jones, D. E.: A Comparison of the Photospheric and Interplanetary Magnetic Fields During the Flight of Mariner IV. *Solar Phys.*, Vol. 7, 1969, p. 478.

**DISCUSSION** J. M. Wilcox I rise to the defense of the sector interpolation in 1964. The physical evidence cited by Doug Jones has always seemed fairly convincing to me, but there is very recent evidence that, from observing the geomagnetic field in the polar regions, a close correlation with the sector polarity is obtained in the sense that in an away sector the field lines leaving the polar region near the north pole have a larger drag on them than would be the case in a toward sector. Using this one again finds the same four-sector polarity through the interval in which the interpolation was made.

#### COMMENTS

E. J. Smith This short contribution deals with the propagation of sector boundaries over widely separated points in space. E. J. Rhodes and I have just finished a study of sector boundaries using Mariner 5 magnetic field data. Mariner 5 was on its way toward Venus at the time. Those measurements were compared with measurements of the interplanetary field near earth by Explorers 33 and 35. It seemed appropriate to show these data at this session because, as you heard this morning, there are several studies under way that attempt to relate the sector boundaries in interplanetary space to solar magnetic fields. In addition, what happens to the sector boundaries as they propagate from the sun to the earth is one way of studying the large scale interactions that are occurring in the solar wind.

Figure 1 shows the essential geometry of the problem. The Mariner trajectory is shown as projected into the plane of the ecliptic. The horizontal direction is the sun-earth direction. Solar rotation numbers are marked along the trajectory. As you can see, the difference between the two spacecraft grew to be as large as about 0.3 AU, and, similarly, the angular separations grew to be substantial. We have used the sector boundaries identified by Wilcox and Colburn to find the corresponding sector boundaries in our data. We then used the corresponding sector boundaries to determine the propagation time between the two points of observation.

The results are shown in figure 2, which is simply a plot of the observed time delay versus the day number of the year. The time delays are represented by points and vertical lines. The lines indicate either a data gap or an uncertainty in identification. The curves

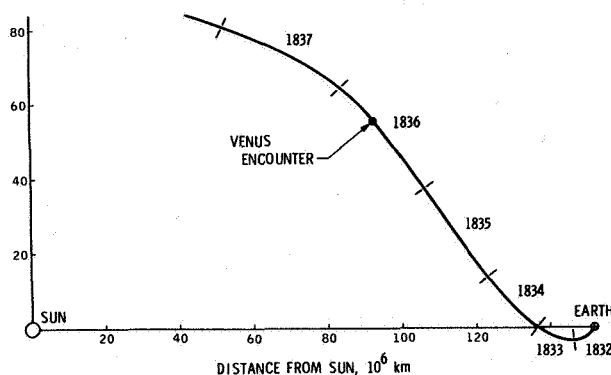


Figure 1 Mariner 5 trajectory projected into the plane of the ecliptic.

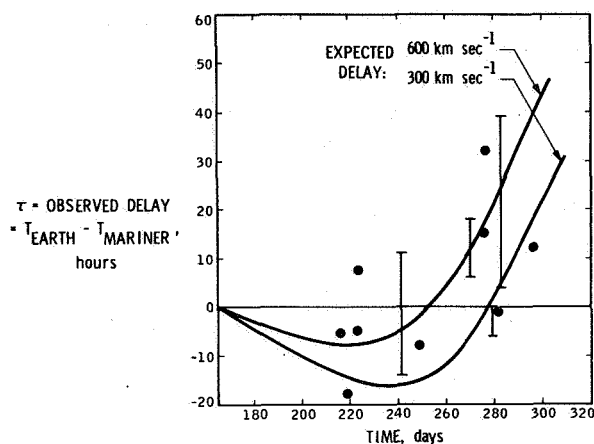
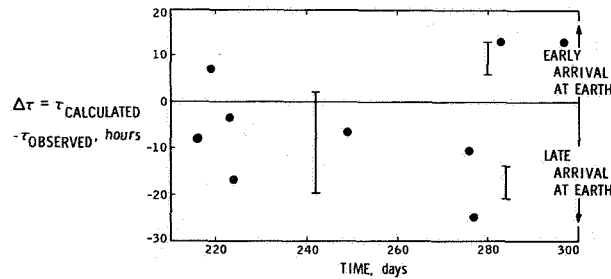


Figure 2. Observed and expected delay times for sector boundaries at Mariner 5 and at the earth.

drawn through the data show the expected time delays corresponding to two solar wind speeds, one at 600 km/sec and the other at 300 km/sec. These values bracketed the minimum and maximum velocities measured at Mariner during this time interval.

There is a general correspondence between the observations and the expectations based on a simple model of the solar wind, namely, assuming constant solar wind speed. But there are very large deviations, some of which are as large as one day. Figure 3 was prepared in an attempt to reduce the scatter somewhat and to investigate the causes of these deviations. We calculated the time delay not on the basis of some average solar wind speed but using the actual speed as measured by the Mariner plasma probe. Knowing when the solar wind carried the sector boundary past Mariner 5, and assuming that the wind speed would be constant for the remaining distance to earth, it was possible to compute the delay time. Plotted here are the residuals, which are the differences between the observed and computed delays, assuming a constant solar wind speed between Mariner 5 and earth. Again, the residuals or deviations are quite large. Several deviations seen here are as large as a day. There appears to be a tendency for more of the sector boundaries to arrive late at earth than early.

We interpret these results from two points of view. First, we believe the reason for the large discrepancies is the interaction between adjacent solar wind streams. There are any number of interaction effects that might be invoked. We are investigating several now. I'm



**Figure 3.** Difference between calculated and observed delay times for sector boundaries observed at Mariner 5 and at the earth. The solar wind velocities observed by Mariner 5 were used in the calculation.

a little partial, myself, to an explanation based on the deflection of the solar wind as a result of these interactions. One need not have a very large deflection, say only  $5^\circ$  or so, to account for the differences in the delays as large as those that are actually being seen.

The other viewpoint concerns the desire to make the sector boundary measurements near earth and extrapolate backwards toward the sun. One has to be careful in doing that because deviations as large as a day would correspond to something like  $10^\circ$  to  $15^\circ$  in longitude on the sun. Of course, how important such errors are, and how significant these deviations are, will depend on what it is you're trying to study.

#### DISCUSSION

*A. J. Dessler* Would you say the fact most of them arrive late means that interactions are all decelerating interactions or wouldn't you? Those interactions between adjacent streams, wouldn't you have as many arriving early as late?

*E. J. Smith* Well, you might think so; I think there probably are several factors involved. But based just on a preliminary investigation I think that the sector boundaries much more commonly than not tend to occur in the velocity minima ahead of the solar wind streams. And I think that then there is a preferential deflection in the solar wind flow. That's the sort of hypothesis I'm investigating now.

*R. L. Carovillano* I wonder if your study might not be able to reflect a little bit on whether the neutral sheet has one shape or another. For example, whether we have something that is fluted, going around azimuthally, or something like an orange peel, or something like that. Various interpretations might be implied by fitting your delay time to various geometries.

*K. H. Schatten* I think these observations point out non-Archimedean spiral nature of the field at times, and that it is only a spiral on the average, and deviations occur. I think we might try to improve the correlations of observed delay times by calculating not just an average Archimedean spiral field but rather, say, using the observed field to get what the shape of the field is as it's going by between the two points, or utilizing the observations of velocity and calculating the field deflection from the gradient in the velocity. And you might try that on these delay times.

*E. J. Smith* That would give you a longitude density, right.

*J. M. Wilcox* You pointed out if one observes the sector boundary at earth and takes it back to the sun, the result is uncertain by plus or minus a day or so. In other words, plus or minus  $15^\circ$ .

*E. J. Smith* That's correct, that's right.

*J. M. Wilcox* It may be worth noting that the observations of the mean solar field that are now in progress will probably help this, because one is then observing directly at the sun. It seems quite likely that we can get the time at which the field goes through zero or, in other words, the time when the sector boundary should be centered near central meridian, up to within a couple of hours; which would greatly facilitate comparisons with other solar features.

## LARGE-SCALE SOLAR MAGNETIC FIELDS AND H-ALPHA PATTERNS *Patrick S. McIntosh*

**ABSTRACT** Coronal and interplanetary magnetic fields computed from measurements of large-scale photospheric magnetic fields suffer from interruptions in day-to-day observations and the limitation of using only measurements made near the solar central meridian. Procedures have been devised for inferring the lines of polarity reversal from H-alpha solar patrol photographs that map the same large-scale features found on Mt. Wilson magnetograms. These features may be monitored without interruption by combining observations from the global network of observatories associated with NOAA's Space Environment Services Center. The patterns of inferred magnetic fields may be followed accurately as far as  $60^\circ$  from central meridian. Such patterns will be used to improve predictions of coronal features during the next solar eclipse.

### INTRODUCTION

Careful interpretation of structures seen on H-alpha solar filtergrams allows the inference of magnetic field patterns within active regions and in areas of extended weak magnetic fields [McIntosh, 1970]. The large-scale distribution of weak magnetic fields is mapped by the dark filaments (fig. 1) and the patterns of fine fibrils which have been called filament channels or neutral bands [Rust, 1970]. These large-scale H-alpha patterns have not received much attention for two reasons: (1) the predilection of solar astronomers for high-resolution photography of small areas of the sun, and (2) the low resolution of most full-disk H-alpha patrol photographs. The limited field of view of the nonpatrol instruments prevents recognition of the large-scale organization of H-alpha structures. The adoption of new high-resolution films in recent years by many of the patrol observatories makes it possible to study the large-scale patterns mapped by fine structures formerly seldom observed on full-disk photographs. The continuity of filaments and filament channels over large areas of the sun, in and out of several active regions, implies that all these features

are physically associated. Examples of extremely long, continuous, longitudinal neutral lines are shown in the synoptic chart of inferred magnetic patterns for a single solar rotation (fig. 2). Magnetograms that display the strength and polarity of the longitudinal component in the magnetic field do not reveal the large-scale associations without ambiguity. The filament channels are apparently responses to patterns of magnetic field lines parallel to the solar surface. They often form a common boundary to many separated areas of longitudinal fields. The absence of measurable longitudinal fields on these boundaries makes the boundaries indistinguishable from areas where the total field vector goes to zero, if only the longitudinal component is recorded.

The studies of the distribution of large-scale magnetic fields have previously been limited by the low resolution of the full-disk magnetograms and the restriction to using measurements within  $40^\circ$  of the center of the disk [Bumba and Howard, 1965b]. The positions of inferred lines of polarity reversal are certainly accurate to better than the 23 arc-sec resolution of the synoptic magnetic charts, and it is possible to obtain usable magnetic field patterns as far as  $60^\circ$  from the center of the disk. It should be possible to monitor the evolution of large-scale magnetic patterns for as many as 10 consecutive

---

*The author is at the National Oceanic and Atmospheric Administration, Environmental Research Laboratories, Boulder, Colorado.*

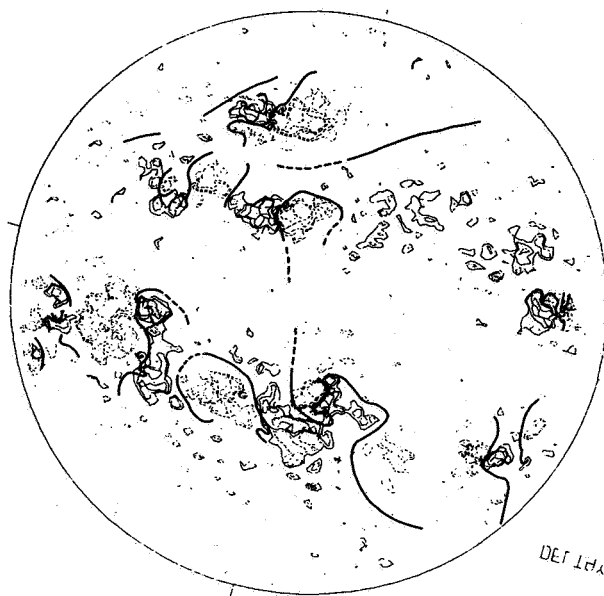


**Figure 1.** An H-alpha filtergram (top) for 4 June 1968 is compared with a Mt. Wilson plot of line-of-sight magnetic fields [McIntosh, 1971]. The heavy lines are the lines of polarity reversal inferred from the H-alpha structures. The dark filaments map most of the polarity reversals, with patterns of parallel fibrils (filament channels) connecting some filaments with the bright active regions. Filtergram from the NASA SPAN observatory operated by NOAA in Boulder, Colorado.

days with time resolution as good as the rate of photography on the solar flare patrol telescopes (as high as 10 sec). The many existing H-alpha telescopes assures that there will be no interruptions in the data such as now hamper studies based on magnetograph data [Altschuler, 1971]. The H-alpha data may reveal patterns of evolution that can be safely extrapolated from one solar rotation to the next, thereby allowing more accurate predictions of the large-scale magnetic fields. Such predictions could provide more accurate estimates of the coronal structures to be expected at times of total solar eclipses [Schatten, 1968]. Inferred magnetic patterns will be used for 1972 eclipse predictions.

Several maps of inferred longitudinal neutral lines have been combined to form the unforeshortened map of the entire sun in figure 2. This synoptic chart bears a strong resemblance to the *Cartes Synoptique* because both include all filaments. This chart also displays large-scale features spaced at regular intervals, mimicking the patterns revealed on synoptic charts of Mt. Wilson magnetograms [Bumba and Howard, 1965b]. Neither *Cartes Synoptique* nor the Mt. Wilson magnetic field charts reveal the continuity of longitudinal neutral lines over such large distances.

Nearly the full variety of forms exhibited by large-scale inferred magnetic patterns are shown in figure 2. A large cell of follower polarity in the northern hemisphere near 0° longitude is bounded by filaments on its

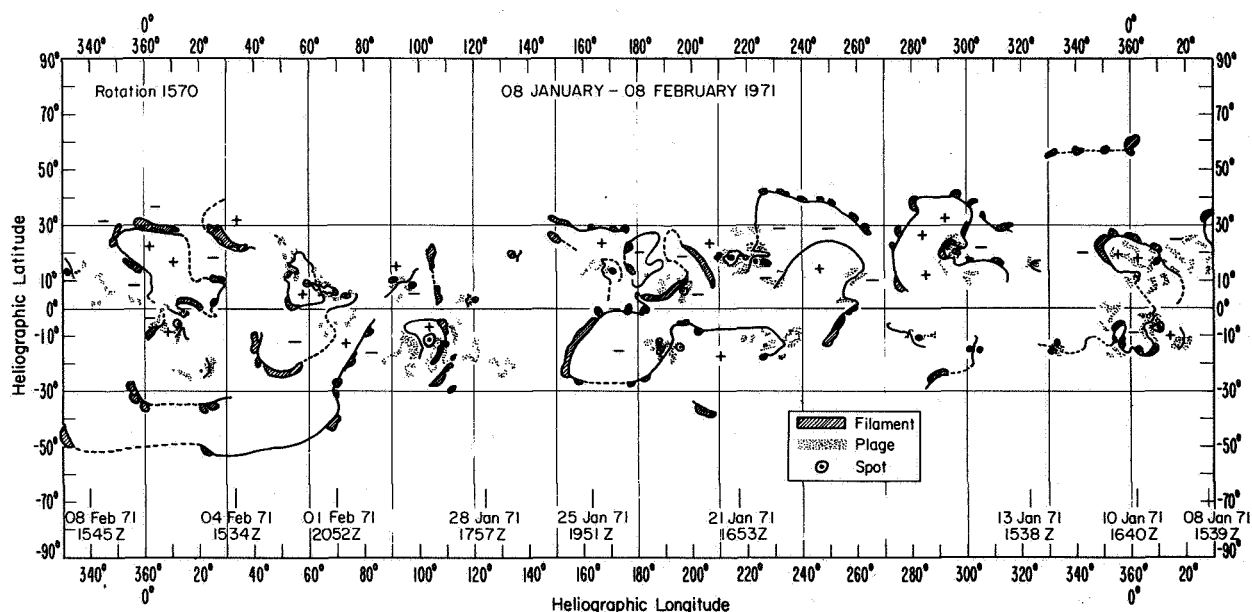


**Figure 2.** Daily maps of inferred lines of polarity reversal were combined to form a synoptic chart representing one solar rotation from 8 January through 8 February 1971. Dotted lines are extrapolations over areas of poorly ordered, or poorly resolved, H-alpha structures.

poleward side. This feature is typical of the areas of following polarity that evolve near areas of persistent active-region formation [Sýkora, 1969], and which have been identified with unipolar magnetic regions (UMRs); see figure 8 in *Bumba and Howard [1965b]*. The eastern, or following, side of the cell is bounded by an inferred line of polarity reversal that continues across the solar equator to form a weak mirror-image of the UMR, a pattern noted by Bumba and Howard in their discussion of UMRs seen in the magnetic field data.

The large cells of follower polarity always evolve from large active centers or complexes of activity, expanding and moving poleward and eastward after the active regions decay. *Bumba and Růžicková-Topolová [1969]* found a close relationship between positions of enhanced coronal emission and these filament-bounded areas of follower polarity. This relationship with active centers conforms to the relationship of coronal helmet streamers to active centers as discussed by *Bohlin [1970]*. *Pneuman [1969]* argues from theoretical grounds that the coronal structure associated with an active region should evolve toward a helmet-streamer form as the follower polarity fields expand into the extended areas studied by *Sýkora [1969]* and *Bumba and Růžicková-Topolová [1969]*. It appears that the coronal development must follow the development of the large, follower-polarity cells that are clearly visible on H-alpha filtergrams.

The large-scale patterns in both the inferred magnetic charts and the Mt. Wilson synoptic charts have typical diameters of about 25 heliographic degrees, in near-perfect agreement with the 300,000-km cell size predicted for the largest scale of solar convection [*Simon and Weiss, 1968*]. Study of the evolution of some of these large-scale features indicates that there are some features that undergo such rapid changes as to be unrecognizable after one solar rotation, while other patterns of similar scale remain little changed for as many as six solar rotations. Poleward migration of follower-polarity magnetic fields can be detected on a day-to-day basis (fig. 3). Note the poleward motion of filaments bounding the "cell" at 0° longitude in figure 2, comparing aspect at right to aspect at left. Proper motions of coherent features 30° in diameter have occurred that clearly exceed the motions attributable to differential rotation. Studies are planned that should determine whether these motions resemble large-scale circulatory patterns deduced by *Ward [1965]* and theorized by *Gilman [1969]*, *Kato and Nakagawa [1969]*, and others.

The study of the large-scale magnetic field patterns associated with the birth and development of an active

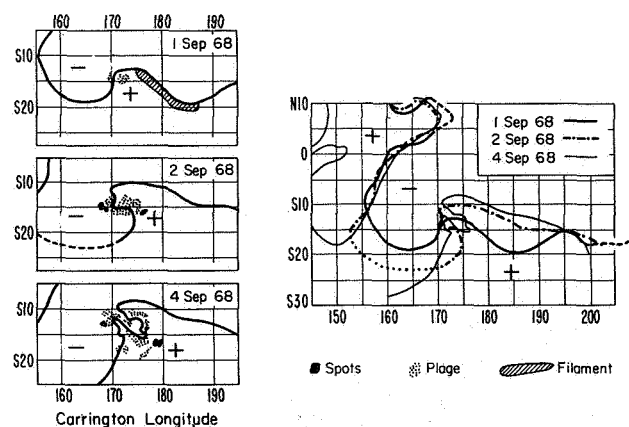


**Figure 3.** The patterns of inferred magnetic fields for a 4-day period near a developing active region are superposed. Large features distant from the activity repeat positions from day to day while rapid motions are evident near and within the active center.

region (fig. 3) showed some behavior that has since proven to be typical. The continuous patterns made up of filaments and filament channels extending over large distances tend to change slowly in time and repeat positions on successive days to within a fraction of a heliographic degree. Within a developing active region the pattern of the inferred polarities changes rapidly, generally becoming most complex at the time of greatest development of the active region.

The repeatability of the positions of the large-scale patterns is significant when an area near east limb is compared with its aspects at central meridian and near west limb. In no way could an eager observer influence the making of the map so that such an accuracy could be artificially produced. This repeatability of inferred patterns provides an additional proof of the validity of the techniques for inferring magnetic fields from H-alpha observations; in particular, it demonstrates the close correspondence of filament channels with the former positions of filaments.

Just as active regions first appear at the borders of supergranulation (30,000 km diameter) [*Bumba and Howard, 1965a*], the large complexes of activity [*Bumba and Howard, 1965b*] may prefer to form at the junction of two or more giant cells outlined by the filaments and filament channels [*Simon and Weiss, 1968*]. Understanding the evolution of large-scale magnetic field patterns could be important to long-range solar-activity forecasting.

The association of large, filament-bounded cells of follower polarity magnetic fields with UMRs, enhanced green-line corona, and helmet streamers implies that



proper interpretation of large-scale H-alpha patterns might lead to inference of interplanetary structures. Wilcox [1968] has shown that the interplanetary magnetic field is dominated by a sector structure corotating with the sun in which the field is predominantly away from the sun for several days (as observed near the earth) and then toward the sun for several days. This interplanetary structure and some of the coronal forms seen at times of eclipse have been successfully modelled by combining photospheric magnetic field measurements with potential theory [Schatten *et al.*, 1969]. Wilcox and Howard [1968] and Wilcox *et al.* [1969] have demonstrated a direct correlation between the interplanetary magnetic field distribution and the pattern of large-scale magnetic fields on the solar surface, finding an average delay of 4.25 days between central meridian passage of the solar source and the magnetic field reversal measured near the earth (Archimedes spiral of solar interplanetary field). Bumba and Obridko [1969] discovered that flare activity correlated closely with the interplanetary sector-boundary positions on the solar surface, with the correlation improving with increasing flare magnitude. The correlation was most striking for proton flares. The great flares and the extended areas of follower-polarity both originate from the large complexes of active centers; therefore, it appears that the follower cells, the UMRs, the coronal intensity, and the helmet streamers should also prefer positions near sector boundaries.

The UMRs were associated with the sources of recurrent geomagnetic activity by Bumba and Howard [1966] and Wilcox and Colburn [1969] demonstrated a strong correlation between geomagnetic activity and the passage of sector boundaries past the earth. The UMR was associated with the extended areas of follower polarity that were usually mirror-imaged in opposite hemispheres [Bumba and Howard, 1965b]. The enclosed cell of follower polarity near 0° longitude in figure 2 plainly has a southern hemisphere counterpart. Such conspicuous crossings of the solar equator by chromospheric markers of polarity reversal can be tentatively associated with the polarity reversals measured by spacecraft near the earth. First attempts at identifying the chromospheric marker of interplanetary sector structures indicate that equator-crossing filaments, filament-bounded cells of following polarity, and combinations of both are the most common features occurring near central meridian 4 days prior to a measurement of interplanetary polarity reversal near the earth. Attempts are being made to forecast sector structures from such features. Early results are encouraging, but there seem to be numerous features crossing the

equator without a measured reversal in the interplanetary fields. It appears that the degree of persistence of an equator-crossing filament (or filament channel) is related to whether that feature is a reliable indicator of the interplanetary structure. The longitude distribution of X-ray flares appears to follow the distribution of the filament-bounded cells of following polarity, with the most persistently active longitudes correlating with the most persistent equator-crossing inferred longitudinal neutral lines.

The prediction of recurrent geomagnetic activity from sector boundary positions depends, at present, on either interplanetary spacecraft or measurements of the solar magnetic polarity averaged over the whole solar disk [Wilcox *et al.*, 1969]. The positions and limited number of interplanetary spacecraft place limits on the reliability and lead time provided by predictions based on their measurements. The solar magnetic polarity measurements allow a 4-day advance notice of the passage of sector boundaries past the earth. If these boundaries can be inferred from the patterns of solar activity in H-alpha, then advance notice may be possible as soon as the appropriate patterns can be identified in the eastern hemisphere of the sun, increasing the lead time of prediction to as much as 8 days.

The correlation of solar activity with sector boundaries is stronger than the correlation with the active heliographic longitudes [Bumba and Obridko, 1969]. This implies that the fundamental source for flare activity is also the source of the interplanetary sectors. The detailed monitoring of large-scale solar magnetic fields through the interpretation of H-alpha patterns will contribute to a greater understanding of how flare-active regions and interplanetary sectors emerge and evolve.

#### ACKNOWLEDGEMENTS

John M. Wilcox has provided advice and encouragement for the pursuit of a relationship between large-scale H-alpha features and the interplanetary sector structures. Bela Scheiber, John E. Allen, and Charles Shanks prepared synoptic charts for the initial studies of the large-scale H-alpha features.

#### REFERENCES

- Altschuler, M.D.: The Geometry of the Coronal Magnetic Field. *Sky and Telescope*, Vol. 41, 1971, p. 146.
- Bohlin, J. D.: Solar Coronal Streamers II: Evolution of Discrete Features from the Sun to 1 AU. *Solar Phys.*, Vol. 13, 1970, p. 153.
- Bumba, V.; and Howard, R.: A Study of the Development of Active Regions on the Sun. *Astrophys. J.*, Vol. 141, 1965a, p. 1492.

- Bumba, V.; and Howard, R.: Large-Scale Distribution of Solar Magnetic Fields. *Astrophys. J.*, Vol. 141, 1965b, p. 1502.
- Bumba, V.; and Howard, R.: A Note on the Identification of 'M' Regions. *Astrophys. J.*, Vol. 143, 1966, p. 593.
- Bumba, V.; and Obridko, V. N.: 'Bartel's Active Longitudes', Sector Boundaries and Flare Activity. *Solar Phys.*, Vol. 6, 1969, p. 104.
- Bumba, V.; and Růžicková-Topolová, B.: Magnetic Fields, Green Corona and Filaments in High Solar Latitudes. *Bull. Astron. Inst. Czech.*, Vol. 20, 1969, p. 63.
- Gilman, P. A.: A Rossby-Wave Dynamo for the Sun, I. *Solar Phys.*, Vol. 8, 1969, p. 316.
- Kato, S.; and Nakagawa, Y.: The Solar Differential Rotation and 'Rossby-Type' Waves. *Solar Phys.*, Vol. 10, 1969, p. 476.
- McIntosh, P. S.: Techniques of Solar Flare Forecasting. AGARD Conference Proceedings No. 49 (Ionospheric Forecasting), edited by Vaughn Agy, Paper 8, 1970.
- McIntosh, P. S.: The Inference of Solar Magnetic Polarities from H-alpha Observations. Paper presented at AIAA Conference on Solar Activity Observations and Predictions, Huntsville, Alabama, Nov. 1970.
- Pneuman, G. W.: Coronal Streamers II: Open Streamer Configurations. *Solar Phys.*, Vol. 6, 1969, p. 255.
- Rust, D.: Magnetic Fields in Quiescent Solar Prominences II: Photospheric Sources. *Astrophys. J.*, Vol. 160, 1970, p. 315.
- Schatten, K. H.: Prediction of the Coronal Structure for Solar Eclipse of September 22, 1968. *Nature*, Vol. 220, 1968, p. 1211.
- Schatten, K. H.; Wilcox, J. M.; and Ness, N. F.: A Model of Interplanetary and Coronal Magnetic Fields. *Solar Phys.*, Vol. 6, 1969, p. 442.
- Simon, G. W.; and Weiss, N. O.: Concentration of Magnetic Fields in the Deep Convection Zone. IAU Symposium No. 35 (*Structure and Development of Solar Active Regions*), D. Reidel Publishing Co., Dordrecht, Holland, 1968, p. 108.
- Sýkora, J.: The Photospheric Magnetic Field Structure and Corona in a Small Complex of Activity. *Bull. Astron. Inst. Czech.*, Vol. 20, 1969, p. 70.
- Ward, F.: The General Circulation of the Solar Atmosphere and the Maintenance of the Equatorial Acceleration. *Astrophys. J.*, Vol. 141, 1965, p. 534.
- Wilcox, J. M.: The Interplanetary Magnetic Field, Solar Origin and Terrestrial Effects. *Space Sci. Rev.*, Vol. 8, 1968, p. 258.
- Wilcox, J. M.; and Colburn, D. S.: Interplanetary Sector Structure in the Rising Portion of the Sunspot Cycle. *J. Geophys. Res.*, Vol. 74, 1969, p. 2388.
- Wilcox, J. M.; and Howard, R.: A Large-Scale Pattern in the Solar Magnetic Field. *Solar Phys.*, Vol. 5, 1968, p. 564.
- Wilcox, J. M.; Severny, A.; and Colburn, D. S.: Solar Source of Interplanetary Magnetic Fields. *Nature*, Vol. 224, 1969, p. 353.

## COMMENTS

*E. C. Roelof* Bob Lin and I have been interested for quite a while in trying to use quite low-energy low-rigidity particles, solar energetic particles, to get some idea of how the field lines above active regions are mapped out to the earth, as sort of a way of doing this independent of the plasma data. The particles we are talking about are 45 keV electrons and 0.3 meV protons. Now, first of all, during an analysis from 1967 to 1969 of the electron data with regard to sector boundaries, the time histories at 45 keV are quite different from what one sees at thermal energies. The electrons just don't seem to know that the sector boundaries are there. These 45 keV electron fluxes are continuous across the boundaries when they are above background.

The story is a bit different for the protons. The protons sometimes undergo a discontinuous jump in intensity, either up or down but these are discontinuous jumps in a "D.C." level. There aren't peaks and therefore one would not say that at these times there is any streaming of the protons out along the sector boundaries, but rather that the sector boundaries are in some way related to proton storage in the corona. However, the 45 keV electrons don't seem to know that the boundaries are around.

We have tried to analyze some peculiar events that we call "core-halo" events. We found one in 1966 and we have found three more in 1967, and we don't seem to be finding any more after that. These are events in which about a day or so after a flare one sees an enhanced particle density coming around as a more or less quasi-stationary structure on the field lines, on the spiral field lines from the sun. There is a narrow core of these

low-energy particles that lasts only perhaps a fraction of a day, a third of a day, and a more extended halo, which can last several days. And harking back to the last solar wind conference, what we have done is take the technique of extrapolating solar wind streams back to the sun using the observed plasma velocity that was originally suggested by Neugebauer and Snyder. Figure 1 shows a mapping in an  $r$ - $\phi$  plot where  $r$  is the radial

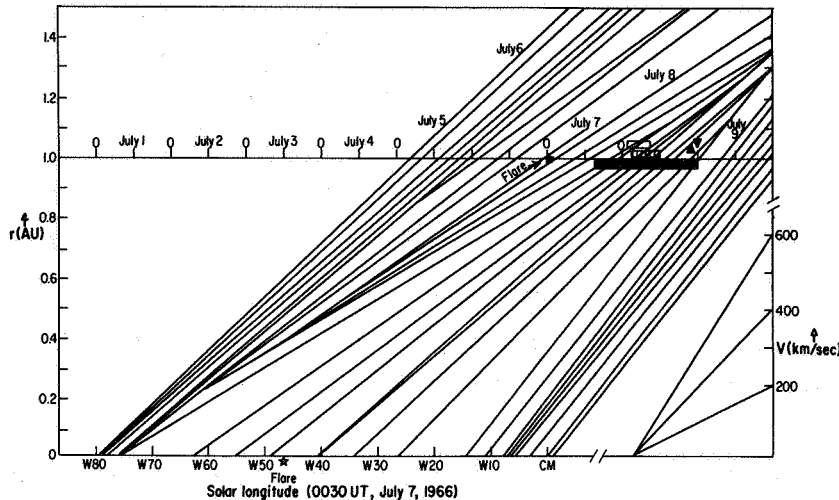


**Figure 1.** Solar wind streams mapped back to the sun (assuming a constant radial velocity). Radial distance from the sun ( $r$ ) is given in AU and solar longitude ( $\phi$ ) (west of central meridian location at 00 UT, 7 July 1966) is given in degrees on the abscissa. The time when the earth is at a given longitude (referred to CM at 00 UT, 7 July 1966) is marked on the line through  $r = 1$  AU. This is also the time when the plotted solar wind velocity was observed.

distance from the sun and  $\phi$  is the solar longitude. For those of you who are unfamiliar with the original paper, a spiral shows up as a straight line in such a plot. This is done for the July 7 flare in figure 1. The white box on the time line indicates the duration of the electron core, the striped box is the proton core, and the filled box is the proton halo. It is delightful to come to a conference and find someone reporting findings related to your own but in another region of energies and densities and particles. Professor Davis was talking about the rarefactions due to the interaction between a fast and a slow speed region of the solar wind. We have found that these core-halo events (all the ones we have found) all occurred during a rarefaction of the solar wind. You can read the solar wind velocities off the slopes of the lines using the key in the lower right corner of the figures.

When we map these stream lines back we are happy with an accuracy of something like  $10^\circ$  or  $15^\circ$  as far as the mapping goes and we claim no more accuracy. In figure 1 you will notice the core and the halo map back along the solar wind stream to the position of the solar flare which occurred at W47 about 00 UT on July 7. But there is an even more interesting phenomenon and that is the termination of the halo. It is accompanied by a sudden commencement of a magnetic storm, and a Forbush decrease occurred at the time when we leave the rarefaction of the low speed stream when there is a rapid transition to the fast stream which, in a naive sense, maybe one could say results in quickly switching the connection for the particles from the flare region quite far to the east where particles are no longer injected from the corona. Now, this is a very fortunate event because there were also Pioneer 6 data available. The same plot can be formed from Pioneer 6 data taken  $45^\circ$  to the west of the earth, and the remarkable thing on figure 2 is that we get the same story, although the data are fragmentary. One can identify the end of the proton core. There were no electron observations available at the end of the proton halo. Once

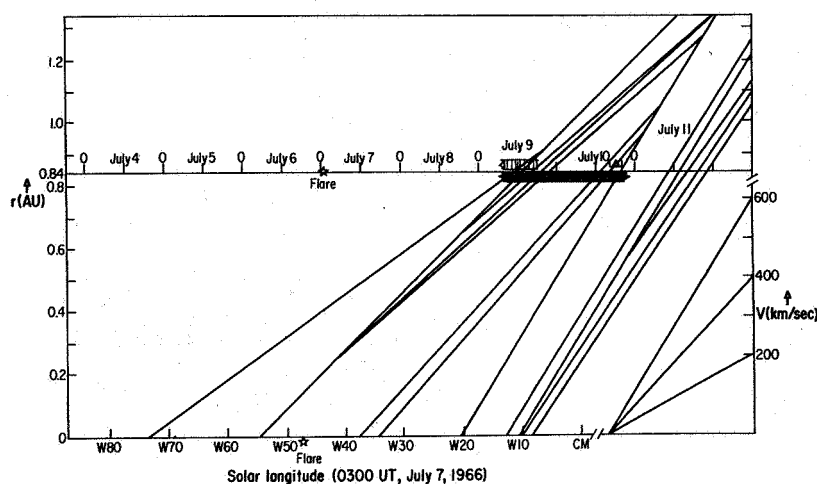


Figure 2. Mapping of solar wind streams as in figure 1 except time line now refers to observations on Pioneer 6 at  $r = 0.84$  AU and  $45^\circ$  to west of earth.

again the proton core is connected back to the vicinity of the flare, whereas the halo again terminates at the time when one goes from the rarefaction into the fast solar wind stream. One also notices that this event, which fits well to this picture of solar stream mapping, cannot be explained by a rigid rotation of some sort of a connecting field structure because the expected rigid corotation rate is something over 80 hr. The actual delay is 45 hr. It shows that this fast stream was evolving. Indeed, it means the solar wind velocity was higher on July 10 when it was detected by Pioneer 6 than it was at earth on July 9. And finally, of course, there is no possibility of explaining these proton fluxes by any sort of a radially moving feature because of the 45-hr time delay.

We have found three other events in 1967 that fit the same pattern of the particles being connected back to the flare region along solar wind streams and the halos occurring in the rarefaction region of the solar wind pattern and ending at the time when one enters the fast stream.

**DISCUSSION** *M. Dryer* Are you saying these particles go out with the shock wave that comes from the flare?

*E. C. Roelof* No, I'm saying these particles are coming out mainly collimated by the interplanetary magnetic field.

*M. Dryer* Which has been changed by the faster flowing plasma?

*E. C. Roelof* Well, the way one interprets those features drawn or the changes in the velocity is in the eye of the beholder. There can be no containment or elimination or shutting off of these particles by such a shock because of the 45 hr delay between the shutting off at earth and at Pioneer 6, which were separated  $45^\circ$  in longitude. So there are shock associations, perhaps there is a shock in the discontinuity in the earth at the time these colliding streams sweep over the earth. But we do not believe this is the fundamental mechanism for what is happening to the particles.

#### COMMENTS

*F. C. Michel* I would like to make a few comments about the filamentary structure of the solar wind, which stands in relation to the wind itself as do the trees to a forest. A lot has been said about the forest, so perhaps it is not inappropriate to make a few comments about the trees. The forest, of course, is the uniform plasma outflow from the sun, recognizing as well that there is some modification that leads to the sector structure. What I would like to talk about is the very fine scale structuring which is seen in

interplanetary magnetometer data. The observations reveal extremely chaotic and variable magnetic fields and, in fact, the famous garden-hose spiral structure is generally seen only in long-term averaging of such data.

Figure 1 is from *McCracken and Ness* [1966]. They describe cosmic ray propagation data in terms of the magnetic field-line topology, and they are essentially describing the interplanetary field in terms of filaments.

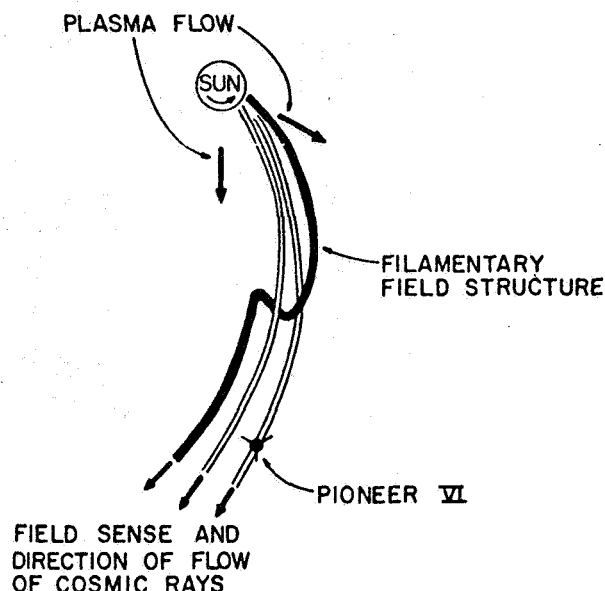


**Figure 1.** A schematic diagram of a few interplanetary filaments, as viewed from the north ecliptic pole and as sampled by Pioneer 6 on December 30, 1965. Compare this figure with the azimuths recorded in in figure 2 [McCracken and Ness, 1966].

Figure 2 shows the data that led them to this description. The solid line indicates a continuation of magnetic field measurements, successive magnetic field vectors added vectorially, while the arrows that are shown as such are the directions of the cosmic ray anisotropies in the solar wind. One sees that the two line up very well, which indicates that the cosmic rays are ducted along the magnetic field lines, as one might well expect. The curve so constructed in figure 2 would not actually represent a *single* magnetic field line but sort of a superposition of many. Nevertheless, it shows that the magnetic field lines meander about quite a bit.

Figure 3 is from a paper by *Bukata and Palmeira* [1967] and shows their picture for the propagation of flare cosmic rays in terms of filamentary structures. In trying to understand this filamentary structure on a basic picture as shown in figure 4 [Michel, 1967], I started with the assumption that the source of solar wind itself is modulated by propagation of energy from below up into the corona to keep it hot enough so it expands outward and forms the solar wind. This mechanism need not be absolutely homogeneous, and the inhomogeneities can be preserved by virtue of the magnetic field structure; consequently, variations in the source (e.g., acoustic energy propagated up from granulations) would lead to local modification of the solar wind source. This modulation would in turn lead to regions of higher or lower density propagating outward.

Figure 5 is a sketch of how this would appear on the large scale. The dotted lines show the expected garden hose geometry, while in fact the flux tube position varies with the propagation velocity as well as its dimensions, owing to spatial and temporal variations in the source function.

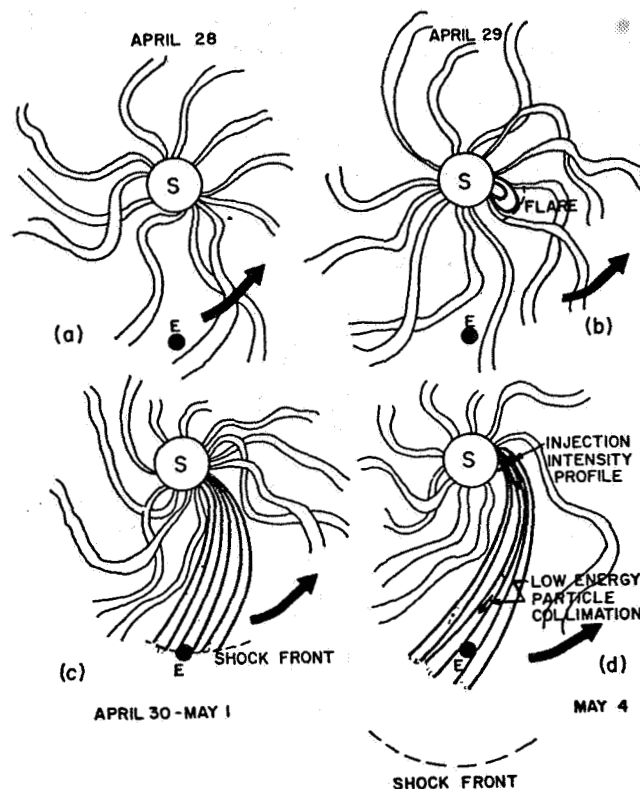
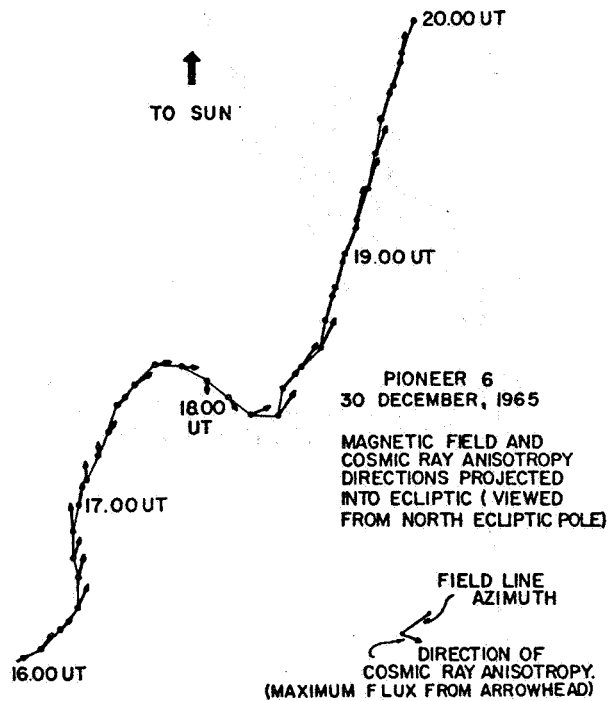


Figure 2. The magnetic field and cosmic-ray azimuths during the interval 1600 to 2000 UT, December 30, 1965. Note the very close correspondence of the two azimuths during the abrupt change in direction around 1800 UT [McCracken and Ness, 1966].

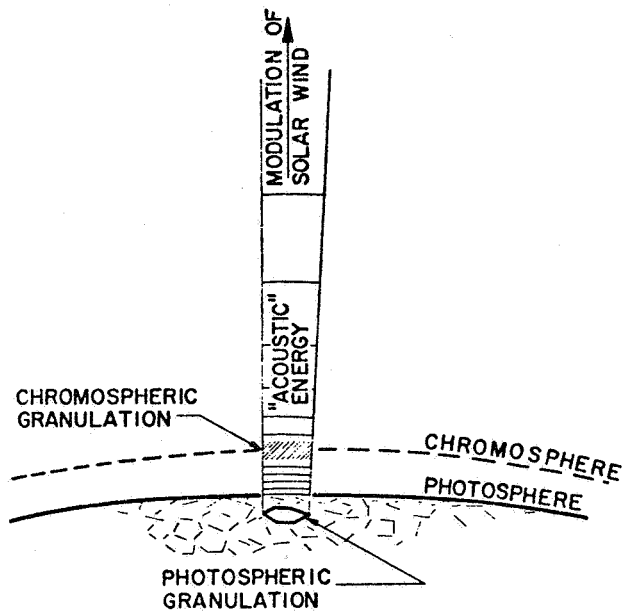
Figure 6 shows the same idea, the filamentary structure is just a small-scale variation. The large-scale sector structure simply refers to the field in the filaments being predominantly of one direction (toward or away from the sun).

Figure 7 is from Bartley *et al.* [1966] showing the "wet spaghetti" model. The basic idea is that one can get large variations in field direction simply by having a tangling of the flux tubes. Thus one might regard the filaments as being distinct individual flux tubes. Jokipii and Parker [1968] have expanded on this idea and discuss how the movement of the source of the flux tube in the photosphere would lead to tangling of the field lines, and this would give, at the earth, a highly variable field wherein the observed field variations are due to encountering first one flux tube, and then another flux tube, and so on. The boundaries between the flux tubes will be tangential discontinuities. These discontinuities have been observed in abundance from many spacecraft and since they are not waves, not shock waves or anything but just flux tubes frozen-in to the solar wind, the total pressure must remain constant as one crosses such a discontinuity. Burlaga [1968] has analyzed magnetometer and particle data to show quantitatively that in fact total field pressure plus gas pressure is indeed constant across these discontinuities.

Finally, the scale for the discontinuities projected down onto the sun is of the correct general size. The scale of fluctuations seen in the solar wind, if projected back to the sun—a reduction factor of about 200—is not quite the same scale as the granulations. It's a little larger, and Newkirk prefers the supergranulation as the more likely characteristic dimension, but the same idea essentially applies. In this way we can understand at least qualitatively some of the detailed phenomena, such as plasma flow out of the ecliptic plane (just flowing along a flux tube) and the abundance of discontinuities on the solar



**Figure 3.** Grossly exaggerated representation of the time-history of the interplanetary magnetic field configuration from late April to early May 1960. Solar particles generated in the flare event of May 4 are being preferentially injected into a single well-ordered magnetic filament created in the west limb flare event of April 29. The presumptuous, highly exaggerated, disordered magnetic filamentary structure depicted for the fields removed from the localized west limb flare activity is presented solely for contrasting the two filamentary magnetic regimes and is not intended to be taken at face value [Bukata and Palmeira, 1967].



**Figure 4.** Hypothetical interrelation between photospheric and chromospheric granulations and the modulations of solar wind flow.

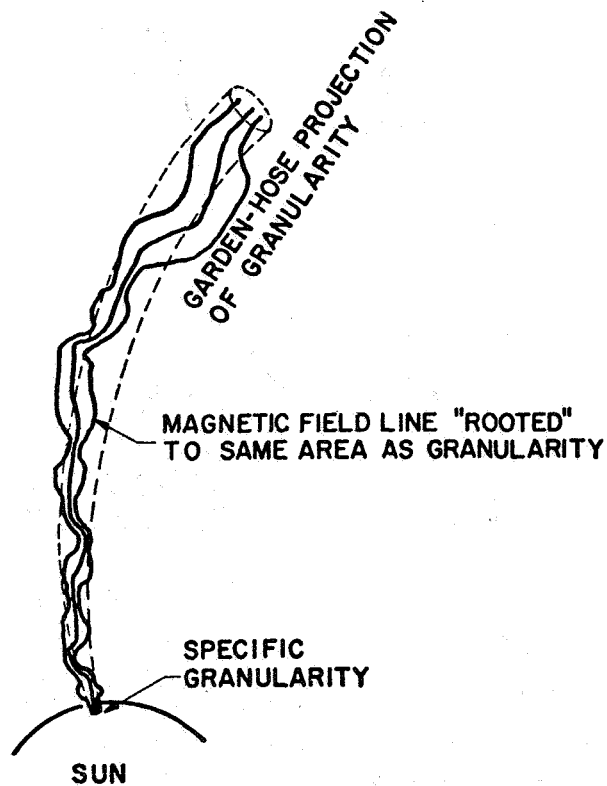


**Figure 5.** Schematic of field-line configuration showing relation between the garden-hose extension of a granulation and the magnetic field lines.

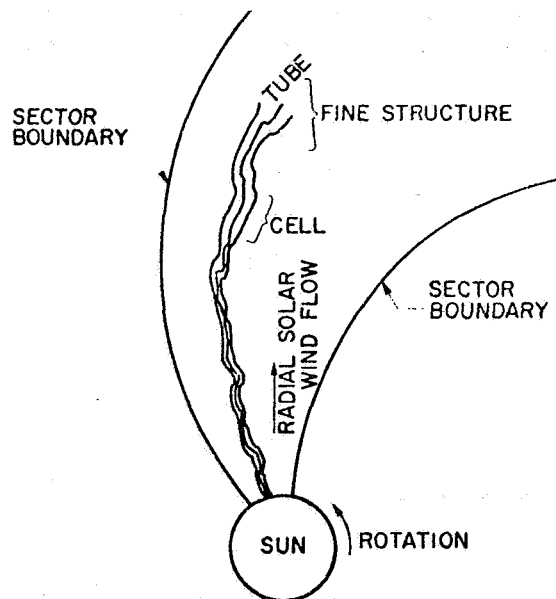


**Figure 6.** Schematic of structure within the solar wind illustrating cellular structure within the interplanetary magnetic field. The field lines passing through a given cell tube lead to the site of cell origin.



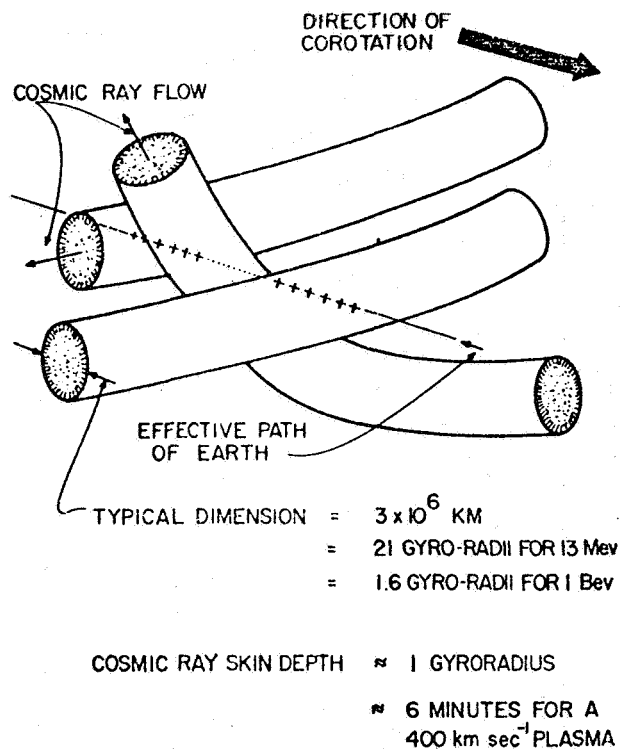


**Figure 7.** *Simplified model of filamentary structure of interplanetary magnetic field. Each filament can be thought of as a bundle of tubes of force. The cosmic rays of low energy are constrained to travel along the filament by the magnetic field [Bartley et al., 1966].*

wind. Thus the structure of the solar coronal rays, which can readily be seen in eclipse photographs, is just the manifestation near the source of the very fine structuring observed locally in the solar wind.

I should remind you of the cosmic-ray arrival time data [Bryant et al., 1965], wherein one takes the energy versus arrival time spectrum and corrects it for the time of flight. There one finds that protons with energies from almost 500 meV down to 2.2 meV have arrival times that all scale as if the particles all followed essentially the same path from the sun to the earth. Of course, that again is consistent with the idea that the basic solar wind structure is filamentary and the effective path length (6 or more astronomical units) results simply from detouring the cosmic rays out along the filaments.

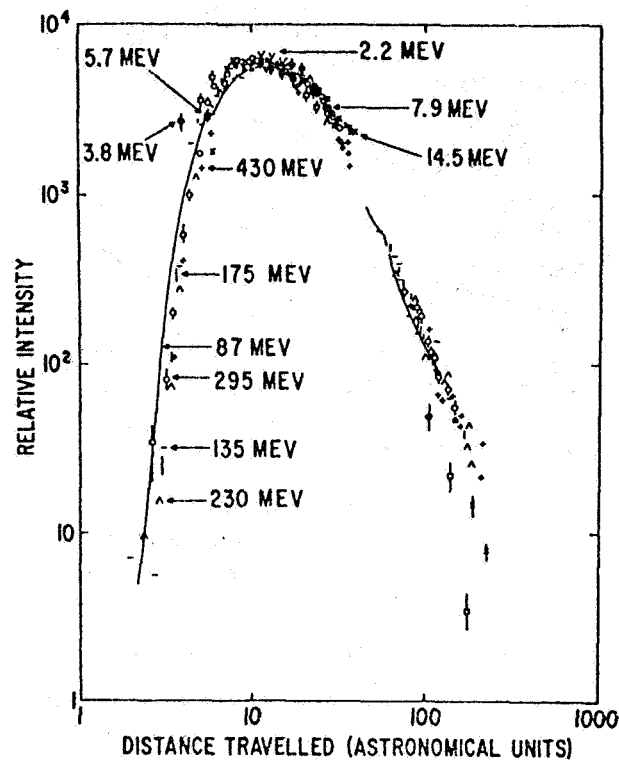


Figure 8. Normalized (same maximum) intensity versus distance traveled (time of observation after flare  $\times$  particle speed) for interplanetary flare protons [Byrant et al., 1965].

#### REFERENCES

- Bartley, W. C.; Bukata, R. P.; McCracken, K. G.; and Rao, U. R.: Anisotropic Cosmic Radiation Fluxes of Solar Origin. *J. Geophys. Res.*, Vol. 71, 1966, p. 3297.
- Bukata, R. P.; and Palmeira, R. A. R.: The Effect of the Filamentary Interplanetary Magnetic Field Structure on the Solar Flare Event of May 4, 1960. *J. Geophys. Res.*, Vol. 72, 1967, p. 5563.
- Burlaga, L.: Micro-scale Structures in the Interplanetary Medium. *Solar Phys.*, Vol. 4, 1968, p. 67.
- Bryant, D. A.; Cline, T. L.; Desai, U. D.; and McDonald, F. B.: Studies of Solar Protons with Explorers XII and XIV. *Astrophys. J.*, Vol. 141, 1965, p. 478.
- Jokipii, J. R.; and Parker, E. N.: Random Walk of Magnetic Lines of Force in Astrophysics. *Phys. Rev. Letters*, Vol. 21, 1968, p. 44.
- McCracken, K. G.; and Ness, N. F.: The Collimation of Cosmic Rays by the Interplanetary Magnetic Field. *J. Geophys. Res.*, Vol. 71, 1966, p. 3315.
- Michel, F. C.: Model of Solar Wind Structure. *J. Geophys. Res.*, Vol. 72, 1967, p. 1917.

*A. J. Dessler* Is there any contradiction between the source surface model that Schatten has talked about with the start of the magnetic field at about one solar radius out and only using part of the solar surface, and your using the granulation?

*F. C. Michel* Well, naively, one would say one is mapping from the granulations out to 1 AU. But, of course, one has to realize that you do have these arcades with the field lines closed, so you don't get all the map, you get chunks cut out of the map where the field lines actually close and the granulations connect to one another. But other than that distortion one essentially maps outward.

*E. C. Roelof* I would just like to point out that we are forced to certain exceptions to what must be a very physical phenomenon, the braiding or random walking of these field lines. And those exceptions are unique low-energy particle events, the examples of which are becoming more and more numerous, in which there are clearly enhanced fluxes whose width is only something like  $3^\circ$  or  $4^\circ$  at the earth. These are not temporal events, these are spatial features that are more or less being quasirigidly rotated in the interplanetary field. We can tell this in multiple spacecraft observations, using two or sometimes three spacecraft. Since these particles have to be stored or be continually accelerated from an active region these field lines must be connecting back to an active region. Consequently, this puts a limit on the random walking or the braiding of these field lines above active regions. This limit, as far as I can see from the low-energy particles, then, is only something like  $3^\circ$  or  $4^\circ$  and this, of course, does not in any sense invalidate the process of a general braiding at the general surface of the sun. It just says there is something peculiar and rather fateful about the mapping of field lines out to the earth above active regions that are producing low-energy particles. But these are exceptions.

*J. M. Wilcox* That last comment calls to mind another possible exception to the random walk process of Jokipii and Parker, namely, the sector boundary, and a particular case where a sector boundary may persist for a year or more, coming back every 27 days. Naively one would think that the random walk process would eat away at that sharp boundary and finally cause it to disappear. One can help the situation somewhat by having an arcade or a loop structure near the photosphere, but then maybe you would get the time up to a month or so. But a year still seems too long. It seems there is something of interest occurring there.

*E. C. Roelof* Well, I didn't mean to give the impression that I thought all the fluctuation was due to the random walk. Some of it is due to just the variations in the sizes of the filaments, and also possibly the most important process is the variation in the velocity, within individual filaments, which will cause certain ones to slip through or meander, and get well ahead of the general trend. So I don't think it is very well sorted out which are the important physical factors there.

*L. Davis* Since the random walk and speed of the field lines came up I just felt that I wanted to remark that these field lines continue deep on down into the sun, and I am worried that they may not walk at random over long periods. They may move at random for short periods, but they may stay somewhat anchored to the same spot and may not accumulate the square root of the distance over weeks and months.

*G. Newkirk* Is there any characteristic size for the noodles in interplanetary space?

*F. C. Michel* Well, I think again that is in the eye of the beholder.

*G. Newkirk* No, that's a question of frequency analysis.

*F. C. Michel* But I think it varies. I don't think there is a single number.

*E. C. Roelof* It's the same old problem we've had for a long time, what do we want to call a filament? The whole problem of the mixing of the data makes it a bit difficult to identify something you wish to call filament. If you plot the field direction you see all sorts of assorted things. So the point of view that I take is let's drop the word *filament* as it's gotten all sorts of meanings now, and concentrate on the other things, the discontinuities and waves, because we've got theory behind us on that. If you look at the

discontinuities, pick them out in space, you find out they are not paired; they have orientations which change from one to the next. And given that situation we have almost completely lost the idea of a filament. So I personally prefer to simply drop the idea of filament and work with the more fundamental ideas of the current sheet and the discontinuities.

I don't recall the author but I do know that a Russian author many years ago suggested that granulation could give rise to small cellular features in the interplanetary magnetic field. The idea is very similar to yours.

*F. C. Michel* If you are willing to say that the discontinuities are boundaries of different filaments, then one can answer the question. I would say they probably run by about once every 30 minutes. We can say that would be plausible. It comes down to about  $10^\circ$  of arc or  $5^\circ$  of arc in the sun, something like that.

## SOLAR LARGE-SCALE POSITIVE POLARITY MAGNETIC FIELDS AND GEOMAGNETIC DISTURBANCES

V. Bumba

Unlike the negative polarity solar magnetic field large-scale regular features that correlate with enhanced solar activity regions, the positive polarity regular formations formed in the weak and old background magnetic fields seem to correlate well with geomagnetically enhanced periods of time (shifted for 4 days), which means that they seem to be the source of the quiet solar wind. This behavior of the large intervals of heliographic longitude with prevailing positive polarity fields may be followed to the end of the 18th cycle, during the declining part of the 19th cycle, and during the first half of the present 20th cycle of solar activity.

### ABSTRACT

### INTRODUCTION

In Chapter 1 (p. 31), we tried to demonstrate some characteristic behavior of the large-scale negative polarity magnetic fields on the sun, and some consequences of the demonstrated properties of these photospheric fields in the interplanetary magnetic fields. We now discuss some characteristics of the large-scale positive polarity distribution that seem to be in a pronounced correlation with the interplanetary field and the geomagnetic disturbances. We use the same observational data as in the earlier discussion, complemented by the geomagnetic character index C9.

*Bumba and Howard* [1969] have mentioned the striking similarity in the 27 days Bartel's geomagnetic data recurrences with the 27 days rotational period of rows and streams of solar magnetic fields of both polarities. In an earlier note [*Bumba and Howard*, 1966] it was shown that the large geomagnetic disturbances with slow commencement tend to correlate with so-called unipolar magnetic regions (UMRs), each of which is one of several morphological characteristics of a very complex magnetic situation connected with the development of a complex of activity in active longitudes. *Ambrož et al.* [1971] recently noted the dynamics of development of so-called "supergiant" structures

in individual polarities of opposite active longitudes to which again the UMRs are in a close relation. Each of the mentioned effects is only one side of this complex pattern developing in the photospheric magnetic fields, and we are only trying to complete this picture by still more information.

### POSITIVE POLARITY DISTRIBUTION

Contrary to the fact that the positive rows and streams on magnetic synoptic charts mounted successively are less pronounced and much broader than the negative polarity streams, the "giant" regular structures (30° to 35° in diameter), which may be accepted as an effect of convective motion in giant cells on the magnetic field redistribution [*Bumba*, 1970], are much better seen in the positive polarity during the preceding 19th cycle of activity (positive was the leading polarity on the more active northern hemisphere). On the other hand, independent of the cycle of activity, the "supergiant" structures (100° to 180° in length) again are better and more often observable in the negative polarity fields.

In heliographic longitude the concentration of opposite polarity fields in streams on opposite sides of the sun is frequently recognized [*Ambrož et al.*, 1971]. As far as the latitudinal distribution is concerned, our synoptic charts suggest that the positive polarity is less widely distributed in heliographic latitudes than the

---

*The author is at the Astronomical Institute of the Czechoslovak Academy of Sciences, Observatory Ondřejov, Czechoslovakia.*

negative one, and that it tends to be more concentrated to the equator in the preceding as well as in the present cycle.

#### CORRELATION OF POSITIVE POLARITY WITH GEOMAGNETIC DISTURBANCES DURING THREE CYCLES

It has been shown that the frequent concentration of opposite polarity fields in streams on opposite sides of the sun or in separated active longitudes is not the only difference between the polarities. If we compare the distribution of fields of the two polarities with the distribution of activity as seen in the synoptic charts made from the Freiburg daily solar maps, we may see good coincidence of activity concentrations with concentrations of negative polarity fields [Ambrož *et al.*, 1971]. If we compare the daily geomagnetic disturbances, shifted 4 days to account for the travel time of solar wind plasma from the sun to the earth, with the magnetic synoptic charts we again see a fairly close

correlation of these magnetic characteristic figures with the positive polarity magnetic features (figs. 1 and 2). This correlation may be seen practically always when the daily geomagnetic character figures C9, published by the Geophysikalisches Institut Göttingen, display the long-lasting strips of enhanced geomagnetic activity with strongly kept 27-day recurrence, as may be observed especially during the decay time of the 19th cycle.

These regular strips of greater values of geomagnetic character figures are common to this phase of solar activity cycles. The same is true of the 18th cycle during the end of which measurements of solar magnetic fields were made (1952–1954) by Babcock and Babcock [1955]. If we redraw their figure 9, the diagram presenting "evidence tending to relate terrestrial magnetic storms of the sequential type to UM regions on the Sun," and take again into account the 4-day travel time of plasma we may see the coincidence of large-scale positive solar fields with the enhanced figures of

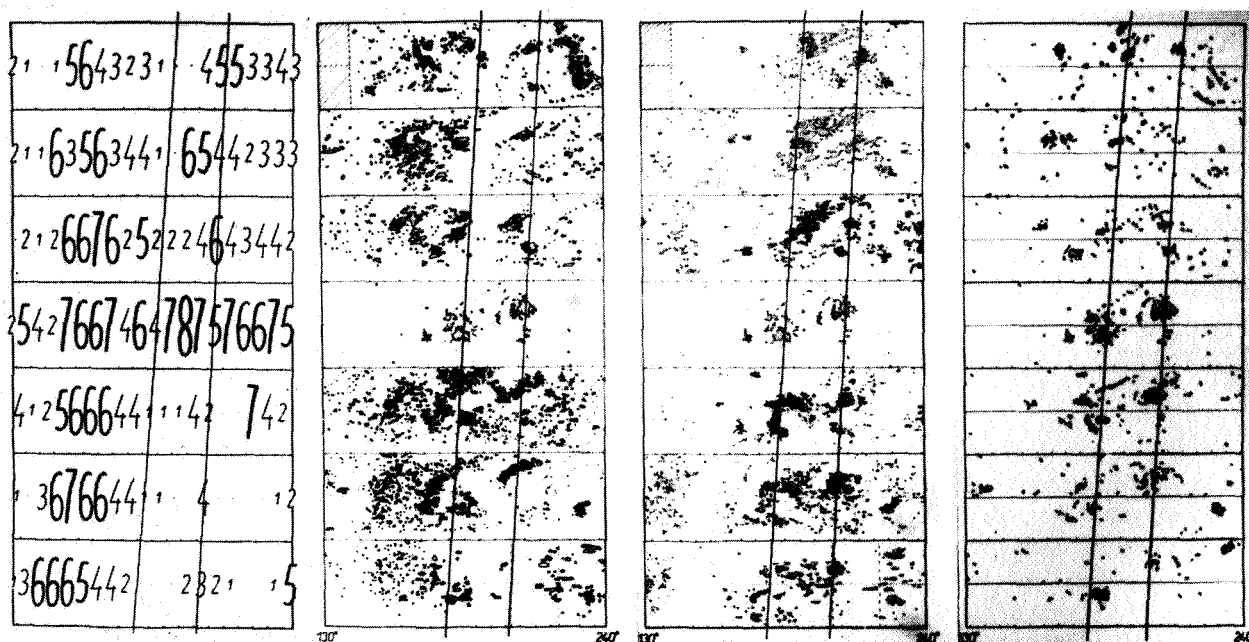


**Figure 1.** Portions of magnetic synoptic charts for rotations 1439–1442, drawn in separated polarities (plus to the left, minus to the right), compared with the large-scale solar activity distribution (Fraunhofer Institute, Freiburg) and the geomagnetic activity distribution (Institut für Geophysik, Göttingen) for the same time interval. (The 4 days needed by the solar wind plasma to arrive at the earth are taken into account.) The close relation of young negative fields to the actual activity, as demonstrated by calcium plages, and the relation of areas of older positive fields to the geomagnetically disturbed days may be seen.

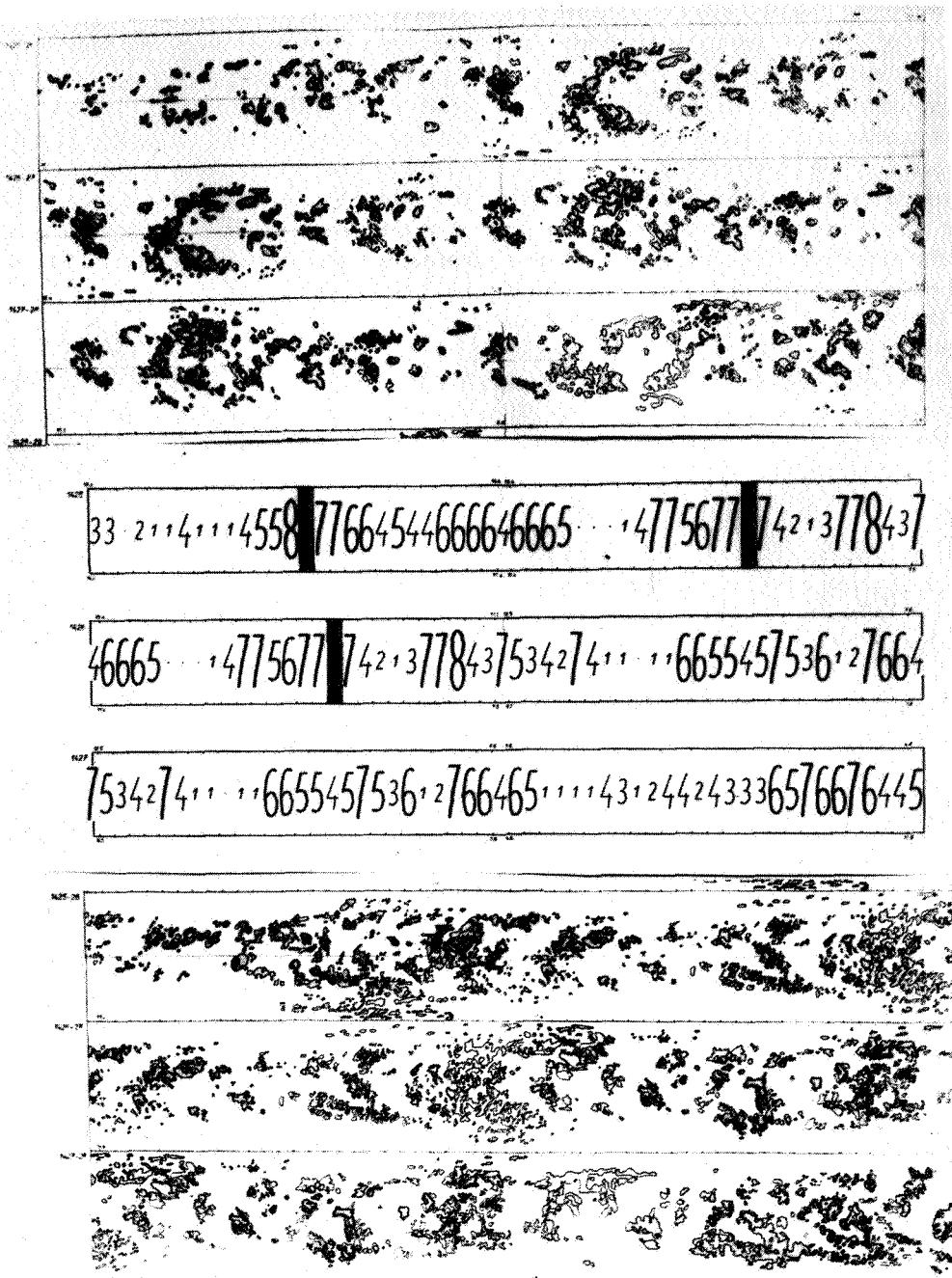


**Figure 2.** The same comparison of different polarity distribution with the geomagnetic activity distribution for rotations 1425–1428 from the preceding cycle. For integration two consecutive maps, one of which is repeated, are overlapped and drawn twice for better visualization of large-scale features. The negative polarity in the upper part of the picture demonstrates well-developed “supergiant structure,” the presence of which diminished the geomagnetic activity. The intervals of enhanced geomagnetic activity (shifted by 4 days) correlate well with the positive polarity large-scale magnetic fields shown in the lower part of the picture.

geomagnetic activity, and relatively good coincidence of regions with prevailing negative polarity features with the time periods of very low geomagnetic activity (fig. 3).

During the growth of the 20th cycle such sequences of enhanced geomagnetic activity may be followed very rarely. But when they are observed, they again tend to correlate mostly with the positive polarity large-scale fields on the sun. The complex situation during the maximum of the 20th cycle will be discussed separately.

During the phase of growth of the present cycle of solar activity the polarity of the interplanetary magnetic field was observed [Wilcox and Colburn, 1970]. Making a histogram (fig. 4) of the geomagnetic character figures distribution in dependence on this polarity we may see that also in the interplanetary space the geomagnetic

disturbances tend to be related more to the positive polarity than to the opposite one, although the positive and negative values are practically equally frequent.

From the histogram of the occurrence frequency of positive and negative polarity in the interplanetary field we may possibly see one more piece of information: the largest secondary maximum of the histogram giving for the frequent time interval of the sector of one polarity of about 6 days—on the sun about  $80^\circ$ —is again in good correlation with the large-scale structures of the field of one polarity on the sun (fig. 5).

#### THE CORRELATION OF GEOMAGNETIC DISTURBANCES WITH THE PHOTOSPHERIC FIELD IN 1968

For the time of about four solar rotations during the first half of 1968, *Severny et al.* [1970] made a detailed

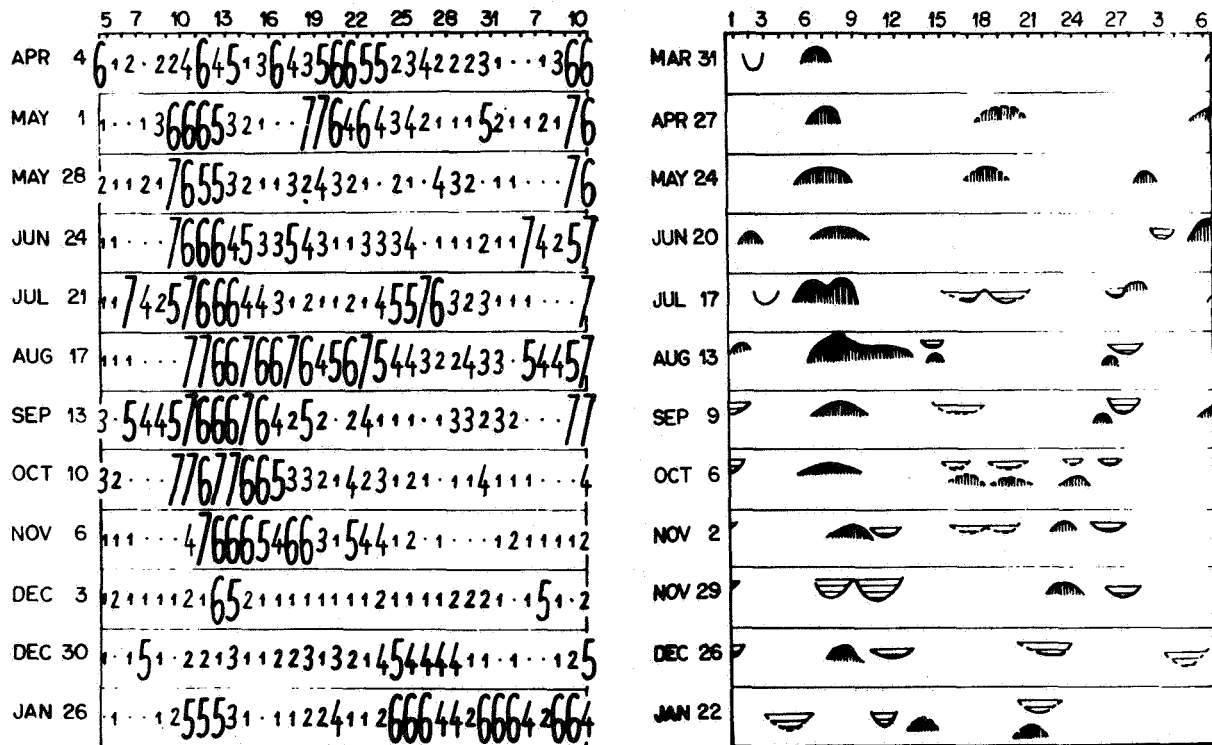


**Figure 3.** Comparison of geomagnetic activity distribution with the large-scale magnetic field distribution of opposite polarities on the sun for the year 1953 (the 18th cycle) [fig. 9, Babcock and Babcock, 1955]. The same manner of daily geomagnetic figures presentation as in figures 1 and 2 was used, taking into account the 4 days of plasma travel time. The positive polarity fields have been indicated by U-shaped convex upward curves with the vertical hatching, the negative polarity fields by convex downward curves and horizontal hatching. The correlation of large-scale positive solar fields with the enhanced geomagnetic activity as well as the coincidence of prevailing negative polarity fields with the calm periods of geomagnetic activity may be seen.



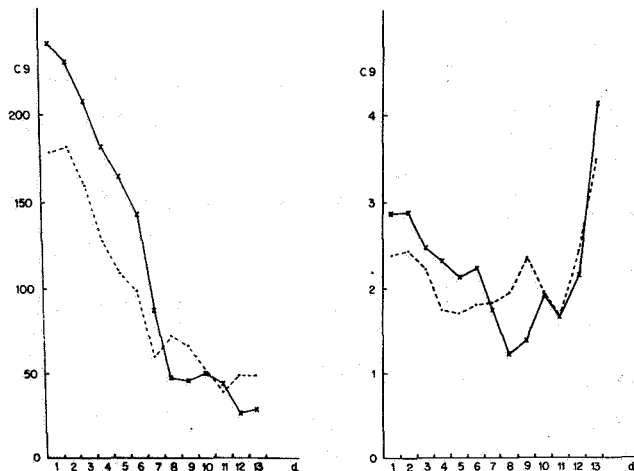


**Figure 4.** The histogram of the geomagnetic character figures distribution in dependence on the polarity of interplanetary magnetic field [Wilcox and Colburn, 1970]. In the left picture the sum of geomagnetic character figures and the length of the sector in days is shown, and in the right picture the mean value of the character figures and the length of the sector in days. The full line represents in both pictures the positive polarity, the dashed line the negative polarity distribution.

comparison of the mean photospheric magnetic field of the sun seen as a star measured at the Crimean observatory with the interplanetary magnetic field observed with spacecraft near the earth. If we correlate the geomagnetic activity shifted for 4 days with the situation on the sun and in interplanetary space in still more detail, we may see that there are enhanced geomagnetic figures in coincidence with both the positive and the negative polarity of solar and interplanetary magnetic fields (fig. 6). Only the separation of both polarities on magnetic synoptic charts and their comparison with solar activity demonstrates that there exists on one side of the sun the normal enhancement of geomagnetic figures due to the large-scale regions of older activity plus polarity in which only smaller solar activity occurs, and on the other side of the sun another enhancement follows the regions of the greater solar activity connected with the prevailing large-scale negative polarity fields. Later we will find that in this negative polarity sector several particle-emitting flares occur, and that the enhanced geomagnetic activity more often starts with sudden commencements.

## CONCLUSIONS

Summarizing the above demonstrated observational data, we may come to the conclusion that there are

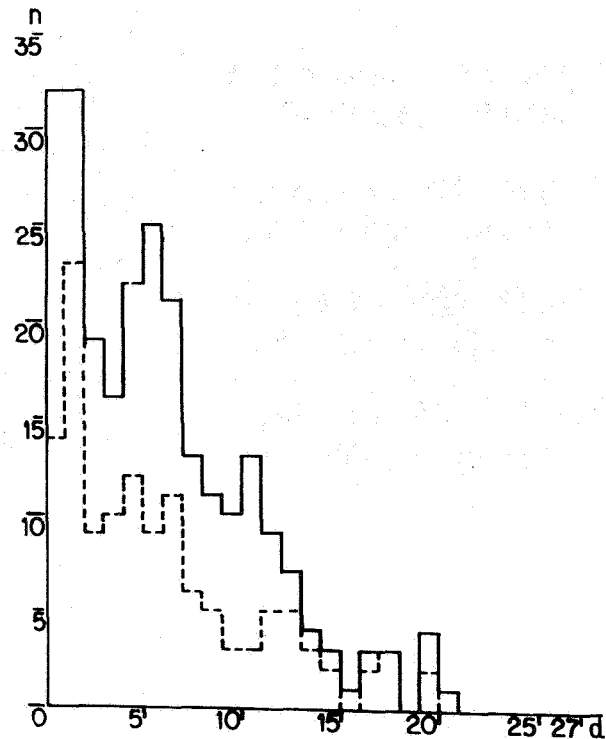


**Figure 5.** The histogram of positive and negative polarity occurrence frequency in the interplanetary magnetic field. The most frequent lengths of sectors may be seen from this picture. Again the full line represents the positive polarity and the dashed line the negative polarity distribution.

large-scale features of opposite polarity magnetic fields on the sun, frequently developed in separated active longitudes. To the negative polarity fields new and great activity formations including large flares are bounded, and they tend to be the source of sudden commencement geomagnetic disturbances. The positive polarity structures, usually with less and older activity, correlate with geomagnetic enhanced periods of time, which means that they are sources of the quiet solar wind.

Because of the more complex situation and new formations in regions with the prevailing negative polarity field, we may expect greater gradients of field, and the lines of force may be more closely bounded to the surface of the sun, connecting not very distant regions of opposite polarity, although certain portions of these lines of force must go farther into the interplanetary space. The positive polarity regions on the sun seem to have less complicated magnetic field situations, and the field lines may go without greater complications farther

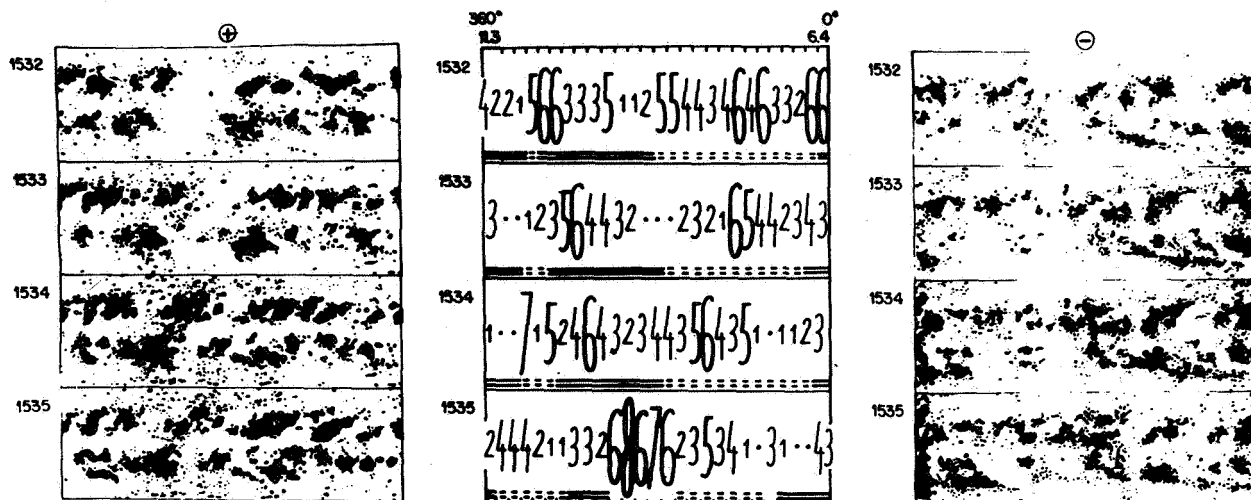


**Figure 6.** Comparison of solar magnetic field opposite polarity distribution with the geomagnetic activity and interplanetary magnetic field distribution as measured by Severny et al. [1970] for the rotations 1532–1535 [1968]. For integration two consecutive magnetic maps, one of which is repeated, are overlapped. The positive polarity is to the left and the negative polarity distribution to the right. In the central part of the picture the daily geomagnetic character figures with the 4-day shift and the positive polarity (full double line) and the negative polarity (dashed double line) of interplanetary field are presented. The predominance of the minus polarity in the right part of the synoptic charts is clearly visible. From the comparison of the plus polarity distribution we may see that in the right part of synoptic charts the positive polarity will be cancelled by the negative polarity, while in the left part of the charts it will be superior to that polarity.

into space. This means that on the sun observed as a star, during the period of negative polarity field observations we may expect enhancement of some spectral lines due to the greater activity, as well as enhanced X- and radio-emission. On the other hand, positive polarity formations on the sun are the source of the undisturbed

solar wind. How far the analogy with the stars may go is a question for further research.

Considerable experimental work is still needed to obtain more information, but we think there are already some problems that require some theoretical approach for interpretation.

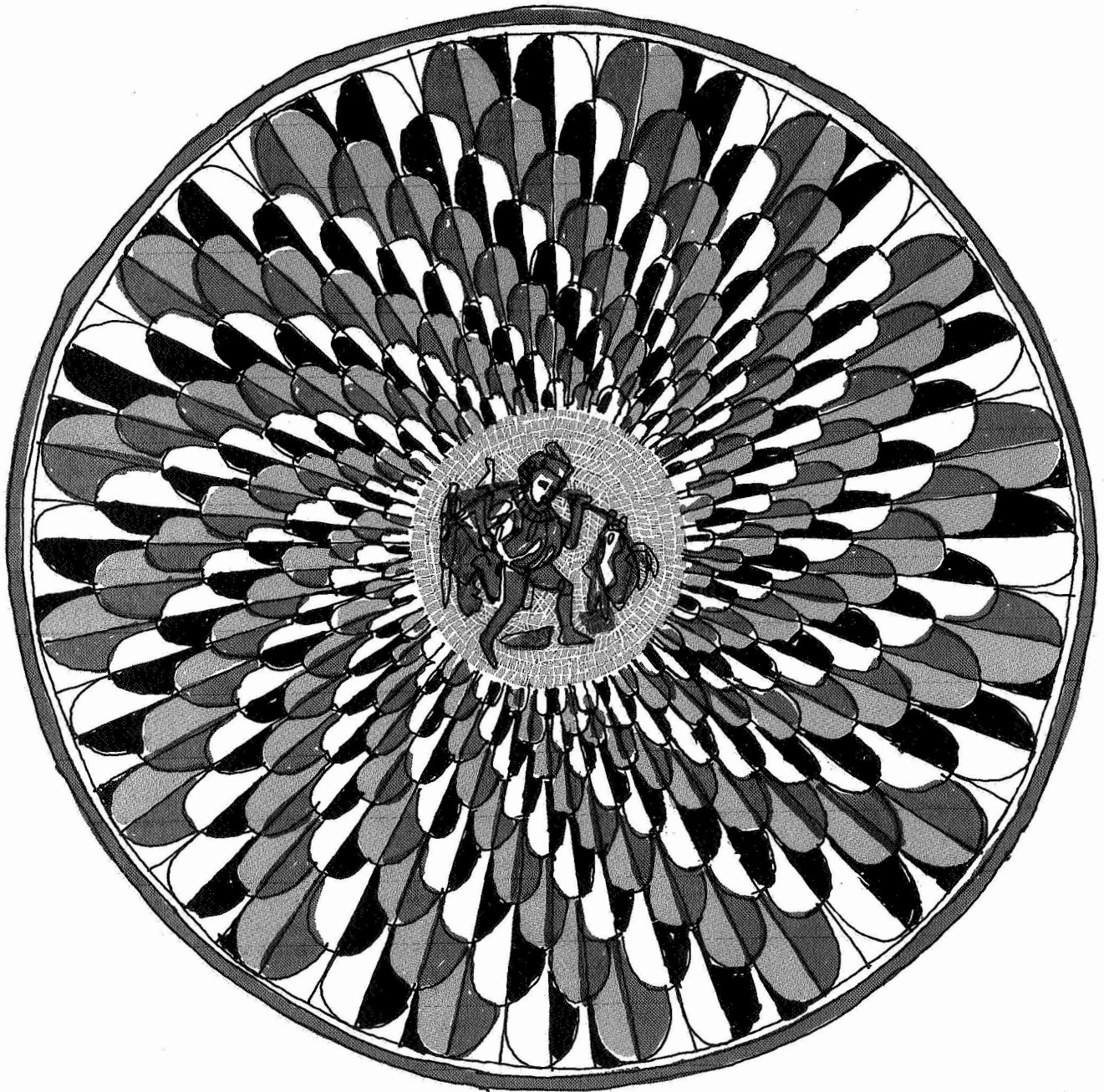
## REFERENCES

- Ambrož, P.; Bumba, V.; Howard, R.; and Sykora, J.: Opposite Polarities in the Development of Some Regularities in the Distribution of Large-Scale Magnetic Fields. *IAU Symposium, No. 43*, edited by R. Howard and D. Reidel, 1971.
- Babcock, H. W.; and Babcock, H. D.: The Sun's Magnetic Field, 1952–1954. *Astrophys. J.*, Vol. 121, 1955, p. 349.
- Bumba, V.: Concerning the Formation of Giant Regular Structures in the Solar Atmosphere. *Solar Phys.*, Vol. 14, 1970, p. 80.
- Bumba, V.; and Howard, R.: A Note on the Identification of "M" Regions. *Astrophys. J.*, Vol. 143, 1966, p. 592.
- Bumba, V.; and Howard, R.: Solar Activity and Recurrences in Magnetic-Field Distribution. *Solar Phys.*, Vol. 7, 1969, p. 28.
- Severny, A. B.; Wilcox, J. M.; Scherrer, P. H.; and Colburn, D. S.: Comparison of the Mean Photospheric Magnetic Field and the Interplanetary Magnetic Field. *Solar Phys.*, Vol. 15, 1970, p. 3.
- Wilcox, J. M.; and Colburn, D. S.: Interplanetary Sector Structure Near the Maximum of the Sunspot Cycle. *J. Geophys. Res., Space Phys.*, Vol. 75, 1970, p. 6366.

*P. McIntosh* The results that I haven't had time to talk about yet agree very well with what Dr. Bumba is presenting—that the times of enhancement of geomagnetic activity in the last several months seem to be coming in between the active longitudes for major flares. These major flares have been coming within the negative polarity sectors. This says, then, that the geomagnetic recurrent storms come in positive sectors. Furthermore, what chance I've had to look at the evolution of the sectors related to what is on the sun seems to imply that the negative sectors are being formed from proton active centers, which again is in agreement with what Dr. Bumba has had to say.

DISCUSSION





# *Chapter III*

Large Scale Features of the Solar Wind Plasma

Theory of the large scale flow structure, formation at the coronal base, solar and interplanetary sources of energy; possible flow dependence upon solar latitude; transport parameters; the heat flux; basic anisotropy of the velocity distribution function.

# PRESENT DEVELOPMENTS IN THEORY OF THE SOLAR WIND *E. N. Parker* An invited review

Current problems and developments in the theory of the large-scale expansion of the solar corona are reviewed. The outstanding question is whether the energy supply to the quiet corona is mainly thermal conduction outward from a region of active heating at its base, or mainly wave propagation outward from the base. It is suggested that the question can be settled only when the properties of the wind can be sampled over a wide range of radial distance from the sun, from far inside the orbit of earth to well beyond. It has been suggested that hydromagnetic waves may drive the expansion of the active corona by direct transfer of momentum as well as energy.

## ABSTRACT

## INTRODUCTION

This paper presents some of the current theoretical work, and outstanding problems, posed by the observations in understanding the quiet solar wind. For a comprehensive coverage of the entire subject the reader is referred to the collected proceedings of this meeting, as well as to the many excellent reviews already in the published literature [Dessler, 1967; Lüst, 1967; Ness, 1968; Axford, 1968; Wilcox, 1968; Hundhausen, 1968, 1970; Holzer and Axford, 1970; see also Parker 1965b, 1967, 1969].

## THE BASIC PROBLEM

A consideration of the energy supply provides the most direct confrontation with the theoretical questions posed by the solar wind. The energy is believed to be supplied by sound, gravity, and hydromagnetic waves generated in or beneath the photosphere by the convection. The question is where, and in what way, the waves are dissipated and the energy transferred to the expanding corona.

For simplicity suppose that the coronal gas is pure hydrogen, neglecting helium and heavier elements. Denote the mass of the hydrogen atom by  $M$ . Denote by  $N(r)$  and  $T(r)$  the number of hydrogen atoms per unit

volume and the temperature, respectively, at a distance  $r$  from the center of the sun. The gas is fully ionized, so the pressure is  $p = 2 NkT$  and the thermal energy density is  $3 NkT$ . Hence, the thermal energy in a volume  $V$  is  $U = 3 NkTV$ . The thermal energy is available, upon expansion of the volume  $V$ , to lift the gas out of the gravitational field of the sun. The gas in the volume  $V$  is bound to the sun by the gravitational potential  $\Phi = -GM_{\odot}MN/r$ . Of course, if the gas expands outward from the sun, more gas crowds in behind to replace it, doing the work  $pV$  on the volume  $V$ . Thus the total energy directly available for escape is the enthalpy

$$E = U + pV = 5 NkTV$$

The ratio of the available energy  $E$  to the gravitational binding energy  $\Phi$  is

$$\frac{E}{|\Phi|} = \frac{5kT(r)r}{GM_{\odot}M}$$

For a coronal temperature of  $2 \times 10^6$ °K this ratio is about 0.5. The thermal energy is only half the amount needed to lift the gas out of the solar gravitational field. Hence, the solar corona expands continually to form the solar wind only because thermal energy  $Q$  is supplied to

---

*The author is with the Department of Physics, University of Chicago, Chicago, Illinois.*

the gas while it is expanding away from the sun [Parker, 1958]. The total energy available is then  $E + Q$ . For the quiet corona and solar wind  $E + Q$  is evidently about 25 percent larger than  $\Phi$ , because it leads to a solar wind at large radial distance with a velocity equal to about half the 600 km/sec escape velocity from the base of the corona.

The addition of energy can be represented in a very simple mathematical way using the conventional polytrope relation  $p = p_0 (N/N_0)^\alpha$  where  $\alpha$  is chosen to be less than the adiabatic value of 5/3. This artifice permits integration of the momentum equations, leading to winds of the general character of the observed solar wind for  $\alpha$  between the isothermal value of 1.0 and about 1.3 [Parker, 1960b]. The effective enthalpy, which now includes the addition of heat  $Q$ , can be written

$$E_{\text{eff}} = \frac{2\alpha}{\alpha-1} NkTV$$

in terms of  $\alpha$ . The polytrope law, however, is only a convenient, and often used, mathematical device for representing the addition of heat. It tells us nothing about the actual mechanisms responsible for the addition.

The total energy flux  $F$  carried by the wind is then the convection of kinetic energy, gravitational potential energy, and the effective enthalpy,

$$F = 4\pi r^2 Nv \left( \frac{1}{2} Mv^2 - \frac{GM_\odot M}{r} + \frac{2\alpha kT}{\alpha-1} \right)$$

where  $v$  is the wind velocity at  $r$  and  $4\pi r^2 Nv$  is the number of atoms streaming away per unit time, a quantity independent of  $r$ .

Thermal conduction outward from the base of the solar corona is obviously one source of heat supply from the inner to the outer corona [van de Hulst, 1953, Chapman, 1957] and was the first explicit mechanism considered in connection with the expansion to form the solar wind [Noble and Scarf, 1963].

In this case, the thermal conduction term must be added to  $F$ :

$$F = 4\pi r^2 Nv \left( \frac{1}{2} Mv^2 - \frac{GM_\odot M}{r} + \frac{2\alpha kT}{\alpha-1} \right) - 4\pi r^2 \kappa(T) \frac{dT}{dr}$$

where the thermal conductivity  $\kappa(T)$  is  $6 \times 10^{-7} T^{5/2}$  ergs/cm sec  $^\circ\text{K}$  [Chapman, 1954]. Noble and Scarf [1963] constructed the first solar wind models using this energy flux. They obtained wind velocities of 300 km/sec and densities of  $7/\text{cm}^3$  at the orbit of earth for a

temperature  $T_0 = 2 \times 10^6$  K in the low corona, in general agreement with observation. However, it was necessary to assume a rather low density  $N_0 = 1-3 \times 10^7/\text{cm}^3$  at the base of the corona. If  $N_0$  is chosen to be as large as observed,  $N_0 \cong 1-2 \times 10^8/\text{cm}^3$ , then much lower wind velocities and higher densities at the orbit of earth result, because the thermal conductivity (which is essentially independent of the gas density) is unable to supply enough energy to maintain the temperature of the expanding coronal gas. The reduced temperature in the outer corona then gives a small wind velocity at large  $r$ , which leads to an increased  $N$  through  $r^2 vN = \text{constant}$  [see discussion in Parker, 1965a, b].

If one wishes the model to fit the observed coronal density at the sun, the temperature must be reduced somewhat near the sun, to give a more rapid decline of density with radial distance, and the temperature must be increased somewhat beyond several solar radii, to give the observed 300 km/sec wind velocity. This would require heating the expanding corona with waves from the sun [Noble and Scarf, 1963; Parker, 1964a; Barnes, 1968, 1969].

The wind velocity can be enhanced and the density reduced somewhat if the thermal conduction from the sun is obstructed at large  $r$  [Parker, 1964a, 1965b]. Then the thermal energy piles up behind the obstruction, raising the temperature and increasing the velocity of the expanding wind gases (whereupon the energy passes the obstruction in the form of enhanced wind velocity). Transverse magnetic fields are the most obvious obstruction to thermal conduction. Beyond the orbit of earth the interplanetary magnetic field is largely transverse and therefore may be expected to furnish an obstruction. The angle  $\theta$  which the spiral field makes with the radial direction is  $\tan \theta = \Omega r/v$  where  $\Omega$  is the angular velocity of the sun ( $\Omega \sim 3 \times 10^{-6}$  rad/sec), so that  $\theta = 45^\circ$  at 0.7 AU (for quiet day wind velocities of the order of 300 km/sec) and is larger than  $45^\circ$  beyond. Thermal conduction is reduced by the factor  $\cos^2 \theta$ , which is already below 0.5 at the orbit of earth. At Mars  $\cos^2 \theta$  is 0.2 or 0.3.

Forslund [1970] has pointed out another effect: that the high thermal conduction flux in the wind leads to skewed electron distributions, producing plasma instabilities and thereby reducing the effective thermal conduction coefficient. The heat from viscous dissipation is a further contributing factor. Recently several authors [Brandt et al., 1969; Gentry and Hundhausen, 1969; Urch, 1969; Cupperman and Harten, 1970] have worked out the effects quantitatively. Unfortunately, the reduction of  $\kappa$  at large  $r$  does not appear to have a sufficiently



large effect to make up the entire difference. The theoretical models fit the density of the wind at the orbit of earth and in the outer corona only with a density as small as  $3-5 \times 10^7/\text{cm}^3$  at the base of the corona, better than the  $1-3 \times 10^7/\text{cm}^3$  required by the simpler models, but still well below the  $1-2 \times 10^8/\text{cm}^3$  observed. The models also predict a thermal conduction flux at the orbit of earth which is several times larger than observed. Consequently, *Hartle and Barnes* [1970] have taken up the formal calculation of models of the corona with energy deposition from the dissipation of hydromagnetic waves from the sun. They show that the wind velocity is increased, and/or the density decreased, if heat is added by wave dissipation in the broad region containing the sonic transition point, where the expansion velocity crosses the speed of sound. The sensitive region is roughly  $2-25 R_\odot$ . With their model it is a simple matter to bring the density at the base of the corona and at the orbit of earth both into line with the observations. They point out that their theoretical model fits the empirical relation

$$T^{1/2} = (0.036 \pm 0.003)v - (5.54 \pm 1.50)$$

between the proton temperature  $T$  (in units of  $10^3^\circ\text{K}$ ) at the orbit of earth and the wind velocity  $v$  (in km/sec) proposed by *Burlaga and Ogilvie* [1970a]. The empirical relation is remarkable in that it applies to both quiet and disturbed times. Hence, from the work of *Hartle and Barnes* [1970] we have a strong case that in quiet times the coronal heating extends out from the sun for several solar radii.

Needless to say, the active corona and solar wind, with velocities two or more times the quiet day values, and densities half or less the quiet values, implies very active heating of the corona, presumably by wave dissipation, out to 0.1 AU or more. The models of *Hartle and Barnes* show what can be done in this respect.

*Burlaga and Ogilvie* [1970b] make the interesting point, too, that the total pressure in the wind  $p + B^2/8\pi$  is generally uncorrelated with wind velocity. And they note that the sum  $p + B^2/8\pi$  varies much less over periods of hours than either  $p$  or  $B^2/8\pi$  separately, suggesting local hydrostatic equilibrium in the wind.

When one goes beyond the gross properties of density and velocity of the wind, considering the individual temperatures and anisotropies of the electrons and protons at the orbit of earth, more detailed models are needed. Treating the ionized hydrogen of the wind as a single gas overlooks the fact that it is mainly the electrons that are responsible for thermal conduction, and they are but weakly coupled by collisions to the

protons. For this reason, the two-fluid models of the solar wind have been developed [*Sturrock and Hartle*, 1966; *Hartle and Sturrock*, 1968; *Hartle and Barnes*, 1970] in which the electron and proton gases are treated separately, with an energy exchange between the two depending on the temperature difference  $T_e - T_p$  and the collision rate  $\nu$ . Thus the total energy flux  $F$  is independent of  $r$ , but the energy fluxes  $F_e$  and  $F_p$  for the electron and proton gases separately satisfy

$$\frac{dF_e}{dr} = -\frac{3}{2} \nu N k (T_e - T_p) 4\pi r^2$$

$$\frac{dF_p}{dr} = +\frac{3}{2} \nu N k (T_e - T_p) 4\pi r^2$$

There is little effect on the wind velocity and density. But the temperature is profoundly affected. With the one-fluid model, the theoretical temperature of the wind at the orbit of earth is of the order of  $2 \times 10^5^\circ\text{K}$  (for  $2 \times 10^6^\circ\text{K}$  at the base of the corona). With the two-fluid model, the calculated electron temperature is  $3 \times 10^5^\circ\text{K}$  and the proton temperature is quite low,  $4 \times 10^3^\circ\text{K}$ . The observed electron temperatures are generally around  $1.5 \times 10^5^\circ\text{K}$  and do not vary much with the level of solar activity. The observed quiet-day proton temperatures are typically  $4 \times 10^4^\circ\text{K}$ , with values as low as  $10^4^\circ\text{K}$  only rarely observed. The proton temperatures increase to  $10^5^\circ\text{K}$ , and more, with the advent of solar activity.

Altogether, then, the one-fluid model gives temperatures that at the orbit of earth are close to the observed electron temperatures. The two-fluid model gives too low a proton temperature and too high an electron temperature. That is to say,  $T_e$  and  $T_p$  are actually tied together more closely than can be accounted for by the Coulomb collisions assumed to couple the two gases in the simple two-fluid theory. *Wolff et al.* [1971] show that inclusion of viscosity can raise the proton temperature to  $4 \times 10^4^\circ\text{K}$ , which agrees with typical quiet-day observations. And, of course, introducing wave dissipation into the two-fluid model near the sun can be made to bring  $T_e$  and  $T_p$  closer together and into rough agreement with the observed values [*Hartle and Barnes*, 1970; *Cuperman and Harten*, 1971].

Consider the thermal anisotropy of the electron and proton gases. The observations at the orbit of earth show 92 percent of the energy flux convected in the form of kinetic energy of the wind and only 4 percent in thermal conduction, whereas the two-fluid model gives over 50 percent in thermal conduction at the orbit of earth [see

discussion in *Hundhausen, 1970*]. The observed anisotropies in the proton temperatures are only 2 to 1, whereas Coulomb collisions alone give 50 to 1.

Thus again the theoretical model can be brought more into line with the observations with liberal doses of wave dissipation toward the sun. Plasma waves may be called on to suppress thermal conduction and thermal anisotropy, and the dissipation of hydromagnetic waves can be called on to supply whatever energy is needed to give the observed velocity and density at the orbit of earth. But the theoretical models that produce quantitative agreement with all presently observable properties of the wind are complicated. Postulating wave dissipation introduces enough arbitrary parameters that the present quiet-day observations can be fitted—probably in more ways than one. It is not evident that a unique theoretical model can be constructed, showing the general quantitative characteristics of the wind at the orbit of earth, without direct observation of the wind over much of the distance between earth and the sun, and beyond the orbit of earth, to establish (1) whether the observed electron anisotropies are, or are not, compatible with the anisotropy deduced from  $\kappa dT/dr$  and the observed  $dT/dr$ ; (2) whether the electron and proton anisotropies at any given position are compatible with the waves observed there; (3) what plasma waves and plasma instabilities are actually present; or (4) what hydromagnetic waves are present. It is likely that quantitative observation of the wind over the regions inside and outside the orbit of earth will show novel features (and inconsistencies in some of our present ideas) that could not possibly have been anticipated from theory and from analysis of observations near the orbit of earth.

One of the fundamental questions that has been a subject of curiosity for a long time is whether the solar corona and wind expand radially outward from the sun, or whether the low latitude corona contributes most of the wind, so that the wind near the equatorial plane is expanding rapidly toward high solar latitudes. If the wind is expanding away from the equatorial plane, the gas density drops more rapidly than the  $1/r^2$  for radial flow. The temperature, density, and velocity of the wind at the orbit of earth could be seriously affected by nonradial expansion.

Another question is the inhomogeneity of the corona near the sun. The structure of the small-scale filaments near the sun is not known with precision, nor is it known to what extent the solar wind arises from filaments, or interfilament regions. Expansion limited to filaments appears to be a necessary part of any pure conduction models that are to fit the high coronal densities near the sun. The filaments expand faster than

$r^2$  with increasing radial distance, thereby reducing the wind density relative to that of the corona. (Dynamical studies of filaments are noted in the last section.)

### THE ROLE OF WAVES

Hydromagnetic waves generated at the sun are a source of heat for the solar corona and solar wind. The degree to which waves heat the quiet-day corona and solar wind is a subject of some discussion, as noted above. Waves generated by wind velocities that vary around the sun—that is, colliding streams—and by wind velocities that vary with time in the rotating frame of the sun, have also been studied by many authors [*Parker, 1963; Jokipii and Davis, 1969; Carovillano and Siscoe, 1969; Siscoe and Finley, 1970; Burlaga et al., 1971*]. These studies consider the waves both as a phenomenon to be observed directly and as a source of heat for the wind. *Belcher [1971]* has recently pointed out another role of waves—namely, supplying momentum directly to the wind.

The expanding corona and wind are stable to small perturbations [*Parker, 1966; Carovillano and King, 1966; Jockers, 1968*], and the propagation of hydromagnetic waves outward from the sun proceeds in a straightforward manner subject to the damping of thermal conductivity, Landau damping [*Barnes, 1966, 1967*], and stochastic fields [*Jokipii and Parker, 1969; Valley, 1971*].

Consider the idealized situation of a solar wind with spherical symmetry about a nonrotating sun. Then the wind velocity and density  $v(r)$  and  $N(r)$  are functions only of  $r$ . The magnetic field is radial and declines outward as  $1/r^2$ . Alfvén waves involving displacements in the  $\phi$  direction are easily treated when the wavelength is small compared to the scale  $r$  of the wind, and it is readily shown [*Parker, 1965b*] that the amplitude of outward propagating waves varies as

$$\begin{aligned}\delta B(r, t) &= \delta B_0 \left( \frac{N}{N_0} \right)^{1/4} \frac{v_0 / C_0 + 1}{v / C + 1} \\ &\quad \exp i\omega \left( t - \int \frac{dr}{v + C} \right) \\ \delta v(r, t) &= -\delta v_0 \left( \frac{N}{N_0} \right)^{1/4} \frac{v_0 / C_0 + 1}{v / C + 1} \\ &\quad \exp i\omega \left( t - \int \frac{dr}{v + C} \right)\end{aligned}$$

where  $C$  is the local Alfvén speed  $B/(4\pi NM)^{1/2}$  and  $r^2 v N = \text{constant}$ . The subscript zero denotes the value at some specified reference level. The waves do work on the wind because of their centrifugal force  $(\delta v)^2/r$  and

their magnetic pressure  $\delta B^2/8\pi r$  exerted on the wind. The forces exerted by the waves are outward, in the same direction as the wind, so that they boost the wind along in its outward flow. The rate at which work is done is [Parker, 1965b]

$$P = \frac{NM\langle\delta v^2\rangle\nu}{r} + \frac{\langle\delta B^2\rangle}{8\pi} \frac{dv}{dr} \text{ erg/cm}^3 \text{ sec}$$

The new point that Belcher [1971] makes is that the work done by the waves directly on the wind can greatly enhance the velocity of the wind. The energy flux  $F$  has added to it the term  $4\pi r^2 \times (1/2)NM\langle\delta v^2\rangle\nu$  representing convection of the kinetic energy, and the term  $4\pi r^2 \times \langle\delta B^2\rangle/8\pi (\nu + C)$  representing the convection and propagation of magnetic energy.

If the wave amplitude  $\delta B$  is nearly as large as the radial field  $B$ , the waves may contribute as much as the pressure gradient to accelerating the wind. For with  $\delta v = \delta B/(4\pi NM)^{1/2}$  it follows that the centrifugal force term  $NM\langle\delta v^2\rangle/r$  is  $\langle\delta B^2\rangle/4\pi r$ , which may be comparable to  $B^2/8\pi r$ . Presumably  $B^2/8\pi$  can be as large as the gas pressure  $2NkT$ , so the driving force of the waves may be as large as the driving force of the pressure gradient. Wave driving can have a large effect on the wind. Belcher suggests that such wave propulsion may contribute to the production of the fast, hot, tenuous winds that sometimes come from the active sun. Presumably the waves would both accelerate the wind, in the manner just described, and heat the wind on dissipation. Clearly, the effect must be included in any comprehensive model of the solar wind.

A final comment is in order concerning the propagation and damping of hydromagnetic waves in the solar wind. Not many years ago there was a general impression that long wavelength hydromagnetic waves (say  $\lambda \sim 10^{11} - 10^{12}$  cm) propagate in the solar wind with but little damping. All the stability calculations mentioned above are based on this idea, using the simple field equations without damping. Then Barnes [1966, 1967] showed that Landau damping dissipates all such waves in distances of 1 AU or less, except for Alfvén waves, which propagate exactly along the field, and magnetosonic waves propagating exactly across the field. Then Jokipii [1967; Jokipii and Parker, 1969] pointed out that the lines of force of the interplanetary magnetic field are stochastic. The mean field follows the usual Archimedes spiral (or radial pattern in the idealized case above), but the individual neighboring lines of force wander (random walk) apart if one follows along the lines. The random walk is the result of turbulence on the sun (granules, supergranules) as well as turbulence in

interplanetary space. In any case, Valley [1971] has shown that Alfvén waves and magnetosonic waves are dispersed in distances of 1 AU by the stochastic nature of the large-scale field. Valley points out, then, that *no hydromagnetic waves escape damping* in distances of 1 AU. This does not entirely exclude waves generated near the sun from reaching the orbit of earth, because such waves are largely convected, rather than propagated, in the solar wind. The Alfvén speed is 0.1–0.2 the wind speed. But the dissipation is a significant effect and must be considered in any model involving waves as a source of either heat or momentum for the wind.

### MISCELLANEOUS TOPICS

Those interested in exospheric models of the solar corona, in which magnetic irregularities are ignored and the outer corona and wind are treated as an aggregate of noninteracting particles (except for the charge-separation electric field), are referred to the recent papers of Jockers [1969] and Hollweg [1970] [see also the discussion and references in Hundhausen, 1970]. It is well known that the moments of the collisionless Boltzmann equation give the ordinary hydrodynamic equations, so that the fluid and free-particle treatments cannot be wholly different [Parker, 1960a]. But the free-particle approach is much more involved, particularly in the question of boundary conditions at the sun, so that only with the recent work, beginning with Brandt and Cassinelli [1966], has it been possible to carry through the exospheric model correctly, obtaining wind velocities of a few hundred km/sec at the orbit of earth. Needless to say the exospheric models lack the mixing of thermal velocities between different directions, and between electrons and protons, that is indicated by observations of the thermal anisotropy and proton temperatures at the orbit of earth.

Siscoe [1970; Parker, 1964b; Carovillano and Siscoe, 1969] has recently looked further into the dynamics of coronal streamers, treating fast and slow streams with solar rotation included. Interest has also arisen recently in solar wind filaments because of the east-west asymmetries that may develop between slow and fast streams [Siscoe et al., 1969], and several theoretical papers treating that aspect have appeared [Carovillano and Siscoe, 1969; Siscoe, 1970; Siscoe and Finley, 1970]. Siscoe and Finley [1969] have shown that the observed  $1^\circ - 3^\circ$  north-south deflections sometimes observed in the wind direction can be explained by 10 to 20 percent pressure variations with solar latitude. The calculations suggest that coronal gas from  $\pm 12^\circ$  solar latitude may arrive at the orbit of earth. Pneuman and Kopp [1970] consider the nonradial expansion in streamers, showing

that it leads to reduced wind densities at the orbit of earth.

It will be recalled that several years ago a number of authors became interested in the decelerating torque exerted by the wind on the rotating sun and on the azimuthal velocity  $v_\phi$  of the wind at the orbit of earth [see review and list of references in Parker, 1969; Wolff *et al.*, 1971]. The torque is approximately the  $10^{30}$  to  $10^{31}$  dyne-cm exerted by the spiral magnetic field [Parker, 1958]. The calculations of the azimuthal velocity in the wind predict  $v_\phi = 1$  to 2 km/sec, whereas observations [Belton and Brandt, 1966; Brandt, 1967; Hundhausen *et al.*, 1968] indicate 5 to 10 km/sec. The error could lie in the difficult analysis of the observations. But if the observational analysis is correct, it suggests perhaps a systematic forward tilt of the magnetic fields in the rotating sun [Schubert and Coleman, 1968]. This puzzle remains unsolved after several years of serious consideration.

This is perhaps the place to note recent research pertaining to some of the fine points in the theory of the solar wind. Questions of unique and convergent solutions including thermal conductivity and/or viscosity have been explored by Eisler [1969a, b], Weber [1970] and Wolff *et al.* [1971]. See also the paper by Whang *et al.* [1966]. Explicit solutions of the polytrope equations have been given by Tyan [1970] and by Holzer and Axford [1970].

Tan and Abraham-Shrauner [1971] have worked out the equations of motion including the pressure anisotropy in the gas and have given numerical solutions that compare well with observations.

Another point of recent interest is the transition from a supersonic to a subsonic wind that occurs if the coronal density is slowly increased while the temperature remains fixed [Parker 1965a]. Calculations show analytic solutions with the temperature declining asymptotically as  $T \sim 1/r^{2/7}$  in the supersonic regime (low-density corona) and  $T \sim 1/r$  in the subsonic regime (high-density corona) with a special isolated supersonic solution  $T \sim 1/r^{2/5}$  [Whang and Chang, 1965] in the transition region between the regular supersonic and subsonic regions. Durney [1971] has recently carried out numerical calculations indicating a range of supersonic solutions with  $T \sim 1/r^{4/3}$  in the transition region. If his conclusion is in fact correct, it indicates a richer field of solutions than previously imagined, and suggests that further investigation may be rewarding.

#### ACKNOWLEDGEMENT

This work was supported in part by the National Aeronautics and Space Administration under grant NASA NGL 14-001-001.

#### REFERENCES

- Axford, W. I.: Observations of the Interplanetary Plasma. *Space Sci. Rev.*, Vol. 8, 1968, p. 331.
- Barnes, A.: Collisionless Damping of Hydromagnetic Waves. *Phys. Fluids*, Vol. 9, 1966, p. 1483.
- Barnes, A.: Stochastic Electron Heating and Hydromagnetic Wave Damping. *Phys. Fluids*, Vol. 10, 1967, p. 2427.
- Barnes, A.: Collisionless Heating of the Solar Wind Plasma, I. Theory of the Heating of a Collisionless Plasma by Hydromagnetic Waves. *Astrophys. J.*, Vol. 154, 1968, p. 751.
- Barnes, A.: Collisionless Heating of the Solar Wind Plasma, II. Application of the Theory of Plasma Heating by Hydromagnetic Waves. *Astrophys. J.*, Vol. 155, 1969, p. 311.
- Belcher, J. W.: A Wave Driven Model of the Solar Wind. *Solar Phys.* 1971.
- Belton, M. J. S.; and Brandt, J. C.: Interplanetary Gas, XII. A Catalogue of Comet-Tail Orientations. *Astrophys. J. Suppl.*, Vol. 13, 1966, p. 125.
- Brandt, J. C.: Interplanetary Gas, XIII. Gross Plasma Velocities from the Orientations of Ionic Comet Tails. *Astrophys. J.*, Vol. 147, 1967, p. 201.
- Brandt, J. C.; and Cassinelli, J. P.: Interplanetary Gas, II. An Exospheric Model of the Solar Wind. *Icarus*, Vol. 5, 1966, p. 47.
- Brandt, J. C.; Wolff, C.; and Cassinelli, J. P.: Interplanetary Gas, XVI. A Calculation of the Angular Momentum of the Solar Wind. *Astrophys. J.*, Vol. 156, 1969, p. 1117.
- Burlaga, L. F.; and Ogilvie, K. W.: Heating of the Solar Wind. *Astrophys. J.*, Vol. 159, 1970a, p. 659.
- Burlaga, L. F.; and Ogilvie, K. W.: Magnetic and Thermal Pressures in the Solar Wind. *Solar Phys.*, Vol. 15, 1970b, p. 61.
- Burlaga, L. F.; Ogilvie, K. W.; Fairfield, D. A.; Montgomery, M. D.; and Bame, S. J.: Energy Transfer at Colliding Streams in the Solar Wind. *Astrophys. J.*, Vol. 164, 1971, p. 137.
- Carovillano, R. L.; and King, J. H.: Dynamical Stability and Boundary Perturbations of the Solar Wind. *Astrophys. J.*, Vol. 145, 1966, p. 426.
- Carovillano, R. L.; and Siscoe, G. L.: Corotating Structure in the Solar Wind. *Solar Phys.*, Vol. 8, 1969, p. 401.
- Chapman, S.: The Viscosity and Thermal Conductivity of a Completely Ionized Gas. *Astrophys. J.*, Vol. 120, 1954, p. 151.

- Cuperman, S.; and Harten, A.: The Solution of One-Fluid Equations with Modified Thermal Conductivity for the Solar Wind. *Cosmic Electrodyn.*, Vol. 1, 1970, p. 205.
- Cuperman, S.; and Harten, A.: The Electron Temperature in the Two Component Solar Wind. *Astrophys. J.*, Vol. 162, 1971, p. 315.
- Dessler, A. J.: Solar Wind and Interplanetary Magnetic Field. *Rev. Geophys.*, Vol. 5, 1967, p. 1.
- Durney, B.: A New Type of Supersonic Solution for the Equations of the Solar Wind. To be published in *Astrophys. J.*, 1971.
- Eisler, T.: Convergent Solutions of the Inviscid Solar Wind Equations. *Solar Phys.*, Vol. 7, 1969a, p. 46.
- Eisler, T.: Asymptotic Solutions of the Viscous Solar Wind Equations. *Solar Phys.*, Vol. 7, 1969b, p. 49.
- Forslund, D. W.: Instabilities Associated with Heat Conduction in the Solar Wind and Their Consequences. *J. Geophys. Res.*, Vol. 75, 1970, p. 17.
- Gentry, R. A.; and Hundhausen, A. J.: A Solar Wind Model with Magnetically Inhibited Heat Conduction (Abstract). *Trans. Amer. Geophys. Union*, Vol. 50, 1969, p. 302.
- Hartle, R. E.; and Barnes, A.: Nonthermal Heating in the Two-Fluid Solar Wind Model. *J. Geophys. Res.*, Vol. 75, 1970, p. 6915.
- Hartle, R. E.; and Sturrock, P. A.: Two-Fluid Model of the Solar Wind. *Astrophys. J.*, Vol. 151, 1968, p. 1155.
- Hollweg, J. V.: Collisionless Solar Wind, I. Constant Electron Temperature. *J. Geophys. Res.*, Vol. 75, 1970, p. 2403.
- Holzer, T. E.; and Axford, W. I.: The Theory of Stellar Winds and Related Flows. *Ann. Rev. Astron. Astrophys.*, Vol. 8, 1970, p. 31.
- van de Hulst, H. C.: The Chromosphere and Corona, in *The Sun*, edited by G. P. Kuiper, Univ. of Chicago Press, Chicago, 1953, p. 304.
- Hundhausen, A. J.: Direct Observations of Solar Wind Particles. *Space Sci. Rev.*, Vol. 8, 1968, p. 690.
- Hundhausen, A. J.: Composition and Dynamics of the Solar Wind Plasma. *Rev. Geophys. Space Phys.*, Vol. 8, 1970, p. 729.
- Jockers, K.: On the Stability of the Solar Wind. *Solar Phys.*, Vol. 3, 1968, p. 603.
- Jockers, K.: Solar Wind Models Based on Exospheric Theory. Max-Planck-Institut für Physik und Astrophysik, Preprint MPT-PAE/Astro 28, 1969.
- Jokipii, J. R.: Cosmic Ray Propagation, I. Charged Particles in a Random Magnetic Field. *Astrophys. J.*, Vol. 146, 1967, p. 380.
- Jokipii, J. R.; and Davis, L.: Long Wavelength Turbulence and the Heating of the Solar Wind. *Astrophys. J.*, Vol. 156, 1969, p. 1101.
- Jokipii, J. R.; and Parker, E. N.: Stochastic Aspects of Magnetic Lines of Force with Application to Cosmic Ray Propagation. *Astrophys. J.*, Vol. 155, 1969, p. 777.
- Lüst, R.: The Properties of Interplanetary Space, in *Solar Terrestrial Physics*, edited by J. W. King and W. S. Newman. Academic Press, New York, 1967, p. 1.
- Ness, N. F.: Observed Properties of the Interplanetary Plasma. *Ann. Rev. Astron. Astrophys.*, Vol. 6, 1968, p. 79.
- Noble, L. M.; and Scarf, F. L.: Conductive Heating of the Solar Wind. *Astrophys. J.*, Vol. 138, 1963, p. 1169.
- Parker, E. N.: Dynamics of the Interplanetary Gas and Magnetic Fields. *Astrophys. J.*, Vol. 128, 1958, p. 664.
- Parker, E. N.: The Hydrodynamic Treatment of the Expanding Solar Corona. *Astrophys. J.*, Vol. 132, 1960a, p. 175.
- Parker, E. N.: The Hydrodynamic Theory of Solar Corpuscular Radiation and Stellar Winds. *Astrophys. J.*, Vol. 132, 1960b, p. 821.
- Parker, E. N.: *Interplanetary Dynamical Processes*, Interscience, John Wiley, New York, 1963.
- Parker, E. N.: Dynamical Properties of Stellar Coronas and Stellar Winds, II. Integration of the Heat-Flow Equation. *Astrophys. J.*, Vol. 139, 1964a, p. 93.
- Parker, E. N.: Dynamical Properties of Stellar Coronas and Stellar Winds, III. The Dynamics of Coronal Streamers. *Astrophys. J.*, Vol. 139, 1964b, p. 690.
- Parker, E. N.: Dynamical Properties of Stellar Coronas and Stellar Winds, IV. The Separate Existence of Subsonic and Supersonic Solutions. *Astrophys. J.*, Vol. 141, 1965a, p. 1963.
- Parker, E. N.: Dynamical Theory of the Solar Wind. *Space Sci. Rev.*, Vol. 4, 1965b, p. 666.
- Parker, E. N.: Dynamical Properties of Stellar Coronas and Stellar Winds, V. Stability and Wave Propagation. *Astrophys. J.*, Vol. 143, 1966, p. 32.
- Parker, E. N.: The Dynamical Theory of Gases and Fields in Interplanetary Space, in *Solar-Terrestrial Physics*, edited by J. W. King and W. S. Newman. Academic Press, New York, 1967.
- Parker, E. N.: Theoretical Studies of the Solar Wind Phenomenon. *Space Sci. Rev.*, Vol. 9, 1969, p. 325.
- Pneuman, G. W.; and Kopp, R. A.: Coronal Streamers, III. Energy Transport in Streamer and Interstreamer Regions. *Solar Phys.*, Vol. 13, 1970, p. 176.

- Schubert, G.; and Coleman, P. J.: The Angular Momentum of the Solar Wind. *Astrophys. J.*, Vol. 153, 1968, p. 943.
- Siscoe, G. L.: Fluid Dynamics of Thin Solar Filaments. *Solar Phys.*, Vol. 13, 1970, p. 490.
- Siscoe, G. L.; and Finley, L. T.: Meridional Motions of Solar Wind. *Solar Phys.*, Vol. 9, 1969, p. 452.
- Siscoe, G. L.; and Finley, L. T.: Solar Wind Structure Determined by Corotating Coronal Inhomogeneities, I. Velocity Driven Perturbations. *J. Geophys. Res.*, Vol. 75, 1970, p. 1817.
- Siscoe, G. L.; Goldstein, B.; and Lazarus, A. J.: An East-West Asymmetry in the Solar Wind. *J. Geophys. Res.*, Vol. 74, 1969, p. 1759.
- Sturrock, P. A.; and Hartle, R. E.: Two-Fluid Model of the Solar Wind. *Phys. Rev. Letters.*, Vol. 16, 1966, p. 628.
- Tan, M.; and Abraham-Shrauner, B.: Solar Wind for a Magnetized Plasma with Tensor Plasma Pressure. To be published in *Astrophys. J.*, 1971.
- Tyan, Y.: An Explicit Solution of Polytrope Solar Wind Equations. *J. Geophys. Res.*, Vol. 75, 1970, p. 6309.
- Urch, I. H.: A Model of the Magnetized Solar Wind. *Solar Phys.*, Vol. 10, 1969, p. 219.
- Valley, G.: Scattering of Hydromagnetic Waves in Stochastic Fields. *Astrophys. J.* (to be submitted).
- Weber, E. J.: Unique Solutions of Solar Wind Models with Thermal Conductivity. *Solar Phys.*, Vol. 14, 1970, p. 480.
- Whang, Y. C.; and Chang, C. C.: An Inviscid Model of the Solar Wind. *J. Geophys. Res.*, Vol. 70, 1965, p. 4175.
- Whang, Y. C.; Lie, C. K.; and Chang, C. C.: A Viscous Model of the Solar Wind. *Astrophys. J.*, Vol. 145, 1966, p. 255.
- Wilcox, J. M.: The Interplanetary Magnetic Field: Solar Origin and Terrestrial Effects. *Space Sci. Rev.*, Vol. 8, 1968, p. 258.
- Wolff, C. L.; Brandt, J. C.; and Southwick, R. G.: A Two Component Model of the Quiet Solar Wind with Viscosity, Magnetic Field, and Reduced Heat Conduction. *Astrophys. J.*, Vol. 165, 1971, p. 181.

**DISCUSSION** *D. B. Beard* I have seen some recent interpretations by our group and others of observations of the *K* component of the solar corona in which the electron density was estimated to be more like  $10^9$  rather than  $10^8 \text{ cm}^{-3}$ . Can you reasonably accommodate the higher figure?

*E. N. Parker* Well, the  $1$  or  $2 \times 10^8$  atoms/ $\text{cm}^3$  I gave is for the quiet corona, because I wanted to discuss the quiet solar wind. The active corona shows densities up to  $10^9$  atoms/ $\text{cm}^3$  and I think all one can say is that it is quite evident there is extensive wave heating, though how extensive nobody knows. Again, one can construct models with the wind expanding away from local regions. These fit the data at the orbit of earth, but they are by no means unique. There are several ways to handle the parameters.

*K. Schatten* I would like to comment on the amount of nonradial flow that Gene Parker discussed. In calculating the coronal magnetic field, for the years 1965 and 1966 we found approximately a 1 to 6 expansion by area or a 1 to 2-1/2 expansion in terms of linear dimension. So for models that include this expansion from local regions it might be worthwhile to use these numbers for the approximate expansion.

*E. N. Parker* What do those numbers mean, again?

*K. Schatten* For a unit solid angle on the sun we determine the magnetic flux and ask what solid angle this flux will extend over at 1 AU. It turns out that the solid angle will be about 6 times as large at 1.0 AU.

*E. N. Parker* How is this determined? It's very interesting.

*K. Schatten* Using the computed magnetic field, according to the coronal magnetic field models, one follows the field vectors from the sun's surface to a 'source' surface at about a solar radius and observes how much area on the sun maps out to how much area at the source surface. One then assumes a radial extension from the source surface to 1.0 AU. The 1 to 6 figure suggests that about 17 percent of the sun's surface is directly connected by field lines to 1 AU.

*E. N. Parker* You're saying that some spots on the sun are the dominant sources of the field at the orbit of earth?

*K. Schatten* Yes. The model of the coronal field does *not* suggest a complete 100 percent direct extension of flux from the sun to 1 AU.

*J. V. Hollweg* I have a question about the damping of Alfvén waves. Is it not reasonable to consider the stochastic nature of the magnetic field as actually due to random Alfvén waves, in which case you wouldn't describe scattering of Alfvén waves off the random field?

*E. N. Parker* It's possible to think of the stochastic nature of the field as due to Alfvén waves, in which case it is wave scattering rather than scattering from an equilibrium field. You get roughly the same answers.

*E. J. Smith* I have a related question. You mentioned the scattering of waves. Where would this become important?

*E. N. Parker* For waves of length 0.01 or 0.1 AU it is important at the orbit of earth. That is, given the estimates of the degree by which the field random walks, the scattering of Alfvén waves is an important effect inside the orbit of earth. Apparently, for waves of almost any dimension less than 1 AU, the scattering takes place as soon as they leave the sun. The distances which a wave will propagate is typically 1 AU, but in making numerical estimates, one must remember that when a wave arrives at the earth, it has not propagated 1 AU. It has been convected for about 4/5 AU, during which time it propagated only about 1/5 AU. So the damping is significant, but not excessive.

*F. W. Perkins* I would like to make a comment for those theorists working themselves out of a job doing solar wind calculations. There's another interesting problem concerning mass loss from stars. Red super giant stars are structured such that the combination of heat and ionization energy for regions just below the surface of these stars is above zero. It's difficult to determine how the flow will come off these stars.

*A. Hewish* I would just like to mention that the best available data on solar winds from radio scintillations indicate complete spherical symmetry up to ecliptic latitudes of  $70^\circ$  and over a range of radial distance of 0.3 to 1 AU. There is limited data on the acceleration of the wind closer to the sun.

*E. N. Parker* By spherical symmetry you mean the velocity of the wind is more or less independent of direction from the sun?

*A. Hewish* The velocity is radial and independent of latitude or distance from the sun in that range.

*G. W. Pneuman* An observation that might pertain to this high density problem is that corona observations of the inner corona during solar eclipse seem to indicate that many regions of very high density may not be taking part in the coronal expansion at all, but are confined in large closed loop structures.

## THE LARGE-SCALE STRUCTURE OF THE SOLAR WIND *John H. Wolfe* An invited review

**ABSTRACT** The large-scale structure of the solar wind is reviewed on the basis of experimental space measurements acquired over approximately the last decade. The observations cover the fading portion of the last solar cycle up through the maximum of the present cycle. The character of the interplanetary medium is considered from the viewpoint of the temporal behavior of the solar wind over increasingly longer time intervals, the average properties of the various solar wind parameters and their interrelationships. Interplanetary-terrestrial relationships and the expected effects of heliographic latitude and radial distance are briefly discussed.

### INTRODUCTION

The purpose of this paper is to review our knowledge of the large-scale structure of the solar wind. This review will be considered from measurements made from 1962 to the present. Results discussed represent data obtained during the fading portion of the last solar cycle (cycle 19) up to approximately the peak of the present cycle. Only proton results will be considered here since they represent the major energy-carrying constituent of the solar wind, and discussions of solar wind composition and solar wind electrons will be covered separately later in the conference. Consideration is given first to the average behavior of the solar wind as observed over many days and up to several solar rotations. The variations in the solar wind are then compared with the large-scale interplanetary magnetic field observations and with the behavior of the solar wind over much longer intervals up through the major portion of a solar cycle. An overall view is given of the average properties of the solar wind, and the interrelationship between solar wind parameters; and interplanetary-terrestrial relationships are discussed along with present speculation of the behavior of the solar wind closer to the sun, far beyond the earth's orbit and at high heliographic latitudes.

### SHORT-TERM VARIATIONS

Short-term variations are defined here to pertain to the solar wind behavior over periods of days and months, as opposed to years for long term variations. Figure 1 is taken from the Mariner 2 results reported by *Neugebauer and Snyder* [1966] and shows the variation in the solar wind velocity and temperature averaged over 3-hr intervals. The data were taken over approximately 4-1/2 solar rotations in late 1962. One of the most interesting features of these results is the great variability in the solar wind over a time period on the order of days. The velocity is observed to rise frequently from a quiescent value between 300 and 350 km/sec up to as high as approximately 700 km/sec, indicating a high degree of temperature inhomogeneity in the solar corona. Note that these high-velocity streams are often asymmetric, showing a sharper rise in velocity on the leading edge with a slower decay in the descending portion. The temperature is observed to be approximately in phase with the velocity, although frequently tending to high values on the leading edge of the stream somewhat prior to the velocity peak. Although some high-velocity streams tend to persist from one solar rotation to the next, they change in width and amplitude and some streams do not repeat at all. The data thus indicate, at least at the time of the Mariner 2 flight, that dramatic coronal changes take place on a time scale of less than one solar rotation. *Neugebauer and Snyder*

---

*The author is at NASA-Ames Research Center, Moffett Field, California.*



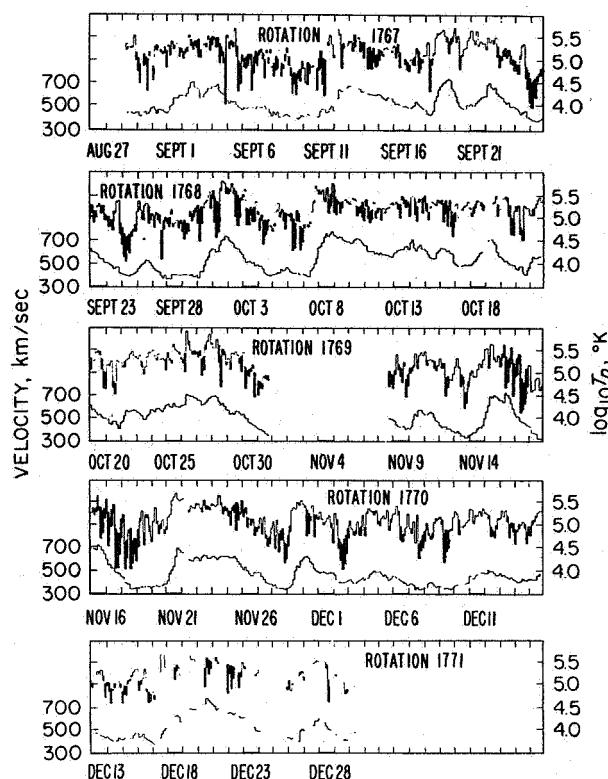


**Figure 1.** Three hour average values of velocity and temperature versus time observed by Mariner 2 in late 1962. The time base is chosen to show the 27-day recurrence features associated with solar rotation.

[1966] also reported the proton number density for this same period of time as shown in figure 2. For comparison purposes the velocity is again plotted here as the darker curve and the density as the lighter curve. The approximate in-phase relationship between velocity and temperature is in contrast to the striking anticorrelation between velocity and density observed here. In addition to the velocity-density anticorrelation, note also a frequent tendency for large increases in density associated with the leading edge of a high-velocity stream. This density pileup is dramatically observed, for example, in the streams beginning September 1, September 30, and October 7.

Three-hour averages of various solar wind parameters obtained during the last two weeks of December 1965 are shown in figure 3. The data are taken from the Ames Research Center plasma probe on Pioneer 6 [Wolfe, 1970] and show the solar wind bulk velocity, proton density and temperature, the two angular components of the flow direction, and the geomagnetic disturbance index  $K_p$ . The angular components of the flow direction

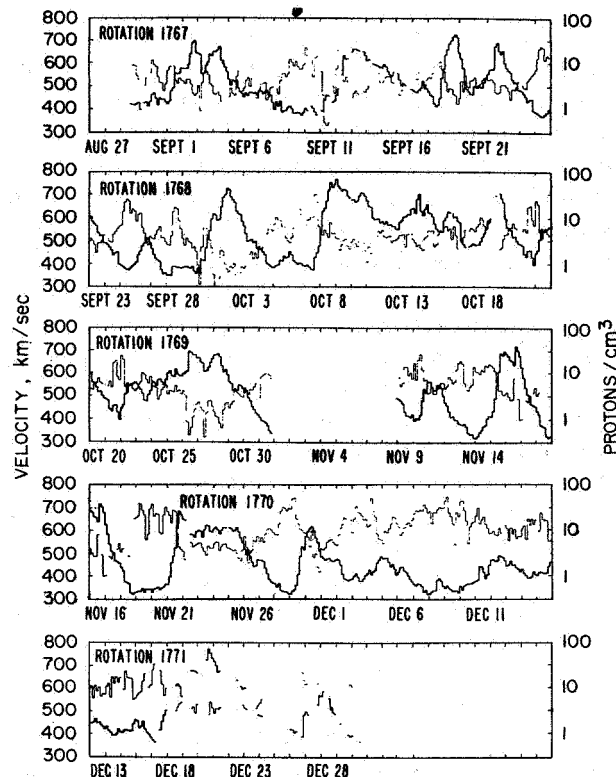


**Figure 2.** Mariner 2 3-hr average values of plasma velocity and proton number density versus time.

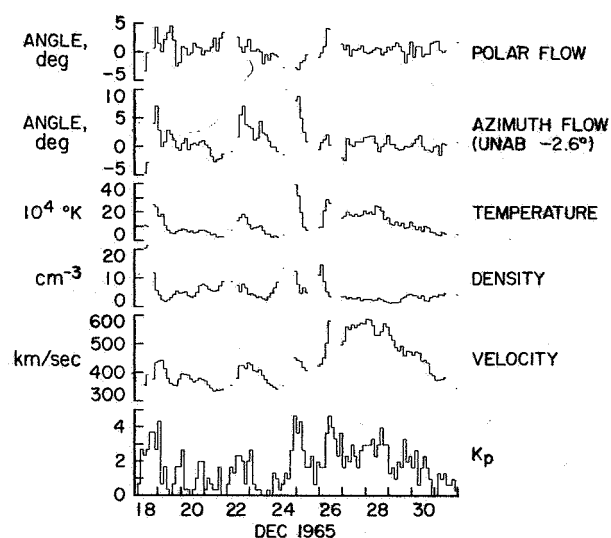


**Figure 3.** Pioneer 6 3-hr average values of velocity, density, temperature, azimuthal flow direction, polar flow direction and  $K_p$  versus time.

are defined in terms of a spacecraft-centered, solar ecliptic coordinate system. The azimuthal flow direction represents the angle of flow in the ecliptic plane with positive angles defined as flow from the west with respect to the spacecraft-sun line and negative angles from the east. This angle has been corrected for the aberration due to the motion of the spacecraft around the sun and has also been corrected for an apparent systematic error of a negative  $2.6^\circ$ . The polar flow direction represents the angle of flow in the plane normal to the ecliptic containing the spacecraft-sun line with positive angles defined as flow from the north and negative from the south. As was the case for the Mariner 2 data, the stream structure in the velocity is quite evident in the Pioneer 6 results. The density is observed to pile up in front of the leading portion of the streams with a sharp temperature rise associated with the positive gradient in the velocity. Also note that associated with the leading edge of each stream, the azimuthal flow angle shows that the flow shifts to a direction first from the east and then from the west across the positive gradient in velocity. This is a very persistent stream feature and is even more dramatically observed in figure 4. These data were also obtained from the Pioneer 6 Ames Research Center plasma probe [Wolfe, 1970] and show the solar wind bulk velocity and flow directions for the first two weeks of January 1966. Note the one-for-one correlation of the east-west shift in the azimuthal flow direction with the positive gradients in velocity. Although large

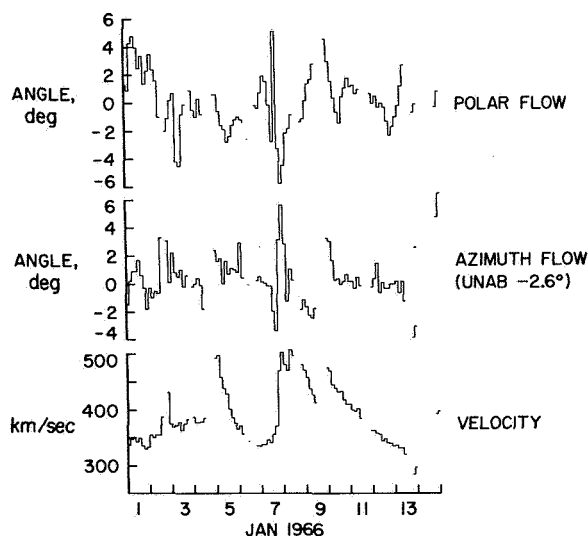
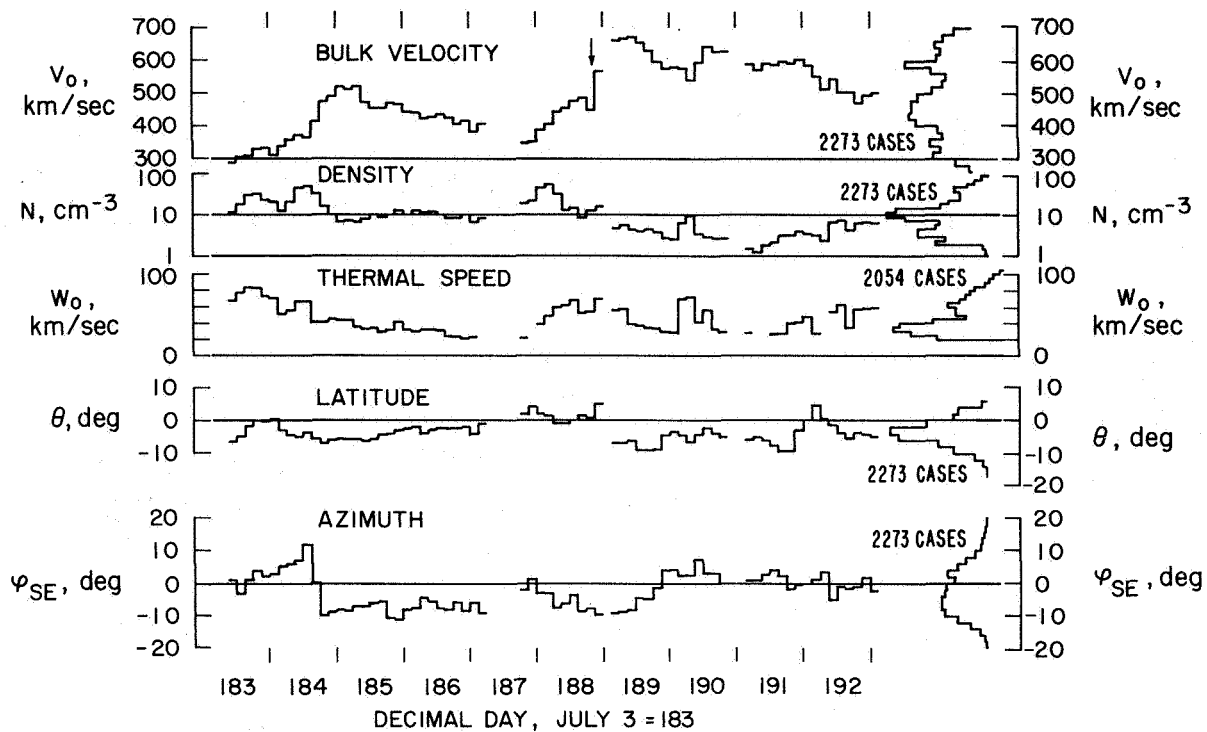


Figure 4. Pioneer 6 3-hr average values of velocity, azimuthal flow direction and polar flow direction versus time.

shifts in the polar flow direction are observed, frequently associated with velocity gradients, there is no particular flow pattern discernible in this angular component.

Similar results obtained during the rising portion of the present solar cycle have been reported by Lyon *et al.* [1968] using Explorer 33 data. Figure 5 shows 3-hr average values of the solar wind bulk velocity; density (logarithmic scale); most probable thermal speed, related to temperature by  $w = (2kT/m)^{1/2}$ ; and the azimuthal and latitude (polar) angles. Note that the azimuthal angle  $\varphi_{SE}$ , has been defined here in a sense opposite to that described for figures 3 and 4. The data were taken over the interval July 3-12, 1966. Again, the influence of the solar wind high-velocity stream structure is apparent. Note the striking examples of the density pileup at the leading edges of the high-velocity streams and the east-west shift in azimuthal flow direction across the positive gradient in velocity.

Short-term variations in solar wind behavior as observed over averages of several hours and considered on a time scale of weeks to months appear to be dominated by the solar wind stream structure. Coronal temperature inhomogeneities suggest (as observed near 1 AU) numerous coronal high-temperature regions that give rise to high-velocity solar wind streams; due to the rotation of the sun, these streams interact with the quiescent plasma associated with the ambient coronal solar wind. The stream interactions manifest themselves as a positive gradient in the solar wind convective velocity associated with the leading edge of the stream, which is typically much steeper than the negative gradient in velocity associated with the trailing portion of the stream. Although the velocity and temperature are observed to be approximately in phase, the steep positive gradient in velocity frequently indicates an interaction mechanism for heating the solar wind gas. Although the velocity and density are approximately anticorrelated, anomalous density pileup is frequently observed in association with the leading edge of the stream, presumably because of a "snowplow" effect as high-velocity plasma overtakes the slower ambient gas. Of particular significance is the east-west shift in the azimuthal component of the solar wind flow direction across the positive gradient in bulk velocity associated with the leading edge of the stream. This azimuthal shift in flow direction is consistent with that expected for the azimuthal stresses set up along the average Archimedian spiral of the interplanetary field, the latter presumably defining the interaction geometry between the high velocity plasma stream and the ambient gas. Note that the westward flow shifts at the positive velocity gradients are



**Figure 5.** Explorer 33 3-hr averages of azimuthal flow direction, latitude flow direction, thermal speed, proton density and bulk velocity versus time.

usually of higher amplitude (in angle) than the eastward flow shifts. There also seems to be a frequent tendency for slight eastward flow associated with the more gradual negative gradient in the velocity on the trailing edge of a stream.

### SOLAR WIND STREAMS AND MAGNETIC FIELD SECTOR STRUCTURE

Results from the IMP 1 satellite [Wilcox and Ness, 1965] indicated the presence of a definite pattern in the dominant polarity of the interplanetary magnetic field. This polarity pattern or sector structure was fairly repetitive over approximately 3 solar rotations observed by the IMP 1 flight. These results are shown in figure 6 where 3-hr averages of the interplanetary magnetic field are plotted starting on November 27, 1963, with the plus symbols representing field lines predominantly outward from the sun and the negative symbols representing field lines predominantly inward toward the sun. The Archimedean spiral lines represent the best-fit sector boundaries separating the different field polarities. The only gross exception to the repeating pattern appears to be the early polarity reversal associated with a geomagnetic storm commencing on December 2, 1963. At the time, Wilcox and Ness [1965] attributed this early

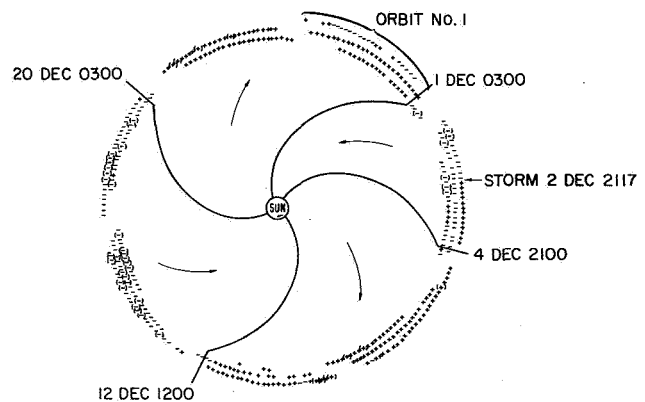


**Figure 6.** IMP 1 interplanetary magnetic field sector structure for approximately three solar rotations starting late November 1963. The pluses represent fields predominantly away from the sun and minuses predominantly toward the sun.

polarity reversal to a higher than expected solar wind velocity associated with the storm.

The obvious next question concerns the relationship between the interplanetary magnetic field sector structure and the high velocity solar wind stream pattern.

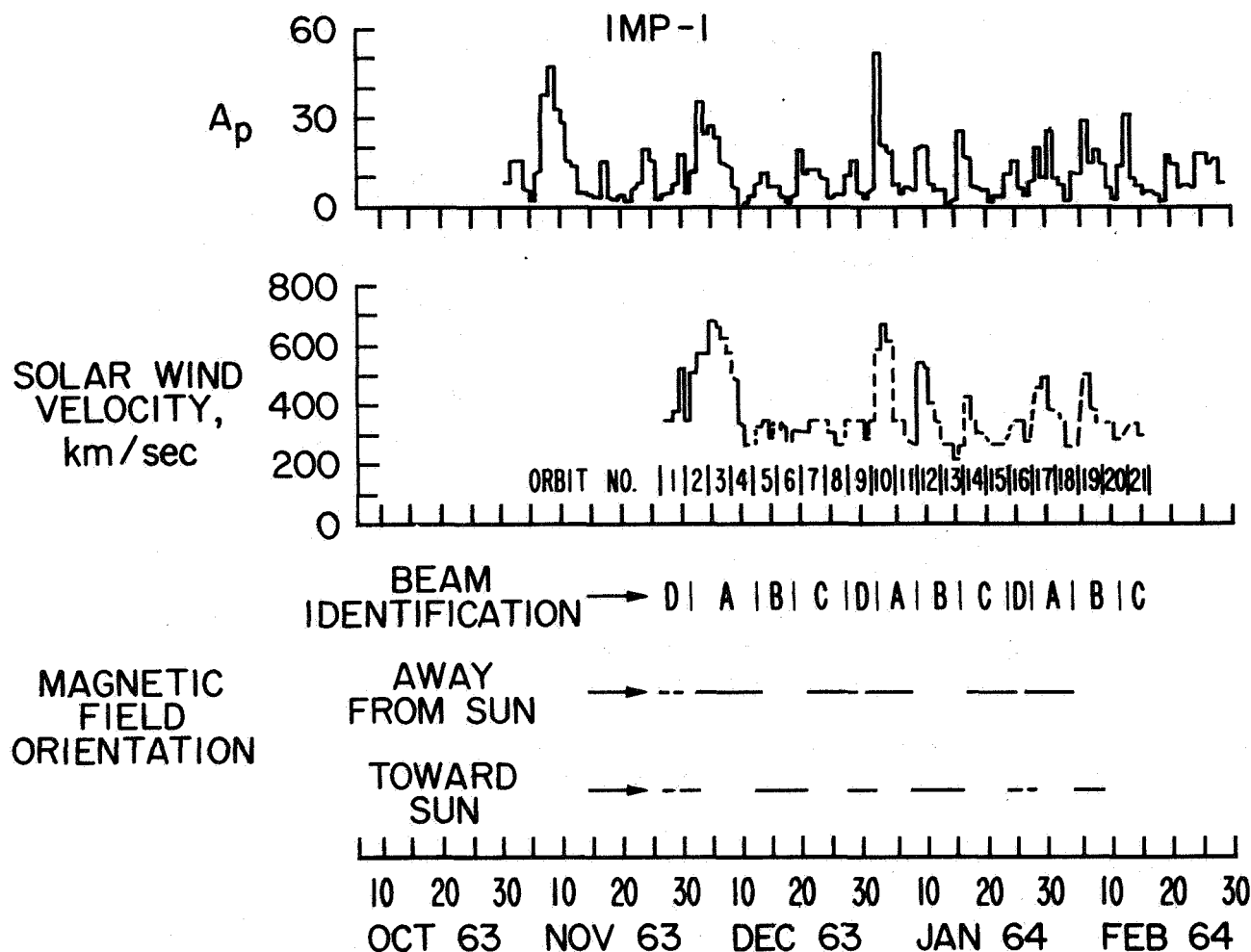


**Figure 7.** Comparison of the IMP 1 solar wind velocity and magnetic field orientation with the  $A_p$  index.

Twenty-four hour average values of the solar wind velocity obtained from the Ames Research Center plasma probe on IMP 1 are shown in figure 7. The dominant orientation of the interplanetary magnetic field is also shown together with the geomagnetic disturbance index  $A_p$ . The recurring solar wind streams are identified by letter. The most striking feature is the almost one-for-one correspondence between the solar wind stream pattern and the magnetic field sector structure. Note that the field changes its dominant polarity near the beginning of each stream and that the width of any given stream and corresponding sector are almost identical. If the solar wind streams define the magnetic sector structure, the earlier than expected polarity reversal on December 2, 1963, can be explained in terms of a change in the solar wind stream width on the successive

solar rotation rather than a change in velocity as discussed previously. This can be seen in figure 7, where the stream identified as A has decreased in width by 2 to 3 days between its first observed occurrence to its recurrence on the next solar rotation, whereas the peak velocity has remained near 700 km/sec. It is interesting to note that although the  $A_p$  index in general follows the solar wind stream structure, the peak velocity frequently tends to lag the peak in  $A_p$  by as much as a day.

Using the method of superposed epoch analysis, Wilcox and Ness [1965] compare the interplanetary magnetic field sectors observed by IMP 1 with preliminary MIT plasma data. The results for solar wind velocity are shown in figure 8 where the ordinate is a 3-hr average value of the solar wind velocity and the abscissa is the position within the four large sectors previously

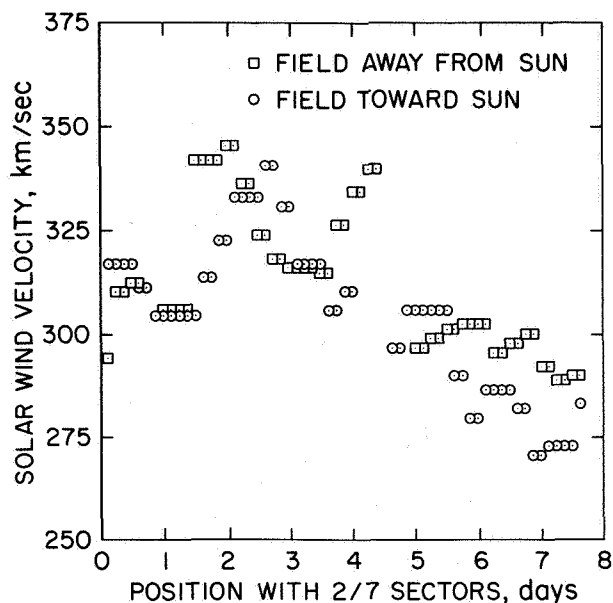


**Figure 8.** Superposed epoch analysis of the magnitude of the solar wind velocity as a function of position within the 2/7 sectors shown in figure 6.

shown in figure 6. Note that both "toward" and "away" sectors are used. It can be seen that the velocity tends to reach a maximum on the order of one fourth to one third of the way through the sector. The second peak near 4 days for the "away" sectors is considered to be an

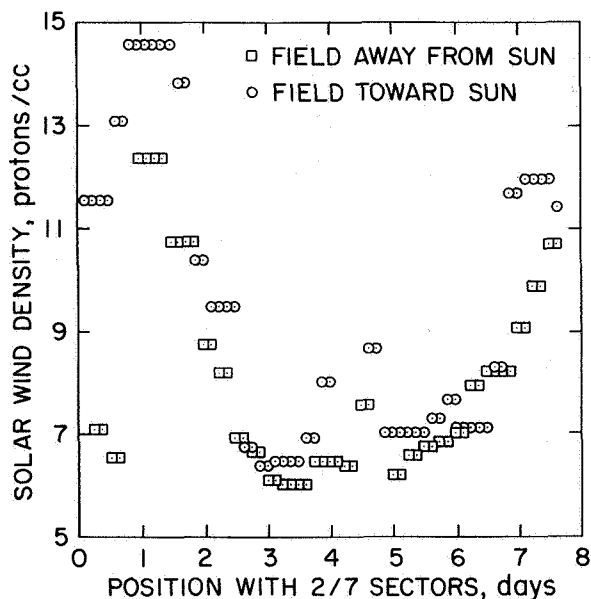


**Figure 9.** Superposed epoch analysis of the solar wind density as a function of position within the 2/7 sectors.

artificial feature related to the perigee passage of the spacecraft near the middle of these "away" sectors. The same analysis was performed for the solar wind density (fig. 9). The density is observed to rise to a maximum value at about one day after the sector beginning, decrease to a minimum near the center, and then rise again at the end of the sector. Note by comparison with figure 8 that the large peak in density at the beginning of the sector coincides with the positive gradient in the velocity, which in turn is associated with the beginning of a new solar wind stream.

Figure 10 shows the sector pattern of the interplanetary magnetic field, as given by Wilcox and Colburn [1969], covering the period from the flight of Mariner 2 in 1962 through Explorer 35 in mid-1968. The sector structure is shown overlaying the daily geomagnetic character index  $C_9$  with light shading indicating sectors with fields predominantly away from the sun and dark shading for sectors with fields predominantly toward the sun. The diagonal bar indicates an interpolated quasistationary structure during 1964. Although it might be argued that the 1964 interpolations could be misleading, it is certainly clear that the sector structure was much more repetitive from one solar rotation to the next up through the IMP 2 flight as compared to after that time. The period from 1965 through mid-1967 is particularly chaotic with no discernible repeating pattern. This period occurred during the steeply rising portion of the present solar cycle (cycle 20) as compared to near solar minimum for the time of the IMP 1 flight. Note that the sector pattern becomes somewhat more regular in 1968 near solar maximum.

The relationship between the solar wind stream structure and the more chaotic interplanetary magnetic field sector pattern associated with the steeply rising portion of the solar cycle is illustrated in figure 11. The solar wind data are taken from Pioneer 6 [Wolfe, 1970] and 24-hr average values of the proton temperature (fitted to an isotropic Maxwellian distribution), number density and velocity have been plotted together with the geomagnetic disturbance index  $A_p$ . The data are shown for slightly more than one solar rotation beginning December 18, 1965. The bar graph at the top gives the interplanetary magnetic field sector structure with the extent of the away ( $A$ ) and toward ( $T$ ) sectors as shown. The vertical lines designate the sector boundaries. As was the case for the IMP 1 results discussed earlier, the sector boundaries appear to be associated with the beginning of new solar wind streams. Here, however, more than one stream is observed to appear within a given magnetic sector. The sector commencing on December 25, 1965, for example, is "classic" in that it is quite similar to that

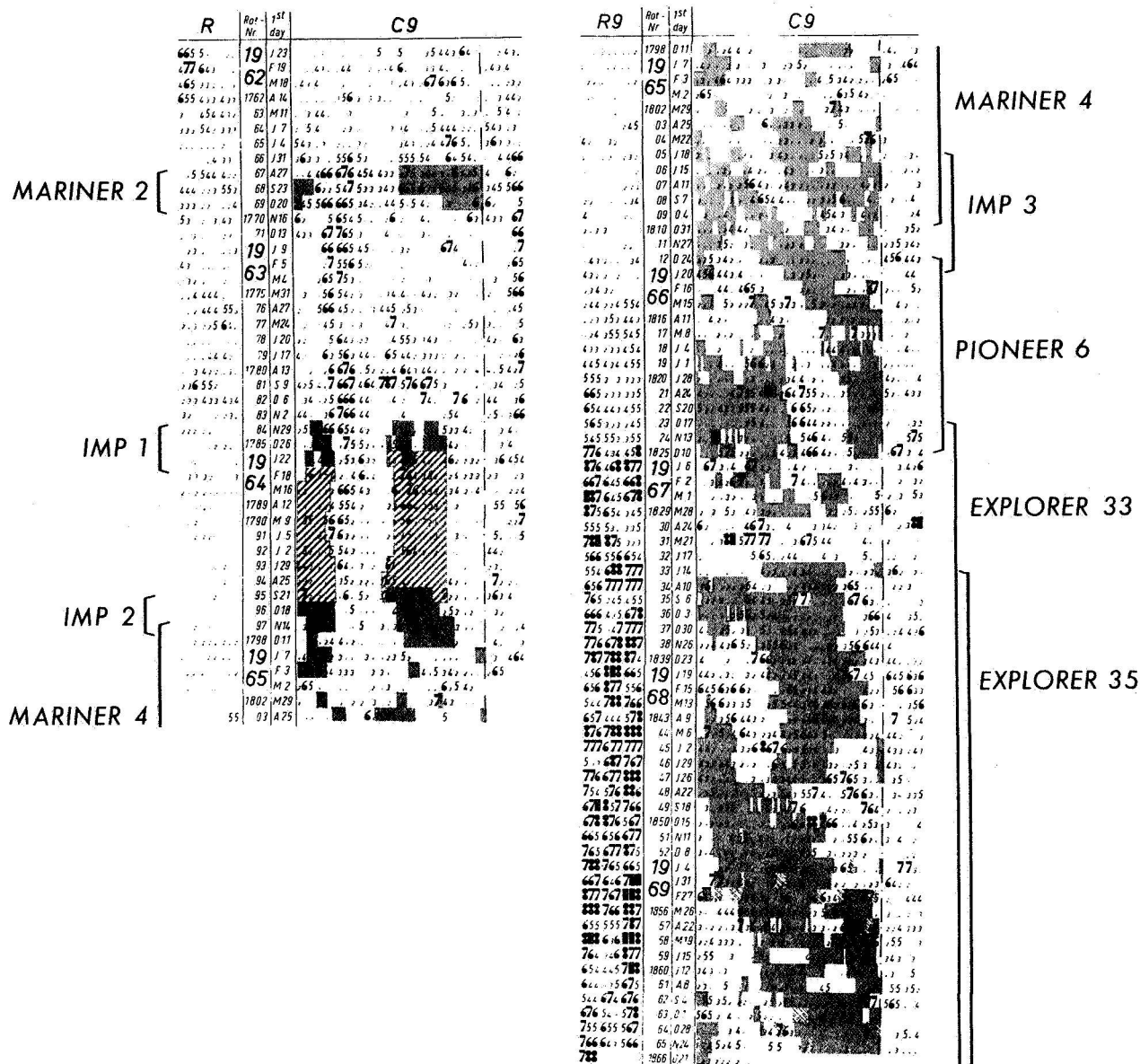


**Figure 10.** Observed sector structure of the interplanetary magnetic field overlaying the daily geomagnetic character index C9. Light shading indicates sectors with field predominantly away from the sun and dark shading indicates sectors with field predominantly toward the sun.

observed by IMP 1 in late 1963. The velocity is observed to peak approximately one-third of the way through the sector with the density high at the extremes of the sector and at a minimum near the center. In addition, the temperature is seen to peak early in the sector and then descend throughout the remainder of the sector. By contrast, the wide sector beginning January 2, 1966, is seen to contain two distinct solar wind streams. Note, however, that when the sector boundaries do occur, they

appear near the beginning of a new solar wind stream.

Another interesting feature of the data is the nature of the solar wind streams themselves and their relationship to geomagnetic activity. Although there is general correlation of temperature and anticorrelation of density with velocity, anomalously high densities and temperatures are observed in association with the positive gradients in velocity that define the leading edge of a solar wind stream. With respect to geomagnetic activity, the

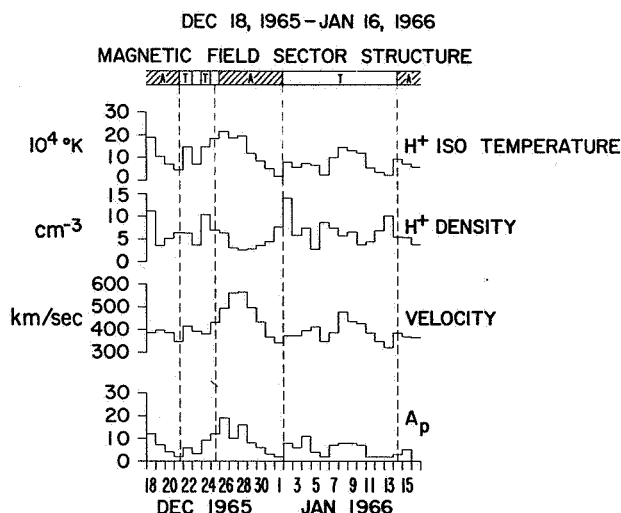


**Figure 11.** Pioneer 6 24-hr average values of the solar wind velocity, proton density and temperature plotted versus time. The interplanetary magnetic field sector structure is shown at the top.

maximum in velocity tends to lag and the density tends to lead the peaks in the  $A_p$  index whereas the temperature appears to be roughly in phase. For the set of data shown here, the correlation coefficient between temperature and  $A_p$  was a surprisingly high 0.88. Although not necessarily cause and effect, it seems apparent that the temperature might be a fairly reliable index of the state of disturbance in the solar wind, which in turn determines the level of geomagnetic activity.

A perhaps even more complex example of the relationship between the solar wind streams and the magnetic field sector structure is shown in figure 12. The plots are similar to the previous figure with the solar wind data taken from Pioneer 7 [Wolfe, 1970] and are shown for slightly more than one solar rotation beginning August 19, 1966. As was the case with Pioneer 6, more than one solar wind stream is observed within a given magnetic field sector. The sector with field predominantly toward the sun that ends on September 4, 1966, contains three distinct solar wind streams. Note again, however, that when the sector boundaries do occur they appear near the beginning of a new solar wind stream. An exception to this appears to be the September 4, 1966, sector boundary. Investigation of the detailed data [Wolfe, 1970] shows, however, that the solar wind stream beginning at this time was somewhat anomalous with a 6-hr "spike" in velocity to values over 530 km/sec associated with this sector boundary. This short-period velocity increase has been washed out in the averaging process in

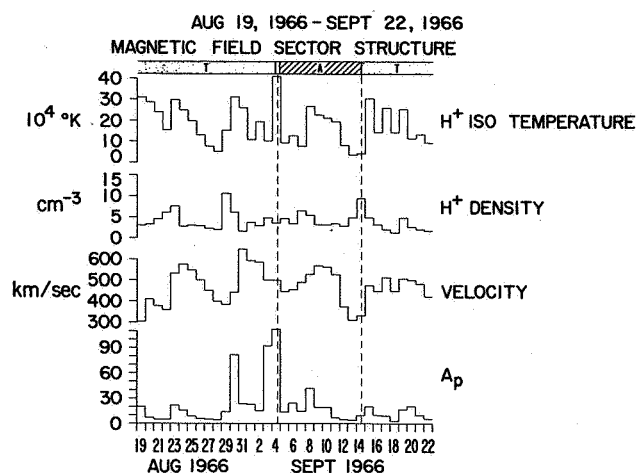


**Figure 12.** Pioneer 7 24-hr average values of the solar wind velocity, proton density and temperature versus time. The interplanetary magnetic field sector structure is shown at the top.

figure 12. The peak in geomagnetic activity on August 30, 1966 illustrates a striking example of the lag, lead and in phase relationship between respectively velocity, density and temperature and the  $A_p$  index.

The interplanetary investigations reported thus far clearly indicate an apparent dominance of the magnetic field sector structure by solar wind streaming. The solar wind high velocity streams are apparently the interplanetary manifestations (observed near 1 AU) of coronal temperature inhomogeneities. According to the classical Parker [1958] model, higher temperature regions in the corona would lead to higher interplanetary solar wind velocities. Due to the rotation of the sun, these higher velocity streams would be expected to interact with the lower velocity gas associated with the quiescent corona. Based on the observed interplanetary magnetic field and solar wind characteristics, it is postulated that an interaction region forms along the Archimedean spiral of the interplanetary magnetic field between the high velocity plasma and the lower velocity gas associated with the quiescent corona. For some hypothetical boundary, perhaps associated with the initial velocity increase at the leading edge of a new stream, the leading ambient gas would be accelerated with the loss of kinetic energy (and therefore velocity) for the higher velocity driving gas, giving rise to the observed asymmetry in the stream velocity profile. Because of the essentially infinite conductivity of the medium, the streams cannot penetrate one another, and the plasma density increases forward of

this hypothetical boundary in a "snowplow" effect. The observed east-west shift in the solar wind azimuthal flow direction is then simply the reaction of the gas to the tangential stresses set up at the interaction boundary. It is quite likely that waves are generated at this boundary that propagate both upstream and downstream in the moving frame of reference of the gas, giving rise to plasma heating throughout the entire interaction region. Since the interaction region is likely to be the most disturbed, it follows that geomagnetic disturbance indices should correlate with interplanetary solar wind ion temperatures. Since the interaction boundary separates different plasma regimes, the change in the dominant interplanetary magnetic field polarity might be expected to most likely occur at this boundary. Finally, the occurrence of more than one solar wind stream in a given magnetic field sector may be simply due to the greater frequency of coronal temperature inhomogeneities and wider magnetic field sectors associated with increased solar activity as compared to the state of the corona closer to solar minimum.

#### LONG-TERM VARIATIONS

We now consider the long-term variations of solar wind characteristics over many solar rotations during the entire period of solar wind observations from 1962 to the present. Figure 13 shows the solar wind velocities and temperatures averaged over each solar rotation as observed by the Vela 2 satellites [Strong *et al.*, 1967] from July 1964 to July 1965. The last value in the velocity averages was taken from the Vela 3 satellite. This time interval included a solar minimum in October 1964, during solar rotation number 1795. Perhaps the most interesting feature of the data is the great variability of the solar wind parameters over the one year period. The 27-day averages of the solar wind velocity range from

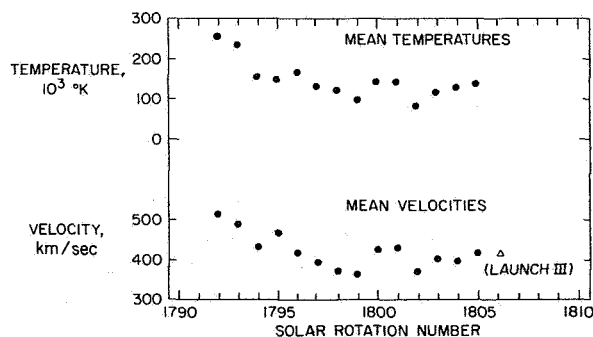


**Figure 13.** Solar wind flow speed and proton temperature averaged over solar rotations as measured on the Vela 2 satellites from July 1964 to July 1965.

slightly over 500 km/sec for rotation number 1792 to approximately 360 km/sec for rotation number 1799 for an overall variation of roughly 140 percent. Similarly, the temperature ranges from approximately  $2.6 \times 10^5$  °K for rotation number 1792 to about  $9 \times 10^4$  °K for rotation number 1802 for an overall variation of almost a factor of 3. It is enticing to speculate that the decline in temperature and velocity from rotation 1792 to 1799 is associated with the decline in solar activity. It should be pointed out, however, that the actual minimum in the sunspot number occurred during rotation number 1795 (October 1964), and the geomagnetic activity in July 1964 and October 1964 was about the same. As will be seen later, the total range in solar wind parameters observed here is not significantly different from that observed throughout the entire portion of the solar cycle observed to date.

The variations in the azimuthal flow direction of the solar wind observed by Vela 2 [Strong *et al.*, 1967] over the same time interval is shown in figure 14. The angles have been averaged over each successive solar rotation with the area of each circle representing the statistical weight for each value. The last value was taken from the Vela 3 satellite as indicated. As was the case for velocity and temperature, great variability in the azimuthal flow direction is observed throughout the one-year period. The values of the average azimuthal flow direction range from a minimum of approximately  $-0.5^\circ$  for rotation number 1793 to a maximum of approximately  $-3.5^\circ$  for

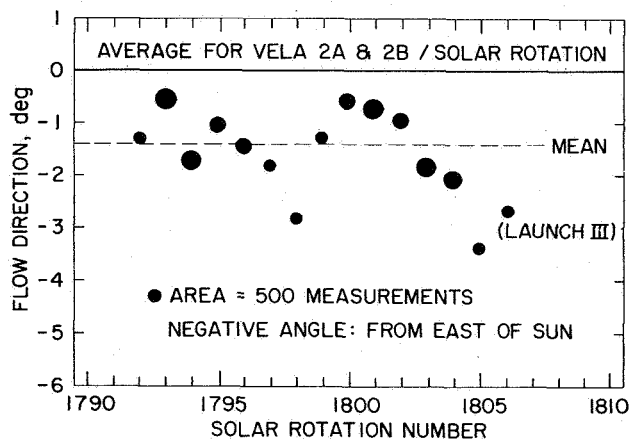


**Figure 14.** Solar wind flow directions averaged over solar rotations as measured by the Vela 2 satellites from July 1964 to July 1965.



rotation number 1805. The overall mean value, indicated by the dashed line, was approximately  $-1.4^\circ$  indicating a mean azimuthal velocity component of about 10 km/sec. Note that negative angles refer to flow directions from east of the sun.

Using the interplanetary magnetic sector structure results from a variety of satellites and deep space probes, *Wilcox and Colburn* [1970] have reported the variation in the synodic rotation period of the interplanetary field from 1963 to 1968. The synodic period is plotted in figure 15 with the smoothed sunspot numbers for the present solar cycle and the mean of cycles 1 through 19. Note that synodic period varies from near 27.0 days close to solar minimum up to 28.0 days at the beginning of the solar cycle and then gradually declines back to 27.0 days at solar maximum. *Wilcox and Colburn* [1970] postulate that the increase from 27.0 to 28.0 days represents the dominance of the interplanetary field by the high solar latitude spot groups associated with the beginning of the solar cycle. The decline in synodic rotation period thereafter is the result of the decrease in latitude of the spot groups as the solar cycle progresses. One might expect then that the synodic period would remain near 27.0 days throughout the remainder of the present solar cycle and not increase until the beginning of the next cycle.

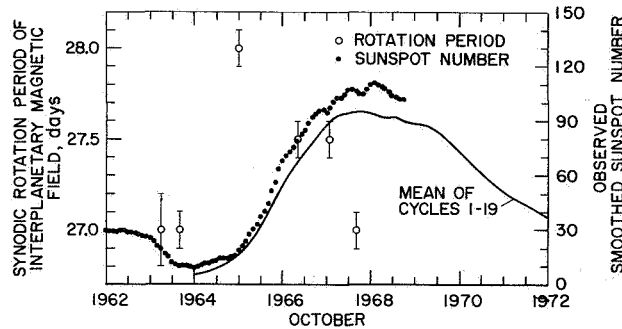


**Figure 15.** Synodic rotation period of the interplanetary magnetic field superimposed on the observed smoothed sunspot number from October 1962 to October 1972.

Table 1 shows selected solar wind parameters reported from the time of Mariner 2 to the present. With respect to the sunspot cycle recalled in figure 15, it is seen that the Mariner 2 observations were obtained during the waning portion of the previous cycle; IMP 2 and Vela 2 observations near solar minimum; Vela 3, Pioneer 6, and Pioneer 7 during the steeply rising portion of the present cycle; Explorer 34 near solar maximum; and finally HEOS 1 slightly past solar maximum. Since the time

**Table 1.** Average and most probable values of the various solar wind parameters from all reported spacecraft measurements

Spacecraft	Institution	$V_{mp}$ km/sec	$V_{AV}$ km/sec	$N_{mp}$ cm $^{-3}$	$N_{AV}$ cm $^{-3}$	$T_{mp}$ 10 $^5$ °K	$T_{AV}$ 10 $^5$ °K	$\phi$ deg	$\theta$ deg	Approximate date
Mariner 2	JPL		504		5.4		1.5 - 1.8			9/62 12/62
IMP 1	MIT	330	360	4	7			+1.5		12/63 2/64
IMP 1	ARC		378							12/63 2/64
Vela 2	LASL	325	420			$\sim 0.5$	1.4	-1.4		7/64 7/65
Vela 3	LASL	$\sim 350$	400	$\sim 4$	7.7	$\sim 0.4$	0.91	-2.5		7/65 7/67
Pioneer 6	MIT		430		6	0.38		-0.9		12/65 2/66
Pioneer 6	ARC	$\sim 340$	422	$\sim 3.2$	5.7	$\sim 0.4$	1.0	+3.0	+0.56	12/65 2/66
Pioneer 7	MIT		460		6	0.66				8/66-10/66
Pioneer 7	ARC		455	$\sim 2.4$	4.4	$\sim 0.5$	1.6	+0.3	+0.34	8/66-10/66
Explorer 34	GSFC	$\sim 390$	438			0.46				6/67-12/67
HEOS 1	ROME	$\sim 390$	409	$\sim 2$	4.3		0.66			12/68-1/70

distributions of velocity, density, and temperature are nongaussian and highly skewed, both the most probable and the average values of these parameters are given in table 1. In addition, the average values (where available) of the components of the flow direction are also given. Here  $\phi$  is the azimuthal component with positive values for flow from west of the sun and  $\theta$  is the polar component of the flow with positive values for flow from north of the sun. The most surprising feature of the data is the absence of any definite trend in any of the parameters with respect to the solar cycle. One is tempted to visualize an increase in the average velocity from the time of IMP 1 near solar minimum up through Pioneer 7 during the rising portion of the cycle and then a decline up through solar maximum. Unless there is a significant increase in velocity with declining solar activity (which seems unlikely), the Mariner 2 velocity average is anomalously high. In addition, the Vela 3 velocity average, which includes the entire rising portion of the solar cycle, is anomalously low compared to the Pioneer 6 and Pioneer 7 averages, which were obtained within the time period of the Vela 3 observations. In addition, the Vela 3 averages are anomalously low with respect to the Vela 2 results, which were obtained at solar minimum.

With the possible exception of the angle  $\phi$ , which is highly susceptible to systematic error, it is hypothesized that the lack of any discernible trend in the various solar wind parameters is primarily due to a sample aliasing problem. It is intended here to consider sample aliasing in a very long term sense. For example, in recalling figure 13, the range in the solar wind velocity averages per solar rotation obtained by Vela 2 for the year period including solar minimum is approximately the same as

the range in averages reported by all spacecraft observations for the better part of an entire solar cycle. This surprising result clearly indicates that any effects on the solar wind parameters due to the solar cycle must indeed be subtle compared to the variations observed from one solar rotation to the next regardless of the time of observations within the entire solar cycle. The inevitable conclusion is that the effects of the solar cycle can only be unfolded through continuous monitoring of the interplanetary medium throughout a complete solar cycle.

### AVERAGE PROPERTIES

The average properties of the various solar wind parameters are best considered from the point of view of their frequency distributions. Figures 16 through 21 show histograms of solar wind velocity obtained from 7 separate spacecraft observations. Figure 16 was obtained from IMP 1 [Olbert, 1968] and covers the time period from December 1963 to February 1964. The velocities shown are 3-hr averages with each bar representing a 20 km/sec velocity interval. Here the most probable velocity was approximately 330 km/sec and the average velocity was 360 km/sec. The velocity histogram shown in figure 17 was obtained from the Vela 2 satellites [Strong *et al.*, 1967] and covers the one-year interval from July 1964 to July 1965. Individual cases have been included here in the velocity intervals shown. The location and widths of the velocity intervals were chosen to coincide with the energy acceptance windows of the Vela 2 plasma analyzers. For these observations, the most probable velocity was approximately 325 km/sec and the average velocity was 420 km/sec. Figure 18 shows the velocity histogram obtained from the Vela 3 measurements [Hundhausen *et al.*, 1970] obtained from July 1965 to November 1967. Here the individual cases are included in 25 km/sec intervals. The Vela 3 results indicate a most probable velocity of approximately 350 km/sec and an average velocity of 400 km/sec. Figure 19 gives the velocity distribution results from Pioneer 6 (lighter curve) from December 1965 to March 1966, and Pioneer 7 (darker curve) from August 1966 to October 1966 [Mihalov and Wolfe, 1971]. The velocities given are individual cases included in 10 km/sec intervals. For Pioneer 6 the most probable velocity was approximately 340 km/sec and the average velocity was 422 km/sec. For Pioneer 7 the most probable velocity was not determined and the average velocity was 455 km/sec. The velocity histogram for Explorer 34 [Burlaga and Ogilvie, 1970a] is shown in figure 20. The results were obtained

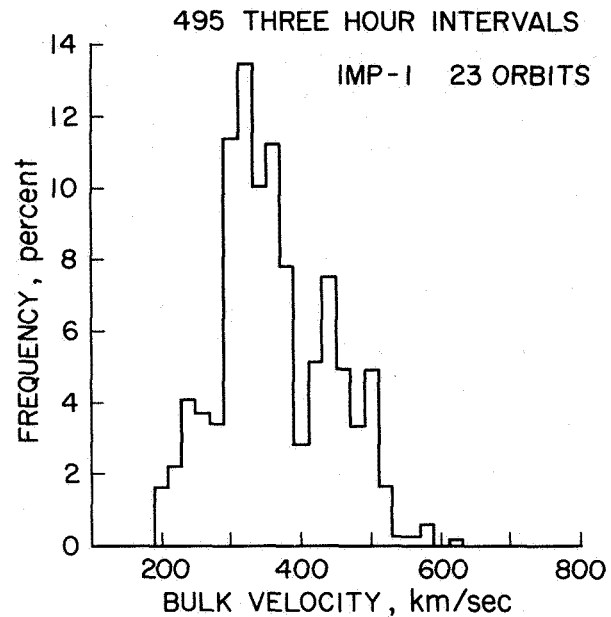


Figure 16. IMP 1 solar wind bulk velocity histogram.

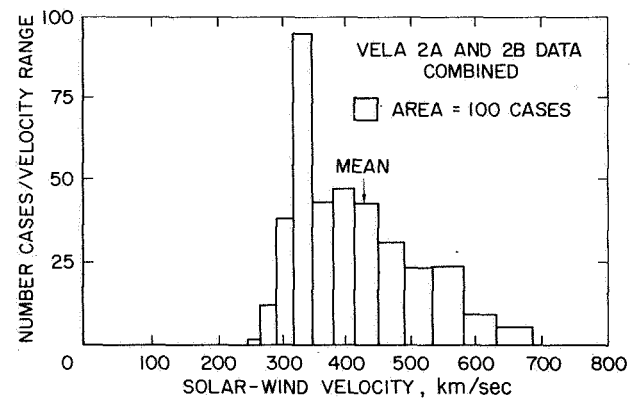


Figure 17. Vela 2 solar wind bulk velocity histogram.

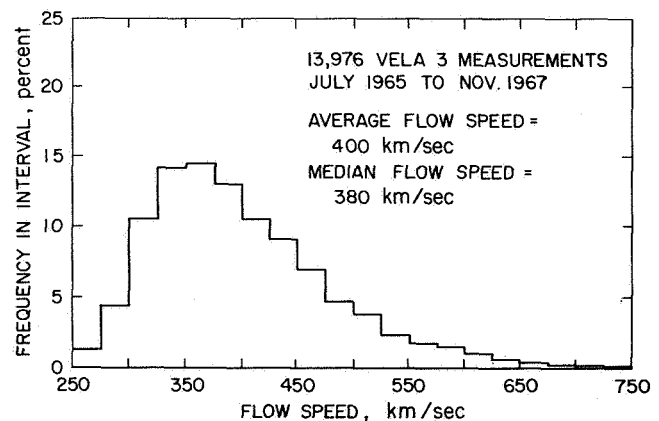


Figure 18. Vela 3 solar wind bulk velocity histogram.

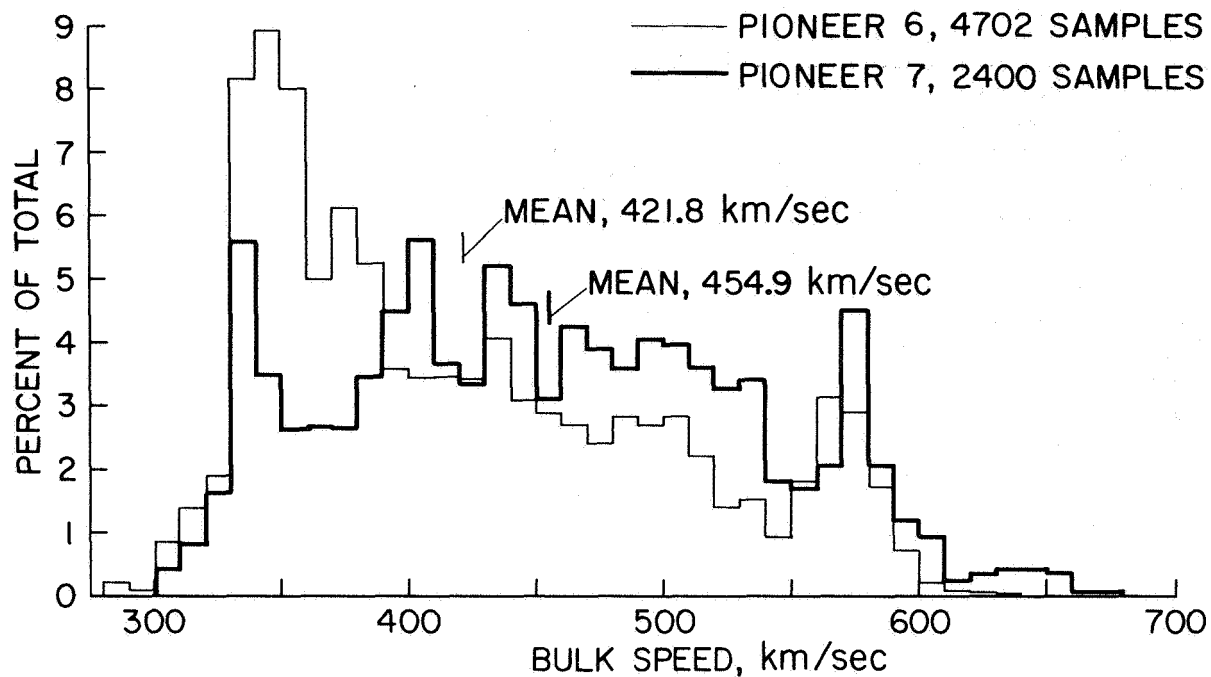


Figure 19. Pioneer 6 and Pioneer 7 solar wind bulk velocity histogram.

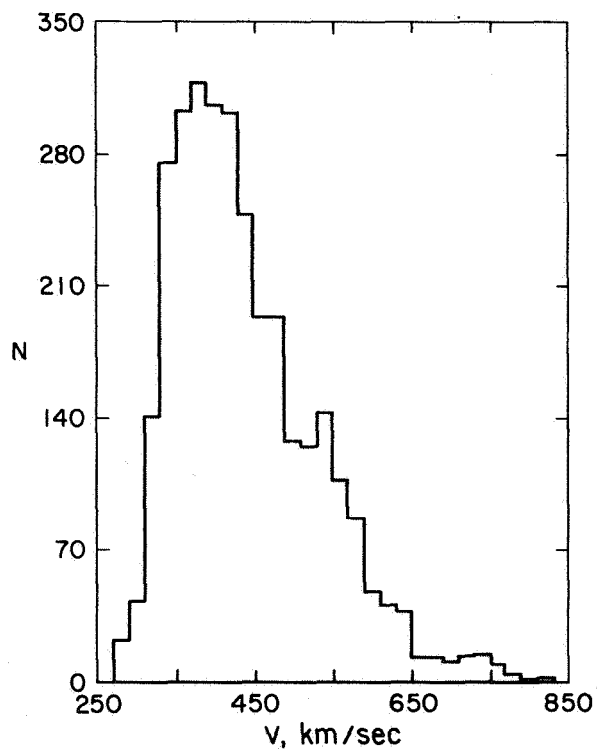


Figure 20. Explorer 34 solar wind bulk velocity histogram.

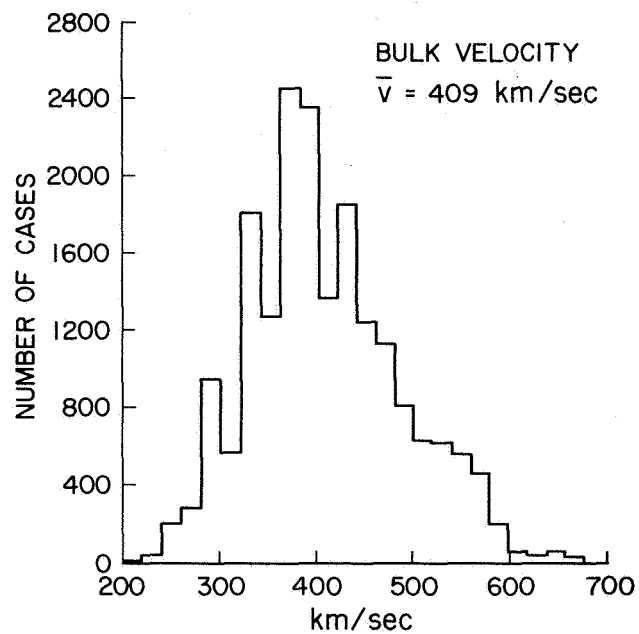


Figure 21. HEOS 1 solar wind bulk velocity histogram.

over the period from June to December 1967. The velocities given are 3-hr averages included in 20 km/sec velocity intervals. Here the most probable velocity was approximately 390 km/sec and the average velocity was 438 km/sec. The last velocity histogram (fig. 21), was obtained from HEOS 1 [Egidi *et al.*, 1970] from 2100 hours of observations in the period from December 1968 to April 1969 and from August 1969 to January 1970. Individual cases are shown in 20 km/sec velocity intervals. For the HEOS 1 results, the most probable velocity was 390 km/sec and the average velocity was 409 km/sec.

The most common feature among the various velocity histograms is the skew in the distributions out to a high velocity tail. This high velocity skewing evidently indicates that, in general, the solar wind exists in the more quiescent state between streams than at the high velocities associated with the peak of the streams themselves. Another contributing factor is the frequent observation of a much more gradual slope for the negative gradient of velocity associated with the trailing edge of the high velocity stream as compared to the steep slope at the leading edge. Comparison of the results of Pioneer 6 and Pioneer 7 in figure 19, for example, shows that the skew is much more pronounced for Pioneer 6. Although the statistics are not as good for the Pioneer 7 data, the detailed parameters (fig. 12) reveal a much higher frequency of streams during the observations of Pioneer 7 than that observed during the time of Pioneer 6 (see fig. 11).

Similar plots of the frequency distributions of the solar wind proton number density from five separate spacecraft observations are given in figures 22 through 25.

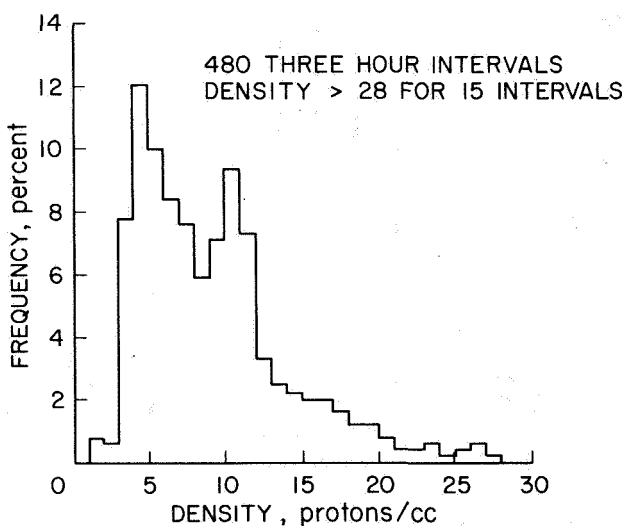


Figure 22. IMP 1 proton density histogram.

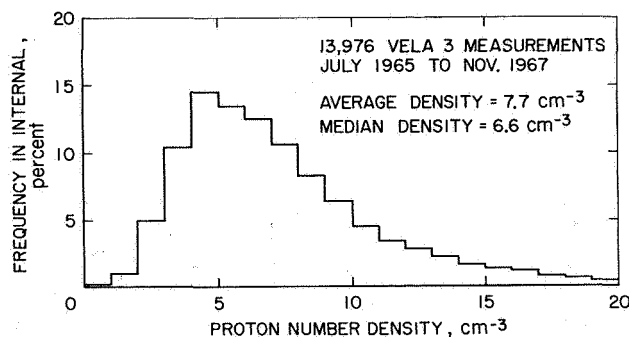


Figure 23. Vela 3 proton density histogram.

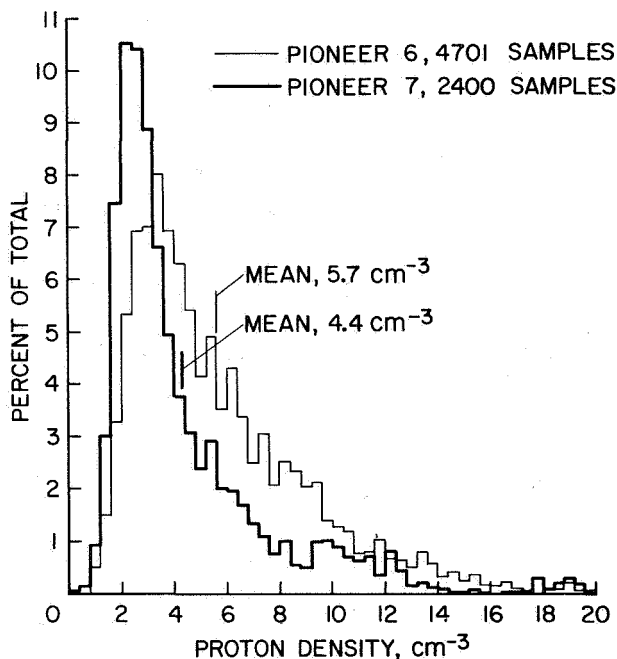


Figure 24. Pioneer 6 and Pioneer 7 proton density histogram.

The density histogram shown in figure 22 was obtained from IMP 1 observations [Olbert, 1968] from December 1963 to February 1964. The results shown are 3-hr average values of the density in 1 proton/cm<sup>3</sup> density intervals. For these data the most probable density was approximately 4 cm<sup>-3</sup> and the average density was 7 cm<sup>-3</sup>. Figure 23 gives the density histogram from the Vela 3 measurements [Hundhausen *et al.*, 1970]. Individual cases were used with a density interval of 1 proton/cm<sup>3</sup>. Here the most probable density was approximately 4 cm<sup>-3</sup> and the average density was 7.7 cm<sup>-3</sup>. The density histograms shown in figure 24 [Mihalov and Wolfe, 1971] were obtained from Pioneer 6 from December 1965 to February 1966 and from

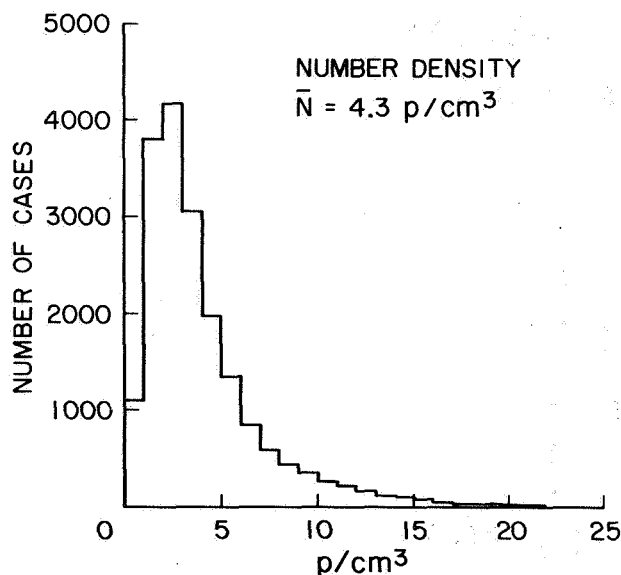


Figure 25. HEOS 1 proton density histogram.

Pioneer 7 from August to October 1966. Individual cases were used here with a density interval of  $0.4 \text{ proton/cm}^3$ . The most probable densities for the Pioneer 6 and Pioneer 7 observations were  $3.2$  and  $2.4 \text{ cm}^{-3}$ , respectively. The corresponding average densities were  $5.7$  and  $4.4 \text{ cm}^{-3}$ . The last density histogram, shown in figure 25, was obtained from the HEOS 1 observations [Egidi *et al.*, 1970] over two time intervals from December 1968 to April 1969 and from August 1969 to January 1970. Individual cases are used and the density interval was  $1 \text{ proton/cm}^3$ . From the HEOS 1 results the most probable density was approximately  $2 \text{ cm}^{-3}$  and the average density was  $4.3 \text{ cm}^{-3}$ .

As was the case for velocity, all the density histograms show a high degree of skewing. Note that the distributions of density all show a tail out to  $20 \text{ cm}^{-3}$  and beyond. The skewing to high values for both the velocity and density might at first be surprising since the velocity and density are expected to be roughly anticorrelated. Careful examination of the data, however, shows that a velocity-density anticorrelation is a gross oversimplification. For example, recalling the Pioneer 6 results shown in figure 11, it is noted that of the 30 days of data presented, only on four of those days did the 24-hr average values of the density exceed approximately  $8 \text{ cm}^{-3}$ . Assuming December 17-18, 1965, was a positive gradient in velocity, these high density averages were all associated with the density pileup region at the leading edge of the solar wind streams discussed earlier. Figure 11 indicates that most of the time outside the pileup regions the density varies between approximately 3 and

$6 \text{ cm}^{-3}$  regardless of velocity. The Pioneer 6 density histogram of figure 24 confirms this result.

Of the three convective properties of the solar wind—bulk speed, number density, and flow direction—the latter is the least well understood. This is probably due to the relatively small variations in the flow directions that one observes and the susceptibility of the measurements to systematic error. Historically, the solar wind flow direction has been considered in terms of its azimuthal and polar components in a solar-ecliptic coordinate system. The azimuthal angle is usually defined as the flow component that lies in the ecliptic and is measured with respect to the spacecraft-sun line. This definition of the azimuthal angle is convenient for most spacecraft since it readily allows the subtraction of the aberration of this angle due to the motion of the spacecraft around the sun. The polar angle is measured with respect to the spacecraft-sun line in the orthogonal plane containing the spacecraft, sun, and ecliptic poles. Figures 26 through 28 show the frequency distribution of the azimuthal component of flow from five separate spacecraft observations. For all histograms shown, negative angles represent flow from east of the sun, positive angles for flow from the west and aberration effects have been removed from all the data. For the case of the Vela 2 data shown in figure 26 [Strong *et al.*, 1967] and the Vela 3 data shown in figure 28 [Hundhausen *et al.*, 1970], the azimuthal angle is measured in the spin plane of the spacecraft, which were tilted with respect to the ecliptic on the order of  $30^\circ$ . The Pioneer data shown in figure 27 [Mihalov and Wolfe, 1971] is in the ecliptic, which coincides with the spin plane of all Pioneer spacecraft. The mean azimuthal flow angles from the Vela 2, Pioneer 6, Pioneer 7, Vela 3A, and Vela 3B measurements are  $-1.4^\circ$ ,  $+3.0^\circ$ ,  $+0.31^\circ$ ,  $-2.52^\circ$ , and  $-0.93^\circ$ , respectively. The  $+3.0^\circ$  value

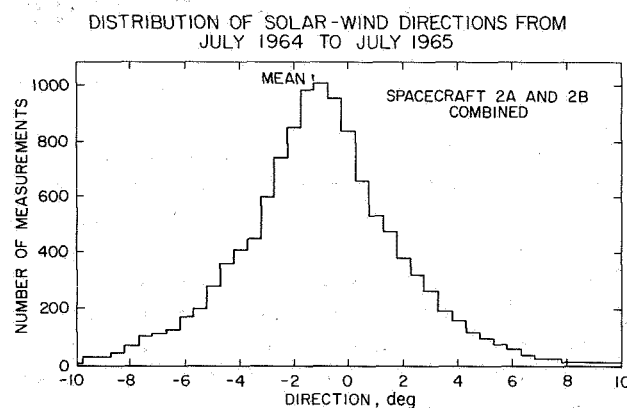


Figure 26. Vela 2 solar wind flow direction histogram.

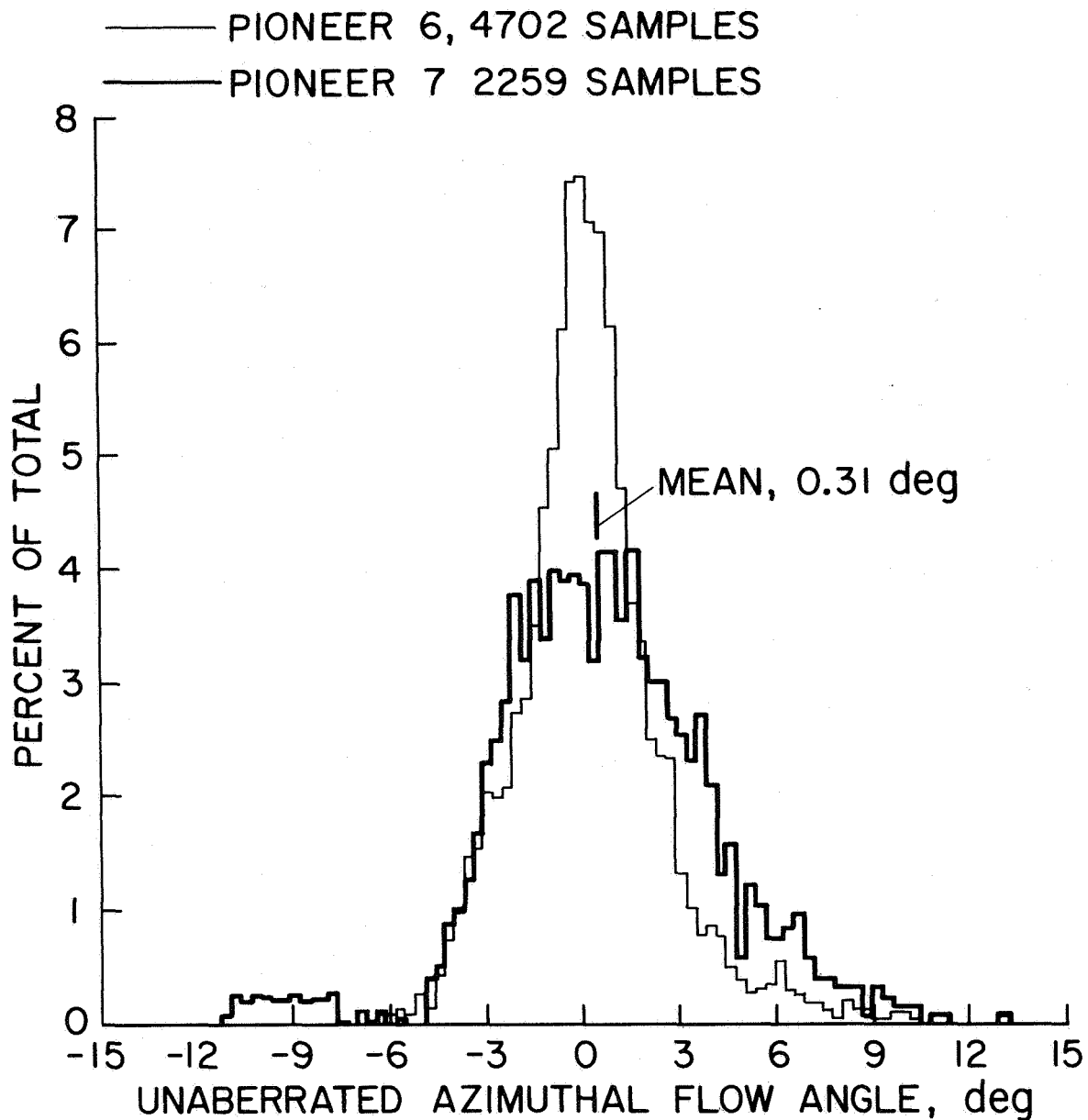


Figure 27. Pioneer 6 and Pioneer 7 azimuthal flow angle histograms.

obtained from Pioneer 6 was considered a possible systematic error and for comparative purposes was subtracted in the histogram in figure 27. The significant variance in the reported mean values of the azimuthal flow direction leads one to suspect systematic error problems. This is particularly supported by the  $1.6^\circ$  difference in the mean values reported by the Vela 3A and 3B observations, which were taken over the same time interval by presumably identically instrumented spacecraft. Long-term sample aliasing due to noncontinuous observations could also be a contributing factor. In any

event, subtle effects on the solar wind azimuthal flow direction due to solar angular momentum (expected to be only a fraction of a degree) must await more accurate measurements from continuously monitored spacecraft. One of the most interesting features of the azimuthal flow direction distributions is the tendency toward skewing in the direction of flow from west of the sun. Although the azimuthal flow histogram is much more symmetric than the velocity or density distributions, the slight skewing appears to be real. The skewing is particularly evident in the Pioneer and Vela 3 data. Although

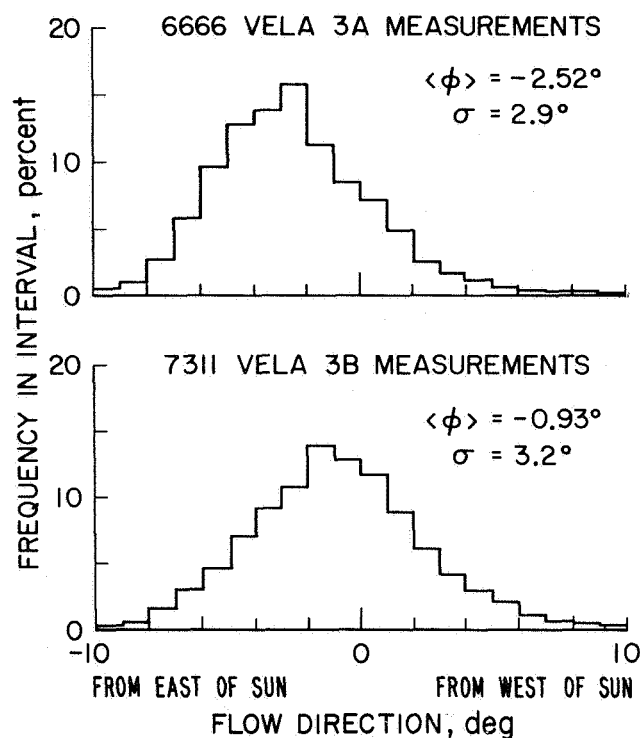


Figure 28. *Vela 3A and Vela 3B flow direction histograms.*

conceivably statistical, it is postulated that the skewness is due to the solar wind stream structure. Recalling the stream structure discussed previously, note that the flow from west of the sun, associated with the leading edge of the stream (positive gradient in velocity) was accompanied by high amplitude shifts in the flow direction from west of the sun whereas the negative gradients in velocity, which were associated with azimuthal flow shifts from east of the sun, were of much lower amplitude and much more gradual. This alone seems adequate in accounting for the skewness observed in the azimuthal flow histograms.

Figure 29 shows the distribution in flow direction from the polar component as observed by Pioneer 6 and Pioneer 7 [Mihalov and Wolfe, 1971]. The polar flow histograms are the most symmetric of any of the solar wind parameter distributions. The mean values are within experimental error of zero, indicating that the polar component of the solar wind flow is symmetric about the ecliptic. Note that the widths of the polar and azimuthal histograms (fig. 27) are comparable and lead to the conclusion that the stresses on the flow do not have any particular preferred orientations.

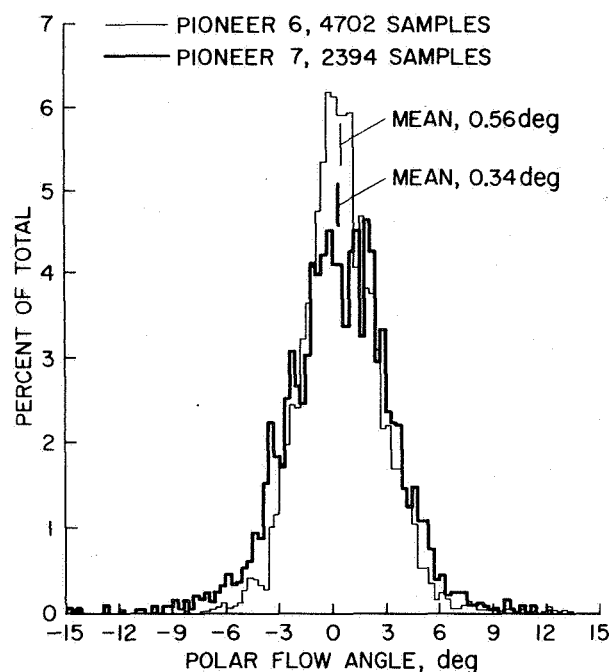


Figure 29. *Pioneer 6 and Pioneer 7 polar flow angle histograms.*

The distributions of the solar wind temperature as observed by six different spacecraft are illustrated in figures 30 through 34. The temperature histogram given in figure 30 was obtained from the Vela 2 results [Coon, 1968] from observations made between July 1964 and July 1965. The most probable and mean temperatures are as indicated. Note the skew in the temperature distribution out to approximately  $6 \times 10^5$  K. Figure 31

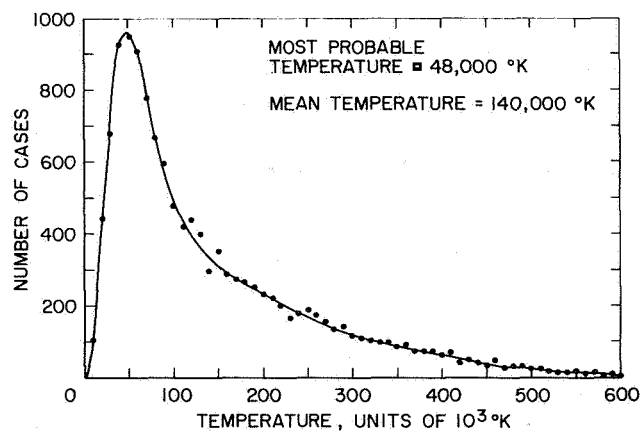


Figure 30. *Vela 2 solar wind proton temperature histogram.*

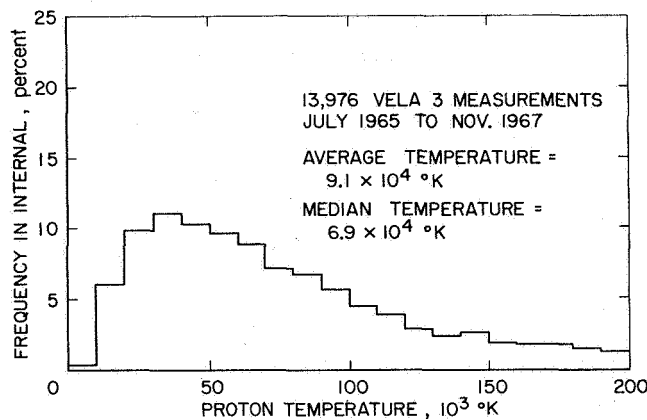


Figure 31. Vela 3 proton temperature histogram.

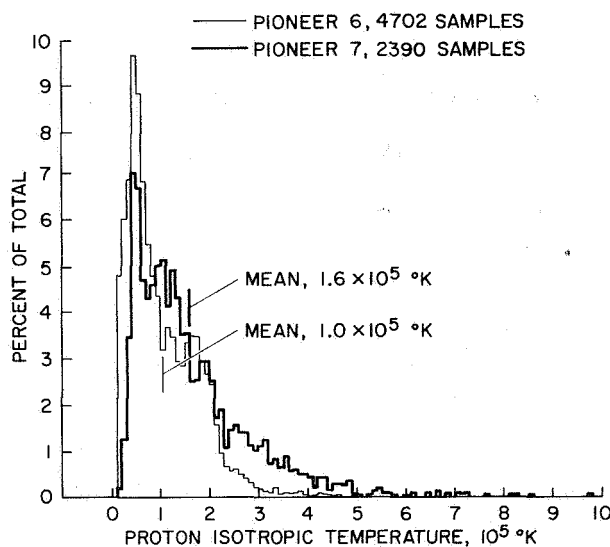


Figure 32. Pioneer 6 and Pioneer 7 proton temperature histograms.

shows the temperature distribution obtained from Vela 3 measurements [Hundhausen *et al.*, 1970] from July 1965 to November 1967. The histogram is plotted out to  $2 \times 10^5$  °K with 9 percent of the measured values greater than this temperature. The most probable temperature here is approximately  $4 \times 10^4$  °K and the average temperature is  $9.1 \times 10^4$  °K. Measurements obtained from Pioneer 6 from December 1965 to February 1966 and Pioneer 7 from August and September 1966 yielded the temperature histograms shown in figure 32 [Mihalov and Wolfe, 1971]. The mean temperatures for the two spacecraft are as indicated. The most probable temperatures for Pioneer 6 and Pioneer 7 were  $0.4 \times 10^5$  °K and  $0.3 \times 10^5$  °K, respectively. Note the tendency for greater skewing toward higher temperatures for the Pioneer 7

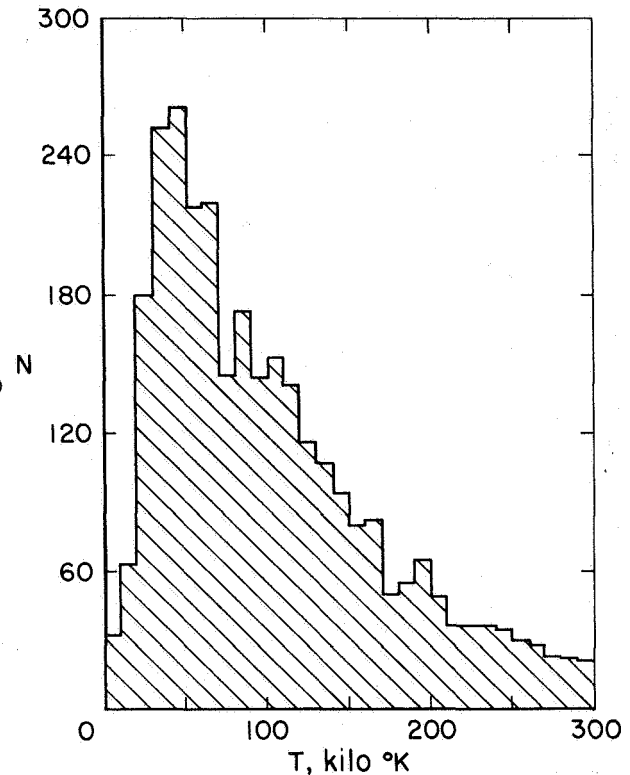


Figure 33. Explorer 34 proton temperature histogram.

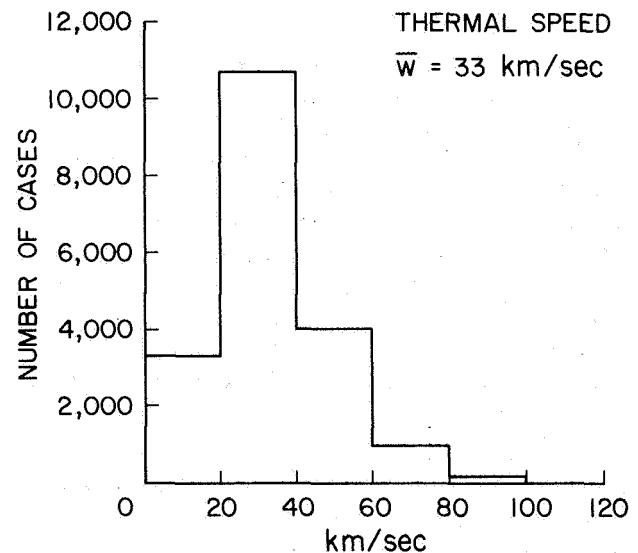


Figure 34. HEOS 1 proton thermal speed histogram.

results as compared to Pioneer 6. This evidently reflects the more highly disturbed character of the interplanetary medium and more complex solar wind stream structure at the time of the Pioneer 7 measurements.

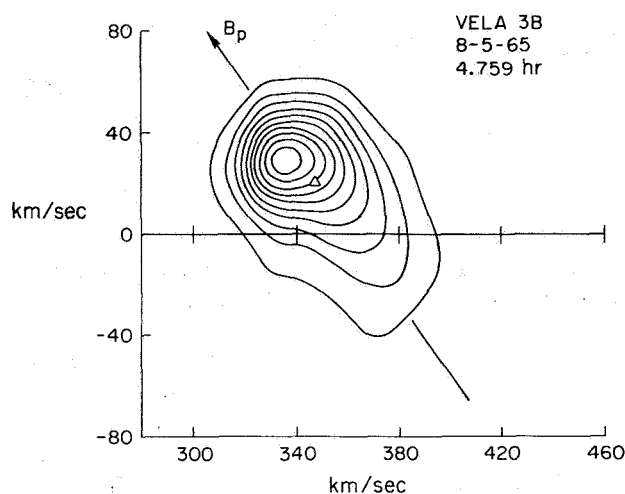


Figure 33 shows the temperature distribution obtained from Explorer 34 measurements [Burlaga and Ogilvie, 1970] taken from June to December 1967. The most probable temperature was approximately  $4.6 \times 10^4$  K. The average temperature was not reported but is estimated here to be near  $10^5$  K. The temperature distribution obtained from HEOS 1 measurements [Egidi et al., 1970] is shown in figure 34. These results were obtained from 2100 hr of observations during two time intervals from December 1968 to April 1969 and from August 1969 to January 1970. The average temperature is about  $6.6 \times 10^4$  K where the temperature  $T$  is related to the thermal speed  $W$ , by  $W = (2kT/m)^{1/2}$ . The most probable temperature is estimated here to be about  $5.5 \times 10^4$  K.

The most common feature of all of the temperature histograms is the large skewing in the distribution forming a long, high temperature tail. The temperature distributions are generally the most skewed of any solar wind parameter. It is interesting to note that although the average temperature varies by almost a factor of 3 among the various observations, the most probable temperatures are all comparable, near  $4\text{--}6 \times 10^4$  K. The above might be explained by differing degrees of complexity in the solar wind stream structure that were present during the various observations. A complex stream structure tends to elevate the high temperature tail leading to a higher average temperature. On the other hand, the solar wind resides a greater percentage of the time in the "between stream" state where the temperatures are lower and comparable regardless of the period of observation.

With the exception of the Vela 3 results, all the temperature histograms shown are plotted in terms of an isotropic temperature. The Vela 3 histogram is plotted using an effective temperature and will be discussed later. An isotropic temperature assumes that the random motions of the protons obey an isotropic maxwellian distribution law. Although valid to a first approximation, this assumption is not strictly true, as illustrated in figure 35 [Hundhausen et al., 1967], which shows contours of constant flux in a plane in velocity space from Vela 3B in August 1965. The contours are plotted in 10 percent increments decreasing outward from the maximum central contour. The abscissa is the velocity radially outward from the sun and the ordinate is the perpendicular velocity in the spin plane of the Vela 3B satellite. At the time of these measurements, the spin plane was tilted approximately  $35^\circ$  with respect to the ecliptic. The arrow represents the orientation of the interplanetary magnetic field projected onto the coordinate plane. The magnetic field orientation was determined by the Goddard Space Flight Center

magnetometer on IMP 3 for the period of the Vela 3B measurements. The triangle near the center of the distribution represents the bulk velocity, which for this case was 347 km/sec in the radial direction and 20 km/sec in the orthogonal direction. The distribution around the bulk velocity is due to the random motions of the protons, and deviations from a circular pattern centered above the bulk velocity are a result of anisotropy. The particular distribution shown in figure 35 is highly anisotropic with an elongated tail symmetric about the magnetic field projection and outward away from the sun.



**Figure 35.** A contour mapping in the Vela 3 spin plane of an example proton velocity distribution function. The small triangle indicates the mean velocity. The  $B_p$  indicates the magnetic field orientation of the time of the measurements.

Assuming the random motion in the distribution shown in figure 35 to be thermal, Hundhausen et al., [1967] derived the polar plot of temperature given in figure 36. The coordinates and magnetic field are as before. For this case, the maximum temperature seems to be near  $120^\circ$  and is approximately  $9.2 \times 10^4$  K. The minimum temperatures lie near the  $30^\circ$  and  $210^\circ$  radial lines. Defining the anisotropy as the ratio of the maximum to minimum temperatures gives, for this case, a value of about 3.4. Comparison of Vela 3 and IMP 3 data at other times seems to confirm that the anisotropy is, in general, aligned with the magnetic field but that the elongated tail is always outward from the sun regardless of the polarity of the field. This elongated tail in the temperature distribution outward from the sun was interpreted as an energy transport or heat conduction away from the sun and estimated to be on the order of  $10^{-5}$  ergs  $\text{cm}^{-2} \text{sec}^{-1}$ . This proton heat conduction is

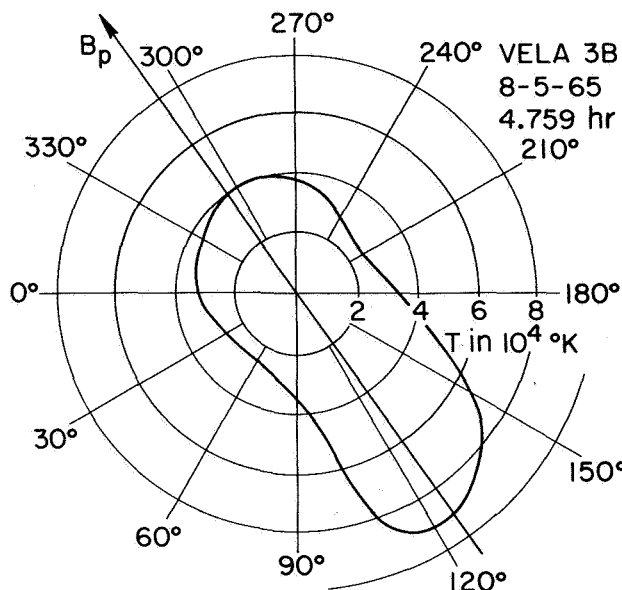


Figure 36. A polar graph of the temperature for the proton distribution function of figure 35.

small, however, compared to the electron heat conduction [Montgomery *et al.*, 1968], which is about three orders of magnitude larger.

The anisotropy value of 3.4 for the case discussed above is unusually high as shown in figure 37 [Hundhausen *et al.*, 1970]. This histogram was obtained from the Vela 3 measurements over the time period from July 1965 to November 1967. The most probable value of the anisotropy is between 1.2 and 1.3 and the average value is about 1.9. Note that only 9.6 percent of the determined anisotropy values are greater than 3.0. The anisotropy arises from simple conservation of the magnetic moment of the proton as the collisionless solar wind flows outward from the sun. Theoretical calculations, however, typically predict anisotropy values generally one to two orders of magnitude greater than those

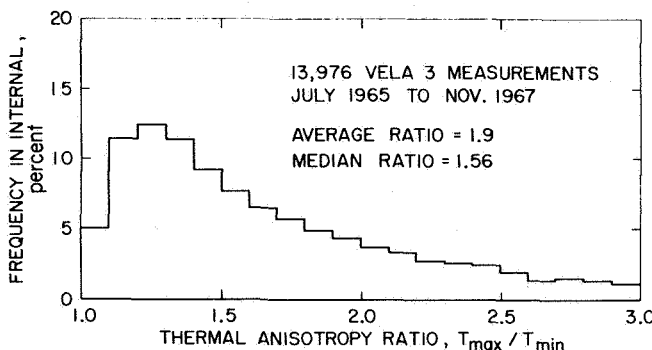


Figure 37. Vela 3 thermal anisotropy histogram.

observed. This clearly indicates that instabilities and wave-particle interactions must play an important role in inhibiting the growth of the anisotropy to such high values.

#### SOLAR WIND PARAMETER RELATIONSHIPS

Up to the present, only the temporal behavior and variance or frequency distribution of the individual solar wind parameters have been dealt with. Consider now a more detailed investigation of the relationships between various solar wind parameters. Figure 38 shows the solar wind proton density as a function of flow speed from measurements made by the Vela 3 satellites [Hundhausen *et al.*, 1970] during the period from July 1965 to November 1967. The density is plotted as the average within a 25 km/sec flow speed interval. For

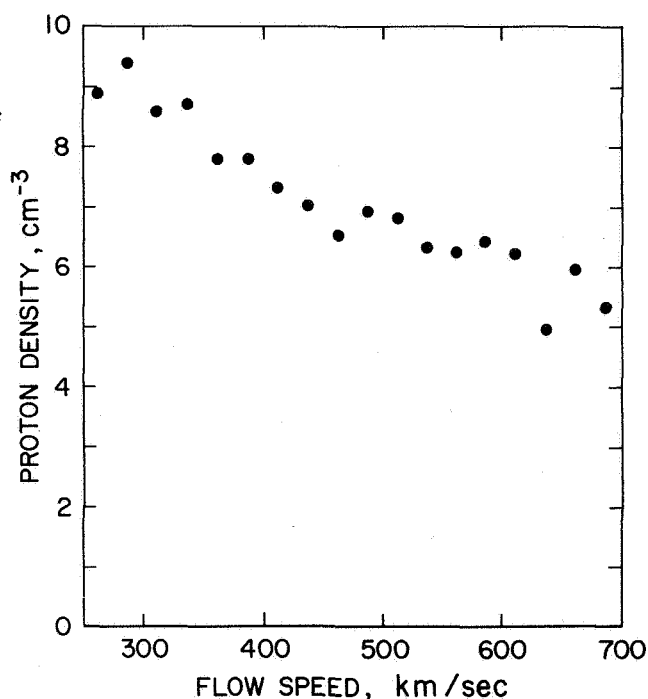


Figure 38. Vela 3 proton density versus solar wind flow speed.

these observations the density is observed to decrease with increasing velocity almost as  $V^{-1}$  (constant flux) up to about 500 km/sec, beyond which the density tends to level off. The relationship between density and velocity observed by the Ames Research Center plasma probe on Pioneer 6 from December 1965 to March 1966 is shown in figure 39. Here the results are presented somewhat differently than in the previous figure with each point representing a 24-hr average value of the proton density and velocity. These results suggest a

12/18/65 - 3/2/66

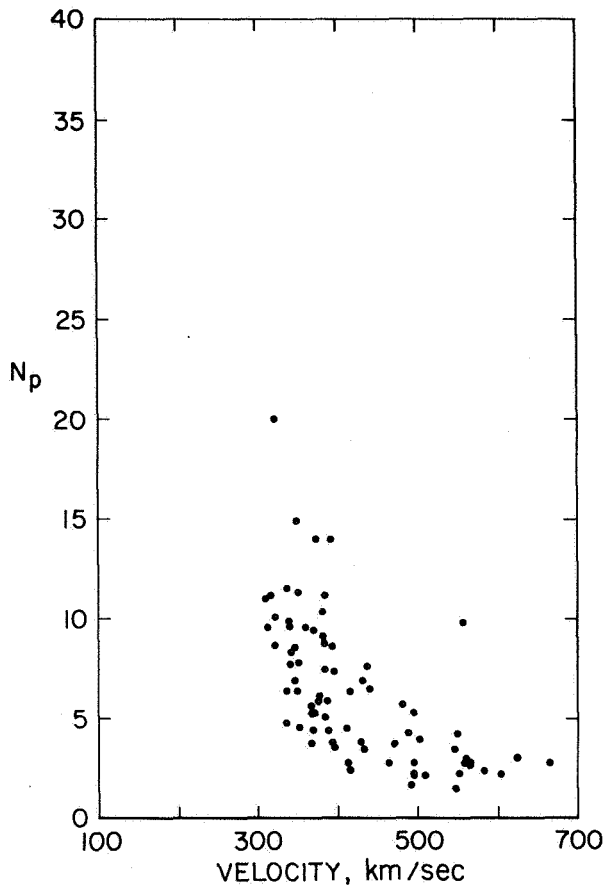


Figure 39. Pioneer 6 proton number density versus velocity.

much more exponential fall off of density with increasing velocity, particularly at the lower velocities. Note the large scatter in the density for low velocities. This can be accounted for by recalling that densities in the range of about  $4$  to  $7 \text{ cm}^{-3}$  are typical of the solar wind in the "between stream" state where the velocity is low. On the other hand, densities greater than  $7 \text{ cm}^{-3}$  are more typical of the "pileup" regions ahead of new streams where the velocity is also relatively low. The exponential character of the density-velocity relationship clearly indicates why the density and velocity frequency distributions both tend to peak at low values with skewing toward the higher values of both parameters. The density-velocity relationship obtained by Explorer 34 [Burlaga and Ogilvie, 1970b] and some average values obtained from several other spacecraft observations are given in figure 40. The Explorer 34 observations cover

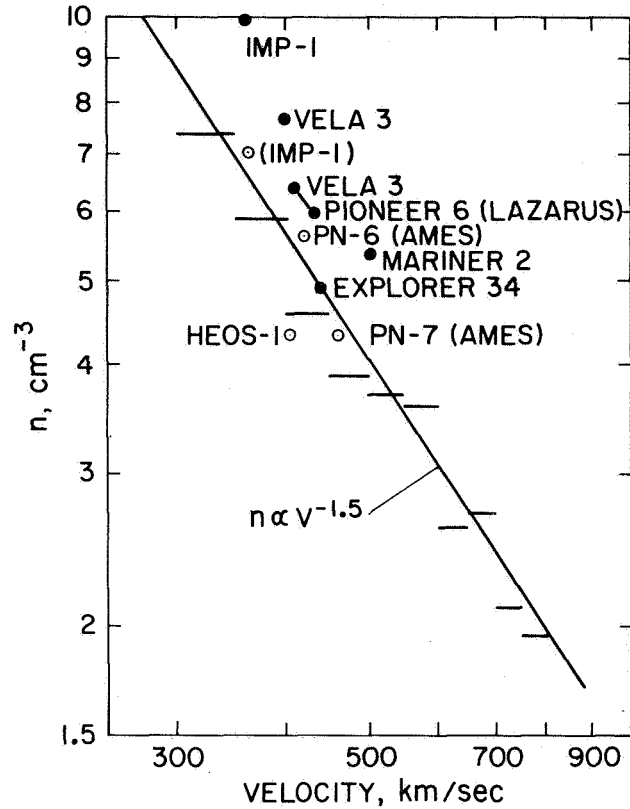
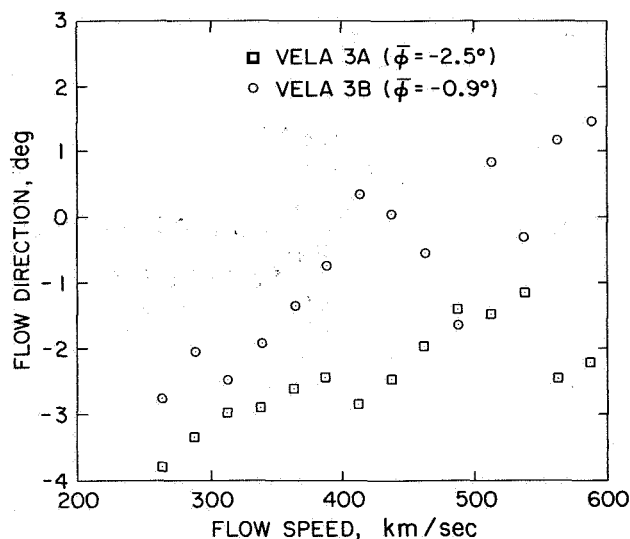


Figure 40. Explorer 34 proton number density versus velocity. Average values from other spacecraft are shown in the circles.

the period from June to December 1967 and the horizontal lines represent the average density within 50 km/sec velocity intervals. The individual points represent the average values of density and velocity for the various spacecraft observations indicated. The open points are further observations that have been added to the original figure of Burlaga and Ogilvie [1970b]. The lower density IMP 1 average is a corrected value [Olbert, 1968] and the higher density IMP 1 point should be ignored. The best-fit curve to the Explorer 34 results indicates a density dependence on velocity of  $V^{-1.5}$ . Although the various observations show some scatter, it is clear that density decreases exponentially with velocity and that on the average the solar wind flux is not a constant. The above must be accounted for by any theory that attempts to determine the solar wind source function.

Consider next the relationship between the solar wind flow direction and velocity. Figure 41 [Hundhausen et al., 1970] gives the average flow direction in the Vela 3A and 3B spin planes as a function of the flow speed in 25 km/sec intervals. The results were obtained from measurements made during the interval from July 1965



**Figure 41.** *Vela 3A and Vela 3B flow directions versus flow speed.*

to November 1967. Since the Vela 3 spin planes are tilted approximately  $35^\circ$  with respect to the ecliptic, then in a solar-ecliptic coordinate system, the flow directions given here contain contributions from both the azimuthal and polar components. Wolfe [1970], however, has shown from Pioneer 6 results that there is no discernible correlation between the polar component and the flow speed; therefore the results shown here presumably reflect only contributions from the azimuthal component. Due to the likelihood of systematic error and for comparative purposes, the obvious trend toward more positive flow with increasing velocity should be considered the important feature of the flow direction-velocity relationship rather than the absolute values. Note in the Vela 3A data the tendency for the return of the flow toward the negative direction at the highest velocities. Although conceivably statistical, this trend is also seen in the Pioneer 6 results [Wolfe, 1970] given in figure 42. Plotted here are 3-hr average values of the azimuthal flow direction and corresponding velocity from measurements made over one complete solar rotation beginning December 18, 1965. The average azimuthal flow direction for this entire time interval was  $+2.6^\circ$  (flow from west of the sun). This average is considered to be possibly a systematic error and has been arbitrarily subtracted from all the data to permit investigation of trends in the azimuthal flow direction with respect to a zero mean. The trend toward more positive flow with increasing velocity is also readily seen in the Pioneer 6 results; however, the return to more nearly radial flow at the higher velocities is quite pronounced.

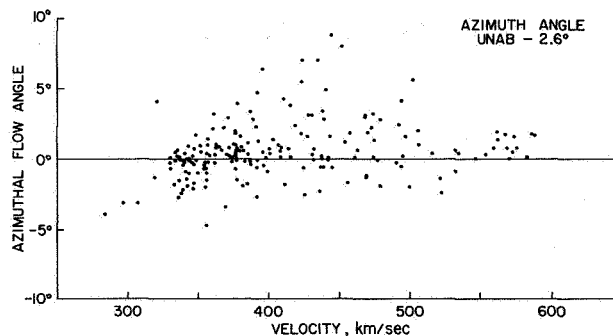


**Figure 42.** *Pioneer 6 3-hr average values of the azimuthal flow angle as a function of velocity.*

Note also the large scatter in azimuthal angles most prominent between about 400 and 450 km/sec. Recalling the more detailed data discussed in connection with the solar wind stream structure, the largest amplitude variations in the azimuthal flow direction (particularly positive) were associated with the leading edge (sharp positive velocity gradient) of a new stream where the velocity was typically on the order of 400-450 km/sec. Recall also that near the peak of the stream (highest velocity) the flow tended to be more radial. Thus, the correspondence between the azimuthal flow direction and velocity seen here seems clearly to be highly dependent on the solar wind stream structure.

Figure 43 [Wolfe, 1970] shows the relationship between the polar and azimuthal flow directions

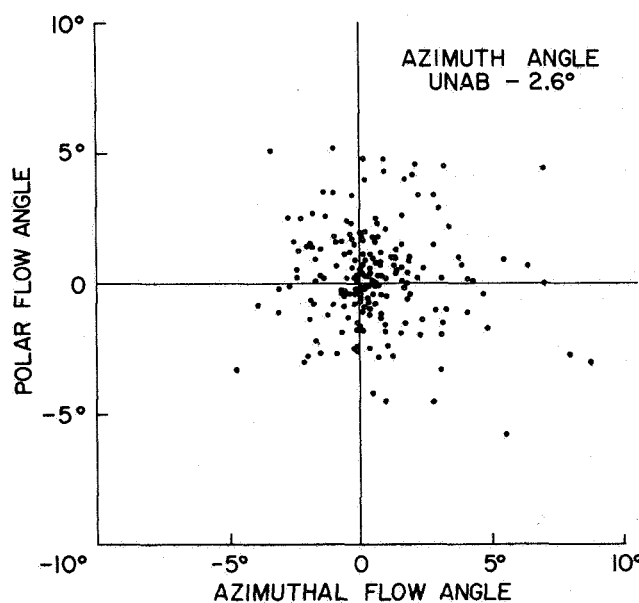


**Figure 43.** *Pioneer 6 polar flow angle as a function of azimuthal flow angle.*

obtained from Pioneer 6 over the same time interval as the previous figure. As before, the azimuthal angles have been corrected by  $2.6^\circ$  for comparative purposes. By inspection it is seen that the polar and azimuthal flow components are completely independent. It is interesting to note, however, that the amplitude in the flow angle variations are comparable for the two components.

The relationship between temperature and velocity is very strong, as indicated by the Vela 3 results shown in figure 44 [Hundhausen *et al.*, 1970]. These results were compiled from observations made from July 1965 to November 1967. The temperatures are averages in 25 km/sec flow speed intervals. A similar strong temperature-velocity relationship is also indicated by Ames Research Center plasma observations from Pioneer 6 during the period December 1965 to March 1966 (fig. 45). The values given are 24-hr averages with the temperature plotted on a logarithmic scale. For reference purposes the square root of  $T$  relationship with velocity determined by Burlaga and Ogilvie [1970a] derived from Explorer 34 observations is also plotted on the Pioneer 6 data. Although the Pioneer 6 results seem to fit this relationship fairly well, there is a great deal of

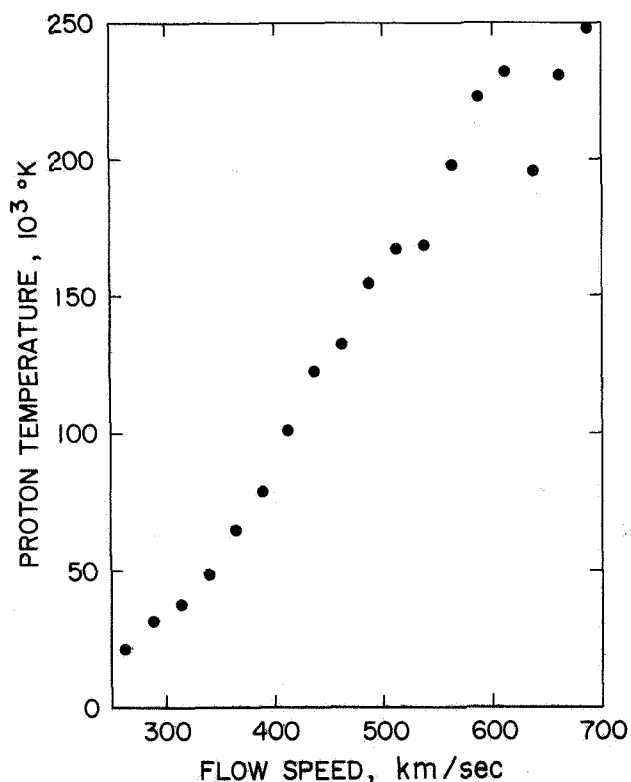


Figure 44. Vela 3 proton temperature versus flow speed.

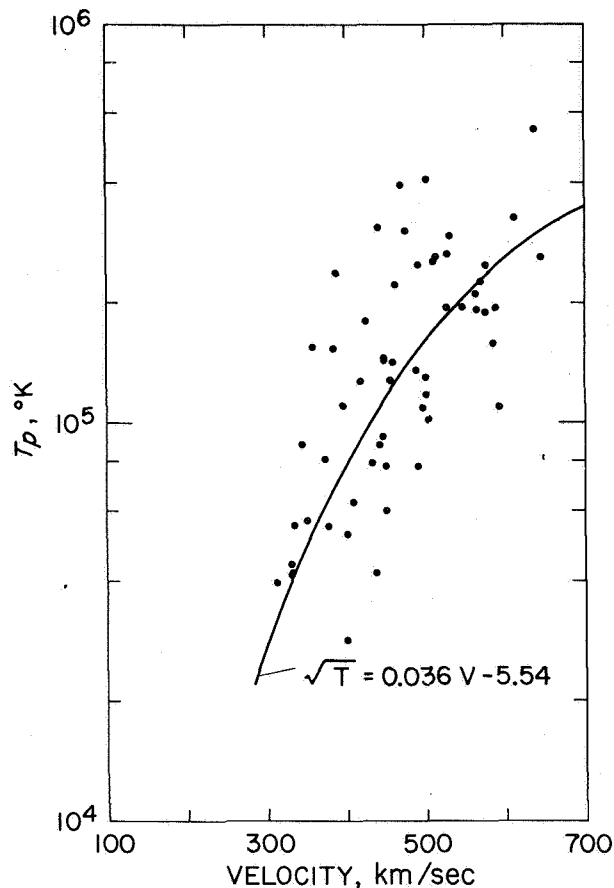


Figure 45. Pioneer 6 proton temperature versus velocity.

scatter, and a linear relationship seems to fit about as well. This is also true for the Vela 3 results of figure 44. Note, however, the particularly large amount of scatter (in the direction of higher temperature with respect to the curve) between about 350 and 500 km/sec. This is conceivably due to the heating one observes associated with the positive gradient in velocity on the leading edge of a solar wind stream where the velocities are typically in this range. Figure 46 shows the relationship between the anisotropy, defined by  $T_{max}/T_{min}$  [Hundhausen *et al.*, 1970], and the flow speed. These results were obtained from Vela 3 measurements over the period from July 1965 to November 1967 with the anisotropy averaged in 50 km/sec flow speed intervals. The average anisotropy is seen to peak near 375 km/sec at a value of approximately 2.0, and to drop off slightly for lower velocities and much more steeply for higher velocities. Hundhausen *et al.* [1970] postulated the fall off of anisotropy for the low velocities as consistent with coulomb collision effects and the decrease in anisotropy

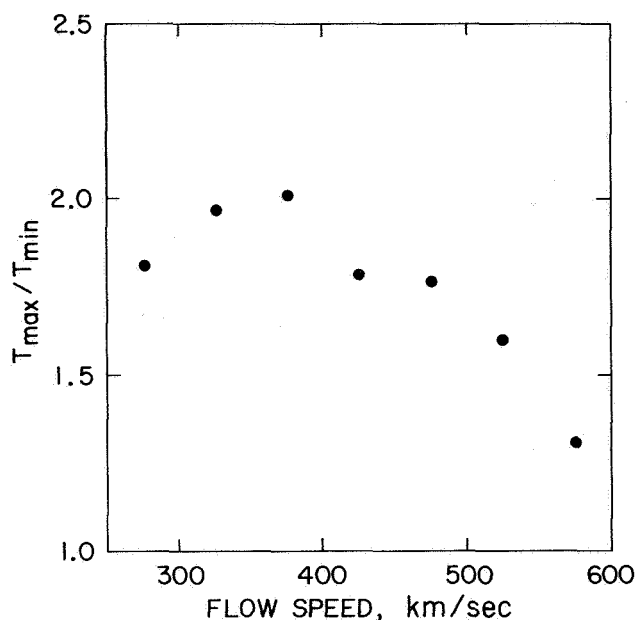


Figure 46. *Vela 3 anisotropy versus flow speed.*

with increasing velocity above 375 km/sec to be the result of the dominance of instabilities associated with a more disturbed medium.

#### INTERPLANETARY-TERRESTRIAL RELATIONSHIPS

The interplanetary-terrestrial relationship that has been sought historically is that between the character of the solar wind and the state of the geomagnetic field. *Snyder et al.* [1963] made the first attempt to establish this relationship on the basis of Mariner 2 observations. Of all the solar wind parameters or combinations thereof, the best correlated parameter with the geomagnetic disturbance index  $K_p$  was the solar wind flow speed. These results are shown in figure 47 where the 24-hr average velocity is plotted against the daily sum of  $K_p$  for that particular day. The results were obtained during the period from late August through late December 1962. The line through the data represents the least-squares linear fit to the points. Although the trend of increasing  $K_p$  with increasing velocity is certainly evident, the large amount of scatter in the data obscures a possibly, strong relationship between velocity and  $K_p$ . Similar results were reported by *Olbert* [1968] from the MIT IMP 1 observations obtained from November 1963 to February 1964 shown in figure 48. The relationship (assumed linear) between velocity and  $K_p$  is somewhat different than the Mariner 2 results, and a large residual scatter remains in the data. The correlation coefficient for these results was approximately 0.8. Figure 49 indicates the

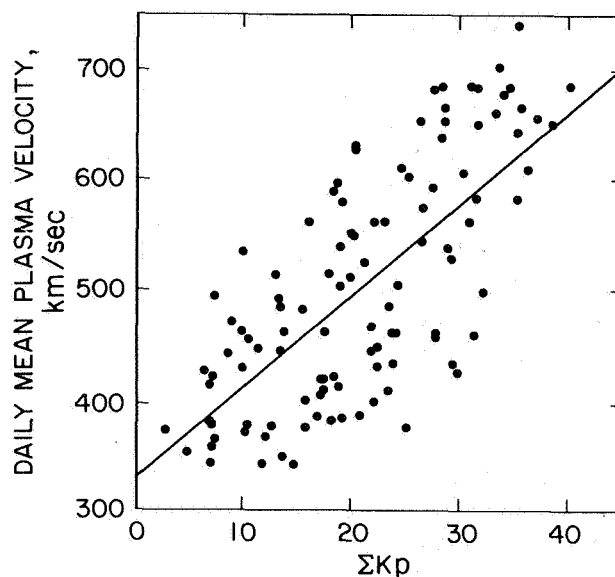


Figure 47. *Mariner 2 scatter diagram of daily mean plasma velocity versus  $\Sigma K_p$ . The line is the least squares linear fit to the points.*

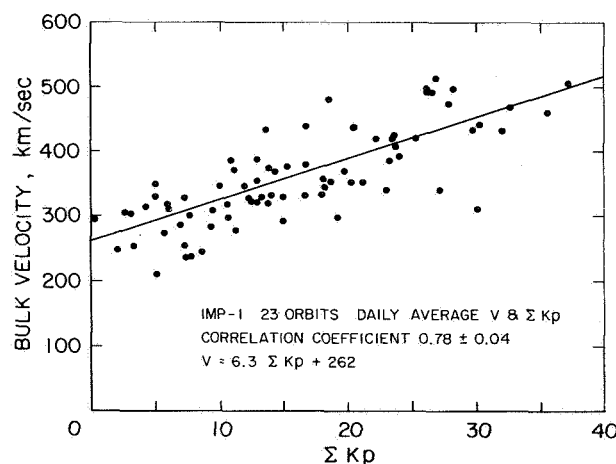
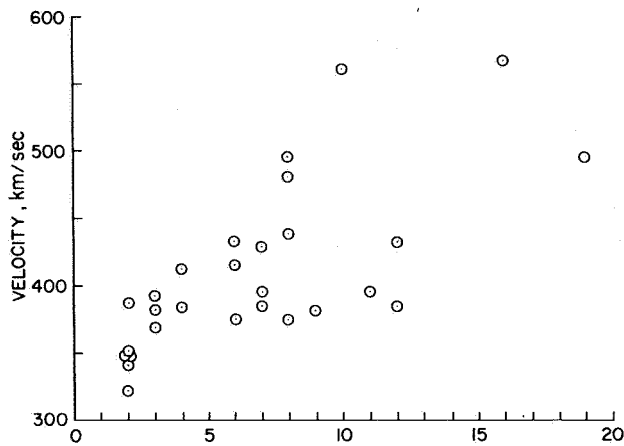


Figure 48. *IMP 1 daily averages of the solar wind velocity plotted versus the daily sum of the  $K_p$  index.*

relationship between the 24-hr average solar wind velocities obtained by Pioneer 6 [*Wolfe*, 1970] and the daily geomagnetic disturbance index  $A_p$ . The correlation coefficient here is approximately 0.7, and as was the case with the Mariner 2 and the IMP 1 results there is again a large scatter in the data. Perhaps the best explanation of the scatter is the frequently observed phase lag between the solar wind velocity and geomagnetic disturbance indices discussed earlier. During the rising portion or



**Figure 49.** Pioneer 6 24-hr average values of solar wind velocity versus the  $A_p$  index.

leading edge of a solar wind stream (positive gradient in velocity), the geomagnetic field tends to be much more disturbed than during the trailing portion (more gradual negative gradient) of the stream. Thus for a given value of solar wind velocity the  $K_p$  or  $A_p$  index would be double valued leading to the scatter observed in figures 47 through 49. As discussed earlier, the density tends to lead the velocity lag, and the temperature is approximately in phase with the daily geomagnetic disturbance index  $A_p$  (or  $\Sigma K_p$ ). Figure 50 gives the 24-hr average values of the Ames Research Center Pioneer 6 solar wind proton temperature observations as a function of the  $A_p$  index. These measurements were obtained over the same period as the previous figure. Even though the correlation coefficient here is approximately 0.9, there is still significant scatter in the data. It is inconceivable that the amplitude of the random motion in the protons should really have any strong effect on the geomagnetic field.

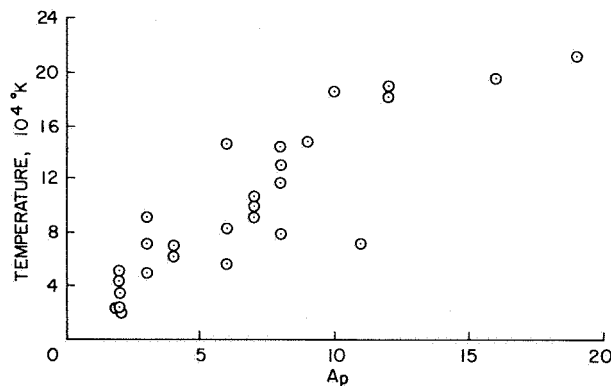


**Figure 50.** Pioneer 6 24-hr average values of proton temperature versus the  $A_p$  index.

What seems more plausible is that the solar wind proton temperature represents a large-scale indication of the degree of disturbance in the interplanetary medium, and that changes in the momentum flux or simply flux fluctuations are conceivably responsible for geomagnetic disturbance. The above, however, can only be confirmed by higher time resolution plasma measurements than are presently available. The result that solar wind proton temperature seems to give the best correlation with geomagnetic disturbance indices is considered here to be an effect, not a cause.

### EFFECTS OF SOLAR LATITUDE AND RADIAL DISTANCE

Unfortunately, space observations to date have been restricted to near the plane of the ecliptic between the orbits of Venus and Mars. In a spherical coronal expansion model, the solar wind density is expected to decrease as the square of the distance. This has been tentatively verified by the Mariner 2 results [Neugebauer and Snyder, 1966] shown in figure 51. Twenty-seven day averages of the daily averages of proton density, flux, and total momentum flux are plotted versus distance from the sun. The slopes for an inverse square relationship are also shown. Considering the variations observed from one solar rotation to the next, the density here seems to fit the expected inverse square relation remarkably well. The Mariner 2 results showed no radial dependence for either the velocity or temperature. This is not unexpected since the radial dependence for these parameters is conceivably much more subtle. As the

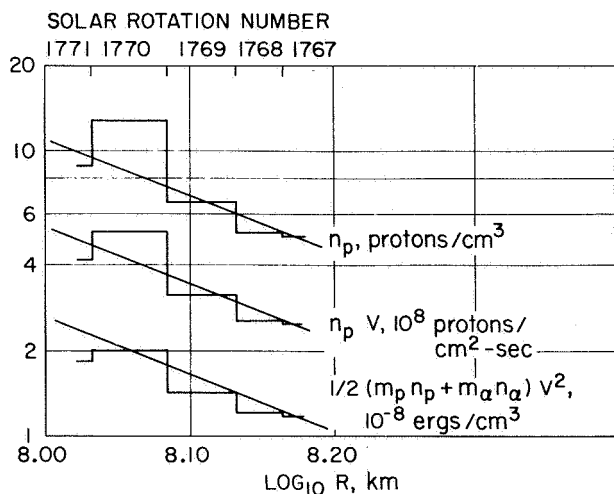


**Figure 51.** Mariner 2 27-day averages of the daily averages of proton number density, proton flux and total momentum flux versus distance from the sun. The slopes for an inverse square relation are also given.

solar wind flows outward from the sun, it is expected to quickly approach a terminal velocity that would be essentially constant beyond the Earth's orbit. The radial variation of the proton temperature is less certain and would be dependent on the proton-heating mechanisms. For example, adiabatic, constant speed expansion with isotropic pressure requires that the proton temperature decrease as  $R^{-4/3}$ , whereas conduction-dominated flow gives an  $R^{-2/7}$  dependence and flow dominated by proton-electron energy exchange has an  $R^{-6/7}$  dependence. It seems likely that these dependencies would be difficult to separate from the temporal variations for observations which only extend over a radial distance of approximately 0.3 AU.

Gosling [1971] compared Pioneer 6 and Pioneer 7 velocity observations during the period from January 1969 to July 1970. Specifically, the velocity observed by one spacecraft was compared to the velocity observed by the other spacecraft after a period corresponding to the corotation delay due to their heliocentric azimuthal separation. Figure 52 shows the results when the two spacecraft are separated in corotation by less than two days. With a few exceptions, most of the points tend to lie close to the equal velocity line, although there is some scatter. When the two spacecraft have a separation of 2 to 4 days (fig. 53), the fit is not as good. A separation of greater than 4 days (fig. 54), indicates a very poor correlation. This implies that there are significant coronal changes taking place on a time scale of a few days (at least at the time of these measurements) and predicts the difficulty of determining the solar wind radial gradients from a single spacecraft. However, one cannot discount the possibility that this is a heliographic

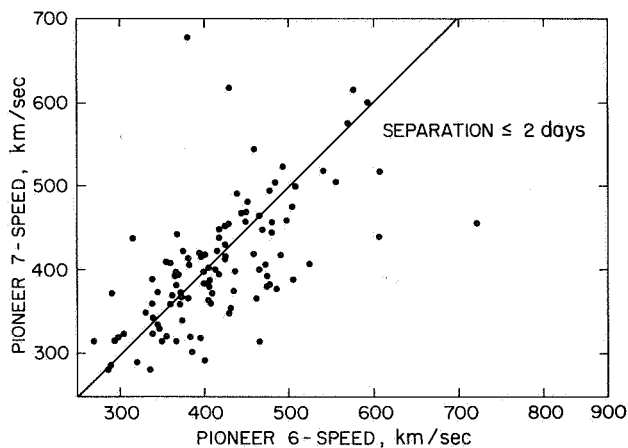


**Figure 52.** Comparison of Pioneer 7 and Pioneer 6 solar wind flow speeds when the two spacecraft are separated by less than 2 days corotation delay.

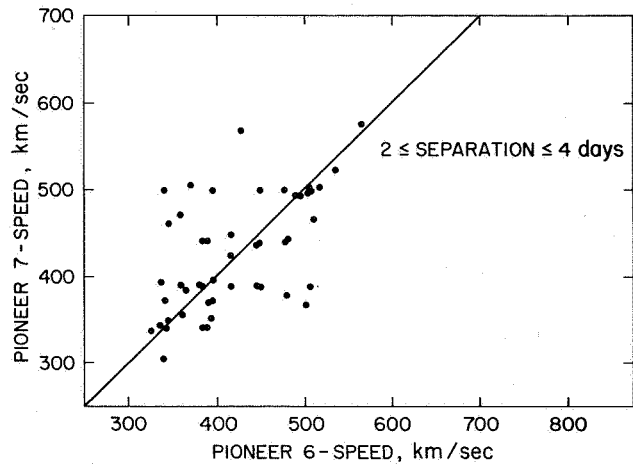


**Figure 53.** Comparison of Pioneer 7 and Pioneer 6 solar wind flow speeds when the two spacecraft are separated by 2 to 4 days corotation delay.

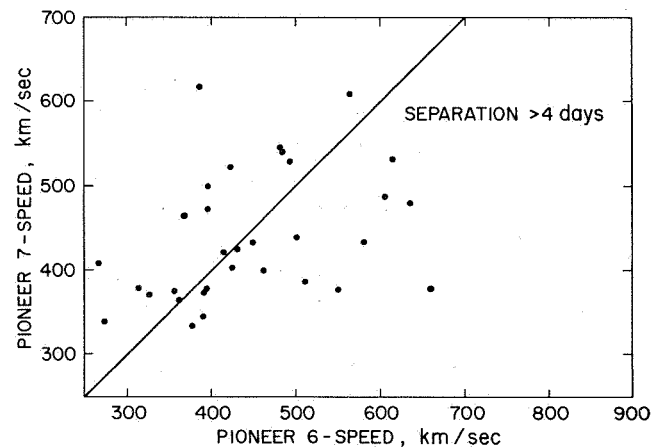


**Figure 54.** Comparison of Pioneer 7 and Pioneer 6 solar wind flow speed when the two spacecraft are separated by greater than 4 days corotation delay.

latitude effect due to the tilt of approximately  $7^\circ$  of the sun's equatorial plane with respect to the ecliptic.

In considering what might be expected in the way of heliographic latitude effects on the solar wind, a coronagraph photo of the March 7, 1970, solar eclipse is shown in figure 55 [Smith, 1970]. This is a composite of three separate pictures with the north pole of the sun at the



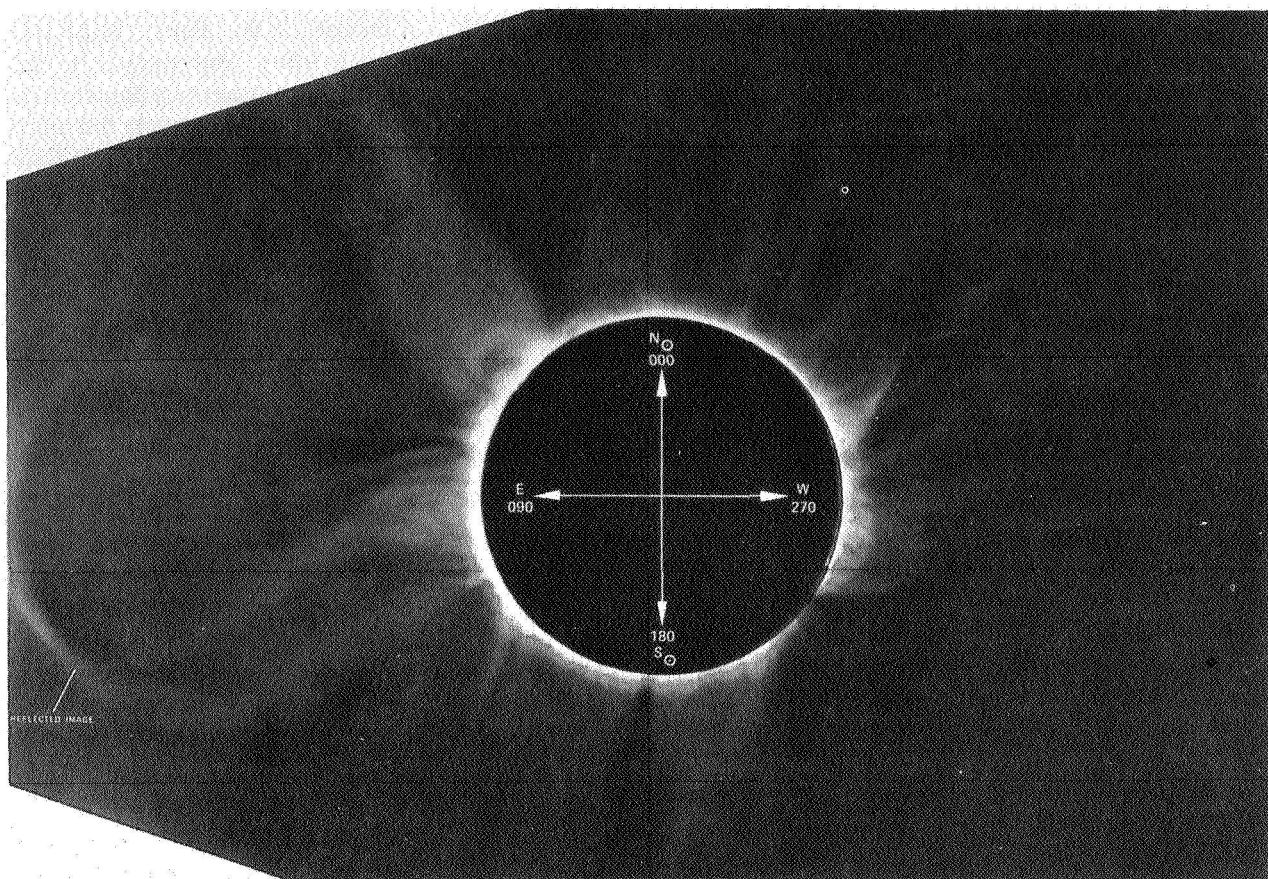


Figure 55. Composite of 3 coronagraph photos of the March 7, 1970 solar eclipse.

top. Note in particular that the coronal streamers are just as prevalent near the solar pole as they are near the equator. If these streamers play an important role in solar wind dynamics, then one might not expect any significant solar wind latitude effects. However, one might expect drastic effects on the character of the stream interactions since with increasing heliographic latitude the interplanetary magnetic field becomes less and less spiraled. The observation of these effects will probably require space measurements up to at least  $30^\circ$  to  $40^\circ$  heliographic latitude.

#### REFERENCES

- Burlaga, L. F.; and Ogilvie, K. W.: Heating of the Solar Wind. *Ap. J.*, Vol. 159, 1970a, pp. 659-670.
- Burlaga, L. F.; and Ogilvie, K. W.: Magnetic and Kinetic Pressures in the Solar Wind. *Solar Phys.*, Vol. 15, 1970b, pp. 61-71.
- Coon, J. H.: Solar Wind Observations, in *Earth's Particles and Fields*, edited by B. M. McCormac, Reinhold, New York, 1968, pp. 359-372.
- Egidi, A.; Formisano, V.; Moreno, G.; Palmiotto F.; and Saraceno, P.: Solar Wind and Location of Shock Front and Magnetopause at the 1969 Solar Maximum. *J. Geophys. Res.*, Vol. 75, 1970, pp. 6999-7006.
- Gosling, J. T.: Variations in the Solar Wind Speed Along the Earth's Orbit. *Solar Phys.*, 1971 (in press).
- Hundhausen, A. J.; Bame, S. J.; and Ness, N. F.: Solar Wind Thermal Anisotropies: Vela 3 and IMP-3. *J. Geophys. Res.*, Vol. 72, 1967, pp. 5265-5274.
- Hundhausen, A. J.; Bame, S. J.; Asbridge, J. R.; and Sydoriak, S. J.: Solar Wind Proton Properties: Vela 3 Observations from July 1965 to June 1967. *J. Geophys. Res.*, Vol. 75, 1970, pp. 4643-4657.
- Lyon, E.; Egidi, A.; Pizzella, G.; Bridge, H.; Binsack, J.; Baker, R.; and Butler, R.: Plasma Measurements on Explorer 33, (1) Interplanetary Region. *Space Research VIII*, edited by A. P. Mitra, L. G. Jacchia and W. S. Newman, North-Holland Publishing Co., Amsterdam, 1968, pp. 99-106.

- Mihalov, J. D.; and Wolfe, J. H.: Average Solar Wind Properties from Pioneers 6 and 7. *Cosmic Electrodynamics*, Vol. 2, 1971, pp. 326-339.
- Montgomery, M. D.; Bame, S. J.; and Hundhausen, A. J.: Solar Wind Electrons: Vela 4 Measurements. *J. Geophys. Res.*, Vol. 73, 1968, pp. 4999-5003.
- Neugebauer, M.; and Snyder, C. W.: Mariner 2 Observations of the Solar Wind, 1. Average Properties. *J. Geophys. Res.*, Vol. 71, 1966, pp. 4469-4484.
- Olbert, S.: Summary of Experimental Results from MIT Detector on IMP-1. *Physics of the Magnetosphere*, edited by R. L. Carovillano, D. Reidel, Dordrecht-Holland, 1968, pp. 641-659.
- Parker, E. N.: Dynamics of the Interplanetary Gas and Magnetic Fields. *Astrophys. J.*, Vol. 128, 1958, p. 664.
- Smith, S.: Solar Eclipse 1970. Bulletin F, National Science Foundation, 1970, p. 157.
- Snyder, C. W.; Neugebauer, M.; and Rao, U. R.: The Solar Wind Velocity and its Correlation with Cosmic-Ray Variations and with Solar and Geomagnetic Activity. *J. Geophys. Res.*, Vol. 68, 1963, pp. 6361-6370.
- Strong, I. B.; Asbridge, J. R.; Bame, S. J.; and Hundhausen, A. J.: Satellite Observations of the General Characteristics and Filamentary Structure of the Solar Wind. *The Zodiacal Light and the Interplanetary Medium*, edited by J. L. Weinberg, National Aeronautics and Space Administration, Washington, D. C., 1967, pp. 365-372.
- Wilcox, J. M.; and Ness, N. F.: A Quasi-stationary Co-rotating Structure in the Interplanetary Medium. *J. Geophys. Res.*, Vol. 70, 1965, pp. 5793-5805.
- Wilcox, J. M.; and Colburn, D. S.: Interplanetary Sector Structure in the Rising Portion of the Sunspot Cycle. *J. Geophys. Res.*, Vol. 74, 1969, pp. 2388-2392.
- Wilcox, J. M.; and Colburn, D. S.: Interplanetary Sector Structure Near the Maximum of the Sunspot Cycle. *J. Geophys. Res.*, Vol. 75, 1970, pp. 6366-6370.
- Wolfe, J. H.: Solar Wind Characteristics Associated with Interplanetary Magnetic Field Sector Structure. *Trans. Amer. Geophys. Union*, Vol. 51, 1970, p. 412.

DISCUSSION *E. R. Schmerling* I have a very naive view of the sun as something that emits the solar wind and has a few small active regions on it. From this view I can see very readily why your curves of velocity and temperature should be skewed towards the high end. If you follow up you can understand why your curves of density are also skewed along the high end. However, you stated that there are inverse relationships between density and velocity and between density and temperature. Would you explain?

*J. H. Wolfe* The skew toward the high end for the density comes primarily from the pileup region near the leading edge of a new stream. The solar wind velocity is fairly low there. The density structure is maybe two or three days wide, whereas the velocity structure is many days wide. Overall the density seems to be "anticorrelated."

*R. H. Dicke* For the solar wind torque calculations one would like the product of the density by the velocity. Is there information about the way the mean values of this product vary through the sunspot cycle?

*J. H. Wolfe* I tried to point out that there doesn't seem to be any systematic variation in that number or in any of the numbers that were shown, with perhaps the exception of the velocity. But in terms of torque on the sun, I think the systematic errors which look to be as much as  $3^\circ$  means that any calculation of momentum is fruitless.

*E. N. Parker* Isn't it true that if you were to plot the logarithm of the density and logarithm of the velocity you would get rid of most of that skewness, which pertains to the question of whether the product is more nearly constant.

*J. H. Wolfe* I think that is probably so.

*E. N. Parker* The percentage changes I think are not skewed.

*J. H. Wolfe* Their product is not a constant value.

*A. J. Hundhausen* I have a few comments that I hope you will find are restrained and positive. Let's start with the solar cycle effects. In a paper recently published in the *Journal of Geophysical Research* Gosling, Hansen, and Bame combined the data from all these different satellites, displaying histograms and giving averages for all the years up to, I think, 1969 or 1970, to get a very similar result. It's very interesting that the highest

velocities were observed near the end of the last solar cycle. There then seems to have been very little change in the yearly average flow speed through the present solar cycle. I think one should emphasize this. In yesterday's discussions of magnetic sectors, changes in the solar wind speed during the solar cycle were evoked. This change doesn't seem to be observed.

Now, considering that decrease in the Vela 2 solar rotation averages of the velocity at or near the very end of the last solar cycle, recall that although something like October-November of 1964 was defined as the beginning of the present cycle, the steady sector pattern observed back in 1963 by IMP 1 appeared to persist until early 1965. In a paper presented yesterday I pointed out that the apparent variations in solar wind density and flow speed with heliographic latitude also appear to begin in early 1965. The new solar cycle may, in fact, have become manifest in the solar wind 6 months after the change in the sunspot pattern.

Finally, with regard to the Vela 3 observations of possible heliographic latitude dependence, the Pioneer 6 and 7 averages and histograms presented here—which I think came from only one or two solar rotations—agree very well with the data I showed yesterday. This limited comparison may not completely confirm the latitude effects, but if this comparison were carried out as Pioneer 6 and 7 get farther from the earth, we would have an independent check as to whether we are seeing latitude effects, time variations, or some instrumental effect.

*J. H. Wolfe* I think in the last few figures I showed that what Gosling had done could be interpreted either way.

*L. Davis, Jr.* You spoke of westerly flow and sometimes it sounded as though you were saying from the west. When you say westerly flow do you mean flow *to* the west or *from* the west?

*J. H. Wolfe* From the west and westerly flow are synonymous. Solar wind people are like weathermen, they talk about the direction from which the wind blows.

*R. Lüst* From this we get that "negative" would be in conformity with corotation and "positive" against corotation.

*J. H. Wolfe* With one exception. At MIT they define it the other way around.

*Unidentified Speaker* You made a point about the raggedness of the velocity distributions and the peak nature. In our experience those peaks usually occur because of the energy channels in the instrument rather than anything occurring in the solar wind.

*J. H. Wolfe* We questioned those peaks on the Pioneer 7, because they were so ragged, and it just didn't make any sense at all with regard to where the channels were. Certainly I think by the time you get nearly to 5000 points, in the histogram, as we had in Pioneer 6, such instrumental effects tend to go away.

*Dr. Newkirk* I'm very perplexed by the lack of any change in the condition of the solar wind over the solar cycle. We do see a significant change in the inner corona. The temperature during sunspot maxima is 30 or 40 percent higher; the densities on the average are a factor of 2 higher. These are averages which are constructed differently from those observed in interplanetary space. But we still see an effect as was pointed out by Jack Gosling and his collaborators in their recent paper.

*J. H. Wolfe* If you are perplexed, then I feel my lecture has been successful this morning. I think we here at Asilomar should discuss current problems and I think the absence of change through the solar cycle is indeed a problem.

*N. F. Ness* I was a bit puzzled about the emphasis you gave to this comparison between Pioneer 6 and 7 data based upon these snapshots of plasma presented in the NOAA Geophysical Data Series. If I understand the data that are deposited there correctly, they are something like a 1-minute picture of peak velocity for each 24-hour time interval. And when you attempt to compare on short time scales, 1 day or 2 days in the vicinity of the earth, such small segments of data I wouldn't be at all surprised if, even on

the same spacecraft with different time intervals, you would get a scatter diagram. I don't understand why you emphasize that those results substantiate a variable solar wind on such a small time scale. In fact, it would seem to me that we can predict on the order of a few days within the vicinity of the earth if we take the right parameter set. Do you have a comment?

*J. H. Wolfe* Yes. I think Gosling went through a fairly extended argument in the paper. I'm just showing a list of the conclusions. Actually, the data are from both MIT and ARC. The data from both seem to agree even though they might have been taken at slightly different times. With regard to the snapshot, the number that the project office gives to Virginia Lincoln is a number that best represents that day. The exact time of the measurement is also given. So there's not a 24 hour uncertainty; you know precisely when it was taken. I think Gosling calculated a time at the other spacecraft based on the corotation delay predicted, and compared those two. I think this sort of thing should be done in greater detail with much better data. So I think your point is well taken. But I think the work Gosling did is valid.

*D. S. Intriligator* I would like to comment on Norman's question. We looked at four solar rotations, two from Pioneer 6 and two from Pioneer 7. We checked this single daily value. We assumed it would not be representative, but we found that instead, on the average, it differed by only 10 percent from the daily average value.

Looking at Pioneer 6 and 7 data from December 1965 to the middle of 1968, we find variations in the number density and velocity that seem to correlate with heliographic latitude.

*P. J. Coleman, Jr.* I would like to suggest that possibly this is another latitude effect because when spacecraft are separated by 4 or 5 days of corotation time they are separated by something like  $6^\circ$ , since both are in the ecliptic plane.

*J. H. Wolfe* Agreed. I said there were two explanations, one that the part of the corona which drives the solar wind can evolve in times like 4 days, and the other that these parameters are sensitive to latitude. Those are the two explanations Gosling gave.

*J. T. Gosling* There are both possibilities. I hope to give a talk after the coffee break where I'll explain a little more, but I think it's primarily a temporal effect.

*A. Hundhausen* I would like to comment on Gordon's question regarding solar activity. We do see more manifestations of solar activity in the solar wind as the solar cycle progresses. However, these manifestations never seem to dominate the transport of energy (or mass) in the solar wind. For instance, individual flare-produced shock waves appear to be an order of magnitude more energetic 2 years after the solar cycle began than at solar minimum. But there are not very many more such shocks, so that the increased activity doesn't influence the characteristics of the solar wind as greatly as one might expect. However, these activity-related solar wind disturbances do have a more subtle effect, as suggested in a comment made yesterday by Ed Smith. In many ways the averages we publish are dominated by the presence of these transient and spatial structures. In particular, the compression at the front of a high speed stream has been emphasized here today. This was recognized as early as 1962 in Neugebauer and Snyder's discussions of Mariner 2 observations. But I think few people have looked closely enough at solar wind observations to realize that a very broad rarefaction often follows this compression. When one averages over time, this rarefaction dominates. The density is low at high velocities because of the presence of this rarefaction. It is a *dynamic* effect. Those attempts, mentioned by Gene Parker, to explain such relationships, as the temperature-velocity relationship, by using steady-state models miss entirely this basic dynamic nature of solar wind variations.

*J. Hirshberg* I wanted to make two points suggesting caution in interpreting the data about the solar cycle. One is about the data on the changes in the velocity. The  $K_p$  indices show that the flight of Mariner 2 occurred during a very active period, not at all

typical of the low part of the solar cycle. The other comment concerns the sector structure. We've been saying that the sector structure was constant during the low part of the solar cycle. But the actual data, without the interpolations on the basis of the  $K_p$ , contain practically no evidence for this as far as I can see. In the early periods the interpolation using  $K_p$  looked good. However, if you do that same thing later on when you have the rapidly changing sector structure the interpolation would not work. So I wonder whether we don't need more data. This is another reason to take measurements continuously, that is to get the sector structure through the last half of a cycle.

*K. H. Schatten* Parker said that the solar wind might not be radial and then Wolfe showed observations suggesting it is. However, I think that Wolfe's observations don't necessarily prove it is radial. There is a large amount of scatter present. If the scatter were related to solar latitude, insofar as the ecliptic is half the time above the solar equator and half the time below it, skewing of the flow could occur and the flow would not be radial although it would appear so from Wolfe's observations.

*M. M. Neugebauer* I think there's a possibility of systematic error in velocity measurements made from earth satellites. We have noticed such an effect in our OGO data. The maximum pressure in the front of a high velocity stream occurs when the velocity is still relatively low. On several occasions we observed the start of a high velocity stream when OGO-5 was in the solar wind; the velocity started to increase and the density was very high. Then the density dropped, the earth's bow shock moved outward, and OGO was not in the solar wind to observe the highest velocity plasma, which could be seen by deep space probes such as Pioneer 9. In John Wolfe's tables of velocity from all the different spacecraft, you will notice that the average velocity was higher at the deep space probes than at the satellites. So I think there may be a systematic effect here; that is, most of the satellites miss the high velocity periods because the bow shock moves out.

## COMMENTS

*D. S. Intriligator* I would like to elaborate on the comment by M. Neugebauer on a possible systematic bias toward lower velocities in plasma data from spacecraft that are earth orbiters. Figure 1 is from a study Neugebauer and I have been doing to look for a radial gradient affecting the solar wind plasma between 0.75 and 1 AU. We have been comparing simultaneous Pioneer 9 and OGO-5 data. The data in figure 1 are from January 24, 25, 1969. OGO-5 is in earth orbit and is located close to the earth. At this time Pioneer 9 is essentially directly in front of the earth at a radial distance of 0.88 AU. The distance between the two spacecraft is, therefore, approximately 16,000,000 km. As indicated on the abscissa there is almost a 12 hr lag between the Pioneer 9 and OGO-5 data. The darker curves are the OGO-5 data and the lighter curves are the Pioneer 9 data. The bottom graph shows the solar wind velocity recorded at each spacecraft. The two curves follow well until there is a jump in velocity observed at Pioneer 9 at ~1800 on January 24. Subsequently, at ~0500 on January 25, OGO-5 was then in the magnetosphere and did not measure this initial interval of higher variations in velocity. There were also several shorter intervals (e.g. ~1200 on January 25) when OGO-5 was in the magnetosphere during a solar wind velocity increase. At ~1200 on January 25 Pioneer 9 recorded an extremely large velocity increase and the velocity remained elevated for more than the next 18 hr as shown at the far right of the figure. The initial velocity increase was seen at OGO-5 at ~2300 on January 25 when the magnetosphere boundary overtook the spacecraft. For more than the next 18 hr OGO was in the magnetosphere. The top graph shows the relative proton flux ( $n_p V$ ). The OGO-5 data display the total proton flux. The Pioneer 9 data indicate the proton flux in the peak energy channel. The two curves have been arbitrarily displaced. The two curves together show that at ~1800 January 24 (Pioneer 9) the flux in the peak energy channel increased. At OGO-5 the total flux most likely dropped suddenly and, therefore, OGO-5 was thrown

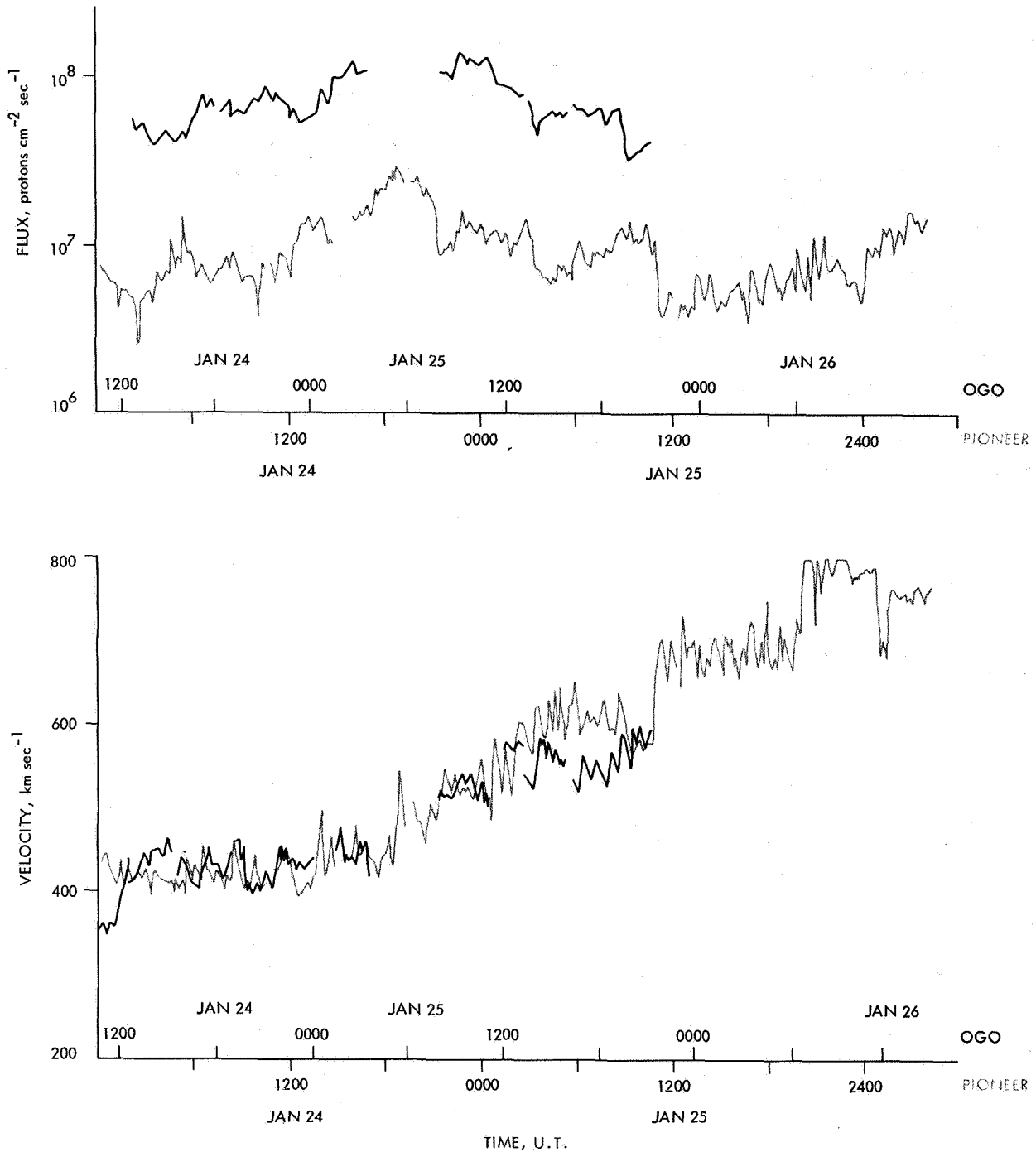


**Figure 1.** Simultaneous Pioneer 9 and OGO-5 data from January 24, 25, 1969. The darker curves are the OGO-5 data and the lighter curves are the Pioneer 9 data. The spacecraft are separated by  $\sim 16,000,000$  km and there is approximately a 12-hr lag time (as indicated on the abscissa) between the event as seen at the two spacecraft. In the top graph the OGO-5 data are the total proton flux and the Pioneer 9 data are the proton flux in the peak energy channel. The two curves have been arbitrarily displaced. The bottom graph indicates the solar wind velocity measured at each spacecraft. Notice the two longer intervals starting at  $\sim 1800$  Jan. 24 (Pioneer 9 time) and at  $\sim 1200$  Jan. 25 (Pioneer 9) when the solar wind velocity increases at Pioneer 9 and OGO-5 enters the magnetosphere. The figure shows (see text) that a sharp increase in solar wind velocity and/or a decrease in solar wind flux causes the magnetosphere to expand so that OGO-5 enters the magnetosphere. There is a definite bias in the OGO-5 data toward intervals of lower solar wind velocity and higher solar wind flux.

into the magnetosphere. At ~1200 January 25 (Pioneer 9 time) the peak flux at Pioneer 9 fell sharply. The total solar wind proton flux in the vicinity of the earth probably dropped suddenly at the time OGO-5 reentered the magnetosphere.

These are not unusual events. From studying 3-½ months of simultaneous data (November 1968 until mid February 1969) we find there are many examples of solar wind velocity increases accompanied by simultaneous decreases in solar wind flux. During many of these intervals OGO-5 is overtaken by the magnetosphere and is no longer in the interplanetary medium. There is a definite bias in the OGO-5 interplanetary data toward both intervals of lower solar wind velocity and higher solar wind flux.

*K. H. Schatten* Are you trying to say that the reduced solar wind flux causes the bow shock and magnetopause to move farther out and that's why OGO is in the magnetosphere? **DISCUSSION**

*D. S. Intriligator* That's right, the bow shock is sensitive to the pressure on it and it moves correspondingly.

*E. J. Smith* In a way I suppose the comment I want to make is a word of caution. Obviously the stream-stream interactions are very important and there are many cases, some of which have been shown today, in which you see the effects of a pileup of the plasma ahead of the solar wind stream. But just to try and provide what I consider to be some balance to the presentation, there are other cases in interplanetary data in which you see rather large increases in the plasma density which are probably not due to any sort of pileup. In particular, there are the increases in the density that occur near the minimum of the solar wind speed. These happen to be the portions of the solar wind in which one is likely to find sector boundaries. If you look only at the plasma data you may not be able to distinguish readily whether the higher density is due to a pileup or not. If you look at the magnetic field data, you will see that during those occurrences the magnetic field magnitude does *not* increase, whereas in regions where there is compression or pileup taking place the magnetic field magnitude should increase along with the density of the plasma. Another difference is that these density increases occur well ahead of the positive gradient regions. There is a substantial delay because the solar wind streams and the high velocity streams, tend to be fairly narrow and that leads to fairly broad valleys or minima in the velocity. It's in these minima that this type of density increase occurs. The increases are then presumably related to something having to do with the origin of that portion of the solar wind, and are not likely to be the result of some kind of stream-stream interaction.

Finally, I might just mention that it's these broad valleys of lower velocity and narrow peaks of higher velocity that cause skewness in many of the histograms that were shown today. A high velocity stream is present for a very short period of time; consequently, you have fewer samples. On the other hand, low velocity regions usually last longer because they are broader in spatial extent, and you get a lot of readings.

## TEMPORAL EVOLUTION OF VELOCITY STRUCTURES IN THE SOLAR WIND

J. T. Gosling

**ABSTRACT** Generally poor correlations have been obtained of solar wind flow speed measurements at one point in the ecliptic plane with measurements at the same point 28 days (one solar rotation) earlier or with measurements at other points in the ecliptic plane separated by  $50^\circ$  or more in solar longitude. This is evidence that either the flow speed is a very sensitive function of solar latitude or that temporal processes *typically* alter the speed of the wind emanating from particular solar regions on a time scale of about 4 days. From a measure of the persistence of the flow speed at the orbit of the earth, it appears that the temporal explanation is more likely to be the correct one.

The daily variation of the solar wind speed at the orbit of the earth is one of the wind's most interesting observational features. For some time now we have been endeavoring to determine the relative importance of solar rotation and true temporal evolution in producing these variations. The present paper reports on the current status of these investigations.

Recently an extensive autocorrelation analysis of the Vela 2 and 3 solar wind speed data for July 1964 through December 1967 was completed [Gosling and Bame, 1972]. One result of that study is shown in figure 1. The upper autocorrelation curve was obtained using daily averages of the data, while the lower curve was obtained from 3-hr averages. The 95 percent confidence limits are derived from the number of *independent* data points used in the calculation of the correlation. For an uncorrelated set of data, 95 percent of the calculated correlation values would fall within  $\pm 1.96 n^{-1/2}$  of zero,  $n$  being the number of independent data points available [Brooks and Carruthers, 1953]. Despite the differences in the averaging intervals, the two autocorrelation curves are remarkably similar. Both curves

exhibit a statistically significant peak near a lag of 28 days, while the daily-average curve exhibits a second small, but significant, peak near the 55-day lag. Although statistically significant, the correlations near 28- and 55-day lags are small, about 0.30 and 0.15, respectively. If we associate these correlations with the solar rotation, we see that there is only a slight tendency for particular speeds measured during one solar rotation to recur 28 days (one solar rotation) later.

The degree of correlation at 28 days is, perhaps, better appreciated by a study of figure 2, which is a scatter plot of  $V(t_0 + L)$  versus  $V(t_0)$  with  $L$  equal to 28 days. Were the solar wind speed pattern stationary in time and the same for latitudes  $\pm 7^\circ$  from the solar equator, then all points in figure 2 would lie along the  $45^\circ$  line drawn. The best fit line  $V_c$  (in the least-squares sense) amply demonstrates that the recurrence tendency is slight. Indeed, the slope of  $V_c$  is a direct measure of the correlation involved.

We should qualify the above comments in two respects. First, there is no *a priori* reason to expect that the solar wind observed near the earth emanates from any particular point on the sun, such as the center of the visible solar disk. If all solar latitudes are allowed, then differential rotation of the sun ensures that a variety of periods from about 27 to 31 days will be present in the data, perhaps at the same time. In fact, when one breaks

---

*The author is at the High Altitude Observatory, National Center for Atmospheric Research, Boulder, Colorado. The National Center for Atmospheric Research is sponsored by the National Science Foundation.*



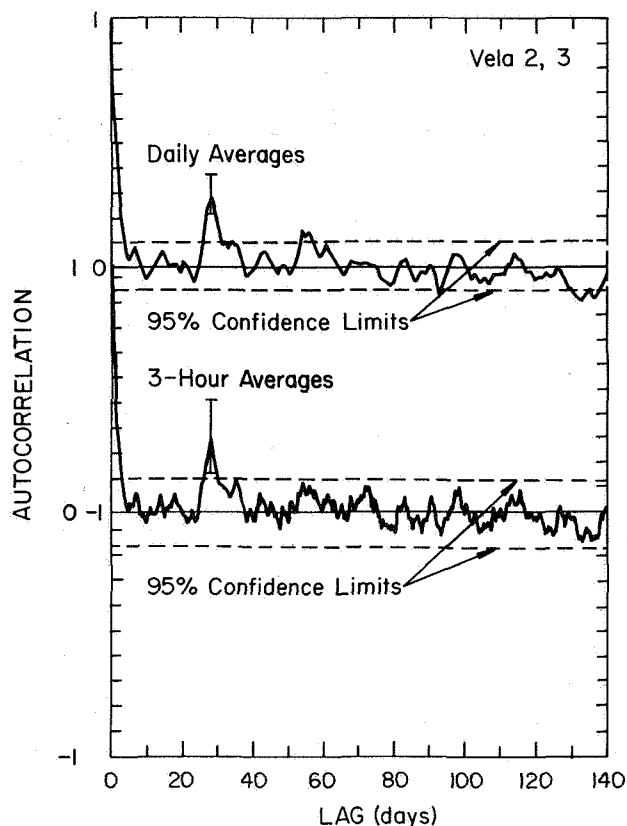


**Figure 1.** Autocorrelation of the solar wind flow speed for the interval July 1964-December 1967 using daily averages (upper curve) and 3-hr averages (lower curve) [from Gosling and Bame, 1972].

the 3½ years of Vela 2 and 3 data into smaller time series, one notes that a variety of recurrence periods seem to be present [Gosling and Bame, 1972]. Such an effect serves to diminish the amplitude of the correlation at any particular lag. Second, analysis of the data taken 6 months at a time reveals that the recurrence tendency waxes and wanes. For some 6-month intervals the peak correlation near 28 days exceeds 0.5; for others, the peak correlation near 28 days is less than 0.1. The average peak correlation near 28 days for the 6-month analysis is 0.37; this value slightly exceeds the 0.30 value derived from treating all the data at once (fig. 1) because the peak correlations occur at a variety of lags near 28 days. Despite the above qualifications, it is nevertheless true for the Vela 2 and 3 data that most speed structures observed on one solar rotation do not reappear on subsequent rotations.

One possible interpretation of this result is that solar wind speed structures are highly constricted in solar

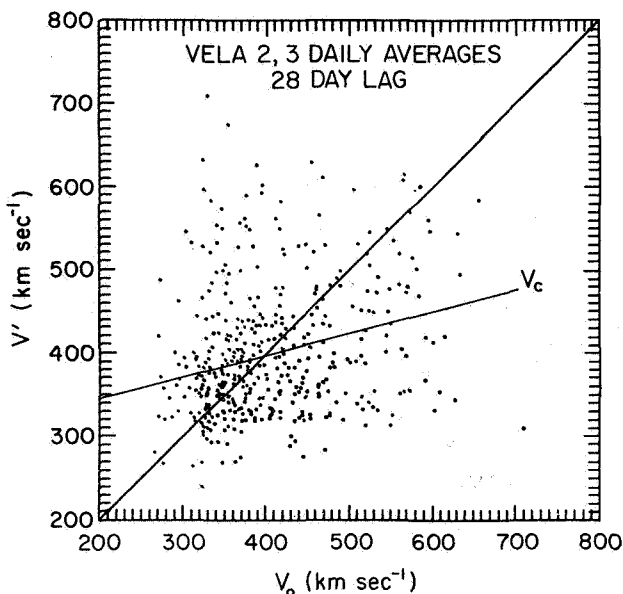


**Figure 2.** Scatter plot of 3½ years of daily average solar wind speeds measured 28 days apart [from Gosling and Bame, 1972].

latitude, with different latitude structures being sampled as the earth in its orbit oscillates  $\pm 7^\circ$  from the solar equator. A more likely interpretation is that most speed structures evolve on a time scale that is short compared to 28 days.

To examine this question further, it is necessary to analyze data taken over an extended period of time by observers stationed at different points along the earth's orbit. The Pioneer 6 and 7 satellites, which were launched into nearly circular orbits about the sun, and the Vela 3, 4, and 5 satellites, which were launched into large, nearly circular orbits about the earth, provide an opportunity for such a study. Figure 3 shows the position of the Pioneer satellites relative to the sun and earth in 1969-1970, the period we shall consider. Sample measurements of the solar wind speed by these satellites were reported routinely in the *Solar Geophysical Reports*, the quantity varying from day to day and from spacecraft to spacecraft. This body of data was combined into a set of daily averages for each spacecraft as described in Gosling, [1971a]. Although the speed values quoted in the *Solar Geophysical Reports* are usually mere "snapshots" of the solar wind speed, they are usually representative for a given day as has been discussed by Wolfe and Intriligator (p.198). This is a consequence both of the speed values quoted being selectively chosen and the very high persistence of the solar wind throughout a day [Gosling and Bame, 1972]. Figure 4 shows histograms displaying the frequency with

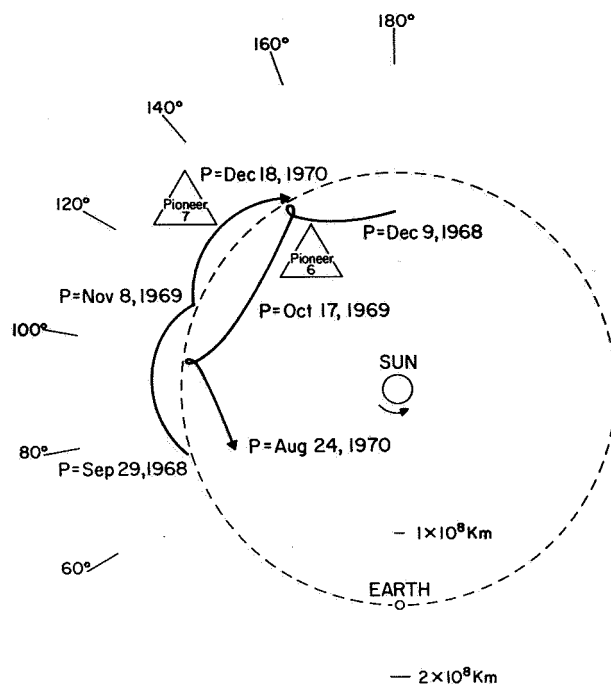


**Figure 3.** Relative positions of Pioneer 6 and 7 to the earth and sun in the ecliptic plane [from Gosling, 1971a].

which different solar wind speeds were measured by the different satellites under consideration. Note that the distributions are quite similar despite wide separations of the satellites along the earth's orbit. From this we can conclude that differences in the calibration of the various instruments aboard the different satellites are small and any lack of correlation between satellites is real rather than instrumental.

If one can assume that the solar wind is emitted uniformly at all pertinent latitudes, that the emission is steady in time, and that the solar plasma moves radially with a constant convective speed near 1 AU, then it should be possible to predict the arrival of solar wind speeds at one satellite on the basis of earlier measurements at another. Comparison of the data will provide a test of the validity of the assumptions. Figures 5 and 6 are scatter plots of the Pioneer 6 and 7 daily measurements against the Vela daily measurements. In constructing these plots the Pioneer data were shifted in time for the expected earth-arrival based on a synodic rotation rate of 27 days; in that sense, the measurements are "simultaneous." Shifts of from 6 to 12 days are involved in these plots. Were there good agreement between the Pioneer predictions and the Vela measurements near the earth, then the points in these plots would cluster close to the 45° line drawn. This does not appear to be the case. In fact, when one calculates the correlation

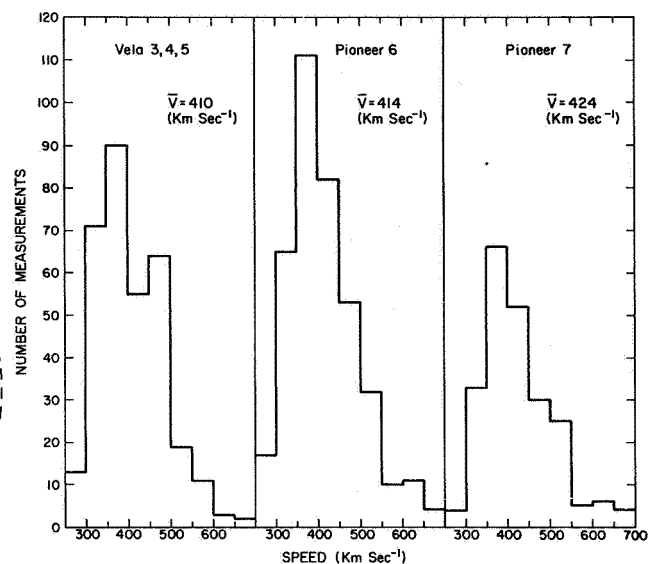


**Figure 4.** Histograms of the daily average solar wind speeds measured by Pioneer 6 and 7 and Vela 3, 4, 5 during 1969-1970. Note the similarities of the histograms including the near equivalence of average ( $\bar{V}$ ) and most probable speeds [from Gosling, 1971a].

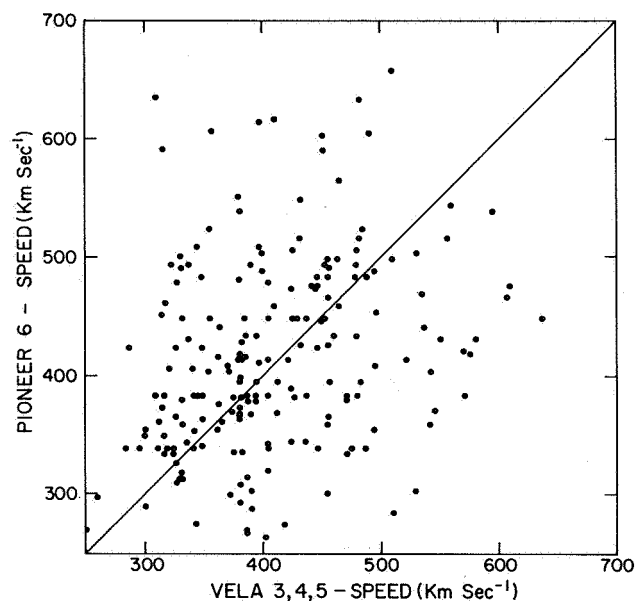


**Figure 5.** Scatter plot of Pioneer 6 and Vela 3, 4, 5 solar wind speed data. The data from the two satellites are simultaneous in the sense discussed in the text. Temporal shifts of 6 to 13 days are involved [from Gosling, 1971a].

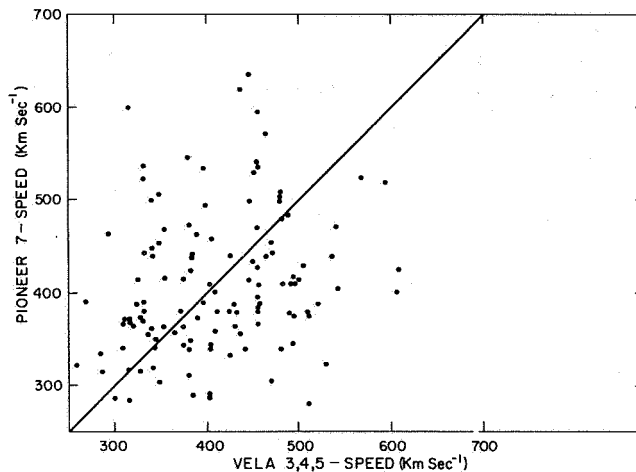


**Figure 6.** Scatter plot of Pioneer 7 and Vela 3, 4, 5 solar wind speed data. The data from the two satellites are simultaneous in the sense discussed in the text. Temporal shifts of 6 to 13 days are involved [from Gosling, 1971a].

coefficients for these plots one finds correlations of 0.37 and 0.29, respectively, for the Pioneer 6 and 7 plots, indicating that this is not a very good way to make predictions of the solar wind speed at the orbit of the earth [Gosling, 1971b].

Using the Pioneer satellites it is possible to show that the degree of correlation between satellites depends on the separation of the satellites. We note that the Pioneer satellites were moving in opposite directions relative to the earth and passed one another in December, 1969. Figure 7 is a scatter plot of the Pioneer 7 data against the Pioneer 6 data for spatial separations of 2 days or less (in the corotation sense). As before, the data have

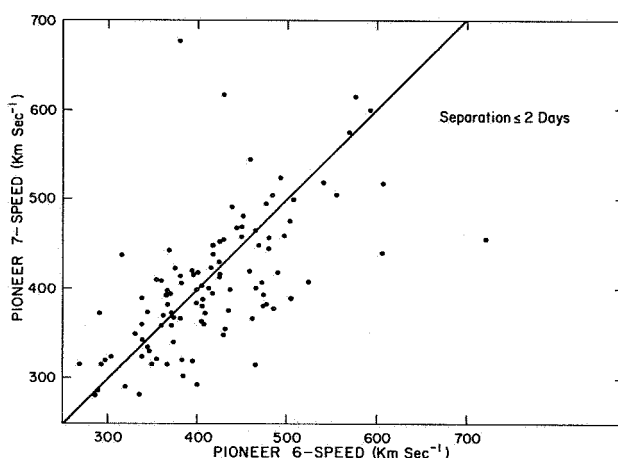


**Figure 7.** Scatter plot of Pioneer 6 and 7 solar wind speed data for satellite separations of less than 2 days in the corotation sense [from Gosling, 1971a].

been shifted in time and are "simultaneous" in the corotation sense. It is evident that here the two sets of data are more closely, although imperfectly, correlated (the correlation coefficient is 0.66). Figure 8 is a corresponding plot of the Pioneer 6 and 7 data for spatial separations greater than 4 days. We see that this plot resembles the Pioneer-Vela plots, although the available number of data points is considerably reduced. The calculated correlation coefficient is 0.28.

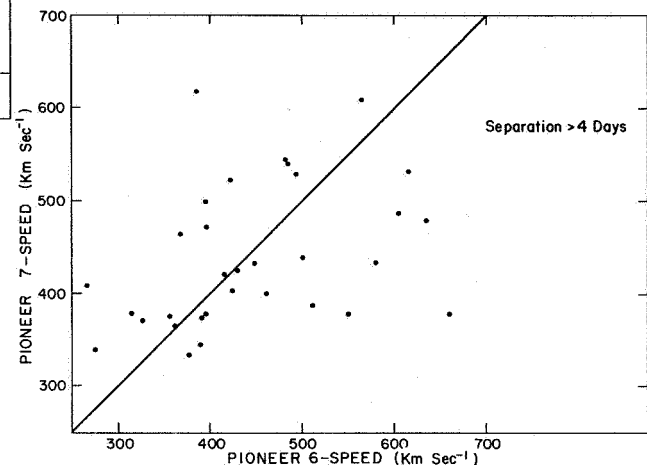


**Figure 8.** Scatter plot of Pioneer 6 and 7 solar wind speed data for satellite separations of 4 days or greater in the corotation sense [from Gosling, 1971a].

We can summarize the above results as follows: the assumption of a steady state, constant velocity solar wind, emitted uniformly over several degrees of solar latitude, flowing nearly radially near 1 AU and corotating with the sun is seldom sufficient for correlation of measurements between observers separated by more than 4 days in the corotation sense; for lesser separations, the correlation improves under these assumptions although remaining imperfect even for separations of 2 days or less. The weakest parts of our assumptions are those of steady state and uniformity with solar latitude. Thus, we can conclude that either temporal evolution processes typically alter the speed of the wind emanating from particular solar regions on a time scale of approximately 4 days and/or the solar wind expansion is a very sensitive function of solar latitude [Gosling, 1971a].

We have already noted that the solar wind speed is quite persistent at the orbit of the earth. Stated another way, closely spaced measurements (in time) are seldom independent of one another. An autocorrelation analysis at short lag times provides a method of establishing the typical time interval over which measurements of the speed demonstrate persistence. Figure 9 displays the autocorrelation of the Vela 2 and 3 speed data near zero

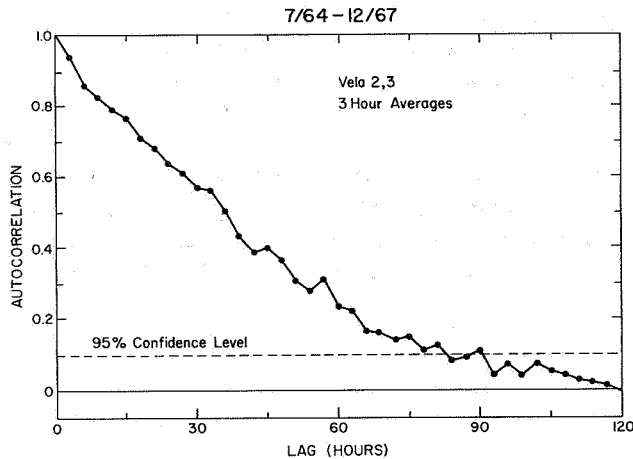


**Figure 9.** Autocorrelation of Vela 2 and 3 3-hr average solar wind speed data near zero lag. Significant correlations extend out to a lag of about 75 hr [from Gosling and Bame, 1972].

lag using 3-hr averages. A statistically significant persistence is observed out to a lag of 75 hr. Thus, on the average, measurements separated by 3 days or more are independent of one another, while those separated by less than 3 days are not. Either temporal evolution of the outer solar atmosphere or solar rotation and a finite spatial scale size of speed structures can be dominant in limiting persistence at the earth. If persistence is limited by solar rotation effects, then emission from the sun must typically be coherent over about  $40^\circ$  ( $13.3^\circ/\text{day} \times 3$  days) in longitude. (The actual scale size back at the sun may be smaller or larger than this depending upon the degree and manner in which the flow departs from the radial.) It seems reasonable to assume that the emission should be coherent over a similar extent in latitude; if so, solar latitude effects are insufficient to explain the results of the Pioneer-Vela study. It is well to note,

## DISCUSSION

*E. C. Roelof* In the proceedings of the Budapest conference on Cosmic Rays in 1969, Balasubrahmanyam, Bukata, Palmeira, and I presented a paper covering one of the periods here, namely the end of 1966. We did an autocorrelation and cross-correlation analysis of the quiet time cosmic ray flux near the earth, and at Pioneer 6, some  $50^\circ$  west of the earth. We detected corotating regions, quasi-rigid regions of cosmic ray variations that seem to be related to your solar wind streams. Just eyeballing your figure, I would say our autocorrelation and cross-correlation curves look very similar to your solar wind auto- and cross-correlation curves. So, maybe even the GEV particles are telling us something about the solar wind.

*J. H. Wolfe* The Pioneer 6 and 7 comparisons you're talking about here are around 1969, 1970, aren't they?

*J. Gosling* The Vela autocorrelation data are 1964 through 1967; the Vela and Pioneer

however, that latitude and longitude effects in the solar wind are fundamentally different owing to solar rotation and the attendant interaction of high and low speed longitudinal structures [Siscoe et al., 1969; Hundhausen, 1971]. If we can neglect such effects, we can conclude that it appears that true temporal processes generally dominate the solar wind speed variations on a time scale of 4 days or greater, with rotational effects becoming increasingly more important at shorter intervals. Stated another way, for an observer rotating with the sun the solar wind speed typically would be "steady" for approximately 2 or 3 days; after about 4 days an entirely new velocity regime would be established. We emphasize that the above represents only a typical situation; as noted earlier, certain velocity structures do endure at the earth for longer than 28 days.

## REFERENCES

- Brooks, C. E. P.; and Carruthers, N.: *Handbook of Statistical Methods in Meteorology*. Her Majesty's Stationery Office, London, 1953, pp. 220, 221, 377.
- Gosling, J. T.: Variations in the Solar Wind Speed Along the Earth's Orbit. *Solar Phys.*, Vol. 17(2), 1971a, p. 499.
- Gosling, J. T.: Predicting the Solar Wind Speed. To be published in *Developments in the Observation and Prediction of Solar Activity*, edited by M. Dryer and P. McIntosh, 1971b.
- Gosling, J. T.; and Bame, S. J.: Solar Wind Speed Variations 1964-1967: An Autocorrelation Analysis. *J. Geophys. Res.*, Vol. 77, 1972, p. 12.
- Hundhausen, A. J., private communication, 1971.
- Siscoe, G. L.; Goldstein, S. B.; and Lazarus, A. J.: An East-West Asymmetry in the Solar Wind. *J. Geophys. Res.*, Vol. 74, 1969, p. 1759.
- Solar Geophysical Data Reports*, U.S. Dept. of Commerce, ESSA (now NOAA), Boulder, Colorado.

correlation study was 1969, 1970. So we're actually comparing data from two different times.

*J. H. Wolfe* We are specifically comparing 6 and 7. What dates were those?

*J. Gosling* That's 1969-70.

*J. H. Wolfe* I think that if you go back to the Mariner 2 and IMP-1 solar wind data, you will find several rotations in which the speed structure was repeated almost identically. In that case an observer rotating with the sun would not see things evolve in 4 days but perhaps could see steady-state conditions throughout the solar rotation.

*J. Gosling* I don't mean to imply that all velocity structures evolve on a time scale of 4 days. I do say that this time scale is typical of the 1964-1967 data and the 1969-1970 data. Even here, however, there are some stationary structures that endure for several solar rotations.

*J. H. Wolfe* These data were taken during an interval of changing sectors rather than during relatively quiet intervals.

*J. Gosling* That's certainly true. Even in these data there are certain periods when the solar wind is more stationary than at other times. From one solar rotation to the next you sometimes see the same feature. Typically, that's not the case, however.

# AVERAGE THERMAL CHARACTERISTICS OF SOLAR WIND ELECTRONS

Michael D. Montgomery

**ABSTRACT** This contribution presents average solar wind electron properties based on a 1 year Vela 4 data sample—from May 1967 to May 1968. Frequency distributions of electron-to-ion temperature ratio, electron thermal anisotropy, and thermal energy flux are presented. The resulting evidence concerning heat transport in the solar wind is discussed.

## INTRODUCTION

As is well known, the information concerning electrons in the solar wind published to date is quite fragmentary [Wolfe and McKibbin 1968; Serbu, 1968; Montgomery *et al.*, 1968; Ogilvie *et al.*, 1971]. Here we present some average solar wind electron properties based on a more extended and significant Vela 4 data sample. The sample to be used covers the year from May 1967 to May 1968. We concentrate on the thermal properties of the electron component of the plasma, in particular, the electron-to-ion temperature ratio, the electron thermal anisotropy, the total pressure anisotropy, and thermal conduction properties.

## ELECTRON-TO-ION TEMPERATURE RATIO

Figure 1 contrasts the proton and electron temperature variation with solar wind speed. Approximately 6000 temperature measurements from the one-year interval defined above are divided into 100 km/sec speed intervals. The averages within each interval are plotted versus solar wind speed. The proton temperature-velocity relationship is essentially the same as has already been published [Burlaga and Ogilvie, 1970; Hundhausen *et al.*, 1970]. In contrast, the electron temperature is almost constant but there is a possible slight increase with velocity. This rise may be due to a small amount of electron heating associated with the interaction region between high- and low-velocity streams [Burlaga *et al.*, 1971; Hundhausen and

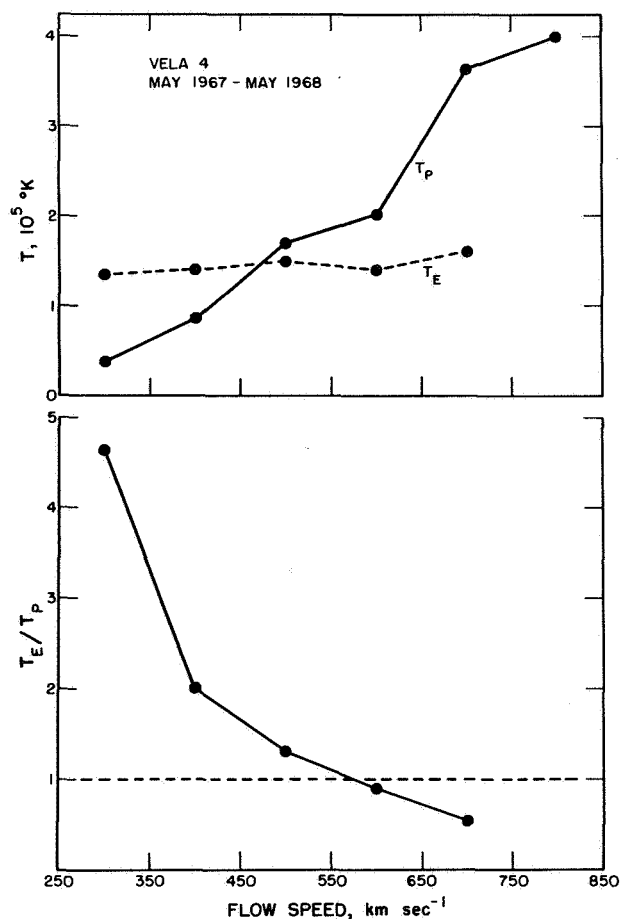


**Figure 1.** Variation of electron and proton temperature with flow speed. Each point represents an average over a 100 km sec<sup>-1</sup> interval.

The author is at the University of California, Los Alamos Scientific Laboratory, Los Alamos, New Mexico.

Montgomery, 1971]. The electron-to-proton temperature ratio is plotted in the lower panel of figure 1. During quiet times (low solar wind speeds) an electron-to-ion temperature ratio of about 4 is a good average. However, since most of the measurements are situated at about 400 km/sec, the overall average temperature ratio is about 2. The fact that the electron temperature in the solar wind is much more constant than the proton temperature can be explained by the relatively high thermal conductivity of the electrons [Hundhausen and Montgomery, 1971].

### ELECTRON THERMAL ANISOTROPY

Figure 2 shows the Vela 4 proton thermal anisotropy distribution. This distribution differs little from that of Vela 3 [Hundhausen *et al.*, 1970]. The Vela 4 average of 1.5 is somewhat smaller than the average of 1.9 from Vela 3, but it must be understood that what is measured is the projection of the temperature ratio onto the plane of analysis [Hundhausen *et al.*, 1967; Montgomery *et al.*, 1970]. Thus, the fact that the spin axis of Vela 4 was always pointed away from earth along a radius vector while that of Vela 3 was nearly perpendicular to the

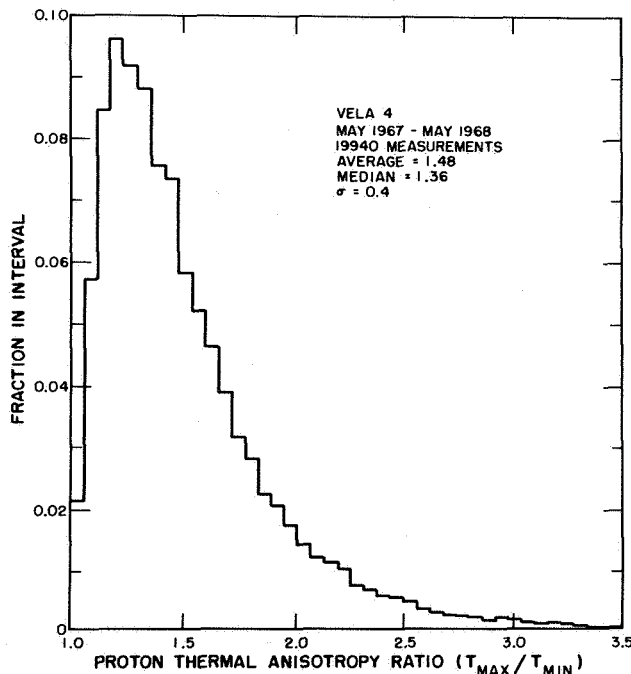


**Figure 2.** Distribution of proton thermal anisotropy. 90 percent of the values are  $< 2.0$ .

ecliptic plane may account for the smaller average Vela 4 value. The histogram showing the distribution of electron temperature anisotropy measured by Vela 4 is

presented by figure 3. It can be easily seen that the average is *much smaller* than for protons—about 1.1. If one takes into account the projection on the analysis plane, the true value could be as high as 1.2.

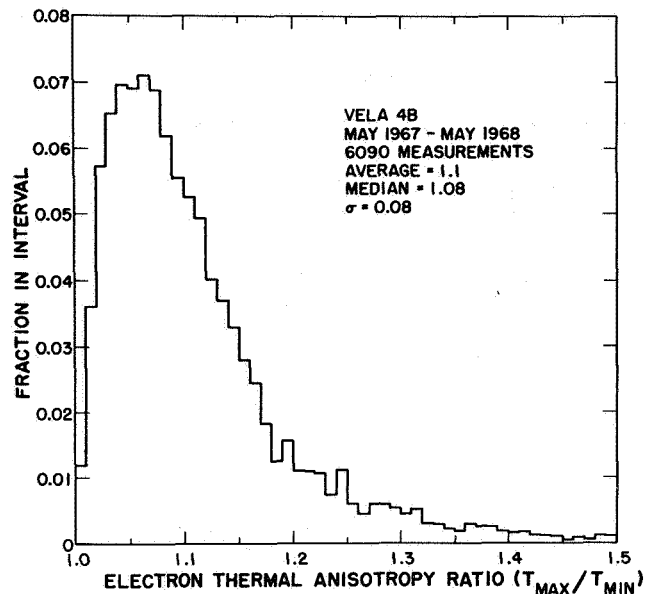


**Figure 3.** Distribution of electron thermal anisotropy. 90 percent of the values are  $< 1.22$ .

### TOTAL PRESSURE ANISOTROPY

For those interested in doing magnetohydrodynamic calculations, the total pressure anisotropy is of major interest. The total pressure anisotropy distribution is given by figure 4. The average is about 1.2; but due to projection, it could be as high as, but probably less than, 1.4. Thus, for most purposes, thermal anisotropies are relatively unimportant in the solar wind.

### THERMAL CONDUCTION

The Vela results concerning thermal conduction are summarized in figure 5. This figure simply shows the measured thermal energy flux distribution where, again, the measured values are really projections onto the spacecraft equatorial plane. The effect of the projection is probably less than about  $\sqrt{2}$ ; that is, the true magnitudes of the energy flux are probably about  $\sqrt{2}$  times greater than indicated. It should be noted that the average value given here of  $\sim 7 \times 10^{-3} \text{ erg cm}^{-2} \text{ sec}^{-1}$  turns out to be less than that given by early samples of Vela 4 data [Montgomery *et al.*, 1968] where a range of  $0.005\text{--}0.02 \text{ erg cm}^{-2} \text{ sec}^{-1}$  was quoted. It is instructive to compare the measured thermal energy flux with what one would expect assuming completely collision

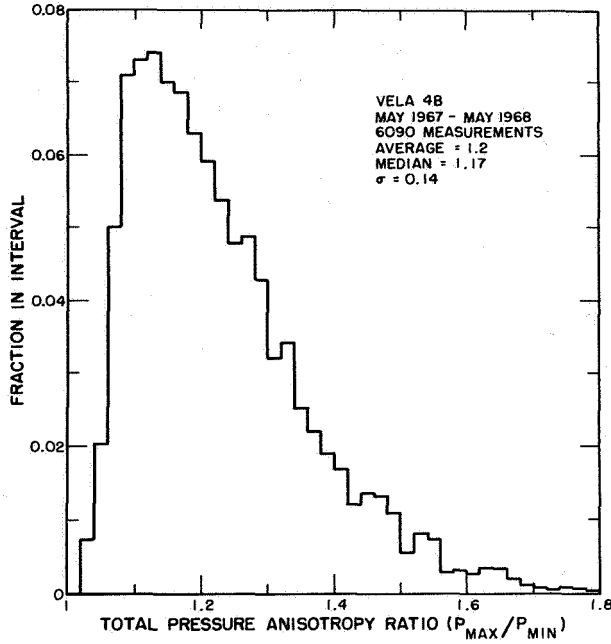


**Figure 4.** Distribution of total pressure anisotropy. 90 percent of the values are  $< 1.42$ .

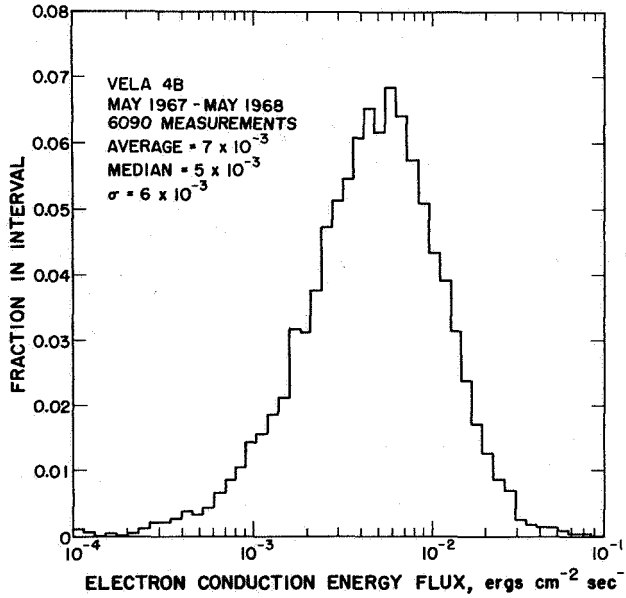


**Figure 5.** Distribution of electron heat conduction flux density.

dominated classical thermal conductivity [Spitzer and Härn, 1953; Forslund, 1970]. This comparison can be carried out with the aid of a dimensionless parameter  $B_T$  that was used as an expansion parameter in the Spitzer-Härn approximation. The Spitzer-Härn approximation is expected to be valid only for  $B_T \ll 1$  [Forslund,

1970]. The parameter  $B_T$  can be defined in two equivalent ways:

$$B_T \equiv \lambda_{mfp} / \lambda_{\nabla T} \quad (1)$$

or

$$B_T \equiv E_F / E_F(sat) \quad (2)$$

where  $\lambda_{mfp}$  is the electron-electron collision mean free path,  $\lambda_{\nabla T}$  is the scale length of the thermal gradient in the solar wind  $(dT/T dr)^{-1}$ ,  $E_F$  is the measured energy flux, and  $E_F(sat)$  is the saturation energy flux defined as the energy flux obtained if the internal energy of the electrons is transported at the electron thermal speed [Parker, 1964]. For this study a conduction-dominated radial temperature dependence of  $T = T_0(r/r_0)^{-2/7}$  and a magnetic field direction of  $45^\circ$  from radial were assumed. Under these assumptions, (1) can be rewritten as

$$B_{T2} = 1.8 \times 10^{-10} T_E^2 / n \quad (3)$$

where  $T_E$  is electron temperature ( $^\circ K$ ) and  $n$  is particle density in  $cm^{-3}$ , and (2) can be rewritten

$$B_{T1} = E_F / V_{th} (3/2) n k T_E \quad (4)$$

where  $V_{th}$  is the electron thermal speed. Both  $B_T$  can be evaluated by measuring  $T_E$ ,  $n$ , and  $E_F$ , and then compared. The results are shown in figure 6 where the dashed histogram represents the distribution of  $B_{T2}$

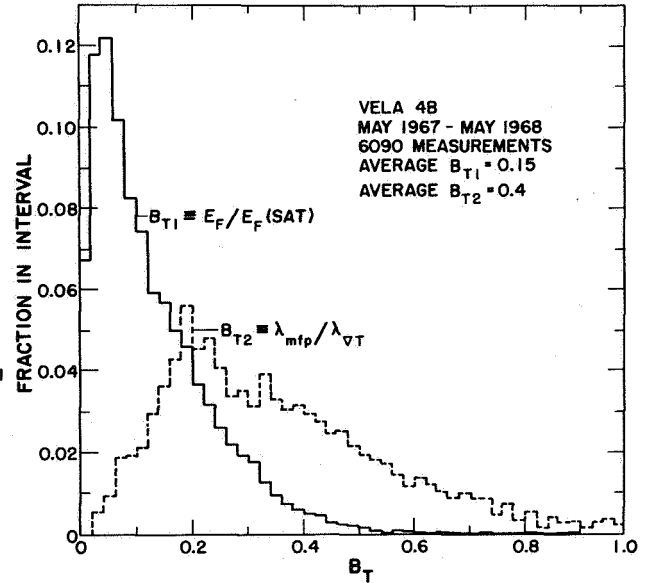


**Figure 6.** Comparison of experimental ( $B_{T1}$ ) and theoretical ( $B_{T2}$ ) heat flux parameters. See the text for definitions and discussion.



evaluated from (3) while the solid histogram represents  $BT_1$  evaluated from (4). It is important to note that there is a significant difference in the average values of  $BT_1$  and  $BT_2$ . In fact, they differ by about a factor of 3. A likely conclusion is that use of the collision-dominated conductivity is probably not valid, and a quasi-collisionless kind of conductivity should be substituted. Other papers in this chapter include some discussion on this point; see Comments by Perkins (p. 215). In addition, since large  $BT$  implies a large skewing of the electron velocity distribution, it is possible that plasma instabilities may contribute to the reduction of the thermal conductivity [Forslund, 1970].

## SUMMARY

A representative one-year sample of Vela 4 solar wind data gives the following results:

1.  $T_E$  is much less variable than  $T_P$ .
2. Thermal anisotropies are much smaller for electrons than for protons.
3. The total pressure anisotropy in the solar wind is small and relatively unimportant for many purposes.
4. The measured thermal energy flux in the solar wind is much smaller than expected on the basis of a collision dominated thermal conductivity. Thus, the actual thermal conductivity of the solar wind is probably significantly less than the classical value. This reduction in conductivity may be due to heat-conduction-generated plasma instabilities.

## ACKNOWLEDGMENTS

The Vela nuclear test detection satellites have been designed, developed, and flown as a part of a joint program of the Advanced Research Projects Agency of the U.S. Department of Defense and the U.S. Atomic Energy Commission. The program is managed by the U.S. Air Force.

## REFERENCES

Burlaga, L. F.; and Ogilvie, K. W.: Heating of the Solar Wind. *Astrophys. J.*, Vol. 159, 1970, p. 659.

## COMMENTS

*J. D. Scudder* The variability of interplanetary magnetic field from its average spiral configuration is exploited in this analysis of data from the OGO-E electron spectrometer to determine the energy flux transport in the rest frame of the plasma in the solar wind. We have proceeded on the hypothesis that the velocity distribution is axially symmetric about the magnetic field direction and roughly time independent on a time scale of several hours, as you have seen indicated in Montgomery's data. The rough time independence of the velocity distribution essentially implies that it is constant in shape when described about the magnetic field direction. Under this hypothesis we have determined the magnitude of the energy transport vector per unit solid angle, which we

Burlaga, L. F.; Ogilvie, K. W.; Fairfield, D. H.; Montgomery, M. D.; and Bame, S. J.: Energy Transfer at Colliding Streams in the Solar Wind. *Astrophys. J.*, Vol. 164, 1971, p. 137.

Forslund, D. W.: Instabilities Associated with Heat Conduction in the Solar Wind and Their Consequences. *J. Geophys. Res.*, Vol. 75, 1970, p. 17.

Hundhausen, A. J.; and Montgomery, M. D.: Heat Conduction and Nonsteady Phenomena in the Solar Wind. *J. Geophys. Res.*, Vol. 76, 1971, p. 2236.

Hundhausen, A. J.; Asbridge, J. R.; Bame, S. J.; Gilbert, H. E.; and Strong, I. B.: Vela 3 Satellite Observations of Solar Wind Ions: A Preliminary Report. *J. Geophys. Res.*, Vol. 72, 1967, p. 87.

Hundhausen, A. J.; Bame, S. J.; Asbridge, J. R.; and Sydorak, S. J.: Solar Wind Proton Properties: Vela 3 Observations from July 1965 to June 1967. *J. Geophys. Res.*, Vol. 75, 1970, p. 4643.

Montgomery, M. D.; Bame, S. J.; and Hundhausen, A. J.: Solar Wind Electrons: Vela 4 Measurements. *J. Geophys. Res.*, Vol. 73, 1968, p. 4999.

Montgomery, M. D.; Asbridge, J. R.; and Bame, S. J.: Vela 4 Plasma Observations Near the Earth's Bow Shock. *J. Geophys. Res.*, Vol. 75, 1970, p. 1217.

Ogilvie, K. W.; Scudder, J. D.; and Sugiura, M.: Electron Energy Flux in the Solar Wind, submitted to *J. Geophys. Res.*, 1971.

Parker, E. N.: Dynamical Properties of Stellar Coronas and Stellar Winds, 2, Integration of the Heat Flow Equation. *Astrophys. J.*, Vol. 139, 1964, p. 93.

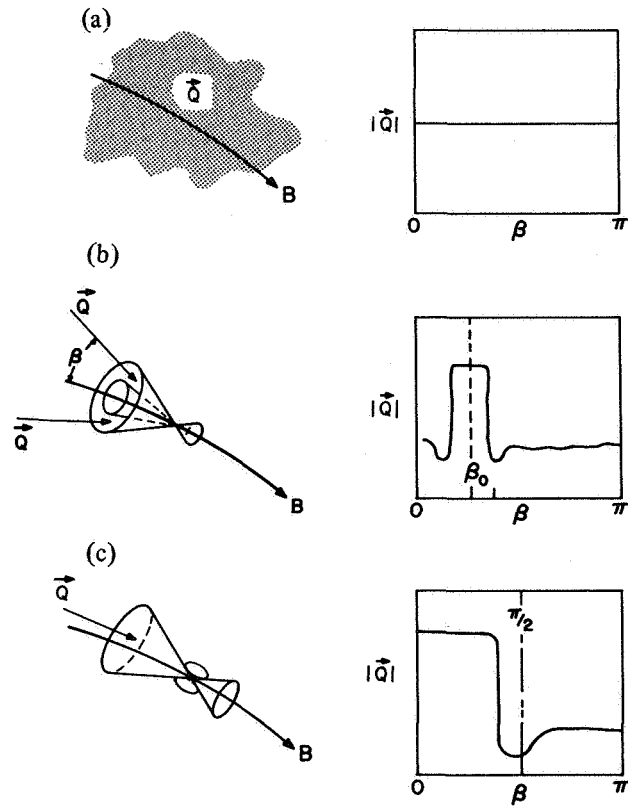
Serbu, G. P.: Low-Energy Plasma Measurements Obtained in Lunar Orbit. *Trans. Amer. Geophys. Union*, Vol. 49, 1968, p. 234.

Spitzer, L., Jr.; and Härm, R.: Transport Phenomena in a Completely Ionized Gas. *Phys. Rev.*, Vol. 89, 1953, p. 977.

Wolfe, J. H.; and McKibbin, D. D.: Pioneer 6 Observations of a Steady-State Magnetosheath. *Planet Space Sci.*, Vol. 16, 1968, p. 953.

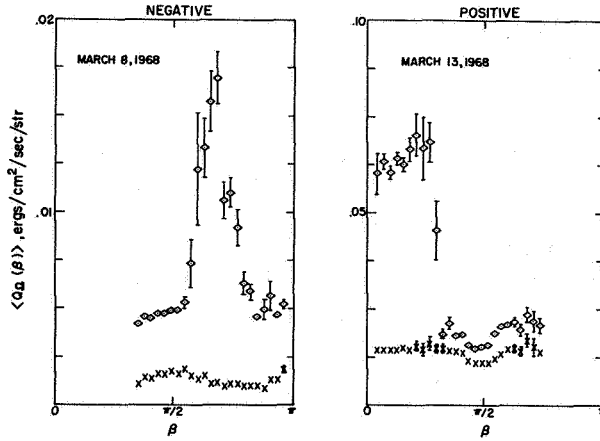
call  $Q_\Omega$ , by computing the third moment of the empirical distribution function. Because of time limitations I will not show you exactly why you would expect this to be non-zero, but you've probably seen it in the literature. The asymmetry of the velocity distribution essentially gives rise to this non-zero character.

Figure 1 is a schematic idealization of what one might expect for energy transport per unit solid angle. If the energy flow were isotropic and one plotted the magnitude of  $Q_\Omega$  versus  $\beta$ , which is the angle the transport direction would make with the magnetic field line, one would get essentially an isotropic picture as indicated in the top panel; if there were some preferred direction for the flow with respect to the field one would see something like the right-hand side of the middle panel; if the preferred direction were that of the magnetic field, one would either see something like the lower panel of this figure or its mirror image in the line  $\beta = \pi/2$  if the interplanetary magnetic field polarity were reversed.



**Figure 1.** Schematic representation of energy flux density  $\langle Q_\Omega(\beta) \rangle$  versus  $\beta$  for various physical situations; (a) energy flux uncorrelated with field direction; (b) correlation with empty cone about field; (c) energy flux filling cone about field line.

If one assembles the data in this manner we see typically something which looks like the lower two panels. Two examples of our data have been plotted in figure 2 with only worst error bars indicated. If the data points don't have error bars on them the errors are too small to show. What one can see in this figure is that the flow direction for the flux is basically outward from the sun, regardless of sector polarity and is controlled by the field direction for a selected time interval when there is a good idea there is *no* bow shock intersection (from the vector magnetic field on the same spacecraft). The rather



**Figure 2.** Plots of  $\langle Q_{\Omega}(\beta) \rangle$ , the differential contributions to the energy flux density per unit solid angle, for angular intervals of  $5^\circ$ . Note that  $\beta$  is the angle between  $\mathbf{v}$  and  $\mathbf{B}$ . Sector polarity as indicated. Diamonds imply  $E_u = 9.9$  keV; crosses,  $E_u = 0.340$  keV.

well-defined cone of energy flux transport per unit solid angle at  $\beta$  less than  $50^\circ$  and the approximate flatness of the step for the positive sector example indicates a uniform population in this cone. The relative minima at  $\pi/2$  suggest some inhibition of energy transport in the transverse direction. A similar example for a negative sector also shows outward flow as well as field control much like the middle panel of figure 1.

On a shorter time scale we can see the same type of phenomena, in figure 3, where we have plotted for the three mutually orthogonal detectors of our spectrometer system the magnitude of  $Q_{\Omega}$  as computed from each one of them. The point to keep in mind here is that this data is for a time period determined as an outward sector; therefore, if the flux transport is along the magnetic field line (if  $\beta$  is small) as in the top detector, the

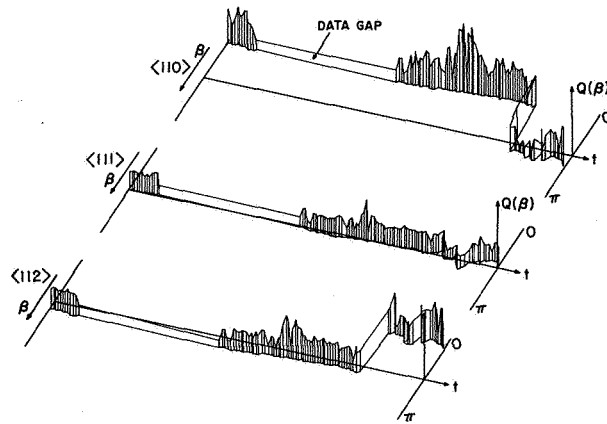


**Figure 3.** Isometric plots for each detector showing that the largest flux is detected by that detector "looking" closest to the magnetic field line, and that this condition is preserved as the magnetic field direction shifts with respect to the triad of directions of the detectors. This is interpreted as showing that the energy flux is greatest along the field direction away from the sun.

amplitude of  $Q_\Omega$  should be large, as it is. If  $\beta \gtrsim \pi/2$  the magnitude of  $Q_\Omega$  is rather small, as it is monitored by detector (111) and, you can see in detector (112) that if the field is shifting from the transverse direction into the forward cone the amplitude of  $Q_\Omega$  the energy flux transport per unit solid angle is increasing as it comes into the forward cone. We have concluded on the basis of this and other examples that the axis of the  $Q_\Omega$  cone (i.e., the energy flux transport cone) is that of the *vectorial* field line, so that on average the *net* energy transport is away from the sun regardless of the sector designation when not on field lines intersecting the shock.

Previous measurements by Montgomery and Ness have shown that  $Q_\Omega$  is parallel to the projection of  $B$  into the plane of their analysis. The result here is basically an extension of their result, using the entire vectorial magnetic field.

The magnitude of the *net* energy flux transport in the plasma frame is just the projection of this vector onto the magnetic field. It is important to note that  $Q_\Omega$  as shown here is an integral over a finite interval of the velocity distribution function. Therefore, it is implicitly a function of the uppermost energy included in the distribution function itself.

In the lower panel of figure 4 we present several curves of  $E$  parallel, that is, the net energy transport in the rest frame of the plasma, versus the upper energy involved in the empirical distribution function. The spectrometer on OGO-5 assembled the velocity distribution function from 10 eV to 10 kV. The curves shown here are for three successive passages in the interplanetary medium near apogee where field line intersection with the bow shock was highly improbable. The important things here are the two domains apparent in these examples. The convergent region of  $E_\parallel(E_u)$ ,  $E_u \sim 210-340$  eV, and the divergent contributions to  $E_\parallel$  above this point. Although  $E_\parallel(E_u)$ ,  $E_u \gtrsim 340$ , shows increasing divergences for the three examples  $E_\parallel(E_u)$ ,  $E_u < 300$  eV, remains relatively insensitive to the modified form of the distribution at higher energies which causes the divergence. We understand this temporal variability of  $E_\parallel$  as being caused by particles associated with a delayed type solar electron event, as has been discussed in the literature by Lin and Anderson. You can see plotted on the top of this same figure the integral electron fluxes above 22 kV and above 45 kV, respectively, from Lin's particle counters on Explorer 35 orbiting the moon. The day when our  $E$  parallel vs.  $E_u$  curve is least divergent corresponds to the point (A) in Lin's fluxes where the integral fluxes above 22 kV are essentially at the quiet background that they have been at for some several days previous. On day 71, when we start to see an increasingly divergent behavior indicating particle populations down as low as 1 kV being influenced we see a thirtyfold enhancement (at point B) of Lin and Anderson type particles between 22 and 45 kV. If we take the spectra that we have on day 71, and we take information that Bob Lin was able to supply us on the spectral index between 25 and 45 kV and piece together the velocity distribution function within the errors of absolute intercalibration, the velocity distributions fit together very nicely. Thus we have an example of the solar wind plasma velocity distribution function merging with some type of transient phenomena.

Also of interest is an experimental value for  $H_\parallel$  predicted by solar wind theories as the heat conduction under quiet solar wind expansion. Among other things, these theories assume a spherically symmetric corona and do not take into account transient energy flow injections. Therefore, it should not be too hard to swallow the idea that  $H_\parallel$ , the heat conduction, as a component of the overall energy flow in the plasma rest frame, should be less than any quantity plotted here. We have identified the value of  $E_\parallel$  in the convergence zone to be the quantity most directly associated with the quiet time heat flux,  $H_\parallel$ . Then  $H_\parallel \lesssim 4 \times 10^{-3}$  erg/cm<sup>3</sup> even during the height of the high energy solar particle fluxes. An absolute upper ground for a very conservative estimate would be  $E_\parallel$  (10 keV) on day 68  $\sim 1.6 \times 10^{-2}$ . These examples are from cases when the magnetic field line does not intersect the bow shock with a high probability. The results that Mike

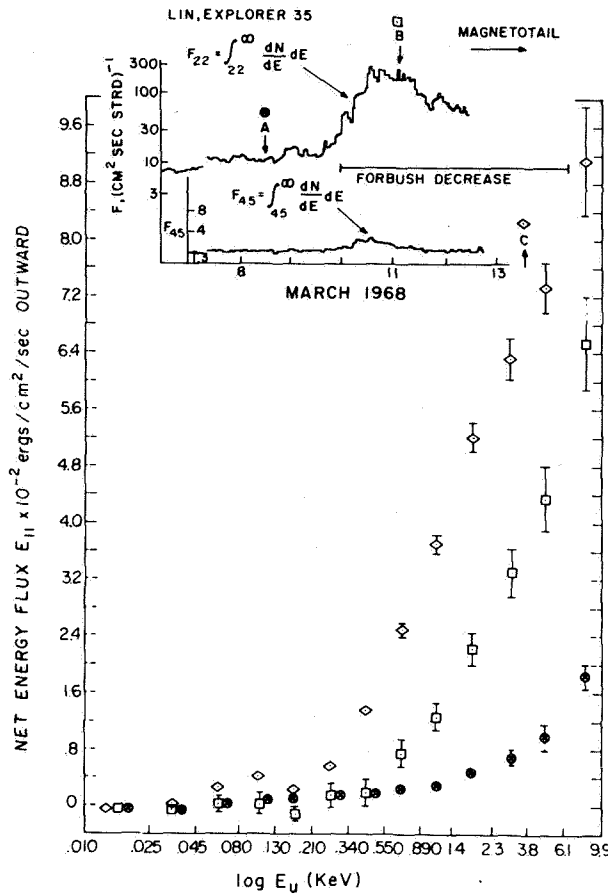


**Figure 4.**  $E_{||}$  as a function of  $\log E_u$  for three periods during a "delayed" electron event (Lin and Anderson, private communication). The circles (pt. A in the inset) refer to a time of low solar electron flux, the squares and diamonds (pt. B, C in the inset) refer to a time of higher solar electron flux. The event is discussed further in the text. Note how extrapolating back to  $E_{||} = 0$  on all three curves crosses the axis between 210–340 eV.

Montgomery has just presented are certainly consistent with this bound. Thus, in addition to our directional conclusions of  $E_{||}$  and also its transient behavior on a scale of several days, this determination shows that  $H_{||}$  is in fact small; it is small even in the sure absence of bow shock contaminations.

#### COMMENTS

*F. W. Perkins* I would like to present some thoughts on how you go about calculating the electron heat conductivity in a collisionless plasma. First of all, in order to describe how to compute the heat conductivity, let's look at the collisionless motion of electrons in the solar wind. The electrons move essentially at constant energy under the influence of an electrostatic radial electric field which occurs in all ionized atmospheres and holds the electron in and at constant magnetic moment  $\mu$ . Therefore the parallel motion of the electrons occurs in sort of a potential well; the bulk of the electrons have an oscillatory motion in the solar wind, bouncing back and forth between an electrostatic reflection on the outside and a magnetic mirror on the inside. A few energetic electrons are sufficiently energetic to overcome the potential barrier and escape; but with the bulk of electrons there is an oscillatory motion with an amplitude of the order of the radial distance  $r$

from the sun and a frequency which I call  $\omega_b \sim V_{the}/r$ , because it bounces back and forth, essentially given by the thermal speed divided by the radial distance  $r$ . The collisionless picture will apply provided this bounce frequency is bigger than the collision frequency.

Let's see how this is reflected in the electron velocity distribution. It is obvious from the last picture that for the bulk of the electrons they must have an essentially even distribution in  $V_{\parallel}$ . There will be a few escaping photoelectrons that override the potential. In the middle of this even distribution in  $V_{\parallel}$  sit the solar wind ions separated by the solar wind velocity. So the ions see most of the electrons drifting backwards. Second, this backward drift is well known to cause a lot of plasma instabilities. This is the type of velocity distribution Forslund used in discussing plasma instabilities associated with thermal conduction. The point I would like to make here is that thermal conduction and temperature gradients aren't really necessary to produce this type of velocity distribution. It's a natural type of velocity distribution the solar wind electrons would get into if the collisions just stopped; and I think it's this type of velocity distribution that is equally important compared with the anisotropies in driving plasma wind instabilities.

Let's see how this all fits in with the heat conductivity  $k$ . Heat conductivity, like a diffusive process, is proportional to the square of the step size times the frequency at which this step size happens, and for the heat conductivity you have to put in the number density. But in the Spitzer conductivity the step size is essentially the thermal speed divided by the coulomb collision frequency. If this step size is longer than the average bounce motion, then the Spitzer conductivity does not apply. If you put the step size together with the coulomb collision frequency you get  $k \propto T_e^{5/2}$ —the neoclassical conductivity. Neoclassical is a word that is creeping into plasma physics literature confusion, which means that you do the right collisionless orbits but you put in the strict coulomb binary collisions. It comes out this way. For the step size we use the radial distance from the sun. For the collision frequency we use the coulomb collision frequency and thus, the scaling properties of this collision frequency are  $k \propto n^2 r^2 T_e^{-3/2}$ . A neoclassical conductivity will really inhibit the heat flow as the density gets lower. But I said that the velocity distribution causes plasma instabilities. And you can estimate the collision frequency associated with those instabilities just by requiring that collision frequencies essentially match an order of magnitude of the time scale in which this velocity distribution is set up. Well, this velocity distribution is set up in essentially one electron bounce time, and so I think that  $\omega_b$  is a good estimate for the collision frequency caused by instability. You use the same step size, you put in the bounce frequency, and this is what I would propose to use as a heat conductivity formula in the solar wind, and it scales like  $k \propto nr T_e^{1/2}$ .

Well, you can always put numbers in the conductivity formulas. If you do it for what I thought about before the talks was a reasonable value, you would get the Spitzer conductivity about a factor of 4 larger than the instability conductivity. You can also estimate the rate at which energy exchange must occur if you have a specific instability in mind. Here I have the ion-sound instability. It occurs at a much faster rate than it would from a coulomb collision of essentially the rate  $V_{SW} r^{-1}$ .

**DISCUSSION** *J. V. Hollweg* I have a comment and a question. The comment is that the electron distribution that you drew compared to the ion distribution looks like it implies a radial current from the sun which would lead to a loss of charge from the sun and therefore can't exist.

The question is, do you calculate electron thermal anisotropies in your model?

*F. W. Perkins* The velocity distribution that I discussed was supposed to have zero net moment compared to the outward going velocity of the solar wind. There were a few high energy escaping photoelectrons precisely equal to the net outward flow of ions. I don't

compute anisotropies. I imagine they would be very small because the electrons are essentially stuck in the solar wind, and execute many bounce motions.

*J. V. Hollweg* On that latter point, this calculation has similarities to a model that Jockers did of an exospheric solar wind. He considered electrons executing bounces, but the bounces were not mirror bounces. Instead the motion was equilibrated with the maxwellian distribution at the source. He found electron thermal anisotropies of the order of 3 which is, of course, much larger than observed.

On your first point, may I ask how the ion sound instability is driven if there is no current. Is it by heat conduction?

*F. W. Perkins* The ion sound instability depends on the slope of the electron velocity distribution in the neighborhood of the ions. It has a positive slope for a backward going wave. This model definitely predicts that backward going waves are unstable. Since the solar wind is both supersonic and super-Alfvénic it also predicts an instability for backward going Alfvén waves. All of this was brought out in Forslund's paper. This is just another way of getting the velocity distribution—perhaps in a way that is more physically motivated.

*Unidentified Speaker* In the previous talk on the energy flux you excluded the cases where the magnetic field lines intersected the bow shock. Can you tell us what happens under those circumstances?

*J. D. Scudder* Figure (A) shows the data for  $E_{\parallel}$  vs.  $E_u$  for an example where bow shock intersection was extremely probable on March 19, 1968 when the bulk speed

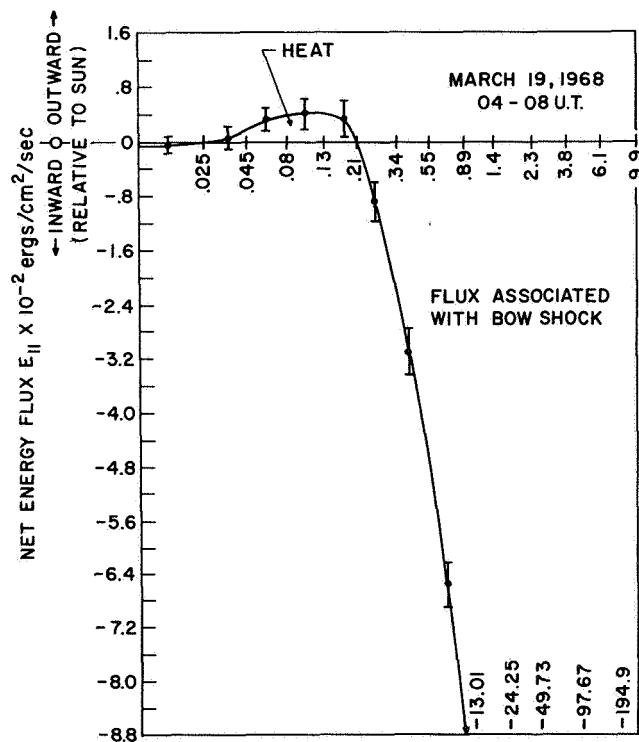


**Figure A.** The net energy flux  $E_{\parallel}$  plotted against  $\log E_u$ , the uppermost energy to which it is calculated. Values of  $E_{\parallel} > 0$  represent flux direction away from the sun, and values  $< 0$  represent flux toward the sun (away from the earth's bow shock) along the magnetic field line. In this example the field almost certainly intersects the earth's bow shock.

was  $\sim 600$  km/sec. We note again the presence of two domains, the convergent and divergent zones. The net heat flux (i.e.,  $E_{\parallel}$  ( $\sim 130$  eV)) is outwardly directed, whereas the divergent higher energy contribution flow is *toward* the sun with extremely large net reverse flows which swamp the outward heat flux at lower energy. So you can see that the magnitude of this reverse transport is quite large; therefore, if there is significant flux coming back up field lines that interfere with velocity distribution calculations in the large, it can tend to reduce the asymmetry of the distribution function and therefore reduce the third moment.

*M. Dryer* I have a question for Mike Montgomery. You showed the temperatures of the protons and the electrons plotted versus the velocity, in which the former increased while the latter stayed fairly constant. Does this indicate that there is a preferential heating of the protons at discontinuities of various kinds?

*M. D. Montgomery* Not necessarily. I think the proper interpretation is that in most nonsteady phenomena in the solar wind, the source strength of local heating is not strong enough to saturate completely the local thermal conductivity. Therefore, the conductivity is enough to spread that heat over a large region and the temperature gradients are small in the electrons, but large in ions.

*F. C. Michel* How is the conductivity related to the heat flux? It seems unlikely that kilovolt electrons, which you (Montgomery) find to contribute most of the heat flux, are going to flow in response to thermal gradients that are the order of only a few electron volts. Such a heat flux may be intrinsic and not generated by thermal gradients.

*M. D. Montgomery* In our distributions, which we believe were taken on field lines that don't connect to the bow shock (we have eliminated such data from the sample), most of the heat flux is carried by the electrons of much smaller energy than that. Most of the energy is carried by electrons of the order of 50 to 100 eV. Now, why this is higher than a few eV I can't tell you.

*J. D. Scudder* The figures we have shown are certainly consistent with the major portion of the heat flux coming from energies below  $\sim 80$  eV, just as Mike has indicated (cf. figs. 4 and A.)



# MODEL FOR ENERGY TRANSFER IN THE SOLAR WIND: MODEL RESULTS

Aaron Barnes and R. E. Hartle

We describe the results of calculations of solar-wind flow in which the heating is due to (1) propagation and dissipation of hydromagnetic waves generated near the base of the wind, and (2) thermal conduction. A series of models is generated for fixed values of density, electron and proton temperature, and magnetic field at the base by varying the wave intensity at the base of the model. This series of models predicts the observed correlation between flow speed and proton temperature for a large range of velocities. The wave heating takes place in a shell about the sun  $\gtrsim 10 R_{\odot}$  thick. We conclude that large-scale variations observed in the solar wind are probably due mainly to variation in the hydromagnetic wave flux near the sun.

## ABSTRACT

Hartle and Barnes (p. 248) describe the formulation of solar-wind models in which hydromagnetic-wave dissipation is part of the energy transport. Here we review the results of these calculations and their implications [Barnes *et al.*, 1971].

The base radius was chosen to be  $2 R_{\odot}$ , as in the investigation by Hartle and Barnes [1970] of the effects of artificially specified heat sources. The base number density, electron temperature, proton temperature, and magnetic field were chosen to be, respectively,  $n_0 = 1.46 \times 10^6 \text{ cm}^{-3}$ ,  $T_{e0} = 1.3 \times 10^6 \text{ }^{\circ}\text{K}$ ,  $T_{p0} = 1.7 \times 10^6 \text{ }^{\circ}\text{K}$ , and  $B_0 = 0.18 \text{ gauss}$ . These values are somewhat different from those used in the earlier work [Hartle and Barnes, 1970] with artificial heat sources, but are still consistent with coronal observations. The choice of proton temperature greater than electron temperature implies preferential heating of the protons below  $r = 2R_{\odot}$ ; this effect is consistent with coronal observation [Newkirk, 1967] and is predicted by D'Angelo's [1968, 1969] model of heating the inner corona. The circular frequency of the hydromagnetic waves was

chosen as  $\omega_0 = 2 \times 10^{-2} \text{ sec}^{-1}$ , which corresponds to the maximum noise in the chromosphere and photosphere [Leighton *et al.*, 1962; Tanenbaum *et al.*, 1969]. The results of these computations ( $n$ ,  $v$ ,  $T_e$ ,  $T_p$  and  $B$  at

**Table 1.** Number density, flow speed, electron and proton temperatures, and magnetic field strength at 1 AU

$F_0$ , erg cm <sup>-2</sup> sec <sup>-1</sup>	$n_E$ , cm <sup>-3</sup>	$v_E$ , km/ sec	$T_{eE}$ , °K	$T_{pE}$ , °K	$B_E$ , $\gamma = 10^{-5}$ gauss
0	20	210	$2.4 \times 10^5$	$8.5 \times 10^3$	3.5
$1.4 \times 10^3$	18	270	$2.3 \times 10^5$	$1.3 \times 10^4$	2.9
$2.2 \times 10^3$	16	290	$2.3 \times 10^5$	$2.0 \times 10^4$	2.8
$3.4 \times 10^3$	15	330	$2.2 \times 10^5$	$3.2 \times 10^4$	2.6
$4.5 \times 10^3$	14	360	$2.2 \times 10^5$	$5.0 \times 10^4$	2.4
$5.2 \times 10^3$	14	370	$2.2 \times 10^5$	$6.2 \times 10^4$	2.4
$5.8 \times 10^3$	14	380	$2.1 \times 10^5$	$7.9 \times 10^4$	2.4
$6.5 \times 10^3$	14	390	$2.1 \times 10^5$	$9.6 \times 10^4$	2.3
$1.2 \times 10^4$	13	430	$2.1 \times 10^5$	$1.7 \times 10^5$	2.2

Aaron Barnes is at the Space Science Division, Ames Research Center, NASA, Moffett Field, California. R. E. Hartle is at the Laboratory for Planetary Atmospheres, Goddard Space Flight Center, NASA, Greenbelt, Maryland.

$r = 1$  AU) are summarized in table 1 [from *Barnes et al.*, 1971]. The subscript  $E$  denotes the value of a quantity at 1 AU. This series of models implies a correlation between  $T_{pE}$  and  $v_E$  that may be compared against the observed correlation. This comparison is indicated in figure 1 [Barnes et al., 1971] where we plot  $T_{pE}^{1/2}$  against  $v_E$  to facilitate comparison with the empirical formula of *Burlaga and Ogilvie* [1970a]. The predicted and observed correlations agree for  $v_E \lesssim 430$  km/sec; most (about 70 percent) solar-wind observations lie in this velocity range [Hundhausen et al., 1970]. The range of agreement can probably be extended to about  $v_E = 450$  km/sec by adjusting the base conditions.

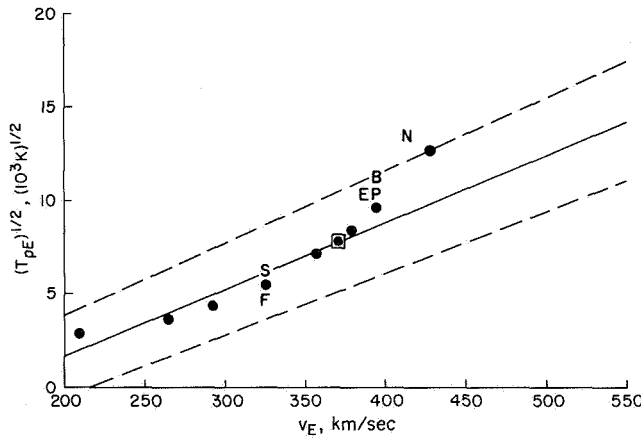


**Figure 1.** Correlation of  $T_{pE}^{1/2}$  and  $v_E$ . The units of  $T_{pE}$  are  $10^3$  °K. Solid and dashed lines are, respectively, the average and variances of the Burlaga-Ogilvie empirical formula. Filled circles (including the boxed one) correspond to models listed in table 1. Letters N, E, P, B correspond to models in which one (and only one) of the boundary conditions is modified from the main series, with  $F_0 \approx 5.2 \times 10^3$  ergs  $\text{cm}^{-2}$   $\text{sec}^{-1}$  (the corresponding main-series point is boxed): for N,  $n_0 = 1.2 \times 10^6 \text{ cm}^{-3}$ ; for E,  $T_{e0} = 1.2 \times 10^6$  °K; for P,  $T_{p0} = 1.6 \times 10^6$  °K; for B,  $B_0 = 0.2$  gauss. Letters S and F correspond to models with the same boundary conditions as the main series, but different wave frequencies; for S,  $\omega_0 = 10^{-2} \text{ sec}^{-1}$  and  $F_0 = 2.9 \times 10^3$  ergs  $\text{cm}^{-2}$   $\text{sec}^{-1}$ ; for F,  $\omega_0 = 4 \times 10^{-2} \text{ sec}^{-1}$  and  $F_0 = 3.9 \times 10^3$  ergs  $\text{cm}^{-2}$   $\text{sec}^{-1}$ . Reprinted courtesy University of Chicago Press © 1971.

Therefore, for the velocity range corresponding to most solar-wind observations, the observed temperature-velocity correlation is obtained for fixed base conditions by varying the single parameter  $F_0$  (the base hydro-magnetic wave energy flux). On the other hand, extension of the computed correlation curve indicates that

the predicted correlation will no longer agree with observation for velocities above 450 km/sec. One reason for this discrepancy may be that high-velocity winds come from coronal regions where the base conditions are different. However, it is also possible that the discrepancy is due to the large wave amplitudes associated with high fluxes ( $F_0 \gtrsim 10^4$  ergs  $\text{cm}^{-2}$   $\text{sec}^{-1}$ ), for at large amplitudes the dissipation rate probably increases, and hence moves the heat source inward; furthermore, at large amplitudes the momentum transfer by wave dissipation can be significant. Both processes will probably increase  $v_E$  more than  $T_{pE}$ , which would improve the agreement between the models and observation.

Table 1 also predicts correlations among the other flow parameters. For example, it indicates an inverse correlation between density and flow speed, which is observed, although the computed densities are systematically higher than what is observed by about a factor 2. The predicted electron temperature does not vary much with flow speed, consistent with observation [Burlaga and Ogilvie, 1970a]; the values of  $T_{eE}$  given in the table are 30 to 40 percent higher than reported measurements, but considerably lower than the values obtained in previous two-fluid calculations [Hartle and Sturrock, 1968; Hartle and Barnes, 1970]. Finally, the calculations predict an inverse correlation between the magnetic field  $B_E$  and the flow velocity; observational studies are not conclusive on this point [Burlaga and Ogilvie, 1970b]. The computed values of  $B_E$  are systematically smaller than observed by about a factor 2.

In summary, the correlations between velocity, density, and proton and electron temperatures are qualitatively consistent with observation, the electron temperature is somewhat higher than reported observations, and the density is high and the magnetic field low by about a factor 2. It may be that modifications in the model, such as the inclusion of nonradial flow and magnetic stresses, will be necessary to improve agreement between the predicted and observed values of density and magnetic field. On the other hand, it is possible that some improvement can be achieved by suitably changing the boundary conditions. We cannot at present make any conclusive remarks about the effects of varying the base conditions, because the large amount of computing time necessary for each model has limited the number of models that we have run. Such an investigation is planned. Some preliminary results on the effects of varying base conditions are indicated in figure 1, where we indicate the effects on the  $(T_{pE}, v_E)$  correlation. The effect of varying the wave spectrum

seems to be moving the  $(T, v)$  pair approximately along the observed correlation line, suggesting that this correlation is not very sensitive to the spectrum. Varying each of the base quantities  $n_0$ ,  $T_{p0}$ ,  $T_{e0}$ ,  $B_0$  tends to move the  $(T, v)$  pair away from the observed correlation, although certainly some variation in these quantities is consistent with observation.

It is established that the observed correlation between proton temperature and flow speed in the solar wind at the orbit of earth can be explained by models in which an efflux of fast-mode hydromagnetic waves is dissipated beyond  $2 R_\odot$ . From this viewpoint, the large-scale variability in the observed  $v_E$  (and corresponding  $T_{pE}$ ) is due primarily to the variability of this efflux (and possibly of its frequency spectrum) rather than variability of density and temperature at the base of the outer corona. The order of magnitude of the postulated efflux ( $10^{27}$  ergs/sec) is quite reasonable when compared with estimates of the power required to heat the inner corona ( $5 \times 10^{27}$  ergs/sec) and the chromosphere ( $5 \times 10^{29}$  ergs/sec) [Osterbrock, 1961]. Since the power that heats the outer corona and solar wind by wave dissipation is fairly small compared with the power required to maintain the inner corona, it seems plausible that the relative large-scale inhomogeneity in the wave flux at  $2 R_\odot$  is greater than the relative inhomogeneities in large-area averages of density and temperature, which would mean that the flow properties of the wind are mainly determined by the wave flux  $F_0$ . Finally, the wave periods chosen in these models (2.5 to 10 min) correspond to maximum photospheric and chromospheric disturbance [Leighton *et al.*, 1962; Tanenbaum *et al.*, 1969]. Altogether, then, the assumptions about the wave flux and spectrum are consistent with what is known about the solar chromosphere and corona.

The proton heating takes place over a very extensive region,  $10\text{--}20 R_\odot$  in radius, as may be seen from figure 2, in which wave efflux and proton heating are plotted against  $r$  for one of the higher velocity models. In this case, half the proton heating takes place beyond  $r = 6.2 R_\odot$ , and the last 10 percent of the proton heating occurs beyond  $r = 14 R_\odot$  (the subsonic-supersonic transition in these models occurs at  $r \sim 6 R_\odot$ ). Half the wave efflux is dissipated inside  $r = 6 R_\odot$ , but 5 percent survives beyond  $r = 15 R_\odot$ . Thus it appears that a (small) fraction of the noise generated by the convective envelope of a late-type star should play a significant role in driving a stellar wind, and, in part, this noise would survive as turbulence many stellar radii from the star.

There is evidence for the existence of a turbulent region about the sun. It has been proposed that observed solar cosmic-ray anisotropies can be understood in terms

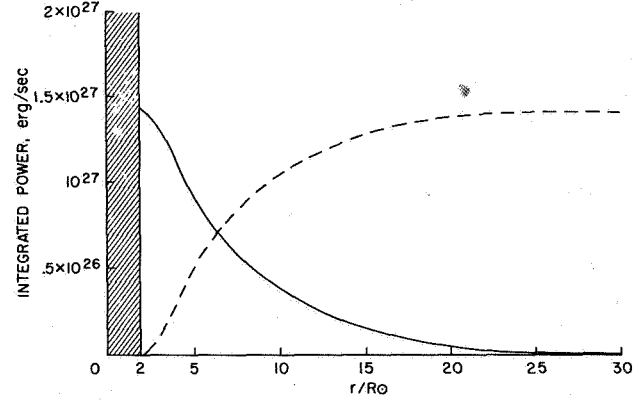


**Figure 2** Profile of the net wave efflux  $4\pi r^2 F_T(r)$  (solid line) and net integrated heating  $4\pi \int_0^r P_p(r') r'^2 dr$  for the protons (dashed line). These curves pertain to the model of table 1 defined by  $F_0 = 5.8 \times 10^3 \text{ ergs cm}^{-2} \text{ sec}^{-1}$ .

of scattering in a turbulent region ( $\sim 20 R_\odot$  characteristic dimension; see Burlaga, 1969). Radio observations suggest that the corona and solar wind are turbulent throughout the region  $r \lesssim 1 \text{ AU}$  [Hewish and Dennison, 1967; Cohen *et al.*, 1967; Jokipii and Hollweg, 1970; Hollweg, 1970a]. Finally, Belcher and Davis [1971] have shown that much of the power in solar wind fluctuations directly observed at 1 AU is due to *outwardly propagating* Alfvén waves. They argued that these waves (net efflux  $\sim 3 \times 10^{24}$  ergs/sec, periods  $10\text{--}10^4$  sec) are very likely the signature of noise generated near the sun.

Assuming that the collisionless heating mechanism of these models is significant in stars other than the sun, it follows that the magnetic field of the star is crucial in determining whether a stellar wind flows. In one sense this is not surprising, since it is generally recognized that a suitably oriented strong magnetic field, through its stresses, might effectively inhibit the expansion of a stellar corona. But it turns out that even a radially oriented magnetic field can play a crucial role. If the energy transport in a stellar corona is purely conductive, then even a rather strong, but radially oriented magnetic field, would not restrict coronal expansion. On the other hand, if the magnetic pressure is substantially higher than particle pressure at the coronal base, dissipation of a sufficiently intense hydromagnetic-wave flux will choke off the flow. This occurs because if  $\beta_p = 8\pi n_0 k T_{p0} / B^2$  is small (about 0.3 or less), the damping rate  $\gamma \propto \exp(-1/\beta_p)$ , so that the damping rate can be very sensitive to  $B_0$ . Hence the heating may be

negligible at the base. But since  $\beta_p$  increases fairly rapidly with distance from the star, dissipation can become strong somewhere beyond the distance at which a purely conductive flow becomes supersonic. There will be strong heating in the region of supersonic flow, which will reduce the flow speed and possibly drive the expansion subsonic. Thus the magnetic field can act as a valve on a supersonic stellar wind.

Finally, we discuss briefly the relationship between the models reported in this paper and some other ideas about energy transport in the solar wind. It has been argued that typically observed values of  $v_E$  and  $T_{pE}$  can be understood without invoking an extended heat source, provided one assumes some collisionless mechanism for proton-electron energy exchange [Cuperman and Harten, 1970b; Hundhausen, 1969; Nishida, 1969]. There are two main difficulties with that view: first, there is no reason to believe that such energy exchange can account for the observed correlation between  $T_{pE}$  and  $v_E$ ; and second, it is not clear what sort of mechanism could produce such energy exchange, although some interesting possibilities have been discussed by Forslund [1970]. It has also been proposed that an external heat source is not required if thermal conduction is inhibited by some mechanism [Hundhausen, 1969; Forslund, 1970]. Again, it seems unlikely that the  $T_{pE}$ - $v_E$  correlation could be explained by such a cutoff of conduction. Furthermore, inhibition of thermal conduction in the region of supersonic flow does not affect the flow very strongly [Cuperman and Harten, 1970a; Holzer and Axford, 1970], its main effect being to reduce the conduction flux and (possibly) the electron temperature at 1 AU. In this connection, it may be noted again that the latter quantities are somewhat higher than their observed values in the present models, so that agreement with observation of these quantities might be improved by allowing for inhibition of thermal conduction. Also, due to our choice of base conditions, the thermal conduction flux at 1 AU is considerably smaller in the present models than in those of Hartle and Sturrock [1968] and Hartle and Barnes [1970]. In the present models, this flux is of order 10 to 30 percent of the flow energy flux at 1 AU.

Being spherically symmetric, the present models do not allow for heating due to collision of fast and slow streams, as proposed by Jokipii and Davis [1969]. Current observational evidence suggests that the main effect of this heating is to produce local "hot spots," rather than large-scale heating, for  $r = 1$  AU. [Burlaga and Ogilvie, 1970a; Belcher and Davis, 1971], although it is quite possible that this effect produces larger scale

heating beyond 1 AU. Hollweg [1970b] has suggested that electron heating may be important in driving the solar wind. The calculations reported here suggest that this is probably not the case, because essentially all the wave energy is dissipated in the proton component. Nevertheless, a certain amount of electron heating might occur; it is possible that this heat would simply be conducted away, but it might also be converted to flow energy. The effects of varying electron heating have not yet been investigated. Further discussion of the relationship between models with external heating and other models may be found in Hartle and Barnes [1970].

## REFERENCES

- Barnes, A.; Hartle, R. E.; and Bredekamp, J. H.: On the Energy Transport in Stellar Winds. *Astrophys. J. Ltrs.*, Vol. 166, 1971, p. 1-53.
- Belcher, J. W.; and Davis, L., Jr.: Large Amplitude Alfvén Waves in the Interplanetary Medium, 2. *J. Geophys. Res.*, Vol. 76, 1971, p. 3534.
- Burlaga, L. F.: Anisotropic Solar Cosmic Ray Propagation in an Inhomogeneous Medium. I. Solar Envelope, Goddard Preprint NASA-GSFC X-616-69-281 (to appear in Proceedings of the Eleventh International Conference on Cosmic Rays), 1969.
- Burlaga, L. F.; and Ogilvie, K. W.: Heating of the Solar Wind. *Astrophys. J.*, Vol. 159, 1970a, p. 659.
- Burlaga, L. F.; and Ogilvie, K. W.: Magnetic and Thermal Pressures in the Solar Wind. *Solar Phys.*, Vol. 15, 1970b, p. 61.
- Cohen, M. H.; Gundermann, E. J.; Hardeback, H. E.; and Sharp, L. E.: Interplanetary Scintillations, 2. Observations. *Astrophys. J.*, Vol. 147, 1967, p. 449.
- Cuperman, S.; and Harten, A.: The Solution of One-Fluid Equations with Modified Thermal Conductivity for the Solar Wind. *Cosmic Electrodyn.*, Vol. 1, 1970a, p. 205.
- Cuperman, S.; and Harten, A.: Noncollisional Coupling Between the Electron and the Proton Components in the Two-Fluid Model of the Solar Wind. *Astrophys. J.*, Vol. 162, 1970b, p. 315.
- D'Angelo, N.: Heating of the Solar Corona. *Astrophys. J.*, Vol. 154, 1968, p. 401.
- D'Angelo, N.: Heating of the Solar Corona. *Solar Phys.*, Vol. 7, 1969, p. 321.
- Forslund, D. W.: Instabilities Associated with Heat Conduction in the Solar Wind and their Consequences. *J. Geophys. Res.*, Vol. 75, 1970, p. 17.
- Hartle, R. E.; and Sturrock, P. A.: Two-Fluid Model of the Solar Wind. *Astrophys. J.*, Vol. 151, 1968, p. 1155.

- Hartle, R. E.; and Barnes, A.: Nonthermal Heating in the Two-Fluid Solar Wind Model. *J. Geophys. Res.*, Vol. 75, 1970, p. 6915.
- Hewish, A.; and Dennison, P. A.: Measurements of the Solar Wind and the Small-Scale Structure of the Interplanetary Medium. *J. Geophys. Res.*, Vol. 72, 1967, p. 1977.
- Hollweg, J. V.: Angular Broadening of Radio Sources by Solar Wind Turbulence. *J. Geophys. Res.*, Vol. 75, 1970a, p. 3715.
- Hollweg, J. V.: Collisionless Solar Wind, 1, Constant Electron Temperature. *J. Geophys. Res.*, Vol. 75, 1970b, p. 2403.
- Holzer, T. E.; and Axford, W. I.: The Theory of Stellar Winds and Related Flows. *Ann. Rev. Astron. Astrophys.* (Palo Alto: Annual Reviews, Inc.) Vol. 8, 1970, p. 31.
- Hundhausen, A. J.; Bame, S. J.; Asbridge, J. R.; and Sydoriak, S. J.: Solar Wind Properties: Vela 3 Observations from July 1965 to June 1967. *J. Geophys. Res.*, Vol. 75, 1970, p. 4643.
- Hundhausen, A. J.: Nonthermal Heating in the Quiet Solar Wind. *J. Geophys. Res.*, Vol. 74, 1969, p. 5810.
- Jokipii, J. R.; and Davis, L., Jr.: Long-Wavelength Turbulence and the Heating of the Solar Wind. *Astrophys. J.*, Vol. 156, 1969, p. 1101.
- Jokipii, J. R.; and Hollweg, J. V.: Interplanetary Scintillations and the Structure of Solar-Wind Fluctuations. *Astrophys. J.*, Vol. 160, 1970, p. 745.
- Leighton, R. B.; Noyes, R. W.; and Simon, G. W.: Velocity Fields in the Solar Atmosphere. I. Preliminary Report. *Astrophys. J.*, Vol. 135, 1962, p. 474.
- Newkirk, G., Jr.: Structure of the Solar Corona. *Ann. Rev. of Astron. and Astrophys.* (Palo Alto: Annual Reviews, Inc.) Vol. 5, 1967, p. 213.
- Nishida, A.: Thermal State and Effective Collision Frequency in the Solar Wind Plasma. *J. Geophys. Res.*, Vol. 74, 1969, p. 5155.
- Osterbrock, D. E.: The Heating of the Solar Chromosphere, Plages, and Corona by Magnetohydrodynamic Waves. *Astrophys. J.*, Vol. 134, 1961, p. 347.
- Tanenbaum, A. S.; Wilcox, J. M.; Frazier, E. N.; and Howard, R.: Solar Velocity Fields: 5-Min. Oscillations and Supergranulation. *Solar Phys.*, Vol. 9, 1969, p. 328.

## COMMENTS

*J. V. Hollweg* I would like to comment on two points that have been mentioned so far this morning. The question of the energy supply to the solar wind, and the observation of Alfvén waves in the solar wind. Along the way I will also comment briefly on the sources of high velocity streams, a possible explanation for the latitude dependence if it exists, a possible explanation for the lack of a solar cycle dependency, and on the paper just presented by Dr. Barnes.

Belcher, Davis, and Smith have recently reported a fairly positive identification of large amplitude Alfvén waves in the solar wind a large fraction of the time. The salient feature of these Alfvén waves is that they are almost always propagating outward from the sun in the frame of reference moving with the plasma. This suggests that their source is below the Alfvénic critical point, and I want to discuss here a particular solar source. That is, the generation of Alfvén waves by the supergranular motions at the solar surface.

The basic idea is fairly simple. The supergranulation is a large scale convective cellular motion at the surface. The motion is mainly horizontal with a time period of 20 to 40 hr, and velocities of the order of 0.5 km/sec. Field lines will be rooted into the solar surface and moved around horizontally by the supergranulation. It's like wiggling the end of a string and you thereby send Alfvén waves up the vertical magnetic field line.

The difficulty with the calculation is that with a 20 to 40 hr wave period you get wavelengths very much longer than the scale heights, so you actually have to solve the wave equation. To simplify things I have taken a biexponential solar chromosphere. In figure 1 the points are taken from observations; I have calculated the model for the biexponential atmosphere shown by the straight line.

Figure 2 shows the calculated Poynting flux you get when you solve the wave equation. This is for a magnetic field of 1 gauss. The horizontal scale is the period of the motion at

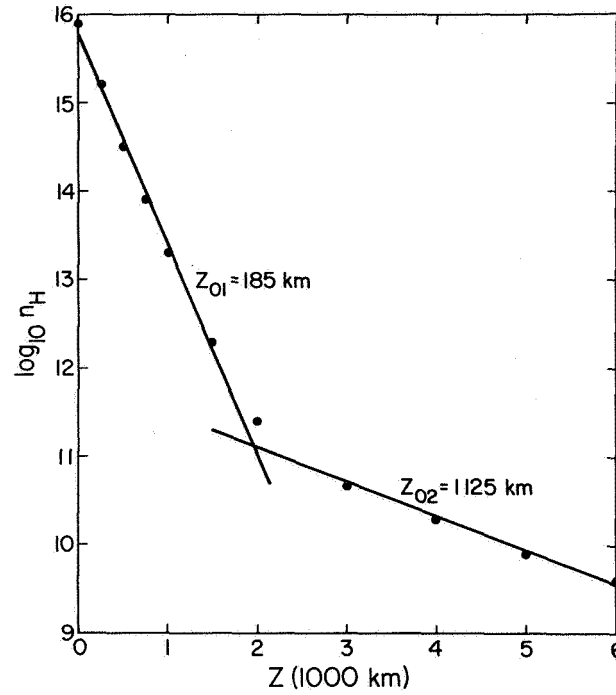


**Figure 1.** The proton concentration in the solar atmosphere as a function of height above the visible edge of the sun. Circles are data points, and the solid lines are the idealized model used in this work.

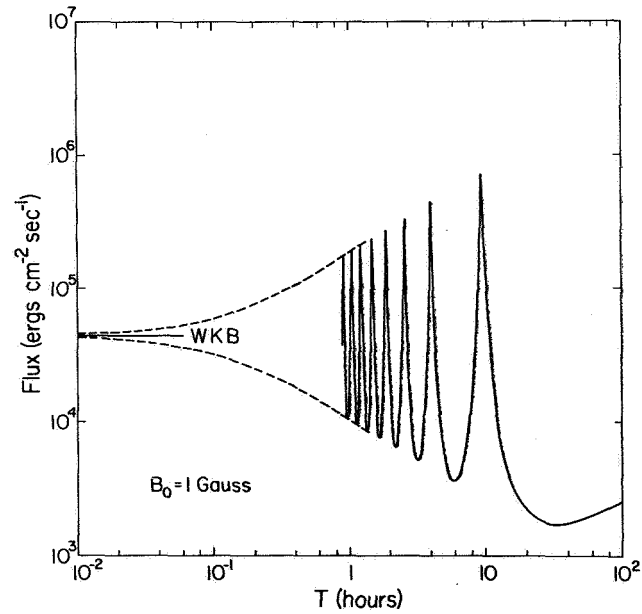


**Figure 2.** The Poynting flux in supergranulation-driven Alfvén waves as function of wave period, for a magnetic field strength of 1 gauss.

the surface in hours. If you are looking at periods of the order of 20 to 40 hr, for a magnetic field of 1 gauss you get energy fluxes of several times  $10^3$  ergs  $\text{cm}^{-2}$   $\text{sec}^{-1}$ .

Figure 3 shows more specifically how this varies with magnetic field. The interesting point is that the energy flux is a very strong function of magnetic field. So if the magnetic field were 2 gauss you would get something like  $5 \times 10^3$  ergs  $\text{cm}^{-2} \text{sec}^{-1}$ . These energy fluxes are of the order of what one would like to have to explain the discrepancy between the original two fluid solar wind model and the observations. With a slightly stronger magnetic field you can get energy fluxes of the order that Dr. Barnes has just presented. This has several consequences. The first is that if there are very subtle variations in the magnetic field strength or in the amplitude of the supergranular motions at the solar surface, you can get a very significant change in the energy flux in these waves, and if these waves should dissipate in the solar wind, high velocity streams would result. Furthermore, if there were a subtle increase in the motion, or in the magnetic field away from the solar equator, one might explain the apparent fact that there are at times more high velocity streams away from the equator.

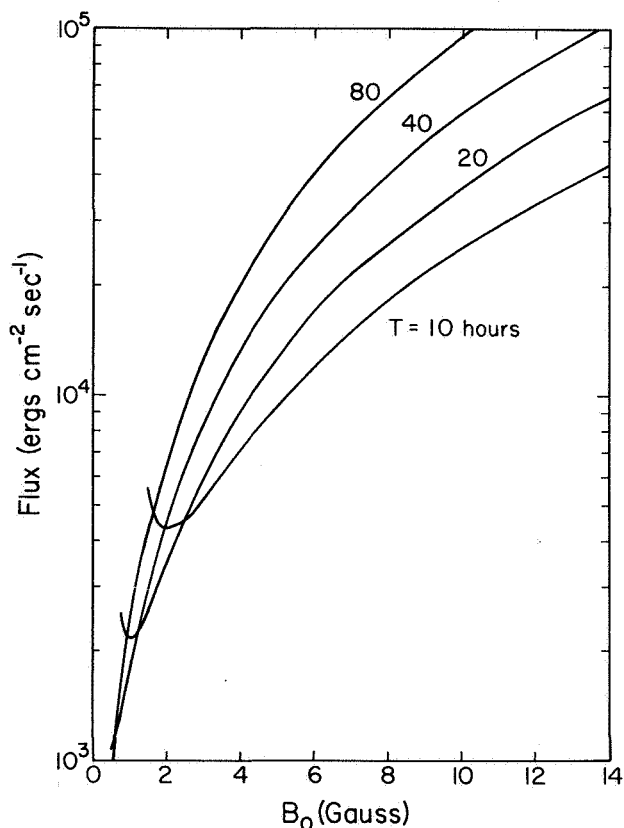


**Figure 3.** *The Poynting flux as a function of solar magnetic field strength, for a variety of wave periods.*

This large flux leads one to expect Alfvén waves to be found in the solar wind, and they are, in fact, observed. I believe that supergranular motions are the source of waves seen by Belcher, Davis, and Smith. However, they take the point of view that the Alfvén waves seen at the earth are the undamped remnant of something else that is going on at the sun, while I would take the point of view that the Alfvén waves are, in fact, primary. I calculate a very large energy flux compared to what is observed at the earth, and this implies that damping occurs in the solar wind.

As to the question of the solar cycle, although one sees variations in the corona with the solar cycle, there may be little or no variation of the supergranulation or of the

average magnetic field with solar cycle, and this would perhaps explain why one doesn't see a great variation in the solar wind energy flux at the earth with solar cycle.

There are a couple of problems. The biggest is that the supergranular periods are 20 to 40 hr and the dominant period that Belcher and Davis see is approximately 2 hr. There are two possible explanations for the discrepancy. One might be to assume that there is really a broad spectrum of motions at the solar surface, and since figure 2 shows an increase of flux toward lower periods one would thus tend to preferentially see the lower periods. The other possible explanation is the following: The supergranular motions at the solar surface are not coherent; each supergranule in a sense generates its own wave. Thus, the waves generated from separate but adjacent supergranules are going to have a tendency to "collide" with each other, and this is going to limit the amplitude of the wave. Since the amplitude can be related to the period, this is in effect a limitation on the wave period.

Another problem is that I predict very large fluxes, while only very small fluxes are seen at 1 AU. So I suggest that damping is going on. The question is, how does this damping occur. I can think of several explanations. One is that large-amplitude Alfvén waves coupled nonlinearly with ion sound waves can damp by Landau damping. This is a possible mechanism. Also, there might be an interaction of magnetic moments with fluctuations of the magnetic field strength and this is another type of Landau damping. Another possibility involves the motion of "colliding waves" again. If  $\delta B/B_0 = \delta v/v_A \gtrsim 0.5$ , then when these waves "collide" they are colliding super-Alfvénically. You would then expect shocks and nonlinear dissipation.

DISCUSSION     *Unidentified Speaker* I would like to ask a question of Dr. Barnes. Does this model overcome the high density problem which Dr. Parker mentioned earlier.

*A. Barnes* We don't know. We started our calculations out at 2 solar radii, where there is no density problem.

*Unidentified Speaker* Can I ask a second question or make a second comment to Dr. Hollweg? We have observed oscillations in the intensity in the corona with a period of approximately 270 sec. Now, whether this is a characteristic of the entire corona or just a freak event we don't really know. Presumably they are associated with the macroscopic observations at the photospheric level.

*J. V. Hollweg* Two hundred seventy sec is 5 min, which is much shorter than the periods I'm talking about. I'm talking about several hours or more. I think that your oscillations may be connected with gravity wave propagation in the chromosphere and there is possibly some coupling. But that is an interesting observation in any case.

*A. J. Hundhausen* I feel compelled to rise and register my standard objection to Barnes's conclusion that his model really agrees well with the solar wind, particularly since he has neglected the difficulty with the density. His model predicts a density at 1 AU that is high by a factor of roughly 3 yet he chooses to emphasize only agreement with proton temperatures, despite the fact that the thermal energy is only a few percent of the energy in the solar wind. I must also object to his contention that those who construct steady models that do not explain dynamic phenomena such as the temperature-velocity relationship should bow their heads in shame. However, I've made these objections before, so I'll leave it at that.

But I would like to mention the model which will soon be published in the *Astrophysical Journal* by Wolfe, Brandt, and Southwick. Theirs is a two-fluid model including an artificial inhibition of the thermal conductivity of electrons. They predict most solar wind parameters that agree better with observations than does the model presented by Barnes, but without any assumption of additional nonthermal heating.



# MAGNETIC LATITUDE EFFECTS IN THE SOLAR WIND C. Richard Winge, Jr., and Paul J. Coleman, Jr.

The Weber-Davis model of the solar wind is generalized to include the effects of latitude. ABSTRACT  
The principal assumptions of high electrical conductivity, rotational symmetry, the polytropic relation between pressure and density, and a flow-aligned field in a system rotating with the sun, are retained. An approximate solution to the resulting equations for spherical boundary conditions at the base of the corona indicates a small component of latitudinal flow toward the solar poles at large distances from the sun as a result of latitudinal magnetic forces.

The purpose of this paper is to demonstrate that even with spherically symmetric boundary conditions at the base of the corona, the magnetic field introduces a small latitude effect in the solar wind that should be measurably significant at large distances. As motivation for a more general development it is useful to consider the magnetic forces predicted by the spiral field approximation of *Parker* [1958]. The magnetic force per unit mass for this model is

$$(\nabla \times \mathbf{B}) \times \mathbf{B} / (4\pi\rho) = -\nabla [B_0^2 / 4\pi\rho_0 \sin^2\theta] \quad (1)$$

where  $B_0$  and  $\rho_0$  are reference values for the magnetic field and density. The total force per unit mass is then given by the negative gradient of the sum of the thermal energy per unit mass, the gravitational energy per unit mass, and the magnetic energy per unit mass (eq. (1)). The thermal term is assumed to be falling adiabatically toward zero at large distances, and the gravitational term is decreasing toward zero; however, for spherical boundary conditions on  $B_0$  and  $\rho_0$ , the magnetic term depends upon  $\sin^2\theta$  and does not decrease explicitly with  $r$ . This suggests that changes in momentum at large distances may be dominated by the magnetic field.

The magnetic torque per unit mass for this model is then

$$\boldsymbol{\tau} = \mathbf{r} \times (d\mathbf{V}/dt) = -(B_0^2 / 4\pi\rho_0) \sin\theta \cos\theta \hat{\phi} \quad (2)$$

which acts to drive the plasma toward the poles, producing a nonzero component of the  $\theta$  component of velocity  $V_\theta$ . For infinite electrical conductivity, the presence of a finite component of  $V_\theta$  implies a finite component of  $B_\theta$  through the process of convection. The assumed field is therefore inconsistent with respect to latitude and requires a more general treatment. It should be noted that the magnetic stress given by this model results because of the  $\phi$  component of the magnetic field. Since this winding of the field is due to solar rotation, the effect demonstrated here may be expected to persist in a more general treatment.

The approach to be described here is identical with that of *Weber and Davis* [1967] except that the equations are generalized to include the effects of latitude through the development of the normal component of momentum. We begin with the steady-state flow equations subject to the following assumptions: (1) neglect viscosity, (2) isotropic thermal conductivity, (3) infinite electrical conductivity, (4) equal electron and proton temperatures, and (5) energy equation may be replaced by the polytropic law. We further assume rotational symmetry and that

---

*The authors are with the Department of Planetary and Space Science and Institute of Geophysics and Planetary Physics, University of California, Los Angeles, California.*

the magnetic field and flow velocity are parallel in a reference system rotating with the sun. A flow-aligned field may be generally represented by

$$\mathbf{B} = \kappa \rho \mathbf{U} \quad (3)$$

where  $\mathbf{U} = \mathbf{V} - \omega_S r \sin \theta \hat{\phi}$  is the flow velocity in the rotating system,  $\mathbf{V}$  is the flow velocity in a fixed system of reference,  $\rho$  is the mass density, and  $\omega_S$  is the solar rotation rate. The condition  $\nabla \cdot \mathbf{B} = 0$ , combined with the equation of continuity, requires  $\kappa$  to be a streamline constant. The physical meaning of  $\kappa$  is obtained by noting that the quantity  $\kappa^2 \rho / 4\pi$  must be unity at the Alfvén point, or  $\kappa^2 = 4\pi / \rho_A$  where  $\rho_A$  is the density at the Alfvén point.

With rotational symmetry the  $\phi$  component of the momentum equation may be directly integrated to obtain  $V_\phi$  as a function of  $r$ ,  $\theta$ , and  $\rho$ , which when combined with the magnetic field as a function of velocity and density (eq. (3)), reduces the problem to one of two-dimensional flow in the  $r\theta$  plane. Given boundary conditions, the unknowns at a general point  $r$ ,  $\theta$  are  $\rho$ ,  $V_r$ , and  $V_\theta$ , which are determined by the equation of continuity, the parallel component of momentum (Bernoulli's equation), and the normal component of momentum. The problem is complicated by the presence of three critical surfaces corresponding to the fast, slow, and Alfvén modes of propagation in the medium.

A particular streamline will be designated by specifying its coordinate  $\theta_O$  at the base of the corona, which is constant along the streamline. There are six required boundary values that must be specified or determined as functions of  $\theta_O$  at the coronal base:  $T_O(\theta_O)$ ,  $\rho_O(\theta_O)$ ,  $V_{rO}(\theta_O)$ ,  $V_{\theta O}(\theta_O)$ ,  $\kappa(\theta_O)$ , and the total  $\phi$  component of angular momentum along the streamline  $L(\theta_O)$ . The requirement that the velocity components be finite at the three critical surfaces supplies three of the required boundary conditions for  $V_{\theta O}$ ,  $\kappa$ , and  $L$ . Further, if  $B_O(\theta_O)$  is specified, then  $V_{rO}$  may be determined through equation (3). Hence, we chose to specify  $T_O(\theta_O)$ ,  $\rho_O(\theta_O)$ , and  $B_O(\theta_O)$ , the magnitude of the total magnetic field at the coronal base.

We find that the best way to cope with the critical surfaces is to integrate the equations along a streamline until the critical point is encountered and then to vary a boundary condition until the streamline that passes through is determined. Because of the differential form of the equations, integration along a streamline is possible only if the previous neighboring streamline is known. Hence, to start the integration, the polar limit of the equations is required. However, the equations at

the pole are not closed and an assumption is necessary to obtain the polar limit. A complete solution to the problem is possible through a process of iteration over the entire set of streamlines; however, techniques we have been able to devise thus far are too costly.

As a first approximation to the solution, we chose to close the equations with the assumption

$$V_\theta / V_r = -\{r [df(r)/dr] / f(r)\} \sin \theta \cos \theta \quad (4)$$

which integrates to

$$\tan \theta_O = f(r) \tan \theta \quad (5)$$

Equation (4) is the lowest order  $\theta$  dependence for which  $V_\theta$  is zero at both the equator and the pole. The radial function  $f(r)$  specifies the shape of the streamlines. Radial flow in the  $r\theta$  plane is given by  $f(r) = 1$  and  $df(r)/dr = 0$ . The function  $f(r)$  is determined by integration of the limit of the normal component of momentum along the polar stream line. In the polar limit we have

$$\partial V_\theta / \partial \theta = -V_r [r df(r)/dr] / f(r) \quad (\theta = 0) \quad (6)$$

$$\partial \theta_O / \partial \theta = f(r) \quad (7)$$

The results of equations (4) and (5) and the polar integration of  $f(r)$  for two sets of constant temperature, density, and magnetic field at the coronal base are presented in tables 1 through 4 and figure 1. Figure 1 shows the radial dependence of  $V_\theta$  along a streamline for the two sets of boundary conditions; tables 1 and 2 tabulate the resulting values at 1 AU, and tables 3 and 4 tabulate the corresponding critical surfaces.

The function  $f(r)$  obtained at the pole is not overly sensitive to reasonable changes in the assumed model to close the equations for constant boundary conditions. The general shape of the curve results from the physics of the problem and is maintained. Since  $V_\theta$  for  $\theta_O = 10^\circ$  may be obtained directly from the polar solution through equation (6), this curve should be in close agreement with an exact solution. The curves for  $\theta_O > 10^\circ$ , however, are contingent upon how well the assumption contained in equation (4) approximates the normal component of momentum at lower latitudes.

The results presented here indicate a modest latitudinal flow toward the poles due to magnetic stresses, which persist out to very large distances from the sun for spherical boundary conditions at the corona. Associated with this flow is a  $\theta$  component of the magnetic field. The radial flow parameters are not

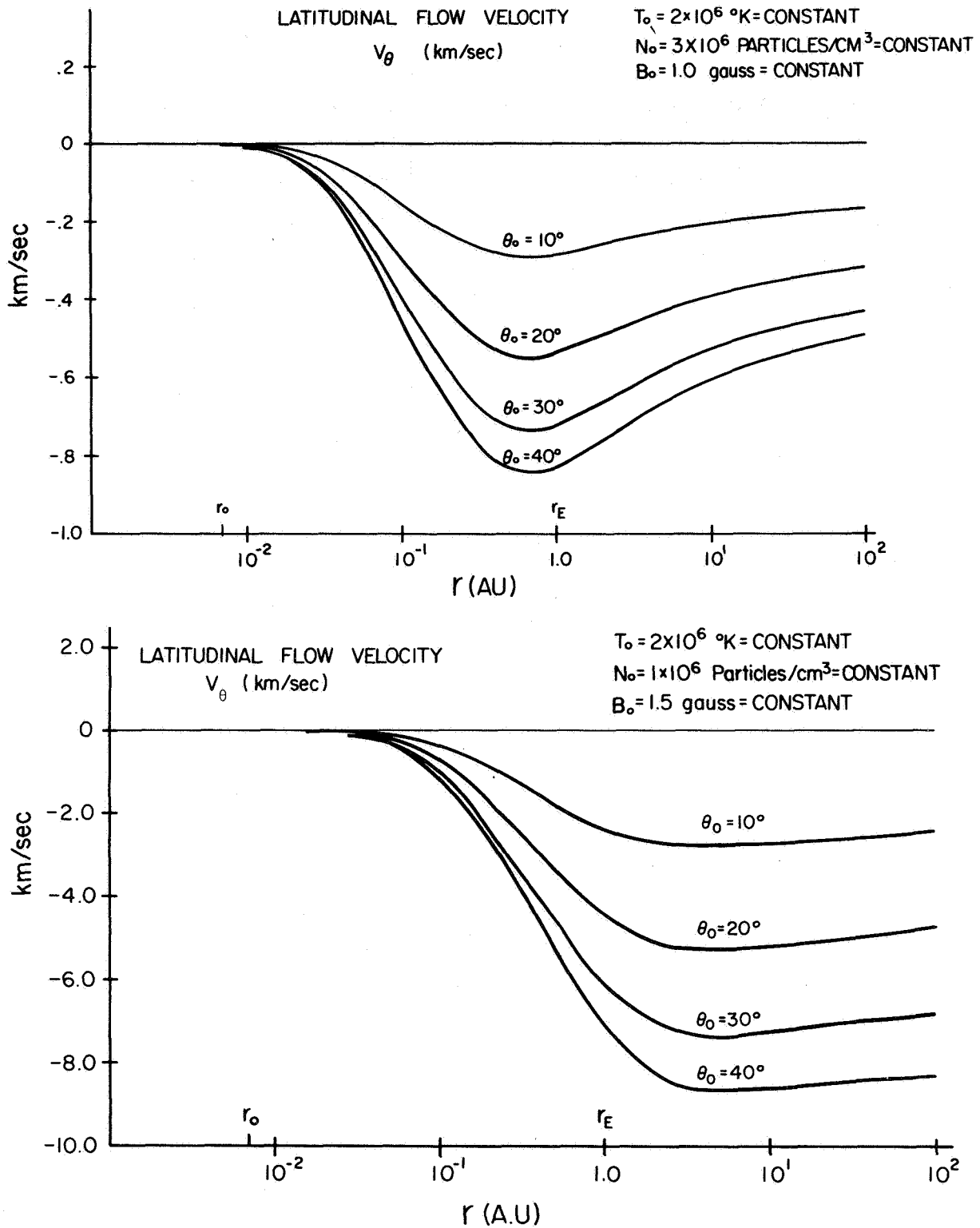


**Figure 1.** Latitudinal flow velocity for two sets of constant boundary conditions at the coronal base,  $r_0 = 1.0 \times 10^{11}$  cm. Curves for  $\theta_0 = 50^\circ, 60^\circ, 70^\circ$  and  $80^\circ$  are nearly identical with the displayed curves for  $40^\circ, 30^\circ, 20^\circ$  and  $10^\circ$ , respectively, and are not shown.

**Table 1.** *Predicted values at 1 AU*[Constant coronal boundary conditions:  $T_o = 2 \times 10^6$  °K,  $N_o = 3 \times 10^6$  particles/cm<sup>3</sup>,  $B_o = 1$  gauss]

$\theta_o$ , deg	$\theta$ , deg	Velocity, km/sec			Magnetic field, $10^{-5}$ gauss			Density, protons/cm <sup>3</sup>	Temperature, °K
		$V_r$	$V_\theta$	$V_\phi$	$B_r$	$B_\theta/B_r$	$B_\phi/B_r$		
10	9.88	403	-0.28	0.19	3.57	$-7.06 \times 10^{-4}$	-0.19	13.6	$3.16 \times 10^5$
20	19.78	403	-0.54	0.37	3.57	$-1.33 \times 10^{-3}$	-0.38	13.6	$3.16 \times 10^5$
30	29.70	403	-0.72	0.53	3.56	$-1.80 \times 10^{-3}$	-0.55	13.6	$3.16 \times 10^5$
40	39.65	403	-0.83	0.68	3.55	$-2.05 \times 10^{-3}$	-0.71	13.5	$3.16 \times 10^5$
50	49.65	403	-0.83	0.81	3.54	$-2.06 \times 10^{-3}$	-0.85	13.5	$3.16 \times 10^5$
60	59.69	403	-0.73	0.91	3.53	$-1.82 \times 10^{-3}$	-0.96	13.5	$3.15 \times 10^5$
70	69.77	404	-0.55	0.98	3.52	$-1.35 \times 10^{-3}$	-1.04	13.5	$3.15 \times 10^5$
80	79.88	404	-0.29	1.03	3.51	$-7.22 \times 10^{-4}$	-1.09	13.5	$3.15 \times 10^5$

**Table 2.** *Predicted values at 1 AU*[Constant coronal boundary conditions:  $T_o = 2 \times 10^6$  °K,  $N_o = 1 \times 10^6$  particles/cm<sup>3</sup>,  $B_o = 1.5$  gauss]

$\theta_o$ , deg	$\theta$ , deg	Velocity, km/sec			Magnetic field, $10^{-5}$ gauss			Density, protons/cm <sup>3</sup>	Temperature, °K
		$V_r$	$V_\theta$	$V_\phi$	$B_r$	$B_\theta/B_r$	$B_\phi/B_r$		
10	9.48	402	-2.37	0.60	6.75	$-5.89 \times 10^{-3}$	-0.18	5.85	$3.28 \times 10^5$
20	19.01	402	-4.50	1.16	6.70	$-1.12 \times 10^{-2}$	-0.36	5.83	$3.28 \times 10^5$
30	28.66	403	-6.15	1.64	6.64	$-1.53 \times 10^{-2}$	-0.53	5.80	$3.28 \times 10^5$
40	38.46	403	-7.13	2.05	6.56	$-1.77 \times 10^{-2}$	-0.69	5.75	$3.27 \times 10^5$
50	48.44	403	-7.27	2.34	6.47	$-1.80 \times 10^{-2}$	-0.83	5.71	$3.27 \times 10^5$
60	58.62	404	-6.51	2.56	6.39	$-1.61 \times 10^{-2}$	-0.94	5.66	$3.27 \times 10^5$
70	68.98	404	-4.81	2.69	6.32	$-1.19 \times 10^{-2}$	-1.03	5.62	$3.26 \times 10^5$
80	79.45	404	-2.64	2.78	6.27	$-6.54 \times 10^{-3}$	-1.09	5.59	$3.26 \times 10^5$

**Table 3. Critical surfaces**

[Constant coronal boundary conditions:  $T_O = 2 \times 10^6$  °K,  
 $N_O = 3 \times 10^6$  particles/cm<sup>3</sup>,  $B_O = 1$  gauss]

$\theta_O$ , deg	Slow mode		Alfvén mode		Fast mode	
	$r_S$ , solar radii	$\theta_S$ , deg	$r_A$ , solar radii	$\theta_A$ , deg	$r_f$ , solar radii	$\theta_f$ , deg
10	4.012	9.997	15.233	9.979	15.239	9.979
20	4.011	19.994	15.226	19.961	15.236	19.961
30	4.010	29.992	15.211	29.947	15.233	29.947
40	4.008	39.991	15.194	39.940	15.230	39.940
50	4.006	49.991	15.174	49.940	15.226	49.940
60	4.004	59.992	15.159	59.947	15.224	59.947
70	4.003	69.994	15.144	69.961	15.221	69.961
80	4.002	79.997	15.136	79.979	15.220	79.979

significantly different from the Parker or Weber-Davis models for latitudinal flow velocities up to about 10 km/sec.

#### ACKNOWLEDGMENTS

This work was supported in part by the National Aeronautics and Space Administration under research grant NGR 05-007-065. A portion of the computer costs was covered by the Regents of the University of

**Table 4. Critical surfaces**

[Constant coronal boundary conditions:  $T_O = 2 \times 10^6$  °K,  
 $N_O = 1 \times 10^6$  particles/cm<sup>3</sup>,  $B_O = 1.5$  gauss]

$\theta_O$ , deg	Slow mode		Alfvén mode		Fast mode	
	$r_S$ , solar radii	$\theta_S$ , deg	$r_A$ , solar radii	$\theta_A$ , deg	$r_f$ , solar radii	$\theta_f$ , deg
10	4.015	9.997	36.043	9.895	36.067	9.895
20	4.013	19.994	35.931	19.803	36.027	19.803
30	4.011	29.992	35.773	29.736	35.977	29.734
40	4.008	39.991	35.578	39.701	35.914	39.698
50	4.003	49.991	35.354	49.703	35.827	49.698
60	4.001	59.992	35.178	59.740	35.781	59.734
70	3.999	69.994	35.020	69.805	35.731	69.803
80	3.997	79.997	34.931	79.896	35.703	79.895

California. The authors are grateful to G. L. Siscoe and G. Schubert for helpful discussions.

#### REFERENCES

- Parker, E. N.: Dynamics of the Interplanetary Gas and Magnetic Field. *Astrophys. J.*, Vol. 128, 1958, p. 664.  
 Weber, E.; and Davis, L., Jr.: The Angular Momentum of the Solar Wind. *Astrophys. J.*, Vol. 148, 1967, p. 217.

# TRANSITION FROM A SUPERSONIC TO A SUBSONIC SOLAR WIND *B. Durney*

**ABSTRACT** The transition from a supersonic to a subsonic corona was investigated by increasing the density  $N_0$  at the base of the corona (initially  $N_0 = 9.3 \times 10^7/\text{cm}^3$ ) while keeping the temperature  $T_0$  there constant ( $T_0 = 2.1 \times 10^6$  °K). For the initial values of  $N_0$  and  $T_0$ , the solution of the inviscid solar wind equations is of the Parker type. As  $N_0$  is increased, Parker type supersonic solutions cease to exist for  $N_0 = N_0^P \sim 1.17 \times 10^8/\text{cm}^3$ . No subsonic solutions exist, however, for  $N_0 < N_0^S$  where  $N_0^S > 3 \times 10^8/\text{cm}^3$ . For  $N_0^P < N_0 < N_0^S$  the solar wind equations permit supersonic solutions which are not of the Parker type, with the temperature varying as  $(1/r)^{4/3}$  for large distances.

The transition region separating supersonic expansions of the solar wind [Parker, 1958] from subsonic expansions [Chamberlain, 1961] has been considered by Parker [1965]. Here we study this transition region for a given value of the temperature at the base of the corona. Chamberlain's notation [1961] will be used throughout this paper; that is, the dimensionless values of the temperature, square of the velocity, and the inverse of the radial distance will be defined as

$$\tau = T/T_1 \quad \psi = mw^2/kT_1 \quad \lambda = GM_\odot m/kT_1 r \quad (1)$$

where  $T_1$  is a reference temperature taken equal to  $2 \times 10^6$  °K,  $w$  the radial expansion velocity,  $m$  the average mass (for a hydrogen-helium mixture 10:1),  $M_\odot$  the mass of the sun, and  $G$  and  $k$  are the gravitational and Boltzmann constants, respectively. The usual momentum and energy equation can then be written as

$$\frac{d\psi}{d\lambda} = \frac{1 - 2\tau/\lambda - d\tau/d\lambda}{0.5(1 - \tau/\psi)} \quad (2a)$$

The author is with the National Center for Atmospheric Research, Boulder, Colorado. The National Center for Atmospheric Research is sponsored by the National Science Foundation.

$$\frac{d\tau}{d\lambda} = \frac{\epsilon_\infty - \frac{1}{2}\psi + \lambda - \frac{5}{2}\tau}{0.5 A \tau^{5/2}} \quad (2b)$$

For  $A$  we take [Chamberlain, 1961]:  $A = 5.8 \times 10^6/C$  where  $C$  is the mass flow given in terms of  $N$ ,  $\psi$ , and  $\lambda$  by  $C = N \psi^{1/2} \lambda^{-2}$  ( $N$  is the total particle density). In equation (2b)  $\epsilon_\infty$  is the residual energy per particle at infinity. For  $\epsilon_\infty \neq 0$  a well-known solution of equations (2a) and (2b) is the Parker supersonic solution. Then for small values of  $\lambda$

$$\tau = D_0 \lambda^{2/7} \left( 1 + \frac{77}{9} \frac{\lambda^{2/7}}{A D_0^{5/2}} + \dots \right) \quad (3)$$

The asymptotic expansion for  $\psi$  is obtained from equation (2b). The parameter  $D_0$  in equation (3) is left undetermined; this allows equations (2) to be solved as follows. Given  $C$  and  $\epsilon_\infty$ , the integration of (2) and (3) is started from small values of  $\lambda$

$$\left( \frac{77}{9} \frac{\lambda^{2/7}}{A D_0^{5/2}} \ll 1 \right)$$

toward the sun; the condition that the numerator and denominator of equation (2a)

$$\phi_1 = 1 - 2\tau/\lambda - d\tau/d\lambda \quad \phi_2 = 0.5(1 - \tau/\psi) \quad (4)$$

should vanish for the same value of  $\lambda(\lambda_c)$  determines then  $D_0$ . This solution is supersonic for large distances and subsonic for  $\lambda > \lambda_c$ . Therefore, given the values of  $C$  and  $\epsilon_\infty$  the integration of equations (2) determines  $N_0$  and  $T_0$  at the base of the corona; that is, the curves  $\epsilon_\infty = \text{constant}$  and  $C = \text{constant}$  are known in the  $N_0, T_0$  plane [Kopp, 1968]. In the present paper,  $C$  and  $\epsilon_\infty$  were adjusted to give the desired value of  $T_0$  ( $T_0 = 2.1 \times 10^6 \text{ K}$ ) and increasing values of  $N_0$  ( $N_0 > 9.3 \times 10^7 / \text{cm}^3$ ). In figure 1,  $D_0$  is plotted versus

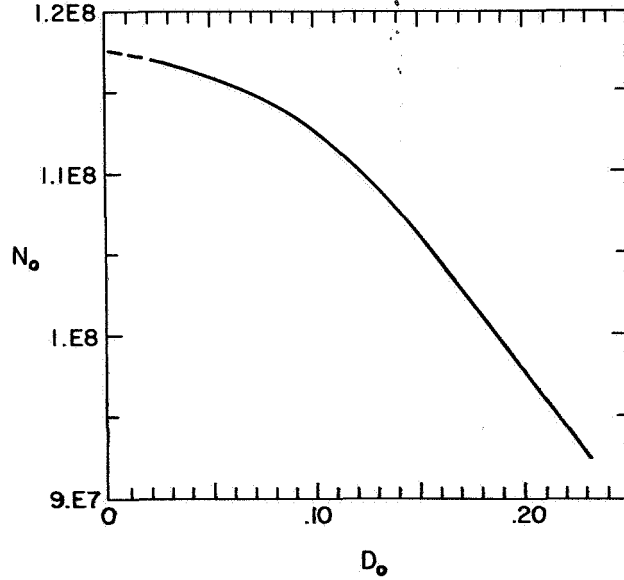


**Figure 1.** Density at the base of the corona versus  $D_0$ . The dotted lines are interpolated values.

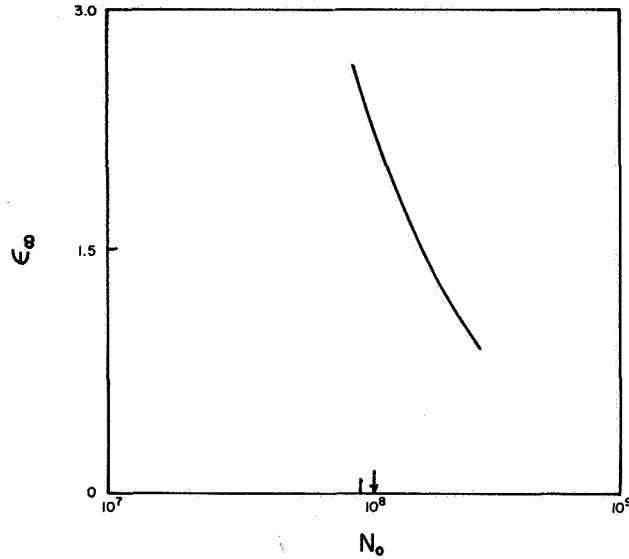


**Figure 2.** Residual energy at infinity versus  $N_0$  for  $T_0 = 2.1 \times 10^6 \text{ K}$ .

$N_0$ ; the dashed curve represents interpolated values. In figure 2,  $\epsilon_\infty$  is plotted versus  $N_0$ . Thus, from figures 1 and 2 it is clear that  $D_0$  vanishes for  $N_0 = N_0^p = 1.17 \times 10^8 / \text{cm}^3$ , that is, for a finite value of  $\epsilon_\infty$ . It is easily seen that the vanishing of  $D_0$  implies that the conductive flux at infinity is zero. Therefore, supersonic solutions of the Parker type cease to exist for  $N_0 > N_0^p$ . However, since for  $N_0 = N_0^p$  the total energy flux at infinity,  $\epsilon_\infty$ , is not zero, it is to be expected from physical grounds that as  $N_0$  is increased the flow will remain supersonic. This was confirmed by numerical calculations. No subsonic solutions were found for  $N_0 < 10^9 / \text{cm}^3$ .

The above considerations led to the search for a supersonic solution of equations (2) with an asymptotic expansion different than that given by equation (3). It was indeed found that the full equations (2) also admit a solution with the following asymptotic expansions

$$\tau = D_0 \lambda^{4/3} [1 + D_1 \lambda + D_2 \lambda^{4/3} + D_3 \lambda^{5/3} + D_4 \lambda^2 + D_5 \lambda^{7/3} + \dots] \quad (5a)$$

$$\psi = \psi_\infty + 2\lambda + C_0 \lambda^{4/3} [1 + C_1 \lambda + C_2 \lambda^{4/3} + C_3 \lambda^{5/3} + C_4 \lambda^2 + C_5 \lambda^{7/3} + \dots] \quad (5b)$$

with

$$\left. \begin{aligned} \epsilon_\infty &= \frac{1}{2} \psi_\infty; C_0 = -5D_0; C_1 = D_1 = -\frac{2}{3\psi_\infty}; \\ C_2 = D_2 &= \frac{5}{3} \frac{D_0}{\psi_\infty}; C_3 = D_3 = 0 \\ C_4 = D_4 &= \frac{8}{9\psi_\infty^2}; \\ D_5 &= -\frac{2D_0}{63} \left[ \frac{175}{\psi_\infty^2} + 22AD_0^{3/2} \right]; \\ C_5 &= \frac{4A}{15} D_0^{5/2} + D_5 \end{aligned} \right\} \quad (6)$$

As in the Parker solutions the parameter  $D_0$  in equation (5) is left undetermined, and equations (2) can again be solved by integrating from small values of  $\lambda$  toward the sun. An iteration procedure was used to determine  $D_0$  so that  $\phi_1(\lambda) = \phi_2(\lambda) = 0$  (cf. eq. (4) for the same value of  $\lambda = \lambda_c$ ). This determines the critical point. The iteration procedure is based on the fact that if  $\phi_1$  vanishes first ( $\phi_1(\lambda_c) = 0$  and  $\phi_2(\lambda) \neq 0$  for  $\lambda < \lambda_c$ ), then  $D_0$  is too

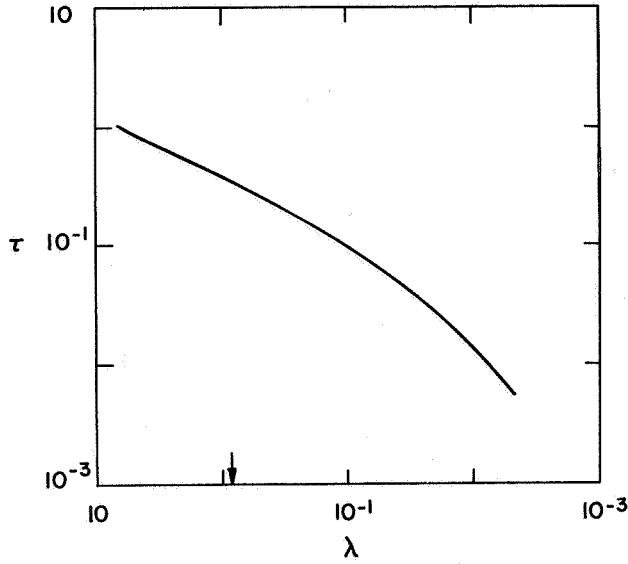


Figure 3.  $\tau$  versus  $\lambda$  for  $C = 5.47 \times 10^4$ ,  $\epsilon_\infty = 0.887$ .

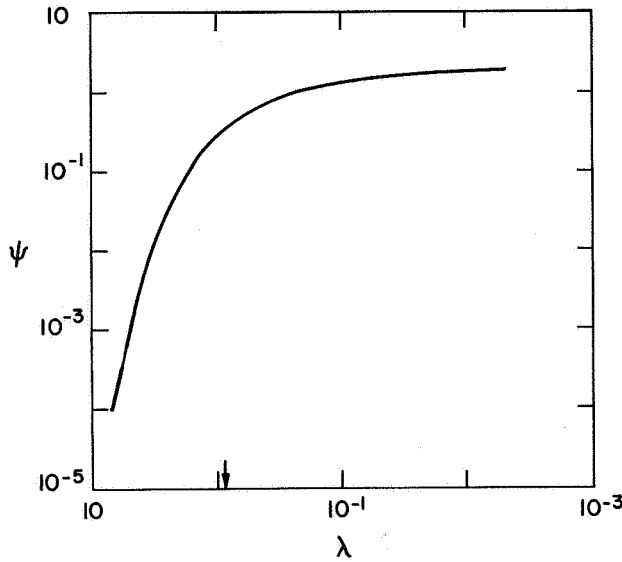


Figure 4.  $\psi$  versus  $\lambda$  for  $C = 5.47 \times 10^4$ ,  $\epsilon_\infty = 0.887$ .

large and it should be decreased; if on the other hand  $\phi_2$  vanishes first, then  $D_0$  is too small and it should be increased. This method allows the critical point  $\lambda_c$  to be known as accurately as desired. Once  $\lambda_c$  is determined a Taylor expansion of  $\tau$  and  $\psi$  in the neighborhood of  $\lambda_c$  can be used to integrate across the critical point. In figures 3 and 4,  $\tau$  and  $\psi$  are plotted versus  $\lambda$  for  $C = 5.47 \times 10^4$ ,  $\epsilon_\infty = 0.887$ . With the help of the asymptotic expansions (5) the integrations were started from

$\lambda = 4.7 \times 10^{-3}$  toward the sun. The arrow indicates the position of the sonic point. For the above values of  $C$  and  $\epsilon_\infty$  the values of the density and temperature at the base of the corona are  $T_0 = 2.1 \times 10^6$  K and  $N_0 = 2.88 \times 10^8/\text{cm}^3$ , respectively. Therefore, to summarize, if the temperature at the base of the corona is assumed constant and equal to  $2.1 \times 10^6$  K, the solution of the solar wind equations is of the Parker type for values of  $N_0 < 1.17 \times 10^8/\text{cm}^3$ . For values of  $N_0$  such that  $1.17 \times 10^8/\text{cm}^3 < N < N_0^s$  ( $N_0^s > 3 \times 10^8/\text{cm}^3$ ) the flow continues to be supersonic but differs from the Parker solution. The asymptotic expansions of the velocity and temperature are now given by equations (5). For  $N > N_0^s$  the flow becomes subsonic. The value of  $N_0^s$  was not determined with great accuracy; the numerical calculations suggest that  $N_0^s \sim 2 \times 10^9/\text{cm}^3$ . Since the integrations are time consuming no supersonic solutions were evaluated for  $N_0 > 3 \times 10^8/\text{cm}^3$ .

As the density at the base of the corona is increased from an initial value of  $N_0 = 9.3 \times 10^7/\text{cm}^3$  and the temperature there is held constant ( $T_0 = 2.1 \times 10^6$  K) there is not a direct transition from a Parker type supersonic flow to a subsonic flow. As  $N_0$  is increased the conductive flux at infinity  $\epsilon_\infty^c$  decreases sharply and vanishes for a finite value of the total energy per particle at infinity  $\epsilon_\infty$ . This is not surprising, since as  $N_0$  increases the mass flow  $C$  also increases, and since  $T_0$  has been kept constant  $\epsilon_\infty$  must decrease. The sharp decrease in  $\epsilon_\infty^c$  arises as more and more of the conductive flux at infinity is converted into kinetic energy of the particles. The Parker type supersonic solutions cease to exist when  $\epsilon_\infty^c$  vanishes. The total energy flux at infinity remaining, however, different from zero, it is to be expected from physical grounds that if  $N_0$  increases still further there will not be an immediate transition to a subsonic flow but rather a transition to a different type of supersonic flow (cf. eqs. (5) and (6)). The expansion becomes adiabatic [Chamberlain, 1961] and the heat conduction flux is much smaller than the internal energy flux [Hundhausen, 1971]. Any further increase in  $N_0$  must now be entirely accounted for by a decrease in the kinetic energy flux at infinity. The velocity reaches a maximum and decreases towards a finite value as  $r \rightarrow \infty$ . Finally, for values of  $N_0$  large enough,  $\epsilon_\infty$  vanishes and the flow becomes subsonic.

#### ACKNOWLEDGMENTS

The author is indebted to Drs. R. A. Kopp, G. W. Pneuman, and E. J. Weber for many illuminating discussions and to Dr. G. Vickers presently at Sheffield



University for carrying out the analytical and numerical calculations for the subsonic solutions.

#### REFERENCES

- Chamberlain, J. W.: Interplanetary Gas, III, A Hydrodynamic Model of the Corona. *Astrophys. J.*, Vol. 133, 1961, p. 675.
- Hundhausen, A. J.: Dynamics of the Outer Solar Atmosphere. *Physics of the Solar System*, edited by S. I. Rasool, Goddard Space Flight Center publication X-630-71-380, 1971.
- Kopp, R. A.: The Equilibrium Structure of a Shock-Heated Corona. Thesis, Astronomy Department, Harvard University, 1968.
- Parker, E. N.: Dynamics of the Interplanetary Gas and Magnetic Fields. *Astrophys. J.*, Vol. 128, 1958, p. 664.
- Parker, E. N.: Dynamics Properties of Stellar Coronas and Stellar Winds, IV, The Separate Existence of Subsonic and Supersonic Solutions. *Astrophys. J.*, Vol. 141, 1965, p. 1463.

## CONVERSION OF MAGNETIC FIELD ENERGY INTO KINETIC ENERGY IN THE SOLAR WIND

Y. C. Whang

**ABSTRACT** The outflow of the solar magnetic field energy (the radial component of the Poynting vector) per steradian is inversely proportional to the solar wind velocity. It is a decreasing function of the heliocentric distance. When the magnetic field effect is included in the one-fluid model of the solar wind, the transformation of magnetic field energy into kinetic energy during the expansion process increases the solar wind velocity at 1 AU by 17 percent. The predicted solar wind conditions at 1 AU are  $u = 302$  km/sec,  $n = 8$  protons/cm<sup>3</sup>,  $T = 1.5 \times 10^5$ °K,  $q = 1.4 \times 10^{-2}$  erg/cm<sup>2</sup>/sec,  $B = 7.3\gamma$ ,  $\phi = 129.5^\circ$ , and  $\beta = 1.58$ . They agree very well with the observed quiet solar wind.

### INTRODUCTION

Since the original application of hydrodynamic equations to the solar wind by *Parker* [1958], a number of theoretical models have been developed to study the solar wind, notably the one-fluid models studied by *Noble and Scarf* [1963] and by *Whang and Chang* [1965], and the two-fluid model by *Sturrock and Hartle* [1966] and by *Hartle and Sturrock* [1968]. The one-fluid model assumed that all types of particles (electrons, proton, helium, etc.) have the same temperature, while the two-fluid model took into consideration the different temperatures for protons and electrons. The inviscid model of *Whang and Chang* predicted a solar wind velocity of 260 km/sec at 1 AU. The solution of *Hartle and Sturrock* predicted a velocity of 250 km/sec at 1 AU. These velocities are about 20 percent below the observed quiet solar wind condition [*Hundhausen*, 1970].

The interplanetary magnetic field has a strong coupling with the dynamics of the solar wind. The magnetic field organizes the collisionless plasma into a continuum in the expansion process of the solar wind. It is well known that when the solar wind flows across a shock wave, the

magnetic field energy flux and the convective thermal energy increase during the *compression* process at the expense of the kinetic energy. In a reverse process, during the magnetohydrodynamic *expansion* of the solar wind, the magnetic field energy as well as the thermal energy is continuously converted into kinetic energy. Therefore, we propose that in a magnetohydrodynamic model of the solar wind, which includes an additional energy source, the predicted solar wind velocity can be increased closer to the observed quiet condition.

Various mechanisms for the additional energy source needed to increase the solar wind velocity have been proposed by many authors. *Barnes* [1968, 1969] proposed that a significant amount of energy is carried by the hydromagnetic waves. The dissipation of hydromagnetic waves adds its energy into the solar wind flow. *Jokipii and Davis* [1969] proposed that the observed long-lived velocity streams are the source of long-wavelength turbulence, which in turn serves as an efficient and variable heat source for the solar plasma. In this paper, we will show that the magnetic field energy flow per steradian is a decreasing function of the heliocentric distance  $r$ . The total decrease of field energy flow from  $r = 2r_0$  to  $r = 1$  AU is about 25 percent of the convective kinetic energy at 1 AU. Therefore, during the expansion process of the solar wind, the conversion of

---

The author is with the Department of Aerospace and Atmospheric Sciences, The Catholic University of America, Washington, D. C.

field energy into kinetic energy increases the solar wind velocity by 17 percent.

The solution of a steady-state magnetohydrodynamic one-fluid model of the solar wind is carried out in this paper. The model assumes that the solar wind velocity is in radial directions away from the center of the sun, and its temperature is isotropic. The solar wind conditions near the equatorial plane predicted by the present solution clearly demonstrate the process of energy conversion in the solar wind on a quantitative basis.

## DECREASE OF THE MAGNETIC FIELD ENERGY FLOW

### Spiral Pattern of the Magnetic Field

The steady-state solar magnetic field is governed by Maxwell's equations

$$\nabla \cdot \mathbf{B} = 0 \quad (1)$$

$$\nabla \times (\mathbf{u} \times \mathbf{B}) = 0 \quad (2)$$

Spherical coordinates  $(r, \psi, \omega)$  are used in this paper;  $\psi$  denotes the colatitude measured from the north pole of the sun. If  $\mathbf{B} = \mathbf{e}_r B_r(r, \psi) + \mathbf{e}_\omega B_\omega(r, \psi)$ , then we can write equations (1) and (2) as

$$\frac{\partial}{\partial r} (r^2 B_r) = 0$$

$$\frac{\partial}{\partial r} (ru B_\omega) = 0$$

These two equations can be integrated to give

$$B_r \propto r^{-2} \quad (3)$$

$$B_\omega \propto (ru)^{-1} \quad (4)$$

which represent the spiral pattern of the solar magnetic field.

### The Poynting Vector

The equation of energy conservation can be integrated once:

$$N \left( m_i \frac{u^2}{2} + 5kT - \frac{m_i GM_\odot}{r} \right) + r^2 q_r + r^2 p_r = F \quad (5)$$

Here  $N = r^2 nu = \text{constant}$ ,  $G$  is the gravitational constant,  $M_\odot$  the mass of the sun,  $q_r$  the radial component of the heat flux, and  $p_r$  the radial component of the Poynting vector

$$\mathbf{p} = \frac{c}{4\pi} \mathbf{B} \times (\mathbf{u} \times \mathbf{B})$$

In the right side of (5),  $F$  is a constant. Thus equation (5) expresses the conservation of the total energy in the steady-state expansion of the solar wind. During the expansion process, energy can be converted from one form into another, but the total energy must be conserved.

The radial component of the Poynting vector is

$$p_r = \frac{u B^2 \sin^2 \phi}{4\pi}$$

Making use of (4), we can express the flow of magnetic field energy per steradian as

$$r^2 p_r \propto u^{-1} \quad (6)$$

The solar wind velocity  $u$  is an increasing function of the heliocentric distance  $r$ . Thus the flow of magnetic field energy per steradian is a decreasing function of  $r$ . Conservation of the total energy flow requires that the field energy be transformed into other forms of energy flow.

### Mechanism of Energy Conversion

The equation of motion for the magnetohydrodynamic expansion of the solar wind is

$$m_i n \frac{D\mathbf{u}}{Dt} = m_i n \mathbf{g} - \nabla (2nkT) + \frac{1}{c} \mathbf{J} \times \mathbf{B} \quad (7)$$

where  $\mathbf{g} = -\mathbf{e}_r GM_\odot/r^2$ . In the right hand side of (7), the magnetic field exerts a force

$$\frac{1}{c} \mathbf{J} \times \mathbf{B}$$

on the moving solar wind flow. The radial component of this force can be written as

$$\frac{B^2 \sin^2 \phi}{4\pi u} \frac{du}{dr}$$

This term is always positive, because  $u$  is an increasing function of  $r$ . The magnetic field exerts a force on the solar wind in the direction of the solar wind velocity.

The rate of work done by this force on a unit volume of the solar wind flow is

$$\frac{B^2 \sin^2 \phi}{4\pi} \frac{du}{dr}$$

The work done on the solar wind flow is used to increase the kinetic energy of the solar wind at the expense of the field energy.

## MAGNETOHYDRODYNAMIC ONE-FLUID MODEL OF THE SOLAR WIND

### Governing Equations

The magnetohydrodynamical expansion of the one-fluid solar wind is governed by a system of two ordinary nonlinear differential equations: The equation of motion

$$\frac{du}{dr} = \frac{u}{r} \frac{4kT}{m_i} - \frac{GM_\odot}{r^2} - \frac{2kr}{m_i} \frac{dT}{dr} - \frac{B^2 \sin^2 \phi}{4\pi m_i n} \quad (8)$$

and the equation of energy conservation

$$r^2 \kappa \cos^2 \phi \frac{dT}{dr} = N \left( m_i \frac{u^2}{2} + 5kT - \frac{m_i GM_\odot}{r} + \frac{B^2 \sin^2 \phi}{4\pi n} \right) - F \quad (9)$$

where the thermal conductivity  $\kappa$  is proportional to  $T^{5/2}$ .

Let us denote conditions at the critical radius by a superscript asterisk. Then we can introduce the following dimensionless variables

$$\begin{aligned} V &= u/u^* \\ \theta &= T/T^* \\ Z &= r/r^* \end{aligned}$$

and dimensionless parameters

$$\begin{aligned} \alpha &= \frac{2Nk}{r^* \kappa^* \cos^2 \phi^*} \\ \gamma &= \frac{GM_\odot}{r^* u^{*2}} \\ H &= \frac{F}{N m_i u^{*2}} \end{aligned}$$

$$\xi = \frac{m_i u^{*2}}{2kT^*}$$

Because the denominator of (8) vanishes at the critical radius, we obtain

$$\xi = 1 + \sin^2 \phi^* \frac{B^{*2}/8\pi}{n^* k T^*} = \frac{1 + 2 \sin^2 \phi^*}{\beta^*}$$

In terms of the dimensionless quantities, we can write the two governing equations, (8) and (9), in dimensionless form,

$$\frac{dV}{dZ} = \frac{V}{Z} \frac{2\theta - \frac{\gamma\xi}{Z} - Z \frac{d\theta}{dZ}}{\xi V^2 - \theta - (\xi-1) \frac{1}{V}} \quad (10)$$

and

$$\frac{d\theta}{dZ} = \frac{\alpha}{Z^2 \theta^{5/2}} \frac{\cos^2 \phi^*}{\cos^2 \phi} \left[ \xi \frac{V^2}{2} + (\xi-1) \frac{1}{V} + \frac{5}{2} \theta - \frac{\gamma\xi}{Z} - \xi H \right] \quad (11)$$

These two ordinary differential equations will suffice to solve for the two dependent variables  $V$  and  $\theta$ .

At the critical radius, equation (11) reduces to

$$\left( \frac{d\theta}{dZ} \right)^* = \alpha \left[ \xi \left( \frac{3}{2} - \gamma - H \right) + \frac{3}{2} \right] \quad (12)$$

Both the denominator and the numerator of equation (10) must vanish simultaneously at  $Z=1$ . When the numerator is zero, we obtain

$$\left( \frac{d\theta}{dZ} \right)^* = 2 - \gamma\xi \quad (13)$$

From the above two equations, we can show that  $\alpha$  is not an independent parameter:

$$\alpha = \frac{\gamma\xi - 2}{\xi(\gamma + H - 3/2) - 3/2} \quad (14)$$

Therefore, the general solutions for  $V$  and  $\theta$  can be expressed in the form

$$\left. \begin{aligned} V &= V(Z, H, \gamma, \xi, \phi^*) \\ \theta &= \theta(Z, H, \gamma, \xi, \phi^*) \end{aligned} \right\} \quad (15)$$

Making use of the l'Hospital's rule, we can calculate  $(dV/dZ)^*$ ; the result is

$$\left(\frac{dV}{dZ}\right)^* = -C_1 + (C_1^2 + C_2)^{1/2} \quad (16)$$

where

$$C_1 = \frac{\alpha + (\xi\gamma - 2)(1 + 2\sin^2\phi^*)}{(6\xi - 2)}$$

$$C_2 = \frac{2 + \alpha\left(\frac{3}{2}\xi\gamma - 5\right) + (\xi\gamma - 2)\left(\frac{5}{2}\xi\gamma + 2\sin^2\phi^* - 7\right)}{(3\xi - 1)}$$

### Numerical Solutions

For any given value of  $\gamma$ ,  $H$ ,  $\xi$ , and  $\phi^*$ , we can use (13) and (16) to calculate the solution for  $V(Z)$  and  $\theta(Z)$  in the  $\epsilon$  neighborhood of the singular point at  $Z = 1$ . Then we can integrate equations (10) and (11) for  $Z > 1 + \epsilon$  and  $Z < 1 - \epsilon$ . The two branches of the numerical solutions join smoothly at the singular point.

The numerical solutions for  $Z > 1$  show the same property as the numerical solutions for the inviscid model of the solar wind [Whang and Chang, 1965]. As  $Z \rightarrow \infty$ , the solution curve is expected to approach the condition  $V = V_\infty$  and  $\theta = 0$  with

$$\frac{V_\infty^2}{2} + \frac{\xi - 1}{\xi V_\infty} = H$$

A solution satisfying this condition when  $H = 3.0$ ,  $\xi = 1.3$ ,  $\phi^* = 176^\circ$ , and  $\gamma = 1.8978$  is obtained as shown in figure 1. The numerical values of this solution in dimensionless form  $V = V(Z)$  and  $\theta = \theta(Z)$  are given in table 1.

Physical interpretation of the numerical solution depends on the choice of the ratio  $r^*/r_0$ . When the critical radius is chosen at between 5 and 6  $r_0$ , the solar wind conditions at 1 AU predicted by the present solution are (fig. 2)  $u = 287\text{--}318$  km/sec and  $T = (1.45 - 1.57) \times 10^5$  °K. In the remaining part of this paper, we will interpret the physical meaning of the solution based on  $r^*/r_0 = 5.5$  (fig. 3). The predicted solar wind conditions at 1 AU are

$$u = 302 \text{ km/sec}$$

$$T = 1.50 \times 10^5 \text{ °K}$$

$$\frac{dT}{dr} = 5.7 \times 10^{-9} \text{ °K/cm}$$

$$\phi = 129.5^\circ$$

$$\beta = 1.58$$

where  $\beta$  is defined as the ratio of  $2nkT$  to  $B^2/8\pi$ .

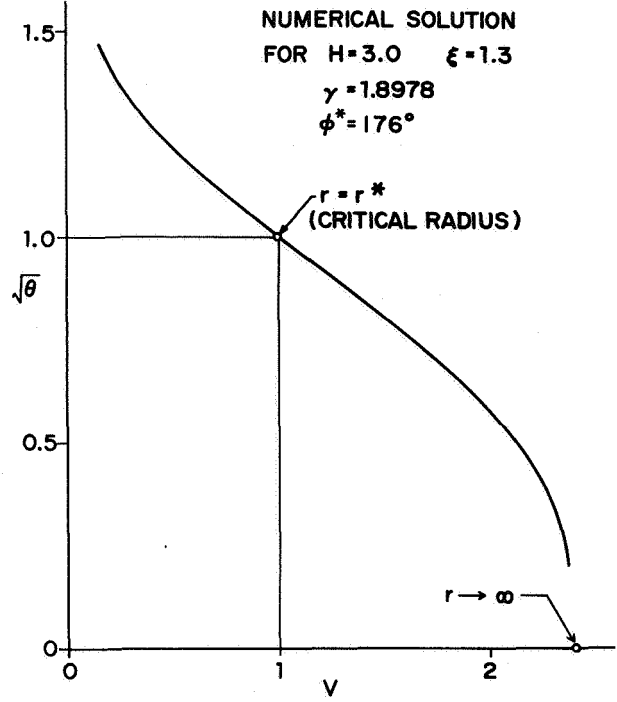


Figure 1. The numerical solution, given in table 1, smoothly passes through the singular point at the critical radius ( $Z = 1$ ), and approaches the condition  $V = V_\infty$  and  $\theta = 0$  as  $Z \rightarrow \infty$ .

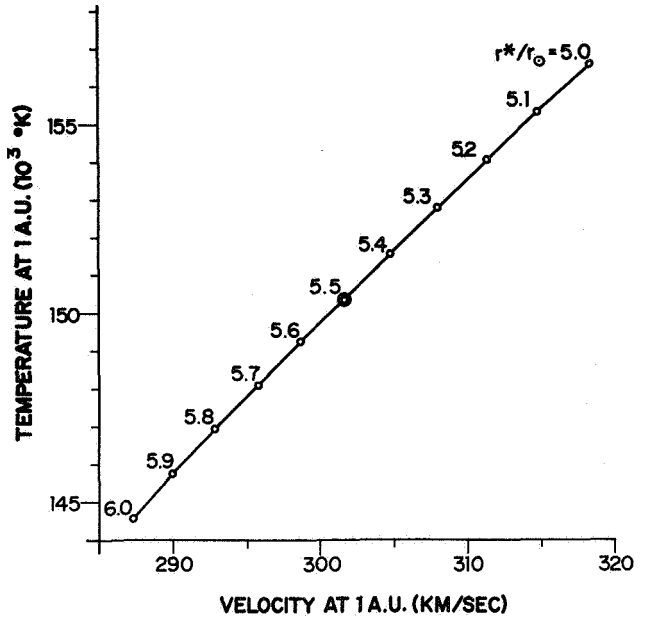


Figure 2. The solar wind conditions at 1 AU predicted by the present solution depend on the choice of the ratio  $r^*/r_0$ . For  $r^*/r_0 = 5.5$ , the present result gives  $u = 302$  km/sec and  $T = 1.50 \times 10^5$  °K at 1 AU.

**Table 1.** Numerical solution for  $H = 3.0$ ,  $\xi = 1.3$ ,  $\phi^* = 176^\circ$  and  $\gamma = 1.8978$

$Z$	$\phi$	$V$	$\theta$	$d\theta/dZ$	$\beta$
0.100	171.3	0.046	3.026	-14.76	0.021
0.126	172.7	0.069	2.704	-10.53	0.020
0.158	174.0	0.105	2.415	- 7.483	0.019
0.200	175.0	0.159	2.157	- 5.294	0.017
0.251	175.7	0.234	1.928	- 3.733	0.017
0.316	176.2	0.331	1.724	- 2.630	0.017
0.398	176.4	0.448	1.544	- 1.853	0.018
0.501	176.5	0.579	1.384	- 1.309	0.019
0.631	176.5	0.719	1.241	- 0.926	0.022
0.794	176.3	0.860	1.114	- 0.657	0.027
1.000	176.0	1.000	1.000	- 0.467	0.033
1.259	175.6	1.134	0.898	- 0.333	0.041
1.585	175.0	1.261	0.807	- 0.237	0.052
1.995	174.2	1.380	0.725	- 0.169	0.067
2.512	173.3	1.489	0.651	- 0.121	0.089
3.162	172.1	1.590	0.585	- $8.61 \times 10^{-2}$	0.118
3.981	170.6	1.682	0.525	- 6.14	0.157
5.012	168.8	1.766	0.472	- 4.38	0.211
6.310	166.5	1.842	0.424	- 3.11	0.283
7.944	163.8	1.911	0.381	- 2.22	0.378
10.00	160.5	1.974	0.343	- 1.58	0.503
12.59	156.6	2.030	0.308	- 1.13	0.661
15.85	152.0	2.081	0.277	- $8.10 \times 10^{-3}$	0.850
19.95	146.7	2.127	0.249	- 5.88	1.063
25.12	141.0	2.169	0.223	- 4.35	1.277
31.62	134.9	2.207	0.199	- 3.27	1.464
39.81	128.8	2.241	0.175	- 2.51	1.588
50.12	122.9	2.271	0.152	- 1.96	1.626
63.10	117.5	2.298	0.130	- 1.53	1.567
79.44	112.7	2.322	0.108	- 1.18	1.424
100.0	108.5	2.342	0.087	- $8.78 \times 10^{-4}$	1.222
125.9	105.0	2.359	0.068	- 6.16	0.997
158.5	102.1	2.372	0.052	- 3.87	0.781

The values of  $u$ ,  $T$ ,  $dT/dr$ ,  $\phi$ , and  $\beta$  calculated above are independent of the constant  $K$  used in the expression for the thermal conductivity  $\kappa = KT^{5/2}$ . However, the proton number density, the magnitude of the magnetic field and the heat flux at 1 AU predicted by

the present solution depend on the value of the constant  $K$  (table 2). When the value of  $K$  is about half of that used in the ordinary expression for the thermal conductivity of fully ionized hydrogen, the predicted  $n$ ,  $B$ , and  $q$  agree very well with the observed solar

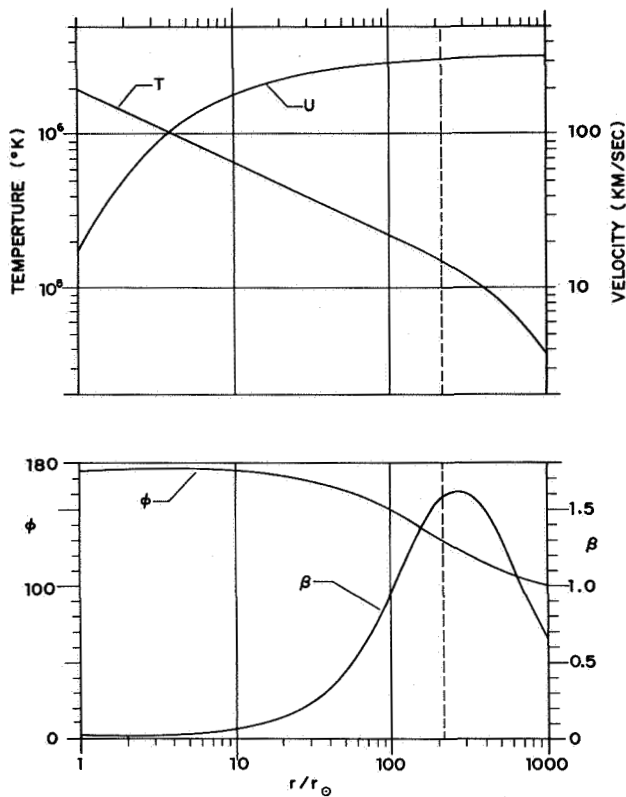


**Figure 3.** The solar wind temperature, velocity, direction angle, and  $\beta$ -value as functions of the heliocentric distance, at 1 AU  $u = 302$  km/sec,  $T = 1.50 \times 10^5$  °K,  $\phi = 129.5^\circ$  and  $\beta = 1.58$ .

**Table 2.** The proton density, the magnitude of the magnetic field, and the heat flux at 1 AU predicted by the present solution

$\kappa/T^{5/2}$ , ergs cm <sup>-1</sup> sec <sup>-1</sup> deg <sup>-7/2</sup>	$n$ , protons cm <sup>-3</sup>	$B$ , gammas	$q$ , ergs cm <sup>-2</sup> sec <sup>-1</sup>
$6.00 \times 10^{-7}$	13.1	9.3	$2.23 \times 10^{-2}$
$4.58 \times 10^{-7}$	10.0	8.1	$1.70 \times 10^{-2}$
$4.00 \times 10^{-7}$	8.7	7.6	$1.49 \times 10^{-2}$
$3.66 \times 10^{-7}$	8.0	7.3	$1.36 \times 10^{-2}$
$2.75 \times 10^{-7}$	6.0	6.3	$1.02 \times 10^{-2}$

wind conditions [Hundhausen, 1970; Ness, 1967]. For  $\kappa = 3.66 \times 10^{-7} T^{5/2}$  erg cm<sup>-1</sup> sec<sup>-1</sup> deg<sup>-1</sup>, the predicted results at 1 AU are  $n = 8$  protons/cm<sup>3</sup>,  $B = 7.3 \gamma$  and  $q = 1.36 \times 10^{-2}$  erg/cm<sup>2</sup>/sec. The predicted  $n$ ,  $B$ , and  $q$  as functions of the heliocentric distance  $r$  are plotted in figures 4 and 5. The density

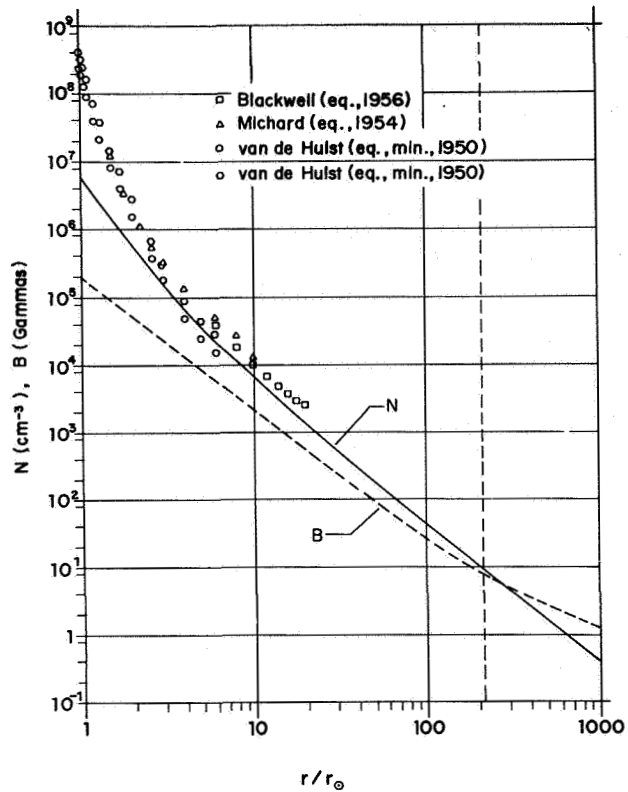


**Figure 4.** The proton density and the magnitude of the magnetic field as functions of the heliocentric distance.

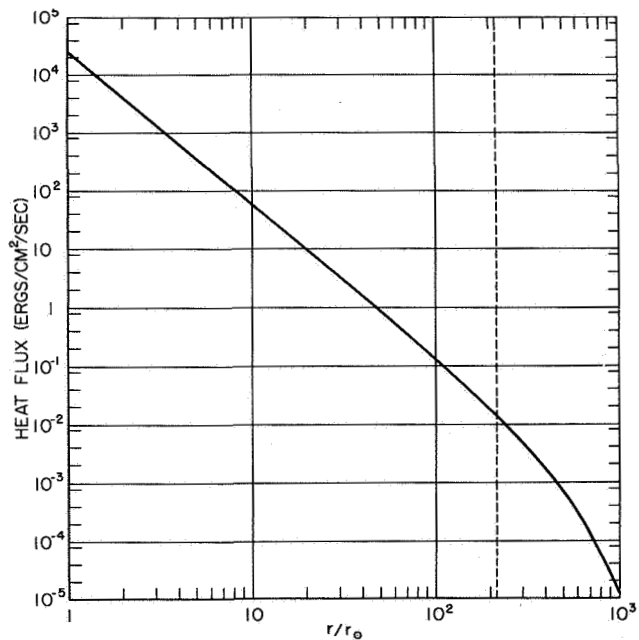


**Figure 5.** The heat flux as a function of the heliocentric distance,  $q = 1.4 \times 10^{-2}$  erg/cm<sup>2</sup>/sec at 1 AU.

curve agrees reasonably well with the observed data in the region  $2 r_{\odot} < r < 20 r_{\odot}$  [van de Hulst, 1950, 1953; Michard, 1954; Blackwell, 1956]. In the region  $r < 2 r_{\odot}$ , the present solution is not expected to be accurate, because the structure of the solar magnetic field is more complicated than the simple model described by equations (3) and (4).

### CONCLUDING REMARKS

The solar wind conditions predicted by the present magnetohydrodynamic model show that when the effect of the solar magnetic field is included in the one-fluid model, we obtain an increase of 17 percent in the solar wind velocity or 37 percent in the convective kinetic energy at 1 AU. The variations of the magnetic field energy flow and the convective kinetic energy flow per steradian as functions of the heliocentric distance  $r$  are plotted in figure 6. The magnetic field energy flow per

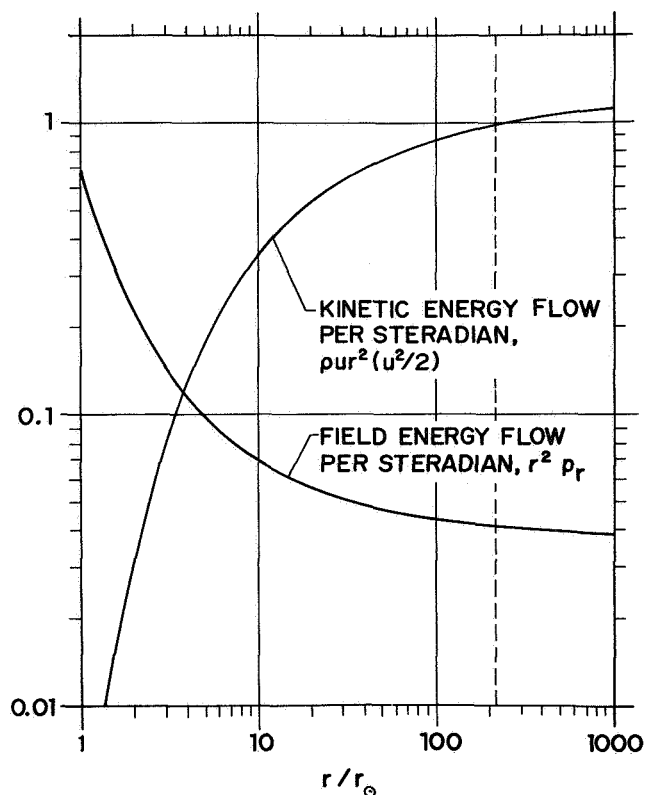


**Figure 6.** The radial flow of magnetic field energy per steradian is a decreasing function of the heliocentric distance. The field energy is converted into the kinetic energy during the expansion of the solar wind. The convective kinetic energy flow per steradian at 1 AU is chosen as unity in this figure.

steradian is a monotonically decreasing function of  $r$ . Using the convective kinetic energy per steradian at 1 AU as a unit, we can see that the total decrease of the magnetic field energy flow from  $r = 2 r_{\odot}$  to  $r = 1$  AU is about 0.35. Conversion of the magnetic field energy into the kinetic energy certainly plays an important role in the expansion process of the solar wind.

Urch [1969] has studied the magnetohydrodynamic one-fluid model of the solar wind. The equations of motion and energy conservation were integrated in a quite different way. He has obtained the numerical solutions for the solar wind after several iterations. The temperatures at 1 AU predicted by Urch are 3 to  $4 \times 10^5$  K, which are too high compared with the observed data.

Recently Wolff *et al.* [1971] have studied the magnetohydrodynamic two-fluid model of the solar wind; their predicted solar wind conditions at 1 AU are very close to the results obtained in this paper. Barnes *et al.* [1971] have also included the magnetic field in their two-fluid model of the solar wind. Because they have dropped out the  $\mathbf{J} \times \mathbf{B}/c$  force term in their equation of motion, the magnetic field force is not doing work on the expanding solar wind. The conversion of magnetic field energy into kinetic energy is not included in their work. They proposed that an energy source due to dissipation of hydromagnetic waves supplies the energy needed to increase the solar wind velocity. Their source of energy is completely different from the magnetic field energy flow (the Poynting vector) discussed here.

### ACKNOWLEDGMENTS

This work was supported by National Aeronautics and Space Administration under Grant No. NGR-09-005-063.

### REFERENCES

- Barnes, A.: Collisionless Heating of the Solar Wind Plasma, I, Theory of Heating of a Collisionless Plasma by Hydromagnetic Waves. *Astrophys. J.*, Vol. 154, 1968, p. 751.
- Barnes, A.: Collisionless Heating of the Solar Wind Plasma, II, Application of the Theory of Plasma Heating by Hydromagnetic Waves. *Astrophys. J.*, Vol. 155, 1969, p. 311.
- Barnes, A.; Hartle, R. E.; and Bredekamp, J. H.: On the Energy Transport in Stellar Winds. *Astrophys. J. Ltrs.*, Vol. 166, 1971, p. L-53.
- Blackwell, D. E.: A Study of the Outer Solar Corona from a High Altitude Aircraft at Eclipse of 1954, June 30. *Mon. Not. Roy. Astron. Soc.*, Vol. 116, 1956, p. 57.



- Hartle, R. E.; and Sturrock, P. A.: Two-Fluid Model of the Solar Wind. *Astrophys. J.*, Vol. 151, 1968, p. 1155.
- Hundhausen, A. J.: Composition and Dynamics of the Solar Wind Plasma. *Rev. Geophys. Space Phys.*, Vol. 8, 1970, p. 729.
- Jokipii, J. R.; and Davis, L. Jr.: Long Wavelength Turbulence and the Heating of the Solar Wind. *Astrophys. J.*, Vol. 156, 1969, p. 1101.
- Michard, R.: Densité's Electroniques Dans la Couronne Externe du 25 Février 1952. *Ann. Astrophys.*, Vol. 17, 1954, p. 429.
- Ness, N. F.: Observed Properties of the Interplanetary Plasma. *Ann. Rev. Astron. Astrophys.*, Vol. 6, 1967, p. 79.
- Noble, L. M.; and Scarf, F. L.: Conductive Heating of the Solar Wind, I. *Astrophys. J.*, Vol. 138, 1963, p. 1169.
- Parker, E. N.: Dynamics of the Interplanetary Gas and Magnetic Fields. *Astrophys. J.*, Vol. 128, 1958, p. 664.
- Sturrock, P. A.; and Hartle, R. E.: Two-Fluid Model of the Solar Wind. *Phys. Rev. Letters*, Vol. 16, 1966, p. 628.
- Urch, I. H.: A Model of the Magnetized Solar Wind. *Solar Phys.*, Vol. 10, 1969, p. 219.
- Whang, Y. C.; and Chang, C. C.: An Inviscid Model of the Solar Wind. *J. Geophys. Res.*, Vol. 70, 1965, p. 4175.
- Wolff, C. L.; Brandt, J. C.; and Southwick, R. G.: A Two Component Model of the Quiet Solar Wind with Viscosity, Magnetic Field, and Reduced Heat Conduction. *Astrophys. J.*, Vol. 164, Pt. I, 1971, p. 181.
- van de Hulst, H. C.: The Electron Density of the Solar Corona. *Bull. Astron. Inst. Neth.*, Vol. 11, 1950, p. 136.
- van de Hulst, H. C.: The Chromosphere and the Corona, in *The Sun*, edited by G. P. Kuiper, Univ. of Chicago Press, Chicago, 1953, p. 259.

## SOME PHYSICAL IMPLICATIONS OF RECENT SOLAR WIND MEASUREMENTS

*S. Cuperman and A. Harten*

**ABSTRACT** The physical implications of the existence at about 1 AU of a quiet solar wind particle flux about 90 percent larger than that suggested in the past [Hundhausen *et al.*, 1970] is investigated within the framework of the two-fluid solar wind model equations.

During the spherically symmetric radial expansion of the quiet solar wind the particle flux is a conserved quantity; therefore, one expects the new piece of observational information to affect strongly the predicted gross features of the solar wind.

It is found that a "pure collisional" two-fluid model provides good particle density and streaming velocity at 1 AU, but predicts too large an electron temperature and too small a proton temperature.

When noncollisional contributions to the transport coefficients are incorporated in the model equations, a complete and satisfactory agreement with the available observations between about  $12 R_{\odot}$  and 1 AU is obtained. Between  $1 R_{\odot}$  and about  $12 R_{\odot}$ , particle densities lower than indicated by observations are found.

Upper limits to the effective coupling between electrons and protons, as well as to the effective proton thermal conductivity, and both upper and lower limits to the effective electron thermal conductivity in the quiet solar wind, required to provide agreement with observations, are given.

### INTRODUCTION

Recently, a statistical description of the solar wind properties observed at 1 AU has been given by Hundhausen *et al.* [1970]. Unlike earlier reports, which covered relatively short time periods, this last analysis is based on the Vela 3 positive-ion data accumulated during a rather long period, extending from July 1965 to Jun 1967. Among the data covering this time period, of special interest are those referring to the "quiet conditions"—to periods during which the solar wind is steady. In this last case, it is possible to compare with theoretical fluid models based on the assumption of a steady flow from a spherically symmetric corona. This, in turn, could help to understand better the basic processes existing in the solar wind.

Thus, Hundhausen and his collaborators selected from the existing data only those referring to time periods when the flow speed lay between 300 and 350 km sec<sup>-1</sup> as being characteristic of the "quiet" or steady solar wind. Their results indicate a rather good agreement between the average proton temperature and the previously found values, namely  $T_{p,E} = (4.4 \pm 1.8) \times 10^4$  °K,  $\pm 1.8$  being the standard deviation. The subscript *E* here represents a distance 1 AU away from the sun. However, the average proton density  $n_E$  is now found to be  $8.7 \pm 4.6$  cm<sup>-3</sup>, which is more than 70 percent larger than the one suggested in the past. Consequently, the proton flux  $n_p v_p$  at 1 AU is found to be  $(3 \pm 1.5) \times 10^8$  cm<sup>-2</sup> sec<sup>-1</sup>, which is to be compared with the value  $1.6 \times 10^8$  cm<sup>-2</sup> sec<sup>-1</sup> indicated by Hundhausen [1968].

Now, it is well known that the particle flow  $J = nvr^2$  (*r* being the radial distance) is a conserved quantity during the spherically symmetric radial expansion of the solar

---

*The authors are with the Department of Physics and Astronomy and The Institute of Planetary and Space Science, Tel-Aviv University, Tel-Aviv, Israel.*

wind. In fact, its actual constant value represents a constraint which any solution of a fluid (or multifluid) model equation should obey. Since in the past, a value  $J_E/r_E^2 = 1.625 \times 10^8 \text{ cm}^{-2} \text{ sec}^{-1}$  has been used in solving two-fluid model equations with allowance for non-collisional contributions to the coupling between the electrons and the protons and to the thermal conductivities [Cuperman and Harten, 1970, 1971], it was of interest to investigate how the previously found results change with the use of the new, much more reliable observational data now available.

Thus, we solved the two-fluid model equations for the spherically symmetric quiet solar wind by the same integration method as described in Cuperman and Harten [1970, 1971] but using the constraint that the proton particle flux  $J = nvr^2$  be everywhere equal to that observed at 1 AU—namely,  $J = J_E = (nvr^2)_E$ —and we took  $(nv)_E = 3 \times 10^8 \text{ cm}^{-2} \text{ sec}^{-1}$  instead of  $1.6 \times 10^8 \text{ cm}^{-2} \text{ sec}^{-1}$ , as in Cuperman and Harten [1970, 1971].

First, we solved the equations by using “pure collisional” coupling between electrons and protons as well as thermal conductivities. Next, we allowed for noncollisional contributions to those quantities, and determined their effective values by requiring the predicted gross features for the solar wind at 1 AU to fit the observations of Hundhausen et al. [1970].

## RESULTS

The solutions of the integration of the two-fluid model equations for the quiet solar wind (with the constraint  $J_E/r_E^2 \equiv (nv)_E = 3 \times 10^8 \text{ cm}^{-2} \text{ sec}^{-1}$ ) obtained are given in table 1 and figures 1 and 2. For convenience, the values obtained in Cuperman and Harten [1970, 1971], using the constraint  $J_E/r_E^2 = 1.625 \times 10^8 \text{ cm}^{-2} \text{ sec}^{-1}$  ( $n_E = 5 \text{ cm}^{-3}$ ,  $v_E = 325 \text{ km sec}^{-1}$ ), are given in parentheses.

Case 1 represents the solution of the model equations with “pure collisional” energy exchange rate between electrons and protons  $\nu$  as well as pure collisional electron and proton thermal conductivities  $K_e$  and  $K_p$ , respectively. As seen, while the agreement of the calculated particle density and the streaming velocity with the observed values are very good, the other gross features predicted for the solar wind at 1 AU are completely unsatisfactory. The predicted electron temperature is about 2.2 times larger, proton temperature about 4 times lower, and electron thermal flux about 25 times higher than the observed values, respectively. It should be noted that the disagreement of the last three quantities with the observations is even worse than in the pure collisional case with  $J_E/r_E^2 = 1.625 \times 10^8 \text{ cm}^{-2} \text{ sec}^{-1}$ , obtained in Cuperman

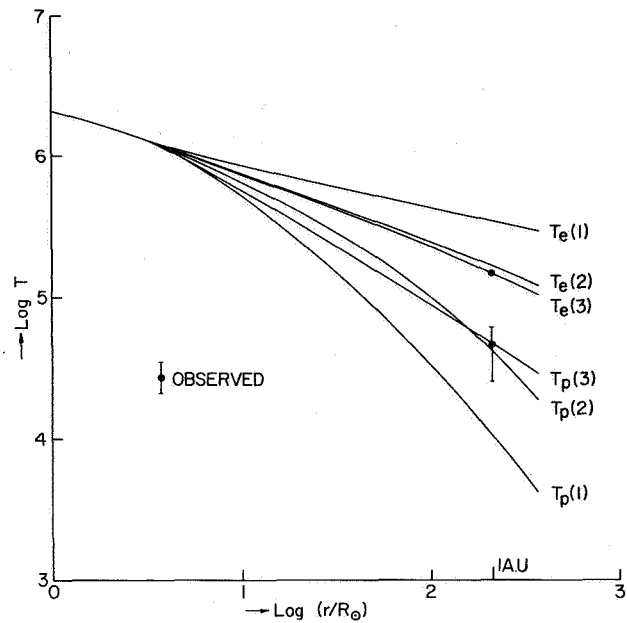


Figure 1. Electron and proton temperature profiles obtained by solving the two-fluid equations with the constraint  $(nv)_E = 3 \times 10^8 \text{ cm}^{-2} \text{ sec}^{-1}$ . The symbols 1, 2, and 3 represent the corresponding cases in table 1.

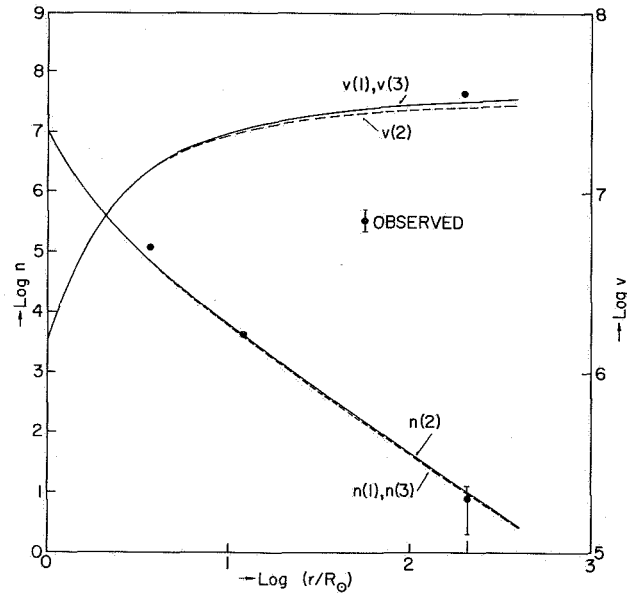


Figure 2. Particle density and radial streaming velocity obtained by solving the two-fluid equations under the same conditions specified in figure 1.

and Harten [1970]. In addition, the values obtained for the particle density at the base of the corona are smaller than those obtained in Cuperman and Harten [1970] and the observed values. Actually, the predicted particle

Table 1. Solutions of the two-fluid equations for the quiet solar wind

Case	$\nu_{mod}$ $\nu$	$K_{e,mod}$ $K_e$	$K_{p,mod}$ $K_p$	$nvr^2$ , $10^8 \text{ cm}^{-2} \text{ sec}^{-1}$	$\frac{r_c}{R_\odot}$	$r = 1R_\odot$		$r = r_c = 12R_\odot$		1 AU					
						$n$ , $10^8 \text{ cm}^{-3}$	$T_e = T_p$ , $10^6 \text{ }^\circ \text{K}$	$\frac{n}{n_{obs}}$	$\frac{n}{n_{obs}}$	$n$ , $\text{cm}^{-3}$	$v$ , $\text{km/sec}$	$T_e$ , $10^5 \text{ }^\circ \text{K}$	$T_p$ , $10^5 \text{ }^\circ \text{K}$	$-K_{e,mod} \frac{dT_e}{dr}$ , $10^{-2} \text{ erg cm}^{-2} \text{ sec}^{-1}$	$-K_{p,mod} \frac{dT_p}{dr}$
1	1 (1)	1 (1)	1 (1)	3 (1.625)	3.832 (5.437)	0.1 (0.24)	2.08 (1.66)	0.5 (0.5)	$\sim 1$ ( $\sim 0.7$ )	9.46 (6.00)	325 (271)	3.40 (2.64)	0.10 (0.16)	24.8 (11.61)	$2.7 \times 10^{-3}$ ( $0.27 \times 10^{-3}$ )
2	30 (30)	0.25 (0.25)	1 (1)	3 (1.625)	3.813 (5.411)	0.1 (0.23)	2.08 (1.67)	0.5 (0.5)	$\sim 1$ ( $\sim 0.7$ )	10.20 (6.33)	302 (256)	1.60 (1.60)	0.45 (0.43)	0.84 (0.75)	$1.43 \times 10^{-3}$ ( $1.30 \times 10^{-3}$ )
3	1 (1)	0.18 (0.20)	2.3 (2)	3 (1.625)	3.838 (5.443)	0.1 (0.24)	2.08 (1.66)	0.5 (0.5)	$\sim 1$ ( $\sim 0.7$ )	9.66 (6.00)	318 (270)	1.47 (1.59)	0.41 (0.43)	0.51 (0.60)	$4.84 \times 10^{-3}$ ( $3.76 \times 10^{-3}$ )
Obser.*	— —	— —	— —	3 (1.625)		$\sim 2.3$ $\sim 2.3$	$\sim 1.2$ $\sim 1.2$		1 1	$8.7 \pm 4.6$ (5)	$\sim 350$ (325)	$\sim 1.5$ ( $\sim 1.5$ )	$4.4 \pm 1.8$ (4)	$< 1$ ( $< 1$ )	— —

\*The observations at 1 AU are taken from Hundhausen et al. [1970]; the values in parentheses are from Hundhausen [1968]. The observations at  $1R_\odot$  are taken from Billings [1966] and those for  $1 < r/R_\odot < 215$  are from Newkirk [1967].

density equals the observed density at about  $12R_\odot$ . Thus, we were able to obtain solutions matching the available observations between about  $12R_\odot$  and 1 AU. As for the agreement between 1 and  $12R_\odot$ , almost unaffected by the modifications to be discussed in the following, we assumed that some more basic physical processes not included in the model equations are required to describe the correct situation prevailing in that region. This point has been strongly emphasized in the literature [Parker, 1969; Hundhausen, 1968], and has also been the object of a discussion in Cupperman and Harten [1970].

As already discussed in Cupperman and Harten [1970, 1971], modification of the transport coefficients in the two-fluid equations could provide satisfactory solutions for all of the characteristics of the solar wind at 1 AU. After systematically investigating the effect of modified (essentially noncollisional) transport coefficients in the two-fluid model equations, we found that the agreement with the observations at 1 AU may be achieved in two ways:

1. By using an "enhanced" energy exchange rate between electrons and protons  $\nu_{mod}$  about 30 times larger than the collisional one (which raises the proton temperature to the observed value but leaves the electron temperature and heat flow almost unchanged) in conjunction with an electron thermal conductivity  $K_{e,mod}$  4 times lower than the collisional one lowering both electron temperature and heat flow to the observed values without further changing the agreement of the proton temperature with the observations (case 2 in table 1).

2. By using an "enhanced" proton thermal conductivity  $K_{p,mod}$  about 2.3 times larger than the collisional one (which, like the enhanced energy exchange rate in case 2, raises the proton temperature at 1 AU to the observed value, without affecting the electron temperature and heat flow) in conjunction with an electron thermal conductivity about 5.5 times lower than the collisional one (which as in case 2, lowers both the electron temperature and the heat flow to the observed values) (case 3 in table 1).

Presumably, the actual situation is intermediate between those corresponding to cases 2 and 3. This indicates the existence of an effective energy exchange rate  $\nu \leq \nu_{mod} \leq 30\nu$ , an effective proton thermal conductivity  $K_p \leq K_{p,mod} \leq 2.3 K_p$ , and an effective electron thermal conductivity  $K_e/5.5 \leq K_{e,mod} \leq K_e/4$ .

Little difference is obtained by comparison of these limit values (namely, 30, 2.3, 4, and 5.5), which are based on a particle flow at 1 AU of  $3 \times 10^8 \text{ cm}^{-2} \text{ sec}^{-1}$ , with the corresponding ones obtained in Cupperman and Harten [1971] (namely, 30, 2, 4, and 5), which were based on a particle flow at 1 AU of  $1.625 \times 10^8 \text{ cm}^{-2} \text{ sec}^{-1}$ .

Thus, the calculations in this work based on the new, and more reliable, statistical value of  $3 \times 10^8 \text{ cm}^{-2} \text{ sec}^{-1}$  for the particle flow at 1 AU give satisfactory solutions for  $n$ ,  $v$ ,  $T_e$ , and  $T_p$  between  $12R_\odot$  and 1 AU, and for  $(K_e dT_e/dr)_E$ , for which observations are available. Between  $1R_\odot$  and  $12R_\odot$  a disagreement with the present observational data exists, which is thought to be due to the absence, in the model equations, of terms describing some additional physical processes present in that region.

#### ACKNOWLEDGMENT

This work was supported by ESSA under contract E-135120.

#### REFERENCES

Billings, D. E.: *A Guide to Solar Corona*, Academic Press, New York, 1966.

Cuperman, S.; and Harten, A.: *Astrophys. J.*, Vol. 162, 1970, p. 315.

Cuperman, S.; and Harten, A.: *Astrophys. J.*, Vol. 163, 1971, p. 383.

Hundhausen, A. J.: *Space Sci. Rev.*, Vol. 8, 1968, p. 666.

Hundhausen, A. J.; Bame, S. J.; Asbridge, J. R.; and Sydoriak, S. J.: *Solar Wind Properties: Vela 3 Observations from July 1965 to June 1967*, University of California, Los Alamos Sci. Laboratory, 1970.

Newkirk, G.: *Ann. Rev. Astron. Astrophys.*, Vol. 5, 1967, p. 213.

Parker, E. N.: *Space Sci. Rev.*, Vol. 9, 1969, p. 325.

# **MODEL FOR ENERGY TRANSFER IN THE SOLAR WIND: FORMULATION OF MODEL**

*R. E. Hartle and Aaron Barnes*

**ABSTRACT** On the basis of conclusions drawn from previous experimental and theoretical evidence, we extend the two-fluid solar-wind model by including the collisionless dissipation of hydromagnetic waves originating at the sun. We generate a series of solar wind models parameterized by the total energy flux of hydromagnetic waves at the base of the model. The resulting properties of propagation and dissipating of hydromagnetic waves on this model are presented.

We interpret the strong positive correlation between observed solar wind speeds  $v_E$  (subscript  $E$  refers to values at 1 AU) and proton temperatures  $T_{pE}$  [Burlaga and Ogilvie, 1970; Hundhausen *et al.*, 1970] as defining a continuum of average macroscopic states. In this case, a realistic model of the wind should be capable of predicting a continuous range of wind speeds and proton temperatures consistent with this  $T_{pE}$ - $v_E$  correlation. Since the wind is frequently observed to blow much faster than the "quiet day" wind, it convects much more energy at some times than at others. We believe that this variability in energy flux reflects the dissipation of varying amounts of nonthermal energy supplied to the system, a view consistent with the  $T_{pE}$ - $v_E$  correlation.

On this basis, we have recently shown [Hartle and Barnes, 1970], in the context of the two-fluid model [Sturrock and Hartle, 1966; Hartle and Sturrock, 1968] that it is possible to choose, *ad hoc*, a class of hypothetical energy deposition functions that give models consistent with the  $T_{pE}$ - $v_E$  correlation. Accordingly, we found that primary energy deposition occurs over an extended region up to about  $25 R_\odot$  from the sun. This result is compatible with the nonthermal heating mechanism suggested by Barnes [1968, 1969];

that is, the collisionless dissipation of fast-mode hydromagnetic waves originating at the sun.

Here we extend our previous model by replacing the artificial heat source with that corresponding to hydromagnetic dissipation. We present some of the properties of propagation and dissipation of hydromagnetic waves as found from a self-consistent treatment of the two-fluid equations with such heating.

This treatment is simplified by assuming that the solar wind is composed of protons and electrons which undergo steady, radial, spherically symmetric expansion. The flow is then described in terms of the proton density  $n$  and flow speed  $v$  (equal to electron density and flow speed), the electron temperature  $T_e$ , and the proton temperature  $T_p$  as functions of the heliocentric distance  $r$ . These profiles are determined by the two-fluid equations of continuity, momentum, and energy given in Hartle and Barnes [1970] by

$$nvr^2 = J = \text{constant} \quad (1)$$

$$nm_p v \frac{dv}{dr} = -\frac{d}{dr} [nk(T_e + T_p)] - \frac{GM_\odot m_p n}{r^2} \quad (2)$$

$$\begin{aligned} \frac{3}{2} n v k \frac{dT_e}{dr} - v k T_e \frac{dn}{dr} - \frac{1}{r^2} \frac{d}{dr} \left( r^2 \kappa_e \frac{dT_e}{dr} \right) \\ = -\frac{3}{2} v_E n k (T_e - T_p) + \mathcal{P}_e \end{aligned} \quad (3)$$

---

*The authors are with the NASA Laboratory for Planetary Atmospheres, Goddard Space Flight Center, Greenbelt, Md., and the Space Science Division, Ames Research Center, Moffett Field, California.*

$$\begin{aligned} \frac{3}{2} n v k \frac{dT_p}{dr} - v k T_p \frac{dn}{dr} - \frac{1}{r^2} \frac{d}{dr} \left( r^2 \kappa_p \frac{dT_p}{dr} \right) \\ = \frac{3}{2} v_E n k (T_e - T_p) + \Phi_p \end{aligned} \quad (4)$$

in terms of the proton and electron masses  $m_p$  and  $m_e$ , the solar mass  $M_\odot$ , the gravitational constant  $G$ , and Boltzmann's constant  $k$ . The electron and proton thermal conduction coefficients,  $\kappa_e$  and  $\kappa_p$ , and the electron-proton energy exchange rate  $\nu_E$  are those of *Braginskii* [1965]. The fast-mode hydromagnetic heat sources are of the form

$$\Phi_{(p)}^{(e)}(r) = \int d^3k \Phi_{(p)}^{(e)}(k, r) \quad (5)$$

$$\Phi_{(p)}^{(e)}(k, r) = (\omega_o - k \cdot v) W(k, r) G_{(p)}^{(e)} \left( \frac{\omega_o - k \cdot v}{k}, e_k, r \right) \quad (6)$$

The local plasma-frame (complex) circular frequency, in terms of the rest-frame (of the sun) frequency  $\omega_o$  and wave vector  $k$ , is given by  $\bar{\omega} = \omega + i\gamma = \omega_o - k \cdot v + i\gamma$  and is related to  $k$  through the dispersion relation [Barnes, 1968]. The factor  $W$  is the energy density spectrum of the waves and  $G$  corresponds to the energy absorption by the protons (electrons) per unit wave energy in the time  $1/\omega$ . The heat functions are based on the assumptions that the velocity distributions are maxwellian, that the wave amplitudes are small enough that linear wave theory is valid, and that  $|\gamma| \ll \omega$ .

The energy deposition term  $G_{(p)}^{(e)}$  is a complicated function of the plasma parameters  $n$ ,  $v$ ,  $T_e$ , and  $T_p$ , the local average magnetic field  $B(r)$ , and the angle  $\theta$  between the wave vector  $k$  and field  $B$ . We assume that the average properties of the magnetic field  $B(r)$  are adequately described by the spiral model of *Parker* [1963]. In the models considered here, the electron energy deposition term  $G_e \approx 0$  since the electron-electron collision frequency is much greater than the source frequency  $\omega_o = 2 \times 10^{-2} \text{ sec}^{-1}$  (see below). The typical dependence of the proton energy deposition term  $G_p$  on  $\theta$  is shown in figure 1 for plasma parameters at the base of one of the models (see below;  $F_o = 5.2 \times 10^3 \text{ ergs cm}^{-2} \text{ sec}^{-1}$  for this case). Here we note that the energy deposition distribution peaks at  $\theta \sim 20^\circ$  and that primary proton heating occurs over the range  $10^\circ \lesssim \theta \lesssim 35^\circ$ .

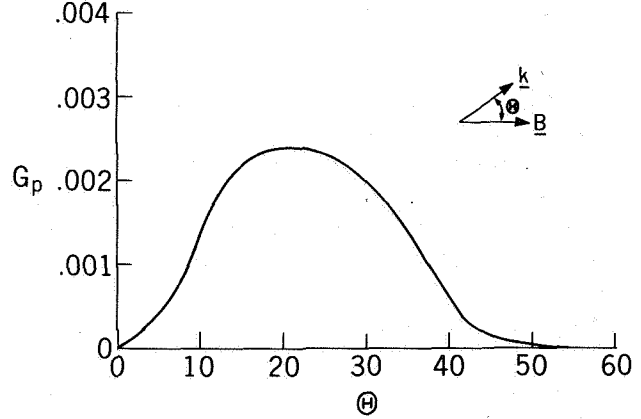


**Figure 1.** Proton energy absorption rate per unit wave energy in time  $1/\omega$  versus  $\theta$ , the angle between the wave vector and magnetic field.

Since the wavelengths in question are small relative to macroscopic scale lengths, we determine the energy density  $W$  of the waves in the approximation of "geometrical hydromagnetics." In this case, the ray paths  $x(s)$  and wave vectors  $k(s)$  ( $s$  is path length along ray) are obtained from Hamilton's equations, the dispersion relation, and the computed profiles  $n$ ,  $v$ ,  $T_p$ ,  $T_e$ , and  $B$ . Then for a given pair  $(x_o, k_o)$  at the base and fixed  $\omega_o$

$$W[k(s), x(s)] = W(k_o, x_o) \exp \int_{s_o}^s \frac{2\gamma_k(s')}{|\partial\omega(s')/\partial k|} ds' \quad (7)$$

where  $\gamma_k = \text{Im } \omega_k$  is the damping decrement and  $\partial\omega/\partial k$  the group velocity, and the integration is along the ray.

The solar-wind models considered here are determined by self-consistent numerical solutions of equations (1) through (7) and the ray equations using a method of iteration similar to that described in *Hartle and Barnes* [1970]. In addition to specifying the magnetic field strength  $B_o$  and the hydromagnetic wave spectrum at the base of the model, the solutions are subject to the usual constraints of specifying the base density and temperatures  $n_o$ ,  $T_{eo}$ ,  $T_{po}$ , requiring the velocity  $v$  to pass continuously through the subsonic-supersonic transition, and requiring  $T_e$  and  $T_p$  to tend to zero as  $r$  goes to infinity. We treat the wave spectrum as a discrete number of rays (six in this work), weighted so that the base intensity is approximately isotropic in the outward directions (zero in the inward directions), and the frequency spectrum is assumed monotonic. The boundary values we choose at the base

$r = 2R_\odot$  are  $n_0 = 1.5 \times 10^6 \text{ cm}^{-3}$ ,  $T_{e0} = 1.3 \times 10^6 \text{ K}$ ,  $T_{p0} = 1.7 \times 10^6 \text{ K}$ , and  $B_0 = 0.18$ , consistent with coronal observations [Newkirk, 1967]. Our selection  $T_{p0} > T_{e0}$ , implying selective proton heating below the base, is consistent with the inner corona heating model of D'Angelo [1968, 1969]. The source frequency is taken to be  $\omega_0 = 2 \times 10^{-2} \text{ sec}^{-1}$ , near the peak of the observed photospheric and chromospheric acoustic spectrum [Leighton et al., 1962; Tanenbaum et al., 1969].

We have calculated a series of models that are parameterized by the remaining free parameter of the system; namely, the total energy flux  $F_0$  of hydromagnetic waves at the base. Three of the resulting ray trajectories are shown in figure 2 in terms of their azimuthal and radial coordinates  $\phi$  and  $r/R_\odot$ . These trajectories, corresponding to a flux  $F_0 = 5.2 \times 10^3 \text{ ergs cm}^{-2} \text{ sec}^{-1}$ , are typical of the class of models we considered and, for purposes of illustration, have been selected so that they all become radial at  $\phi = 0$ . The base emission angles  $\theta_e \equiv \cos^{-1}(\mathbf{k} \cdot \hat{r}/k)$ , between the wave vectors and the radial direction, are  $0^\circ$ ,  $15^\circ$ , and  $45^\circ$ . We note that the ray with emission angle  $\theta_e = 0$  propagates radially while the remaining rays refract toward the radial direction, becoming essentially radial at 10 or  $12 R_\odot$ . In addition, we observe that the refraction becomes stronger as the emission angle increases.

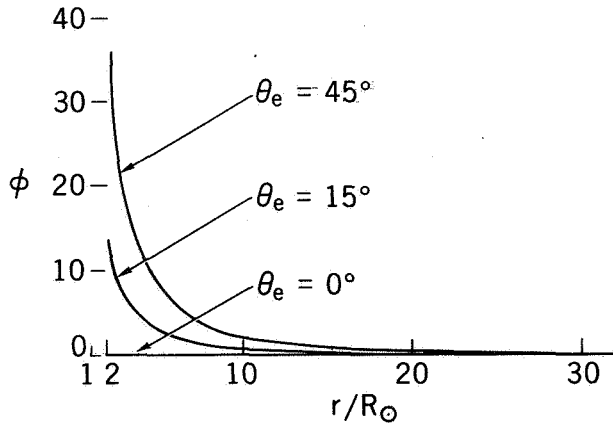


Figure 2. Ray trajectories in equatorial plane.

Let us now consider the damping of these rays. The peak amplitude of the energy deposition term  $G_p$  increases strongly with  $\beta_p = 8\pi n k T_p / B^2$ ; for example, the damping rate  $\gamma \propto \exp(-1/\beta_p)$  when  $\beta_p \lesssim 0.1$ . Nevertheless, since the shape of the energy deposition term  $G_p$  of figure 1 is essentially the same for the range of parameters of interest, we can get a qualitative

indication of where the relative damping between rays takes place by considering the angles  $\theta$  each wave vector makes with the magnetic field. The  $\theta$  profiles corresponding to the rays of figure 2 are shown in figure 3. In this case, the ray with emission angle  $\theta_e = 45^\circ$  should lose a significant portion of its energy at radii less than about  $6 R_\odot$  since it passes through the range  $10^\circ < \theta < 35^\circ$  where the damping is strongest (damping will be relatively weak for  $r \lesssim 2.5 R_\odot$ ). The intermediate ray,  $\theta_e = 15^\circ$ , will not damp as strongly near the base, resulting in a more extended heating region. Finally, the radial ray corresponds to the most extended dissipation since it has relatively low values of  $\theta$  throughout. The rays dissipate at similar rates beyond about  $12 R_\odot$  where they are essentially radial. In this region  $\theta$  increases with the spiral angle, resulting in increasing deposition rates with  $r$ ; here the remaining portion of the wave energy is lost.

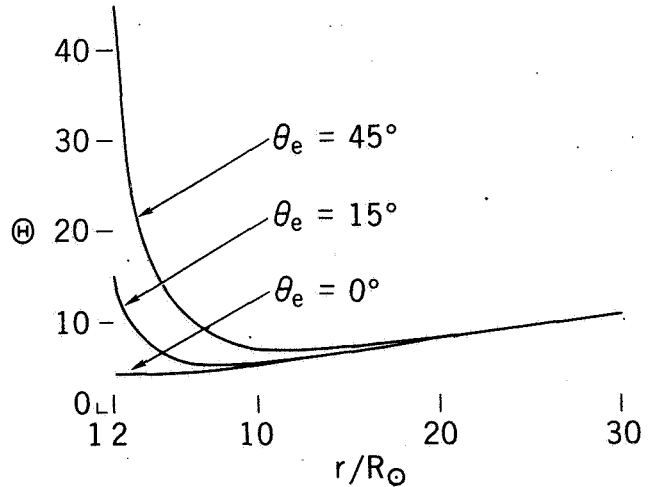
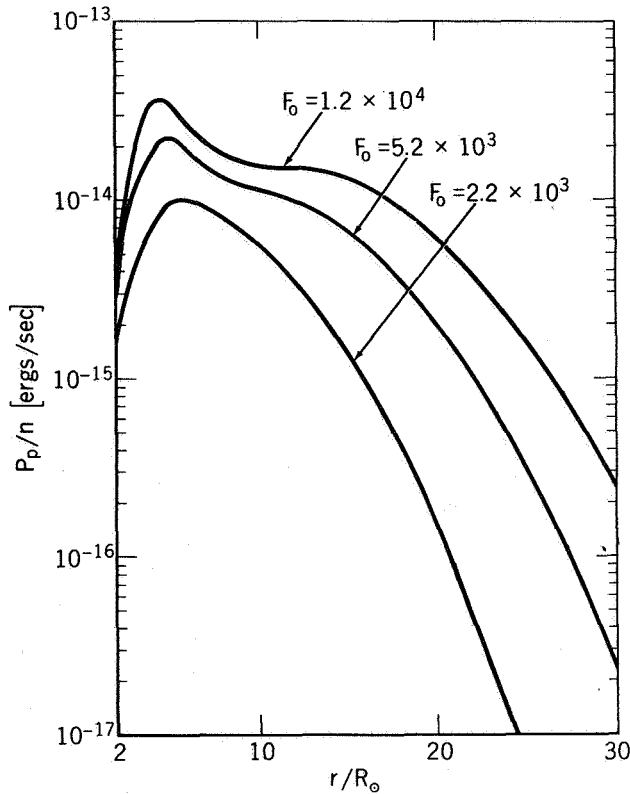


Figure 3. Angle  $\theta$  between the wave vector and magnetic field versus radial position  $r/R_\odot$ .

Upon summing the heat contribution from each ray we obtain the proton heat source  $P_p$  on this model. The resulting energy deposition distributions are shown in figure 4 corresponding to three models with  $F_0 = 2.2 \times 10^3$ ,  $5.2 \times 10^3$ , and  $1.2 \times 10^4 \text{ (ergs cm}^{-2} \text{ sec}^{-1})$ , which result in wind speeds  $v_E = 290$ ,  $370$ , and  $427 \text{ (km sec}^{-1})$  and proton temperatures  $T_{pE} = 2 \times 10^4$ ,  $6.2 \times 10^4$ , and  $1.7 \times 10^5 \text{ (K)}$ , respectively. These models are consistent with the  $T_{pE} - v_E$  correlation as discussed earlier by Barnes and Hartle (p. 219). For clarity, we normalized the heat profiles by the density to give the heating rate per proton. In each model hydromagnetic heating is important over an extensive region of  $20$ – $30 R_\odot$  in radius. Beyond this region,  $P_p$  decays





**Figure 4.** Normalized proton heat sources  $P_p/n$  versus radial position  $r/R_\odot$ .

rapidly and other terms in the proton heat equation become dominant.

When the energy flux  $F_0$  is increased, we note in figure 4 that there is an overall increase in the heat profile resulting in both increased wind speeds  $v_E$  and proton temperatures  $T_{pE}$  at 1 AU. This is consistent with our previous model [Hartle and Barnes, 1970], which demonstrated that heating in the region of subsonic flow ( $r \lesssim 5-7 R_\odot$ ) primarily raises the wind speed at 1 AU and heating in the supersonic flow region primarily raises the proton temperature at 1 AU. Also consistent with a requirement of our previous model is the inward motion of the heat source peak with increasing flux  $F_0$ . This variation in the peak is related to the fact that increased heating raises  $\beta_p = 8\pi nkT_p/B^2$ , which in turn raises the damping rate  $\gamma \propto \exp(-1/\beta_p)$ , leading to a relatively larger rate of energy deposition near the base.

## REFERENCES

- Barnes, A.: Collisionless Heating of the Solar-Wind Plasma, I, Theory of the Heating of Collisionless Plasma by Hydromagnetic Waves. *Astrophys. J.*, Vol. 154, 1968, p. 751.
- Barnes, A.: Collisionless Heating of the Solar-Wind Plasma, II, Application of the Theory of Plasma Heating by Hydromagnetic Waves. *Astrophys. J.*, Vol. 155, 1969, p. 311.
- Braginskii, S. I.: Transport Processes in a Plasma, in *Reviews of Plasma Physics*, Vol. 1, edited by M. A. Leontovich, Consultants Bureau, New York, 1965, p. 205.
- Burlaga, L. S.; and Ogilvie, K. W.: Heating of the Solar Wind. *Astrophys. J.*, Vol. 159, 1970, p. 659.
- D'Angelo, N.: Heating of the Solar Corona. *Astrophys. J.*, Vol. 154, 1968, p. 401.
- D'Angelo, N.: Heating of the Solar Corona. *Solar Phys.*, Vol. 7, 1969, p. 321.
- Hartle, R. E.; and Sturrock, P. A.: Two-Fluid Model of the Solar Wind. *Astrophys. J.*, Vol. 151, 1968, p. 1155.
- Hartle, R. E.; and Barnes, A.: Nonthermal Heating in the Two-Fluid Solar Wind Model. *J. Geophys. Res.*, Vol. 75, 1970, p. 6915.
- Hundhausen, A. J.; Bame, S. J.; Asbridge, J. R.; and Sagdorak, J.: Solar Wind Proton Properties: Vela 3 Observations from July 1965-June 1967. *J. Geophys. Res.*, Vol. 75, 1970, p. 4643.
- Leighton, R. B.; Noyes, R. W.; and Simon, G. W.: Velocity Fields in the Solar Atmosphere, I, Preliminary Rep. *Astrophys. J.*, Vol. 135, 1962, p. 474.
- Newkirk, G., Jr.: Structure of the Solar Corona, in *Annual Review of Astronomy and Astrophysics*, Vol. 5, edited by L. Goldberg, D. Layzer, and J. G. Phillips, Annual Reviews, Inc., Palo Alto, Calif., 1967, p. 213.
- Parker, E. N.: *Interplanetary Dynamical Processes*. Interscience, New York, 1963.
- Sturrock, P. A.; and Hartle, R. E.: Two-Fluid Model of the Solar Wind. *Phys. Rev. Letters*, Vol. 16, 1966, p. 628.
- Tanenbaum, A. S.; Wilcox, J. M.; Frazier, E. N.; and Howard, R.: Solar Velocity Fields: 5-min Oscillations and Supergranulation. *Solar Phys.*, Vol. 9, 1969, p. 328.

## A GAS-DYNAMIC CALCULATION OF TYPE II SHOCK PROPAGATION THROUGH THE CORONA

Roger A. Kopp

**ABSTRACT** An approximate analytic theory of acoustic shock propagation in nonuniform media is used to determine the motion of a flare-generated shock wave in the corona. The shock is followed from the time it strikes the chromosphere-corona transition region (density interface) out to  $5 R_{\odot}$  under the assumption that the corona in this region is approximately in hydrostatic equilibrium. In the actual corona, the situation would apply to the case of slow-mode shock propagation along a radially diverging magnetic field.

The strength of the shock incident on the transition region from below determines the ejection velocity of eruptive prominence material, as well as the initial velocity of the coronal shock. The calculation is applied to one well-documented case of a related flare spray, moving type IV isolated source, and type II burst. It is shown that a chromospheric shock of the appropriate strength to produce the observed prominence and type IV velocities strengthens as it moves out in the corona by an amount sufficient to account for the observed high velocity of the type II burst.

### INTRODUCTION

It is now regarded as a well-established fact that type II solar radio bursts are the direct result of flare-generated shock waves traveling outward through the corona [Wild, 1969, 1970]. Whether such waves are primarily acoustic (slow mode) or magnetohydrodynamic (fast mode) in character, however, is still an open question. Many workers have relied on magnetic effects to explain certain features of the bursts, such as band-splitting [Sturrock, 1961], although nonmagnetic explanations are frequently available as well [McLean, 1967].

If the waves are acoustic in nature, then rather large shock Mach numbers are required to produce the observed burst velocities of the order of 1000 km/sec [Weiss, 1965]. Nevertheless, at least low in the corona the material motions following a flare, as evidenced by the underlying eruptive prominence (or so-called "flare

spray"), appear to be largely channeled along magnetic lines of force. Observational evidence for magnetic fields influencing the motion of a type II source at higher levels has been presented by Kai [1969]. However, at least in some cases shock propagation must occur across field lines if one is to explain the Moreton-wave phenomenon as the intersection of a type II wave front with the chromosphere [Wild, 1969; Uchida, 1970].

Occasionally associated with a type II burst and prominence eruption, but occurring later in time and having a much longer duration, is a moving burst of type IV. Smerd and Dulk [1970] distinguish three subclasses of type IV: the isolated source, the expanding arch, and the advancing front. Here we are concerned only with the first of these, for which it appears that the source moves outward along predominantly open magnetic field lines [Smerd and Dulk, 1970; Dulk and Altschuler, 1971].

Type IV bursts of the "isolated source" variety are relatively infrequent; Smerd and Dulk [1970] have identified possibly eight examples observed with the 80-MHz radioheliograph during the period February

---

*The author is at the High Altitude Observatory, National Center for Atmospheric Research, Boulder, Colorado. The National Center for Atmospheric Research is sponsored by the National Science Foundation.*

1968 to April 1970. Particularly well observed was the event of March 21, 1970, reported by *Sheridan* [1970]: Following a flare of importance 2N near the east limb at 00<sup>h</sup> 23<sup>m</sup>, a large eruptive prominence was seen in  $H\alpha$  to leave the flare location with a velocity of 260 km/sec. It reached a height of  $0.3 R_{\odot}$  above the photosphere before fading from view. Simultaneously, radiospectrograph records indicated a type II burst with a velocity of order 1500 km/sec [*Smerd and Dulk*, 1970]. Type II bursts are frequently observed to occur in pairs after large flares, presumably the result of multiple shocks being emitted by the flaring region. This was the case with the event being described. We refer here to the second, and stronger, burst.) A short time after the prominence faded, a type IV source appeared at  $r = 1.9 R_{\odot}$  and subsequently moved outward to a distance of more than  $5 R_{\odot}$  with a constant 290-km/sec velocity, whereupon it fragmented and slowly faded away. The source velocity was comparable to that measured for the prominence eruption; extrapolation backwards in time showed that both left the sun during the flash phase of the flare.

*Sheridan* [1970] suggested that the outward-moving prominence material excited the type IV source near the  $r = 1.9 R_{\odot}$  level. However, such an interpretation does not account for the nearly equal velocities of the source and the prominence ejecta. Alternatively, we may conjecture that the flare spray and the type IV source are simply different manifestations of the same material, the ejected "blob" becoming visible at 80 MHz only after the prominence fades in  $H\alpha$  and rises significantly above the 80-MHz plasma level in the corona.

Here we show, by means of a simple model, that a relationship exists between the velocities of the eruptive prominence and moving type IV isolated source (here assumed to be the same) and that of the type II burst. We postulate that these three phenomena are the natural consequence of a single flare-initiated shock traversing the solar atmosphere. In the model, the velocity of the flare spray is taken as a measure of the strength of the shock at the top of the chromosphere. With this information and knowledge of the coronal density structure, the shock strength and velocity may then be calculated as functions of height in the corona. As an example, we apply the calculation to the event observed by *Sheridan* [1970].

### SHOCK-WAVE CALCULATIONS

The shock wave emitted by the flare during its flash phase is assumed to propagate vertically upward, or nearly so, through the chromosphere. Here we will be concerned with its motion only after the shock reaches the "top" of the chromosphere. By that time we assume

it to be a slow mode shock traveling along the magnetic field.

The atmosphere ahead of the shock is characterized by large gradients of temperature and density. It is convenient to divide the calculation of the subsequent shock motion into two parts, corresponding roughly to regions with large or small temperature gradients.

#### Shock Interaction with the Transition Region

The shock immediately encounters the chromosphere-corona transition region, where the preshock atmospheric density drops abruptly by more than 2 orders of magnitude over a radial distance of less than a scale height. We idealize this region to be a sharp density interface (infinite temperature gradient), with equal pressures above and below.

The interaction of a slow-mode shock with a density interface is shown schematically by an  $(x, t)$  diagram in figure 1. Regions 0 and 3 represent the undisturbed chromosphere and corona, respectively, separated by the contact discontinuity  $CC'$ . When the chromospheric

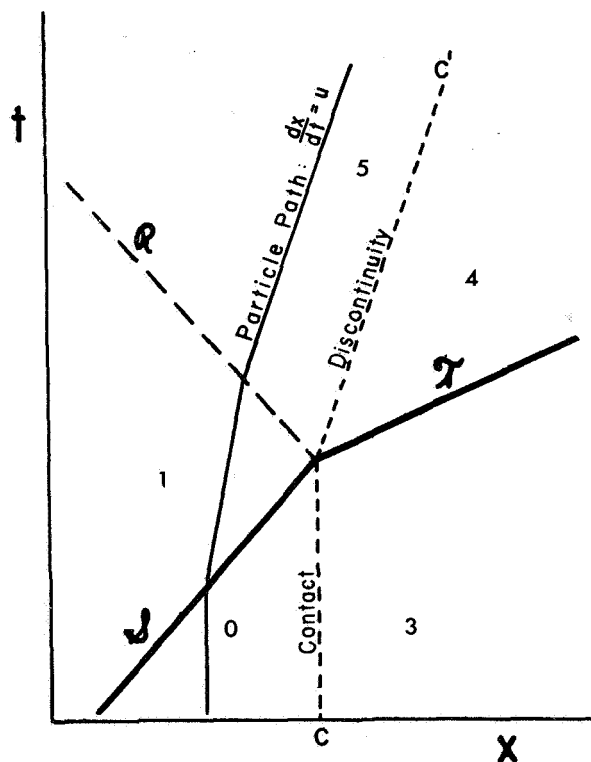


Figure 1. A distance-time  $(x, t)$  diagram of a plane shock wave,  $\mathcal{S}$ , impinging normally upon a contact discontinuity  $CC'$ . The case shown here is that of the shock entering a region of lower density, for which (assuming equal specific heat ratios) the reflected wave,  $\mathcal{R}$ , is a rarefaction.

shock  $\mathcal{S}$  strikes the interface, it sets the latter in motion. At the same time a transmitted shock  $\mathcal{T}$  and a reflected rarefaction wave  $\mathcal{R}$  propagate away from the contact surface in the directions shown. Region 1 indicates the shocked chromospheric gas, region 4 the shocked coronal gas, and region 5 the shocked chromospheric gas, which has been somewhat recooled by the downward-propagating rarefaction wave.

In this picture the  $H\alpha$  prominence eruption is identified with chromospheric material immediately below the ascending interface (region 5); the velocity of the interface  $v_5$  corresponds to that of the prominence.

This shock wave-density interface model of a flare spray is similar to that proposed by *Osterbrock* [1961] for spicules, except that a much stronger disturbance is involved here. There are six nontrivial, independent algebraic relations between the state variables in the five regions of the  $(x, t)$  diagram (the trivial ones being  $p_0 = p_3$ ,  $v_0 = v_3 = 0$ ,  $p_4 = p_5$ , and  $v_4 = v_5$ ). Apart from differences in notation, they have been given by *Osterbrock*. Together with the known properties of the undisturbed chromosphere and corona, these relations completely determine the shock-interface interaction in terms of the strength of the incident shock. Solution by iteration is straightforward.

As a numerical example, we assume a chromospheric temperature  $T_0 = 7 \times 10^3$  °K, a coronal temperature  $T_3 = 1.5 \times 10^6$  °K, and a 10:1 hydrogen-helium ratio (mean molecular weight  $\mu = 0.609$ ). The specific heat ratio  $\gamma$  is taken to be 5/3 on both sides of the interface. Table 1 shows the results of a calculation in which the strength of the chromospheric shock was adjusted to

obtain an interface velocity of about 290 km/sec corresponding to the eruptive prominence-moving type IV source velocity of the event of March 21, 1970 [*Sheridan*, 1970].

#### Shock Propagation in the Corona

As the transmitted coronal shock moves away from the sun it traverses a medium with continuously varying properties, which cause additional changes in its strength. To describe the motion of the shock in the corona we use the method of *Whitham* [1958], which was applied to the case of a spherical shock in a gravitational atmosphere by *Kopp* [1968]. For a corona in hydrostatic equilibrium this theory yields the following total differential equation for shock Mach number  $M$ :

$$\frac{1}{M} \frac{dM}{dr} = \eta \left\{ \frac{1}{\xi + \zeta} \left[ (\zeta^2 + \xi\zeta - 1) \frac{g(r)}{a^2} - \xi\zeta \frac{1}{A} \frac{dA}{dr} \right] - \xi \frac{1}{a} \frac{da}{dr} \right\} \quad (1)$$

In this equation,  $r$  denotes distance from the center of the sun,  $g(r) = GM_\odot/r^2$  is the gravitational acceleration,  $a = (\gamma RT/\mu)^{1/2}$  is the velocity of sound, and  $(1/A)/(dA/dr)$  is the rate of geometric spreading of the wave. In addition,

$$\xi = \frac{2}{\gamma + 1} \left( M - \frac{1}{M} \right) = \frac{\text{postshock gas velocity}}{\text{preshock sound velocity}}$$

$$\zeta = \left[ \frac{(\gamma - 1)M^2 + 2}{(\gamma + 1)M^2} \phi \right]^{1/2} = \frac{\text{postshock sound velocity}}{\text{preshock sound velocity}}$$

Table 1. Shock-density interface calculation

Preshock	Chromosphere	$T_0 = 7 \times 10^3$ °K
	Corona	$T_3 = 1.5 \times 10^6$ °K
Flare spray	$v_5 = 288.1$ km/sec	
	$T_5 = 1.10 \times 10^5$ °K	
	$\rho_{\text{spray}}/\rho_{\text{chromosphere}} = 0.47$	( $\rho$ = density)
Chromospheric shock Mach number	$M = 14.26$	( $v = 179.8$ km/sec)
Coronal shock Mach number	$M = 2.48$	( $v = 457.8$ km/sec)

and

$$\eta = \frac{\gamma + 1}{2} \left( \frac{2\xi M^2}{\phi} + \frac{1 + M^2}{M} \right)^{-1}$$

where

$$\phi = \frac{2\gamma}{\gamma + 1} M^2 - \frac{\gamma - 1}{\gamma + 1} = \frac{\text{postshock pressure}}{\text{pres shock pressure}}$$

Since  $\xi > 0$  and  $\zeta > 1$ , we have that  $\xi^2 + \xi\zeta - 1 > 0$ , so that the first term in equation (1) corresponds to a strengthening of the shock as it moves into regions of lower density. Similarly, the second term yields a weakening of the wave due to geometric attenuation, and the third term indicates the effect of a coronal temperature gradient on the shock.

Equation (1) predicts changes in shock strength resulting only from nonuniform properties of the pre-shock gas. In addition, changes occur in response to disturbances overtaking the shock from the rear. These include (1) re-reflected waves generated by the changing shock strength itself, and (2) waves produced by variations in the motions of the shock "driver." The basis of *Whitham's* [1958] method is that the first of these disturbances can be neglected in an approximate description of the shock motion. For the coronal shock under consideration here, we suggest that the "driver" waves can be neglected as well, since the observed constancy of the type IV velocity implies a continuously driven type II shock.

Equation (1) can be numerically integrated for a corona of known temperature and for a shock of known geometrical spreading. Again, as an example, we adopt a constant coronal temperature of  $1.5 \times 10^6$  K ( $a = 184.6$  km/sec). Using the transmitted shock strength, from the interface calculation,  $M_0 = 2.48$ , as an initial condition, and assuming a slow-mode shock channeled along a radially diverging magnetic field  $[(1/A)(dA/dr) = 2/r]$ , we obtain the radial dependence of shock speed shown in figure 2. Then the path of the shock in the  $(r, t)$  diagram can be found from

$$t(r) = a^{-1} \int_{R_0}^r \frac{dr}{M(r)} \quad (2)$$

where  $t = 0$  corresponds to the time when the shock leaves the transition region ( $r = R_0$ ). The shock path for the above example is shown in figure 3.

The most striking aspect of this calculation is the rapid strengthening of the shock below about  $2 R_0$ . Beyond  $r = 2 R_0$  the shock speed varies by only about 20

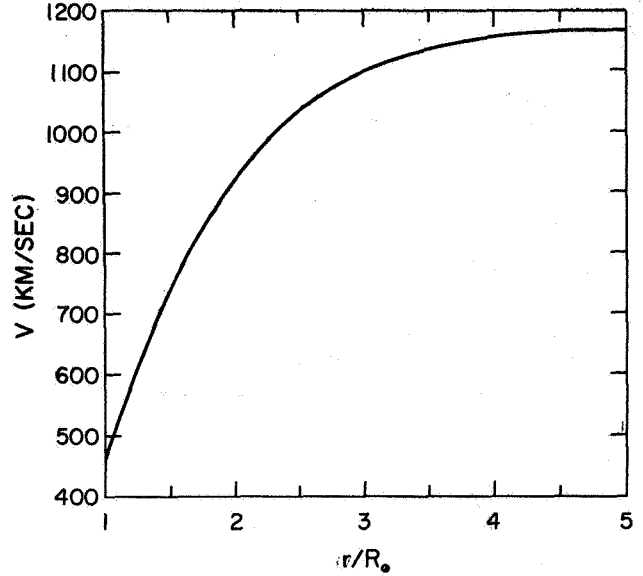


Figure 2. Shock velocity versus height in a  $1.5 \times 10^6$  °K corona, assuming a radially diverging geometry and a driven shock.

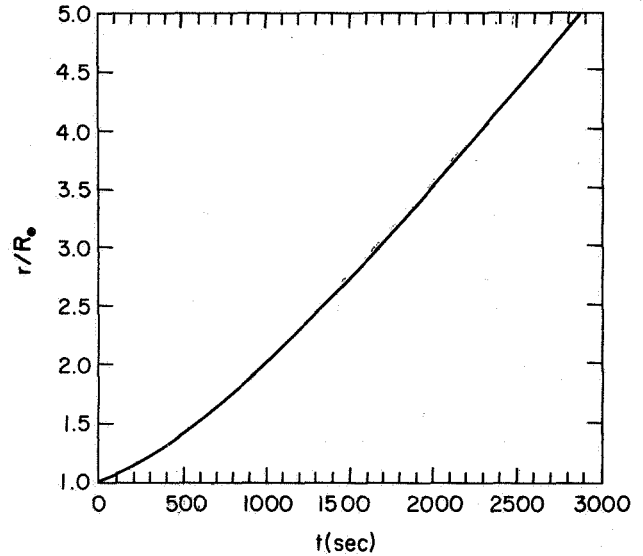


Figure 3. Shock path  $r(t)$  corresponding to figure 2.

percent of its maximum value of 1165 km/sec, which occurs near  $4.8 R_0$ . Evidently, the gravitational and area terms in equation (1) nearly balance each other over a rather broad region.

Considering the uncertainties inherent in deducing type II source velocities from dynamic spectra [Zaitsev, 1969; Van Bueren and Kuperus, 1970], the maximum

shock speed obtained by this calculation is in reasonable agreement with the observed type II velocity for the event of March 21, 1970 [Smerd and Dulk, 1970; cf. previous section].

## DISCUSSION

We have seen that the eruptive prominence, moving type IV isolated source, and type II burst associated with a particular flare may all be the result of a flare-initiated shock wave traveling outward along the magnetic field. When the shock strikes the transition region, the chromospheric material set in motion by the shock continues to rise into the corona and initially becomes visible as the ascending  $H\alpha$  prominence, in the manner proposed by Osterbrock [1961]. Later, as the  $H\alpha$  emission fades and the material passes the 80-MHz plasma level in the corona, it appears as a moving source of type IV emission.

The major predictions of the shock-interface calculation are that:

1. A strong slow-mode shock is required in the upper chromosphere to produce a flare spray of the observed velocity. Such a shock could result either from intense heating in the flaring region or from rapid growth of a weak flare-initiated shock as it runs outward through chromospheric layers of successively lower density.
2. The kinetic temperature of the rising prominence ( $\sim 10^5$  K) greatly exceeds that of the chromosphere, whereas the density is somewhat less. This may account for the eventual disappearance of the spray in  $H\alpha$  as a new statistical equilibrium becomes established at the higher temperature.
3. The transmitted shock is of intermediate strength. In particular, its velocity is too low to match that of a type II burst.

The flare-excited shock continues into the corona, where the outward-decreasing density leads to its re-strengthening and acceleration to typical type II velocities. The observed constancy of the type IV source velocity out to distances of several solar radii lends credence to the postulate that the type II shock is steadily driven from below.

The derived shock speeds depend, of course, on the assumed values of the coronal temperature and the geometrical spreading factor. For example, a higher coronal temperature would decrease the initial rate of strengthening of the shock through the "scale-height" term in equation (1). Moreover, the shock Mach number would then reach its maximum value closer to the sun. In spite of the increased speed of sound in the corona, the result would be a lower shock velocity.

It would be extremely interesting to follow the motion of such a shock to large distances from the sun ( $r > 5 R_\odot$ ), as it is possible that type II shocks may be detected as collisionless interplanetary shock waves at 1 AU. Such a calculation is tractable at the present time, although it requires explicit consideration of the expansion state of the preshock atmosphere.

## ACKNOWLEDGMENTS

The author wishes to thank Drs. G. Dulk and G. Newkirk, Jr., for several illuminating discussions. Mrs. Nancy Werner kindly assisted with the numerical calculations, and Mr. V. Pizzo offered valuable technical assistance.

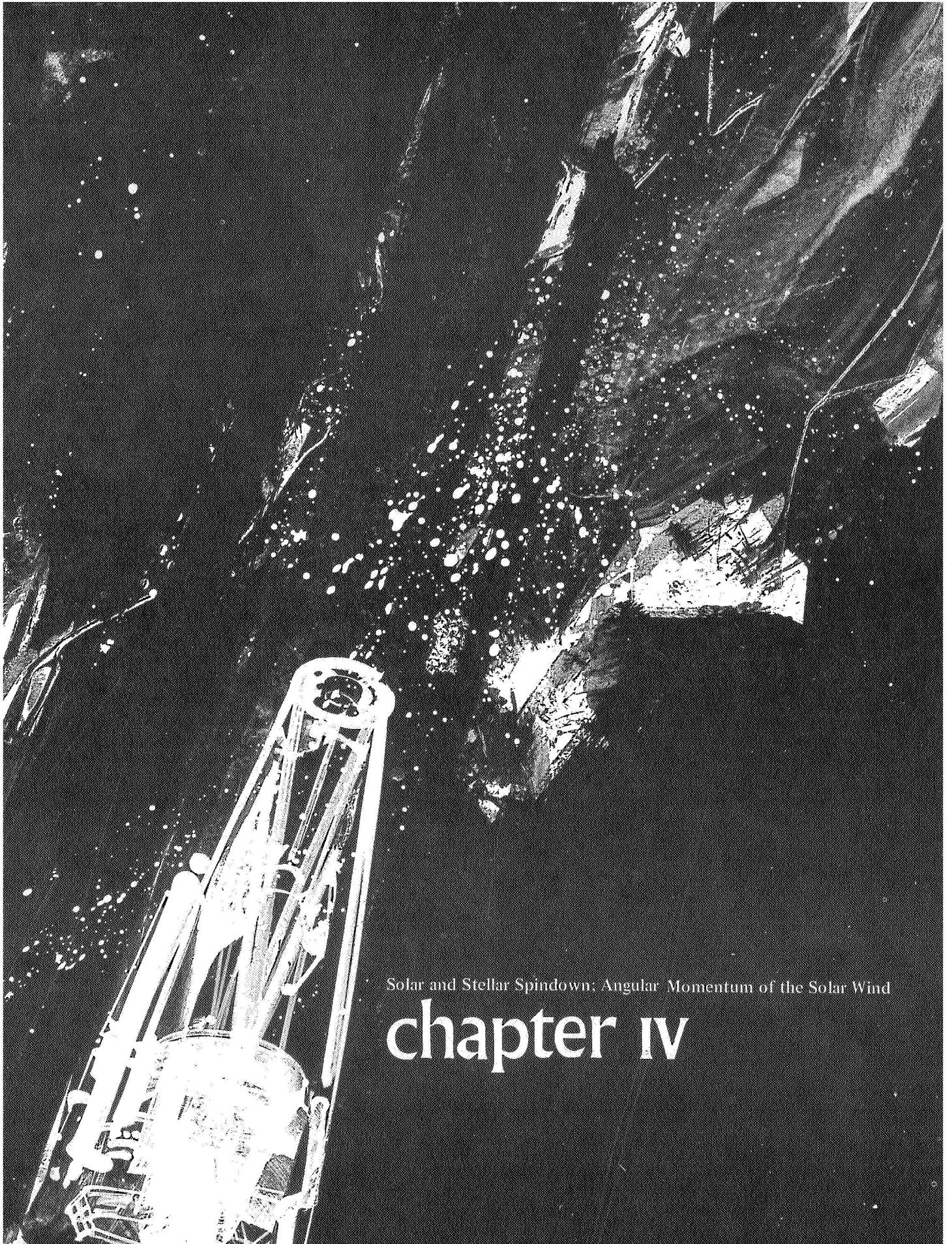
## REFERENCES

- Dulk, G. A.; and Altschuler, M.: A Moving Type IV Radio Burst and Its Relation to the Coronal Magnetic Field. Submitted to *Solar Phys.*, 1971.
- Kai, K.: Radio Evidence of Directive Shock-Wave Propagation in the Solar Corona. *Solar Phys.*, Vol. 10, 1969, p. 460.
- Kopp, R. A.: The Dynamical Structure of a Shock-Heated Corona. Ph.D. Thesis, Harvard University, 1968.
- McLean, D. J.: Band Splitting in Type II Solar Radio Bursts. *Proc. Astron. Soc. Australia*, Vol. 1, 1967, p. 47.
- Osterbrock, D. E.: The Heating of the Solar Chromosphere, Plages, and Corona by Magnetohydrodynamic Waves. *Astrophys. J.*, Vol. 134, 1961, p. 347.
- Sheridan, K. V.: 80 MHz Observations of the Movement of a Type IV Source Out to  $6 R_\odot$  from the Centre of the Sun. *Proc. Astron. Soc. Austr.*, Vol. 1, 1970, p. 376.
- Smerd, S. F.; and Dulk, G. A.: 80-MHz Radioheliograph Evidence on Moving Type IV Bursts and Coronal Magnetic Fields. IAU Symposium No. 43 (Solar Magnetic Fields, Paris, Aug. 31-Sept. 4, 1970).
- Sturrock, P. A.: Spectral Characteristics of Type II Solar Radio Bursts. *Nature*, Vol. 192, 1961, p. 58.
- Uchida, Y.: Diagnosis of Coronal Magnetic Structure by Flare-Associated Hydromagnetic Disturbances. *Publ. Astron. Soc. Jap.*, Vol. 22, 1970, p. 341.
- Van Bueren, H. G.; and Kuperus, M.: On the Determination of the Velocity of the Exciters of Type II Solar Radiobursts. *Solar Phys.*, Vol. 14, 1970, p. 208.
- Weiss, A. A.: The Nature and Velocity of the Sources of Type II Solar Radio Bursts. *Aust. J. Phys.*, Vol. 18, 1965, p. 167.

- Whitham, G. B.: On the Propagation of Shock Waves Through Regions of Non-Uniform Area or Flow. *J. Fluid Mech.*, Vol. 4, 1958, p. 337.
- Wild, J. P.: Radio Evidence of Instabilities and Shock Waves in the Solar Corona, in *Plasma Instabilities in Astrophysics*, edited by D. G. Wentzel and D. A. Tidman, Gordon and Breach, New York, 1969, p. 119.
- Wild, J. P.: Some Investigations of the Solar Corona: The First Two Years of Observation with the Culgoora Radioheliograph. *Proc. Astron. Soc. Austr.*, Vol. 1, 1970, p. 365.
- Zaitsev, V. V.: Parameters for Shock Waves Generating Type II Solar Radio Bursts and for Coronal Magnetic Fields. *Soviet Astron.-AJ*, Vol. 12, 1969, p. 610.







Solar and Stellar Spindown: Angular Momentum of the Solar Wind

## chapter IV

Round table discussion on problems of solar and stellar  
spindown and theory and observational evidence of the  
angular momentum of the solar wind.

## EVIDENCE FOR AN ANGULAR MOMENTUM FLUX IN THE SOLAR WIND

*R. P. Kraft* As an observational astronomer who watches the stars I feel somewhat remote from most of the proceedings that have gone on so far in the conference. Most of us in astronomy usually think that first there is the solar wind, then the physics of the solar wind, and next speculation, then wild speculation, and finally there is astronomy. But after hearing the activities of the last couple of sessions I am not so sure that that is the correct order any more.

### OPENING REMARKS

This afternoon we will divide the discussion into three parts and begin with a discussion of *evidence for an angular momentum flux in the solar wind*. There will be a summary introductory report by A. J. Hundhausen and, additional contributions, and open discussion, including the floor and members of the round table. I would like to conclude this part after about an hour. It is entirely possible that we will reach the conclusion that there is no angular momentum flux in the solar wind and consequently we can all go out and have a beer because the rest of the afternoon does not matter. However, I rather anticipate that we will not end on that note.

We will pass then onto the second part of the discussion, which concerns *evidence for changes in the angular velocity of the surface regions of the sun and stars*, and its relation to stellar efflux. This will start with a summary introductory talk by me, and some subsequent remarks by others. Then we will have further discussion, round table and floor. The ultimate session this afternoon will consist of *evidence for the distribution of angular velocity inside the sun and stars*; there we will have an introductory talk by Leon Mestel, followed by remarks and open discussion as before.

### INTRODUCTION

*A. J. Hundhausen* The rationale for this strange union of solar wind specialists and more traditional astronomers stems from the fortuitous location of the sun. Not only can the solar rotation rate be measured with considerable precision, but observations of solar wind particles and magnetic fields can be used to infer the loss rate of angular momentum from the sun. This loss, resulting in a small nonradial velocity component of the solar wind plasma, implies a torque that tends to slow the rotation of the sun.

The observations of the angular momentum carried by the solar wind began, as did many other facets of solar wind research, with the study of comet tails. Under the assumption that an ionic comet tail is aligned with the

solar wind velocity (in the rest frame of the comet) comet tail direction observations can be used to infer the direction of flow of the solar wind. This method has been used in deducing the mean nonradial velocity component of the solar wind by J. C. Brandt and his colleagues [*Brandt, 1970*]. This deduction is based on the difference in orientation of the tails of two different classes of comets (direct and retrograde) and thus does not depend on any "absolute calibration" of the radial direction. The resulting mean nonradial velocity component at 1 AU falls in the range from 6.6 to 8.8 km/sec (depending on how comet observations at heliocentric distances other than 1 AU are transformed to this position) in the direction of corotation with the sun. As the

mean radial velocity of the solar wind is  $\sim 400$  km/sec, this implies that the solar wind flow deviates from the radial by  $1^\circ$  or  $2^\circ$ . The difficulties in measuring this nonradial velocity component, using either comet tail observations or the direct, *in situ*, plasma observations stem from the small size of this deviation from radial flow.

The direct determination of the nonradial component of the solar wind velocity requires measurement of the solar wind flux as a function of angle. The first such observations used to infer a mean nonradial velocity component were made on the twin Vela 2 spacecraft (launched in July 1964) and reported in papers published by the Vela group in 1967.

Figure 1 (from Strong *et al.* [1967]) is a histogram of the measured flow directions (projected into the ecliptic plane) determined from Vela 2 data acquired

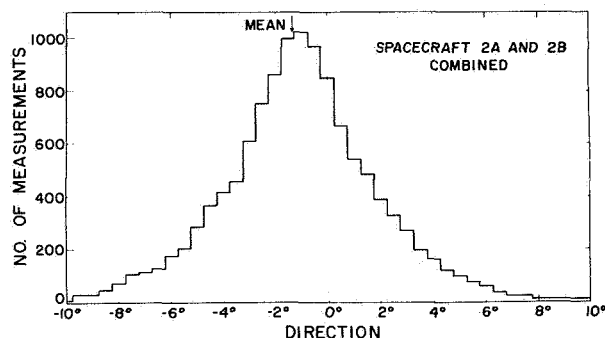


**Figure 1** A histogram of the solar wind flow directions observed by the twin Vela 2 spacecraft between July 1964 and July 1965 [Strong *et al.*, 1967]. Negative angles correspond to flow from the east of the sun, positive angles to flow from the west of the sun.

between July 1964 and July 1965. The sign convention used in these data is that negative angles are flow from east of the sun (i.e., rotation in the same sense as that of the photosphere), positive angles are flow from west of the sun (i.e., rotation in the opposite sense as that of the photosphere). The mean direction of flow of the solar wind implied by these observations is from  $1.35^\circ$  east of the sun. This is equivalent to an azimuthal velocity component of about 8 km/sec in the same sense as the solar rotation.

The Vela 2 observations are thus in basic agreement with Brandt's conclusions and, as we shall see a bit later, imply a considerable angular momentum loss from the sun. The problem in interpreting these observations is

the accuracy of the  $0^\circ$  orientation; that is, do we really know when the Vela detector system is pointing at the sun? This is the "absolute calibration" problem referred to earlier (see Wolfe, p. 184). An analysis of the possible systematic errors in the Vela detector system led to the conclusion that the solar direction was probably accurate to  $\sim 0.7^\circ$ , equivalent to a probable systematic error of about 4 km/sec in the mean nonradial velocity component. With a probable error of this size, one would have to concede that an error as large as the  $1.5^\circ$  mean deviation from radial flow itself could not be ruled out.

Figure 2 (from Hundhausen *et al.* [1970]) shows histograms of the flow directions observed on the next set of Vela spacecraft, launched in July 1965. The plasma detectors on these Vela 3 spacecraft are similar to those on Vela 2. If all of the Vela 3 data (from the two-year period July 1965 to July 1967) are averaged together, the mean flow is from  $1.5^\circ$  east of the sun, in excellent agreement with the Vela 2 result. However, figure 2 has unfortunately been drawn to display the observations from each Vela 3 spacecraft separately, and we discover that these two supposedly identical detector systems lead to mean directions that differ by  $1.6^\circ$ . Thus not only did our Vela 3 observations confirm the mean flow

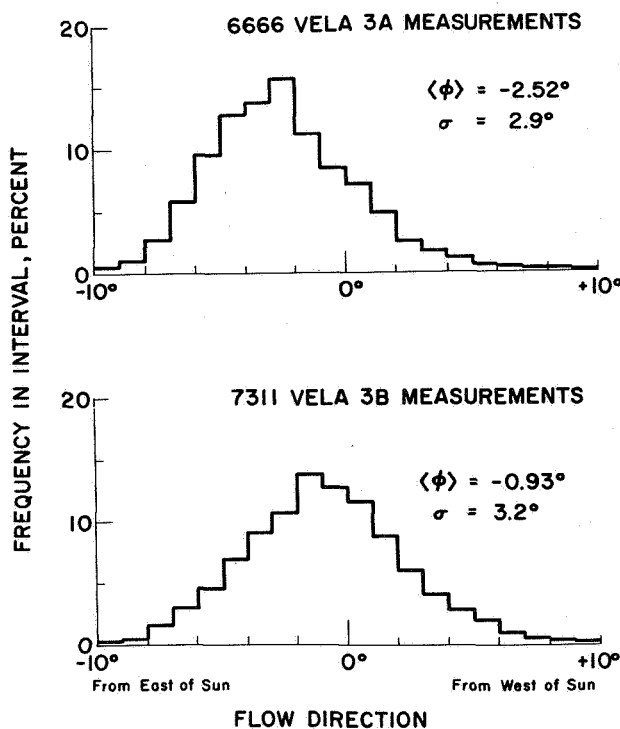


**Figure 2** Histograms of the solar wind flow directions observed by each Vela 3 spacecraft between July 1965 and July 1967 [Hundhausen *et al.*, 1970].

direction observed by Vela 2, but also gave direct support to our concession that an error as large as the result was possible.

The latter conclusion was also supported by the publication of flow direction observations made on the IMP-1 spacecraft in 1963 [Egidi *et al.*, 1969]. The mean flow deduced from these data was also  $1.5^\circ$  from the radial, but from *west* of the sun. This would imply a solar rotation in the opposite sense from the solar photosphere.

All observations are displayed in a "stationary" frame of reference, with the orbital motion of the spacecraft (and earth) about the sun subtracted from the observed nonradial velocities. The results described above constitute all the published observations on solar wind flow direction as determined by direct spacecraft measurements. J. H. Wolfe has presented (p. 184) previously unpublished results from Pioneers 6 and 7 data acquired over several solar rotations. These observations led to mean flow directions appearing to come from  $0.3^\circ$  west of the sun.

A. J. Lazarus will shortly discuss a set of flow direction observations made on Mariner 5 (p. 265). I don't want to steal his thunder, but I must admit I know his observations agree well with the Vela results and with Brandt's comet observations. Thus, we have a set of independent observations that are in agreement in finding a solar wind flow direction at  $\sim 1.5^\circ$  from east of the sun, or an azimuthal flow component of  $\sim 8$  km/sec. I might be tempted to claim a triumph for the democratic process, but I think that any of this group of observers would concede that the uncertainties in our results could be as large as the final mean values. Nonetheless, let us explore the implication of a mean nonradial velocity component of  $\sim 8$  km/sec at 1 AU. The angular momentum flux density carried by the solar wind plasma at 1 AU is then  $6.3$  dyne cm/cm<sup>2</sup>. Computation of the torque on the sun requires some assumption regarding the variation of the angular momentum flux density with solar latitude, as all of the observations are made near the ecliptic plane, within  $\pm 7^\circ$  of the solar equator. Assuming either a uniform flux over  $\pm 30^\circ$  of solar latitude or a flux that varies as the cosine of the heliographic latitude leads to a torque of  $\sim 10^{31}$  dyne cm. For anyone unfamiliar with torques of this magnitude, some physical feeling comes from computing the braking time for the sun under such a torque. If the sun were rotating as a solid body this torque would result in a braking time of about  $3 \times 10^9$  years. That, of course, is approximately equal to the generally accepted lifetime of the sun and means that such a torque could have a significant braking effect in a solar lifetime.

Let us next briefly discuss the theoretical models of the transfer of solar angular momentum to the solar wind, as I think that some reluctance to accept the observations of an 8 km/sec nonradial velocity component near 1 AU stems from an apparent discrepancy between the theories and observations. E. N. Parker pointed out some time ago that a rough estimate of the angular momentum of the solar wind could be obtained by assuming that the solar magnetic field drags the coronal plasma in rigid corotation until the outward flow speed is greater than the Alfvén speed and then assuming conservation of angular momentum at larger heliocentric distances. Application of this idea leads to an azimuthal flow speed component of about 1 km/sec at 1 AU, a result an order of magnitude less than the observations described above. The magnetic force was incorporated into a quantitative model by Weber and Davis [1967], and figure 3 shows the azimuthal velocity component  $v_\phi$  predicted by their model as a function of heliocentric distance.

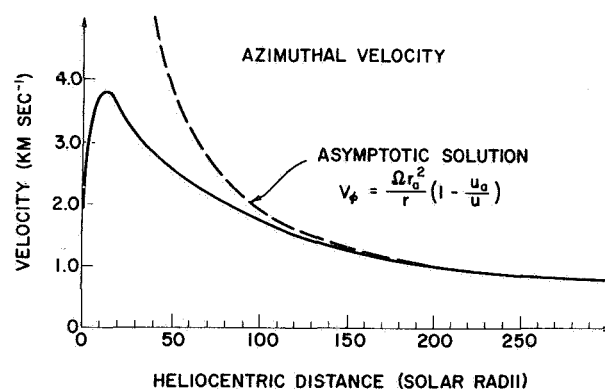


Figure 3 The nonradial component of solar wind velocity as a function of heliocentric distance predicted by the model of Weber and Davis [1967].

Rigid corotation of the plasma ( $v_\phi \propto r$ ) is maintained by the magnetic field for only a very short distance from the sun. However, the magnetic field does continue to transfer angular momentum to the plasma and at large heliocentric distances, the Weber and Davis solution approaches that predicted by Parker (as described above) and shown by the dashed line of the figure. The nonradial velocity component predicted at 1 AU ( $215 R_\odot$ ) was again near 1 km/sec.

The Weber and Davis model assumed a polytropic law relating temperature to density, as described by Parker (p. 162). Brandt *et al.* [1969] have incorporated the same magnetic force into a model in which the energy



equation is actually integrated. This model gives a different variation in the radial expansion speed with heliocentric distance, and thus obtains a different nonradial velocity, 2.5 km/sec at 1 AU. The difference between these two results indicates that the models are quite sensitive to the detailed manner in which the solar wind is heated (thus determining the detailed radial velocity variation). You may recall that some sign of a lack of universal agreement has emerged as to how the solar wind is heated. It should be clear at this point that such uncertainties feed back into the angular momentum problem and lead to uncertainties in the theoretical value of the angular momentum and azimuthal flow speed at 1 AU.

The problem can become much more complicated than in the simple models thus far considered. A logical next step is to include viscosity in the computations. A model including viscosity was derived by *Weber and Davis* [1970]. In fact, this particular model also included an anisotropy in the pressure tensor, as anisotropic thermal motions do imply a flux of angular momentum. This effect was put in the model in a rather crude manner by simply assuming a variation of the anisotropy magnitude with heliocentric distance. I should point out also that the *total* pressure tensor, as M. D. Montgomery has shown (p. 208), is not very anisotropic when observed near 1 AU, because the electrons are hotter than the protons and nearly isotropic. Now, this particular model predicts an azimuthal flow speed component at 1 AU of 6 km/sec. This larger transfer of angular momentum to the solar wind is largely due to the viscous force at some tens of solar radii. Six kilometers per second is in fair agreement with the lowest value given by Brandt's comet study, and one might consider the theory and observations to be approaching a common ground.

A viscous model has also been developed by *Wolff et al.* [1971]. The Weber and Davis' model, including viscosity, again used a polytropic index to avoid having to integrate the energy equation. *Wolff et al.* [1971] integrated the energy equation with a thermal conductivity modified by the presence of the magnetic field. The latter predicts a nonradial velocity component at 1 AU of only 1.5 to 2.0 km/sec. The basic reason for this difference is the strong dependence of viscosity on the proton temperature and the by now familiar uncertainties as to how the proton temperature is actually determined in the solar wind.

There are many other ways of complicating the models. For example, there are known to be fluctuations or waves in the interplanetary medium. *Schubert and Coleman* [1968] have pointed out that these waves also

carry angular momentum from the sun and that interaction with the particles can ultimately transfer that angular momentum to the plasma, producing a larger nonradial velocity. There has been some debate at this conference about the role of nonsteady phenomena and nonspherical flows in the solar wind. If the expansion from the sun is not spherically symmetric, there are new possibilities for increasing the corotation of the coronal and having a large angular momentum in the solar wind. A rough model including such effects has recently been published by *Sakurai* [1971].

In summary, solar wind observations do give some evidence for an important loss of solar angular momentum in the expansion of the solar wind. These observations are difficult, not always in agreement, and should still be approached with a healthy skepticism. The theoretical models connecting solar rotation and the nonradial flow of the solar wind are oversimplified, sensitive to the unknown mechanisms of heating the plasma, and deserve a similar skepticism.

## REFERENCES

- Brandt, J. C.: *Introduction to the Solar Wind*. W. H. Freeman and Co., San Francisco, 1970.
- Brandt, J. C.; Wolff, C.; and Cassinelli, J. P.: Interplanetary Gas XVI, A Calculation of the Angular Momentum of the Solar Wind. *Astrophys. J.*, Vol. 156, 1969, p. 1417.
- Egidi, A.; Pizzella, G.; and Signorini, C.: Measurements of the Solar Wind Direction With the Imp 1 Satellite. *J. Geophys. Res.*, Vol. 74, 1969, p. 2807.
- Hundhausen, A. J.; Bame, S. J.; Asbridge, J. R.; and Sydoriak, S. J.: Solar Wind Proton Properties: Vela 3 Observations From July 1965 to July 1967. *J. Geophys. Res.*, Vol. 75, 1970, p. 4643.
- Sakurai, T.: Quasi-Radial Hypervelocity Approximation of the Azimuthally Dependent Solar Wind. *Cosmic Electrodyn.*, Vol. 1, 1971, p. 460.
- Schubert, G.; and Coleman, P. J., Jr.: The Angular Momentum of the Solar Wind. *Astrophys. J.*, Vol. 153, 1968, p. 943.
- Strong, I. B.; Asbridge, J. R.; Bame, S. J.; and Hundhausen, A. J.: Satellite Observations of the General Characteristics and Filamentary Structure of the Solar Wind. *Zodiacal Light and Interplanetary Medium*. J. Weinberg, ed., NASA SP-150, 1967.
- Weber, E. J.; and Davis, L., Jr.: The Angular Momentum of the Solar Wind. *Astrophys. J.*, Vol. 148, 1967, p. 217.

Weber, E. J.; and Davis, L., Jr.: The Effect of Viscosity and Anisotropy in the Pressure on the Azimuthal Motion of the Solar Wind. *J. Geophys. Res.*, Vol. 75, 1970, p. 2419.

Wolff, C.; Brandt, J. C.; and Southwick, R. G.: A Two-Component Model of the Quiet Solar Wind With Viscosity, Magnetic Field, and Reduced Heat Conduction. *Astrophys. J.*, Vol. 165, 1971, p. 181.

## COMMENTS

**A. J. Lazarus** I would like to comment on the points that Hundhausen has brought out. First of all, on IMP-1, where the average flow direction was reported to be from the west, there is a possibility of bias, as he said, because the IMP-1 orbit was unfortunatously commensurate with the passage of the interaction regions between high and low speed streams. It turned out that we missed some of the low velocity plasma nearly every time. That plasma occurred just before the higher speed plasma and (as we now know) it probably would have appeared to be coming from east of the sun. Therefore, the data could very well be biased so that the average flow was from the west. But it is very difficult to prove this without having some comparison spacecraft.

My second comment involves our average direction measurement from Pioneer 6. A photoelectric effect existed when measuring electrons and looking at the sun. On the other hand, it does enable us to check on the sun direction. We used that information to analyze the Pioneer 6 data and find that our experiment responded as if the pulse from the spacecraft sun sensor was offset by approximately  $2.5^\circ$ . Taking that offset into account, the average flow direction we get is very close to radial.

Table 1 shows 1-hr averages of data from the Mariner 5 spacecraft that went in toward Venus. These values in turn are averaged over the six solar rotations for which we have

**Table 1.** *Solar wind properties observed on Mariner 5 (averaged over solar rotations)*

Solar rotation	$\bar{R}$ (AU)	$\bar{V}_r$	$\bar{V}_n$	$\bar{V}_t$	Angular momentum flux density		Flux/ $d\Omega$ =	Proton flux/ $d\Omega$
					$Nm_p V_r V_t R$	$B_r B_t R/4\pi$	Sum $\times \bar{R}^2$	
					(dyne-cm/cm <sup>2</sup> )		(dyne-cm)	
1832	1.0	392	-1.8	0.84	$3.0 \times 10^3$	$0.9 \times 10^3$	$8.7 \times 10^{29}$	$6.7 \times 10^{34}$
1833	.95	373	-1.3	5.2	5.3	.8	12	5.8
1834	.87	438	-1.3	8.5	6.1	1.4	13	5.1
1835*	.80	441	-4.1	7.7	9.3	1.6	16	5.0
1836	.73	417	-3.1	11.2	7.7	2.5	12	4.5
1837*	.68	415	-5.3	11.0	8.4	2.2	11	4.5

\*Data missing from a portion of the solar rotation.

data. The first columns show the radial distance from the sun, and the averages over the solar rotations of the radial, normal, and tangential components of the velocities. The components are taken relative to the solar equatorial plane. Positive values indicate corotating flow — from east of the sun. For each rotation we've averaged the two contributions to the angular momentum flux density. For the contribution from the particles we have taken the average of the product of the number density  $N$ , the proton mass  $m_p$ , the radial velocity  $V_r$ , the tangential velocity  $V_t$ , and the distance from the sun  $R$ . The next column shows the contribution of the anisotropic pressure produced by the magnetic field. These are combined to obtain the flux per solid angle by multiplying the sum by  $R^2$  for the various rotations. The values range from 9 to  $16 \times 10^{29}$  dyne cm. Two of the solar rotations are incomplete. It is very important to obtain complete solar rotations because when the high-low speed stream combination moves over the spacecraft, the

tangential component of velocity first arrives from the east and then from the west, and this must be properly averaged out by examining the behavior of all the contributions to the angular momentum flux. For comparison the table also includes the proton flux per solid angle, which is seen to vary with decreasing solar distance.

A conclusion to be drawn from this is that there does appear to be a net angular momentum flux from the sun. It is consistent with Brandt's values and gives a slowing torque on the sun. If you calculate the net slowing torque by assuming that most of the contributions would come from solar wind flow between solar latitudes of  $\pm 30^\circ$ , the net result is a slowing torque of  $7 \times 10^{30}$  dyne cm.

We believe the errors are roughly  $\pm 4$  km/sec ( $\pm 0.5^\circ$ ) for an individual measurement of tangential velocity and approximately  $\pm 2$  km/sec for the average systematic error. As you get closer to the sun, the tangential velocity increases, reducing the effect of systematic error. On the other hand, the only check that we have is during the first solar rotation. The spacecraft was rolled about the sun-spacecraft line and during that time we could see the apparent azimuthal flow direction relative to the sun-spacecraft line change as the spacecraft rotated. This enabled us to find an effective alinement error of  $0.5^\circ$  of our instrument relative to the sun-spacecraft line. But there is no way of checking this later in the flight. So it is conceivable that there could have been some drift, but the numbers do seem to be consistent. (These comments appeared in extended form in a paper by Goldstein and Lazarus in *Astrophys. J.*, Vol. 168, 1971, p. 571.)

## DISCUSSION

*J. H. Wolfe* I did want to add one point to Lazarus' comment regarding the Pioneer 6 sun pulse offset of  $2.5^\circ$ . If true, then our overall average of  $3^\circ$  means we are still  $0.5^\circ$  west. Could you indicate the sun pulse offset on Pioneer 7?

*A. J. Lazarus* I think about  $5.5^\circ$ .

*J. H. Wolfe* Well, if it's  $5.5^\circ$  on Pioneer 7 and our average is  $0.3^\circ$  . . .

*A. J. Lazarus* Okay, this is a very complicated business. Pioneer 7 spent some time within the magnetosheath; it then went outside the shock, came back through the tail of the earth, and then out into solar wind. Now, what you need to do is be sure that you have data from a complete solar rotation taken out in the solar wind and then we can compare values. We must compare by solar rotation. If we examine the bias due to looking at the sun inadvertently through the photoelectric effect and correct our data for that, it is consistent with the plasma coming radially. But uncertainties in Pioneer data are greater than uncertainties in Mariner 5 data from which I quoted. So we could certainly have been off by  $\pm 0.5^\circ$ , perhaps even twice that, on Pioneers 6 or 7.

*J. H. Wolfe* What I still don't understand is that since we did not correct our Pioneer 7 data in terms of the azimuthal histogram for any supposed error in the sun pole, the curve I showed this morning should have been shifted over about  $5^\circ$ .

*A. J. Lazarus* You've got to look at exactly what solar rotation that was.

*J. H. Wolfe* Do you agree with that statement?

*A. J. Lazarus* If you took the data from the time when you were out in the solar wind and if the  $5.5^\circ$  bias, which we know is in our data, was also in your data, then it should be shifted over  $5.5^\circ$ , as you stated. It's a very subtle difference; you're trying to measure small angles, you have to be sure that you get a completely unbiased sample. It's very difficult.

*J. H. Wolfe* I agree. The point I would like to make is that there are systematic errors that tend to creep into a spacecraft measurement in terms of instrumental alinement, etc. If you have an internal photo effect, how well do you know it? Can you calibrate it in the laboratory convincingly?

*A. J. Lazarus* There are two points I want to be clear on; what I should really make claims for are our data and not yours. Our data are corrected by what we know is the



alinement from the pure geometry of the instrument; we know what our alinement is relative to the sun by looking at the photo effect. We are quite sure of that. It's very difficult to be off — to be off by  $0.5^\circ$  is absolutely as far as I can say we would be off. Now, when our data are corrected by that, we get flow consistent with  $v_r$  within the accuracy of our measurements, which is not as great as Mariner 5. I can't say whether or not you had the same bias to your instrument. What we would have to do is compare data for the same solar rotation at the same time and see what happens.

*J. H. Wolfe* I would just like to reiterate the three points Hundhausen made. I think that the data taken in space today with regard to the average flow direction should be looked upon with skepticism. I say it is in error from one measurement to the next. We see it in our own.

I think the idea of when you sample the data is very important. Probably measurements taken over at least a year are required to get an understanding of this. And, finally, sampling problems with regard to tracking are exceedingly important in getting a good average.

*A. J. Hundhausen* Well, I was hesitant to put that  $1.5^\circ$  up there, but now I feel pretty good about it. I think that what this points out is that there is a real problem because of the need for an absolute measurement. The roll maneuver of Mariner 5 was very important in this consideration. Now, it's easy to tell people how to design spacecraft, but if this is a real important physical problem, rolling, and the ability to make this kind of calibration in space, is something that we should consider in the future.

*J. H. Wolfe* Was the experiment on when you went through the roll maneuver?

*A. J. Lazarus* Yes.

*J. H. Wolfe* In the scientific format?

*A. J. Lazarus* Yes. We didn't know this kind of measurement could be made when we planned the experiment. Looking at the data, during the roll maneuver by chance we could make the determination.

*R. H. Dicke* All remarks so far have been connected with the particle flux of angular momentum. Let's not forget that the twisted negative field also contributes to the transport of momentum. The magnetic stress must be added to the velocity stress.

Second, I take great comfort from the fact that computations using the measured stress tensor provide results that agree within a factor of 2 with that obtained from the Alfvénic radius, though they are quite different. The Alfvénic radius is perhaps  $20 R_\odot$  and the other measurement is taken at  $\sim 100$  AU. That these two ways of looking at the problem show agreement within a factor of 2 I think is something to take comfort from and not be worried about.

*L. Mestel* I want to take up that point of Dicke's. If I understand the situation correctly, the difficulty in detailed comparison of the theory with observation, in particular the 1 km/sec as compared with 10 km/sec, is not that the theory predicts too little angular momentum loss. As Dicke points out, there is angular momentum loss transport by the twist in the field, an old idea going back to 1955 or 1956. The difficulty is that one has gotten used to thinking that the Alfvénic surface, the Alfvénic point on the particular stream line, is a water shed and that inside of it the transport is essentially by magnetic stresses and not too far beyond the transport is by plasma and the magnetic stresses can be ignored. At great distance the latter is true, but it is because the increase of velocity in the Parker model is so slow, going perhaps as the square root of log distance; although one is well beyond the Alfvénic point still the simple models we use do predict that the magnetic stresses, the twist in the field, transport most of the angular momentum.

*R. H. Dicke* It's only about 20 or 30 percent.

*L. Mestel* Well, depending on which model you're using. I think that's the difference.

*A. J. Lazarus* I'm sorry, I didn't point out that my figure has both the magnetic field

contribution and the particle contribution, and the magnetic field contribution is about one-fourth of the total.

*J. C. Brandt* There is one other object in the solar system amenable to wind sock type analysis, and that is the earth's magnetic tail. Such analyses have been carried out and to explain the aberration angle requires azimuthal velocity of about 7.5 km/sec. This work has been carried out by Behannon. So another independent piece of information exists for velocities of the kind we are talking about.

## COMMENTS

*E. J. Weber* The torque exerted on the sun by the expanding solar wind is of considerable importance to astrophysics. Yet, while general features of the azimuthal motion of the steady-state solar wind and the resulting torque on the sun are quite well understood theoretically [*Weber and Davis*, 1967], angular velocities at 1 AU predicted by this and similar other models differ significantly from those inferred from the observed deflections of comet tails [*Brandt and Heise*, 1970] and from certain plasma velocity measurements on satellites [*Hundhausen*, 1970]. The observationally determined values of the azimuthal velocity are subject to large uncertainties, especially those obtained from plasma measurements on spacecraft. Since the solar wind flows nearly radially at 1 AU, one attempts to determine deviations from this direction of the order of  $1^\circ$  to  $2^\circ$ . The degree of uncertainty is best illustrated by the average values of the angle between the radial velocity  $u$  and the velocity vector in the direction  $(ue_r + v_\phi e_\phi)/(u^2 + u_\phi^2)^{1/2}$  as determined from plasma measurements on different spacecrafts. These values are indicated in table 1. Very recently, *Lazarus and Goldstein* [1971] have presented results for the plasma angular momentum, the torque due to the magnetic field as well as other pertinent data obtained on Mariner 5. Their results are given in terms of averages over solar rotations, in particular for rotations 1832 to 1837.

**Table 1.** Average values of angle between the radial velocity and the projection of the total velocity vector into the  $r$ - $\phi$  plane [data are from Wolfe; see p. 183]

Spacecraft	Average angle, deg
IMP 1	-1.5
Vela 2	+1.4
Vela 3A	+2.5
Vela 3B	+0.9
Pioneer 6	-3.0
Pioneer 7	-0.3

We can define the following constants of the motion, for the mass flux, the "total angular momentum" flux and the magnetic flux per steradian:

$$c = \rho ur^2 \quad (1)$$

$$l = \Omega r_A^2 c \quad (2)$$

$$b = r^2 B_r \quad (3)$$

where the symbols used are the same as those in *Weber and Davis* [1967]. Furthermore, there are two contributions to the total angular momentum flux

$$l = \Omega r_A^2 c = r[v_\phi - (B_r/4\pi\rho u)B_\phi]c \quad (4)$$

where the first term represents the contribution due to the angular momentum of the plasma, and the second term represents the torque due to the presence of the magnetic field. In the region between the earth and Venus where the Mariner 5 measurements were obtained, the radial velocity of the solar wind has very nearly its asymptotic value  $u_\infty$ . *Weber and Davis* [1967] have shown that for this case, the two components of  $l$  are given by

$$rv_\phi = \frac{l}{c} \left(1 - \frac{u_A}{u_\infty}\right) = \Omega r_A^2 \left(1 - \frac{u_A}{u_\infty}\right) \quad (5)$$

and

$$-\frac{B_\phi B_r}{4\pi\rho u} r = \frac{l}{c} \left(\frac{u_A}{u_\infty}\right) = \Omega r_A^2 \left(\frac{u_A}{u_\infty}\right) \quad (6)$$

respectively. Furthermore, we know that at the radial Alfvénic critical point  $M_A^2 = 1$ , which implies that

$$u_A = \frac{b^2}{4\pi cr_A^2} \quad (7)$$

We have used the above relations to determine  $r_A$ ,  $u_A$ ,  $b$ , and  $B_r$  from the values given by *Lazarus and Goldstein* [1971]. The results are shown in table 2. Note that the position of the radial Alfvénic critical point falls into the region predicted by *Weber and Davis*

**Table 2.** Theoretical solar wind properties determined from Mariner solar wind data.

Solar rotation	Distance from sun AU	Observed radial velocity $\bar{u}$ 10 <sup>7</sup> cm sec <sup>-1</sup>	Values obtained from model				Observed magnetic field magnitude $ \bar{B} $ $\gamma$	$\bar{B}_r/ \bar{B} $
			$\bar{r}_A$ $r_\oplus$	$\bar{u}_A$ 10 <sup>7</sup> cm sec <sup>-1</sup>	$\bar{b}$ $\gamma \times \text{AU}^2$	$\bar{B}_r$ $\gamma$		
1832	1.00	3.94	21.1	0.91	2.6	2.6	5.9	0.43
1833	0.95	3.73	26.7	0.48	2.2	2.4	6.6	0.37
1834	0.87	4.38	30.0	0.83	3.0	4.0	7.6	0.52
1835	0.80	4.41	33.2	0.66	3.0	4.6	9.5	0.49
1836	0.73	4.17	30.3	1.04	3.2	6.1	11.5	0.54
1837	0.68	4.15	29.0	0.79	2.7	5.8	11.3	0.51

[1967], but they also determined the radial velocity  $u_A$  to be 332 km sec<sup>-1</sup> with  $u_\infty = 425$  km sec<sup>-1</sup>. Thus with the specific boundary values used, the model predicted a total angular momentum flux that was largely due to the torque associated with the

magnetic field, as indicated in figure 1. This particular result is partially due to the model itself and partially due to the specific boundary conditions used. The model employs a polytrope relationship instead of a full energy equation, which will result in a radial solution that rises relatively rapidly close to the sun; thus in general we would expect to calculate from the model a  $u_A$  that is too high. This could be changed by using a model with a different energy equation [Brandt *et al.*, 1969] for which the radial velocity rises much more slowly. However, even with such a model it is not quite apparent that one can obtain radial velocities as low as required by the data in table 2. These values could only be explained if there would be a very significant energy flux due to waves and other factors, even at  $30 r_\odot$ .

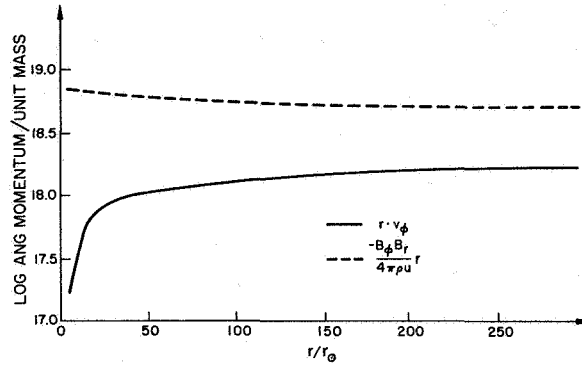


Figure 1. Comments on recent observations of the angular momentum flux in the solar wind.

Since the corrections to the actual radial velocity due to the inclusion of the azimuthal velocity and the magnetic field are only second-order effects – very small – we can assume that we know a radial solution of the solar wind and thus the plasma density everywhere. The density at the critical point is given by

$$\rho_A = 4\pi c^2/b^2 \quad (8)$$

and thus increasing the magnetic flux  $b$  will decrease  $\rho_A$  and move the critical Alfvénic point farther away from the sun. This also implies that  $(u_A/u_\infty)$  is increasing and thus the fraction of the total angular momentum flux due to the angular momentum associated with the plasma will decrease. The value of  $5\gamma$  assumed for  $B_r$  at 1 AU in the numerical calculations by Weber and Davis [1967] as well as by Brandt *et al.* [1969] is somewhat larger than the average value of about  $3\gamma$  observed near the orbit of earth. Using this low value for  $B_r$ , we would obtain a density at the critical Alfvénic point that is larger by approximately a factor of 2. This would imply that the total angular momentum flux removed from the sun would be smaller, but that a larger fraction would be carried away at 1 AU by the plasma itself.

In summary, we wish to point out that while there is some discrepancy between the observed azimuthal plasma velocities at 1 AU and the values predicted by calculations from the models, the differences are not too large and not that significant due to the

great uncertainties associated with the observational results. The anisotropy in the pressure tensor due to the nonalignment of the magnetic field vector with the plasma flow direction will also produce an increase in the predicted azimuthal velocity as has been shown by Weber [1970], using a rather simple, heuristically derived model for the anisotropic pressure. More refined models for the radial motion of the solar wind which take into account heating due to waves (see Barnes' discussion, p.219) may result in densities that fall off much more slowly and, correspondingly, in radial velocities that increase much less rapidly than predicted by presently used models. We may thus obtain even with a radial magnetic field of only  $3\gamma$  at 1 AU a torque on the order of  $10^{30}$  dyne cm steradian<sup>-1</sup> and thus a significant torque on the sun. At the same time one would find that at 1 AU the angular momentum associated with the plasma would account for the major portion of this torque. Finally we can see from equation (8) that if over the solar cycle  $b$  varies significantly while  $c$  remains relatively constant, the position of the Alfvénic critical radius will shift and the torque on the sun can vary significantly.

An accurate determination of the azimuthal motion of the solar wind at 1 AU is thus of prime importance, since it would not only give us more information on the spindown of the sun, but it would also provide us indirectly, and in conjunction with a theoretical model, information about the properties of the solar wind at the radial Alfvénic critical point.

## REFERENCES

- Brandt, J. C.; Wolfe, C.; and Cassinelli, J. P.: Interplanetary Gas. XVI. A Calculation of the Angular Momentum of the Solar Wind. *Astrophys. J.*, Vol. 156, 1969, p. 1117.
- Brandt, J. C.; and Heise, J.: Interplanetary Gas. XV. Nonradial Plasma Motions From the Orientations of Ionic Comet Tails. *Astrophys. J.*, Vol. 159, 1970, p. 1057.
- Hundhausen, A. J.: Composition and Dynamics of the Solar Wind Plasma. *Rev. Geophys. and Space Phys.*, Vol. 8, 1970, p. 729.
- Lazarus, A. J.; and Goldstein, B. E.: Observation of the Angular Momentum Flux Carried by the Solar Wind. Submitted to *Astrophys. J.*, 1971.
- Weber, E. J.; and Davis, L., Jr.: The Angular Momentum of the Solar Wind. *Astrophys. J.*, Vol. 148, 1967, p. 217.
- Weber, E. J.: The Torque on the Interplanetary Plasma due to its Anisotropy. *Solar Phys.*, Vol. 13, 1970, p. 240.

**J. C. Brandt** Well, in reply to something you said, Ed, I don't really disagree. I think that the instant we understand how energy is inserted low in the solar atmosphere we'll have to develop other models. Our two-fluid model with viscosity gives a velocity of about 2 km/sec. We could have made it 3 km/sec had we been willing to spend another two weeks on the computer. I personally suspect that if you dump in more energy, you will get a higher azimuthal velocity. And that's the only real sense of disagreement I would have with you.

I think the model we now have is a perfectly good representation of the quiet solar wind and has only one "fudge" factor in it. All we've had to "fudge" was the electron conductivity. The model reproduces the azimuthal velocity, which is low. It reproduces both the proton and electron temperature, the density, and the radial velocity. We're a little high on the magnetic field, but I don't think that would seriously influence our results.

**E. J. Weber** But if you're slightly high in the magnetic field you just have too much stress in the magnetic field versus the plasma. That is just really what you are fighting. And I think the whole idea is again not a disagreement. The important point is what the radial velocity is at the stage when the Alfvénic critical point is reached. If you have a fast

## DISCUSSION

flow, you might push it out — get more angular momentum. But you then also decrease the difference between  $u_\infty$  and  $u_a$  at the critical point. If that's the case, then, I just say it ought to be inversely correlated to the more quiet zone.

*J. C. Brandt* The other point I would like to make is that in treating viscosity it is very important to go immediately to the two-fluid model. I think Hundhausen hinted at this. To be more specific, the coefficient of the viscosity is so dependent on temperature that you must correctly use the lower temperature. And then you open up another Pandora's box, which I will open and shut immediately, of the question of what the viscosity in the solar wind really is. I personally have good reasons to believe that at quiet times the normal value that one would get out of Spitzer's book is correct. I also have good reason to suspect that at the hotter times with larger velocities that value will be in error by orders of magnitude. So this is a problem that has to be I think taken into account.

*C. P. Sonett* When you carry out a plasma experiment you get a three-dimensional distribution function; sometimes it has a high energy tail. In the latter case, fitting procedures are needed. The typical way is to fit a Maxwellian velocity distribution, subtracting off the high-energy tail. A further problem is the  $\text{He}^{++}$  contribution, and I guess sometimes one can even see a little bit of  $\text{He}^+$ . When done, one comes up with some sort of a mean velocity. It seems to me that in the process of carrying out this rather involved set of trial fits there is room for considerable margin.

*E. J. Weber* I think if you really want to go into that detail with the helium at the present stage, then any relationship between the models and actual nature is purely coincidental because the models are just too simple to have all these very fine features in there. I don't know of any model that has all the helium  $\text{He}^+$  and  $\text{He}^{++}$ . If you do that you get into trouble because there isn't just a single critical point but a lot of them — not only that, but more than one branch, as I showed you once before. So the problem I think becomes insoluble.

*A. J. Hundhausen* I think your question is do we know well what we are doing when dealing with data analysis. I think that's the entire question. However, I would like to point out that in the Vela data I don't think the problems with high-energy tails or helium really interfered with our determination of the proton distribution. Further, the analysis has been done as far as I know in these results by two different methods: bimaxwellian fitting and a more empirical piece-wise gaussian fitting that does show the basic asymmetries in the proton distribution function. When the latter is true, of course, one must use the mean, and that's what has been used. And my guess of the error from the difficulties unfolding in the distribution function is that it's not going to amount to a degree and a half. You can see that by looking at the contour plots that were shown this morning (Hundhausen, fig. 2, p. 262).

*J. H. Wolfe* I think that typically where the errors seem to show up in the end product is usually density more than anything else. And that the flow directions and velocities and so forth are less susceptible to the error.

*C. P. Sonett* I hoped when we set the conference up that this particular subject would be explored because it seems critical; the numbers we are dealing with are quite small. In addition, what is the proper definition of bulk velocity? Is it the most probable or the mean?

*A. J. Hundhausen* The first moment of the distribution function [mean value].

*C. P. Sonett* What do you do now about things like the heat flux, which throws in a skewness?

*A. J. Hundhausen* When done right it is taken into account in the calculation; you really reconstruct the distribution function and recompute a mean.

*C. P. Sonett* What sort of estimate is there that lends confidence to the validity the very small values used in estimates of the angular momentum?

*A. J. Hundhausen* Well, I've given my answer.

*R. P. Kraft* Can some person in the audience comment on this?

*J. D. Mihalov* At Ames Research Center we've studied the errors associated with the reduced Pioneer 6 and 7 Ames plasma probe data. One of the results is that the most probable formal statistical error for the unaberrated azimuthal flow angles normalized to a chi square of one is  $0.9^\circ$  and this seems to be comparable to the size of some of the theoretical flow angles mentioned previously.

*I. B. Strong* I would like to agree with Hundhausen except for one thing. I think the Vela data have been measured in three different ways. Recall that the Vela 2 data, shown first, were reduced by a simple gaussian fit to the distribution. Since then, this has been done on Vela 3 by bimaxwellian fit and integration over the whole distribution function. Although not published, I've done this for the Vela 2 data. It seems to give the same answer within 10 percent as the very crude methods. So I think the worry about the exact method is valid, but it doesn't seem to make too much difference whether the same data are treated in different ways.

*R. Lüst* I have a question for the table, namely, what about the various observations of comets and what we have heard here, that there's a tail, a gas magnetic tail; my impression from the solar wind data is that the question is still completely open — I mean, we are uncertain that the theory can explain the observations. Is it not true that one should be very cautious about comet magnetic tail observations since they rely on such few comets? There could also be a strong time effect.

*J. C. Brandt* The uncertainty in one observation is quite large, of course, and this is because in addition to the radial velocity of 400 km/sec, the comet velocity of about 40 km/sec, and an azimuthal velocity of somewhere between 5 and 10 km/sec, there is superimposed a random isotropic velocity of 30-50 km/sec. This comes out of the data quite well. However, I have a sample distributed over many years beginning in 1889 of 600-800 observations, and it is quite true that a given observation must be taken with great reserve; in fact, you can't derive anything from one observation. But for a large group the radial velocity, the azimuthal velocity, and a peculiar velocity separate from this quite naturally. The peculiar velocity can be checked directly without any assumptions about the comet by looking at the relatively small sample of comets ( $\sim 100$ ), where we can view the comet tail orientation exactly in the plane of the orbit. To a very good approximation, the radial velocity separates, and the azimuthal velocity has almost no effect at all. You then see the dispersion in velocities perpendicular to the plane of the orbit, and the entire picture falls together, I think, quite well. I might add that the spacecraft dispersions and the comet dispersions agree quite well, and the average radial velocity that comes from the sample of comets is 450 km/sec — again in very good agreement with the spacecraft measurements. So, from the viewpoint of other checks, I see no reason to doubt the comet observations. It doesn't mean there are not difficulties in it, it doesn't mean there might not be an error, but there is no obvious source of error I've been able to turn up in the last 5 years.

*E. J. Weber* I don't know what the present state of comet theory is but I recall that there was some work done at the Max-Planck Institute by Biermann and others. They say that if there's a mass loading you get a big shock wave developing ahead of the comet. If that's the case, then I think we have to be very careful about whether the comet really represents a weather vane in the wind.

Further there may be a mechanism around the comet forbidding transfer or changing the magnetic stress inherent in the solar wind into actual plasma motion. If you transfer by some mechanism, then Brandt's numbers come out right. In other words, if you assume something like  $9 \times 10^{29}$  dyne-cm, the plasma motion comes out to be about 9 km/sec. So I think it's of the right order in that respect, except I don't know of any mechanism; I just say it's a possibility.

*G. Siscoe* In these discussions about the angular momentum flux, there are really two different physical quantities used. One is the average transverse component of the speed, the other is the average angular momentum of the flux, which is the product of the transverse component of the speed, the radial component of the speed, and the density. So to go from one to the other would you have to make some assumptions about the correlation coefficient between the transverse component and the mass flux? That's one thing, at least, that the solar wind people could answer, what the correlation coefficient is between  $B_\phi$  and  $\rho B_r$ ; if that's a large number you cannot go directly from average  $B_\phi$  to angular momentum flux.

*F. C. Michel* If I understand correctly, you indicated that you could get more angular momentum deposited in the particles than in the fields. But I didn't understand whether that was the result of an actual calculation or a proposed idea. And I would be a little conservative about that because within the assumptions of the calculation you would have no angular momentum transfer if the field were taken to zero. Consequently, almost all the angular momentum initially resides in the field and to get the bulk of the angular momentum ultimately deposited in the particles at 1 AU means the field must be willing to surrender the bulk of its angular momentum; it may be a little more difficult than proposed to actually find the state that accomplishes that.

*E. J. Weber* I did not imply that this happens to plasma in general — that is, to the plasma you measure in spacecraft. I just say this might be a possibility for explaining the comet tail data, because at the comet there are shock lines, there is interaction, there is something similar to a magnetosphere, a magnetosheath possibly.

*H. Schmidt* I think one doesn't have to worry about inferences on the aberration of the comet tails from shocks and plasma dynamics because an average interplanetary magnetic field line is delayed in the visible comet tail by a day or more, and it has a width of, say, 100,000 km at the most. So it is an extremely good weather vane in the solar wind. From that respect, no matter what the complicated dynamics of a bow shock of a comet is, the visible tail is a very good weather vane.

*J. C. Brandt* If we can show the first slide (fig. 1) I think we will see very convincing evidence of this. This is a plot of angular dispersion made in three different ways. One was stolen from the Vela group, Strong *et al.*'s data. I simply divided their distribution in their viewing plane in half, folded them over, and then made the same calculation from the comet data. The dashed line is the dispersion of angles around the mean in the plane of the comet, and the dotted line is the dispersion viewed perpendicular to the plane. You

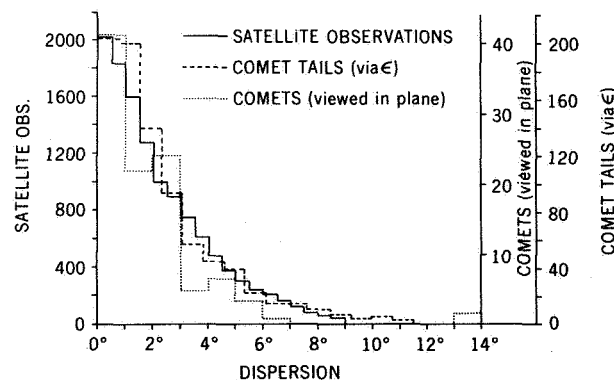


**Figure 1** Contributions of the plasma angular momentum and the torque due to the magnetic field to the total torque on the sun as calculated by Weber and Davis [1967].



can see that although the curves are ragged they are essentially similar. This means we are observing the same plasma directions, and it encourages you as far as the comet observations are concerned, because it means that the comets do in fact respond rather well to changes in the solar wind plasma direction, so that an individual comet that may have some peculiar structure probably does not bias the distribution of angles.

*G. Siscoe* I realize what I said wasn't altogether understood. The quantities to be measured are  $B_\phi$ ,  $B_r$ , and density. But there also must be added a correlation coefficient between  $B_\phi$  and the mass flux.

*M. Dryer* I want to make a comment with regard to the theoretical interaction of the solar wind with, let us say, a magnetosphere or a comet. Some recent work applicable to the meridian plane containing the solar wind magnetic field and velocity vector includes the magnetic field explicitly, not implicitly, the way we've done it in the past. So if you take the magnetic field and pass it through the bow shock, and it refracts or whatever, the pressure is going to be asymmetrical. This harks back to suggestions made a long time ago by Walters. Now, what effect this asymmetrical pressure is going to have on the overall wind sock angle is still not quite clear. I agree completely with Brandt and Schmidt that the wind sock does respond to the solar wind. I just want to point out there might be a small bias introduced due to the asymmetrical calculation that is limited to the plane including the velocity and the magnetic field vectors.

#### COMMENTS

*L. Davis and I. Strong* As we have seen from Brandt's figure, the flow direction of the solar wind as deduced from the space probe and comet tail observations shows substantial dispersion about the mean velocity (extreme deviations of nearly  $10^\circ$  and a half-width at half maximum of about  $3^\circ$  to  $5^\circ$ ). Is this variability dominated by the now well-known deflections produced in the interaction regions between fast and slow streams? Alternative possibilities are that it may be due to: (1) effects derived from variations in the radial flow parameters that lead to a variation in the steady-state azimuthal velocity; (2) more or less random fluctuations due to Alfvén waves or other oscillations in the plasma; (3) random uncertainties in the observations.

To the extent that the first possibility accounts for the variability, its theoretical explanation is qualitatively very easily understood. In any case, it poses no problem in any purely theoretical investigation of the angular momentum loss of the sun. It suggests that in determining the observed angular momentum loss one might do better to reject all data that might be contaminated with this deflection produced by stream-stream interaction than to try to uniformly sample the fluctuations.

If alternative possibility (1) is the most likely, theorists should attempt to meet the challenge of providing a quantitative explanation. Any theory that predicts only a small range of azimuthal velocities will be unsatisfactory. What is needed is a theory that quite easily gives a range of velocities as one makes nominal variations in the boundary conditions but perhaps does not allow a unique determination of conditions at the sun from the observations at 1 AU.

The effects of alternative (2) can presumably be eliminated by choosing a suitable averaging period.

## EVIDENCE FOR CHANGES IN THE ANGULAR VELOCITY OF THE SURFACE REGIONS OF THE SUN AND STARS

### INTRODUCTION

*R. P. Kraft* If we are willing to believe that there is an angular momentum flux from the sun carried by the solar wind, then we can ask the question: Is there any direct observational evidence that the outer layers of the sun have indeed slowed down — that the torque corresponding to this angular momentum flux acting for a long time will lead to a deceleration of the observable outer layers of the sun? Obviously we cannot get such evidence very directly from the sun itself. But by placing the sun in the context of stellar evolution perhaps we can say something if we are willing to believe that the sun is a typical star.

To do this I want to remind you in 5 minutes, if I can, of the relationship between stellar rotation, stellar evolution, and the basic problem of the HR diagram. The HR diagram is the fundamental diagram of stellar astronomy. In it, astronomers plot the effective temperature  $T_e$  of a star against its luminosity  $L$ , where  $L = 4\pi R^2 \sigma T_e^4$ , where  $R$  is the radius and  $L$  is in units of energy (erg/sec). For a large sample of stars in the vicinity of the sun we find that the overwhelming majority (~90 percent) lie in a narrow band, called the *main sequence*, running diagonally across the diagram. The sun is a member of this band. There are a few stars in the lower left-hand corner of the diagram called *white dwarfs*. There are also a few up at the top right-hand side of the diagram (say 5 percent to 10 percent), which are called *giants* and *supergiants*.

The leading task of observational stellar astronomy is to explain why this diagram is not everywhere dense — why there aren't points all over it. Now it is an observed fact that luminosities of main sequence stars are a monotone increasing function of mass. So if we go up along the main sequence we go to stars of larger and larger mass; thus there is a mass luminosity relation along that sequence in which luminosity goes more or less as the

third or fourth power of the mass. The interpretation of this observation is that stars somehow arrive on this main sequence, which then represents a locus of points of stars of different mass burning hydrogen in equilibrium — that is, converting hydrogen into helium. The rate at which the nuclear processes take place depends critically upon a high positive power of the central temperature and density, and these in turn depend on the total mass of the star. Consequently, stars high on the main sequence burn out their critical hydrogen supply first, and therefore evolve into the giant region. Theoretical calculations bear this out. One computes an evolving stellar model in which stars start out on the main sequence chemically homogenous, burn up a critical hydrogen supply in the central region, and move rapidly in the HR diagram to the giant domain. Then they may burn helium for a while, or perhaps hydrogen also in shell sources. Eventually they contract, exhaust their nuclear energy sources, and wind up in the degenerate white dwarf domain. Before you get to the main sequence you have a period of gravitational contraction, with stars moving in from the right-hand side of the HR diagram, simply in a state of gravitational contraction. The time scales involved here for the sun, for example, are of the order of  $10^8$  years for the gravitational contraction. The hydrogen burning lifetime on the main sequence is of the order of  $10^{10}$  years, and subsequent stages — the red giant episode and presumably the dwarfs — spend most of their time on the main sequence.

What this has to do with stellar rotation is simply the issue of whether the e-folding time for significant changes in rotational velocities of stars owing to the action, let us say, of winds similar to the solar wind is short, long, or of the same order as the nuclear or the gravitational time for the star. If it is very much longer, the problem is of no interest. If it's very much shorter

than these critical times, especially the nuclear time, of course, then one has an interesting problem.

Rotation can be described in relation to the topology of the HR diagram. I draw a roughly vertical line, intersecting the main sequence just above the position of the sun, in the region of what are called the *F*-type stars. To the left of this line one has the domain of rapid rotation, in which stars have rotational velocities up to a few hundred km/sec. To the right of this line one has the domain of slow rotation. This includes the main sequence and giants. Thus the main sequence from just above the sun on down is a domain of slow rotation, and the upper main sequence above middle *F* is a domain of rapid rotation.

Figure 1 shows the post main sequence evolutionary tracks from the work of Iben and others. These stars

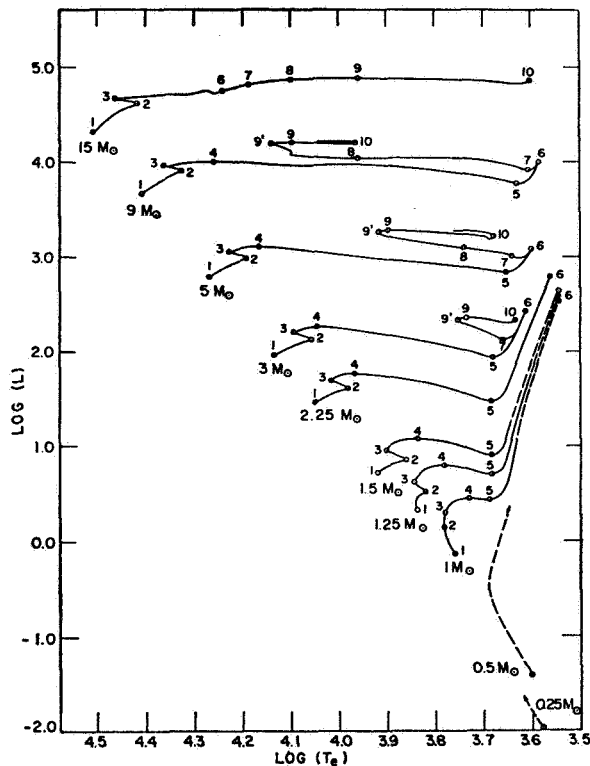


**Figure 1.** Post main sequence evolutionary tracks showing progression from the main sequence (starting points on the left) toward the red giant stage for different solar masses [adapted from Iben and others].

have exhausted their critical hydrogen supply and have moved on to the right in the HR diagram to become giants. Essentially their radii swell up at an almost constant luminosity. One can understand the slow rotation for these stars if angular momentum is essentially con-

served, because the radii of the giants are much larger on the average than the radii of the main sequence stars.

Referring to the main sequence, figure 2 shows the distribution of mean rotational velocities along the main sequence.  $V_{\sin i}$  refers to the mean value (over a large sample of stars) of the rotational velocity projected on the line of sight (recall that a spectrograph measures only the radial component of motion);  $V$  refers to the

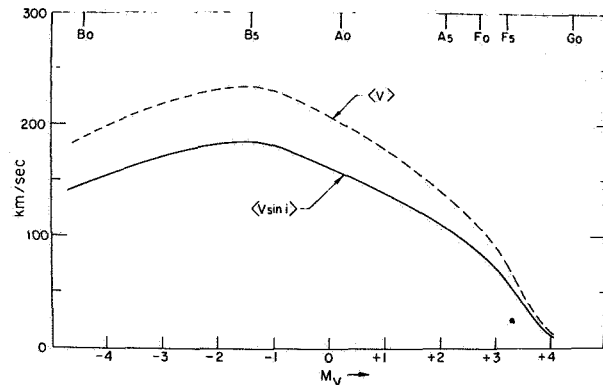


**Figure 2.** Distribution of mean line-of-sight rotational velocities as a function of absolute magnitude as a representation of luminosity together with the mean rotation based upon the assumption of a random distribution of rotational directions.

mean true value, assuming a random orientation of rotational axes. The abscissa is absolute magnitude, a logarithmic measure of luminosity. Higher luminosity stars are to the left. The rotations go up to a few hundred km/sec on the average, reach a maximum where stars have temperatures of the order of 15,000° or 20,000° ( $M_V = -1$ ), and then decline rapidly in middle *F* spectral class, near  $M_V = +\beta$ . The sun on this diagram would be at  $M_V = +4.7$ , and the rotations there on the average along the main sequence become very slow. This region between  $M_V = +2.5$  and  $M_V = +4$  is the "break" in rotations on the main sequence that I will be returning to several times in this talk.

Figure 3 shows the same thing in terms of specific angular momentum  $J = J/M_e$ , where  $M_e$  is the mass of a star. The momentum  $J$  is shown as a function of  $M_e$  along the main sequence, assuming that the stars are rigid rotators. It is seen that  $J$  varies roughly as  $M_e^{2/3}$  down to masses just a little larger than the sun's; then  $J$  takes a sharp drop. Thus the stars of solar rotation have angular momentum densities that are very low in contrast to the stars higher up on the main sequence, if we take the surface rotational velocity as characteristic of the total rotation. The figure also shows that if you

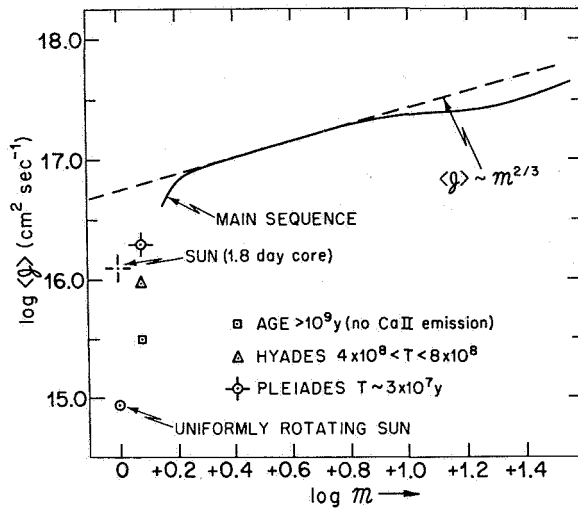


**Figure 3.** Specific angular momentum versus absolute magnitude for two solar models, the Pleiades, Hyades, and Ca II emission-free objects.

put all the angular momentum in the solar system back into the sun, of course, you get up to the extension of the specific angular momentum line for the more luminous stars. On the other hand, if you restored the angular momentum of the sun by assuming it had a rapidly rotating core, then you would also restore the sun back up to the relation  $J \sim M_e^{2/3}$ . It should be remembered, of course, that the relation  $J \sim M_e^{2/3}$  is statistical in character because, at a given  $M_e$ , stars do, in fact, have a very wide range of true rotational velocities.

One may ask first of all, why are all stellar rotations so slow, even those of the upper main sequence. If you try to contract a piece of the interstellar medium with the differential galactic rotation in it and a mass equal to one solar mass, and ask that angular momentum be conserved, you will wind up with a surface rotational velocity exceeding the speed of light when the mass has solar dimensions. So somewhere in the early stages of contraction you've got to get rid of a lot of angular momentum, and even the most rapidly rotating main sequence stars have a velocity of only a few hundred km/sec. Thus only about 1 percent of the initial angular momentum winds up even in the most rapidly rotating star, and there has to be a lot of angular momentum dumped in the early stages of stellar evolution. In addition, after you dispose of most of the angular momentum, there is finally the question of the origin of the break on the main sequence in early *F* where rotation takes a nosedive and gets extremely slow. And one would imagine that this might have something to do with the existence of an angular momentum flux in the solar wind.

Now, Wilson showed from an extensive amount of work that one index of stellar chromospheric activity was correlated with stellar age; that is, when stars first arrive on the main sequence after gravitational contraction, they give evidence for a large degree of chromospheric activity as measured by the strength of the ionized calcium (Ca II) emission at the bottom of the *K*-line, which, as you know, arises in the chromosphere. The body of evidence Wilson assembled strongly suggests, and indeed I think proves that, as a star sits on the main sequence burning up its hydrogen supply, its chromosphere tends to die away with time, in the sense that the Ca II emission gradually dies away with time. The first work was based on stars of the general field in the vicinity of the sun. Later, Wilson confirmed the result by studying the stars in galactic cluster where age dating can be obtained from the nuclear time of the turnoff on the main sequence. Young clusters like the Pleiades, which has an age of  $3 \times 10^7$  years, were found to have strong Ca II emission. As you go to the Hyades with an age of  $5 \times 10^8$  years, the Ca II emission weakens. When you look at typical field stars with Ca II emission, the strengths are similar to those of the Hyades or are weaker. As you go on toward stars that don't have any Ca II emission, they are the ones that on the average have the oldest nuclear ages.

Now, the other thing Wilson was able to show is that, as you go up the main sequence, the Ca II emission rather abruptly disappears in middle *F*. So among main sequence stars, Ca II emission is confined to those from just above the sun on downwards; the ones above middle *F* do not show it. Now it is remarkable that the main sequence location where Ca II emission disappears is the same as that where the rotational velocities take a nosedive. It is also the same place where stars begin, as one passes down the main sequence, to develop an outer convection zone owing to the mid-ionization of hydrogen.

The picture that develops from all this is essentially the following: One imagines that a star arrives on the main sequence after gravitational contraction. One postulates that if the star arrives on the main sequence below middle *F* then, because the outer part of the star has a well-developed hydrogen convection zone, there is acoustic heating of the chromosphere and of the corona; therefore, a wind exists owing to coronal evaporation, which then is capable, if coupled to a magnetic field, of carrying away angular momentum. On the other hand, if the star arrives on the main sequence somewhat above middle *F* the convection zone disappears — that is, the structure of the star does not permit an external hydrogen

convection zone — in which case there is no acoustic hearing, no corona, no wind, and therefore there is no torque exerted by outflowing gas. A few years ago, I looked for observational confirmation of this picture. One predicts that if you looked at field stars below middle *F* with strong Ca II emission or looked at stars in young galactic clusters below middle *F* you would on the average find them rotating more rapidly than older stars like the sun. In other words, what one would look

for is a systematic decay of rotational velocity of the surface regions of stars with advancing age. Since the clusters give a nuclear age-dating of the stars, you simply assemble them into age groups, observe them for rotation, and see if in fact the mean rotation systematically declines with advancing age.

Consider first the field emission-line stars shown by Wilson to be younger than those without emission. In figure 4, these are compared in a pseudoHR diagram.

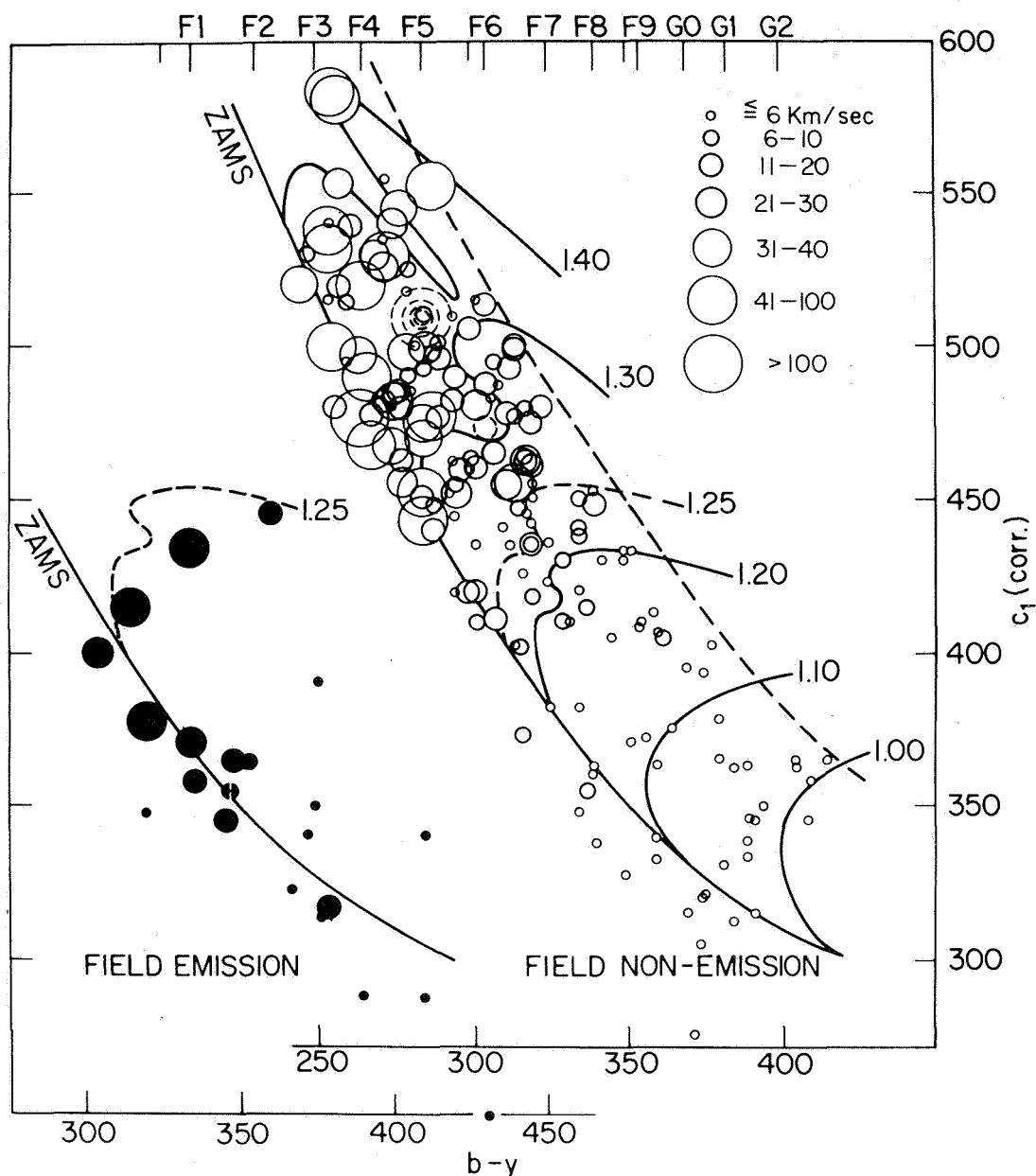


**Figure 4.** Strömgren diagram representation of the HR diagram for both field emission and field emission-free stars of variable solar mass [from *Ap. J.*, Vol. 150, 1967, p. 551].

The color ( $b-y$ ) increases with decreasing surface temperature; the quantity  $C$  is related to the luminosity in the sense that luminosity increases upward. Filled circles refer to emission-line stars and open circles to nonemission line stars. Rotational velocities are proportional to the sizes of the dots. The break in rotation corresponding to stars of middle  $F$  type is apparent. Figure 4 shows what happens in clusters. In the Pleiades there are large rotations and in the Hyades intermediate rotations. The field stars have emission lines of strength similar to the Hyades; both have rotations much larger than the non-emission-line old stars in the solar vicinity.

This finding is summarized in figure 5. If at a given mass you make a cut in the rotational velocity, the Pleiades are highest, field emission and Hyades stars are next, and then the field nonemission stars have the lowest velocities. Figure 6 shows the theoretical justification for the statement that the existence of the convection zone is related to the production of a stellar wind. The thickness of the outer hydrogen convection zone in main sequence stars is given as a function of surface temperature from work of Baker. Alpha is the ratio of mixing length to scale height and is only of interest to people who worry about convection theory. In any event, you see that the zone gets thinner and thinner as you go up the main sequence. Eventually, the convection zone disappears and one would then argue there is

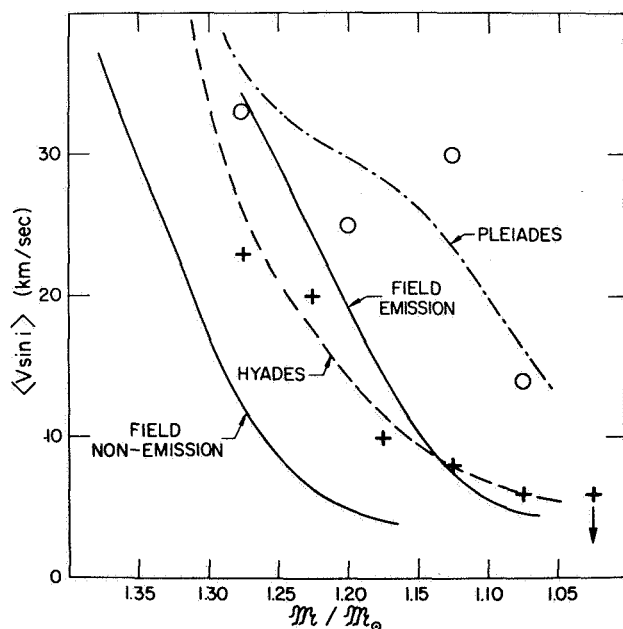


**Figure 5.** Line-of-sight rotational surface speeds as a function of mass normalized to the sun [from *Ap. J.*, Vol. 150, 1967, p. 551].

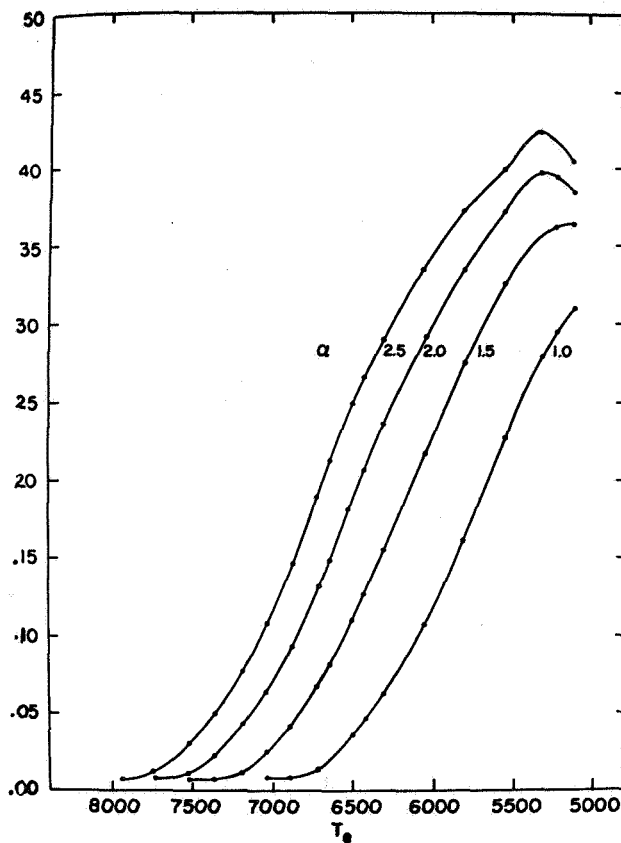


**Figure 6.** Normalized hydrogen convection zone thickness as a function of surface temperature,  $T_e$ .  $\alpha$  is the ratio of mixing length to scale height (adapted from Baker).

no acoustic heating, no corona, and therefore no wind for stars above middle  $F$ .

Table 1 gives the mean rotation as a function of age. One has first the type of star, the mean age, the mean rotational velocity, and the specific angular momentum  $J$  assuming uniform rotation. The value of  $J$  corresponding to  $J \sim M_e^{2/3}$  is also given. According to Dicke, the

**Table 1.**  $\langle v \rangle$  as a function of age for stars of mass  $M = 1.2 M_{\odot}$  and for the sun

Star	Approximate average age (yr)	$\langle v \rangle$ (km/sec)	$\log J$
Field nonemission	$3 \times 10^9$	6	15.5
Hyades cluster	$4 \times 10^8$	18	16.0
Pleiades cluster	$3 \times 10^7$	39	16.3
Sun (uniform)	$5 \times 10^9$	2	15.0
Sun (1.8 day core)	$5 \times 10^9$	2	16.2

torque exerted by the wind has acted only to slow down the external convection zone and perhaps a small portion of the radiative region. If the Dicke model is correct, it predicts a certain relationship between the abundances of Li and Be; see Dicke, p. 290.

Olin Wilson has shown that the Ca II emission dies away with time when a star occupies a certain position on the main sequence. Now, this is essentially a statistical statement, averaged over time. There are two ways in which the Ca II emission in a star might change. One is the very short-term secular variation that might be

induced by stellar rotation. That is, if the emission comes from a few localized plages on the surface, then you might expect it to be modulated by stellar rotation. Essentially nothing about that is known from stellar astronomy observations.

A second kind of modulation of the Ca II emission might come from solar cycles — that is, the stellar analogs of what the solar cycle is — since we know that the strength of the Ca II emission integrated over the solar surface would certainly be a function of phase in the solar cycle.

*R. P. Kraft* I think we could allow now about 5 to 10 min on discussion of these two talks on the observational side of stellar astronomy. DISCUSSION

*J. V. Hollweg* In the sun the Ca emission is closely related to supergranulation and, although you spoke of acoustic heating I think these emissions are also consistent with heating by supergranulation driven Alfvén waves, which I discussed this morning.

*R. P. Kraft* Yes, I realize there's been quite a bit of discussion about these points. I didn't mean to imply acoustical heating was in question. Also, lack of time prohibited any real discussion about the problem of the relation between solar Ca emission as it would be seen integrated over the whole disk and Ca emission in stars, which is, after all, the only way you can observe stars. That's a rather difficult question that sometimes solar physicists also balk at answering, answering how much comes from plages and — well, they don't always want to tell you exactly.

*A. Barnes* I was wondering whether there are any observations of Ca enhancement in stars that have detectable magnetic fields.

*O. C. Wilson* Offhand, I can't think of any, because the stars in which magnetic fields have been found are all earlier types — that is, up to *F* in general.

*R. P. Kraft* It's rather a very interesting point that if you put out of consideration binary stars among the stars in the domain of the HR diagram, where the rapid rotators lie, I think you can make a pretty good case for the statement that the only stars in slow rotation in that part of the HR diagram are in fact the stars with magnetic fields.

*C. P. Sonett* Could you give some kind of idea what the bound is? Because, if I recall correctly, there's a limit imposed by line broadening turbulence and rotation.

*R. P. Kraft* That's a very difficult question, one of the things that make it very hard to determine stellar rotations, when down to solar rotational velocities; there is a great deal of discussion in non-LTE circles about the meaning of turbulence, but it is true that there are other sources of line broadening that become competitive with rotation in the range less than 5 km/sec. So trying to disentangle rotation from other effects does begin to be difficult.

*C. P. Sonett* How small a magnetic field can you determine?

*R. P. Kraft* The field strengths that can be determined by the longitudinal Zeeman effect are limited to about 500 gauss. Under that one can't really say anything with certainty. That's about the difference between the left- and right-hand circularly polarized spectra, leading to about  $1 \mu$  on a typical plate. Under that, you can't say much for that kind of a field.

*J. M. Beckers* It also calls for a variation of calcium emissions which could be stellar rotations. From the emission and principal possibilities and various velocities that have been observed, can you see any variations?

*O. C. Wilson* I only get to the observatory maybe three or four nights each month, and also there are gaps due to weather and so on, so I cannot say. There are some variations that take place occasionally in the course of days or certainly weeks, but I

don't have a dense enough array of points so far to establish any periodicity. The only things that look as if they might be periodic are these long-term effects that Kraft showed on the screen here.

*R. P. Kraft* Some years ago the Russian astronomer Chiginov discovered sinusoidal variations in brightness of a dwarf  $M$  type star with Ca and H emission lines (one would judge it to be a young  $M$  star); the variations in amplitude sometimes also show a phase shift. Similar variations in integrated broadband photometry have been found in other dwarf  $M$  type stars with emission lines, but not in dwarf  $M$  type stars without emission lines. This has been interpreted as a rotational modulation of a spotted surface. The periods tended to be of the order of a few days and the rotational velocities are not unreasonable — that is, 10 or 15 km/sec. But, of course, it remains to be seen whether that is the correct interpretation of the effect.

*D. S. Intriligator* When you showed the pairs of the possible stellar cycles, in each case they weren't necessarily unrelated; it's just they were out of phase. If that is true, that's quite interesting.

*O. C. Wilson* That's correct. In the 1961 Cygnus pair, I think there is just an out-of-phase relationship. In the other, I could not see anything (well, with four points) but random scatter in the case of the faint member.

*D. S. Intriligator* Unless it's just out of phase the other way.

*O. C. Wilson* Well, it went up and went down, then went up.

*L. Mestel* I would like to ask for confirmation from the floor on the following. Fitting the observed velocities for the young cluster and the sun does imply a nonlinear dependence of the rate of loss of angular momentum on the angular velocity. I seem to remember Conti was quoted as saying this some years back. It would be very interesting in that it would, I think, give a broad hint of the magnetic field that is doing the braking, and, therefore, its strength should depend on the angular velocity and so one obtains a braking rate that is not linear.

*M. M. Conti* The only data we have is for the Hyades, the Pleiades, and the sun, where we have the ages. If these are plotted logarithmically one obtains a reasonable linear relation of just about three points and two of them at one end.

*L. Mestel* What is the index?

*M. M. Conti* I'm sorry, I don't remember the number.

*R. Dicke* I suppose you want to hear a comment on the initial rotation of  $1.0 M_{\odot}$  mass stars; how much is known about that. I understand it's very little.

*R. P. Kraft* Well, it is true that all this work on rotations was done at about  $1.2 M_{\odot}$ . You see, the decline in rotation along the main sequence is very sharp, and you soon get down to where these troubles exist that Sonett was talking about; there are all kinds of observational reasons the stars are getting fainter, and you have to go higher dispersions to resolve the rotational velocity. Well, all the light is disappearing. You disperse the spectrum out still more and with less and less light. So you know less and less about stellar rotations, the fainter you go. And the difference even between stars of  $1.2 M_{\odot}$  and of one is exceedingly difficult to handle. So we really don't know as much as we should.

## COMMENTS

*B. Durney* The angular velocity of the sun is calculated as function of time assuming that the initial angular momentum is given by extrapolating the main sequence values of stars with mass greater than  $1.2 M_{\odot}$  [Kraft, 1968]. The angular momentum loss is assumed to be proportional to  $\omega(\omega/\Omega_{\odot})^n$  with  $n = 2$  where  $\omega$  is the angular velocity and  $\Omega_{\odot}$  is the sun's angular velocity. Two cases are considered: (1) rigid rotation; and (2) mixed outer shell coupled with a rapidly rotating interior only by viscosity [Dicke, 1970c]. A comparison is made between the computed values of  $\omega$  and the observed angular velocities of  $1 M_{\odot}$  stars [Kraft, 1967]. With the help of the simplest



approximations the time dependence of the magnetic field is estimated for the case of rigid rotation and found identical to that obtained by *Skumanich* [1971] from the variations of the intensity of Ca II emission with age.

The well-known *Dicke and Goldenberg* [1967] experiment measuring the difference in flux between the equator and the pole at the limb of the sun has been interpreted by *Dicke* [1970a, b, c] as resulting from an oblateness of the surfaces of constant density which define the limb of the sun. For vanishing magnetic and velocity fields, surfaces of constant potential and density coincide. The oblateness of surfaces of constant potential has been attributed by Dicke to a gravitational quadrupole moment caused by a rapidly rotating core. It is well established [*Kraft*, 1967, 1968] that stars with mass larger than  $1.2 M_{\odot}$  arrive at the main sequence in rapid rotation and that stars with convection zones are subsequently slowed down by the torque exerted by the solar wind. The angular momentum loss of the sun from this torque is given by *Weber and Davis* [1967]:

$$\frac{dJ}{dt} = \frac{2}{3} r_a^2 \omega \frac{dM}{dt} \quad (1)$$

where  $\omega$  is the angular velocity,  $r_a$  the Alfvénic point, and  $dM/dt$  the solar wind mass flow.

It will be assumed that the angular momentum of the sun when it arrived at the main sequence is given by extrapolating the angular momentum of stars without convection zones [*Kraft*, 1968; *Dicke*, 1970b]. Assuming uniform rotation, the present solar wind torque slows down the sun with an e-folding time of about  $10^{10}$  years. Thus, if  $\omega$  is independent of  $r$ , equation (1) can be written

$$\frac{d\omega}{dt} = -\alpha\omega, \quad \alpha = \frac{1}{4\pi} \frac{r_a^2 (dM/dt)}{\int \rho r^4 dr} \quad (2)$$

with  $\alpha(t = 5 \times 10^9 \text{ yr}) \sim 10^{-3}$ , where the unit of time is  $10^7 \text{ yr}$ . There is little doubt that the sun's angular momentum loss was much larger in the past. The Alfvénic point  $r_a$  and presumably also to some lesser extent the mass flow (the properties of the convection zone have not changed significantly in  $5 \times 10^9 \text{ yr}$ ) depend on the average solar magnetic field at the surface. The sun's magnetic field is generated by a dynamo mechanism [*Leighton*, 1969; *Parker*, 1970] driven by differential rotation, which in itself is the result of the interaction of rotation with convection [*Durney*, 1971]. Thus, ultimately the torque exerted by the solar wind is a function of the angular velocity [*Spiegel*, 1968, 1971]. Following Spiegel we write:

$$r_a^2 \frac{dM}{dt} \propto \left( \frac{\omega}{\Omega_{\odot}} \right)^n \quad (3)$$

The proportionality factor can be evaluated from the present known angular momentum loss of the sun. Equation (2) can thus be written:

$$\frac{d\omega}{dt} = -10^{-3} \omega \left( \frac{\omega}{\Omega_{\odot}} \right)^n \quad (4)$$

As described earlier, the initial value for the angular momentum ( $J_0$ ) will be assumed to be given by extrapolating the main sequence values of stars with mass greater than  $1.2 M_{\odot}$  [*Kraft*, 1968]. This gives  $\omega(t=0) = 65 \Omega_{\odot}$ . Table 1 gives  $\omega$  as function of time

**Table 1.** Angular velocity as function of time

$t(10^7)$ years	$n = 1$		$n = 2$		$n = 3$	
	$\omega \times 10^{-5}$ (a) Rigid rotation	$\omega \times 10^{-5}$ (b) Rotating shell coupled with the core	$\omega \times 10^{-5}$ (a) Rigid rotation	$\omega \times 10^{-5}$ (b) Rotating shell coupled with the core	$\omega \times 10^{-5}$ (a) Rigid rotation	$\omega \times 10^{-5}$ (b) Rotating shell coupled with the core
0.1	18.5	8.12	13.7	6.95	4.3	2.6
1	17.5	7.64	6.1	3.66	2	1.5
3	15.6	6.77	3.6	2.32	1.4	1.09
10	11.3	4.88	2	1.39	0.92	0.81
40	5.2	2.36	1	0.84	0.58	0.61
100	2.5	1.35	0.64	0.67	0.43	0.53
200	1.3	0.95	0.45	0.58	0.34	0.49
300	0.91	0.8	0.37	0.54	0.3	0.46
400	0.69	0.72	0.32	0.51	0.27	0.44
500	0.56	0.68	0.287	0.49	0.25	0.43

(in units  $10^7$  yr) for  $n = 1, 2, 3$ . The column “rotating shell coupled with the core” was computed by assuming that the outer shell is coupled with the core only by viscosity. In this outer shell the angular velocity is constant across the convection zone and varies as  $1/r^2$  for  $r_{con} > r > 0.54 R_\odot$  where  $r_{con}$  is the inner radius of the convection zone. The equation for  $\omega$  (the angular velocity at the surface) is now [Dicke, 1970c).

$$\frac{d\omega}{dt} = -2.5 \times 10^{-3} \omega \left( \frac{\omega}{\Omega_\odot} \right)^n \quad (5)$$

$$- \frac{4\sqrt{2\pi} v_c \rho_c r_c^2}{M_{r_c}} 1.78 \times 10^7 \int_0^t \frac{d\omega/d\tau}{(t-\tau)^{1/2}} d\tau$$

where the subindex “c” refers to values at the core surface ( $r_c = 0.54 R_\odot$ ) and  $M_{r_c}$  is the mass contained in the outer shell ( $r > 0.54 R_\odot$ ). The factor  $1.78 \times 10^7$  is introduced by the time unit of  $10^7$  yr. Equation (5) was solved by Dicke for a torque that depends exponentially on time. In the present case, it can be solved numerically by iteration. The initial angular velocity at the surface was taken equal to  $28.5 \Omega_\odot$ , and  $\omega(r, t = 0) = \omega(r_c, 0)$  for  $r < r_c$ . With these values of  $\omega$  the angular momentum at  $t = 0$  is equal to  $J_0$ .

For the case of rigid rotation and with the help of very crude approximations the time dependence of the magnetic field can be estimated as follows: In the first approximation the mass flow  $C = dM/dt$  will depend on the total amount of mechanical heating absorbed by the corona. The corona is heated predominantly by shock waves [Osterbrock, 1961; Kopp, 1968] having their origin in the convection zone which has not changed much during the sun’s lifetime. We assume therefore that the mass flow  $C$  is independent of time. Even for modest magnetic fields the Alfvénic point is at much larger distance than the sonic point and therefore the velocity at the Alfvénic point  $u_a$  should not depend strongly on  $B$ ; we assume thus that also  $u_a \sim \text{constant}$ .

Now, the Alfvénic point is defined by

$$\frac{4\pi\rho_a u_a^2}{B_a^2} = \frac{4\pi C^2}{B_a^2 r_a^4 \rho_a} = \frac{4\pi C^2}{B_\odot^2 r_\odot^4 \rho_a} = 1 \quad (6)$$

where  $B_\odot$  is the magnetic field at the base of the corona and  $r_\odot$  is the radius of the sun. From equation (6), and from the assumptions that  $C$  and  $u_a$  are in the first approximation independent of time we obtain

$$r_a^2 \propto \frac{1}{\rho_a} \propto B_\odot^2$$

Equation (3) (with  $n = 2$ ) shows that  $r_a^2 \propto \omega^2$  and therefore

$$B_\odot \propto \omega \quad (7)$$

From equation (4) ( $n = 2$ ) and from the initial value of  $\omega$  ( $\omega \sim 65 \Omega_\odot$ ) it is easily seen that  $\omega$  will be proportional to  $1/t^{1/2}$  for  $t \gg 10^6$  yr. Therefore,

$$B_\odot \propto 1/t^{1/2} \quad (8)$$

for  $t \gg 10^6$  yr. This is exactly the dependence of the magnetic field on time found by Skumanich from the observed variations of Ca II emission with age.

The dependence of the magnetic field on angular velocity given by equation (7) differs from that suggested by Cowling [1965]. However, even the dependence of differential rotation on  $\omega$  is not simple [Durney, 1971]. In relation to the magnetic field and keeping in mind Leighton's model for the solar cycle, differential rotation and the "tilt" of the axis of the sunspot groups depend on  $\omega$ . It is unlikely, however, that the strong dependence of  $\omega$  on  $r$  required by Leighton's model is real [Durney, 1971]. Perhaps the concentration of the magnetic flux by convection as suggested by Weiss [1964] should be included explicitly. The above considerations suggest that a reliable theoretical estimate of the dependence of  $B$  on  $\omega$  is difficult.

We discuss now the dependence of the angular velocity on time as given in table 1. Consider the case  $n = 2$ . For the Hyades ( $t = 3$ )  $\omega \sim 1.4 \times 10^{-5}$  [Kraft, 1967] and even the case of "rotating shell coupled with the core" gives too large an angular velocity. The angular velocity for the Pleiades ( $t = 40$ ) is about  $0.84 \times 10^{-5}$  (in perfect agreement with case 2). However, its age is the subject of some discussion and could be as large as  $t = 90$  [van den Heuvel, 1969]. The perfect agreement between the angular velocity of the sun and the case of rigid rotation for  $n = 2$  is, of course, accidental. It is easy to understand on the other hand why case 2 gives angular velocities for  $t = 500$  that are too large. Initially the viscous stresses at the core surface ( $r = r_c$ ) are negligible and only the outer shell is slowed down, greatly reducing the angular momentum loss. At  $t \sim 20$  the torque exerted by the core becomes significant; from then on the angular velocity decreases slowly. It should be noted from table 1 that the angular velocity decreases initially very fast. For the case of rigid rotation and  $n = 2$ , the sun is already rotating in about 2 days for  $t = 3 \times 10^7$  yr. Even if during the Hayashi phase the primordial magnetic field was destroyed, since the star is convective, a dynamo mechanism would have generated a magnetic field that could have initially coupled the inner core ( $r < 0.54 R_\odot$ ) with the outer shell. The sun could have rapidly lost angular momentum without a large amount of lithium destruction. Since it was likely that the magnetic field was subsequently expelled from the interior by magnetic buoyancy (enhancing possibly the initial angular momentum loss) the core and the outer shell could have decoupled giving rise to the observed lithium depletion [Danziger, 1969; Wallerstein and Conti, 1969].

#### ACKNOWLEDGEMENTS

The author is grateful to Dr. R. A. Kopp for illuminating discussions and to Mrs. Nancy Werner for performing the numerical calculations.

## REFERENCES

- Cowling, T. G.: *Stellar and Solar Magnetic Fields*. R. Lüster, ed., North-Holland Publishing Co., Amsterdam, 1965.
- Danziger, I. J.: Observational Time-Scales for Depletion of Lithium in Main Sequence Stars. *Astrophys. Letters*, Vol. 3, 1969, p. 115.
- Dicke, R. H.; and Goldenberg, H. M.: Solar Oblateness and General Relativity. *Phys. Rev. Letters*, Vol. 18, 1967, p. 313.
- Dicke, R. H.: The Solar Oblateness and the Gravitational Quadrupole Moment. *Ap. J.*, Vol. 159, 1970a, p. 1.
- Dicke, R. H.: The Rotation of the Sun. IAU Colloq. No. 4, *Stellar Rotation*. A. Sletteback, ed., Reidel, Holland, 1970b.
- Dicke, R. H.: Internal Rotation of the Sun. *Ann. Rev. Astron. Astrophys.*, L. Goldberg, ed., Annual Reviews, Inc., Palo Alto, Calif., 1970c.
- Durney, B.: Differential Rotation, Meridional Velocities, and Pole-Equator Difference in Temperature of a Rotating Convective Spherical Shell. *Ap. J.*, Vol. 163, 1971, p. 353.
- Kopp, R. A.: The Equilibrium Structure of a Shock-Heated Corona. Thesis, Harvard Univ., 1968.
- Kraft, R. P.: Studies of Stellar Rotation. V. The Dependence of Rotation on Age Among Solar Type Stars. *Ap. J.*, Vol. 150, 1967, p. 551.
- Kraft, R. P.: *Stellar Rotation in Stellar Astronomy 2*. H. U. Chiu, R. Warasila, and J. Remo, eds., Gordon and Breach, New York, 1968.
- Leighton, R. B.: A Magneto-Kinematic Model of the Solar Cycle. *Ap. J.*, Vol. 156, 1969, p. 1.
- Osterbrock, D. E.: The Heating of the Solar Chromosphere, Plages, and Corona by Magnetohydrodynamic Waves. *Ap. J.*, Vol. 134, 1961, p. 347.
- Parker, E. N.: The Origin of Solar Magnetic Fields. *Ann. Rev. Astron. Astrophys.*, L. Goldberg, ed., Annual Reviews, Inc., Palo Alto, Calif., 1970.
- Spiegel, E. A.: The Mixing of Lithium. *Highlights of Astronomy*, L. Perek, ed., Reidel, Holland, 1968.
- Spiegel, E. A.: A History of Solar Rotation in Physics of the Solar System, S. I. Rasool, ed., NASA publication, in press.
- Skumanich, A.: On the Physical Calibrations of Stellar Chromospheres (private communication).
- van den Heuvel, E. P. J.: The Ages of Hyades, Praesepe, and Coma Clusters. *Pub. Astron. Soc. Pacific*, Vol. 81, 1969, p. 815.
- Wallerstein, G.; and Conti, P. S.: Lithium and Beryllium in Stars. *Ann. Rev. Astron. Astrophys.*, L. Goldberg, ed., Annual Review, Inc., Palo Alto, Calif., 1970.
- Weber, E. J.; and Davis, L., Jr.: The Angular Momentum of the Solar Wind. *Ap. J.*, Vol. 148, 1967, p. 217.
- Weiss, N. O.: Magnetic Flux Tubes and Convection in the Sun. *Mon. Not. Roy. Astron. Soc.*, Vol. 128, 1964, p. 225.

# EVIDENCE FOR THE DISTRIBUTION OF ANGULAR VELOCITY INSIDE THE SUN AND STARS

## INTRODUCTION

*L. Mestel* We have heard that the solar wind is steadily removing angular momentum from the solar surface via magnetic coupling. We now ask how the internal rotation field of the sun responds to this surface stress. We know that the sun has a deep subphotospheric convection zone, surrounding a radiative core. We shall assume that there are only modest variations of angular velocity within a convective zone, though we should note that there is at least one model of nonisotropic turbulence that, in principle, could allow a marked inward variation [Biermann, 1951, 1958; Kippenhahn, 1963]. We now ask whether the radiative core also steadily adjusts its angular velocity to stay more or less in step with the outer regions, or whether a steep inward angular velocity gradient is built up, as in Dicke's [1970, 1971] model, which has the core rotating some ten times faster than the convective zone.

One feels that a necessary condition for the persistence of the Dicke model is the absence of even a modest primeval magnetic field coupling the core and zone, for torsional hydromagnetic waves would iron out nonuniformities in rotation in a time much shorter than the solar lifetime. I personally am doubtful if this is a plausible assumption; however, I shall act as an *advocatus diaboli* and discuss the equilibrium and stability of the Dicke model in strictly nonhydromagnetic terms. The complications that arise are a justification for the claim I once made that the magnetic field is one of the great simplifying features of astrophysics.

Howard *et al.* [1967] and later Bretherton and Spiegel [1968] suggested that the Dicke model would be destroyed by a process analogous to Ekman pumping that is responsible for the rapid "spindown" in a coffee cup. In an incompressible (or barotropic) fluid the condition of hydrostatic support requires that the centrifugal force be conservative, so that the angular velocity must be a function only of distance  $\tilde{\omega}$  from the axis.

Such a law is inconsistent with the no-slip boundary condition at the bottom of the cup, so that a dynamically driven circulation is set up, with viscous force balancing Coriolis force in the thin Ekman boundary layer. Continuity forces the flow to extend through the bulk, yielding a very short spindown time.

The treatment of this problem contrasts markedly with that customary for a nonbarotropic stellar gas, obeying the law  $p \propto \rho T$ . A nonconservative field of centrifugal force, such as Dicke's, can be balanced hydrostatically by suitable variations of  $\rho$  and  $T$  over isobaric surfaces. The consequent breakdown in radiative equilibrium yields buoyancy forces that drive a slow circulation [Eddington, 1929; Sweet, 1950; Baker and Kippenhahn, 1959; Mestel, 1965]. The circulation speeds are normally of the order of the Kelvin-Helmholtz contraction speed times the factor  $r|\nabla(\Omega^2 \tilde{\omega})|/g$ , where  $g$  is the gravitational acceleration. If  $\Omega$  is slowly varying, this factor is essentially  $\Omega^2 \tilde{\omega}$ , but in a region of large rotational shear, as in the transition between Dicke's core and the convection zone, the circulation speeds will be much faster and will act to reduce the gradient. But before concerning ourselves with processes dependent on heat transport, we want to be sure that there is no analog of Ekman suction, yielding a much shorter spindown time. In fact, if the angular velocity gradient is too large it is impossible to satisfy the condition of hydrostatic support without the density gradient becoming locally positive and so unstable; the thermally driven Eddington-Sweet circulation is replaced by a dynamically driven flow if the scale of variation of  $\Omega$  is less than

$$d_c \simeq r[(\Omega^2 \tilde{\omega}/g)(\lambda/r)]^{1/2} \quad (1)$$

where  $\lambda$  is the local scale height. This is the analog of the layer thickness through which Ekman-pumped currents can travel against the effect of stable stratification

[Holton, 1965]. One is therefore led to consider a model in which a rapidly rotating core and a slowly rotating envelop do coexist, with the transition region between them never smaller than  $d_c$ . The evolution of the angular velocity field in the core would be given by the Eddington-Sweet currents, with the sharp  $\Omega$  gradient and any variations of molecular weight playing an important role. However, a much shorter spindown time could result if the transition layer were to become unstable. One would then arrive at a picture in which the slow but persistent braking of the star would drive a weak turbulence in the radiative core, which would keep the whole sun rotating more-or-less uniformly [Spiegel, 1968].

Let us therefore adopt a Dicke-type model, and study possible instabilities [see Spiegel and Zahn, 1970, for a recent survey]. If the fluid is inviscid and incompressible (with  $\Omega$  necessarily a pure function of  $\tilde{\omega}$ ), a celebrated criterion due to Rayleigh applies; for stability against axisymmetric disturbances, we require

$$(1/\tilde{\omega}^2)(d/d\tilde{\omega})(\Omega^2 \tilde{\omega}^2) > 0 \quad (2)$$

The angular momentum per unit mass must increase away from the rotation axis. However, there exist some nonaxisymmetric unstable modes even if condition (2) holds [Howard and Gupta, 1962]. Other nonaxisymmetric instabilities occur if

$$(d/d\tilde{\omega})[(1/\tilde{\omega})(d/d\tilde{\omega})(\Omega \tilde{\omega}^2)] = 0 \quad (3)$$

“inflectional instabilities” [Lin, 1955].

The principal modification in astrophysical applications is the stabilizing effect of a density stratification. In a zone that is stable against convection the density gradient is subadiabatic, and energy is required to drive adiabatic motions against gravity. The Richardson criterion for the stability of shear flow [Chandrasekhar, 1961] sets a lower limit to  $|\Omega/(d\Omega/d\tilde{\omega})|$ , which turns out to be of the order of the Holton thickness (1). However, in the Dicke model  $\Omega$  is a function of displacement  $z$  parallel to the rotation axis as well as of  $\tilde{\omega}$ ; the surfaces of constant angular momentum are not cylinders. Such models are sometimes subject to rapidly growing “baroclinic instabilities,” discussed by Hoiland [Ledoux, 1958] and more recently by James and Kahn [1970] who call them “sliding instabilities” because they involve motion of gas elements along either isobars or isentropes. They occur if the local angular momentum gradient  $\mathbf{h}$  lies in the shaded region (fig. 1), where  $\mathbf{p}$  is the direction of the pressure gradient and  $\mathbf{s}$  the direction of the negative entropy gradient. It appears that some Dicke-type models with the surfaces of constant angular momentum, as in figure 2, would violate the stability criterion, but others, as in figure 3, would not.

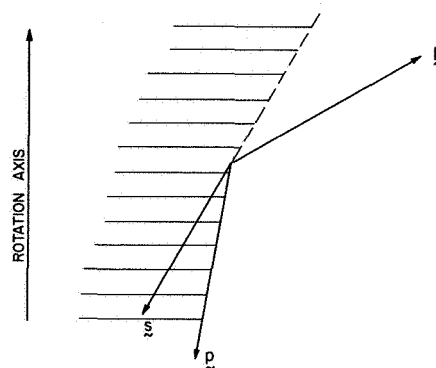


Figure 1. Schematic of angular momentum gradient,  $\mathbf{h}$ ;  $\mathbf{p}$  is the direction of the pressure gradient, and  $\mathbf{s}$  is the direction of the negative entropy gradient in a star for the condition of “sliding instabilities” to not be met. The converse takes place when  $\mathbf{h}$  lies in the shaded region.

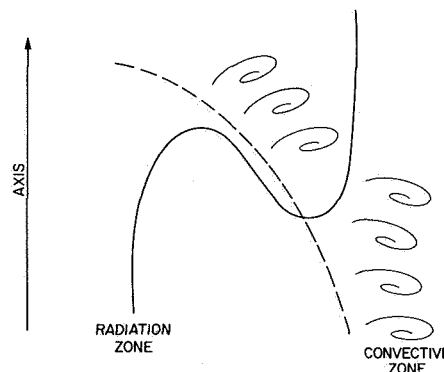


Figure 2. Dicke sun with a surface of constant angular momentum conceptually illustrated by the folded line crossing the radiative-convective transition. (The line is a cut in a surface of rotational symmetry about the axis. This condition might violate stability against the “sliding instability.”)

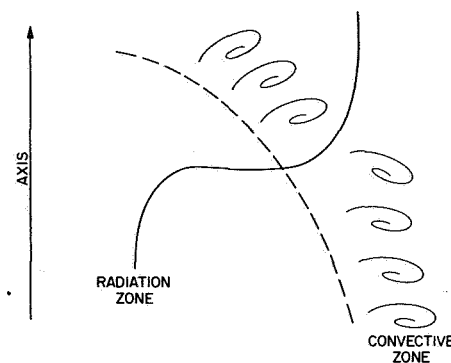


Figure 3. Dicke sun under the condition where stability is satisfied. The definitions of the figure elements are the same as those in figure 2.

So far we have assumed adiabatic motions. As soon as we allow for finite transport processes the whole situation changes. In stellar interiors the ratio of viscosity to thermal conductivity is very low ( $\approx 10^{-6}$ ), so that viscous effects can often (though not always) be ignored compared with heat flow. *Townsend* [1958] and *Yih* [1961] showed how radiative transfer can remove the stabilizing effect of stratification, so that for a completely stable state conditions (2) and (3) replace the Richardson criterion. The reason is that when temperature perturbations are smoothed out, the stabilizing effect of buoyancy is simultaneously removed [*Moore and Spiegel*, 1964]. More recently, *Goldreich and Schubert* [1967] and *Fricke* [1968], again ignoring viscosity, have shown that another necessary condition for the absence of "secular" (dissipation-dependent) instabilities is  $\partial\Omega/\partial z = 0$ , or angular momentum constant on cylinders. We have noted that this is a condition for the equilibrium of an incompressible star. *Fricke* [1969a] summarizes these results by the prescription: to determine which states of a real star are *secularly* stable, solve the problem of the *equilibrium* and *dynamical* stability of the corresponding inviscid, incompressible system.

It is then clear that even Dicke models that are not subject to baroclinic instabilities are certainly secularly unstable on the Goldreich-Schubert-Fricke criterion. However, it is still not generally agreed what asymptotic state the star reaches, and in what time scale. *Colgate* [1968] and *Kippenhahn* [1969] argue that the developed weak turbulence that follows from secular instabilities takes in general at least a Kelvin-Helmholtz time to alter substantially the overall angular momentum distribution. More recently, *James and Kahn* [1970] have proposed that an arbitrary initial rotation law rapidly approaches a state with the surfaces of constant angular momentum either cylinders or isentropes. The secular instabilities to which such a model is subject are suppressed by the much more rapid baroclinic instabilities which they themselves generate. *James and Kahn* [1971] also have studied the evolution of the junctions between the isentropes and cylinders, where the breakdown in radiative equilibrium leads to locally large Eddington-Sweet velocities; they conclude that the time for overall redistribution of angular momentum is the average Eddington-Sweet time, and this would be just about comparable with the solar lifetime if Dicke's internal rotation is correct. However, the subject remains controversial.

I have assumed that there are no inward gradients of mean molecular weight  $\mu$ . It has been known for many years that a very modest  $\mu$  gradient will suppress the Eddington-Sweet circulation [*Mestel*, 1953, 1957;

*Kippenhahn*, 1967], and that the growth of  $\mu$  in the center of a star is normally able to prevent the circulation from homogenizing the star. Similarly a  $\mu$  gradient will kill secular instabilities [*Goldreich and Schubert*, 1968]. The  $\mu$  gradient that can be built up during the early solar lifetime clearly depends on the rate at which instabilities develop and mix matter and angular momentum (see Dicke's discussion of the lithium problem, p. 290). *Fricke* [1969b] finds that the maximum oblateness due to internal rotation that can be obtained from a rotation field satisfying the secular stability requirements (including the effect of  $\mu$  gradients) is a factor 4 less than Dicke's value. But if we can tolerate secularly unstable rotation laws, because we have grounds for believing that the consequent angular momentum diffusion time is at least as long as the Kelvin-Helmholtz time, then a  $\mu$  gradient can be built up that will stabilize the Dicke model for the much longer nuclear lifetime of the sun. To return to a point made earlier, those who accept the arguments but do not like the Dicke model might very well claim that the conclusion is an argument in favor of magnetic coupling between core and envelope.

## REFERENCES

- Baker, N.; and Kippenhahn, R.: *Zeits. f. Astrophys.*, Vol. 48, 1959, p. 140.  
 Biermann, L.: *Zeits. f. Astrophys.*, Vol. 28, 1951, p. 304.  
 Biermann, L.: *Electromagnetic Processes in Cosmical Physics*. Vol. 248, B. Lehnert, ed., Cambridge Univ. Press, Cambridge, 1958.  
 Bretherton, F. P.; and Spiegel, E. A.: *Astrophys. J.*, Vol. 153, Pt. 2, 1968, p. L77.  
 Chandrasekhar, S.: *Hydrodynamic and Hydromagnetic Stability*. Oxford Univ. Press, Oxford, 1961.  
 Colgate, S. A.: *Astrophys. J.*, Vol. 153, Pt. 2, 1968, p. L81.  
 Dicke, R. H.: *Astrophys. J.*, Vol. 159, 1970, p. 1.  
 Dicke, R. H.: *Ann. Rev. Astr. Astrophys.*, Vol. 8, 1971, p. 297.  
 Eddington, A. S.: *Mon. Not. R. Astr. Soc.*, Vol. 90, 1929, p. 54.  
 Fricke, K.: *Zeits. f. Astrophys.*, Vol. 68, 1968, p. 317.  
 Fricke, K.: *Astron. and Astrophys.*, Vol. 1, 1969a, p. 388.  
 Fricke, K.: *Astrophys. Lett.*, Vol. 63, 1969b, p. 219.  
 Goldreich, P.; and Schubert, G.: *Astrophys. J.*, Vol. 150, 1967, p. 571.  
 Goldreich, P.; and Schubert, G.: *Astrophys. J.*, Vol. 154, 1968, p. 1005.  
 Holton, J. R.: *J. Atmos. Sci.*, Vol. 22, 1965, p. 402.  
 Howard, L. N.; and Gupta, A.: *J. Fluid Mech.*, Vol. 14, 1962, p. 463.

- Howard, L. N.; Moore, D. W.; and Spiegel, E. A.: *Nature*, Vol. 214, No. 5095, 1967, p. 1297.
- James, R. A.; and Kahn, F. D.: *Astron. and Astrophys.*, Vol. 5, 1970, p. 232.
- James, R. A.; and Kahn, F. D.: *Astron. and Astrophys.*, Vol. 12, 1971, p. 332.
- Kippenhahn, R.: *Astrophys. J.*, Vol. 137, 1963, p. 664.
- Kippenhahn, R.: *Zeits. f. Astrophys.*, Vol. 67, 1967, p. 271.
- Kippenhahn, R.: *Astron. and Astrophys.*, Vol. 2, 1969, p. 309.
- Ledoux, P.: *Handbuch der Physik*, Vol. 51, S. Flügge, ed, (Berlin: Springer-Verlag), 1958, p. 605.
- Lin, C. C.: *The Theory of Hydrodynamic Stability*. Cambridge Univ. Press, Cambridge, 1955.
- Mestel, L.: *Mon. Not. R. Astr. Soc.*, Vol. 113, 1953, p. 716.
- Mestel, L.: *Astrophys. J.*, Vol. 126, 1957, p. 550.
- Mestel, L.: *Stellar Structure*. Vol. 465, L. H. Aller and D. B. McLaughlin, eds., Chicago Univ. Press, Chicago, 1965.
- Moore, D. W.; and Spiegel, E. A.: *Astrophys. J.*, Vol. 139, 1964, p. 48.
- Spiegel, E. A.: *Highlights of Astronomy*. L. Perek, ed., (Reidel: Dordrecht-Holland), 1968.
- Spiegel, E. A.; and Zahn, J. P.: *Comments on Astrophysics and Space Physics*, Vol. 2, 1970, p. 178.
- Sweet, P. A.: *Mon. Not. R. Astr. Soc.*, Vol. 110, 1950, p. 548.
- Townsend, A. A.: *J. Fluid Mech.*, Vol. 4, 1958, p. 361.
- Yih, C.-S.: *Phys. Fluids*, Vol. 4, 1961, p. 806.

### COMMENTS

**R. Kraft** I would like to go back to the issue of the Li and Be abundances in the sun, to remind you of what Mestel said, that in comparison with young stars the solar Li abundance is very low. The solar Be abundance, however, is appropriate in making these comparisons. One knows that Li can be destroyed at a temperature somewhat higher than the base of the external convection zone, but that to destroy Be requires still higher temperature. So one imagines now there must be some way to mix the subadiabatic sub-convection zone material. And the issue is whether the turbulence that can be set up by the spindown process may be sufficient.

**R. H. Dicke** Mestel raised the question of stability that is a source of worry in connection with a rapidly rotating core in the sun. The instabilities in question are thermally driven: the Eddington-Sweet thermally driven currents and Goldreich-Schubert, and Fricke types of mild turbulence also driven by thermal effects. I will take the following viewpoint: Assume that the Goldreich-Schubert-Fricke instability holds and then calculate the turbulent transfer of angular momentum out of a star when despinning. This amounts to a turbulent diffusion of angular momentum. The same turbulent diffusion of angular momentum out of the star implies a turbulent diffusion of Li and Be downward into the interior, where these elements are burned. The two effects are boot strapped together: observe the rotation, and you should be able to say what is happening to the abundances of Li and Be. By observing rotations and abundances of Li and Be we decide whether or not this instability exists. This is program 1. I have another program after that, which is to use the "observed" depletion of Li in the sun as a basis for some conclusions about the present solar wind torque.

I assume that the thermally driven turbulence at the condition of marginal instability, after averaging  $\Omega \sin^2 \theta$  over spherical surfaces, leads to  $\Omega \sim r^{-n}$ , where  $0 < n \leq 2$ . The Goldreich-Schubert instability results in a function  $\Omega(r)$  in reasonable accord with the above equation with  $n \simeq \Omega_0/\Omega$  where  $\Omega_0$  refers to the present surface rotation of the sun. For isotropic diffusion the transport of angular momentum is controlled by the diffusion equation

$$(\partial/\partial r)[D\rho r^4(\partial\Omega/\partial r)] = \rho r^4(\partial\Omega/\partial t)$$

where  $D$  is the diffusivity of the turbulent diffusion. Assuming marginal instability  $\Omega(r, t)$  is known everywhere in the interior if the surface rotation  $\Omega_s(t)$  is known. Integration gives  $D(r, t)$ .



The next step is to ask what controls the diffusion of lithium. Let's designate the abundance of Li, Be, or whatever the isotope is by the symbol  $F$ . The corresponding diffusion equation is

$$(\partial/\partial r)[D\rho r^2(\partial F/\partial r)] = \rho r^2(\partial F/\partial t)$$

The diffusivity  $D$  is the same as before. To emphasize the point, we know, or at least we assume that we know, the time dependence of surface rotation. As the rotation rate of the surface of the star decreases the variation of the angular velocity of the stellar interior is known as a function of time and position from the condition of marginal instability. Instead of the usual interpretation of the diffusion equation, it is interpreted as a first-order differential equation for  $D$ . We solve that differential equation, substitute the resulting diffusivity  $D$  in the diffusion equation for Li (or Be), and solve the differential equation to obtain the depletion of Li (or Be) at the surface. The stellar rotation and the depletion of the isotope ( $\text{Li}^6$ ,  $\text{Li}^7$ , or  $\text{Be}^9$ ) are boot strapped together. The relation is  $F/F^* = (\Omega_s/\Omega_s^*)^\Lambda$  where the asterisks ( $F^*$  and  $\Omega^*$ ) refer to original values on the main sequence, and  $\Lambda$  is an eigenvalue derived from the solution of the differential equation for  $F$  as an eigenvalue problem. Figure 1 shows  $\Omega$  for marginal instability calculated from the

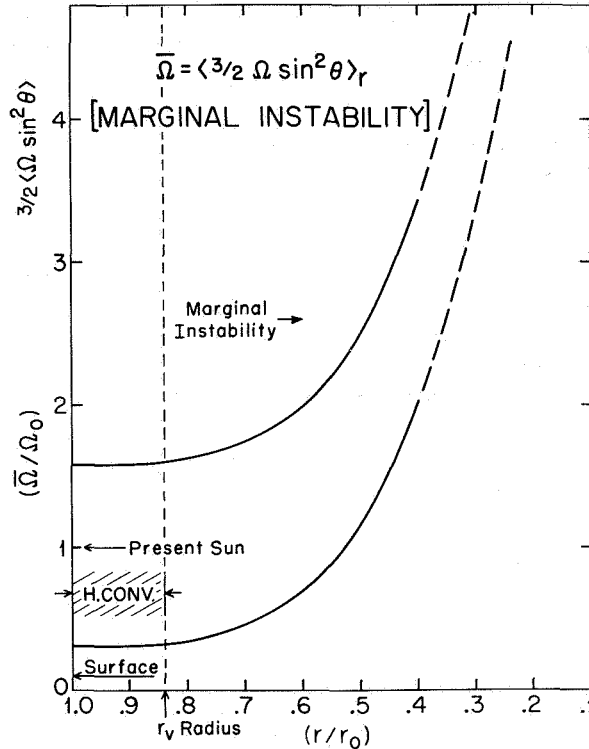


Figure 1.  $\Omega(r)$ , after averaging over spherical surfaces.

Goldreich-Schubert dispersion relation. Table 1 gives  $\Lambda$  for three different values of  $n$ ,  $n = 1/2$ , 1, and 2. The values of  $\Lambda$  given in table 1 are all so great that there should be no lithium or beryllium in the Hyades for which Kraft has measured a rotational slowing by a factor 2; that is,  $\Omega/\Omega^* = 1/2$ . On the contrary, we do see  $\text{Li}^7$  and  $\text{Be}^9$ , from which I conclude that this turbulence does not extend down deep in the star and the Goldreich-Schubert instability does not occur deep in the star.

**Table 1.**  $\Lambda$  eigenvalue for deep lying mild turbulence

	Li <sup>6</sup>	Li <sup>7</sup>	Be <sup>9</sup>
$n$	$r_b = 0.63$	0.58	0.47
1/2	237	140	46
1	174	100	31.3
2	222	120	33
2 (2nd mode)	1460	780	212
$\Lambda = \gamma\tau$			

The next question is whether the instability exists at all or whether it exists only part way down. Since we don't at the moment have any other explanation for the depletion of lithium I'm going to try on for size the idea that the lithium is depleted as a result of angular momentum being transported by means of this turbulence – angular momentum flowing out of the star into a stellar wind – but that the turbulence is terminated at a certain radius (which we will call  $r_c$ ) because of a slight jump in the mean molecular weight ( $\Delta\mu \sim 2 \times 10^{-3}$ ). As was noted by *Goldreich and Schubert* [1967], such a molecular weight jump provides a means for turning off the turbulence. Incidentally, when you turn off the turbulence you also turn off the circulation currents at that point; they both terminate.

Figure 2 shows a hypothetical way of obtaining the molecular weight jump. In the process of stellar contraction in the core, density goes quite high. But increased density in the core ought to result in increased angular velocity in the core. The curve marked "after core contraction" shows the high angular velocity of the interior leading to an angular velocity gradient that may exceed the instability limit. Goldreich-Schubert turbulence and circulation currents may occur inside the core, and if there is any extra helium as a result of hydrogen burning while this mixing is occurring, extra helium may be mixed throughout the core while the core's angular velocity tends to become uniform. As noted before, the jump in molecular weight required to stabilize is only  $\sim 2 \times 10^{-3}$ , which is very small. There is a possibility that one ends up with a stabilized boundary at  $r \cong 0.55$  with the region  $0.55 < r < 0.84$  being the thermally driven turbulent region. Outside is the hydrogen convective zone where angular momentum is moved convectively. These are the assumptions we make.

Table 2 shows the eigenvalue  $\Lambda$  discussed earlier, but now the turbulence is assumed to be cut off at  $r_c$ . The tabulated values are for various assumptions about cutoff radius and the index  $n$ . These have been chosen in such a way as to give reasonable values for the depletion rate for Li<sup>7</sup>. It is found that the cutoff can never go deep enough to deplete Be<sup>9</sup>. For a reasonable depletion of Li<sup>7</sup>, Li<sup>6</sup> should be essentially completely burned. If you reduce Li<sup>7</sup> by a factor of 5 the Li<sup>6</sup> ought to be out of sight.

In attempting to apply this situation to the sun or stars of precisely  $1 M_\odot$ , one runs into the problem indicated before. We don't have observations giving the slowing of rotations of  $1 M_\odot$  stars. But we do have the stars that Kraft has observed at  $1.2 M_\odot$ , and we see that their rotations have decreased with time; we also have the lithium abundances decreasing with time. When you boot strap these two together you find a best fit; you get the best explanation for the depletion of Li<sup>7</sup> if you take  $n \sim 2$ . For  $\Omega \gg \Omega_0$ , this is much too large a value of  $n$  to be associated with the Goldreich-Schubert threshold, and some modification of the Goldreich-Schubert effect is required, perhaps by nonrotational motion of the fluid such as a slight oscillation of the core.

For the sun we are stopped for lack of observations and don't know what to do. So we

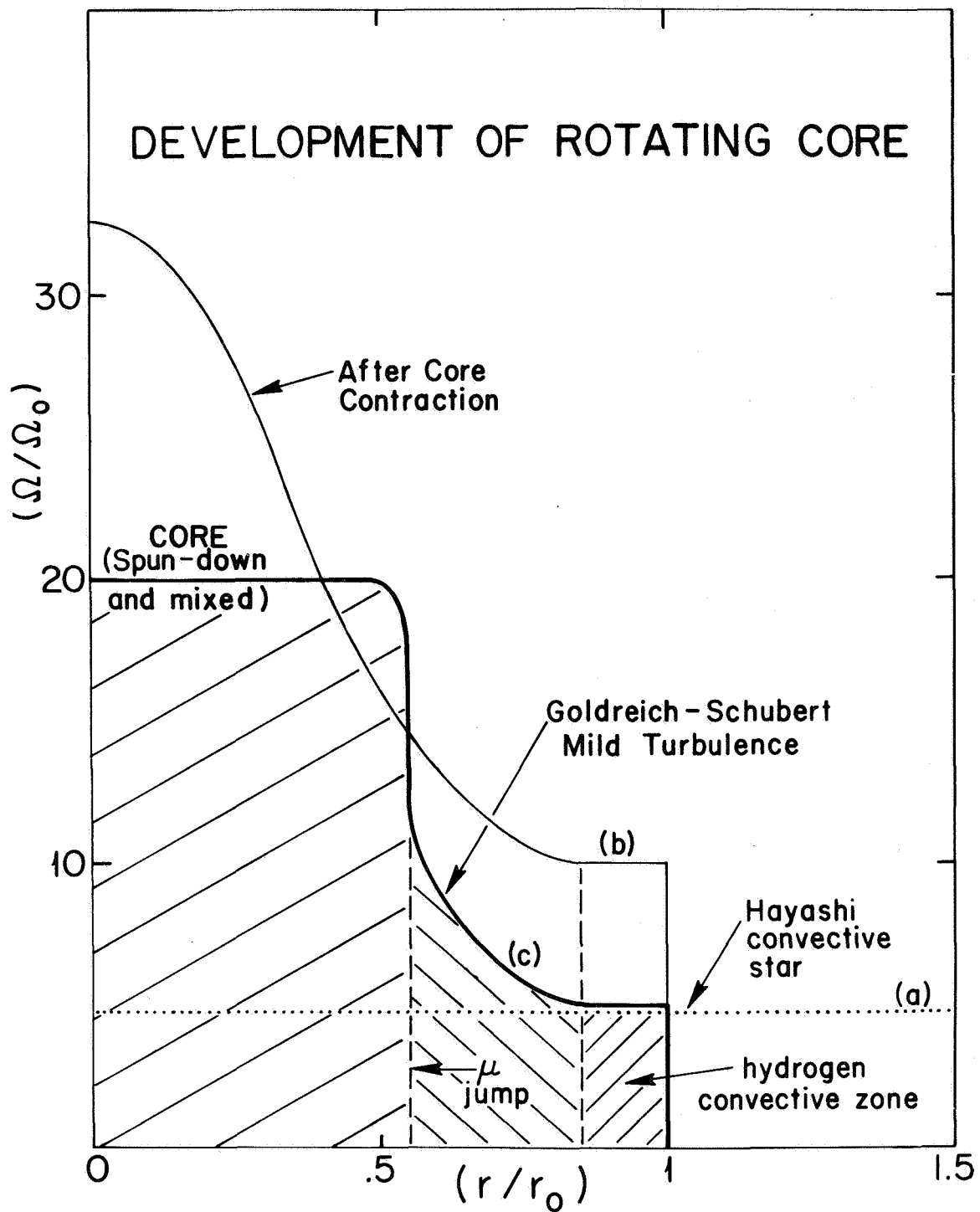


Figure 2. Hypothetical rotational history for the sun.

Table 2.  $\Lambda$  eigenvalue with turbulence quenched at  $r_c$

$n$	$r_c$	Li <sup>6</sup>	Li <sup>7</sup>
		$r_b = 0.63$	0.58
2	0.578	5.265	0.901
	.57	6.01	1.633
	.56	5.97	2.372
	↓	52.3	20.5
	↓	145.0	55.8
	.55	8.0	3.013
	.53	10.33	4.376
1	.50	14.57	6.772
	0.578	9.64	1.761
	2nd mode	70.3	20.98
	.57	10.9	3.30
	.56	12.5	4.48
	.55	14.2	5.61
	2nd mode	100.5	43.5
1/2	0.578	18.6	3.48
	2nd mode	134.9	40.36
	.57	20.75	6.45
	.56	23.63	8.70

$$\Lambda = \gamma\tau$$

take a new approach. After all, we have, or at least we think that we have, a rough value for the solar wind torque. We can insert that to give the flow of angular momentum inside the sun, from which we can calculate a present rate of decrease of Li<sup>7</sup> at the surface of the sun.

Figure 3 shows lithium abundance in meteorites in the Pleiades, coma cluster, the Hyades, and the sun. There's some argument concerning the abundance in the sun, but I would guess the best value is about [Li<sup>7</sup>] ~ 0.8. There is a problem if you take as the solar wind torque density  $6 \times 10^{29}$  dyne cm/sr, which for an isotropic solar wind is  $\sim 5 \times 10^{30}$  dyne cm total, and attempt to calculate the rate at which Li<sup>7</sup> should be decreasing. One must decide whether angular momentum is coming from deep inside the star or only from an outer shell with inner radius  $r_c$  as a result of the slowing of the shell. If it comes from slowing of the outer shell alone, the rate of decrease of Li<sup>7</sup> with time is given by the dashed line (1). If angular momentum arises in the deep solar interior, the rate of decrease of Li<sup>7</sup> is given by (2).

But I forgot an important point, that if you do have a rapidly rotating core for which there may be viscous diffusion of angular momentum from the core, you can't say exactly how much it is. You can give an upper bound because the initial steepness of the angular velocity gradient in the young sun cannot exceed a certain amount without also exceeding the Richardson criterion for instability to ordinary dynamically driven turbulence. The assumption of an initially steep angular velocity gradient provides a takeoff point for the solution of the viscous diffusion problem to obtain the diffusion of angular momentum. Adding viscous diffusion as a source of angular momentum gives lines lying between (1) and (2). You can calculate a value for the flux of angular momentum from the core, hence a *lower bound* on the angular rotation of the core, by adding the right amount of core angular momentum flux to obtain the correct present values for the

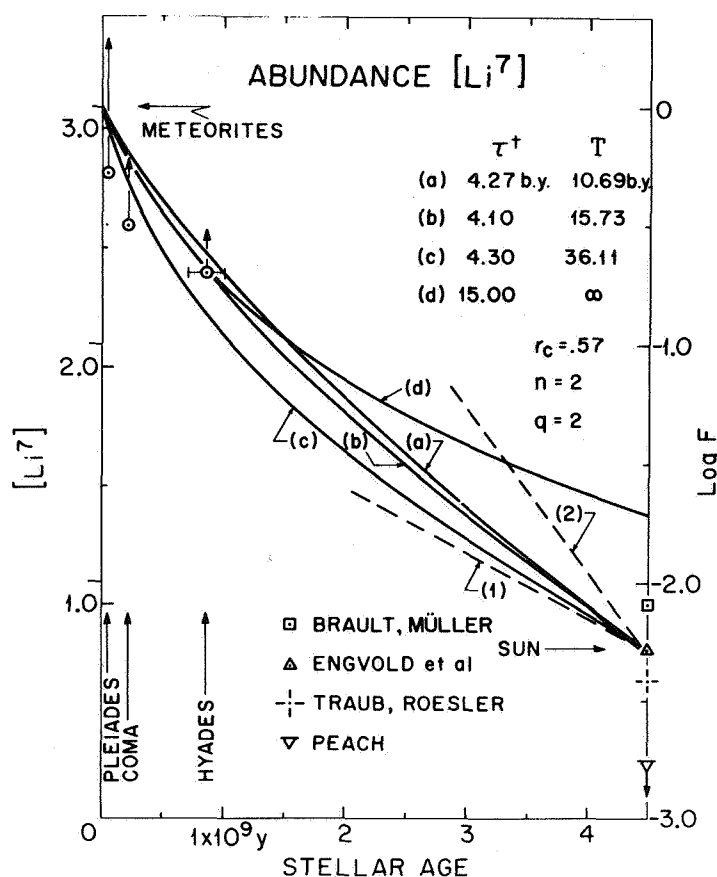


**Figure 3.**  $[Li^7]$  and  $\log F$ , logarithmic depletion of  $Li^7$ . The curves (a), (b), and (c) are integrations applicable to the sun. Curve (d) is an interpretation applicable to Kraft's stars of mass 1.2. The associated angular velocity curves (surface angular velocity as function of time) are given in figure 4.

abundance of lithium and the angular velocity at the sun's surface. Curves a, b, and c of figures 3 and 4 give integrations for  $\log F$  and  $\Omega$  calculated in this way. Corresponding *lower bounds* for the angular velocity of the core are included in figure 5.

Now let me turn the problem around another way. Ask yourself the following: suppose we know nothing whatever about the solar wind torque, know nothing whatever about the location of the radius  $r_c$  except to say that it is somewhere in the zone of  $Li^7$  burning. It is found that to obtain the correct values for the present abundance of  $Li^7$  and surface angular velocity the present solar-wind torque is  $\sim 4 \times 10^{30}$  dyne cm if the torque is proportional to the square of the solar angular velocity. For a torque proportional to the solar angular velocity, the calculated solar-wind torque is roughly a factor of 2 greater. These are surprising results. The present value of the solar-wind torque implied by the loss of lithium in the sun is quite insensitive to detailed assumptions and is quite close to the "observed" solar-wind torque. Another interesting result is that the maximum value for the angular momentum flux (by viscous diffusion) from a core rotating rapidly enough to account for the solar oblateness ( $20 \Omega_0$ ) is  $3.5 \times 10^{30}$  dyne cm. The close correspondence with the calculated torque (from lithium depletion),  $4 \times 10^{30}$  dyne cm, and the "observed" torque,  $5 \times 10^{30}$  dyne cm, suggests that the present source of angular momentum for the solar wind may be viscous diffusion from a rapidly rotating core.

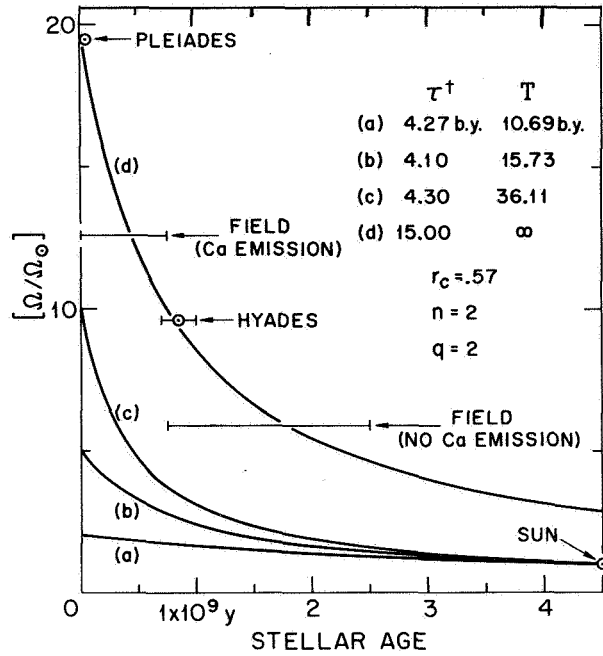


Figure 4. With various assumptions concerning the initial main-sequence value of the surface angular velocity, the time dependence is calculated. The curves of figures 3 and 4 assume that the solar-wind torque is proportional to the square of the angular momentum. (a), (b), and (c) are applicable to the sun and (d) refers to Kraft's stars.

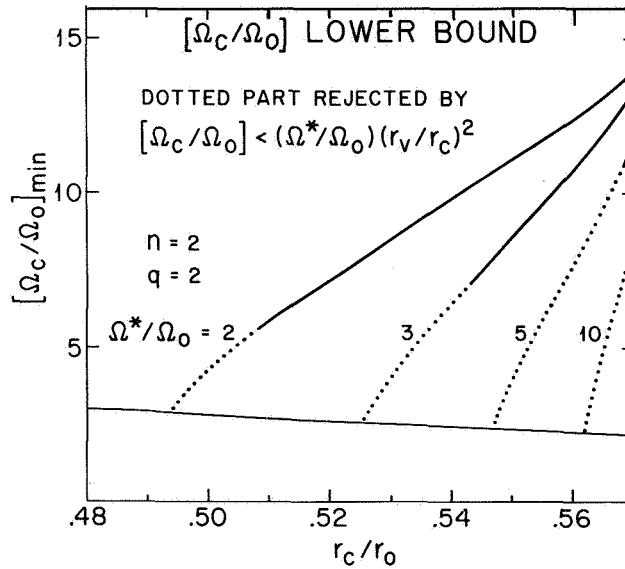


Figure 5. Lower bounds for the angular velocity of the solar core obtained assuming viscous diffusion of angular momentum from the core. The corresponding angular momentum flux is that required by integrations such as (a), (b), and (c) of figures 3 and 4. The interpretation of the solar oblateness of  $\Delta r/r \sim 5 \times 10^{-5}$  as the effect of a rapidly rotating core requires an angular velocity of  $\sim 20 \Omega_0$  for  $r_c \sim (1/2)r_0$ .

## REFERENCE

Goldreich, P.; and Schubert, G.: Differential Rotation in Stars. *Ap. J.*, Vol. 150, 1967, p. 571.

## COMMENTS

*E. Schatzman* There are a number of questions related to this discussion concerning the transport of matter or momentum, including the question of whether we can apply a diffusion equation. I would like to give a number of ideas concerning the possibility of an observational test of this transport inside the sun and possibly in stars, by detailed analyses of the abundances of certain isotopes at the surface of the sun or in the solar wind. If we consider the different nuclear reactions that can take place inside the sun, first there is  $H^2$  burning which can be neglected because it takes place in the very outer layers.

Next there are  $Li^6$ ,  $Li^7$ ,  $Be^9$ ,  $B^{10}$ , and very deep inside the sun  $He^3$  formation by the reaction  $D^2 + p \rightarrow He^3$  together with  $C^{13}$  burning which takes place at the very core of the sun. Now, what we have to do irrespective of whether turbulent transport from the inside has taken place, is to compare some initial abundances to the observed one. We don't know the initial abundances of the sun and can only make guesses, the validity of which I am not certain. I shall discuss this briefly.

In units of  $\log N_H = 12$ , where  $N_H$  is the abundance of hydrogen, the initial value of  $\log N_{Li^7} = 3$ . Assuming earth abundances, then the initial value for  $Li^6$  in these units  $\sim 1.9$ . Now, if we consider the spallation ratio, if produced by spallation of carbon or nitrogen, the value would be about 2.7, that is to say, about one-half the abundance of  $Li^7$ .

In regard to  $Be^9$  there are some difficulties. Again using earth abundance for Be, a value of  $\sim 1$  is obtained whereas using the spallation ratio yields  $\sim 1.7$ . For  $B^{10}$  the spallation ratio should be 3.3. These numbers are to be compared to what observations?

For lithium, we can take three for the initial value and the observed value is depleted by a factor of a hundred; this can be explained by turbulent transport from the lower boundary of the convective zone to the place where Li is being burned.  $Li^6$  is not observed and probably has an abundance less than one-twentieth of  $Li^7$ , that is,  $\log N_{Li^6} \sim 0.3$ . Using the values 1 and 0.3, we have compatibility with the turbulent process in which the time scale is proportional to the square of the distance over which the transport takes place. For  $Be^9$  with an observed value of 0.7-1, depending on interpretation of the profile of the spectral lines of Be, based upon the earth abundance, no burning exists, in which case we would have the case raised by Professor Dicke. On the other hand, using the spallation value for the initial concentration of Be we note depletion by an appreciable factor, which could also be explained by a turbulent transport. For  $Be^{10}$  we know that  $\log N < 2.7$ , given by the limit of visibility of the spectral lines. This is a depletion by a small factor, if any, perhaps 4, and this is also compatible with transport. But the real clue concerning this problem rests with  $He^3$  and the  $C^{13}$ .  $He^3$  has not been observed spectroscopically, but we have solar wind observations and I want to refer here to Professor Geiss' measurements on the surface of the moon for which he reports a value of  $He^4/He^3 \sim 2 \times 10^3$ . Now, what is the initial value? Perhaps it corresponds to the very lowest value which has been obtained in meteorites, which is  $\sim 4$  or  $5 \times 10^3$ . So there is a possibility that the present  $He^3$  concentration is larger than the  $He^3$  concentration in the solar wind say a few million years ago. This can be interpreted also as due to turbulent transport and in fact we have two ways of estimating the rate at which the turbulent transport takes place. One is by considering the rate at which the  $He^3$  concentration increases with time at the surface of the sun, and the other one is the absolute value of the present abundance of  $He^3$  at the surface of the sun, if it is assumed that  $He^3$

is being produced at the center by thermonuclear reactions. Now, this represents one of the possibilities for testing the turbulent transport from the center to the surface. And just from orders of magnitude we also obtain a turbulent diffusion coefficient  $d \sim 10^3$ .

$C^{13}$  is also interesting because if we take the earth abundance ratio  $C^{12}/C^{13} \sim 80$ , do we observe in the sun the same or possibly a smaller ratio? This cannot be considered as settled. Suppose  $C^{12}/C^{13} > 80$  can be explained by  $C^{13}$  burning at the center of the sun because the  $C^{12}/C^{13}$  ratio in the carbon cycle is about 4. This is an increase and seems to go the other way around, but we have to remember that the carbon is essentially turned into nitrogen during the carbon cycle, which means finally the destruction of carbon in favor of nitrogen and consequently a greater destruction of  $C^{13}$  than  $C^{12}$ . If the ratio is larger than 80, this could possibly give an indication of the presence of turbulent transport from the center to the surface of the sun. I don't mean at all that this is a demonstration which has taken place because as you can judge, there are a number of difficulties concerning the initial abundances which are present.

#### COMMENTS

*A. Ingersoll* I want to discuss the question of whether the oblateness measurements that *Dicke and Goldenberg* [1967] made do indicate that the core of the sun is rotating rapidly, or whether there is an equally attractive alternate possibility. Dicke and Goldenberg looked at the shape of the sun in visible light, and there are really three ways that the sun might look oblate in visible light. The first possibility is that the equipotentials, gravitational plus centrifugal, are oblate, which would be the case if the interior of the sun were rotating rapidly. The second and third are variations of the possibility that the solar equator is somehow hotter than the poles. If the equator were hotter, it would also be brighter, and this might be confused with an oblateness because of the limitations of seeing in the earth's atmosphere.

I divide this hotter-equator possibility into two categories because the first of these, the one considered and rejected by Dicke and Goldenberg, is that the equator of the sun is hotter at all depths by a certain amount of  $\Delta T$ . This would be like saying that the equivalent temperature of the sun is greater at the equator than it is at the poles, or that the radiant flux is greater at the equator than it is at the poles. Their measurements suggest that this is an unlikely possibility, although I do not feel that it can be conclusively ruled out.

The second possibility, which Spiegel and I have proposed [*Ingersoll and Spiegel*, 1971], is that the equator of the sun is hotter only in the chromosphere but not in the photosphere. This possibility is much easier to confuse with a real oblateness. To show why this is so, I must digress to define certain aspects of the Dicke-Goldenberg experiment. They took an image of the sun and projected it onto a perfectly circular occulting disk, slightly smaller than the solar image. The radial angular distance from the edge of the disk to the mean solar limb is  $\delta$ , and they did their experiments for  $\delta \approx 6.5''$ ,  $12.8''$ , and  $19.1''$ . In each case, they scanned around the edge of the disk, measuring all the light that was coming from beyond the occulting disk, and looked for an increase in flux at the equator relative to that at the poles. This difference in flux is the signal they used to infer the solar oblateness. The important thing about this quantity  $\delta$  is that for each of the three possibilities that I mentioned earlier, there is a different relationship between signal amplitude and  $\delta$ .

First, if the sun is truly oblate, then the signal is approximately independent of how much sun is in the field of view, and therefore, the signal amplitude is proportional to  $\delta^0$  — that is, independent of  $\delta$ . In this case the signal simply depends on the difference between the equatorial and polar radii of the sun, and not on how much sun is occulted. Next, if the equivalent temperature of the sun is greater at the equator than at the poles, then the signal amplitude is proportional to the fraction of the solar disk in the field of view — that is, to  $\delta^1$ . From the data taken at the three values of  $\delta$ , Dicke and Goldenberg



concluded that this was very unlikely. What Spiegel and I pointed out is that if the equator is hotter than the poles, but only in an optically thin part of the sun's atmosphere, then the dependence on  $\delta$  is intermediate between these two and is proportional to  $\delta^{1/2}$ . Here we postulate an equatorial temperature excess in parts of the sun's atmosphere that can be seen even on the extreme limb — that is, in the very top of the photosphere and in the chromosphere. In this case, each emitter in the field of view contributes as much to the signal as any other, and the number of emitters in the field of view is simply proportional to the solar surface area exposed from the edge of the occulting disk to the limb, and this is proportional to  $\delta^{1/2}$ .

Figure 1 is our reworking of the Dicke and Goldenberg data. We have plotted signal

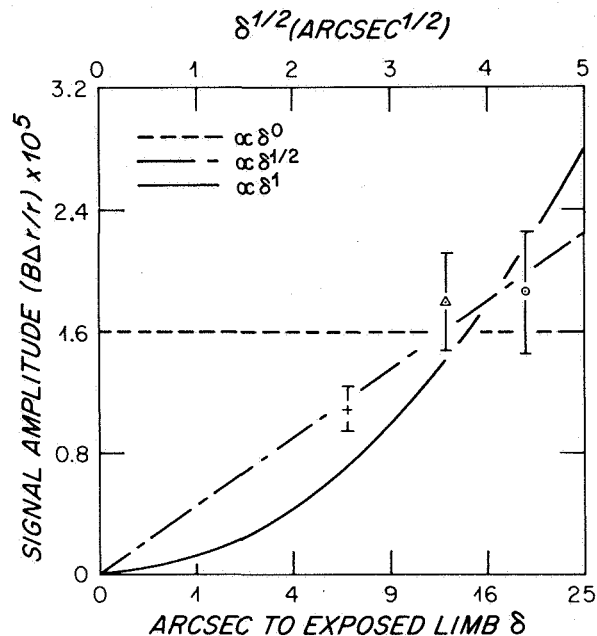


**Figure 1** Signal amplitude versus  $\delta^{1/2}$  after correction for surface rotation. Units are  $B\Delta r/r$ , where  $B$  is relative brightness at the occulting disk, and  $\Delta r/r$  is measured oblateness [Dicke and Goldenberg, 1967]. Error bars give the square root of variance for each  $\delta$ . Curves illustrate three possible dependences on  $\delta$ .

amplitude versus  $\delta^{1/2}$ , for  $\delta = 6.5''$ ,  $12.8''$ , and  $19.1''$ , which are the three values of  $\delta$  used in the experiments. The three lines drawn represent the three possibilities: signal amplitude  $\propto \delta^0$ ,  $\delta^{1/2}$ ,  $\delta^1$ . Actually, the signal due to a true oblateness would not be exactly  $\propto \delta^0$ , but would depend on the brightness at the edge of the occulting disk, and this brightness increases slightly with  $\delta$ . So a true oblateness is consistent with these data. Dicke and Goldenberg ruled out the parabola, signal  $\propto \delta^1$ . The curve shown corresponds to  $\Delta T_e \approx 5^\circ \text{ K}$  — that is, to a  $5^\circ$  excess in the equivalent temperature of the sun at the equator relative to that at the poles. Obviously, it would be very interesting to measure that somehow — I suppose by sending a satellite over the poles. The line on the graph labeled  $\delta^{1/2}$  corresponds to what Spiegel and I suggested, with

$$\tau_0 \Delta T \approx 0.3^\circ \text{ K}, \quad \tau_0 \ll 0.1$$

Here  $\Delta T$  is the required temperature difference between equator and poles, which is restricted, we assume, to an optically thin layer. And  $\tau_0$  is the value of the optical depth at the level below which this temperature difference is assumed to vanish. The restriction  $\tau_0 \ll 0.1$  simply ensures that this layer is optically thin. Examination of figure 1 shows that this possibility fits the Dicke and Goldenberg data quite well.

Now if Spiegel and I are correct in our interpretation, and if the chromosphere really is hotter at the equator than it is at the poles, the heat source for the equatorial chromosphere must be greater than the heat source for the polar chromosphere by a specific amount. This excess mechanical flux upward at the equator must be whatever is necessary to supply the excess emission implied by the relation  $\tau_0 \Delta T \approx 0.3^\circ \text{ K}$ . The required excess flux is  $\Delta F \approx 2.5 \times 10^7 \text{ ergs/cm}^2/\text{sec}$ , which is comparable to what many people believe is the total mechanical and hydromagnetic energy flux into the chromosphere. So if our interpretation is correct, then we have to be prepared either for a mechanical heating of the chromosphere, which is larger than what most people believe, or a variation in this heating from equator to pole, which is comparable in magnitude to the heating itself.

## REFERENCES

- Dicke, R. H.; and Goldenberg, H. N.: Solar Oblateness and General Relativity. *Phys. Rev. Ltrs.*, Vol. 18, 1967, p. 313.  
 Ingersoll, A.; and Spiegel, E.: Temperature Variation and the Solar Oblateness. *Ap. J.*, Vol. 163, 1971, p. 375.

**DISCUSSION**     *R. H. Dicke*     There are three points I would make. First, the question was raised as to whether a general temperature difference of the photosphere between the equator and the pole could account for the observations. The measurements were made with three different amounts of limbs exposed, which lead to a light flux ratio of approximately 1.0 to 2.5 between the smallest and the greatest amount. Under an oblate sun hypothesis these two signals have a ratio of about 1.0 to 1.2 and when we renormalize (correct the signal of the biggest exposure by a factor of 1.2 downward), the observations are satisfactory. I can't believe that they would be satisfactory if we had reduced the signal by a factor 2.5. There would then be a sizable discrepancy in those three curves. I don't think that's possible.

On the question of a hot layer, I think one must go far above an optical depth of 0.1 to make the scheme work. For levels above 0.01 you need at least a  $40^\circ$  temperature difference between the equator and the pole. For this case, I think that the signal could be sufficiently close to what we observed that this might be a satisfactory way of accounting for the signals. On the other hand, one has to make a physically reasonable statement. There are two requirements to be satisfied. One is the requirement of energy balance for the necessary steady state — the problem of getting excess energy at the equator into the particular layer, the upper photosphere, to heat it up enough to give the excess radiation. And the other requirement is one of dynamic balance for the necessary steady state. There may be several ways this can be done; the one that's been suggested by the authors, which is to require that the angular velocity increase outward in the upper photosphere with a scale height of about 1,500 km, may well be in difficulty with what is known observationally about the rotation of the sun at various levels. So I would say that insofar as the observations are concerned it is possible that one could account for them in this way, but I haven't seen a coherent physical statement of how such a physical state would be maintained or dynamically balanced.

*A. Ingersoll*     The first point Dicke raised was that he didn't feel that the data could be consistent with a temperature difference between equator and poles that extended

deep into the atmosphere of the sun. Now, that really hinges on whether you feel that the parabola can be made to fit the three data points, the parabola being the solid line in the graph I showed earlier.

*R. Dicke* I don't know how you got these points. The paper didn't list them — the paper didn't even give the normalization ratios that you would have had to know to compute these points; the ratios weren't in the paper.

*A. Ingersoll* We assumed that the values of  $\delta$  and the values of the photospheric brightness at the edge of the occulting disk were those which you gave in your paper. We used the limb darkening curve you gave in your paper —

*R. Dicke* We didn't give a limb darkening curve.

*A. Ingersoll* Well, not in *Dicke and Goldenberg* [*Phys. Rev. Letters*, 18, 31, 1967], but in *Dicke* [*Ap. J.*, 159, 1, 1970] from which we took these values.

*R. Dicke* But those were not observations, but a theoretical limb darkening curve from a theoretical paper.

*A. Ingersoll* Let me put it this way: All the data we got for making this graph came from various papers you have written; we consulted no others for this.

Now, the second point, I guess, was the question of the dynamical balance. If we are to accept the fact that the parabola does not fit the data, then the temperature difference between the equator and pole is concentrated only in the chromosphere, and it is true that you need to balance the forces implied by this horizontal temperature difference. The most likely way is that angular velocity should be increasing with height. We calculate that if angular velocity increases by  $\sim 5$  percent in 100 km over some 100-km region near the temperature minimum, that would be enough. So there's another observation that should be made in order to test this observation.

*E. Schatzman* There is a very well-known solar oblateness in the meter wavelength that corresponds to a structure of the corona, but very high in the corona. The oblateness is considerable. So might there be a relation between your assumption concerning the chromosphere and what has been observed at meter wavelength?

*R. H. Dicke* It seems to me that the postulate of the increasing angular velocity does fit observations; that is, one sees angular velocity increase with height in the chromosphere. The sign is correct for the chromosphere and consequently may be correct for the upper photosphere where the balance is actually needed if the upper photosphere is to be extended on the equator with a higher temperature. So it's not a question of whether the idea is qualitatively wrong but whether in fact it is quantitatively right. (Ed. note: See comment by Livingston, p. 304).

## COMMENTS

*C. P. Sonett* We have carried out extensive calculations regarding a mechanism for early electrical heating of meteorite parent bodies with the view to obtaining clues about the early solar system especially the question of the pristine solar spin rate and evolving conditions in the solar nebula just after condensation of the primary objects. The proposed mechanism and the calculations which have been carried out are based upon the following observational evidence. Certain classes of meteorites, particularly the iron-nickels and achondrites, has been exhaustively studied for evidence of cooling from elevated temperatures [*Wood*, 1964; *Goldstein and Short*, 1967]. The iron-nickels show evidence for cooling rates which range approximately from  $1-10^\circ$ /million years indicating that at the time of the cooling cycle these objects were at depths within parent bodies to several hundred km radius. Some error might accrue in these estimates on the basis that for the nickel-irons the diffusion of Ni across grain boundaries between kamacite and taenite, both of which are Ni-Fe phases, varies from the values used because of "doping" of the matrix by trace elements which can adversely affect diffusion coefficients. However,

the basic phenomenon cannot be avoided by this argument; only the rates can be modified, which means that the parent body sizes would have to be adjusted. On the other hand, it has been argued that because Si grains are found within a metallic matrix, that primordial condensation is required to form the meteorite bodies. Here we assume that the parent body heating mechanism is correct. There are compelling reasons for believing that, for example, the Widmanstätten patterns in the irons could only be produced by a well-behaved cooling from an elevated temperature.

The time setting for the cooling cycle is early in the chronology of the solar system. This is established, at least for Weekeroo Station, by *Wasserburg et al.* [1965], who dated Si inclusions as about 4.6 billion years old. Thus, at least on this basis, the heating and cooling episodes are very early. To explain a heating episode for parent bodies of the restricted sizes postulated, since the event appears to have taken place very early, requires either fossil radionuclides or some exotic form of heating. Long-lived radioactives are ruled out because their energy-deposition rates are too low for the short time scales proposed. Similarly, accretional heating released by the potential through which objects fall in accreting would be ruled out because of the small size of the bodies and the small gravitational energy *Sonett* [1969].

The classical means of heating of parent bodies has been based on a class of extinct isotopes thought to have been present during the formative period of the solar system. That such isotopes were present is clear from both the presence of  $\text{Xe}^{129}$  from the decay of  $\text{I}^{129}$ , Xe components from  $\text{Pu}^{244}$  fission decay and the appearance of fission tracks in meteoritic matter. Although the existence is verified for these cases, the speculated level of activity assignable to these isotopes is far below that required for the heating cycle. Other nuclides have been popular candidates in the past. Perhaps the most prevalent has been  $\text{Al}^{26}$  hypothesized to have arisen in spallations associated with the early sun. However, the most recent tests show no evidence for this isotope [*Schramm et al.*, 1970], and thus the hypothesis is not well supported.

In view of the lack of strong evidence for radioisotopic heating, the study of the fossil residues remains a fundamental requisite for understanding of the cosmochemical formative processes leading to the condensation into material bodies, but the source of the heating cycle appears to require a separate explanation.

*It seems likely that the early sun was spinning rapidly* and that it was endowed with at least a modest magnetic field. These conditions arise quite naturally from the trapping of field in the Hayashi contraction and the spinup due to condensing angular momentum from the primordial cloud. If we associate the contractive period with the precursor phase of an early star prior to a *T* Tauri efflux of mass, then conditions are quite naturally established for the establishment of strong electric fields in the expanding cloud, a result of the combination of high spin, magnetic field, and plasma outflow [*Sonett et al.*, 1970].

The conditions just described can lead to strong electrical currents flowing through planetary objects, the circuit being completed through the surrounding "solar wind." Electromagnetically the interaction is classified as transverse magnetic (TM) and has been discussed extensively in the literature [*Sonett and Colburn*, 1967; *Schubert and Schwartz*, 1969]. Its application to the present cases, forming in effect a linear unipolar generator, requires that the electrical impedance along the current streamlines through the body be sufficiently small so that strong currents can flow. On the other hand, too low an impedance will result in the formation of a steady-state magnetohydrodynamic bow shock wave ahead of the body facing into the direction from which the flow of plasma comes.

To provide an appropriate impedance, we invoke the well-known exponential dependence of the bulk electrical conductivity of rocky matter on the reciprocal temperature.

Extensive calculations have been made involving parameterization of the problem. Significant heating due to Joule losses from the current system are found. It is clear that because the currents close through the surface of the body that the crustal temperature is a crucial aspect of the heating, and that a sufficiently elevated temperature is required. To provide this it is only necessary to consider further the general properties of *T* Tauri objects, which are often endowed with an infrared excess attributed to dust-induced opacity. We term the enclosure a *hohlraum* and invoke an interior surface temperature to this enclosing matter; thus, the planetary object "sees" a background temperature sufficient to maintain an adequate bulk electrical conductivity [Sonett *et al.*, 1970].

Although this all may appear as unduly complicated, the effects required appear to be commonly hypothesized or observed in what are thought to be early stars. Their parametric association, numerically adjusted to provide significant heating, has shown that only quite modest requirements must be placed on the system to provide the heating cycle.

We now turn the problem around to discuss the spindown issue. *It is clear that a rapidly spinning sun must eventually be braked so that the present epoch spin rate is achieved* [Durney, Chap. 4, p. 282]. Although the calculations referenced use an exponentially decreasing field and magnetic braking, some other shaping of the field decay is equally appropriate and angular momentum can also be shed by the outflowing gas. Thus, in the present calculations, the field and spin damping are represented in an integral sense only, and the instantaneous rates cannot easily be determined. However, the evidence is strong that some form of heating other than fossil nuclides is required if the heating cycle continues to be maintained as a viable requirement.

The electrical problem is complicated by the additional presence of a TE (transverse electric) mode of interaction, which simply stated is due to eddy current generated from the action of  $\dot{B}$ , the time rate of change of the interplanetary magnetic field seen in the frame comoving with the planet [Schubert and Schwartz, 1969]. The tendency would be to associate this mode more with turbulence in the outflowing gas which in turn is reflected in magnetic field disturbances. This mode also has the simplification that the *hohlraum* is not required as the current system is toroidal closing wholly within the planet. Calculations are in progress to determine the efficiency of the TE mode and the coupled action of both the TE and TM modes together with a modest addition of radioactives, which are known to inhibit the later stages of the heating by the TM mode.

Figure 1 shows the heating of small bodies as a function of their radius. The peak temperatures are achieved in times of the order of 0.5 million years for the larger cases,

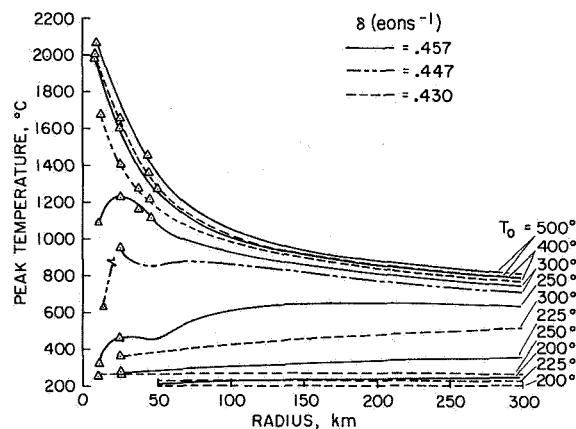


Figure 1. Peak core temperature versus parent body radius.

while for the very small objects of 10- to 25-km radius the peak heating of the core is achieved in a much shorter time, so that a relaxation begins to take place and the interior cools long before the overall induction process is completed.

The clue to the high solar spin rate is carried in the requirement for the large electric field at the site of the parent body which then leads to the large induction. The very substantial electric field in turn is strongly dependent upon the winding up of the interplanetary field into a tight Parker spiral because of the large spin. Thus, the evidence for early heating of parent bodies leads quite naturally to the condition where the sun was endowed with a high spin rate during its early history. Although the specific spin rate at a given time cannot be presently foretold, it is clear that the elements of the overall theoretical treatment leading to better understanding of this are intrinsically carried in the thermal history of these small bodies, provided that electrical heating proves to withstand the test of further examination.

#### REFERENCES

- Goldstein, J. I.; and Short, J. M.: Cooling Rates of 27 Iron and Stony-Iron Meteorites. *Geochim. Cosmochim. Acta.*, Vol. 31, 1967, p. 1001.
- Schramm, D. N.; Tera, F.; and Wasserburg, G. J.: The Isotopic Abundance of  $^{26}\text{Mg}$  and Limits on  $^{26}\text{Al}$  in the Early Solar System. *Earth and Planet. Science Letter*, Vol. 10, 1970, p. 44.
- Schubert, G.; and Schwartz, K.: A Theory for the Interpretation of Lunar Surface Magnetometer Data. *The Moon*, Vol. 1, 1969, p. 106.
- Sonett, C. P.: Fractionation of Iron: A Cosmogonic Sleuthing Tool. I. Radioisotope Heating. *Comm. Astrophys. Space Phys.*, Vol. 1, 1969, pp. 6, 41.
- Sonett, C. P.; and Colburn, D. S.: Establishment of a Lunar Unipolar Generator and Associated Shock and Wake by the Solar Wind. *Nature*, Vol. 216, 1967, p. 340.
- Sonett, C. P.; Colburn, D. S.; Schwartz, K.; and Keil, K.: The Melting of Asteroidal-Sized Bodies by Unipolar Dynamic Induction From a Primordial T Tauri Sun. *Astrophys. and Sp. Sci.*, Vol. 7, 1970, p. 446.
- Wasserburg, G. J.; Gurnett, D. S.; and Frondel, C.: Strontium-Rubidium Age of an Iron Meteorite. *Science*, Vol. 150, 1965, p. 1814.
- Wood, J. A.: The Cooling Rates and Parent Bodies of Several Iron Meteorites. *Icarus*, Vol. 3, 1964, p. 429.

#### COMMENTS

*W. C. Livingston* Spectroscopic observations made on the solar disk near the equatorial limbs consistently indicate an increase of angular velocity as we pass outward through the sun's atmosphere. The chromosphere, as revealed by  $\text{H}\alpha$ , appears to rotate 5 to 8 percent faster than the underlying photosphere as represented by the metallic lines [*Livingston*, 1969]. Because manifestations of magnetism such as sunspots, filaments (or prominences), and plages corotate with the spectroscopic photosphere, it has been suggested that we are observing in  $\text{H}\alpha$  the "superrotation" of neutral matter that can flow independent of magnetic constraints. (The term *superrotation* is borrowed from aerodynamics where it is used to describe an analogous condition in the atmosphere of the earth and Venus [*King-Hele*, 1970; *Gierasch*, 1970].) As a working hypothesis we propose the existence of an east to west wind whose lower boundary is the photosphere and whose upper extent is unknown.

Seeking additional evidence of this superrotating wind, in 1968 we began to obtain

prominence spectra. The structure of prominences undoubtedly is dominated by magnetic forces, so one would not expect to find any degree of superrotation in these objects. However, some early work by *Evershed* [1935] suggested some peculiarities in their spectroscopic rotation rates.

Our spectra are taken with the slit placed normal to the limb and generally at a position angle such that the height of the  $H\alpha$  emission is at a maximum. Records are taken in both  $H\alpha$  and  $Ca^+K$ . Figure 1 illustrates a phenomenon often found on our spectra. At the top of the line, corresponding to the upper edge of the prominence, the weakened emission typically becomes diffuse and exhibits an abrupt displacement in wavelength, indicating line-of-sight motions differing from the main body below. By analogy with smoke escaping from the confines of a stack, we picture gas escaping from the magnetic confines of a prominence to be picked up and accelerated by a wind. Indeed, in the majority of cases within our limited sample this displacement is in agreement with an east to west superrotating wind [*Livingston*, 1971]. Further examples are

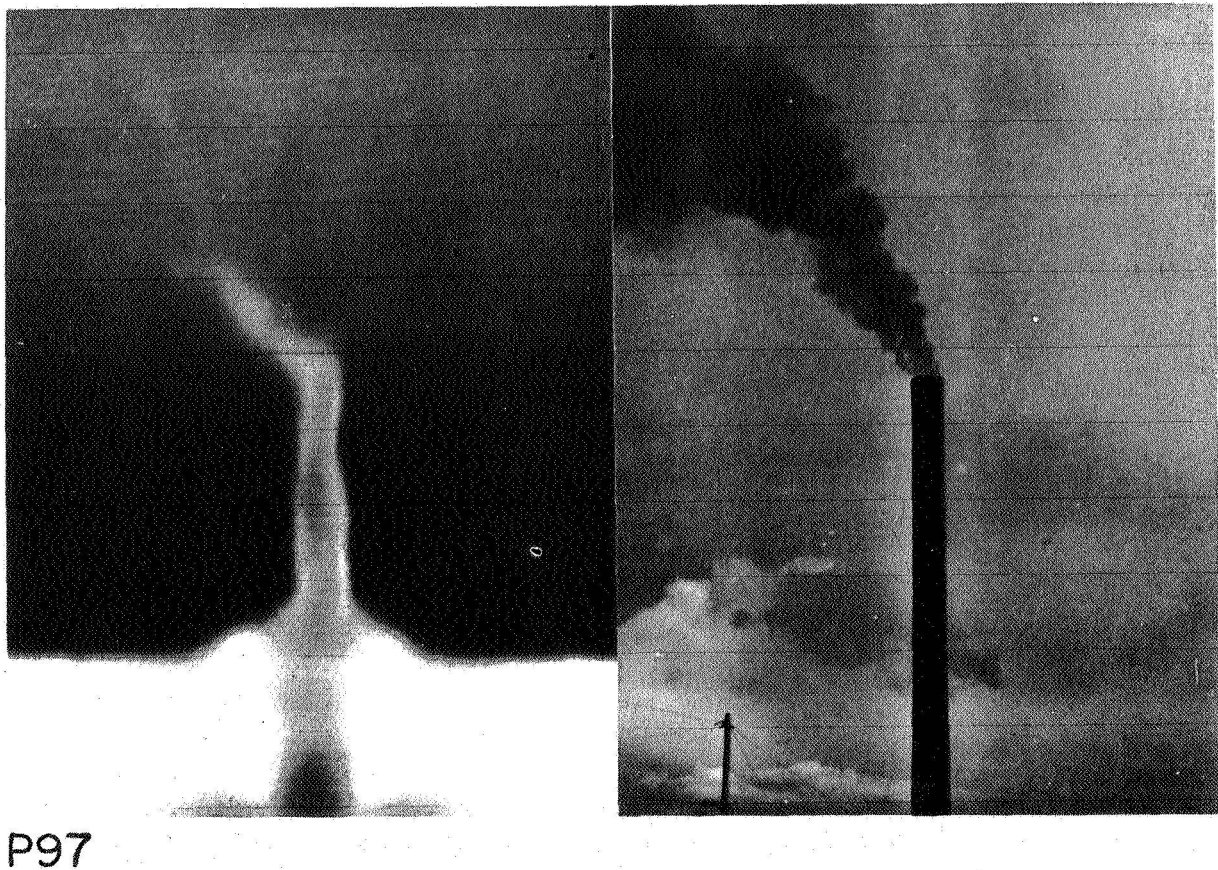


Figure 1. Spectrum of solar prominence in  $Ca^+K$  3933, slit perpendicular to the limb. Magnetic constraints of the main body of the prominence is analogous to the smoke stack with gas escaping at the top and caught up in the prevailing wind.

given in figure 2. The magnitude of the displacement ranges from a few km/sec to as much as 50 km/sec.

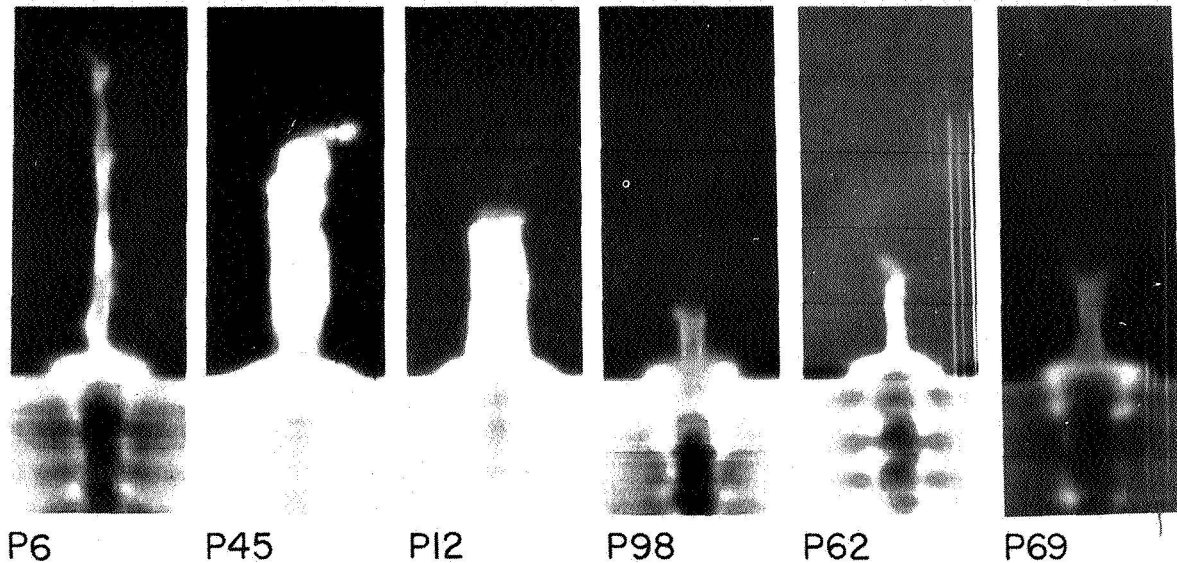


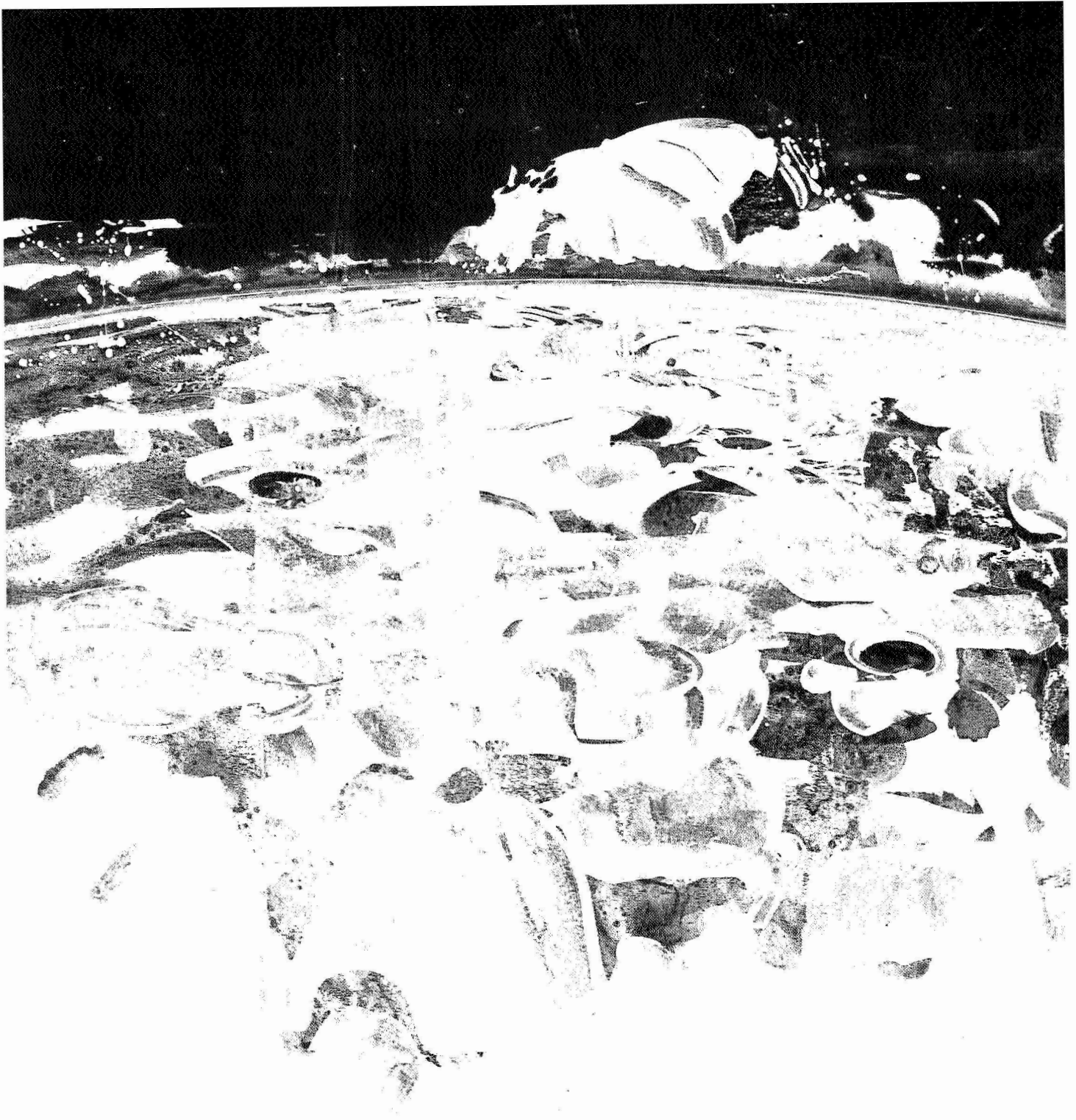
Figure 2. Examples similar to figure 1 taken in both  $H\alpha$  and  $Ca^+K$ . In all cases (except the ambiguous last) the Doppler displacement of the upper emission is compatible with a hypothetical east-west wind.

In summary, both disk and prominence spectra suggest the existence of systematic east to west flow patterns at the chromospheric level. Whether or not such a superrotating surface wind of neutral gas would interact with the solar wind plasma remains to be studied. We can note that any interaction would be in the forward direction and counter to the backward drag of the Archimedes spiral.

#### REFERENCES

- Evershed, J.: The Solar Rotation and Shift Towards the Red Derived From the H and K Lines in Prominences. *Mon. Notic. Roy. Astron. Soc.*, Vol. 95, 1935, p. 503.
- Gierasch, P. J.: The Four-Day Rotation in the Stratosphere of Venus: A Study of Radiative Driving. *Icarus*, Vol. 13, 1970, p. 25.
- King-Hele, D. G.: Super-rotation of the Upper Atmosphere at Heights of 150-170 km. *Nature*, Vol. 226, 1970, p. 439.
- Livingston, W. C.: On the Differential Rotation With Height in the Solar Atmosphere. *Solar Phys.*, Vol. 9, 1969, p. 448.
- Livingston, W. C.: Solar Rotation: Direct Evidence From Prominences for a Westward Wind. Submitted to *Solar Phys.*, 1971.





## CHAPTER V

Microstructure, "Turbulence" and Hydromagnetic Waves in the Solar Wind

The observational evidence from measurements, theory of the formation, convection, propagation, and dissipation; problems of Fourier analysis.

## MICROSTRUCTURE OF THE INTERPLANETARY MEDIUM *L. F. Burlaga* An invited review

High time resolution measurements of the interplanetary magnetic field and plasma reveal a complex microstructure which includes hydromagnetic wave and discontinuities. This paper discusses the identification of hydromagnetic waves and discontinuities, their statistical properties, their relation to large-scale structure, and their relative contribution to power spectra. **ABSTRACT**

### INTRODUCTION

This review is an up-to-date description of the microstructure of the solar wind and its relation to the large-scale structure. The term *microstructure* refers to the features with a scale length of  $\approx 0.01$  AU or less and the fluctuations with Doppler-shifted periods of  $\lesssim 1$  hr.

The basic problems concern the interpretation of high time resolution data in terms of hydromagnetic waves and discontinuities. The process of interpreting magnetic field and plasma measurements is not straightforward, and several controversies have developed. Questions to which this review is addressed include: Are the frequently observed discontinuities in the direction of  $\mathbf{B}$  predominantly tangential or rotational? Are power spectra levels due to discontinuities, Alfvén waves, and/or some other type of structures? Are microscale fluctuations related to  $\beta$ ? What are filaments?

Theoretical results and ideas concerning the physical processes that occur on the microscale and cause the microscale features are reviewed by Barnes later in this chapter (p.333). *Burlaga* [1971] reviews the theory of hydromagnetic waves and discontinuities appropriate for the solar wind, and the experimental evidence for the existence of such waves and discontinuities in the solar wind.

### DISCONTINUITIES

Discontinuous changes in the magnetic field and plasma parameters are frequently observed on the microscale. It

is generally agreed that these are hydromagnetic discontinuities. There are several types of hydromagnetic discontinuities [*Landau and Lifshitz*, 1960; *Jeffrey and Taniuti*, 1964; *Colburn and Sonett*, 1966; *Hudson*, 1970; *Burlaga*, 1971]. They are fast shocks, slow shocks, contact discontinuities, rotational discontinuities, and tangential discontinuities. Most types have been identified in the solar wind [*Burlaga*, 1971].

Given a complete set of measurements,  $n_p$ ,  $n_\alpha$ ,  $T_p^\parallel$ ,  $T_p^\perp$ ,  $T_\alpha^\parallel$ ,  $T_\alpha^\perp$ ,  $\mathbf{V}$ , and  $\mathbf{B}$ , made with a time resolution of several seconds at four or more spacecraft, the interpretation of the measured discontinuities is relatively simple [*Hudson*, 1970]. Such complete measurements have never been made, however. In practice, it is necessary to introduce an operational definition of a discontinuity that describes the incomplete measurements. This is usually subjective and somewhat arbitrary, but ideally it is sufficiently clear and quantitative that it can be used by different observers with different data to identify the same type of discontinuities.

The operational definitions of discontinuities that appear in the literature are given below, followed by discussion of the nature of these discontinuities (such as tangential or rotational). The statistical properties of these discontinuities and their morphology also are discussed. The concept of a *filament* is related to that of a discontinuity. The history of filaments is reviewed.

### Definitions

Several definitions of discontinuities have been used,

*The author is at the Laboratory for Extraterrestrial Physics, NASA Goddard Space Flight Center, Greenbelt, Maryland.*

primarily based on magnetic field measurements. These are as follows:

*Filament-discontinuity.* Ness *et al.* [1966] were the first to observe the frequent occurrence of discontinuities in the magnitude and direction of interplanetary magnetic field. Examples from Pioneer 6 are shown in figure 1. Note the scale. These discontinuities were not defined quantitatively.

*Directional discontinuities* [Burlaga and Ness, 1968; Burlaga, 1969]. This term was introduced in reference to the type of discontinuities discussed by Ness *et al.* [1966]. It refers to changes in the magnetic field direction  $\geq 30^\circ$  that occur in less than 30 sec and are preceded and followed by relatively uniform fields. A more detailed operational definition is given by Burlaga [1969]. Some examples from Pioneer 6 are shown in figure 2, which shows 30-sec averages plotted on a scale of 1 hr.

*Simple discontinuities* [Siscoe *et al.*, 1968]. In studying Mariner 4 data, it was observed that the

magnetic field components sometimes change from one more or less steady direction to another in a time short compared with the time that it previously or subsequently remains nearly constant, as shown by the examples in figure 3. Siscoe *et al.* [1968] called such changes "simple discontinuities." Other types of rapid changes identified by Siscoe *et al.* are also shown in figure 3. For computational purposes, they required that  $|\mathbf{B}(t_2) - \mathbf{B}(t_1)| \geq 4\gamma$  for simple discontinuities. They found that most of the transitions associated with simple discontinuities had durations of less than 15 sec.

*Possible tangential discontinuity* [Turner and Siscoe, 1971]. This type of discontinuity was identified using plasma points obtained at 5-min intervals and corresponding magnetic field averages. The resolution is an order of magnitude lower than that used for identifying the discontinuities discussed above. The procedure for identifying this type of discontinuity is as follows: (1) select intervals in which the density changes by  $\geq 20$  percent between two consecutive readings; (2) select the

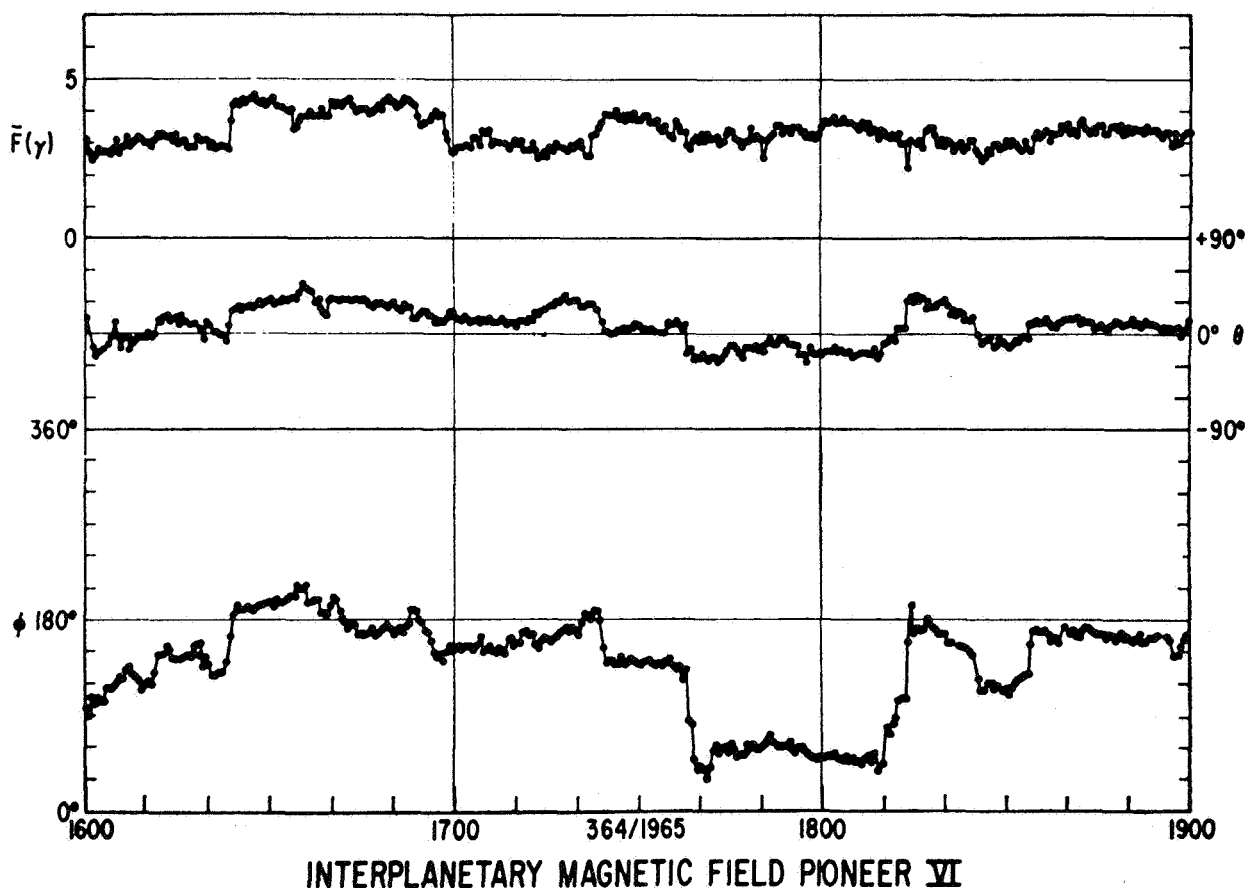
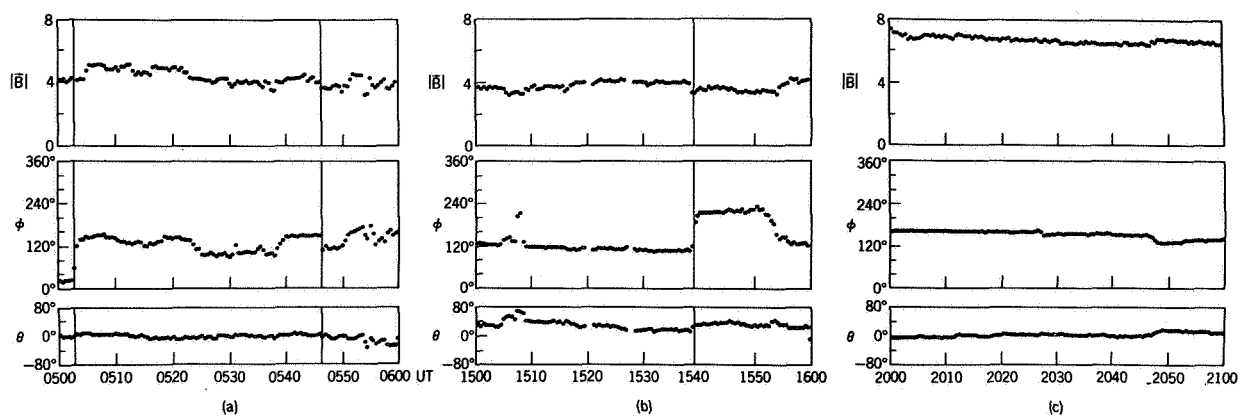
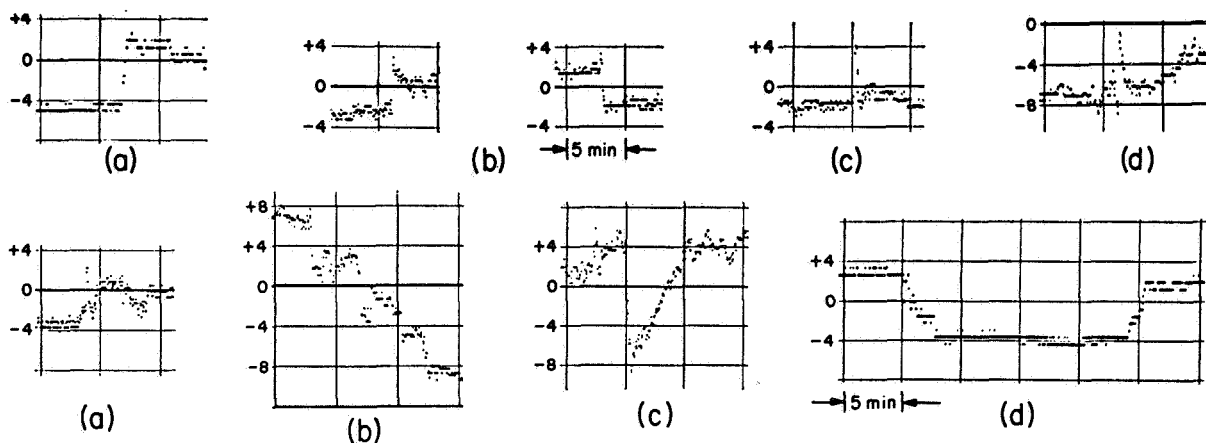


Figure 1. Filament discontinuities.  $F$  is the magnetic field intensity and  $\theta$  and  $\phi$  are solar ecliptic latitude and longitude of  $\mathbf{B}$ . The field is plotted versus universal time.



**Figure 2.** *Directional discontinuities. Three examples of directional discontinuities are shown by the vertical lines. Note the small changes in (c) and the gradual changes in (a) and (b) which are not directional discontinuities.*



**Figure 3.** *Simple discontinuities and other types. Simple discontinuities are shown in (a), spiked discontinuities in (b).*

subset for which the density is nearly constant for the three measurements before the discontinuity and for the three measurements after the discontinuity; (3) select those discontinuities for which the magnetic field direction changes by a sufficiently large amount, meaning that the larger of  $\sin^{-1}(3\sigma_1/B_1)$ ,  $\sin^{-1}(3\sigma_2/B_2)$ , where  $\sigma_1$  and  $\sigma_2$  refer to standard deviations in the measurements of the components [Turner and Siscoe, 1971], should be less than the angle between  $B_1$  and  $B_2$ ; and (4) eliminate those discontinuities with a shock signature.

*Possible rotational discontinuities* [Turner and Siscoe, 1971]. This is based on 5-min magnetic field averages and plasma measurements made at 5-min intervals. The selection procedure is as follows: (1) choose changes in the bulk speed  $\Delta V > 25$  km/sec between consecutive measurements; (2) eliminate those discontinuities for

which the bulk speed changed appreciably in the 15 min before or after the discontinuity; (3) eliminate those discontinuities across which the magnetic field intensity changed; (4) require that the change in the magnetic field direction be sufficiently large, as discussed above for possible tangential discontinuities; and (5) choose those for which  $\Delta \mathbf{V} \cdot \Delta \mathbf{B} \geq 0.7 |\Delta \mathbf{V}| |\Delta \mathbf{B}|$ .

*Sharply crested Alfvén waves, abrupt Alfvén waves* [Belcher and Davis, 1971]. These terms are used by Belcher and Davis without a definition. They call a rotational discontinuity a “sufficiently sharp crested Alfvén wave” (see fig. 4).

*Appreciable discontinuities* [Quenby and Sear, 1971]. This refers to field magnitude changes  $> 20$  percent and direction changes  $\geq 30^\circ$ .

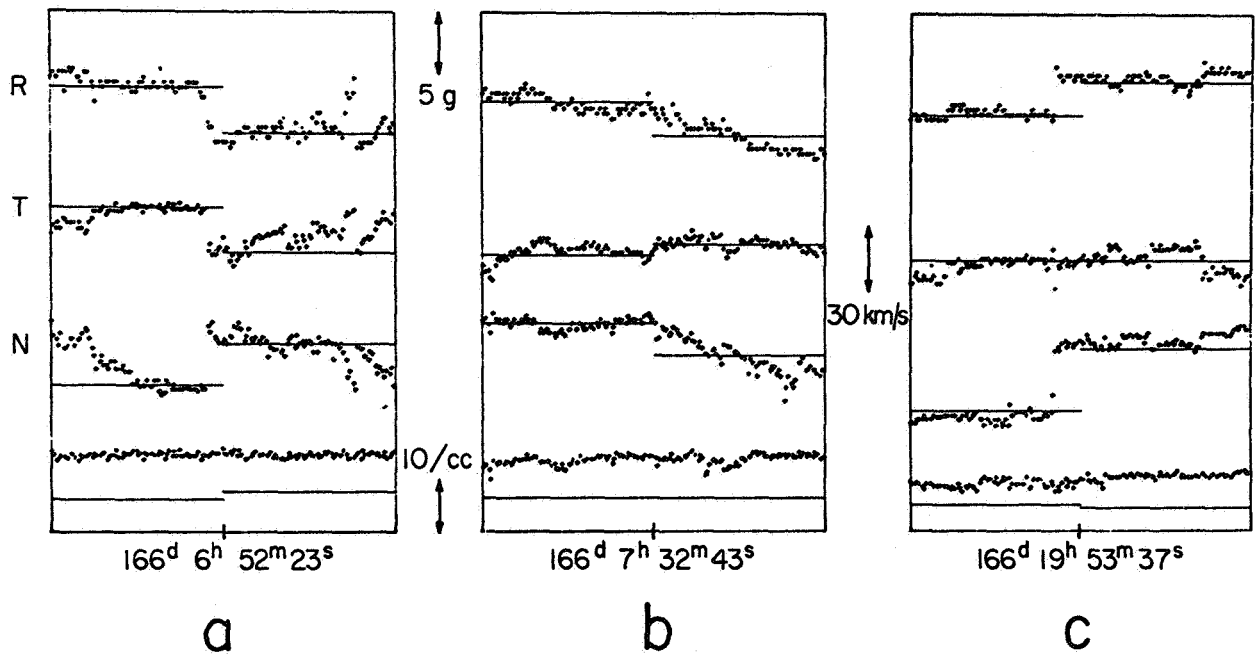


**Figure 4.** "Sufficiently sharp-crested Alfvén waves." The time scale is  $\approx 10$  min. The dots show the components of  $\mathbf{B}$  in RTN coordinates [Belcher and Davis, 1971]. The corresponding velocity components are shown by the horizontal lines, normalized to give the fits shown here. The density is shown by the horizontal lines at the bottom.

It is clear from the definitions and from figures 1, 2, and 3, that filament discontinuities, directional discontinuities, and simple discontinuities are similar. Further similarities are discussed below. The definitions of *possible tangential discontinuities* and *possible rotational discontinuities* are very restrictive and are likely to give two distinct sets. The definitions of the terms *filaments*, *directional discontinuities*, and *simple discontinuities* do not distinguish between tangential and rotational discontinuities [Burlaga, 1969].

#### The Nature of Discontinuities

The discontinuities are likely to be shocks, rotational discontinuities, tangential discontinuities, or a combination of these. The number of shocks is sufficiently small that they can be considered negligible. One question then is: What is the ratio of tangential to rotational discontinuities for each of the classes defined above?

Ness *et al.* [1966] suggested that filament discontinuities are all tangential. Some supporting evidence from simultaneous cosmic ray and magnetic field data was given by McCracken and Ness [1966].

Burlaga [1971] showed that most (but not necessarily all) directional discontinuities observed in the period December 18 to 25, 1965, were tangential. The argument is as follows. The discontinuities are probably either tangential, rotational, or a mixture of both. If they are rotational, then necessarily they satisfy the condition

$$\mathbf{V}_2 - \mathbf{V}_1 = \pm \left( \frac{\mathbf{B}_2}{\rho_2} - \frac{\mathbf{B}_1}{\rho_1} \right) \left( \frac{\rho_1}{4\pi} \right)^{1/2} \times A, \equiv QA$$

where  $A = 1$  for an isotropic plasma and  $A \approx 0.9 \pm 0.1$  for the anisotropies typically measured in the solar wind.

The above condition is not satisfied for most of the directional discontinuities (fig. 5). The peak occurs at 0 rather than at  $\pm 0.9$ . Thus most of the discontinuities are not rotational; they must be tangential. Burlaga shows that the fraction of rotational discontinuities in the set of directional discontinuities must be less than 0.25. Smith *et al.* [1970] have recently suggested that the ratio is greater than 0.5.

Siscoe *et al.* [1968] analyzed the structure of current sheets associated with *simple discontinuities* and concluded that they correspond to tangential discontinuities

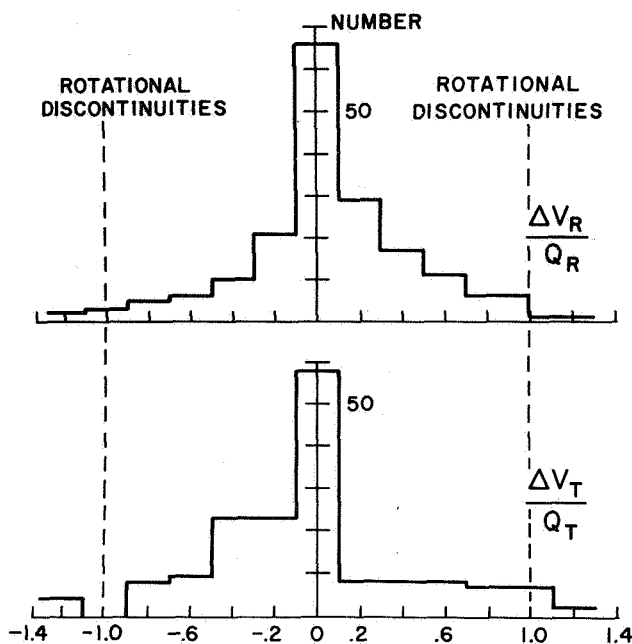


**Figure 5.** If most directional discontinuities were rotational, then the distribution of  $\Delta V_i / Q_i$ , where  $Q_i \equiv 21.8 \left( \frac{B_{1i}}{n_1} - \frac{B_{2i}}{n_2} \right) \sqrt{n}$  would be peaked at  $\pm 0.9$ . The fact that it is peaked at zero implies that most directional discontinuities are not rotational discontinuities.

rather than rotational discontinuities. The reason for the difference between this result and that of *Smith et al.* [1970] is not clear.

In view of the many constraints involved in using both plasma and magnetic field data in the definition of possible tangential discontinuities, there is little reason to doubt that most are in fact tangential. Similarly, most probable rotational discontinuities are indeed likely to be rotational, if they can actually be classified as discontinuities. They should be studied with higher time resolution data.

The nature of the appreciable discontinuities discussed by *Quenby and Sear* [1971] has not been studied directly using both plasma and magnetic field measurements. They suggest from a theoretical argument based on cosmic ray measurements that most appreciable discontinuities are rotational.

#### Statistical Properties of Discontinuities

**Directional and simple discontinuities.** The basic distributions are for  $B_1/B_2$ ,  $\omega$  (the angle between  $B_1$  and  $B_2$ ), the time interval between successive discontinuities, and the directions  $\hat{n} = B_1 \times B_2 / |B_1 \times B_2|$ .

The distributions of  $B_1/B_2$  for planar simple discontinuities and  $(B_1 - B_2) / \max(B_1, B_2)$  for directional discontinuities are shown in figure 6. It is clear that for

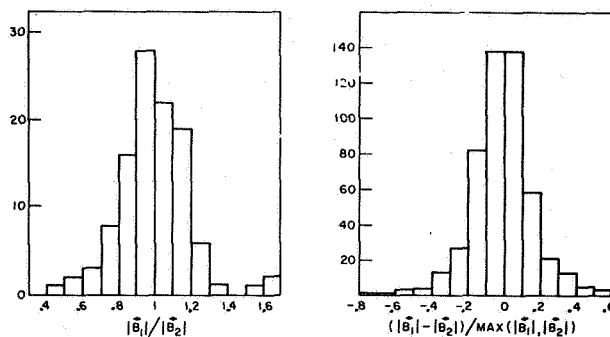


**Figure 6.** Change in magnetic field intensity across simple discontinuities (left) and directional discontinuities (right).

both types, the most probable case is that the magnetic field intensity  $B$  does not change across the discontinuity; and increases and decreases in  $B$  are equally probable.

The distribution of  $\omega$  for directional discontinuities is shown in figure 7. An empirical fit gives

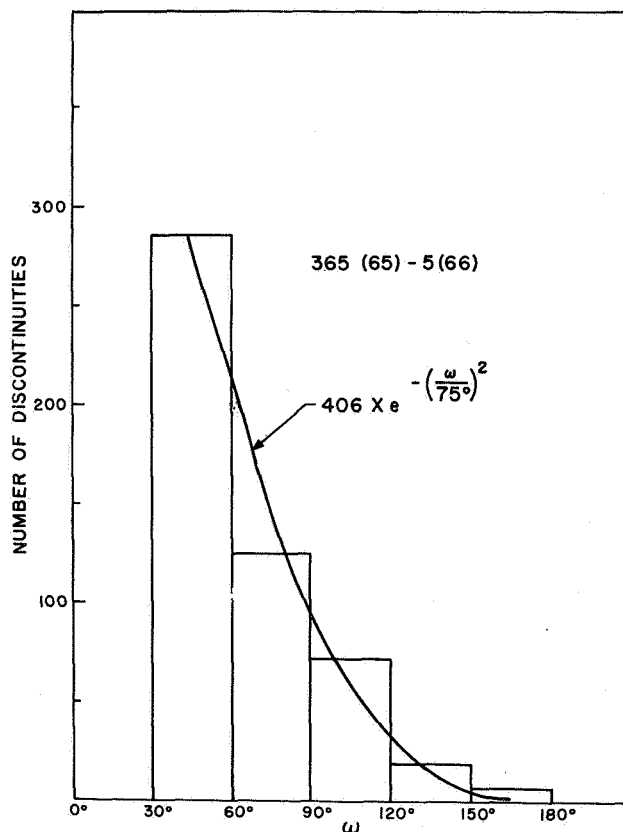


**Figure 7.** Distribution of  $\omega$  for directional discontinuities.

$dN/d\omega \sim \exp-(\omega/75^\circ)^2$ . Clearly, most directional discontinuities have small  $\omega$ . The lower limit  $\omega = 30^\circ$  is a result of the definition of a directional discontinuity and was used to avoid confusing discontinuities and the fluctuations that are usually present. The corresponding distribution of  $\omega$  for simple discontinuities is shown in figure 8. For  $\omega > 60^\circ$  it is very similar to that for directional discontinuities. The decrease for  $\omega < 50^\circ$  is due to the selection criterion,  $|B_2 - B_1| > 4\gamma$ . Note that for the usual case,  $B_1 = B_2 \approx 5\gamma$ , this criterion gives a discontinuity with  $\omega \geq 50^\circ$ .

The distribution of time intervals between successive directional discontinuities is given in figure 9 for four classes of these discontinuities, those with  $30^\circ < \omega \leq 60^\circ$ ,  $60^\circ < \omega \leq 90^\circ$ ,  $90^\circ < \omega \leq 120^\circ$ ,  $120^\circ < \omega \leq 150^\circ$ . The distributions are of the form that would be expected if they occurred with a Poisson distribution. They occur at the rate of  $\approx 1/\text{hr}$ . The probability of finding a simple discontinuity in any time interval  $T$  is shown in figure 10. The probability of finding a simple discontinuity in an arbitrary 5-min interval is 0.1. Thus, they occur at the rate of  $\approx 1/\text{hr}$ . Again we find that the characteristics of directional discontinuities and simple discontinuities are very similar.

The distribution of "normals" for directional discontinuities is shown in figure 11. They tend to be perpendicular to the spiral direction and out of the ecliptic plane. The distribution of "normals" of the current sheets associated with simple discontinuities is shown in figure 12 from *Siscoe et al.* [1968]. Here a sector-dependent asymmetry is also shown. Although figures 11 and 12 are not directly comparable, it is clear that the normal tends to be out of the ecliptic in both cases. The orientation of  $\hat{n}$  with respect to the spiral field is not clearly shown by the projection in figure 11.

The distributions described above show that directional discontinuities and simple discontinuities have essentially the same statistical properties. Since their definitions are also similar, and since different, independent analyses show that each type consists predominantly of tangential discontinuities, we may infer that directional discontinuities and simple discontinuities are essentially equivalent.

*Possible tangential discontinuities.* One expects the properties of these discontinuities to be similar to directional and simple discontinuities, since physically they seem to be the same. However, one expects "probable tangential discontinuities" to occur less frequently because of the more stringent requirements involved in their definition.

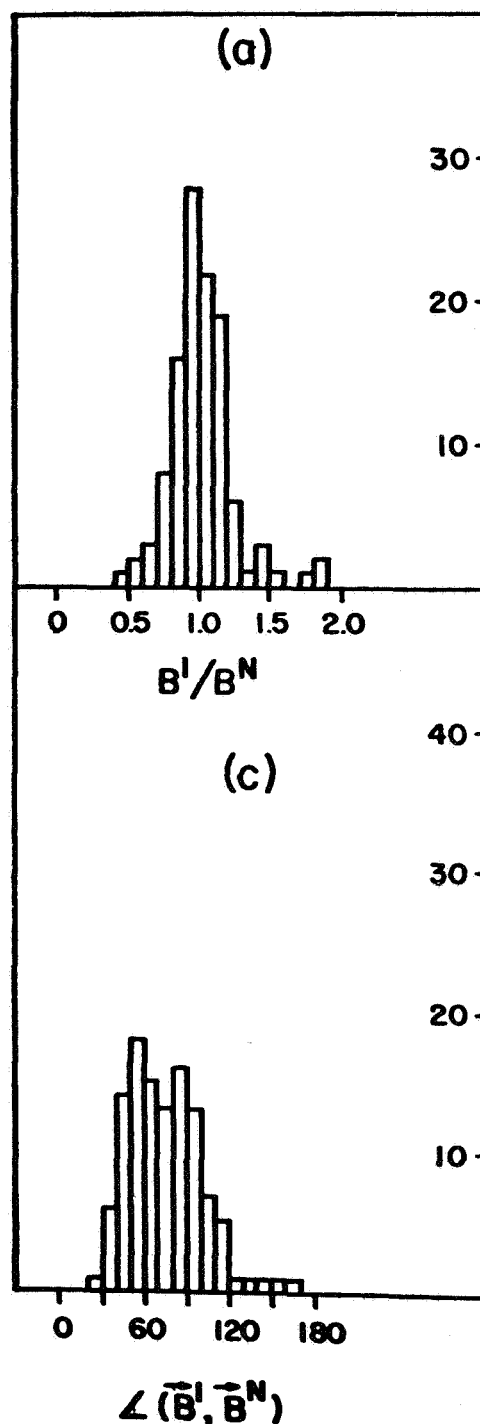
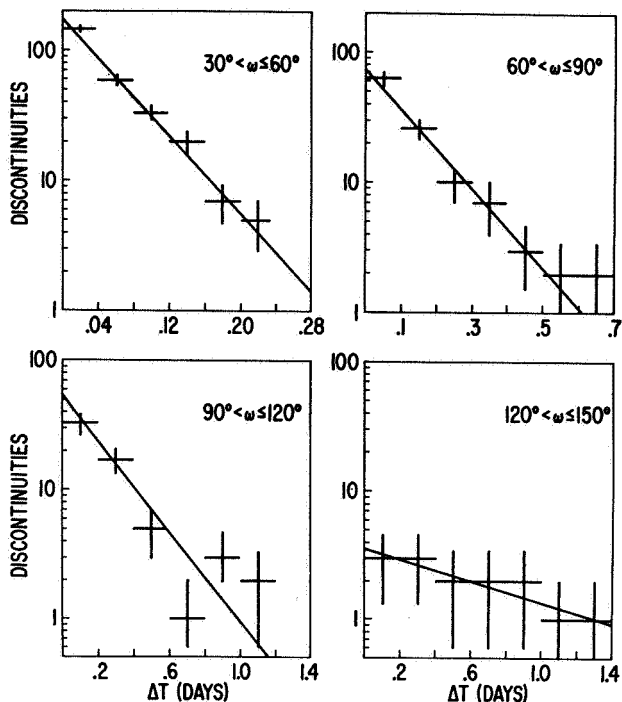


Figure 8. Distribution of magnitude changes (a) and  $\omega$  (c) for simple discontinuities.

The rate at which possible tangential discontinuities passed Mariner 5 is  $\approx 1/25$  hr, which is to be compared to  $\approx 1/\text{hr}$  for simple and directional discontinuities.





**Figure 9.** Distribution of time intervals between successive directional discontinuities.

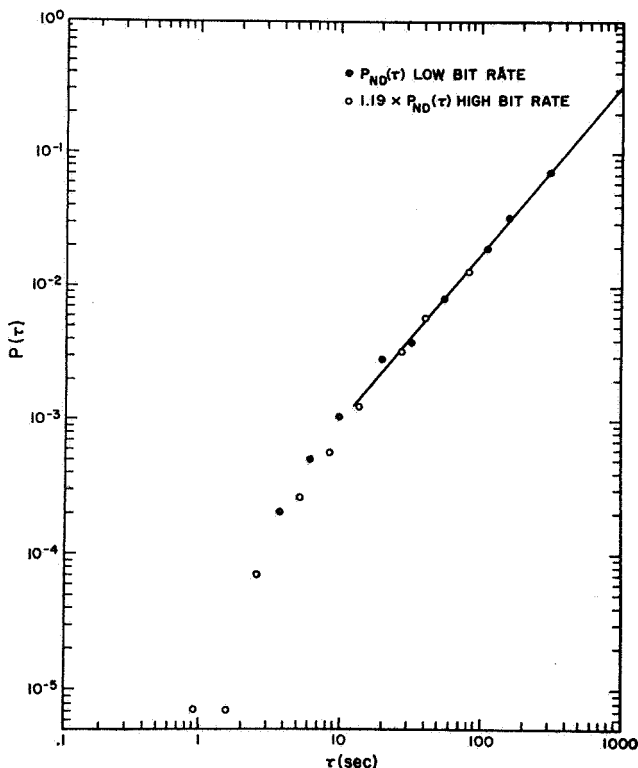


**Figure 10.** Probability of finding a simple discontinuity in any time interval  $\tau$ .

#### SIMPLE DISCONTINUITIES 12/16/65–1/5/66

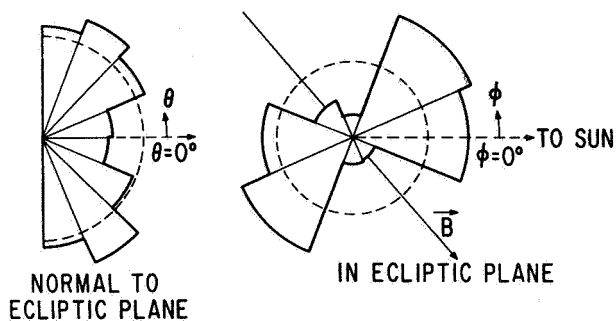


**Figure 11.** Distribution of the vectors  $\mathbf{B}_1 \times \mathbf{B}_2 / |\mathbf{B}_1 \times \mathbf{B}_2|$  for directional discontinuities.

Turner and Siscoe [1971] did not give the distributions of  $B_1/B_2$  and  $\omega$  for possible tangential discontinuities. The distribution of the polar angles of the normals normalized to obtain the number per unit solid angle is shown in figure 13. The normals of possible tangential discontinuities tend to be normal to the spiral direction and in the ecliptic plane. Recall that the “normals” associated with directional discontinuities also tend to be normal to the spiral direction, but they tend to be out of the ecliptic.

**Possible rotational discontinuities.** Forty of these were found in 40 days of data from Mariner 5, but most occurred in three intervals of  $5 \pm 1$  days. Thus, the maximum rate is  $\approx 0.1/\text{hr}$  which is only 10 percent of the rate of directional and simple discontinuities. Most of the time the rate is much less than this. Although the ratio of possible rotational discontinuities to possible tangential discontinuities is  $\approx 1$ , it does not mean that this is the ratio of rotational to tangential discontinuities in the set of directional discontinuities. One can only say that at times up to 10 percent of the directional discontinuities might be possible rotational discontinuities.

The  $\omega$  and  $B_1/B_2$  distributions were not given by Turner and Siscoe [1971]. The distribution of average normals for three subsets of discontinuities is given in figure 13. This is different from that of probably tangential discontinuities.

**Changes in plasma parameters at discontinuities.** The early models assumed that the plasma parameters change across most magnetic field discontinuities. This is probably not so, but the matter has not been studied extensively. Burlaga [1968] found no change in  $n$ ,  $V$ , or  $T$  across directional discontinuities with  $B_1 \approx B_2$ , which according to figure 6 is the most probable case. Changes in plasma parameters do sometimes occur, however. Burlaga classified discontinuities according to changes in

# INTERPLANETARY MAGNETIC FIELD

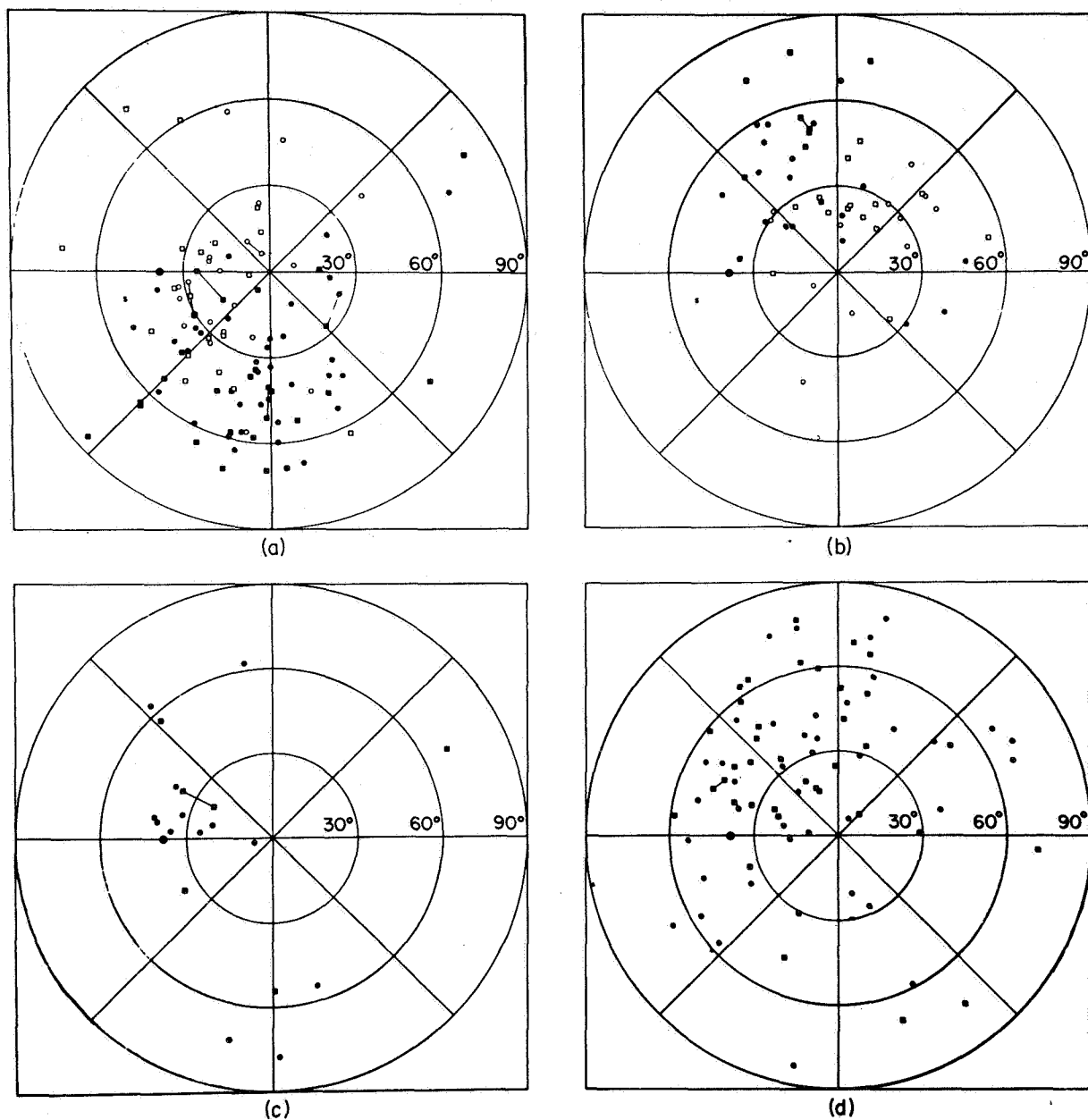


**Figure 12.** Distribution of current sheet normals associated with simple discontinuities.

$B$ ,  $n$ , and  $T$ , as shown in table 1. The symbol  $(+, -, 0)$  implies an increase in  $B$ , a decrease in  $n$ , and no change in  $T$ . The other symbols have similar meaning. Nine of the 13 possible signatures were found in the Pioneer 6 data. This scheme may be useful for discussing the statistical properties of discontinuities when more data become available. It has been used to discuss interaction of discontinuities with the earth [Burlaga, 1970b]. Hudson [1970] has pointed out that it cannot be used for identifying tangential or rotational discontinuities in

an anisotropic medium such as the solar wind. Recently, Burlaga and Chao [1971] showed that the discontinuities in  $B$  which they selected ( $\geq 20$  percent in  $\lesssim \min$ ) are essentially always accompanied by changes in  $n$  and possibly  $T$  (fig. 14). However, figure 6 shows that the probability of such a change in  $B$  across a directional discontinuity is small.

## Morphology of Simple and Directional Discontinuities

This section aims to present a mesoscale ( $\approx 1$  AU)

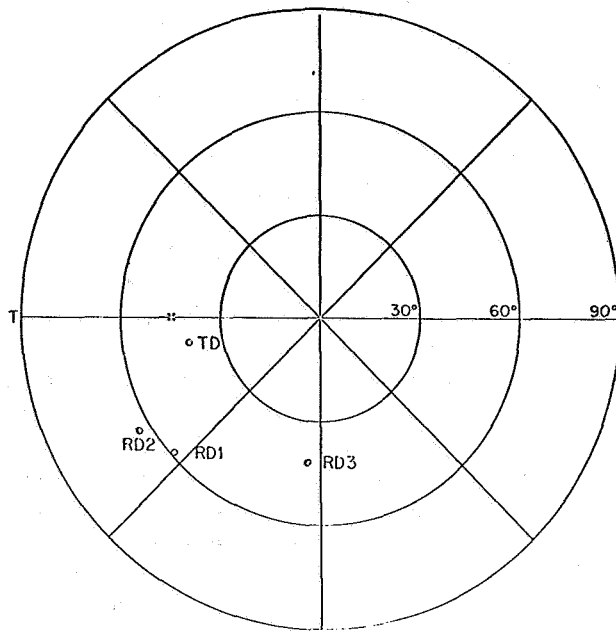


Figure 13. Average normals for "probable tangential discontinuities" and "probable rotational discontinuities."

Table 1. Tangential discontinuities

T0	( 0 0 0 ) <sup>a</sup>		
T2	( + - 0 ) <sup>a</sup>	( 0 + - ) <sup>a</sup>	( - 0 + ) <sup>a</sup>
	( - + 0 ) <sup>a</sup>	( 0 - + )	( + 0 - ) <sup>a</sup>
T3	( + - + ) <sup>a</sup>	( + + - ) <sup>a</sup>	( - + + )
	( - + - ) <sup>a</sup>	( - - + )	( + - - )

<sup>a</sup>Observed in Pioneer 6 data

picture of the topology of the discontinuity surfaces and the variations of plasma parameters between them. This is intended to be a zeroth approximation; details must be supplied by later work.

The separations between discontinuity surfaces can be approximately described by the distribution of time intervals between successive discontinuities, since the discontinuities are convected past the spacecraft at the solar wind speed. This is an approximate description since the solar wind speed changes, but it is a good

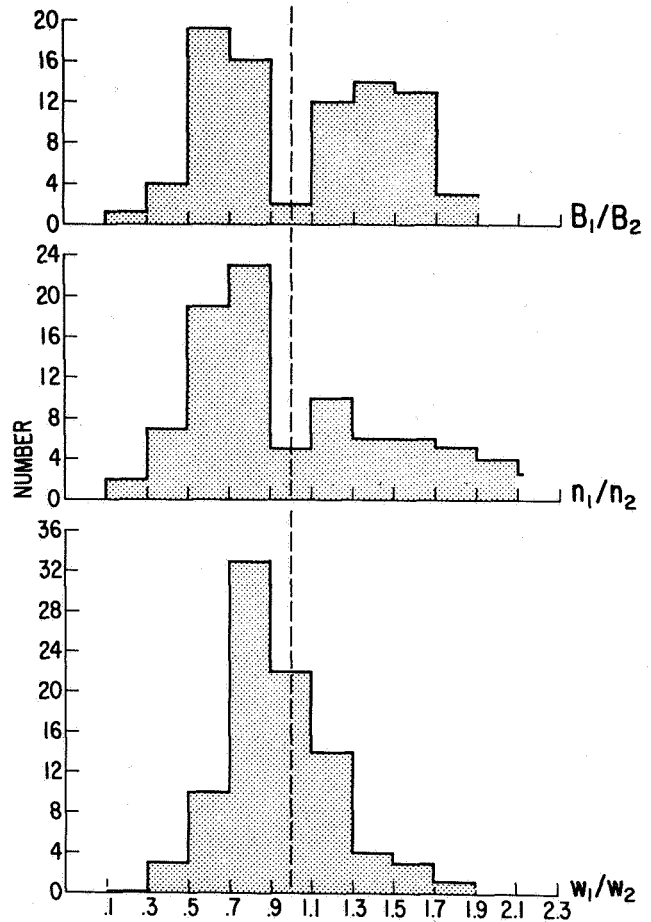


Figure 14. Changes in  $n$  associated with changes in  $|B|$  across discontinuities.

zeroth approximation because the changes are seldom greater than 50 percent. Figure 9 from Burlaga [1969] shows such a distribution of time intervals for four classes of directional discontinuities. The corresponding mean separations in space are shown in figure 15.

The topology of individual surfaces can be studied only with multiple spacecraft observations. Burlaga and Ness [1969] and Ness [1966] discuss one exceptional surface seen by Pioneer 6 and IMP 3, which was planar and unchanged over a distance of 0.01 AU. Burlaga and Ness [1969] studied six surfaces, each of which was observed at three spacecraft, Explorers 33, 34, and 35. These are shown in figure 16 where it is seen that some of them do show an appreciable curvature over distances of  $100 R_E = 0.005$  AU. These are probably atypical; the curvature is likely to be larger for most discontinuities.

If it is assumed that the surfaces are plane, then their orientations can be computed very simply using the formula  $\hat{n} = \mathbf{B}_1 \times \mathbf{B}_2 / |\mathbf{B}_1 \times \mathbf{B}_2|$  and measurements

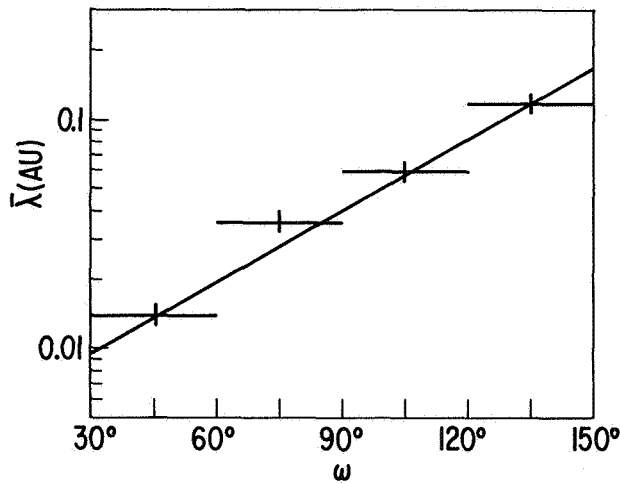


Figure 15. Average separation of directional discontinuities.

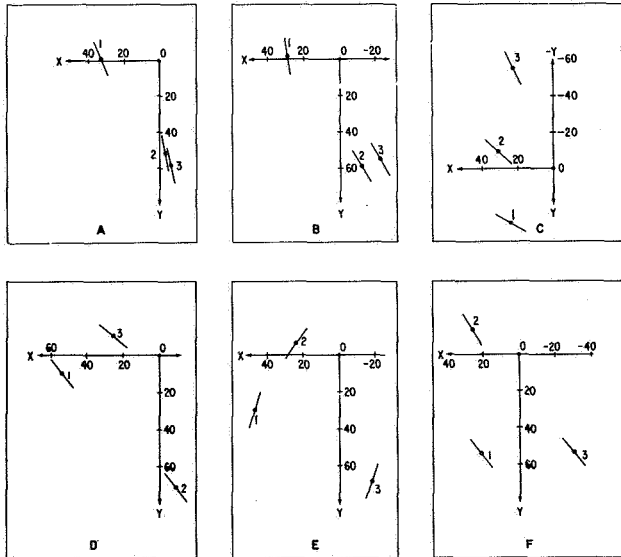


Figure 16. Multi-spacecraft observations of discontinuity surfaces. Each panel describes one surface. Each dot represents the position of a spacecraft. The earth is at the origin and units are earth radii. The line segments are ecliptic plane intersection of the discontinuity surface, compiled from  $\hat{n} = \mathbf{B}_1 \times \mathbf{B}_2 / |\mathbf{B}_1 \times \mathbf{B}_2|$ . The surface first passed spacecraft 1, then spacecraft 2, and finally spacecraft 3.

from just one spacecraft. This procedure shows (unpublished results) that the surfaces associated with directional discontinuities intersect at a distance  $\approx 0.01$  AU from the earth-sun line. This should not be surprising, since the autocorrelation length of  $\mathbf{B}$  is  $\approx 0.01$  AU. The result does not imply that directional discontinuities are

not tangential. Rather, it implies that the surfaces are appreciably curved on a scale of  $\approx 0.01$  AU.

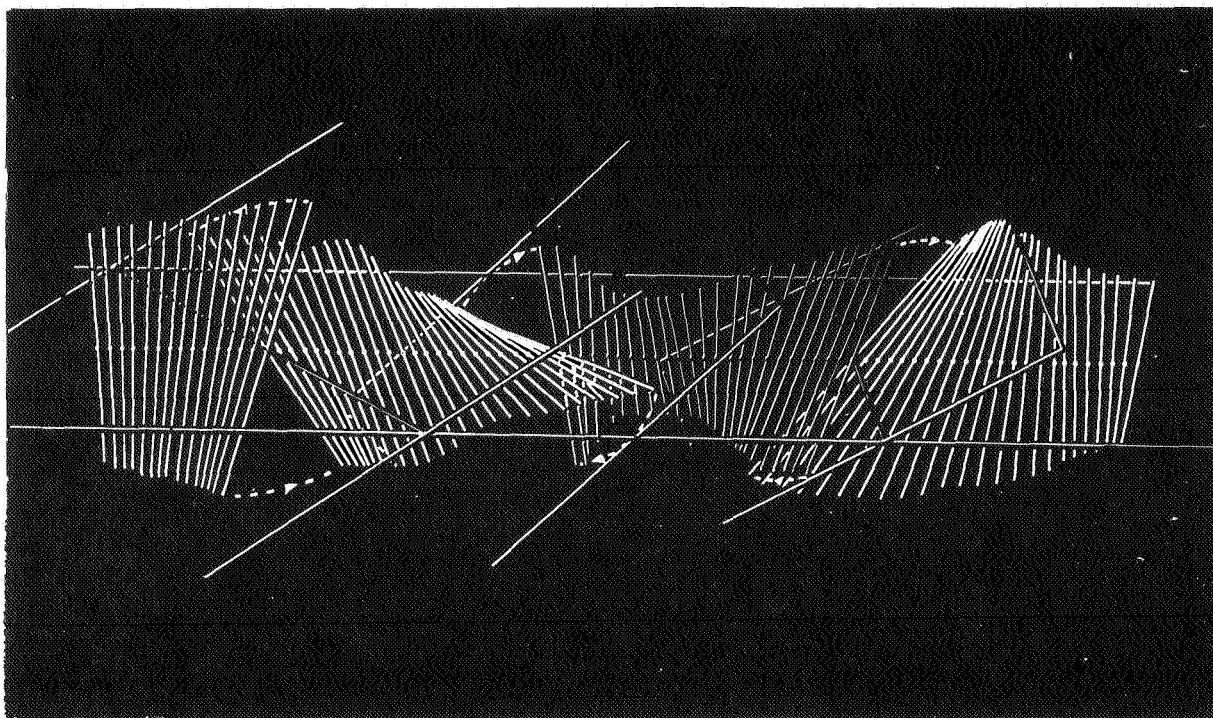
The picture that is suggested by the above results is illustrated in figure 17. There are numerous discontinuity surfaces (current sheets) in space, separated by  $\approx 0.01$  AU. Although the surfaces are shown as planar in figure 17 for simplicity, they are actually appreciably warped and bent on the scale of the figure. Successive discontinuity surfaces are not parallel, but they do tend to scatter about the spiral field direction. The magnetic field direction changes discontinuously across each of the surfaces and varies appreciably between adjacent surfaces. The magnetic field directions are shown as straight line segments in figure 17, but in reality are appreciably bent and "distorted" on the scale shown there. In reality, they are probably additional discontinuities between the directional discontinuities that have  $\omega < 30^\circ$  or are obscured by fluctuations and noise.

Figure 17 gives only a rough approximation to reality. There are infinitely many variations of detail, and complexities not yet mentioned. The way that surfaces connect with one another (if they do so) and their extent toward the sun is unknown. The cosmic ray measurements of McCracken and Ness [1966] suggest that the magnetic field lines on either side of a discontinuity go directly to the sun; but this does not necessarily imply a similar extent of the current sheet.

The density, temperature, and bulk speed usually do not change across the discontinuity surfaces, but such changes do occasionally occur. The plasma parameters sometimes also vary *between* the discontinuity surfaces. Thus, if one were to use a color code to map plasma parameters in figure 17, he would probably find a weak relation between the color pattern and the directional discontinuities.

#### Relations Between Discontinuities and Mesoscale Structure

Siscoe *et al.* [1968] noted that there was a pronounced north-south, sector-dependent asymmetry in the distribution of current sheet normals (fig. 12). They suggested that this is due to velocity shears acting in tangential discontinuities. Another interpretation was given by Siscoe and Coleman [1969]. Subsequently, however, Turner and Siscoe [1971] offered the hypothesis that the north-south asymmetry is due mainly to rotational discontinuities. This is based on the assumption that more than half of the discontinuities in Siscoe *et al.* [1968] are rotational. At the moment, there is no evidence to support this assumption. The results of Burlaga [1970b] argue against it if the discontinuities studied by Siscoe *et al.* [1968] are directional discontinuities. Obviously, the problem needs further study.



**Figure 17.** *Simplified view of three discontinuity surfaces and magnetic fields between them illustrating how a 0.05 AU segment of the solar wind might look (see text).*

*Burlaga* [1970a] could not find a relation between the rate of occurrence of directional discontinuities and positive bulk speed gradients. This implies that most of these discontinuities are not caused by the gradients.

#### **Variation of Discontinuities with Distance from the Sun**

The only work on this subject is that of *Burlaga* [1970a] which is based on the Pioneer 6 data of Ness for the region between 0.8 and 1.0 AU. He found that (1) the "density" of discontinuities (number passing the spacecraft per hour) was possibly 35 percent less at 0.8 AU than at 1.0 AU, but this difference could be due to the higher quality data near the earth; and (2) the distributions of  $\omega$ , the change in the direction of  $B$  across a discontinuity, were essentially identical at 0.8, 0.9, and 1.0 AU. The conclusion is that most discontinuities originate within 0.8 AU and their characteristics do not change very much between 0.8 and 1.0 AU.

#### **Filaments**

The concept of a filament is widely used, but never precisely defined. This has caused much confusion. The concept has evolved appreciably during the last 10 years, so a historical discussion is appropriate.

The idea that filaments might exist in the solar wind seems to go back to *Parker* [1963], who suggested that they would be the result of an assembly of fine streamers or temperature striations in the corona. Parker pictured the streamers as more or less discrete flow tubes separated by regions of material with different density, temperature, and magnetic field intensity. The scale of these filaments was set at  $\approx 0.01$  AU. Radio observations of Hewish (p. 477) have been interpreted as evidence for such filaments, but this interpretation has been questioned by *Jokipii and Hollweg* [1970]. The observation of filamentary structure in comet tails was also interpreted as evidence for filaments in the solar wind, but more recent work [*Kubo et al.*, 1970] suggests that this might result from turbulence, instabilities, or some other mechanism. The early observations by Explorer 10 showed regions of plasma with density 7 to 20/cm<sup>3</sup> and  $B \approx 10 \gamma$  alternating at approximately hour intervals with higher field regions (20  $\gamma$ ) with no detectable plasma. This was said to be evidence for filaments in the solar wind, but more recent observations suggest that Explorer 10 was alternately inside and outside the magnetosheath.

With the advent of high time resolution magnetic field

data from Pioneer 6, Mariner 4, and other spacecraft, the concept of filaments was rejuvenated. Ness [1966] pointed to two kinds of filaments: those bounded by pairs of nearly identical directional discontinuities (fig. 11) and those characterized by less abrupt changes in magnetic field intensity (fig. 18). It was suggested [McCracken and Ness, 1966] that the interplanetary field could be viewed as bundles of intertwined filaments bounded by tangential discontinuities (directional discontinuities) and extending to the sun. This has been referred to as the "spaghetti" model. Support of this model was given by Siscoe *et al.* [1968], who on the basis of Mariner 4 data suggested that the shape of the filamentary tubes is elliptical.

Michael [1967] proposed an alternate model, with "entropy fluctuation cells," but this has not been discussed further in the literature. Burlaga [1969] pointed out that such filaments are exceptions rather than the rule at 1 AU and suggested that the interplanetary medium should be regarded as discontinuous rather than filamentary. Figure 19 shows a day of Ness's Pioneer 6 magnetic field data with a number of clearly defined directional discontinuities, but it would be difficult for two observers to agree on how it might be divided into filaments. The point is that there is

generally no obvious pairing of directional discontinuities. This does not imply that filaments bounded by similar directional discontinuities never occur, only that they are relatively rare. Siscoe *et al.* [1968] found only nine pairs of nearly identical simple discontinuities separated by 2 to 30 min in the Mariner 4 data. "Filaments" of the kind shown in figure 18 are not uncommonly seen behind driven shocks. These structures resemble more closely than any others the type described by Parker [1963]; but their nature might be different. Again, they are the exception rather than the rule.

The current situation is that the term *filament* has many meanings. It seems more appropriate to describe the solar wind near 1 AU as discontinuous rather than filamentary. This does not exclude the presence of waves, fluctuations, or turbulence. Pairs of simple discontinuities and pairs of directional discontinuities do sometimes occur, but their significance is not certain.

#### Waves and Fluctuations

Linear hydromagnetic theory predicts three types of waves: fast, slow, and Alfvén waves. It is possible that all three types are present at one time or another in the solar wind as well as larger amplitude nonlinear waves. The observed waves are very seldom periodic and frequently nonlinear, and they are probably coupled

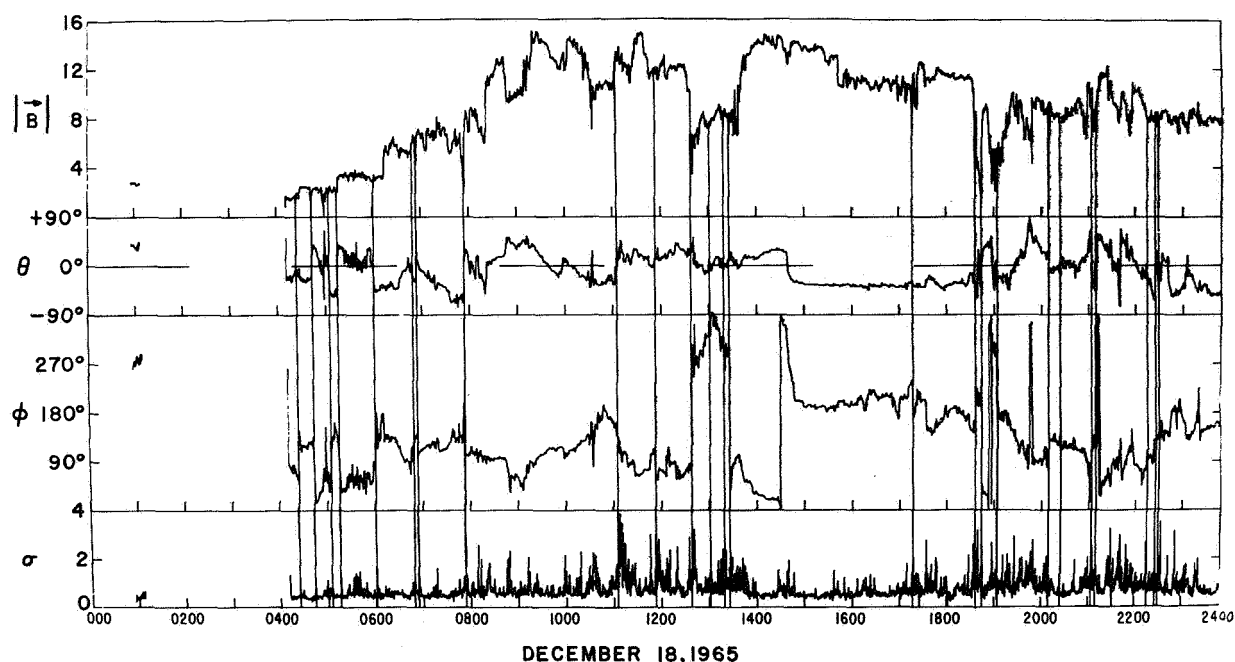


Figure 18. "Filaments" in B.

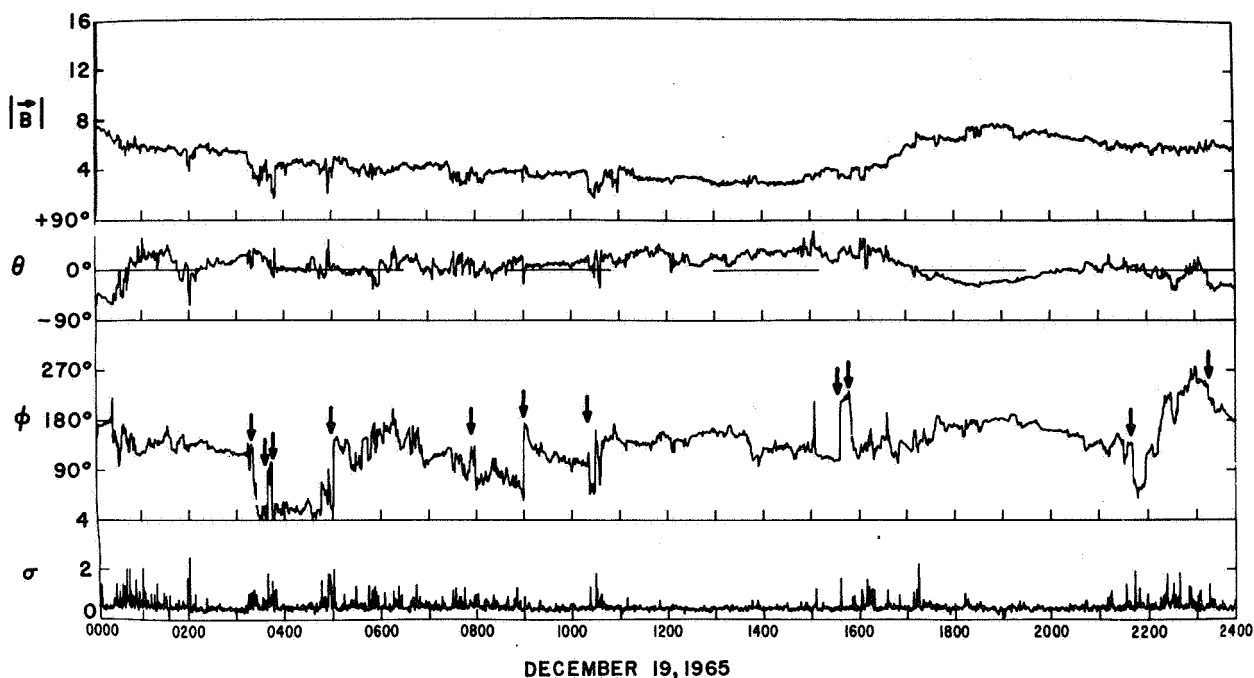


Figure 19. Directional discontinuities and filaments. The directional discontinuities are marked by arrows. How would one divide this interval into filaments?

with one another. The interpretation of the observations is thus intrinsically complicated and is further hindered by incomplete plasma observations. The usual approach is to study the fluctuations in the magnetic field and try to interpret them, with the limited available plasma data and/or with idealized models, in terms of the linear hydromagnetic theory.

Much confusion has resulted from the loose or erroneous use of words and definitions. Here we review the various types of waves and fluctuations that have been mentioned in the literature, discuss the interpretation of power spectra and the controversy concerning microscale fluctuations, and present a hypothetical model of the relation between the bulk speed and fluctuations and evidence for the variation of fluctuations with distance from the sun.

#### Types of Waves and Fluctuations

**Periodic Alfvén waves.** *Unti and Neugebauer* [1968] searched Mariner 2 data for *sinusoidal* changes in the direction of  $B$  that satisfy the conditions for Alfvén waves. One (but only one) such wave, with a Doppler-shifted period of 30 min, was found [Burlaga, 1971]. Such waves do not play an important role in the general structure of the solar wind at 1 AU, but their existence is of fundamental physical significance.

**Periodic waves.** *Burlaga* [1968] found a few sinusoidal wave trains with Doppler-shifted periods of  $\approx 5$  min in the Pioneer 6 magnetic field data of Ness. These were compressive waves, probably magnetoacoustic and fast waves [Burlaga, 1971]. Again, only a few periodic waves were found in  $\approx 6$  months of data, so they are not basic to the general structure of the solar wind at 1 AU.

**Large-amplitude aperiodic Alfvén waves.** *Belcher et al.* [1969] found in the Mariner 5 data that the bulk speed and radial component of  $B$  were strongly correlated 30 percent of the time (fig. 20), and argued that the fluctuations during these times were primarily Alfvén waves. An example of such a wave train is shown in figure 21. Note that this plot is based on 5-min averages.

The basic criterion which *Belcher and Davis* [1971] and *Belcher et al.* [1969] use to identify Alfvén waves is a strong correlation ( $> 0.8$ ) between  $V$  and  $B_R$ . They consider three subclasses of Alfvén waves:

1. **Pure waves.** Waves are called "pure" if there is no power in  $B$ —i.e., no compression oscillations—and the wave is linear. Such a condition seldom, if ever, occurs in the solar wind. Strictly speaking, an Alfvén wave is linear and is characterized by a constant  $B$ , so it must be a pure wave. Thus, intervals of pure Alfvén waves seldom, if ever, occur in the solar wind.

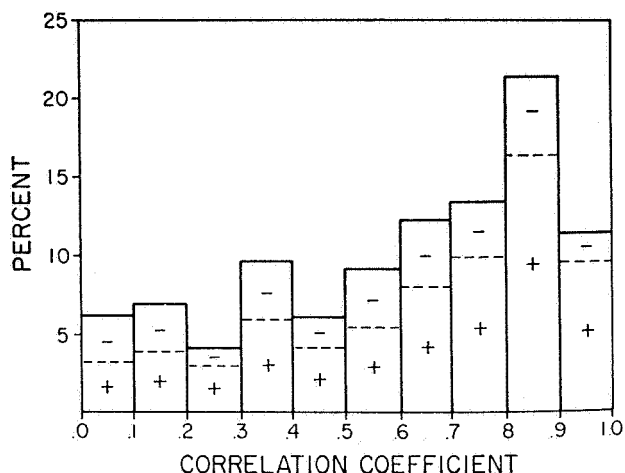


**Figure 20.** Correlation between  $V$  and  $B_R$ . Thirty percent of the time the correlation coefficient was  $>0.8$  in the period June 14 to November 21, 1967.

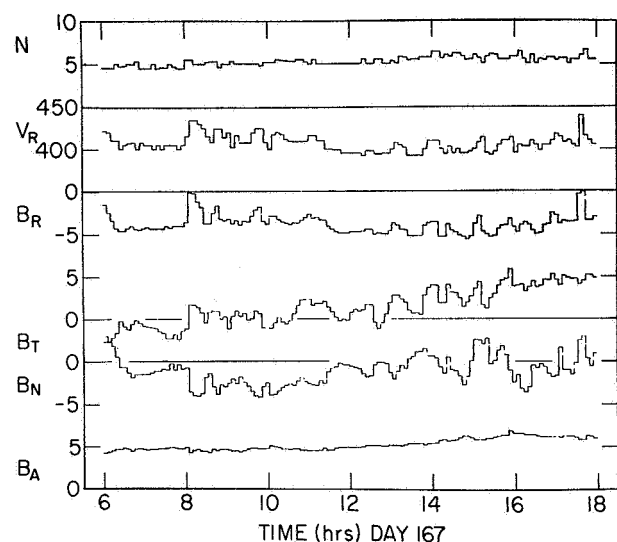


**Figure 21.** Aperiodic Alfvén waves. The density  $N$ , bulk speed  $V_R$ , magnetic field components  $B_R$ ,  $B_T$ ,  $B_N$ , and magnetic field intensity are plotted versus time on a scale of 12 hr.

2. *Almost pure waves.* These are periods when the power in  $B$  is judged to be much less than that in the components of  $B$ . Belcher (private communication) expects the power in the magnitude to be at least an order of magnitude below the power in the components, with a correlation between  $\delta V$  and  $\delta B$  above 0.8, for almost pure waves. There may also be some

nonlinear coupling with other modes. Belcher and Davis [1971] sometimes refer to almost pure waves as pure waves.

3. *Good waves.* These show a correlation between  $\delta V$  and  $\delta B$ , but are presumably accompanied by changes in  $B$  as well. These seem to be the most common type of large-amplitude aperiodic Alfvén waves.

Physically, there is no such thing as an almost pure Alfvén wave or a good Alfvén wave. When Belcher and Davis [1971] use these terms they are referring to the fraction of the power that is contributed by Alfvén waves. It might be better to stop using these terms and refer instead to power levels and correlation coefficients.

Most aperiodic Alfvén waves move away from the sun, as shown by figure 22 from Belcher et al. [1969].

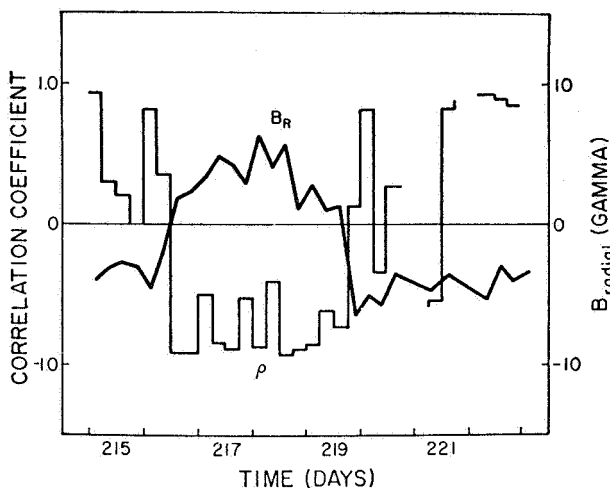


**Figure 22.** Correlation coefficient and  $B_R$  versus time. The anticorrelation indicates outward propagating waves during the period shown here.

Belcher and Davis further distinguished between “sharply crested waves” and “smooth waves.” The distinction was not defined operationally, and it depends on the time scale used (Belcher, private communication).

*Fluctuations.* This is a general term, seldom defined, which is used to describe nearly any kind of change in  $B$ . Consider a time series  $B(t)$ . For a given interval this may be written  $B(t) = B_A V + B'(t)$  where  $B_A V$  is the average over that interval. The term “fluctuation” refers to  $B'(t)$ . Here we use the term for that which is described by the power spectrum of  $B(t)$ . Obviously,  $B(t)$  contains shocks, tangential discontinuities, sector boundaries, Alfvén waves, aperiodic Alfvén waves, and many other phenomena besides. However, the power spectrum may



be dominated by only one of these structures and the dominant type may change with time. This is discussed more precisely below.

**Microscale fluctuations.** *Burlaga et al.* [1969] noted that there are certain isolated periods, usually an hour or two in length, in which there are large, high-frequency (minutes) fluctuations in both the magnitude and direction of  $\mathbf{B}$ . These are illustrated in figure 23.

*Belcher and Davis* [1971] also used the term *microscale fluctuations*, but they refer to a phenomenon distinctly different from that described by *Burlaga et al.* [1969]. The microscale fluctuations of Belcher and Davis have frequencies in the range  $1/(4.2 \text{ hr to } 10 \text{ min})$ , and they occur more or less continuously. They seem to be essentially the same as the fluctuations discussed above. Belcher and Davis use variances to describe the fluctuations.

**Abrupt Alfvén waves.** Belcher and Davis use this term to describe three discontinuous or nearly discontinuous

changes in  $\mathbf{B}$  (in the sense defined earlier, which were correlated with  $\mathbf{V}$  in accordance with the relation  $\delta\mathbf{B} = \pm D\delta\mathbf{V}$ . They consider abrupt Alfvén waves to be identical to rotational discontinuities. Belcher and Davis stated that such changes occur at the rate of one per hour; however, they presented no evidence to support this remark.

### Fluctuations and Power Spectra

**Observations.** The standard techniques of spectral analysis are used to describe the magnetic field time series and its relation to other time series such as  $V_R(t)$ . This method of analyzing interplanetary magnetic field fluctuations was used by *Coleman* [1966a] in his analysis of Mariner 2 data. The basic results are as follows:

1. The power spectra of  $B_r$ ,  $B_\theta$ ,  $B_\phi$ , and  $\mathbf{B}$  for 24-hr periods have the approximate form  $f^{-\alpha}$ ,  $1 \lesssim \alpha \lesssim 2$ , in the range  $10^{-5}$  to  $10^{-2}$  Hz.

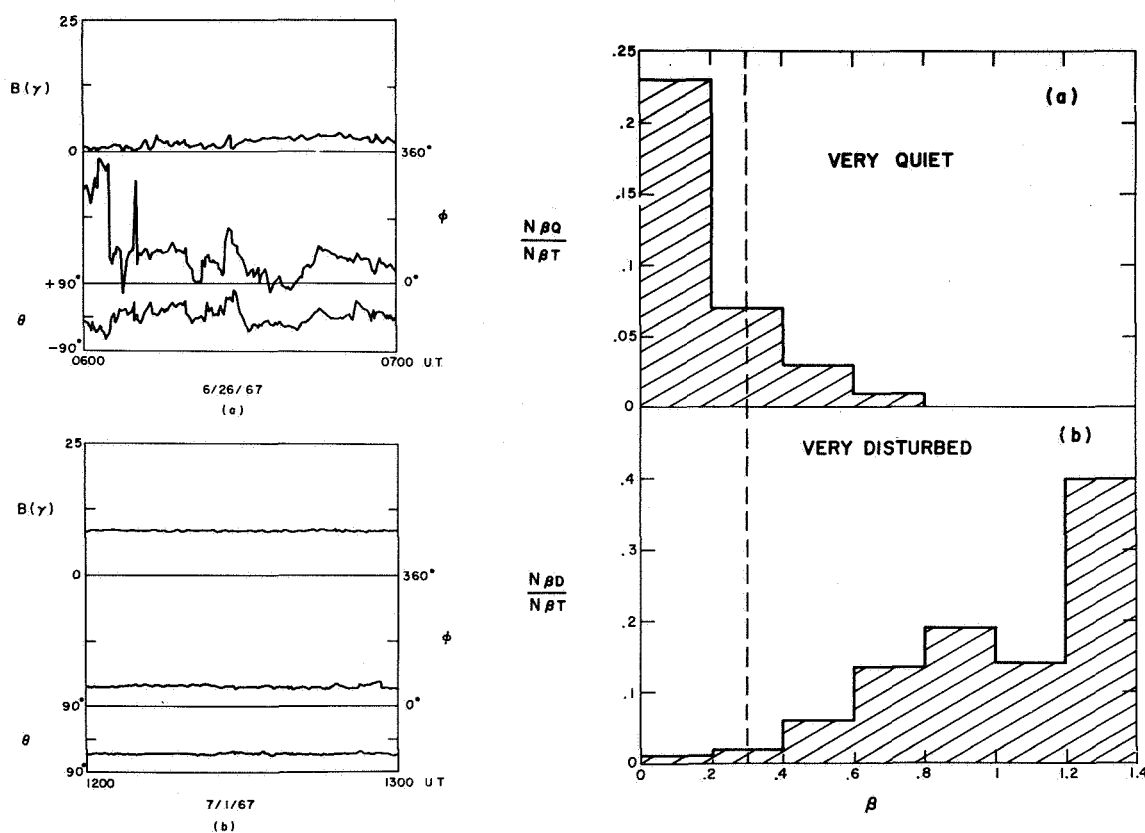


**Figure 23.** Microscale fluctuations and relation to  $\beta = 8\pi nkT/B^2$ . *Burlaga et al.* [1969] considered only two extreme conditions: very quiet (b) and very disturbed (a) on a scale of 1 hr. The very disturbed periods show large, "rapid" fluctuations in both the magnitude and direction of  $\mathbf{B}$ . The very quiet periods occur when  $\beta$  is small, the very disturbed periods when  $\beta$  is large.

2. Power levels range from  $(10^3 \text{ to } 50) \gamma^2/\text{Hz}$  at  $10^{-3} \text{ Hz}$ .
3.  $P(B_\theta) > P(B_\phi) > P(B_r) > P(|B|)$ —that is, the fluctuations are primarily transverse rather than compressional, and the largest fluctuations are normal to the ecliptic plane. The power in compressional oscillations was typically one-half to one-third that of the power in the components. All six intervals examined by Coleman showed fluctuations in  $|B|$ .
4.  $V_r$  and  $B_r$  were correlated. Their phase difference was  $\approx 180^\circ$  when  $B_A V$  was away from the sun and  $\approx 0^\circ$  when  $B_A V$  was toward the sun. The magnitude of the square of the coherence between  $V_r$  and  $B_r$  was between 0.05 and 0.49 in the range 1 to 50 cycles per day (cpd); it was typically 5 to 8 times larger than that for  $(V_r, B_\theta)$   $(V_r, B_\phi)$  and  $(V_r, B)$ , although all pairs showed significant coherences.
5. The ratios  $P(B_i)/P(V_r)$ ,  $i = r, \theta, \phi$ , were essentially independent of frequency in the range 1 to 50 cpd.

Power spectra from Mariner 4 covering the range  $3 \times 10^{-4}$  to  $0.5 \text{ Hz}$  for six 24-hr intervals in the period December 7, 1964, to January 2, 1965, were reported by Siscoe *et al.* [1968] (fig. 24). They show the same general characteristics, (1) to (3) above, found by Coleman. Siscoe *et al.* [1968] distinguished active, intermediate, and quiet times; they found an order of magnitude more power at active times than at quiet times (fig. 24).

Belcher and Davis [1971] report that they computed power spectra and cross spectra for the high data rate part of the Mariner 5 mission to Venus, and obtained results similar to those of Coleman [1966a]. The spectra are not published, however.

*Interpretation of power spectra.* Power spectra are simply statistical descriptions of time series. Their physical interpretation is not straightforward since they do not contain phase information. There are at least four contributors to the power spectra.

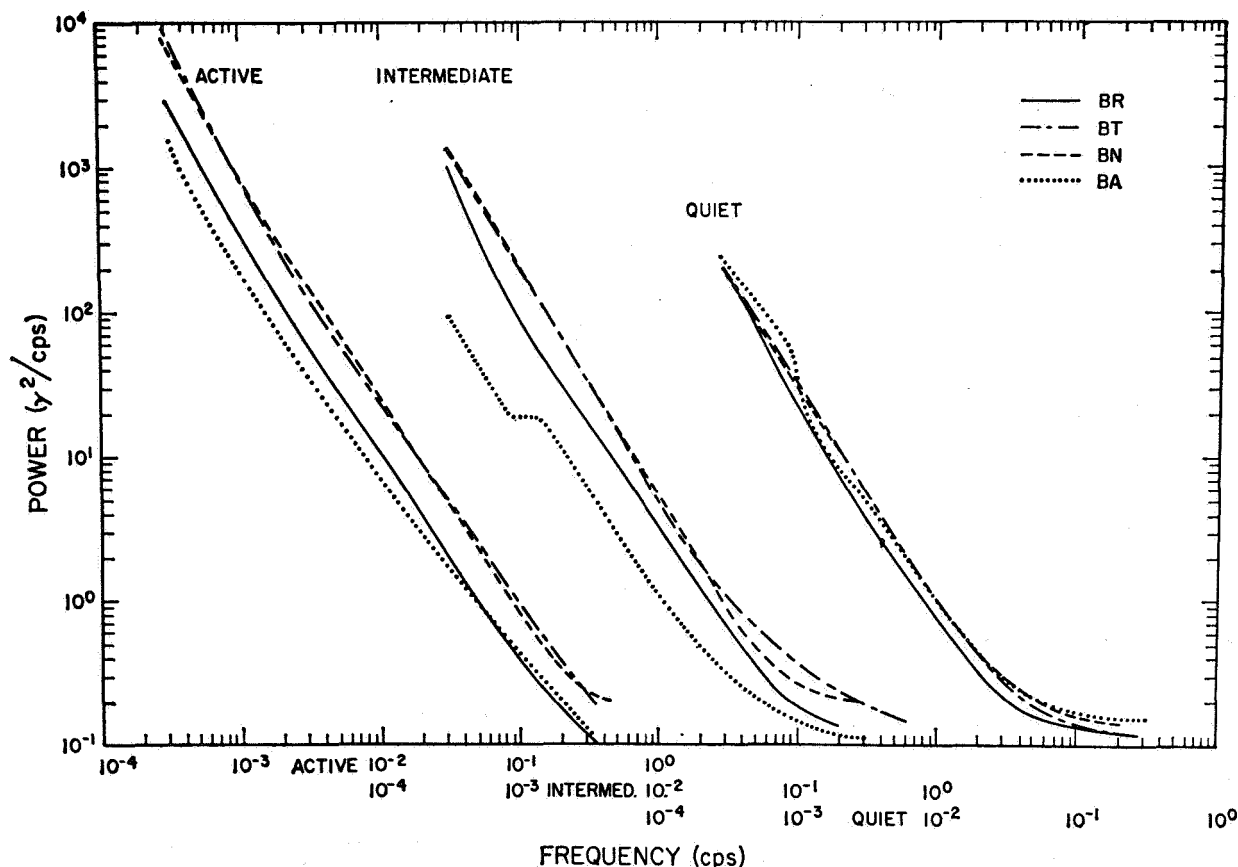


Figure 24. Mariner-4 power spectra showing relative power in the magnetic field intensity  $B_A$  and components.  $N$  is the direction normal to the ecliptic,  $R$  the radial direction and  $T$  in the direction of the earth.

Coleman [1966b, 1967] examined the possibility that linear MHD waves are dominant. He concluded that typical spectra are probably due to fast hydromagnetic waves or a mixture of fast waves and Alfvén waves. He could not exclude either of these two possibilities. He did exclude the possibility that the spectra were due to pure Alfvén waves alone, because he always found a significant amount of power in  $|B|$ , amounting to nearly one-third or one-half that in the other components. The results of Siscoe *et al.* [1968] could be interpreted similarly.

Belcher and Davis [1971] imply that “nearly pure” nonlinear, aperiodic, Alfvénic waves dominate the power spectrum  $\approx 30$  percent of the time. By “nearly pure,” Belcher and Davis mean that the power in  $|B|$  and  $n$  was judged to be much less than that in the components, but not necessarily zero. This seems to be the case in figure 24, for example. The observations of Belcher and Davis that there is a strong correlation between  $V_r$  and  $B_r$  and that the coherence indicates outward-going waves were also made by Coleman. In effect, Belcher and Davis have taken the further step of discussing the subset of spectra for which  $P(B)/P(B_i)$  is very small. This process selects intervals where the ratio of Alfvén waves to compressive waves is large. Referring to figure 24 from Siscoe *et al.* [1968], this subset would occur at times of intermediate activity. This is consistent with remarks in Belcher and Davis [1971].

Coleman [1967, 1966b] assumed that the power in  $B$  was due to some kind of wave. He inferred that fast waves were the principal contributors. A compressive wave implies a positive correlation between  $n$  and  $B$ . Such a correlation was not examined by Coleman. However, Burlaga and Ogilvie [1970b] showed that changes in magnetic and thermal pressures tend to be anticorrelated on a scale of 0.01 AU. This is illustrated for a particular period in figure 25, which shows many

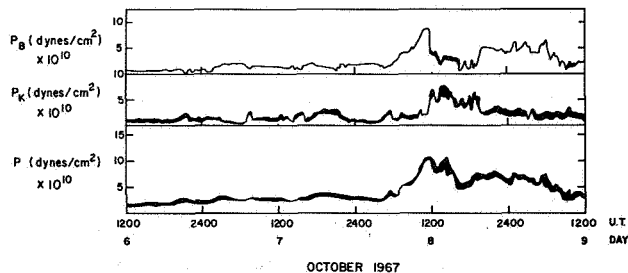


Figure 25. The magnetic pressure  $P_B$  and thermal pressure  $P_K$  tend to be anticorrelated on a scale of 0.01 AU, tending to keep the total pressure  $P_T$  constant on the scale, even though  $P_T$  changes on a larger scale. The anticorrelation suggests static features. These will contribute to the power spectrum of  $B$ .

changes in the magnetic pressure  $P_B = B^2/(8\pi)$  accompanied by opposite changes in the thermal pressure  $P_K \equiv nk(T + T_e)$ . Thus, it is possible that much of the power in  $B$  is due to convected structures (not necessarily discontinuities).

Sari and Ness [1969] showed that there are also times when the power levels in the components of  $B$  are due primarily to discontinuities. This is shown in figure 26,

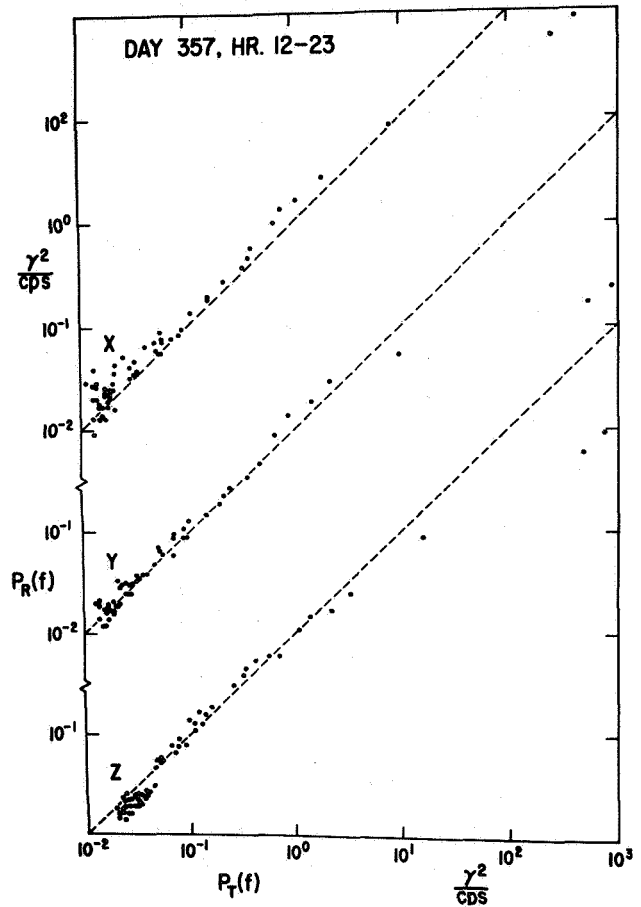


Figure 26. Discontinuities may dominate the power spectrum. The observed power  $P_R$  equals the power  $P_T$  computed from the observed discontinuities for the period indicated. Thus, the discontinuities alone can account for all of the power at this particular time.

which compares the observed power in the interval 1200–2400 UT on December 23, 1965, with the power computed from the discontinuities that were present. Clearly, the observed power can be accounted for by the discontinuities alone. The actual power spectrum for this time is shown in figure 27. The spectrum has the form  $f^{-2}$ , as predicted for a series of discontinuities. The power levels are rather low and geomagnetic

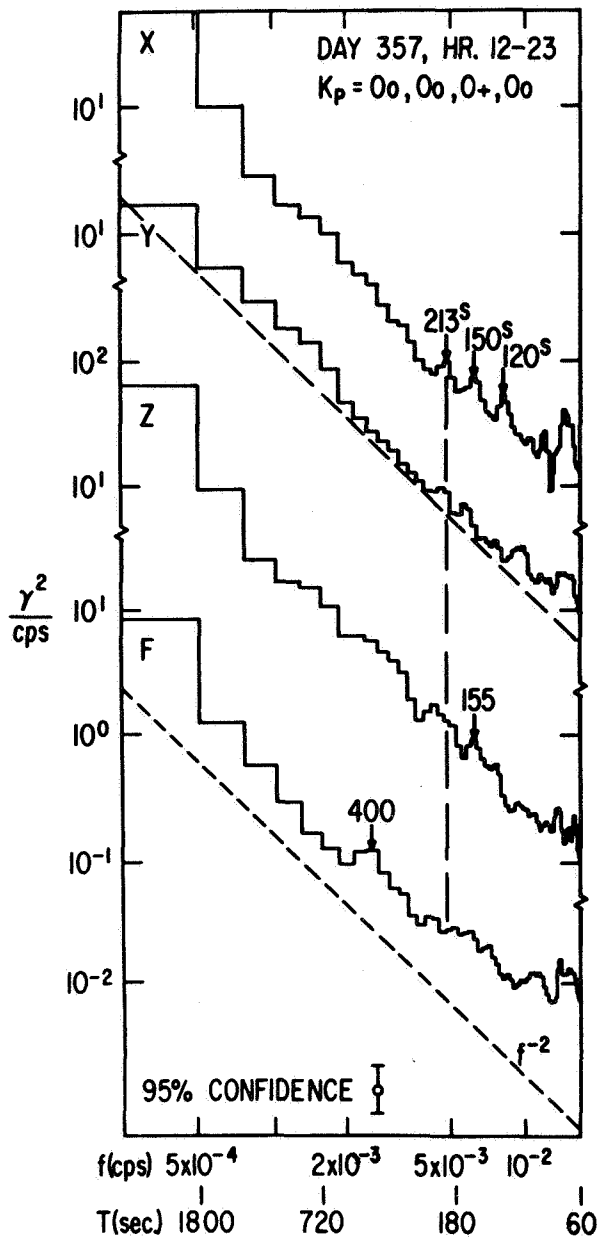


Figure 27. The observed power spectra for the period discussed in figure 26. The slopes are  $-2$ , as predicted for discontinuities.

activity, as indicated by  $K_p$ , was very low. The solar wind speed at that time was decreasing from 375 to 350 km/sec. Siscoe *et al.* [1968] also considered the possibility that discontinuities might dominate the spectrum, but found no evidence for it. Belcher *et al.* [1970] have challenged the results of Sari and Ness [1969]; see the reply by Ness *et al.* [1970]. Actually, they challenged a misinterpretation of the results in Sari and Ness, namely that discontinuities *always* dominate the power

spectrum. Sari and Ness [1970] themselves show that discontinuities are not always dominant. It seems to be agreed [Belcher *et al.*, 1970], that discontinuities can dominate the spectrum at times; the evidence is that given by Sari and Ness [1969].

#### Microscale Fluctuations of Burlaga *et al.* [1969]

The most important feature of these fluctuations is a strong correlation with the local value of  $\beta \equiv 8\pi nkT_p/B^2$ , as shown in figure 23. Very disturbed intervals are associated with high  $\beta$ , very quiet conditions with low  $\beta$ . The high  $\beta$  were due primarily to high temperatures.

Microscale fluctuations such as those shown in figure 23 are not common features of the data; out of  $\sim 2500$  hr examined, only 126 hr contained such fluctuations. Hour intervals with such fluctuations tend to be isolated. Less than 24 percent of such disturbed intervals occurred in pairs, and less than 20 percent in groups of more than 3-hr intervals.

Belcher and Davis [1971] challenged the result of Burlaga *et al.* [1969]. They assumed that the power in microscale fluctuations is measured by  $\sigma_{s1}$ , the square root of the 3-hr average of the 168.75-sec total variances in the magnetic field components. They found a low correlation between  $\sigma_{s1}$  and  $\beta$  ( $-0.12$ ), and suggested that this implies a conflict with the results of Burlaga *et al.* [1969]; an alternative, and correct, inference is that  $\sigma_{s1}$  is not a good measure of the type of fluctuations studied by Burlaga *et al.*

Burlaga *et al.* [1969] inferred that microscale fluctuations are generated locally. Belcher and Davis [1971] suggested that microscale fluctuations are generated by nonlocal properties such as stream structure.

#### Relation of Fluctuations to Bulk Speed of the Solar Wind

Many characteristics of the solar wind can best be organized and understood in reference to the bulk speed. Here we shall attempt to relate fluctuations and waves to the bulk speed. Unfortunately, little has been published on this as yet.

Neugebauer and Snyder [1966a, 1967] and Davis *et al.* [1966] showed that the 3-hr variances of the magnetic field from Mariner 2 were sometimes appreciably larger than average at the leading edge of high speed streams—where the bulk speed increases. The interpretation is that the fluctuations are abnormally large there. As pointed out earlier, it is not clear what physical characteristics  $\sigma$  really measures. Moreover, the magnitude of  $B$  also increases at positive bulk speed gradients,

so it is not clear that the relative level of activity  $\sigma/B$  is unusually high there. As shown by *Belcher and Davis* [1971], there is a strong correlation between  $\sigma$  and  $B$ .) Nevertheless, it is probably true that the power levels are unusually high in the interaction regions. Figure 28 from

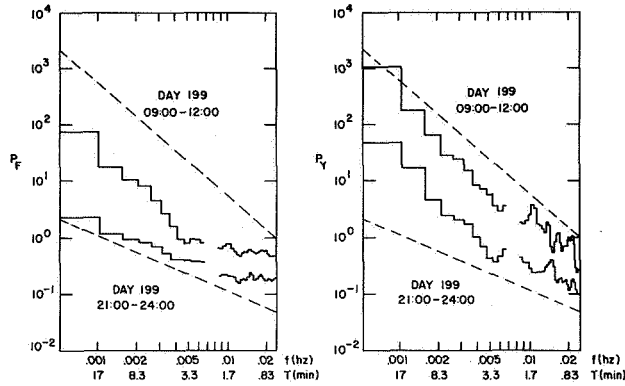


**Figure 28.** Power inside and outside an interaction region. The left panel shows power in  $|B|$ , the power in the right panel shows power in one of the ecliptic plane components. The top histogram in each panel is the power in the interaction region.

*Burlaga et al.* [1971] compares the power in the longitudinal and transverse fluctuation in an interaction region with that just outside the interaction region. The power is an order of magnitude higher in the interaction region. *Belcher and Davis* give some examples of the greater disturbances in  $B$  in interaction regions. They state that the largest Alfvénic fluctuations are found in interaction regions, but it is not clear how they identify Alfvén waves in an interaction region where  $|B|$  fluctuates appreciably. In any case, no matter how one measures the fluctuations, it is generally true that the magnetic field is highly disturbed in the interaction regions, both compressive and transverse fluctuations being present.

*Belcher and Davis* [1971] state that there is no discernible pattern of association between the presence of aperiodic Alfvén waves and high speed streams or sectors; i.e.,  $\rho$  is not related to the large-scale structure of the solar wind. However, *Belcher and Davis* offer the interesting hypothesis that the largest amplitude “pure” aperiodic Alfvén waves are found in high speed streams and on their trailing edges. This might be due to an association of such waves with high temperatures, since  $T$  is related to  $V$  [*Neugebauer and Snyder*, 1966b; *Burlaga and Ogilvie*, 1970a].

The lowest wind speeds are probably relatively free of magnetic field fluctuations, although the evidence to

support this is rather meager. *Belcher and Davis* state that Alfvén waves in low speed regions have smaller amplitude and are “less pure” than elsewhere. The intervals of low fluctuation intensity in *Sari and Ness* [1970] were associated with low bulk speeds.

In summary, the relation between fluctuations and bulk speed is poorly understood, but published results suggest the following working model. There are large fluctuations in  $B$  at positive gradients, presumably representing inward and outward propagating transverse and compressive waves generated there. There are transverse waves in the high speed streams and on their trailing edges whose intensity is proportional to the proton temperature. They may be remnants of a wave-heating process near the sun [*Alfvén*, 1947; *Parker*, 1963; *Burlaga and Ogilvie*, 1970a; *Hartle and Barnes*, 1970; *Belcher and Davis*, 1971; *Barnes et al.*, 1971]. Between streams, where the solar wind is in its base state in which there is presumably little or no wave heating beyond  $2 R_\odot$  [*Burlaga and Ogilvie*, 1970a; *Barnes et al.*, 1971], wave-like fluctuations in  $B$  but not discontinuities might be essentially absent. Again, this is a tentative working model, and further work is needed to substantiate it (fig. 29). *Hundhausen* [1970] discusses some of the problems with the Hartle-Barnes model.

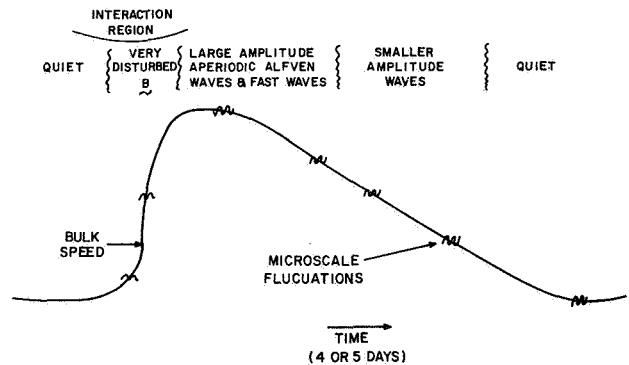


**Figure 29.** Hypothetical model of relations between the waves and fluctuations and the bulk speed.

#### Variation with Distance from the Sun

The only report of changes in the characteristics of fluctuations (as measured by power spectra) with distance from the sun is that of *Coleman et al.* [1969] based on Mariner 4 measurements over the distance 1 to 1.43 AU made in the period November 28, 1964, to July 14, 1965. The basic result is shown in figure 30, which gives the ratio of the power at 1.43 AU,  $[P_i(A)]_2$ , to that at 1.00 AU,  $[P_i(A)]_1$ , as measured by  $k$ , where  $[P_i(A)]_2/[P_i(A)]_1 = (1.43)^{-2k}$ . The positive  $k$  imply a

decrease of power with increasing distance from the sun. The decrease is seen in all components and at all frequencies in the range  $\approx 10^{-6}$  to  $\approx 10^{-2}$  Hz. The power in the magnetic field intensity decreases appreciably less rapidly than the power in the components. Thus, the ratio of power in the compressive fluctuations to that in the transverse fluctuations increases with distance from the sun. In other words, the compressive mode tends to become dominant and the Alfvén mode less significant as one moves away from the sun and earth. This assumes that the observed variations are not temporal changes.

Coleman *et al.* [1969] report that the average field intensity decreases as  $(r/r_0)^{-1.25}$ . This decrease is more rapid than that of the square root of the power. Thus, the magnetic field becomes increasingly disturbed and disordered as one moves from 1.0 to 1.4 AU. This result tends to support models of cosmic ray propagation that postulate a diffusing shell near the earth and beyond [Lüst and Simpson, 1957; Burlaga, 1969].

Figure 30 shows that the power in the fluctuations in  $B_\theta$ , normal to the ecliptic plane, decreases more rapidly than that in the ecliptic plane components  $B_r$  and  $B_\phi$ .

If the compressional oscillations studied by Coleman *et al.* [1969] are related to  $\beta$  as the microscale fluctuations studied by Burlaga *et al.* [1969], then one

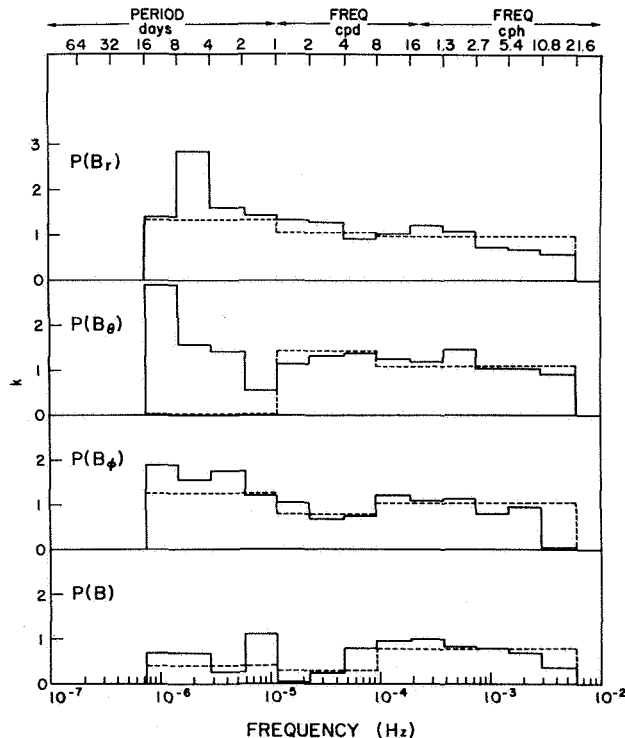


Figure 30. Ratio of the power densities at 1.4 and 1 AU, as parameterized by  $k$  (see text).

would expect the power in these fluctuations to be maximum just beyond the orbit of Mars (fig. 31). The

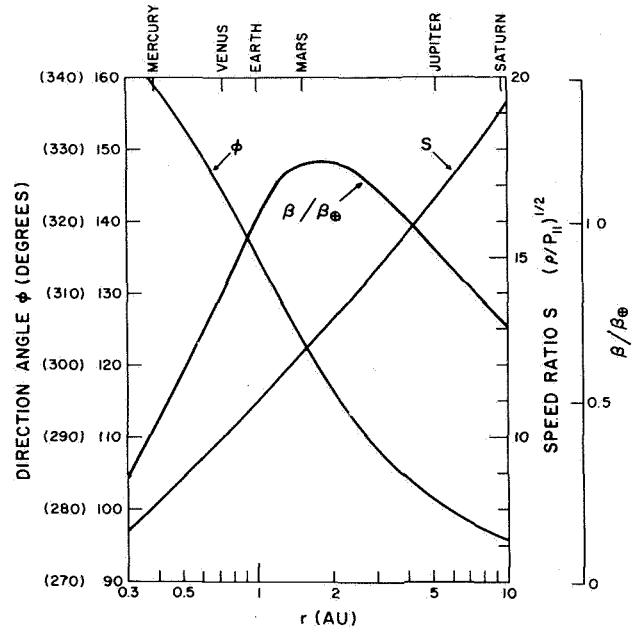


Figure 31. Variation of  $\beta$  with distance from the sun, relative to  $\beta$  at earth. The spiral angle and  $(\rho/P_\parallel)^{1/2}$  are also shown. The results are based on Whang's model of the solar wind.

figure indicates the corresponding shell should extend somewhat farther outward from Mars than inward toward the earth, unless other effects associated with the spiral angle  $\phi$  or sound speed ratio  $S$  become important. This hypothesis also implies a decrease in the power in compressional oscillations as one moves from earth to Venus (a point that could be tested with existing data), and it implies that this power would be very small at the orbit of Mercury and closer to the sun (a point that will be tested in 1973 and 1974 when the MVM and Helios spacecraft are launched.)

## SUMMARY

There are numerous tangential discontinuities in the solar wind, more or less evenly distributed between 0.8 and 1.0 AU. The discontinuity surfaces are separated by  $\approx 0.01$  AU and are probably appreciably bent and curved on that scale. They tend to be aligned along the spiral direction, but the orientation changes from one surface to the next. There is generally no obvious pairing, so it is more appropriate to say that the solar wind is discontinuous than to say that it is filamentary. Filamentary forms do sometimes occur, however. Most discontinuities are characterized by changes in the magnetic field

direction with little or no change in the magnitude. When the magnitude does change, there is usually a corresponding opposite change in the plasma density. Rotational discontinuities may occur at the rate of  $\approx 1/\text{day}$ , corresponding to separations  $\approx 0.25$  AU. *Belcher and Davis* [1971] and *Smith et al.* [1970] suggested that rotational discontinuities occur at the rate of  $1/\text{hr}$  but they gave no evidence for this. The observations discussed by *Burlaga* [1970a] and by *Siscoe et al.* [1968] suggest that tangential discontinuities are present every day. The failure of *Belcher and Davis* [1971] to observe tangential discontinuities is probably due to the fact that they used 5-min averages (or longer), which would tend to obscure any microstructural discontinuities that were present.

Sinusoidal waves are very seldom seen in the solar wind, but random fluctuations seem to be the rule. These fluctuations are best described by power spectra when there is little damping of them. The principal contributors to the power are probably (1) Alfvén waves, (2) fast waves, (3) static structures in which  $B$  and  $n$  are anticorrelated, and (4) discontinuities. Discontinuities dominate the power spectra occasionally in the range  $\approx 5 \times 10^{-4}$  to  $\approx 10^{-2}$  Hz, but probably they usually make only a small contribution. Usually the power in  $B$  is only a fraction ( $\leq 0.3$ ) of that in the components, and fluctuations in  $V$  are often correlated with the fluctuations in  $B$ . This has led *Belcher and Davis* [1971] to imply that Alfvén waves are the principal contributors to the typical power spectrum. Coleman has pointed out that pure Alfvén waves are never present for periods of 12 hr or more, since there is always appreciable power in  $B$ , and he suggested that the compressive fluctuations are due to fast waves. The relative contribution of fast waves and static structures to the power in  $B$  remains to be determined, however.

Little is known about the relation of discontinuities and fluctuations to the large-scale structure. There is evidence that discontinuities show a sector-dependent north-south asymmetry, and they are not associated with positive bulk speed gradients. It has been suggested that fluctuations can be related to the bulk speed, having the largest amplitudes when the speed is high and decreasing amplitudes with decreasing speeds. This hypothesis fits in nicely with the idea that the fluctuations originate in the region close to the sun which heats and accelerates the solar wind. But a comprehensive study of the relation between power levels or wave amplitudes and bulk speed has not yet been made. There appears to be more than average power in both transverse and compressional oscillations at positive bulk speed gradients, presumably due to the collision of a high speed

stream with slower plasma, but the fluctuations generated in this way do not propagate away from the interaction region.

There are also isolated "patches" of enhanced, high frequency transverse and compressional fluctuations, which are correlated with  $\beta$ , some of which might be due to local instabilities.

Very little is known about the radial dependence of discontinuities and fluctuations. No significant radial dependence of discontinuities has been observed between 0.8 and 1.0 AU. A relative increase of compressional fluctuations from 1.0 to 1.4 AU has been suggested, and might be related to an increase with  $\beta$ . Basically, however, the question of radial dependence will not be answered until observations from deep space probes are available.

We now know more or less how to interpret  $B(t)$  in terms of hydromagnetic structures. The next step will be to analyze discontinuities and power spectra for extended periods of time, to relate these results to the larger scale structures of the solar wind, and to identify the origin of these structures.

#### ACKNOWLEDGMENTS

The author wishes to thank N. Ness and K. Ogilvie for their comments on the manuscript, and J. Belcher, L. Davis, and E. Smith for helpful discussions. Dr. Y. C. Whang kindly provided figure 31.

#### REFERENCES

- Alfvén, H.: Granulation, Magnetic-Hydrodynamic Waves, and the Heating of the Solar Corona. *Mon. Notic. Roy. Astron. Soc.*, Vol. 107, 1947, p. 211.
- Barnes, A.; Hartle, R. E.; and Bredekamp, J. H.: On the Energy Transport in Stellar Winds. Submitted to *Astrophys. J.*, 1971.
- Belcher, J. W.; Coleman, P. J., Jr.; Davis, L., Jr.; Jones, D. E.; and Smith, E. J.: Waves and Discontinuities in the Solar Wind. Preprint, 1970.
- Belcher, J. W.; and Davis, L., Jr.: Large Amplitude Alfvén Waves in the Interplanetary Medium: 2. *J. Geophys. Res.*, Vol. 76, 1971, p. 3534.
- Belcher, J. W.; Davis, L., Jr.; and Smith, E. J.: Large-Amplitude Alfvén Waves in the Interplanetary Medium: Mariner 5. *J. Geophys. Res.*, Vol. 74, 1969, p. 2302.
- Burlaga, L. F.: Microscale Structures in the Interplanetary Medium. *Solar Phys.*, Vol. 4, 1968, p. 67.
- Burlaga, L. F.: Directional Discontinuities in the Interplanetary Magnetic Field. *Solar Phys.*, Vol. 7, 1969, p. 57.

- Burlaga, L. F.: On the Nature and Origin of Directional Discontinuities. NASA-Goddard Space Flight Center Preprint X-692-70-462; Submitted to *J. Geophys. Res.*, 1970a.
- Burlaga, L. F.: Discontinuities and Shock Waves in the Interplanetary Medium and Their Interaction with the Magnetosphere. NASA-Goddard Space Flight Center Preprint X-692-70-95, 1970b.
- Burlaga, L. F.: Hydromagnetic Waves and Discontinuities in the Solar Wind. NASA-Goddard Space Flight Center Preprint X-692-70-95, in press, *Space Sci. Rev.*, 1971.
- Burlaga, L. F.; and Chao, J. K.: Reverse and Forward Slow Shocks in the Solar Wind. NASA-Goddard Space Flight Center Preprint X-692-71-66, to be published, 1971.
- Burlaga, L. F.; and Ness, N. F.: Macro- and Micro-Structure of the Interplanetary Magnetic Field. *Can. J. Phys.*, Vol. 46, 1968, p. S962.
- Burlaga, L. F.; and Ness, N. F.: Tangential Discontinuities in the Solar Wind. *Solar Phys.*, Vol. 9, 1969, p. 467.
- Burlaga, L. F.; and Ogilvie, K. W.: Heating of the Solar Wind. *Astrophys. J.*, Vol. 159, 1970a, p. 659.
- Burlaga, L. F.; and Ogilvie, K. W.: Magnetic and Thermal Pressures in the Solar Wind. *Solar Phys.*, Vol. 15, 1970b, p. 61.
- Burlaga, L. F.; Ogilvie, K. W.; and Fairfield, D. H.: Microscale Fluctuations in the Interplanetary Magnetic Field. *Astrophys. J.*, Vol. 155, 1969, p. L171.
- Burlaga, L. F.; Ogilvie, K. W.; Fairfield, D. H.; Montgomery, M. D.; and Bame, S. J.: Energy Transfer at Colliding Streams in the Solar Wind. *Astrophys. J.*, Vol. 164, in press, 1971.
- Colburn, D. S.; and Sonett, C. P.: Discontinuities in the Solar Wind. *Space Sci. Rev.*, Vol. 5, 1966, p. 439.
- Coleman, P. J., Jr.: Variations in the Interplanetary Magnetic Field: Mariner 2, 1, Observed Properties. *J. Geophys. Res.*, Vol. 71, 1966a, p. 5509.
- Coleman, P. J., Jr.: Hydromagnetic Waves in the Interplanetary Plasma. *Phys. Rev. Letters*, Vol. 17, 1966b, p. 207.
- Coleman, P. J., Jr.: Wave-like Phenomena in the Interplanetary Plasma: Mariner 2: *Planet. Space Sci.*, Vol. 15, 1967, p. 953.
- Coleman, P. J., Jr.; Smith, E. J.; Davis, L., Jr.; and Jones, D. E.: The Radial Dependence of the Interplanetary Magnetic Field: 1.0-1.5 AU. *J. Geophys. Res.*, Vol. 74, 1969, p. 2826.
- Davis, L.; Smith, E. J.; Coleman, P. J.; and Sonett, C. P.: in *The Solar Wind*, edited by R. J. Mackin, Jr., and Marcia Neugebauer. Pergamon Press, 1966, p. 35.
- Hartle, R. E.; and Barnes, A.: Nonthermal Heating of the Solar Wind. *J. Geophys. Res.*, Vol. 75, 1970, p. 6915.
- Hudson, P. D.: Discontinuities in an Anisotropic Plasma and Their Identification in the Solar Wind. *Planet. Space Sci.*, Vol. 18, 1970, p. 1611.
- Hundhausen, A. J.: Composition and Dynamics of Solar Wind Plasma. *Rev. Geophys. Space Phys.*, Vol. 8, 1970, p. 724.
- Jeffrey, A.; and Taniuti, T.: *Non-linear Wave Propagation*. Academic Press, London, 1964.
- Jokipii, J. R.; and Hollweg, J. V.: Interplanetary Scintillations and the Structure of Solar Wind Fluctuations. *Astrophys. J.*, Vol. 160, 1970, p. 745.
- Kubo, H.; Kawashima, N.; and Itoh, T.: Simulation Experiment on the Tail of Type 1 Comets. *J. Geophys. Res.*, Vol. 75, 1970, p. 1937.
- Landau, L. D.; and Lifshitz, E. M.: *Electrodynamics of Continuous Media*. Pergamon, London, 1960.
- Lüst, R.; and Simpson, J. A.: Initial Stages in the Propagation of Cosmic Rays Produced by Solar Flares. *Phys. Rev.*, Vol. 108, 1957, p. 1563.
- Michael, F. C.: Model of Solar Wind Structure. *J. Geophys. Res.*, Vol. 72, 1967, p. 1917.
- McCracken, K. G.; and Ness, N. F.: The Collimation of Cosmic Rays by the Interplanetary Magnetic Field. *J. Geophys. Res.*, Vol. 71, 1966, p. 3315.
- Ness, N. F.: Simultaneous Measurements of the Interplanetary Magnetic Field. *J. Geophys. Res.*, Vol. 71, 1966, p. 3319.
- Ness, N. F.; Burlaga, L. F.; Ogilvie, K. W.; and Sari, J. W.: Comments on Waves and Discontinuities in the Solar Wind. NASA-Goddard Space Flight Center Preprint X-692-70-460, 1970.
- Ness, N. F.; Scarce, C. S.; and Cantarano, S.: Preliminary Results from the Pioneer 6 Magnetic Field Experiment. *J. Geophys. Res.*, Vol. 71, 1966, p. 3305.
- Neugebauer, M.; and Snyder, C. N.: in *The Solar Wind*, edited by R. J. Mackin, Jr., and Marcia Neugebauer. Pergamon Press, London, 1966a, p. 21.
- Neugebauer, M.; and Snyder, C. W.: Mariner 2 Observations of the Solar Wind, 1, Average Properties. *J. Geophys. Res.*, Vol. 71, 1966b, p. 4469.
- Neugebauer, M.; and Snyder, C. W.: Mariner 2 Observations of the Solar Wind Relation of Plasma Properties to the Magnetic Field. *J. Geophys. Res.*, Vol. 72, 1967, p. 1823.
- Parker, E. N.: *Interplanetary Dynamical Processes*. Interscience, New York, 1963.



- Quenby, J. F.; and Sear, S. F.: Interplanetary Magnetic Field Irregularities and the Solar Proton Diffusion Mean Free Path During the February 25, 1969 Event. *Planet. Space Sci.*, Vol. 19, 1971, p. 95.
- Sari, J. W.; and Ness, N. F.: Power Spectra of the Interplanetary Magnetic Field. *Solar Phys.*, Vol. 8, 1969, p. 155.
- Sari, J. W.; and Ness, N. F.: Power Spectral Studies of the Interplanetary Magnetic Field. Proc. 11th Int. Conf. on Cosmic Rays, Vol. 2. *Acta Phys. Acad. Sci. Hungar.*, Vol. 29, Suppl. 373, 1970.
- Siscoe, G. L.; and Coleman, P. J., Jr.: On the North-South Asymmetry in the Solar Wind. *Solar Phys.*, Vol. 8, 1969, p. 415.
- Siscoe, G. L.; Davis, L., Jr.; Coleman, P. J., Jr.; Smith, E. J.; and Jones, D. E.: Power Spectra and Discontinuities of the Interplanetary Magnetic Field: Mariner 4. *J. Geophys. Res.*, Vol. 73, 1968, p. 61.
- Smith, E. J.; Belcher, J.; Davis, L., Jr.; and Coleman, P. J., Jr.: The Identification of Interplanetary Field Fluctuations as Traveling Waves (Abstract). *EOS*, Vol. 51, 1970, p. 412.
- Turner, J. M.; and Siscoe, G. L.: Orientations of 'Rotational' and 'Tangential' Discontinuities in the Solar Wind. *J. Geophys. Res.*, Vol. 76, 1971, p. 1816.
- Unti, T. W.; and Neugebauer, M.: Alfvén Waves in the Solar Wind. *Phys. Fluids*, Vol. 11, 1968, p. 563.

*J. R. Jokipii* Would you care to estimate the relative contributions to the power spectrum, say at periods of about 10 min, of the tangential discontinuities and the rotational or wave type? DISCUSSION

*L. F. Burlaga* We will have to look at the data to find out.

*C. P. Sonett* I was under the assumption that Alfvén waves are linear, no matter what their amplitude. Am I correct?

*L. F. Burlaga* I see heads nodding yes, and heads shaking no. I think that shows the problem. What are we going to call an Alfvén wave? Perhaps Professor Davis can give us his opinion.

*L. Davis* I will give my own personal definition of an Alfvén wave. I start with perhaps the oldest definition, which implies an incompressible fluid in which the wave amplitude is not important and Alfvén waves of very high amplitude are possible. Historically, I think the Alfvén wave in a plasma came next. This is usually derived by a linearized treatment, and the restriction to small amplitude is probably important. However, the Alfvén disturbance does not produce any compression of the plasma and you can't tell from the behavior of the fluid whether or not it is compressible. There is a second-order change in field strength which changes the total pressure; if the medium is compressible, large-amplitude Alfvén waves will be modified. The observations in space reveal waves which have the characteristics of Alfvén waves in their correlation between velocity and magnetic field fluctuations, but they are large amplitude and the plasma in space is not incompressible. I would still like to characterize them as Alfvén waves, using an extended definition of the term, although I agree that we have to explore the problem mathematically much more than we have.

Turning now to a question of my own, there seems to be considerable confusion as to the dividing line between microscale and mesoscale structures. Is a feature with a length of approximately 0.01 AU that takes a half hour to go by microscale or mesoscale? In the discussion we just heard there was some indication that the 1 hr referred to the length of the plot that was used, not to the length of the feature, and that the feature had to be significantly shorter than an hour. This is a matter that the people who invent these definitions should make clear to those who want to use them.

*L. F. Burlaga* Let us agree to use the term *microscale* to refer to features with a scale length of  $\approx 0.01$  AU or less, and fluctuations with Doppler-shifted periods  $\lesssim 1$  hr. *Mesoscale* features are from 1 to  $\sim 100$  hr.

*M. Dryer* I recall a definition of rotational discontinuities, given by Landau, in which the Alfvénic Mach number normal to the discontinuity is equal to 1 on both sides of the discontinuity. If no component of the field gives unity Alfvén Mach number normal to the discontinuity, then the discontinuity is a *tangential* or *contact* discontinuity.

*L. F. Burlaga* I know that's a necessary condition for an isotropic medium. I don't know if it's sufficient to define a rotational discontinuity.

*M. Dryer* I guess what I'm trying to advocate is the use of some of these fundamental descriptions as given in the classical literature.

*L. F. Burlaga* The trouble is, Murray, that the data are not mathematically precise. We might have, say, a nonzero normal component that is less than the experimental uncertainties. In this case we can't distinguish between a rotational and tangential discontinuity. That's why we used directional discontinuities and other simple discontinuities which showed relatively large changes. I think the accuracy of the data is sufficient that we can test the necessary conditions in such cases.

*M. Dryer* In your first figure there's a small perturbation. Is that a rotational discontinuity?

*L. F. Burlaga* If there is a component of  $B$  normal to the discontinuity surface, then it is probably a rotational discontinuity. The rotational part is then the projection of  $B$  in the plane of the discontinuity surface. If it's a tangential discontinuity, there is no component of  $B$  normal to the surface or the current sheet.

*L. Davis* Is it strictly a question of whether there's a normal component?

*L. F. Burlaga* No, that's just one necessary condition. There are others. The condition that I was referring to in figure 5, the histogram, is the necessary condition that relates the change in velocity to the change in the field. Essentially, it is the type of condition that you see for an Alfvén wave:  $\Delta V$  is proportional to  $\Delta B$ . The proportionality constant involves the Alfvén speed. That is a necessary condition for a rotational discontinuity. What I showed is that that condition is not generally satisfied for the directional discontinuities, therefore they are not rotational.

*L. Davis* I think part of our confusion arises because the term *rotational discontinuity* is used in a variety of ways and some of us are trying to find out how you are using it.

*L. F. Burlaga* I'm using it the way Landau and Lifshitz used it.

*C. P. Sonett* If these waves are nonlinear, then I would assume that they must steepen with time and ultimately become shocks, infinitesimal or finite shocks, depending on the particular situation. I suppose this depends also on their lifetime.

*L. F. Burlaga* I don't know if they necessarily do steepen. It's been argued that Alfvén waves don't steepen into shocks, and I think that's just one of the questions one must answer by a nonlinear treatment.

*D. S. Intriligator* In reference to your illustration of the power spectra for the different components of the magnetic field, a similar analysis for the velocity of the plasma shows no comparable effect as a function of whether the intervals are quiet or disturbed. We find that, in general, the level of power and the slope is the same for each component of the velocity,  $V_r$ ,  $V_\theta$ , and  $V_\phi$ .

*L. F. Burlaga* That would imply, then, that they are not Alfvén waves? Do you agree?

*D. S. Intriligator* We haven't yet looked at the simultaneous power spectra for the magnetic field.

*P. A. Sturrock* Have any structures been detected similar to the "solitary waves" discussed by Adlam and Allen, *Phil. Mag.* 3, 448, (1958) and others?

*F. L. Scarf* I think there are certain structures seen near the bow shock that look very much like these solitary pulses that they discussed. I would, however, like to defer this discussion. Our program includes many more talks on Alfvén waves and other low-frequency turbulence in the solar wind, so we will all have an opportunity to continue with the questions and comments later.

## MICROSCALE FLUCTUATIONS IN THE SOLAR WIND *Aaron Barnes*

An invited review

Theoretical constraints on the interpretation of fluctuations (either propagating or stationary) in the interplanetary medium are reviewed, with emphasis on the important differences between the properties of hydromagnetic waves (and stationary structures) in collisionless and in collision-dominated plasmas, and on the possible roles of Landau damping and nonlinear effects in determining the interplanetary fluctuation spectrum. Hypotheses about the origins of the fluctuations and their influence on the large-scale properties of the solar wind are reviewed.

### ABSTRACT

### INTRODUCTION

There are three main reasons for interest in fluctuations in the solar wind. One, of course, is that by studying waves or other fluctuations we can hope to learn their origins, and consequently learn something about the solar wind or even the sun itself. Second, the interplanetary fluctuations may participate actively in the large-scale dynamics of the solar wind. Finally, the solar wind, as well as other regions accessible by spacecraft, provide an opportunity to study plasma fluctuations under conditions very different from those in any terrestrial laboratory.

Much recent discussion has been directed at the question of the nature of microfluctuations (length scale  $\lesssim 0.01$  AU) in the interplanetary medium. In particular, there is disagreement among observers about the following two questions: (1) Are these fluctuations associated with waves propagating relative to the solar wind, or are they simply structures that are stationary in the local solar-wind rest frame? (2) Do these fluctuations vary smoothly in space, or are they principally discontinuities—structures whose length scale is comparable to or smaller than the proton gyroradius ( $\sim 100$  km at 1 AU)? The two questions are logically separate, since both waves and stationary structures of sufficiently short length scale can appear as discontinuities. The resolution of these questions is necessary for

understanding the sources of the fluctuations and their role in solar wind dynamics. In view of the present uncertainties, it is desirable to review what theoretical constraints can be placed on the interpretation of the observed fluctuations.

These constraints will be one of the topics discussed here. We consider mainly fluctuations of hydromagnetic scale in the sense that their characteristic dimension is long compared with the proton gyroradius (period  $\gtrsim$  a few seconds in the spacecraft frame at 1 AU). Presumably these fluctuations correspond to observed discontinuities for sufficiently short length scale. We first review the physical processes that can influence the fluctuation spectrum away from its sources. It will be seen that collisionless dissipation and nonlinear effects may be of extreme importance in this respect. We then consider the various possible sources of fluctuations in the solar wind, and some of the ways in which fluctuations can influence the large-scale properties of the wind.

### HYDROMAGNETIC FLUCTUATIONS

By definition, a hydromagnetic wave in a magnetized conducting medium is a propagating fluctuation whose characteristic time and length scales are long compared with, respectively, the gyrofrequencies and mean Larmor radii of the particles that make up the medium. Implicit in this definition is the assumption that the periods and

---

*The author is at the Space Science Division, Ames Research Center, NASA, Moffett Field, California.*

wavelengths of the fluctuations are short in comparison with the time and length scales for significant changes in the average properties of the medium. Just as large-scale motions in an ordinary gas are associated with sound waves, the large-scale motions in a magnetized conducting fluid are associated with hydromagnetic waves. We can expect such processes as the violent stirring in the solar photosphere, chromosphere and corona, or the collision between fast and slow solar-wind streams, among others, to be associated with the generation of hydromagnetic waves.

The simplest approach to the theory of hydromagnetic waves is through the equations of magnetohydrodynamics [Kantrowitz and Petschek, 1966; Landau and Lifshitz, 1960]. Although these equations (which describe the behavior of collision-dominated ionized gases) cannot properly be used to describe hydromagnetic waves in the solar-wind plasma, where collisionless effects are important, they do provide a useful set of concepts and definitions that help to order the complexities of the collisionless theory. Hence, it is useful to review briefly the main results of the MHD theory of hydromagnetic waves.

First, consider the case in which the amplitudes of the fluctuations are small enough that the MHD equations can be linearized with the usual assumptions that the electrical conductivity of the medium is infinite and that the fluctuations are thermally adiabatic. The self-consistent solutions of the MHD equations admit three true wave modes (the Alfvén mode, and the fast and slow magnetoacoustic modes) and two classes of stationary fluctuations (the so-called entropy wave and the tangential pressure balance). The Alfvén wave is transverse and involves no compression of the fluid or magnetic field. The fast and slow magnetoacoustic waves generally involve compressions of both the fluid and magnetic field; in the limit of strong magnetic field the fast mode propagates with the Alfvén speed for all directions of propagation, and in the limit of weak magnetic field the fast mode becomes a sound wave. The entropy wave is a static structure involving variation of fluid density and temperature, but not of pressure, magnetic field or velocity. The tangential pressure balance can occur only for variations that are transverse to the magnetic field and for which the total pressure (fluid plus magnetic) does not fluctuate.

When finite-amplitude effects are significant, the fast and slow magnetoacoustic waves behave like sound waves in the sense that they can steepen and form shocks. On the other hand, the Alfvén wave is more like an elliptically polarized electromagnetic wave. Even when its amplitude is large, it retains many of its

small-amplitude features: It is noncompressive, and the relation between velocity and magnetic-field fluctuations is the same as in the linearized theory. The finite-amplitude Alfvén wave may have any polarization consistent with constant magnitude of the fluctuation field (hence, for example, linear polarization is forbidden). It does not steepen to form shocks in a homogeneous medium.

There are other important nonlinear effects. Nonlinear wave decay and mode coupling may occur, even for the Alfvén wave. In the case of the magnetoacoustic modes, there are shock waves. In the limit of zero wavelength, the Alfvén wave is known as the *rotational* discontinuity, the entropy wave as the *contact* discontinuity, and the tangential pressure balance as the *tangential* discontinuity. Being stationary structures, the entropy wave and tangential pressure balance are not subject to steepening effects, but may be unstable under some circumstances.

### COLLISIONLESS HYDROMAGNETIC WAVES

The preceding magnetohydrodynamic picture must be modified in situations in which collisionless effects are important—when the wave frequencies are large compared with the Coulomb collision frequencies of the plasma particles. In this sense the protons, and to a large extent the electrons, are collisionless with respect to most interesting hydromagnetic waves throughout the solar wind. For example, at 1 AU protons are collisionless with respect to waves of period shorter than about 12 hr (as measured in the spacecraft frame), and electrons are collisionless with respect to periods shorter than about 3 hr. At heliocentric distance  $r = 2R_{\odot}$ , protons and electrons are collisionless with respect to wave periods shorter than about 10 min, and 20 sec, respectively. Hence, to understand hydromagnetic waves in the solar wind, a collisionless theory is required.

The wave mode that is least changed by collisionless effects is the Alfvén wave [Stepanov, 1958; Barnes, 1966; Tajiri, 1967]. In the limit of small amplitude, this wave is transverse, and its energy flux (as viewed in the rest frame of the plasma) is always parallel to the mean magnetic field direction. Its phase velocity follows from the dispersion relation

$$\begin{aligned} \left[ \frac{\omega}{k_{\parallel}} \right]^2 &= \frac{B^2}{4\pi\rho} \left[ 1 + \frac{4\pi}{B^2} (P_{\perp} - P_{\parallel}) \right] \\ &= C_A^2 \left[ 1 + \frac{4\pi}{B^2} (P_{\perp} - P_{\parallel}) \right] \end{aligned}$$

Here  $\omega$  is the circular frequency and  $k_{\parallel}$  is the component of the wave vector parallel to the magnetic field,  $B$  is the magnetic field strength,  $\rho$  is the mass density,

$P_{\parallel, \perp}$  are the components of total fluid pressure transverse and parallel to the magnetic field direction, and  $C_A$  is the usual Alfvén speed. The collisionless character of the plasma appears only through the pressure anisotropy. As is well known, this mode becomes nonresonantly unstable if  $P_{\parallel}/P_{\perp}$  is large enough that the right-hand side of the preceding expression is negative. Counterstreaming of different ion species along the magnetic field lines can produce similar effects. If a significant high-energy tail of the proton velocity distribution is present, the Alfvén mode can be further modified by wave-particle cyclotron resonance, with consequent damping or growth of the wave.

As in the MHD theory, the collisionless Alfvén mode is not greatly modified by finite-amplitude effects [Barnes and Suffolk, 1971]. It is still noncompressive, the usual relation between velocity and magnetic-field fluctuations still holds, and the magnetic field associated with the wave is of constant magnitude. Its polarization is indeterminate, except for the requirement that the magnitude of the fluctuating field be constant, which of course rules out plane polarization. These conclusions are valid for Alfvén waves of arbitrary amplitude. It may also be shown that these statements are valid even when relativistic effects are important (although the dispersion relation is somewhat modified by relativity). In particular, the criterion for the firehose instability is unchanged by relativity and finite-amplitude effects.

However, just as in the MHD case, the fact that large-amplitude Alfvén waves are very much like their small-amplitude counterparts does not mean that the large-amplitude waves may be superposed as in the linearized theory. Two large-amplitude Alfvén waves interact in a nonlinear manner, generating turbulence in other wave modes. In fact, a large-amplitude Alfvén wave may be unstable against decay, an effect that may be of importance for understanding solar-wind turbulence.

Although the properties of the Alfvén mode in a stable plasma do not depend much on whether the plasma is collisionless or collision-dominated, the collisionless magnetoacoustic modes differ radically from their MHD counterparts. This difference is due to the strong resonant wave-particle energy exchange that can occur in the collisionless case, usually resulting in strong collisionless damping of magnetoacoustic modes [Stepanov, 1958; Barnes, 1966; Tajiri, 1967]. The resonant interaction of importance here involves particles whose motion along the magnetic field is such that they see the wave frequency Doppler shifted to zero—that is,  $v_{\parallel} = \omega/k_{\parallel}$ , where  $v_{\parallel}$  is the component of particle velocity along the magnetic field,  $\omega$  is the circular

frequency of the wave, and  $k_{\parallel}$  is the component of the wave vector along the magnetic field. This kind of resonance is usually called Landau resonance, as opposed to cyclotron resonance, which occurs when the resonant particles see the wave frequency Doppler shifted to an integral multiple of their gyrofrequency. Cyclotron resonance is normally negligible for hydromagnetic waves, but Landau resonance is not.

Physically, the resonant acceleration is due to the fact that in a collisionless plasma a gradient in *magnitude* of the magnetic field accelerates the guiding center of a particle along the magnetic field [Barnes, 1967]. This acceleration tends to produce a small charge separation and an associated electric field parallel to the magnetic field; this electric field, which also contributes to the resonant energy exchange, is proportional to the gradient in the magnetic field magnitude, and vanishes if this gradient vanishes. Hence the resonant energy exchange depends on the presence of fluctuations in magnetic field magnitude in the wave. Therefore, this interaction will occur for magnetoacoustic waves, but not for Alfvén waves, because the Alfvén mode is associated with fluctuations in *direction*, but not magnitude, of the magnetic field.

Consider a stable collisionless hydrogen plasma whose components have bi-maxwellian velocity distributions. In such a plasma the resonant acceleration always produces damping of the waves. An example of this damping is shown in figure 1. The theoretical damping rate per unit frequency  $|Im(\omega)/Re(\omega)|$  is plotted as a function of propagation direction, for small-amplitude magnetoacoustic waves in plasmas whose proton and electron temperatures are equal and isotropic. The resonant heating and consequent damping are maxima for directions of propagation such that  $\omega/k_{\parallel}$  is roughly

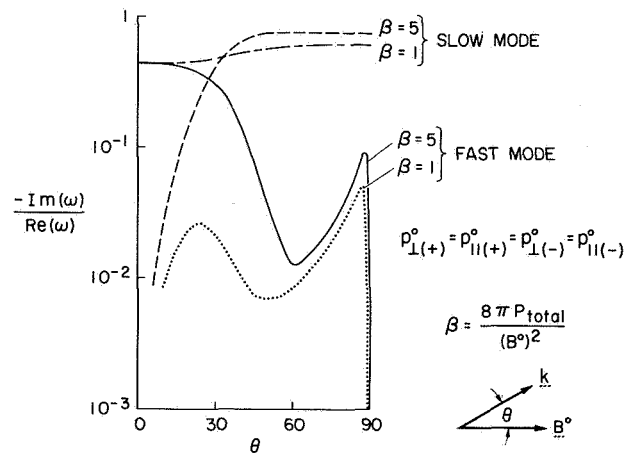


Figure 1. Damping rate versus propagation direction for magnetoacoustic waves in two isotropic plasmas.

equal to the proton and electron thermal speeds. The resonant heating, especially for the ions, is sensitive to average plasma conditions, because the heating rate is largely determined by the number of particles available for resonance. For maxwellian proton distributions, the proton heating rate per unit wave energy for the least-damped mode is roughly proportional to  $\exp - [1/\beta_p \cos^2 \theta]$  where  $\beta_p = 8\pi n_p K T_p / B^2$ ,  $n_p$  and  $T_p$  are the proton number density and temperature,  $B$  is the magnetic field strength, and  $K$  is Boltzmann's constant. Thus the damping depends strongly on  $\beta_p$ , the ratio of the proton pressure to magnetic pressure. If  $\beta_p \gtrsim 1$ , the damping is strong, but as  $\beta_p \rightarrow 0$ , the damping becomes exponentially weak. This dependence is illustrated below:

$\beta_p$	Characteristic time of strongest proton damping
1	$\sim 2$ wave periods
0.5	$\sim 10$ wave periods
0.2	$\sim 200$ wave periods

If one takes typical solar-wind parameters at 1 AU as number density  $n = 7$  protons  $\text{cm}^{-3}$ , proton temperature  $T_p = 4 \times 10^4$  K, and magnetic field  $B = 5 \times 10^{-5}$  gauss, the resulting  $\beta_p = 0.4$ . The observational study of *Burlaga et al.* [1969] indicates that this parameter can range from less than 0.1 to more than 5.0. If we suppose that  $\beta_p \sim 0.3$  to 0.5 for most of the distance between the sun and the orbit of earth, compressive hydromagnetic waves will be damped out in 10 to 100 wavelengths. Thus it is unlikely that magnetoacoustic waves of wavelength  $\lesssim 0.01$  AU (spacecraft wave period  $\lesssim 1$  hr) could propagate from the sun to the earth. Presumably any magnetoacoustic waves in the solar wind near 1 AU are of relatively local origin.

In this connection it should be noted that this damping mechanism can be modified by distortion of the proton or electron velocity distributions. In particular, it is possible to distort the velocity distributions in such a way that the sign of the damping rate is changed — that is, the wave amplitude grows. The possibility that such a process actually generates waves in the interplanetary medium will be discussed later.

### COLLISIONLESS STATIONARY STRUCTURES

It is also important to consider how the absence of collisions modifies the MHD picture of stationary, nonpropagating structures—namely, the tangential pressure balance (or tangential discontinuity) and the “entropy wave” (or contact discontinuity). It turns out

that the tangential pressure balance is essentially the same in collisionless as in collisional plasma. One can easily show from the guiding-center theory that equilibrium obtains for plane variations transverse to the magnetic field in an infinite plasma if

$$\begin{aligned} \nabla(P_{\perp} + B^2)/8\pi &= 0 \\ J_{\parallel}^D B &= (P_{\perp} + B^2/4\pi)\mathbf{e} \cdot \nabla \times \mathbf{e} \end{aligned}$$

Here  $P_{\perp}$  is the total fluid pressure (including the electrons) transverse to the magnetic field  $\mathbf{B}$ ,  $\mathbf{e}$  is the unit vector in the direction of  $\mathbf{B}$ , and  $J_{\parallel}^D$  is the current parallel to  $\mathbf{B}$  due to motions of the particle guiding centers along the field lines. The first equation is the usual transverse pressure balance condition, and the second equation specifies the current required to support the shear in the magnetic field. It should be reemphasized that this equilibrium is possible only if all gradients are transverse to the magnetic-field direction. Components of flow velocity  $\mathbf{V}$  and pressure  $P_{\parallel}$  along the magnetic field direction are unrestricted, although the values of these and other quantities can affect the stability of the equilibrium [*Northrup and Birmingham* 1970].

On the other hand, the MHD theory of the entropy wave (or contact discontinuity) is essentially irrelevant to collisionless plasmas. This is fairly obvious physically, because an entropy wave would have a component of magnetic field parallel to its density gradient, permitting particles to diffuse along the gradient [*Colburn and Sonett*, 1966]. The hypothetical entropy wave would disappear in a time of order  $T \sim L \cos \mu / v_{th}$  ( $L$  is the length scale of the density gradient,  $v_{th}$  is the proton thermal velocity, and  $\mu$  is the angle between the magnetic field and the direction of the density gradient). This time might be increased somewhat by plasma collective effects if the gradient is sufficiently steep, but we would not expect the order of magnitude of the eradication time to be changed by such processes. If we take  $L \sim 0.01$  AU and  $v_{th} \sim 40$  km/sec, then  $T \sim 2 \times 10^4$  sec  $\sim 6$  hr is small compared with the characteristic solar wind flow time ( $\sim 4$  days).

Furthermore, it has been shown formally that in collisionless plasmas in the limit of small amplitudes, there are no stationary structures (other than the tangential pressure balance) whose length scale is long compared with the Debye length ( $\sim 10$  m in the solar wind) [*Barnes*, 1971]. Hence a true entropy wave simply cannot exist in a collisionless plasma. However, it

is also true that the dispersion relation for hydromagnetic waves in collisionless plasmas admits solutions whose frequencies are purely imaginary [Barnes, 1966; Tajiri, 1967]. Such fluctuations do not propagate, but damp out in a deadbeat manner, in time  $T$  mentioned above. Barberio-Corsetti [1969] has pointed out that these rapidly damped fluctuations are in a sense the analog of entropy waves for collisionless plasmas. The damping time is so short that such structures are not likely to be found in the solar wind.

### NONLINEAR EFFECTS

In our discussion of waves we have not considered the nonlinear coupling between the various wave modes. Mathematical analysis of such effects is very complicated, and we are far from having a good understanding of the role played by nonlinear phenomena in solar wind fluctuations. The most pessimistic viewpoint would be that the solar wind is so turbulent (or otherwise disordered) at 1 AU that existing theories are hopelessly inadequate for understanding the observed fluctuation spectra. While this may be so, it seems more likely that some useful information can be gained by applying available theories of weak plasma turbulence to this problem.

For example, we may inquire what role nonlinear processes play in determining the power spectra of magnetic fluctuations near 1 AU. Figure 2 shows typical power spectra from Explorer 33. Although there is disagreement among observers about the detailed character of interplanetary fluctuations, and in particular of their power spectra, certain features seem to be established as typical. One such feature, indicated here, is the fact that the power in fluctuations of the magnitude of the magnetic field is normally smaller than the power in fluctuations of direction by about a factor of 10. These fluctuations could be due to stationary structures or to waves. The point to be emphasized at the moment is that to the extent that these fluctuations are waves, they must be either (1) Alfvén waves, or (2) magnetoacoustic waves propagating very nearly parallel to the magnetic field. They cannot be magnetoacoustic waves propagating obliquely to the magnetic field, because then the power in fluctuations of magnitude would be comparable to that in fluctuations of the various components.

It is further agreed that correlations of magnetic and plasma fluctuations indicate that Alfvén waves are often present in the interplanetary medium at 1 AU. On the other hand, there are no reported observations of magnetoacoustic waves. This fact, together with the fact that power in directional fluctuations is usually much greater than in magnitude fluctuations, indicates that obliquely propagating magnetoacoustic waves are

present, if at all, at intensities considerably lower than the intensities of transverse waves. The relative absence of compressive waves is easily understood in terms of the linearized theory, which tells us that magnetoacoustic waves are Landau damped while Alfvén waves are not. We have further noted that the Vlasov-Maxwell equations admit large-amplitude Alfvén wave solutions. Unless for some reason nonlinear effects inhibit the magnetoacoustic Landau damping, the above picture is self-consistent as far as it goes. On the other hand, it is possible that several nonlinear effects could provide an alternate explanation of the dominance of Alfvén over magnetoacoustic waves at 1 AU.

One obvious possibility is that decay into other, possibly higher frequency, wave modes, rather than Landau damping, accounts for the relative absence of magnetoacoustic waves. The details of such a process have never been analyzed, at least in a context that is clearly appropriate for solar wind fluctuations. However, it is possible to make at least crude order-of-magnitude estimates of nonlinear effects. Since the solar wind usually appears randomly disordered, rather than organized into neatly ordered wave packets, it seems reasonable to ask what one would expect from the "random-phase" approximation of weak-turbulence theory [Tsytovich, 1970; Sagdeev and Galeev, 1969]. In this approximation one expects the rate  $\gamma_{NL}$  of nonlinear decay from one mode into another to be of order

$$|\gamma_{NL}| \lesssim \omega(\Delta B/B)^2$$

where  $\omega$  is the circular frequency of the wave,  $\Delta B$  is the wave amplitude, and  $B$  is the magnetic field strength. This expression should be taken as an upper limit on  $|\gamma_{NL}|$ , and even this upper limit is uncertain by at least a factor of 10. If we take  $\Delta B/B \sim 0.1$ , then  $|\gamma_{NL}| \lesssim 0.01 \omega$ . Hence, it seems plausible that a wave in the solar wind might be significantly modified by nonlinear processes in 100 wave periods or less.

Therefore, large-amplitude magnetoacoustic waves may undergo significant dissipation by nonlinear decay into other wave modes, as well as by Landau damping. On the other hand, why do the transverse waves not decay into compressive waves, resulting in a sizable intensity of compressive waves? A tentative answer is that the magnetoacoustic Landau damping rate  $|\gamma_o| \gg |\gamma_{NL}|$ ; if this is so, the nonlinear decay of transverse waves would be strongly inhibited. Another interesting possibility is the following. Recent theoretical work by Rogister [1970] suggests that magnetoacoustic waves propagating along the magnetic field may be much more stable against nonlinear decay than

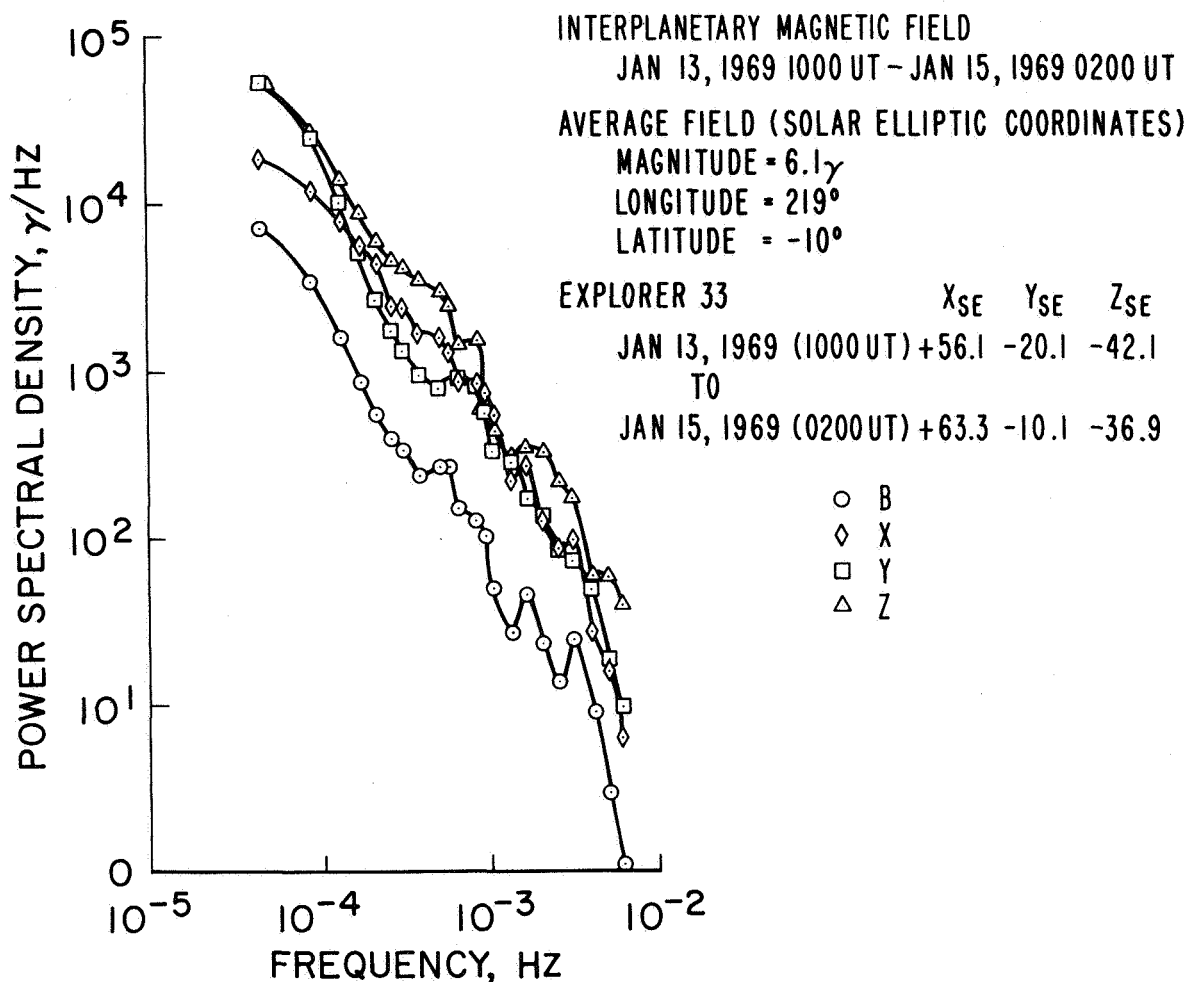


Figure 2. Typical power spectra of the interplanetary magnetic field, illustrating that power in transverse fluctuations is greater than in compressive fluctuations.

magnetoacoustic waves propagating in other directions. If this theory is applicable to solar wind fluctuations, then since fast magnetoacoustic waves propagating parallel to the magnetic field are essentially identical to Alfvén waves propagating in the same direction, one might suppose that the solar wind turbulence spectrum initially consisted of large-amplitude compressional waves, which subsequently decay, leaving only magnetoacoustic waves propagating parallel to the magnetic field. The resulting spectrum might be similar to the observed solar wind spectrum. This picture of solar wind turbulence may not be realistic, for at least two reasons: (1) Rogister's theory is in a sense analogous to "fixed-phase" wave-mode coupling theories and may not be appropriate to the solar wind fluctuations, which appear to be randomly disordered; and (2) even if Rogister's theory is applicable to the solar wind, the flow tends to convect waves so that their wave vectors become parallel

to the wind velocity and hence oblique with respect to the magnetic field, and so the effect of the nonlinear decay would be to obliterate the entire magnetoacoustic spectrum. Therefore, the transverse fluctuations, if they are waves rather than stationary structures, must be Alfvén rather than magnetoacoustic waves. In principle, this statement is subject to direct observational test, since the direction of phase propagation of an elliptically polarized plane wave can be determined (except for sign) as the direction of zero fluctuation of magnetic field; in general the direction of phase propagation of an Alfvén wave will be different from the magnetic field direction.

We have considered the following question: Given the fact that waves or other fluctuations exist in the solar wind, how are the fluctuations affected by the presence of the solar-wind plasma and of other fluctuations? We have seen that plasma kinetic theory gives us useful, but so far incomplete, insight into this question.



For example, we have seen that of the five classes of magnetohydrodynamic fluctuations only two, the Alfvén wave and the tangential pressure balance, are likely to exist in appreciable quantity in the microstructure of the wind. On the other hand, it is quite conceivable that nonlinear effects significantly modify the fluctuation spectra, but in ways that are obscure at present.

### SOURCES OF THE FLUCTUATIONS

Even if we had a complete knowledge of the intrinsic properties of solar wind fluctuations, we could not explain the observed fluctuations without knowledge of their sources. Obviously, the sources of stationary structures and of hydromagnetic waves would be very different. Nevertheless, in both cases possible sources may be conveniently placed into three broad classes: (1) the source is at or near the sun; (2) the source is some large-scale process in the interplanetary medium far from the sun; and (3) the source is some instability intrinsic to the solar wind flow far from the sun.

One area in which considerable systematic study has been made deals with the possibility that solar wind fluctuations at 1 AU are stationary structures, originating at the sun, which are convected out in the wind [Siscoe, 1970; Siscoe and Finley, 1969, 1970; Carovillano and Siscoe, 1969]. These fluctuations are stationary in the local rest frame of the solar wind, but they also corotate with the sun, like the magnetic sector structure. However, these fluctuations involve the large-scale structure of the wind, and may not have a very direct relation with the microstructure of the wind. Nevertheless, stationary microstructures may in fact originate at the sun. Thin, twisted filaments (of thickness  $\sim 10^6$  km) or other topological arrangements of magnetic field coming from the sun have been suggested [Ness, 1968; Burlaga, 1969]. Such an arrangement of stationary structures is a plausible consequence of the random walk of field lines rooted in the solar supergranulation [Jokipii and Parker, 1969]. In addition, there is some direct evidence that the statistical properties of stationary structures do not vary much between about 0.8 and 1.0 AU [Burlaga, 1971], which suggests that their source is nearer the sun than 0.8 AU. In particular, this conclusion is consistent with the hypothesis of solar origin of stationary structures.

It is also possible that stationary structures in the interplanetary medium could originate in the relaxation of some large-scale dynamical process or instability that takes place far from the sun. One possibility would be that stationary structures originate in regions of interaction between fast and slow streams; however, Burlaga

[1971] suggests that this hypothesis is not supported by observational data. Otherwise, the possible nonsolar origin of stationary fluctuations seems not to have been studied in detail.

Consider now the possible sources of hydromagnetic waves. The most obvious hypothesis is that the waves originate at the sun itself. This idea very naturally explains the recent observations that a substantial fraction of the power in solar wind fluctuations may be identified with Alfvén waves whose propagation direction relative to the plasma is *away from the sun* [Belcher *et al.*, 1969; Belcher and Davis, 1971]. If one assumes this wave efflux to be distributed in a spherically symmetric fashion, the net energy efflux is  $\sim 3 \times 10^{24}$  ergs/sec, small compared with the estimated  $5 \times 10^{27}$  ergs/sec in waves that heat the inner corona [Osterbrock, 1961]. In addition, only Alfvén waves originating near the sun would be able to reach the orbit of earth, because of the strong Landau damping of magnetoacoustic waves. The wave periods (in the spacecraft frame) range from  $\sim 2$  hr down at least to 10 min (and probably less); Alfvén wave intensities tend to be higher in fast solar wind streams than in slow ones. All these properties (propagation direction, wave intensity, wave mode, wave period, and intensity-flow speed correlation) are qualitatively consistent with the interpretation of these waves as the remnants of a hydromagnetic wave flux and the coronal base, which supplies a significant part of the solar wind energy.

Another large-scale process that may very well be a strong source of hydromagnetic waves in the solar wind is the collision between fast and slow streams. Most waves from this source would be generated in the region from 0.5 to 3 AU [Jokipii and Davis, 1969]. Observations indicate that the interaction regions are highly disturbed, with a large amount of power in compressive fluctuations [Belcher and Davis, 1971]. Presumably these compressive fluctuations are at least partly magnetoacoustic waves, which are Landau damped before they can propagate far from the interaction region. The wave dissipation produces heating of the gas; the heating appears to be restricted to the locality of the interaction region, at least at 1 AU [Burlaga and Ogilvie, 1970; Belcher and Davis, 1971].

Waves also can be generated locally when the solar wind encounters a planetary obstacle. For example, 30-sec period waves observed upstream of the earth's bow shock can be interpreted as hydromagnetic waves generated upstream of the earth's bow shock by cyclotron-resonant instability of a high-energy stream of protons traveling back upstream from the shock [Fairfield, 1969; Barnes, 1970; Rogister, 1970]. This process is illustrated

in figure 3. Waves generated at point *B* upstream are convected back downstream toward the bow shock, resulting in a region of enhanced turbulence. It should be pointed out that an alternate explanation of these waves is that they are whistlers generated at the bow shock and essentially standing in the wind, so that their frequency is Doppler shifted to the observed value of *Perez and Northrop* [1970]. This particular question, as

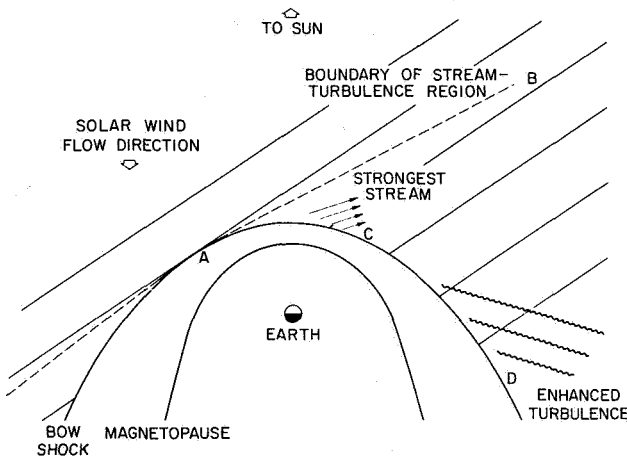


**Figure 3.** Schematic representation of generation of hydromagnetic waves upstream of the earth's bow shock, by protons streaming from the shock. Straight solid lines represent interplanetary magnetic field lines.

well as questions about the character of other interesting, high frequency waves upstream of the bow shock, has not yet been definitely resolved. In any case, it seems clear that waves should be generated locally in the solar wind whenever it encounters a planetary obstacle. Also, the fact that waves and, very likely, distorted particle velocity distributions exist upstream of the earth's bow shock emphasizes that caution must be used in interpreting solar wind data from earth orbiting spacecraft. In particular, data taken at times when the spacecraft is located on an interplanetary magnetic field line that intersects the bow shock can be contaminated by shock-produced effects.

Besides the previously mentioned sources of hydromagnetic waves in the solar wind, it is probable that such waves can be produced by a variety of processes intrinsic to the flow of the wind. The possible influence of nonlinear effects on the solar wind fluctuation spectrum has already been mentioned. Another possibility would be the Kelvin-Helmholtz instability, which can sometimes occur when two streams in tangential pressure

balance slip past one another. However, the observational study of *Burlaga and Ogilvie* [1970] indicates that this instability is probably not a significant source of heating in the wind, so that this mechanism is probably not a significant source of waves in the wind.

Another interesting possible source of hydromagnetic waves is microinstability of solar wind electrons due to distortion of their velocity distribution by thermal conduction [*Forsslund*, 1970; *Perkins and Spight*, 1970]. In particular, *Forsslund* [1970] has suggested that two hydromagnetic wave modes can be generated in this way. For example, it is conceivable that ion-acoustic waves, including the slow-mode hydromagnetic wave, could be generated by conductive instability if the ratio of electron to proton temperature is sufficiently high. *Forsslund* has suggested that this process occurs at a heliocentric distance  $r = 10 R_{\odot}$  for temperature distributions of the bare two-fluid model of the solar wind. On the other hand, this particular instability probably would not occur for temperature distributions corresponding to models with external heating. *Forsslund* has also suggested that fast-mode hydromagnetic waves might be generated by conductive instability in the vicinity of 1 AU, by the inverse of the Landau-damping process discussed earlier. However, it seems unlikely that any fast-mode waves produced in this way would be easily observable, for several reasons. First, *Forsslund's* mechanism generates fast-mode waves only for a fairly narrow range of propagation directions ( $\leq 15^{\circ}$ ); waves produced in this way would eventually be refracted outside this narrow production cone, into other directions where Landau damping occurs, and therefore such waves probably would not be observable long after they were generated. Second, the fastest growth rate of this process occurs for waves whose frequency is of the order of the proton gyrofrequency; and since the growth time of a microinstability is usually also a measure of its quenching time, it is likely that very little power in hydromagnetic waves will be generated by the instability. Probably the main effect of this instability would be to keep the electron velocity distribution near the marginally stable configuration, possibly with an associated "fizz" of noise whose characteristic frequency is comparable to the proton gyrofrequency. Altogether, then, it appears that although the thermal conduction instabilities considered by *Forsslund* may conceivably have nonnegligible effects on thermal conduction and electron-proton energy exchange, they are not likely to produce readily observable hydromagnetic waves in the solar wind.

It is conceivable that other microinstabilities could generate hydromagnetic waves in the solar wind. For

example, instabilities like the firehose associated with pressure anisotropy can generate hydromagnetic waves, at least in principle. Waves by anisotropy would be generated preferentially in higher- $\beta$  regions of the wind. According to the work of *Burlaga et al.* [1969] regions of high  $\beta$  tend to be associated with enhanced microfluctuations, which would be consistent with their being waves generated by anisotropy-driven microinstabilities. On the other hand, *Belcher and Davis* [1971] argue that enhanced fluctuations are better correlated with colliding-stream regions (which are often, but not always, regions of high  $\beta$ ), and that the fluctuations are generated by the large-scale, stream-stream interaction rather than anisotropy. From a theoretical standpoint, anisotropy-driven instabilities generate higher frequency or shorter wavelength waves more abundantly than hydromagnetic waves; probably the main effect of anisotropy-driven instability is to maintain the anisotropies in a marginally stable state, and to generate a relatively weak background of high frequency, short wavelength noise.

Altogether, it appears quite likely that most hydromagnetic waves in the solar wind are generated in large-scale processes. Observations at 1 AU are consistent with the generation of a large fraction of the waves at the sun; in addition, other large-scale processes, notably the collision of fast and slow streams, contribute to the observed fluctuations. Interaction of the wind with a planetary obstacle may account for local generation of hydromagnetic waves. The fluctuation spectrum of the wind may be significantly affected by nonlinear processes. Other small-scale processes, such as microinstabilities, are probably a relatively minor source of hydromagnetic waves.

## RELATION TO LARGE-SCALE PROPERTIES OF THE WIND

Hydromagnetic waves may influence the large-scale properties of the wind in a number of important ways. For example, heating due to Landau damping of magnetoacoustic waves, whatever their source, can have a significant effect on the flow. It has been shown that a model in which heating is due to thermal conduction and dissipation of an efflux of magnetoacoustic waves of  $\sim 4$ -min period generated at the sun can explain the observed correlation between proton temperature and flow speed at 1 AU for a large range of flow speeds [*Barnes et al.*, 1971; *Hartle and Barnes*, 1971; *Barnes and Hartle*, 1971]. *Jokipii and Davis* [1969] have suggested that the damping of magnetoacoustic waves generated by the collision of fast and slow streams is significant for solar wind heating. Observational evidence

indicates that this process probably produces local rather than global heating at 1 AU [*Burlaga and Ogilvie*, 1970]; *Belcher and Davis*, 1971], but this process may well produce larger scale effects beyond 1 AU.

Besides heating, the dissipation and even the simple propagation of hydromagnetic waves produce a force on the wind. It is possible that this sort of "radiation pressure" has a significant effect on the flow of the wind, especially if it acts in the region of supersonic flow. *Belcher* [1971] has developed a polytropic model of the solar wind which includes pressure due to the propagation of Alfvén waves outward from the sun. These waves do not damp locally, but gradually lose energy because they do work on the wind as they propagate outward. Although that model in its present form is probably not realistic in detail, it does show that radiation pressure from hydromagnetic waves may significantly accelerate the wind.

Fluctuations in the solar wind are related to many other problems of great current interest. Hydromagnetic waves or other fluctuations may participate in the transport of angular momentum from the sun [*Schubert and Coleman*, 1968; *Siscoe*, 1970]. Scattering and diffusion of cosmic rays are caused by fluctuations in the interplanetary medium [*Jokipii*, 1971]. Scintillation and scattering of signals from radio sources are produced by interplanetary fluctuations [*Hewish and Dennison*, 1967; *Cohen et al.*, 1967; *Jokipii and Hollweg*, 1970; *Hewish*, 1971]. Some of these problems, which are far beyond the scope of this discussion, are considered in other chapters.

One last topic should be mentioned briefly here. There are numerous observations of interplanetary fluctuations of shorter length scale and higher frequency than hydromagnetic-scale fluctuations. [see review by *Scarf*, 1970]. By combination of higher frequency magnetic and electric field measurements, some progress has been made in identifying the modes of various fluctuations, at least to the extent of distinguishing electrostatic from electromagnetic oscillations.

Higher frequency waves (period  $\sim 2$  sec) as well as hydromagnetic waves are generated in the upstream solar wind by the earth's bow shock [*Russell et al.*, 1971]. Probably the noise generated by microinstabilities due to anisotropy or to saturation of thermal conduction will be predominantly at frequencies comparable to or greater than the proton gyrofrequency. High-frequency noise will probably be found in most regions of rapid change, like shock fronts or colliding-stream regions.

Although the smaller-scale fluctuations normally contribute a small fraction of the total fluctuation energy in the wind, such fluctuations probably can have some

effect on the large-scale structure of the wind. For beyond a heliocentric distance of about  $10 R_{\odot}$ , wave-particle interactions probably have significant influence on transport phenomena, perhaps completely dominating Coulomb collisions [Eviatar and Schulz, 1970; Newman and Sturrock, 1969]. Modification of thermal conduction and proton-electron energy exchange by various collisionless mechanisms have been considered [Forslund, 1970; Perkins and Spight, 1970]. Eviatar and Wolf [1968] have discussed a possible collisionless viscous interaction between the solar wind and the earth's magnetosphere. It is conceivable that some such viscous mechanism could affect the heating, and especially the angular momentum transport of the wind.

To conclude, it is clear that the study of microscale fluctuations, both of hydromagnetic and smaller scale, is of great importance. The microscale fluctuations present an opportunity to directly observe waves in a plasma whose fluid pressure is not small compared with its magnetic pressure. Furthermore, observed fluctuations may provide major clues for understanding important large-scale effects in the solar wind. Considerable progress, partly theoretical but mainly observational, has been made in these areas in the past several years. I think that we may expect even greater advance in our understanding of the nature, origin, and effects of solar wind fluctuations in the near future. Again, most of this progress will probably come from observation, partly from new instrumentation, new spacecraft missions, partly from analysis of data from existing spacecraft, and hopefully from multiple satellite experiments.

#### ACKNOWLEDGEMENTS

I am grateful to Dr. Bruce Smith for providing the power spectra of figure 2, and to Dr. Patrick Cassen for his comments on the first draft of this review.

#### REFERENCES

- Barberio-Corsetti, P.: Entropy Mode Identification. *Bull. Amer. Phys. Soc.*, Vol. 14, 1969, p. 1019.
- Barnes, A.: Collisionless Damping of Hydromagnetic Waves. *Phys. Fluids*, Vol. 9, 1966, p. 1483.
- Barnes, A.: Stochastic Electron Heating and Hydromagnetic Wave Damping. *Phys. Fluids*, Vol. 10, 1967, p. 2427.
- Barnes, A.: Theory of Generation of Bow-Shock-Associated Hydromagnetic Waves in the Upstream Interplanetary Medium. *Cosmic Electrodyn.*, Vol. 1, 1970, p. 90.
- Barnes, A.; and Suffolk, G. C. J.: Relativistic Kinetic Theory of the Large-Amplitude Transverse Alfvén Wave. *J. Plasma Phys.*, in press, 1971.
- Barnes, A.: Theoretical Constraints on the Micro-scale Fluctuations in the Interplanetary Medium. *J. Geophys. Res.*, in press, 1971.
- Barnes, A.; Hartle, R. E.; and Bredekamp, J. H.: On the Energy Transport in Stellar Winds. *Astrophys. J.*, Vol. 166, 1971, p. L53.
- Barnes, A.; and Hartle, R. E.: Model for Energy Transfer in the Solar Wind: Model Results (proceedings of this meeting), 1971.
- Belcher, J. W.: Alfvénic Wave Pressures and the Solar Wind. *Astrophys. J.*, Vol. 68, 1971, p. 509.
- Belcher, J. W.; and Davis, L., Jr.: Large Amplitude Alfvén Waves in the Interplanetary Medium: II. *J. Geophys. Res.*, Vol. 76, 1971, p. 3534.
- Belcher, J. W.; Davis, L., Jr.; and Smith, E. J.: Large Amplitude Alfvén Waves in the Interplanetary Medium: Mariner 5. *J. Geophys. Res.*, Vol. 74, 1969, p. 2302.
- Burlaga, L. F.: Directional Discontinuities in the Interplanetary Magnetic Field. *Solar Phys.*, Vol. 7, 1969, p. 54.
- Burlaga, L. F.: On the Nature and Origin of Directional Discontinuities. *J. Geophys. Res.*, Vol. 76, 1971, p. 4360.
- Burlaga, L. F.; and Ogilvie, K. W.: Heating of the Solar Wind. *Astrophys. J.*, Vol. 159, 1970, p. 659.
- Burlaga, L. F.; Ogilvie, K. W.; and Fairfield, D. H.: Microscale Fluctuations in the Interplanetary Magnetic Field. *Astrophys. J.*, Vol. 155, 1969, p. L171.
- Carovillano, R. L.; and Siscoe, G. L.: Corotating Structure in the Solar Wind. *Solar Phys.*, Vol. 8, 1969, p. 401.
- Cohen, M. H.; Gundermann, E. J.; Hardebeck, H. E.; and Sharp, L. E.: Interplanetary Scintillations, 2, Observations. *Astrophys. J.*, Vol. 147, 1967, p. 449.
- Colburn, D. S.; and Sonett, C. P.: Discontinuities in the Solar Wind. *Space Sci. Rev.*, Vol. 5, 1966, p. 439.
- Eviatar, A.; and Schulz, M.: Ion-Temperature Anisotropies and the Structure of the Solar Wind. *Planet. Space Sci.*, Vol. 18, 1970, p. 321.
- Eviatar, A.; and Wolf, R. A.: Transfer Processes in the Magnetopause. *J. Geophys. Res.*, Vol. 73, 1968, p. 5561.
- Fairfield, D. H.: Bow-Shock-Associated Alfvén Waves in the Upstream Interplanetary Medium. *J. Geophys. Res.*, Vol. 74, 1969, p. 3541.
- Forslund, D. W.: Instabilities Associated with Heat Conduction in the Solar Wind and Their Consequences. *J. Geophys. Res.*, Vol. 75, 1970, p. 17.
- Hartle, R. E.; and Barnes, A.: Model for Energy Transfer in the Solar Wind: Formulation of Model (proceedings of this meeting), 1971.

- Hewish, A.: The Spectrum of Plasma-Density Irregularities in the Solar Wind. *Astrophys. J.*, Vol. 163, 1971, p. 645.
- Hewish, A.; and Dennison, P. A.: Measurements of the Solar Wind and the Small-Scale Structure of the Interplanetary Medium. *J. Geophys. Res.*, Vol. 72, 1967, p. 1977.
- Jokipii, J. R.: Propagation of Cosmic Rays in the Solar Wind. *Rev. Geophys. Space Phys.*, Vol. 9, 1971, p. 27.
- Jokipii, J. R.; and Davis, L., Jr.: Long Wavelength Turbulence and the Heating of the Solar Wind. *Astrophys. J.*, Vol. 156, 1969, p. 1101.
- Jokipii, J. R.; and Hollweg, J. V.: Interplanetary Scintillations and the Structure of Solar-Wind Fluctuations. *Astrophys. J.*, Vol. 160, 1970, p. 745.
- Jokipii, J. R.; and Parker, E. N.: Stochastic Aspects of Magnetic Lines of Force with Application to Cosmic-Ray Propagation. *Astrophys. J.*, Vol. 155, 1969, p. 777.
- Kantrowitz, A.; and Petschek, H. E.: *Plasma Physics in Theory and Application*, edited by W. B. Kunkel, Ch. 6. McGraw-Hill, New York, 1966.
- Landau, L. D.; and Lifshitz, E. M.: *Electrodynamics of Continuous Media*. Pergamon Press, New York, 1960.
- Ness, N. F.: Observations of the Interplanetary Plasma. *Ann. Rev. Astron. Astrophys.*, Vol. 6, 1968, p. 79.
- Newman, C. E.; and Sturrock, P. A.: Electrical Conductivity of a Collisionless Plasma in a Weakly Turbulent Magnetic Field. *Phys. Fluids*, Vol. 12, 1969, p. 2553.
- Northrop, T. G.; and Birmingham, T. J.: Stability of Tangential Discontinuities. *Solar Phys.*, Vol. 14, 1970, p. 226.
- Osterbrock, D. E.: The Heating of the Solar Chromosphere, Plages and Corona by Magnetohydrodynamic Waves. *Astrophys. J.*, Vol. 134, 1961, p. 347.
- Perez, J. K.; and Northrop, T. G.: Stationary Waves Produced by the Earth's Bow Shock. *J. Geophys. Res.*, Vol. 75, 1970, p. 6011.
- Perkins, F. W.; and Spight, C.: Magnetic Field Effects on the Ion-Acoustic Instability in the Solar Wind (abstract). *EOS*, Vol. 51, 1970, p. 412.
- Rogister, A.: Parallel Propagation of Nonlinear Low Frequency Waves in High  $\beta$  Plasma, submitted for publication, 1970.
- Russell, C. T.; Childers, D. D.; and Coleman, P. J., Jr.: OGO-5 Observations of Upstream Waves in the Interplanetary Medium: Discrete Wave Packets. *J. Geophys. Res.*, Vol. 76, 1971, p. 845.
- Sagdeev, R. Z.; and Galeev, A. A.: *Nonlinear Plasma Theory*. Benjamin, New York, 1969.
- Scarf, F. L.: Microscopic Structure of the Solar Wind. *Space Sci. Rev.*, Vol. 11, 1970, p. 234.
- Schubert, G.; and Coleman, P. J., Jr.: The Angular Momentum of the Solar Wind. *Astrophys. J.*, Vol. 153, 1968, p. 943.
- Siscoe, G. L.: The Solar Wind Problem with Fluctuations. *Cosmic Electrodyn.*, Vol. 1, 1970, p. 51.
- Siscoe, G. L.; and Finley, L. T.: Meridional (North-South) Motions of the Solar Wind. *Solar Phys.*, Vol. 9, 1969, p. 452.
- Siscoe, G. L.; and Finley, L. T.: Solar Wind Structure Determined by Corotating Coronal Inhomogeneities, 1, Velocity-Driven Perturbations. *J. Geophys. Res.*, Vol. 75, 1970, p. 1817.
- Stepanov, K. N.: Kinetic Theory of Magnetohydrodynamic Waves. *J. Exp. Theor. Phys. (U.S.S.R.)*, Vol. 34, 1958, p. 1292; (English Tr.: *Soviet Phys. JETP*, Vol. 7, 1958, p. 892).
- Tajiri, M.: Propagation of Hydromagnetic Waves in Collisionless Plasma, II, Kinetic Approach. *J. Phys. Soc. Jap.* Vol. 22, 1967, p. 1482.
- Tsytovich, V. N.: *Nonlinear Effects in Plasma*, Plenum Press, New York, 1970.

*J. V. Hollweg* I wish to point out that if one is careful, the idea that the nonlinear Alfvén wave can be linearly polarized is also very reasonable. If you consider a linearly polarized Alfvén wave propagating parallel to the average magnetic field,  $B_0$ , the wave magnetic field fluctuation is perpendicular to  $B_0$ . If this is some kind of sinusoid, this configuration implies that there is a variation of magnetic field pressure. This would lead, in general, to steepening of the wave; then I agree it is questionable whether you can talk about an Alfvén wave. However, it turns out that this steepening appears only in third-order terms, so if you are content to say that you're talking only about first- and second-order terms, there is no change in the Alfvén wave profile and one can consider this wave to be exactly an Alfvén wave to second order. There is an additional effect, though, to second order, and this is if you manipulate some of the equations you get a wave equation that has the properties of an ion-sound wave (this implies density

## DISCUSSION

fluctuations and velocity fluctuations parallel to the direction of propagation) on the left-hand side, and a driving term proportional to the gradient of the magnetic field pressure of the Alfvén wave on the right-hand side. These second-order density fluctuations lead to steepening, but only in the third order.

It turns out that for  $\beta$  of the order of a half or a third or so, which is perhaps typical of the conditions near the orbit of the earth, you get a resonance with the sound waves and therefore very large density fluctuations. At that point my calculations break down, but nevertheless the density fluctuations can be large. But still to second order it's an Alfvén wave.

*A. Barnes* As I said, there's an exact solution for the Vlasov-Maxwell equations for all directions of propagation, which gives an Alfvén wave and this includes  $\theta = 0$ . It sounds as if you have established equations that indicate something about the mode coupling between the Alfvén waves and the acoustic waves and, of course, such coupling is well known to occur. Would you agree?

*J. V. Hollweg* Somewhat. But I don't think it's ever been described specifically. Furthermore, strictly speaking I have not considered *coupling* between Alfvén waves and ion acoustic waves, but rather how Alfvén waves *drive* acoustic waves. There is a difference.

*W. C. Feldman* I'm a bit confused about some of the formulas I've seen here for large-amplitude Alfvén waves. The problem concerns the anisotropy. With small-amplitude Alfvén waves the energy density of the magnetic field fluctuation should be in equipartition with the energy density of the plasma fluctuation. For large-amplitude waves, there are cases in which the magnetic energy density fluctuation is larger than the plasma energy density fluctuation, an effect that has been ascribed to anisotropy. When you look at the formulas there is a factor  $(P_{\perp} - P_{\parallel})$  divided by the energy density of the magnetic field. So for the large amplitudes, I would like to know which magnetic field to choose—the unperturbed or the perturbed? If it is the unperturbed  $B$ , how do you compute the temperature anisotropy that should be determined by the total magnetic field, especially for the large-amplitude fluctuations.

*A. Barnes* I'm not sure I understand the question. In the limit of small amplitude, of course, you get the kinetic part of the energy of the Alfvén waves from a standard formula. The energy of a small-amplitude plasma wave, of course, is magnetic energy plus the energy associated with the thermal and kinetic energy of the waves. In the case of an Alfvén wave, the total energy turns out to be exactly  $\langle \Delta B^2 \rangle / 4\pi$  for the isotropic case, and you can work out what it is for the anisotropic case. The difference is that there is a term that involves the difference between the pressures just as you would expect. I don't remember what the numbers are but they are such as to make the total energy go to zero just when the firehose instability would take place. For an Alfvén wave this would mean that the mechanical part of the wave energy is less when  $P_{\parallel}$  is greater and  $P_{\perp}$  is less than the magnetic energy. This is for the small-amplitude case. I don't really know how to define the wave energy for large wave amplitudes.

*H. J. Volk* When you talked about decay of waves, did you mean the three-wave decay process?

*A. Barnes* I mean anything that actually occurs. But what I basically had in mind was a three-wave process.

*H. J. Volk* Then gamma, the growth rate you gave, which you say is proportional to  $\Omega(\Delta B/B)^2$ , should be, as I recall, proportional to  $\Delta B/B$ . Second, near the orbit of earth  $\Delta B/B$  is the order of 1 so the growth rates would be much greater than yours and the fluctuation level at the orbit of earth would probably have nothing to do with what happens at the sun.

*A. Barnes* I believe there are two different questions here. First of all, there are two different classes of three-wave decays: those that occur when the waves are in fixed phase

and those that occur when the waves are in random phase. For fixed phase waves the growth rate is proportional to  $\Delta B/B$ . For random phase it is proportional to  $(\Delta B/B)^2$ . This, by the way, is essentially the formula that Parker used yesterday for a related process, which you could look at as the three-wave decay between Alfvén waves, magnetoacoustic waves, and maybe tangential pressure balance or something like that. So if you assume that the appropriate theory to use is for the solar wind random phase theory, then  $(\Delta B/B)^2$  is correct. Second, I think I said that the amount of power in the fluctuations at earth  $\Delta B/B$  can range from less than 0.1 to 1.0. Perhaps some of the experimentalists would like to comment on this, but it seems to me that from the data I have seen that  $\Delta B/B$  on the order of 0.1 is typical, though certainly it can be as great as 1.0, in which case the nonlinear decay may be much larger than I said it would be. The decay is proportional to  $(\Delta B/B)^2$ , after all, and so it's a very sensitive function that varies quite a bit.

The other point, however, is that the expression I wrote is an upper limit. It doesn't include the dynamics, the cross section, for the wave-wave interaction, and it may be that a detailed analysis of these things would show smaller growth rates in some cases.

*N. F. Ness* In connection with the question from observational data, if the fluctuations are normalized, and if you were to use a discontinuity as defined by *Siscoe et al.*, the threshold value was  $4\gamma$  out of an ambient field average of something like  $5\gamma$ . If you were to use the  $30^\circ$  definition or the larger of Burlaga's, then you would have a relative amplitude ratio of 0.5. If you look at the time scale plots of Belcher and Davis (figs. 1, 2, p. 383) you find that the fluctuations are of approximately equal amplitudes throughout the ambient magnetic field for the period ranges studied. Generally I think that  $\Delta B/B$  at the periods you are considering is on the order of unity. This includes periods up to about 1 hr.

*F. C. Michel* I have a comment on these damping rates. Basically, there are two simple approximations one can make. One can describe the interplanetary medium as being made up of frozen-in fluctuations that are just convected out. Or one assumes that the medium is homogeneous with superimposed waves. Both of these are extreme approximations. Now, for the frozen-in approximation, at least in the filamentary picture, there are filaments unwinding or moving relative to one another. For example, if all filaments were radial except one that wiggled back and forth, this wiggle would tend to straighten out and behave in a sense as a propagating wave. Whether or not one calls this a wave is a matter of taste. I personally think the filamentary picture is preferable. But, the damping rates come from the picture of a homogeneous plasma and a monochromatic wave. I think that the short times appropriate for the damping time of a uniform plasma wave in a homogeneous medium are not appropriate for the time that it would take the filaments to rearrange and become uniform.

*A. Barnes* I agree. The time scales I gave for dissipation of hydromagnetic waves are probably quite a bit shorter than those for filaments to rearrange themselves. The latter would be on the order of the flow time between the sun and earth, right? And the homogeneous theory is applicable only if the length scale of the fluctuation is short compared with the scale height of the solar wind.

*L. Davis* I believe that a reasonable way to investigate whether  $\Delta B/B$  is 1.0 or 0.1 is through variance over periods of say 3 hr. I think it's worth trying to make a somewhat finer division than this because I think the effects vary more or less as the square. As I recall, it is rare that the square root of the variance over a period of something like 3 hr approaches the value of 4 or  $5\gamma$  typical of the field strength. I think  $\Delta B/B$  about 0.7 for these very disturbed times is a somewhat better characteristic value than 1. The square of that is 0.5 and on these curves which rise very steeply, the difference between 0.5 and 1.0 for  $(\Delta B/B)^2$  is probably significant.

*N. F. Ness* I think that the use of the standard deviation to measure  $\Delta B/B$  for these

nonlinear wave modes is not correct. One should look at the time history and look at the amplitude, peak to peak, relative to the magnitude of the field to obtain a correct estimate.

#### COMMENTS

*D. W. Forslund* Barnes mentioned (p. 340) that there are a number of micro-instabilities in the solar wind that occur due to the heat flux and velocity space anisotropies. I would like to review briefly some of their properties and how they may arise.

A number of properties of the plasma were described earlier in studies of the large-scale structure of the steady-state solar wind. In particular, there are at least three properties that illustrate how the dynamics of the expansion can cause a departure of the plasma from thermodynamic equilibrium. One simple case is that proton temperature is distinct from that of the electrons because of the weak collisional coupling. A second effect arises if there are few collisions between the proton components—that is, a velocity anisotropy between the components parallel and perpendicular to the magnetic field. This can arise in the electron component also if collisions or wave interactions are sufficiently weak. A third effect arises in any model one chooses—collisionless, exospheric, one-fluid, or even two-fluid magnetohydrodynamic. There exists a heat flux outward from the sun (unless an isothermal approximation is made). This effect appears microscopically as a third moment of the electron and ion distribution functions.

I shall describe briefly how these last two types of velocity space anisotropy give rise to plasma instabilities. In particular, the plasma, if it can, will try to destroy these departures from thermodynamic equilibrium, since they are a free energy source on a microscopic scale. How might one determine the various ways the plasma in the solar wind can tap the free energy, relax closer to an equilibrium thermodynamic state, and in a sense approach the properties of a one-fluid model? The important thing to recall, as Perkins mentioned earlier (Chap. 3, p. 215), is that the transport properties of the plasma can be altered due to instabilities. A model analysis shows “feedback” superimposed on the steady-state dynamic expansion of the solar wind with the possibility of giving better agreement with observation of the large scale features. In particular, the recent model of *Brandt et al.* [1969] illustrates how an alteration of the heat flux, by arbitrarily modifying the transport coefficients, can make the model calculations agree better with observation.

Turning now to the process by which a heat flux may give rise to instabilities, assume a spherically symmetric model including a spiral magnetic field and no net electric charge flow out from the sun. Hence, on the average, the current parallel to the magnetic field is zero, which taken with the fluid equations may be written as

$$0 = j_{\parallel} + \sigma_1 \left( E + \frac{\cos \psi}{ne} \frac{dp}{dr} \right) + K_1 \cos \psi \frac{d\Theta_e}{dr}$$

where  $j_{\parallel}$  is the parallel current,  $\sigma_1$  the electrical conductivity,  $K_1$  the usual transport coefficient,  $\psi$  the angle of  $\mathbf{B}$  with the radial direction,  $n$  the number density,  $p$  the pressure, and  $\Theta_e$  the electron temperature. For zero current one has to balance the current from the temperature gradient with the current from the effective electric field. The dimensionless parameters that enter into the determination of the transport coefficients  $A_E$  are complex, but basically they can be thought of as corresponding to the electric field normalized to the runaway field—the field in which the electrons will be accelerated freely. We also define the quantity  $B_T$ , the ratio of the mean free path for collisions to the scale length of the temperature gradient, in this case the scale length of the solar wind. The zero current condition requires that  $A_E = 0.35 B_T$ . For collisional heat conduction, these two parameters must be small compared to unity, which in fact they are not in the solar wind. As Montgomery has shown (Chap. 3, p. 210), there is a significant discrepancy between the observed value of  $B_T$  and that predicted by Spitzer-Härm theory.



Within linear transport theory the equilibrium electron distribution function is given by

$$F_e = f_e^0(\nu) \left\{ 1 + [A_E D_E(\nu) + B_T D_T(\nu)] \cos \theta \right\}$$

where  $\theta$  is the angle of  $\nu$  with respect to the gradients, the function  $f_e^0(\nu)$  is the maxwellian distribution, and the transport parameters  $A_E$  and  $B_T$  multiply the perturbed distribution functions  $D_E$  and  $D_T$  describing the current flow and the heat flux. Figure 1 illustrates the way in which the distribution gives rise to instability. The third moment of

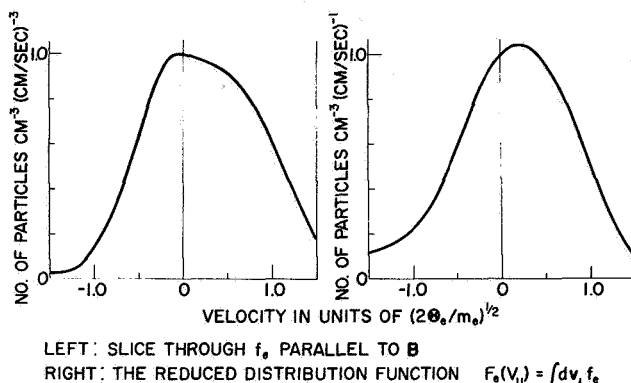


**Figure 1.** Linearized electron distribution function in a combined electric field and temperature gradient.  $B_T = 0.9$ ,  $A_E = 0.32$ .

the electron distribution function averaged over velocities perpendicular to  $\mathbf{B}$  shifts the peak of the distribution away from the protons even though they have a net velocity that matches the proton flow speed. Free energy then exists due to the shift of this peak. That is, if waves can exist in the region between the electron and ion peaks they can extract some of the heat flux energy from the electrons and produce turbulence. We have described here how a heat flux instability can arise for a collisionally driven distribution function, but as Parker pointed out earlier (Chap. 3), collisions are not absolutely necessary for instability to occur. In collisionless exospheric models a distribution function very similar to that in figure 1 can arise. At a given distance from the sun there will be a velocity cutoff for trapping electrons, as Perkins has pointed out (p. 215), due to an electrostatic potential barrier at large radius from the sun and a magnetic mirror at small radius. Above that velocity a flux of escaping electrons gives rise to a shift of the electron peak away from the average velocity, again generating a local source of free energy.

Table 1 summarizes briefly some solar wind model values for  $B_T$  as well as the observational values. Recall that in these models or in the actual solar wind the heat flux increases with  $B_T$ . Close to the sun ( $\sim 10R_{\odot}$ ) values of  $B_T \sim 0(0.1)$  exist for a number of models. At 1 AU,  $B_T$  generally becomes very large, implying that the heat-conduction law will break down because of purely collisionless expansion effects or wave-particle interactions that arise from instabilities. The observations give significantly smaller values for  $B_T$ . In the observations of Montgomery (Chap. 3, p. 210), the actual value of  $B_T$  was less than 0.2 on the average, significantly lower than that from model calculations,

**Table 1.** Table of  $B_T$  for various solar wind models

MODEL	$ B_T $	
	10 $R_\odot$	215 $R_\odot \approx 1$ A.U.
HARTLE and STURROCK [1968]	$\sim 0.4$	$\sim 1.5 \quad \psi = 0^\circ$
WHANG and CHANG [1965]	$\sim 0.1$	$\sim 0.8 \quad \psi = 0^\circ$
BRANDT et al. [1969]	$\sim 0.3$	$\sim 1.8 \quad S = 2/7 \quad \psi = 55^\circ$
		$\sim 2.6 \quad S = 2/5$
OBSERVATIONS	—	$\sim 0.26 \quad S = 2/7 \quad \psi = 45^\circ$
$T \sim 10^5$ °K, $n \sim 5$ cm $^{-3}$	—	$\sim 0.5 \quad S = 2/5$

indicating that the models are actually not very good and should be modified. By reducing the value of  $B_T$  in their model, Brandt *et al.* [1969] obtained much better agreement with observations at 1 AU.

Figure 2 summarizes the instabilities that can arise. A number of waves can be driven

ION-ACOUSTIC WAVES

$$(k \approx 0, \frac{T_e}{T_i} \gg 1) \quad |B_T| > 4.3 \left[ \left( \frac{m_e}{2m_i} \right)^{1/2} + \frac{1}{\sqrt{2}} \left( \frac{T_e}{T_i} \right)^{3/2} e^{-\frac{T_e}{2T_i} - \frac{3}{2}} \right] \geq 0.07$$

ELECTROSTATIC ION CYCLOTRON WAVES

$$\frac{T_e}{T_i} \geq 1 \quad |B_T| > 1.3 \left( \frac{T_i}{T_e} \right)^{3/2}$$

MAGNETOACOUSTIC WAVES

$$|B_T| > \frac{2}{\beta_e^{1/2}} \left( \frac{m_e}{m_i} \right)^{1/2} \sim \frac{0.04}{\beta_e^{1/2}}$$

ION CYCLOTRON WAVES

$$|B_T| > \frac{1}{\beta_i^{1/3}} \left( \frac{m_e}{m_i} \right)^{1/2} \sim \frac{0.02}{\beta_i^{1/3}}$$

**Figure 2.** Conditions for instability.

unstable provided that they can exist in the valley between the electrons and ions of figure 1. Ion-acoustic waves are most easily excited if the ions are very cold. For electrons much hotter than ions, the critical  $B_T$  for ion acoustic waves is shown at the top of figure 2. If the ions are very cold, the second term is small and for  $B_T > 0.07$ , ion-acoustic waves are unstable. This is very easily satisfied in all the models very near the critical radius and close to the sun (table 1), implying that the heat conduction should be modified there in a manner perhaps similar to what Brandt *et al.* [1969] did.

A number of other waves can be driven unstable as indicated in figure 2. The formulas are approximate but show that as the plasma  $\beta$  increases the critical value for  $B_T$  decreases. Thus, these waves will presumably grow farther out in the solar system than will the ion-acoustic waves, although actually they are still unstable fairly close to the sun.

Figure 3 summarizes some numerical results obtained recently for the electromagnetic and electrostatic ion-cyclotron waves driven unstable by a current. This is relevant here since a 1-to-1 correspondence exists between current-driven instabilities and heat-conduction instabilities with the two differing by a numerical factor of the order of unity. Here we show the  $\beta$  dependence of the critical drift velocity for electrostatic ion-cyclotron waves with  $T_e = T_i$ . As  $\beta$  is increased the critical drift speed increases slowly, but in the

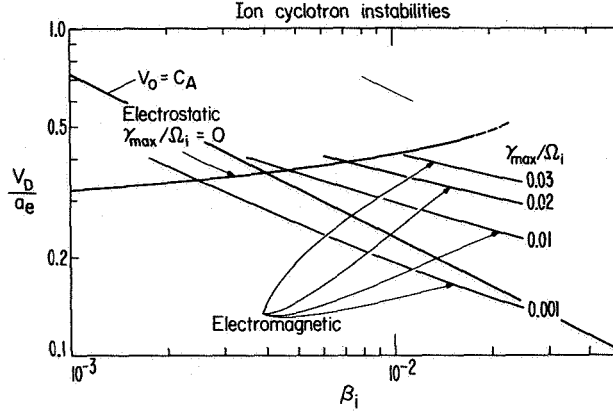


**Figure 3.** Marginal stability curve for the electrostatic ion cyclotron wave as a function of  $\beta$  for  $T_e/T_i = 1$  and contours of maximum growth rate of the electromagnetic ion cyclotron wave versus  $\beta$  for  $T_e/T_i = 1$ ;  $V_D$  is the electron drift velocity or net shift in the electron peak from that of the ions;  $a_e$  is the electron thermal velocity.

neighborhood of  $\beta = 0.01$  it starts to rise more sharply. Figure 3 also shows the maximum growth rate contours of the electromagnetic ion-cyclotron wave obtained by numerically searching the full hot plasma electromagnetic dispersion relation. Note that these contours drop to very low drifts as  $\beta$  increases;  $\beta \sim 0.01$  is probably typical when close to the critical radius and analytically depends exactly on what kind of model is used. At any rate, near  $10 R_\odot$  the electromagnetic ion-cyclotron mode may indeed be unstable along with the ion-acoustic wave and cause modification of the transport coefficients. These results need to be extended to  $\beta = 1$  to determine more carefully what happens as one approaches the orbit of earth.

Thus we see that there are a moderate number of instabilities that can take place due to heat conduction. With the exception of the ion-acoustic mode, the most unstable modes have wavelengths about that of the ion gyroradius, although most of the instabilities can grow at very long wavelength but at reduced rates of growth. What sort of turbulence they produce is uncertain, but one would expect a peak at around the ion gyroradius.

I would next like to discuss the instabilities that can occur from the proton and electron anisotropy created by the nearly adiabatic expansion of the plasma out from the sun. It is known that a very large anisotropy,  $T_\perp \ll T_\parallel$ , should develop which in turn should destabilize Alfvén waves, thus reducing the anisotropy, more closely approaching the values found in the solar wind. We have recently looked at finite gyroradius effects on these instabilities more carefully, both analytically and numerically and by searching the electromagnetic dispersion relation over a range of wave numbers  $k_\parallel$ , propagation angles, anisotropies, and  $\beta$ , and by studying the maximum growth rates. We have uncovered several interesting effects. [Kennel and Scarf, 1968] discussed the case for waves propagating exactly along the field lines, but we have recently looked at the oblique firehose instability, which has zero real frequency at large angles to  $\mathbf{B}$  and continues to have zero frequency as one approaches finite gyroradius. For  $T_\perp \ll T_\parallel$  and zero real frequency, the condition for marginal stability

$$\beta_+ A_+ (k_\parallel^2 R_{L\parallel}^2)^{-1} Z' \frac{1}{k_\parallel R_{L\parallel}} + \beta_- A_- \geq 2$$

is found where  $\beta_+$  is the proton pressure along the field relative to the magnetic pressure,  $A_+$  is the proton anisotropy  $1-T_\perp/T_\parallel$ ,  $R_{L\parallel}$  is the proton gyroradius, and  $Z'$  is the plasma-dispersion function, involving only parallel wave numbers. The electron anisotropy enters in the usual firehose fashion. In the asymptotic long wavelength limit the coefficient of  $\beta_+ A_+ \rightarrow 1$ , giving the usual criterion for firehose instability. However, for finite gyroradius, this coefficient has a maximum of 1.65, thus reducing the anisotropies and  $\beta$ , which can give rise to instability. As will be shown later, this may be significant. For the parallel whistler mode one can also show that this occurs at finite gyroradius, as indicated by *Kennel and Scarf* [1968] and also more recently by *Hollweg and Völk* [1970]. In particular, one can derive an expression from Kennel and Scarf if the anisotropy  $A_+ \gtrsim 0.1$

$$\beta_+ A_+ + \beta_- A_- - 2 \geq -\frac{1}{2} k_\parallel^2 R_{L\parallel}^2 \beta_+ A_+$$

Here the left-hand side of the expression is the normal firehose criterion. The finite gyroradius effect destabilizes the firehose—that is, permits it to function for parameter values below the hydromagnetic firehose limit. Since both modes have lower thresholds at finite gyroradius, the nonlinear evolution will stabilize these waves and reduce the anisotropy before the hydromagnetic limit is reached. Thus, in the firehose case, it appears that the short wavelength turbulence is very important.

Figure 4 is a scatter plot of proton pressure anisotropy from *Eviatar and Schulz*

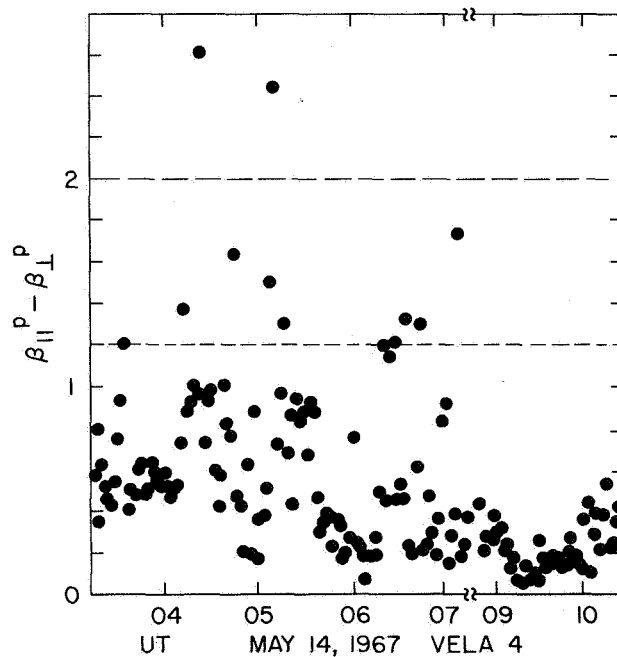


**Figure 4.** Contribution of protons to  $\beta_\parallel - \beta_\perp$  during a typical time period (*Eviatar and Schulz*).

[1970] using the Vela 4 data. The hydromagnetic firehose limit is indicated by the top dashed line assuming isotropic electrons. Weakly anisotropic electrons will drop the line somewhat. From this line, one would draw the conclusion that the plasma is rarely near the firehose limit. However, with the inclusion of the factor 1.65, the marginal stability line drops down to the lower dashed line, and the firehose instability may develop more frequently in the solar wind.

In figure 5 we have plotted contours of maximum growth rate obtained numerically for the  $k_{\parallel}$  instability, with  $\beta$  along the magnetic field plotted horizontally and the anisotropy plotted vertically. The normal firehose limit is given by the right-hand dashed line. The growth rate contours with very small values are the *Kennel and Scarf* [1968] mode with phase velocities out on the tail of the proton distribution. Going to the right one moves continuously over the firehose instability. We can see that this parallel mode operates at fairly low  $\beta$ , but a key question is whether or not it can isotropize the body of protons.

Finally, I should mention that if one includes the combination of heat flux and anisotropy, a number of these modes have even lower threshold, implying that at least in some states of the solar wind these instabilities are almost certainly present and should be included in a complete model either in the form of transport coefficients in a fluid model or in some more detailed way as, for example, in an exospheric model.

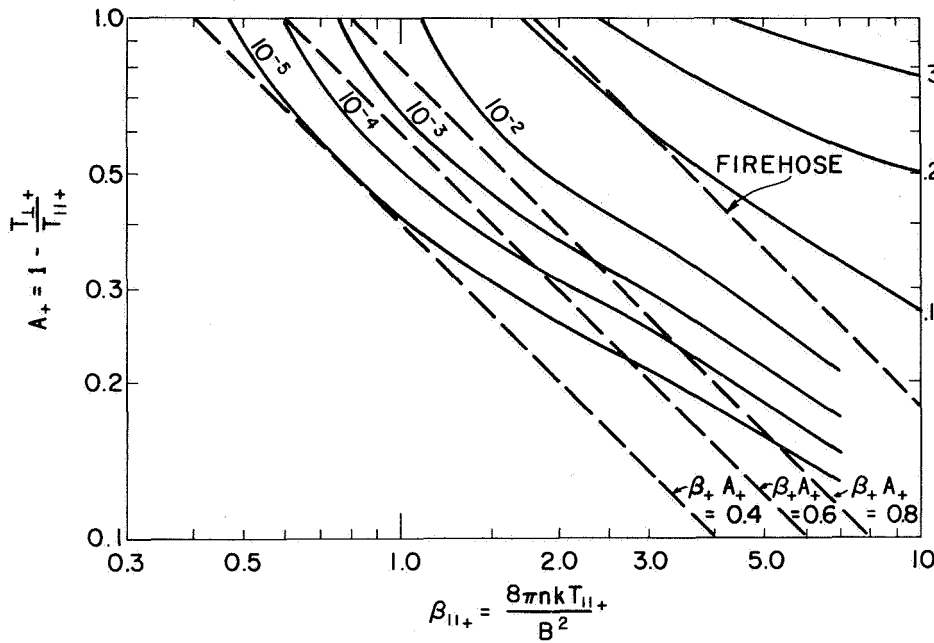


Figure 5 Maximum growth rates of Whistler mode anisotropy instability in units of  $\Omega_+$  for  $\beta_- A_- = 0.2$ .

#### REFERENCES

- Brandt, J.; Wolff, C.; and Cassinelli, J.: The Angular Momentum of the Solar Wind. *Astrophys. J.*, Vol. 156, 1969, p. 1117.  
 Eviatar, A.; and Schulz, M.: Ion-Temperature Anisotropies and the Structure of the Solar Wind. *Plan. Space Sci.*, Vol. 18, 1970, p. 321.  
 Hollweg, J., Völk, H. J.: New Plasma Instabilities in the Solar Wind. *J. Geophys. Res.*, Vol. 75, 1970, p. 5297.  
 Kennel, C. F.; and Scarf, F. L.: Thermal Anisotropies and Electromagnetic Instabilities in the Solar Wind. *J. Geophys. Res.*, Vol. 73, 1968, p. 6149.

#### COMMENTS

*H. J. Volk* Forslund has discussed (p. 346) heat current instabilities and anisotropy-induced instabilities. Hollweg, Pilipp, and I have been working on anisotropy instabilities to see whether one can, without heat current, reduce the proton anisotropy and at the same time heat the protons, because it turns out from the fluid models that the protons always come out too cool. This then is in some contrast to the model of *Kennel and Scarf*

who used, as we do, parallel propagating hydromagnetic waves. Because in their model—although this is the most likely candidate to reduce the proton anisotropy—at the same time the protons are cooled, and this is not in line with the two-fluid model. So we include an electron anisotropy and try to see whether the *electrons*, which are hot and anisotropic, can both lower the anisotropy and heat the protons.

In the right-hand side of figure 1 we have plotted  $\tilde{\omega}_i$ , the imaginary part of  $\omega$  (the growth rate) versus  $\tilde{\omega}_r$ , which is the real frequency. Both are normalized to the proton gyrofrequency. This is a numerical calculation. I show you that particular case, although it does not involve the best parameter one could choose, to demonstrate what one obtains in general. Starting for small  $k$ , the firehose is excited in this particular example, and then the curve turns down; there we come to the Kennel and Scarf mode. For still larger  $k$  the curve turns back and up and develops into a negative frequency, left-hand mode. It is clear that in the left-hand mode the protons are in cyclotron resonance and therefore will be heated. However, if you look at the parameters they are quite stringent. In this particular example, the ratio of parallel to perpendicular temperature of the protons is equal to 5. We took the  $\beta$  of the protons equal to 2 and the ratio of electron to proton parallel temperatures as also being equal to 2. And we need a rather large electron anisotropy  $(T_{\parallel}/T_{\perp})_e$  which we took in this case to be 1.8, which is much larger than observed under average conditions. So this is then rather unrealistic. If one now includes a heat current, one can reduce the electron anisotropy somewhat. This radiation can easily bring the plasma below the firehose limit, which is nice, but the electron anisotropy still remains at about 1.5, which is quite high. We then conclude that although one can show that this instability not only heats the protons, but also reduces their anisotropy, this mechanism generally won't work and that you rather should take heat current induced instabilities like those discussed by Forslund, or you heat the protons by, say, the Barnes mechanism or any other wave mechanism. Thus, my conclusion would be that probably the Kennel and Scarf mechanism is the best one, besides perhaps the oblique firehose case, to reduce proton anisotropy, and the couplings between electrons and protons should rather be done by the heat current rather than trying to eliminate energy by introducing electron anisotropies.

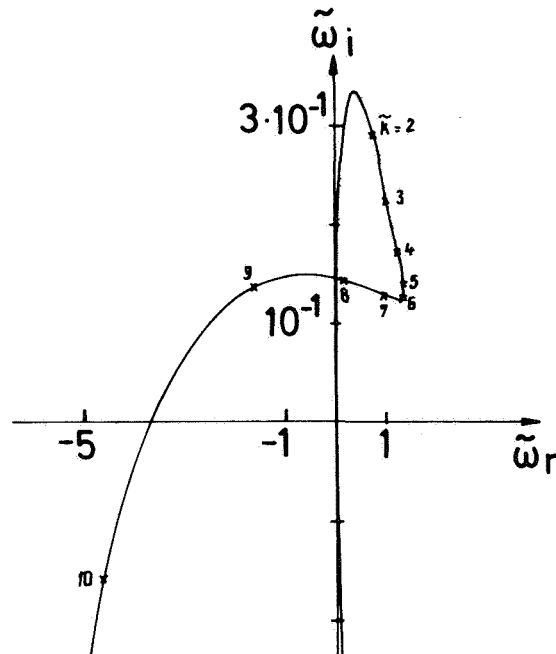


Figure 1.

# ELECTRON PLASMA OSCILLATIONS IN THE NEAR-EARTH SOLAR WIND: PRELIMINARY OBSERVATIONS AND INTERPRETATIONS

R. W. Fredricks, F. L. Scarf, and  
I. M. Green

We report here some preliminary results and conclusions of a study of electric field oscillations in the upstream solar wind. The OGO-5 orbits discussed are on the dusk (three) and on the dawn (one) sides of the earth-sun line. It is concluded that there are electron streams with  $E \gtrsim 700$ –800 eV produced at or near the bow shock. These streams penetrate the incoming solar wind plasma at least out to  $23 R_E$ , and generate quasi-electromagnetic waves at  $\omega \sim \omega_{pe}$  and  $|k| \gtrsim \omega_{pe}/v_B$  where  $v_B$  is the streaming speed of the suprathermal electrons. The streams (as inferred from the wave levels) occur without regard to dawn-dusk location, as opposed to the low-frequency MHD upstream disturbances driven by backstreaming protons, which show a definitely strong preference for the dawn-noon sector. The presence of the suprathermal electron streams and associated wave turbulence indicates that some near-earth electron distributions are probably not representative of true solar wind distributions far away from the earth.

## ABSTRACT

## INTRODUCTION

Electric field fluctuations at or near the local electron plasma frequency have been observed regularly by the plasma wave detector experiment (PWDE) aboard OGO-5 in regions upstream from the bow shock; details of the PWDE instrumentation are given by Crook *et al.* [1969]. The sources of these oscillations at or near  $\omega_{pe}$  are suprathermal electron beams in the upstream region, as described experimentally in a recent paper by Scarf *et al.* [1971] and interpreted theoretically in a paper by Fredricks *et al.* [1971a].

Scarf *et al.* [1971] showed the time correlations of the appearance of signals in the PWDE 30-kHz electric field channel and the detection of suprathermal electrons of  $E \gtrsim 700$  to 800 eV by the LEPEDea probe, when OGO-5 was in the upstream region on March 11, 1968. Also, they showed that the local number density  $n_o$  computed from data gathered by the JPL plasma probe aboard OGO-5 was consistent with the frequency of the wave phenomena simultaneously detected by the PWDE,

provided the wave frequency  $\omega \sim \omega_{pe} = (4\pi n_o e^2/m)^{1/2}$ .

For the most commonly encountered plasma conditions near earth, the solar wind number density ranges from 1 to  $10 \text{ cm}^{-3}$ , with occasional excursions up to perhaps 60 or  $70 \text{ cm}^{-3}$ . Thus, the local plasma frequency ( $f_{pe} = \omega_{pe}/2\pi$ ) in the near-earth solar wind commonly is 10 to 30 kHz, with occasional excursions up to some 70 kHz ( $f_{pe} \sim 9\sqrt{n_o}$  kHz). Since the OGO-5 PWDE has narrowband electric field channels at 14.5, 30, and 70 kHz, along with a broadband channel covering 1 to 22 kHz, and a magnetic field channel only at 70 kHz (narrowband), the most commonly generated E-field fluctuations (10 to 30 kHz) have no simultaneous B-field data; thus, it is not possible to say whether the waves generated by the streams of  $E \gtrsim 700$  to 800 eV electrons are electrostatic (longitudinal), electromagnetic (transverse), or quasiaelectromagnetic (mixed longitudinal and transverse) modes. The bulk speed corresponding to 800 eV is  $v_B \sim 5 \times 10^9 \text{ cm-sec}^{-1}$ . Thus  $v_B/c \sim 0.06$ , so that for a wave of phase speed comparable to  $v_B$  the index of refraction  $|kc/\omega| \sim 16$ . This index is large, but not large enough to assume that waves generated by the interaction between streaming, suprathermal electrons

---

The authors are at the Space Sciences Laboratory, TRW Systems Group, Redondo Beach, California.

and the cooler (10–20 eV) solar wind plasma will be purely longitudinal.

With this latter fact in mind, *Fredricks et al.* [1971a] have shown that quasiaelectromagnetic waves should be generated by 700–800 eV electron streams even if the random energy (or beam temperature) is also 700–800 eV. Quasitransverse modes of initial growth rate  $\gamma/\omega_{pe} \sim 5 \times 10^{-4}$  and frequency  $\omega/\omega_{pe} \sim 0.9996$  can be generated by beams as tenuous as  $n_B/n_0 \sim 10^{-3}$ . The waves couple to the beam such that  $\mathbf{k} \cdot \mathbf{v}_B/\omega_{pe} \sim 1.45$ . If  $k_{\parallel}$  and  $k_{\perp}$  are the components of  $\mathbf{k}$  along and across the beam direction ( $\mathbf{v}_B/v_B$ ), then for  $k_{\perp}/k_{\parallel} < 10^{-1}$ , the solutions of *Fredricks et al.* [1971a] yield quasitransverse modes with a measurably large  $B$  component. Wherever the solar wind density  $n_0$  has been high enough to allow beams to excite 70 kHz fluctuations, both  $E$  and  $B$  components have been observed [*Scarf et al.*, 1970a].

The theory of the generation of the upstream plasma

oscillations is discussed by *Fredricks et al.* [1971a]. *Fredricks et al.* [1971b] also have given an extensive statistical survey of the distributions in space and time of the upstream oscillations. Here we present briefly some preliminary results extracted from a study based on 31 orbits of OGO-5 as a means of illustrating a very important point: namely, that near the earth the solar wind is clearly disturbed by backstreaming electrons over the entire sunlit hemisphere as mapped by OGO-5.

## EXPERIMENTAL RESULTS

A study of electric field fluctuations has been made for orbits 106 to 151 of OGO-5. This covers the time period December 2, 1968, to early April 1969, and local times (at apogee) from about 1600 to about 0800 hr. The maximum, minimum, average, and standard deviation of all electric and magnetic field channels of the PWDE were obtained for each 3.23-min (193.536-sec) experiment cycle [*Crook et al.*, 1969]. We present here a few

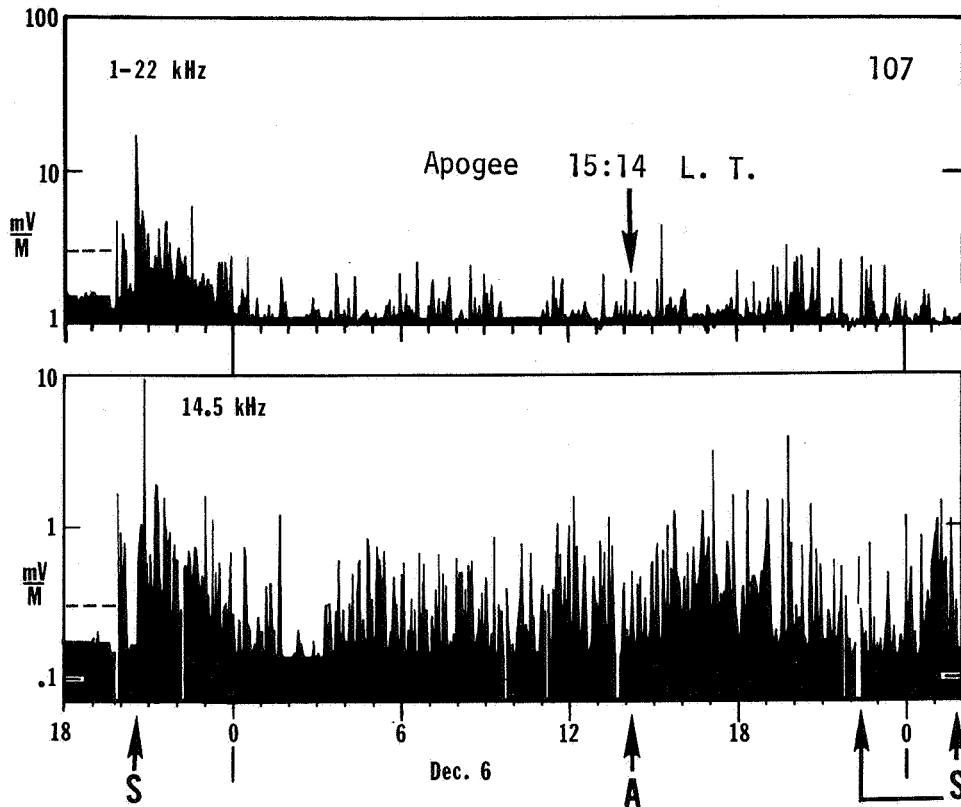


**Figure 1.** Upstream electric field fluctuating levels measured on orbit 107 of OGO-5. The bow shocks and apogee are indicated by S and A, respectively. The maximum value of the electric field in the 1–22 kHz broadband each 3.23 min is plotted in the top panel, while the maximum and minimum values (bottom of panel) are plotted for the  $14.5 \pm 1.1$  kHz narrowband channel in the lower panel. More details are given in the text. Abscissa is universal time.



illustrative data plots extracted from this more extensive study.

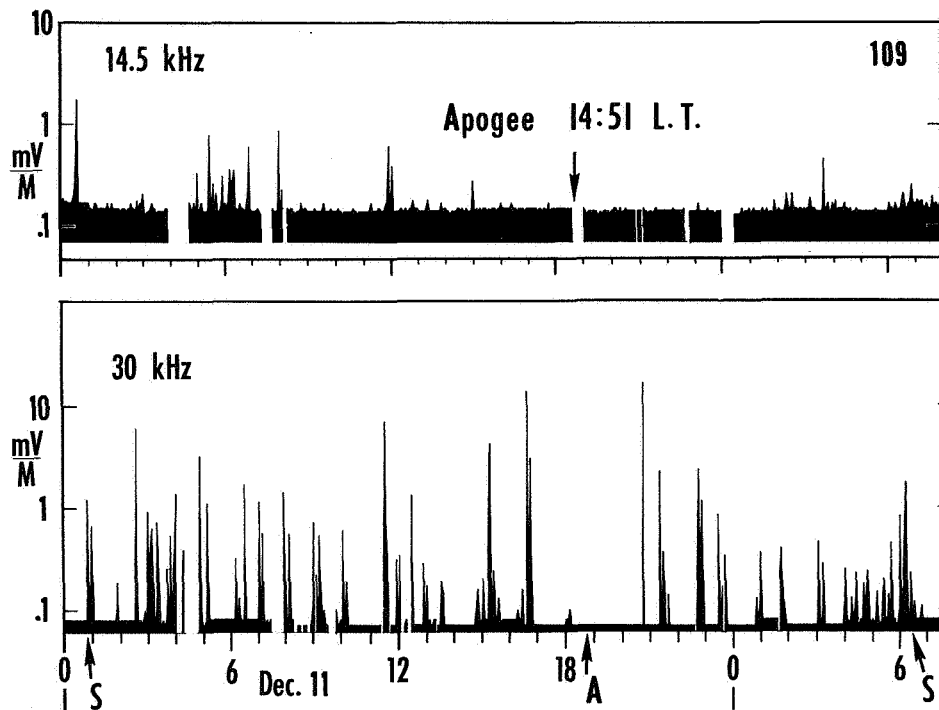
The three channels most frequently active in the upstream region, from the last outbound to the first inbound encounters with the bow shock, are the  $14.5 \pm 1.1$ -kHz and  $30 \pm 2.25$ -kHz narrowband electric field channels, and the 1- to 22-kHz broadband electric field channel. As noted previously, those channels cover the expected range of the normal solar wind plasma frequency.

Figure 1 shows the 1- to 22-kHz broadband and the 14.5-kHz electric field channels for the portion of orbit 107 beyond the bow shocks. Encounters with the last outbound and first inbound bow shock are marked by an *S* at the two extremes of the plot, while apogee is denoted by *A*. This particular orbit, with apogee at 1514 hr local time, was entirely on the dusk side of the earth-sun line. The 30-kHz channel remained inactive throughout, while the 14.5-kHz narrowband and the 1- to 22-kHz broadband channels contained activity over practically the entire interplanetary portion. The 1- to 22-kHz plot shows only the maximum value each 3.23 min, while the 14.5-kHz data are maximum and minimum ( $\sim 0.07$  mV/M) values each 3.23 min. As discussed by Scarf *et al.* [1971], the field values in figures 1

through 4 assume a signal at the center frequency of the narrowband filters, and they are therefore lower limits, since signals at frequencies away from the center frequency suffer attenuation.

A relatively inactive orbit is described in figure 2. Here the 14.5- and 30-kHz narrowband maximum-minimum (max-min) data are plotted for orbit 109. The broadband 1- to 22-kHz channel remained at or very near threshold during the interval covered by figure 2. Although comparison of figure 2 with figures 1 and 3 (below) shows the relative quietness of orbit 109, there is sporadic wave activity throughout, indicating the presence of at least occasional suprathermal electron streams.

Figure 3 shows the 1- to 22-kHz broadband and 30-kHz narrowband channels for portions of orbit 110 while OGO-5 was in the interplanetary regime. Again, shocks are marked by *S*, and apogee at 1451 hr local time by *A*. Negligible activity was present in the 14.5-kHz *E*-field channel on this orbit. The simultaneous response of the 1- to 22-kHz broadband channel indicates that the true local wave frequency was probably between 22 and 30 kHz, or in the rolloff region of both filter characteristics, and far enough above



**Figure 2.** Upstream electric field fluctuation (max-min) levels measured each 3.23 min on orbit 109 of OGO-5 in  $14.5 \pm 1.1$  kHz and  $30 \pm 2.25$  kHz narrowband channels. Broadband channel was near or at threshold for this orbit. More detail in text.

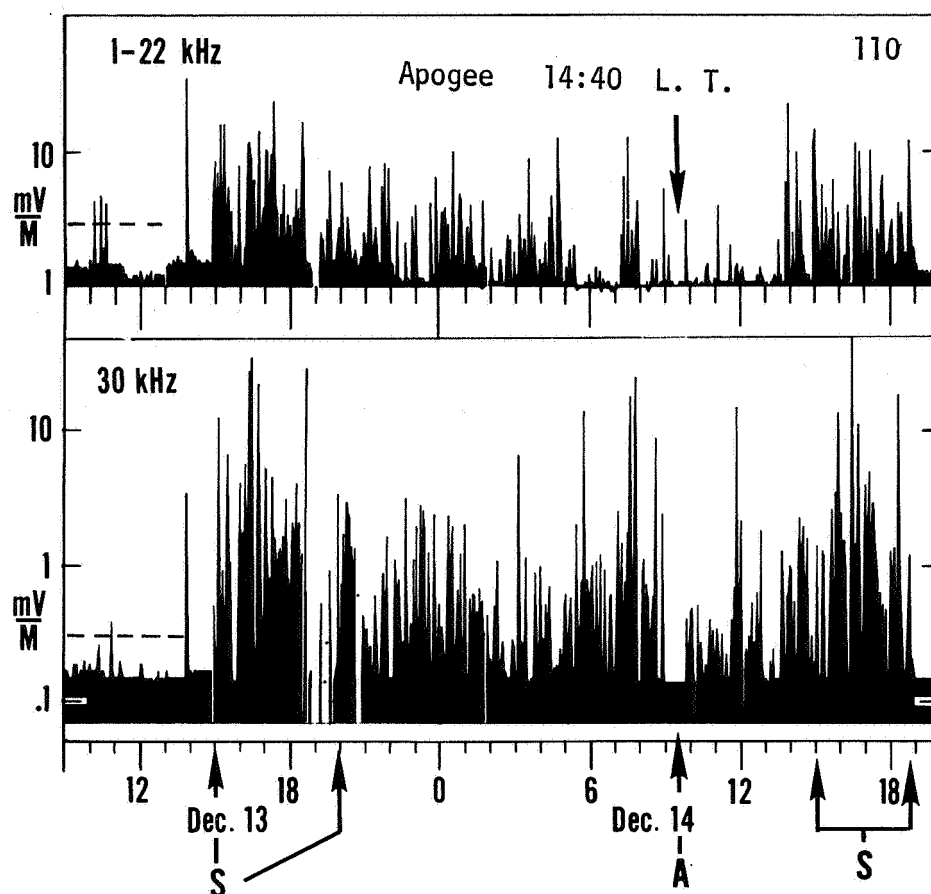


**Figure 3.** Upstream electric field fluctuation levels measured on orbit 110 of OGO-5. The 1-22 kHz broadband shows only maximum value each 3.23 min, while 30 kHz narrowband plot shows max-min.

14.5 kHz to be undetectable in that channel. These considerations imply that a very strong signal between 22 and 30 kHz was generated by electron streams interacting with a solar wind of density on the order of 6 to 10  $\text{cm}^{-3}$ , while for orbit 107 (fig. 1) the solar wind density was on the order of 2 to 3  $\text{cm}^{-3}$ .

Figure 4 shows the 1- to 22-kHz broadband and the 14.5- and 30-kHz narrowband max-min plots for orbit 145 of OGO-5, with apogee at 0826 hr local time. Thus, this orbit was on the dawn side of the earth-sun line. It is noteworthy that all three channels in figure 4 show significant levels of wave activity. Again, a great deal of wave turbulence near  $\omega_{pe}$  occurred, while some of the broadband activity was caused by waves exciting the 3- and 7.35-kHz narrowband channels (not shown). These latter waves are associated with backstreaming protons [Scarf *et al.*, 1970b] and also with MHD disturbances seen by the dc magnetometers. Such proton-related electrostatic waves are rarely observed on orbits lying

duskward of the earth-sun line, which is consistent with observations of Fairfield [1969], Russell *et al.* [1971], and others that upstream MHD waves are found with large statistical predominance in the dawn-to-noon local time sector.

## DISCUSSION

Based on studies of electric field fluctuations measured by the PWDE aboard OGO-5, and by an extrapolation of the previously reported direct correlations of LEPDEA and low energy plasma probe data with those of PWDE, it is apparent that very significant wave-particle interactions are present in the near-earth solar wind. This region therefore must be considered as disturbed upstream by the presence of the earth and its magnetosphere.

Some important aspects of these observations are summarized as follows:

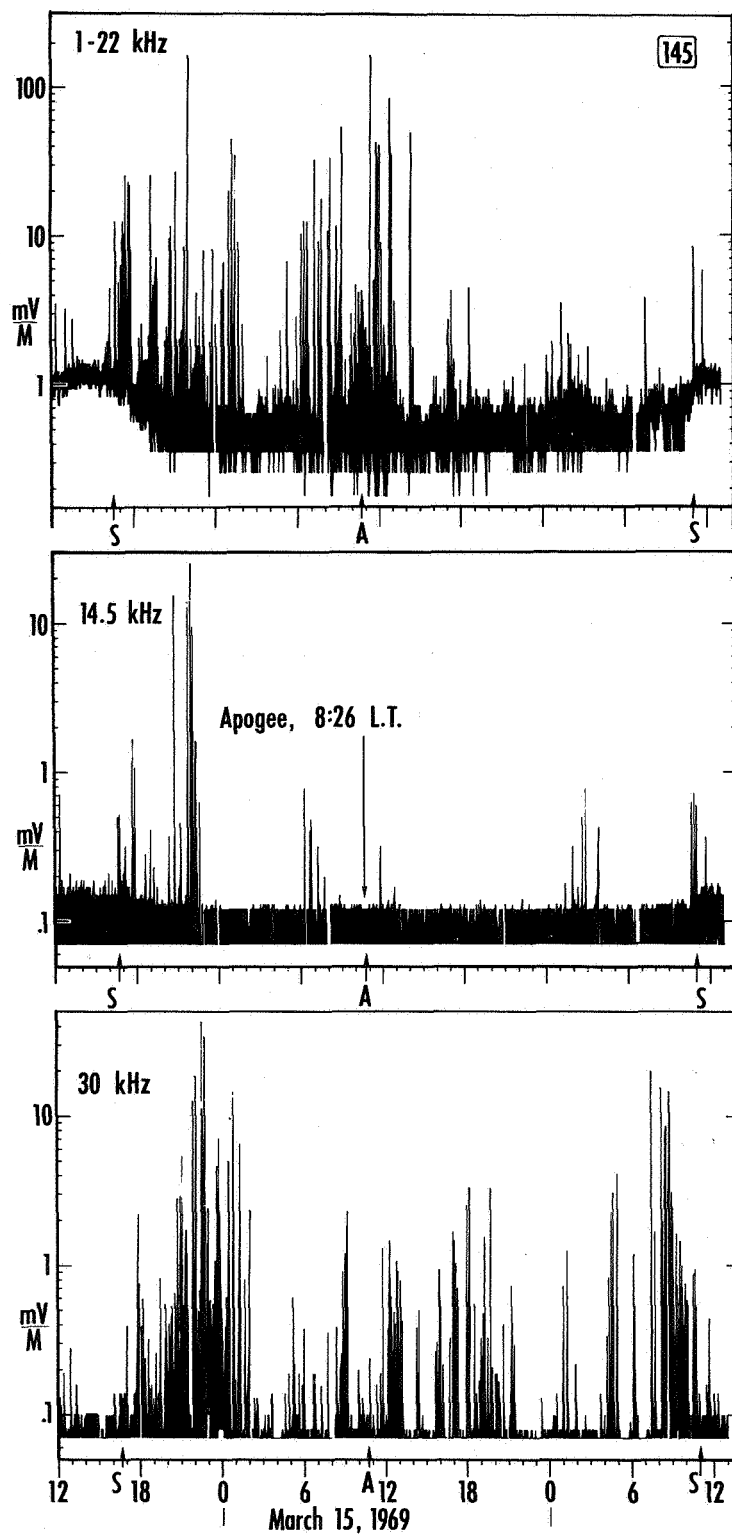


Figure 4. Upstream electric field fluctuation max-min levels on orbit 145 of OGO-5. Details in text.

1. Suprathermal electron streams appear to be generated by the solar wind-earth interaction, either at the bow shock or near it.
2. These streams penetrate the solar wind on both dusk and dawn sides of the earth-sun line, where they produce a significant level of wave turbulence at or close to the local electron plasma frequency.
3. The fluctuation level, or energy density in the waves,  $\langle E^2 \rangle / 8\pi$ , is several orders of magnitude above the solar wind thermal level ( $\sim 1 \mu\text{V}/M$ ), but less than the total available directed energy density in the streams. Equipartition with  $\langle E^2 \rangle / 8\pi \sim n_B m v_B^2 / 2$  implies  $E \sim 200 \text{ mV}/M$  wherever both wave and particle data have been available to estimate these quantities.
4. The waves are most probably quasi-electromagnetic modes driven by the electron streams, and the resulting wave turbulence levels are locally important to any heat flow or energy balance considerations.
5. Strong waves are observed even at apogee ( $\sim 23 R_E$ ), and no orbit has been found to be completely devoid of such disturbances at or near  $\omega_{pe}$ , although some are more quiet than others.
6. When these waves are present it is unlikely that measurements of electron energy spectra in near-earth orbits are trustworthy replicas of deep-space solar wind electron distributions, because of the wave-particle effects described here.

#### ACKNOWLEDGMENTS

The work reported here was supported by the National Aeronautics and Space Administration, Goddard Space Flight Center, OGO Project, under contract number NAS 5-9278. We are very grateful to Marcia Neugebauer of JPL and L. A. Frank of the University of Iowa for furnishing supporting particle data, which have been central to understanding the data reported here.

#### DISCUSSION

*K. Schindler* In connection with these large anisotropies of electrons in front of the bow shock discussed by Fredricks, it may be of interest that one can excite whistlers, by sufficiently large electron anisotropy, if they go obliquely to the magnetic field. The existence of such a nonresonant instability has recently been established in studies by myself and others.

*F. Perkins* I have several questions. The first question is for Bob Fredricks. Is the energy in these plasma waves sufficient to cause the electron heating that is felt to be important in front of shocks?

*R. W. Fredricks* No, I don't think so. These waves have high phase speeds corresponding to electrons in the part of the tail that is quite far away from the main body of the solar wind distribution and therefore these waves do not do much heating. However, if these effects last long enough the integrated result could be some nonresonant scattering.

*F. Perkins* Perhaps the coupling could come if the waves propagate in an inhomogeneous plasma, and consequently change their wavelength and the location of the

#### REFERENCES

- Crook, G. M.; Scarf, F. L.; Fredricks, R. W.; Green, I. M.; and Lukas, P.: The OGO-5 Plasma Wave Detector; Instrumentation and In-Flight Operation. *IEEE Trans. Geosci. Elec. GE-7*, Vol. 2, 1969, p. 120.
- Fairfield, D. H.: Bow Shock Associated Waves Observed in the Far Upstream Interplanetary Medium. *J. Geophys. Res.*, Vol. 74, 1969, p. 3541.
- Fredricks, R. W.; Scarf, F. L.; and Frank, L. A.: Non-Thermal Electrons and High Frequency Waves in the Upstream Solar Wind, 2, Theoretical Interpretations. Submitted to *J. Geophys. Res.*, 1971a.
- Fredricks, R. W.; Scarf, F. L.; and Green, I. M.: Electric Field Fluctuations Beyond the Bow Shock to  $23 R_E$ . Submitted to *J. Geophys. Res.*, 1971b.
- Russell, C. T.; Childers, D. D.; and Coleman, P. J., Jr.: OGO-5 Observations of Upstream Waves in the Interplanetary Medium: Discrete Wave Packets. *J. Geophys. Res.*, Vol. 76, 1971, p. 845.
- Scarf, F. L.; Fredricks, R. W.; Green, I. M.; and Neugebauer, M.: OGO-5 Observations of Quasi-Trapped Electromagnetic Waves in the Solar Wind. *J. Geophys. Res.*, Vol. 75, 1970a, p. 3735.
- Scarf, F. L.; Fredricks, R. W.; Frank, L. A.; Russell, C. T.; Coleman, P. J., Jr.; and Neugebauer, M.: Direct Correlation of Large Amplitude Waves with Suprathermal Protons in the Upstream Solar Wind. *J. Geophys. Res.*, Vol. 75, 1970b, p. 7316.
- Scarf, F. L.; Fredricks, R. W.; Frank, L. A.; and Neugebauer, M.: Non-thermal Electrons and High Frequency Waves in the Upstream Solar Wind, 1, Observations. Submitted to *J. Geophys. Res.*, 1971.

resonance in velocity space. At any rate, I would like to mention that there is some evidence that the heat conduction instability occurs because of anisotropy of the ion velocity distribution. The heat conduction instabilities all give diffusion on the backward part of the ion velocity distribution. The backward part seems to be much colder than the forward part and one can argue that this is circumstantial evidence for the occurrence of the heat conduction instability.

Last, I would like to ask Dave Forslund whether the electromagnetic ion cyclotron instability, that seems to be so easily set off, has a significant component of plasma density fluctuations with it so that it might be relevant to the radio star scintillations.

*D. W. Forslund* It may have some density fluctuation. I haven't checked it in detail, but our computations show that there is a significant electric field in the direction of  $\mathbf{k}$ . In fact, it can be larger than the component perpendicular to  $\mathbf{k}$  even though the electromagnetic part is polarized as required for an electromagnetic wave. I suspect that the large  $\mathbf{E}$  field in the direction of  $\mathbf{k}$  should cause some density fluctuations.

*M. Montgomery* I have a couple of questions for Bob Fredricks. First, your figures indicate that the plasma frequency noise was present most of the time. Are you implying, then, that the electron streams in the bow shock are observed most of the time? Is there a direct and consistent correlation between the noise and the upstreaming electrons?

*R. W. Fredricks* There is insofar as we have been able to determine from simultaneous LEPEDea measurements. Whenever the waves are seen there are bursts of these electron fluxes above 380 V with this characteristic. But this correlation study is limited to early March 1968 data when Frank's instrument was on. Unfortunately, there was a failure in his instrument on March 12, 1968. Therefore, I am extrapolating because during the interval covered by the simultaneous measurements the waves were always associated with the disturbed electron distribution.

*M. Montgomery* Do you mean correlated with the upstreaming electrons? Can we assume then from your data that most of the time when OGO-5 is outside the bow shock there were upstreaming electrons present?

*R. W. Fredricks* There are many bursts of electrons, but there can be time intervals of minutes when none occurs. One point that I didn't mention is that when we see these high-frequency electron plasma frequency waves there are no correlations with magnetic perturbations of any size.

*M. Montgomery* That brings to mind the next question I was going to ask. That is, when you see these noise bursts, what is the field configuration? Is the field configuration consistent with OGO-5 being on a line of force connected with the bow shock?

*R. W. Fredricks* I haven't done a systematic study yet, I can't answer that question. But there seems to be no systematic difference between the dawn and dusk quadrants. This is not true of the proton generated noise, which seems to be concentrated on the dawn side of the earth sun line.

*M. Montgomery* And then the last question is, from the LEPEDea measurements can you estimate the amount of energy flux being carried away from the shock?

*R. W. Fredricks* I haven't calculated it yet. I don't know.

*M. Montgomery* That is a relatively important quantity to know.

*R. W. Fredricks* This does indicate when this is going on the local heat flux vector could be pointing in some arbitrary direction. It doesn't have to be from the sun or back towards the sun.

*M. Montgomery* It worries me a little bit that you see it so much of the time, especially when the magnetic field line upon which OGO-5 is located is not likely to be connected to the bow shock.

*R. W. Fredricks* Well, I believe I have an answer for that, but right now I don't want to commit myself to a statement that there is *no* field alignment correlation. This requires a further study.

## MAGNETIC FIELD MERGING IN THE SOLAR WIND *Karl Schindler*

**ABSTRACT** Magnetic field merging in the solar wind is discussed in terms of steady-state merging, which involves a steady flow field, and of spontaneous merging, which involves an instability such as the tearing instability. Spontaneous merging is found to be much more effective than steady-state merging.

### INTRODUCTION

It is generally believed that magnetic field merging takes place in the neutral sheet of the geomagnetospheric tail [Dungey, 1961; Axford *et al.*, 1965; Coppi *et al.*, 1966; Dessler, 1968]. The question has been raised [Dessler, 1970] of whether one would expect similar processes to occur in the interplanetary sector boundaries. Merging of magnetic lines of force is of interest because it governs the topology of the magnetic field and thereby, for instance, electron heat conduction; also, the electric fields involved can accelerate particles inside the neutral sheet.

Available satellite observations seem to be consistent with the concept of an ideal sector structure within 1 AU [Wilcox and Ness, 1965]. Therefore, we may state the problem of field line merging in the solar wind in the form of two questions: Why is merging unimportant within 1 AU? Do we or don't we expect more merging at larger heliocentric distances? There is no final answer to these questions as yet. This note approaches the problem from a particular viewpoint and gives some preliminary answers that could perhaps serve as a basis for further discussion.

It seems convenient to distinguish between *steady-state* merging, which involves a steady flow field, and *spontaneous* merging, which involves an instability such as the tearing instability [Schindler and Soop, 1968].

Both types of merging have been suggested for the magnetospheric tail, and it is quite possible that both

occur under suitable circumstances. For instance, there is increasing evidence that the neutral sheet has a fine structure that can be consistently explained by assuming spontaneous merging [Schindler and Ness, 1971].

Similarly, for sector boundaries we cannot *a priori* exclude either type of merging. However, on the basis of the simple estimate given at the end of this note, it seems that steady-state merging is less important than spontaneous merging for the solar wind. We therefore concentrate on processes involving neutral sheet instabilities to see in what way and to what extent they might lead to merging of magnetic field lines across the sector boundaries.

### SPONTANEOUS MERGING

Let us consider stability of a static one-dimensional neutral sheet separating regions of homogeneous magnetic field with opposite field directions. It is easy to show that such neutral sheets are stable against perturbations that keep the magnetic field strictly frozen into the plasma—that is,  $\mathbf{E} + \mathbf{v} \times \mathbf{B} = 0$ . This implies that at the neutral plane ( $B = 0$ ) the electric field has to vanish. It is a characteristic property of neutral sheet instabilities that this constraint is violated, allowing for a finite electric field in the neutral sheet.

Table 1 gives some properties of a number of neutral sheet instabilities. It is evident that the two tearing instabilities are those with the largest wavelengths and hence they are more likely to give rise to macroscopic effects. Table 2 indicates how tearing can be stabilized.

---

*The author is at the European Space Research Institute, Frascati, Rome, Italy.*

**Table 1.** *Neutral sheet instabilities*

Mode	Driven by	Geometry	Approximate growth rate	Reference
Collision-free tearing	Electrons passing neutral plane	$k_B L < 1$ $k_j L < \left(\frac{a_i}{L}\right)^{1/4} \sqrt{k_B L}$	$k v_{th_e} \left(\frac{a_e}{L}\right)^{3/2}$	[Laval et al., 1966]
Resistive tearing	Finite resistivity	$k_j \approx 0$	$\frac{\eta}{\mu_0 L^2} \left(\frac{\mu_0 v_A}{k \eta}\right)^{2/5}$ $S^{-1/4} < kL < 1$	[Furth et al., 1963]
Resistive rippling	Spatial variation of resistivity	$k_B = 0$	$\frac{\eta}{\mu_0 L^2} \left[ \left(\frac{L \eta'}{\eta}\right)^2 \frac{k L^2 \mu_0 v_A}{\eta} \right]^{2/5}$ $S^{-2/7} < kL < S^{2/3}$	[Furth et al., 1963]
Resistive gravitational interchange	Finite resistivity and external force	$k_B = 0$	$\frac{\eta}{\mu_0 L^2} \left( \frac{L  \rho_0' }{\rho_0} \frac{k L^3 \mu_0 g}{\eta v_A} \right)^{2/3}$ $S^{-1/4} G^{1/8} < kL < S^{1/2} G^{-1/4}$ $G < 1, (kL)^2$ $G > (kL)^{-2/5} S^{-2/5}, (kL)^{-8/5} S^{-2/5}$	[Furth et al., 1963]
Fried-Weibel (collision-free)	Temperature anisotropy	$k_B \approx 0$	$\frac{v_{th_e}}{a_e} \left( 1 - \frac{T_\perp}{T_\parallel} \right)_e^{5/4}$	[Fried, 1959; Weibel, 1959]

$S = \frac{\mu_0 L v_A}{\eta}$	$\rho_0$	mass density
$G = \frac{L^2 g  \rho_0' }{V_A^2 \rho_0}$	$L$	neutral sheet width
$\mu_0$	$\eta$	resistivity
$v_A$	$g$	acceleration due to external force
$v_{th}$	$'$	derivative normal to the sheet
	$R$	wave number
	$a$	Larmor radius
	$T$	temperature

Subscripts  $e, i, B, j, \perp, \parallel$  refer to electrons, ions, direction of the magnetic field  $\mathbf{B}$ , direction of the electrical current  $\mathbf{j}$ , direction perpendicular and parallel to  $\mathbf{B}$ .

The average electron temperature anisotropy in the solar wind works in the direction of stabilization. However, since the average anisotropy is small, there may be times during which the isotropy is reversed, such that the tearing wave can grow. Also it seems possible to visualize nonlinear perturbations that grow even in the linearly stable regime. Of course, we do not assume a normal field component at the outset, because that should be the result of merging. Nor do we have to worry about boundaries in the solar wind.

The problem becomes more involved when we look at

the nonlinear properties of tearing. Quasilinear stabilization is effective for extremely small initial perturbations [Biskamp et al., 1970], and it may not be important if the initial perturbation is larger or if the spectrum is sufficiently narrow. Under suitable conditions a single mode will grow and field loops will start to coalesce by forming larger loops from smaller ones. This process is much faster than the original tearing [Biskamp and Schindler, 1971]. When sufficiently large concentrations of the electrical current are formed, it is conceivable that magnetohydrodynamic pinch instabilities will set in,

**Table 2.** Properties related to the stabilization of collision-free tearing

1. Temperature anisotropy (linear theory) [Coppi and Rosenbluth, 1968; Laval and Pellat, 1968]

$$(T_{\parallel} - T_{\perp} / T_{\parallel})_e > a_e / L$$

2. Normal magnetic field component (linear theory?)

3. Boundary stabilization:

Boundary at a few neutral sheet widths [Furth, 1968]

4. Nonlinear effects

- a. Quasi-linear stabilization at

$$B/B_0 \sim ka_e(a_e/L)^2$$

[Biskamp et al., 1970]

- b. Single mode dynamics

Loop merging [Biskamp and Schindler, 1971]

$$\gamma \sim \min \begin{cases} kv_{the} \sqrt{a_e/L} (\log \sqrt{L/a_e})^{-1/2} \\ kv_{thi} \end{cases}$$

MHD pinch-instabilities

$$\gamma \sim kv_{thi}$$

$\gamma$  growth rate,  $B$  absolute value of magnetic field perturbation; other quantities as in table 1.

which may stop further loop growth. Because of the large growth rate for coalescence of loops, a firm answer cannot be given at the present time.

Let us therefore explore the consequences of the hypothesis that, in an infinite system, tearing would grow indefinitely. In a finite system with a convective flow superimposed, as there is both in the solar wind and in the magnetosphere, the occurrence of merging would then depend on the ratio of the growth time of the tearing instability and the characteristic time of convective flow across the system.

Figure 1 gives the critical heliocentric radius  $R^*$  at which tearing will occur as a function of the width  $L$  of the sector boundary.  $R^*$  is given by

$$\int_{R^*}^{\infty} \frac{\gamma(R)}{v_{sw}} dR = 1$$

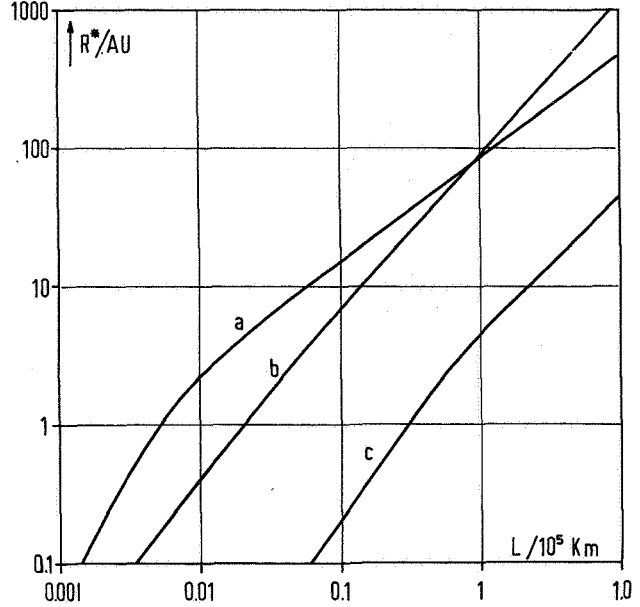


**Figure 1** Heliocentric distance  $R^*$  at which tearing may occur as a function of the width  $L$  of the sector boundary: (a) resistive, (b) collision-free, and (c) collective-resistive tearing with  $v_{eff} = 10^{-3} \omega_{pi}$  (see also text).

To evaluate the radial dependence of the growth rate  $\gamma$  a very simple solar wind model is chosen. The velocity  $v_{sw}$  is constant (500 km/sec), and the magnetic field lines form Archimedean spirals. For  $R < 1$  AU the electron temperature scales as  $R^{-2/5}$ ; going to  $T_e \sim R^{-2/7}$  would not change the results significantly [Forsslund, 1970]. For  $R > 1$  AU we assume adiabatic electron cooling with a specific heat ratio of 5/3. Note that  $L$  does not vary with distance in an Archimedean spiral field.

The collision-free tearing curve does not use the standard sheet pinch growth rate [Laval et al., 1966], which was derived for a situation where the plasma density drops to zero outside the neutral sheet, but a more general form that applies to situations such as the solar wind:

$$\gamma \sim kv_{the} \frac{(c/\omega_{pe})^2}{\sqrt{a_e} L^{3/2}}$$

The notation is explained in the captions of tables 1 and 2. For  $L = 10^5$  km, which is close to the upper limit  $L = 1.5 \times 10^5$  km [Wilcox and Ness, 1965], tearing would become important only for  $\geq 100$  AU. Smaller widths would lead to tearing closer to the sun. To have tearing at 1 AU, one would need sector boundaries as thin as 2000 km. More experimental information on the width of sector boundaries is necessary before one can cite this fact as a possible reason for the absence of tearing for



$R \lesssim 1$  AU. Within roughly 100 AU, resistive tearing based on electron-ion collisions requires even smaller values of  $L$ , for instance,  $L \sim 500$  km for  $R^* \sim 1$  AU. For  $R > 100$  AU, resistive tearing is more effective than the collision-free mode.

Resistive tearing may also be produced if small-scale electrostatic fluctuations are present, leading to an effective collision frequency  $\nu_{eff}$ . Choosing  $\nu_{eff} = \epsilon \omega_{pi}$ , the curve  $c$  in figure 1 corresponds to  $\epsilon = 10^{-3}$ . The same curve holds for arbitrary values of  $\epsilon$  if we reinterpret the abscissa as measuring the quantity  $10 L/\epsilon^{1/3}$  instead of  $L$ . More experimental observation on the fluctuation level is necessary before the importance of collective-resistive tearing can be firmly evaluated.

Although we are not concerned here with the magnetosphere it may be interesting to note that for a neutral sheet width of  $1 R_E$ , a characteristic length along the tail of  $100 R_E$ , and a convection speed of  $5 \cdot 10^6$  cm/sec, the growth time of the (collision-free) tearing instability is about equal to the characteristic time for convection. Therefore, also in the magnetosphere convection may be responsible for limiting the growth of tearing.

It remains to visualize the field configuration a spatially growing tearing mode would give. Figure 2

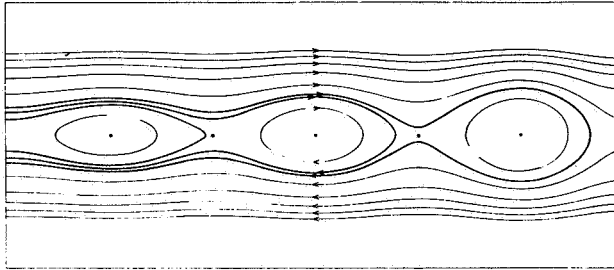


**Figure 2** Qualitative picture of field lines of a neutral sheet configuration with a spatially growing tearing mode. Note field line merging (heavy field lines).

shows what one qualitatively obtains by replacing time in a typical tearing mode perturbation by the space coordinate (divided by the flow velocity) along the field lines. It is evident that by this process field lines of neighboring sectors merge, thereby more and more decoupling the out-flowing plasma magnetically from the sun.

### STEADY-STATE MERGING

To estimate the importance of steady-state merging, we compare the characteristic time  $\tau$  with the resistive tearing growth time. We obtain  $\tau$  from

$$\frac{d\psi}{dt} = - \oint_s \eta \mathbf{j} \cdot d\mathbf{s}$$

where  $\psi$  is the magnetic flux through a closed integration path  $s$  moving with the plasma. With  $d\psi/dt \sim \delta\psi/\tau = \kappa\psi/\tau$  ( $\kappa$  being the fraction of the total flux dissipated after time  $\tau$ ) we estimate

$$\tau \sim \kappa \frac{sL\mu_0}{\eta}$$

where  $s$  is the characteristic length of a flux tube of one polarity. We compare with resistive tearing (growth rate  $\gamma$ ) by estimating

$$\gamma\tau \sim \left( \frac{L\omega_p^2 \nu_A}{c^2 \nu} \right)^{1/2} \frac{\kappa s}{L}$$

Both processes are expected to have roughly the same macroscopic effect if  $\kappa \sim L/s$ . Thus we find for solar wind conditions at 1 AU

$$\gamma\tau \sim 3 \times 10^5$$

### CONCLUSIONS

From the above, spontaneous merging clearly is much more effective than the corresponding steady-state process. Note that spontaneous merging is not expected to be as regular as shown in figure 2, which is only given to illustrate the field line topology. In fact, one might rather expect a turbulent structure. The present conclusions must remain tentative, however, until more experimental data (such as the width of sector boundaries) and theoretical information (such as the long-time asymptotic behavior of the tearing instability) are available.

### REFERENCES

- Axford, W. I.; Petschek, H. E.; and Siscoe, G. L.: Tail of the Magnetosphere. *J. Geophys. Res.*, Vol. 70, 1965, p. 1231.
- Biskamp, D.; Sagdeev, R. Z.; and Schindler, K.: Non-Linear Evolution of the Tearing Instability of the Geomagnetic Tail. *Cosmic Electrodyn.*, Vol. 1, 1970, p. 297.
- Biskamp, D; and Schindler, K.: Instability of Two-Dimensional Collisionless Plasma with Neutral Points. Submitted to *Plasma Phys.*, 1971.
- Coppi, B.; Laval, G.; and Pellat, R.: Dynamics of the Geomagnetic Tail. *Phys. Rev. Letters*, Vol. 16, 1966, p. 1207.
- Coppi, B.; and Rosenbluth, M. N.: Model for the Earth's Magnetic Tail, in *Stability of Plane Plasmas*, ESRO SP-36, 1968.

- Dessler, A. J.: Correction to a Paper by A. J. Dessler, "Magnetic Merging in the Magnetospheric Tail." *J. Geophys. Res.*, Vol. 73, 1968, p. 1861.
- Dessler, A. J.: The Role of the Geomagnetic Tail in Substorms. Invited review presented at the STP Symposium, Leningrad, U.S.S.R., May 11-20, 1970.
- Dungey, J. W.: Interplanetary Magnetic Field and the Auroral Zones. *Phys. Rev. Letters*, Vol. 6, 1961, p. 47.
- Forslund, D. W.: Instabilities Associated with Heat Conduction in the Solar Wind and Their Consequences. *J. Geophys. Res.*, Vol. 75, 1970, p. 17.
- Fried, B. D.: Mechanism for Instability of Transverse Plasma Waves. *Phys. Fluids*, Vol. 2, 1959, p. 337.
- Furth, H. P.: The External Region of the Tearing Mode, in *Stability of Plane Plasmas*, ESRO SP-36, 1968.
- Furth, H. P.; Killeen, J.; and Rosenbluth, M. N.: Finite-Resistivity Instabilities of a Sheet Pinch. *Phys. Fluids*, Vol. 6, 1963, p. 459.
- Laval, G.; and Pellat, R.: Stability of the Plane Neutral Sheet for Oblique Propagation, in *Stability of Plane Plasmas*, ESRO SP-36, 1968.
- Laval, G.; Pellat, R.; and Vuillemin, M.: Proceedings of the Conference on Plasma Physics and Controlled Nuclear Fusion, Culham 1965, Vol. II, International Atomic Energy Agency, Vienna, 1966, Paper CN-21/71.
- Schindler, K.; and Ness, N. F.: Neutral Sheet Fine Structure. Paper presented at the AGU Meeting, April 12-16, Washington, D.C., 1971.
- Schindler, K.; and Soop, M.: Stability of Plasma Sheaths. *Phys. Fluids*, Vol. 11, 1968, p. 1192.
- Weibel, E. S.: Spontaneously Growing Transverse Waves in a Plasma Due to an Anisotropic Velocity Distribution. *Phys. Rev. Letters*, Vol. 2, 1959, p. 83.
- Wilcox, J. M.; and Ness, N. F.: Quasi-Stationary Corotating Structure in the Interplanetary Medium. *J. Geophys. Res.*, Vol. 70, 1965, p. 5793.

## DISCUSSION

*M. Dryer* Karl, did I understand you to say that the merging will take place independent of the boundary conditions but rather depending on the modes that caused the resistivity? The boundary conditions do not matter?

*K. Schindler* Yes, in a certain sense. You see I was just quoting or trying to quote the existing models for merging. And there are particular classes that depend very highly on boundary conditions, such as the slow fields of this type. We may have this locally somewhere in the solar wind, but this is the exception rather than the rule because the solar wind models don't have these particular situations as they probably have it in the magnetosphere. So tentatively I have excluded these classes for this discussion.

## COMMENTS ON THE MEASUREMENT OF POWER SPECTRA OF THE INTERPLANETARY MAGNETIC FIELD

Christopher T. Russell

Examination of the possible sources of noise in the measurement of the power spectrum of fluctuations in the interplanetary magnetic field shows that most measurements by fluxgate magnetometers are limited by digitization noise whereas the search coil magnetometer is limited by instrument noise. The folding of power about the Nyquist frequency or aliasing can be a serious problem at times for many magnetometers, but it is not serious during typical solar wind conditions except near the Nyquist frequency. Waves in the solar wind associated with the presence of the earth's bow shock can contaminate the interplanetary spectrum in the vicinity of the earth. However, at times the spectrum in this region is the same as far from the earth. Doppler shifting caused by the convection of waves by the solar wind makes the interpretation of interplanetary spectra exceedingly difficult.

### ABSTRACT

### INTRODUCTION

The interplanetary magnetic field has been probed by many spacecraft, and it has been popular to calculate the power spectrum of the fluctuations in the interplanetary magnetic field with the hope of gaining some insight into the physical processes occurring in the solar wind. Power spectra have been obtained from Pioneer 5 [Coleman, 1964], Mariner 2 [Coleman, 1966], OGO-1 [Holzer *et al.*, 1966], Mariner 4 [Siscoe *et al.*, 1968], Pioneer 6 [Sari and Ness, 1969], Mariner 5 [Belcher and Davis, 1971] and OGO-5 [Childers *et al.*, 1971]. Although the calculation of power spectra is quite straightforward analytically, there are many technical difficulties involved in determining the power spectrum of solar wind fluctuations. They stem mainly from the fact that the magnetic field and its fluctuations are quite small. Thus, it is possible that noise sources inherent in the measurement process could significantly add to the measured power spectrum. In addition, since many instruments have much wider pass bands than the bandwidth of the power spectrum being measured, noise from outside the nominal frequency band of the

spectrum may be folded into the spectrum. This effect, called *aliasing*, in some cases can alter the spectrum significantly. Further, a spectrum measured in the solar wind may not be truly representative of the interplanetary medium if it is measured near the earth, since waves, apparently radiated from the earth's bow shock, are present for large distances (up to  $46 R_E$ ) from the shock in the solar wind [Fairfield, 1969; Russell *et al.*, 1971]. Here we examine the extent that these problems have affected measured interplanetary spectra, and in this light construct a meaningful typical interplanetary spectrum. Finally, we shall make some comments on the interpretation of interplanetary power spectra, mainly as a guide to the uninitiated.

### INSTRUMENT NOISE LEVELS

Since the interplanetary field is so small, approximately  $10^{-4}$  of that at the surface of the earth, one of the first questions that might be asked is whether the inherent noise levels of the magnetometers are comparable to the noise being measured. In particular, we would like to compare the spectrum of the instrument noise with the measured interplanetary spectrum. Unfortunately, very

*The author is at the Institute of Geophysics and Planetary Physics, University of California at Los Angeles.*

few magnetometer experimenters have made this comparison. Usually, at best, an rms amplitude noise over some bandwidth is quoted with no clue as to the distribution of the noise over this band. Figure 1 shows instrument noise levels for the OGO-3 search coil magnetometer [Russell *et al.*, 1970] and for two fluxgate magnetometers, which were backup units for two different deep space missions. Also on this figure is a curve representing a typical quiet spectrum of one component of the interplanetary field in this frequency range. The justification for this curve will be given later.

We see that the noise spectrum of both fluxgate

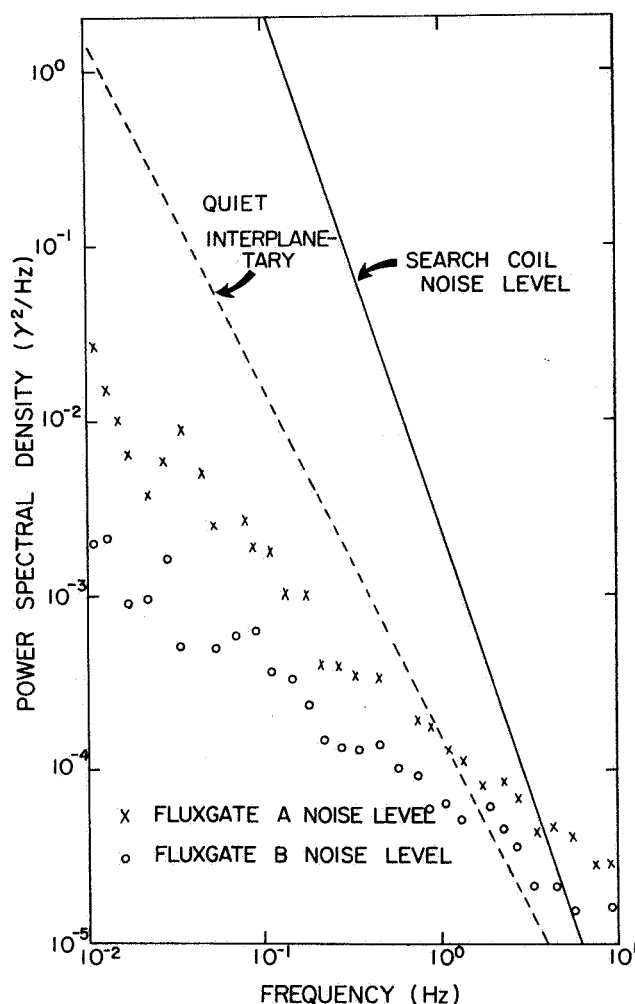


**Figure 1.** The instrument noise levels of three magnetometers. Fluxgates A and B were not flown aboard spacecraft but served as backup units for space missions. The search coil noise level is that of the OGO-3 instrument [Russell *et al.*, 1970]. The dashed line is an extrapolation of the quietest interplanetary power spectrum obtained by Siscoe *et al.* [1968] assuming an  $f^{-2}$  spectral dependence.

magnetometers has a frequency dependence proportional to  $1/f$  whereas the search coil noise has a  $1/f^3$  spectral dependence. The inverse cube dependence of the search coil noise results from a  $1/f$  noise in field derivative units  $(\gamma/\text{sec})^2/\text{Hz}$  (the search coil measures the derivative of the field), which is converted to field units  $\gamma^2/\text{Hz}$  by dividing by  $(2\pi f)^2$ , where  $f$  is the frequency in hertz. The interplanetary power spectrum, however, is proportional to  $1/f^2$ . Due to their different slopes all three spectra cross. The fluxgates intersect the quiet interplanetary spectrum at about 1 Hz. Thus, to the extent that these are representative of fluxgate magnetometers in actual operation in space, fluxgates should be able to measure the quiet interplanetary spectrum to about 1 Hz. Since the search coil noise spectrum crosses the fluxgate noise spectrum at about 4 Hz, the search coil is the better high-frequency instrument. We note, however, that the search coil does not intersect our hypothesized quiet interplanetary spectrum until 15 Hz. Thus, to the extent that fluxgates A and B are typical of fluxgates used on actual missions we would expect that the quiet interplanetary spectrum from 1 to 15 Hz remains unmeasured. We shall see in fact our assumption for the quiet interplanetary spectrum must not extend to frequencies much above 1 Hz and in reality the entire interplanetary magnetic spectrum above 1 Hz remains unobserved. In addition there are other sources of noise which limit the detection of the interplanetary spectrum at lower frequencies.

### ALIASING

Aliasing is the folding of power about the Nyquist frequency (half the sampling frequency) into the analysis band during spectral analysis of discretely sampled time series. It does not create any power not originally present in the signal, but since it adds power from outside the analysis band it can have drastic consequences on the measured spectrum. The way to avoid this addition of power due to aliasing is to remove any power above half the sampling frequency from the signal to be measured *before* the data are sampled by the telemetry system. Many times this has not been done on interplanetary magnetometers. Table 1 lists the Nyquist frequency and the upper cutoff frequency of the instrument for a number of magnetometers which have made measurements in the interplanetary medium. The entries are ranked according to ratio of these two frequencies. A large ratio indicates a possible serious aliasing problem. Many of the numbers used in the constructing of this and succeeding tables can be found in Ness [1970].

To examine the effect of aliasing on measured spectra, let us assume that the ratio  $R$  in table 1 equals  $2K + 1$

**Table 1.** The Nyquist frequency (half the sampling frequency), the upper frequency cutoff of the instrument's passband, and the ratio of these two frequencies for spacecraft probing the interplanetary medium

Spacecraft	Nyquist frequency, Hz	Upper cutoff frequency, Hz	Ratio
IMP 1, 2, 3	0.025	5.0	200
IMP 4, 5	0.20	12.0	60
Explorer 33, 35 <sup>a</sup>	0.10	5.0	50
Mariner 2	0.0135	0.33	24
Pioneer 6, 7, 8	0.33	5.0	15
Mariner 5	0.119 <sup>b</sup>	0.80	6.7
Mariner 4	0.159 <sup>b</sup>	0.80	5.0
Pioneer 9	1.7	1.7	1.0
Explorer 33, 35 <sup>c</sup>	0.08	0.05	0.63
OGO 5 <sup>d</sup>	0.43	0.22	0.50
	3.54	1.77	0.50
	27.8	13.9	0.50
OGO 1,3 <sup>e</sup>	2.2	0.8	0.36
	17	0.8	0.05
	139	70	0.50

<sup>a</sup>GSFC magnetometer

<sup>b</sup>Calculated from average sample rate for high telemetry rate

<sup>c</sup>Ames Research Center magnetometer

<sup>d</sup>UCLA fluxgate magnetometer

<sup>e</sup>Search coil magnetometer

where  $K$  is integral. Then, it is easy to show that the measured power spectrum  $P'(f)$  after aliasing is

$$P'(f) = P(f) + \sum_{n=1}^k [P(2nf_N - f) + P(2nf_N + f)]$$

where  $0 \leq f \leq f_N$ ,  $f_N$  is the Nyquist frequency and  $P(f)$  is the true spectrum at frequency  $f$ . Figure 2 shows the result of aliasing for a magnetometer with  $R = 51$  for  $1/f$  and  $1/f^2$  spectra. We see that the effect of aliasing is significant over the whole frequency band for the  $1/f$  spectrum but is significant from only about  $0.5 f_N$  to  $f_N$  for the  $1/f^2$  spectrum. Table 2 lists the additional power added to the spectrum at various frequencies for these two spectra and a  $1/f^3$  spectrum. We note the aliasing

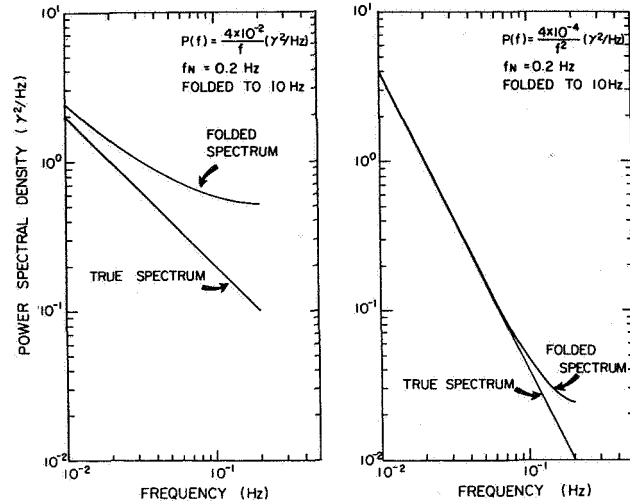


**Figure 2.** The effect of aliasing on digitized time series for a spectrum proportional to  $f^{-1}$  and one proportional to  $f^{-2}$  when the Nyquist criterion for reconstructing the spectrum is violated. In this example signals up to 10 Hz were allowed to fold into the analysis band of 0-0.2 Hz.

**Table 2.** The additional power added to the true spectrum by aliasing, for a magnetometer whose bandwidth is 50 times greater than the analysis band allowed by the sampling rate, for three spectra with slopes proportional to  $f^{-1}$ ,  $f^{-2}$  and  $f^{-3}$

$f/f_N$	Additional $1/f$ , percent	Folded $1/f^2$ , percent	Power $1/f^3$ , percent
0.01	3.8	0	0
0.10	38	0.9	0
0.25	96	5.0	0.5
0.50	195	23	5.0
0.70	279	33	19
0.80	323	73	35
0.90	370	103	62
1.00	420	145	110

always at least doubles the power at the *Nyquist* frequency.

In the vicinity of the Nyquist frequencies of the instruments listed in table 1, the typical spectrum of the interplanetary field has at least a  $1/f^2$  dependence. Thus aliasing should only be a problem during typical interplanetary conditions in the vicinity of the Nyquist frequency. However, the instrument noise levels for the fluxgate magnetometers shown in figure 1 had  $1/f$  dependences. This noise is subject to aliasing, too. Examining table 2 we see that the noise level at the Nyquist frequency was raised by a factor of 5 in this example due to aliasing. Thus, for those instruments with much larger upper cutoffs than Nyquist frequencies we must reinterpret our conclusions about their capability to resolve the quiet interplanetary spectrum. Examining figure 1, we see that this spectral folding of the instrument noise would limit them to measurements below from about 0.1 to 0.2 Hz.

#### DIGITAL NOISE

The process of digitizing the magnetic field data adds further noise to the spectrum. This noise is subject to aliasing also, but in this case the folded power cannot be removed in the instrument design. The rms noise due to the digitization process can easily be shown to be  $D^2/12$ , where  $D$  is the size of a digital window [Bendat and Piersol, 1966]. To understand how this noise affects a measured spectrum, however, we must determine how it is distributed over the power spectrum. The most straightforward way to accomplish this is to compare two spectra of the same time series: one digitized with a large digital window, and one digitized with an extremely small digital window. For this purpose, time series were generated with a random number generator with a gaussian distribution of amplitudes. These time series were then filtered with a digital single section low-pass filter with a corner frequency below the analysis band. The time series thus formed had a  $1/f^2$  power spectrum.

Figure 3 shows two power spectra of the same time series with digital windows of  $10^{-5} \gamma$  and  $0.5 \gamma$ . The spectra were computed from 2048 points with 50 degrees of freedom. We note that there were only 315 steps between digital windows in the coarsely digitized time series. The horizontal line is the power spectral density to be expected if the digitization noise of  $0.021 \gamma^2$  were spread uniformly over the analysis band of 0.5 Hz. The most obvious feature of figure 3 is that

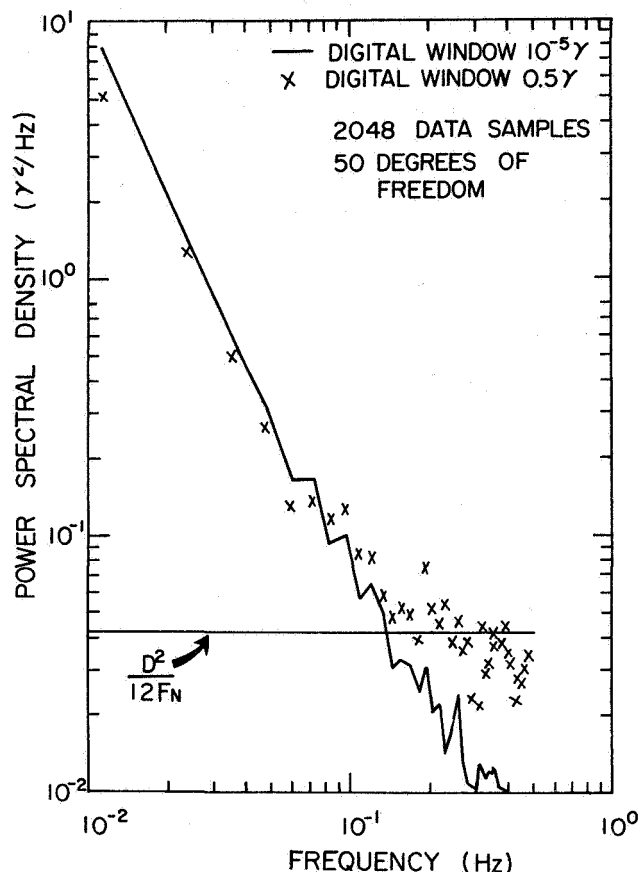
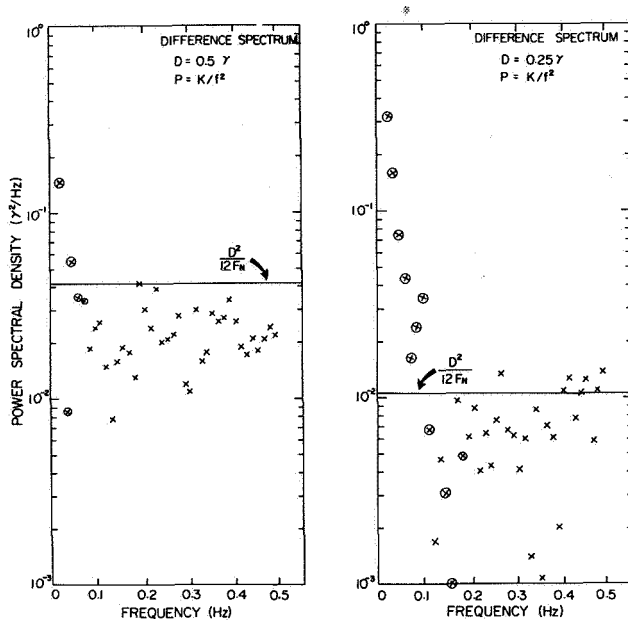


Figure 3. Two spectra of the same time series: one sampled with a digital window of  $0.5 \gamma$  and one sampled with a digital window of  $10^{-5} \gamma$ . The original spectrum was proportional to  $f^{-2}$ . The horizontal line is the power expected if the rms digital noise,  $D^2/12$ , due to the digital window ( $D = 0.5 \gamma$ ), were spread uniformly over the band 0 to  $f_N$  where  $f_N$  is the upper frequency of the analysis band, the Nyquist frequency.

the spectrum of the coarsely digitized signal deviates strongly from the finely digitized spectrum at high frequencies and approaches the line expected if the noise were spread evenly across the band ( $D^2/12f_N$ ). A surprising feature is that at low frequencies the coarsely digitized power spectrum is less than that of the finely digitized power spectrum. In other words, at low frequencies the digitization process has consistently reduced the power, whereas at high frequencies it has raised the power. This is not a chance event, but has been observed in every test case.

Figure 4 shows the difference between these two



**Figure 4.** The difference between two pairs of spectra of a random time series with an  $f^{-2}$  spectral shape. One spectrum of each pair had a digital window of  $10^{-5} \gamma$ . The other spectrum had a digital window of  $0.5 \gamma$  in the first case and  $0.25 \gamma$  in the second case.

power spectra on a semilog plot together with a second test case. The second test case was performed on a different random time series but with the same spectral shape and integrated power. However, for the second case, the coarse digital window was set at  $0.25 \gamma$ . This coarsely digitized time series had 705 digital steps in the 2048 points. The circled points indicate that the coarse digitization spectrum was less than the fine digitization spectrum. We see that at high frequencies the formula  $D^2/12f_N$  is a good predictor of the digitization noise added to the spectrum, but that at low frequencies digitization actually reduces the power spectral density.

In table 1 we ranked magnetometers by the amount of spectral folding present. Table 3 also ranks these instruments but this time by their digital noise level as calculated from  $(D^2/12f_N)$ . This table is not as revealing as it may seem at first, because a digital noise level for a magnetometer with a high Nyquist frequency, will alter the apparent shape of the spectrum much more than the same noise level for a magnetometer with a low Nyquist frequency. This is illustrated more clearly in figure 5 where the digital noise level is plotted as a horizontal

**Table 3.** The digital window, Nyquist frequency and digital noise level for spacecraft probing the interplanetary medium. The digital noise level given assumes that the digital noise is spread uniformly across the analysis band

Spacecraft	Digital window, $\gamma$	Nyquist frequency, Hz	Digital noise level, $\gamma^2/\text{Hz}$
Mariner 2	0.7	0.0135	3.02
IMP 1, 2, 3	0.8	0.025	2.13
Mariner 4	0.7	0.159 <sup>a</sup>	0.26
Explorer 33 <sup>b</sup>	0.5	0.10	0.21
Explorer 33, 35 <sup>c</sup>	0.4	0.08	0.17
Mariner 5	0.4	0.119	0.11
IMP 5	0.4	0.2	$6.7 \times 10^{-2}$
Pioneer 6	0.5	0.33	$6.3 \times 10^{-2}$
IMP 4	0.32	0.20	$4.3 \times 10^{-2}$
Explorer 35 <sup>b</sup>	0.19	0.10	$3.0 \times 10^{-2}$
Pioneer 7, 8	0.25	0.33	$1.6 \times 10^{-2}$
Pioneer 9	0.40	1.75	$7.6 \times 10^{-3}$
OGO 5 <sup>d</sup>	0.125	0.43	$3.0 \times 10^{-3}$
	0.125	3.47	$3.8 \times 10^{-4}$
	0.125	27.78	$4.7 \times 10^{-5}$

<sup>a</sup>Calculated using average sample rate at highest telemetry rate

<sup>b</sup>GSFC magnetometer

<sup>c</sup>Ames Research Center magnetometer

<sup>d</sup>UCLA fluxgate magnetometer

line for each of the magnetometers listed in table 3, from the magnetometer's Nyquist frequency to our assumed typical quiet interplanetary spectrum. If the interplanetary field were "quiet" and digital noise were the only noise source present in the measured spectra, then we would expect that spectra derived by these various magnetometers would follow the dashed line at low frequencies and asymptotically approach the horizontal noise line given for that magnetometer at high frequencies. Naively, we could interpret the length of

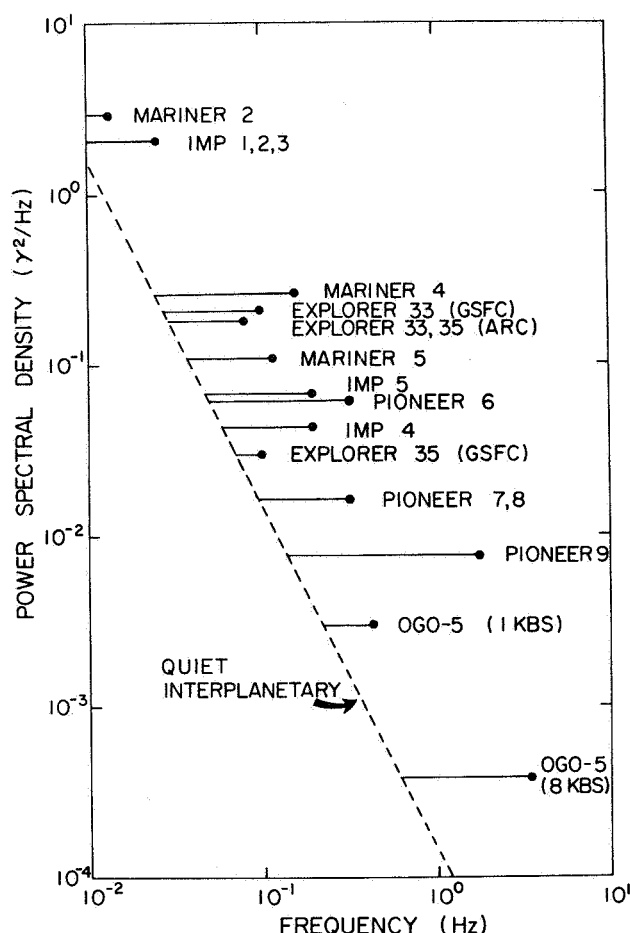


**Figure 5.** The digital noise level and Nyquist frequency of a majority of the magnetometers which have measured the interplanetary magnetic field. The horizontal line marks the digital noise level. The dot marks the Nyquist frequency. The dashed line shows the expected quiet interplanetary spectrum.

the horizontal lines as the amount of wasted telemetry during quiet conditions in the interplanetary medium. However, conditions are not always quiet nor do all these spacecraft remain solely in the interplanetary medium. Figure 5 does not show the noise level of the UCLA OGO-5 fluxgate magnetometer at its highest telemetry rate because from figure 1 we expect that the instrument noise level is greater than the quiet interplanetary spectrum above 1 Hz. Similarly, the digitization noise level of the OGO-1 and 3 search coil magnetometer is not shown because its instrument noise level is greater than its digital noise level except in its two low gain states.

## MEASUREMENT OF THE INTERPLANETARY FIELD NEAR THE EARTH

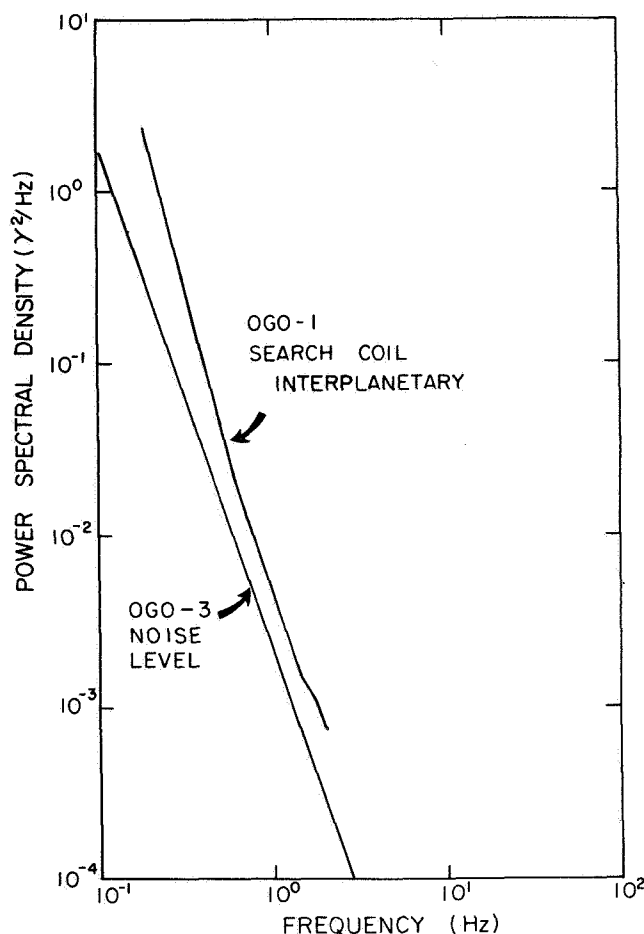
It is now well established that near the earth but upstream from the bow shock, waves are present in the interplanetary medium that are not present far from the earth [Fairfield, 1969; Russell *et al.*, 1971]. While these waves do not apparently affect the average magnetic field strength [Fairfield, 1969], they do increase the power in the frequency range from  $10^{-2}$  to 1 Hz. Although the waves are seldom present unless the field line simultaneously threads both the satellite and the bow shock, it is difficult in practice to determine whether a particular field line intersects the shock because of the variability of the position of the shock and the uncertainty in the direction of the field due to the presence of the waves. Thus, even when the orientation of the interplanetary field is known, care must be exercised in the interpretation of interplanetary spectra obtained near the earth. However, from figure 5, we see that to extend our knowledge of the interplanetary spectrum much above 0.1 Hz we must examine near-earth data.

Figure 6 shows a power spectrum obtained in the interplanetary medium by the OGO-1 search coil magnetometer [Holzer *et al.*, 1966]. We see that it is at least a factor of 2 higher than the noise level of the similar instrument on OGO-3 but has a very similar slope. The increased power at low frequencies could be due to interference near the OGO-1 spin frequency of 0.08 Hz, which was not present in OGO-3 search coil magnetometer data. Besides the possibility that this spectrum simply shows the noise level of the magnetometer, there is the possibility that this spectrum was contaminated by bow shock associated waves. This spectrum was obtained near the earth (the apogee of OGO-1 was  $24 R_E$ ), and no data were available on the orientation of the interplanetary magnetic field at this time. Furthermore, this spectrum differs significantly from others measured in the same region.

Figure 7 shows power spectra of the three components of the interplanetary magnetic obtained by the UCLA OGO-5 fluxgate magnetometer in solar ecliptic coordinates calculated from 24,500 points with 500 degrees of freedom. At the time of this measurement, the interplanetary field measured upstream from the bow shock by both Explorer 33 and 35 magnetometers had a roughly constant solar ecliptic longitude of  $260^\circ$  and a latitude that varied from about  $0^\circ$  to  $20^\circ$ . Using this orientation and extrapolating from the OGO-5 solar ecliptic position of (9.5, -10.8, 15.2) the field line did not intersect the average position of the bow shock.

Thus, it is reasonable to assume that this spectrum is





**Figure 6.** A comparison of the OGO-1 search coil measurement of the spectrum of the interplanetary magnetic field [Holzer et al., 1966] with the noise level of a similar instrument on board OGO-3 [Russell et al., 1970].

unaffected by the presence of upstream waves and represents a true interplanetary spectrum at 1 AU. However, one spectrum cannot be considered "typical" and further work is being undertaken to establish what the typical spectrum is. However, we note that during this spectrum the solar wind velocity was approximately 400 km/sec and the density was  $3.3 \text{ cm}^{-3}$  and both quantities were changing only slowly over the course of the day [J. Binsack, private communication 1970]. In other words, the solar wind was average during this period of time.

#### POWER SPECTRAL DENSITY OF THE INTERPLANETARY MAGNETIC FIELD

Having discussed the possible errors in the measurement of the interplanetary power spectrum, we will now put

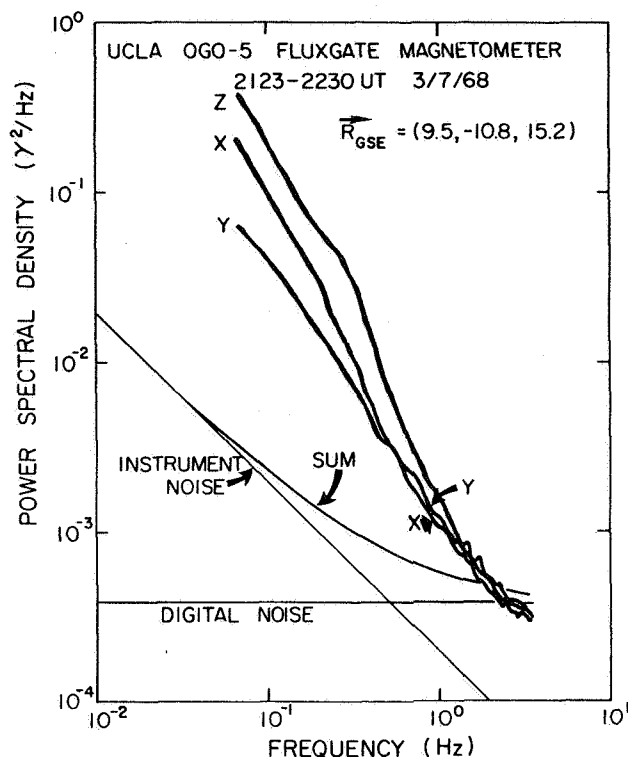


**Figure 7.** Power spectra of the three solar ecliptic coordinates of the interplanetary magnetic field obtained by the UCLA OGO-5 fluxgate magnetometer from 2123 to 2230 UT on March 7, 1968. At this time, the field line through OGO-5 did not intersect the expected position of the bow shock. The expected instrument noise level, the digital noise level, and their sum are also shown.

together what we feel is the best estimate of the interplanetary power spectrum. This is shown in figure 8. At the lowest frequencies ( $10^{-6}$  to  $10^{-4}$  Hz), to define accurately the power spectrum requires continuous data in the interplanetary medium for many days. Earth orbiting spacecraft cannot acquire such continuous data. Of the two series of interplanetary probes, the Mariner series and the Pioneer series, spectra have been published for the lowest frequencies only for the Mariner 2 [Coleman, 1968] and Pioneer 6 data [Sari and Ness, 1969]. However the normalization of the power spectra of Sari and Ness [1969] are obviously incorrect and so we have used the Mariner 2 data in figure 8. Mariner 2 was launched during a very active period of time and inward toward Venus. These two effects would tend to increase the power observed and indeed the Mariner 2 curve appears to be somewhat high. We note that since tables 1 and 2 indicate a possible spectral

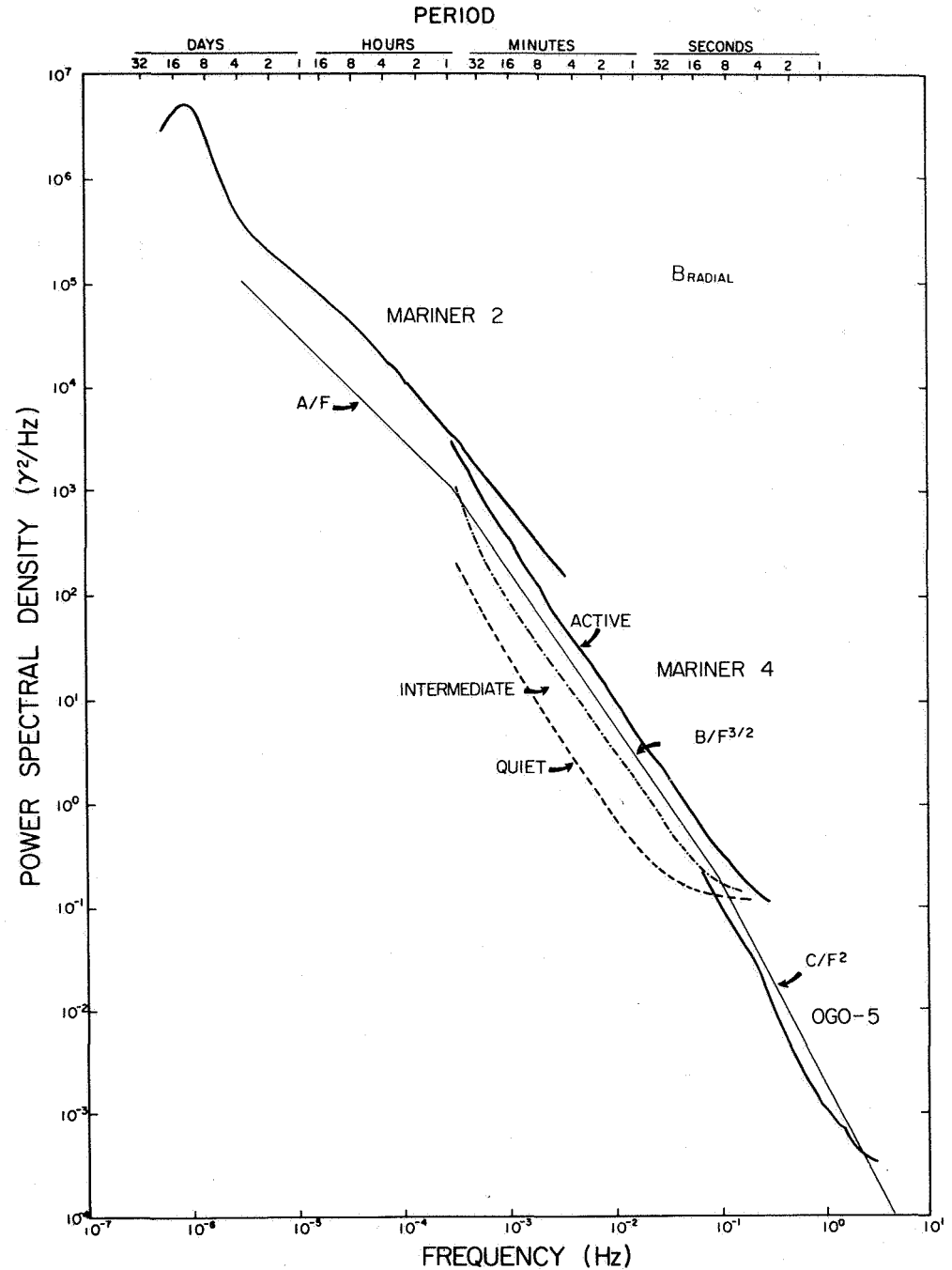


**Figure 8.** A composite spectrum of the radial component of the interplanetary magnetic field as observed on Mariner 2 [Coleman, 1968], on Mariner 4 [Siscoe et al., 1968], and on OGO-5. Three spectra showing the range of variability of the interplanetary spectrum are shown for Mariner 4. Since the Mariner 2 data are consistently higher than the Mariner 4 data in the overlapping range of frequencies, it is assumed that the Mariner 2 data were obtained during an unusually disturbed period of time, and the typical spectrum has lower power. Three straight line segments have been drawn with slopes of  $-1$ ,  $-1.5$ ,  $-2$  to roughly represent the expected average spectrum near 1 AU.

folding problem, we have plotted the Mariner 2 data only to one-quarter of its Nyquist frequency.

At the intermediate frequencies, the Mariner 4 [Siscoe *et al.*, 1968] data have been used because these data have been analyzed to show the range of variability of the spectrum. Active, intermediately active and quiet spectra are shown. We note that the Mariner 4 spectra asymptotically approach a value of about  $0.1 \gamma^2/\text{Hz}$  at high frequencies, which is a factor of 2 lower than our estimate of the digitization noise in table 3. This is possibly because the Mariner 4 data samples are not equi-spaced as we have assumed in the calculation of the digital noise level. Finally, at the highest frequencies we have used the OGO-5 power spectrum shown in figure 7, which, as suggested in the previous section, appears to be typical of average solar wind conditions since it joins smoothly with the intermediate activity spectrum of Mariner 4. We note that although we have chosen to plot only the power in the radial component on this figure, the other components have similar spectral form.

On this figure we have drawn three straight lines with slopes of  $-1$ ,  $-1.5$ , and  $-2$  with changes in slope occurring at  $3 \times 10^{-4}$  and  $10^{-1}$  Hz. We see that these straight lines are roughly parallel to the spectrum in the three frequency ranges. The two breaks in the spectrum are somewhat arbitrary, however, and *Sari and Ness* [1969] claim that the break between  $f^{-3/2}$  and  $f^{-2}$  occurs at about  $5 \times 10^{-4}$  Hz. However, this is not clear from their data since they present no spectra that cover the region of their hypothesized change in slope.

Since *Russell et al.* [1970] showed that power spectra obtained in the interplanetary medium from 1 to 140 Hz with the search coil magnetometer were at the instrument's noise level, there must be a further increase in the slope of the spectrum possibly from  $f^{-2}$  to  $f^{-3}$  above 1 Hz. However, no other limits on the possible spectrum above 1 Hz can be determined with the present data.

#### THE INTERPRETATION OF POWER SPECTRA OF THE INTERPLANETARY MAGNETIC FIELD

It is tempting to interpret the changes in slope in figure 8 as changes in allowed wave modes, and the like. However, all power spectra obtained in the interplanetary medium are measured in a frame of reference that is moving at a very high velocity relative to the plasma rest frame. For example, a 340-km/sec solar wind with a number density of  $4 \text{ cm}^{-3}$  and a magnetic field of  $5 \gamma$  is streaming past a spacecraft with a velocity of 6 times the Alfvén velocity. Thus, waves propagating in the solar wind are severely Doppler shifted. The amount of Doppler shifting depends on the size of the component of the solar wind parallel to the phase velocity of the

wave. If a wave is propagating perpendicular to the solar wind velocity, therefore, the Doppler shifting is zero. However, if a wave with phase velocity less than that of the solar wind (most electromagnetic waves under typical solar wind conditions) is propagating parallel or antiparallel to the solar wind it will be severely Doppler shifted. Waves propagating parallel to the solar wind will be Doppler shifted to higher frequencies maintaining their sense of polarization, and waves propagating antiparallel to the solar wind will be Doppler shifted to lower frequencies if their phase velocity is greater than half the solar wind velocity and to higher frequencies if their phase velocity is less than half the solar wind velocity. In both antiparallel propagation cases, however, the wave polarization observed in the satellite frame is reversed unless the phase velocity is greater than the solar wind velocity. In short, then, the fact that the solar wind is flowing past the observer and is, in fact, usually super Alfvénic and supersonic, mixes the power spectrum of the signal in the plasma rest frame as well as mixing cross correlations between components. Thus, it is not simple to interpret these power spectra.

To understand the physical processes occurring in the magnetic field, such as which wave modes are present, it is essential to perform cross correlations with other plasma parameters.

At present there is some controversy as to the importance of discontinuities versus waves in determining the interplanetary power spectrum [Sari and Ness, 1969; Belcher *et al.*, 1970]. Step functions in the magnetic field, whether they are propagating as waves or whether they are simply convected with the solar wind velocity, will both contribute to a  $1/f^2$  spectrum at high frequencies. (We note that the low-frequency spectrum, below approximately the frequency corresponding to the average spacing of the discontinuities, need not be proportional to  $1/f^2$ .) Furthermore, there is no necessity that the natural wave spectrum between discontinuities *not* be proportional to  $1/f^2$ . Thus, the spectral shape of the interplanetary spectrum provides no simple answer to this controversy. To distinguish between propagating and nonpropagating structures requires examination of both the field and plasma behavior. We note the anisotropies in the solar wind plasma distributions further complicate these identifications [Hudson, 1970].

#### SUMMARY

From our examination of the noise levels of two typical fluxgate magnetometers, it appears that most power spectra of the interplanetary field fluctuations are limited by digital noise rather than instrument noise.

However, we have no guarantee that all magnetometers are this quiet. The OGO-1 and 3 search coil magnetometer, however, is limited by its inherent noise level rather than digital noise; in fact, the spectrum of this noise level is greater than the power spectrum of the average interplanetary magnetic field at 1 AU. We note, however, the search coil magnetometer is a more sensitive instrument than the fluxgate magnetometer above about 4 Hz.

From our test cases, it appears that digital noise is distributed uniformly over the power spectrum at least at high frequencies. However, at low frequencies digitization actually reduced the power. Although this undoubtedly altered the power spectra obtained in the interplanetary medium, its effect is small (fig. 3) and cannot account for the observed changes in slope.

Aliasing could be a problem in the creation of power spectra from the data for many of the interplanetary magnetometers. However, due to the observed natural spectrum of interplanetary fluctuations this should only be a serious problem for frequencies above one-half the Nyquist frequency.

Although the interplanetary spectrum near the earth can be contaminated by waves associated with the earth's bow shock, we can combine OGO-5 data with the Mariner 2 and 4 interplanetary spectra to create the spectrum from about  $5 \times 10^{-6}$  Hz to 1 Hz, if care is taken to exclude times when the magnetic field line threads both OGO-5 and the shock front. The spectrum of the radial component is approximately proportional to  $f^{-1}$  up to  $3 \times 10^{-4}$  Hz; then it is proportional to  $f^{-3/2}$  up to about  $10^{-1}$  Hz; and finally it is proportional about  $f^{-2}$  up to at least 1 Hz. It is quite probable that the spectrum undergoes another change in slope above 1 Hz.

Finally, we stress the difficulty in interpreting the power spectrum of the interplanetary magnetic field by itself. Doppler shifting mixes frequencies and different physical processes can result in the same spectrum. Cross correlations with simultaneous plasma data are necessary. Multispacecraft studies could also be very fruitful.

#### ACKNOWLEDGMENTS

We wish to thank J. Binsack of MIT for providing us with the results of the Explorer 33 and 35 plasma experiment in advance of publication, and also D. Hei of the National Space Science Data Center for providing us with the Explorer 33 and 35 Ames Research Center magnetometer data submitted by D. S. Colburn. This work was supported by the National Aeronautics and Space Administration contract NAS 5-9098.

#### REFERENCES

- Belcher, J. W.; and Davis, L., Jr.: Large Amplitude Alfvén Waves in the Interplanetary Medium: 2. *J. Geophys. Res.*, Vol. 76, 1971, p. 3534.
- Belcher, J. W.; Coleman, P. J., Jr.; Davis, L., Jr.; Jones, D. E.; and Smith, E. J.: Waves and Discontinuities in the Solar Wind. *Space Phys.* Preprint, California Institute of Technology, 1970.
- Bendat, J. S.; and Piersol, A. G.: *Measurement and Analysis of Random Data*, Chap. 7, John Wiley and Sons, New York, 1966.
- Childers, D. D.; Russell, C. T.; and Coleman, P. J., Jr.: OGO-5 Observations of Upstream Waves in the Interplanetary Medium: Statistical properties, in preparation, 1971.
- Coleman, P. J., Jr.: Characteristics of the Region of Interaction Between the Interplanetary Plasma and the Geomagnetic Field: Pioneer 5. *J. Geophys. Res.*, Vol. 69, 1964, p. 3051.
- Coleman, P. J., Jr.: Variations in the Interplanetary Magnetic Field: Mariner 2, 1, Observed properties. *J. Geophys. Res.*, Vol. 71, 1966, p. 5509.
- Coleman, P. J., Jr.: Turbulence, Viscosity and Dissipation in the Solar Wind Plasma. *Astrophys. J.*, Vol. 153, 1968, p. 371.
- Fairfield, D. H.: Bow Shock Associated Waves Observed in the Far Upstream Interplanetary Medium. *J. Geophys. Res.*, Vol. 74, 1969, p. 3541.
- Holzer, R. E.; McLeod, M. G.; and Smith, E. J.: Preliminary Results from the OGO-1 Search Coil Magnetometer: Boundary positions and magnetic noise spectra. *J. Geophys. Res.*, Vol. 71, 1966, p. 1481.
- Hudson, P. O.: Discontinuities in an Anisotropic Plasma and their Identification in the Solar Wind. *Planet. Space Sci.*, Vol. 18, 1970, p. 1611.
- Ness, N. F.: Magnetometers for Space Research, Goddard Space Flight Center, Report X-690-70-78, 1970.
- Russell, C. T.; Holzer, R. E.; and Smith, E. J.: OGO-3 Observations of ELF Noise in the Magnetosphere, 2. The nature of the equatorial noise. *J. Geophys. Res.*, Vol. 75, 1970, p. 755.
- Russell, C. T.; Childers, D. D.; and Coleman, P. J., Jr.: OGO-5 Observations of Upstream Waves in the Interplanetary Medium: Discrete Wave Packets. *J. Geophys. Res.*, Vol. 76, 1971, p. 845.
- Sari, J. W.; and Ness, N. F.: Power Spectra of the Interplanetary Magnetic Field. *Solar Phys.*, Vol. 8, 1969, p. 155.
- Siscoe, G. L.; Davis, L.; Coleman, P. J., Jr.; Smith, E. J.; and Jones, D. E.: Power Spectra and Discontinuities of the Interplanetary Magnetic Field: Mariner 4. *J. Geophys. Res.*, Vol. 73, 1968, p. 61.

## POWER SPECTRA OF THE INTERPLANETARY MAGNETIC FIELD NEAR THE EARTH

*D. D. Childers and C. T. Russell*

Power spectra of the interplanetary magnetic field measured by near-earth satellites upstream from the earth's bow shock are free from terrestrial contamination provided the field at the satellite does not intersect the bow shock. Considerable spectral enhancement for the range of frequencies 0.01 to 1.00 Hz, due to turbulence caused by the shock, may occur if the field observed at the satellite intersects the shock. This turbulence occurs frequently in both the morning and afternoon quadrants. In the frequency band from 0.07 to 1 Hz, this noise decreases in amplitude with radial distance from the shock with an attenuation length of  $4 R_E$ .

### ABSTRACT

### INTRODUCTION

Since the first measurements of the interplanetary medium, power spectra of the interplanetary field have been calculated to characterize the nature of the fluctuations observed [Coleman, 1966, 1967, 1968; Siscoe *et al.*, 1968; Sari and Ness, 1969]. Not only was it hoped that the power spectrum would lead to insight into the physical processes occurring in the solar wind, but also that the power spectrum could be related to the diffusion of energetic particles from cosmic rays [Jokipii, 1966] to solar electrons [Lin, 1970]. For a 1-GeV cosmic ray, fluctuations at frequencies of the order of  $10^{-4}$  Hz are important in the diffusion process, but for a 40-keV electron frequencies near 1 Hz are dominant. Thus, it is necessary to know the spectrum of the interplanetary magnetic fluctuations over a wide frequency range.

Clearly, earth-orbiting spacecraft that enter the magnetosheath and magnetosphere every few days are not capable of determining the spectrum below frequencies of the order of  $10^{-4}$  Hz. Thus necessarily our knowledge of this low frequency portion of the interplanetary spectrum has come from deep space probes such as Mariner 2 [Coleman, 1966, 1967, 1968], Pioneer 6

[Ness *et al.*, 1966; Sari and Ness, 1969], and Mariner 4 [Siscoe *et al.*, 1968]. These spacecraft have also returned information up to frequencies from  $10^{-2}$  to  $10^{-1}$  Hz; because of the remoteness from the earth of these probes; however, their telemetry rates have not permitted an examination of the spectrum at higher frequencies.

Recent near-earth spacecraft, such as the OGO series, have had a much higher telemetry rate and thus can extend the spectrum to much higher frequencies. However, the interplanetary magnetic field beyond the earth's bow shock is not always free from the fluctuations associated with the interaction of the solar wind with the earth. To the extent that we are interested in examining the spectrum of waves in the interplanetary medium at 1 AU due to strictly solar wind related processes, these waves contaminate the interplanetary spectrum.

In this paper, we use data obtained in the near-earth interplanetary medium by the UCLA OGO-5 fluxgate magnetometer to show how the spectrum is altered by these so-called "upstream waves," and where this contamination is observed. A detailed description of this magnetometer has been given by Aubry *et al.* [1971], but a few relevant facts will be mentioned here. First, OGO-5 has an apogee of  $24 R_E$  and thus at maximum is only  $10 R_E$  from the earth's bow shock. Second, the

---

*Dr. Childers is with the UCLA Department of Planetary and Space Science. Dr. Russell is with the UCLA Institute of Geophysics and Planetary Physics.*

data are digitized to within  $\pm 1/16 \gamma$ , and the data used in this paper have a Nyquist frequency (1/2 the sampling frequency) of 3.47 Hz. This results in a digital noise level of  $\sim 3 \times 10^{-4} \gamma^2/\text{Hz}$ , which is the limiting noise level for the data presented here.

We first compare OGO-5 spectra calculated both in the presence and absence of upstream waves with previous deep space measurements. We then show examples of the kinds of waves encountered in this region. Finally, we will present a map of the region of occurrence of these upstream waves and obtain an attenuation length for the higher frequency components of these waves.

### COMPARISON OF OGO-5 AND MARINER 4 POWER SPECTRA

Figure 1 shows the power spectra of the radial components (in a heliocentric spherical coordinate system) of both typical quiet and disturbed magnetic fields for both the near-earth region upstream from the earth's bow shock (referred to below as the upstream region), observed with OGO-5, and the distant interplanetary region (but with a heliocentric distance of about 1.0 AU) observed on the Mariner 4 spacecraft. The Mariner spectra have been taken from *Siscoe et al.* [1968]; the flattening of the spectra at high frequencies is due to digitization noise. The interval of the OGO quiet spectrum is 2123 to 2223 UT, March 7, 1968. Above 0.07 Hz this spectrum has been computed from the digitally sampled data using 486 degrees of freedom per spectral estimate; the lower frequency portion has been computed from time-averaged data using 20 degrees of freedom per estimate. For this interval, OGO-5 was on the morning side of the sun-earth line at an average geocentric distance of  $20.9 R_E$  and at a sun-earth-satellite (SES) angle of  $63.1^\circ$ . For the disturbed OGO spectrum the interval 0856 to 1035 UT, March 10, 1968, was used; again, OGO-5 was on the morning side, but at an average geocentric distance of  $19.6 R_E$  and at an SES of  $66.7^\circ$ . The same techniques for computing the spectra as just outlined are employed, but the degrees of freedom per estimate are 40 and 810 for the low- and high-frequency parts of the spectrum, respectively.

A comparison of the two quiet spectra of figure 1 reveals that they agree rather well: They both exhibit, in general, roughly the same power law dependence on frequency in the region of frequency overlap, viz.,  $P(f) \propto f^{-1.5}$ , and the power levels are similar. However, above 0.1 Hz, the OGO spectrum becomes steeper, obeying  $P(f) \propto f^{-2}$ . Closer inspection of this typical quiet OGO spectrum reveals that, for the overlapping frequencies, its power level actually is intermediate between the two Mariner spectra. The Mariner disturbed

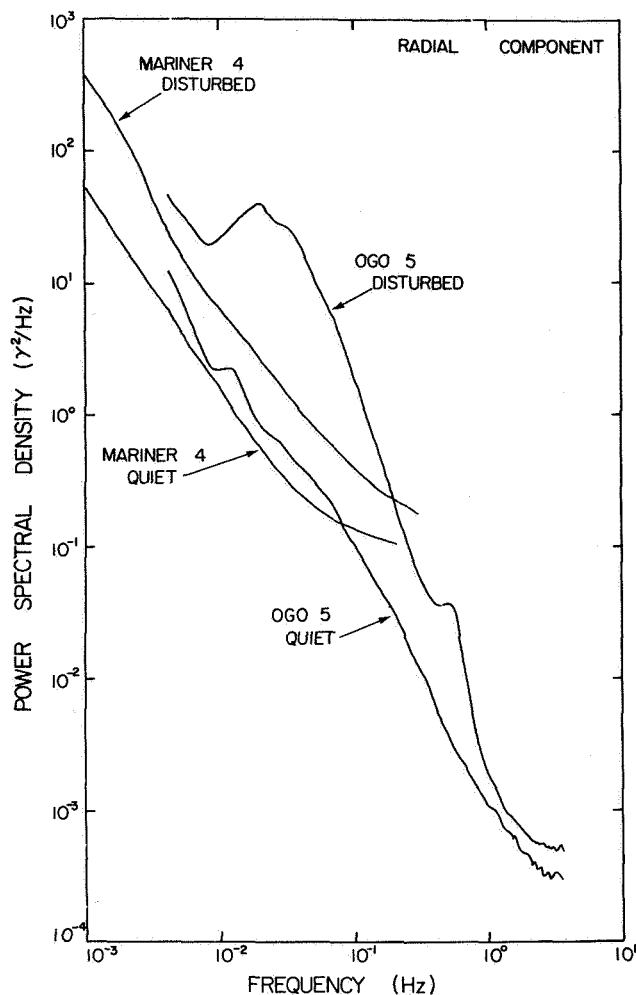


**Figure 1.** Comparison of the power spectra of near-earth interplanetary fields, observed with OGO-5, with the spectra of interplanetary fields far from the earth, observed with Mariner 4 [Siscoe et al., 1968]. Spectra of the radial components, in a heliocentric spherical coordinate system, of both typical quiet and typical disturbed fields measured at both spacecraft are shown. The Mariner 4 spectra are taken from figure 2(a) of Siscoe et al. [1968]. The OGO-5 quiet spectrum was obtained from 2123 to 2223 UT, March 7, 1968, while the disturbed spectrum was obtained 0856 to 1035 UT, March 10, 1968.

spectrum also has a power law exponent  $\gamma \approx 1.5$ , where  $P(f) \propto f^{-\gamma}$ . Since the quiet OGO spectrum has the same power law exponent, at least up to 0.1 Hz, as do the two Mariner spectra, and since its power level lies within the range of the quiet and disturbed Mariner spectra which are characteristic of the interplanetary field far from the

earth, it is evident that at times OGO-5 data can be used to extend our knowledge of the interplanetary spectrum.

However, when the near-earth field is disturbed, its spectrum can be quite different from the typical 1 AU interplanetary spectrum. Examining the two disturbed spectra reveals that the OGO spectrum is significantly enhanced in power over the Mariner spectrum for most of their common frequency range,  $0.004 < f < 0.5$  Hz. This enhancement peaks around  $f = 0.03$  Hz; below  $f = 0.008$  Hz the OGO spectrum appears to fit onto the Mariner spectrum rather well. At frequencies above that of the low-frequency spectral peak, the OGO spectrum exhibits a power law exponent of  $\gamma \gtrsim 3$ , except, of course, that part of the spectrum around the peak at  $f = 0.55$  Hz; on the other hand, the Mariner spectrum has  $\gamma \approx 1.5$ . The low-frequency spectral peak is typical of disturbed OGO spectra, but, although the high frequency peak is a common feature of disturbed upstream fields, it does not always occur. The significance of both these spectral peaks will be discussed later.

From an examination of many such spectra we have found that the following characteristics distinguish disturbed upstream fields from distant interplanetary fields: (1) the upstream spectra are significantly enhanced over those of interplanetary fields for periods  $T$  ranging from the order of seconds to just over 100 sec; (2) this spectral power peaks at periods typically from 20–30 sec; and (3) at frequencies above the peak the power law exponent for the spectrum is  $\gamma \gtrsim 3$ , as compared to typical interplanetary values  $\gamma \approx 1.5$ .

### UPSTREAM WAVES

The power spectrum of disturbed upstream interplanetary fields shown in figure 1 was noted to have two spectral peaks. We first consider the low-frequency peak, which is a typical feature of disturbed fields observed near the earth. *Fairfield* [1969] has studied the properties of waves in the interplanetary field, in the 0.01 to 0.05-Hz frequency range, associated with the earth's bow shock. Figure 2 compares one of *Fairfield's* [1969] power spectra, computed from the IMP-4 (Explorer 34) magnetometer data, with the OGO-5 spectrum of the same disturbed interval shown in figure 1. Only the spectra of components transverse to the average field during their respective intervals are displayed. The two spectra agree very well. They both peak at  $f \approx 0.03$  Hz and have similar power law exponents for higher frequencies. This is to be expected, of course, because they were both obtained near the earth under similar conditions. Any significance in the higher power level for the OGO spectrum can be attributed to the fact that the IMP 4 is farther upstream.

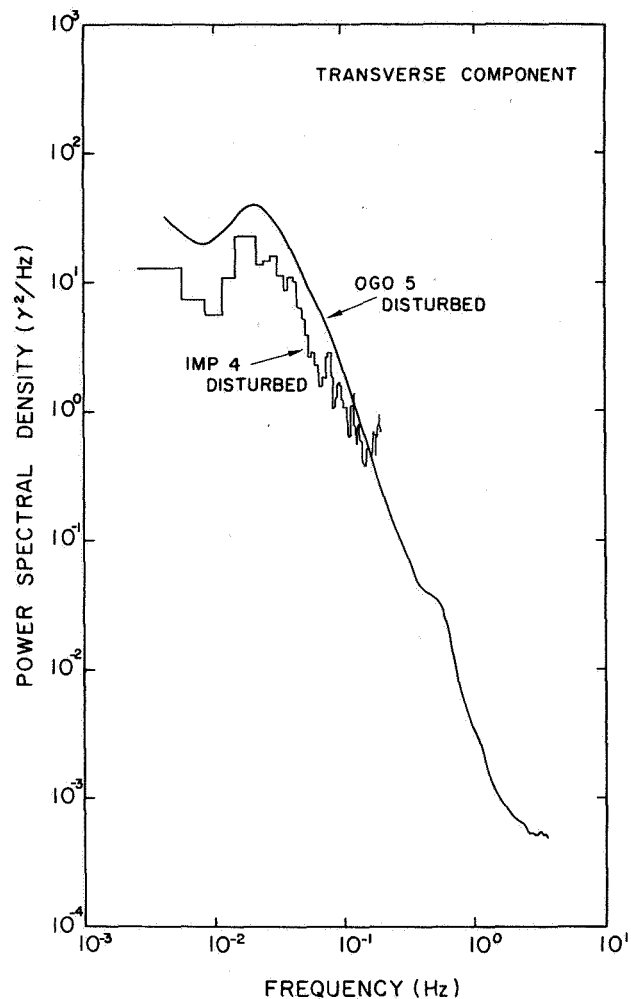


**Figure 2.** Comparison of the power spectra of disturbed fields observed with OGO-5 with those observed with IMP 4 [Fairfield, 1969]. Shown are spectra for a component transverse to the average field direction in each case. The OGO-5 spectrum is for the same interval displayed in figure 1 (0856 to 1035 UT, March 10, 1968), while the IMP 4 spectrum is for the interval from 0102 to 0129 UT on July 3, 1967.

*Fairfield* [1969] showed convincingly that these waves are associated with the earth's bow shock. Among other things, he found that these waves occur only when the interplanetary field observed at the satellite intersects the bow shock. More recently, these same conclusions have been reached by *Greenstadt et al.* [1970], who used simultaneous field observations of Vela 3A and Explorer 33 to study the occurrence properties of these upstream waves. Since it is improbable that hydromagnetic waves could travel to the position of the satellite against the solar wind flow velocity, and since particles

reflected at the shock have been observed moving along field lines into the solar wind [see, for example, Anderson, 1968, 1969; Asbridge *et al.*, 1968; Frank and Shope, 1968], we attribute these waves to an unspecified instability of the reflected particles.

Before considering the high-frequency peaks, it is perhaps instructive to examine the spectra of all three components of the disturbed OGO fields. Figure 3 shows the spectra of all components in a heliocentric spherical coordinate system for the same interval, 0856 to 1035 UT, March 10, 1968, as shown in figures 1 and

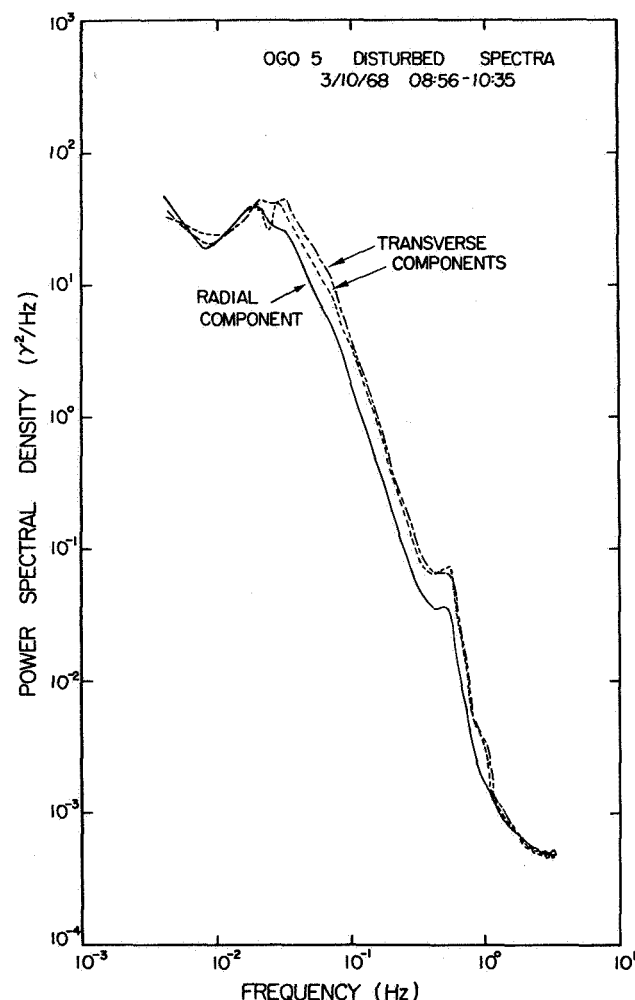


**Figure 3.** OGO-5 power spectra of all three vector components for the period 0856 to 1035 UT March 10, 1968. Spectra are for the radial and transverse components in a heliocentric spherical coordinate system. The solid line represents the radial component, the uniformly dashed line the azimuthal component, and the other dashed trace the northward component.

2. Clearly, the spectra of the two transverse components of the field are similar to that of the radial component in almost every detail; however, the transverse spectra are seen to have more power than the radial spectrum. This feature, which was noted by Siscoe *et al.* [1968] to occur also for distant interplanetary fields, is rather typical of the disturbed upstream fields.

The spectral peak at  $f = 0.55$  Hz occurs on all three spectra; the cross-spectral coherences at  $f = 0.55$  Hz are very large among all three components, with the largest coherence being 91 percent for the two transverse components. For these particular spectra, these peaks at  $f = 0.55$  Hz are caused by the occurrence of several discrete wave packets of a class that has been analyzed in some detail by Russell *et al.* [1971]. Some of these packets for this interval are illustrated in figure 4. Note

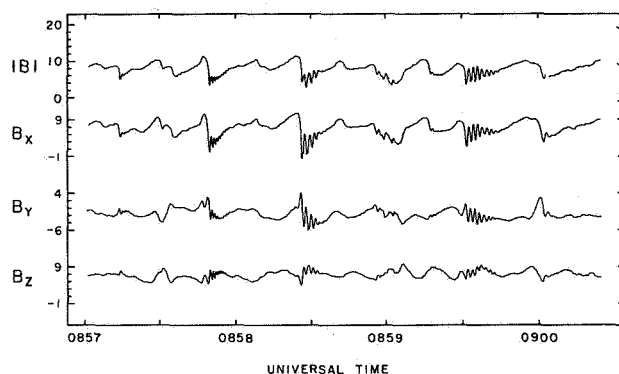


**Figure 4.** Discrete wave packets occurring in association with irregular low-frequency waves on March 10, 1968, while the satellite was at 19.1  $R_E$  and at a sun-earth-satellite angle of  $67.5^\circ$ .

that low-frequency fluctuations of the type discussed earlier occur here along with these high frequency wave packets. Russell *et al.* [1971] have found that the discrete wave packets are more likely to occur when the lower frequency turbulence is present, which explains in part why the high-frequency (0.1 to 1.0 Hz) spectral peaks are rather common features of disturbed upstream fields. Often high-frequency spectral peaks occur in upstream spectra which are due, not to discrete wave packets, but rather to continuous waveforms as illustrated in figure 5. These waves, too, are associated with the occurrence of the low-frequency turbulence, of which another example is shown superposed on the high frequency fluctuations in figure 5. However, we emphasize that, although these higher frequency spectral peaks are very common among disturbed upstream spectra, they do not occur all the time.



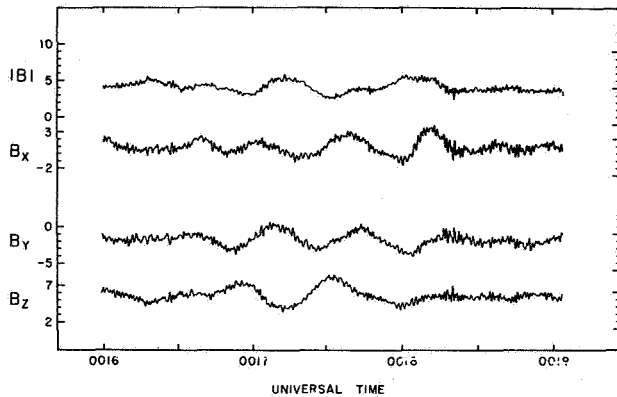


**Figure 5.** Continual high frequency waves simultaneous with quasi-sinusoidal low-frequency waves on March 8, 1968, while the satellite was at  $21.9 R_E$  and at a sun-earth-satellite angle of  $61.3^\circ$ .

#### SPATIAL PROPERTIES OF THE UPSTREAM TURBULENCE

On the average, the interplanetary field lies along the Parker spiral angle, and field lines upstream from the bow shock on the afternoon side of the earth do not intersect the bow shock. Thus, upstream waves usually are not present in this region. Deviations from the spiral angle occur frequently enough, however, that even here upstream waves are seldom entirely absent for periods of more than 5 hr (at the OGO-5 orbit). Thus far, the data shown have been obtained entirely on the morning side of the earth. Figure 6 shows power spectra obtained on the afternoon side of the earth while OGO-5 was at a geocentric distance of  $19.9 R_E$  and a SES of  $59.3^\circ$ . We see that, when waves are observed in this region, the spectra are the same as on the morning side as shown in figure 3.

The major difference between the morning and afternoon sides of the upstream region is not in the spectral character of the waves but in their frequency of occurrence. This becomes evident when we attempt to map the average amplitude of the turbulence upstream from the shock. We decided to construct such a map from the amplitudes in the frequency range from 0.07 to approximately 1 Hz, because this quantity was available as a minutely average from the regular OGO-5 data processing. Although this frequency range does not include the spectral peak at  $\sim 0.03$  Hz, it is thought that the average behavior of the turbulence can be obtained from the amplitudes at slightly higher frequencies.

To make this map, we used data from the first 1-1/2 years of OGO-5 operation containing over 1200 hr in the interplanetary medium. Only data for times during

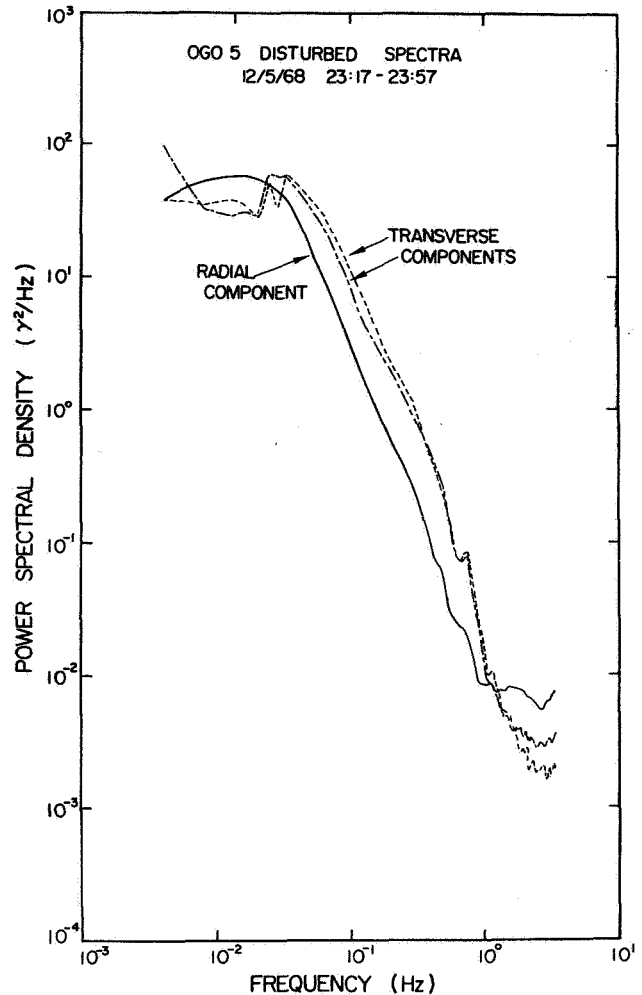


**Figure 6.** OGO-5 power spectra of disturbed upstream fields observed on the afternoon side of the sun-earth line for the interval 2317 to 2357 UT on December 5, 1968. The spectra are shown in the heliocentric coordinate system described in figure 3.

which the satellite was within  $40^\circ$  azimuth of the solar magnetospheric (GSM) equatorial plane were used. The azimuthal angle is defined here in a geocentric spherical coordinate system that used the solar direction (GSM X axis) as the polar axis; the GSM Y axis, which is perpendicular to both the GSM X axis and the earth's magnetic dipole axis and points generally oppositely to the earth's orbital motion, is the reference axis for this azimuthal angle.

Figure 7 shows the results of this mapping. The vertical axis represents the geocentric distance, in earth radii, along the solar direction of observation point, while the horizontal axis is of the distance perpendicular to this direction; the outer curve represents the OGO-5

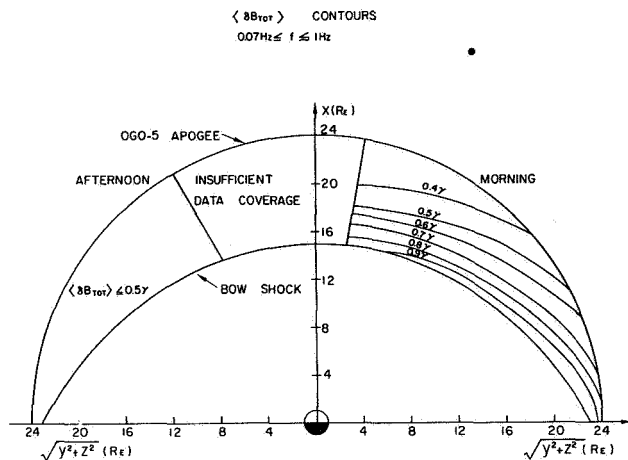


**Figure 7.** A contour map of the average rms amplitudes of magnetic field turbulence, in the frequency range  $0.07 \leq f \leq 1$  Hz, observed upstream of the average position of the earth's bow shock (inner curve). The outer curve represents the OGO-5 apogee at  $24 R_E$ .

apogee, at  $24 R_E$ , while the inner curve is of the average bow shock position (no aberration of the shock position is assumed). On the afternoon side no contours are shown, since within our statistical accuracy no unambiguous spatial dependence of wave rms amplitudes was found. However, we were able to conclude from our data that the average rms field amplitude in this region is about  $0.5 \gamma$  or less, and thus the region is marked. No data coverage is available near the subsolar point (the X axis) from the OGO-5 orbit.

In the morning region, however, there is an unambiguous spatial dependence of the average wave amplitudes. The contours of the average amplitudes range from  $0.4 \gamma$  up to  $0.9 \gamma$ , and these contours roughly parallel the shock front. Furthermore, the amplitude is greatest near the shock and decreases with increasing distance from the shock. This further illustrates that the source of the energy for these waves comes from some process in the earth's bow shock.

To examine the significance of these contours, it was recalled that Fairfield [1969] reported that the occurrence of the lower frequency waves ( $0.01 < f < 0.05$  Hz) at the IMP 4 is consistent with the concept of a source at the shock transmitting information—waves or, most probably, particles—along interplanetary field lines threading the shock to the satellite position, where this information is then responsible in some way for the observed fluctuations. He measured the propagation velocity of such information along field lines to be about 2.7 times the solar wind velocity. We can apply this result to our contours of wave fields in a slightly higher

frequency range, as shown in figure 8. As illustrated in the inset, we assume a typical spiral field angle of  $45^\circ$  to the X axis; the information streams out along the field at a velocity of  $2.7 V_{SW}$ . In the shock frame the solar wind velocity adds to this, resulting in a velocity direction in this frame of  $25.5^\circ$  to the negative Y axis (or, equivalently,  $64.5^\circ$  to the solar direction). Lines of this direction are shown sketched across the region containing the  $0.5 \gamma$  and  $0.8 \gamma$  contours. We also make three further assumptions: (1) the contours will be assumed to be axially symmetric about the X axis (on the morning side only); (2) the shock will be assumed to be uniformly distributed with information radiators, hence the equispaced lines; and (3) any turbulence generated upstream of a particular contour by this or any other shock-associated mechanism and convected past the contour will be ignored. We then find that the distances from the average shock position to the two contours along these information lines, over the region in which both contours are connected by the lines, to be remarkably constant. The mean distance along these information lines for the  $0.8 \gamma$  contour is  $1.6 R_E$ , and for  $0.5 \gamma$  contour it is  $5.6 R_E$ . Since the power ratio of the wave fields represented by these contours is roughly  $e$ , we therefore find that the attenuation length of the turbulence field, for frequencies 0.07 to the order of

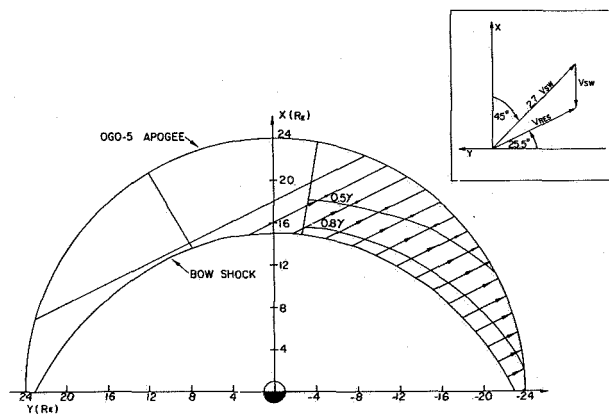


**Figure 8.** In the inset it is shown schematically that information propagating upstream along the interplanetary field, at a typical spiral field angle of  $45^\circ$  to the sun-earth line (X axis), with a velocity of  $2.7 V_{SW}$  appears in the shock frame to propagate at a resultant angle of  $25.5^\circ$  to the Y axis. The rest of the figure is a reproduction of the  $0.8\text{-}\gamma$  and  $0.5\text{-}\gamma$  contours from figure 7, along with information lines at  $25.5^\circ$  to the Y axis superposed. The distances from the shock position to the  $0.8\text{-}\gamma$  and  $0.5\text{-}\gamma$  contours are  $1.6 R_E$  and  $5.6 R_E$ , respectively.

1 Hz, is approximately  $4 R_E$ . This is to be contrasted with Fairfield's [1969] estimate of an attenuation length of approximately  $15 R_E$  for the turbulence at lower frequencies of 0.01 to 0.05 Hz.

## SUMMARY

We have shown that it is possible to calculate power spectra of the interplanetary magnetic field, free of any evident terrestrial contamination from data obtained by spacecraft such as OGO-5, which probe the interplanetary medium in the vicinity of the earth's bow shock. However, to avoid terrestrial contamination of the spectra, the measurements must be performed for times during which the field line threading the satellite does not intersect the bow shock.

When the observed field at the satellite does intersect the shock, then the power spectra may be substantially enhanced at frequencies from about 0.01 to 1 Hz, with a peak in power occurring at frequencies from 0.01 to 0.05 Hz. This spectral enhancement is a consequence of turbulence generated by some shock-associated process, probably by particles reflected at the bow shock and traveling against the solar wind along field lines. Because of deviations of the interplanetary field from its average spiral angle, these upstream effects are observed often in the afternoon upstream region, as well as in the morning hemisphere. In the afternoon quadrant at the OGO-5 orbit, the effect of these deviations is such as to make periods of greater than five hours duration during which these upstream waves are absent very rare.

From our OGO-5 data, we estimate the attenuation length of the high frequency components, from 0.07 to about 1 Hz, of the shock-associated turbulence to be about  $4 R_E$ . However, low-frequency shock-associated waves have been observed as far as  $46 R_E$  from the average bow shock position [Fairfield, 1969]. Therefore, power spectra of the interplanetary field can be contaminated by terrestrial effects at considerable distances upstream from the bow shock.

## REFERENCES

- Anderson K. A.: Energetic Electrons of Terrestrial Origin Upstream in the Solar Wind. *J. Geophys. Res.*, Vol. 73, 1968, p. 2387.
- Anderson, K. A.: Energetic Electrons of Terrestrial Origin Behind the Bow Shock and Upstream in the Solar Wind. *J. Geophys. Res.*, Vol. 74, 1969, p. 95.
- Asbridge, J. R.; Bame, S. J.; and Strong, I. B.: Outward Flow of Protons from the Earth's Bow Shock. *J. Geophys. Res.*, Vol. 73, 1968, p. 5777.
- Aubry, M. P.; Kivelson, M. G.; and Russell, C. T.: Motion and Structure of the Magnetopause. *J. Geophys. Res.*, Vol. 76, 1971, p. 1673.
- Coleman, P. J., Jr.: Variations in the Interplanetary Magnetic Field: Mariner 2, 1. Observed Properties. *J. Geophys. Res.*, Vol. 71, 1966, p. 5509.
- Coleman, P. J., Jr.: Wave-like Phenomena in the Interplanetary Plasma: Mariner 2. *Planet. Space Sci.*, Vol. 15, 1967, p. 953.
- Coleman, P. J., Jr.: Turbulence, Viscosity, and Dissipation in the Solar-Wind Plasma. *Astrophys. J.*, Vol. 153, 1968, p. 371.
- Fairfield, D. H.: Bow Shock Associated Waves Observed in the Far Upstream Interplanetary Medium. *J. Geophys. Res.*, Vol. 74, 1969, p. 3541.
- Frank, L. A.; and Shupe, W. L.: A Cinematographic Display of Observations of Low-Energy Proton and Electron Spectra in the Terrestrial Magnetosphere and Magnetosheath and in the Interplanetary Medium (Abstract). *Trans. Amer. Geophys. Union*, Vol. 49, 1968, p. 279.
- Greenstadt, E. W.; Green, I. M.; Inouye, G. T.; Colburn, D. S.; Binsack, J. H.; and Lyon, E. F.: Dual Satellite Observations of Earth's Bow Shock, II, Field Aligned Upstream Waves. *Cosmic Electrodyn.*, Vol. 1, 1970, p. 279.
- Jokipii, J. R.: Cosmic Ray Propagation, 1, Charged Particles in a Random Magnetic Field. *Astrophys. J.*, Vol. 146, 1966, p. 480.
- Lin, R. P.: Observations of Scatter-Free Propagation of ~40-keV Solar Electrons in the Interplanetary Medium. *J. Geophys. Res.*, Vol. 75, 1970, p. 2583.
- Ness, N. F.; Searce, C. S.; and Cantarano, S.: Preliminary Results from the Pioneer 6 Magnetic Field Experiment. *J. Geophys. Res.*, Vol. 71, 1966, p. 3305.
- Russell, C. T.; Childers, D. D.; and Coleman, P. J., Jr.: OGO-5 Observations of Upstream Waves in the Interplanetary Medium: Discrete Wave Packets. *J. Geophys. Res.*, Vol. 76, 1971, p. 845.
- Sari, J. W.; and Ness, N. F.: Power Spectra of the Interplanetary Magnetic Field. *Solar Phys.*, Vol. 8, 1969, p. 155.
- Siscoe, G. L.; Davis, L., Jr.; Coleman, P. J., Jr.; Smith, E. J.; and Jones, D. E.: Power Spectra and Discontinuities of the Interplanetary Magnetic Field: Mariner 4. *J. Geophys. Res.*, Vol. 73, 1968, p. 61.

## CORONAL ALFVÉN WAVES AND THE SOLAR WIND *J. W. Belcher*

**ABSTRACT** The observed properties of coronal Alfvén waves in the solar wind at 1 AU are briefly reviewed, with some theoretical discussion of their probable effects on the dynamics of the expanding solar corona. It is concluded that coronal Alfvén waves can have a major influence on both the small- and large-scale properties of the solar wind at 1 AU.

The interplanetary medium is a highly conducting, essentially collisionless plasma with approximate equipartition between thermal and magnetic field energy densities. Spacecraft measurements of the fine scale structure of the medium (scale lengths on the order of 0.01 AU and less) offer a unique opportunity to study the physics of such plasmas observationally. Of particular astrophysical interest are their wave and turbulence properties. When interplanetary field data were first obtained more than 8 years ago, the microscale structure (scale lengths on the order of 0.01 AU and less) was found to be quite irregular, and it seemed plausible [Davis, 1966] that many of the observed features were propagating as Alfvén or magnetoacoustic waves. Coleman [1967, 1968] carried out an extensive spectral and cross-spectral analysis of the Mariner 2 plasma and field data, and concluded that Alfvén waves propagating away from the sun in the rest frame of the wind could account for a substantial fraction of the fluctuations. This statistical analysis did not give patterns of occurrence of the waves or explicit examples of the wave forms. Unti and Neugebauer [1968] were the first to isolate a specific example of a quasi-periodic Alfvénic wave form. Belcher *et al.* [1969], in a preliminary analysis of Mariner 5 plasma and magnetometer data, identified outwardly propagating Alfvénic wave trains as frequently occurring phenomena, although for the most part they are nonsinusoidal and aperiodic.

Figure 1 is an example [Belcher and Davis, 1971] of

one such wave train, with a length of about 0.25 AU. As in the preliminary analysis, a fluctuation is identified as an Alfvén wave if it satisfies

$$\mathbf{b} = \pm(4\pi\rho)^{1/2} \mathbf{v} \quad (1)$$

where  $\mathbf{b}$  is the vector perturbation in the magnetic field (the deviation from the average),  $\mathbf{v}$  is the perturbation in the velocity, and  $\rho$  is the mass density of the plasma. Fluctuations in the field strength  $B$  and the density during such periods are relatively small, as would be expected for the transverse Alfvén mode. Figure 2 is a very high time resolution plot of three 10-min periods at times indicated on figure 1. At this resolution, the waves can appear either abrupt (2i, 2iii) or more gradual (2ii). The gradual changes predominate, with the more sharply crested waves occurring on the order of once per hour. The best examples of such waves (as in fig. 1) are found in high-velocity, high proton temperature, solar wind streams (fig. 3). Belcher and Davis [1971] have argued that the waves are generated at or near the sun, and are closely related to the dynamical processes that produce the hot, high velocity streams. Of course there are many other structures which contribute to the interplanetary microscale fluctuations (such as shocks, tangential discontinuities, and polarity reversals), but a careful study of 130 days of good field and plasma data from Mariner 5 indicates that Alfvén waves dominate the microscale fluctuations on the order of 50 percent of the time [Belcher and Davis, 1971]. They are thus a major source of fluctuations in the solar wind at scale lengths on the order of 0.01 AU and less.

---

The author is at the Center for Space Research, M.I.T., Cambridge, Massachusetts.

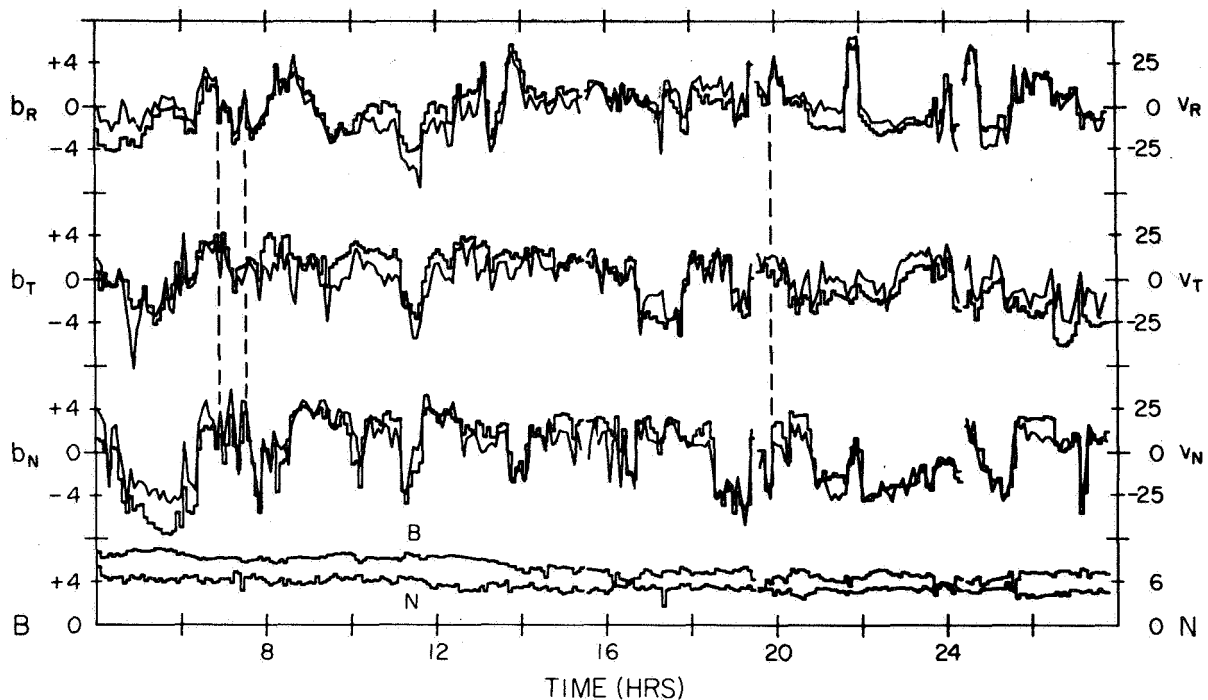


**Figure 1.** Twenty-four hours of magnetic field and plasma data demonstrating the presence of nearly pure Alfvén waves. The upper six curves are 5.04-min velocity components in km/sec (diagonal lines) and magnetic field components in gamma (horizontal and vertical lines), with a scale ratio of approximately  $(4\pi Nm_p)^{1/2}$ . Twenty-four hour averages have been subtracted. The polarity during this period is negative and the correlation positive, indicating outward propagation. The lower two curves are field strength and proton number density. RTN components are solar polar coordinates.

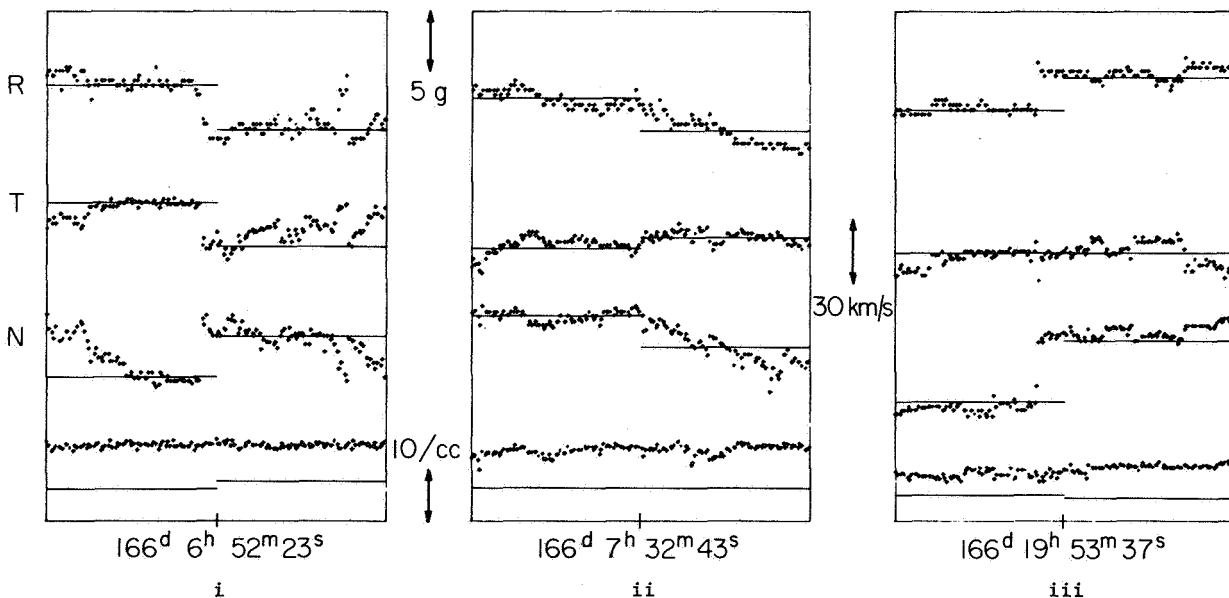


**Figure 2.** Expanded plots of three 10-min periods of figure 1 at the times indicated by vertical dotted lines there. The points are high rate field data, the bars are 5.04 min plasma readings with the same scale ratio as in figure 1 and arbitrary zeroes. The lower set of bars are density readings, and the lowest points are field strengths.

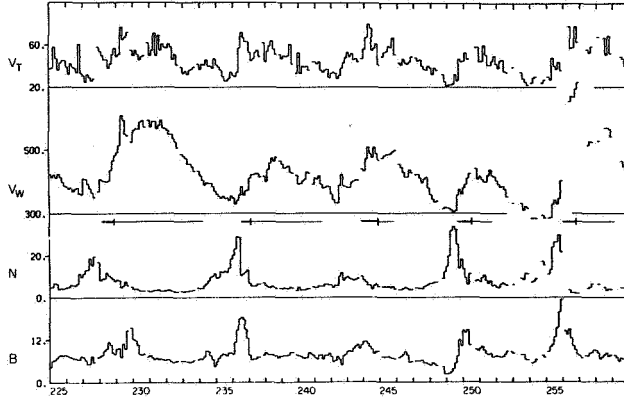


**Figure 3.** Thirty-five days of Mariner 5 data plotted using 3-hr averages and showing the large scale stream structure of the solar wind.  $B$  is the magnetic field strength ( $\gamma$ ),  $N$  is the proton number density ( $\text{cm}^{-3}$ ),  $V_W$  is the radial proton bulk velocity (km/sec), and  $V_T$  is the most probable proton thermal speed (km/sec). The best examples of the outwardly propagating Alfvén waves (light bars) are found in high velocity streams and on their trailing edges. The largest amplitude waves (heavy bars) are found at the leading edges of high velocity streams.

Assuming that the outwardly propagating waves observed at 1 AU are in fact generated at or near the sun (and this seems almost certain), we would like to point out some of the more obvious effects they will have on the dynamics of the expanding solar corona, assuming no wave damping. The waves contribute to the efflux of energy away from the sun, and they will do work on the wind as they propagate and are convected outward into interplanetary space [Parker, 1965]. Consider a one-fluid polytrope model of the solar wind for a non-rotating sun (radial field lines). With the assumption that the Alfvénic wavelengths are small compared to scale heights, we can write an expression for the transverse Alfvénic fluctuations as a function of  $r$

$$\left. \begin{aligned} \delta \mathbf{B}(r, t) &= \mathbf{e}_t \delta B(r) \exp[i(\omega t - kr)] \\ \delta \mathbf{V}(r, t) &= \pm \frac{\delta \mathbf{B}(r, t)}{(4\pi\rho)^{1/2}} \\ \omega &= k(V + V_A) \end{aligned} \right\} \quad (2)$$

with the WKB amplitude [Parker, 1965] given by

$$\delta B(r) = \delta B_o \left( \frac{\rho}{\rho_o} \right)^{3/4} \frac{(1 + V_A^o/V_o)}{(1 + V_A/V)} \quad (3)$$

where the subscript  $o$  refers to an arbitrary reference level. This expression is for outwardly propagating Alfvén waves with no damping (dissipation of wave energy directly into thermal energy);  $V$  is the radial solar wind speed,  $V_A$  is the Alfvén velocity, and  $\rho$  is the solar wind density.

The total energy flux across a sphere of radius  $r$ , including Alfvén waves, is given by

$$F = 4\pi r^2 \left[ V \left( \frac{1}{2} \rho V^2 + \frac{\alpha}{\alpha - 1} p + \rho \Phi \right) + \frac{1}{2} \left( \frac{1}{2} \rho \delta V^2 \right) V + \frac{1}{2} \frac{\delta B^2}{4\pi} (V + V_A) \right] \quad (4)$$

where  $\Phi$  is the gravitational potential and  $p$  is the thermal pressure. The first term in parentheses contains the familiar terms evaluating the kinetic energy density associated with the radial motion, the sum of the enthalpy and the energy transported by thermal conduction, and the gravitational energy. The terms in the second and third parentheses are due entirely to the presence of the waves. The second is the wave kinetic energy density convected by the bulk velocity and the third is the radial component of the Poynting vector. Using the WKB wave amplitudes given above, we can write an expression for the wave energy flux as a function of  $r$ :

$$F_{\text{wave}}(r) = 4\pi r_o^2 \frac{\delta B_o^2}{8\pi} V_A^o \left( 1 + \frac{V_o}{V_A^o} \right)^2 \frac{1 + \frac{3}{2} M_A}{(1 + M_A)^2} \left\{ M_A = \frac{V}{V_A} = \frac{V_o}{V_A^o} \left( \frac{\rho_o}{\rho} \right)^{1/2} \right\} \quad (5)$$

where  $M_A$  is the solar wind Alfvén mach number and is a monotonically increasing function of  $r$ . It can easily be shown that  $F_{\text{wave}}(r)$  is a monotonically decreasing function of  $r$ , approaching 0 as  $r \rightarrow \infty$ . Since the total energy flux  $F$  must remain constant, there is thus a continual transfer of energy flux from the waves to the wind.

We can heuristically understand the mechanism which produces this energy transfer by considering the  $1/c \mathbf{J} \times \mathbf{B}$  term in the equation of motion. In the Parker radial field model, this term is identically zero. With Alfvén waves, however, it is proportional to

$(\mathbf{k} \times \delta \mathbf{B}) \times (\mathbf{B}_0 + \delta \mathbf{B})$ , where  $\mathbf{B}_0$  is the radial background field,  $\mathbf{k}$  is the radial propagation vector, and  $\delta \mathbf{B}$  is the Alfvénic perturbation (transverse to the radial). The  $(\mathbf{k} \times \delta \mathbf{B}) \times \mathbf{B}_0$  term in this expression is also transverse to the radial, and produces the  $\delta \mathbf{V}$  perturbation. The  $(\mathbf{k} \times \delta \mathbf{B}) \times \delta \mathbf{B}$  term, however, is in the radial direction. If the wave amplitude were not a function of  $r$ , this second order term would average to zero over one cycle of the waves. However, since the wave amplitude is a function of  $r$ , there is a small nonzero average over one wave cycle, and thus a net acceleration of the plasma in the radial direction. The radial equation of motion becomes

$$\rho V \frac{\partial V}{\partial r} = -\rho \frac{\partial \Phi}{\partial r} - \frac{\partial}{\partial r} \left( p + \frac{\delta B^2}{8\pi} \right) \quad (6)$$

The waves exert an effective pressure on the wind (analogous to a radiation pressure), which serves to increase the streaming velocity. Thus the energy flux in the waves decreases as  $r$  increases away from the sun, with a corresponding increase in the plasma streaming motion.

Having determined that outwardly propagating Alfvén waves can do work on the solar wind, we turn to the question of the importance of this effect on the large-scale solar wind dynamics. Consider a reference level  $r_0 = 10^6$  km. At this level,  $V_A^0 \gg V_0$ , so that the wave energy flux here is given by

$$F_{\text{wave}}(r_0) = 2.2 \times 10^{33} \frac{\epsilon B_0^3}{(N_0)^{1/2}} \text{ ergs/sec} \quad (7)$$

where  $\epsilon = 1/2 (\delta B_0/B_0)$ , and  $N_0$  is the proton particle density. If we take representative values of  $B_0$  and  $N_0$  of 1 gauss and  $2 \times 10^7 \text{ cm}^{-3}$ , respectively, we find that

$$F_{\text{wave}}(r_0) = \epsilon (5 \times 10^{29}) \text{ ergs/sec} \quad (8)$$

This flux estimate is to be compared to estimates of the energy flux due to thermal conduction from the lower corona on the order of  $2 \times 10^{27}$  ergs/sec, and of the energy flux in the solar wind at 1 AU on the order of  $10^{27}$  ergs/sec. Even small amplitude waves at  $10^6$  km ( $\epsilon \ll 1$ ) are associated with large energy fluxes because of the high Alfvén velocity. Note the strong dependence of  $F_{\text{wave}}(r_0)$  on  $B_0$ ; small changes in  $B_0$  at  $10^6$  km cause large variations in the wave energy flux for fixed values of  $\epsilon$  and  $N_0$ . In this simplified model, all of the wave energy flux is eventually transferred to

increased plasma streaming motion, so that the effect of the waves on the large scale solar wind dynamics can be quite large.

Figure 4 shows the results of numerical solutions of Equation 3. The reference level  $r_0$  is  $10^6$  km, with fixed values of  $N_0$  and  $B_0$  ( $2 \times 10^7 \text{ cm}^{-3}$  and 1 gauss) and variable  $T_0$ , with  $\alpha = 1.228$ . Shown are the wind velocity

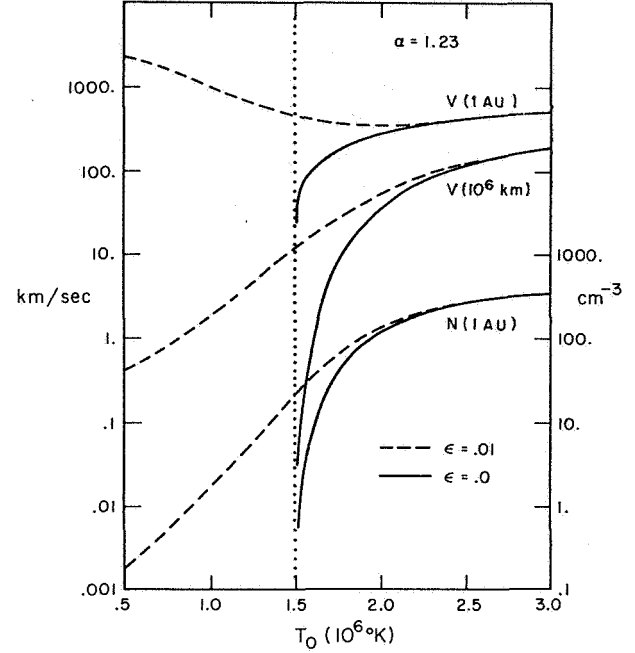


**Figure 4.** The solar wind velocity  $V$  at 1 AU and  $10^6$  km, and the proton particle density  $N$  at 1 AU, as functions of the temperature  $T_0$  at  $10^6$  km, for two values of  $\epsilon$ .

at  $10^6$  km and at 1 AU, and the solar wind particle density  $N$  at 1 AU, as functions of  $T_0$ , for two values of  $\epsilon$  (0. and 0.01). For  $\epsilon = 0$ , and this value of  $\alpha$ , the Parker wind solutions do not exist below  $T_0 = 1.5 \times 10^6 \text{ K}$ . The inclusion of the wave energy flux ( $\epsilon \neq 0$ ) results in the existence of wind solutions for ranges of coronal reference temperatures  $T_0$  below  $1.5 \times 10^6 \text{ K}$ , as the Alfvén waves provide the additional energy needed to lift the coronal plasma out of the solar gravitational field. Note that the wave-dominated solutions can easily produce a combination of high velocities ( $\sim 700 \text{ km/sec}$ ) and low densities ( $\sim 2 \text{ cm}^{-3}$ ) at 1 AU for reasonable conditions at  $10^6$  km, something impossible to do in Parker polytrope models with no waves. There are some fairly important deficiencies in this model that should be mentioned. The observed wave length spectrum of the Alfvén waves at 1 AU ( $\sim 5 \times 10^6$  km and less) implies that the WKB assumption is only approximately satisfied

near the sun. Also,  $\delta B/B$  typically increases by a factor of 20 to 50 between  $10^6$  km and 1 AU, so that even small-amplitude waves at  $10^6$  km will tend to become nonlinear ( $\delta B/B \approx 1$ ) by 1 AU. This will introduce nonlinear and wave damping effects not included in the model. With these deficiencies in mind, the model is a reasonable first attempt to determine the effects of coronal wave pressures on the dynamics of the wind.

In summary, it is clear from both the observations and the simplified model discussed above that coronal waves generated at or near the sun can have a major effect on both the small and large-scale structure of the interplanetary plasma at 1 AU. At the small scale they provide a major source for the interplanetary microscale fluctuations, and at the large scale they are almost certainly a dominant factor in the dynamics of the high-velocity streams, as has been suggested many times before.

## REFERENCES

- Belcher, J. W.; and Davis, L., Jr.: Large Amplitude Alfvén Waves in the Interplanetary Medium: II. *J. Geophys. Res.*, in press 1971.
- Belcher, J. W.; Davis, L., Jr.; and Smith, E. J.: Large Amplitude Alfvén Waves in the Interplanetary Medium: Mariner 5. *J. Geophys. Res.*, Vol. 74, 1969, p. 2302.
- Coleman, P. J., Jr.: Wave-like Phenomena in the Interplanetary Plasma: Mariner 2. *Planet. Space Sci.*, Vol. 15, 1967, p. 953.
- Coleman, P. J., Jr.: Turbulence, Viscosity, and Dissipation in the Solar Wind Plasma. *Astrophys. J.*, Vol. 153, 1968, p. 371.
- Davis, L., Jr.: Models of the Interplanetary Fields, in *The Solar Wind*, edited by R. J. Mackin, Jr., and M. Neugebauer. Pergamon Press, New York, 1966, p. 147.
- Parker, E. N.: Dynamical Theory of the Solar Wind. *Space Sci. Rev.*, Vol. 4, 1965, p. 666.
- Unti, T.W.J.; and Neugebauer, M.: Alfvén Waves in the Solar Wind. *Phys. Fluids*, Vol. 11, 1968, p. 563.

## ACKNOWLEDGMENTS

The author is greatly indebted to H. S. Bridge, A. J. Lazarus, and C. W. Snyder for the use of their Mariner 5 plasma data, and to P. J. Coleman, L. Davis, Jr., D. E. Jones, and E. J. Smith for the use of Mariner 5 magnetometer data, and for helpful comments and discussions. In particular, the author is indebted to L. Davis, Jr. for invaluable comments on all phases of this work.

## DISCUSSION

*A. Barnes* What was the total energy efflux at the base of the corona (fig. 4) of Belcher for  $\epsilon = 0.01$ ?

*J. Belcher* For that value I think it's on the order of  $2 \times 10^{27}$  ergs/sec. The Alfvén velocity is very high there, so even small-amplitude waves can carry a tremendous amount of energy into the plasma at the Alfvén velocity.

*Unidentified Speaker* In connection with the identification of the source region for the Alfvén waves, is it necessary that the source be very close to the sun? From the comments this morning in the theoretical discussion, the decay times are e-folding times for these waves. As such that they can propagate only a relatively short distance, and it seems to me that the observations only require that the source be closer to the sun than the point of observation, but not that they be within the critical surface. Do you have a comment on that, John?

*J. Belcher* Yes. Typically, any source of fluctuations, for example, stream-collisions, will generate waves propagating in all directions. If this source is outside the Alfvénic critical point, all the waves are swept out or convected, so you'll see waves going in both directions. However, if the source is inside the Alfvénic critical point you will only see the waves that propagate outward into the solar wind because the waves that propagate inward can propagate faster than they are being convected and they can move back toward the sun. Incidentally, the Alfvénic critical point, at which the solar wind velocity exceeds the local Alfvén velocity, is located at 10 to 20  $R_\odot$ .

*E. J. Smith* I would like to make a couple of brief comments having to do with the identification of the different types of discontinuities in interplanetary space. Len



Burlaga (p. 315) mentioned an analysis of his that indicates that certain classes, namely, the rotational discontinuities, occur at most, say, 25 percent of the time, at least in the data samples taken. Now, I feel, rightly or wrongly, that I have been partly responsible for this controversy and I know that there is a fundamental legal principle in English law that silence is usually interpreted as assent. So I thought I would take a couple of minutes to indicate that I do not necessarily assent. The method of analysis I have used is different from the one Burlaga has used. I don't think we've heard the last word about this matter of discontinuities yet. I'm certainly not about to give it now. However, those of you who are interested in this controversy might be interested in both the technique I'm using and, more importantly, the results that have been obtained so far.

Figure 1 is just an attempt to remind those of you who haven't been through this

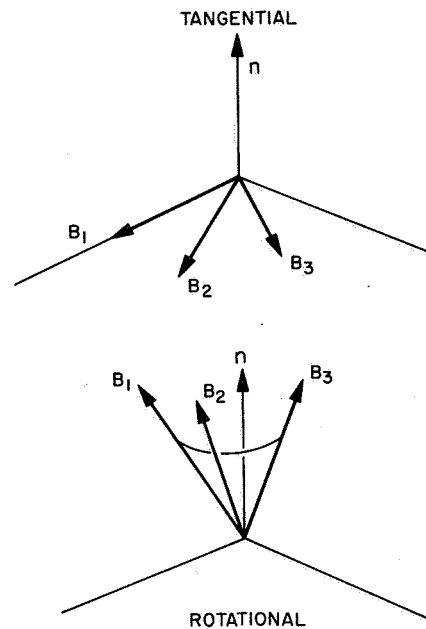


**Figure 1.** *Field changes across tangential and rotational discontinuities.*

recently of one way of viewing the distinction between the two types of discontinuities. The upper half of the figure shows how the field changes across a tangential discontinuity: It tends to rotate in the plane of the discontinuity, although it may change magnitude as well as direction. The fact that it rotates in the plane of discontinuity, as this drawing indicates, implies that there is no normal component to the magnetic field. At a rotational discontinuity, on the other hand, the field rotates in a cone about the normal to the plane of the discontinuity and consequently there is a normal component to the field. This distinction is borne out by the type of analysis discussed by, for example, Landau and Lifshitz. Using this rather simple approach I have analyzed the discontinuities from the Mariner 5 data as a basis for determining: (1) the direction of the normal to the plane of the discontinuity, and (2) whether there is a component of the magnetic field that is essentially constant and parallel to that direction.

Figure 2 is a histogram of the results obtained so far. The relative percentages of the number of cases for which the magnitude of the normal component relative to the total field has ratios indicated on the abscissa extend all the way up to one. As you can

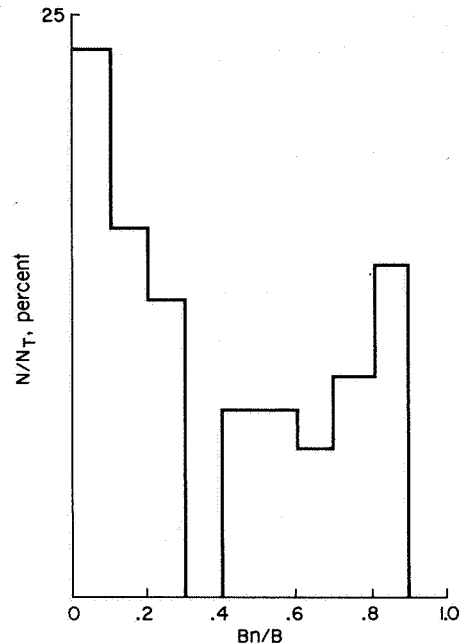


**Figure 2.** *Distribution of the normal components of the set of discontinuities analyzed.*

appreciate, in a  $5$  to  $10\gamma$  field, when you get up to this end of the axis, the values of the normal components are very large. They can be  $5\gamma$  or larger. The important thing about this distribution function, the most obvious feature, is that it has a double hump. There is obviously no narrowly defined classification, for example, two  $\delta$  functions, one at zero and the other for a finite, normal component. Nevertheless, you see very clearly that there appear to be two broad classes of discontinuities. There is some overlap where one ends and the other begins, and this introduces some uncertainty into the exact statistics that you end up with. The point is that I have chosen those discontinuities for which the normal component is  $0.4$  or more of the field magnitude on the two sides. Then it turns out that on the basis of this classification there is about an equal number of rotational and tangential discontinuities. That's been a consistent result which I've been obtaining with this method looking at different sets of data. There are other ways of checking this, which is what I'm doing now. Certainly the method Burlaga used, based on simultaneous plasma data, can be a very powerful one, and that is another way of now testing to see whether this classification is indeed the correct one or not.

There are other properties of discontinuities that should be mentioned. One of the important ones is that for a rotational discontinuity the magnitude of the field should remain constant at all times. The magnitude of the field may or may not be constant for tangential discontinuities. Now, based on this classification, all discontinuities selected as being rotational display a change in the magnitude of the field which is less than  $0.1$  of the total field.

*J. R. Jokipii* How do you determine the shock normal from one spacecraft?

*E. J. Smith* The normal to the discontinuity? I use a technique that a number of people have used for various purposes. It is the so-called "variance method." The distribution of the individual vectors is assumed to form an ellipsoid, which may degenerate into a plane. The variance analysis determines the principal axes of that ellipsoid, or equivalently, the eigenvalues and eigenvectors. The direction in which the variance is a minimum is taken to be the normal to the discontinuity. I then look at the individual discontinuities in the principal axis coordinate system and see the extent to which there is a nonnormal magnetic field component. This is a technique that Siscoe used to study discontinuities. Sonnerup also used it in studying the magnetopause, if you are familiar with those applications.

*F. C. Michel* Do you make this computation once for each discontinuity or do you select several and impose some consistency relation—for example, that successive discontinuities should tend to be parallel?

*E. J. Smith* I do this analysis on each individual discontinuity, and I use the vector fields on both sides as well as some vectors inside the current sheet. I do the analysis on that whole set, which is about 2 to 3 min of data.

*F. C. Michel* The field for rotational discontinuities should be the same on both sides unless the plasma pressure changes, and statistically such changes should average out. Thus, the average field before the discontinuity should equal that after it. Shock waves, for example, would not have that property.

*E. J. Smith* The classification really has nothing to do with the constancy of the magnetic field magnitude. I just use that as a test afterwards.

*N. F. Ness* I want to ask two specific questions: (1) How many discontinuities were in the sample you showed for the distribution of  $B_N/B$ , and (2) what was the average time interval of the data set used to define the discontinuity?

*E. J. Smith* The histogram that I showed contains a little over 60 discontinuities, and they are fairly large. I tried to pick examples where the field was relatively quiet both before and after the discontinuities, so there wouldn't be any large variations which might tend to obscure the identification of normal components. These occur on the average once every 6 hr. As I said earlier, the actual analysis interval is something like 3 min. The discontinuities, of course, are very abrupt, and consequently the transition occurs in less than 3 min.

*K. Schindler* It seems to me that your classification still might contain quite a number of weak shock waves, whereas Burlaga's doesn't.

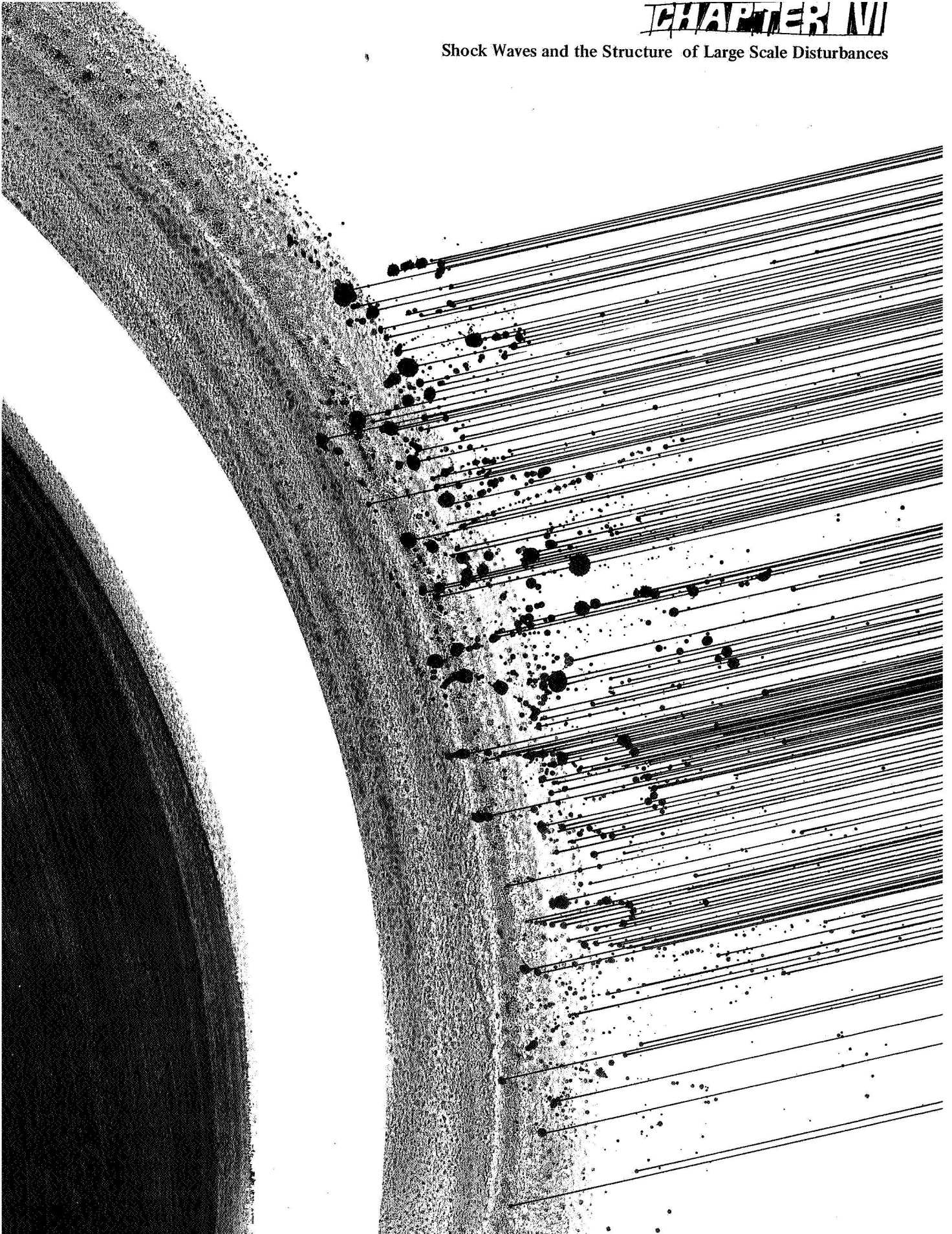
*E. J. Smith* I suppose it's possible that some shocks have been included. However, in looking at the discontinuities I have always tried to be careful to avoid shocks and I have used the plasma data for that. I look at the plasma velocity and see whether it's changed and also look to see the extent of the change in the magnitude whenever there's been a change in the magnitude of the field.

*A. Barnes* If possible I would like to jump back to the question Norman Ness raised before about Alfvén waves propagating out from the sun. I think there may be a bit of confusion on this point. This morning I wrote down an equation (p. 337) that indicated the decay of Alfvén waves might be very significant. I should point out that the equation is based on an estimate for bounds that include the value zero. The only solid calculation on this point that I know of is the one Gene Parker mentioned yesterday, which was performed by George Valley. His conclusion is that many Alfvén waves originating at the sun could probably reach the earth but with considerable attenuation. There is one other point. For most of the distance between the earth and sun, or at least half the distance,  $\Delta B/B$  will be smaller than at the earth even though the energy efflux in the Alfvén waves is larger than at 1 AU.



# CHAPTER VI

## Shock Waves and the Structure of Large Scale Disturbances



The geometry of flare and beam initiated shock disturbances; compositional differences in the shocked and driver gas; energy considerations, coplanarity theorems and multiple satellite determinations of geometry; multiple shocks and shock pairs; interactions of shocks and surfaces of discontinuity.

# INTERPLANETARY SHOCK WAVES AND THE STRUCTURE OF SOLAR WIND DISTURBANCES

A. J. Hundhausen

An invited review

Observations and theoretical models of interplanetary shock waves are reviewed with emphasis on the large-scale characteristics of the associated solar wind disturbances and on the relationship of these disturbances to solar activity. The sum of present day observational knowledge indicates that shock waves propagate through the solar wind along a broad, roughly spherical front, ahead of plasma and magnetic field ejected from solar flares. Typically, the shock front reaches 1 AU about two days after its flare origin, and is of intermediate strength (Mach number of  $\sim 2$ ). Not all large flares produce observable interplanetary shock waves; the best indicator of shock production appears to be the generation of *both* type II and type IV radio bursts by a flare. Theoretical models of shock propagation in the solar wind can account for the typically observed shock strength, transit time, and shape. Both observations and theory imply that the flare releases a mass of  $\sim 5 \times 10^{16}$  gm and an energy of  $\sim 1.6 \times 10^{32}$  ergs into the shock wave on a time scale of hours. This energy release estimate indicates that the shock wave is a major energy loss mechanism for some solar flares. **ABSTRACT**

## INTRODUCTION

The existence of interplanetary shock waves was inferred from the short rise times of geomagnetic sudden impulses [Gold, 1955] before the era of direct interplanetary observations. Quantitative theoretical models of shock propagation through an ambient interplanetary medium were shortly thereafter developed by Parker [1961]. Since the first direct observation of such a shock by the Mariner 2 spacecraft in 1962 [Sonett *et al.*, 1964], considerable effort, both theoretical and observational, has been directed to the study of interplanetary shock waves. Most of this effort has concentrated on the detailed, local characteristics of the shock front. In contrast, here we emphasize the relationship of interplanetary shocks to the large-scale solar wind disturbances of which they are part and to the solar activity thought to produce the entire phenomenon. For purposes

of this discussion the following terminology is used: *shock* is the surface discontinuity at which plasma properties change abruptly; a *solar wind disturbance* is any large-scale perturbation of ambient or quiet solar wind conditions; a *shock wave* is a solar wind disturbance with a shock at its leading edge. These phenomena are discussed in reviews by Wilcox [1969] and Hundhausen [1970a, b].

## A QUALITATIVE DESCRIPTION OF SOLAR WIND DISTURBANCES

Classical studies of solar-terrestrial relationships have pointed to the existence of two classes of interplanetary disturbances: transient disturbances following some solar flares, and recurrent (at 1 AU) disturbances thought to be produced by long-lived active regions (the so-called "M regions"). We present here qualitative descriptions of the interactions (leading to the formation of shocks) of these two types of disturbances with a steady, spherically symmetric, ambient solar wind. These descriptions will prove useful in organizing later discussions of quantitative theoretical models and of shock observations.

---

*This paper was prepared while the author was at the University of California Los Alamos Scientific Laboratory, Los Alamos, New Mexico. Present Address is High Altitude Observatory, National Center for Atmospheric Research, Boulder, Colorado.*

Figure 1 illustrates the plasma and magnetic field characteristics expected in a steady, structureless solar wind near the solar equatorial plane. At heliocentric distances greater than 10 to  $20R_{\odot}$ , solar wind models predict an almost radial plasma flow at nearly constant speed [Parker, 1963, 1969]. The expansion of the highly conductive plasma and the rotation of the sun

combine to produce the familiar spiral pattern of the interplanetary magnetic field lines [Parker, 1963, pp. 137–138]. Figure 1(a) shows the plasma and field configuration in a frame of reference stationary with respect to the solar system. Figure 1(b) shows the same configuration in a frame of reference rotating with the sun; in this latter frame both the field lines and flow streamlines are Archimedes spirals for a constant expansion speed.

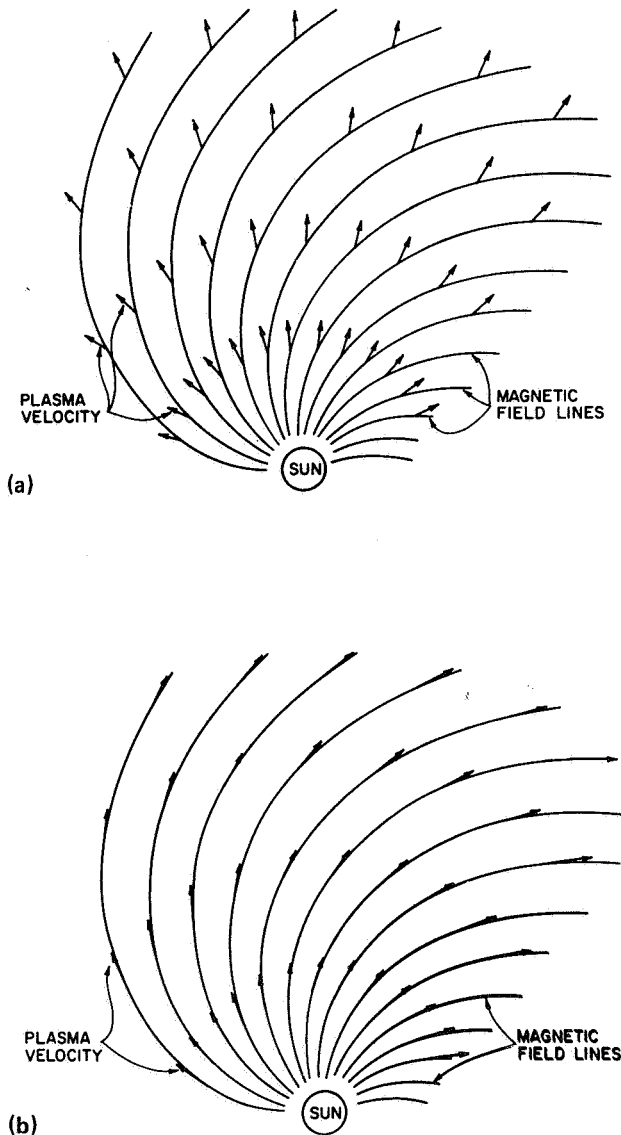


**Figure 1.** The plasma flow and magnetic field line configurations near the solar equatorial plane for a spherically symmetric, steady solar wind. Part (a) shows the flow pattern in a stationary frame of reference, while part (b) shows the same pattern in a frame of reference rotating with the sun.

#### Flare-Associated Solar Wind Disturbances

Optical, radio, particle observations all indicate that material is explosively ejected by large solar flares. Consider a volume of this material, presumably plasma from the chromosphere or low corona, moving rapidly outward into a slower ambient solar wind. Figure 2 shows a hypothetical cross section (in the solar equatorial plane) of the resulting solar wind disturbance at a time when it has traveled well out into interplanetary space. The shape given the disturbance in the drawing assumes some lateral expansion; theoretical and observational arguments for this effect are given in later sections. The ambient solar wind plasma and magnetic field lines must be compressed and pushed aside by expanding flare ejecta (the high electrical conductivity of the plasma prevents rapid interpenetration of the plasmas). If the speed of the ejected material exceeds the ambient solar wind speed by more than the local sound (or Alfvén) speed, a shock front will form at the leading edge of the compressed ambient plasma shell.

The nature of the boundary between the compressed ambient solar wind and the flare ejecta depends somewhat on details of the flare process. If the flare region was also a source of the ambient solar wind, the magnetic field lines in the flare plasma must connect to the ambient field. However, for the configuration shown in figure 2, this connection would take place only on a small part of the boundary, as shown just above and to the right of the flare site. Most of the boundary surface separates plasmas from different solar source regions, as well as with different time histories. Thus, the material on the two sides of the boundary might be expected to have different thermodynamic and chemical properties. Further, magnetic field lines would not cross such a region of the boundary, which must then form a tangential discontinuity within the interplanetary plasma and magnetic field [Colburn and Sonett, 1966]. If the flare region was not a source of the ambient solar wind, the entire boundary surface would separate plasma from different source regions and would be expected to be a tangential discontinuity; this situation is entirely different from that illustrated by Parker [1963] for a



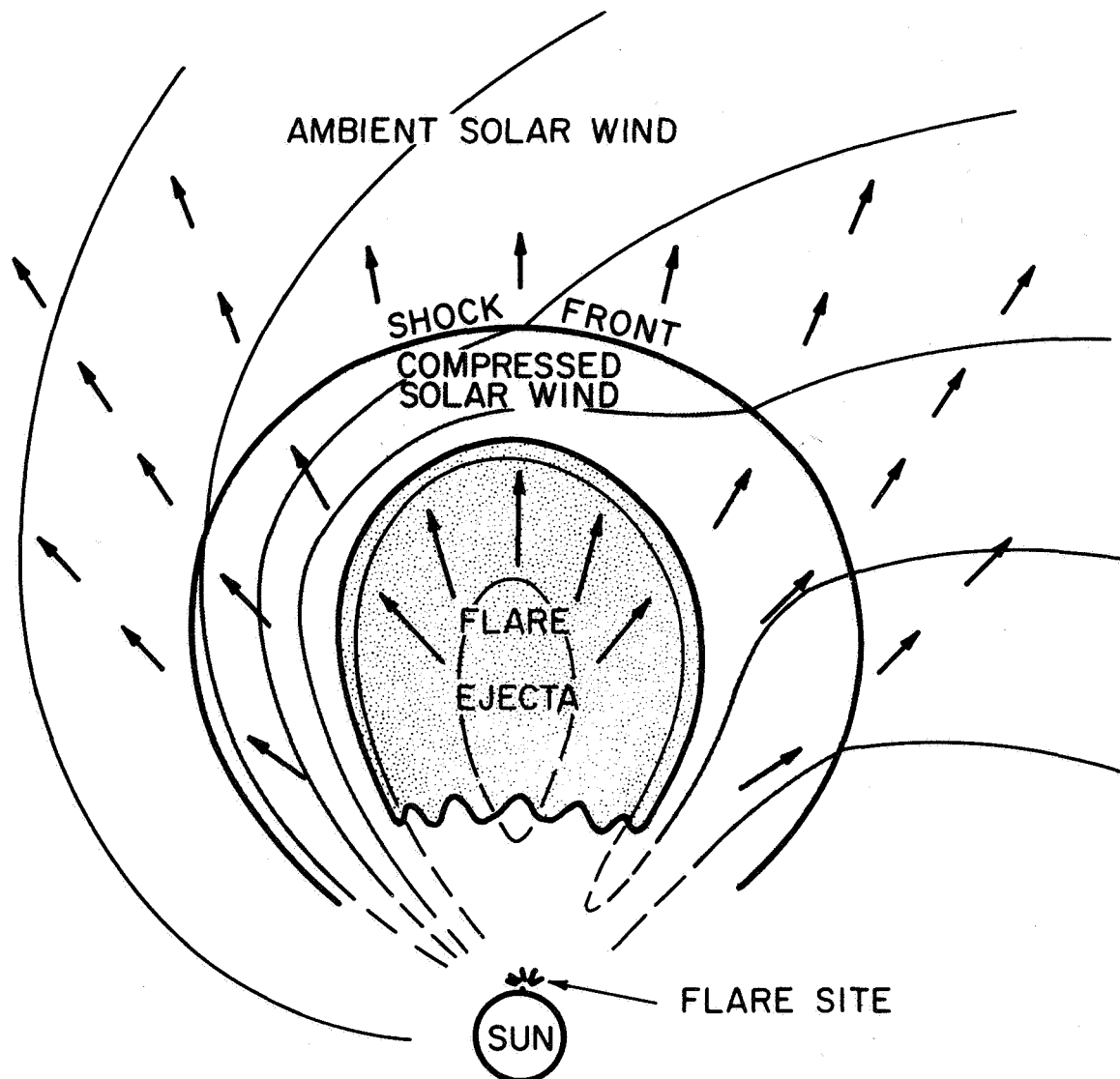


**Figure 2.** A qualitative sketch, in equatorial cross section, of a flare-produced solar wind disturbance, propagating into an ambient solar wind similar to that shown in figure 1. The arrows again indicate the plasma flow velocity and the light lines indicate the magnetic field. The rotation of the sun has been neglected in drawing a configuration symmetric about the flare site.

spherically symmetric wave, where the entire boundary is crossed by the field lines [Colburn and Sonett, 1966]. The rarity of collisions in the tenuous interplanetary plasma leads to extremely slow diffusion normal to magnetic field lines. The expected tangential nature of the boundary discontinuity would then help to preserve any thermodynamic or chemical differences between the ambient and flare plasmas.

The magnetic field and plasma structure within the flare ejecta depends strongly on the details of the flare process. The magnetic field lines must connect back to

the flare site (with a current sheet extending through the body of the ejecta as well as along its boundary) unless some diffusion of the plasma relative to the field lines, or "reconnection" of the field lines [Petschek, 1966] were to occur. Reconnection is a distinct possibility, as some theories of solar flares employ this process as the basic flare mechanism; for example, figure 3 shows the magnetic field configurations assumed and produced in the flare model of Sturrock [1967]. Such reconnection would produce closed magnetic loops within the flare plasma, as shown by the dashed field line of figure 2.

This configuration has been advocated by Gold [see the numerous discussions following relevant papers in *MacKin and Neugebauer, 1966*]. If some of the ejected material moves outward more rapidly than that near the tangential discontinuity (due either to acceleration of the former or deceleration of the latter) a second shock might form within the flare ejecta. This would be a "reverse" shock, moving toward the sun relative to the plasma but convected outward by the rapid plasma motion [*Sonett and Colburn, 1965*].

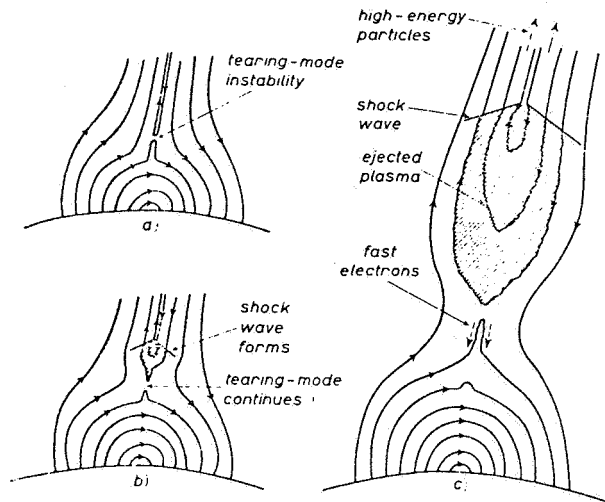


**Figure 3.** Coronal magnetic field configurations in the solar flare model of Sturrock [1967]. Closed magnetic field loops are formed within the flare ejecta (c) by the field line reconnection process taken to be the basic energy mechanism in the model.

#### Steady, High-Speed Solar Wind Streams

Solar wind observations such as those by *Neugebauer and Snyder [1966]* indicate that some streams of high speed solar wind, presumably emanating from specific centers of solar activity, persist long enough to be present on several successive solar rotations. Consider such a steady stream of solar wind flowing radially outward, with high, constant speed, from a source rotating with the sun. Figure 4 shows a hypothetical cross section of this stream (in the solar equatorial plane) viewed in the frame of reference rotating with the sun. In this frame, as in figure 1(b), the flow is along Archimedes spirals, with the magnetic field lines along the flow streamlines. The flow of a slow ambient wind, assumed to exist ahead of the fast stream, is along more tightly wound spirals that must eventually intersect the high speed stream. The high electrical conductivity of the plasma again prevents interpenetration, and the ambient plasma must be compressed and deflected to

ultimately flow parallel to the interface with the fast stream. If the inflow of the ambient plasma relative to this interface exceeds the local sound speed, a shock wave should form at the leading edge of the compressed ambient plasma region. The resulting flow pattern is steady in the frame of reference rotating with the sun. Figure 5 shows this pattern transformed into a stationary frame of reference, wherein the entire shock wave would appear to rotate counterclockwise about the sun.

The structure of the magnetic field and plasma in this shock wave is, in many ways, similar to that already described for flare-associated disturbances. The boundary between the compressed ambient solar wind and the high speed stream should again be a tangential discontinuity separating plasma and magnetic fields from two different solar source regions. The material on the two sides of the boundary might again be expected to have different thermodynamic and chemical properties, preserved because of the slow rates of diffusion across the field lines. A second or reverse shock could again form within the high speed stream if material is flowing toward the tangential discontinuity [*Colburn and Sonett, 1966*].

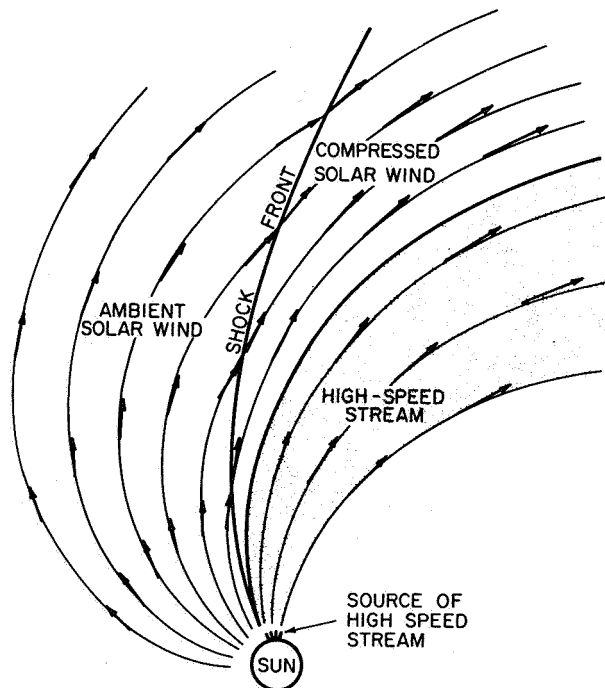


**Figure 4.** A qualitative sketch, in equatorial cross section, of a steady, localized stream of high speed solar wind interacting with a slow, ambient solar wind similar to that shown in figure 1. The interaction is shown in a frame of reference rotating with the sun. The arrows again indicate the plasma flow velocity and the light lines indicate the magnetic field.

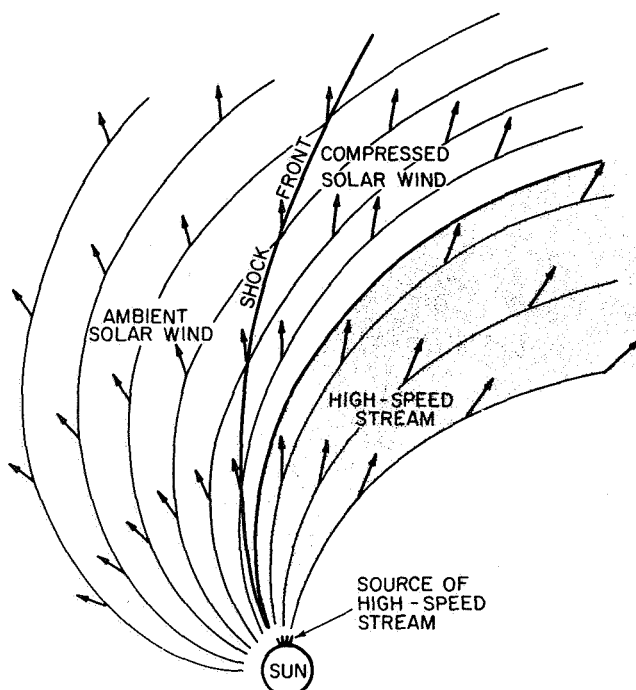


Figure 5. The interaction of figure 4, shown here in a stationary frame of reference.

#### Distinctions Between Flare-Associated and Steady-Stream Solar Wind Disturbances

Despite the many similarities between the flare-associated solar wind disturbance of figure 2 and the steady-stream disturbance of figure 5, several differences exist that might permit an observational distinction between the two classes. The most obvious of these is the shape of the shock front. For flare-associated disturbances the shock front is expected to be roughly symmetric about the radial direction from the flare site, while for steady-stream disturbances the shock front is more nearly aligned with the spiral interplanetary field lines. Observations of a single disturbance by several widely separated spacecraft, or the observation and statistical analysis of many shock orientations by a single spacecraft [Hirshberg, 1968] might be used to distinguish these two geometries. A still more fundamental difference exists in the basic topology of the field lines intersecting the shock front. For flare-associated disturbances the field lines in the preshock, ambient plasma all lead outward toward interstellar space, while for the steady-stream disturbance the field lines in the preshock, ambient plasma connect back to the sun. Observations of galactic cosmic rays, whose high energies make them tracers of large-scale magnetic field geometry, might be capable of distinguishing the two topologies.

In pursuing either of these suggested tests, as is done in a later section, one should always bear in mind that

these two classes of disturbances are idealized extremes. Intermediate classes, in which plasma is emitted from a solar source for about the same time required for its transit to an observer, could well occur and would be expected to display configurations between these two extremes. Further, solar flares occur in active regions, and thus might occur preferentially near the sources of high-speed streams; a correlation of this basic nature has been reported by Bumba and Obridko [1969]. The transient disturbances produced by such flares would be distorted by the lack of symmetry in the ambient medium into a configuration quite different from that shown in figure 2. We present some evidence later that solar wind disturbances appearing to be flare associated also show some characteristics of steady-stream emission.

#### THEORETICAL MODELS OF SOLAR WIND DISTURBANCES

Quantitative theoretical models have been developed for some aspects of the solar wind disturbances qualitatively described in the preceding section. Most attention has concentrated on the propagation of flare-associated shock waves under the assumption of spherical symmetry; as such models have recently been reviewed in some detail [Hundhausen, 1970b; Hundhausen and Montgomery, 1971], only a brief summary of some useful results is given here. The present discussion will then focus on the propagation of nonspherical, flare-associated shock waves, on the formation of shock waves in steady-stream disturbances, and on the effect of the high thermal conductivity of interplanetary electrons on both classes of solar wind disturbances.

##### Flare-Associated Shock Waves

Theoretical models of transient disturbances propagating through an ambient solar wind are most easily derived if both the ambient medium and the disturbances are assumed to be spherically symmetric (plasma properties are then functions only of the time  $t$  and heliocentric distance  $r$ ). Parker [1961, 1963] obtained spherical shock wave solutions of the adiabatic fluid equations (neglecting magnetic forces and solar gravity) by similarity techniques that assume basic dependence on the parameter  $\eta = tr^{-\lambda}$ . Any feature of these solutions that is at position  $r_0$  at time  $t_0$  moves with time as  $r = r_0 (t/t_0)^{1/\lambda}$ . The solutions are connected to the ambient medium by assuming a *strong* shock at the leading edge of the disturbances.

Figure 6 shows the density versus position (normalized to the shock location) for two of Parker's shock waves, with a ratio of specific heats  $\gamma = 5/3$  and an ambient

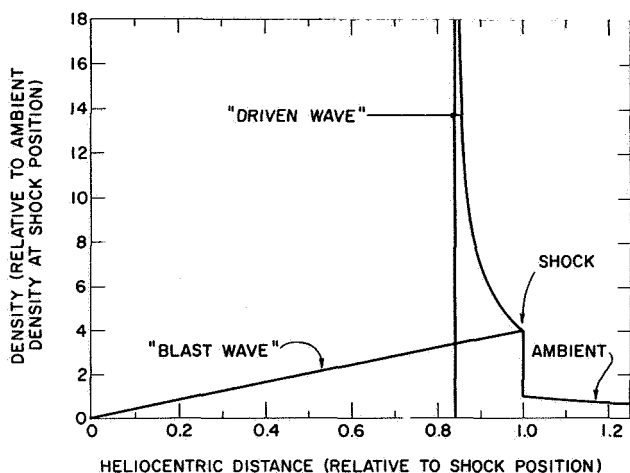


**Figure 6.** Similarity solutions for the propagation of spherically symmetric shock waves in the solar wind. The "driven wave" has an energy increasing linearly with time, while the "blast wave" has a constant energy [adapted from Parker, 1961].

density proportional to  $r^{-2}$ . The density change by a factor of 4 at the shock location indicates the assumption of infinite shock strength. The solution labeled *driven wave* corresponds to  $\lambda = 1$ ; the density rises monotonically behind the shock with a singularity as  $r \rightarrow 0.84$ , the position of the vertical line on figure 6. This wave moves with constant speed, and can be shown to have an energy increasing linearly with time. It represents the wave pushed (or driven) ahead of a steadily expanding "piston" (located at the singularity). The solution labeled *blast wave* corresponds to  $\lambda = 3/2$ ; the density falls monotonically behind the shock. This wave moves with steadily decreasing speed, and can be shown to have constant energy. It represents the wave produced by an explosion at  $r = 0, t = 0$ , with no further addition of energy thereafter. This class of "blast wave" solutions (approached by disturbances with energy input occurring over a time short compared to the transit time to a position of interest) has an interesting and useful characteristic; the properties of the wave (e.g., shock speed, transit time to a given radius) depend only on the total energy of the disturbance. The classification of solar wind disturbances as "driven" or "blast" waves will prove useful in the next section. Physically, the driven wave can be thought of as a disturbance whose properties are determined by the nature of the initiating signal at the sun, while the blast wave can be thought of as a disturbance whose properties are determined by interaction with the ambient medium.

Extensions of Parker's basic similarity solutions have been carried out by Simon and Axford [1966], Lee and

Balwanz [1968], Lee and Chen [1968], and Lee et al., [1970]. Korobeinikov [1969] has derived similarity solutions in which the assumption of infinite shock strength is somewhat relaxed, these solutions being valid to first order in the ratio of the ambient solar wind speed to the shock speed. However, all of these similarity theories of interplanetary shock waves basically apply to strong shocks. Observations (to be discussed in the next section) reveal that most interplanetary shocks are of intermediate strength. The applicability of the similarity solutions to solar wind conditions is therefore questionable.

This difficulty can be overcome by numerical integration of the fluid equations for shocks of arbitrary strength. Hundhausen and Gentry [1969a, 1969b] thus obtained spherical wave solutions of the adiabatic fluid equations (again neglecting magnetic forces, but including solar gravity). Figure 7 shows the density versus

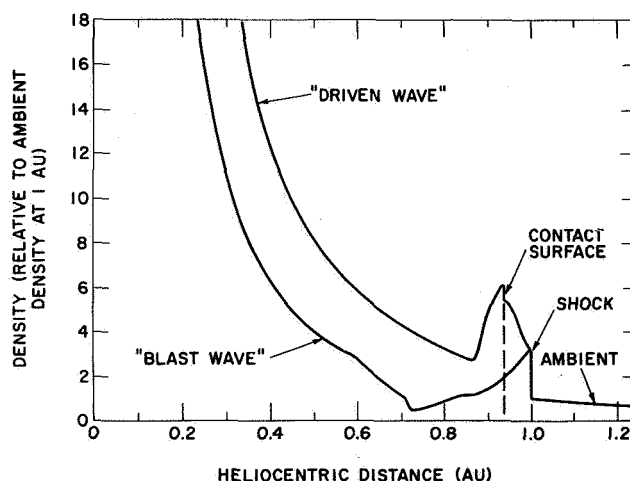


**Figure 7.** Numerical solutions for the propagation of spherically symmetric shock waves in the solar wind. The "driven wave" and "blast wave" cases correspond to the same basic definitions used in figure 6 [adapted from Hundhausen and Gentry, 1969a].

heliocentric position (in AU) for two of these shock waves, with a ratio of specific heats  $\gamma = 5/3$  and an ambient adiabatic solar wind with a flow speed of 400 km sec<sup>-1</sup> and a density of 12 protons cm<sup>-3</sup> at 1 AU. The density change of less than a factor of 4 at the shock location indicates the finite strength of the shock. The solution labeled *driven wave* shows a monotonic density rise behind the shock until a contact surface, separating the compressed ambient solar wind from the gas ejected in the initial disturbance at  $t = 0$ , is reached. This interface requires special treatment in the numerical integrations, and its properties are only qualitatively

indicated in figure 7. However, there is no density singularity as found at the "piston" interface in the similarity solutions (the latter appears to be due to the assumption of zero temperature in the similarity theory). The wave moves with nearly constant speed, and has an energy increasing linearly with time. It is thus analogous to the driven wave of similarity theory, representing a wave pushed by a continuous output of driver gas from the sun (forming a new steady state, shown in figure 7 for  $r < 0.83$  AU). It differs from the similarity solution of figure 6 in that it considers the flow at heliocentric distances within the contact surface. The numerical solution labeled *blast wave* in figure 7 shows a monotonic decrease in density for some time after the shock, with an eventual increase to the original ambient profile (approximately proportional to  $r^{-2}$ ) at  $r \approx 0.6$  AU. This wave moves with steadily decreasing speed and has a constant total (including gravitational) energy. It is thus analogous to the blast wave of similarity theory, representing a wave produced by a short-duration explosion at  $t = 0$ , followed here by a return to ambient conditions. As in similarity theory, the properties of this impulsively generated class of waves depend only on the total energy in the disturbance [Hundhausen and Gentry, 1969a]. The numerical blast waves differ from those of similarity theory in that the density rarefaction following the shock does not extend all of the way back to the sun.

Figure 8 shows a more detailed comparison of the density (normalized here to the ambient density at any heliocentric radius) versus heliocentric position (normalized to one at the leading-edge shock) for the driven wave solutions derived numerically by Hundhausen and Gentry [1969b] and using similarity theory by Simon and Axford [1966]. Both solutions shown involve a new steady flow at small heliocentric distances that is faster than the flow near the contact surface separating the ambient and "driver gas." Both solutions thus include a "reverse shock" (at  $S_2$  in the numerical solution and at the innermost  $S$  in the similarity solution) within the driver gas, as mentioned in the qualitative discussion of the preceding section. Hundhausen and Gentry [1969b] demonstrated that this configuration will be observed at a given heliocentric position in interplanetary space only if the initiating solar disturbance persists for more than 10 percent of the transit time of the resulting interplanetary shock wave to that position.

The optical emission from nearly all solar flares comes from an area of less than  $10^{-3}$  of a hemisphere [Smith and Smith, 1963, pp. 61–63]. Hence the theoretical models described above, all of which assume spherical symmetry of the flare-associated solar wind disturbance,

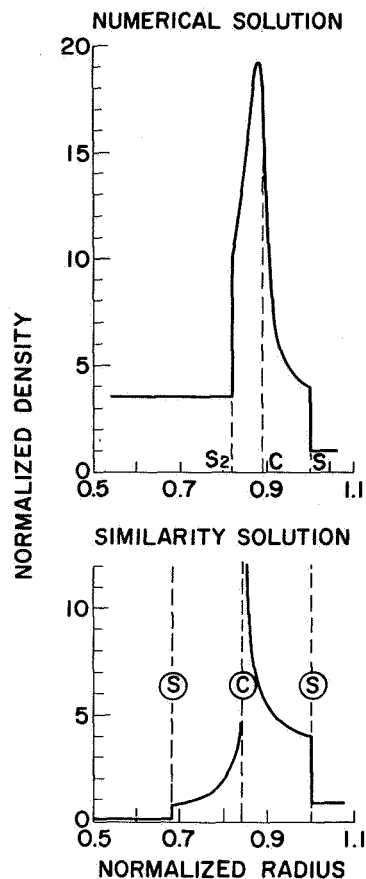
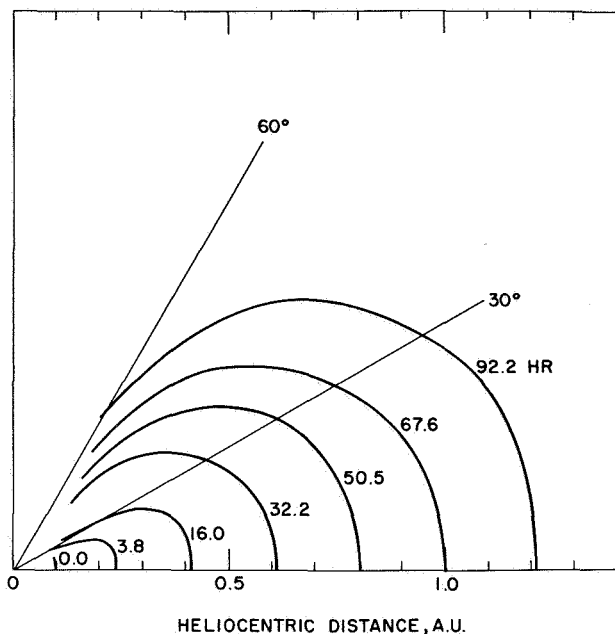


Figure 8. Numerical and similarity solutions showing the existence of a "reverse shock pair" in the solar wind [Hundhausen and Gentry, 1969b].

can only roughly approximate reality. De Young and Hundhausen [1971] have considered a radially moving flare ejecta confined to a thin spherical shell (at  $r = 0.1$  AU) within a cone of half-angle  $\theta$  (with symmetry axis above the flare site). The propagation of this disturbance into a spherically symmetric, adiabatic ambient solar wind is followed by numerical integration of the hydrodynamic equations. As the energy of the disturbance is constant, it is of the blast wave class defined above. Figure 9 shows the shape of the resulting shock front at several times (in hr) after introduction of a flare ejecta with  $\theta = 15^\circ$  and an energy of  $2.8 \times 10^{30}$  ergs. The wave slows and expands laterally in propagating to 1 AU; upon arrival at this distance, 67.6 hr after initiation at 0.1 AU, the shock fills a cone with half angle of nearly  $60^\circ$ . The transverse expansion becomes important when the wave is beyond  $r \approx 0.4$  AU because interaction with the ambient medium has considerably slowed and weakened the shock; the high pressure produced behind the front can then produce



**Figure 9.** The shock configuration as a function of time (indicated in hours) produced by a shell of flare ejecta initially confined to a cone with half-angle  $15^\circ$  at a heliocentric distance of 0.1 AU [De Young and Hundhausen, 1971]. On arrival at 1 AU, the disturbance has expanded laterally to fill a cone with half angle of  $\sim 60^\circ$ .

lateral expansion at a significant fraction of the shock propagation speed.

Figure 10 shows the shapes of the shock fronts (on reaching 1 AU) produced by flare ejecta of the same energy but subtending different half angles when introduced at  $r = 0.1$  AU. For  $\theta < 15^\circ$ , the shock shapes are almost identical; the shock is roughly spherical with radius  $\sim 0.5$  AU, but centered at 0.5 AU. Thus, for small initial angles, the nonspherical blast waves display an extension of the characteristic of spherical blast waves noted above. The shock shape, as well as the shock speed and transit time, depends on the energy of the initial disturbance, not on such details as the initial angular extent. This characteristic again illustrates the dominant role of the interaction with the ambient medium in determining the properties of blast waves.

#### Steady, High-Speed Streams

Theoretical models of solar wind disturbances produced by steady, high-speed streams are most logically considered in the frame of reference rotating with the sun (as in fig. 4), wherein the flow is steady although not spherically symmetric (in this sense, the system is at an opposite extreme from the transient, spherical models described earlier). Viewed in this frame, the interaction

of a slow ambient solar wind with the high-speed stream is the deflection of a nonuniform, supersonic flow by an impenetrable, curved surface.

No thorough quantitative treatment of this interaction has yet been published. The most pertinent theoretical work in the literature treats corotating, linear perturbations of a uniform ambient flow [Carovillano and Siscoe, 1969; Siscoe and Finley, 1970]. Figure 11 shows the perturbation of the density  $\rho$ , the radial velocity component  $V_r$ , and the azimuthal velocity component  $V_\phi$  produced at 1 AU by the introduction of a localized, radial, high-speed stream on a source surface at  $r = 0.1$  AU [Carovillano and Siscoe, 1969]. The abscissa is in units of time for a stationary observer, or, equivalently, the azimuthal angle within the steady structure in the rotating frame (fig. 4). The interaction of the ambient solar wind with the high speed stream has

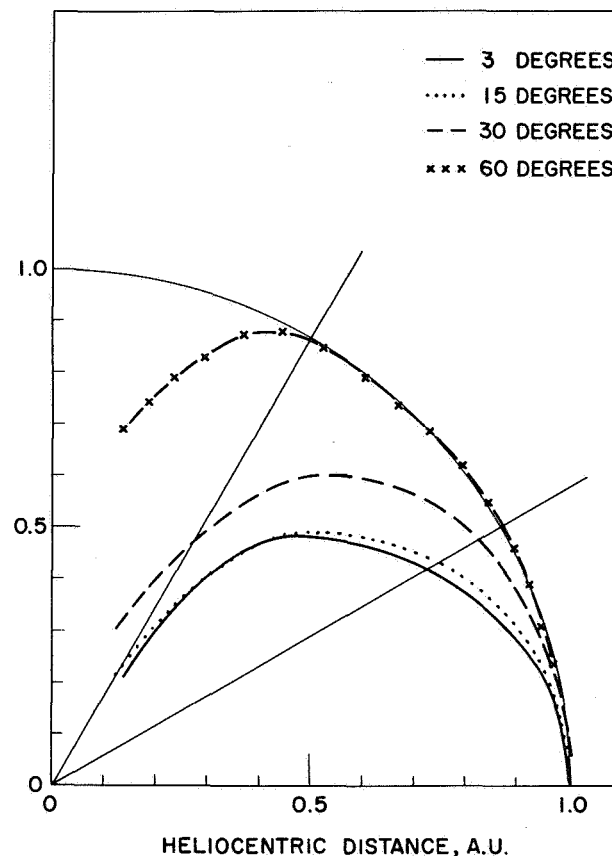


**Figure 10.** The interplanetary shock configurations produced by flare ejecta that were initially confined to cones with different half-angles  $\theta$  at 0.1 AU. For  $\theta \lesssim 15^\circ$ , the initial half angle has little influence on the configuration near 1 AU [De Young and Hundhausen, 1971].

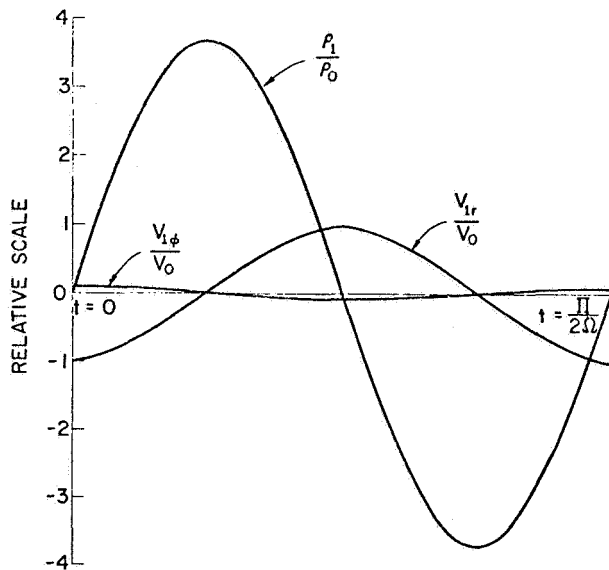


**Figure 11.** The linear perturbations in the density  $\rho$ , radial velocity component  $v_r$ , and azimuthal velocity component  $v_\phi$  produced at 1 AU by a steady high-speed stream, rotating with the sun, introduced at 0.1 AU. The abscissa is the time in a stationary frame of reference rotating with the sun (as in figure 4) [Carovillano and Siscoe, 1969].

produced the expected density compression and rarefaction in the leading and trailing halves of the disturbance, as well as a small azimuthal velocity component. The nonlinear steepening of the leading edge of the density compression would be expected to ultimately produce a shock. Mori [1970] has discussed this process and estimated the heliocentric position of shock formation as a function of the difference in speeds of the ambient solar wind and high-speed stream. This treatment involves several drastic simplifying assumptions (e.g., one-dimensional flow) and does not consider momentum exchange implicit in the interaction of the streams. Its applicability to the actual phenomenon is thus questionable.

#### Possible Effects of Heat Conduction on Solar Wind Disturbances

For the sake of tractability, all the theoretical models described above have assumed an adiabatic flow of plasma. However, it is expected that the interplanetary plasma is a highly efficient heat conductor. Parker [1963] pointed out that the "thermal equilibration time" in the hot plasma behind an interplanetary shock is of the order of  $10^4$  sec, much shorter than the expected transit time of a flare-produced shock wave to 1 AU. This implies that the flow behind the shock would be more nearly isothermal than adiabatic. Hundhausen

and Montgomery [1971] have extended this analysis to more general solar wind conditions, arguing that a nearly steady balance will exist between heat conduction and any solar wind heating mechanism persisting on a time scale longer than  $\sim 4 \times 10^4$  sec. In fact, the heat conductivity of interplanetary electrons is so large that only a small electron temperature gradient is required to dissipate the energy released at a typical interplanetary shock or in the typical interaction of slow and fast solar wind streams. Heat conduction must then prevent any large rise in electron temperatures associated with such disturbances and ultimately affect their large-scale structure. In the case of flare-produced shock waves, heat conduction should broaden the entire wave structure [Parker, 1963]. In the case of steady streams, heat conduction might even prevent the formation of shocks in front of high-speed streams.

#### OBSERVATIONS OF SOLAR WIND DISTURBANCES

Many detailed observations of interplanetary shock waves have been reported in the literature and discussed in the reviews by Wilcox [1969] and Hundhausen [1970a, b]. The emphasis here will be on placing the observations within the context of the large-scale structure of solar wind disturbances. After some illustration of the difficulties encountered in relation specific interplanetary shock waves to specific solar activity, some pertinent observations are presented (with reference to the reviews already mentioned for most details) and a general description of a typical flare-associated disturbance synthesized from the various pieces of observational evidence.

##### The Relationship Between Interplanetary Shock Waves and Solar Activity

The study of solar-terrestrial relationships was pursued long before any direct observations of the intervening medium were possible. Statistical correlations of solar and geomagnetic activity provided both some general cause-and-effect relationships and some specific inferences regarding the geometry of interplanetary disturbances. Unfortunately, interpretation of such indirect studies was not always unambiguous. To cite only a recent example, Bell [1961] has found that over half of the major flares (basically important 2+ or greater) from the years 1937 through 1959 produced a geomagnetic storm within three days, while Ballif and Jones [1969] have advocated geomagnetic storms "can be accounted for entirely by the effects of interplanetary streams," with no consideration of emissions from individual flares being necessary. One might conclude that the heritage of the presatellite era is a mixture of wisdom and confusion.

Direct interplanetary observations of shock waves and

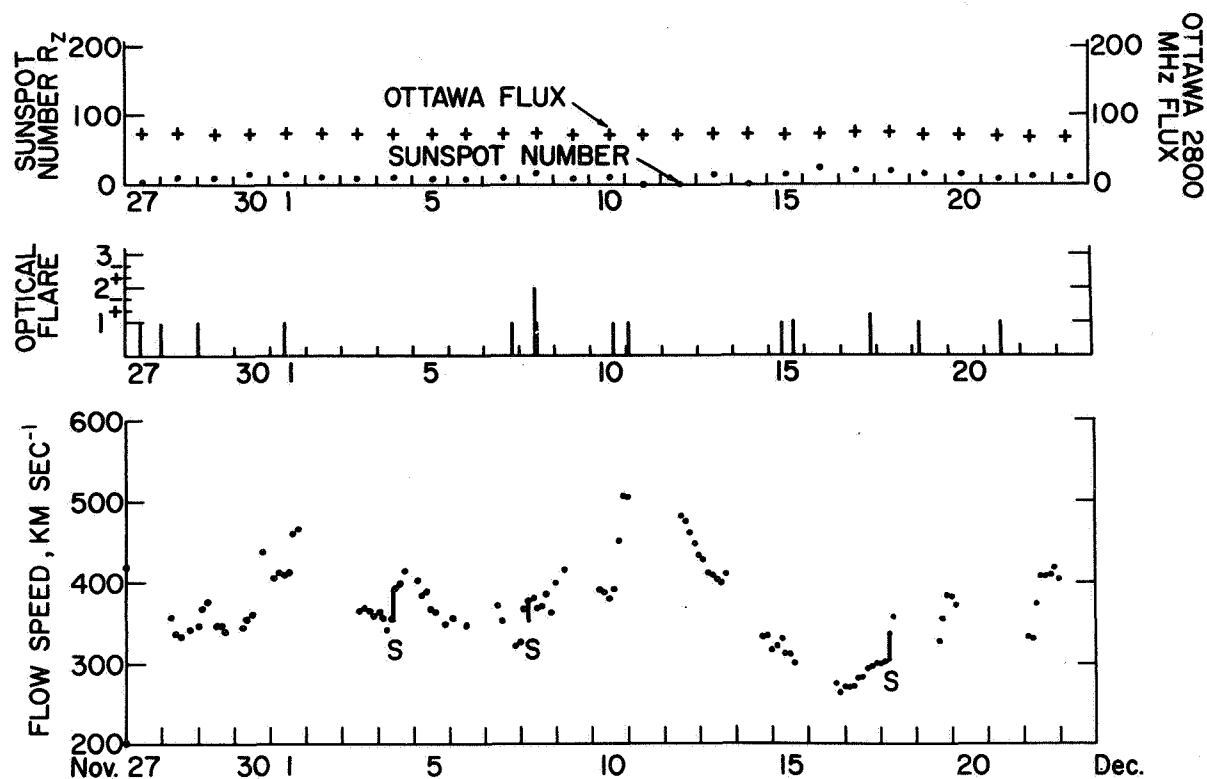


Figure 12. A summary of solar and interplanetary observations made during the 27-day solar rotation period 27 November to 24 December 1965. Zurich sunspot number, Ottawa 2800 MHz radio flux, optical flare observations (with importance rating denoted by the length of the vertical line), and the 3 averages of the solar wind speed observed on Vela 3 satellites are shown as functions of time. Interplanetary shock waves detected in the Vela 3 observations are denoted by the vertical bars (indicating the observed change in flow speed) and the letter S along the flow speed curve.

correlations of these observations with indices of solar and geomagnetic activity have added to this heritage. Some observed shock waves can be reasonably attributed to large solar flares, others can be attributed only to small flares, and some have no reasonable flare associations. A few large flares appear to produce no interplanetary shock waves. The relationship between solar activity and solar wind disturbances is still, in fact, imperfectly understood. A few illustrations of specific difficulties are in order.

Figure 12 summarizes solar and interplanetary observations from a 27-day solar rotation period in late 1965. Daily values of the Zurich sunspot number  $R_z$  and the Ottawa index of 2800-MHz solar radio flux, taken from *Solar-Geophysical Data* [1967], are shown in the first frame. Solar flares listed in the same compilation are shown in the second frame by vertical lines whose lengths denote optical importance. Three-hour averages of the solar wind speed observed by Vela 3 spacecraft

[Bame *et al.*, 1971] are shown in the lowest frame; interplanetary shocks discernible in the Vela data are indicated by a vertical bar, indicating the observed change in flow speed, and the letter S along the flow speed versus time curve.

The low level of solar activity during this period can be judged from the low sunspot numbers and radio fluxes. Only 14 solar flares of importance 1 or greater, including only one flare rated at importance 2 by a single station, were reported during these 27 days. The Vela solar wind observations detected three small interplanetary shock waves; other shocks might have gone undetected during gaps in spacecraft telemetry. None of the three observed shock waves appears to be recurrent [Hundhausen *et al.*, 1970] or associated with a high speed stream of the nature described by Neugebauer and Snyder [1966]. Reasonable flare associations can be proposed for the 3 December and 18 December shocks, but these associations must of necessity involve flares of importance 1



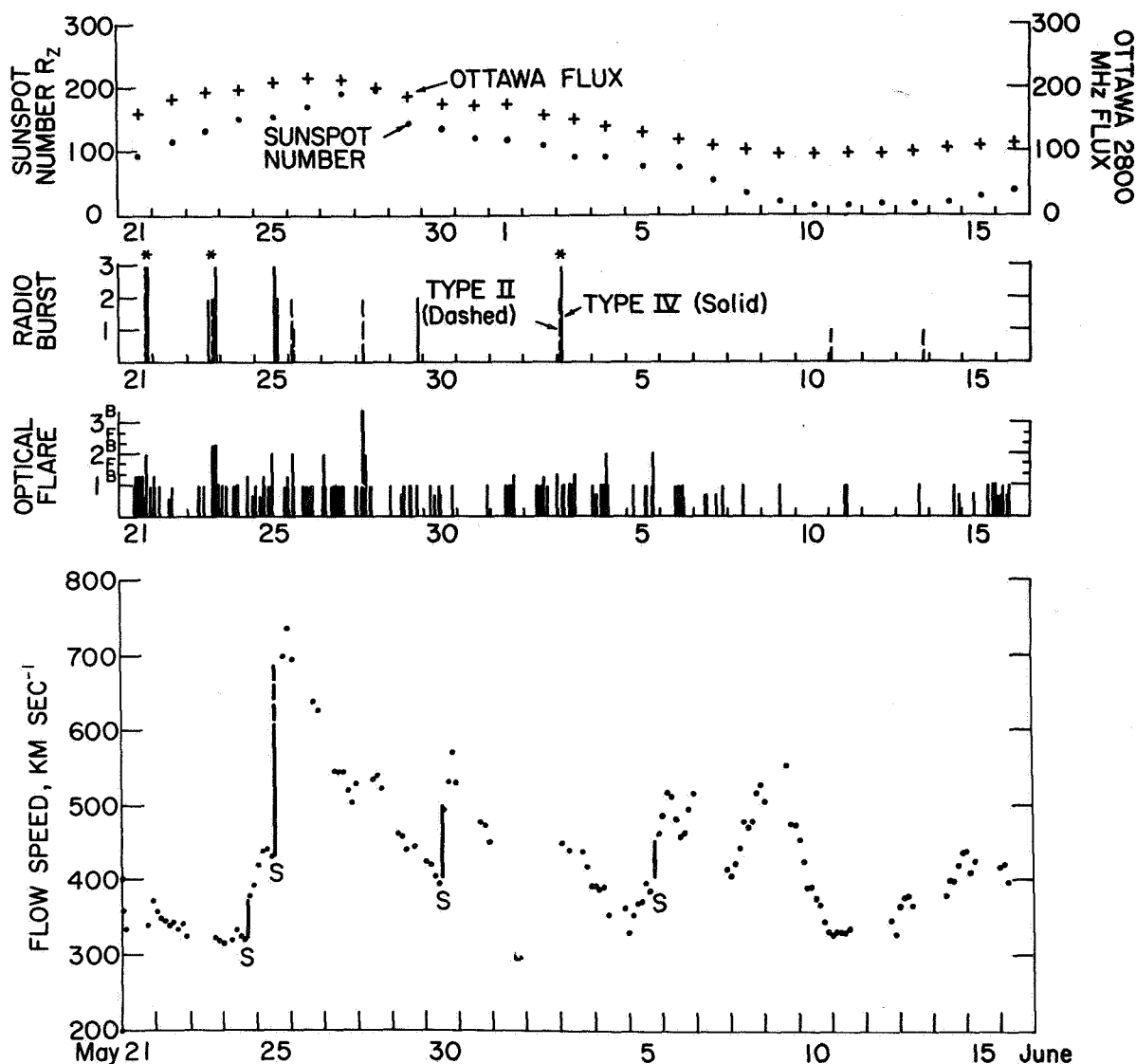


Figure 13. A summary of solar and interplanetary observations made during the 27-day solar rotation period 21 May to 17 June 1967. Type II and type IV radio bursts, indicated by dashed and solid lines (whose lengths again denote importance), respectively, have been added to the data shown in figure 12. Simultaneous type II and type IV bursts are emphasized by asterisks above the events.

(i.e., flares with optical emission from a rather small area). Even during this time of low solar activity, there is no unambiguous relationship between the observed solar activity and interplanetary disturbances.

Figure 13 summarizes solar and interplanetary observations from a solar rotation in mid-1967. In addition to the information given in the previous example, figure 13 includes type II and type IV radio bursts from the compilations in *Solar-Geophysical Data* [1967] and the

*Quarterly Bulletin on Solar Activity* [1967]. The bursts are shown by vertical lines, dashed for type II, solid for type IV, whose lengths indicate importance on the scale (based on maximum intensity) used in the above sources.

Solar activity was at a much higher level during this rotation than during the previous example, as attested by the higher sunspot numbers and 2800-MHz radio fluxes. This difference is manifested in the reporting of 147 importance 1 flares, 12 importance 2 flares, and 2

importance 3 flares during the May-June 1967 solar rotation. It may then be somewhat surprising to find that Vela 3 and Vela 4 satellites detected only four interplanetary shock waves during this rotation. None of the solar wind disturbances related to these shocks appears to be recurrent. Any attempt at flare associations encounters a problem completely different from the paucity of flares in the previous example; in the present example there are many more flares (even many more major flares) than observed interplanetary shock waves.

Consideration of the radio burst data might be expected to help in clarifying flare associations, as type II and type IV bursts are generally attributed to flare-related coronal processes and have been statistically related to geomagnetic storms. In particular, the occurrence of "a combined type II-type IV burst, which indicates a shock front moving ahead of a plasma cloud through the solar corona" [Kundu, 1965, p. 553], has a very high correlation with geomagnetic activity. Three such combinations, hereafter referred to as II-IV radio burst pairs, occurred during the solar rotation under discussion and are indicated on figure 13 by asterisks above the vertical lines denoting the bursts. Each burst pair can be associated with a solar flare and was followed within three days by an interplanetary shock wave observation at 1 AU. Consideration of the radio burst data thus leads to an entirely reasonable set of flare-radio burst-interplanetary shock associations: an importance 2N flare and a II-IV burst pair on 21 May with the interplanetary shock observed on 24 May, one of several importance 2B flares and a II-IV burst pair on 23 May with the interplanetary shock observed on 25 May; and an importance 1 flare and a II-IV burst pair on 3 June with the interplanetary shock observed on 5 June. It is curious that the last of these associations favors an importance 1 flare over two later importance 2 flares as the origin of the June 5 shock. The only remaining interplanetary shock from this rotation period, that of 30 May, can be assigned a reasonable association with an importance 3 flare and simultaneous type II burst (but with no reported type IV burst) on 28 May. Thus use of a combination of optical flare and radio burst data brings some order out of the original chaos, leading to a highly plausible association for each observed interplanetary shock wave. The conclusion remains, as stated earlier, that some large solar flares (importance 2 or greater) do not produce interplanetary shock waves.

Further evidence for the usefulness of combined type II-type IV radio bursts in assigning flare associations, as well as a devastating proof that all is not simple, can be found in observations from two successive solar rota-

tions at a level of solar activity intermediate between the examples already discussed. Figure 14 shows sunspot number, 2800-MHz radio flux, type II and type IV radio bursts, optical flares, and solar wind speeds for a solar rotation in February 1967. Two interplanetary shock waves were observed by Vela 3 satellites, each following an importance 2 or 3 flare and a simultaneous II-IV burst pair by the canonical two to three days. The pattern of successful associations of such events was broken on 22 February when a new active region, associated with the plage area McMath 8704, appeared on the east limb of the sun. Figure 15 extends the solar and interplanetary observations through the transit of this active region across the visible solar hemisphere. Many flares, including five with importance ratings as high as 2, were observed within the active region. Four II-IV radio burst pairs, presumably related to some of these flares, were reported during the transit of McMath 8704. Yet no interplanetary shock waves were detected by the Vela 3 satellites; in fact, no major solar wind disturbance is revealed in the flow speed data of figures 14 and 15 for the entire period of transit. Despite a high level of optical flare and radio burst activity, despite the high general level of activity evidenced by the sunspot numbers and 2800-MHz radio fluxes, this active region produced very little perturbation of the solar wind at 1 AU. The interval from 22 February to 16 March is, in fact, the most extended interval of undisturbed solar wind (characterized by low and relatively steady flow speeds) observed by the Vela 3 satellites between July 1965 and June 1967.

Despite the ample demonstration afforded by the above examples of our imperfect understanding of the relationship between solar activity and interplanetary disturbances, some hope can be salvaged from the frequent correlations between the combination type II-type IV radio bursts and observed interplanetary shock waves. For example, during the first 6 months of 1967, 17 II-IV burst pairs were reported. Nine of the burst pairs were followed within one to three days by an interplanetary shock wave discernible in Vela 3 data; eight of these bursts could be related to simultaneous solar flares that occurred at solar longitudes within  $51^\circ$  of central meridian. Eight of the 17 reported burst pairs were not followed by observed interplanetary shock waves; of these, 3 could be related to flares at solar longitudes greater than  $51^\circ$  from central meridian, while 4 could be related to flares in the infamous McMath 8704 discussed above. Thus 60 percent of the II-IV radio burst pairs related to flares within  $\sim 50^\circ$  of central meridian, a restriction similar to those derived in some indirect studies such as that by Akasofu and Yoshida

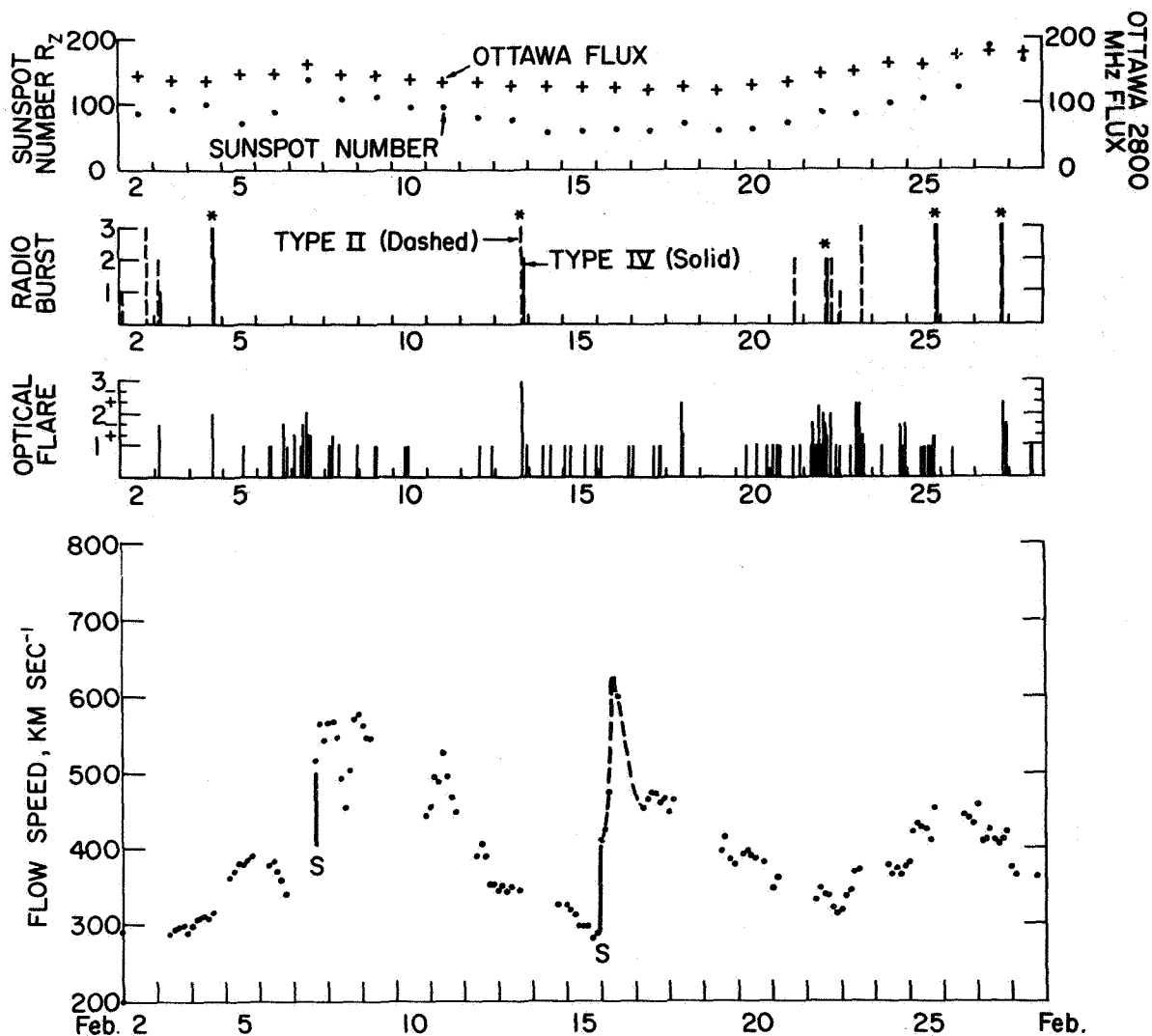


Figure 14. A summary of solar and interplanetary observations made during the 27-day solar rotation period 2 February to 1 March 1967.

[1967], were followed by an observed interplanetary shock wave. Particular active regions, such as McMath 8704, however, can be completely anomalous. A test on the necessity of II-IV burst pairs for the occurrence of interplanetary shock waves (the discussion above tests sufficiency) yields a similar result. During the first half of 1967, 9 of the 15 interplanetary shock waves detected by Vela 3 satellites were preceded (within three days) by reported II-IV radio burst pairs (note that daily gaps do exist in solar spectral observations). This latter test works much less well for the solar rotation from late 1965, discussed as the first example above. In fact, *Hundhausen* [1970b] and *Hundhausen et al.* [1970] list 7 shock observations from the last half of 1965, while not one II-IV burst pair is reported from these 6 months.

However, the shock waves observed in late 1965 were found to be an order of magnitude less energetic than those observed in early 1967; if radio emission were similarly less energetic in 1965, bursts might have occurred but fallen below the threshold of observation. The correlation of radio burst and solar wind observations clearly deserves further and more detailed study.

#### Local Properties of Interplanetary Shocks

The properties of 27 individual interplanetary shocks observed on various satellites between October 1962 and February 1969 are tabulated in the review by *Hundhausen* [1970b]. Table 1 summarizes the dynamic properties of the "typical" shock drawn from this sample. Relevant to the present discussion are the

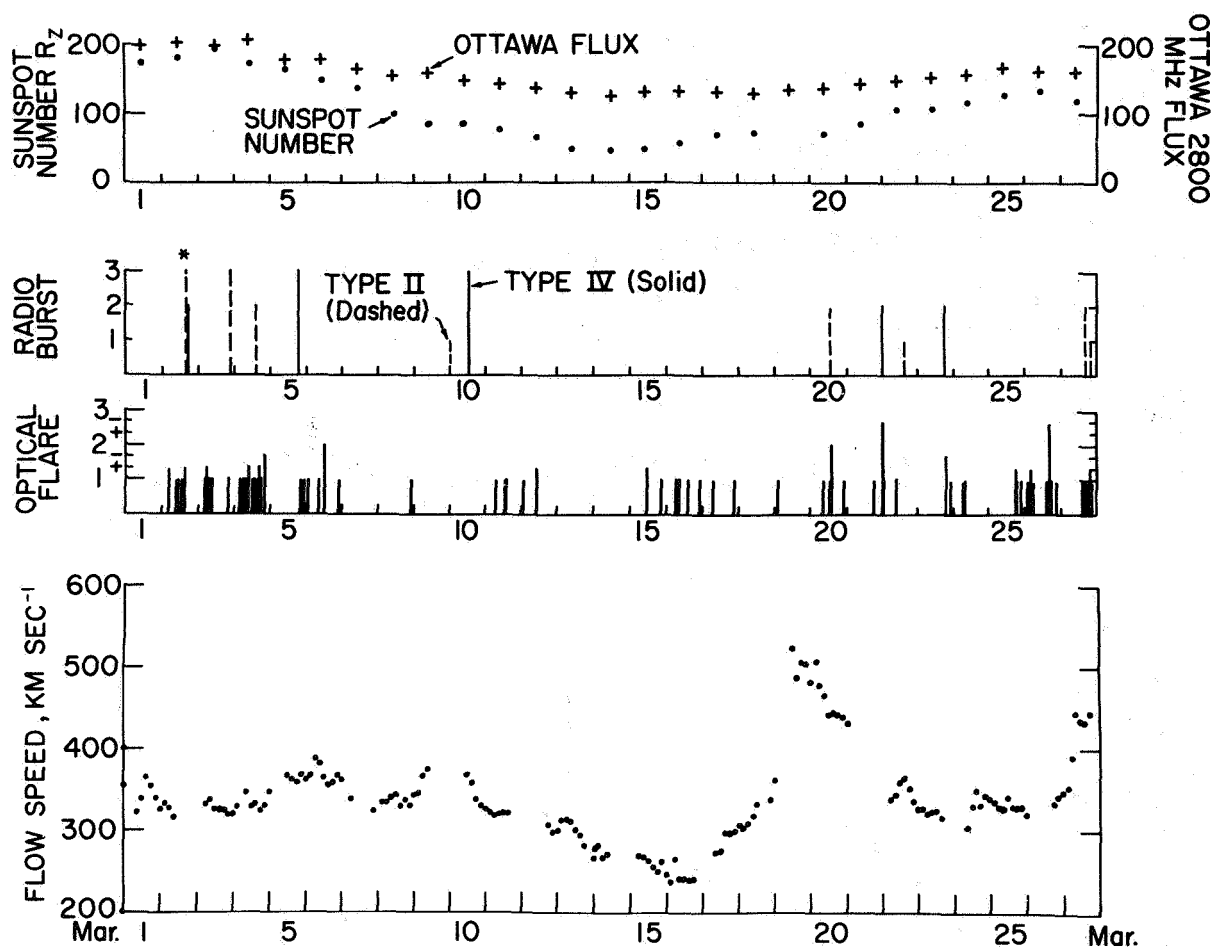


Figure 15. A summary of solar and interplanetary observations made during the 27-day solar rotation period 1 March to 28 March 1967.

following conclusions:

1. Interplanetary shocks are not strong (of high Mach number) but rather of intermediate strength. Two implications follow from this conclusion. First, theoretical models that assume strong interplanetary shocks must be applied to solar wind disturbances with some caution. Second, the motion of a shock through interplanetary space is largely the result of the general outward flow of the solar wind plasma rather than the propagation of the shock relative to the plasma. The geometric configuration of the shock wave will then be *strongly* influenced by irregularities in the plasma flow. In particular, the large-scale shock shape can be greatly distorted from the idealized configurations of figures 2 and 5 by a spatial structure of the *ambient* solar wind.
2. Both the similarity and numerical models of interplanetary shock propagation yield relationships between transit time to a given heliocentric distance

Table 1. Dynamical properties of the typical interplanetary shock observed near 1 AU (based on the tabulation in [Hundhausen, 1970b])

Flow speed of preshock plasma	390 km sec <sup>-1</sup>
Flow speed of postshock plasma	470 km sec <sup>-1</sup>
Shock propagation speed relative to stationary observer	500 km sec <sup>-1</sup>
Shock propagation speed relative to ambient solar wind	110 km sec <sup>-1</sup>
Mach number (sonic or Alfvén)	2 to 3
Transit time from the sun	55 hr

and the energy in the shock wave, valid for "blast-wave" or impulsively generated disturbances. These relationships have been used to infer shock wave

energies from transit times by *Dryer and Jones* [1968], *Hundhausen and Gentry* [1969a], *Korobeinikov* [1969], and *De Young and Hundhausen* [1971]. The 55-hr average transit time given in table 1 leads to an energy estimate of a few times  $10^{32}$  ergs from similarity theory, or of a few times  $10^{31}$  ergs (at 1 AU) from the numerical computations. These estimates assume that the typical interplanetary shock wave is of the blast wave class, and are dependent on both the models and flare associations. A comparison with more directly derived shock wave energies is presented later in this paper.

The local orientations of interplanetary shocks are of special interest as indicators of large-scale shock configurations. A basis for deriving shock orientations from spacecraft observations of the vector magnetic fields,  $\mathbf{B}_1$  in the preshock or ambient plasma, and  $\mathbf{B}_2$  in the postshock plasma, is the so-called "coplanarity theorem." Application of Maxwell's equations and momentum conservation to a compressive shock front in a medium with isotropic pressure tensor shows [Colburn and Sonett, 1966] that the shock normal must lie in the plane defined by  $\mathbf{B}_1$  and  $\mathbf{B}_2$ . *Chao* [1970] has demonstrated that this theorem remains valid in an anisotropic medium if the pressure tensor is symmetric about the magnetic field (as one would expect on the basis of physical symmetry arguments). As  $\Delta\mathbf{B} = \mathbf{B}_2 - \mathbf{B}_1$  must lie in the plane of a shock (to satisfy  $\nabla \cdot \mathbf{B} = 0$ ), it follows that the shock normal is parallel to  $\Delta\mathbf{B} \times (\mathbf{B}_1 \times \mathbf{B}_2)$ . Thus, in principle, observation of the preshock and postshock magnetic fields is sufficient to determine a shock orientation. This technique was applied to actual observations by *Sonett et al.* [1964] and *Ogilvie and Burlaga* [1969]. In practice, however, the coplanarity method does not usually lead to an accurate determination of shock orientation; fluctuations in the fields of the preshock and postshock plasmas and the small change in field direction that occurs at many shocks conspire to produce large uncertainties in the computed normal. *Ogilvie and Burlaga* [1969] were forced to use observations from two spacecraft to derive acceptable normals for several shocks despite the availability of magnetic field observations.

Using both coplanarity and dual-satellite observations *Ogilvie and Burlaga* [1969] derived six shock normals, which gave the first direct statistical evidence regarding shock configurations near 1 AU. These normals clustered about the radial from the sun, with a  $20^\circ$  average deviation therefrom. This distribution is qualitatively consistent with expectations for the shock configuration of figure 2—that is, the flare-produced case. *Taylor* [1969] combined the  $\Delta\mathbf{B}$  observed by the IMP 3

magnetometer at 8 "possible shocks" (no unambiguous identification was possible due to the lack of plasma data) having reasonable flare associations with the assumption that the normal was parallel to the ecliptic plane. The resulting shock orientations are shown in figure 16 at a position (on the circle representing 1 AU)

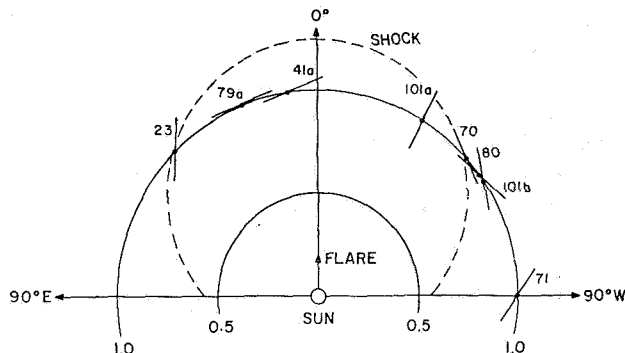
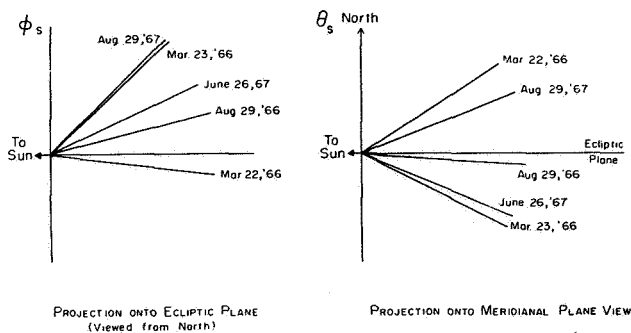


Figure 16. The orientations of eight shock surfaces inferred from IMP 3 magnetometer data, each plotted at the heliocentric longitude of observation relative to the associated flare [Taylor, 1969].

corresponding to the solar longitude of each actual observation, relative to the site of the associated flare. All of the shocks except that labeled 101a are consistent with shock propagation over a broad front roughly symmetric about the flare site. The dashed line on figure 16 is a circle of radius 0.75 AU centered at 0.5 AU, judged by Taylor to be a reasonable representation of the shock configuration implied by the IMP 3 observations. A similar configuration was proposed by *Hirshberg* [1968] from a statistical study of geomagnetic sudden commencements and solar flares.

Two more complex techniques for derivation of shock normals have been proposed to reduce the uncertainties inherent in the coplanarity method. *Chao* [1970] has used the time delay between observations of a shock at two different locations to improve the shock orientations and propagation speeds derived from detailed data obtained at one position. Figure 17 shows five shock normals, determined by Chao from Mariner 5 and Pioneer 6 or 7 data. These normals cluster at approximately an average direction about  $20^\circ$  from the radial, with a spread similar to that obtained by *Ogilvie and Burlaga* [1969]. *Lepping and Argentiero* [1970] combine mass and momentum conservation with Maxwell's equations to derive an overdetermined system of equations in the plasma densities, flow speeds, and magnetic field components of the preshock and postshock plasmas. A least-squares fit of these equations to plasma and magnetometer data, accumulated before and after shock



**Figure 17.** The orientations of five shock normals derived by Chao [1970]. The angle  $\theta_s$  is solar ecliptic latitude, while  $\phi_s$  is solar ecliptic longitude.

passage at a single spacecraft, then reduces the effects of fluctuations within the accumulation periods and yields a more accurate shock orientation. This technique has been applied to only a few actual observations.

#### Characteristics of the Postshock Plasma

The plasma observed after the passage of an interplanetary shock wave is initially the compressed ambient solar wind and ultimately the flare ejecta or high-speed stream responsible for the solar wind disturbance. The properties of these two regimes of postshock plasma are influenced both by the original (near-sun) properties of the ejecta or stream and by the interaction with the ambient solar wind. The shock propagation models described in the preceding section suggest a classification scheme for the dynamical properties of flare-associated disturbances based on the dominance of one or the other of these influences. In the "driven waves," the continual addition of mass, momentum, and energy to the disturbance dominates the dynamics of its propagation and results in a negligible interaction with the ambient plasma. This extreme case is characterized at a given position by continued increases in density and flow speed after the abrupt increases at shock passage. In the "blast waves," the finite mass, momentum, and energy in the disturbance are ultimately less than those in swept-up ambient plasma, so that the interaction with the ambient dominates the dynamics of wave propagation. This extreme case is characterized at a given position by steady decreases in density and flow speed after the abrupt increases at the shock. Although no similar quantitative foundation exists for steady-stream disturbances, a similar classification scheme, based on mass, momentum, and energy fluxes, can be envisioned. The concepts of driven and blast waves will prove useful in organizing observations of the postshock plasma and provide some evidence regarding the duration of energy

release in a solar flare. The thermodynamic and chemical characteristics of the ejecta or steady stream would be expected to be retained, as discussed earlier, regardless of the dynamical evolution of the disturbance.

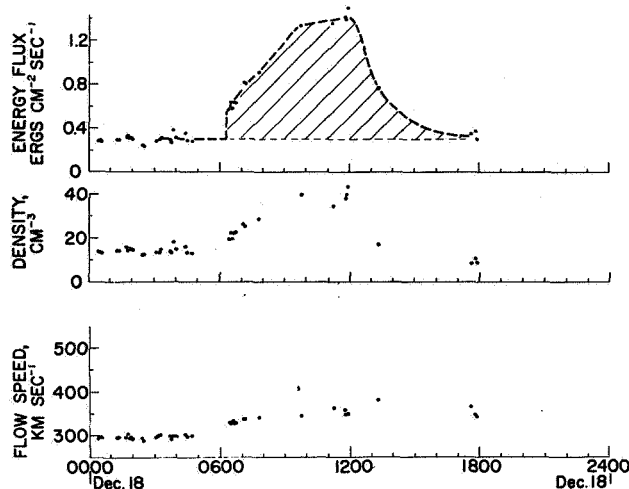


**Figure 18.** The solar wind density, flow speed, and kinetic energy flux density observed on 18 December 1965 [Hundhausen et al., 1970].

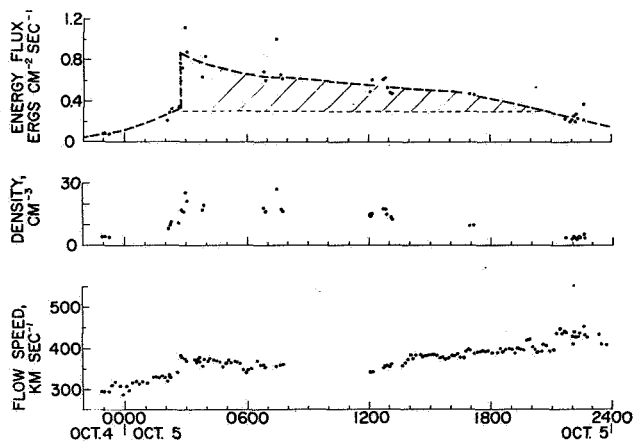


**Figure 19.** The solar wind density, flow speed, and kinetic energy flux density observed on 5 October 1965 [Hundhausen et al., 1970].

Figures 18 and 19 present contrasting examples of solar wind disturbances observed by the Vela 3 satellites [Hundhausen et al., 1970]. The proton density, flow speed, and (for future use) energy flux density are shown as functions of time for 18 December (fig. 18) and 5 October (fig. 19), 1965. The occurrence of a shock during the data gap near 0600 UT on figure 18 can be inferred from a geomagnetic sudden commencement and is confirmed by direct magnetic field observations from the IMP 3 satellite [Taylor, 1969]. As both

the density and flow speed continued to rise for some 6 hr after this shock, the disturbance of 18 December qualitatively fit the pattern of postshock plasma variations expected for a driven wave. A shock is clearly indicated in figure 19 by the abrupt rises in density and flow speed just before 0300 UT. As both quantities decreased for some six hours after the shock, the disturbance of 5 October qualitatively fit the pattern of post shock plasma variations expected for a blast wave. The numerical shock propagation models of *Hundhausen and Gentry* [1969a, b] predict a driven wave-like disturbance profile near 1 AU if energy release near the sun persists for more than  $\sim 20$  percent of the transit time, a blast wave-like disturbance profile if energy release persists for less than  $\sim 8$  percent of the transit time, and an intermediate disturbance profile (in which the density rises but the flow speed falls after shock passage) for intermediate durations of energy release. The observation of both driven and blast wave profiles, along with transit times in the range 40 to 60 hr, thus implies that energy release by flares must occur on time scales varying from less than 1 hour to several hours. It has generally been found [*Ogilvie and Burlaga*, 1969; *Hundhausen*, 1970a, b; *Lazarus et al.*, 1970] that the driven wave or intermediate disturbance profiles are most commonly observed near 1 AU.

Despite the general resemblance of the 5 October solar wind disturbance (fig. 19) to a blast wave, the rise in flow speed after 1200 UT is a distinct deviation from the expected pattern. High speed, low-density solar wind was, in fact, observed for several days after this shock. *Hundhausen et al.* [1970] have emphasized that such a persistent stream of high-speed solar wind is observed after most interplanetary shocks (figs. 12 through 14 illustrate this generality) and used a classification scheme for solar wind disturbances based on the rising or falling nature of the postshock energy flux (as shown in figs. 18 and 19). This interpretation of flare-associated disturbances involves a two-stage origin; an enhanced mass and energy injection into the solar wind by the flare, with a duration on the few hour time scale deduced above, followed by a flow of high-speed, low-density solar wind from the general region of the flare for several days thereafter. The persistent high speed stream would be distorted by solar rotation and, despite its flare-related origin, assume some resemblance to the steady-stream configuration of figures 4 and 5.

No observations of a distinct thermodynamic nature of the flare ejecta or steady stream have been reported. Of some interest in this respect are limited observations showing only small changes in the electron temperature

at and following an interplanetary shock wave [*Hundhausen*, 1970d] and only a minor elevation of the electron temperature in regions where high-speed streams overtake slower solar wind [*Burlaga et al.*, 1971]. *Hundhausen and Montgomery* [1971] have interpreted these results as an effect of heat conduction on solar wind disturbances, as discussed in the preceding section.

Numerous observations do indicate a chemical difference between the compressed ambient solar wind and flare ejecta. The appearance of plasma unusually rich in helium 5 to 12 hr after passage of a shock has been reported by *Gosling et al.* [1967], *Bame et al.* [1968], *Ogilvie et al.* [1968], *Lazarus and Binsack* [1969], *Ogilvie and Wilkerson* [1969], *Hirshberg et al.* [1970], and *Bonetti et al.* [1970]. Figure 20 illustrates this

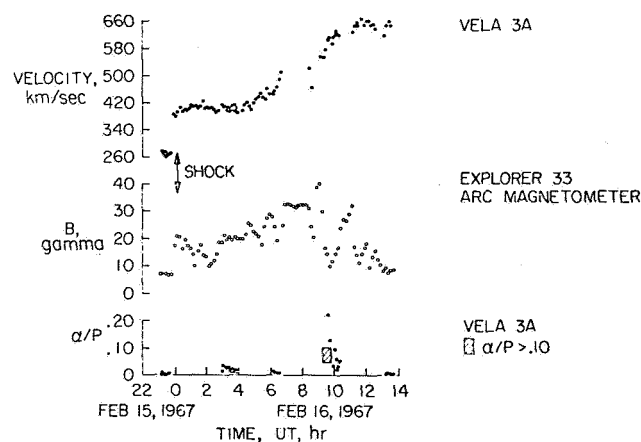


**Figure 20.** Solar wind speed, interplanetary magnetic field strength, and the ratio of helium and hydrogen number densities observed on 15-16 February 1967. The shaded area on the lower frame indicates observation of a helium-hydrogen density ratio greater than 0.1 [*Hirshberg et al.*, 1970].

phenomenon with Vela 3 plasma data and Explorer 33 magnetic field data obtained during the solar wind disturbance of 15-16 February, 1967 [*Hirshberg et al.*, 1970]. The ratios of helium and hydrogen number densities in the plasma observed before the shock and for some 9 hours after the shock were in the range 1 to 2 percent. At 0920 UT, the Explorer 33 magnetometer detected the passage of a tangential discontinuity, discernible in figure 20 as a sudden decrease in the magnitude  $B$  of the magnetic field. The plasma following the discontinuity was observed by Vela 3 to have an extremely high helium content, with individual density ratio determinations as high as 22 percent. The helium

content remained above 10 percent for 30 min (indicated by the shaded area on the lowest frame of fig. 20). *Hirshberg et al.* [1970] interpreted the sudden appearance of helium-rich plasma as the arrival of the flare ejecta, separated from the compressed ambient solar wind by the expected tangential discontinuity. The ambient plasma and flare ejecta presumably owe their different chemical compositions either to origins in different regions of a chemically inhomogeneous chromosphere and corona or to their different time histories in expanding from the sun to 1 AU.

One further possible feature of the postshock plasma flow, the reverse shock expected on the basis of the qualitative discussion and quantitative models given earlier, has been the subject of some observational interest. The existence of a small number of reverse shocks has been reported [*Burlaga*, 1970; *Binsack*, 1970], but none has been clearly related to large-scale solar wind disturbances. The apparent rarity of reverse shocks is puzzling, as the high-speed, low-density stream observed to follow most shocks gives precisely the flow condition that should lead to reverse shock formation [*Sonett and Colburn*, 1965; *Hundhausen and Gentry*, 1969b; *Hundhausen et al.*, 1970]. Perhaps some energy dissipation mechanism, such as heat conduction, inhibits formation of the shock.

#### Mass and Energy in Solar Wind Disturbances

The energy in a typical flare-associated solar wind disturbance was estimated at the beginning of this section by using a theoretical relationship between energy and transit time and a mean transit time inferred from flare associations. More direct estimates of the mass as well as the energy can be derived from spacecraft observations at a given heliocentric distance  $r$  by integrating the excess of the mass or energy flux (through the sun-centered sphere of radius  $r$ ) above the ambient value throughout the solar wind disturbance. *Hundhausen et al.* [1970] have applied this technique to Vela 3 and Vela 4 shock wave observations made between August 1965 and July 1967. The flux through the 1 AU sphere was estimated from the observed flux density by assuming that the deviations from ambient conditions were uniform within a  $\pi$  solid angle. This assumption is in reasonable accord with the theoretical shock shapes of *De Young and Hundhausen* [1971], described in the preceding section, or the observational inferences of *Hirshberg* [1968] and *Taylor* [1969], described earlier in this section. The integration over time is illustrated in figures 18 and 19 by the shaded areas under the energy flux density curves. Analysis of 19 nonrecurrent solar wind disturbances led to mass

estimates ranging from  $5 \times 10^{15}$  to  $1.5 \times 10^{17}$  gm, with an average of  $3 \times 10^{16}$  gm, and to energy estimates ranging from  $5 \times 10^{30}$  to  $2 \times 10^{32}$  ergs, with an average of  $5 \times 10^{31}$  ergs. The latter value, independent of any theoretical models or specific flare associations, is in excellent agreement with the estimate based on the models of *Hundhausen and Gentry* [1969a] and the 55-hr mean transit time to 1 AU given in table 1. The energy released at  $1 R_{\odot}$  (corrected from the 1 AU values for the work done against solar gravity) ranges from  $1.7 \times 10^{31}$  to  $5 \times 10^{32}$  ergs, with an average of  $1.1 \times 10^{32}$  ergs. These mass and energy estimates will be discussed in the context of solar flare physical processes in the next section.

#### Multiple Satellite and Integral Observations

An obvious means of determining the large-scale structure of a solar wind disturbance would be the combination of observations made at several spacecraft separated by distances comparable to the scale size of the disturbance. Unfortunately, only two such multiple satellite observations of an interplanetary shock wave have been reported in the literature. *Lazarus and Binsack* [1969], using Explorer 33 and Pioneer 6 observations, found a significant deviation from spherical symmetry in a shock associated with the 7 July 1966 proton flare. The distortion of the shock wave was attributed to the presence of a spatial structure (related to a magnetic sector) in the ambient solar wind. *Lazarus et al.* [1970] have combined observations from Mariner 5 and Explorer 34, separated by 0.1 AU in heliocentric distance, of an 11 August 1967 solar wind disturbance. A similar disturbance profile, resembling that expected in a driven wave, swept past both spacecraft.

A related technique for the direct observation of the structure of solar wind disturbances involves the Stanford radio propagation experiment, flown on several Pioneer spacecraft, which determines the total electron content along the propagation path between the spacecraft and the earth. The passage of the high-density cloud following an interplanetary shock across this path provides an integrated density measurement from which the gross features of the cloud can be inferred. For example, data obtained from Pioneer 6 on 9 July 1966 indicated the passage of the cloud associated with a shock observed directly by an onboard plasma probe [*Lazarus and Binsack*, 1969]. *Landt and Croft* [1970] have attempted to reconstruct the geometry of the cloud by assuming the presence of two outward moving regions with densities of  $140 \text{ cm}^{-3}$  and  $50 \text{ cm}^{-3}$ , values derived from the direct observations. Figure 21 shows the three postshock plasma clouds that could have



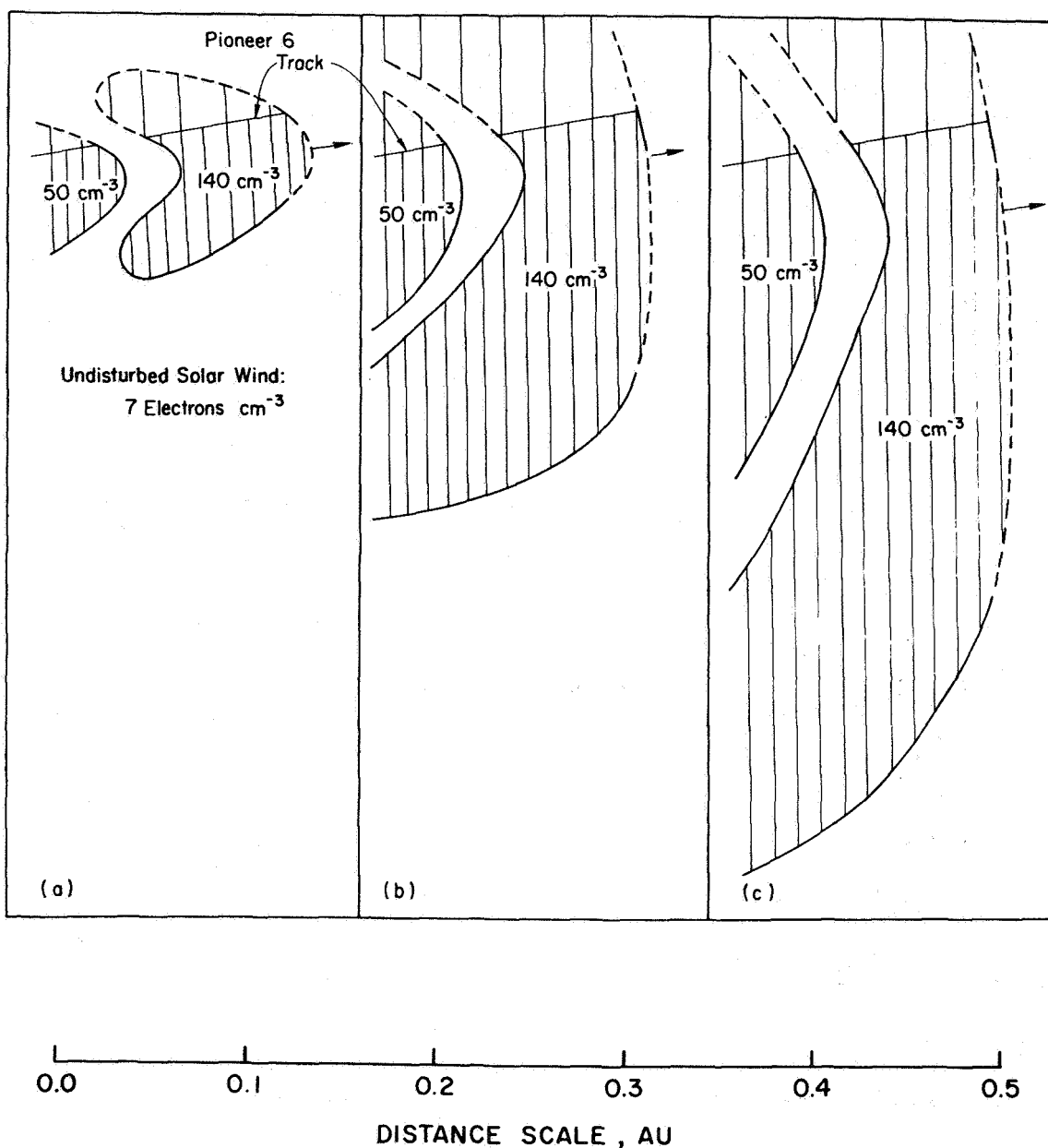


Figure 21. Three possible plasma cloud shapes inferred from Pioneer 6 radio propagation observations made on 9 July 1966 [Landt and Croft, 1970].

produced the observed total density signals. Although no objective choice can be made among the three, Landt and Croft [1970] favored the disturbance of intermediate size (fig. 21(b)). This disturbance has a characteristic size of several tenths of an AU, and is in basic agreement with the other inferences regarding the geometries of solar wind disturbances presented above.

#### Conclusions

The observations described in this section point to

several conclusions regarding the nature and structure of the solar wind disturbances related to interplanetary shock waves. The distributions of observed shock normals are basically consistent with the configuration expected qualitatively (fig. 2) and predicted quantitatively (fig. 10) for a flare-produced disturbance. The ordering in solar longitude of sudden commencements or observed shock fronts relative to the sites of associated flares (fig. 16) and the plasma cloud shape inferred from the integrated electron density (fig. 21) both lead to this

same consistency. None of these pieces of observational evidence is consistent with the expected steady stream-produced shock configuration (fig. 5). In fact, no single directly observed shock has been positively attributed to a steady high speed stream, and most observed recurrent streams [Neugebauer and Snyder, 1966; Hundhausen *et al.*, 1970] do not appear to be preceded by shocks. We can only conclude that shocks produced by steady high speed streams are difficult to observe or identify, or are extremely rare. Our present observational knowledge appears to apply to flare-produced solar wind disturbances.

Figure 22 is an attempt to synthesize this knowledge and add some precision to our earlier qualitative

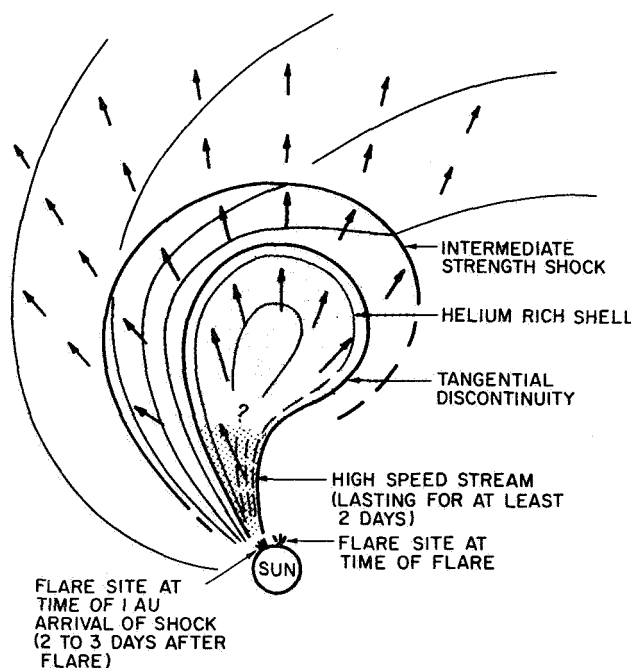


**Figure 22.** A sketch, in equatorial cross section, of the observed features of a flare-produced solar wind disturbance (compare with fig 2.).

description (fig. 2) of a flare-produced disturbance, hereafter considered to be near 1 AU. The shape of the shock at the leading edge of the disturbance is much as previously drawn. The shock is of intermediate strength, propagating through interplanetary space at  $\sim 500 \text{ km sec}^{-1}$ . The region of compressed ambient solar wind behind the shock is 0.1 to 0.2 AU thick. The tangential discontinuity that separates the compressed ambient plasma from the flare ejecta is sometimes followed by a thin shell ( $\sim 0.01$  AU thick) of helium-rich material. A localized stream of high-speed, low-density solar wind usually follows the flare ejecta: in the two to three days

required for the shock wave to reach 1 AU this stream is expected to be distorted into a spiral configuration by solar rotation. Reverse shocks within the flare ejecta or high-speed stream appear only rarely.

Thus many properties of a flare-produced solar wind disturbance are indicated (although in some cases only tentatively) by presently available observations. Many equally interesting properties remain undetermined. For example, there is virtually no observational evidence related to the possible existence of closed field lines within the flare ejecta (as denoted by the question mark on fig. 22). We further note that most of the observations used in this synthesis date from the rising portion of the present solar cycle. These observations do indicate some changes within the cycle—that is, the changes in the energies of disturbances. The large-scale structures of solar wind disturbances might also undergo detailed or gross changes. Clearly, much remains to be learned from future observations.

## THE PHYSICS OF SOLAR FLARES

If most interplanetary shock waves are produced by solar flares, as deduced in the preceding section, it is reasonable to attempt to use observations of these waves to infer characteristics of flares. In particular, the estimates of the mass and energy in observed shock waves imply some constraints on the mass and energy release in the flare phenomenon. Before pursuing these implications, a specific warning regarding selection effects is in order.

Both the statistical correlation of solar and geomagnetic activity and the specific relationships between solar and interplanetary observations indicate that not all solar flares, nor even all large solar flares, produce observable interplanetary shock waves. Further evidence for this conclusion has been found in the observation of three transient Faraday rotations of a polarized microwave signal transmitted from Pioneer 6 to earth while the spacecraft moved through occultation by the solar corona [Levy *et al.*, 1969]. Schatten [1970] associated each of these events with a specific 1B to 1F flare and interpreted the observed rotation in terms of the expansion and subsequent contraction of a "coronal magnetic bottle" into the microwave transmission path, as illustrated in figure 23. The plasma within the closed field structure or bottle was inferred to be expanding outward at  $\sim 200 \text{ km sec}^{-1}$  from the delay between the associated flare and the onset of the observed rotation (for the transmission path near  $10R_{\odot}$ ). This expansion is hypothesized to be slowed and ultimately stopped by the tension in the magnetic field lines. After cooling by radiation and heat conduction, the magnetic bottle

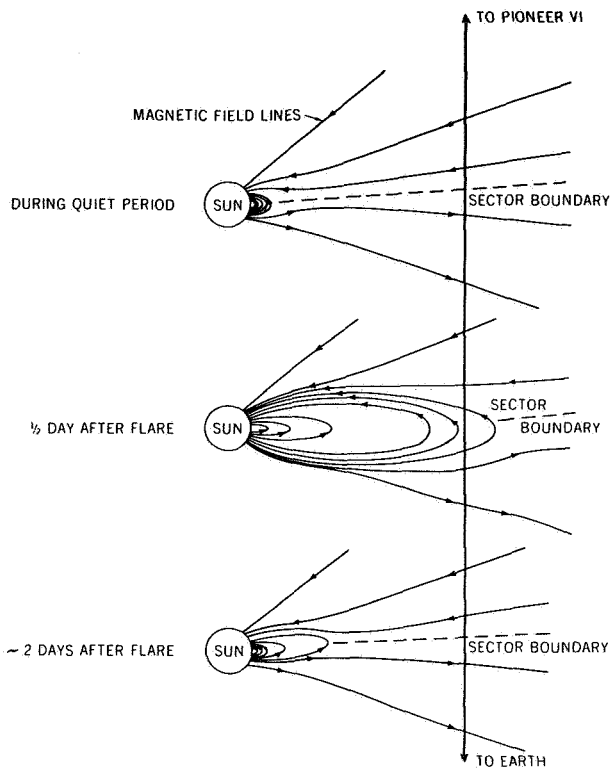


**Figure 23.** The coronal magnetic field configurations proposed by Schatten [1970] to account for the transient Faraday rotations of a microwave signal transmitted from Pioneer 6 during occultation by the solar corona.

presumably contracts to a configuration similar to that of the preshock stage. The energy of the plasma within the structure is estimated to be of the order of  $10^{30}$  ergs, one to two orders of magnitude smaller than that in the interplanetary shocks discussed in the preceding section.

This situation could lead to selection effects; that is, the (unknown) characteristics that allow some flares to produce interplanetary shock waves might not be typical of all flares. In fact, the shock wave mass and energy observations hint that some such selection does take place. Figure 24 shows the estimates of the mass and equivalent energy at  $1R_{\odot}$  for the 19 solar wind disturbances analyzed by Hundhausen *et al.* [1970]. No observation can fall below the dashed line, as an energy of  $1.92 \times 10^{15}$  ergs  $\text{gm}^{-1}$  has been added to each value derived at 1 AU to account for the work done against solar gravity in transit to the latter distance. Remarkably, all the observations fall in a limited region just above this line, near an equivalent energy per mass of 3 keV per H atom or a temperature of  $\sim 10^7$  K. This grouping could be interpreted as evidence that all flares

produce flare ejecta with essentially the same temperature. However, a completely different interpretation can be proposed. Suppose rather that flares produce ejecta with an effective energy (kinetic plus thermal) per mass distributed about an average that is less than that required for escape to 1 AU against solar gravity, as shown in figure 25. The solar wind disturbances observed at 1 AU would have an equivalent energy (with the gravitational correction back to  $1R_{\odot}$ ) per mass distributed as indicated by the shaded area under the curve of figure 25, producing an effect similar to that noted in figure 24. In fact, this latter interpretation is in accord with the earlier conclusion that most flares do not produce interplanetary shocks observed at 1 AU. It neglects such important complications as heat conduction or the magnetic forces invoked by Schatten. However, the remarkable ordering of figure 24 in terms of the energy per mass may indicate that solar gravity is a dominant factor in limiting the escape of flare ejecta into interplanetary space.

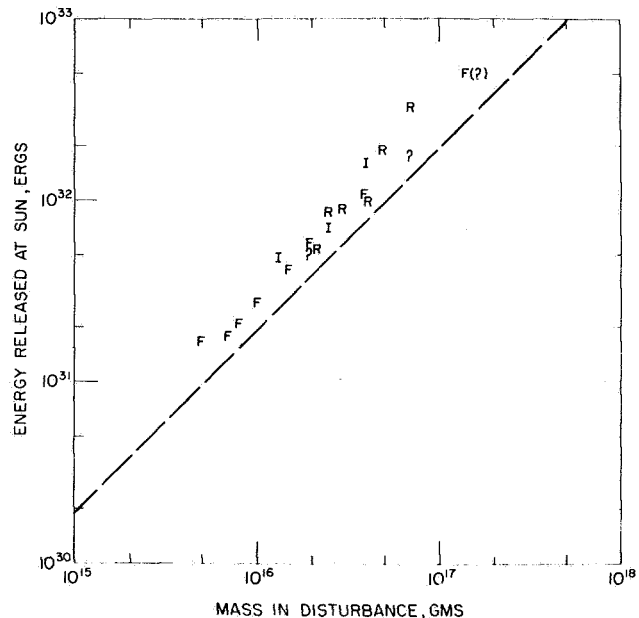


**Figure 24.** The mass and equivalent energy at 1 solar radius in 19 interplanetary shock waves analyzed by Hundhausen *et al.* [1970]. The behavior of the post-shock energy flux is denoted by the symbols R (rising), F (falling), I (intermediate), or ? (undetermined) for each event. The dashed line indicates the gravitational correction added to the energy determined at 1 AU.

With these possible selection effects in mind, let us finally consider the implications of the interplanetary observations with respect to the mass and energy releases

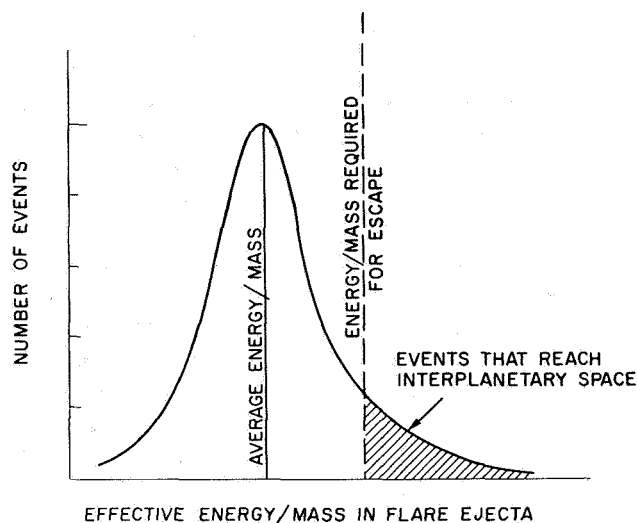


**Figure 25.** The effect of solar gravity on flare ejecta whose energy per mass are distributed about an average less than the energy per mass required for escape to 1 AU in the solar gravitational field.

in solar flares. Of the 19 solar wind disturbances considered by *Hundhausen et al.* [1970], six have highly plausible associations with optical flares accompanied by type II and type IV radio bursts (five of these associations were discussed among the examples at the beginning of the preceding section). Table 2 summarizes this set of solar-interplanetary associations. Five of these flares were of importance 2 or greater, and could thus be described as large flares. The average optical duration of

all six flares was 130 min, comparable to the several hour time scale for energy deposition deduced from interplanetary shock profiles, as well as typical of large flares [*Bruzek*, 1967]. The average mass of the associated solar wind disturbances was  $4.5 \times 10^{16}$  gm, while the average equivalent energy at  $1R_{\odot}$  was  $1.6 \times 10^{32}$  ergs.

The rates of mass and energy addition to the solar wind implied by these mass, energy, and time scale estimates are respectively  $6 \times 10^{12}$  gm sec<sup>-1</sup> and  $2 \times 10^{28}$  ergs sec<sup>-1</sup>. The rates of coronal mass and energy loss in the quiet solar wind are  $1 \times 10^{12}$  gm sec<sup>-1</sup> and  $3 \times 10^{27}$  erg sec<sup>-1</sup> [*Kuperus*, 1969; *Hundhausen*, 1971]. Thus solar flares, despite having an area of  $\lesssim 10^3$  of the total sun, can for a short time supply mass and energy to the solar wind with a total flux greater than that of the entire undisturbed corona.

The optical emission from a large solar flare comes from a volume of  $\sim 10^{28}$  cm<sup>3</sup> wherein the electron density is  $\sim 10^{13}$  cm<sup>-3</sup> [*Bruzek*, 1967]. Thus the mass within the luminous volume is  $\sim 2 \times 10^{17}$  gm. *Bruzek* [1967] has estimated the mass in visible flare-associated ejections to be  $\sim 2 \times 10^{16}$  gm. Thus the mass ejected into interplanetary space,  $\sim 5 \times 10^{16}$  gm as deduced above, is roughly equal to that in the visible ejections and an appreciable fraction ( $\sim 1/4$ ) of that within the flare region (note that these conclusions differ from those of *Bruzek*, who estimated a much smaller mass in the interplanetary shock wave.) Mass ejection on this scale must be expected to produce large changes in the chromosphere and corona near the flare site.

**Table 2.** Associations of flares and radio bursts with interplanetary shock waves analyzed in *Hundhausen et al.* [1970]

Flare				Radio Bursts		Interplanetary Shock Wave			
Date	Imp.	Duration	Position	Type	Duration	Date	Time	Mass(gm)	Energy at Sun (erg)
Feb. 4	2	1641-1902	N11E40	II IV	1708-1728 1705-1846	Feb. 7	1640	$4 \times 10^{16}$	$1.6 \times 10^{32}$
Feb. 13	3	1749-2130	N20W10	II IV	1803-1820 1829-2438	Feb. 15	2345	$5 \times 10^{16}$	$1.9 \times 10^{32}$
May 3	2B	1537-1926	N25E51	II IV	1548-1603 1603-1650	May 7	0100	$3 \times 10^{16}$	$0.9 \times 10^{32}$
May 21	2N	1919-1945	N24E39	II IV	1923-1945 1923-2100	May 24	1730	$4 \times 10^{16}$	$1.1 \times 10^{32}$
May 28	3B	0527-0712	N28W33	II	0545-0552	May 30	1430	$7 \times 10^{16}$	$3.3 \times 10^{32}$
June 3	1N	0243-0342	N24E14	II IV	0243-0250 0235-0450	June 5	1915	$4 \times 10^{16}$	$1.1 \times 10^{32}$

Table 3 compares the average energy at  $1R_{\odot}$  in an interplanetary shock wave, as deduced above, with other energy losses from a large (3+) flare; the tabulation is based on the energy estimates (some valid only to an order of magnitude) given by Bruzek [1967], with correction of typographic errors and adoption of the shock wave energy derived herein. All loss processes other than optical emission and the interplanetary shock wave are negligible despite their interest as indicators of physical phenomena. The shock wave appears to carry away about half of the energy released in a flare, with most of the remainder radiated at optical wavelengths. This is in contrast to the energy balance for normal chromospheric and coronal conditions, wherein only about 1 percent of the total energy loss is due to the ambient solar wind flow. The total energy released by the flare must be at least  $2 \times 10^{32}$  ergs. This requires a specific energy release of  $2 \times 10^4$  ergs  $\text{cm}^{-3}$  from the luminous volume of a flare. A comparison with the normal chromospheric thermal energy density of 5 ergs  $\text{cm}^{-3}$  and the normal coronal energy density of 1 erg  $\text{cm}^{-3}$  illustrates the magnitude of the problem to be faced in any model of energy storage and release by a solar flare.

#### ACKNOWLEDGEMENTS

Informative discussions with Drs. S. J. Bame and M. D. Montgomery of the Los Alamos Scientific Laboratory, Dr. J. T. Gosling of the High Altitude Observatory, Dr. L. F. Burlaga of NASA Goddard Space Flight Center, and Prof. A. J. Lazarus of the Massachusetts Institute of Technology are acknowledged.

This work was performed under the auspices of the U.S. Atomic Energy Commission.

#### REFERENCES

- Akasofu, S. I.; and Yoshida, S.: The Structure of the Solar Plasma Flow Generated by Solar Flares. *Planet. Space Sci.*, Vol. 15, 1967, p. 39.
- Ballif, J. R.; and Jones, D. E.: Flares, Forbush Decreases, and Geomagnetic Storms. *J. Geophys. Res.*, Vol. 74, 1969, p. 3499.
- Bame, S. J.; Asbridge, J. R.; Hundhausen, A. J.; and Strong, I. B.: Solar Wind and Magnetosheath, Observations During the January 13-14, 1967, Geomagnetic Storm. *J. Geophys. Res.*, Vol. 73, 1968, p. 5761.
- Bame, S. J.; Asbridge, J. R.; Felthausen, H. E.; Gilbert, H. E.; Hundhausen, A. J.; Smith, D. M.; Strong, I. B.; and Sydoriak, S. J.: A. Compilation of Vela 3 solar wind observations, 1965 to 1967. *Los Alamos Scientific Laboratory LA-4536*, Vol. 1, 1971.
- Bell, Barbara: Major Flares and Geomagnetic Activity. *Smiths. Contr. to Astrophys.*, Vol. 5, 1961, p. 69.

**Table 3.** *Estimated energy releases in a large solar flare*

Process	Energy (ergs)
H-alpha emission	$10^{31}$
Line emission (including H $\alpha$ )	$5 \times 10^{31}$
Continuum emission	$8 \times 10^{31}$
Total optical emission	$10^{32}$
Soft X-rays (1 to 20 Å)	$2 \times 10^{30}$
Radio burst	$10^{25}$
Energetic protons ( $E > 10$ MeV)	$2 \times 10^{31}$
Solar cosmic rays ( $E = 1$ to 30 GeV)	$3 \times 10^{30}$
Visible ejections	$10^{31}$
Interplanetary shock wave	$1.6 \times 10^{32}$

- Binsack, J. H.: Average Properties of the Solar Wind as Observed by Explorers 33 and 35. *Eos. Trans. Amer. Geophys. Union*, Vol. 51, 1970, p. 413.
- Bonetti, A.; Moreno, G.; Candidi, M.; Egidi, A.; Formisano, V.; and Pizzella, G.: Observation of Solar Wind Discontinuities from February 24 to February 28, 1969. *Interrelated Satellite Observations Related to Solar Events*, edited by V. Manno and D. E. Page, D. Reidel, Dordrecht, 1970, p. 436.
- Bruzek, A.: Physics of Solar Flares, the Energy and Mass Problem. *Solar Physics*, edited by J. N. Xanthakis, Interscience, New York, 1967, p. 399.
- Bumba, V.; and Obridko, V. N.: "Bartels' Active Longitudes," Sector Boundaries and Flare Activity. *Solar Phys.*, Vol. 6, 1969, p. 104.
- Burlaga, L. F.: A Reverse Hydromagnetic Shock in the Wind. *Cosmic Electrodyn.* Vol. 1, 1970, p. 233.

- Burlaga, L. F.; Ogilvie, K. W.; Fairfield, D. H.; Montgomery, M. D.; and Bame, S. J.: Energy Transfer at Colliding Streams in the Solar Wind. *Astrophys. J.*, Vol. 164, 1971, p. 137.
- Carovillano, R. L.; and Siscoe, G. L.: Corotating Structure in the Solar Wind. *Solar Phys.*, Vol. 8, 1969, p. 401.
- Chao, J. K.: *Interplanetary Collisionless Shock Waves*. MIT center for Space Research preprint CSR TR-70-3, 1970.
- Colburn, D. S.; and Sonett, C. P.: Discontinuities in the Solar Wind, *Space Sci. Rev.*, Vol. 5, 1966, p. 439.
- DeYoung, D. S.; and Hundhausen, A. J.: Non-spherical Propagation of a Flare-Associated Interplanetary Blast Wave (abstract), *J. Geophys. Res.*, Vol. 76, 1971, p. 2245.
- Dryer, M.; and D. L. Jones: Energy Deposition in the Solar Wind by Flare-Generated Shock Waves. *J. Geophys. Res.*, Vol. 73, 1968, p. 4875.
- Gold, T.: *Gas Dynamics of Cosmic Clouds*, edited by H. C. van de Hulst and J. M. Burgers, North-Holland Publishing Co., Amsterdam, 1955, p. 103.
- Gosling, J. T.; Asbridge, J. R.; Bame, S. J.; Hundhausen, A. J.; and Strong, I. B.: Measurements of the Interplanetary Solar Wind During the Large Geomagnetic Storm of April 17-18, 1965. *J. Geophys. Res.*, Vol. 72, 1967, p. 1813.
- Hirshberg, J.: The Transport of Flare Plasma from the Sun to the Earth. *Planet. Space Sci.*, Vol. 16, 1968, p. 309.
- Hirshberg, J.; Alksne, A.; Colburn, D. S.; Bame, S. J.; and Hundhausen, A. J.: Observation of a Solar Flare Induced Interplanetary Shock and Helium-Enriched Driver Gas. *J. Geophys. Res.*, Vol. 75, 1970 p. 1.
- Hundhausen, A. J.: Solar Wind Disturbances Associated with Solar Activity, in *Intercorrelated Satellite Observations Related to Solar Events*, edited by V. Manno and D. E. Page, D. Reidel, Dordrecht, 1970a.
- Hundhausen, A. J.: Composition and Dynamics of the Solar Wind Plasma. *Rev. Geophys. Space Phys.*, Vol. 8, 1970b, p. 729.
- Hundhausen, A. J.: Dynamics of the Outer Solar Atmosphere. Los Alamos Scientific Laboratory Preprint LA-DC-11911 (to be published in the proceedings of the Fourth Summer Institute for Astronomy and Astrophysics, Stony Brook) 1970c.
- Hundhausen, A. J.: Shock Waves in the Solar Wind. *Particles and Fields in the Magnetosphere*, edited by B. M. McCormac, D. Reidel, Dordrecht, 79, 1970d.
- Hundhausen, A. J.; and Gentry, R. A.: Numerical Simulation of Flare-Generated Disturbances in the Solar Wind. *J. Geophys. Res.*, Vol. 74, 1969a, p. 2908.
- Hundhausen, A. J.; and Gentry, R. A.: The Effects of Solar Flare Duration on a Double Shock Pair at 1 AU. *J. Geophys. Res.*, Vol. 74, 1969b, p. 6229.
- Hundhausen, A. J.; Bame, S. J.; and Montgomery, M. D.: The Large Scale Characteristics of Flare-Associated Solar Wind Disturbances, *J. Geophys. Res.*, Vol. 75, 1970, p. 4631.
- Hundhausen, A. J.; and Montgomery, M. D.: Heat Conduction and Nonsteady Phenomena in the Solar Wind. *J. Geophys. Res.* Vol. 76, 1971, p. 2236.
- Korobeinikov, V. P.: On the Gas Flow Due to Solar Flares. *Solar Phys.*, Vol. 7, 1969, p. 463.
- Kundu, M. R.: *Solar Radio Astronomy*. Interscience, New York, 1965.
- Kuperus, M.: The Heating of the Solar Corona. *Space Sci. Rev.*, Vol. 9, 1969, p. 713.
- Landt, J. A.; and Croft, T. A.: Shape of a Solar Wind Disturbance on July 9, 1966, Inferred From Radio Signal Delay to Pioneer 6. *J. Geophys. Res.*, Vol. 75, 1970, p. 4623.
- Lazarus, A. J.; and Binsack, J. H.: Observations of the Interplanetary Plasma Subsequent to the July 7, 1966 Proton Flare. *Ann. IQSY*, Vol. 3, 1969, p. 378.
- Lazarus, A. J.; Ogilvie, K. W.; and Burlaga, L. F.: Interplanetary Shock Observations by Mariner 5 and Explorer 34. MIT Center for Space Research preprint CSR-P-70-36, submitted to *Solar Phys.*, 1970.
- Lee, T. S.; and Balwanz, W. W.: Singular Variations Near the Contact Discontinuity in the Theory of Interplanetary Blast Waves. *Solar Phys.* Vol. 4, 1968, p. 240.
- Lee, T. S.; and Chen, T.: Hydromagnetic Interplanetary Shock Waves. *Planet. Space Sci.*, Vol. 16, 1968, p. 1483.
- Lee, T. S.; Chen, T.; and Balwanz, W. W.: Hydromagnetic Theory for Disturbances Following an Ideal "Solar Thermal Explosion." *E&S, Trans. Amer. Geophys. Union*, Vol. 51, 1970, p. 414.
- Lepping, R. P.; and Argentiero, P. D.: Improved Shock Normals Obtained From Combined Magnetic and Plasma Data from a Single Spacecraft. NASA Goddard Space Flight Center Preprint X-692-70-276, 1970.
- Levy, G. S.; Sato, T.; Seidel, B. L.; Stelzried, C. T.; Ohlson, J. E.; and Rusch, W. V. T.: Pioneer 6: Measurement of Transient Faraday Rotation Phenomena Observed During Solar Occultation. *Science*, Vol. 166, 1969, p. 596.
- Mackin, R. J.; and Neugebauer, Marcia: *The Solar Wind*, Pergamon Press, New York, 1966.
- Mori, Y.: Shock Wave Hypothesis on Sudden Commencements of 27-Day Recurrent Geomagnetic Disturbances. *Sci. Rep. of Tohoku Univ., Series 5*, Vol. 19, 1970, p. 135.

- Neugebauer, M.; and Snyder, C. W.: Mariner 2 Observations of the Solar Wind, 1, Average Properties. *J. Geophys. Res.*, Vol. 71, 1966, p. 4469.
- Ogilvie, K. W.; and Burlaga, L. F.: Hydromagnetic Shocks in the Solar Wind. *Solar Phys.* Vol. 8, 1969, p. 422.
- Ogilvie, K. W.; and Wilkerson, T. D.: Helium Abundance in the Solar Wind. *Solar Phys.*, Vol. 8, 1969, p. 435.
- Ogilvie, K. W.; Burlaga, L. F.; and Wilkerson, T. D.: Plasma Observations on Explorer 34, *J. Geophys. Res.*, Vol. 73, 1968, p. 6809.
- Parker, E. N.: Sudden Expansion of the Corona Following a Large Solar Flare and the Attendant Magnetic Field and Cosmic Ray Effects. *Astrophys. J.*, Vol. 133, 1961, p. 1014.
- Parker, E. N.: *Interplanetary Dynamical Processes*. Interscience, New York, 1963.
- Parker, E. N.: Theoretical Studies of the Solar Wind Phenomenon. *Space Sci. Rev.*, Vol. 9, 1969, p. 325.
- Petschek, H. E.: Reconnection and Annihilation of Magnetic Fields. *The Solar Wind*, edited by R. J. Mackin and M. Neugebauer, Pergamon Press, New York, 1966, p. 221.
- Quarterly Bulletin on Solar Activity*, Eidgen-Sternwarte, Zurich, 1967.
- Schatten, K. H.: Evidence for a Coronal Magnetic Bottle at 10 Solar Radii, *Solar Phys.*, Vol. 12, 1970, p. 484.
- Simon, M.; and Axford, W. I.: Shock Waves in the Interplanetary Medium, *Planet. Space Sci.*, Vol. 14, 1966, p. 901.
- Siscoe, G. L.; and Finley, L. T.: Solar Wind Structures Determined by Corotating Coronal Inhomogeneities: I. Velocity Driven Perturbations. *J. Geophys. Res.*, Vol. 75, 1970, p. 1817.
- Smerd, S. F.: Radio Evidence for the Propagation of Magnetohydrodynamic Waves Along Curved Paths in the Solar Corona. *Proc. Astron. Soc. Australia*, Vol. 1, 1970, p. 305.
- Smith, H. J.; and Smith, E. V. P.: *Solar Flares*. Macmillan, New York, 1963. *Solar-Geophysical Data*, U. S. Govt. Printing Office, Washington, D. C., 1965, 1967.
- Sonett, C. P.; Colburn, D. S.; Davis, L. Jr.; Smith, E. J.; and Coleman, P. J., Jr.: Evidence for a Collision-Free Magnetohydrodynamic Shock Wave in Interplanetary Space. *Phys. Rev. Lett.*, Vol. 13, 1964, p. 153.
- Sonett, C. P.; and Colburn, D. S.: The  $SI^+$  -  $SI^-$  Pair and Interplanetary Forward-Reverse Shock Ensembles. *Planet. Space Sci.*, Vol. 13, 1965, p. 675.
- Sturrock, P. A.: *Solar Flares*. *Plasma Astrophysics*, Academic Press, New York, 1967.
- Taylor, H. E.: Sudden Commencement Associated Discontinuities in the Interplanetary Magnetic Field Observed by IMP 3. *Solar Phys.*, Vol. 6, 1969, p. 320.
- Wilcox, J. M.: Solar Wind Disturbances Associated with Solar Flares. *Solar Flares and Space Research*, edited by Z. Svestka and C. De Jager, North-Holland, Amsterdam, 1969.

*C. P. Sonett* In the case of the reverse shock it was pointed out some years ago that there are basically two mechanisms that could be thought of by which to make them. One was the method mentioned by Hundhausen—that is, by increasing velocity in the driver gas. Another one is by the interaction of the shock wave with a tangential discontinuity, so that there is one wave reflected and one transmitted; under certain conditions the reflected wave will be a shock wave.

*M. Dryer* I want to ask one question and make one comment. I'm a bit puzzled about the question of the mass coming out from the sun, and thought there might be a contradiction in what was said in the first part of the talk, namely, about the gas being compressed and then later making an experimental integration of the mass and then saying that all of the mass came from the sun.

*A. J. Hundhausen* The whole point is if you had a steady ambient solar wind and put a blip in it all of it will eventually come out. So you continuously integrate and you have subtracted the ambient off correctly. You don't have to identify which is compressed gas and which is the original because the total ultimately passes through the sphere. The trick is that you subtracted the ambient off.

*M. Dryer* Except you're making a readjustment in the density distribution of that mass.

## DISCUSSION

*A. J. Hundhausen* Yes, I'm just obtaining an integral. Now, of course, it's an estimate of the mass and energy. You would have to know what the real ambient value was and of course you don't know because it's been swept up, so one assumes it's the same as just before the shock. That's one of the limitations in the accuracy of the calculation.

*M. Dryer* The basis for the question was the suggestion by Hirshberg that the enriched helium represented the flare ejecta that followed the first shock by a number of hours.

*A. J. Hundhausen* In that case, including only that material, you get just about the same answer.

*M. Dryer* The second point is the comment regarding the type II radio bursts. May I show one slide (fig. 1) which is of a type II radio burst published by *Smerd* [1970] using the 80-MHz radio heliograph at Culgoora. This type II burst, which extends over more than  $180^\circ$  came from a flare that occurred about  $20^\circ$  behind the west limb. It would be very interesting if there is any information at 1 AU following this flare. The point I want to make is that this may be anomalous, but it is very suggestive that the use of spherical models is not too bad.

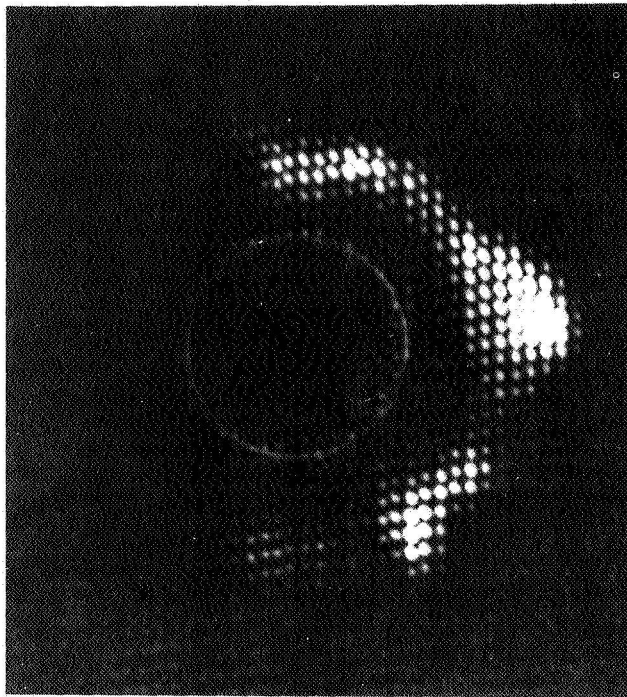


**Figure 1** *Radioheliogram (Culgoora, Australia), at 80 MHz, of a series of type II radio bursts following a flare beyond the west limb on 30 March 1969, 0250 UT [Smerd, 1970].*

*A. J. Hundhausen* How do you know where this is along your line of sight?

*M. Dryer* There were some time developments of this, and so I can't really say. This radio heliogram is in the plane perpendicular to the line of sight.



*J. Hirshberg* I did want to mention there is a small amount of magnetic field data when we suspect ejecta is being seen; in the very few cases looked at the field does not lie in the plane of the equator of the sun but makes very large angles as you would expect.

*A. J. Hundhausen* You have complicated the problem by making it truly three dimensional. What I really should have said is there is no consistent idea about how the variation within the blob really goes.

*J. Hirshberg* Well, we haven't really been able to look back to see whether it closes or continues to be connected.

*P. McIntosh* I know that at least two of the events in your list were white light flares with visible shock waves in  $H\alpha$ . Now, since white light flares are surely a bit deeper than the other flares, doesn't this allow you to get a little more particle ejecta than in the normal flare?

*A. J. Hundhausen* I must confess that I have in the past appeared as a skeptic regarding everybody's flare associations. This is the closest I have ever gotten to seeing anything definite. I think that any study of these observations has to be made very carefully. In fact, if they are white light flares you may be able to estimate the energy since that is the major source of energy emission other than the interplanetary shock wave; that's a fruitful thing to study.

*R. J. Hynds* Do I understand that if you put in the observed shock velocity near the earth, then work out the transit times, you get good agreement between the measures? Because I remember someone some years ago did a mean transit time and he came out with about 40 hr, which implies a mean velocity of about 1000 km, which implies that over a large fraction of an AU it is presumably moving at several 1000 km.

*A. J. Hundhausen* If you use 1 AU, of course, you imply something like 80 hr. The associations I've got are on the order of 60 or 70 hr, which I don't think is too bad an agreement. Remember that the shock wave can be moving faster close to the sun and in fact some of the observations indicate 1000 km/sec. I think that's roughly what you get from the type II bursts. If waves of the mass and energy that we have determined here do start at 1000 km/sec they are very quickly slowed down in passing through the denser parts of the corona and come out near 500 km/sec most of the way, which I think explains why the difference isn't too great. There may be some deceleration on the way out.

*Unidentified Speaker* The shortest transit time observed is about 16 hr. Could you then cope with such an extreme example?

*A. J. Hundhausen* No. That's why I'm skeptical about flare associations.

*P. A. Sturrock* I would like to comment on the mass problem. One has the problem of trying to understand both the source of the energy and the source of the mass in a flare. We don't know where the mass comes from, but it most probably comes from the chromosphere, not the corona. On the other hand, the magnetic energy is stored primarily in the corona, not the chromosphere. I think this paradox is related to the problem of understanding hard and soft X-ray bursts. A picture that has emerged recently is as follows: The beginning of the magnetic field reconnection gives rise to a stream of high energy particles. When these impinge on the chromosphere, they give rise to the hard X-ray bursts. They also evaporate a large mass of gas, which then gives rise to the soft X-ray burst. I suggest that the evaporation extends slightly ahead of the reconnection. Then that part of the plasma becomes trapped in the closed magnetic field lines, giving the soft X-rays, and part of the plasma is trapped in the reconnected open magnetic field lines and is subsequently ejected from the sun. Some confirmation of this hypothesis is provided by the fact that the mass of gas needed to explain the soft X-ray burst of a large flare is comparable with the mass of gas needed to explain a flare-produced shock wave in the solar wind.

*Unidentified Speaker* As far as accounting for the effects, I suggest that we already

have some evidence in the comparison of magnetic fields and type III bursts. We do see examples where these are channeled by the magnetic field.

*T. G. Cowling* Can one imagine a burst that does not proceed radially out and so that one would expect to have a certain proportion of the bursts missing the places immediately above the point of origin. One does know that something of that sort seems to effect cosmic ray eruptions from flares. I was wondering if there was anything similar in regard to ordinary flares. And whether there might be some radio observations that might support such an effect.

*J. Hirshberg* One of these shocks we are talking about caused a geomagnetic storm. So if we are getting things shooting out in one direction in any systematic way in the same manner, for example, as cosmic rays, we should see some east-west asymmetry in the geomagnetic storm sudden commencements, and we don't see more than a degree or two.

COMPARISON OF DEEP SPACE AND NEAR-EARTH OBSERVATIONS OF PLASMA TURBULENCE AT SOLAR WIND DISCONTINUITIES

F. L. Scarf, R. W. Fredricks and  
I. M. Green

An invited review

We use simultaneous observations of plasma waves from the electric field instruments on Pioneer 9 and OGO 5 to illustrate the difference between near-earth and deep space conditions. It is shown that the experimental study of true interplanetary wave-particle interactions is difficult to carry out from an earth orbiter because the earth provides significant fluxes of nonthermal particles that generate intense plasma turbulence in the upstream region.

ABSTRACT

INTRODUCTION

The first extensive measurements of interplanetary parameters were made on the deep space probe Mariner 2. However, most of the experimental information on the solar wind and its interface with the earth has actually come from instrumentation on near-earth satellites such as IMP, OGO, Vela and HEOS. The early Explorer 18 observations suggested that the bow shock represents an abrupt outer boundary of the earth's influence. Therefore, the upstream region was tacitly considered to represent undisturbed interplanetary plasma, essentially identical to that expected in the absence of the earth. Nevertheless, even in 1963-1964, it was known that there were some significant large-scale perturbations associated with the magnetospheric obstacle, and several early reports described nonthermal electron observations upstream from the shock [Anderson *et al.*, 1965; Anderson, 1968].

During the past few years it has become clear that the earth does disturb a vast region in the solar wind. Detectable geomagnetic tail phenomena [Ness *et al.*, 1967; Wolfe *et al.*, 1967; Mariani and Ness, 1969; Intriligator *et al.*, 1969; Scarf *et al.*, 1970a] and wake effects [Siscoe *et al.*, 1970] exist at least 500-1000  $R_e$  downstream, and some direct upstream magnetospheric perturbations are found to extend to the orbit of the

moon [Fairfield, 1968; Freeman *et al.*, 1970] and beyond.

Ahead of the earth the perturbations involve supra-thermal electrons and protons produced near the bow shock. These particles flow upstream and they generate large-amplitude electromagnetic and electrostatic plasma turbulence [Scarf *et al.*, 1970b, 1971]. The presence of these nonthermal particles is extremely significant for a number of reasons. For instance, the upstream flow can frequently involve a reversal of the local heat flux moment so that the region is predominantly "heated" by mechanisms originating near the earth. This makes it difficult to measure the actual interplanetary heat conduction, and the modifications can also drastically influence the local solar wind stability properties [Forsslund, 1970]. Moreover, we know that the waves associated with upstream protons can produce local density modulations having wave periods near 20 to 60 sec, in a geocentric frame [Scarf *et al.*, 1970b]. These inhomogeneities are then convected downstream toward earth, and they ultimately produce a variable pressure on the entire magnetosphere. It is tempting to speculate that this large-scale upstream beam-plasma instability directly produces the pc micropulsations and short period disturbances that are correlated with changes in the solar wind flux magnitude [Gringauz *et al.*, 1971].

Since December 1967 it has been possible to monitor low-frequency interplanetary plasma turbulence with instruments on Pioneer 8, OGO 5, and Pioneer 9. These plasma wave detectors provide sensitive diagnostics that

---

The authors are at Space Sciences Laboratory, TRW Systems Group, Redondo Beach, California.

indicate when nonthermal plasma distributions are present, and the measurements give additional information on the magnitude and extent of the interplanetary perturbations produced by the magnetosphere. In fact, since no high sensitivity plasma probes or ac search coil magnetometers have yet been flown in deep space, these simple plasma wave instruments presently provide almost the only information on changes in the microstructure of the solar wind with increasing distance from earth. In this report we illustrate the difference between near-earth and deep space conditions using simultaneous Pioneer 9 and OGO 5 observations. We also discuss the geocentric radial variation in high-frequency turbulence, and comment on the value of the solar-terrestrial physics (STP) mission proposed in the recent NAS-NRC study [National Academy of Sciences-National Research Council, 1971].

## OBSERVATIONS

The well documented cosmic ray event of November 18, 1968, was produced by a west limb flare and the associated interplanetary shock reached 1 AU at about 0900 UT on November 20, 1968 [Lincoln, 1970]. At this time Pioneer 9 was approximately 2.5 million km from earth and OGO 5 was just upstream from the bow shock. Thus, on November 20, the two spacecraft were clearly in a good position for a comparison between deep-space and near-earth observations. We therefore use these measurements to illustrate the main complexities associated with proximity to the earth's magnetosphere.

The actual positions of OGO 5 and Pioneer 9 are shown in figure 1. The OGO spacecraft detected the shock many minutes before Pioneer did, and this suggests that the shock normal was tilted far from the radial direction. Ungstrup *et al.* [1972] have examined the shock front geometry using data from OGO 5, Pioneer 9, and Explorer 35, and their report contains a comprehensive account of the analysis. The main result of interest here is the verification that the shock detected on Pioneer at 0929:30 UT was the same as the one detected near 0902 UT on OGO 5.

Figure 2 shows low-frequency electric field amplitude ranges, along with dc magnetic field measurements from the two spacecraft. The Pioneer 9 magnetometer results were supplied by Drs. C. P. Sonett, D. S. Colburn, and E. Ungstrup, and the plotted points are 28-sec averages; however, preliminary offset values were used here and the curves may still be subject to some small corrections. The OGO 5 field values in figure 2 are 1-min averages from the UCLA magnetometer, and the data were furnished by Drs. C. T. Russell and P. J. Coleman, Jr.

On November 20, the Pioneer 9 spacecraft was

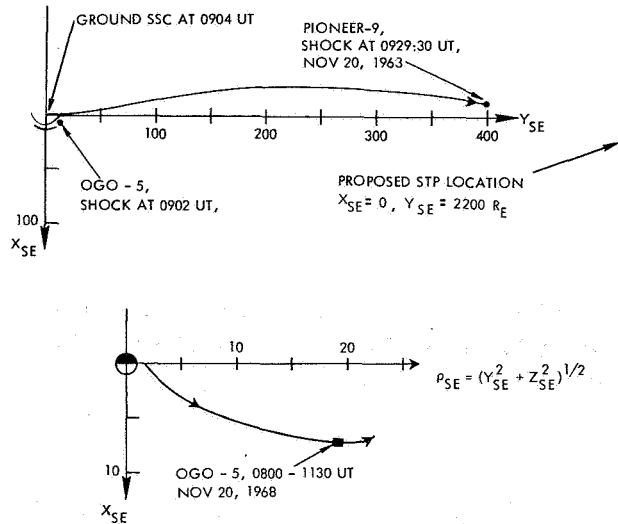


**Figure 1.** (a) The Pioneer 9 trajectory from launch to November 20, 1968, and OGO 5 location at 0902 UT on November 20. We indicate here when the solar terrestrial physics (STP) probe might be located. (b) The OGO 5 trajectory for November 20, 1968, in rotated geocentric solar ecliptic coordinates.

transmitting at its highest telemetry rate (512 bits/sec) so that the 400-Hz potential amplitude was sampled every 7 sec. However, the unbalanced and asymmetric dipole does have a sun-oriented photosheath response that produces a fairly strong spin modulation [Scarf *et al.*, 1968]. We therefore display here 5-min ranges that clearly show the true shifts in 400-Hz wave levels; near 0930 UT, the small arrows mark the actual locations of the Pioneer 9 maxima. During this period, OGO 5 was transmitting at its lowest telemetry rate (1 kilobit/sec), and the 560-Hz electric field strength was sampled once per 1.18 sec for 27.6 sec. As described by Crook *et al.* [1969], six other frequency channels are examined during successive 27.6-sec intervals and the instrument returns to the 560-Hz channel every 3.23 min. There were no special-purpose telemetry transmissions on November 20, 1968.

In figure 2, the time scales are shifted to align the interplanetary shock encounters, and the last dashed vertical line marks passage of this discontinuity. The B-field magnitude profiles displayed here are remarkably similar in the region surrounding the shock encounter. We see that the low-frequency electric field levels also changed characteristically as the shock front passed each spacecraft.

Before the shock (0910–0930 UT on Pioneer 9, 0840–0900 UT on OGO 5) the wave levels were quite low, each instrument detected a noise “spike” at the

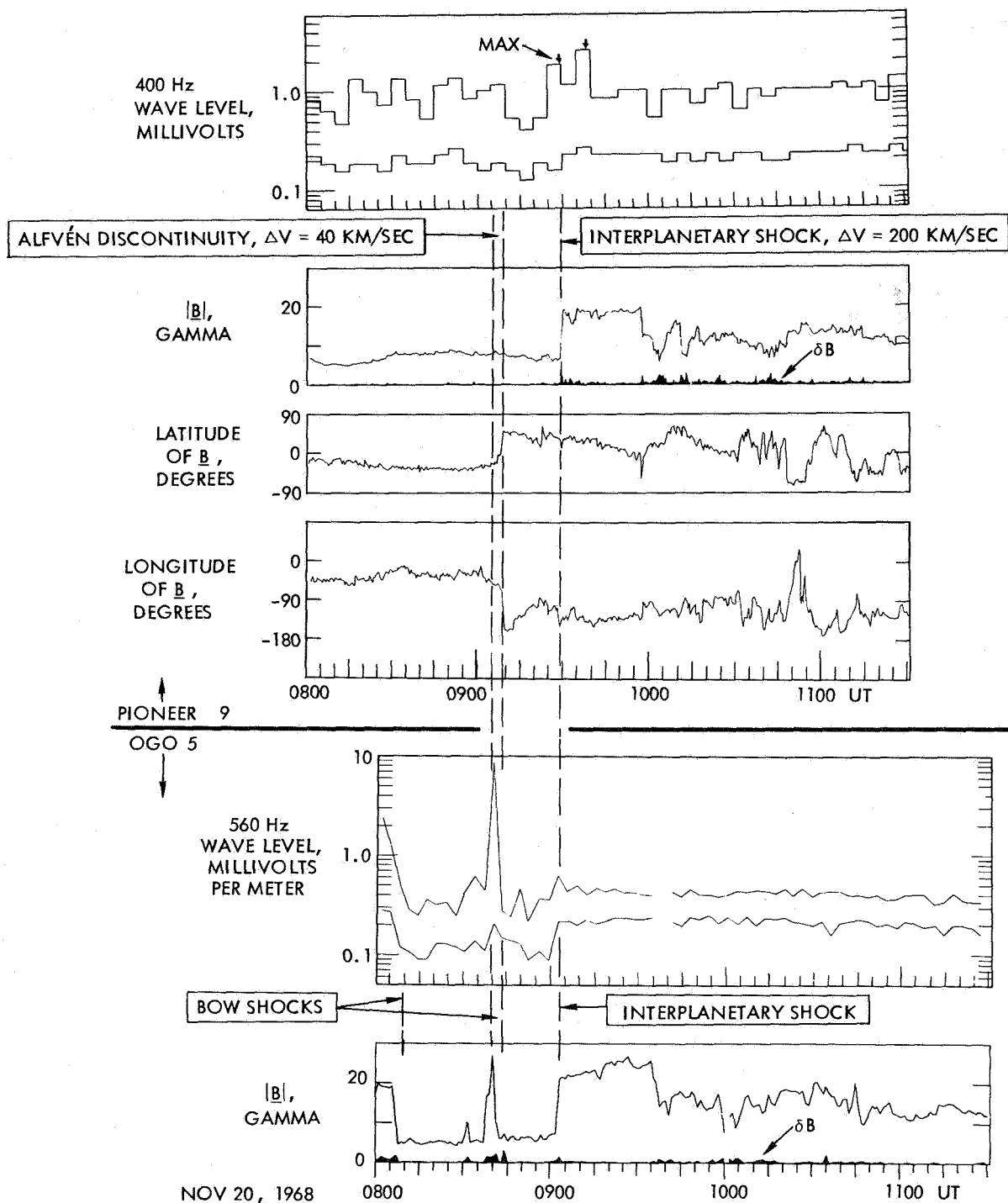


Figure 2. Simultaneous Pioneer 9 and OGO 5 field and wave data for 0800–1130 UT on November 20, 1968. The time scales are shifted to align the interplanetary shock encounters (third vertical dashed line). The first two vertical lines represent passage of interplanetary discontinuities; however, their appearance at the same relative times (with respect to the shock) is complete coincidence. The Pioneer 9 event at 0905–0910 UT was an Alfvén discontinuity, while the event responsible for the brief OGO 5 return to the magnetosheath (0838–0842 UT) was a contact discontinuity.

shock encounter, and enhanced postshock noise levels were observed on both spacecraft for many hours afterward. There are, of course, some striking differences. For instance, on Pioneer 9 two noise spikes were detected in the 400-Hz channel, but only one in the OGO 560-Hz channel; however, when the second peak would have been encountered by OGO 5, the plasma wave spectrum analyzer was not sampling the 560-Hz channel output. We demonstrate below that a corresponding second noise peak was actually detected by the OGO instrument in a higher frequency channel. It is also clear that if a 1-m effective antenna length is assumed for Pioneer, then the average OGO and Pioneer wave levels in the two channels were not identical, but the relative variations were quite similar.

We have analyzed many interplanetary shock encounters on Pioneer 8, Pioneer 9, and OGO 5, and the results displayed in figure 2 are fairly typical. The shock is generally "announced" by a brief noise spike, and enhanced low-frequency plasma turbulence is then detected for an extended period after encounter [Siscoe *et al.*, 1971].

The first pair of vertical dashed lines in figure 2 marks times when additional abrupt shifts in the low-frequency turbulence levels were detected. It is evident that each spacecraft observed a change at the *same relative* time with respect to the shock encounter. One might therefore be led to speculate that some sort of precursor preceded each shock encounter by a fixed distance equal to 20 to 25 min travel time in the solar wind. However, it can be demonstrated that this interpretation is not possible; the interplanetary shock speed must have been much higher than speeds of any other discontinuities, so that fixed precursor standoff distances could not be maintained.

The basic point is that the interplanetary shock of November 20, 1968, was a strong fast-mode forward shock [see Colburn and Sonett, 1966, for definitions]. As noted on figure 2, the peak velocity detected by the ARC plasma probe on Pioneer 9 jumped by about 200 km/sec [J. H. Wolfe and D. S. Intriligator, private communication]. The field magnitude increased, and on OGO it was evident that the density also jumped as the shock passed by [M. Neugebauer, private communication]. Discontinuities of this type must propagate rapidly through the plasma and they must overtake slower discontinuities.

The early Pioneer 9 event at 0905–0910 UT is clearly identifiable as a slow Alfvén discontinuity, with a small velocity jump, a field rotation, and no change in  $|B|$  or  $N$ . On close inspection we find that an interplanetary discontinuity also swept by OGO 5 between 0838 and

0842 UT, and this produced brief encounters with the bow shock and magnetosheath. At OGO there were negligible changes in interplanetary field latitude and longitude surrounding these brief bow shock encounters; moreover, the JPL plasma probe data show that the OGO discontinuity did *not* involve a velocity jump, but the pressure changed because of a sharp drop in the helium-to-hydrogen ratio between 0838 and 0842 UT [M. Neugebauer, private communication]. Thus, OGO 5 encountered a contact discontinuity about 25 min before the shock, while Pioneer encountered an Alfvén discontinuity at the same relative time. At OGO the change in Mach number apparently allowed the bow shock to move outward for a short period.

We conclude that it was complete coincidence that OGO and Pioneer both detected a discontinuity 25 min before the shock encounter. Indeed, the Pioneer 9 plasma probe also showed a large helium-to-hydrogen ratio for an extended period that ended near 0615 UT. With an effective corotation speed of 330 km/sec, this contact discontinuity would have encountered the earth near 0840 UT, in accordance with observations.

Thus, events combined fortuitously so that more order is suggested by figure 2 than actually was present in the solar wind at the time. The correct conclusions to be drawn from the observations of figure 2 are: (1) various forms of discontinuities produce large changes in low-frequency electric field turbulence levels; (2) a near-earth encounter with an interplanetary discontinuity can appear as a multiple bow shock crossing; (3) at low frequencies (400 and 560 Hz) the electric field noise enhancements generated near a standing bow shock are much more intense than those produced at a propagating interplanetary shock front.

The last conclusion is qualified by the restriction to certain frequency channels, and it is instructive to consider the measurements in all available channels. The Pioneer 9 instrument has only the 400-Hz channel, a qualitative broadband ( $f \lesssim 100$  Hz) wave level indicator, and a 30-kHz channel. On OGO 5 we also have information available on levels for electric field waves with frequencies centered at 1.3, 3.0, 7.3, 14, 30, and 70 kHz. Figure 3 compares the Pioneer and OGO lower frequency outputs; the broadband wave level plotted is the equivalent amplitude for a 100-Hz sine wave, and the measurement is repeated every 56 sec.

Figure 3 reveals great complexity with rapid temporal variation in the turbulent electric field spectrum near earth. Although the magnetosheath was only encountered between 0838 and 0842 UT, large-amplitude noise enhancements were continuously detected after about 0815 UT, with peak levels in the 1.3-kHz and 3-kHz

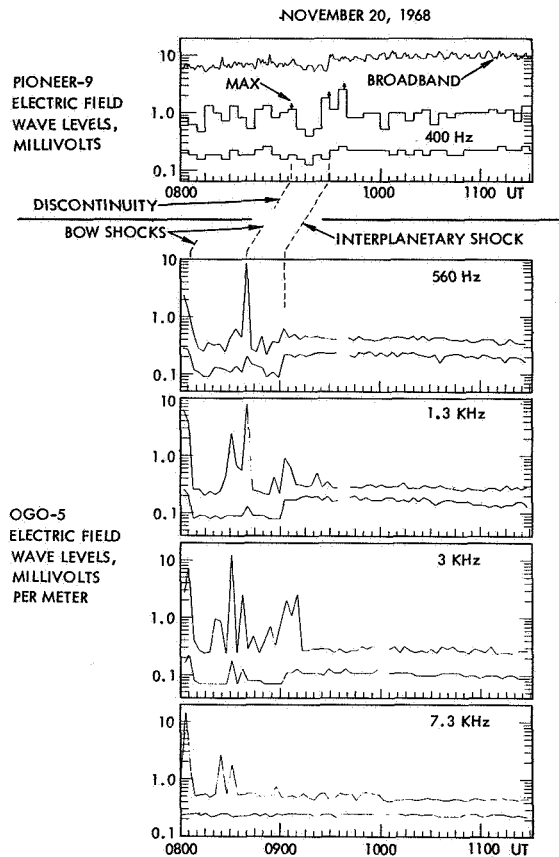


**Figure 3.** Comparison of low-frequency plasma turbulence near earth and in deep space. These results indicate that: (a) the interplanetary shock electric field spectrum is peaked at a higher frequency than a standing shock spectrum; (b) large amplitude electrostatic turbulence develops throughout the upstream region; (c) the source of this turbulence is swept away through interplanetary shock.

channels. We interpret this as evidence that suprathermal protons with  $E \approx 5$  keV were present, but since no high-sensitivity plasma probes were operating on OGO during the November 20 interval, there is no direct information on this point. However, for other periods it has been shown that enhanced midfrequency electric field turbulence in the upstream region is correlated with the presence of suprathermal protons [Scarf *et al.*, 1970b].

The OGO 5 observations at the interplanetary shock itself clearly reveal the inadequacy of the simple Pioneer 9 instrument with a single 400-Hz channel. It is evident from figure 3 that near the standing bow shocks (about 0805, 0838, and 0842 UT) the output from the 560-Hz channel is fairly representative; however at the propagating shock front the 560-Hz turbulence level is

significantly lower than that detected in the 1.3- and 3-kHz channels.

These bandpass channel responses suggest a shift in the plasma turbulence spectrum with shock speed past the spacecraft, but analysis of the special purpose telemetry or waveform output is needed if this suggestion is to be verified. Unfortunately, no special purpose transmissions were available on November 20, 1968, and this statement applies for a fair number of additional interplanetary shock encounters near apogee. The OGO 5 special-purpose data link suffered a degradation early in the flight and after mid-April 1968 the highest quality broadband data were acquired at moderate spacecraft altitudes. For this reason, we turn to an early interplanetary shock encounter to describe the turbulent electric field spectrum.

Near 1320–30 UT on April 5, 1968, OGO 5 was outbound in the magnetosheath with  $r \approx 21 R_e$  and local time  $\approx 0630$ . An interplanetary shock swept by at 1326:40 UT, and the spacecraft was suddenly in the solar wind. The lowest panel in figure 4 shows the

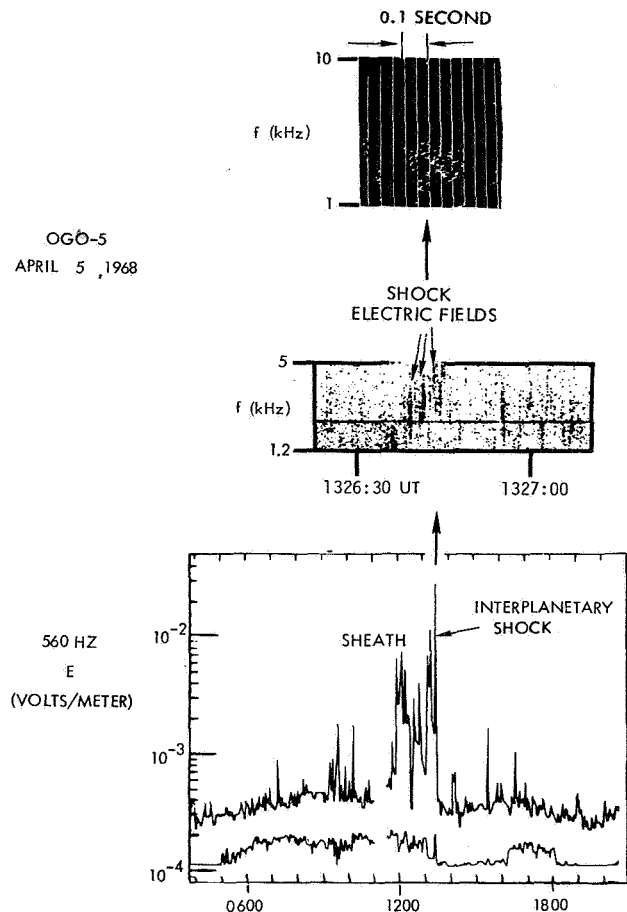


**Figure 4.** High-resolution spectral analysis of electrostatic turbulence at an interplanetary shock front.

560-Hz channel ranges, and the central panel contains a broadband frequency-time diagram of the shock turbulence (the horizontal line is a spacecraft interference tone at 2.46 kHz). At the top of figure 4 we display individual spectral sweeps taken every 50 msec in the neighborhood of the interplanetary shock.

It can be seen that the spectral peak in the April 5 shock spectrum is at a frequency well above 400 Hz or 560 Hz, consistent with the inference drawn from the bandpass channel data of figure 3. *Fredricks et al.* [1968; 1970a, b] have analyzed a number of bow shock encounters in a similar manner, and they found generally lower turbulence frequencies for these standing shocks. It does appear that the turbulent electric field spectrum for a propagating shock is similar to that observed at the bow shock, but that it is shifted in frequency. This suggests that Doppler effects are important, and it tells us that the Pioneer 8 and 9 low-frequency channels give incomplete information on electrostatic wave generation at discontinuities.

Before leaving the discussion of the lower frequency waves, we return to figure 3 and comment briefly on the postshock OGO 5 observations. The first point to note is that a double noise enhancement, with the two peaks separated by about 8 min, is evident in both sets of data. On Pioneer 9 the 400-Hz channel was sampled uniformly and the first noise spike at 0929:45 UT was followed by a somewhat larger one at 0937:45 UT. Similarly, the first 560-Hz noise enhancement was detected at 0902:44 UT, and a subsequent 3-kHz peak was found at 0910:06 UT. Thus it appears that this interplanetary shock did have a complex turbulence profile with two distinct enhancements.

The final point of interest concerns the postshock absence of sporadic 1.3- and 3-kHz noise enhancements. If these bursts are actually associated with upstream protons as suggested earlier, then the observations would seem to suggest that the suprathermal proton halo is swept away by the advancing shock front.

A similar effect is found when we examine the high-frequency electron-mode wave levels. The 30-kHz electric field ranges of November 20, 1968, for Pioneer 9 and OGO 5 are shown in figure 5. In the initial report on Pioneer 8 [*Scarf et al.*, 1968] it was observed that an interference problem associated with the sheath and the unbalanced dipole sensor degraded the inflight sensitivity of the 22-kHz channel. On Pioneer 9 a similar problem was present at 30 kHz and, as shown, the inflight threshold is quite high. Nevertheless, the OGO 5 plasma wave instrument did detect many bursts with  $E \gtrsim 700 \mu V/m$  between 0800 and 0900 UT on November 20, and these should also have been detectable

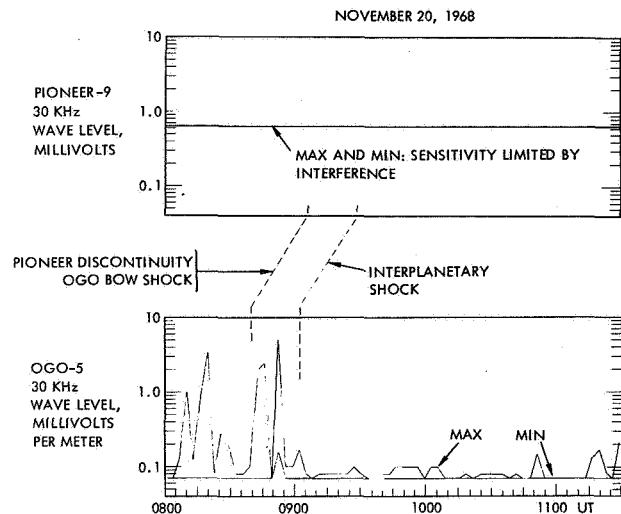


**Figure 5.** Comparison of high-frequency noise bursts near earth and in deep space. Although the Pioneer 9 30-kHz sensitivity is limited by inflight interference many of the OGO 5 signals would have been detectable on Pioneer if they were present at  $400 R_e$ .

on Pioneer 9 if they were present in deep space. The absence of any such signals suggests that the 30-kHz noise bursts are actually a near-earth phenomenon.

Detailed analysis tends to confirm this conjecture. In a recent study [*Scarf et al.*, 1971] it was demonstrated that these bursts have wave frequencies nearly equal to the local electron plasma or upper hybrid frequencies. It was also shown that the oscillations are produced when nonthermal electrons with energies greater than 700 to 800 eV flow upstream.

One aspect of the data from figure 5 supports this interpretation; that is, the abrupt end to the OGO 5 high-frequency wave activity at about 0900–0905 UT can be attributed to the shock front sweeping away these nonthermal upstream electrons. Indeed, during the 0905–1100 UT period the 30 kHz wave activity was about as minimal as we have ever seen it in the upstream solar wind, but toward the end of the period shown in figure 5 somewhat larger signals were detected.

The Pioneer 9 near-earth observations at 30 kHz also tend to confirm this interpretation of the high frequency bursts. The spacecraft entered the magnetosheath at about 1530 UT on November 8, 1968, and the bow shock region was traversed between 0110 and 0315 UT on November 9, when Pioneer was in an engineering format related to a spin-axis reorientation. The lower part of figure 6 shows the near-earth trajectory in rotated geocentric solar ecliptic coordinates, and 56-sec 30 kHz wave level ranges for the period 0315–0645 UT



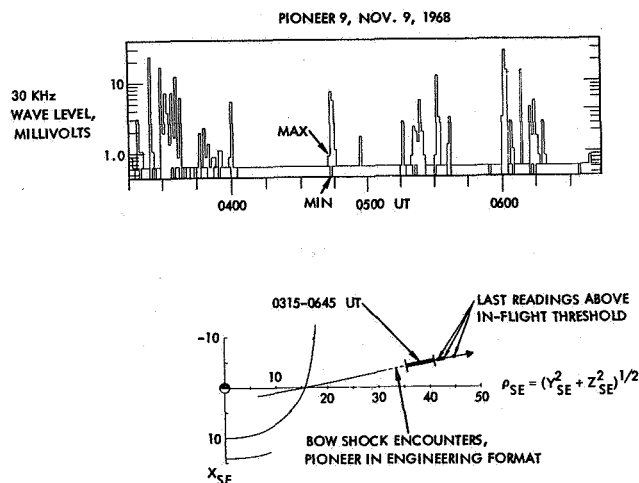


**Figure 6.** High-frequency observations on Pioneer 9 in the near-earth region. Except for the four additional points designated on the trajectory plot, the data in the top panel represent all the above-background 30-kHz measurements made on Pioneer 9. We conclude that high-frequency activity of this type is associated with proximity to the earth and bow shock.

on November 9 are displayed in the top panel. If we use an effective antenna length of about 1 m for Pioneer, it is clear that on November 9 the Pioneer instrument detected many 30 kHz noise bursts at least as strong as those measured by OGO 5 on November 20. However, these readings are virtually the *only* above-threshold values detected by the Pioneer 9 instrument after launch. In fact, only four additional 56-sec segments had above-background readings; their locations are marked on the trajectory plot. Although the inflight threshold for the 30 kHz channel of Pioneer 9 is unfortunately quite high, it can be stated that *all* detectable activity was confined to the region within  $50 R_e$  of earth. This again strongly suggests that the earth's magnetosphere and bow shock are the sources for the nonthermal electrons that produce these waves.

## DISCUSSION

We have seen that characteristic changes in low-frequency interplanetary plasma wave turbulence levels are associated with the passage of solar wind discontinuities such as fast forward shocks, and Alfvén and contact discontinuities. Striking changes in the electric

field noise levels are also associated with reverse and slow shocks, and accounts of these observations will be reported elsewhere. These results have a number of significant physical implications, and several examples can readily be cited. For instance, *Dryer* [1970] and *Eviatar and Dryer* [1970] recently pointed out that turbulent conductivity can drastically affect local conditions near interplanetary shocks and driver pistons. In another area, *Lanzerotti and Robbins* [1969] discussed the effects of electric field turbulence on energetic solar proton and alpha particle distributions. The plasma turbulence may also provide interplanetary acceleration, cross-B diffusion, and quenching of thermal anisotropies and heat flux.

One severe difficulty associated with the experimental study of these wave-particle interactions from an earth orbiter arises because the earth itself provides significant fluxes of nonthermal particles that generate intense plasma turbulence in the upstream region. We have illustrated these effects here by analyzing simultaneous Pioneer 9 and OGO-5 data for the period surrounding the interplanetary shock encounter of November 20, 1968.

The problem raised by the upstream noise halo is solved if the instruments are carried far enough from earth, but missions using conventional heliocentric probes such as Pioneer 9 face a different set of problems. The earth-spacecraft range continually increases, and after a few months the tracking schedule necessarily has large gaps in time, with low information rates between the gaps. Moreover, the deep space measurements are not necessarily well correlated with terrestrial events when the spacecraft-earth distance becomes large.

The solar-terrestrial physics (STP) mission is designed so that a probe will be located at a fixed but large distance from earth; a possible location is indicated in figure 1. At such a range, high bit rates and continuous tracking should be available, and no upstream effects will be present. Thus, the STP probe can provide a suitable platform for the study of interplanetary wave-particle interactions, and experiments on this spacecraft could also measure true interplanetary heat conduction and other subtle features of the undisturbed solar wind. Finally, a probe stationed in this location would be able to detect corotating interplanetary disturbances well before the events reach earth, and the mission would therefore provide firm information on the cause and effect relations in solar-terrestrial physics.

## ACKNOWLEDGMENTS

We are grateful to Drs. D. S. Colburn, P. J. Coleman, Jr., D. S. Intriligator, M. Neugebauer, C. T. Russell, C. P. Sonett, E. Ungstrup, and J. H. Wolfe for allowing us to display and describe their field and plasma data. This research was supported by the National Aeronautics and Space Administration under Contracts NASW-2113, NAS5-9278 (OGO Project at GSFC) and NAS2-4673 (Pioneer Project at ARC).

## REFERENCES

- Anderson, K. A.; Harris, H. K.; and Paoli, R. J.: Energetic Electrons In and Beyond the Earth's Outer Magnetosphere. *J. Geophys. Res.*, Vol. 70, 1965, p. 1039.
- Anderson, K. A.: Energetic Electrons of Terrestrial Origin Upstream in the Solar Wind. *J. Geophys. Res.*, Vol. 73, 1968, p. 2387.
- Colburn, D. S.; and Sonett, C. P.: Discontinuities in the Solar Wind. *Space Sci. Rev.*, Vol. 5, 1966, p. 439.
- Crook, G. M.; Scarf, F. L.; Fredricks, R. W.; Green, I. M.; and Lukas, P.: The OGO-V Plasma Wave Detector; Instrumentation and In-Flight Operation. *IEEE Trans. Geosci. Elec.*, GE-7, Vol. 2, 1969, p. 120.
- Dryer, M.: Some Effects of Finite Electrical Conductivity On Solar Flare-Induced Interplanetary Shock Waves. *Cosmic Elec.*, Vol. 1, 1970, p. 348.
- Eviatar, A.; and Dryer, M.: Finite Conductivity and Interplanetary Piston-Driven Shock Waves. *Cosmic Elec.*, Vol. 1, 1970, p. 371.
- Fairfield, D. H.: Simultaneous Measurements On Three Satellites and the Observation of the Geomagnetic Tail at 1000  $R_E$ . *J. Geophys. Res.*, Vol. 73, 1968, p. 6179.
- Forslund, D. W.: Instabilities Associated with Heat Conduction in the Solar Wind and Their Consequences. *J. Geophys. Res.*, Vol. 75, 1970, p. 17.
- Fredricks, R. W.; Kennel, C. F.; Scarf, F. L.; Crook, G. M.; and Green, I. M.: Detection of Electric-Field Turbulence in the Earth's Bow Shock. *Phys. Rev. Lett.*, Vol. 21, 1968, p. 1761.
- Fredricks, R. W.; Coroniti, F. V.; Kennel, C. F.; and Scarf, F. L.: Fast Time-Resolved Spectra of Electrostatic Turbulence in the Earth's Bow Shock. *Phys. Rev. Lett.*, Vol. 24, 1970a, p. 994.
- Fredricks, R. W.; Crook, G. M.; Kennel, C. F.; Green, I. M.; Scarf, F. L.; Coleman, P. J.; and Russell, C. T.: OGO-5 Observations of Electrostatic Turbulence in Bow Shock Magnetic Structures. *J. Geophys. Res.*, Vol. 75, 1970b, p. 3751.
- Freeman, J. W., Jr.; Balsiger, H.; and Hills, H. K.: Preliminary Results From the Lunar Ionosphere Detector. *Rice Univ. Preprint*, Jan. 1970.
- Gringauz, K. I.; Solomatina, E. K.; Troitskaya, V. A.; and Shchepetnov, R. V.: Variations of Solar Wind Flux Observed by Several Spacecraft and Related Pulsations of the Earth's Electromagnetic Field. *J. Geophys. Res.*, Vol. 76, 1971, p. 1065.
- Intriligator, D. S.; Wolfe, J. H.; McKibbin, D. D.; and Collard, H. R.: Preliminary Comparison of Solar Wind Plasma Observations in the Geomagnetospheric Wake at 1000 and 500 Earth Radii. *Planet. Space Sci.*, Vol. 17, 1969, p. 321.
- Lanzerotti, L. J.; and Robbins, M. F.: Solar Flare Alpha to Proton Ratio Changes Following Interplanetary Disturbances. *Solar Phys.*, Vol. 10, 1969, p. 212.
- Lincoln, J. V.: Data on Cosmic Ray Event of November 18, 1968 and Associated Phenomena. *Report UAG-9, World Data Center A*, April, 1970.
- Mariani, F.; and Ness, N. F.: Observations of the Geomagnetic Tail at 500 Earth Radii by Pioneer 8. *J. Geophys. Res.*, Vol. 74, 1969, p. 5633.
- National Academy of Sciences-National Research Council Report: Priorities for Space Research, 1971-1980, March, 1971.
- Ness, N. F.; Searce, C. S.; and Cantarano, S.: Probable Observations of the Geomagnetic Tail at  $10^3 R_E$  by Pioneer 7. *J. Geophys. Res.*, Vol. 72, 1967, p. 3769.
- Scarf, F. L.; Crook, G. M.; Green, I. M.; and Virobik, P. F.: Initial Results of the Pioneer 8 VLF Electric Field Experiment. *J. Geophys. Res.*, Vol. 73, 1968, p. 6665.
- Scarf, F. L.; Green, I. M.; Siscoe, G. L.; Intriligator, D. S.; McKibbin, D. D.; and Wolfe, J. H.: Pioneer 8 Electric Field Measurements in the Distant Geomagnetic Tail. *J. Geophys. Res.*, Vol. 75, 1970a, p. 3167.
- Scarf, F. L.; Fredricks, R. W.; Frank, L. A.; Russell, C. T.; Coleman, P. J., Jr.; and Neugebauer, M.: Direct Correlations of Large Amplitude Waves with Suprathermal Protons in the Solar Wind. *J. Geophys. Res.*, Vol. 75, 1970b, p. 7316.
- Scarf, F. L.; Fredricks, R. W.; Frank, L. A.; and Neugebauer, M.: Non-thermal Electrons and High Frequency Waves in the Solar Wind: Part 1, Observations, submitted to *J. Geophys. Res.*, 1971.
- Siscoe, G. L.; Scarf, F. L.; Intriligator, D. S.; Wolfe, J. H.; Binsack, J. H.; Bridge, H. S.; and Vasyliunas, V. M.: Evidence for a Geomagnetic Wake at 500 Earth Radii. *J. Geophys. Res.*, Vol. 75, 1970, p. 5319.

Siscoe, G. L.; Scarf, F. L.; Green, I. M.; Binsack, J. H.; and Bridge, H. S.: Very-Low-Frequency Electric Fields in the Interplanetary medium: Pioneer 8 *J. Geophys. Res.*, Vol. 76, 1971, p. 828.

Wolfe, J. H.; Silva, R. W.; McKibbin, D. D.; and Mason, R. H.: Preliminary Observations of a Geomagnetic Wake at 1000 Earth Radii *J. Geophys. Res.*, Vol. 72, 1967, p. 4577.

Ungstrup, E.; Colburn, D. S.; and Sonett, C. P.: in preparation, 1972.

*Roelof* Is my memory correct for this particular flare, the November 18, 1968, flare that it had a west limb origin, about 78°W? DISCUSSION

*Scarf* Yes, this was a west limb flare. The arrival of this flare at the earth was accompanied by an increase in the proton flux that Lanceratti has attributed to a local acceleration process (private communication). I don't know if this describes it any further but the data are tabulated by Virginia Lincoln; this is the flare that originated on the 18th because of the big cosmic ray event and the shock arrived at the earth on the 20th.

*Roelof* So if we go back to the geometries presented by Hundhausen then this is a very broad sort of a bubble (being from a west limb flare) to be detectable as a shock at earth.

*Scarf* Well, it arrived in a very strange way, i.e., at OGO before Pioneer. So it certainly is not in the direction of corotation, it's highly oblique.

## COROTATING SHOCK STRUCTURES *K. W. Ogilvie*

**ABSTRACT** Consideration of observed interplanetary shocks leads to the conclusion that a corotating forward shock has not been unambiguously identified at 1 AU. A reverse shock identified in September 1967 is a likely candidate for a corotating structure.

When the speed of the solar wind increases, the plasma in the high speed stream overtakes the slower plasma in front (fig. 1). Along the line A-A there is a velocity discontinuity, in the limit, but in fact as we have seen the speed change may take place in a thin region where the pressure is raised above that of the surrounding. Dessler and Fejer [1963] suggested that a pair of shock waves would be formed along the positions of the dotted lines. Razdan *et al.* [1965] investigated this configuration also and proposed that the structure would include shocks which were oppositely directed, that is, a forward shock (2) propagating generally in the direction of convection, and a backward propagating, but outwardly convected, shock (1). Thus, a spacecraft at the point X would see, in sequence, a forward shock, followed by a rapidly rising bulk speed and density, then probably one or more discontinuities, and lastly a reverse shock in the high speed stream characterized by an increase in the speed in the fixed frame. If the increase in speed is due to a stream of material more or less continuously emitted by the sun, then when the solar wind speed drops again at the other edge of the stream no collision takes place, and presumably no shocks form. Rather there is a rarefaction region of low pressure, which is the analog of the high pressure region A. Thus since the structure corotates counterclockwise, it is quite different from a flare-associated disturbance when the shock travels outward in a more or less radial direction.

The reverse shock (1) is propagating in the plasma toward the sun, while being convected away from it by

the solar wind flow. Since its net motion is outward, a solar origin for it cannot be ruled out *a priori*, but this seems unlikely since the Alfvén speed is higher nearer the sun and observations of these shocks would make it likely that disturbances can give rise to shocks in the interplanetary medium. Hundhausen and Gentry [1969]

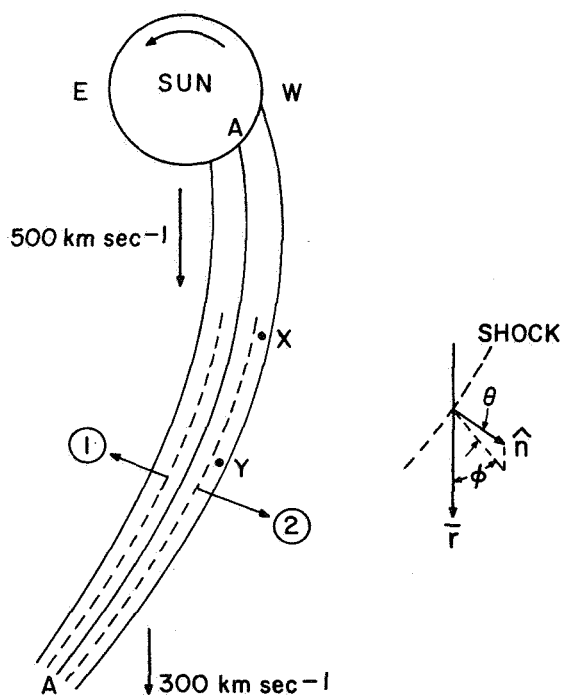


**Figure 1.** Schematic representation of corotating stream with forward and reverse shocks 1, 2. The angles  $\theta$  and  $\phi$  made by the shock normal with respect to the radial direction and the ecliptic plane are shown inset.

*The author is at the Laboratory for Extraterrestrial Physics, NASA Goddard Space Flight Center, Greenbelt, Maryland.*

on the basis of quite realistic model calculations conclude that flare-associated forward-reverse shock pairs are not likely; they would require solar flares of too long duration.

Thus if we observe with a plasma detector, we expect corotating streams to give rise to a signature such as that shown in figure 2. A rather general theoretical treatment

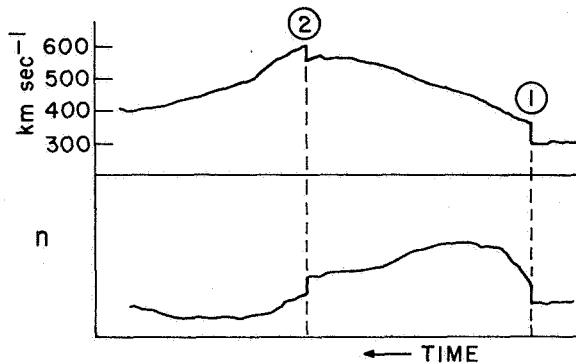


Figure 2. Hypothetical observations of a corotating shock event as observed by a spacecraft at point X in figure 1.

by Carovillano and Siscoe [1969] and Siscoe and Finlay [1970] shows that the density and azimuthal velocity perturbations increase with radial distance for large colliding corotating structures;  $\Delta n/n$  increases and eventually becomes  $\sim 1$ . Thus, there is probably a critical heliocentric distance inside which no shocks will form. In the absence of (2) the profiles look quite like the predictions of Hundhausen and Gentry [1968 and 1969] for the driven shock case, and quite like the observed postshock flows observed by Explorer 34, for example, and shown in figure 3.

Razdan *et al.* [1965] have linked  $SI^+ - SI^-$  pairs observed in terrestrial magnetograms with corotating M region beams and suggested that the  $SI^+ - SI^-$  pair be associated with the two shocks (1) and (2) above. However, Gosling *et al.* [1967] and Burlaga and Ogilvie [1969], among others have shown that geomagnetic impulses, though closely associated with interplanetary structures, do not necessarily indicate the passage of shocks. Ssc's are usually associated with shocks, and SIs with discontinuities, but the classification scheme is not

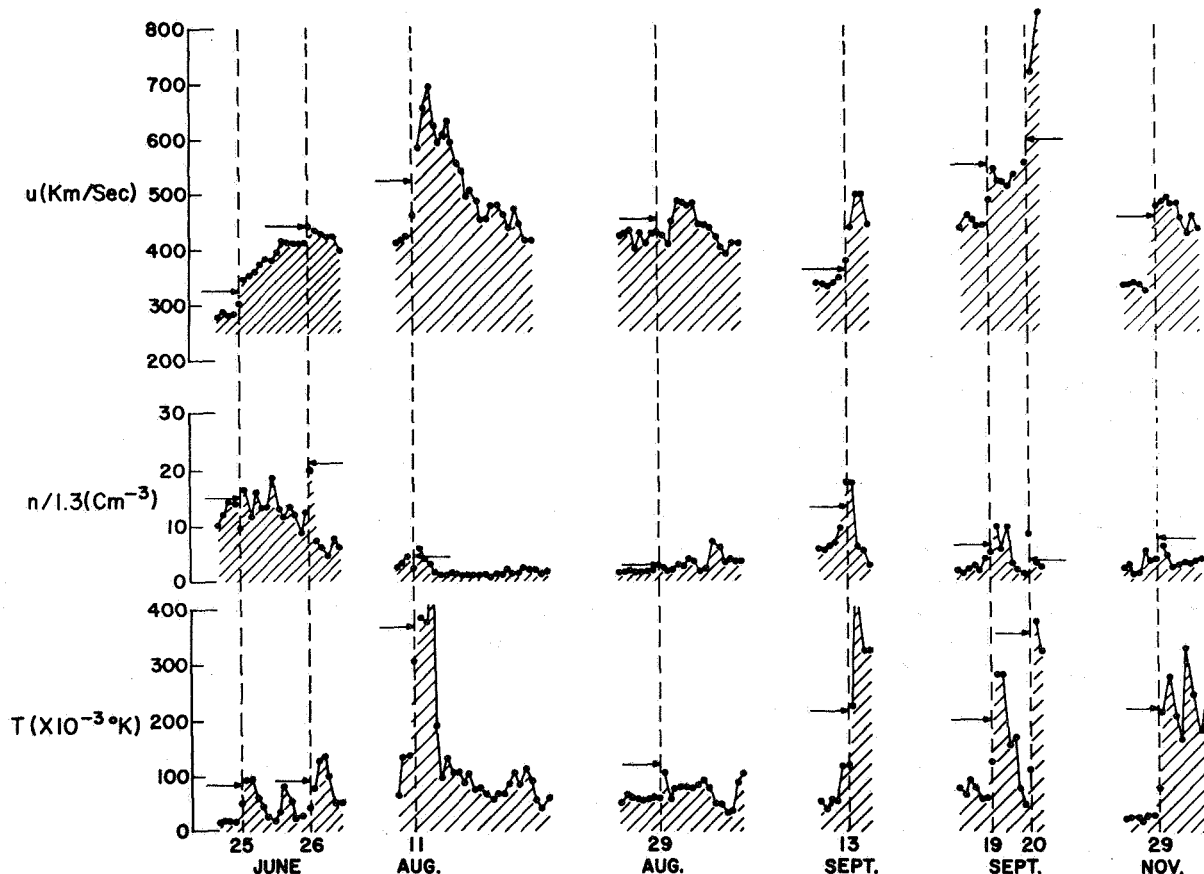
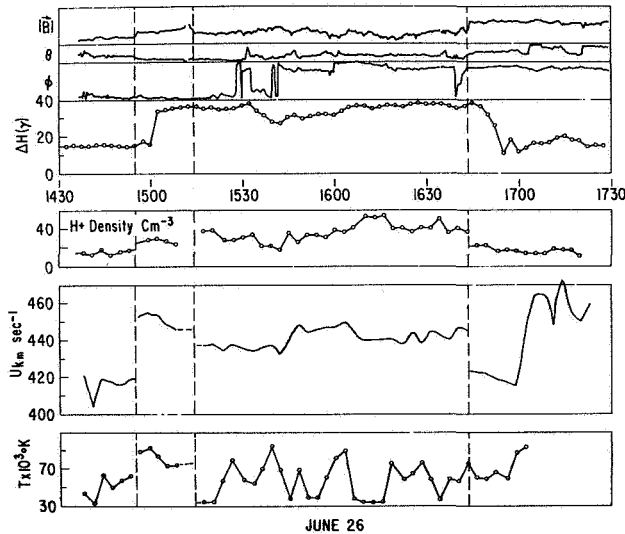


Figure 3. Profiles for bulk speed  $u$ , density  $n$ , and temperature  $T$  observed by Explorer 34 at the times of interplanetary shocks in 1967.

very precise. The structure causing one  $SI^+-SI^-$  pair has been observed by *Ogilvie et al.* [1968]. The positive impulse was due to a shock and the negative one to an apparent convected discontinuity. The shock was observed by Explorer 34 on 26 June 1967, and was apparently not flare associated. The normal direction [Chao, 1970] had values of  $\theta$  and  $\phi$  of  $-23^\circ$  and  $+24.9^\circ$ , respectively. The angles  $\theta$  and  $\phi$  are defined in figure 1, and the event illustrated in figure 4. Examination of the



**Figure 4.** Geomagnetic (upper) and spacecraft (lower) observations of the  $SI^+-SI^-$  event described in the text. Note that the  $SI^-$  impulse at about 1640 does not have the correct signature for a reverse shock. Compare with figure 6.

Kp diagram shows increased geomagnetic activity both 27 and 54 days previously, and a shock 27 days before, on 30 May 1967. Information about the normal direction is not available for this previous shock, and it could be a fortuitous time association, since a large flare (3B) occurred at 0530 on the 28th, although there seems to have been a corotating region. At any rate, since the nature of this event is not certain, we can say that an  $SI^+-SI^-$  pair does not *always* arise in the way envisioned by *Razdan et al.* [1965]. Such a pair does not *necessarily* have two shocks associated with it.

Distinguishing between flare-associated shocks and corotating shocks is difficult. There are differences, however; the normal to the shock (2) makes a large azimuthal angle to the radial direction ( $\phi \approx 45^\circ$ ). This is not an exclusive property of the corotating case if one adopts the *Hirshberg* [1968] idea of a flare-associated shock "standing off" from projected material, the shock having a radius  $\sim 0.6$  AU. If the axis of this projected

material is in a direction making a large heliocentric angle with the line on which the observer is situated, the angle  $\phi$  could be large. We would then be encountering the "side" of the shock; furthermore, in this case flare association might be even harder to establish than usual, because of the large angle between the angular coordinate of the point of observation and the heliocentric coordinate of the flare. Such an event might easily be mistaken for a corotating structure.

A corotating shock should be associated with a structure that appears at 27-day intervals, or at corresponding times at other heliographic longitudes. Such corotating structures are not infrequently observed, an example being one seen at earth at May 28, 1968, and Pioneer 6 on June 10, Pioneer 7 on June 20, and Pioneer 8 on June 23 before reaching the earth again on June 25, where it caused an SC, figure 5.

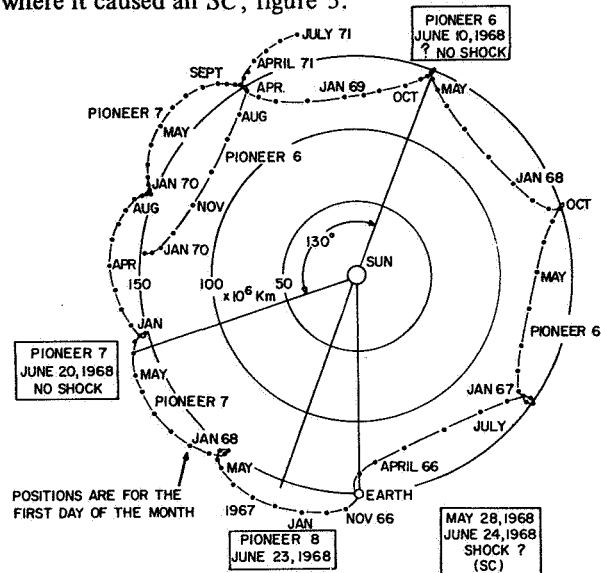


**Figure 5.** Positions of Pioneer spacecraft during the May-June 1968 corotating stream.

Examination of the data from these sources within  $\pm 1$  day of the appropriate times does not confirm a corotating shock; the data are incomplete. Thus, although the corotating nature of the disturbance is confirmed from radio observations of interplanetary scintillation [Dennison and Wiseman, 1968], a corotating shock was not observed.

A corotating shock should have a normal with  $\phi \approx 45^\circ$  or  $215^\circ$ . For our present purposes we disregard values of  $\phi$  between 0 and  $20^\circ$ , to remove those characteristic of radial shocks, so our criterion becomes  $20^\circ < \phi < 90^\circ$ . The value of  $\theta$  is apparently not significant for this classification.

There should be no plausible flare association, and we use this criterion to rule out shocks from the list given

by Hundhausen [1970]. Table 1 lists the remaining examples; where there is a conflict between two values of  $\phi$ , as for June 26 and August 29, 1967, the largest published values are given. The shock of August 11, 1967 [Lazarus *et al.*, 1970] can be eliminated at once since it is impossible to decide on the basis of evidence whether it was flare associated or not; thus, it is a possible example of a corotator, with low reliability. The event of August 29, 1967, occurred at a time when a sector boundary crossed the earth's heliocentric longitude, at the beginning of the life of the sector. At the

**Table 1.** Shock normals for four events

Date	$\phi$	
March 23, 1966	43°	Evidence of corotating structure poor. Close to sector boundary. Transit time to earth consistent with $\phi$
June 26, 1967	25°	
August 11, 1967	large	Insufficient data. [Lazarus <i>et al.</i> , 1970]
August 29, 1967	43°	Close to sector boundary.

next rotation of the sector, on September 28, 1968, the rise in bulk speed was preceded by a number of discontinuities, but none of them appears to have been a shock. The evidence for this event being a corotator is thus not very good. The evidence for the March 23, 1966 event as a corotating structure is not very convincing either.

This leaves the June 26, 1967 shock as perhaps the most likely example from this list, as discussed above, and the low probability we can assign to this case is indicative of the uncertainty in the existence of corotating shocks.

An observed shock perhaps more likely to be associated with a corotating event, and not included in Hundhausen's list, is the reverse shock reported by Burlaga [1970] which took place on 28 September 1967. It was not associated with a solar event, and the shock surface was perpendicular to the ecliptic plane and aligned along the spiral direction ( $\phi = 225.6^\circ$ ). The direction of the normal was determined by time-of-passage observations from Explorers 33, 34 and 35, and can thus be regarded as determined to an accuracy of  $\sim 10^\circ$ . The direction of propagation was towards the sun, and the "signature" of the event unequivocal, figure 6. There is evidence for a high speed stream with a

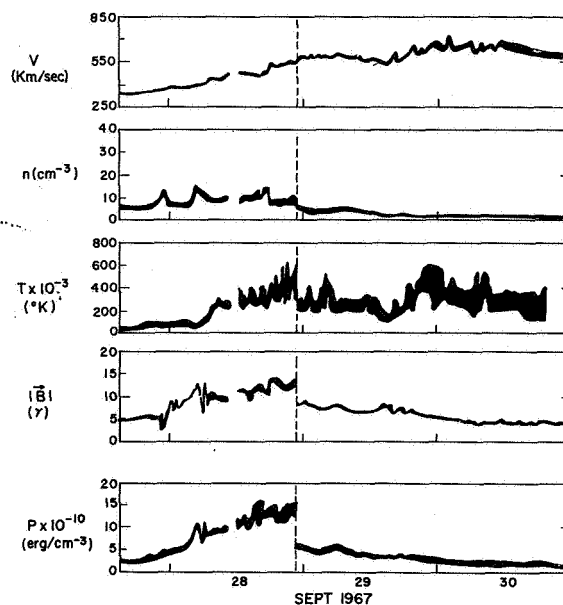


**Figure 6.** Explorer 34 observations of reverse hydro-magnetic shock, from Burlaga [1970].

maximum 29 days after the time of the shock. It was close to the boundary of a sector of rotation period 27.5 days persisting for the rest of 1967 [Wilcox and Colburn, 1970]. It thus appears that a good method to detect the existence, at this time uncertain, of corotating shocks, might be to search for reverse shocks, a procedure which avoids the problem of flare association. It has been clear for a long time that many corotating streams do not have shocks, forward or reverse, associated with them. It may be that observation of such shocks will become more common at greater heliocentric distances, where the relative perturbations have grown larger, especially around solar minimum when confusion by the effects of flare associated shocks will be less.

## REFERENCES

- Burlaga, L. F.: *Cosmic Electrodynamics*, Vol. 1, 1970, p. 233.
- Burlaga, L. F.; and Ogilvie, K. W.: *J. Geophys. Res.*, Vol. 74, 1969, p. 2815.
- Carovillano, R. L.; and Siscoe, G. L.: *Solar Phys.*, Vol. 8, 1969, p. 401.
- Chao, J.: Thesis, MIT 1970.
- Dennison, P. A.; and Wiseman, M.: *Proc. ASA*, Vol. 4, 1968, p. 142.
- Dessler, A. J.; and Fejer, J. A.: *Planet. Space Sci.*, Vol. 11, 1963, p. 505.
- Gosling, J. T., et al.: *J. Geophys. Res.*, Vol. 72, 1967, p. 3357.
- Hirshberg, J.: *Planet. Space Sci.*, Vol. 16, 1968, p. 309.

Hundhausen, A. J.; and Gentry, R. A.: *J. Geophys. Res.*, Vol. 74, 1968, p. 2908.

Hundhausen, A. J.; and Gentry, R. A.: *J. Geophys. Res.*, Vol. 74, 1969, p. 6229.

Hundhausen, A. J.: *Rev. Geophys.*, Vol. 8, 1970, p. 729.

Lazarus, A. J.; Ogilvie, K. W.; and Burlaga, L. F.: *Solar Physics*, Vol. 13, 1970, p. 232.

Ogilvie, K. W.; Burlaga, L. F.; and Wilkerson, T. D.: *J. Geophys. Res.*, Vol. 73, 1968, p. 6809.

Razdan, H.; Colburn, D. S.; and Sonett, C. P.: *Planet. Space Sci.*, Vol. 13, 1965, p. 1111.

Siscoe, G. L.; and Finlay, L. T.: *J. Geophys. Res.*, Vol. 75, 1970, p. 1817.

Wilcox, J. M.; and Colburn, D. S.: *J. Geophys. Res.*, Vol. 75, 1970, p. 6366.



## SHOCK PAIR OBSERVATION *J. K. Chao, V. Formisano and P. C. Hedgecock*

On day 84, 1969, the HEOS 1 satellite observed a shock pair connected with a plasma bulk velocity increase from 400 to  $\sim 750$  km/sec. Both shocks were fast shocks. The forward shock had a Mach number of 1.7, the reverse shock had  $M_{fast} = 1.4$ . The time interval between the two shocks was 7 hr, 10 min. The time delay between HEOS 1 and Explorer 35 reverse shock observation ( $20 \pm 6$  min) agrees with the computed time delay ( $11 \pm 4$  min).

### INTRODUCTION

The HEOS 1 satellite was launched December 5, 1968, and provided good plasma and magnetic data for almost 2 years. Because of its elongated orbit, it was able to observe the solar wind for a high percentage of time. Plasma and magnetic data concerning a shock pair observation are shown in this paper.

The shock pairs have been theoretically studied by *Sonett and Colburn* [1965] and *Hundhausen and Gentry* [1969]. Experimentally they have been studied indirectly from sudden impulses observed in the ground station magnetograms by *Razdan et al.* [1965], but to our knowledge no direct observation has been published. The forward shocks have been observed more frequently in the solar wind. A reverse shock was recently reported by *Burlaga* [1970].

Instrument details and data analysis are reported by *Bonetti et al.* [1969] and *Hedgecock* [1970].

### PLASMA OBSERVATIONS

Plasma observations are shown in figure 1, which gives plasma bulk velocity  $V_p$ ; proton number density  $N_p$ ; proton most probable thermal speed  $W_p$ ; the value of the index  $K$  assumed for the distribution used to fit the data and total energy density, proton thermal energy density, electron thermal energy density (assumed to be

three times greater than that of protons), and magnetic energy density. Periods when  $\alpha$  particles were observed are indicated with a thick line.

$$F_K(W) = \frac{K!}{K^{3/2} [K - (3/2)!] \pi^{3/2} W_o^3} \frac{1}{[1 + (W^2/KW_o^2)]^{K+1}} \quad (1)$$

The bulk speed shows an increase over 10 hr from 400 km/sec to almost 750 km/sec. This increase starts gradually from 0400 UT (400 km/sec) to 0645 (450 km/sec) then shows a complicated discontinuous structure. As we shall see later two fast shocks are present in this structure: one observed at 0645 UT and another at 1355 UT. Plasma parameters for the discontinuities are given in table 1.

The proton number density shows a large increase before the high speed plasma, at the beginning of the velocity gradient. The thermal speed reaches very high values when the bulk speed gradient is observed. Correspondingly, the total energy density, very steady before the first shock, becomes very large and very fluctuating within the velocity gradient. It should be remembered, however, that the "ad hoc" hypothesis that electron thermal energy density is three times proton thermal energy density will enhance the fluctuations due to tangential discontinuities rather than cancel them, as it should if the total pressure is balanced.

*Drs. Chao and Formisano are at the Laboratorio Plasma Spaziale, University of Roma, Rome; Dr. Hedgecock is at the Imperial College of Science and Technology, London.*

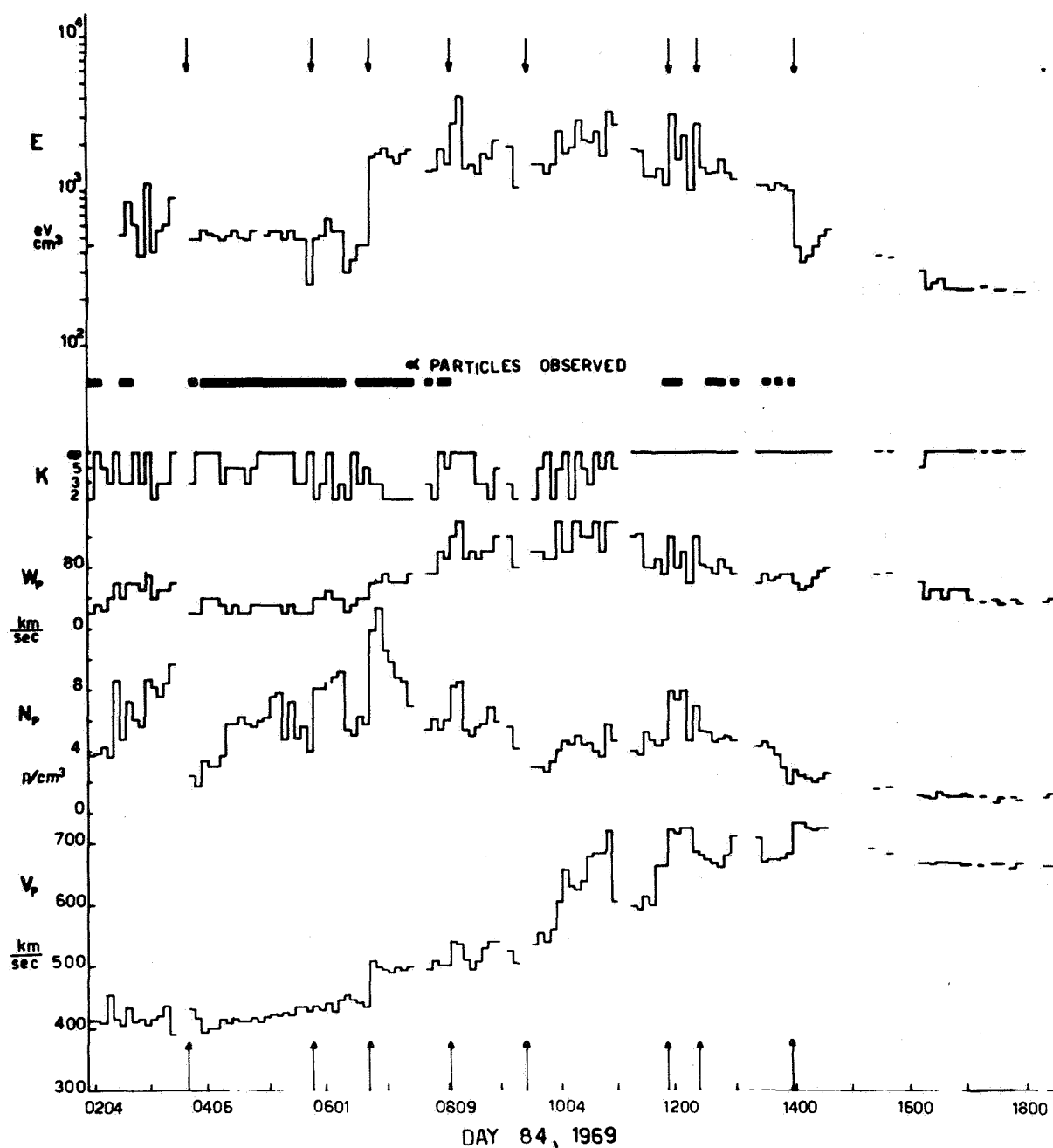


**Figure 1.** Plasma time history during the shock pair period, day 84, 1969. From the bottom are given plasma bulk velocity (note the very compressed scale) proton number density  $N_p$ , most probable thermal speed and total energy density (see text). Periods of  $\alpha$  particles observations are indicated. Arrows indicate eight discontinuities discussed in the text.

The distribution function is constantly maxwellian ( $K = \infty$ ) when high speed plasma is observed, while it shows a long high energy tail ( $K = 2$ ) just after the first shock.

Alpha particles were observed during few short periods of time. Figure 2 shows the  $\alpha$  particle bulk velocity  $V_\alpha$ , number density  $N_\alpha$ , and most probable thermal speed  $W_\alpha$  time history during the first shock crossing. As has

Table 1. Data from HEOS 1

Time	$B_1$	$B_2$	$V_1$	$V_2$	$N_1$	$N_2$	$W_1$	$W_2$	$\theta_{B1}$	$\phi_{B1}$	$\theta_{B2}$	$\phi_{B2}$	$\phi_{V1}$	$\phi_{V2}$	$T_e \times 10^5$		
0339	9.6	14.0	390	430	9.8	2.4	60	20	30°	60°	20°	60°			1.5	2.3	D
0548	13.0	10.0	425	430	3.8	8.0	20	40	5°	60°	-5°	75°			1.5	2.0	D
0645	10.0	18.0	430	510	6.0	12.5	40	60	-35°	80°	-35°	80°	-4.5°	-6.1°	1.5	Negative	Sf
0811	20.0	14.5	500	530	5.8	8.2	90	120	-20°	85°	-70°	90°			1.5	1.6	
0930	13.5	19.0	505	535	4.1	2.9	80	100	50°	130°	80°	230°			1.5	Negative	
1155	18.0	12.0	660	720	4.7	7.9	70	120	70°	170°	20°	200°			1.5	Negative	
1230	15.3	19.6	685	670	6.9	5.2	120	80	-10°	180°	38°	205°			1.5	1.6	D
1355	17.5	9.5	710	750	1.9/4.0 (*)	2.6/2.5 (*)	70	60	20°	210°	20°	185°	-1.3°	-18.8°	1.5	21	Sr

D discontinuity (total pressure is balanced).

S shocks (total pressure not balanced; Sf, forward shock; Sr, reverse shock).

(\*) single value and average value (—) are given.

been already pointed out in general by *Formisano et al.* [1970a], in this case the behavior of the  $\alpha$  particles is not simple. No relevant velocity change is observed for  $V_\alpha$  when the shock is observed, while a large discontinuity is observed 12 min before the shock:  $V_\alpha$  goes from 432 km/sec (0615 UT) to 515 km/sec (0632 UT) (two measurements are missed in between). This abrupt increase of  $V_\alpha$ , however, is observed together with a decrease of  $N_\alpha$ , if we compare the  $N_\alpha$  value observed two measurements before; since the data gap is partially due to low  $\alpha$  particles fluxes, an increase of  $N_\alpha$  together with the increase of velocity  $V_\alpha$  cannot be excluded. An increase of  $N_\alpha$  is observed for a short period in coincidence with the proton shock.

No electron measurements were available. However, assuming for charge neutrality  $N_e \simeq N_p$  and  $T_e = 1.5 \times 10^5$  °K on one side of the considered discontinuities, the electron temperature was computed on the other side in order to balance the pressure on both sides of the discontinuities [Burlaga and Chao, 1971]. As shown in table 1, four out of eight cases gave a very reasonable electron temperature on side two; these were called *tangential discontinuities*. In three cases, the electron temperature became negative, meaning that the pressure on side two was already much higher than on side one. The 0645 UT event will be shown later, as a forward shock. The last discontinuity needed an increase of the electron temperature of a factor of 20 on side two

for the total pressure being balanced. The expected side two electron temperature is therefore very unlikely. This discontinuity will be shown later as a reverse shock.

We are left with two discontinuities observed at 0930 UT and 1155 UT for which it is difficult to balance the pressure. As we will see later from the magnetic field, both of them have a very different character as observed by HEOS 1 and Explorer 35. Therefore, we may tentatively conclude that these are two discontinuities in a nonsteady state. However, wave energy should also be taken into account in balancing the energy density across the discontinuities.

#### MAGNETIC FIELD OBSERVATIONS

HEOS 1 magnetic field observations are shown in figure 3. The satellite had just crossed the laminar structure of earth-bow shock studied by *Formisano et al.* [1970b]. The spikes observed in the magnetic field intensity at 0220 UT and 0357 UT are very short magnetosheath observations due to the fast moving bow shock.

The magnetic field intensity shows a very clear structure that can be described as follows:

1. *The preceding "square wave."* From 0339 UT to 0548 UT magnetic field intensity is very large (14 $\gamma$ ) and very steady. A sharp tangential discontinuity is observed at 0425 UT;  $\theta$  changes from +20° to 30° while B remains constant. It is not clear whether this structure is related to the proton bulk velocity gradient and the shock pair.

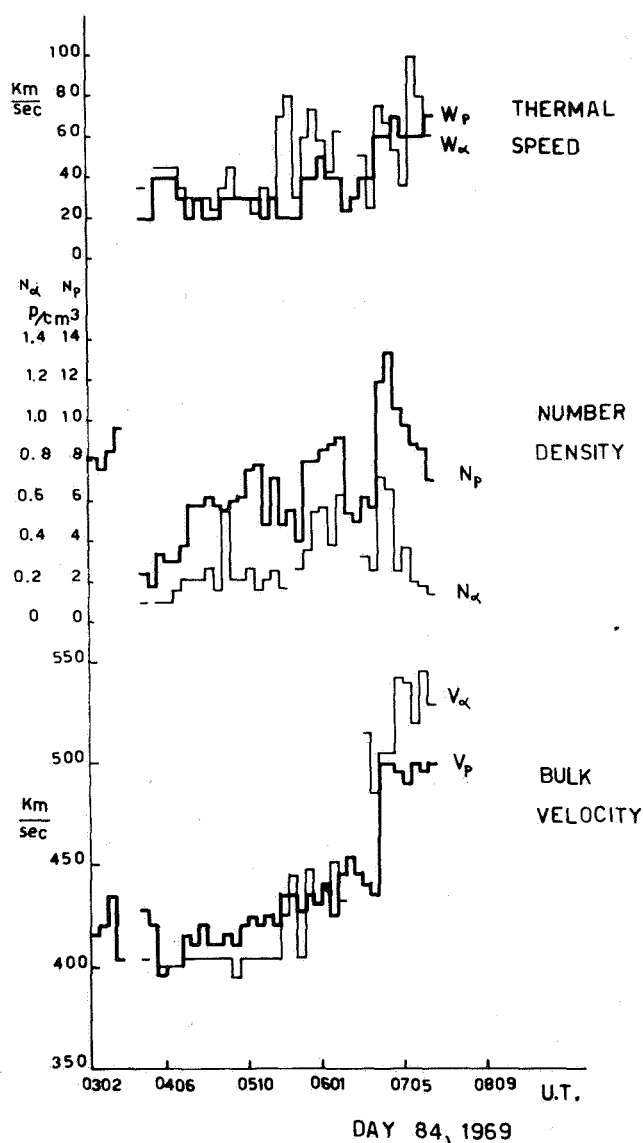


**Figure 2.** Alpha particles and proton parameters across the forward shock. Thick lines are for protons, thin for  $\alpha$  particles. Note that two measurements give high speed  $\alpha$  particles before the proton shock.

2. *The shock pair.* Magnetic field intensity shows the forward shock at 0645 UT when the field magnitude abruptly changes from  $10\gamma$  to  $18\gamma$ . After the shock,  $B$  increases until it reaches  $22\gamma$ ; later at 0811 UT,  $B$  decreases suddenly to  $14.5\gamma$ . From 0811 to 0930 UT both magnetic field intensity and direction are very turbulent and show large fluctuations. From 0930 to 1155 UT only the magnetic field direction shows large fluctuations. A second depression of magnetic field intensity of  $\sim 5\gamma$  is observed between 1155 and

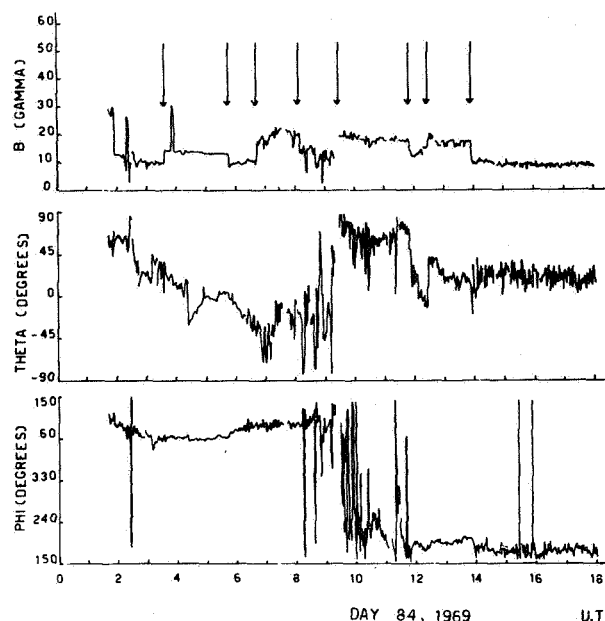


**Figure 3.** HEOS 1 magnetic field during the shock pair period, day 84, 1969. The satellite just left the bow shock at 0158 UT. (Two short magnetosheath periods are shown later by the magnetic field intensity as spikes.) Arrows indicate the eight discontinuities discussed in the text.

1230 UT. The reverse shock finally reaches the satellite at 1355 UT.

Figure 4 shows the magnetic field observed by Explorer 35. The position of the satellite is shown in figure 5; it was around the moon at  $\sim 79^\circ$  from the earth-sun line on the evening side.

Explorer 35 magnetic field observations show the same general configuration as for HEOS 1. However, a few important differences should be noted:

1. The reverse shock is observed at UT 1415, 20 min later than the HEOS 1 observation.
2. The second "depression" of the magnetic field intensity, clearly identified by the changes of the direction, is observed between UT 1234 and 1303:39 $\pm$ 33 min later than HEOS 1. The amplitude of this magnetic field intensity depression is now  $2\pm 2.5\gamma$  instead of  $5\gamma$ .
3. A data gap between 0606 and 0652 UT does not allow a comparison between time observation of the two satellites for the forward shock.
4. The first "depression" of the magnetic field intensity is only partially observed because of a data gap; the observed part looks different for the HEOS 1 observations.

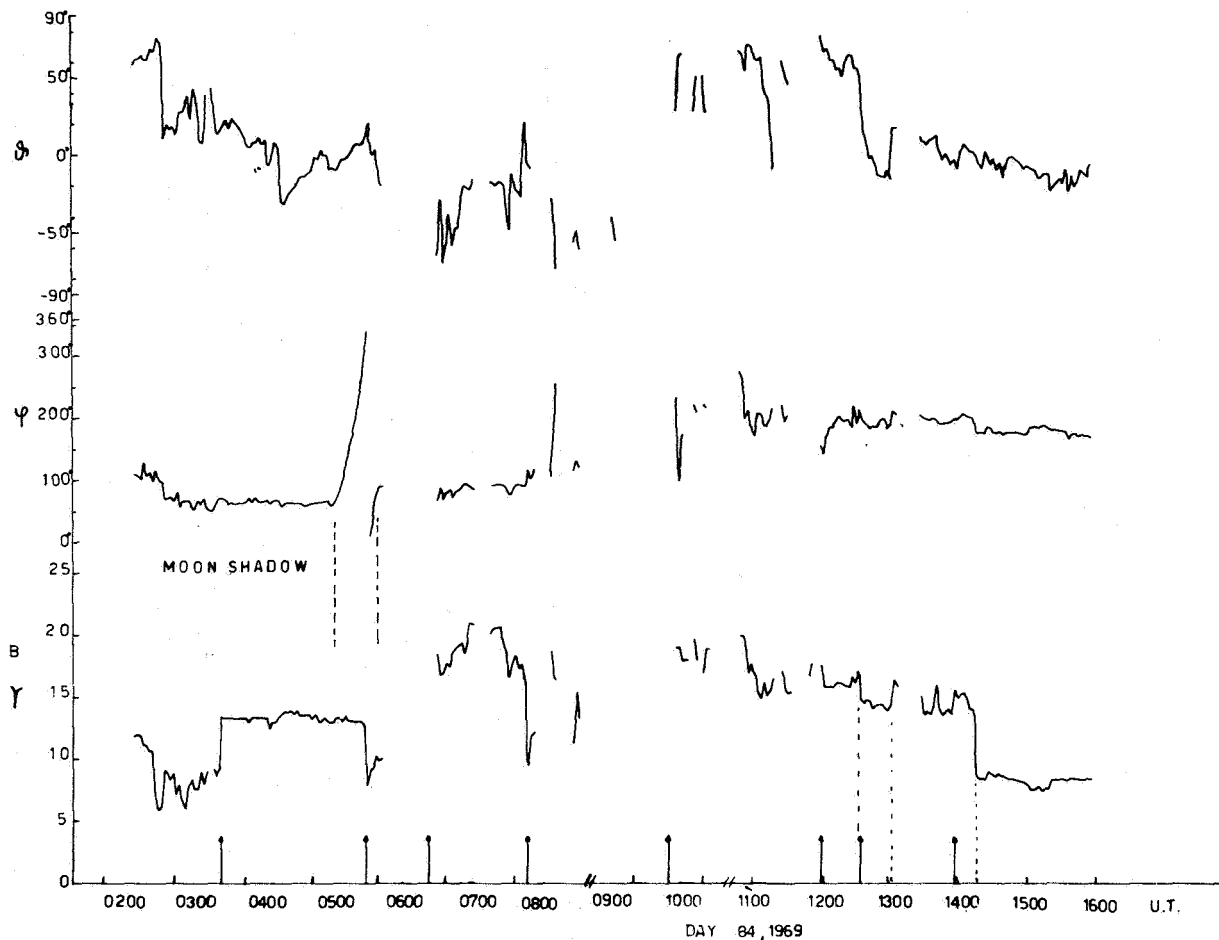


**Figure 4.** Explorer 35 magnetic field during the shock pair observation, day 84, 1969. Arrows indicate the eight discontinuities discussed in the text at the observation time of HEOS 1. Between 0500 and 0600 UT the magnetic field direction is altered by the moon's shadow.

### THE FORWARD SHOCK

The procedure described by Chao [1970] was used to obtain a set of 14 parameters (see table 2) ( $B_{R1}$ ,  $B_{T1}$ ,  $B_{N1}$ ,  $B_{R2}$ ,  $B_{T2}$ ,  $B_{N2}$ ,  $V_{R1}$ ,  $V_{T1}$ ,  $N_{N1}$ ,  $V_{R2}$ ,  $V_{T2}$ ,  $V_{N2}$ ,  $n_1$ ,  $n_2$ ); these satisfy the Rankine-Hugoniot equations for an isotropic plasma and are close to the observed average values on both sides of the discontinuity (table 2). We will call this set of parameters the *computed parameters* associated with the discontinuity. When these computed parameters are within the uncertainty of the corresponding average values, we have shown that the present event is a shock.

In table 2 we use the RTN coordinates in which the  $R$  axis is out from the sun and parallel to the sun-earth line, the  $T$  axis is the direction of the motion of the earth, the  $R$ - $T$  plane is parallel to the ecliptic, and the  $N$  axis is northward and perpendicular to the ecliptic.

The polar coordinates are also used in table 2. The "computed parameters" and the measured average values are given. The close agreement shows that the observed parameters and changes are consistent with the Rankine-Hugoniot equations.

In principle, using the Rankine-Hugoniot equations, it is possible to solve for 1 of the 12 known parameters as a function of the remaining 11 [Chao and Olbert, 1970].

It should be noted that the  $N$  component of the solar wind bulk velocity was not available, therefore we assume that  $V_{N2}$  is zero. We can solve for  $V_1$  as a function of ( $B_1$ ,  $B_2$ ,  $V_3$ ,  $n_1$ ,  $n_2$ ). Then, the measured parameters  $B_1$ ,  $B_2$ ,  $V_2$ ,  $n_1$ ,  $n_2$  are allowed to vary independently within their uncertainties for computing the  $V_1$  value. When the computed value of  $V_1$  is within the uncertainties of its measured average value,

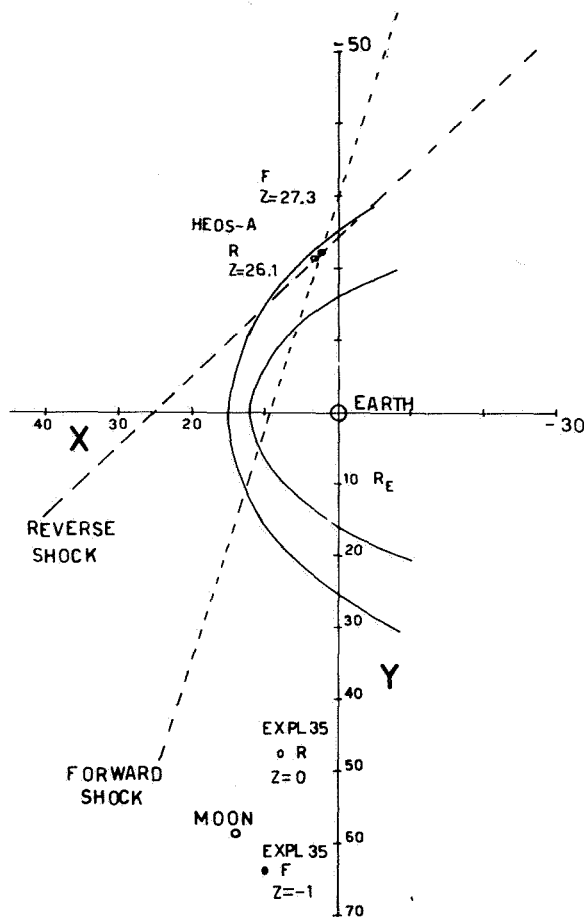


**Figure 5.** HEOS A and Explorer 35 relative positions at the forward (F) and reverse (R) shock observation. The X-Y plane is the plane of the ecliptic, the Z component is also given each time. Dashed lines are the intersections of the two-plane assumed shock surfaces with a plane parallel to the ecliptic plane.

then this computed value can be regarded as a prediction. Table 2 shows that the predicted and observed values of  $V_1$  are in good agreement.

It should be noted that the solution gives a reasonable component of solar wind bulk velocity perpendicular to the ecliptic plane, unknown from the data. This shock is a perpendicular shock for the following reasons:

1. The magnetic field does not change in direction across the discontinuity but change in strength by a factor of  $1.9 \pm 0.1$ .
2. The ratio of number densities across the perpendicular shock equals the ratio of magnetic field strength (i.e.,  $B_1/B_2 = N_1/N_2$ ) as it should.

The shock velocity in an RTN frame of reference is given in table 3 together with other basic shock parameters. In this table,  $V_s$  is the shock velocity in

RTN coordinate,  $\hat{n}$  is the shock normal in RTN and solar ecliptic coordinates  $\theta$ ,  $\phi$ , and  $V_n^*$  is the normal component of the flow to the shock front expressed in the shock frame of reference;  $\theta_{B,n}$  is the angle between  $B$  and  $\hat{n}$ ;  $M_A$  is the Mach number based on the total magnetic field intensity and  $\hat{n} \cdot M_{fast}$  is the Mach number based on the fast mode magnetosonic wave propagating along the shock normal. The fast Mach number is 1.7; that is, it fulfills the necessary condition for a shock pair to develop ( $M > 1.5$ ) found by Hundhausen and Gentry [1969].

From the shock normal and shock speed the time delay between HEOS 1 and Explorer 35 observations was computed.

The Explorer 35 shock distance was  $14.4 R_e \pm R_e$  and the time delay predicted is 2.6 min. The time delay observed, because of data gap, has to be  $-39 < \tau < 7$  min; therefore there is no inconsistency.

Figure 5 shows the intersection of the shock surface with a plane parallel to the ecliptic and passing through the HEOS 1 position.

### THE REVERSE SHOCK

The best-fit procedure also has been used for the reverse shock, with very good agreement obtained between predicted and observed parameters (table 4). The shock Mach number was 1.4. The shock was moving backward along its normal with a speed of 160 km/sec. The Alfvén Mach number was now computed using only the normal component of  $B$  to the shock surface.

From the shock normal and shock velocity the time delay between HEOS 1 and Explorer 35 observations has been computed. The Explorer 35 to shock distance was  $40.8 R_e$  and the time delay predicted was 11 min. It should be remembered, however, that because of the geometry of the problem (fig. 5) an error as small as  $7^\circ$  for the shock normal would give 2 min of error on the time delay. Another  $\sim 2$  min can be attributed to a 10 percent error on the shock velocity. The time delay is therefore  $11 \pm 4$  min. The observed time delay is  $20 \pm 6$  min.

From the basic shock parameters we see that in this case electron temperature almost does not change across the discontinuity. The forward and reverse shocks cannot be tangential discontinuities. If they were tangential discontinuities the predicted time delay between HEOS 1 and Explorer 35 disagrees with the measured delay time.

The best-fit method gives a possible value for the plasma anisotropy on both sides of the discontinuity:  $\xi = 1 - (\beta_{\parallel} - \beta_{\perp})/2$  is 0.0 in the preshock region and becomes 0.6 in the postshock region. This parameter had been assumed equal to 1 for the forward shock analysis.

**Table 2.** *Computed and averaged parameters for the forward shock*

Parameter	Computed values		Average values	
	Preshock	Postshock	Preshock	Postshock
$B$	-1.4, -8.1, -5.7	-2.3, -13.2, -13.4	-1.4, -8.1, -5.7	-2.3, -13.2, -13.4
(gamma)	10(-35°, 80°)	19(-35°, 80°)	10(-35°, 80°)	19(-35°, 80°)
$V$ , km/sec	429, 0, -19	504, -25, 0	429, -6, 0	504, -25, 0
	430 (-2.5°, -0°)	510 (0°, 2.1°)	430 (0°, 0.5°) (*)	510 (0°, -2.7°) (*)
$N$ , P/cm <sup>3</sup>	6.00	11.0	6.0±20%	12.5±20%
$W$ , km/sec	40	60	40±10 km/sec	60±10 km/sec

Explorer 35 to shock distance 14.4  $R_e$ .

Explorer 35 to HEOS 1 time delay predicted 2.6 min.

Explorer 35 to HEOS 1 observed time delay  $-31 < \tau < 7$  min.

(\*) without aberration.

**Table 3.** *Basic shock parameters*

Forward shock			Reverse shock	
$V_s$ , km/sec	548, -142, 130		251, -257, 71	
$\hat{n}_{RTN}$ ( $\theta, \phi$ )	0.929, -0.294, 0.224 13°, 162.4°		0.684, -0.703, 0.195 11°, 134.0°	
$V_n^*$	Preshock	Postshock	Preshock	Postshock
	185	100	199	166
$\theta_{B, n}$	90°	90°	45°	66°
$M_A$	2.07(*)	0.8(*)	6.4	2.1
$M_{fast}$	1.7	0.67	1.4	0.7
$T_e \times 10^5$ °K	2±1	3±1	2±1	1±1
$\xi$	1	1	0.0±0.2	0.6±0.2

(\*) Using the intermagnetic field intensity.

**Table 4.** *Computed and averaged parameters for the reverse shock*

	Computed values		Average values	
	Preshock	Postshock	Preshock	Postshock
<b>B</b>	8.9, 0.0, 3.3	14.2, 5.8, +5.6		
<b>(gamma)</b>	9.5 (20°, 180°)	17.1 (20°, 202°)	9.5 (20°, 185°)	17.5 (20°, 210°)
<b>V, km/sec</b>	734, -123, 0	723, -92		
	745.0 (0°, -6.5°)	715 (0.1°, 0.7°)	750 (0°, -6.5°) (*)	710 (0°, +1°) (*)
<b>N, P/cm<sup>3</sup></b>	2.3	4.0	2.5±20%	4.0±20%
<b>W, km/sec</b>	60	70	60±10 km/sec	70±10 km/sec

Explorer 35 to shock distance  $40.8 R_e \pm 7.5 R_e$ .  
 HEOS 1 to Explorer 35 predicted time delay 11 min  $\pm 4$ .  
 HEOS 1 to Explorer 35 observed time delay 20 min  $\pm 6$ .  
 (\*) without aberration.

## DISCUSSION

A shock pair observed by HEOS 1 and Explorer 35 has been studied. This shock pair also produces the classical  $SI^+$  and  $SI^-$  pair in the H component of the geomagnetic field reported by most equatorial ground stations.

The shock analysis described by Chao [1970] has given a Mach number of 1.7 for the forward shock and 1.4 for the reverse shock. It seems therefore verified the necessary condition suggested by Hundhausen and Gentry [1969] for the forward shock Mach number ( $M_p > 1.5$ ).

We suggest that the two magnetic field intensity "depressions" observed between 0811 and 0930 UT, 1155 and 1230 UT, be interpreted as decay of two discontinuities where the shocks were generated. Indeed the general structure of two shocks with two "depressions" in the magnetic field intensity has been verified on Pioneer 8 data. A statistical study made by some of the authors is in progress. With this assumption, and using the shock speeds relative to the ambient plasma (154 km/sec for the forward shock, 160 km/sec for the reverse shock) it is possible to compute the distance from the satellite where the shocks were generated.

The reverse shock has been observed by HEOS 1 1.5-2 hr after the assumed generation point. This time interval corresponds to a distance of  $4.9 \cdot 10^6$  km using an average

plasma velocity of 680 km/sec and has been covered by the shock with its velocity of 160 km/sec in 510 min, which corresponds to a distance of  $20.8 \cdot 10^6$  km using the average plasma velocity.

For the forward shock, assuming as a generation point the discontinuity observed at 0930 UT, we obtain an age of 536 min corresponding to a distance of  $16.1 \cdot 10^6$  km, using an average plasma speed of 500 km/sec.

The two shocks appear to be generated within the solar wind at a distance of 0.13 or 0.10 AU from the satellite toward the sun.

## ACKNOWLEDGMENTS

We are very grateful to Drs. N. Ness and L. F. Burlaga of the Goddard Space Flight Center for providing unpublished magnetic data from Explorer 35. We thank also the S-58 Belgian experimenters and Prof. Coutrez who provided unpublished data for the solar wind direction and Dr. Signorini who helped in their analysis.

We are indebted, also, to the other people of the Laboratorio per il Plasma nello Spazio of Rome, who have participated in the development of the solar wind experiment.

This research has been supported by the Consiglio Nazionale delle Ricerche of Italy. The HEOS 1 magnetic field experiment was supported by the British Science Research Council.



## REFERENCES

- Bonetti A.; Moreno, G.; Cantarano, S.; Egidi, A.; Marconero, R.; Palutan, F.; and Pizzella, G.: Solar Wind Observations with the ESRO Satellite HEOS 1 in December 1968. *Nuovo Cimento B*, Vol. 64, 1969, p. 307.
- Burlaga, L. F.; and Chao, J. K.: Reverse and Forward Slow Shocks in the Solar Wind. Preprint, 1971.
- Burlaga, L. F.: A Reverse Hydromagnetic Shock in the Solar Wind. *Cosmic Electrodyn.*, Vol. 1, 1970, p. 233.
- Chao, J. K.: Interplanetary Collisionless Shock Waves. MIT Center for Space Research Preprint CSR TR-70-3, 1970.
- Chao, J. K.; and Olbert, S.: Observation of Row Shocks in Interplanetary Space. *J. Geophys. Res.*, Vol. 75, 1970, p. 6394.
- Formisano, V.; Hedgecock, P. C.; Moreno, G.; Sear, J.; and Bollea, D.: Observations of Earth's Bow Shock for Low Mach Numbers. Preprint L.P.S.-70-13. Submitted to *Planet. Space Sci.* 1970a.
- Formisano, V.; Moreno, G.; and Palmiotto, F.:  $\alpha$ -Particles Observations in the Solar Wind. *Solar Phys.*, Vol. 15, 1970b, p. 479.
- Hedgecock, P. C.: The Solar Particle Event of February 25, 1969, in *Intercorrelated Satellite Observations Related to Solar Events*, edited by V. Manno and D. E. Page. D. Reidel, Dordrecht-Holland, 1970, p. 419.
- Hundhausen, A. J.; and Gentry, R. A.: Effects of Solar Flare Duration on a Double Shock Pair at 1 AU. *J. Geophys. Res.* Vol. 74, 1969, p. 6229.
- Razdan, H.; Colburn, D. S.; and Sonett, C. P.: Recurrent  $SI^+ - SI^-$  Impulse Pairs and Shock Structure in  $M$ -Region Beams. *Planet. Space Sci.*, Vol. 13, 1965, p. 1111.
- Sonett, C. P.; and Colburn, D. S.: The  $SI^+ - SI^-$  Pair and Interplanetary Forward-Reverse Shock Ensembles. *Planet. Space Sci.*, Vol. 13, 1965, p. 675.

## A TWO-SPACECRAFT TEST OF A SINGLE SPACECRAFT METHOD OF ESTIMATING SHOCK NORMALS

*R. P. Lepping*

**ABSTRACT** By assuming the validity of a subset of the Rankine-Hugoniot conservation relations for interplanetary (IP) shocks in an isotropic medium it has been demonstrated, in principle, that improved shock normals can be calculated by using a least-squares technique on combined magnetic field and plasma data from a single spacecraft. The scheme devised by *Lepping and Argentiero* [1971] uses those six conservation relations not involving pressure and temperature. This paper deals with a test of the scheme by examining in detail a shock across which the magnetic field changed direction by a small amount ( $\approx 10^\circ$ ). On January 26, 1968 at about 1430 UT this shock was observed by the plasma and magnetic field instruments in Explorers 33 and 35. The spacecraft were 76.6 and 56.9  $R_e$  sunward of the earth, respectively (and 43.5  $R_e$  from each other), and therefore well outside the earth's bow shock region, a necessary condition for a valid test. It was assumed that an IP shock's surface is locally plane over dimensions of about 100  $R_e$ . Using this assumption and the known geometrical configuration of the positions of the spacecraft with respect to the earth at the times of the shock onset. The orientation of an "observed" normal was ascertained, and least squares best-estimate normals were then calculated for each spacecraft using three different time intervals of data in each case: 9, 12, and 18 min, before and after onset. This was repeated using only the magnetic field data and the conventional coplanarity theorem for further comparison. For the 18 min data interval it was shown that the best-estimate normals for Explorers 33 and 35 agree with each other within less than  $3^\circ$ , and correspond to the observed normal within its angular uncertainty due to the time uncertainty of the earth's sudden commencement.

### INTRODUCTION

In this paper we test a single spacecraft method of estimating shock normals by cross checking the results of the method applied independently to the data of two interplanetary spacecraft located about 44  $R_e$  from each other. The method, devised by *Lepping and Argentiero* [1971], uses a six-equation subset, equations not involving temperature or pressure, of the eight-equation Rankine-Hugoniot conservation relations for interplanetary (IP) shocks in an isotropic medium. They showed in principle that improved normals can be calculated by employing a least-squares technique to best fit the combined magnetic field and plasma data from a single

spacecraft to three equations of the six-equation subset, after transformation to an arbitrary frame of reference. The remaining three equations are used explicitly to obtain the direction of the normal and, provided the average preshock plasma velocity is sufficiently accurate, the speed of the shock. The reasons for ignoring the equations containing temperature or pressure are:

1. The proton data for these parameters usually show the poorest approximation to a step function of all the shock parameters.
2. Use of these parameters would require electron data that are not always available.
3. Probably most importantly, the energy flux equation, which does not take into account possible heat flow across the shock front [*Hundhausen and Montgomery*, 1971], is of questionable validity.

---

*The author is at the Laboratory for Extraterrestrial Physics  
NASA Goddard Space Flight Center Greenbelt, Maryland.*

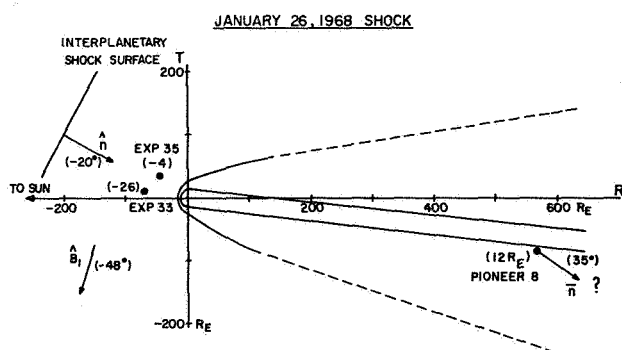


**Figure 1.** The positions of Explorers 33 and 35 and Pioneer 8, at the time of the January 26, 1968 shock, shown in the ecliptic R-T plane. Also shown are the best-fit IP normal  $\hat{n}$  and preshock magnetic field direction  $\hat{B}_1$ , as well as a roughly estimated normal (using average magnetic fields) at Pioneer 8. Quantities in parentheses refer to the direction perpendicular to the ecliptic plane in either degrees or  $R_e$ . The question mark (?) at Pioneer 8 refers to the large uncertainty (error cone  $17^\circ$ ) of the normal's estimate at that location.

## OBSERVATIONS AND DISCUSSION

This paper deals in detail with a shock whose associated magnetic field changed direction by a small angle ( $\approx 10^\circ$ ) across the shock transition zone. On January 26, 1968, at about 1430 UT this shock was observed by Explorers 33 and 35 with an  $88.8 \pm 3.6$ -sec time delay between them (fig. 1). At about 1441 UT a sudden commencement was observed on earth. Approximately 2 hr later (1634 UT) Pioneer 8, located about  $570 R_e$  behind the earth near the earth's tail, observed the shock after some deflection of its normal's direction. Notice that the IP shock normal was southward by  $20^\circ$  but at the Pioneer location it had become northward by  $\approx 35^\circ$  (95 percent certainty error cone angle is  $17^\circ$ ). Only Explorer 33 was significantly out of the ecliptic plane and was  $26 R_e$  below it. The IP shock normal  $\hat{n}$  was almost perpendicular ( $\approx 70^\circ$ ) to the preshock magnetic field direction  $\hat{B}_1$ . Therefore, little change of direction of the magnetic field would be expected as the shock passed the two spacecraft. The quantities  $\hat{n}$  and  $\hat{B}_1$  are best-fit values, whose estimates will be discussed below.

Figure 2 shows superimposed magnetic field data from Explorers 33 and 35 around the time of the shock. There was essentially no change in  $\theta$  across the shock surface and only about  $10^\circ$  change in  $\phi$ . The horizontal lines represent the average of the two individual Explorer 33 and 35 best estimate values. The length of these lines indicate the 18-min time intervals, before and after

## JANUARY 26, 1968 SHOCK OBSERVATIONS MAGNETIC FIELD DATA EXPLORER 33 ..... EXPLORER 35 —

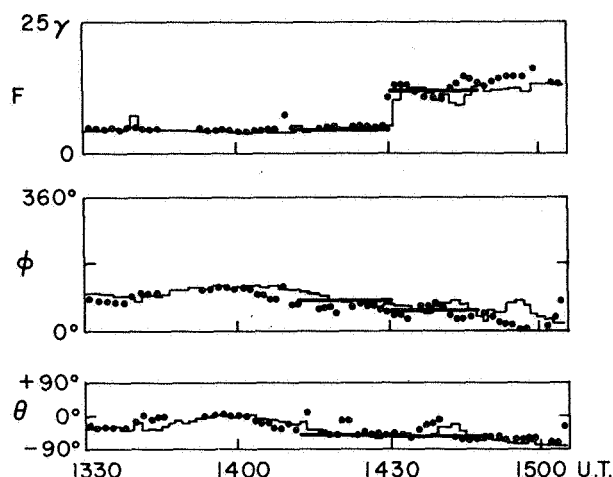


**Figure 2.** Superimposed magnetic field data for Explorers 33 and 35.  $F$  is the magnitude,  $\phi$  is the azimuthal angle measured counterclockwise in the ecliptic plane from  $\phi = 0^\circ$  in the direction of the sun, and  $\theta$  is the angle of inclination measured positive northward from the ecliptic.

shock onset, that were used in the best fit calculation. All six best-fit magnetic field parameters seem to have reasonable values when compared to straightforward averages allowing for deviations equal to the rms deviations for each. Notice the occurrence of a periodic structure before and especially after the shock. Behind the shock the oscillations, occurring over 30 min or so, are clearly out of phase between the Explorer 33 and 35 observations.

Figure 3 shows the plasma data also superimposed from Explorer 33 and 35 observations. The horizontal lines in the preshock case are simply averages of the dual spacecraft data. However, plasma velocity differences are obtained from the best-fit scheme and these along with the added preshock averages yield the postshock "best-fit" values shown. Again the lines represent an 18-min interval before and after the shock. Notice that the periodic structure after the shock, which was rather clear in the magnetic field data, also appears here, except the wavelike signature is not now quite as well defined.

Table 1 gives the best estimate values of the IP shock parameters for the two spacecraft and average values of these best estimates. The subscripts 1 and 2 refer to pre- and postshock, respectively, and the RTN coordinate system, centered at the spacecraft of interest, refers to the unit vectors:  $\hat{R}$  radially away from the sun in the

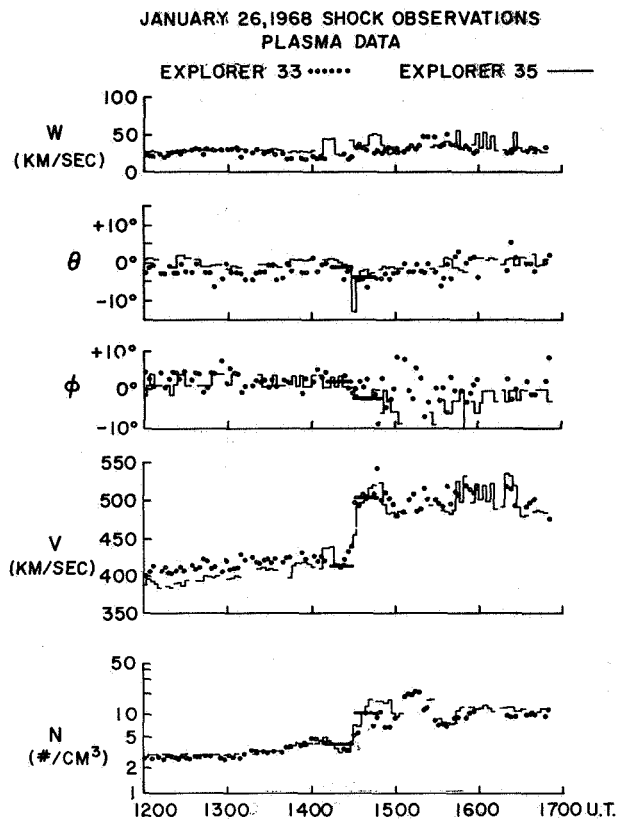


**Figure 3.** Superimposed plasma data for Explorers 33 and 35.  $W$  is the thermal speed and  $V$  is the magnitude of the bulk plasma velocity, whose direction is designated by  $\theta$  (same as fig. 1) and  $\phi$  ( $\phi = 0^\circ$  in antisolar direction).  $N$  is the plasma number density.

ecliptic plane, and  $\hat{T}$  perpendicular to  $\hat{R}$  and lying in the ecliptic such that  $\hat{R} \times \hat{T} = \hat{N}$  is normal to the ecliptic and "northward."  $W = (W_R, W_T, W_N)$  is the plasma bulk velocity difference  $V_2 - V_1$ . The  $N$ s are the number densities and  $n_R, n_T$ , and  $n_N$  are the components of the shock unit normal. The Alfvén Mach numbers for pre- and postshock were 8.5 and 5.5, respectively; these compare well with those of previously studied IP shocks [Hundhausen, 1970]. The best estimate Explorer 33 and 35 normals (calculated from the 18-min interval) differed by less than  $3^\circ$ . The associated calculated shock speeds were 507 and 520 km/sec, respectively, giving an average value of 513 km/sec. An average preshock plasma bulk velocity  $V_1 = (426, 17.4, -7.0)$  km/sec from the data of both spacecraft was used.

## TWO-SPACECRAFT TEST

The best-fit IP normal was checked for accuracy by comparing its angular displacement from two fixed and

**Table 1.** January 26, 1968, shock parameters best estimate values for the 18-minute interval

Parameter	Best Estimate Explorer 33	Value Explorer 35	Average of best estimate for Explorers 33 and 35
$B_{1R} (\gamma)$	-1.59	-0.24	-0.92
$B_{1T}$	-3.16	-3.07	-3.12
$B_{1N}$	-3.49	-3.83	-3.66
$B_{2R}$	-5.15	-3.41	-4.28
$B_{2T}$	-6.60	-6.09	-6.35
$B_{2N}$	-7.54	-8.26	-7.90
$W_R$ (km/sec)	78.6	85.6	82.1
$W_T$	-37.0	-35.0	-36.0
$W_N$	-28.3	-24.2	-26.3
$N_1$ (#/cm <sup>3</sup> )	4.19	4.45	4.32
$N_2$	9.67	10.52	10.1
$n_R$	0.826	0.850	0.838
$n_T$	-0.440	-0.416	-0.428
$n_N$	-0.352	-0.324	-0.338

intersecting lines in space. These lines were: first, the segment between Explorers 33 and 35 and, second, that between Explorer 33 and the earth; they intersected at  $47^\circ$ . Each of these angles can be calculated in two ways: first, by a straightforward calculation using the best estimate normal, which gives the *calculated* check angles; and second, by assuming, for dimensions of about 100  $R_e$ , (1) a plane shock front, and (2) a constant shock speed (513 km/sec) and constant normal. The latter are the *observed* check angles. The calculated and observed check angles can then be compared.

In the case of the Explorer 33-35 line the observed and calculated angles were  $80.5^\circ$  and  $84.1^\circ$ , respectively, giving less than a  $4^\circ$  difference. In the case of the Explorer 33-earth line the observed and calculated angles were  $47^\circ$  and  $44^\circ$ , respectively, giving approximately a  $3^\circ$  difference. The sudden commencement (SSC) time at earth was taken to be 1441 UT, giving an 11-min delay. If 1440 UT is taken as the SSC time, giving a 10-min delay, the angles become  $52^\circ$  and  $44^\circ$ , respectively, an

$\approx 8^\circ$  difference. Assumptions (1) and (2) for the region from Explorer 33 to the earth, even over the path from the bow shock encounter to the earth, are justified within an angle error of  $8^\circ$  or so, because the shock effectively spends only about one-tenth of its total Explorer 33-earth travel time in this latter region.

The (95 percent certainty) error cone angle associated with the normal was  $7.6^\circ$ , which is consistent with the check angles, or is perhaps somewhat conservative.

#### COMPARISON OF ANALYSIS-INTERVALS

To obtain some understanding of the importance of using the proper time interval around the shock for the shock analysis, other time intervals, as well as the 18-min interval, were used. Henceforth, the term *best estimate* refers only to a given analysis-interval for a given spacecraft, and not necessarily to the *final* best estimate of the IP normal. Figure 4 shows, for the three separate input data intervals, estimates of the January IP shock normal, as projected on the R-T plane, for Explorers 33 and 35. The results of both the *average magnetic field*

*method* (coplanarity theorem) and the *best estimate method* (auxiliary use of plasma data) of estimating the IP normal are shown. The latter are represented by either dashed (Explorer 33) or solid (Explorer 35) arrows, and the former by dashed or solid lines. The following features should be pointed out:

1. There is a large ( $70^\circ$ ) spread of the average normals but a reasonably narrow ( $14^\circ$ ) spread of the best estimate normals over the three time intervals.
2. Lengthening the time interval of data around the shock for use in calculating the normal does not necessarily improve the estimate, even within the short range considered here (up to 18 min).
3. For each given time interval the best estimate normals between Explorers 33 and 35 are closer together than the average normals.
4. The 18-min interval was clearly the "proper" choice of interval giving a few degrees difference between the Explorer 33 and 35 best estimate normals.

Figure 5 corresponds to figure 4 except now the estimates of the IP normal are projected into the R-N

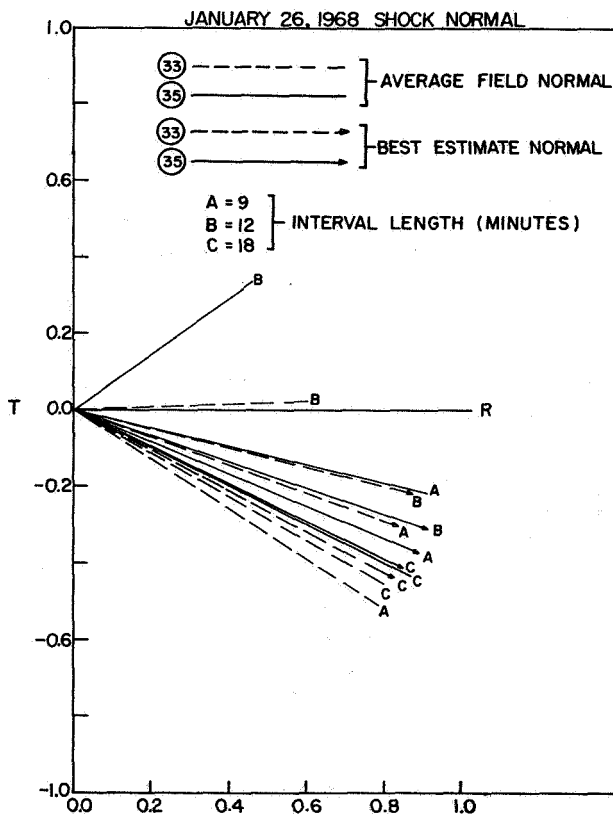


Figure 4. Estimates of the January 26, 1968, shock normal from Explorers 33 and 35 data and projected into the R-T plane. Both average-field and best-fit methods are shown, each for three separate data intervals.

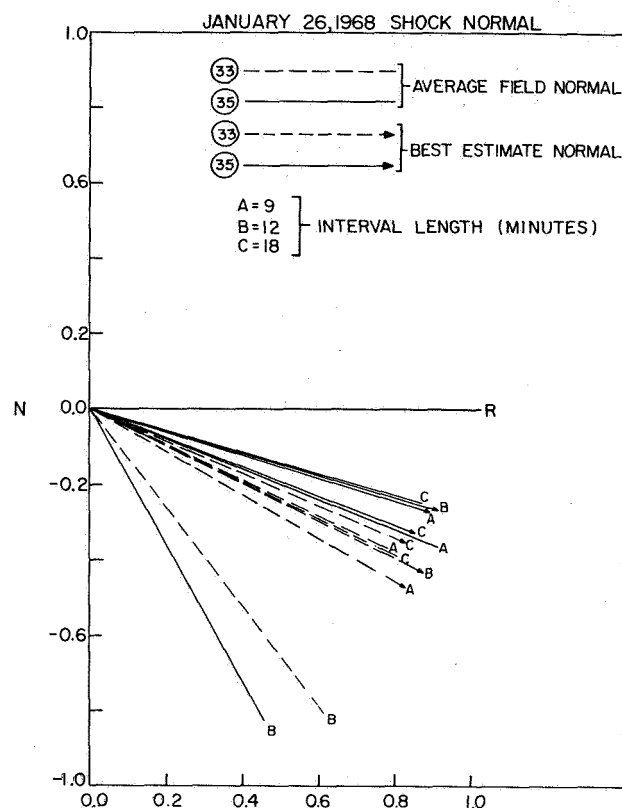


Figure 5. Estimates of the January 26, 1968, shock normal from Explorers 33 and 35 data and projected into the R-N plane.

plane. All the above comments again hold except for (3). In (1) the spread angle for the average normals becomes  $46^\circ$  but that for the best estimate spread remains  $14^\circ$ .

If one had been satisfied with only 12 min (B interval) of data around the shock and had not taken advantage of the available plasma data (or did not have such data) one might have been led into a false sense of certainty about the results because of the relatively good agreement between the results of the two spacecraft for this time interval.

## CONCLUSIONS

We have accurately estimated an interplanetary shock normal and have shown its direction to be significantly different from the  $\hat{R}$  direction both in inclination angle  $\theta$  and azimuthal angle  $\phi$  ( $\theta = -20^\circ$ ,  $\phi = 153^\circ$ ); the ecliptic plane projection was approximately along the average magnetic field spiral direction. There was no obvious solar flare associated with this shock. The shock may or may not have originated at the sun but it *probably did not start as a spherical front near the sun unless the front was severely distorted over 1 AU*. The periodic structure occurring behind the shock as seen especially in the magnetic field data is no doubt, in part, responsible for the fact, stated above, that lengthening the analysis interval does not necessarily improve the

estimate of the normal. A proper analysis-interval is probably one that encompasses, as exactly as possible, two oscillations if such quasiperiodic structure exists after the shock, or at most should be limited to the interval just up to the first obvious discontinuity appearing after the shock.

## ACKNOWLEDGMENTS

I wish to thank Dr. N. F. Ness for the magnetic field data and Dr. J. Binsack and Mr. H. Howe of MIT for the plasma data used in this study. I am grateful to my colleagues at Goddard Space Flight Center for helpful suggestions and comments.

## REFERENCES

- Hundhausen, A. J.: Composition and Dynamics of the Solar Wind Plasma. *Rev. Geophys. Space Phys.*, Vol. 8, no. 4, 1970, esp. pp. 786-87.
- Hundhausen, A. J.; and Montgomery, M. D.: Heat Conduction and Non-steady Phenomena in the Solar Wind. Preprint from Los Alamos Scientific Laboratory of the University of California, LA-DC-11938, 1971.
- Lepping, R. P.; and Argentiero, P. D.: A Single Spacecraft Method of Estimating Shock Normals. *J. Geophys. Res.*, 1971. (in press)

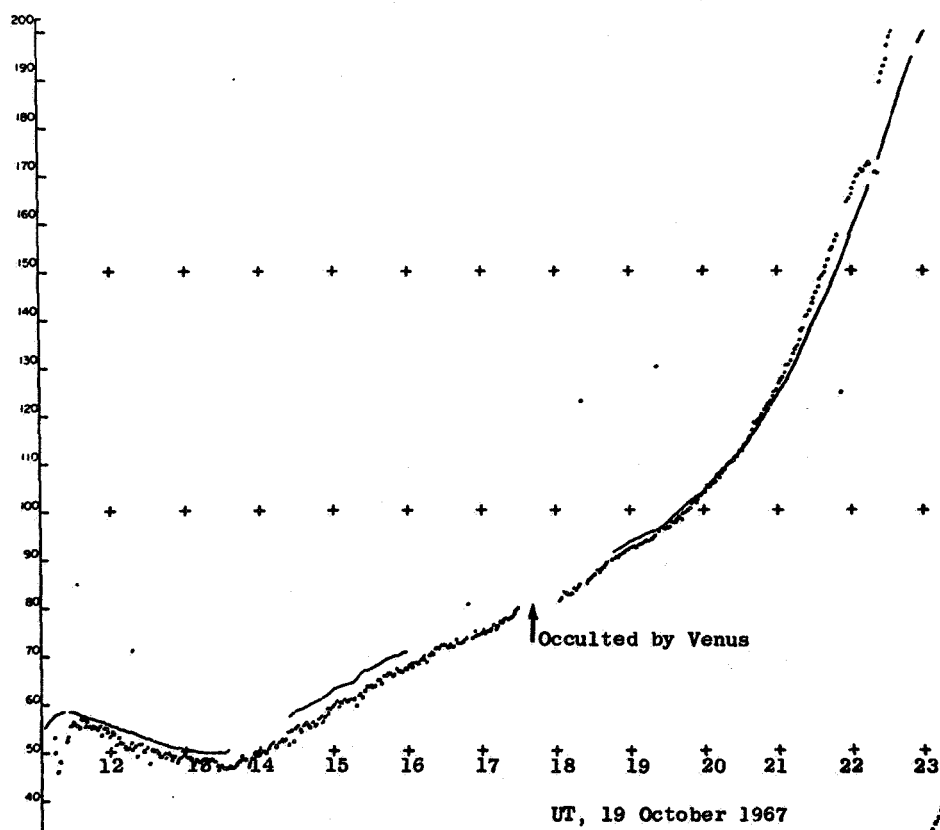
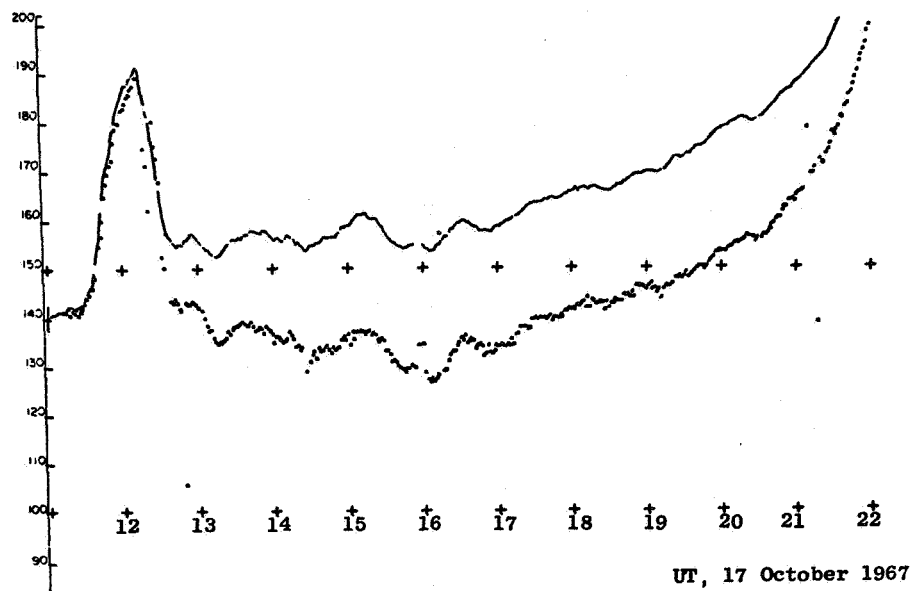
## COMMENTS

*Dr. T. A. Croft* Many people have said there is a need for comparison of data among spacecraft and a need for diagnostics to tell whether observed events are corotating or outward-convecting. I would like to point out that such data are available from Mariner 5 and Pioneers 6, 7, 8, and 9 on which there is a radio propagation experiment that measures the average electron density from earth to the spacecraft. Figure 1 shows a good example of the data derived from the experiment. The bottom curve shows the data obtained during occultation of Mariner 5 by Venus. On the top you see a similar record obtained two days earlier. The significance of this slide is that the fluctuating-density events in the earlier record *must* be due to outward-convecting irregularities in the electron number density; they cannot be due to a corotating event. You can eliminate that possibility by considering how long a corotating event would stay in the path, the "corotation delay," and these fluctuations are too rapid.

If some of you are trying to analyze a particular event, we might be able to offer some diagnostic help like that shown here. You can determine whether we might help you by considering the following: Did the event occur when Mariner 5 was between earth and its occultation by Venus? (We stopped tracking it a month later.) For Pioneer 6, the spacecraft had to be within 1 AU of the earth for our equipment to operate, and I should point out that Pioneer 6 has gone around the sun and is now operating again, within 1 AU. Pioneer 7 was about the same as 6; it works only out to 1 AU, but Pioneers 8 and 9 have operated since their launch and are continuously operating now. They work well at 2 AU.

The experiment can only help you if one of these spacecraft is at least 0.1 AU away from earth and it has to be above Stanford's horizon to operate, so it can only obtain measurements half of every day.

If we can help anyone in this kind of diagnostic work, we would be glad to do so.



## DISCUSSION

*E. C. Roelof* I would like to add some support to Ogilvie's identification of a possible corotating shock on September 28, 1967, from three spacecraft analyses that I carried out with Tom Cornelius, Tom Armstrong, and Jim Van Allen. As I read Keith's slide his candidate for a corotating shock comes at the termination of a 0.3 MeV corotating proton event that we identified at all three spacecraft as its being corotating by several signatures that we developed including a velocity anisotropy, and the demand, of course, the obvious demand for similar spatial profiles at the three spacecraft. So this looks like a supporting piece of evidence.

*D. W. Forslund* I just wanted to mention something in connection with the observations Scarf presented earlier. There has been important research done lately on a collisionless dissipation mechanism that may occur near discontinuities or in interplanetary shocks and is particularly important in laboratory shocks. This mechanism is an instability driven by currents flowing perpendicular to the magnetic field; that is, whenever a sharp magnetic field gradient exists one has an instability due to electron cyclotron waves driven unstable by inverse Landau damping, provided the relative drift is greater than the ion thermal speed. Figure 1 illustrates the basic idea of how it works. The diagram shown here is a plot of roots of the dispersion relation, with the wave frequency  $\omega$  plotted vertically and the wave number  $K$  plotted horizontally. The horizontal branches are Bernstein modes, which propagate exactly perpendicular to the magnetic field and in the absence of ion drift are undamped. And if one has ions flowing relative to the electrons as indicated by the diagonal line in the diagram where the two dashed diagonal lines indicate the ion thermal spread, the ions resonant with the phase velocities of the Bernstein modes drive the electrons unstable as indicated by the mode distortion and growth rates indicated along the curves in units of the electron gyrofrequency. The curves at the bottom are the growth rates for each harmonic. The solid curve on the right of the ion drift line is the slow ion acoustic root which is stable as indicated by the negative growth rates. We've done fully nonlinear studies of the instability and show it causes strong electron and ion heating through a nearly steady turbulent resistance and probably most important for the applications here a significant cross field diffusion, hence reducing the magnetic field gradient which is driving the instability and hence implying there would be a minimal thickness to any discontinuity or shock that would be observed.

*J. R. Spreiter* We've been hearing of using MHD relations to interpret interplanetary shocks and of the existence of slow shock waves. This brings up an interesting question that I don't think any mention has been made of today. That is, in addition to satisfying the conservation equations, slow shock waves must satisfy an evolutionary condition or else they can't occur according to the MHD theory. Now, this evolutionary condition is the MHD counterpart of the entropy-must-rise statement of gas dynamics, but it isn't exactly identical. It would be interesting in doing this type of MHD interpretation, particularly the slow shock waves, to inquire whether the evolutionary conditions are being satisfied.

*S. Olbert* I didn't show the two shocks I promised. They are slow shocks and the analysis has been published. We've checked exactly the question of evolutionary character of these shocks. The crude way of testing is the following: After you have analyzed orientation, the speed, and checked every consistency observation and theoretical prediction from MHD approximations, you can then determine the pressure of the plasma, electrons and protons put together; you can then ask the basic question, what are the Mach numbers relative to the slow mode ahead of the shock and behind the shock? And it has to come out that the Mach number ahead of the slow shock relative to the slow mode is larger than one, smaller than one. Furthermore, the main Mach number has to be smaller than one on both sides of the shock, and if these conditions are all satisfied you can then demonstrate that the evolutionary conditions are satisfied. This has been tested in the two shocks shown.



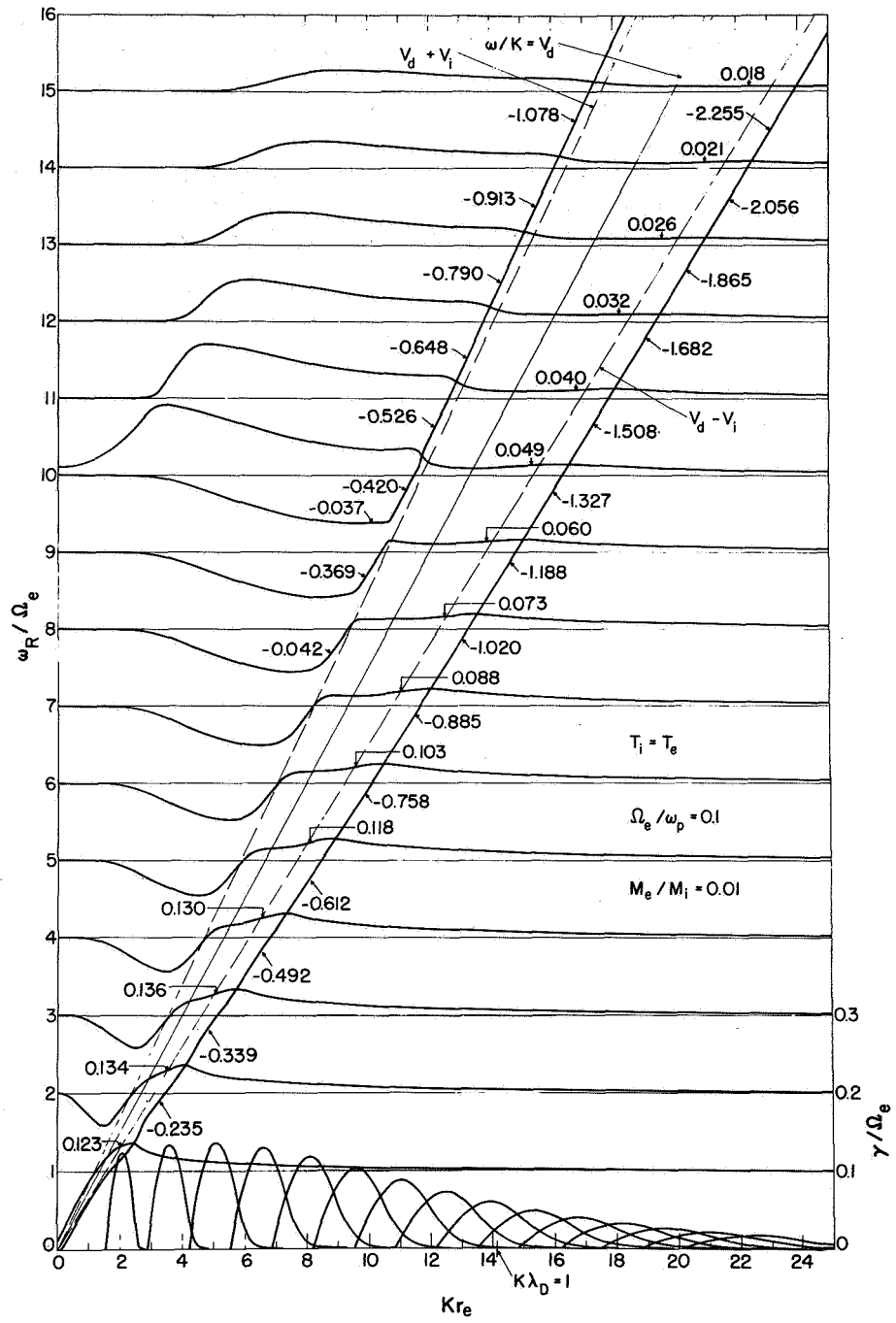


Figure 1. Frequency versus wave number diagram for electron cyclotron waves driven unstable by ion streaming relative to electrons across a magnetic field.

*G. L. Siscoe* One question relating to the heat flux problem is whether there is a flux of heat away from the shock. Isn't there a simple way to test that? Because if the density jump ever gets to be bigger than 4 for very high Mach number shock, you know there's some heat flux away. Has anyone seen density jumps bigger than 4 here at the earth's bow shock?

*S. Olbert* No, the strongest shock we have seen of the 4 shocks we have shown are in the increasing order of strength. The biggest you have seen was the first one. And the biggest jump density in interplanetary space I have ever seen was  $13/4.4$ .

## INTERPLANETARY DOUBLE-SHOCK ENSEMBLES WITH ANOMALOUS ELECTRICAL CONDUCTIVITY

Murray Dryer

Similarity theory is applied to the case of constant velocity, piston-driven, shock waves. **ABSTRACT** This family of solutions, incorporating the interplanetary magnetic field as developed by Lee and Chen for the case of infinite electric conductivity, represents one class of experimentally observed, flare-generated shock waves first described by *Hundhausen et al.* [1970]. This paper discusses the theoretical extension to flows with finite conductivity (presumably caused by unspecified modes of wave-particle interactions). Solutions, including reverse shocks, are found for a wide range of magnetic Reynolds numbers from one to infinity. Consideration of a zero and nonzero ambient flowing solar wind (together with removal of magnetic considerations) enables the recovery of the earlier similarity solutions of *Parker* [1963] and *Simon and Axford* [1966] as well as the numerical simulations of *Hundhausen and Gentry* [1969a]. For the magnetic case, it is shown that negligible joule heating occurs until the conductivity drops to more than 10 orders of magnitude below the solar wind's classical value of approximately  $10^4 (\Omega - m)^{-1}$ . It is shown that even substantial joule heating has a negligible effect on the gross features of the double-shock ensemble. A limited comparison with observations suggests that flare energetics can be reasonably estimated once the shock velocity, ambient solar wind velocity and density, and ambient azimuthal Alfvén Mach number are known.

### INTRODUCTION

Early speculations and theoretical studies of interplanetary shock waves [*Parker*, 1963] were quickly confirmed by spacecraft observations (for several excellent reviews, see *Hundhausen*, 1970a, b). It is now well known that Alfvén waves as well as discontinuities on large ( $> 0.01$  AU) and small ( $< 0.01$  AU) scale lengths, respectively, exist in the solar wind [*Burlaga*, 1968, 1971; *Belcher et al.*, 1969]. This paper is concerned with a theoretical study of shock waves and contact surfaces. Such ensembles were suggested [*Carmichael*, 1962; *Sonett and Colburn*, 1965] to be responsible for sudden commencements, positive and negative magnetic impulses, and substorms. On the basis of simultaneous

solar wind and ground observations, *Hirshberg et al.* [1970a, b] suggest, that contact surfaces following a number of shock waves may be associated with substorms and may be identified by an enriched  $\alpha$ -particle abundance presumably traceable back to the flare plasma itself. Since *Sonett and Colburn's* suggestion that these two discontinuities should be followed by a rearward-facing (or reverse) shock wave, a number of theoretical and experimental studies have examined this ensemble.

*Sturrock and Spreiter* [1965] considered the forward-reverse shock ensemble from a steady-state point of view without consideration of the magnetic field. By considering Hugoniot conditions, they arrived at a class of allowable configurations for what might be called the "shock-tube" analogy in one-dimensional, ordinary gas-dynamics. This study was extended by *Schubert and Cummings* [1967, 1969] who included a transverse

---

The author is at the Space Environment Laboratory, National Oceanic and Atmospheric Administration, Environmental Research Laboratories, Boulder, Colorado.

magnetic field in an infinitely conducting plasma. In comparing their analysis with a potential experimental (Mariner 2) candidate for an ensemble [Neugebauer and Snyder, 1967], they showed that the peak in the proton density did lead the peak in the magnetic field strength as predicted by their shock jump calculations. Because of the time-invariant aspect, however, their study precluded any temporal variation. This suggested identification must therefore be considered inconclusive.

Time dependence was explicitly considered for the forward shock by Parker [1963], who employed similarity theory without consideration of the magnetic field or the kinetic energy of the undisturbed, ambient solar wind. A prominent feature of this spherically symmetric solution was the infinite value of density at the position of the contact discontinuity, or "piston." Korobeinikov and Nikolayev [1970] have referred to a similar solution. Simon and Axford [1966] extended this similarity solution to include the flow that extends from the "piston" back to the reverse shock. The transverse magnetic field was explicitly considered for an infinitely conducting fluid by Lee and Chen [1968] and extended by Dryer [1970] and Eviatar and Dryer [1970] to the case of a fluid with finite conductivity. Significantly, these latter solutions also considered the explicit presence of the undisturbed solar wind through which the forward shock moves with arbitrary speed as described by Lee [1965]. Lee et al. [1970] then proceeded to extend the infinitely conducting solution to the flow between the "piston" and the reverse shock. This paper reexamines the study performed earlier [Dryer, 1970] and extends the entire ensemble (comprising the reverse shock, contact discontinuity, and forward shock) so that it includes the more physically realistic presence of finite conductivity.

Related studies including consideration of the ambient solar wind but without the magnetic field were made by Hundhausen and Gentry [1969a, b]. Their numerical simulation studies considered the superposition of arbitrary disturbances (initiated at 0.10 AU) on a typical steady solar wind model. They concluded that a flare that continues to exert a constant momentum, hence a linear (with time) increase of energy, on the "piston" for longer than  $\sim 5$  hr would produce the double-shock ensemble, which would persist to earth's orbit. Conversely, they showed that rarefaction waves emanating from the flare extend to the propagating reverse shock and thereby weaken and eventually cause it to disappear when the flare ceases its activity prior to 5 hr. Thus, they further suggested that the ensemble would rarely be observed at 1 AU.

Experimental observations of the double shock are inconclusive. Hundhausen et al. [1970], for example, report observations of a number of piston-driven shocks but make no identification of possible associated reverse shocks. One might conclude that the latter were dissipated prior to their arrival at 1 AU. It is known, however, that reverse shocks must exist. Burlaga [1970] reports the first unambiguous identification of a reverse shock on 18 September 1967 by using simultaneously measured plasma and field data from Explorer 34 instruments. Identification of a piston, or *contact discontinuity*, and forward shock as part of a possible ensemble, however, was not attempted. Hundhausen [1970b] has suggested that Lazarus et al. [1970] may have observed an ensemble on 11 August 1967; he also reports the possible identification of a reverse shock, using Vela 4B plasma data only, on 5 July 1967. It is of great interest to note that the first interplanetary shock ever observed [by Mariner 2; Sonett et al., 1964] on 7 October 1962, as mentioned above, may have been part of ensemble as suggested by Schubert and Cummings [1967, 1969]. Also, the suggestion by Hirshberg et al. [1970a, b] that the contact discontinuity might be identified by the anomalous  $H_e^{++}/H^+$  abundance may prove useful.

It is clear, then, that further study, both theoretical and experimental, is required to provide unambiguous evidence, including simultaneous magnetic field measurements, of this class of flare-generated shock waves.

Additional, but still limited, evidence of piston-driven shocks has been given by the VLF electric field observations of Pioneers 8 and 9 [Scarf et al., 1970; Scarf and Siscoe, 1971; and Siscoe et al., 1971]. These authors have suggested that significant wave-particle interactions occur for a substantial time scale (hr) following the passage of interplanetary shock waves. Dryer [1970] has shown, as a result, that associated anomalous electrical conductivity could be incorporated into the theory. The presence of nonclassical resistivity has already been discussed from several points of view [Sagdeev, 1967; Speiser, 1970], which include stochastic "collisions" of electrons with fluctuating electric fields and even "non-noise" effects due to electron inertial effects.

Here we first demonstrate the character of the piston-driven shock for a wide range of magnetic Reynolds numbers (that is, anomalous electrical conductivity) as a basis for estimating how low  $\sigma$  should be before significant departure from the infinitely conducting solution takes place. A second purpose is to examine a typical double-shock ensemble from the theoretical point of view for both  $\sigma = \infty$  and  $\sigma \neq \infty$ .

## ANALYSIS

The nomenclature used for the piston-shock problem is identical to that used in the basic problem considered by Parker (fig. 1). It should be noted that the deformed magnetic field illustrated for the spherical model in figure 1 indicates the presence of a *contact discontinuity*

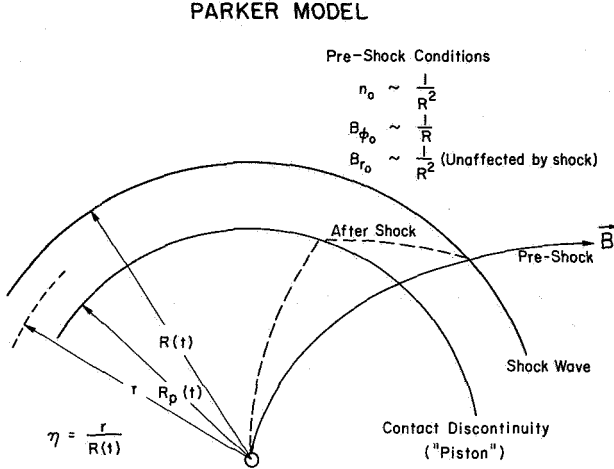


**Figure 1.** Sketch and nomenclature of the shock wave-piston combination as proposed originally by Parker [1963]. The special case of a constant velocity combination gives rise to a reverse shock (not shown here) which follows the piston.

(as distinguished from the tangential and rotational types) at the piston; that is, there is a component of  $\mathbf{B}$  normal to the piston. More realistic nonspherical configurations, however, may require a *tangential* discontinuity over most of its surface [Hundhausen, 1971]. The reverse shock, which causes another kink in the field, is not shown.

The time-dependent partial differential equations, including the Lorentz force, joule heating, and magnetic diffusion, are given in figure 2. Except for the use of Ampere's law on the right side of the energy equation, these equations are identical to those used in the earlier study [Dryer, 1970], which considered the electric field in an explicit way. Figure 3 shows the equations [Lee and Chen, 1968] that are used to transform the equations into ordinary differential equations. The boundary conditions at the shock and piston are also shown. The crossed-out terms in the jump conditions are permitted under the assumption that the inverse of the transverse ambient Alfvén Mach number (squared) is

$$\begin{aligned} \frac{\partial \rho}{\partial t} + \frac{\partial(\rho u)}{\partial r} + \frac{2\rho u}{r} &= 0 \\ \frac{\partial u}{\partial t} + u \frac{\partial u}{\partial r} + \frac{1}{\rho} \frac{\partial p}{\partial r} &= -\frac{1}{\rho \mu} B_\phi \left( \frac{\partial B_\phi}{\partial r} + \frac{B_\phi}{r} \right) \quad (\text{MKSQ UNITS}) \\ c_v \left( \frac{\partial}{\partial t} + u \frac{\partial}{\partial r} \right) \ln p p^{-\gamma} &= \frac{1}{\rho T} \frac{J^2}{\sigma} = \left\{ \frac{\sigma}{\rho T} (\bar{\mathbf{E}} + \bar{\mathbf{V}} \times \bar{\mathbf{B}})^2 \right. \\ &\quad \left. - \frac{1}{\rho T \sigma \mu^2} (\nabla \times \bar{\mathbf{B}})^2 \right\} \\ \frac{\partial B_\phi}{\partial t} + \frac{1}{r} \frac{\partial}{\partial r} (r u B_\phi) &= \frac{1}{\mu \sigma} \left( \frac{\partial^2 B_\phi}{\partial r^2} + \frac{2}{r} \frac{\partial B_\phi}{\partial r} \right) \end{aligned}$$

Where:  $\bar{\mathbf{V}} = (u, 0, 0)$   
 $\bar{\mathbf{B}} = (B_r, 0, B_\phi)$   
 $\bar{\mathbf{E}} = (0, E_\theta, 0)$

**Figure 2.** Basic time-dependent equations of mass, momentum, energy conservation and induction for a finitely conducting plasma which is permeated by a magnetic field. Gravitational attraction to the sun is negligible and therefore neglected. Thermal conduction and viscosity are not considered.

TRANSFORM P.D.E. TO O.D.E. BY USING THE FOLLOWING SIMILARITY TRANSFORMATIONS (LEE & CHEN):

$$\begin{aligned} \rho &= \rho_0 \psi(\eta) \\ u &= (V - u_0) \phi(\eta) \\ p &= \gamma^{-1} \rho_0 (V - u_0)^2 f(\eta) \\ B_\phi &= B_{\phi 0} b(\eta) \end{aligned} \quad \begin{aligned} \eta &= \frac{r}{R(t)} \\ \text{Where: } V &= \frac{dR}{dt} = \text{Shock Velocity} \\ u_0 &= \text{Undisturbed Solar Wind Velocity} \end{aligned}$$

BOUNDARY CONDITIONS:

<p>At Shock:</p> $\begin{aligned} [\rho u] &= 0 \\ [\rho u^2 + p + \frac{B_\phi^2}{2\mu}] &= 0 \\ [\rho u v_\phi - \frac{B_r B_\phi}{\mu}] &= 0 \\ \left[ \frac{\gamma}{\gamma-1} \frac{p}{\rho} + \frac{1}{2} (u^2 + v_\phi^2) + \frac{B_\phi^2}{\mu \rho} - \frac{B_r B_\phi}{\mu \rho} \frac{v_\phi}{u} \right] &= 0 \\ [B_r] &= 0 \\ [u B_\phi - v_\phi B_r] &= 0 \end{aligned}$	<p>At Piston:</p> $\begin{aligned} u_p &= \frac{dR_p}{dt} \\ &= \frac{d[\eta_p R(t)]}{dt} \\ &= \eta_p V \\ \phi_p &= \left( \frac{V}{V - u_0} \right) \eta_p \\ &= k \eta_p \end{aligned}$
--	---

**Figure 3.** Similarity transformation equations and boundary conditions for a double-shock ensemble which propagates into an ambient plasma which moves radially with a velocity  $u_0$ . The crossed-out terms in the shock jump equation may be omitted if  $M_{A\phi}^{-2} < 1.0$ .

small compared to one. It is also important to note that the parameter  $k = V/(V - u_0)$  allows consideration of any shock velocity  $V$  superimposed on a solar wind of velocity  $u_0$ . The value  $k = 1$  reproduces the similarity solutions (neglecting the Lorentz force, joule heating,

and induction equation) found by *Parker [1963]* and *Simon and Axford [1966]*. The reverse shock problem is solved by noting that  $V_R$  (the reverse shock velocity) is less than the new value of the solar wind velocity  $u_0$  through which it is moving, and thus  $k < 1$ ; whereas the forward shock (velocity =  $V_F$ ) problem is solved for  $\eta \leq 1$  the reverse shock problem is solved for  $\eta \geq 1$  as noted by *Lee [1965]*. The latter solution is then "folded over" to match the discontinuity where the pressures and velocities must be matched in this "two-point" boundary-value problem.

The ordinary differential equations are given in figure 4 which also gives the definitions of the transverse Alfvén Mach number and magnetic Reynolds number.

$$\begin{aligned}
 & \text{O. D. E.} \\
 & (k\eta - \phi) \frac{\psi'}{\psi} - \phi' + \frac{2(k\eta - \phi)}{\eta} = 0, \quad (\gamma' = \frac{d(\gamma)}{d\eta}) \\
 & (k\eta - \phi) \psi \phi' - \frac{1}{\gamma} f' - M_{A\phi}^{-2} b(b' + \frac{b}{\eta}) = 0 \\
 & (k\eta - \phi) \left[ \frac{f'}{\gamma} - \frac{\gamma \psi'}{\psi} \right] - 2k(\gamma - 1) = \begin{cases} -\gamma(\gamma - 1)(\frac{E_\theta}{uB_\phi})^2 R_M M_{A\phi}^{-2} \frac{(\phi b)^2}{f} \\ -\gamma(\gamma - 1) R_M^{-1} M_{A\phi}^{-2} \frac{1}{f^2} [(\eta b)']^2 \end{cases} \\
 & (k\eta - \phi) \frac{b'}{b} - \phi' + \frac{k\eta - \phi}{\eta} = -R_M^{-1} \left[ \frac{b''}{b} + \frac{2b'}{\eta b} \right]
 \end{aligned}$$

Where:  $k = \frac{V}{V - u_0} = \text{Constant}$   
 $M_{A\phi} = \frac{V - u_0}{B_{\phi 0} / (\mu \rho_0)^{1/2}} = \text{Constant}$   
 $R_M = R(V - u_0) \mu \sigma = \text{Constant or } R_M(\eta)$

**Figure 4.** Ordinary differential equations which result when the transformation shown in figure 3 is applied to the partial differential equations in figure 2. Note that  $M_{A\phi}$  must be constant as required by the radial dependence of  $B_{\phi 0}$  and  $\rho_0$ , hence the constancy of  $V - u_0$ . The lower (equivalent) joule heating term is used in this paper. A perfect gas with polytropic exponent  $\gamma$  is assumed.

The upper term on the right side of the energy equation (containing the electric field explicitly) was considered in the earlier work [*Dryer, 1970*]. It was found, however, that numerical instabilities were introduced when the product  $(\gamma - 1)(1 - E_\theta / uB_\phi)^2 R_M$  exceeded 100. The results discussed in this paper are found with the use of the lower expression on the right side of the energy equation. Further details are given in the appendix.

The earlier solutions examined the introduction of anomalous conductivity near the piston [*Dryer, 1970*], as well as near the forward shock [*Eviatar and Dryer,*

1970]. The present results (noting the persistent, disturbed conditions behind shocks as observed by the VLF electric field measurements) assume the conductivity to be less than classical *everywhere* between the piston and the two shocks (thus,  $R_M$  is taken as constant within this region). Similarity is therefore maintained from a mathematical sense; from a physical view, the fact that  $R \sim \text{time}$  requires that  $\sigma \sim (\text{time})^{-1}$ . It is not known if the latter requirement (namely, that the conductivity at a given  $\eta$  decreases with time) is justified on physical grounds. The following results, however, are found assuming that the restrictions (spherical symmetry, applicability to the vicinity of the solar equatorial plane,  $\sigma \sim t^{-1}$ ) are not important in the determination of basis features of the double-shock problem.

## RESULTS

### Nondimensional Parameters between the Piston and Forward Shock

The effect of  $k$  is shown in figure 5 for a typical case

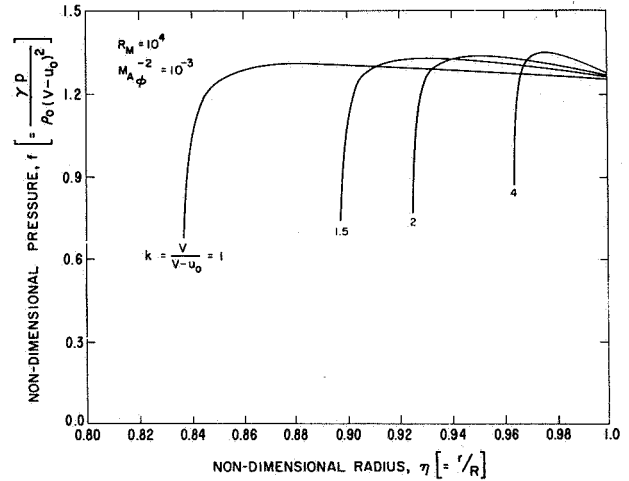


**Figure 5.** The effect of the relative velocity between the forward shock and solar wind velocities on the non-dimensional pressure distribution,  $f$ , for anomalous electrical conductivity ( $R_M = 10^4$ ,  $M_{A\phi}^{-2} = 10^{-3}$ ).

where  $M_{A\phi}^{-2} = 10^{-3}$  and  $R_M = 10^4$ . The nondimensional pressure  $f$  is shown to achieve a physically meaningful value for  $k = 1.0, 1.5, 2.0$ , and  $4.0$ . It is recalled that the pressure goes to zero at the piston (the minimum value of  $\eta$  for each case) when the fluid is infinitely conducting [*Lee and Chen, 1968*]. The polytropic

exponent  $\gamma = 5/3$  is used for all of the calculations in this paper.

The effect of finite conductivity (again for the pressure) is shown in figure 6 for the special case  $k = 2$ .

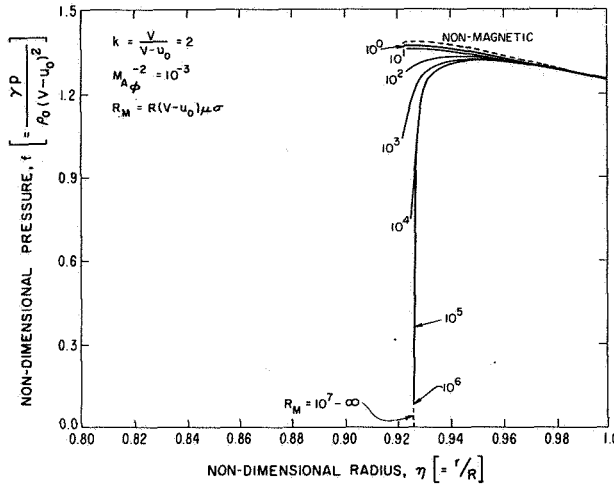


**Figure 6.** The effect of anomalous conductivity on the nondimensional pressure distribution  $f$  for  $k = 2$ . Note that the nonphysical result for infinite electrical conductivity is gradually eliminated as the conductivity is first assumed to be classical (at 1 AU and a typical relative velocity of 100 km sec<sup>-1</sup>,  $R_M = 10^{14}$ ) and then increasingly "anomalously" low. The nonmagnetic case is shown as the limiting pressure distribution for  $k = 2$ ,  $M_{A\phi}^{-2} = 0$ , and  $\gamma = 5/3$ .

The result noted above for infinite conductivity is shown. A similar result, hardly discernible from the case where  $\sigma = \infty$ , is found when a classical value ( $\sigma = 10^4$  mhos  $m^{-1}$ ) is taken for typical solar wind conditions wherein  $R_M = 10^{14}$  at 1 AU. A decrease of eight orders of magnitude produces a small, but finite, pressure at the piston. However, more realistic piston pressures are found with additional decreases of the conductivity. The result for the limiting nonmagnetic case was found by considering the equations of motion without the magnetic terms or induction equation; the Parker [1963] and Simon and Axford [1966] solutions are recovered when  $k = 1$ .

The nondimensional density results for  $\psi$  are shown in figure 7, again for  $k = 2$ . The infinite density at the piston for the nonmagnetic case is clearly shown. Significant decreases are shown at the piston for the cases of infinite and anomalous conductivities. Note that finite, but still large, density increases (a factor of 20 over the ambient value) at the piston are found by the nonmagnetic numerical solutions [cf. Hundhausen and

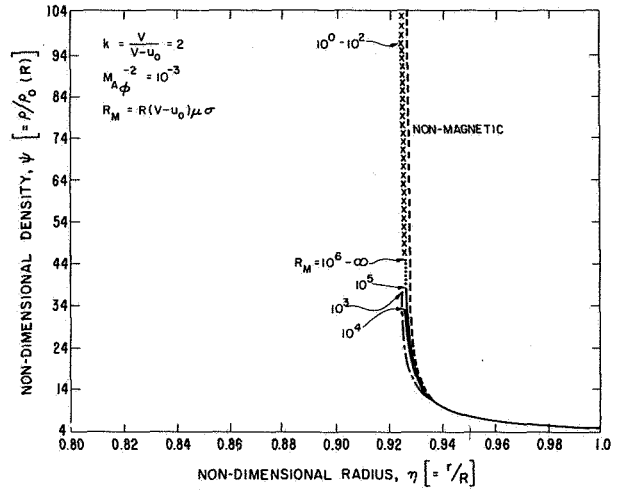


**Figure 7.** The effect of anomalous conductivity on the nondimensional density distribution  $f$  for  $k = 2$ . The density is infinite at the piston for the nonmagnetic case, reminiscent of the same result for  $k = 1$  found by Parker [1963] and Simon and Axford [1966]. Conversely, the density is finite at the piston for the case of infinite conductivity [Lee and Chen, 1968]. The nonmagnetic case is recovered as the conductivity approaches zero.

Gentry, 1969b]. The important role of the magnetic field is suggested by the results for moderately low values of  $\sigma$  in figure 7.

The nondimensional magnetic field is shown in figure 8 where we note that maximum joule heating will be

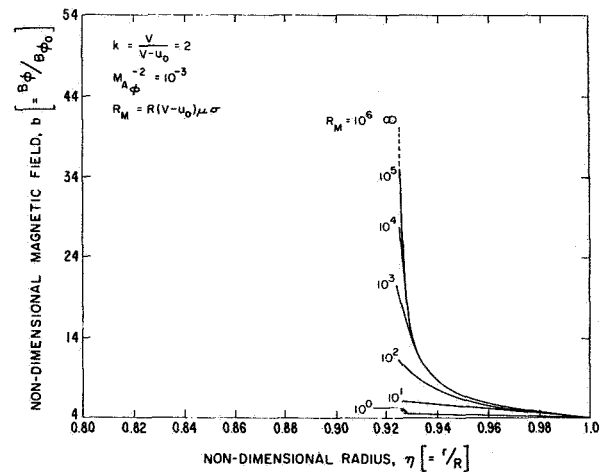


**Figure 8.** The effect of anomalous conductivity on the nondimensional azimuthal magnetic field distribution  $b$  for  $k = 2$ .

expected near the piston. The expected rise in temperature is clearly demonstrated in figure 9. The non-

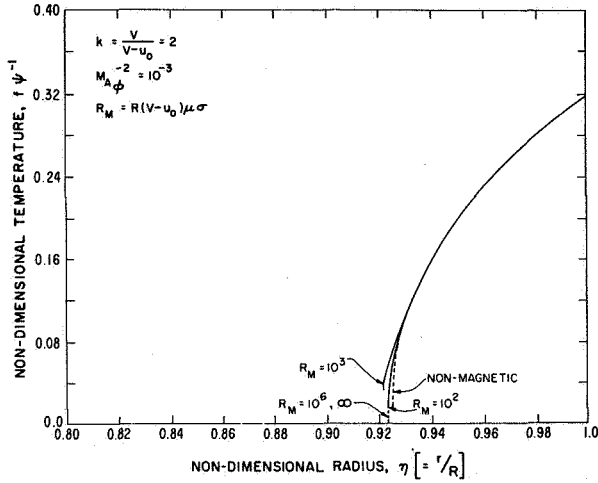


**Figure 9.** The effect of anomalous conductivity on the nondimensional temperature distribution  $f\psi^{-1}$  for  $k = 2$ .

dimensional velocity is shown in figure 10 where no change is seen in the magnitude of the convective velocity when the conductivity is decreased by many orders of magnitude. This velocity insensitivity is anticipated since the joule heating is expected to affect the relative magnitudes of the magnetic and thermal energy densities with a minor effect on the kinetic energy density.

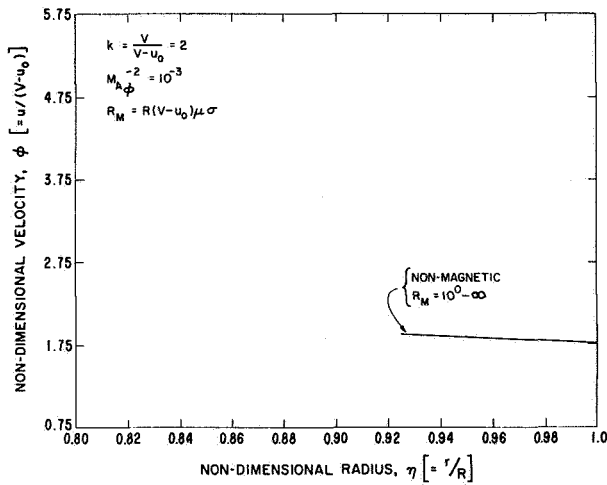


**Figure 10.** The effect of anomalous conductivity on the nondimensional velocity distribution  $\phi$  for  $k = 2$ .

### Energy Budget

The relative energies in the disturbed plasma are now examined explicitly for the flow between the forward shock and the piston. Figure 11 shows the integral for the three energies—kinetic, thermal, and magnetic—contained between these two boundaries and formed within a unit solid angle of 1 steradian. The second and

$$E(t) = \int_{r_p}^{R(t)} \left[ \frac{1}{2} \rho u^2 + \frac{p}{\gamma-1} + \frac{B_\phi^2}{2\mu} \right] r^2 dr / \text{STERADIAN}$$

$$= \rho_0 R^3 (V-u_0)^2 L$$

$$\text{Where } L = \int_{\eta_p}^1 \left[ \frac{\psi \phi^2}{2} + \frac{f}{\gamma(\gamma-1)} + \frac{b^2}{2M_{A\phi}^2} \right] \eta^2 d\eta$$

$$= \text{FUNCTION OF } (k, M_{A\phi}, R_M)$$

**Figure 11.** Energy integral for the sum of kinetic, thermal, and magnetic energies contained between the piston and the forward shock. A similar integral, not given here, may be written for the disturbed plasma between the reverse shock and the piston.

third lines in the figure are found by applying the similarity transformations given in figure 3. The parameter  $L$  is seen to be a function of  $k$ ,  $M_{A\phi}$ , and  $R_M$ . For a given shock observation, the energy is found directly once the following parameters are measured: the ambient transverse field  $B_\phi^0$ , the shock velocity  $V$ , ambient solar wind velocity  $u_0$ , ambient density  $\rho_0$ , and, of course, the forward shock position  $R$ . A similar calculation is made for the flow between the piston and the reverse shock to complete the total energy contained within the disturbed plasma and thus equal to the mechanical energy released during the flare process.

The energy budgets for several values of  $M_{A\phi}^{-2}$  ( $10^{-2}$ ,  $10^{-3}$ ) are given for  $1 \leq R_M \leq \infty$  and  $k = 1.0, 1.5, 2.0$ , and  $4.0$  in figures 12, 13, 14, and 15, respectively. The nonmagnetic result is shown on the left side of each figure for comparison. Of greatest interest is the observation that the electrical conductivity must be reduced (say, at 1 AU, from the  $10^4$  mhos  $m^{-1}$  figure mentioned previously) by more than 6 orders of magnitude before the joule heating can effectively raise the thermal energy density at the expense of the magnetic. In fact, further reduction of this anomalous conductivity causes even the kinetic energy density to decrease by several percent.



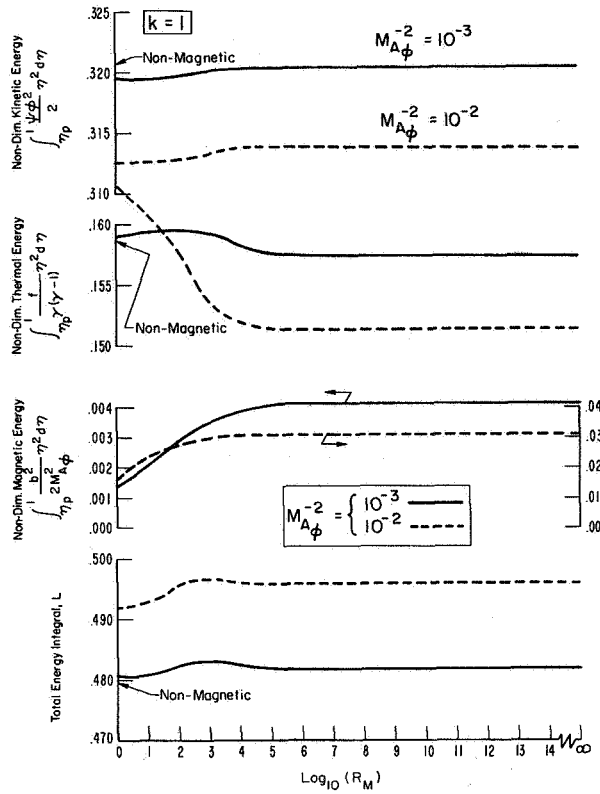


**Figure 12.** The effect of magnetic Reynolds number on the energy budget within the piston–forward-shock combination for several values of  $M_{A\phi}^{-2}$  when there is no solar wind ( $k = 1$ ).

A second observation is also of interest: for the hypothetical case of  $u_0 = 0$ —that is,  $k = 1$ —the nonmagnetic budget shows that the ratio of kinetic energy density to thermal energy density is 2:1. This ratio shifts predominately in favor of the kinetic energy when  $k > 1$ ; that is, when the solar wind is turned on so that the ambient flux is “shocked” and incorporated into the budget of the disturbed flow. A third observation is concerned with the range of this computation’s validity: as  $M_{A\phi}^{-2}$  approaches 1, the need to consider the transverse equation of momentum arises as discussed by Lee and Chen [1968]. As a result, the present solution is expected to be valid to values of  $M_{A\phi}^{-2}$  as high as  $10^{-1}$  after which  $L$  diverges rapidly.<sup>1</sup>

<sup>1</sup>In this connection, figure 6 and table II of Dryer [1970] are in error for values of  $M_{A\phi}^{-2}$  other than  $10^{-3}$ . As shown here (figs. 12–15), the value of  $L$  increases slowly at first as  $M_{A\phi}^{-2}$  is increased.

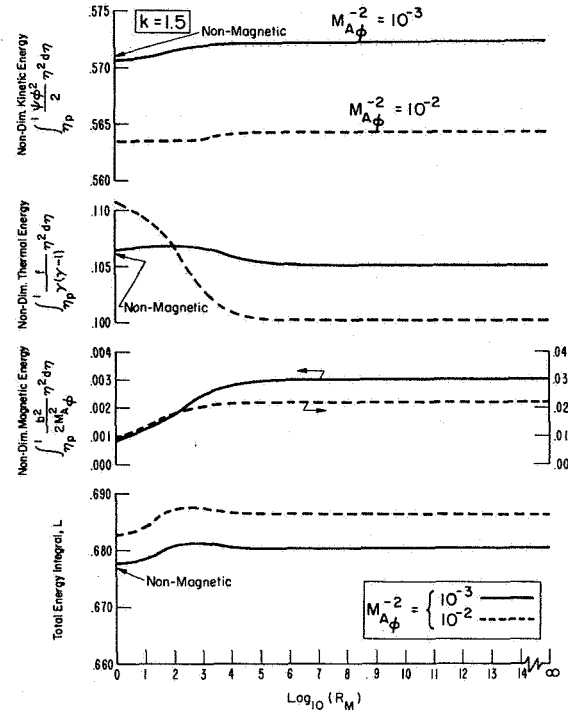


**Figure 13.** The effect of magnetic Reynolds number on the energy budget within the piston–forward-shock combination for several values of  $M_{A\phi}^{-2}$  when  $k = 1.5$ .

The kinetic energy flux in the disturbed plasma has been experimentally measured between the forward shock and the piston (and, possibly, behind it in some cases where the data are inconclusive) by Hundhausen *et al.* [1970] for a number of shocks (approximately six events). Their results for two of these cases are shown on the right side of figure 16. Also shown, for comparison, are the theoretical results (which include the thermal and magnetic energies) found by neglecting the possible presence of the disturbed flow between the piston and the reverse shock. Note that agreement is good for the 15 February 1967 shock but not for the 18 December 1965 shock. It is possible that the discrepancy is due to the decreased validity of the theory because  $M_{A\phi}^{-2}$  is close to 1; an additional contributing factor may be the lack of detailed data during the early years of plasma measurements.

#### Double-shock Structure

“Snapshots” of the nonmagnetic double-shock structure have been presented by Hundhausen and Gentry

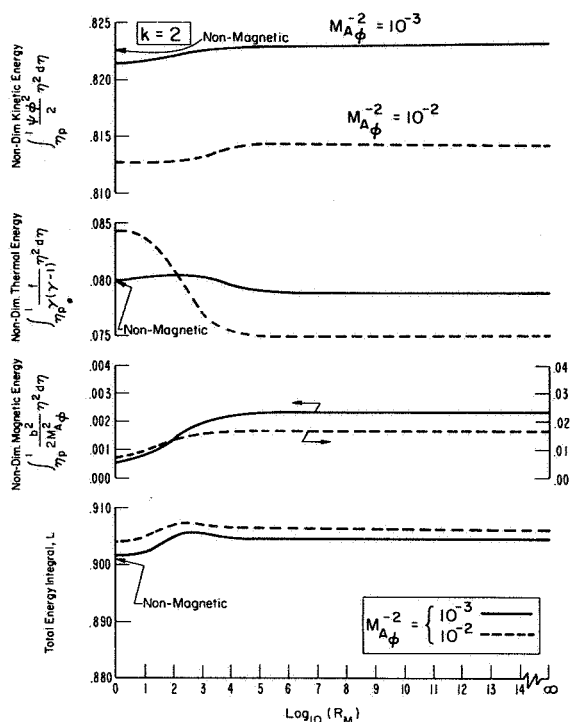


**Figure 14.** The effect of magnetic Reynolds number on the energy budget within the piston-forward-shock combination for several values of  $M_{A\phi}^{-2}$  when  $k = 2$ .

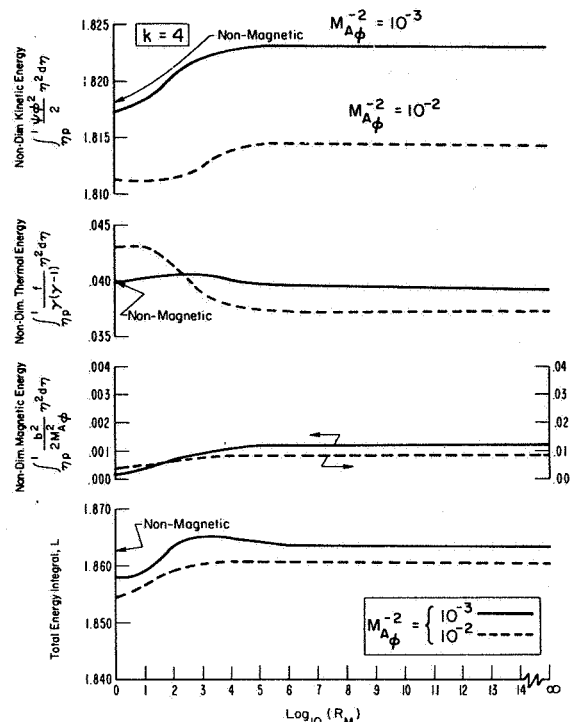


**Figure 15.** The effect of magnetic Reynolds number on the energy budget within the piston-forward-shock combination for several values of  $M_{A\phi}^{-2}$  when  $k = 4$ .

[1969a] and compared with the similarity results of *Simon and Axford* [1966] in a more detailed study [*Hundhausen and Gentry*, 1969b]. The analysis discussed above is now extended to relax the earlier similarity assumptions of (1) zero solar wind velocity and (2) nonmagnetic considerations. The assumption of negligible thermal energy density in the ambient solar wind (both in front of the forward shock and in the “new” solar wind which follows the reverse shock) is retained in view of the dominant presence of the kinetic energy flux.

For the purpose of presenting additional “snapshots” (in the present case, spatial distributions of all parameters as a function of the nondimensional radius  $\eta = r/R$ ), a specific candidate for a double-shock structure is chosen. The case in point is concerned with the 29 August 1966 shock reported by *Chao* [1970] and others. This case is chosen only in order to provide typical values of ambient number density and velocity  $n_0$  and  $u_0$ , forward shock velocity  $V$ , and azimuthal magnetic field component  $B_{\phi_0}$ , which are required by the theory. A detailed comparison of the experimental (plasma and field) data with the theory is presently nearing completion [*Dryer et al.*, 1971]. The present

Shock	Reference	k	$M_{A\phi}$	$R_M$	L	E ERGS	(E) <sub>EXP</sub> ERGS
18 Dec '65	Hundhausen, Bame, & Montgomery (1970), JGR  Taylor, (1969) Solar Phys.	3.4	1.2	$10^{14}$	1.5	$5 \times 10^{31}$	$1.4 \times 10^{31}$
15 Feb '67	Hirshberg et al. (1970) JGR  Hundhausen (1970) Ann. Geophys.	2.2	6.6	$10^{14}$	.95	$11 \times 10^{31}$	$9 \times 10^{31}$

**Figure 16.** Comparison of theoretical and experimental estimates for the energy in the disturbed plasma caused by two flares.  $E$  is found from the equation in figure 11 and the experimentally determined parameters listed above, assuming classical conductivity.  $(E)_{\text{Exp}}$  includes only the kinetic energy flux [*Hundhausen et al.*, 1970]. (Assumed: Solid angle =  $\pi$  ster)

discussion is limited to the theoretical results for the spatial distribution of all parameters as a function of nondimensional radius  $\eta$ .

The following values were found from data provided by *N. F. Ness* and *J. H. Wolfe* [private communications] and *Chao* [1970]:  $n_0 = 4.0 \text{ cm}^{-3}$ ,  $u_0 = 345 \text{ km sec}^{-1}$ ,  $V = 467 \text{ km sec}^{-1}$ , and  $B_{\phi_0} = 0.74\gamma$ . The shock velocity is almost identical with that found by *Hundhausen* [1970a, p. 470]. Thus,  $k = 3.83$  and  $M_{A\phi}^{-2} = 4.41 \times 10^{-3}$ ; and the polytropic exponent  $\gamma$ , is assumed to be  $5/3$  for this example. Infinite electrical conductivity and a low value of anomalous conductivity are examined.

The flow between the piston and forward shock is directly found by the method and parameters noted above. The second part of the flow in our "two-point" boundary value problem is determined uniquely once the "new" solar wind values of density and ambient magnetic field are specified behind the reverse shock. The "new" solar wind is assumed to obey the "old" requirements:  $n_0 \sim r^{-2}$  and  $B_{\phi_0} \sim r^{-1}$ . Thus, we are free to specify new constants of proportionality under the restriction that: (1) the density in the new coronal expansion will be greater than its original value had the disturbance not come by [cf. *Hundhausen and Gentry*, 1969b]; and (2) the hotter coronal base condition will require a higher plasma velocity, which in turn will cause the magnetic topology to become more nearly radial. Hence  $B_{\phi_0}$  will be less than its original value at the same (as yet undetermined) position. The new constants of proportionality, then, are arbitrarily chosen to be twice and  $2/3$  the original values for the density and azimuthal magnetic field components, respectively, for this example. An iterative computation is then performed until the essential boundary conditions at the common piston are satisfied: equality of total pressures and velocity on contiguous sides of the piston. The final results of this iteration produce a new solar wind velocity,  $u_0 = 519 \text{ km sec}^{-1}$ , within which the reverse shock velocity propagates outward at a velocity of  $437 \text{ km sec}^{-1}$ . (The familiar analogy is that of the child who tries to walk unsuccessfully *down* an "up" escalator and arrives at the top at a later time than his brother who decides to walk *up* the moving stairs.) The resulting values of  $k$  and  $M_{A\phi}^{-2}$  are  $-5.34$  and  $2.18 \times 10^{-3}$ , respectively, for the reverse shock-piston part of the flow.

The spatial distributions of velocity, density, thermal pressure, temperature, and azimuthal magnetic field are given as a function of the nondimensional radius  $\eta$  in figures 17, 18, 19, 20, and 21, respectively. Note that the disturbed plasma occupies a region of space  $0.935 \leq \eta \leq 1.00$ , which represents nearly 20 percent of the volume encompassed by the forward shock at any time for the combination of the three parameters:  $k$ ,  $M_{A\phi}^{-2}$  and  $\gamma$  given above. When finite conductivity is

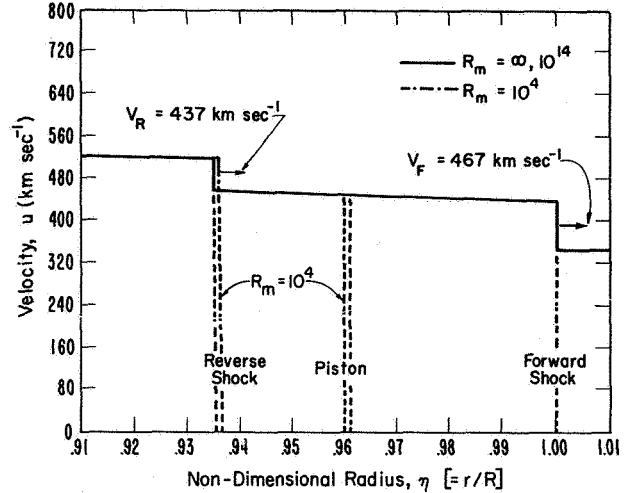


**Figure 17.** Velocity distribution within the double-shock ensemble described in the text.  $V_F$  and  $V_R$  refer to the forward and reverse shock velocities, respectively. The values shown here refer to the time when the forward shock was first detected by Pioneer 7 on 29 August 1966 at  $R = 1.01 \text{ AU}$ . Note the imperceptible change (shown in exaggerated form) in piston and reverse shock positions when  $R_m$  is reduced. The reverse shock velocity, found as part of the iterative procedure, is insensitive to the degree of anomalous conductivity chosen for the piston-reverse shock computation.

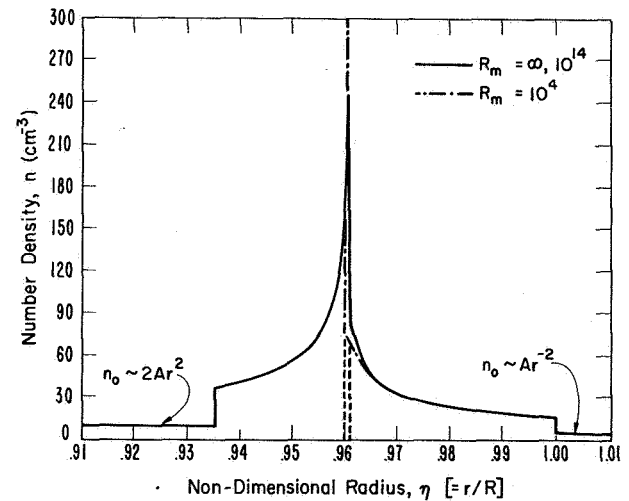


**Figure 18.** Number density distribution within the double-shock ensemble described in the text.  $A$  is a constant of proportionality for the undisturbed solar wind.

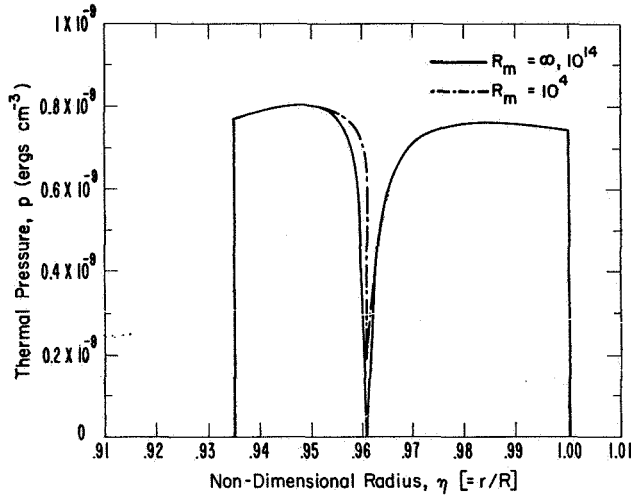


**Figure 19.** Thermal pressure distribution within the double-shock ensemble described in the text. Note that anomalous electrical conductivity removes the non-physical pressure at the piston.

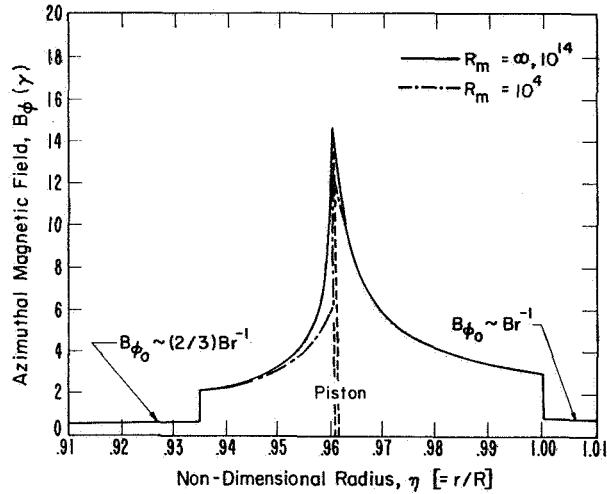


**Figure 20.** Temperature distribution within the double-shock structure described in the text. Note that anomalous electrical conductivity removes the non-physical temperature at the piston.

“turned on,” the piston moves slightly rearward and the reverse shock moves imperceptibly forward as shown in slightly exaggerated form in figure 17.

Several general comments are made with respect to each plasma parameter. In figure 17 it is seen that the velocity jump ( $\sim 100 \text{ km sec}^{-1}$ ) at the forward shock is followed by a very gradual increase until the reverse shock is encountered. A smaller velocity change is seen at the latter position. Figure 18 shows, for infinite con-

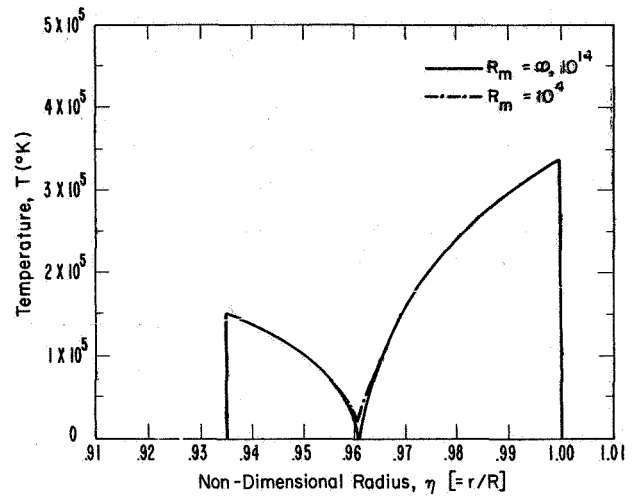


**Figure 21.** Azimuthal magnetic field magnitude within the double-shock ensemble described in the text. Note that  $\beta (=p/(B^2/2\mu))$  contiguous to the piston on the reverse shock’s “side” is greater by nearly an order of magnitude than its value on the forward shock’s “side.” The sums of the two pressures, however, are identical at the piston itself, as required. “B” is a constant of proportionality for the undisturbed solar wind ahead of the forward shock wave.

ductivity, a precipitous density increase on the reverse shock’s “side” of the piston. Figures 19 and 20 (for the infinite-conductivity case) show the nonphysical zero pressure and temperature, respectively, at the piston. The assumption of anomalous conductivity, however, removes this physically unrealistic condition. Figure 21 shows a maximum compression of the azimuthal magnetic field on both sides of the piston where the topology of the field approaches that for a contact discontinuity, as suggested in figure 1. When the electrical conductivity, is decreased by 10 orders of magnitude, however, the peaks of *all* precipitous changes of thermodynamic and magnetic properties at the piston are still present. One expects that thermal conduction and viscous dissipation would change this picture. The piston “boundary layer” would be expected to be “smeared” with the introduction of these additional transport properties, as in the case of earth’s magnetopause. As noted earlier, work presently in progress [Dryer *et al.*, 1971] compares these results with experimental data (for a double-shock candidate) observed by an essentially inertial observer (Pioneer 7). A statistically valid test of the theory, however, will require a much larger experimental sample than those discussed herein as well as in the existing literature on piston-driven shocks.

## CONCLUDING REMARKS

It has been shown that similarity theory can be applied to constant velocity, double-shock wave ensembles with explicit consideration of the interplanetary magnetic field and ambient solar wind kinetic energy flux. It has also been shown that nonphysical results for thermal pressure and temperature at the piston for the case of infinite electrical conductivity were removed in a gradual way by permitting the introduction of an increasingly larger degree of anomalous electrical conductivity within the shocked plasma. The consequent joule heating produces significant conversion from magnetic to thermal energy when the conductivity decreases by more than 10 orders of magnitude below the classical value. Other anomalous transport properties, such as thermal conductivity and [collisionless] coupling of various species, may also be present; but no consideration of these possibilities has been taken into account. Furthermore, there is no requirement (in this magnetogasdynamic analysis to specify the nature of the mechanism(s) required for the anomalous conductive property. It is theoretically possible to determine, indirectly, the order of magnitude of the anomalous conductivity by making detailed measurements of all plasma parameters. These measurements would be made either at an inertially stationary observation point (as a function of time) or at a number of radially spaced points (preferably located within a unit solid angle of  $\pi$  steradians centered at the sun and including the responsible flare).

In this connection, the conductivity level might be inferred from the level of the density and magnetic field magnitudes in the vicinity of the piston, which in turn may include a rich supply of alpha particles as a last vestige of the flare itself [Hirshberg *et al.*, 1970a, b]. The problem of unambiguous identification of reverse shocks has been pointed out by Burlaga [1970] since they are expected to be weaker than forward shocks and diffusive in their gross structure [Hundhausen *et al.*, 1970]; as a result, their identification requires detailed information (high resolution) on both plasma and field.

It is noted by Hirshberg *et al.* [1970b] that most of the piston-driven shocks in their study (identified by high alpha/proton abundances) exhibited shock velocities at 1 AU that were about 0.8 the average speed required by tentative flare-shock time delays. The implication is that these shocks moved outward from the sun at nearly constant velocity; hence the present assumption of constant velocity is justified. A more serious limitation of the theory is the spherically symmetric assumption. Criticism of this assumption would indeed be justified if measurements of a particular ensemble were made near the boundaries of a highly

collimated ejection. Measurements near the central radius of the flare, however, would be expected to be amenable to comparison with theory inasmuch as the effect would be equivalent to a spherical ejection as noted by DeYoung and Hundhausen [1971], who performed numerical studies of nonspherical, nonmagnetic blast waves. Also, at least one remarkable west-limb event observed by the Culgoora 80-MHz radioheliograph on 30 March 1969 [Smerd, 1970] gave rise to an unambiguous shock-associated type II burst that clearly exhibited a greater-than-180° extent projected on a plane perpendicular to the line of sight. It is not known, of course, if this was a unique event or whether similar events are common.

Finally, comparison of magnetic field and density distributions for the complete ensemble (figs. 18 and 21) shows that an inertial observer would first see a peak in the former followed by a peak in the latter parameter. This result differs from the time-independent analysis of Schubert and Cummings [1969].

## ACKNOWLEDGMENTS

It is a pleasure to thank N. F. Ness and J. H. Wolfe for the use of their unpublished data, and G. H. Endrud for programming the equations on the computer. Discussions with T. S. Lee and T. Chen were very beneficial and are gratefully acknowledged.

## APPENDIX: Computational Details

Here we briefly summarize essential details involved in the solution of the transformed equations of motion and the induction equation. The basic equations, with the usual symbols for the dependent variables, are shown in figure 2. The transformation equations are given in figure 3. The boundary conditions at the shock, neglecting the ambient internal energy, are:

$$f(\eta_s) = \frac{2\gamma}{\gamma + 1} \quad (A1)$$

$$\psi(\eta_s) = \frac{\gamma + 1}{\gamma - 1} \quad (A2)$$

$$\phi(\eta_s) = k - \frac{\gamma - 1}{\gamma + 1} \quad (A3)$$

$$b(\eta_s) = \frac{\gamma + 1}{\gamma - 1} \quad (A4)$$

The equations are integrated from the shock  $\eta_s$  to the piston position  $\eta_p$ . The latter is found when  $\eta_p = \phi/k$  (fig. 3).

The transformed equations are shown in figure 4 where the single and double primes indicate ordinary first and second derivatives, respectively, with respect to

$\eta$ . Some comments are now made for the two cases of infinite and finite electrical conductivity:

#### Solution for the Infinite-Conductivity Case

The infinite conductivity case is formed from the basic equations when  $R_M = \infty$ . The equations then take the following form:

$$\phi' = \frac{2f}{\eta\gamma} \frac{\gamma\alpha - \eta k(\gamma-1)}{M_A^{-2} b^2 + f - \alpha^2 \psi} \quad (A5)$$

$$b' = \frac{b}{\alpha} \left[ \phi' - \frac{\alpha}{\eta} \right] \quad (A6)$$

$$\psi' = \frac{\psi}{\alpha} \left[ \phi' - \frac{2\alpha}{\eta} \right] \quad (A7)$$

$$f' = \frac{f}{\alpha} \left[ 2k(\gamma-1) + \gamma \left( \phi' - \frac{2\alpha}{\eta} \right) \right] \quad (A8)$$

where  $\alpha = k\eta - \phi$ , and  $\eta_s = 1$  at the shock wave.

A Runge-Kutta fourth-order technique was used to integrate this set of equations. The same basic procedure was used for both the forward and the reverse shock calculations with one exception:  $k < 1$  for the reverse shock, so that problem was solved for  $\eta \geq 1$ . For the reverse shock case, values for the shock velocity and the solar wind velocity behind the shock were iterated until the bulk velocity and the total pressure matched the same parameters for the forward shock case at the piston. The reverse shock solution was then translated to match the forward shock at the piston.

#### Solutions for the Finite-Conductivity Case

The equations are second order and nonlinear in  $b$  in the finite conductivity case; thus, a boundary condition for  $b'$  is required. No independent relationship for  $b'$  is known, so an approximation was made by solving for  $b'$  in terms of  $b''$ :

$$b' = \frac{b\phi' - \frac{\alpha b}{\eta} - \frac{b''}{R_M}}{\alpha + (2/R_M\eta)} \quad (A9)$$

This equation is the same as (A6) in the infinite conductivity case when  $R_M \rightarrow \infty$ .

Reasonable values of  $b''$ , as suggested by results from the infinite conductivity case, were substituted into (A9) to provide the required boundary condition. For lower values of  $R_M$ , values of  $b''$  were selected to provide a smooth change in all variables between the limiting cases of infinite conductivity and nonmagnetic flow.

The Runge-Kutta fourth-order solution of the second-order set of equations proved to be unstable for high

values of  $R_M$ . An approximate solution was obtained by a first-order solution for  $b$  with  $b' = b'(b'')$  [eq. (A9), using the value of  $b''$  from the previous step in the calculations]. This approximate solution corresponded very closely with the infinite conductivity case at  $R_M = 10^{14}$ .

No such approximation was made for solutions with low values of  $R_M$ . To reduce the truncation error, however, a Ricatti transformation [ $b' = eb$ ] was applied. For the reverse shock case, the two solutions matched at  $R_M = 10^6$ .

The same basic procedure used in the infinite conductivity case was applied to calculate the reverse shock and to match total pressures and bulk velocities at the piston. Total CDC 3800 computer time is less than 4 min for the complete double-shock ensemble.

#### REFERENCES

- Belcher, J. W.; Davis, L. Jr.; and Smith, E. J.: Large Amplitude Alfvén Waves in the Solar Wind. *J. Geophys. Res.*, Vol. 74, 1969, p. 2302.
- Burlaga, L. F.: Micro-scale Structures in the Interplanetary Medium. *Solar Phys.*, Vol. 4, 1968, p. 67.
- Burlaga, L. F.: A Reverse Hydromagnetic Shock in the Solar Wind. *Cosmic Electrodyn.*, Vol. 1, 1970, p. 233.
- Burlaga, L. F.: Discontinuities and Shock Waves in the Interplanetary Medium and Their Interaction with the Magnetosphere. *Proc. Leningrad Symp. Solar-Terrest. Phys.*, May 11-20, 1970, D. Reidel Publishing Company, Dordrecht-Holland, 1971 (in press).
- Carmichael, H.: Discussion following paper by A. J. Dessler, Hydromagnetic Picture of Earth Storms. *J. Phys. Soc. Japan*, Vol. 17 (Supp. A-II), 13, 1962. (Proc. Int. Conf. Cosmic Rays and the Earth Storm, Kyoto, 4-15 Sept. 1961).
- Chao, J. K.: Interplanetary Collisionless Shock Waves. *Massachusetts Institute of Technology Report CSR TR-70-3*, February 1970.
- DeYoung, D. S.; and Hundhausen, A. J.: Non-spherical Propagation of a Flare-Associated Interplanetary Blast Wave. *J. Geophys. Res.*, Vol. 76, 1971, p. 2245.
- Dryer, M.; Smith, Z. A.; Endrud, G. H.; and Wolfe, J. H.: Some Observations of the August 29, 1966, Interplanetary Shock Wave by Pioneer 7, (abstract), *EoS Trans., Amer. Geophys. Union*, Vol. 52, 1971, p. 336.
- Dryer, M.: Some Effects of Finite Electrical Conductivity on Solar Flare-Induced Interplanetary Shock Waves. *Cosmic Electrodyn.*, Vol. 1, 1970, p. 348.
- Eviatar, A.; and Dryer, M.: Finite Conductivity and Interplanetary Piston-Driven Shock Waves. *Cosmic Electrodyn.*, Vol. 1, 1970, p. 371.

- Hirshberg, J.; Alksne, A.; Colburn, D. S.; Bame, S. J.; and Hundhausen, A. J.: Observation of a Solar Flare Induced Interplanetary Shock and Helium-Enriched Driver Gas. *J. Geophys. Res.*, Vol. 75, 1970a, p. 1.
- Hirshberg, J.; Asbridge, J. R.; and Robbins, D. E.: The Helium-Enriched Interplanetary Plasma from the Proton Flares of August/September, 1966 (abstract). *EoS Trans. Amer. Geophys. Union*, Vol. 51, 1970b, p. 818.
- Hundhausen, A. J.: Composition and Dynamics of the Solar Wind Plasma. *Rev. Geophys. Space Phys.*, Vol. 8, 1970a, p. 729.
- Hundhausen, A. J.: Solar Wind Disturbances Associated with Solar Activity. *Intercorrelated Satellite Observations Related to Solar Events* (Proc. Third ESLAB/ESRIN Symp. Noordwijk, The Netherlands, Sept. 16-19, 1969), edited by V. Manno and D. E. Page, D. Reidel Publishing Company, Dordrecht-Holland, 1970b.
- Hundhausen, A. J.; and Gentry, R. A.: Numerical Simulation of Flare-Generated Disturbances in the Solar Wind. *J. Geophys. Res.*, Vol. 74, 1969a, p. 2908.
- Hundhausen, A. J.; and Gentry, R. A.: Effects of Solar Flare Duration on a Double Shock Pair at 1 AU. *J. Geophys. Res.*, Vol. 74, 1969b, p. 6229.
- Hundhausen, A. J.: Interplanetary Shock Waves and the Structure of Solar Wind Disturbances. Presented at the Solar Wind Conference, Asilomar, California, 21-26 March 1971. (this volume).
- Hundhausen, A. J.; Bame, S. J.; and Montgomery, M. D.: Large-Scale Characteristics of Flare-Associated Solar Wind Disturbances. *J. Geophys. Res.*, Vol. 75, 1970, p. 4631.
- Korobeinikov, V. P.; and Nikolayev, Yu. M.: Shock Waves and Magnetic Field Configurations in Interplanetary Space. Symp. Solar-Terrestrial Physics, Leningrad, USSR, May 11-20, 1970 (abstract I 4-7).
- Lazarus, A. J.; Ogilvie, K. W.; and Burlaga, L. F.: Interplanetary Shock Observations by Mariner 5 and Explorer 34. *Solar Phys.*, Vol. 13, 1970, p. 232.
- Lee, T. S.: Unsteady Flows in an Unsteady Environment. *Phys. Fluids*, Vol. 8, 1965, p. 1266.
- Lee, T. S.; and Chen, T.: Hydromagnetic Interplanetary Shock Waves. *Planet. Space Sci.*, Vol. 16, 1968, p. 1483.
- Lee, T. S.; Chen, T.; and Balwanz, W. W.: Hydromagnetic Theory for Disturbances Following an Ideal "Solar Thermal Explosion" (abstract). *EoS Trans. Amer. Geophys. Union*, Vol. 51, 1970, p. 414.
- Neugebauer, M.; and Snyder, C. W.: Mariner 2 Observations of the Solar Wind; 2: Relation of Plasma Properties to the Magnetic Field. *J. Geophys. Res.*, Vol. 72, 1967, p. 1823.
- Parker, E. N.: *Interplanetary Dynamical Processes*. Chap. 8, 1963, Interscience Publishers, New York.
- Sagdeev, R. Z.: On Ohm's Law Resulting from Instability. *Magneto-Fluid and Plasma Dynamics, Proc. Symp. in Applied Mathematics*, Vol. 18, 1967, p. 281.
- Scarf, F. L.; Green, I. M.; Siscoe, G. L.; Intriligator, D. S.; McKibbin, D. D.; and Wolfe, J. H.: Pioneer 8 Electric Field Measurements in the Distant Geomagnetic Tail. *J. Geophys. Res.*, Vol. 75, 1970, p. 3167.
- Scarf, F. L.; and Siscoe, G. L.: The Pioneer 9 Electric Field Experiment: Part 2, Observations between 0.75 and 1.0 AU. *Cosmic Electrodyn.*, Vol. 2, 1971.
- Schubert, G., and Cummings, W. D.: The Double Shock Wave Structure in the Solar Wind. *J. Geophys. Res.*, Vol. 72, 1967, p. 5275.
- Schubert, G.; and Cummings, W. D.: Effect of High Electron-Proton Temperature Ratios on the Double Shock Wave Structure in the Solar Wind. *J. Geophys. Res.*, Vol. 74, 1969, p. 897.
- Simon, M.; and Axford, W. I.: Shock Waves in the Interplanetary Medium. *Planet. Space Sci.*, Vol. 14, 1966, p. 901.
- Siscoe, G. L.; Scarf, F. L.; Green, I. M.; Binsack, J. H.; and Bridge, H. S.: Very-Low-Frequency Electric Fields in the Interplanetary Medium: Pioneer 8. *J. Geophys. Res.*, Vol. 76, 1971, p. 828.
- Smerd, S. F.: Radio Evidence for the Propagation of Magnetohydrodynamic Waves Along Curved Paths in the Solar Corona. *Proc. ASA*, Vol. 1, 1970, p. 305.
- Sonett, C. P.; and Colburn, D. S.: The  $SI^+$  -  $SI^-$  Pair and Interplanetary Forward-Reverse Shock Ensemble. *Planet. Space Sci.*, Vol. 13, 1965, p. 675.
- Sonett, C. P.; Colburn, D. S.; Davis, L., Jr.; Smith, E. J.; and Coleman, P. J., Jr.: Evidence for a Collision-Free Magnetohydrodynamic Shock in Interplanetary Space. *Phys. Rev. Lett.*, Vol. 13, 1964, p. 153.
- Speiser, T. W.: Conductivity Without Collisions or Noise. *Planet. Space Sci.*, Vol. 18, 1970, p. 613.
- Sturrock, P. A.; and Spreiter, J. R.: Shock Waves in the Solar Wind and Geomagnetic Storms. *J. Geophys. Res.*, Vol. 70, 1965, p. 5345.

DISCUSSION *A. Hundhausen* There's one problem, in the choice of the data chosen. One expects a reverse shock because there is a flow from behind which is catching up with something already out in front of it. It seems you picked data where, in general, the velocity is decreasing with time. That would seem to me a rather highly unlikely candidate for a reverse shock.

*M. Dryer* That was quite right. We picked this as something to get our feet wet. I have data (not shown) which indicates the kinetic energy flux calculated the way you have suggested in the paper with Bame and Montgomery and indeed the kinetic energy flux does decrease with time. So this may have been—probably was—a blast wave.

*D. S. DeYoung* Did you include gravitational effects in your, symmetry solution?

*M. Dryer* No.

*D. S. DeYoung* So your temperature in the ambient medium before the shock arrives has to be zero; is that right?

*M. Dryer* That's right, and after the reverse shock has gone.

### COMMENTS

*D. S. DeYoung* I have a brief report on some calculations similar to those introduced this afternoon by Art Hundhausen. He described nonspherically symmetric numerical simulations of flare associated disturbances propagating into the interplanetary medium. All the calculations he discussed were done in a blast wave limit, which in this context means that the duration of the disturbance was much less than the propagation time to 1 AU and that the energy in the disturbance remained constant after initialization. I would like to discuss briefly some additional results obtained from essentially the same numerical method but which explore initial conditions other than this blast wave limit. The geometry is the same as previously discussed with spherical symmetry in the ambient solar wind and an axisymmetric flare associated disturbance. The most obvious case opposite to a blast wave is, of course, a driven disturbance. Such a case was simulated in an ambient solar wind identical to the one used for the blast calculations, a wind with a radial velocity at 1 AU of 400 km/sec, a number density of 12 and a temperature of about  $3.5 \times 10^4$  K, again at 1 AU. The same half-angle of  $15^\circ$  was subtended by the initial cone of disturbance material so that comparison could be made with the blast wave case. The driven disturbance (driven here really should be in quotation marks) is initialized as follows: The shock velocity was set at 1000 km/sec at 0.1 AU just as in the blast wave case, but as the disturbance then propagated outward in a radial direction, a flux of material was maintained flowing outward across the innermost radial boundary, again at 1000 km/sec. This outflow kept on until the shock front associated with the disturbance reached 1 AU; it is in this sense that I meant "driving" to be in quotation marks—that is, we have no piston, we are really just leaving the disturbance turned on, and it is thus not "driven" in the classical sense.

It should be remembered that leaving the disturbance turned on for such a long time represents an extreme case, and one would not expect to find such an event actually occurring on the sun. The transit time to 1 AU for this disturbance is about 40 hours, which gives a total mass for this event of  $10^{17}$  grams and a total kinetic energy of about  $10^{32}$  ergs. This is the mass and energy contained in the disturbance when its associated shock front reaches 1 AU.

The driven case arrives at 1 AU in about two-thirds the time required for the comparable blast wave. The radial velocity along the disturbance symmetry axis decreases most rapidly at small heliocentric distances for both the blast and the driven case, but the amount of deceleration is quite different. By the time the shock wave reaches 1 AU for the blast wave case the shock velocity is half its initial value, whereas the driven shock suffers only a 25 percent loss. The deceleration of both disturbances is strongest at small heliocentric distances because of the strong radial dependence of the ambient solar wind



density, which produces the greatest momentum transfer from the front to the ambient medium in regions close to the sun.

The decrease in transit time for the driven case can be understood in terms of the increased mass and energy present in the disturbance. These two parameters also affect the shape of the shock front at 1 AU in that they determine whether the dynamics of the disturbance at 1 AU is dominated by momentum or by pressure. It is useful to calculate the so-called equal mass radius, which is the distance from the sun at which the mass of the ambient solar wind contained in the disturbance cone is equal to the total amount of mass we have injected into the disturbance by the time the front passes 1 AU. If this radius is much less than 1 AU we expect the disturbance to have transferred most of its momentum to the ambient solar wind, to have been slowed considerably, and to have the shock front propagating more or less uniformly in all directions due to a high, uniform pressure behind the front. This is just what is seen in the blast wave case, with its slow-moving, broad shock front at 1 AU. If the equal mass radius is of the order of 1 AU, then the front is expected to be more rapidly moving, to be propagating primarily due to the directed momentum of the ejected flare associated material, and for the front to be more narrow and streamlined. This is what is seen in our driven case here. Although there is always some uncertainty in the angle subtended by the cone of disturbance material, for the driven case the cone angle is between  $30^\circ$  and  $45^\circ$ , giving an equal mass radius of about 0.8 AU. Another factor which contributes to a narrower shock front at 1 AU is the decrease in transit time of the driven disturbance, which allows less time for the hot, high pressure material directly behind the strong shock front to undergo expansion transverse to the original motion of the ejected material.

Another possible initial condition for a flare-associated disturbance is that in which the flare produces simply a hot region of gas at base of the corona. This material would not have an extraordinarily large radial velocity; in fact, it would share the same radial velocity and possibly the same density as the ambient solar wind, but it would simply be hotter. This condition can be simulated with the present method, and was done so with the same ambient solar wind and with the same half-angle for the cone subtended by the disturbance. In this case we inserted at 0.1 AU a disturbance of the same density and radial velocity as in the steady state solar wind but increased the temperature by a factor of 10, giving a temperature in the disturbed region of  $10^7$  deg. Having so initialized the situation, the disturbance was allowed to freely propagate upwards as this warm level rose in the solar wind. The results are shown in figure 1.

The total energy in this disturbance is  $10^{30}$  ergs, though it's mostly in the form of heat. This energy is not totally out of reason when compared to energies derived by other means. Note that the front takes a long time to reach 1 AU, and that when it does so, it is again roughly spherically shaped, but the center of the sphere tends to lie much more closely to the solar point rather than at some point further out along the symmetry axis. This may or may not imply poor agreement with observations, because there are certain irregularities in the shape, but certainly this is a broader front than one gets with either the driven or the blast wave case.

The heated bubble is an extremely low velocity disturbance, which is essentially convected out with the ambient solar wind. The transit time of this disturbance to 1 AU is generally in excess of what is usually thought. I recall a transit time of around 55 hr as being much more typical. Here the transit time is more like 73 hr.

Figure 2 shows a blast wave case with a disturbance containing 25 percent helium. The same initial energy was used, so that the initial shock velocity is a little less. What happens here is exactly what one would expect. There is early deceleration, perhaps not quite as strong due to the greater momentum per unit mass of the disturbance, but there are no real surprises here. What one would want to investigate next, I think, is a driven case with helium in the driving gas, to see what differences would result.

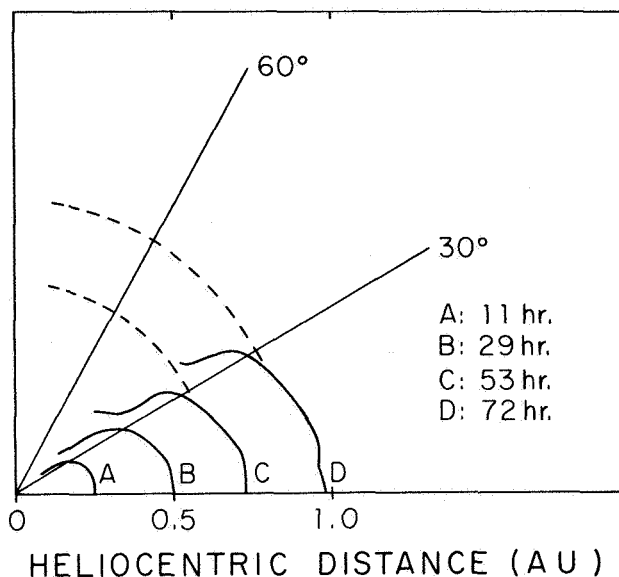


**Figure 1.** Shock front shape as a function of heliocentric distance for the thermally initiated disturbance. The times shown are hours elapsed since release of the disturbance at 0.1 AU. The dashed lines are reference circles centered on the sun, and the symmetry axis is along the bottom of the figure.

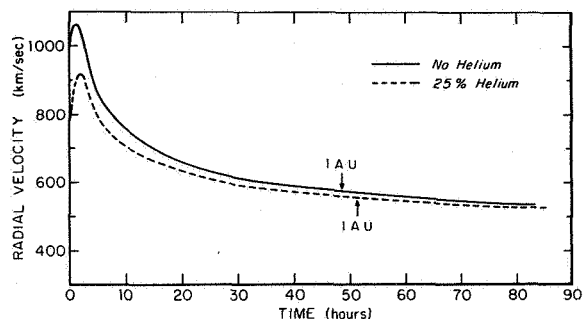


**Figure 2.** Radial velocity of the shock front along the symmetry axis as a function of elapsed time for disturbances with and without He. The arrows indicate the time at which the disturbance passes 1 AU. The ambient solar wind speed at 1 AU is  $400 \text{ km/sec}^{-1}$ .

**DISCUSSION** *J. Hirshberg* In comparing these calculations with observations you assume that the solar wind is spherically symmetric, while in the real case we have fast streams in the sectors, so we don't really expect to see these shapes very easily in any particular case.

*D. S. DeYoung* Yes. That's particularly true for disturbances that are of low initial energy and tend to be convected out with the ambient solar wind, where they can be highly distorted by any inhomogeneities that exist there.

*G. Newkirk* How formidable a job would it be to include the magnetic field in a couple of very simple configurations?

*D. S. DeYoung* I don't know what your scale of formidability is. It would not be too easy.

*G. Newkirk* Would it exceed your patience?

*D. S. DeYoung* Probably not.

*G. Newkirk* The configurations one would want would be where the event is collimated by the field or by the magnetic bubble.

*D. S. DeYoung* It would require major revisions in the code, but I don't think it's beyond the pale of one's imagination to do so in time.

*G. Newkirk* One of the things we know about flares is that they are associated very closely with the magnetic field.

*M. Dryer* I think it might be possible to take a magnetic field, just the line with the local velocity vector. It's completely artificial because the magnetic field in theory doesn't affect the flow. It would be the same kind of calculation John Spreiter and I have done for the interaction of the solar wind with the magnetosphere.

Would you agree to that, John?

*J. Spreiter* Not wholly. It is true that if the flow is steady, and the field is aligned with the flow in, say, the oncoming stream, it will remain aligned everywhere else, but the flow quantities are affected by the magnetic field. In particular, in some ranges of Mach

number and Alfvén Mach number, the hydromagnetic flow may be very different from the related gasdynamic flow. In fact, you can even have instances in which the MHD flow looks like gasdynamic flow going the other way; in other words, Mach waves extend upstream instead of downstream. For high Alfvén Mach number, however, the MHD and gasdynamic flows may not look terribly different.

*A. J. Hundhausen* One thing I advise in judging formidability is that the calculations we have done here are entirely in the range where the kinetic energy in the flow dominates. The real interest in magnetic channeling is done very low down in the corona where the ambient flow is subsonic and it may be quite a different problem.

*D. S. DeYoung* It is possible that you could match up these two regimes. You could do a low beta calculation close down where the field is high, then match it to this type later on.

*W. I. Axford* In this bubble business you have to really let the bubble go right from the bottom, I'm afraid, because you're depending very much on the potential energy of the bubble. If you let it already go from  $20 R_{\odot}$ , which is where you started, there is essentially no potential energy left. What you've got to play with is the gravitational energy or the escape energy of all the gas that the bubble takes up. At the bottom of the corona where the velocity is 600 km/sec, if you're sharing that among fewer particles you've got a very large amount of energy to play with. But if you start higher the escape velocity decreases to  $\sim 100$  km/sec, so there is really no source of energy available to give the buoyancy.

*D. S. DeYoung* Yes, but there is so little to run into that I think the density gradient in the ambient solar wind will result in a lot of transverse expansion anyway; it may present a much more nearly spherical front centered on the sun.

*W. I. Axford* That's true. It's a very complicated problem. That's why I hope you're doing it again. But the problem is rather like having a balloon and if you want to get it to pop out of the atmosphere you grease it very well and then start it at the bottom, not halfway up, or perhaps like a cork in a barrel; if you really want the cork to pop out of the water you pull it way down and then you let it go; you don't start it near the surface.

## COMMENTS

*E. J. Smith* The other day I presented some results from a study of sector boundaries that we are carrying out using Mariner 5 magnetometer data. Another aspect of the study deals with the physical characteristics of the sector boundary, specifically the changes in the plasma and magnetic field observable at high time resolution. There have been discussions of vector boundaries over the past few days on several occasions and I thought some of you might like to see what they look like close up.

This aspect of the analysis is much less well developed than the results I presented the other day, so I want to add a word of caution. First of all, I'm just going to show how the magnetic fields change across the sector boundary. Furthermore, I have selected for presentation a certain subset of sector boundaries which have some particularly interesting structure; I don't want to leave the impression that these are necessarily the only type of sector boundaries to be found. On the other hand, the boundaries to be shown are frequently occurring. I would estimate that we see them in over half the cases studied. As will be seen, we have studied enough examples to be able to prepare some histograms.

Figure 1 deals with the magnitude of field changes. In carrying out this analysis we have been particularly interested in determining the extent to which the properties of the sector boundaries are like the neutral sheet in the earth's magnetotail with which everyone nowadays is familiar. I have chosen three examples of the magnetic field magnitude and a histogram is shown below. As you will notice, these are for time intervals of about 2 hr. I've tried to align these three examples of sector boundaries so

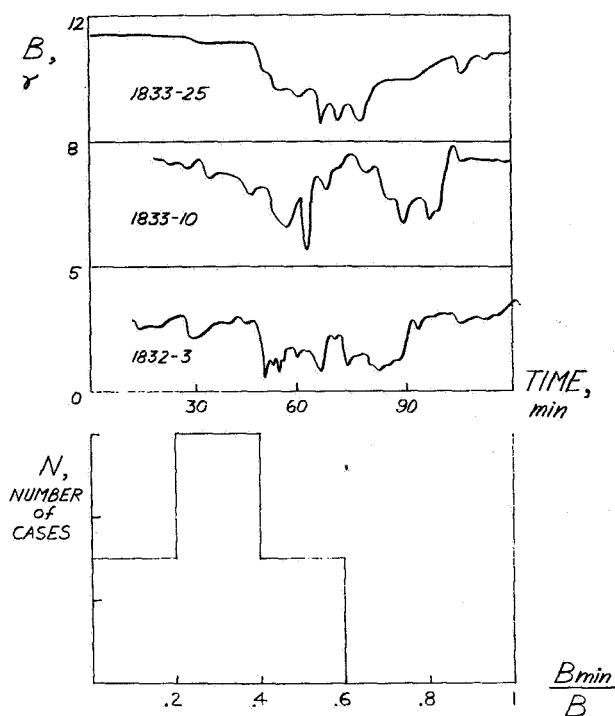


**Figure 1.** Changes in interplanetary field magnitude at three sector boundaries.

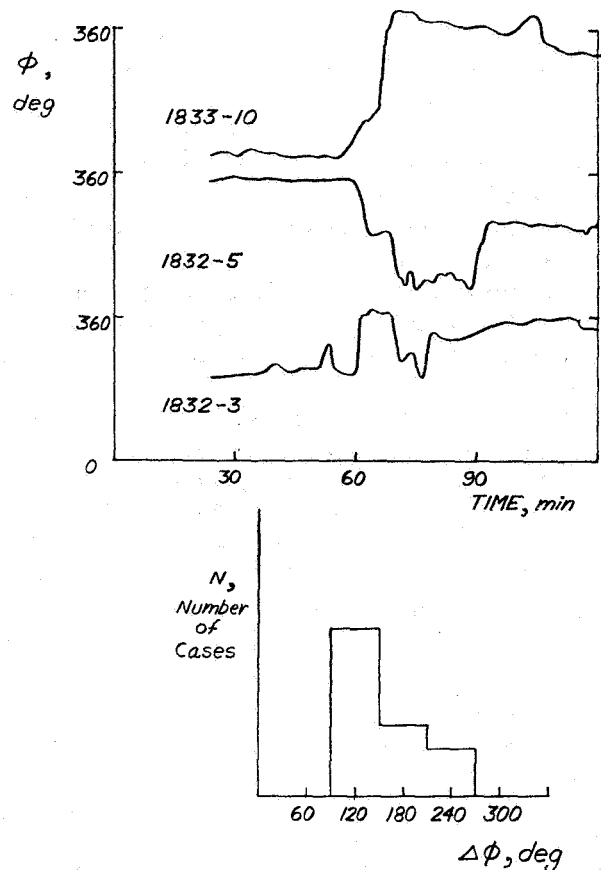


**Figure 2.** Changes in the direction of the interplanetary field at three sector boundaries.

that they can be compared. The identification numbers are our way of designating the sector boundaries in terms of the day number of solar rotation in which they occurred. The most obvious and interesting feature is the marked depression in the magnitude of the magnetic field. This is probably what most people have in mind when they think about the sector boundary as some kind of a simple neutral sheet.

The polarity usually changes in the vicinity of the magnitude change, but need not be coincident with it. On some occasions the direction of the field will start before the depression in the field and in some cases it will finish afterwards. In other cases the change in the field, particularly if it is an abrupt change in the direction of the field, can occur inside the field depression. There is certainly not a one-to-one correspondence between the two. Figure 2 shows some changes that tend to occupy somewhat different time intervals. The scales on the figure are variable because they were chosen at different times. They are 0 to 5γ, 0 to 8γ, and 0 to 12γ.

The histogram at the bottom of the figure shows the ratio of the minimum value to the magnitude of the field essentially ahead of the sector boundary. The differences in magnitude are not great on the two sides, and as you can see, the most probable value turns out to be about 0.3. This result is apparently similar to what is found in the earth's magnetotail where, based on published results, the field rarely ever goes to 0 but it is typically reduced to a value which is less than 40 percent of the magnetotail field. So far, so good.

Figure 2, then, gives us some examples and a histogram indicating how the field

direction changes. Each is scaled  $360^\circ - 0$  to  $360^\circ$  in each case. Some of the changes are very abrupt whereas others are quite slow. There is some irregularity; however, I am impressed by the result that the changes themselves are typically not  $180^\circ$ . One change is substantially larger, while two others are smaller, as shown more clearly by the histogram. The rotation of the magnetic field across the sector boundary is shown in intervals from 10 to 30 min. I should point out that these plots are in the principal axis system, so you're looking down on the plane in which the rotation of the field tends to occur. The histogram shows no particular preference for a change of  $180^\circ$  or for antiparallel, oppositely directed fields on the two sides of the sector boundary. In fact, there does seem to be more of a tendency for the angle through which the fields rotate to be less than  $180^\circ$ . I thought this was an intriguing observation and I would like to suggest an explanation for it.

Figure 3 illustrates the basic idea, which is relatively simple. It is based on the effect of a wind shear on the two sides of the sector boundary. The sector boundary is represented by the horizontal plane in this diagram. I have assumed a relative motion of the solar wind parallel to the sector boundary on the two sides. In this case the velocity is higher in the upper half of the figure. For the sake of illustration, I have also assumed a gradient in that direction. One can draw other configurations, but they simply indicate that wind shears of this kind would indeed lead to a displacement of the field line on one side of the sector boundary relative to its location on the other.

Having looked at the Mariner plasma data, the existence of a velocity change across the sector boundary seems to be a very common kind of phenomena. This hypothesis is one which I have only been considering for only a short period of time, but since I have been here at this conference I have found that it is, of course, not a new idea. You may recall the other day that Professor Cowling made a comment about the concept of the neutral sheet. He asked at that time about the possibility of wind shears. I spoke to him about this afterward and he said that people who had worked on neutral sheet problems in connection with solar flares had found that in that case shearing motions were very important in many of their models. This is obviously just a hypothesis at this point; if it is borne out by more careful analysis, many of you who are interested in neutral sheets, sector boundaries, and such things as field-line merging may want to consider some of the implications of these shearing motions and of the fields not being simply antiparallel as they are in the earth's magnetotail.

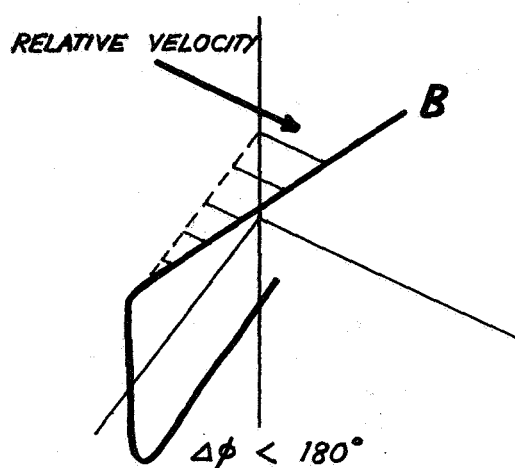


Figure 3. Effect of a solar wind shear on the relative field direction on two sides of a sector boundary.

## THE NATURE OF STREAM-STREAM INTERACTION IN THE LARGE-SCALE STRUCTURE OF THE SOLAR WIND *T. S. Lee*

**ABSTRACT** The stream-stream interaction between a slow solar wind and its leading faster solar wind is considered. A hydrodynamic model comprising double-layered rarefactions and recompressions is proposed toward understanding the observed large-scale structure near the trailing portion of a high-speed stream.

This paper considers the problem of solar wind stream-stream interaction, and introduces additional discussions concerning the interpretation of the quasistatic large-scale solar wind structure.

It is now well inferred from near-earth direct monitoring measurements that, over several consecutive rotations of the sun the solar wind, at times, may possess a near-stable corotating structure. Longitudinal and, to a much lesser extent, latitudinal variations in the solar wind strength appear to be the basic cause. Geomagnetic disturbances often exhibit periodicities, some of which implicate a clear association with solar rotation. Long sequences of the stronger among these—the recurrent storms—were first attributed to the so-called *M* regions on the solar surface by *Bartels* [1932]. His view, which incorporates quasipermanent narrow beams of corpuscular radiation, was long held although observational identifications of these regions were lacking. *Dessler and Fejer* [1963] reconsidered this view and proposed that these storms are generated by corotating nonuniformities resulting from the interaction between a slow-wind region and an overtaking-wind region. *Razdan et al.* [1965] examined their model hypothesis and showed that the basic idea is hydrodynamically viable with respect to the expected implications at 1 AU.

The general premise of regarding longitudinal gradients in solar wind strength near the sun responsible for the corotating wind variations in the interplanetary region is

very reasonable. In addition, the particular picture of one steady wind overtaking another appears to provide useful clues to the dynamical complexities near the leading portion of a high speed stream. Here, the key ideas of a solar wind interface (tangential discontinuity) and accompanying compressions, bounded by perhaps two shock waves, go far toward giving overall interpretations to many observations, as discussed by Dr. Davis in his presentation yesterday.

Phenomena related to the trailing portion of a strong wind have not received adequate considerations in the literature. *Sarabhai* [1963] thought that the decrease in velocity results in the formation of a cavity, or region of reduced density, behind the *M* region beam. Although the suggestion is inherently interesting, it is actually difficult to see how the model is arrived at through his given hydrodynamic arguments. We would like to reopen the discussion and try to indicate a different model concept for limited considerations in the following.

The question is raised: what appropriate hydrodynamic structures may connect two steady solar winds, departing from each other? If we allow ourselves the luxury of disregarding the secondary nonradial motions generated in the context of corotating interactions viewed in the solar equatorial plane, then the problem is grossly similar to its sister problem in the context of spherical flow in which a fast steady expanding flow pulls away from a trailing slow steady expanding flow. Here, one is easily tempted to argue that a more or less simple and smooth rarefaction region would be created, a conclusion generally associated with experiences with laboratory planar flows. However, the conditions of the

---

*The author is at the Electrical Engineering Department, University of Minnesota, Minneapolis, Minn.*

solar wind are sufficiently different to warrant separate considerations for this type of stream-stream interaction. It is interesting to point out that there exist classes of hydrodynamic solutions to the spherical problem mentioned above [Lee, to be published]. They correspond to specific model assumptions made on the solar winds: invariant mass flow rate per steradian and invariant streaming and sound velocities. Not all of these have been scrutinized and cataloged, but one has sufficient bearing on our present consideration that a qualitative description of its main features may shed some light on the original problem.

When a fast wind moves ahead, leaving a trailing slow wind behind, it tends to expand inward on account of its inherent specific thermal energy density. At the same time, the slower wind left behind tends to expand outward. Thus rarefaction waves of respectively decelerative and accelerative nature are generated. First consider the drastic case where the separation of the two steady winds takes place at a sufficiently high relative velocity. Since the specific thermal energy densities for the two winds are both finite, the edges of the two expansion waves cannot meet, thus creating a vacuum. This sequence of wind-rarefaction-vacuum-rarefaction-wind would characterize the structure of the basic stream-stream "noninteraction." [The reader will find it interesting to compare this picture with Sarabhai's, 1963, picture.] Consider next the probably more realistic case where the relative separating velocity is less drastic so that the two rarefaction waves begin to interfere with each other. In figure 1, we have sketched the configuration of the total interaction as projected on the solar equatorial plane. Here, we consider the interference to be only moderate such that it is confined spatially to the regions to the two sides of the interface discontinuity (tangential discontinuity as shown). We note that the interference interaction is basically analogous to the leading edge interaction discussed earlier, except that the double-layered recompression here results from a collision between the expanded extensions of the two winds which, if it were not for compressibility, would depart from each other permanently. It follows that respectively inward-looking and outward-looking shock waves are expected in the flow. Thus the trailing-edge interaction may have a structure composed of regions of fast wind region-rarefied region (fast wind)-recompressed region (fast wind)-recompressed region (slow wind)-rarefied region (slow wind)-slow wind region. In this model picture, five flow discontinuities—two rarefaction fronts, two shock waves and an interface discontinuity—combine to give demarcations to the flow field.

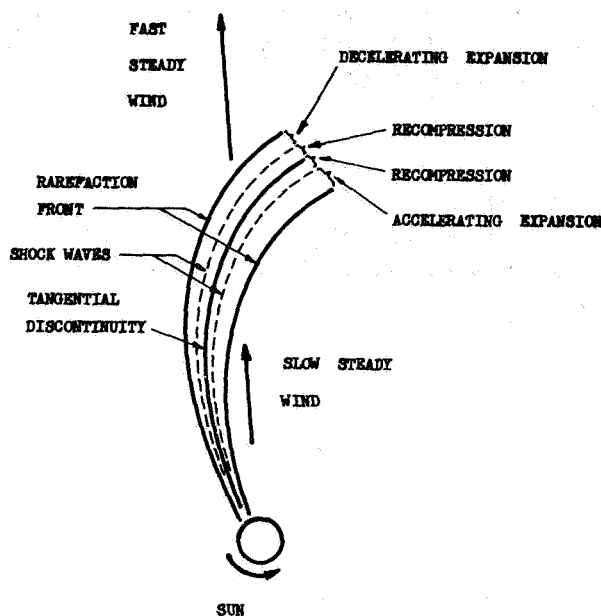


Figure 1. Configuration of stream-stream interaction at the trailing portion of a fast steady wind. This wind and its following slow steady wind are joined through an assemblage of unsteady wave regions encompassing double-layered expansions and recompressions. The discontinuities comprise the sequence of rarefaction front—shock wave—tangential discontinuity—shock wave—rarefaction front.

In the above, we have outlined the essential physical arguments for a specific class of stream-stream interaction. Depending on quantitative specifications on the two interacting solar winds, other possible modes of flow connections may be predicted. We refrain from discussing them here.

If the more complete view is taken that close to the sun the longitudinal strength of the solar wind varies alternately from strong to weak, to strong, and so forth, we should see, of course, leading-edge and trailing-edge types of stream-stream interaction. According to our discussions, plasma compression can be expected at both the leading and trailing portions of a stream. Thus, the mere presence of locally high density does not necessarily imply the arrival of any new enhanced "stream" or "beam." Here, we are being reminded that the occasional detections of density enhancement occur near the minimum of the corresponding time-profiles of the velocity, an interesting fact already observed by Dr. Smith in a comment following Dr. Wolfe's paper yesterday. Finally, the durations of density enhancements of both leading-edge and trailing-edge interactions

are expected from our model considerations to be followed by high (by local comparisons) velocities in the solar wind, in good agreement with the usual observations.

#### REFERENCES

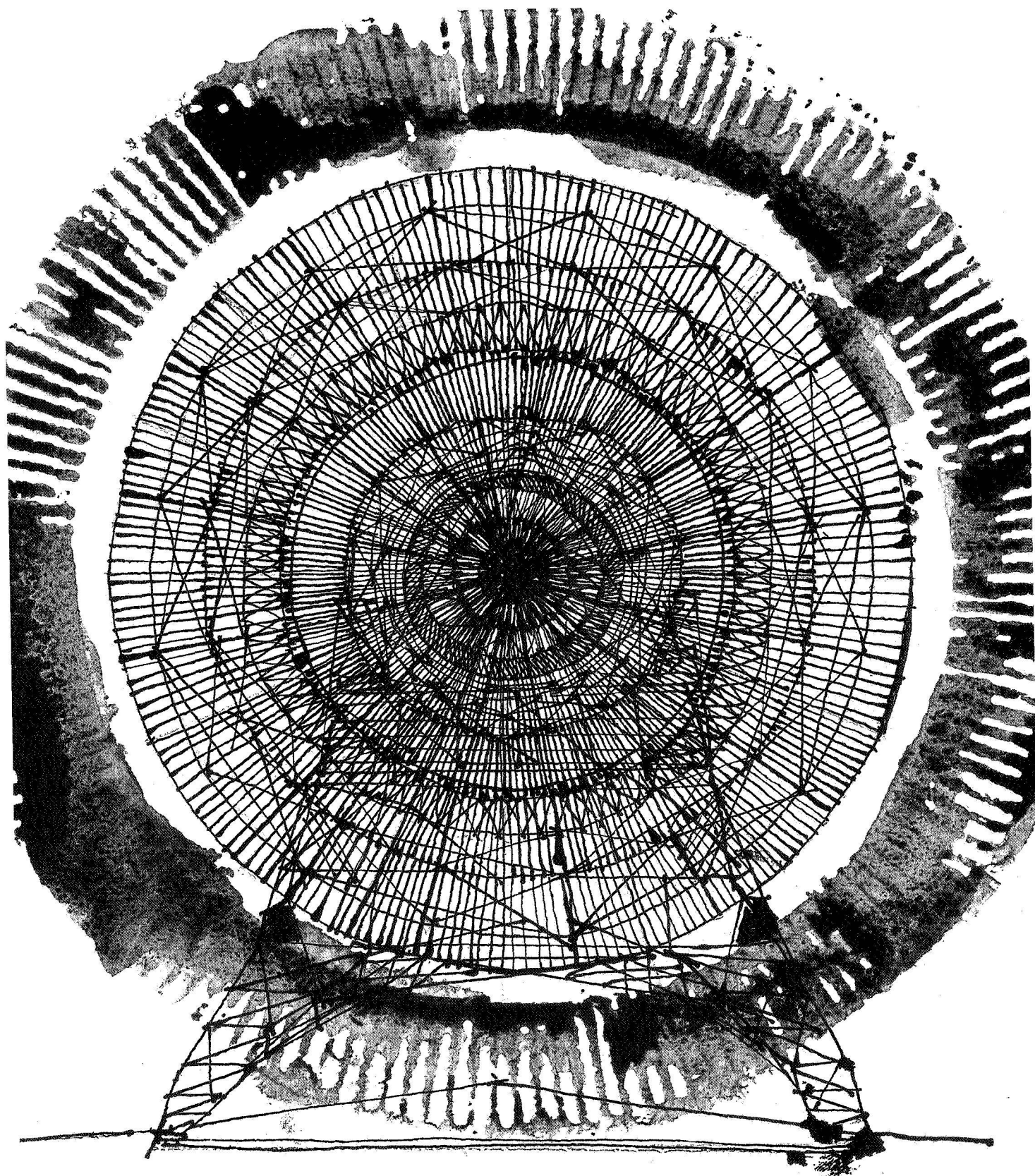
Bartels, J.: Terrestrial Magnetic Activity and Its Relations to Solar Phenomena. *Terr. Magn.*, Vol. 37, 1932, pp. 1-52.

Dessler, A.J.; and Fejer, J. A.: Interpretation of  $K_p$  Index and M-Region Geomagnetic Storms. *Planet. Space Sci.*, Vol. 11, 1963, pp. 505-511.

Razdan, H., Colburn, D. S.; and Sonett, C. P.: Recurrent  $SI^+$  -  $SI^-$  Impulse Pairs and Shock Structure in M-Region Beams. *Planet. Space Sci.*, Vol. 13, 1965, pp. 1111-1123.

Sarabhai, V.: Some Consequences of Nonuniformity of Solar Wind Velocity. *J. Geophys. Res.*, Vol. 68, 1963, pp. 1555-1557.





## CHAPTER, VII

Radio Observations of the Solar Wind

Scattering and scintillation observations of natural radio sources; satellite observations of phase and group path differentials and of Faraday notation; observations at high heliographic latitudes and at a range of distances from the sun.

# OBSERVATIONS OF THE SOLAR PLASMA USING RADIO SCATTERING AND SCINTILLATION METHODS

A. Hewish

An invited review

Observations of the solar plasma using the interplanetary scintillation technique have been made at radial distances of 0.03 to 1.2 AU. The solar wind is found to be independent of ecliptic latitude and radial distance, except close to the sun where acceleration is observed. Plasma density irregularities on a scale near the proton gyro radius, which modulate the mean density by about 1 percent, are present throughout the observed range of radial distance. **ABSTRACT**

## INTRODUCTION

Radio waves traversing the solar plasma are scattered by irregularities of plasma density. Measurements of the angular spectrum of the scattered radiation now exist in the range 0.025 AU to nearly 0.5 AU. Alternatively, for compact radio sources that illuminate the plasma with sufficient coherence the interference of the scattered waves produces a diffraction pattern at the earth. This is the phenomenon of *interplanetary scintillation*.

Studies of the motion and correlation of the diffraction pattern observed at spaced sites give information about the solar wind and the plasma irregularity wave number spectrum. The temporal variations observed at a single site give corresponding, but less complete, information about the wave number spectrum if a drift velocity is assumed. In addition, measurement of the fraction of the incident radiation scattered gives information about the density modulation caused by the irregularities. The importance of these techniques is that they permit study of the solar wind at radial distances and ecliptic latitudes not yet accessible to spacecraft. They also provide evidence of structure on a smaller scale than has been revealed by space probes in interplanetary space.

This paper is a survey of the current observational situation using radio scattering methods. Other methods for studying the solar plasma include Faraday rotation,

time delays in pulses from pulsars, and differential group and phase path measurements from spacecraft. Such techniques give data on the mean plasma density and large-scale irregularities. These latter methods will not be considered.

## SCINTILLATION PARAMETERS AND THE SOLAR PLASMA

The relation between observed scintillation parameters and the plasma irregularities is illustrated in figure 1. We assume the density variations to be time stationary and described by a wave number power spectrum  $G(k_1, k_2, k_3)$ . If the medium is convected past a space probe at velocity  $V$  (along  $k_1$ ) then the wave number components giving rise to temporal fluctuations of angular frequency  $\omega = k_1 V$  lie in the sheet  $\mathbf{k} \cdot \mathbf{V} = \omega$ . Hence the temporal power spectrum  $H(\omega)$  of the density fluctuations seen by a spacecraft is a two-dimensional strip scan of  $G(k_1, k_2, k_3)$ . For a power law irregularity spectrum, as discussed by Cronyn [1970],  $H(\omega)$ , will consequently be flatter than  $G(k)$ .

Consider next the phase modulation imposed on a plane radio wave incident along  $k_3$ . The phase variations will have a two-dimensional spectrum proportional to  $G(k_1, k_2)$ . This will also define the angular spectrum of the scattered radiation when the scattering is weak. In what follows we consider only the weak scattering case; in practice, this condition may be realized by observing at a sufficiently short wavelength.

The intensity diffraction pattern at the earth is again

*The author is at Mullard Radio Astronomy Observatory, Cavendish Laboratory, Cambridge, England.*

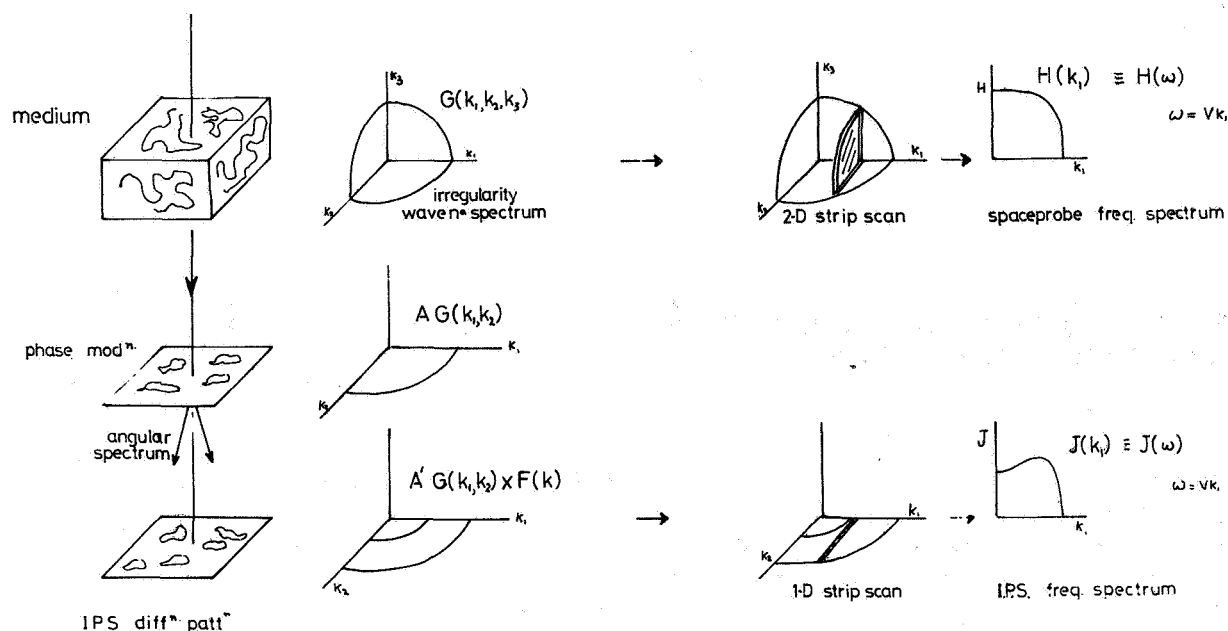


**Figure 1.** Relation between the wave number spectrum of plasma density irregularities and power spectra as measured by space-probe and scintillation techniques.

proportional to  $G(k_1, k_2)$  but it is multiplied by a factor  $F(k) = \sin^2(k^2 z \lambda / 4)$ , where  $\lambda$  is the radio wavelength and  $z$  the distance of the medium from the earth.  $F(k)$  arises from Fresnel "filtering" which removes low wave number components from the diffraction pattern. Measurements at spaced sites permit determination of the autocorrelation function and drift velocity of the medium, while the temporal power spectrum  $J(\omega)$  at a single site is given by a one-dimensional strip scan of  $G(k_1, k_2)F(k)$ .

Another important observational parameter is the scintillation index  $m$ , defined as the rms variation of intensity in the diffraction pattern divided by the mean intensity. Since  $m^2 \propto \lambda^2 F(k)G(k_1, k_2)dk_1, dk_2$  [Salpeter, 1967], it is clear that the scintillation index gives information about the magnitude of the plasma density variations.

When considering effects due to integration along an extended line of sight it is useful to define the scattering power  $S'$  of the medium. We put  $d(m^2) = S^2(z)dz$  where  $dz$  is an element of the line of sight. It is assumed that the distance  $z$  from the earth to this element is so great that, the diffraction pattern is unaffected by Fresnel filtering. Thus  $S$  depends on the medium alone and we have  $S^2 \propto \lambda^2 G(k_1, k_2)dk_1 dk_2$ ; of course,  $S$  will vary with radial distance from the sun.

## THE WAVE NUMBER SPECTRUM OF THE IRREGULARITIES

Observations of interplanetary scintillation were originally interpreted in terms of irregularities having a size of the order of 100 km at a distance of 0.5 to 1.0 AU [Dennison and Hewish, 1967; Cohen et al., 1967]. This conclusion has recently been questioned by authors who have suggested that a power law spectrum  $G(k) \propto k^{-n}$  may be more appropriate [Jokipii and Hollweg, 1970; Lovelace et al., 1970; Cronyn, 1970]. A detailed comparison of observation and theory shows that a power law spectrum cannot, in fact, describe the irregularities [Hewish, 1971; Little, 1971; Lotova and Chashey, 1971]. Since this point is important, the evidence refuting a power law spectrum will be summarized.

Measurements now exist at frequencies ranging from 26 to 2700 MHz, and it is interesting to see how the observed parameters should behave under different assumptions about the irregularity spectrum. In figure 2 we show the general behavior of the Fresnel filter  $F(k)$  at 81 MHz and 2695 MHz, where the approximation

$$F(k) = \sin^2\left(\frac{k^2 z \lambda}{4}\right) \quad k < \sqrt{\frac{2\pi}{z\lambda}}$$

$$= \frac{1}{2} \quad k > \sqrt{\frac{2\pi}{z\lambda}}$$

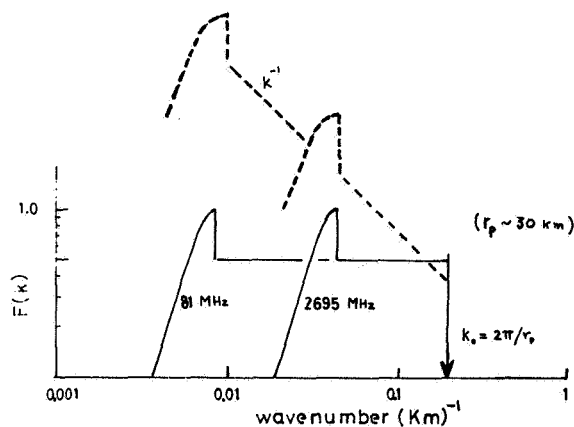
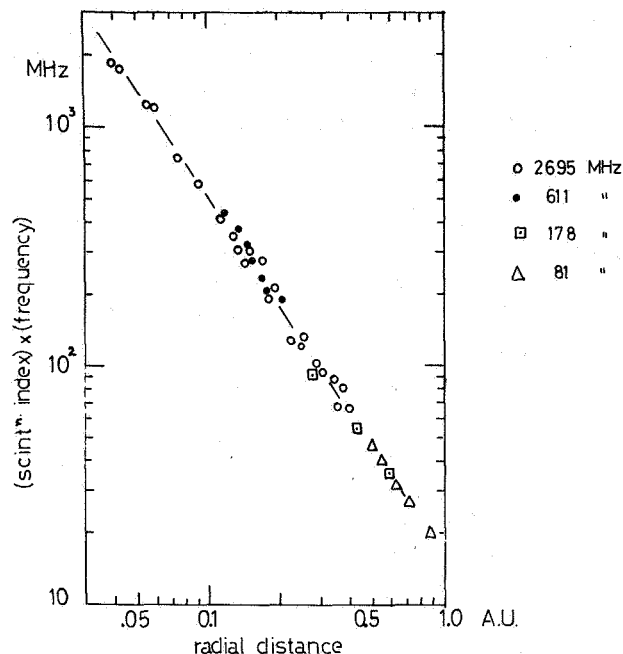


**Figure 2.** Approximate form of the Fresnel filter for a one-dimensional spectrum.  $k_0$  is an assumed upper limit to the spectrum set by the proton gyroradius. The dashed curve shows the effect of filtering on a  $k^{-1}$  spectrum.

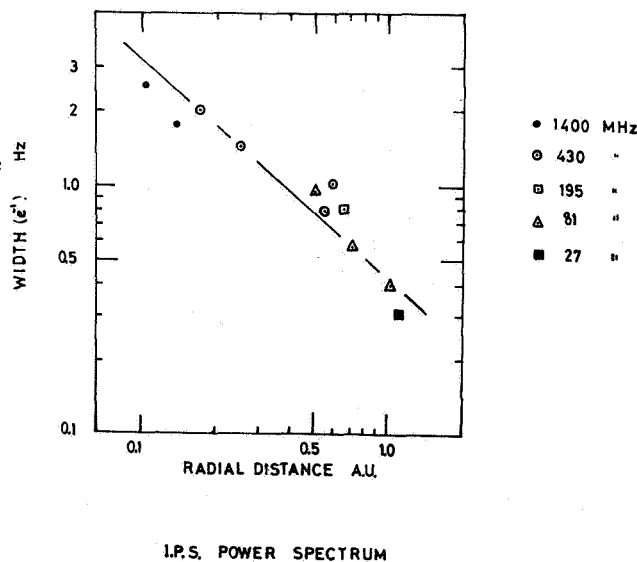
has been adopted. For the actual solar plasma it is likely that  $G(k)$  has an upper bound  $k$  set by the proton gyroradius, and this is shown for a gyroradius of 30 km, appropriate to conditions at 0.5 AU. Now for a spectrum  $G(k) \propto k^{-n}$  it is clear that the diffraction pattern will be dominated by wave numbers in the vicinity  $k \sim \sqrt{2\pi/2\lambda}$ , just greater than the Fresnel cutoff. Thus the autocorrelation function of the pattern and also  $J(\omega)$  will have widths that scale approximately as  $\lambda^{1/2}$  and  $\lambda^{-1/2}$ , respectively. In addition, for a power law spectrum,  $m$  will vary with  $\lambda$  and we have  $m \propto \lambda^2$  for Jokipii and Hollweg's [1970] model, or  $m \propto \lambda^{1.5}$  for the spectrum suggested by Lovelace *et al.* [1970].

Figure 3 shows observations of  $m$  taken at widely different frequencies on a number of sources by different observers; for convenience, the product  $m \times$  radio frequency is plotted. These data refer to solar elongations greater than the critical value at which "turnovers" due to the finite angular size of the source become apparent [Little and Hewish, 1966]. The results indicate  $m \propto \lambda^{1.0 \pm 0.05}$ , which is not compatible with a power law spectrum. We also note that this wavelength dependence confirms the weak scattering assumption.

Further evidence may be drawn from observations of the temporal power spectrum  $J(\omega)$ , which approximates to a gaussian form except at distances within 0.2 AU [Cohen *et al.*, 1967]. Various measurements of the width (to  $e^{-1}$ ) of  $J(\omega)$  at different radio frequencies are illustrated in figure 4. The spectrum undoubtedly varies with solar distance, but the



**Figure 3.** Dependence of scintillation index upon distance from the sun at different radio frequencies.



**Figure 4.** Width of the scintillation temporal power spectrum. 195-, 430-, and 1400-MHz data from Cohen *et al.* [1967]; 81.5-MHz data from Symonds [1970] and 27-MHz data from Cronyn [1970].

observations indicate that  $J(\omega)$  is not a function of the observing frequency. Once again, this is not compatible with a power law spectrum.

To find a spectrum that agrees with the observations we note that the relation  $m \propto \lambda^{1.5}$  implies that the Fresnel factor  $F(k)$  cannot modify  $G(k)$  to any significant extent. This will be true only if  $G(k)$  does not increase appreciably in the range of  $k$  between the Fresnel cutoffs at the extreme radio frequencies. Within the observational limits, this criterion is satisfied by  $G(k) = \text{const}$  for  $k < k_c$ ; alternatively, the strip scan of  $F(k) G(k_1, k_2)$  shown in figure 1 might peak at some wave number higher than the Fresnel cutoff at the highest frequency.

Until more refined data become available it is probably simplest to assume a gaussian spectrum, although this may not be spherically symmetrical. It is clear, however, that the small irregularity sizes deduced from scintillation data correspond to a real plasma scale length, rather than to some limit imposed by diffraction theory. As such, they constitute a regime quite separate from the much larger irregularities detected by space probes.

Scintillation data, of course, do not preclude the existence of large-scale density structure having wave numbers less than the Fresnel cutoff at the lowest observational frequency. Such structure will merely deviate the wave front without producing scintillation. However, it will contribute to the angular spectrum. As shown below, observations of scintillation close to the sun indicate scale sizes in good agreement with those inferred from angular spectrum data. This means that the angular spectrum is not greatly influenced by large-scale irregularities and it follows that some limit can be placed on the density variations in large irregularities. This limit is estimated in a later section.

Having established that the observed scale of the diffraction pattern is representative of the irregularities themselves, we can deduce that the variation of scale size with radial distance, implicit in figure 4, is also real. In figure 5 we combine all the data, including measurements of both the correlation distance of the diffraction pattern at spaced sites and the temporal spectra at a single site. When the latter are used a solar wind of 330 km/sec has been assumed. Also included, close to the sun, are values derived from angular spectrum measurements at low frequency, combined with values of  $m$  at high frequency, as described by Hewish and Symonds [1969]. All the measurements are in reasonable agreement and indicate a scale that increases approximately linearly with radial distance within the observational uncertainty. Further evidence, based on the sharp reduction of scintillation index close to the sun when the finite angular size of radio sources becomes important, suggests that a somewhat steeper variation gives a better fit to  $m$  versus solar elongation

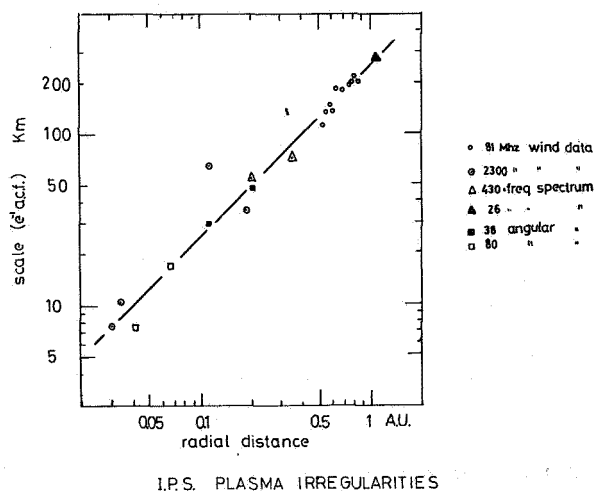


**Figure 5.** The width of the autocorrelation function of the scintillation diffraction pattern obtained by different methods. 2300 MHz and 81.5 MHz data from spaced-site observations [Symonds, 1970; Little, 1971], 430 MHz and 27 MHz points from temporal power spectra [Cohen et al., 1967; Cronyn, 1970]; 38 MHz and 80 MHz points from interferometric angular spectrum measurements [Hewish and Symonds, 1969].

curves. [Cohen and Gundermann, 1969; Readhead, 1971]. Model fitting gives best agreement for  $l \propto R^{1.5}$ , and the scatter in figure 5 barely precludes this law. More data are needed to improve the determination of scale size for radial distances within 0.2 AU.

There is evidence that the irregularities show spatial anisotropy. Early spaced-site observations by Dennison [1969] indicated an axial ratio of  $\sim 1.8:1$  extended roughly radially from the sun. More recent measurements using larger baselines by Symonds [1970] show axial ratios of the same order for individual occasions, but with no significantly preferred direction. Certainly some anisotropy is expected since angular spectrum measurements closer to the sun indicate filamentary irregularities significantly aligned in a radial direction [Hewish and Wyndham, 1963; Harries et al., 1970].

#### VARIATION OF SCATTERING POWER WITH RADIAL DISTANCE

The relation between scintillation index  $m$  and radial distance in figure 3 shows that  $m \propto R^{1.5 \pm 0.05}$  over distances from a few solar radii to 1 AU. Since the observations measure the integrated scattering along a line of sight, it is important to derive the corresponding radial variation of scattering power  $S$  of the medium itself.

Since  $m^2 \propto \int S^2(z) dz$ , where  $z$  is distance along a

line of sight extending from the earth to infinity, the solution of this integral equation is required. Now  $m$  varies with  $R$  as a simple power law  $m \propto R^{-1.5}$  and hence we obtain  $S^2 \propto R^{-4.0}$ , giving  $S \propto R^{-2}$ . For a plasma in which the electron density variations have an rms value  $\Delta N$  and a correlation distance  $\ell$ , we also have  $S \propto \lambda \Delta N \ell^{1/2}$  [Chandrasekhar, 1952]  $\Delta N \ell^{1/2} \propto R^{-2}$ . The implication of this result will be discussed later.

The law  $S \propto R^{-2}$  allows an estimate to be made of the relative importance of different portions of the line of sight in determining the parameters of the solar plasma by scintillation methods. Calculations using this law are illustrated in figure 6, which indicates the relative weight of each element along the line of sight. Because the

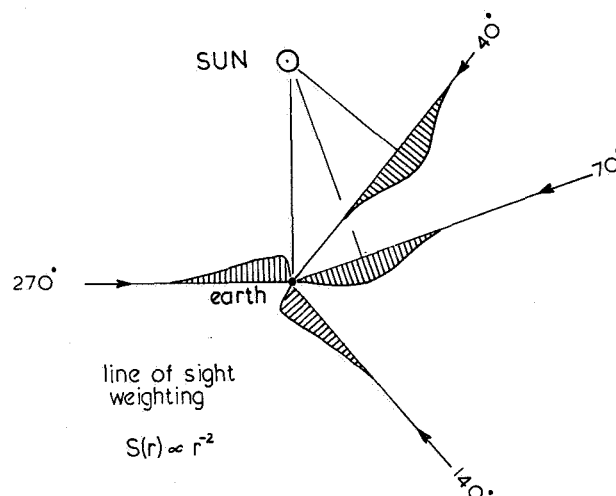


**Figure 6.** Relative contribution of different elements of the line of sight to the total scintillation.

radial variation of  $S$  is pronounced, lines of sight at elongations less than  $90^\circ$  effectively sample the solar plasma over a small region centered on the point of closest approach to the sun. For elongations exceeding  $90^\circ$ , on the other hand, the earth is imbedded in the irregularities that scatter most strongly and thus it is not possible to sample the solar plasma at distances greater than about 1.5 AU.

### THE SOLAR WIND VELOCITY

Observations of the solar wind using the spaced-site method have been made for a number of years [Dennison and Hewish, 1967; Vitkevich and Valsov, 1970]. No evidence has yet been obtained for a departure from strictly radial outflow. Recently, Symonds [1970] used three sites as shown in figure 7. Working on a number of radio sources to achieve a greater coverage of ecliptic

latitude and solar distance, he obtained the measurements shown in figure 8. Detailed examination of the day-to-day variations of velocity for different radio sources suggests the presence of localized streams in which the velocity may differ significantly. The high velocity peak in late September on 3C287, for example, appears to be related to a class 3 solar flare that occurred on September 25.

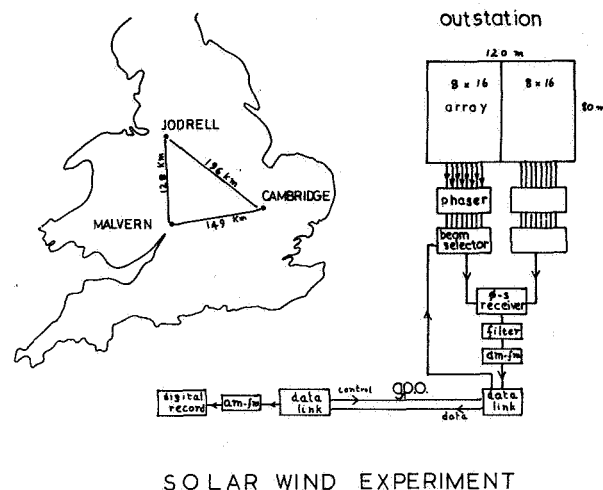


**Figure 7.** Schematic diagram of the Cambridge solar wind experiment.

Averaging the data shown in figure 8 to investigate the solar wind as a function of ecliptic latitude and radial distance reveals no significant departure from a uniform spherical outflow at constant velocity. The results are illustrated in figure 9. The velocity histogram for all the data is compared with space-probe data for the same observing period in figure 10. The histograms are generally similar, but our data give a mean velocity of 330 km/s as compared with 397 km/s for spacecraft measurements. Integration along the line of sight must give a mean value somewhat lower than the true velocity and part of the difference can arise in this way, but the weighting function shown in figure 6 scarcely can account for all the discrepancy. Most of our data refers to ecliptic latitude  $> 20^\circ$ , which is not the region sampled by spacecraft, but figure 9 gives no evidence of systematic effects that might be relevant. It will be interesting to see whether more extensive scintillation data continue to show significantly lower velocities.

Some observations close to the sun, where the solar wind should be accelerating, have been made by Ekers and Little [1971] using two sites spaced by 16 km and

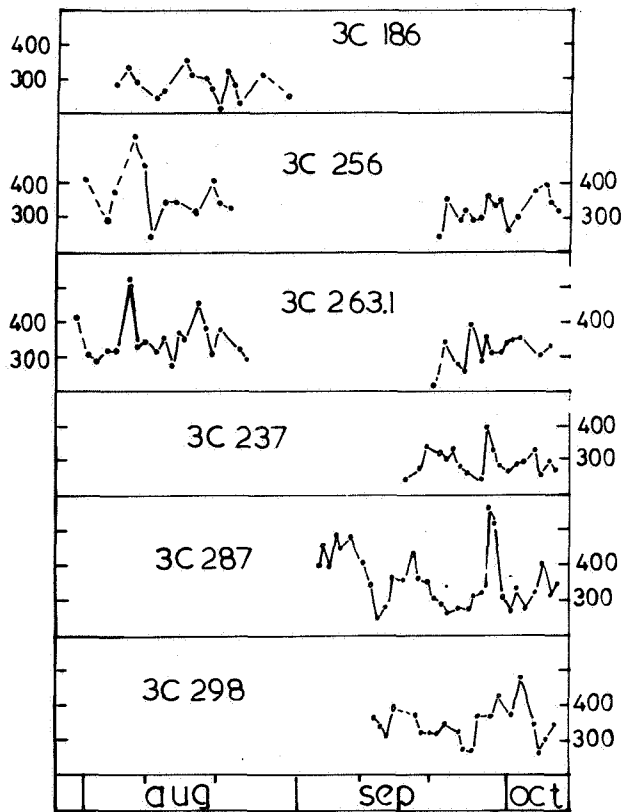


**Figure 8.** Solar wind observations obtained from spaced-site observations of scintillation on a variety of sources.

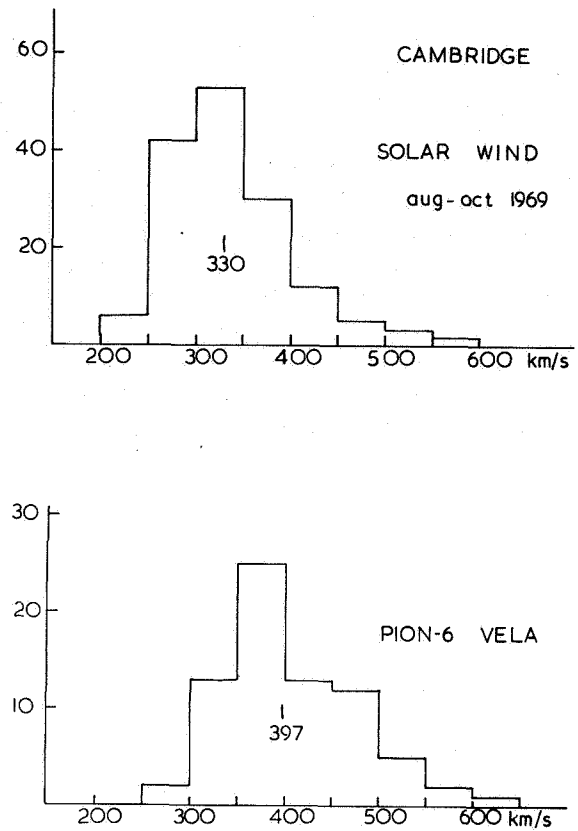


**Figure 10.** Histogram of Cambridge solar wind data compared with space-probe measurements for the same period.

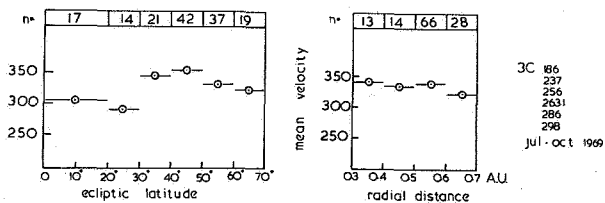


**Figure 9.** Average solar wind velocity as a function of ecliptic latitude and distance from the sun. Horizontal bars and the numbers above denote the averaging interval and the number of independent measurements included.

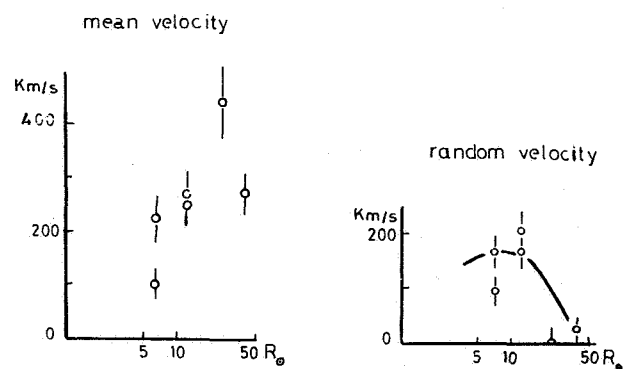


**Figure 11.** Solar wind observations close to the sun obtained by Ekers and Little [1971].

22 km. Their results are shown in figure 11, and the increase of mean velocity with distance agrees with a Parker model for  $T \sim 1 \times 10^6$  °K. A significant random velocity component was also found at  $10 R_{\odot}$ , but this decreased rapidly with distance and was insignificant



beyond about  $30 R_{\odot}$  (0.14 AU). This finding is consistent with other observations at greater distances that have given no evidence for turbulent velocities greater than the small spreading due to variation of projected velocity across the line of sight.

### EVIDENCE FOR COROTATING STRUCTURE

In view of the well-known sector structure of the magnetic field about the sun, it is natural to seek similar effects as revealed by plasma irregularities. Some observations of day-to-day variations of scintillation index have already been used to suggest the presence of corotating structure, but the data have not been sufficiently extended to establish the effect conclusively [Burnell, 1969; Dennison and Wiseman, 1968]. It seems probable that if such structure exists, its presence might be most readily detected by observing at elongations exceeding  $90^\circ$  where the line of sight runs almost parallel to the local spiral magnetic field, rather than perpendicular to it as is the case at small elongations. At 81.5 MHz it is possible to measure  $M$  at all solar elongations, and daily observations for two months on suitably disposed sources made by Houminer [1971] are shown in figure 12. Variations of  $m$  on a time scale of several days are clearly evident and there is a time shift between corresponding features observed on the two sources. This time shift is entirely consistent with a corotating structure, and there is evidence that features repeat with a 27-day period, but more extended data are needed for detailed analysis.

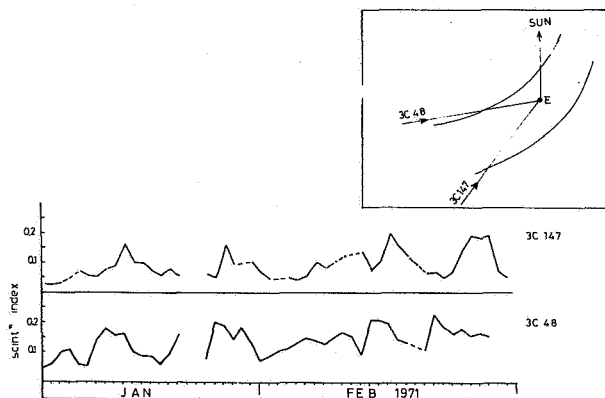


**Figure 12.** Day-to-day variation of scintillation index on 3C 147 and 3C 48 showing time-displaced correlation indicating the presence of corotating structure.

### CONCLUSIONS

Results obtained from a study of the solar plasma by interplanetary scintillation techniques show that the solar wind appears to be independent of ecliptic latitude for radial distances of 0.4 to 1.0 AU. Small-scale irregularities of plasma density are a notable feature at all distances from a few solar radii to the earth. Both the scale and density modulation of the irregularities vary systematically with distance from the sun and their origin is so far unexplained.

It is difficult to account for the irregularities by density variations associated with "frozen-in" magnetic field irregularities which are imposed near the sun and then convected outward. Since the radial variation of  $B^2$  is considerably faster than that of kinetic pressure  $NkT$ , this type of irregularity is progressively smoothed out with increasing distance from the sun. Some type of plasma instability that continually generates density fluctuations on a scale close to the proton gyroradius appears to be necessary. It is natural to inquire whether the increase of scale size with distance varies in the same way as the proton gyroradius. We have  $r_p \propto B^{-1} T^{1/2}$  and putting  $B \propto R^{-2}$ ,  $T \propto R^{-1/2}$ , gives  $r_p \propto R^{1.75}$ , which is somewhat steeper than the observed behavior.

With regard to the density modulation produced by the irregularities, the observations described earlier give  $\Delta N \propto R^{1/2} R^{-2}$ . Also  $R^{1.0}$  (see fig. 5) so that  $\Delta N R^{-2.5}$ . For a gaussian irregularity spectrum the observed scintillation index  $m$  corresponds to  $\Delta N = 4.10^{-2} R^{-2.5} \text{ cm}^{-3}$  where  $R$  is in AU [Little, 1971]. This value is about 1 percent of the mean density at 1 AU.

It is interesting to compare  $\Delta N$  derived from scintillation with the value that might be expected from space-probe measurements of plasma-density power spectra. Taking the data of Intriligator and Wolfe [1970] and extrapolating their spectrum linearly to 1 Hz (appropriate to scintillation scales) gives  $\Delta N$  about ten times larger than our value above. Evidently, the irregularity power spectrum must steepen considerably in the range  $10^{-3}$  to  $10^{-1}$  Hz before flattening out in the region of 1 Hz.

We now consider the upper limit that angular scattering data impose on the density in large-scale irregularities as mentioned earlier. It has already been shown [Hewish and Symonds, 1969] that the angular spectrum determined by interferometer measurements within 0.2 AU is consistent with the observed autocorrelation function of the diffraction pattern. Similar evidence may be drawn from the agreement of scale sizes determined by both methods in figure 5, where the uncertainty is within a factor of 2. It follows that the angular deviations

produced by large-scale irregularities are less than, or of the same order as, those caused by the small-scale irregularities. Now the angular deviation produced by irregularities varies as scale size<sup>-1/2</sup>; thus, irregularities of scale 50 km with  $\Delta N \sim 2$ , as derived from scattering and scintillation studies at 0.2 AU, would produce the same angular deviations as irregularities of scale  $5 \times 10^5$  km with  $\Delta N \sim 200$ . The latter value is comparable to the mean electron density at 0.2 AU. It follows that the large-scale irregularities detected by space probes cannot significantly modify the radio-scattering properties of the interplanetary medium, which are dominated by the small-scale features.

It is evident that radio scattering and scintillation techniques using a variety of modes of observation and analysis yield very good agreement. Such measurements provide information that forms a valuable complement to that obtained by *in-situ* space observations.

## REFERENCES

- Chandrasekhar, S.: A Statistical Basis for the Theory of Stellar Scintillation. *Monthly Notices Roy. Astron. Soc.*, Vol. 112, 1952, p. 475.
- Burnell, S. J.: Enhancements of Interplanetary Scintillation, Corotating Streams and Forbush Decreases. *Nature*, Vol. 224, 1969, pp. 356-357.
- Cohen, M. H.; and Gundermann, E. J.; Hardebeck, H. E.; and Sharp, L. E.: Interplanetary Scintillations, 2. Observations. *Astrophys. J.*, Vol. 147, 1967, pp. 449-466.
- Cohen, M. H.; and Gundermann, E.: Interplanetary Scintillations, 4. Observations Near the Sun. *Astrophys. J.*, Vol. 155, 1969, pp. 645-663.
- Cronyn, W. M.: The Analysis of Radio Scattering and Space-Probe Observations of Small-Scale Structure in the interplanetary Medium. *Astrophys. J.*, Vol. 161, 1970, pp. 755-763.
- Dennison, P. A.; and Hewish, A.: The Solar Wind Outside the Plane of the Ecliptic. *Nature*, Vol. 213, 1967, pp. 343-346.
- Dennison, P. A.: Observation of Fine Structure in the Interplanetary Medium. *Planet. Space Sci.*, Vol. 17, 1969, pp. 189-195.
- Dennison, P. A.; and Wiseman, M.: Preliminary Observations of the Effects of a Corotating Stream on Interplanetary Scintillation. *Proc. Astron. Soc. Australia*, Vol. 1, 1968, pp. 142-145.
- Ekers, R. D.; and Little, L. T.: The Motion of the Solar Wind Close to the Sun. *Astron. Astrophys.*, Vol. 10, 1971, pp. 310-316.
- Harries, J. R.; Blesing, R. G.; and Dennison, P. A.: 80 MHz Observations of Coronal Broadening of the Crab Nebula. *Proc. Astron. Soc. Australia*, Vol. 1, 1970, p. 319-320.
- Hewish, A.: The Spectrum of Plasma Irregularities in the Solar Wind. *Astrophys. J.*, Vol. 163, 1971, pp. 645-647.
- Hewish, A.; and Wyndham, J. D.: The Solar Corona in Interplanetary Space. *Monthly Notices Roy. Astron. Soc.*, Vol. 126, 1963, pp. 469-487.
- Hewish, A.; and Symonds, M. D.: Radio Investigation of the Solar Plasma. *Planet. Space Sci.*, Vol. 17, 1969, pp. 313-320.
- Houminer, A.: Corotating Plasma Streams Revealed by Interplanetary Scintillation. *Nature*, Vol. 231, 1971, pp. 165-167.
- Intriligator, D. S.; and Wolfe, J. A.: Preliminary Power Spectra of the Interplanetary Plasma. *Astrophys. J.*, Vol. 162, 1970, pp. L187-190.
- Jokipii, J. R.; and Hollweg, J. V.: Interplanetary Scintillation and the Structure of Solar Wind Fluctuations. *Astrophys. J.*, Vol. 160, 1970, pp. 745-753.
- Little, L. T.: Small Scale Plasma Irregularities in the Interplanetary Medium. *Astron. Astrophys.* Vol. 10, 1971, pp. 301-305.
- Little, L. T.; and Hewish, A.: Interplanetary Scintillation and its Relation to the Angular Structure of Radio Sources. *Monthly Notices Roy. Astron. Soc.*, Vol. 134, 1966, pp. 221-237.
- Lotova, N. A.; and Chashey, I. V.: On the Spectrum of the Small Scale Irregularities in the Interplanetary Plasma. Lebedev Institute preprint 11, 1971.
- Lovelace, R. V. E.; Salpeter, E. E.; Sharp, L. E.; and Harris, D. E.: Analysis of Observations of Interplanetary Scintillations. *Astrophys. J.*, Vol. 159, 1970, pp. 1047-1055.

Readhead, A.: Interplanetary Scintillation of Radio Sources at Metric Wavelengths, II Theory. *Mon. Notic. Roy. Astron. Soc.*, 1971, In Press.

Salpeter, E. E.: Interplanetary Scintillations 1, Theory. *Astrophys. J.*, Vol. 147, 1967, pp. 433-448.

Symonds, M. D.: An Investigation of the Solar Wind Near Sunspot Maximum. 1970 Cambridge Ph.D. dissertation.

Vitkevitch, V. V.; and Vlasov, V. I.: Solar Wind Observations. *Soviet Astron.* Vol. 13, 1970, p. 669.

*J. C. Brandt* I would point out that the latitude variation that one gets in solar wind velocity from the comets also implies absolutely no significant variation. We had a disagreement with you on the earlier data published, but I am happy to see now that has been resolved also.

## DISCUSSION

*K. H. Schatten* I would like to comment on the random velocity that you observed. I noticed that it dropped down to near zero right past where the Alfvén point is. I was thinking perhaps it might be related to these coronal magnetic bottles that may exist close to the sun. We found a transport time that would provide a velocity of the order of 200 km/sec, and we suppose these bottles were then sort of held stationary by the magnetic tension and then maybe pulled back to the sun. Your random velocities there were of the same order as your velocities, suggesting that some things were stationary and some were moving around. We might get random velocities of that magnitude. So this is what you may be seeing close to the sun. Do you have any comment on that?

*A. Hewish* Can you accommodate that within the fact that you also have a mean derivative of the same order of magnitude? You see, at the place where the random motions were around 200 km/sec the mean solar wind was also around that value. Would that be appropriate for a magnetic bottle?

*K. H. Schatten* Well, we observed them to be on the order to 200 km/sec, but presumably they stopped meantime between the sun and perhaps 10  $R_{\odot}$  distance out.

*A. Hewish* I'm still a little bit bothered. Might not the solar plasma in the bottle be slowing down as you approach the limit of the bottle? But apparently we see acceleration smoothly on out. Although there is a random velocity component, there is a mean acceleration behind it all.

*K. H. Schatten* Well, there's a mean acceleration of the solar wind.

*A. Hewish* Yes, there is. Magnetic bottles will be okay under those conditions, will they? Okay.

*W. M. Cronyn* I have two questions. First of all with regard to pattern lifetimes in the random velocities, I notice that the size of your observing triangle seems to be approaching the limits imposed by the size of the island you are located on. Do you think that the correlations are still sufficiently high that it would be worthwhile to go to substantially longer base lines to see if possibly you could see any decay in the pattern lifetimes, either as a result of velocity smearing or actual decay in the medium? The second question is about the scintillation index. If the scintillation index for small or relatively small elongation angles is a parallel function of radial distance from the sun then it seems to me that by the time one gets out to observations of an elongation angle of 90° one is only integrating through half of the total effective path line relative to the inner measurements, and therefore one might expect that the scintillation index would be some roughly 30 percent lower than such an extrapolation would indicate. But these measurements at 1 AU were taken at a longer wavelength, and the fact that there didn't seem to be any 30 percent drop might indicate that there is a stronger than linear dependence on wavelength. Would you comment on that?

*A. Hewish* Well, let's take your first question first. With regard to the scale size of the pattern and whether it's worthwhile to go to longer base lines, I think we reached the limit, not only because we're going to hit the sea in all directions but also that we are running out of correlation in the pattern. When the wind is not blowing along the line of

two sights the correlation that you get on the other one is usually poor. But, of course, if you wanted to determine the lifetime of the pattern it might well be worth going to a very long base line because you do know that the solar wind is strictly radial. This is something I didn't mention in my talk. We can't measure radial flow angles with great accuracy. But there is no evidence that they are other than within  $\pm 10^\circ$  from the radial direction. So if you assume a strictly radial outflow from the sun you can arrange your source that you're looking at to have the pattern drifting in that direction and can do a transcontinental correlation if you feel like it.

With regard to the other question about the spherical integration and should the scintillation index drop as you come out to  $90^\circ$ , yes, of course it should drop. These effects are not very noticeable, but if you follow around the scintillation index from elongations of  $0^\circ$  to  $180^\circ$  you can perform the spherical integration and find out precisely what it should do. In fact curve fitting the observations to calculations of that sort gives an extremely good fit right around to  $180^\circ$ . So within the sampling range I showed on that slide [fig. 12], which is roughly speaking within 1.5 AU, there is no hint that we are other than following the same radial variation.

*J. R. Jokipii* I have just one comment on this last point, then I want to ask a question. I'll be talking in a little while about this fitting of the scintillation index versus elongation to the sun. I was going to comment on the earlier point. I think one of the very interesting points about the work by Ekers and Little is that we do see this turbulence down where the solar wind is apparently being driven by hydromagnetic waves. It might be worthwhile for some of the experts on this to see if they can get some quantitative estimates, and see whether this is actually telling us that there are indeed waves close to the sun which are driving the solar wind. This may be the interpretation of the Ekers and Little result.

*D. S. Intriligator* I just wanted to say that I thought that the histograms comparing the interplanetary scintillation velocity with the spacecraft measurements were really remarkably good. Since the two spacecraft data you lumped together were Pioneer 6 and Vela, which at that time were actually separated by more than  $120^\circ$  with respect to the sun, they were really measuring quite different sorts of plasma.

*L. Davis* I would like to ask a brief question about these fluctuating velocities you see near the sun. What is the rough frequency of these observations? What frequencies are you sensitive to? And supposing one assumes fluctuations near the sun perpendicular to the radial direction, will you see velocities of that kind at all or do you see mainly velocities parallel to the radial direction?

*A. Hewish* Well, one only sees the resultant component across the line of sight. But with regard to the actual spectrum, I can't put a number on this immediately, but I think they were able to take out to about 20 Hz in the power spectra. Does that answer your question?

*L. Davis* Can you go down to 1 Hz? Can you go down to 0.1 Hz?

*A. Hewish* Oh, yes, that part is easy. But not much below 0.1 Hz because you run into other difficulties.

*J. V. Hollweg* The order of magnitude of the velocities that you showed looked very much like the Alfvén speed at the appropriate distances. I think around  $7 R_\odot$  the Alfvén speed is something like 200 km/sec, and then at  $50 R_\odot$  it would be down to maybe 75 km/sec or so. So this might be consistent with hydromagnetic waves.

*A. Hewish* Would you expect them to accelerate?

*J. V. Hollweg* The local Alfvén velocity is decreasing as you go out.

*E. N. Parker* I was very much interested in your remark that you felt the high frequency oscillations, the 100- and 200-km variations, were something distinct from the large-scale fluctuations. Could you repeat the arguments that lead you to believe they are distinct? For instance, if you were to extrapolate the spacecraft power spectrum would it

decrease at high wave number and leave your high frequency stuff as a spike, or what is the basis for the distinction?

*A. Hewish* Well, I'll come back to this. We shall be hearing more about trying to fit our data to spacecraft data, but my basic argument is as follows: In the presence of a spectrum that is a steep power of wave number, if you take the existing spacecraft data, which give a wave number dependence of about  $k^{-1}$  or slightly faster, then the medium itself is varying as  $k^{-3}$ . If you take a simple analysis, now, that means that in our two-dimensional work on the ground we would be dealing with a wave number spectrum in our diffraction pattern that is going as wave number to the  $-2$ , if you take the space data. Now, when you look at widely different wavelength variations you are really sampling the spectrum at points governed by the Fresnel cutoff, which varies as the square root of the wavelength  $\sqrt{k}$  so that by observing over a wide range of wavelength if the scale size of your pattern is a function of the observing wavelength you are essentially sampling that wave number spectrum at different points. Now, I can find no evidence of a variation that would support a steep power law in that spectrum. I say from our scintillation data that the wave number spectra that we are observing on the ground is more or less flat. It certainly can't be sloping as much as  $k^{-1}$ , and  $k^{-2}$  is what you would get if you extrapolate spacecraft data. That is the basic argument, and I guess there will be discussion on this as we go along.

*K. H. Schatten* With regard to the comment concerning the Alfvén velocity being similar to your random velocity, the magnetic bottle is essentially a big Alfvén wave where the plasma pushes out the magnetic field and then it moves back and pushes the plasma in. So I think that would be consistent with the velocities being on the order of the Alfvén velocity as you move out.

*J. V. Hollweg* Would you describe the bottle, though, as a turbulent motion or as a systematic moving out and back, rather than a hopping back and forth?

*K. H. Schatten* I think it would be a systematic moving out and back, but I don't think we have enough evidence to say one way or the other.

*A. Barnes* One thing I don't quite clearly understand is whether the random velocities are essentially different in velocity measured at the same time but for different scale sizes, or whether they are measurements taken at different times and these represent temporal fluctuations. Or is it some mixture of these?

*A. Hewish* In the analysis of drifting diffraction patterns you can determine both a regular drift component of velocity and at the same time in the same analysis you can determine to what extent the diffraction pattern is changing as it moves. The rate at which the pattern changes as it moves is customarily defined in terms of a random velocity component, but really what it is saying is that the diffraction pattern is bubbling, boiling, as it moves along and that if the random velocity was comparable to the mean velocity, then by the time the pattern has moved one scale length it's a different pattern. So it's a measure of the non time-stationary property of the medium.

*G. Newkirk* Is it possible to combine these observations, which are essentially total power observations, with polarization measurements, or do the same thing for different states of polarization in order to see the fluctuations in the direction of the long axis of the singularities in space?

*A. Hewish* Well, for radio polarization, of course, you have to have a polarized source, and we are not looking really at polarized sources. Some quasars do indeed have a percentage of polarization. But what you want is a completely linearly polarized source to do work of this kind. But in any case I would not really expect any difference because we are dealing here with weak scattering and I think the sense of polarization is going to be quite irrelevant.

## COMMENTS

*W. A. Coles* I would like to describe briefly the work being done on interplanetary scintillations at UC San Diego. We have made regular three-station observations at 74 MHz since June 1970. These data are not completely analyzed, in the sense that we haven't calibrated or normalized them to our satisfaction. The estimated drift velocity of the scintillation pattern can depend heavily on accurate normalization, so we are not prepared to present velocity measurements at this time.

Our data show exponential behavior in both power spectra and cross-power spectra and corresponding to this, the correlation functions are distinctly bell-shaped rather than gaussian as is often assumed. Our observing system consists of three array antennas located near San Diego (fig. 1) and connected to the laboratory at UCSD by commercial telephone lines. The three stations are separated by roughly 100 km.

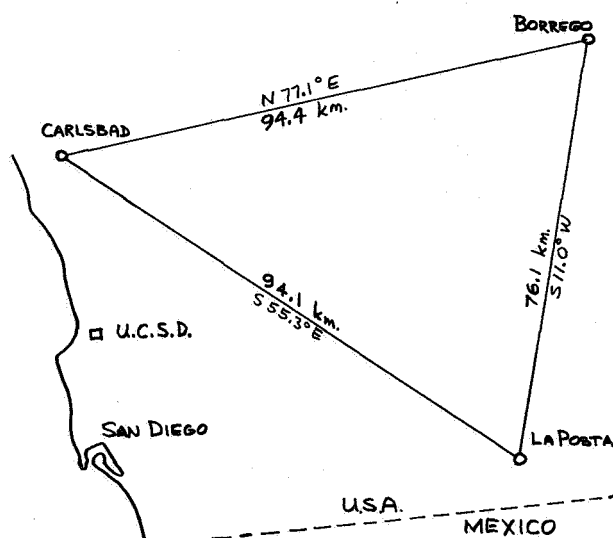
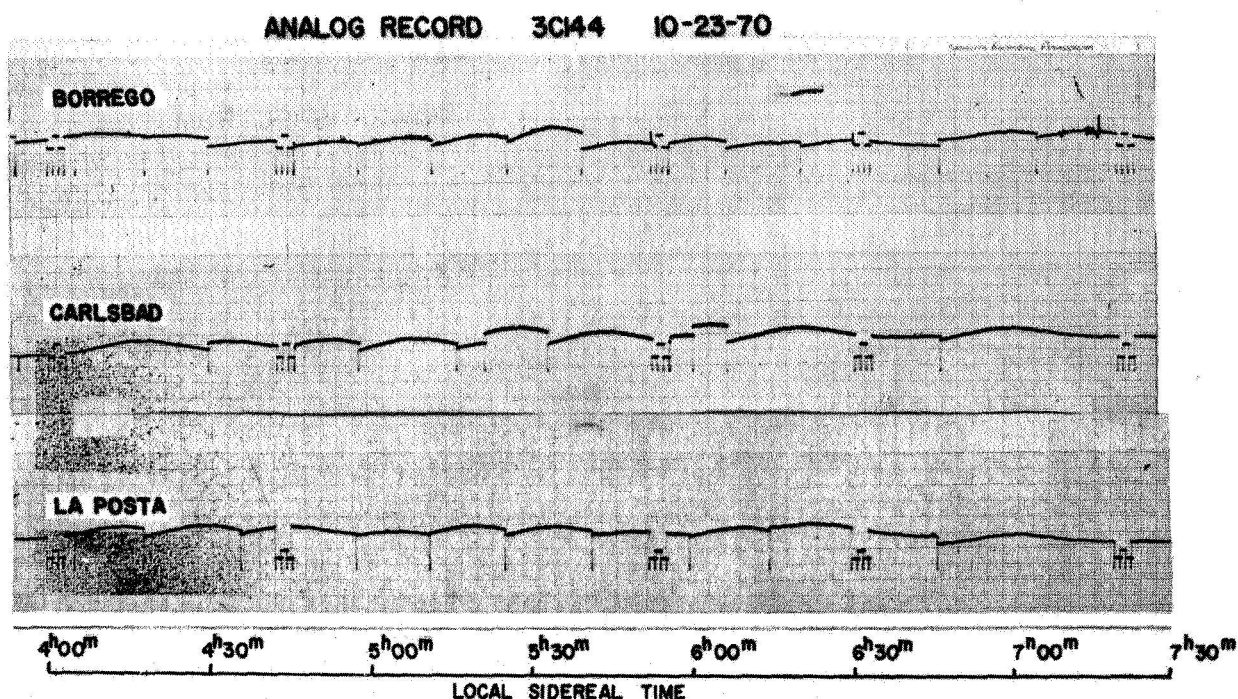


Figure 1. Geometry of observation sites.

The received data are digitized and processed by a Sigma 5 computer, which also controls the antennas and the receivers. Each antenna is a square phased array of 256 elements, 70 m on a side. The beam efficiency is about 60 percent corresponding to some 3,000 m<sup>2</sup> of effective area. The feed system, which will operate over bands of several megahertz, forms 512 discrete pencil beams, each 3.5° in diameter. Figure 2 shows one day's observations on 3C 144 as recorded. The receivers are switched from beam to beam as the source drifts through the pattern causing the obvious modulation on each record. Since the sites are not identical, the switching times are chosen to maximize the time during which all three sites have a strong enough signal to analyze.

The receiver design is straightforward except that special care has been taken to reduce intermodulation interference, because at 74 MHz one is fairly close to the television band. The receiver parameters, such as bandwidth and gain, are remotely controllable. Normally, the receivers operate in a total power mode, since the gain variation is much slower than the scintillation rate. For longer observations such as drift scan calibrations the radiometer mode is used. The telephone lines have limited dynamic range, so a controllable offset voltage has to be added to data before transmission. Telephone line data are filtered and read into the Sigma 5 for preliminary processing. The data are also



**Figure 2.**  $3\frac{1}{2}$  hr drift scans taken from the three sites in figure 1.

recorded on magnetic tape since frequent interference and limited reliability prohibit real-time data reduction without some backup storage. The computer operates on a time-sharing mode so that the observations and reductions may be done simultaneously.

The basic sensitivity limitation for scintillation observations is estimation error for strong sources. For example, the scintillation variance for 3C 144 and 3C 273 is much greater than the variance due to the noise. This being the case, about 20 min of data is required to obtain an adequate spectral estimate regardless of the source strength. For weaker sources the time required increases greatly since it goes as the fourth power of the source flux. Under optimal conditions for our observing system a 10-flux unit source would be considered strong. So that will give us a large number of sources to look at. At present two of the three antennas are about five times worse than that, primarily because of excessive losses in the feed system. This loss is being eliminated by the use of multiple preamplifiers distributed throughout the feed system.

The data analysis consists of calculations of power spectra, cross-power spectra, and their Fourier transforms, the covariance functions. Most of the effort required to produce a good set of results goes into such problems such as editing, interference rejection, timing, and calibration. Because the beams from the three sites do not all point exactly in the same direction the effective gain for cross-covariance differs from that for autocovariance, and this makes normalization more critical. After the spectra are computed they are fitted to a gaussian or an exponential shape and from the shape parameters, the pattern scale sizes, orientation, and velocity are determined. A typical rough power spectrum is shown in figure 3. The scintillation represents an enhancement at the low frequency end between 0 and 2 Hz. There was little ionospheric scintillation on this particular day.

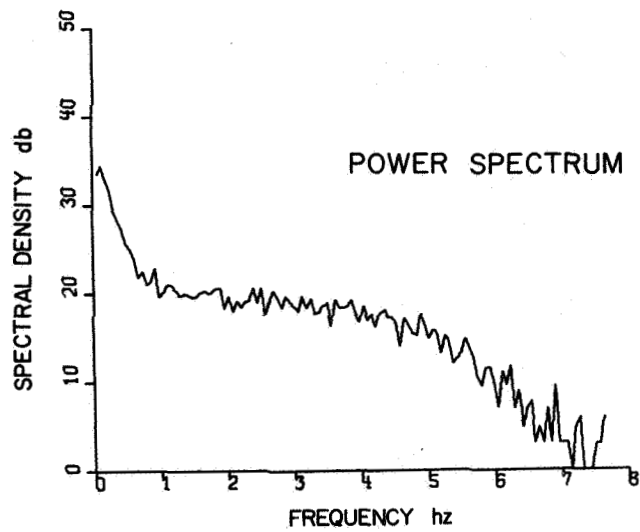


Figure 3. A typical power spectral density.

Figure 4 shows the cross-covariance functions for three-site observations. The cross-covariances have the same shape as the autocovariances, but they are delayed by an amount that is small compared to their width. Figure 5 shows a cross-power spectrum for two sites, which gives a good idea of the signal-to-noise ratio and the estimation errors

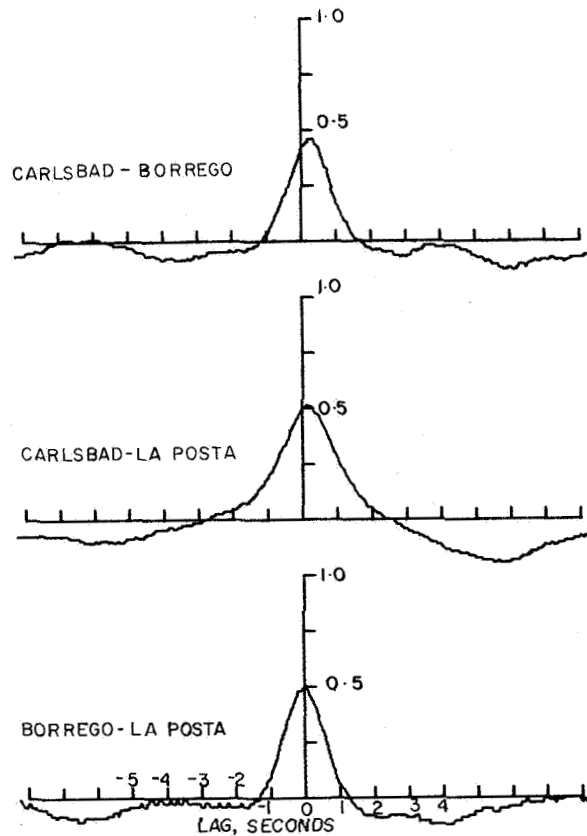


Figure 4. Cross covariances for three site observations.



involved. Considered as a measure of the amount of correlated power between the two sites, figure 5 shows that interference and system noise and telephone line effects are essentially negligible. There is a smooth, approximately exponential decay in the cross-power spectrum down to 0 at about 2 Hz.

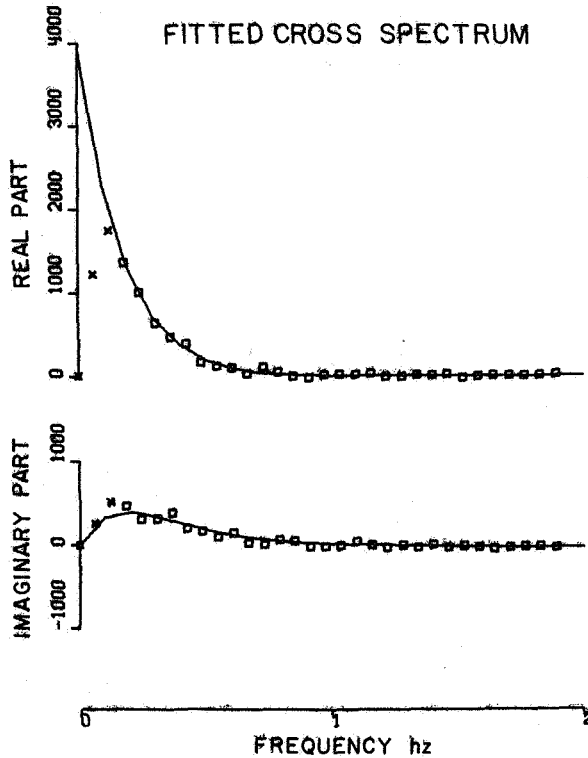


Figure 5. A cross-power spectrum for two sites.

Figure 6 shows the spectra for the three sites and the cross spectra between them, with a "best-fit" exponential drawn over the data. One can see that these "fitted" functions all agree within the estimation error, and that the spectra all match the exponential shape well.

Figure 7 shows spectra for three different days on source 3C114 shortly before it was occulted by the sun. The shape of the spectrum remains rather accurately exponential but the width of it increases as the elongation decreases.

The reason that we weren't prepared to present velocity measurements and the reason we are careful about normalization is that we are not presently satisfied that the intensity pattern is indeed "frozen" as was assumed in the work described by Dr. Hewish. If it were, the velocity would be the site separation divided by the displacement of the cross-correlation function. This "apparent" velocity could then be used to estimate a scale size by multiplying it with the width of the autocorrelation function. An independent measure of the scale size comes from the magnitudes of the cross-correlations between the sites at zero time lag. If these two don't agree, then a significant time change must have occurred in the pattern. Alternatively, one can assume that there is a time change, estimate the decay time, and see if it is indeed comparable with the drift time. But it is more difficult to get amplitudes than time lags in cross-correlation functions, and therefore it is better to estimate the scale size in these two different ways.

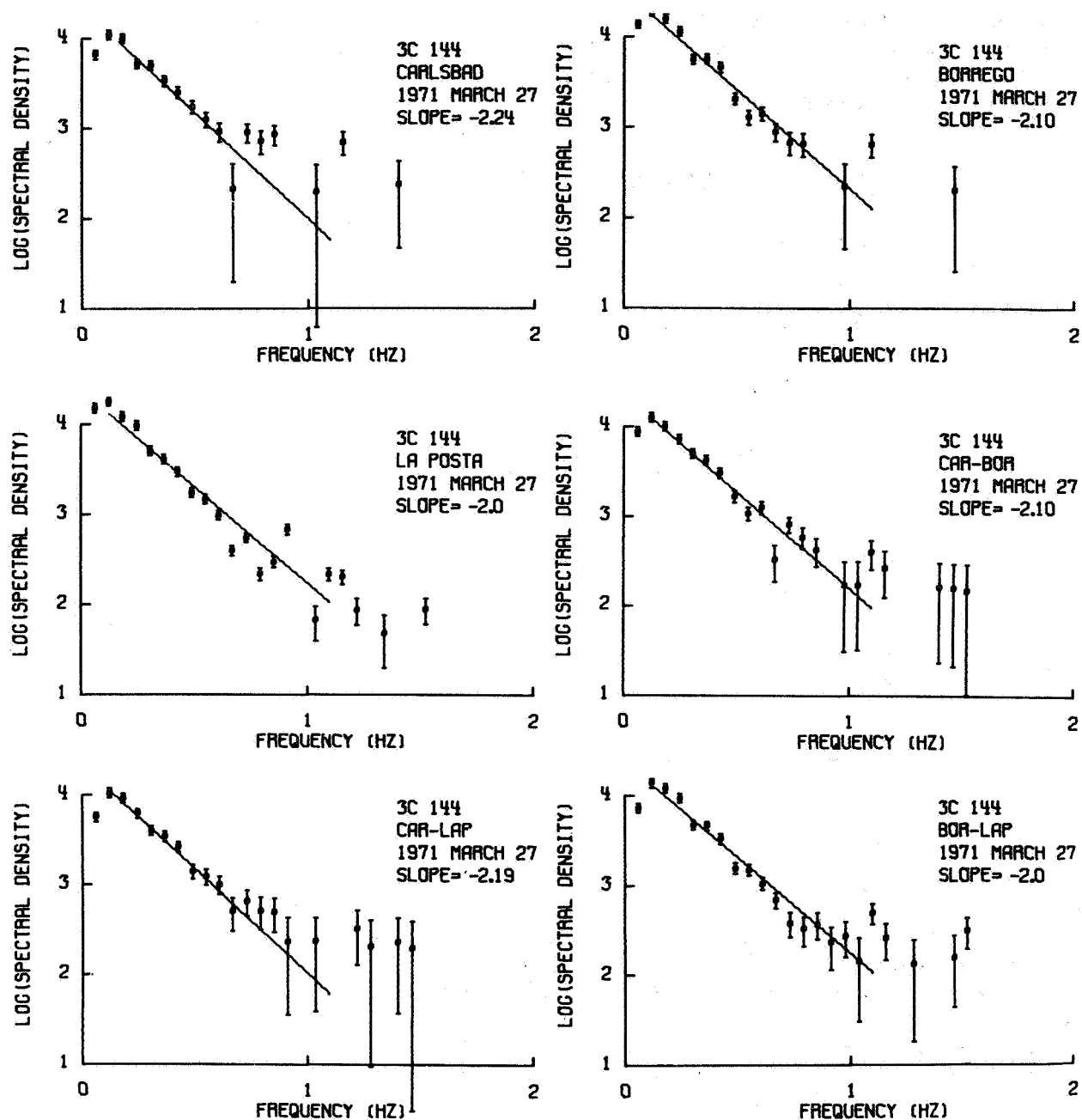


Figure 6. Auto and cross spectra with exponential fits for the three sites of figure 1.

Another point, which was mentioned by previous speakers, concerned the effect of integrating along the line of sight. Contributions from equal path lengths add into the final result as the square of the density variation. Hence one might expect high density regions to dominate the scintillation. Now it is known that high density tends to be correlated with low velocity, so one may tend to observe lower velocities on the average than would a space probe. Furthermore, the presence of several streams with different velocities will cause the pattern to appear to rearrange itself. However, if one then

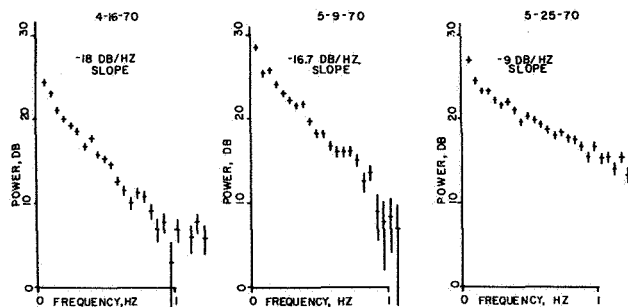


Figure 7. Spectra taken over three different days of 3C 144 just prior to occultation by the sun.

calculates the velocity assuming that this is a rearrangement it will tend to be biased below the average of the velocities along the line of sight.

*A. Hewish* From the cross correlograms you showed on the slide (fig. 4) there seemed to be a significant tendency for the correlation to become negative as you dropped away from the central maximum. If this is real, it would suggest some quasiperiodic nature in the irregularities. Do you regard these below-zero indications as significant?

DISCUSSION

*W. A. Coles* No, I am not sure they are statistically significant. Those raw correlations I presented in fact are zero mean, because the dc has to be subtracted off the power spectra analysis, anyhow. And we simply correct for that when we fit them to the curve.

*E. C. Roelof* If the scale sizes at 1 AU are coming out to be the order of a proton gyroradius, this from my simple-minded point of view would sort of suggest that this is not a fluid phenomenon, this is more a kinetic phenomenon. If that is the case then wouldn't one expect these patterns to be quite dynamic and nonstationary? And if so, then why does one seem to derive a well-ordered velocity comparable to the spacecraft velocities?

*W. A. Coles* Well, you're asking questions which I would prefer to be answered by a plasma physicist. We are simply saying what we observed and we would like somebody to explain it. Can you say why structures on a time scale of 200 km should not last for the required 0.6 sec or 0.3 sec for which we see them?

# WAVELENGTH DEPENDENCE OF THE INTERPLANETARY SCINTILLATION INDEX

*J. V. Hollweg and J. R. Jokipii*

**ABSTRACT** Published observations of the interplanetary scintillation index  $m_z$  are shown to vary with wavelength in a manner consistent with a smooth, power law spectrum of plasma fluctuations. This is in contrast to recent work arguing that the data require a spectrum with two separate regimes. It is concluded that published observations of  $m_z$  are consistent with either type of density spectrum.

A problem of considerable interest in the physics of the solar wind is the relation between interplanetary scintillation of radio sources and the structure of the solar wind turbulence. In particular, it is hoped that interplanetary scintillations can be used to help determine the structure of the solar wind in regions not accessible to direct measurement.

A reasonable first approximation to the scintillation problem is given by the "thin-screen" model in which the fluctuating solar wind plasma is replaced by a thin, phase-changing screen perpendicular to the direction of propagation of the wave. The intensity fluctuations are then built up by interference as the wave propagates to the observer. The observer is situated at a distance  $z$  from the plane of the screen. In the solar wind, the equivalent screen is assumed to be placed at the point of nearest approach of the ray path to the sun, since this is where the effect of the solar wind is greatest, and then  $z$  is of the order of 1 AU. As the fluctuations are carried out from the sun at the solar wind velocity  $V_w$ , the intensity fluctuations in the plane of the observer are also convected at the wind velocity. Hence, the spatial variations in intensity with wavelength  $\lambda$  are seen as temporal fluctuations with time  $\sim \lambda/V_w$ .

Of interest, then, is the wave number spectrum of intensity fluctuations in the plane of the observer, at a distance  $z$  from the phase-changing screen, and the

relation of this spectrum to the power spectrum of density fluctuations in the solar wind. A thorough discussion of this problem is given by *Salpeter* [1967]

Let  $\delta\rho(\mathbf{r})$  be the fluctuation in solar wind plasma density about its mean. Then the power spectrum of density fluctuations is defined as

$$P_\rho(\mathbf{q}) = \int d^3\zeta \langle \delta\rho(\mathbf{r}) \delta\rho(\mathbf{r} + \zeta) \rangle e^{i\mathbf{q} \cdot \zeta} \quad (1)$$

Similarly, if  $\delta I(\mathbf{r})/\langle I \rangle$  is the relative fluctuation in radio intensity in the plane of the observer, as discussed above, we may define the power spectrum of intensity fluctuations as

$$m_z^2(\mathbf{q}) = \frac{1}{\langle I \rangle^2} \int d^2\zeta \langle \delta I(\mathbf{r}) \delta I(\mathbf{r} + \zeta) \rangle e^{i\mathbf{q} \cdot \zeta} \quad (2)$$

where the integration is carried out over the entire plane. It may be shown [*Jokipii*, 1970] that if the scintillation index  $m = (\langle \delta I^2 \rangle)^{1/2} / \langle I \rangle \ll 1$ , the two spectra are related by

$$m_z^2(q_x, q_y) = 4 \sin^2 \left[ \frac{(q_x^2 + q_y^2) z}{2k} \right] \frac{C}{k^2} P_\rho \quad (q_x, q_y, q_z = 0) \quad (3)$$

where  $k$  is the wave number of the electromagnetic wave,  $z$  is the distance from the screen to the observer,

*The authors are with the Physics Department of the California Institute of Technology, Pasadena, California.*

and  $C$  is a constant.

Note that the dependence of the  $\sin^2$  factor on  $(q_x^2 + q_y^2)$  states quite generally that plasma fluctuations much larger than the Fresnel scale  $\sim \sqrt{z/k}$  are not effective in causing scintillations. Using typical values for the parameters,  $z \approx 1$  AU and  $k$  corresponding to 100-MHz radio waves, one finds that the Fresnel scale is of the order of 200 km. Using this fact, *Jokipii and Hollweg* [1970] pointed out that the observed scintillation scales of a few hundred km or so are quite consistent with the observed dominant solar wind scales of the order of  $10^6$  km [*Intriligator and Wolfe*, 1970].

Here we briefly consider the wavelength dependence of the scintillation index  $m$  to see whether or not observations of  $m$  can be used to rule out certain forms of the spectrum  $P_\rho(\mathbf{q})$ . *Hewish* [1971] has argued that the data rule out a smooth variation of  $P_\rho(\mathbf{q})$  from the small values of  $q$  corresponding to the dominant density scales to the higher values relevant to scintillation. We shall argue that the available data do not force such a conclusion. From equation (2), one easily derives

$$m^2 = \frac{\langle \delta I^2 \rangle}{\langle I \rangle^2} = \frac{1}{4\pi^2} \iint_{-\infty}^{\infty} dq_x dq_y m_z^2(q_x, q_y) \quad (4)$$

Now assume  $P_\rho(\mathbf{q})$  is isotropic, so that  $m_z^2(q_x, q_y) = m_z^2(q)$ , with  $q = \sqrt{q_x^2 + q_y^2}$ . Then equation (4) becomes

$$m^2 = \frac{2}{\pi} \frac{C}{k^2} \int_0^\infty q \sin^2 \left( \frac{q^2 z}{2k} \right) P_\rho(q) dq \quad (5)$$

We consider a simple power law for  $P_\rho(q)$ . Let

$$P_\rho(q) = A q^{-\alpha_3} \quad (6)$$

where the subscript 3 is used to emphasize that this is a three-dimensional spectrum. It is possible that a better representation of the actual situation in the solar wind would be given by a power law spectrum with a cutoff at some wave number  $q_0$ . This interesting case is not considered further here. For a given value of  $\alpha_3$ , the temporal spectrum observed on a spacecraft [*Intriligator and Wolfe*, 1970] would be

$$P_\rho(f) = B f^{-(\alpha_3 - 2)} \quad (7)$$

[*Hollweg*, 1970], where  $f$  is frequency.

If  $P_\rho(q)$  has the form given in equation (6), it is then a simple matter to substitute this into equation (5) to obtain, for  $2 < \alpha_3 < 6$ ,

$$m^2 = -\frac{A}{\pi} \frac{C}{k^2} (2) \left( \frac{\alpha_3}{2} - 2 \right) \left( \frac{z}{2k} \right)^{-\left(1 - \frac{\alpha_3}{2}\right)} \Gamma \times \left( 1 - \frac{\alpha_3}{2} \right) \cos \left[ \frac{\pi}{2} \left( 1 - \frac{\alpha_3}{2} \right) \right] \quad (8)$$

The wavelength dependence of  $m_z$  follows immediately as

$$m \propto k^{-(1/2 + \alpha_3/4)} \propto \lambda^{(1/2 + \alpha_3/4)} \quad (9)$$

Thus with  $\alpha_3 \sim 3$ , as observed [*Intriligator and Wolfe*, 1970], we expect  $m \propto \lambda^{1.25}$ . This is in contrast to a gaussian density fluctuation spectrum, which leads to  $m \propto \lambda$ .

*Hewish* [1971] has argued forcibly that the available published data required  $m \propto \lambda^{1 \pm 0.05}$ . He uses this to infer that there are two regimes in the density power spectrum, a long-wavelength regime that contains most of the power and a separate short wavelength regime that causes the observed scintillations. Between these regimes he postulates little or no spectral power. This view, of course, is consistent with the arguments of *Jokipii and Hollweg* [1970] concerning the dominant scale of the density fluctuations.

Such a spectrum, if true, would be of considerable interest physically. Hence we decided to check whether, indeed, the data used by *Hewish* actually rule out a dependence such as that given in equation (9) with  $\alpha_3 = 3$ . We find that they do not. Following the procedure outlined by *Hewish* [1971], we utilized the data reported by *Bourgeois* [1969], *Harris and Hardebeck* [1969], and *Hewish and Symonds* [1969].

The idea is that if  $m \propto \lambda^a$ , then  $m\nu^a$  (where  $\nu = c/\lambda$ ) should be independent of frequency. Unfortunately, reliable simultaneous measurements of  $m$  at different frequencies do not exist. We must instead compare measurements obtained at different times and at different elongations. Since the characteristics of the solar wind vary from day to day, there is considerable spread in the data. Nevertheless, if  $m\nu^a$  is plotted as a function of source elongation, data obtained for different observing frequencies should fall, within the aforementioned spread in the data, on a smooth curve. Figure 1(b) shows a plot of  $m\nu$  versus elongation. The data fall on a smooth curve, and one might be tempted to conclude that, in fact,  $m \propto \lambda^{1.0}$  [*Hewish*, 1971]. But figure 1(a) shows the same data, with  $m\nu^{1.25}$  plotted against elongation. The data points again lie on a smooth curve. We conclude that within the uncertainties of the data,  $m \propto \lambda^{1.25}$  is as good as  $m \propto \lambda$ . To put this more quantitatively, the mean square deviations of the points

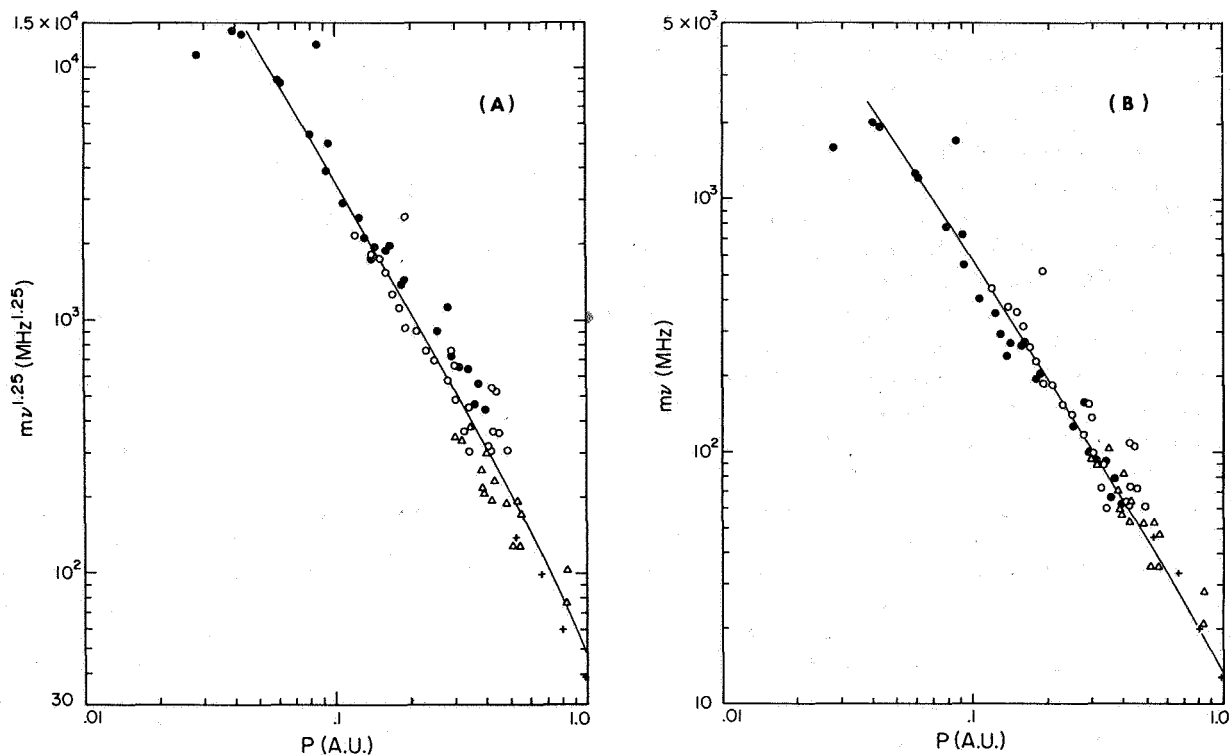


**Figure 1.** Scintillation index  $m$  multiplied by  $\nu^{5/4}$  (curve a) and by  $\nu$  (curve b) versus source elongation.  $P$  is the closest distance of the ray path to the sun. Solid circles are 3C279 at 2695 MHz [Bourgois, 1969]; open circles are CTA 21 at 611 MHz [Harris and Hardebeck, 1969]; triangles are 3C138 at 178 MHz; and crosses are 3C287 at 81.5 MHz [Hewish and Symonds, 1969].

from the smooth curves for  $m\nu$  and  $m\nu^{1.25}$  versus elongation, are 20 and 23, respectively, in arbitrary units.

We therefore conclude that the published scintillation indices at various frequencies do *not* force the conclusion that  $m$  is proportional to  $\lambda$ . Hence smooth, power law, density spectra are consistent with the published scintillation index measurements, in contrast to the conclusions published by Hewish [1971]. Hopefully, improved measurements will make it possible to resolve this question in the near future.

#### ACKNOWLEDGMENTS

We are grateful to L. Davis, Jr., and D. Intriligator for helpful discussions. This work was supported, in part, by the National Aeronautics and Space Administration Grant NGR 05-002-160.

#### REFERENCES

- Bourgois, G.: Scintillations Interplanétaires des Radio-sources à 2695 MHz. *Astron. and Astrophys.*, Vol. 2, 1969, p. 209.
- Harris, D.E.; and Hardebeck, E. G.: Interplanetary Scintillations. V. A Survey of the Northern Ecliptic. *Astrophys. J. Suppl.*, Vol. 19, 1969, p. 115.
- Hewish, A.: The Spectrum of Plasma-Density Irregularities in the Solar Wind. *Astrophys. J.*, Vol. 163, 1971, p. 645.
- Hewish, A.; and Symonds, M. D.: Radio Investigations of the Solar Plasma. *Planet. Space Sci.*, Vol. 17, 1969, p. 313.
- Hollweg, J. V.: Angular Broadening of Radio Sources by Solar Wind Turbulence. *J. Geophys. Res.*, Vol. 75, 1970, p. 3715.
- Intriligator, D. A.; and Wolfe, J. H.: Preliminary Power Spectra of the Interplanetary Plasma. *Astrophys. J.*, Vol. 162, 1970, p. L187.
- Jokipii, J. R.: On the "Thin Screen" Model of Interplanetary Scintillations. *Astrophys. J.*, Vol. 161, 1970, p. 1147.
- Jokipii, J. R.; and Hollweg, J. V.: Interplanetary Scintillations and the Structure of Solar Wind Fluctuations. *Astrophys. J.*, Vol. 160, 1970, p. 745.
- Salpeter, E. E.: Interplanetary Scintillations. I. Theory. *Astrophys. J.*, Vol. 147, 1967, p. 433.

*A. Hewish* I just have one comment I should like to make before handing over. I knew we were going to have some discussion on this point and my only comment here is that I don't think you can stretch the data to find  $\lambda^{1.25}$ . Now, this at the moment we can regard as a matter of opinion and leave it there. But you did, I think, dismiss somewhat quickly the evidence I brought forward on the power spectrum. There is a great deal of evidence on the wavelength dependence of the power spectrum, and I find no evidence that the scale size as we measured it is a function of the observing wavelength. This would certainly be true in the case of a spectrum such as you suggest.

*J. R. Jokipii* I will say that I was not aware of all the evidence that was available. The main point that had been made prior to this meeting and in the literature was that one could use these two types of curves to make the decision. And I was just trying to point out that I at least did not want to make the decision.

*B. Rickett* Dr. Jokipii, on the curve you showed was that a straight line you draw with  $\lambda$  to the 1.25 or was it a smooth curve?

*R. A. Jokipii* A smooth curve. There is no particular reason to expect it to be any particular shape. If I could have gotten a figure 8 through the points I would have regarded that as just as good.

#### COMMENTS

*D. S. Intriligator* I have been asked to review the space observation that everybody has been referring to this morning: the power spectra of the number density fluctuations of the protons in the solar wind. First, I would like to briefly discuss the motivation for our doing this. As you have heard this morning, from the interplanetary scintillation data one finds that the scale size for the interplanetary plasma is around 100 to 200 km, which is really quite small. From previous power spectra of the magnetic field done by *Coleman* [1966] and others a scale size was found of approximately  $10^6$  km. The difference between these magnetic field scale sizes and the ones inferred for the plasma from the interplanetary scintillation data is approximately four orders of magnitude. *Jokipii and Hollweg* [1970] suggested that direct spacecraft observations of the fluctuations of the proton number density of the solar wind plasma might yield scale sizes similar to those that had been found for the magnetic field. Those are the data we have. We have direct observations of the number density fluctuations in the solar wind and we find that we can set a limit—a lower limit—to the scale size of fluctuations for the solar wind plasma and that in fact it is at least  $10^6$  km. So it is different from the scale size inferred from the interplanetary scintillation data by approximately four orders of magnitude. I don't feel this is inconsistent with the interplanetary scintillation data because we are just measuring two different frequencies of the plasma. At this time our measurements, as you have heard several times already, cannot be directly connected with this interplanetary scintillation scale size. There are several possibilities: the 100 to 200 km could relate to the inner scale of the large-scale turbulence that we observed or it could be related to a different plasma regime. The data at this point do not necessarily distinguish between the two. Next I will review the data that we have. Some have been published [*Intriligator and Wolfe*, 1970].

Figure 1 shows nine power spectra that were obtained from Pioneer 6 solar wind data from the Ames Research Center plasma probe. Each of the spectra represents approximately one-half day's worth of data. We feel that the variation in power levels of these data sets is relevant and that it represents the lower frequency power fluctuations associated with the solar stream structure you heard about earlier during the week. The sectors and the high velocity streams are a few days wide and in general the time between our data sets is a few days. Since these data were taken, we have run many more power spectra, and we find the same conclusion, that the slope for the most part is the same, it approximately goes as  $f^{-1.3 \pm 0.1}$ , but that the level of power of the different curves does vary depending on the fluctuations that are going on in the plasma at that time.

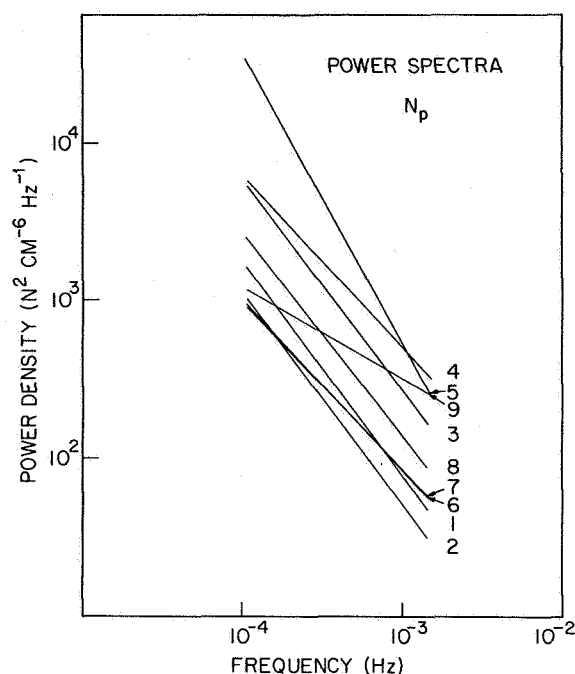


**Figure 1.** Power spectra of  $N_p$ , the number density of protons in the solar wind, for each of the nine data sets listed in table 1.

The way we get our limit to the scale size of the turbulence of the solar wind plasma is that the curve in figure 1 is rising at  $10^{-4}$  Hz. A frequency of  $10^{-4}$  Hz corresponds to a scale size of  $10^6$  km. Since this curve has not turned over yet—in other words, the two-point correlation function has not fallen to zero—there clearly is a lot of power here and that this is associated with the scale size of at least  $10^6$  km. The interplanetary scintillation data are off the figure to the far right and we are not looking at this regime.

Table 1 gives some of the specifics associated with each of the nine data sets in figure 1. It shows that the data were taken between December 21, 1965, and January 13, 1966. As noted, we have filled in consecutively between all of these; we also have extended the data for essentially 2-1/2 solar rotations from the launch of Pioneer 6 and the 2 months after the launch of Pioneer 7. Unlike the interplanetary scintillation data, our data are not constrained primarily by telephone lines and noise but rather by tracking gaps. The only criteria we used in selecting these data sets was that each set be of equal length (100 possible data points, about half a day) and that the number of data gaps during the interval be 20 or less. We have a data point every 7 min so each data set is  $\sim 11.6$  hr. There are two types of data gaps. The first is the interval when there was no tracking of the spacecraft. The other results from the “aliasing” of the time series of the plasma data. That is, during the time (the 7-min interval) we are trying to measure the exact solar wind parameters (number density, temperature, and velocity) the plasma parameters are changing so fast that meaningful parameters such as number density cannot be obtained. In table 1 the equivalent degrees of freedom reflects the amount of data gaps in the data and also the distribution of the gaps. This was just taken the standard way using the *Blackman and Tukey* [1959] method. The equivalent degrees of freedom is, of course, smaller than the degrees of freedom one would obtain if there were no data gaps. Column 4 of table 1 lists the slopes of each of the curves in figure 1. Calculating the mean slope from nine individual slopes listed yields a slope of  $f^{-1.3 \pm 0.1}$  for the frequency range



**Table 1.** Relevant parameters for each of the nine data sets used in this analysis. Number of the data set in column (1) refers to number of the corresponding curve plotted in figure 1. Column (2) is the date the observations were made by the Ames Research Center solar wind plasma probe on Pioneer 6. The "equivalent" number of degrees of freedom, listed in column (3), reflects the presence of the number of data gaps and their distribution within each data set [Blackman and Tukey, 1959]. Column (4) lists the slope for each of the individual data sets shown in figure 1. Columns (5) and (6) list the average number density of protons in the solar wind and the average bulk velocity, respectively.

Data set	Observation date	Equivalent number of degrees of freedom	Slope	Average proton number density, $\text{cm}^{-3}$	Average streaming velocity, $\text{km sec}^{-1}$
1	Dec. 21, 1965	15.6	-1.4	6.7	340
2	Dec. 22-23, 1965	12.9	-1.3	4.3	421
3	Dec. 24-25, 1965	17.6	-1.3	7.3	435
4	Jan. 3-4, 1966	10.2	-1.1	6.5	378
5	Jan. 6-7, 1966	10.9	-1.8	10.7	337
6	Jan. 8-9, 1966	9.6	-1.1	6.3	456
7	Jan. 10-11, 1966	11.6	-1.1	3.8	409
8	Jan. 12, 1966	11.6	-1.3	7.1	345
9	Jan. 12-13, 1966	10.2	-0.6	10.0	335

shown. As mentioned, more recently we have studied a number of other data sets and found similar results.

Figure 2 is the same spectrum that Jokipii just showed, and it indicates the mean slope of  $f^{-1.3 \pm 0.1}$  obtained from the nine data sets where the points are the averaged power of the individual data points at each of the difference frequencies. Since we consider the changes in the level of the power between the nine spectra to be real, reflecting the lower frequency variations in the solar wind stream structure (the high velocity streams, etc.), it would be wrong to take a slope that would average these out. Therefore, the line calculated in this curve is the mean of the slopes of the individual curves. In other words, this reflects the fact that the slopes for most of the data sets are similar but the levels of power are different at these frequencies. Since the slope is still rising at  $10^{-4}$  Hz this is evidence that the scale size of turbulence for the solar wind protons is at least  $10^6$  km. This is similar to the scale size obtained from the magnetic field measurements but differs

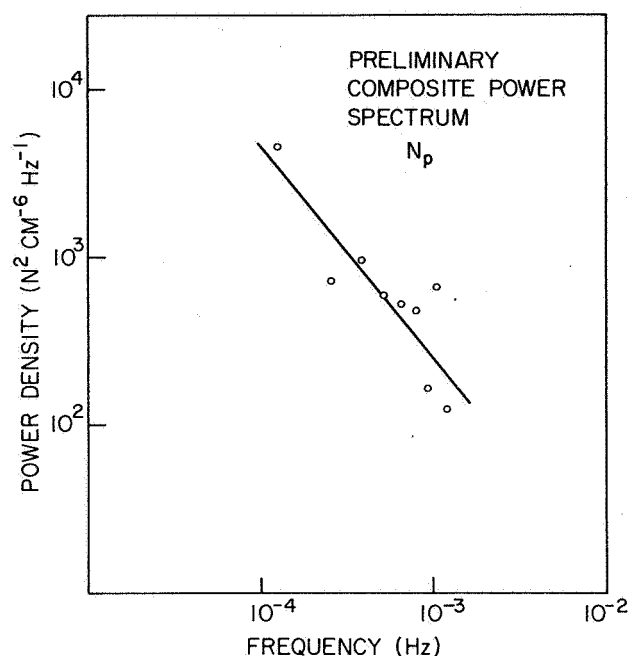


**Figure 2.** Preliminary composite power spectrum of  $N_p$  for December 1965 and January 1966. The individual data points represent the average value [Blackman and Tukey, 1959; Coleman, 1966] of the number density fluctuations in the solar wind at each of the frequencies shown and are based on the nine data sets in figure 1. The curve was obtained by calculating the mean slope from the slopes of the nine data sets.

from that previously inferred from the interplanetary scintillation measurements by four orders of magnitude.

Recently we have performed many other power spectral analyses. We have continued to run the number density spectra, and we have also looked at other quantities. For example, we have calculated the power spectra of the different components of the solar wind velocity ( $V_r$ ,  $V_\theta$ , and  $V_\phi$ ). These are also the first power spectra of this type that have ever been run since previously all of the power spectra have been for the solar wind speed not velocity. That is, they assume that the velocity is completely radial. The Ames Research Center plasma probe can measure the three components of the velocity. We have used this data to obtain power spectra for these different quantities. This has been done for a number of data intervals; figures 3 and 4 show the results for two of the data sets.

In general, the slope of the curves  $V_r$ ,  $V_\theta$ , and  $V_\phi$  in figure 3 are quite similar to the slope we found for the power spectrum of the number density. We find that just as the power spectrum of the number density in the frequency range  $\sim 10^{-4}$  Hz to  $10^{-3}$  Hz varies as  $f^{-1.3}$  the spectra of  $V_r$ ,  $V_\theta$ ,  $V_\phi$  vary as  $f^{-1.0}$ .

Figure 4 is from December 26 and 27, 1965, and it shows the same quantities as figure 3. The slope of the number density and the power of number density versus frequency, as well as for  $V_r$ ,  $V_\theta$ , and  $V_\phi$ . As in figure 3, the slopes of the spectrum for the three velocity components are quite similar. This is what I noted yesterday in reference to Burlaga's paper (p. 309); we have looked at 30 half-day intervals for the velocity, and in these data there are no systematic differences between the curves of  $V_r$ ,  $V_\theta$ , and  $V_\phi$ : they all generally fall together; sometimes the  $V_\theta$  curve lies a little above the  $V_\phi$ , as in the previous figure, or it's vice versa. It doesn't seem to matter.

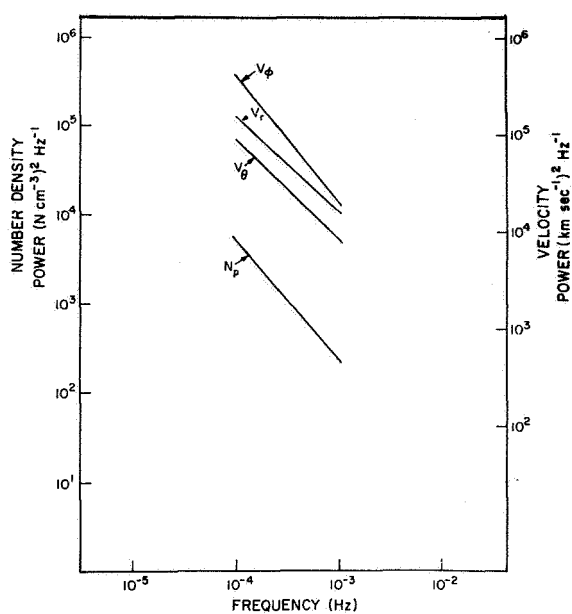


**Figure 3.** Power spectra from December 24-25, 1965 (data set 3 in figure 1) for the number density and the three components of solar wind velocity  $V_r$  (the radial component),  $V_\theta$  (perpendicular to the ecliptic plane), and  $V_\phi$  (in the ecliptic plane). The left ordinate refers to the power associated with the number density spectrum. The right ordinate refers to the power spectra of the components of solar wind velocity.

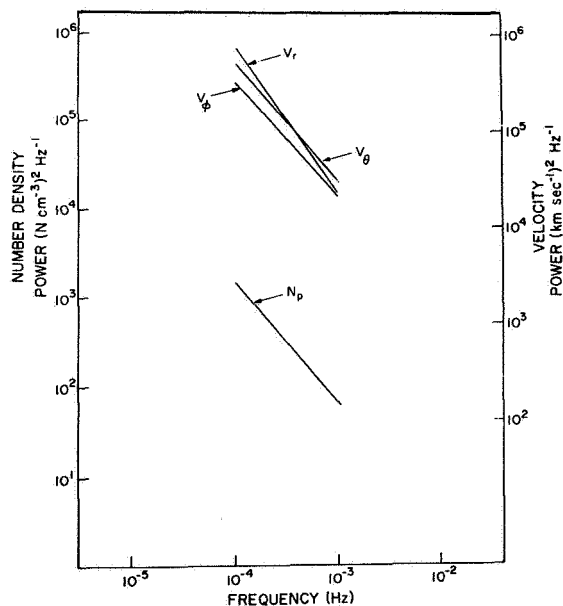


**Figure 4.** Power spectra from December 26-27, 1965, for the number density and the three components of solar wind velocity. The ordinates are the same as those in figure 3, and the data are also from an 11.6-hr time interval.

## REFERENCES

- Blackman, R. B.; and Tukey, J. W.: *The Measurement of Power Spectra*. New York, Dover Publications, 1959.
- Coleman, Paul J., Jr.: Variations in the Interplanetary Magnetic Field: Mariner 2, 1, Observed Properties. *J. Geophys. Res.*, Vol. 71, 1966, pp. 5509–5531.
- Intriligator, D. S.; and Wolfe, J. H.: Preliminary Power Spectra of the Interplanetary Plasma. *Astrophys. J.*, Vol. 162, 1970, pp. L187–L190.
- Jokipii, J. R.; and Hollweg, J. V.: Interplanetary Scintillations and the Structure of Solar-Wind Fluctuations. *Astrophys. J.*, Vol. 160, 1970, pp. 745–753.

**DISCUSSION**    *A. J. Hundhausen* I think if one looks at observed plasma properties as a function of time one indeed sees a good bit of wiggling up and down in anything one measures. Some of this may in fact be due to real fluctuations in the solar wind. And I think if you look at much data, you decide some of it might be due to instrumental problems and, in fact, I would state the opinion that when one talks about density one is on rather precarious grounds. I vaguely recall a comment by somebody from Ames in the panel Tuesday afternoon that such problems as how one fits one's data often show up most clearly in the density. Now, when one goes ahead and takes power spectra for the time series of observations I think one should give consideration to this other possible source of fluctuations. I would like to ask if you have given hard analysis to the possibility that all these fluctuations may in fact be due to problems in time, problems in accuracy in recording your spectra, or curve-fitting problems.

*D. S. Intriligator* The two reasons we have gaps is either from data gaps due to tracking or from data we did feel was aliased. The data that I looked at are detailed least-squares iterations of the fit to the plasma parameters using our calibration function. If there was any doubt as to how good the fit was that point was deleted.

*N. F. Ness* I have a general comment about the presentation of power spectra results. The point is that in the computations of the results you presented the implication is that it is a continuous function of frequency, barring the fact that your computer processing extends it by an order of magnitude over the real Nyquist frequency for the data. In fact, of course, one is making a spectral estimate over a finite frequency interval, and one should be presenting experimental results in spectral estimates more in the nature of a histogram. And associated with that would be appropriately presented not just degrees of freedom, which is a little bit difficult to convert to the appropriate scaling, but something like the 95 percent confidence limits in the spectral estimates. This would then permit one to at least judge the statistical significance of the data at hand. This is a general comment for you and for other people who present power spectra, but without this concept of what you are really computing. It's a discrete set of numbers; it's not a continuum. And leaving out the error bars, you know, when you present averages as has been done also here, is a little bit misleading as to what the data set really means.

                  The question I have is motivated by a presentation given yesterday by Chris Russell on the possible effects of aliasing of power spectra depending on the spectral slope. Now, for spectral slopes of about minus one and with folding factors of something much less than I think you have present in the data, your sampling rate gives you a Nyquist frequency of about 0.001 Hz. That is about three orders of magnitude removed from the kind of frequency I think is relevant to the scintillation measurements. So I don't believe the slopes you are deriving are correct, and I suspect the levels you are quoting are not correct either.

*D. S. Intriligator* Well, I would like to add one more dimension to the dimensions that you put in here about discrete points. That is very true, but as I tried to point out, we feel that you can wash out a very important effect, which is the change as a function of time of the levels of power. If we were to take a histogram of the points, disregarding the time intervals we were taking, it would be like comparing apples and bananas. It's important to keep in mind that the plasma parameters and the magnetic field parameters do reflect lower frequency solar stream structures, and that you have to understand exactly what it is that you're averaging for. Now, it's true, it's clearly true, that we are separated from the interplanetary scintillation data by three orders of magnitude. On the other hand, as Parker and Jokipii and some others have so often told us, one of the interesting problems in astrophysics is the scale size of turbulence, and it does affect many problems, and that is specifically the motivation for this work that we have done. We are looking at the astrophysical implications of space physics data and the scale size of turbulence in the interplanetary medium, and we find that we can set a lower limit to it of at least  $10^6$  km.

## COMMENTS

*J. V. Hollweg* Dr. Intriligator has just presented evidence that the power spectra for density fluctuations in the solar wind tend to resemble the power spectra obtained for magnetic field fluctuations. Since it is now known that Alfvén waves play a fairly important role in the fluctuations in the solar wind, it is interesting to inquire whether Alfvén waves can have density fluctuations associated with them. This is a point that I think quite a few people have some small misconceptions about. I just want to point out that it is fairly reasonable. The top line in figure 1 is an equation for the component of velocity parallel to the direction of propagation of an Alfvén wave and also parallel to the average magnetic field. The only point is that if you take a linearly polarized Alfvén wave

$$\vec{k} \parallel \vec{B}_0: \quad \rho \left( \frac{\partial v_z}{\partial t} + v_z \frac{\partial v_z}{\partial z} \right) = - \frac{\partial}{\partial z} \left( \delta p + \frac{\delta B_x^2}{8\pi} \right)$$

$$\text{LET } \delta B_x = \delta B_x^{(0)} \cos k(z - v_A t)$$

$$\text{THEN } \delta p = \delta p^{(0)} \cos 2k(z - v_A t)$$

$$\frac{\delta p^{(0)}}{\rho^{(0)}} = \frac{(\delta B_x^{(0)} / 2B_0)^2}{1 - v_S^2 / v_A^2}$$

$$\text{AT 1 a.u.: } (\delta B_x^{(0)} / 2B_0)^2 \sim 12.5\%$$

**Figure 1.** Alfvén waves and density fluctuations.  $v_A$  is the Alfvén speed and  $v_S$  the sound speed.

with the fluctuating component of magnetic field in one direction, the x direction, say, then there's a fluctuation in the pressure associated with the magnetic field, and this term will tend to drive compressional oscillations. You just put in some other equations, fool around a bit, and it turns out if you put in, say, a cosine wave for the Alfvén wave then you find that the density fluctuations are also a cosine, but at twice the frequency. The amplitude of the density fluctuations normalized with respect to the average density

depends on the magnitude of the Alfvén wave squared, and then there is an interesting resonant denominator which indicates that what one is really doing is driving sound waves or ion sound waves and that when the two-phase speeds become equal there is a resonance and really a coupling between the waves. The numerator represents in a sense the average or the magnitude of the density fluctuations. If you look at the space-probe data at 1 AU, and if you take naively one of the components you get about 12.5 percent. Thus one can have, if you have a linearly polarized Alfvén wave, a fairly substantial fluctuation in the density associated with it. The question is, of course, whether the waves are at times linearly polarized or, as perhaps might be more often the case, circularly polarized, or something similar.

Figure 2 illustrates this normalized density fluctuation, and it shows that there is a resonant peak and near the earth you can get a rather large contribution.

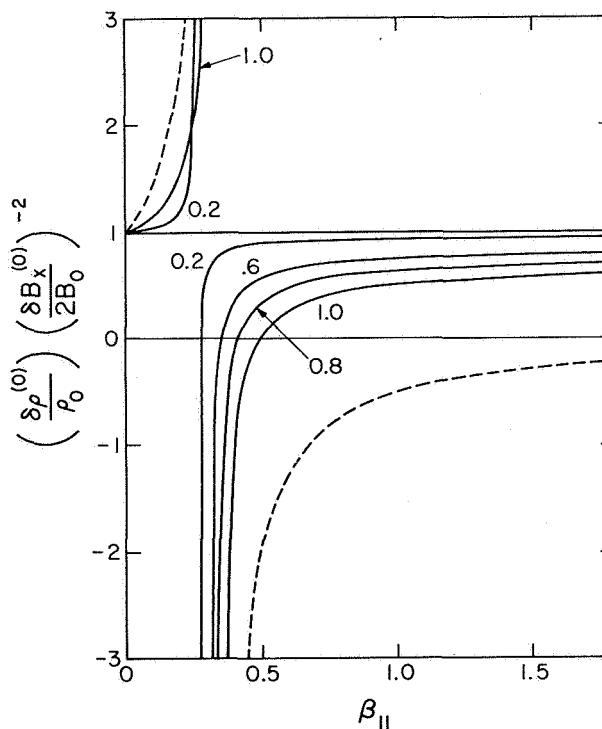


**Figure 2.** Normalized density fluctuation versus  $\beta_{\parallel} = 4\pi m_o K T_{\parallel} / B_o^2$ . The dashed lines are for an adiabatic equation of state with  $\gamma = 3$ ; solid lines are for the double adiabatic (CGL) equation of state.

**DISCUSSION** *B. Rickett* Do the density fluctuations driven from these Alfvén waves depend on the wavelength of the Alfvén waves?

*J. V. Hollweg* No. As long as you're really talking about Alfvén waves for which the phase speed is not dependent on the wavelength, then no, it doesn't.

*A. Barnes* As we discussed yesterday, I'm not quite sure whether the effect that you find should be called mode coupling or not, but whether it is or not first let me ask you, as I understand it, this is strictly an MHD theory, is that right?

*J. V. Hollweg* Right.

*A. Barnes* Now, when you do these nonlinear calculations, sometimes the effect of Landau damping can significantly modify the results that you get. This is certainly true

for mode coupling. Do you have any comments on what the effects might be? Because you're generating acoustic waves which, of course, in general are pretty rapidly Landau damped.

*J. V. Hollweg* There is a little funny problem of words here. Yesterday I used the words "mode coupling" and that is really not strictly correct. What you wind up with is on the left-hand side of an equation you have the wave equation for sound waves. On the right-hand side you have a driving term that is due to the Alfvén wave. This driving term is going with the Alfvén speed, so what you generate is something that looks like a sound wave but it's going at the Alfvén speed. So one really isn't generating an ion sound wave because that would go at the ion sound speed; instead one has a sort of a driven ion sound wave going at the Alfvén speed. There will be Landau damping, but this will be smaller than one would expect for the ion sound wave as long as the Alfvén speed is larger than the ion sound speed. So that the resonance that you get is out on the tail of the distribution function, or farther out on the tail of the distribution function than you would expect for really an ion sound wave. So near the earth this might be important, but farther in the Landau damping will be smaller.

*A. Barnes* Yes, what you say is true, the damping will probably be smaller than for a real ion sound wave. But if beta is of the order one-half or so it can still be a pretty strong effect, because the Alfvén speed is not all that far out on the tail of the distribution.

*J. V. Hollweg* I haven't calculated yet how fast the Landau damping would go for these things. If it did get fast near the earth it wouldn't be all that bad. It would sort of heat up plasma a bit, and damp out the Alfvén waves and that wouldn't bother me. I don't think it would particularly affect the density fluctuations because it would still go into the sound wave.

## SPECTRA AND CROSS SPECTRA OF SOLAR WIND PARAMETERS FROM MARINER 5

*B. Goldstein and G. L. Siscoe*

**ABSTRACT** The spectra of the radial ( $V_R$ ) and nonradial ( $V_T$ ,  $V_N$ ) velocity components of the solar wind, the proton density ( $\rho$ ) and the proton thermal speed ( $W$ ), show increasing power with increasing period up to a period of about 1 day. The powers tend to level off above 1 day except for that of  $V_R$ , which continues to increase up to a period of 10 days. At all periods, the power in  $V_R$  is greater than that in  $V_T$ ,  $V_N$ , and  $W$ , and the difference becomes very large at the longest periods because of the increasing power in  $V_R$ . The powers in  $V_T$ ,  $V_N$ , and  $W$  are similar at all periods.

The cross spectra reveal a sharp change in behavior at periods above and below approximately 1 day, suggesting that two distinct types of physical processes must dominate above and below this dividing period. In general, the coherences at the long periods are larger than at the short periods suggesting that the physical situation in the long period regime may be simpler than in the short period regime where multiple processes appear to be required to account for the low coherences. At periods less than 1 day, the cross spectra are consistent with the presence of intermediate hydromagnetic waves propagating outward in the frame of reference of the wind and with nonpropagating constant pressure fluctuations. However, one or more other processes are required to account for all the observed correlations. At periods greater than 1 day, the models of corotating structure and the spherically symmetric two-fluid model jointly appear capable of accounting for most of the correlations.

### INTRODUCTION

The Mariner and Pioneer series of space probes have allowed measurements of solar wind parameters over long time intervals. These measurements occur in deep space away from the influence of the earth's magnetosphere or the lunar wake. The data are therefore well suited for long-time, statistical studies of the interplanetary environment.

From the Mariner series, spectra of the magnitude and components of the magnetic field and of the solar wind speed have been presented for the period range 74 sec to 2 hr [Coleman, 1967] and for the period range 74 sec to

27 days [Coleman, 1968]. Spectra of the field magnitude and components from Mariner 4 have been given for the period range 3 sec to 1.4 hr [Siscoe *et al.*, 1968] and for the range 100 sec to 27 days [Coleman *et al.*, 1969]. In general, the Pioneer probe tracking coverage was poorer than on the Mariner missions and long-time analysis is therefore more difficult. Spectra of the field magnitude and components from Pioneer 6 for the period range 1 min to 1 hr have been given [Ness *et al.*, 1966; Sari and Ness, 1969, 1971]. Power spectra of the solar wind density in the period range  $10^3$  to  $10^4$  sec have also been presented [Intriligator and Wolfe, 1970].

The spectra all show increasing power with increasing period up to a period of approximately 1 day. On a log power versus log period plot in the less-than-one-day range, the curves approximate straight lines with slopes

---

*B. Goldstein is at the Center for Space Research, Massachusetts Institute of Technology, Cambridge, Massachusetts. G. L. Siscoe is with the Department of Meteorology, University of California, Los Angeles, California.*



in the range 1 to 2. The exact slope depends on which variable is considered and also to a lesser extent on the solar wind conditions at the time of observations. The magnitude of the power at a given period is much more sensitive to solar wind conditions (weather) than is the slope. Those spectra extending to periods greater than 1 day, which include the magnetic field magnitude and components and the solar wind speed, show a tendency for the power to level off with increasing periods and in some cases to decrease beyond a period of approximately 10 days.

There have been fewer presentations of cross spectra of interplanetary parameters. *Coleman* [1967] has given the coherence and phase of the cross spectra between the solar wind speed and the radial component of the magnetic field in the period range approximately 12 min to 2 hr from Mariner 2 data. This same information has been given from Mariner 4 data in the period range 10 min to 4.2 hr [Belcher and Davis, 1971]. The results from both spacecraft show significant coherences and nearly constant phases over most of the displayed period ranges. The cross spectrum between the radial and transverse solar wind velocity components from Pioneer 6 data in the period range 10 hr to 4 days has been presented [Siscoe et al., 1969b]. High coherences, especially at the long period end, and constant phases also were found.

Spectral and cross spectral information are useful both for concisely displaying important statistical properties of solar wind parameters and for trying to understand the physical nature of their fluctuations. Efforts to interpret solar wind fluctuations with the help of spectral information include descriptions in terms of turbulence [Coleman, 1968], of hydromagnetic waves [Coleman, 1967; Belcher and Davis, 1971], of discontinuities [Sari and Ness, 1969, 1971], and of fast stream-slow stream interactions [Siscoe et al., 1969b]. From the variety of interpretations it seems likely that different physical processes may dominate at different times and in different frequency regimes. We might expect the situation to be clarified by incorporating more variables and by greater use of cross spectral analysis.

A correct physical description of solar wind fluctuations is needed for application to related fields. Assumptions about their nature have already been made to estimate the angular momentum flux of the solar wind [Schubert and Coleman, 1968], to interpret the interplanetary scintillation of radio sources [Dennison and Hewish, 1967; Cohen et al., 1967; Hewish and Symonds, 1969; Jokipii and Hollweg, 1970], and to determine cosmic ray diffusion coefficients [see recent review by Jokipii, 1971]. The level of geomagnetic activity as

measured by the  $K_p$  index is known to be well correlated to fluctuations in the period range 1 min to 3 hr of the interplanetary magnetic field [Ballif et al., 1967, 1969], and to larger scale features recognized as the solar wind sector structure [Wilcox and Ness, 1965]. Even prior to direct solar wind measurements, geomagnetic activity was believed due to time variations of the solar corpuscular radiation [Bartels, 1957; Chapman and Bartels, 1962; and Chapman, 1963].

This paper extends the statistical analyses of interplanetary parameters by giving spectra of plasma parameters and cross spectra between plasma and field parameters from Mariner 5 data over a large period interval (10 min to approximately 10 days.). We concentrate primarily on the plasma parameters since the magnetic field has been well treated. However, cross spectra with the magnetic field are also needed for a complete analysis.

## RESULTS FROM MARINER 5

Mariner 5 collected solar wind data from June 14, 1967, to November 21, 1967. The data telemetry changed from a "high" to "low" rate 40 days into the mission. Solar wind plasma parameters were obtained with a modulated grid Faraday map of the type described by Lazarus et al. [1967]. The data are being reduced to provide the solar wind velocity vector and the proton density and temperature. At the present stage of analysis the temperature is calculated assuming an isotropic, Maxwellian distribution; thus, it is only a rough measure of the thermal condition of the protons. A complete set of plasma parameters is determined every 5.04 min at the high data rate and 20.16 min at the low rate. The vector magnetic field was measured with a helium magnetometer [Connor, 1968] at a high data rate of three vector measurements every 12.6 sec and every 50.4 sec at the low rate. In the following analysis the magnetic field data were averaged over the plasma sampling interval to provide commensurate data sets.

The magnetic and velocity vector components are given in coordinates ( $R, T, N$ ) based on a spherical, polar coordinate system ( $r, \theta, \varphi$ ) with the solar rotation axis the polar axis such that  $V_R = V_r$ ,  $V_T = V_\varphi$ , and  $V_N = -V_\theta$ .

The data record covers a 140-day interval, the first 40 days at the high data rate and the remainder at the low rate. Throughout the interval there was an approximately 80 percent data coverage. The missing data occurred mostly in small intervals except near the end of the mission when there were large gaps. Two methods were used for estimating the error in the power spectra. First, a white noise (random) spectrum was sampled with a data rate and gap sequence to duplicate that of

Mariner 5. A spectrum of this record should be constant over the period range 10 min to 40 min and then jump at 40 min to a constant value, four times the old one, and remain constant for all longer periods. The jump at 40 min is due to the change in sampling rate (a factor of 4 after 40 days) and is an example of the effect of aliasing. The spectrum of the random signal is given in figure 1 and shows the features just mentioned. The spectrum is reasonably flat between 10 and 40 min and between 40 min and 10 days with a jump of about a factor of 4 at 40 min. The rise above 10 days is apparently due to data gaps, since a spectrum obtained with the same sampling sequence but with no data gaps shows no rise. Thus, although the spectra and cross

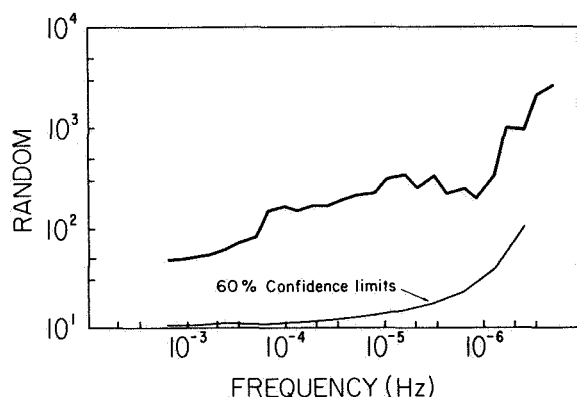


**Figure 1.** The power spectrum of a white noise signal with a sampling and gap sequence duplicating that of Mariner 5. The jump at a period of 40 min corresponds to the change in data sampling rate 40 days into the mission and is an example of the effect of aliasing. The increase in power above a period of 10 days is due to data gaps. Also shown for comparison on following spectra are the 60 percent confidence limits.

spectra go up to a period of about 80 days, accurate results are claimed only for the interval 10 min to 10 days. It should be noted that all the spectra near 40 min are sufficiently steep that the effect of aliasing, evident for a flat spectrum, is not very important.

The second method estimates the confidence limits assuming an equivalent number of degrees of freedom equal to  $2N/m$ , where  $N$  is the number of points in the data record and  $m$  is the number of points in the period interval [Blackman and Tukey, 1959]. In this estimate  $n=9$ , but  $N$  varies from  $10^4$  to 40 as the data are progressively averaged over larger nonoverlapping intervals to obtain the spectrum over a large period

interval. The use of different values of  $N$  leads to the 60 percent confidence limit, which is analogous to one standard deviation, shown as the bottom line in figure 1. It increases from 0.02 decade at 10 min to 1 decade at 28 days. It is 0.13 decade at 10 days. This curve can be viewed as the  $\pm$  error limits on the subsequent spectra.

The estimate of errors in the cross spectra is more difficult, and we have relied primarily on the behavior of the phase as an indication of significance. If the phase is nonrandom from one estimate to the next over a sizable period range, it may be assumed that a real correlation is being observed. The same criterion may be applied to the coherence. It will be seen that persistent phases and coherences do exist in many of the cross spectra.

Figure 2 shows the spectra of the three solar wind velocity components. They exhibit the usual increase with period in the range 1 to 2 at periods less than 1 day. At greater periods the powers tend to level off,

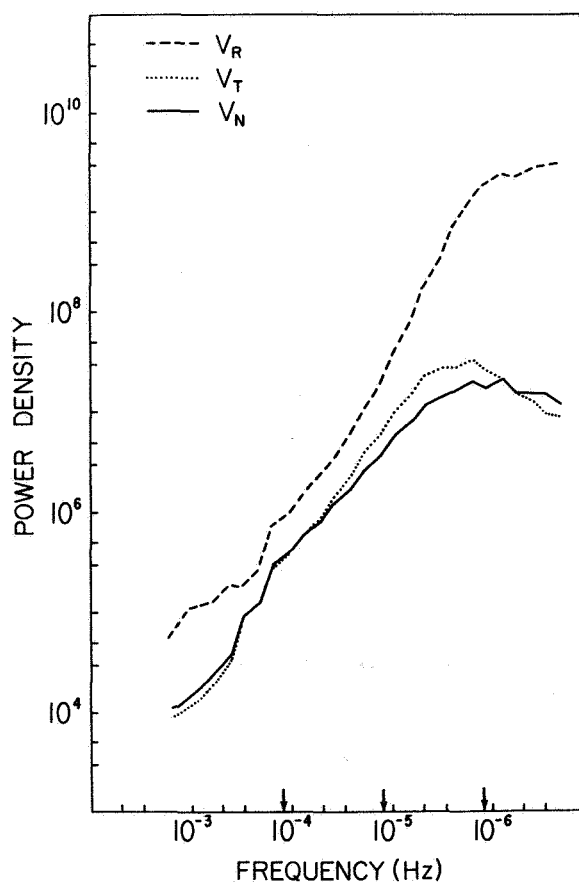


**Figure 2.** Spectra of solar wind velocity components,  $V_R$ ,  $V_T$ , and  $V_N$ . The arrows on the horizontal axis locate the periods of 0.1 day, 1 day, and 10 days. The units for the spectral density are  $(\text{km/sec})^2/\text{Hz}$ .

much sooner in the case of the nonradial components, resulting in considerably higher power in  $V_R$  at the long periods. At periods less than 1 day, the powers in the two nonradial components are seen to be approximately equal and to be less than the power in  $V_R$  by approximately a factor of 2. This is opposite to the behavior of the magnetic field components, for which all previous studies have shown the power in  $B_R$  to be less than in the two non-radial components by approximately a factor of 2 for periods less than 1 day.

As complimentary information to the spectra, it is useful also to give the averages and standard deviations over the entire data interval of each variable. These are

Variable	Average	Standard Deviation
$V_R$	426 km/sec	87.9 km/sec
$V_T$	7 km/sec	17.9 km/sec
$V_N$	-2.6 km/sec	14.8 km/sec

Figure 3 compares the spectra of the three solar wind parameters  $V_R$ , the proton thermal speed  $W$ , and proton density  $\rho$ . The spectrum of  $W$  is very similar in shape and amplitude to those of the nonradial velocity components given in figure 2. All three spectra have a similar shape except that the slope of the density is steeper at short periods. All the velocity spectra, including the thermal speed, have slopes near 1 at short periods and steeper slopes at longer periods up to the turnover near 1 day. The density slope at periods less than 1 day is nearly constant at approximately 1.3. The values for  $V_R$  and  $\rho$  can be compared with results from other spacecraft, referenced earlier, and are found to be consistent.

The averages and standard deviations of the density and thermal speed are:

Variable	Average	Standard Deviation
$\rho$	9.2 $\text{cm}^{-3}$	5.6 $\text{cm}^{-3}$
$W$	44.8 km/sec	13.5 km/sec

It should be noted that the difference in the absolute values of the spectra of  $V_R$  and  $\rho$  is due to different units and not different levels of fluctuations. In fact, there is relatively more fluctuation in  $\rho$  than in  $V_R$  as indicated by comparing averages and standard deviations.

The tendency of the power spectra to change slope near a period of 1 day suggests that there may be interesting differences in the physical processes dominating above and below that period. This suggestion is dramatically confirmed by the cross spectral results. Figure 4 is the cross spectrum between radial speed and density, which shows a sudden change in both the coherence and phase beginning at a period near 8 hr. The change in the phase is very sudden, but the coherence increases from less than 0.1 to greater than 0.8 in the

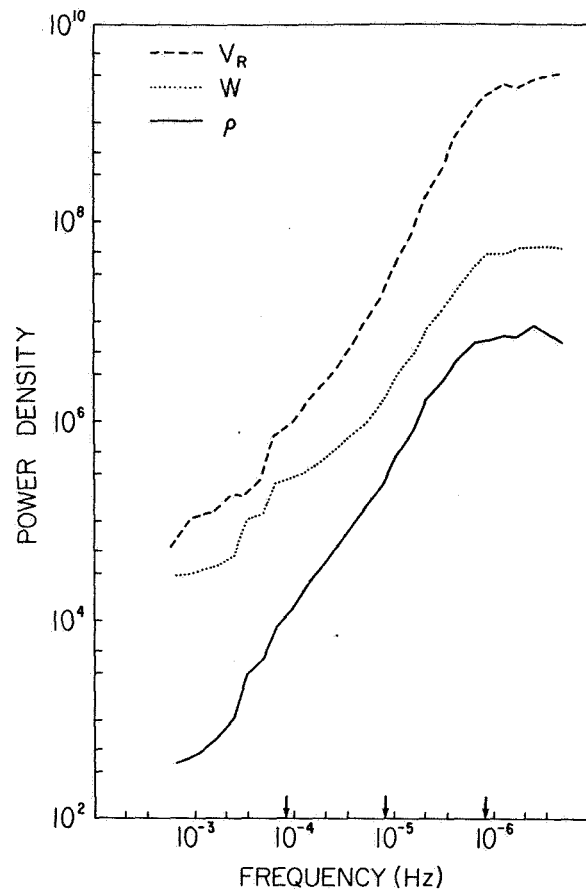
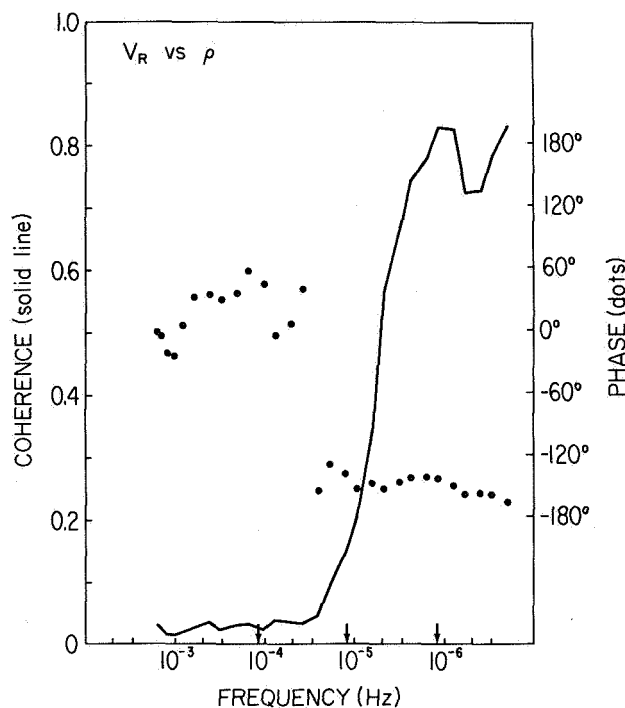


Figure 3. Spectra of  $V_R$ , proton thermal speed  $W$ , and proton density  $\rho$ . Units for  $V_R$  and  $W$  same as in figure 1 and for  $\rho$ ,  $(\text{cm}^{-3})^2/\text{Hz}$ .

range 8 hr to 10 days. Although the coherence at periods less than 8 hr is very small, the tendency of the phase to cluster near  $0^\circ$  indicates the presence of a definite but weak mechanism correlating  $V_R$  and  $\rho$ . The change from near  $0^\circ$  to near  $-150^\circ$  phase strikingly signals the presence of different mechanisms above and below the 1-day period.

Figures 5 and 6 give the cross spectra between  $V_R$  and the proton thermal speed and between  $V_R$  and  $V_T$ . The coherence of the former again exhibits a large contrast between the values above and below approximately 1 day. However, the coherence between  $V_R$  and  $V_T$  becomes large at 0.1 day. In both cases the phases do not change across most of the period range. Over the whole range,  $V_R$  is in phase with  $W$  and out of phase with  $V_T$  up to a period of about 6 days, when it suddenly becomes in phase. If there are different mechanisms correlating these parameters above and below 1 day, they do so with the same phase up to 6 days. Alternatively, it may be a single mechanism that



**Figure 4.** Cross spectrum between  $V_R$  and  $\rho$ . A positive phase angle means the first of the two variables listed leads the second.

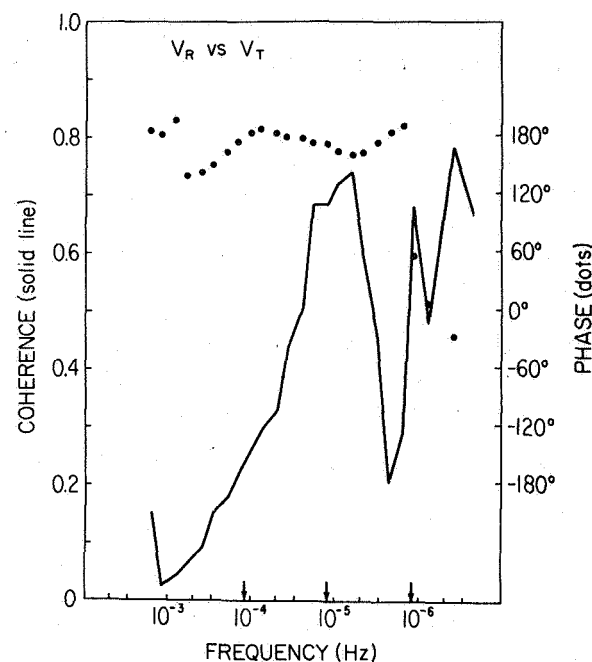


**Figure 6.** Cross spectrum between  $V_R$  and  $V_T$ . A positive phase angle means the first of the two variables listed leads the second.

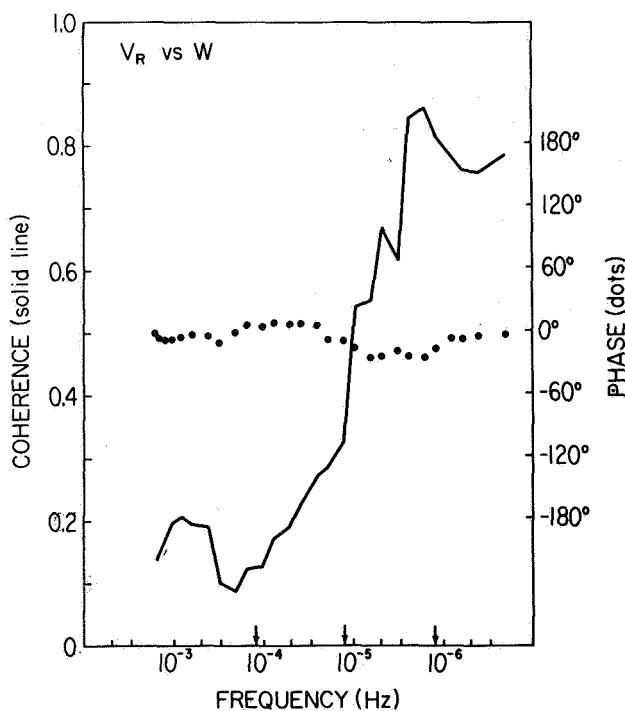


**Figure 5.** Cross spectrum between  $V_R$  and  $W$ . A positive phase angle means the first of the two variables listed leads the second.

dominates at the longer periods but is a less dominant process at the shorter periods where other processes that do not correlate these parameters may dominate. The cross spectra between  $V_R$  and  $V_N$  and between  $V_T$  and  $V_N$ , not shown here, do not reveal any large coherence in any particular period band, although a nearly constant phase over a broad period band, especially for the  $V_R - V_N$  case, suggests that the low level of coherence is related to a definite process.

The last example involving purely plasma parameters (fig. 7) is a cross spectrum between  $V_R$  and the combination  $\rho W^2$ , the proton thermal pressure. The distinct short and long period regimes in this case are marked by a change from low to high coherence and from nearly random phase to a fairly definite phase of  $-90^\circ$  at the long periods. Since  $W$  is the least well-determined quantity, small changes in it may not be very significant. The power spectra show that there is relatively little variation at short periods. Hence, the lack of coherence and the random phase at short periods shown in figure 7 may not be accurate. However, we believe the results at long periods, which involve large changes in  $W$ , are accurate.

Figures 8 through 11 involve correlations between plasma and magnetic field variables. Figures 8 and 9 correlate the  $R$  and  $N$  components of the magnetic and

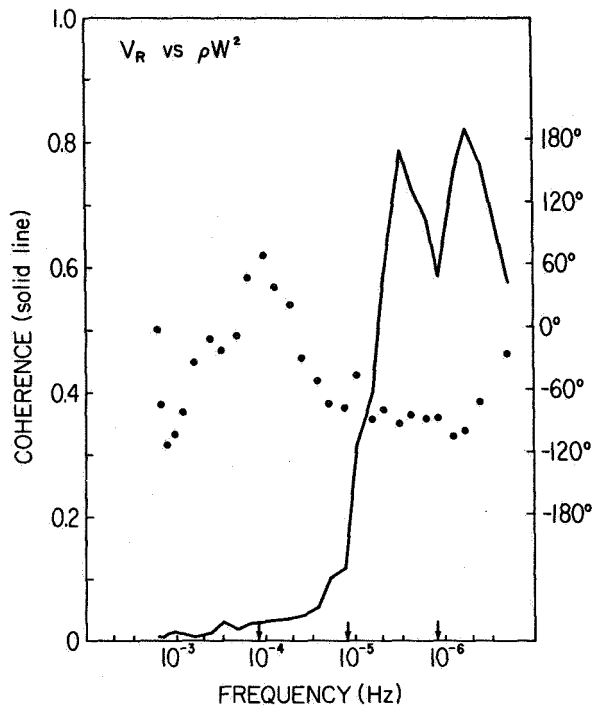


**Figure 7.** Cross spectrum between  $V_R$  and  $\rho W^2$ . A positive phase angle means the first of the two variables listed leads the second.

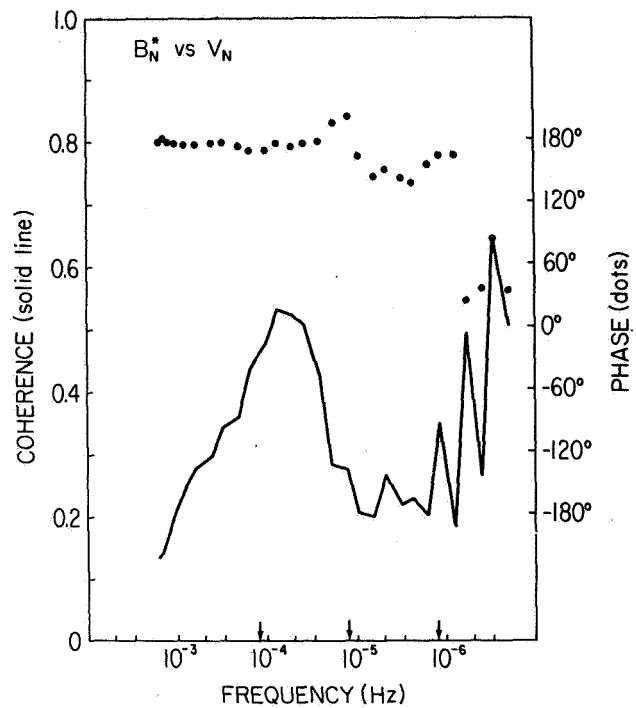


**Figure 9.** Cross spectrum between  $B_N^*$  and  $V_N$ . A positive phase angle means the first of the two variables listed leads the second.

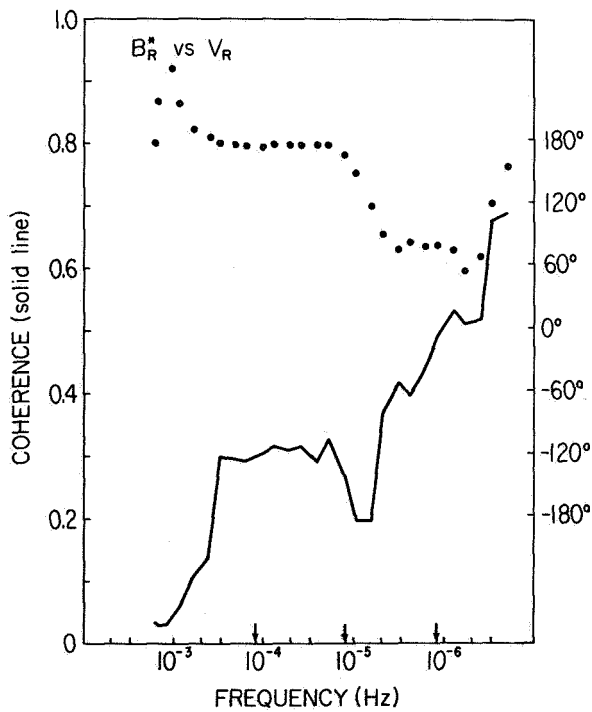


**Figure 8.** Cross spectrum between  $B_R^*$  and  $V_R$ . A positive phase angle means the first of the two variables listed leads the second.

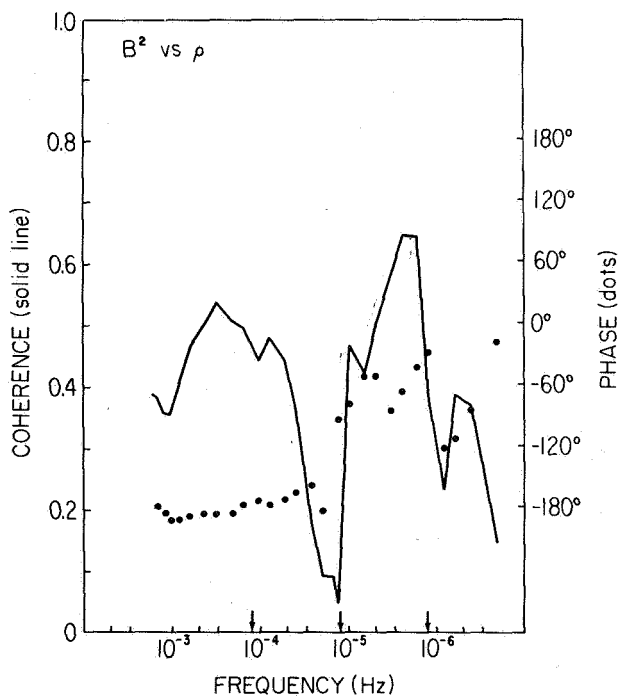


**Figure 10.** Cross spectrum between  $B^2$  and  $\rho$ . A positive phase angle means the first of the two variables listed leads the second.

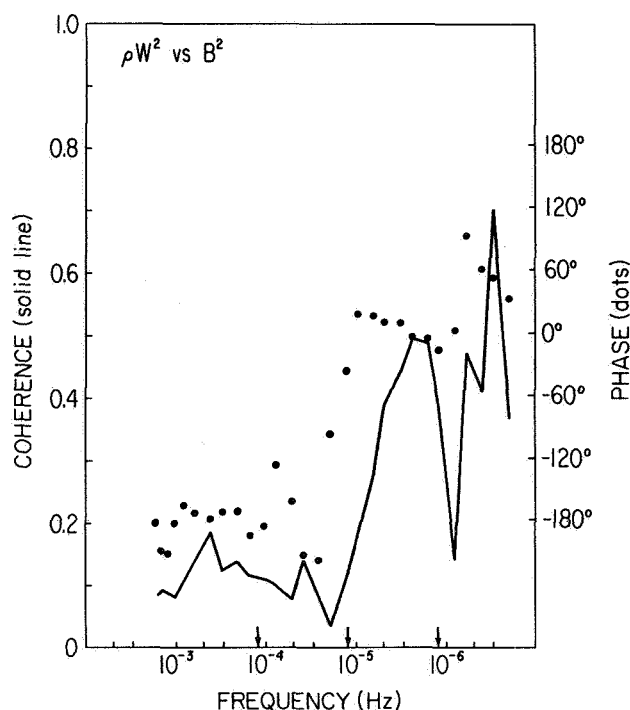


**Figure 11.** Cross spectrum between  $\rho W^2$  and  $B^2$ . A positive phase angle means the first of the two variables listed leads the second.

velocity fields. Variations due to changes in the polarity of the large scale magnetic field (sector structure) were removed by projecting each magnetic vector in the data set onto the spiral direction based on the simultaneously measured solar wind speed, and reversing the vector if the projection was negative. The result produces the effect of an always outward directed polarity. The operation is signified by an asterisk over the field components. Both figures show moderately large coherences in the short period regime and persistent phases near  $180^\circ$ . The long period regime is different in the two cases with high coherence and a change to near  $+90^\circ$  in the  $R$  component and low coherence with little phase change in the  $N$  component. The changeover in the  $R$  component again occurs at a period near 1 day.

Figure 10 is a cross spectrum between  $B^2$  and  $\rho$ . Again, these independently measured quantities show a dip in coherence and a change in phase at a period near one day. An important feature of this cross spectrum to note for later discussion is the high coherence of short periods and definite  $180^\circ$  phase.

Figure 11 is a cross spectrum between the proton thermal pressure and the magnetic field pressure. Again, the division near 1 day is evident, separating low coherences but a definite phase near  $180^\circ$  at short

periods and higher coherences with a definite phase near  $0^\circ$  at the long periods. We note here again that the short period results may be inaccurate because of the uncertainty in  $W$  at short periods.

## CONCLUSIONS

A major result of the present analysis, most clearly revealed in the cross spectra, is the demonstration of two distinctive regimes, divided approximately at a period of 1 day, within the period band studies, 10 min to 10 days. The division is indicated by dramatic changes in both the coherences and phases at the dividing period. As a general rule, the coherences at the long periods tend to be the largest. This may reflect the existence of more competing processes at the short periods. Values of 0.8 occur in many of the cross spectra in the band above 1 day, suggesting that a single, very dominant process may be operating there. That the solar wind behavior might be essentially different in different period ranges was recognized by *Burlaga and Ness [1968]* who suggested division of phenomena into microstructure ( $\leq 1$  hr), mesostructure (1 hr to  $10^2$  hr), and macrostructure ( $>10^2$  hr), although the single division suggested by the cross spectra is somewhat different. We attempt in this section to relate the cross-spectral results to specific physical mechanisms. There has been considerable discussion in the literature of solar wind processes, so the main task is to identify which of these may be operating in which period regime.

### The Short Period Regimes

Consider first periods less than 1 day. Previous waveform analysis of the Mariner 5 plasma and field data [*Belcher et al.*, 1969; *Belcher and Davis*, 1971] have confirmed the presence of intermediate hydromagnetic waves. They find that for periods of less than several hours, the intermediate waves dominate in the variations of the velocity and magnetic field at least 50 percent of the time. Since intermediate waves do not modulate the density or temperature, this is consistent with the low coherences at short periods between  $V_R$  and  $\rho$  (fig. 4),  $V_R$  and  $W$  (fig. 5), and  $V_R$  and  $\rho W^2$  (fig. 7). It is also consistent with the moderate coherences at short periods between  $B_R^*$  and  $V_R$  (fig. 8) and  $B_N^*$  and  $V_N$  (fig. 9). The phase in the last two figures,  $180^\circ$  in both cases, is consistent with outward propagating waves in the frame of reference moving with the solar wind [*Belcher et al.*, 1969]. This is also the situation found in the previous studies. Thus, the assumption of outward propagating intermediate waves dominating about 50 percent of the time explains the short period coherences and phases involving the velocity and magnetic field components.

It was noted by *Belcher and Davis* [1971] and emphasized by *Burlaga and Ness* [1968] that many of the fluctuations occurring at less than 1 day periods cannot be intermediate waves since they involve changes in density, temperature, or magnetic pressure. A study by *Burlaga et al.* [1969] of fluctuations involving pressure changes in the period range 1 min to 1 hr shows that they tend to conserve the total pressure, which is the sum of the thermal and magnetic pressures. Such constant pressure variations will not propagate but will be statically convected by the wind. Thus, there will be no associated modulation of the velocity. This is the hydromagnetic extension of the constant pressure, non-propagating entropy fluctuations in ordinary hydrodynamics, in which the density and temperature vary out of phase in such a way as to keep the total pressure constant. The present cross spectral results at short periods are consistent with the presence of this type of variation. The low coherence between  $V_R$  and  $\rho$  and  $V_R$  and  $W$  have already been noted. Further support is given by the short-period, high coherence, anticorrelation between  $B^2$  and  $\rho$  shown in figure 10. The anticorrelation implies either static pressure variations or slow mode hydromagnetic waves. If the latter are responsible, then the small coherence between  $V_r$  and  $\rho$  implies essentially equal amounts of outward and inward propagating waves, in contrast to primarily outward propagating intermediate mode waves. The present analysis cannot select between the two possibilities, but the predicted strong damping of slow mode waves [*Barnes*, 1968, 1969] favors the first possibility.

In summary, for periods of less than 1 day, many of the cross spectral results can be understood in terms of two mechanisms: outward propagating, intermediate mode hydromagnetic waves and nonpropagating, constant pressure variations. Although the results do not uniquely select these mechanisms, they are the ones that are not strongly damped.

### The Long Period Regimes

The generally larger coherences in the long period regimes suggest a simpler interpretation than for the short period situation. First, note, that for all the solar wind variables most of the power in fluctuations occurs at the long periods. Hence, the correlative studies of solar wind parameters previously reported should show the same general correlations as are exhibited in the long period regime of the present cross spectral results. These general correlations, summarized recently by *Hundhausen et al.* [1970], show that:  $V_R$  and  $\rho$  tend to be anticorrelated [*Neugebauer and Snyder*, 1966];  $V_R$  tends to be anticorrelated with  $V_T$  [*Siscoe et al.*,

1969b]; and  $V_R$  and  $W$  tend to be positively correlated [*Neugebauer and Snyder*, 1966; *Strong et al.*, 1966; *Hundhausen et al.*, 1967; *Coon*, 1968; *Burlaga and Ogilvie*, 1970]. Each instance is seen to agree with the long period regime phases given in figures 4, 5 and 6: namely,  $V_r - \rho$ ,  $-160^\circ$ ;  $V_r - V_T$ ,  $180^\circ$ ; and  $V_R - W$ ,  $0^\circ$ .

Theoretical explanations for some of the general correlations have appeared, and they should also apply to the cross spectral features in the long period regime. The explanations thus far put forth have been based on two different assumptions, corotating inhomogeneities and quasistatic changes in spherically symmetric models. In the first, variations in solar wind parameters are assumed to be associated with long-lived coronal inhomogeneities, and they will therefore be time stationary in a frame of reference corotating with the sun. The second assumes that observed variations are due to different boundary conditions to a spherically symmetric expansion. Both assumptions require that any intrinsic time changes be on a time scale long compared to a "flow time" or approximately the transit time between the sun and earth (4 to 5 days). The two approaches should give similar results in the longest period range. However, the assumption of corotating structure can be used at periods shorter than 4 to 5 days since any change in the symmetric model must be an intrinsic time change and this is not true for the corotation model. Where the spherically symmetric model is valid, it should yield better results since it is physically more sophisticated.

The existing corotation models sacrifice physical sophistication to include the complication of an extra spatial variable. They have been used primarily to describe the interaction of adjacent, long-lived fast and slow streams—so-called "stream-stream interactions." These interactions appear capable of accounting for the  $V_R - V_T$  and  $V_R - \rho W^2$  phases. In these models, the first arises out of nonradial deflections of the streams as they interact along their spiral interface and the second from a pressure compression at the interface in a preceding-slow-stream interaction and a pressure rarefaction at the interface of a preceding-fast-stream interaction [*Siscoe et al.*, 1969a, b; *Carovillano and Siscoe*, 1969; *Siscoe and Finley*, 1970]. The  $180^\circ$  phase between  $V_R$  and  $V_T$  can be restated in more familiar terms: fast streams tend to come from the west and slow streams from the east. The  $-90^\circ$  phase between  $V_R$  and  $\rho W^2$  means that the thermal pressure tends to maximize on the rising slopes and to minimize on the falling slopes of the velocity variations.

The stream-stream interaction model does not explain the  $V_R - \rho$ ,  $V_R - W$ , or  $\rho - W$  phases. These reflect the

coronal boundary conditions for the flow, and for these the spherically symmetric models may be more appropriate, although *Burlaga et al.* [1971] believe that the  $\rho - W$  phase may also be primarily the result of the stream-stream interaction. The latest attempt to explain the  $V_R - W$  phase ( $0^\circ$ ) is by *Hartle and Barnes* [1970]. They find that with a two-fluid model, agreement with the more explicit, empirical  $V_R - W$  relationship of *Burlaga and Ogilvie* [1970] can be obtained if nonthermal heating of the solar wind occurs over an extended range of 2 to  $25 R_\odot$  heliocentric distance.

In summary, it appears that most of the cross spectral phases in the long period regime can be explained as being due either to the stream-stream interaction or to changes in the amount of heat deposited in the solar wind within  $25 R_\odot$  of the sun. However, there are still some uncertainties in this assessment, especially with regard to the  $\rho - W$  phase.

The question still remains as to why there are two distinctive period regimes separated at approximately a period of 1 day. One possibility can be formulated in terms of strong damping of compressional waves in a collisionless plasma [*Barnes*, 1968, 1969]. Compressional waves are believed to damp in only a few wave periods. The situation at periods less than 1 day may be due to all compressional waves in this regime having been damped in transit to earth. This idea is consistent with the small  $V_R - \rho W^2$  coherence at short periods. The compressions at periods greater than 1 day, due perhaps to the stream-stream interaction, are of longer period and may not have had time to damp in the 4- to 5-day transit time to earth. If this is the explanation, future missions to Mercury and Jupiter should find that the cross-over period becomes shorter close to the sun and longer at greater distances.

#### ACKNOWLEDGMENTS

We thank A. J. Lazarus for providing the plasma data and E. J. Smith, L. Davis, P. J. Coleman, and D. E. Jones for providing the magnetic field data. This work was supported in part by the National Aeronautics and Space Administration under contracts NGL-22-009-372 (MIT) and NGR-05-007-304 (UCLA), and in part by the Atmospheric Sciences Section of the National Science Foundation, NSF Grant GA-13554 (UCLA).

#### REFERENCES

- Ballif, J. R.; Jones, D. E.; Coleman, P. J., Jr.; Davis, L., Jr.; and Smith, E. J.: Transverse Fluctuations in the Interplanetary Magnetic Field: A Requisite for Geomagnetic Variability. *J. Geophys. Res.*, Vol. 72, 1967, p. 4357.
- Ballif, J. R.; Jones, D. E.; and Coleman, P. J., Jr.: Further Evidence on the Correlation Between Transverse Fluctuations in the Interplanetary Magnetic Field and  $K_p$ . *J. Geophys. Res.*, Vol. 74, 1969, p. 2289.
- Barnes, A.: Collisionless Heating of the Solar Wind Plasma. 1, Theory of the Heating of Collisionless Plasma by Hydromagnetic Waves. *Astrophys. J.*, Vol. 154, 1968, p. 751.
- Barnes, A.: Collisionless Heating of the Solar Wind Plasma. 2, Application of the Theory of Plasma Heating by Hydromagnetic Waves. *Astrophys. J.*, Vol. 155, 1969, p. 311.
- Bartels, J.: The Geomagnetic Measures for the Time-Variations of Solar Corpuscular Radiation, Described for Use in Other Geophysical Fields. *Annals of the International Geophysical Year*, Pergamon Press, New York, 1957, p. 227.
- Belcher, J. W.; Davis, L., Jr.; and Smith, E. J.: Large Amplitude Alfvén Waves in the Interplanetary Medium: Mariner 5. *J. Geophys. Res.*, Vol. 74, 1969, p. 2302.
- Belcher, J.; and Davis, L., Jr.: Large Amplitude Alfvén Waves in the Interplanetary Medium: II. *J. Geophys. Res.*, Vol. 76, 1971, p. 3534.
- Blackman, R. B.; and Tukey, J. W.: *The Measurement of Power Spectra from the Point of View of Communication Theory*, Dover Pub., New York, 1959.
- Burlaga, L. F.; and Ness, N. F.: Macro- and Micro-structure of the Interplanetary Magnetic Field. *Can. J. Phys.*, Vol. 46, 1968, p. 5962.
- Burlaga, L. F.; Ogilvie, K. W.; and Fairfield, D. H.: Microscale Fluctuations in the Interplanetary Magnetic Field, *Astrophys. J.*, Vol. 155, 1969, p. L171.
- Burlaga, L. F.; and Ogilvie, K. W.: Heating of the Solar Wind. *Astrophys. J.*, Vol. 159, 1970, p. 659.
- Burlaga, L. F.; Ogilvie, K. W.; Fairfield, D. H.; Montgomery, M. D.; and Bame, S. J.: Energy Transfer at Colliding Streams in the Solar Wind. *Astrophys. J.*, Vol. 164, 1971, p. 137.
- Carovillano, R. L.; and Siscoe, G. L.: Corotating Structure in the Solar Wind. *Solar Phys.*, Vol. 8, 1969, p. 401.
- Chapman, S.; and Bartels, J.: *Geomagnetism*. Oxford University Press, London, 1962, p. 850.
- Chapman, S.: Solar Plasma, Geomagnetism and Aurora. *Geophysics, The Earth's Environment*, Gordon and Breach, New York, 1963, p. 373.
- Cohen, M. H.; Gunderman, E. J.; Hardebeck, H. E.; and Sharp, L. E.: Interplanetary Scintillations, II, Observations. *Astrophys. J.* Vol. 147, 1967, p. 449.



- Coleman, P. J., Jr.: Wave-like Phenomena in the Interplanetary Plasma: Mariner 2. *Planet. Space Sci.*, Vol. 15, 1967, p. 953.
- Coleman, P. J., Jr.: Turbulence, Viscosity, and Dissipation in the Solar Wind Plasma. *Astrophys. J.*, Vol. 153, 1968, p. 371.
- Coleman, P. J., Jr.; Smith, E. J.; Davis, L., Jr.; and Jones, D. E.: The Radial Dependence of the Interplanetary Magnetic Field: 1.0-1.5 ACI. *J. Geophys. Res.*, Vol. 74, 1969, p. 2826.
- Connor, B. V.: Space Magnetics: Mariner 5 Magnetometer Experiment. *IEEE Trans. Magnetics*, MAG-4, 1968, p. 391.
- Coon, J. H.: Solar Wind Observations. *Earth's Particles and Fields*, edited by B. M. McCormac, Reinhold, New York, 1968.
- Dennison, P. A.; and Hewish, A.: The Solar Wind Outside the Plane of the Ecliptic. *Nature*, Vol. 213, 1967, p. 342.
- Hartle, R. E.; and Barnes, A.: Nonthermal Heating in the Two-Fluid Solar Wind Model. *J. Geophys. Res.*, Vol. 75, 1970, p. 6915.
- Hewish, A.; and Symonds, M. D.: Radio Investigation of the Solar Plasma. *Planet. Space Sci.*, Vol. 17, 1969, p. 313.
- Hundhausen, A. J.; Bame, S. J.; and Ness, N. F.: Solar Wind Thermal Anisotropies: Vela 3 and Imp 3. *J. Geophys. Res.*, Vol. 72, 1967, p. 5265.
- Hundhausen, A. J.; Bame, S. J.; Asbridge, J. R.; and Sydoriak, S. J.: Solar Wind Proton Properties: Vela 3 Observations from July 1965 to June 1967. *J. Geophys. Res.*, Vol. 75, 1970, p. 4643.
- Intriligator, D. S.; and Wolfe, J. H.: Preliminary Power Spectra of the Interplanetary Plasma. *Astrophys. J.*, Vol. 162, 1970, p. L187.
- Jokipii, J. R.; and Hollweg, J. V.: Interplanetary Scintillations and the Structure of Solar Wind Fluctuations. *Astrophys. J.*, Vol. 160, 1970, p. 735.
- Jokipii, J. R.: Propagation of Cosmic Rays in the Solar Wind. *Rev. Geophys. and Space Phys.*, Vol. 9, 1971, p. 27.
- Lazarus, A. J.; Bridge, H. S.; Davis, J. M.; and Snyder, C. W.: Initial Results from the Mariner 4 Solar Plasma Experiment. *Space Res.*, Vol. 7, 1967, p. 1296.
- Ness, N. F.; Searce, C. S.; and Cantarano, S.: Preliminary Results from the Pioneer 6 Magnetic Field Experiment. *J. Geophys. Res.*, Vol. 71, 1966, p. 3305.
- Neugebauer, M.; and Snyder, C. W.: Mariner 2 Observations of the Solar Wind. 1, Average Properties. *J. Geophys. Res.*, Vol. 71, 1966, p. 4469.
- Sari, J. W.; and Ness, N. F.: Power Spectra of the Interplanetary Magnetic Field. *Solar Phys.*, Vol. 8, 1969, p. 155.
- Sari, J. W.; and Ness, N. F.: Power Spectral Studies of the Interplanetary Magnetic Field. *Proc. 13th Int. Conf. Cosmic Rays*, Budapest, Hungary, 1969. *Akadémiai Kiadó Budapest*, 1971.
- Schubert, G.; and Coleman, P. J., Jr.: The Angular Momentum of the Solar Wind. *Astrophys. J.*, Vol. 153, 1968, p. 943.
- Siscoe, G. L.; Davis, L., Jr.; Coleman, P. J., Jr.; Smith, E. J.; and Jones, D. E.: Power Spectra and Discontinuities of the Interplanetary Magnetic Field: Mariner 4. *J. Geophys. Res.*, Vol. 73, 1968, p. 61.
- Siscoe, G. L.; Turner, J. M.; and Lazarus, A. J.: Simultaneous Plasma and Magnetic Field Measurements of Probable Tangential Discontinuities in the Solar Wind. *Solar Phys.*, Vol. 6, 1969a, p. 456.
- Siscoe, G. L.; Goldstein, B.; and Lazarus, A. J.: An East-West Asymmetry in the Solar Wind Velocity. *J. Geophys. Res.*, Vol. 74, 1969b, p. 1759.
- Siscoe, G. L.; and Finley, L. T.: Solar Wind Structure Determined by Corotating Coronal in Homogeneities. 1, Velocity-Driven Perturbations. *J. Geophys. Res.*, Vol. 75, 1970, p. 1817.
- Strong, I. B.; Asbridge, J. R.; Bame, S. J.; Heckman, H. H.; and Hundhausen, A. J.: Measurements of Proton Temperatures in the Solar Wind. *Phys. Rev. Lett.*, Vol. 16, 1966, p. 631.
- Wilcox, J. M.; and Ness, N. F.: Quasi-stationary Corotating Structure in the Corotating Medium. *J. Geophys. Res.*, Vol. 70, 1965, p. 5793.

C. P. Sonett I would say that the turnover in your spectra at around  $10^{-6}$  Hz is very comforting; it shows that the sun rotates about once every 27 days. DISCUSSION

J. R. Jokipii Is it possible that the reason the radial power continued to go up was that you were beginning to get away from the turbulent regime and into the stream structure?

G. L. Siscoe That seems to be consistent with this break at 1 day. The  $V_R$  really represents the corotating part of the variations, and it is certainly a dominant part of the corotation picture. And when one looks at the calculations that determine  $V_T$  and  $V_N$  from variations in the  $V_R$  the theory says that  $V_T$  and  $V_N$  should be much less, so it is consistent with that.

*L. Davis* In connection with the two or more mechanisms that seem to be operating at periods of the order of an hour or so—that is, all the periods of less than 1 day—do these have to be operating simultaneously, or from the way the data are analyzed would you get the same result if for a period of 1 to 2 days you had what we would call good Alfvén waves, and that was the dominant mechanism for a couple of days, then the next couple of days there were practically no Alfvén waves and you had a completely different mechanism, would that produce the kind of thing that—

*G. L. Siscoe* Yes, yes. I think that's what we should like to do next, that is to break up this 140-day interval into subintervals that look homogeneous in some respect, and see if we can identify dominant processes in subintervals.

*N. F. Ness* For periods of less than 1 day it is obviously not a pure Alfvén mode, because there are other processes evident in this statistical summary.

# EVIDENCE FOR A CONTINUOUS, POWER LAW, ELECTRON DENSITY IRREGULARITY SPECTRUM

Willard M. Cronyn

There is a controversy over the spectral form of the irregularities in electron density that cause interplanetary scintillation (IPS) of small angular diameter radio sources. The intensity scintillation technique always yields an "irregularity scale size," which is of the order of the first Fresnel zone for the wavelength at which the observations are taken. This includes not only the radio wavelength measurements of the structure of the interplanetary medium, with which we are most concerned here, but also radio wavelength measurements of the irregularity structure of the ionosphere and interstellar medium, and optical wavelength measurements of the irregularity structure of the atmosphere. The reasons are relatively straightforward. The fundamental question with regard to the interplanetary medium is: Is the scale size we determine from the analysis of IPS data an artifact of Fresnel diffraction, or is it a physically meaningful parameter of the irregularity structure and just coincidentally on the order of the radius of the first Fresnel zone?

## ABSTRACT

## THEORY

We use the "thin screen" model for scattering in the interplanetary medium [Salpeter, 1967]. Because of the inverse-square law dependence of electron density on heliocentric distance, we assume with reasonable confidence that the scattering takes place in a slab located at the distance of closest approach to the sun of the observer-source ray trajectory. We further assume that the effect of the slab, which introduces phase perturbations across the front of an advancing plane wave, is equivalent to a single, thin scattering screen located at the exit plane of the slab. The screen introduces exactly the same phase perturbations as the thick slab. For observations within  $60^\circ$  of the sun, the screen may be taken to be roughly 1 AU from an observer on the earth.

The basic theoretical problem is to relate the electron density irregularity structure as described by, say, a three-dimensional wave number spectrum  $F_{ns}(K_x, K_y, K_z)$ , to the two-dimensional wave number spectrum  $F_\phi(K_x, K_y)$  that describes the phase structure

in the screen. In turn,  $F_\phi$  must be related to the two-dimensional intensity wave number spectrum  $F_{Is}(K_x, K_y)$  in the observer's plane. Finally,  $F_{Is}$  must be related to the temporal spectrum of the intensity fluctuations  $F_{It}(\nu)$  seen by an observer as the two-dimensional intensity pattern is convected across his plane at the velocity of the solar wind.

The relevant equations for the power spectra are as follows:

$$F_\phi(K_x, K_y) = 2\pi r_e^2 \lambda^2 L F_{ns}(K_x, K_y, 0) \quad (1)$$

$$F_{Is}(K_x, K_y) = \mathcal{F}(K_x, K_y) F_\phi(K_x, K_y) \quad (2)$$

$$F_{It}(\nu) = 2\pi U^{-1} \int_0^\infty F_{Is}(2\pi \nu |U, K_y) dK_y \quad (3)$$

where

- $r_e$   $2.8 \times 10^{-18}$  km
- $\lambda$  radio wavelength
- $L$  effective slab thickness
- $U$  solar wind velocity

The author is at the Space Environment Laboratory, National Oceanic and Atmospheric Administration, Boulder, Colorado.

and  $\mathcal{F}$  is the Fresnel filtering function:

$$\mathcal{F}(K_x, K_y) = 4 \sin^2 [(K_x^2 + K_y^2)/K_f^2] \quad (4)$$

where

$$K_f = \text{spatial Fresnel wave number} \\ = \sqrt{4\pi/\lambda z} \approx (110 \text{ km})^{-1} \lambda_m^{-1/2}$$

for a scattering screen at  $z = 1 \text{ AU}$  from the observer, with  $\lambda_m = \lambda$  in meters. As a temporal fluctuation frequency,  $K_f$  appears as  $\nu_f$ :

$$\nu_f = 0.5 (U/350 \text{ km} \cdot \text{sec}^{-1}) \lambda_m^{-1/2} \quad (5)$$

where again the irregularities are assumed to be 1 AU from the observer.

For  $K_r^2 = K_x^2 + K_y^2 < K_f^2$ ,  $\mathcal{F}$  imposes fourth-power filtering on the density irregularity spectrum as  $\mathcal{F} \approx [2^{1/2} K_r/K_f]^4$ ,  $K_r < K_f$ . Thus for typical meter wavelength observations, one would not expect to see significant intensity fluctuations arising from structure larger than  $\sim 110 \text{ km}$ . In terms of the temporal spectrum  $F_I(\nu)$ , even if the spectrum were power law at frequencies higher than  $\nu_f$ , with an index  $\beta + 1$  so that  $F_I(\nu) \propto \nu^{-\beta-1}$ , at temporal frequencies lower than  $\nu_f$  one would expect to see a rather flat spectrum; the scale of the spectrum would therefore be on the order of  $\nu_f$ .

## OBSERVATIONS

Unfortunately, very few measurements of the spectral index have been made for scintillation spectra. *Lovelace et al.* [1970] computed spectra for observations taken with the Arecibo dish; see *Lovelace* [1970] for significant refinements of the power-law spectral index. The signal-to-noise ratio was sufficient to establish the spectral form as a power law (for  $\nu > \nu_f$ ) rather than gaussian. *Lovelace's* estimate of  $\beta$  is 1.6 for observations from 0.2 to 0.5 AU. The spectra are rather flat at frequencies below  $\nu_f$ .

As a further indication that Fresnel effects are determining the scale of the intensity spectrum, table 1 summarizes the scale of intensity spectra at various wavelengths and solar elongations; the scale is defined as  $\nu_{2I}$ , the square-root second moment of the spectrum—that is,

$$\nu_{2I} = \sqrt{\int_0^\infty \nu^2 F_{It}(\nu) d\nu}$$

The Fresnel frequency, also is given; note that  $\nu_{2I}$  and  $\nu_f$  differ by factors of less than 2. A detailed explanation of the difference would require information about the power law index for  $\nu > \nu_f$ , the axial ratio of the

irregularities, and various other parameters about which we unfortunately have little or no information. As has been suggested [*Cronyn*, 1970], it is important to evaluate the spectral index of scintillation spectra, in addition to the more usual parameters of scale and scintillation index.

Another indication that we are dealing with a continuous power law spectrum of irregularities is provided by a comparison of the electron density spectrum deduced from IPS spectra with the proton density spectrum from space-probe measurements. For a power law irregularity spectrum, the relationship between an intensity scintillation spectrum  $F_{It}(\nu)$  and a space probe density spectrum  $F_{nt}(\nu)$  may be shown [*Cronyn*, 1971] to be given by:

$$F_{nt}(\nu) = \left. \frac{3.7 \nu F_I(\nu) \Gamma(\beta/2 + 1)}{\beta \rho (U/350 \text{ km} \cdot \text{sec}^{-1}) \lambda_m^2 \Gamma(\beta + 1/2)} \right\} \quad (6) \\ \nu > \nu_f$$

where

- $\beta$  spectral index for space-probe spectrum;  $\beta + 1$  is spectral index for temporal intensity spectrum  $F_I(\nu)$
- $\Gamma$  the gamma function
- $\rho$  observer — source ray trajectory distance of closest approach to the sun in AU

**Table 1.** IPS spectral scales and estimated Fresnel frequencies

$\rho$ , AU	$\lambda$ , m	$\nu_{2I}$	$\nu_f^*$	Reference
0.06 – 0.14	0.11	2.2 – 1.3	1.5	<i>Cohen and Gundermann</i> [1969]
0.04 – 0.14	0.21	2.5 – 1.2	1.1	<i>Cohen and Gundermann</i> [1969]
0.14 – 0.60	0.70	1.2 – 0.7	0.6	<i>Cohen and Gundermann</i> [1969]
>0.34	1.54	0.6	0.4	<i>Cohen et al.</i> [1967]
>0.55	3.70	0.5	0.3	<i>Dennison</i> [1969]

\*Computed according to equation (5) with  $U = 350 \text{ km/sec}$

Taking  $\beta = 1.6$ ,  $U = 350 \text{ km} \cdot \text{sec}^{-1}$ , fixing the absolute power spectral density of  $F_f(\nu)$  from the scintillation index as given by Hewish [1971], and assuming that  $F_{nt}(\nu)$  may be extrapolated to much lower frequencies than  $\nu_f$  gives:

$$F_{nt}(\nu) = 1.4 \times 10^{-3} \nu^{-1.6} (\text{electrons/cm}^3)^2 \text{Hz}^{-1}$$

(7)

at 1 AU from the sun; for a detailed discussion, see Cronyn [1971]. This estimate of the power spectral density for electron density irregularities agrees remarkably well with  $F_{nt}(\nu)$  measured for proton density irregularities [Intriligator and Wolfe, 1970]: at  $\nu = 10^{-3} \text{ Hz}$ , equation (7) gives  $F_{nt}(\nu) = 100$ , while  $I$  and  $W$  measure 250; at  $\nu = 10^{-4} \text{ Hz}$ ,  $F_{nt} = 5.1 \times 10^3$ , while  $I$  and  $W$  measure  $4.6 \times 10^3$ .

The only evidence that contradicts the continuous power law irregularity model is the wavelength dependence of the scintillation index, which Hewish has discussed at this conference and elsewhere [Hewish, 1971]. The linear wavelength dependence which Hewish argues for would rule out the power law spectrum. However, as Hollweg and Jokipii have pointed out (p. 495), the dependence can be  $m \propto \lambda^\alpha$ , where  $\alpha$  could be at least as high as 1.25 because the data have substantial scatter. For  $\beta = 1.6$ ,  $\alpha$  would theoretically have to be 1.4.

## CONCLUSIONS

There is evidence that for  $\nu > \nu_f$  the intensity spectrum is a power law indicating a power law electron density spectrum. At frequencies less than  $\nu_f$  the spectra flatten out, as one would expect because of Fresnel filtering. It would therefore appear to be unreasonably fortuitous for the flattening to represent the intrinsic irregularity spectrum, especially since the plasma density irregularities tend to again be described by a power law spectrum at still lower values of  $\nu$ . In any case, the relatively small difference between  $\nu_{2I}$  and  $\nu_f$  is an indication that Fresnel filtering is having a pronounced effect. Finally, there is the very interesting indication that extrapolation to large scales of the very small-scale electron density structure actually agrees very well with measured proton density spectra. Thus, the conclusion we must draw is that the small-scale electron density structure is power law, that it may be smoothly extrapolated to much larger scale sizes, and that the wavelength dependence of the scintillation index can probably accommodate such a spectrum.

## ACKNOWLEDGMENTS

I am grateful to A. Hewish, D. S. Intriligator, and J. R. Jokipii for helpful discussions. This research was supported through an NAS-NRC Postdoctoral Research Associateship in the Space Environment Laboratory of the National Oceanographic and Atmospheric Administration.

## REFERENCES

- Cohen, M. H.; Gundermann, E. J.; Hardebeck, H. E.; and Sharp, L. E.: Interplanetary Scintillations. II. Observations. *Astrophys. J.*, Vol. 147, 1967, p. 449.
- Cohen, M. H.; and Gundermann, E. J.: Interplanetary Scintillations. IV. Observations Near the Sun. *Astrophys. J.*, Vol. 155, 1969, p. 645.
- Cronyn, W. M.: The Analysis of Radio Scattering and Space-Probe Observations of Small-Scale Structure in the Interplanetary Medium. *Astrophys. J.*, Vol. 161, 1970, p. 755.
- Cronyn, W. M.: Interplanetary Plasma Density Fluctuations: Agreement Between Space Probe and Radio Scattering Observations. 1971 (in preparation).
- Dennison, P. A.: Observations of Fine Structure in the Interplanetary Medium. *Planet. Space Sci.*, Vol. 17, 1969, p. 189.
- Hewish, A.: The Spectrum of Plasma-Density Irregularities in the Solar Wind. *Astrophys. J.*, Vol. 163, 1971, p. 645.
- Intriligator, D. S.; and Wolfe, J. H.: Preliminary Power Spectra of the Interplanetary Plasma. *Astrophys. J.*, Vol. 162, 1970, p. L187.
- Lovelace, R. V. E.; Salpeter, E. E.; Sharp, L. E.; and Harris, D. E.: Analysis of Observations of Interplanetary Scintillations. *Astrophys. J.*, Vol. 159, 1970, p. 1047.
- Lovelace, R. V. E.: *Interplanetary Scintillations* (Ph D thesis), Cornell Univ., Sept. 1970.
- Salpeter, E. E.: Interplanetary Scintillations. I. Theory. *Astrophys. J.*, Vol. 147, 1967, p. 433.

DISCUSSION     *G. Newkirk* I would like to ask a question about the physics of all of this, which seems not to have been discussed very thoroughly at the present time. We have given a great deal of attention as to whether or not the spectral index at long wavelength can be carried down to short wavelength. Whether or not it does, the significance of this is what escapes me, and I wonder if someone could say a couple of words as to what we might expect if, for example, we have a medium dominated by turbulence, what we might expect if we have a medium dominated by waves.

*F. W. Perkins* I would like to answer Dr. Newkirk's question to some extent. I think what the spacecraft are observing apparently is outward going Alfvén waves that are probably left over from the processes that are heating the solar wind. Meanwhile, what is being measured in the interplanetary scintillations are smaller scale fluctuations that are characteristic of the microturbulence processes that are playing the role of cushions in the plasma. From what we know about these microprocesses they seem to occur most readily in the sense of velocity deviations from Maxwellian velocity distributions that are less for waves around the ion cyclotron frequency and for wavelengths in the order of the ion gyroradius. These waves have one characteristic signature that could possibly be found in the data, that is, their phase velocities go inward along the magnetic field whereas the waves observed by spacecraft seem to have an outward going phase velocity.

## COROTATION OF AN INTERMITTENT SOLAR WIND SOURCE *Thomas A. Croft*

The measured electron content of the solar wind in mid-1970 exhibited a region of relatively high electron density that reappeared at intervals of about 27.8 days. It is shown that the repeating event cannot be reconciled with the concept of a long-enduring steady flow, even though the recurrence period is close to the rotation period of the sun. This evidence of transients is inferred from the short duration of each appearance of the interval of higher density; each should last for roughly one corotation interval if it is caused by a steady stream. The radio path was approximately 0.8 AU long, and the corotation interval exceeded 3 days. **ABSTRACT**

Other aspects of the content data patterns support the view that such transient events are common in the solar wind. The mid-1970 repeating event is an unusually good example of the intermittent character of flow regions in the solar wind that fluctuate on a time scale of days but endure as identifiable regions for many months. A sputtering corotating source of thin solar plasma streams could explain this series of events; it could also be explained in terms of a stream that is steady in density and speed but undulating north-south so that it passes into and out of the 0.8 AU radio path in a matter of a day or less.

### INTRODUCTION

Observations of the solar wind and of its effects on the earth over the past six or seven decades have revealed a 27-day recurrence pattern, roughly in synchronism with the rotation of the sun. This "corotation" has been manifested in many parameters measured by spacecraft during the last decade, and consequently it is now generally believed that there are corotating flow regimes in the solar wind that endure for several solar rotations. A definitive early work on this subject was given by *Bartels* [1932] and more recent knowledge has been summarized by *Wilcox* [1968]. The 27-day repetition is clearly seen in interplanetary electron content measurements obtained by the radio propagation experiment on the Pioneer spacecraft [*Croft*, 1971].

When solar wind measurements are compared on successive rotations, it is seldom found that the detailed

patterns in the data repeat; rather, it is found that the general character of the data patterns is repetitious. For example, a chaotic region will reappear on successive rotations, but individual fluctuations within that region are not observed to be faithfully reproduced. Similarly, quiet periods in the data will be observed for several successive rotations at 27-day intervals.

The Pioneer electron-content measurements permit the observer to discriminate in some cases between data fluctuations caused by temporal changes in the solar wind and those caused by corotation of the steady-state pattern through the volume of space in which the measurement takes place. In other words, temporal fluctuations can be separated from spatial fluctuations. From such analyses [*Croft*, 1971], the author has concluded that there are isolated sources of solar plasma corotating with the sun but that they typically sputter; that is, they eject plasma intermittently on a time scale of approximately a day. This general conclusion was supported by a number of observed patterns in the data.

---

*The author is at the Center for Radar Astronomy, Stanford University, Stanford, California.*

A particularly convincing piece of evidence is presented here. It is shown that in mid-1970 in the vicinity of Carrington longitude  $50^\circ$  on the sun there was an intermittent source of plasma that endured for at least four solar rotations. The corotation of this region is inferred from the fact that it appears at very nearly the right time on each of several successive rotations. Its intermittent character is inferred from the fact that the duration of each content increase is too short to be explained in terms of a corotating steady stream.

#### EXPERIMENTAL METHOD

The electron content of the solar wind has been measured by a radio propagation technique employing special receivers placed aboard Pioneers 6, 7, 8, 9, and also aboard Mariner 5. Only the results obtained from Pioneers 8 and 9 will be employed here. The measurement technique has been explained most thoroughly by Koehler [1968] and most recently by Croft [1971].

The experiment can operate only when one of the Pioneers is above our horizon (once a day for each spacecraft) and only during times when the telemetry from the craft is being monitored by the NASA Deep Space Network. Two coherent signals at 49.8 and 423.3 MHz are transmitted to the craft from a 150-ft (46-mr) paraboloid antenna located near the Stanford campus. Both signals are phase modulated at about 8 kHz, and at the spacecraft the phase difference between the modulations is measured and encoded by a special receiver. Later, after the results of the measurement are telemetered to earth and analyzed, we derive the differential group delay at the two frequencies, and this is roughly proportional to the electron content from earth to the spacecraft along the radio path. The underlying physical mechanism is the decrease in group velocity brought about by free electrons in the solar wind; the phase velocity is increased by a nearly equal amount, and to take advantage of this fact we monitor changes in the phase delay by observing the relative radio frequency of the two carrier signals which reach the spacecraft.

To quantize this measurement, the higher frequency is multiplied by 2/17 and then subtracted from the lower frequency and the remaining signal is used to drive a counter. Fluctuations in the solar wind cause changes in the content on the path that are manifested in counter rates of approximately 1 Hz or less. The status of the counter is periodically telemetered to earth and subsequently the succession of counts is analyzed to determine the phase delay and, from this, the electron content along the path. This process involves integration and consequently the derived content includes an unknown additive constant, which is determined by

comparing the phase delay to the group delay. The phase delay measurement provides finer resolution and it is less affected by nonlinearities in the earth's ionosphere; the group delay provides total content measurements (since there is no unknown constant) and also the group delay measuring system operates when the signal strength is too weak to permit reliable interpretation of the counter.

Both group and phase delay measurements thus yield electron content from the surface of the earth to the spacecraft, and this includes the content of the ionosphere and magnetosphere, which is unwanted. To eliminate this component, it is necessary to measure it and subtract it from the total, the Pioneer content. The measurement is accomplished by observing the Faraday rotation angle of signals from geostationary satellites on a continuous basis. Ionospheric and magnetospheric content is then inferred from the rotation angle; this yields the content along the line of sight to the geostationary satellite, not to the Pioneer where it is needed.

Two different computer algorithms have been devised for computing the content along the desired line of sight from measured content along geostationary lines of sight. These calculations work best when several geostationary lines are simultaneously monitored. If only one such line is monitored, then the calculation makes use of an assumed constant slab thickness of the ionosphere coupled with a geographic variation in the critical frequency following the numerical maps provided by the ionospheric predictions of NOAA. An alternative algorithm makes use of the assumption that the ionospheric structure is fixed relative to the sun, and that the earth revolves within this ionosphere without modifying it. Both algorithms are used because it has been found that each has strengths and weaknesses and the best result is achieved by human examination of the two derived solutions and comparison to the Pioneer-measured total content. The ionospheric processing is relevant to the following discussion because the errors involved in the calculation are the largest source of error in the entire experiment. The only comparable source of error is the nonlinear relation between ionospheric content and propagation delay, which is troublesome when the spacecraft are viewed near the horizon in the daytime.

Because the size of the ionospheric errors is independent of the distance from earth to the sun-orbiting spacecraft, it follows that the percentage accuracy of the interplanetary content measurement improves as the spacecraft recede from earth. For the time interval to be discussed here, Pioneer 8 was between 0.75 to 0.9 AU and Pioneer 9 between 1.5 to 1.8 AU from the earth.



Under these circumstances, the ionospheric error is typically less than 10 percent of the interplanetary content. However, the processing for these particular data is only of the manual "quick-look" variety, using a single geostationary satellite as an ionospheric monitor and ignoring the Pioneer phase delay measurement. Later, we hope to execute our computer processing of the full data set and recover much fine structure that is lost in the presentation given here. For the purpose of this paper, however, the "quick-look" data provide the necessary evidence.

### DISCRIMINATION BETWEEN TEMPORAL AND SPATIAL CHANGES

The Pioneer spacecraft stay near the orbit of the earth; some move ahead and some fall behind the earth, and thus over a period of time the earth-spacecraft distances increase to a maximum value of roughly 2 AU when the spacecraft are at superior conjunction. For the time interval of interest here, Pioneer 8 was approximately 0.8 AU behind the earth and Pioneer 9 was twice that distance ahead. Figure 1 shows the positions of the spacecraft, sun, and earth, together with other features referred to later in discussing the results obtained. The

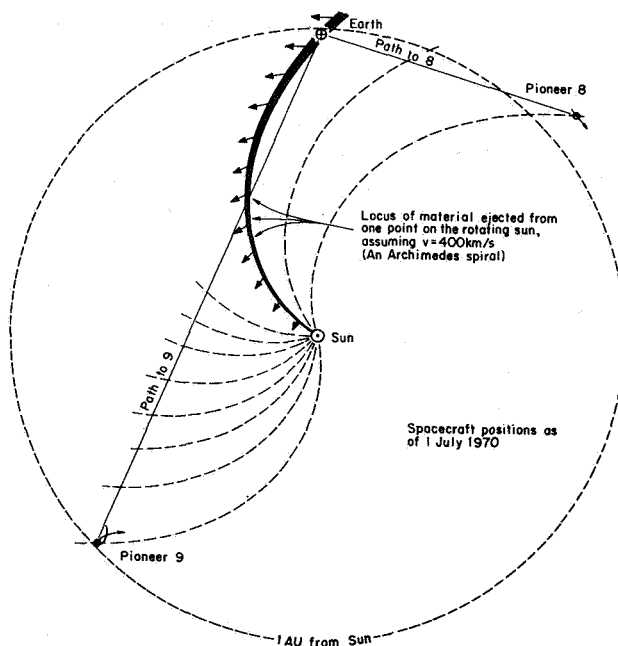


**Figure 1.** Relative positions of Pioneers 8 and 9 and of the sun and earth in mid-1970 as seen projected into the ecliptic plane and viewed in a frame that rotates with the earth once per year. Electron content is measured along the paths shown, and the steady stream response (SSR) is the content-time function due solely to the hypothetical thin plasma jet.

most striking feature of the sputtering solar plasma source observed at  $50^\circ$  longitude was the timing of the appearance of its plasma along the Pioneer 8 path. Consequently, the method for discriminating between spatial and temporal effects is discussed here in relation to Pioneer 8 content measurements along the 0.8 AU path trailing the earth.

Electron content is the line integral of free electron number density along the radio path; when divided by the length of the path, the quotient is the spatial average of density on the path. If the solar wind consisted only of fully ionized hydrogen, then this quotient would represent the solar wind density. The presence of a few percent helium and the observed fluctuations in the percentage [Hundhausen, 1970] prevent us from relating electron density to solar wind density with an accuracy better than about 5 percent.

The test between spatial and temporal changes is based on the logic outlined below.

#### Assume No Temporal Changes

If we assume that there are no temporal changes, the flow pattern of the solar wind (its total distribution of velocity and density) never changes in a frame which rotates with the sun. Differential rotation is not of importance in this test and will thus be ignored. Plasma from a single source is then distributed along the familiar Archimedes spiral having a curvature that depends on the flow velocity.

#### Calculate the Content-Time Function: The Steady Stream Response

We calculate the recognizable characteristics of the content versus time pattern that must follow from the assumed steady-state flow. One consequence of the assumption is that the density measured at a point fixed in space relative to the sun would undergo exact repetition at the rotation rate. Therefore, at any given distance from the sun, one could determine density versus longitude as a single-valued function.

If there were an anomalously high-density plasma stream in the corotating flow structure, then the stream would follow the spiral configuration except for distortion due to interaction with the neighboring flow regimes if they have a different velocity. This distortion should be small since the anomalous stream is of relatively high density. If such a hypothetical stream rotated through a radio path whose content was being monitored, then the content would be observed to rise when the stream entered the path and fall when the stream left the path. This is illustrated in figure 1. For the duration of the increased content, the magnitude of the increase would be proportional to the stream density

at the point (or points) where it crosses the radio path and also proportional to the *length* of the radio path immersed in the stream. The duration of the increase, the *corotation delay*, is easily calculated if the stream velocity is known; the author prefers the term *corotation interval* because in some applications the term *delay* is inappropriate.

The effect of such a hypothetical thin, corotating steady-state stream has been calculated once per solar rotation throughout the lifetime of Pioneers 8 and 9. This calculated content-time function will be called the *steady stream response* (SSR). It is analogous to impulse response in the sense that the steady stream would appear as an impulse in the density-longitude function that one could obtain from measurements at fixed heliocentric distance. If the velocity of the solar wind were the same everywhere, the SSR would be even more closely analogous to impulse response; one could obtain the spatially averaged density measurement of the Pioneer system by convolving the SSR with the density-longitude function, dividing by distance to convert content to density.

With the reservations noted above, and provided that the solar wind is in steady state, one can consider that the radio propagation experiment on Pioneer spacecraft is a measuring system having the SSR as its impulse response. The input function is density versus longitude, measured at 1 AU. Taking this view, one can see that a long radio path in interplanetary space should yield density-time curves that are smoothed in relation to the path length. Longer paths produce smoother data because the SSR becomes very long, and its effect, when it is convolved with the input function, is to smooth that function. As an extreme example, one can consider an SSR which is rectangular—that is, one that increases to a fixed value and remains at that level until its abrupt termination. The convolution of such a rectangle with the input function has a smoothing effect much like that which would be obtained by taking the running mean of the data over the duration of the rectangle. Short pulses in the input function then assume a broad form having a width comparable to the convolving rectangle. (However, in relation to Pioneer 9, we shall see, that paths exceeding roughly 1 AU have an SSR that does not produce the same degree of smoothing.)

#### Compare Data for Irregularities

We compare the real data to the character of hypothetical steady-state data to find features inconsistent with the steady-state restrictions. The most obvious of these inconsistent features are pulses that are short relative to the corotation interval and have a magnitude large relative to the content before and after; such pulses are

inconsistent with the idea of prior convolution with the SSR. The appearance of a short pulse indicates some kind of temporal change in the solar wind; that is, as viewed in a corotating frame of reference, the distribution of density was undergoing change. From the content data alone, it cannot be decided which of several forms of temporal change were the cause of individual observed fluctuations. However, it appears credible to the author that these transient phenomena are outward traveling irregularities in the solar wind. The identification of the character of such irregularities is an extensive subject in itself, and is under study by J. A. Landt, who is presenting some of his conclusions at this symposium (p. 598). One particularly large event has been described in the literature [Landt and Croft, 1970].

#### DISCRIMINATION TESTS ON MID-1970 CONTENT DATA

Beginning in April 1970, there was a period of intensive operation of Pioneers 8 and 9 to gather background data as Pioneer 9 approached superior conjunction and the interesting events associated with the occultation of the radio path by the solar corona. This minimized the major source of ambiguity in our data, which is its intermittent character, a disadvantage that is most pronounced when operations are conducted on only a few of the daily opportunities. The most useful data for the purpose of steady-state testing are those taken at times when observations are conducted almost everyday. There was one such period enduring for roughly nine solar revolutions in 1968; these data have been presented by Croft [1971]. However, the 1968 measurements were taken with Pioneer 8 at a time when the corotation delay was only a few hours; consequently, the steady-state tests could not be conclusively applied in that interval. Beginning in 1970, however, the commencement of daily operation revealed great structural detail in the flow patterns and, in particular, it revealed the repetitive fluctuations that will be discussed here.

The average density measured during five rotations of the sun is shown in figure 2. The average along the path to Pioneer 8 is plotted upward and that to Pioneer 9 is plotted downward. It is readily observed that the Pioneer 9 density is the higher of the two, and this is attributable to the fact that the path to Pioneer 9 lies nearer the sun where the density is higher.

Note that figure 2 includes a scale showing the Carrington longitude of the central meridian of the sun. Because the earth's orbit is not quite circular, the length of one Carrington rotation changes with the season from a minimum of roughly 27.19 to a maximum of about 27.34 days. The time scale is fixed throughout and

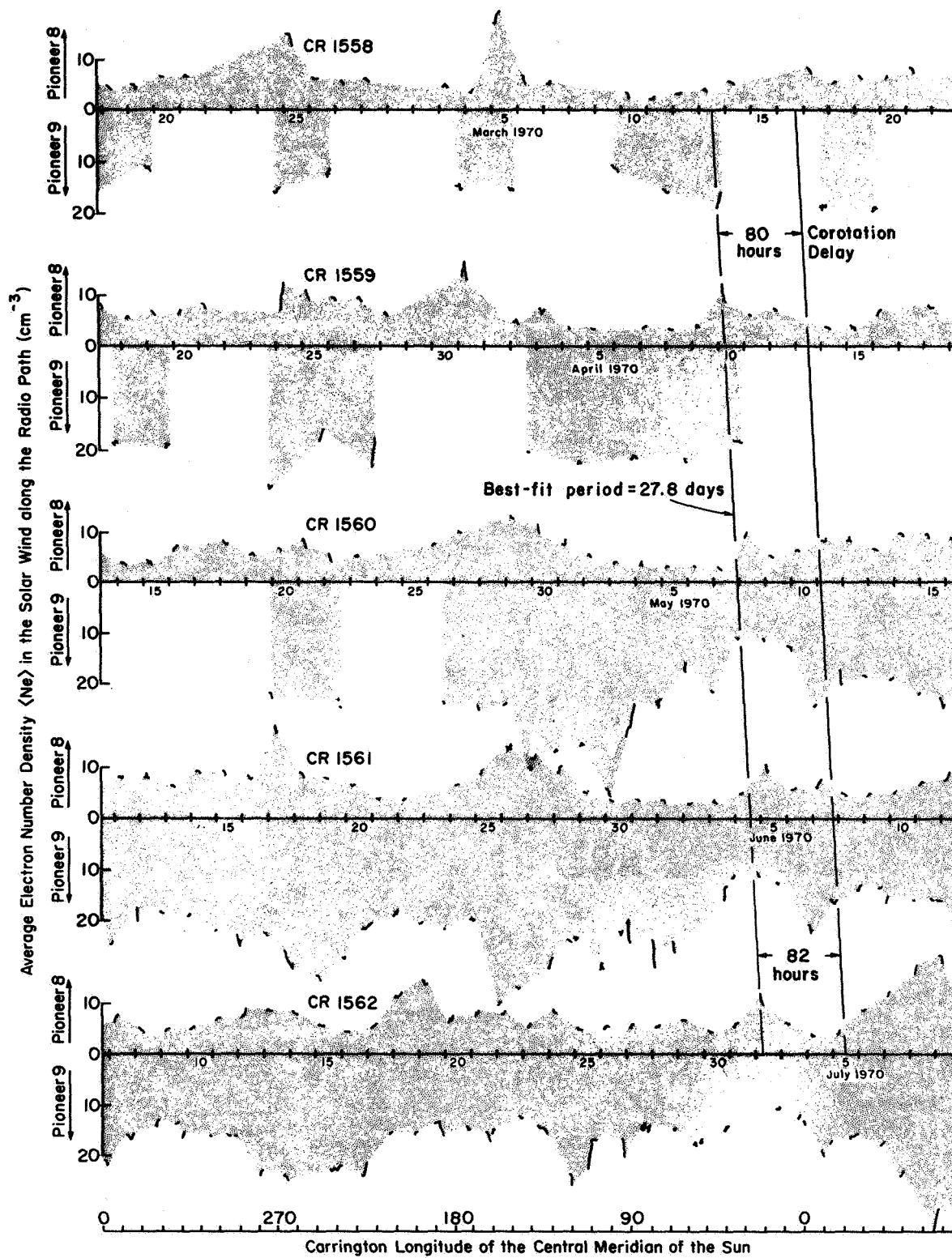


Figure 2. Average density of the solar wind along the line from earth to Pioneer 8 (plotted upward) and to Pioneer 9 (plotted downward). Short-line segments show plotted hourly points as measured, and the intervening shading is a visual aid spanning all data gaps of 4 days or less. The long vertical lines enclose pulses in the Pioneer 8 data.

consequently the longitude, as plotted, is a slight approximation. If used without compensation, errors of up to about 0.1 day can be found, but it should be pointed out that this is only a third the error that is inherently ignored when the Bartels 27-day rotation numbering system is used as a basis for plotting successive rotations. In the context of this discussion, such errors are negligible, but the variation can make a difference when the data are statistically analyzed in a search for long-term trends.

While there are several features on figure 2 that are inconsistent with the concept of steady flow, attention here is directed to the pulses shown in Pioneer 8 data on the second through fifth rotations in the longitude interval from  $0^\circ$  to  $40^\circ$ . If we assume that these bursts of plasma required 4 days to travel from the sun to reach the radio path, then their source near the sun must be located at a Carrington longitude of about  $50^\circ$ . All four peaks reached their maximum value at the Carrington synodic rotation period plus or minus 0.9 day. However, if we allow freedom to fit a period to the data, it happens that the four peaks recur each 27.8 days with a tolerance of only plus or minus 0.2 day. Even this slight tolerance could be eliminated if one were free to fill in the missing data without restriction.

Since the 27.8-day period provides the best fit to these four pulses, it will be used here in the test for the possibility of steady-state flow. An important distinction must be made between the rotation rate used for testing and the rotation rate believed to be correct. This seeming contradiction is due to the nature of the test, which is negative rather than positive; we are attempting to prove that temporal fluctuation occurred by showing that steady-state flow cannot have occurred. To make this negative proof convincing, we must illustrate the impossibility of steady-state flow using any rotation period reasonably close to 27 days. After the testing is concluded and it is found that steady-state flow did not occur, then we may revert to the Carrington period or to any other period thought to be likely.

There is one interesting sidelight to the choice of the 27.8-day period; it happens that there was a slight pulse during Carrington rotation 1564 and two other more marked pulses during rotations 1554 and 1555, all of which correlate with the four pulses under consideration if one assumes the 27.8-day period. Further, in mid-1969 during Carrington rotations 1547-9, regions of higher density occurred that also are consistent with recurrence of this feature at the 27.8-day rate. The physical reality of such alignments remains to be determined; at this time, we are in the process of

extracting the statistics of these observations through objective mathematical processes.

For the five Carrington rotations that appear on figure 2, the SSRs are similar, varying somewhat in dimension but not enough to affect the tests discussed here. As examples, two SSRs for Pioneer 8 and one for Pioneer 9 are plotted on figure 3. At other times during the events depicted on figure 2, there was negligible change in the SSRs insofar as these steady-state tests are concerned. The variation in the Pioneer 8 SSR between the two examples plotted will serve to illustrate the magnitude and character of the changes that occur in an interval of three rotations, or about 82 days.

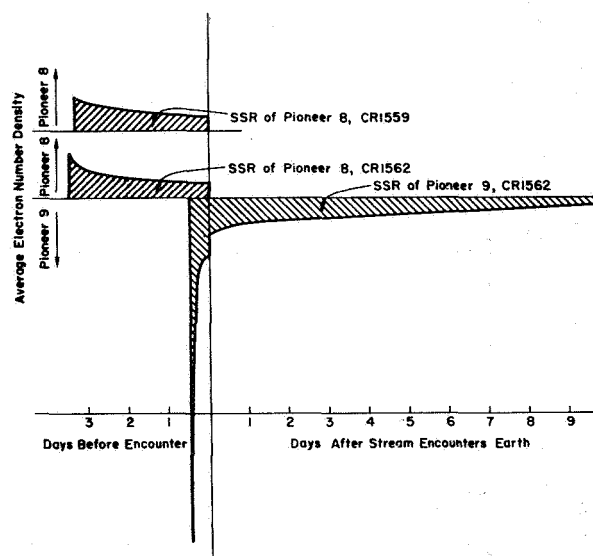


**Figure 3.** The steady stream response (SSR) of the Pioneer 8-Pioneer 9 measuring system in mid-1970. This is the average electron number density versus time along the radio paths caused by a steady stream from a source rotating at the Carrington period. In this example, a flow speed of 400 km/sec was assumed and 1-hr integrations were performed.

There is a qualitative difference between the SSRs of Pioneers 8 and 9; the Pioneer 8 SSR is roughly a rectangle, while that for Pioneer 9 starts with a sharp, short pulse containing more than 20 percent of the total area defined by the SSR. The sharp onset of the function is attributable to the fact that the corotating spiral stream first encountered the Pioneer 9 path broadside, before the stream hit either earth or Pioneer 9. This can be visualized on figure 1. Thus, at the beginning of the influence of the stream, the measured content is very high because the length of the path inside the stream is at a maximum just after the point of

tangency. There is a sharp drop in the Pioneer 9 SSR which coincides with the termination of the Pioneer 8 SSR; prior to the drop, the plasma stream crossed the Pioneer 9 path in two separate regions. At the moment of the drop, the stream strikes the earth; thereafter, the stream is not intercepted by the Pioneer 8 path, and also the single crossing of the Pioneer 9 path occurs at more nearly perpendicular incidence, with the attendant short immersed path length and low content. There are a number of interesting facets to this calculation of the SSR, which are described in a paper now in preparation.

Little has been said of the testing of Pioneer 9 data for possible steady-state causation. This is because the Pioneer 9 SSR contains the large, short initial feature, and when such a function is convolved with another function, sharp features in the second function are comparatively well preserved. Consequently, steady-state tests are more subtle. However, the Pioneer 8 SSR is much like a rectangle and so its convolving effect is similar to the action of a running mean. In the resulting content measurement, pulses should not occur having a duration less than the corotation interval.

The observed content variation on April 10, 1970, when the first of the four repeating pulses occurred, exhibits a high rate of decrease, which could only occur at the termination of the effect of a steady stream—a view inconsistent with the measurements of the preceding three days when the content was relatively low. If we neglect this sharp drop on April 10 and attribute it only to the chance coincidence of a transient event at the beginning of the passage of a steady stream, then it *would* be possible to reconcile the April 10 onset with the steady-state hypothesis since the density stays high for the following two (or three) days.

However, the second occurrence on May 8 is seen to be an isolated, high value occurring among a series of daily values which are relatively undisturbed, although exhibiting a slight rising tendency. The maximum permissible rate of decrease of content over a period of several days is limited by the SSR; the measured content can only decrease at the same proportional rate as the SSR in the unlikely event that the steady-state flow is followed by a region in which there is a vacuum. No such region has ever been detected in the solar wind, and it must be inferred that if there is steady-state flow, the content can never decrease at a proportional rate equal to (or faster than) the SSR. Yet, from May 8 to 9, the content decreases by a factor of 2. Clearly this is inconsistent with steady-state flow.

At the third occurrence on June 5, the rate of decrease for several hours was again too great to be explained in terms of steady flow, and the drop from June 5 to 6 is

also excessive. Notice the slight increase on the following day; if the source of this family of pulses is a single sputtering source, then we should expect to see outbursts more than once in a single rotation on some occasions, and on other occasions we should not see it at all. Perhaps the slight increases observed on June 7 and on April 12 are reappearances of the same sputtering source on rotations 1559 and 1561. A trend that supports this view is the observation that the second appearance in each of these two rotations is less pronounced than the first appearance. This would be expected because the SSR decreases by roughly a factor of 2 during the corotation interval. The decrease is attributable to the rotation of the spiral stream so that it encounters the radio path at more nearly perpendicular incidence (fig. 1). The length of path inside the stream is then shorter, and consequently the content is decreased. This same mechanism would act to decrease the size of content pulses caused by sputtering plasma streams, so that reappearances would cause smaller content pulses.

The final appearance of the recurring pulse is on July 2, although it is possible that the upward trend on July 1 is an indication that the interplanetary content may have begun its increase on that earlier date. Again, steady-state flow can be ruled out because of the high rate of decrease from July 2 to July 3 and to July 4. The observed rate is too high even if one assumes the existence of a steady, thin plasma stream followed by pure vacuum.

#### A POSSIBLE CAUSE OF THE REPEATING PULSE

We have shown that the repetitious event on figure 2 cannot be reconciled with steady flow. There are no clues presently available to the author that permit definition of the character of the corotating region. It is possible that other spacecraft measurements will provide such clues and permit us to determine the details of these detected temporal changes.

These data are consistent with their possible causation by a single source corotating with the sun and near its surface at a Carrington longitude of roughly  $40^\circ$  to  $50^\circ$ . However, this source cannot be steady but must eject plasma at a rate that varies on a time scale of approximately one day. The flow from the source is not necessarily extinguished between outbursts, but its density must change, and if this occurs, it seems likely that the velocity of the stream also changes. Such a behavior would explain the variation of the location of the pulses observed over a time span of roughly one corotation interval. In fact, if the Carrington rotation rate is assumed, and if one wishes to include the primary and secondary pulses mentioned earlier, then it is

necessary to include all pulses over a period of 4 days; this amount of variation could easily be explained in terms of a stream width of  $10^\circ$ , or in terms of varying velocity, which could change the earth-sun transit time by  $\pm 0.5$  day. See, for example, the velocity distributions of Gosling *et al.* [1970].

It is not necessary to consider that the sputtering source is ejecting plasma clouds that are discrete entities with sharply defined leading edges. Rather, one can explain these measurements in terms of a unending stream of varying density. Of course, if velocity varies also, then bunching will often occur and sharp leading edges may occur.

There is at least one alternative explanation, which is quite different: In principle, it is possible to explain these observations in terms of a flow of plasma that is steady in density and velocity, but which undulates north-south and east-west by approximately  $10^\circ$ , heliocentric. If the stream is sufficiently narrow, then it can pass in and out of our radio path in a north-south direction, and it would be visible only for a period of roughly 4 days on each rotation. The author finds this explanation to be less credible than that of the intermittent source, but the judgment is subjective and therefore it is suspect.

Other features in figure 2 are relevant to this discussion. Notice the faithful reproduction of the 27-day content pattern from rotation 1560 to 1561, except the pulse on May 17. We have made this kind of measurement continuously for over 5 years and this particular pair of rotations exhibits the best structural match that we have found.

On rotations 1560 through 1562, notice that there is a tendency for pulses to occur on the Pioneer 9 path about 2 days after the Pioneer 8 pulses under scrutiny here. The three Pioneer 9 pulses are more closely synchronized to the Carrington rotation period than are the Pioneer 8 pulses and, because of the impulsive character of the Pioneer 9 SSR, this may be a clue that the source region near the sun actually rotates at nearly the Carrington rate.

There are other Pioneer 8 pulses in figure 2 that exhibit rates of increase followed by rates of decrease at short intervals inconsistent with the steady-state flow. Some notable examples are those on February 25, March 5, March 31, May 17, and June 19. The interested reader can find more examples in figure 3 of Croft [1971].

## CONCLUSIONS

It is seen that a recurring transient increase in the measured solar wind content cannot be attributed to a corotating flow having steady velocity and density. The

sequence of events can be most readily explained if the causative mechanism is the corotation of an intermittent source that ejects a narrow plasma stream of variable density and, perhaps, of variable velocity. However, on the basis of the data available, we cannot rule out the possibility that these events are caused by a steady flow that undulates in the north-south direction so that it can enter and leave the Pioneer radio path on a time scale of approximately one day. The intermittent flow concept has been indicated by other patterns in the Pioneer content measurements, but this series of events in mid-1970 appears to offer the most conclusive evidence of the existence of sputtering, corotating regions.

## REFERENCES

- Bartels, J.: Terrestrial-Magnetic Activity and its Relations to Solar Phenomena. *Terr. Magn. Atmos. Elec.*, Vol. 37, No. 1, 1932, pp. 1-51.
- Croft, T. A.: Corotating Regions in the Solar Wind, Evident In Number Density Measured by a Radio-Propagation Technique. *Radio Sci.*, Vol. 6, 1971, p. 55.
- Gosling, J. T.; Hansen, R. T.; and Bame, S. J.: Solar Wind Speed Distributions: 1962-1970. *J. Geophys. Res.*, Vol. 76, 1971, p. 1811.
- Hundhausen, A. J.: Composition and Dynamics of the Solar Wind Plasma. *Rev. Geophys. Space Sci.*, Vol. 8, 1970, p. 729.
- Koehler, R. L.: Radio Propagation Measurements of Pulsed Plasma Streams from the Sun Using Pioneer Spacecraft. *J. Geophys. Res.*, Vol. 73, 1968, p. 4883.
- Landt, J. A.; and Croft, T. A.: Shape of a Solar Wind Disturbance on July 9, 1966, Inferred from Radio Signal Delay to Pioneer 6. *J. Geophys. Res.*, Vol. 75, 1970, p. 4623.
- Wilcox, J. M.: The Interplanetary Magnetic Field. Solar Origin and Terrestrial Effects. *Space Sci. Rev.*, Vol. 8, 1968, p. 258.

## ACKNOWLEDGMENTS

The National Aeronautics and Space Administration supported this work under Contract NAS 2-4672 and Grant NGR 05-020-407. The data were gathered under the leadership of Professor V. R. Eshleman and the measurements were taken under the direction of H. T. Howard, supported by a series of NASA grants and contracts in addition to those cited above.

*J. H. Binsack* I have two points. One, I'm just curious why most of your data points on your graphs seem to be vertical.

*T. A. Croft* The data form that I am showing is what we call our interim process data, and still has a lot of ionospheric error in it. In the days for which I discussed this impulse the ionospheric error I could see was not very large, but there are on some rotations periods when the ionospheric error is large and it has a diurnal variation.

*J. H. Binsack* Have you removed the effect of the earth's plasmasphere?

*T. A. Croft* We measure the Faraday rotation to Geostationary Satellites and from that infer that content, and then map it over to the Pioneer line of sight.

*J. H. Binsack* My point is this, that as I recall your heliocentric plot Pioneer 8 was coming out on the dusk side of the earth. That is just in the region where the plasmasphere has this notorious bulge which is very responsive to geomagnetic activity. It can increase its integrated electron content in a very short time period, perhaps shorter than what you can obtain from your geostationary satellite normalization factors. My point is that perhaps the increased density or response function that you do find along the ray path to Pioneer 8 is solely due to the plasma bulge in the plasmasphere. Could you comment on that?

*T. A. Croft* Yes. The impulse response I showed was calculated without that effect in it. The amount of variation that can be attributed to this effect is roughly  $5 \times 10^{16}$  electrons/m<sup>2</sup>, and for the distance to Pioneer 8 that is not a very big effect. By the time we divide by the distance and express that in terms of average density on the path, that amount of error is not very big. The typical error in just the ionospheric portion can be quite a bit larger than that. I think that is important. But I think the ionospheric error in this data form is even bigger. But during the pulses that you saw here I think the errors are roughly about on the order of 10 percent, and not enough to invalidate these arguments about the intermittency of flow.

*J. T. Gosling* I'd just like to repeat a point that I made several days ago. When you do a statistical analysis of a large amount of so-called corotating streams, you find out that this type of event in terms of repeating velocity structures is very very rare. I think you probably make the same point looking at your data, that a structure that comes back again and again is a fairly rare event.

*T. A. Croft* I think I disagree with you, but it may be semantics. I see very very clear and consistent repetition of regions of differing character. There will be a chaotic region and a quiet region, and that will repeat consistently and very often. But individual fluctuations on the time scale of a day almost never repeat. Would you agree that if you see a chaotic 4 days of data on one rotation you will usually see relative chaos on the next rotation during those four days?

*J. H. Binsack* Sometimes yes, sometimes no.

*A. J. Lazarus* How do your intensity peaks compare with the spacecraft measurements of plasma density?

*T. A. Croft* Well, the best comparison we've had is yours, and the correlation wasn't very good. The reason is that you are measuring at a point, and we are measuring the average over a long distance. Unless we analyze in terms of this steady state response, and consider that you're measuring the input function and we are measuring the output function, we can't do very well. The only data we have to work with to do the job here are your Mariner 5 and our Mariner 5 data. And it is not clean enough yet to do that.

## COMMENTS

*N. F. Ness* At the risk of causing some indigestion, I suppose, I'm going to mention power spectra again. I hope it won't upset lunch.

There was a discussion this morning about estimating slopes of power spectra in which I tried to point out that because of the manner in which power spectra are computed, there

are associated uncertainties with slopes that can be very quantitatively specified. What I have sketched in figure 1 is what one computes standardly from any time series or it could be a spatial parameter. It is the power spectral density, which is measured in units of amplitude squared per unit frequency as a function of frequency. But it could be

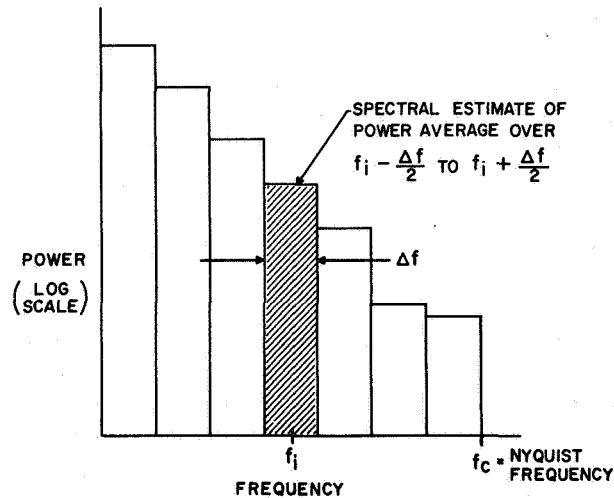


**Figure 1.** Power spectra results yield estimates of amplitude squared over a finite frequency band  $\Delta f$ .

presented as a function of wavelength. The important point here is that the actual quantity computed in fact is an estimate averaged over an elementary frequency interval  $\Delta f$  centered at frequency  $f_i$ . The value of  $\Delta f$  is determined by the number of estimates you make  $M$  and the Nyquist frequency  $f_c$  as  $\Delta f = f_c/M$ .

Now, depending on how many of these estimated points you have—and, of course, the number of sample points—then each of those estimated averages has associated with it a statistical confidence limit determined by the degrees of freedom  $k$ . This value depends on the number of sample points  $N$  and  $M$  as  $k = 2N/M$ . As  $k$ , the number of degrees of freedom, increases the confidence becomes higher, and these uncertainties become less. Usually  $k$  is assumed to relate to a chi-square distribution to determine the size of the confidence limits.

In lots of the graphs we've seen here today, *no one* presents these confidence limits, and *no one* tells us the degrees of freedom, and *no one* tells us what the resolution is in the frequency domain. As an example, I've sketched in figure 2 a very simple spectrum drawn through the averages. As you can see, two straight lines fit through all those points equally well. The question is, which one of those do you want to use? Well, I don't know how the people who presented these continuous straight lines or curves have constructed their power spectrum.

I suggest that in presenting experimental results on the power spectrum of fluctuations one be careful to include these kind of statistical estimate uncertainties with the confidence limits clearly indicated so that the reader can judge for himself whether or not the slope you have chosen is the maximum or minimum and how certain you are of that slope.



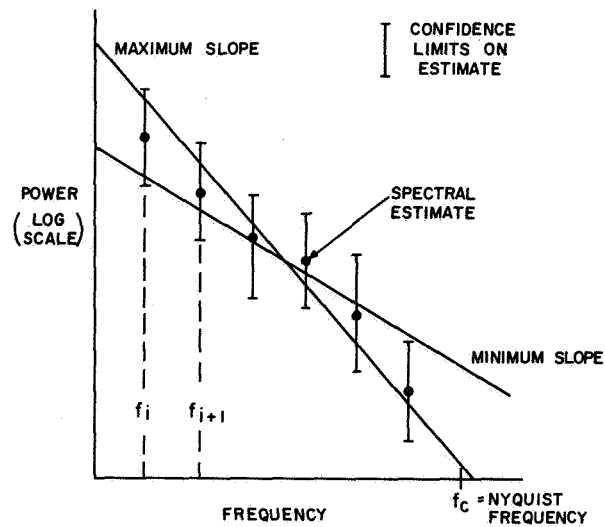


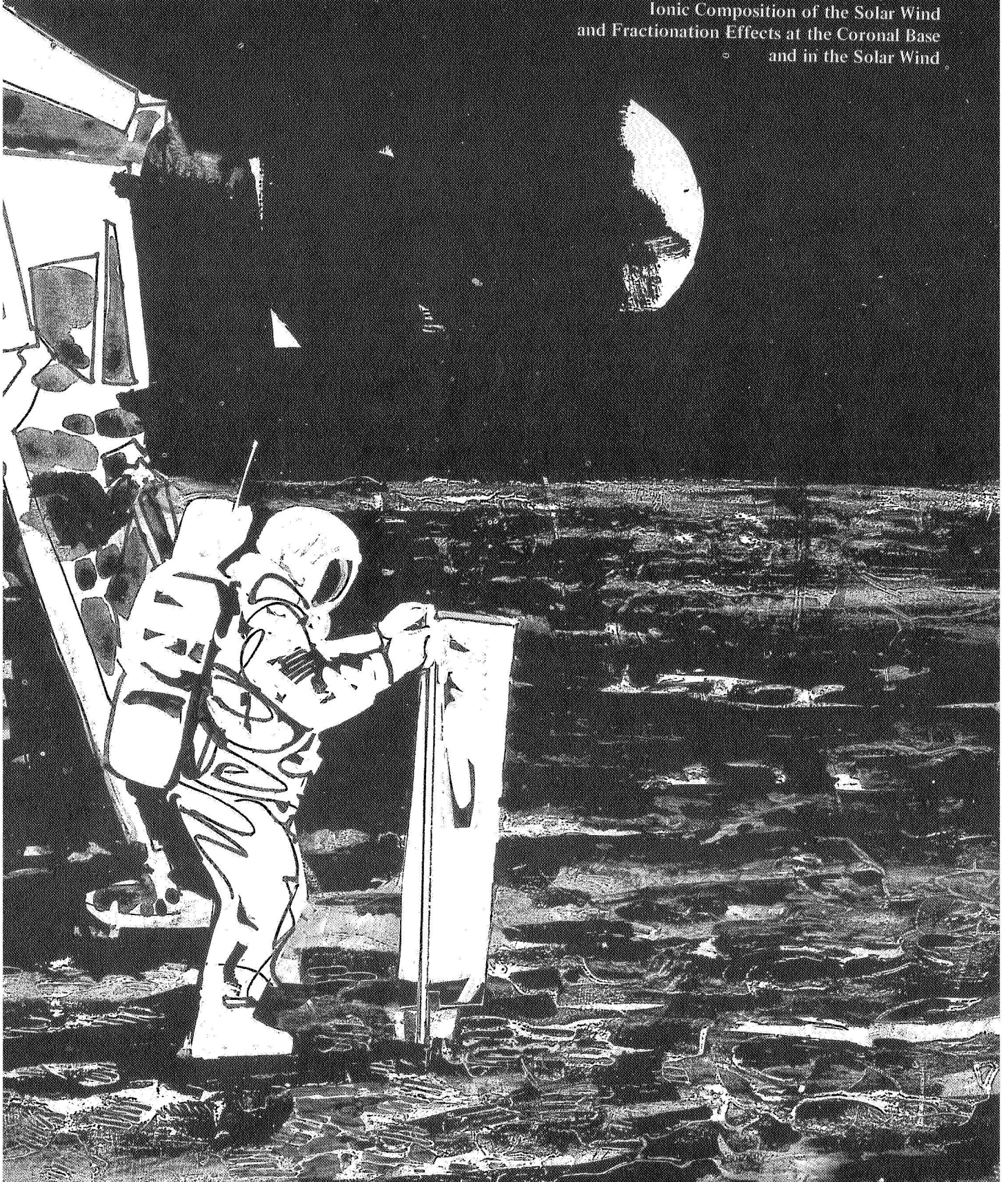
**Figure 2.** *Finite length time series yield spectral estimates with statistically determined uncertainties.*

As a side comment, I didn't quite understand Siscoe's remark about the variability in the confidence limits, because these, if plotted on a log scale, have the same amplitude. So generally it is very convenient to present your spectra with log of the spectral density either linearly or logarithmically as a function of the frequency so that these confidence limits then don't have to have error bars of different height associated with each point.



# CHAPTER VIII

Observational Evidence and Theory of the  
Ionic Composition of the Solar Wind  
and Fractionation Effects at the Coronal Base  
and in the Solar Wind



The chemical and ionic composition of the solar wind as deduced from direct measurements from space probes and from Apollo experiments; the theory of fractionation of species in the solar corona; the existence of  $\text{He}^3$ .

# SPACECRAFT OBSERVATIONS OF THE SOLAR WIND COMPOSITION *S. J. Bame* An invited review

Solar wind composition studies by means of plasma analyzers carried on various spacecraft are reviewed. The average ratio of helium to hydrogen over the solar cycle is close to 0.045; values as low as 0.0025 and as high as 0.25 have been observed. High values have been observed following solar flares and interplanetary shock waves when the flare gas driving the shock arrives at the spacecraft. Ions of  $^3\text{He}^{+2}$ ,  $^{16}\text{O}^{+6}$ , and  $^{16}\text{O}^{+7}$  have been observed with Vela 3 electrostatic analyzers. Further measurements with Vela 5 analyzers have shown the presence of  $^{14}\text{N}^{+6}$ ,  $^{28}\text{Si}^{+7}$  to  $^{28}\text{Si}^{+9}$ , and  $^{56}\text{Fe}^{+7}$  to  $^{56}\text{Fe}^{+12}$  ions. The relative abundance of oxygen, silicon, and iron in the solar wind of July 6, 1969, was 1.00, 0.21, and 0.17, which is very similar to reported values for the corona. The ratio of helium to oxygen is variable; the average value of He/O is close to 100, but values between 30 and 400 have been observed.

## ABSTRACT

## INTRODUCTION

Continued expansion of the solar corona into interplanetary space forms the solar wind, which contains material recently a part of the outer convective zone of the sun. Photospheric matter is transported through the chromosphere into the million degree lower corona where the atoms are highly ionized. As the coronal density falls with increasing distance from the solar surface, interactions between particles decrease; at the same time the expansion velocity increases, and at relatively small distances from the sun the ionization state and composition become fixed, or "frozen in." For example, the ionization state of oxygen is expected to be virtually fixed at a heliocentric distance of about  $1.5 R_{\odot}$  and remain the same as the solar wind flows out beyond 1 AU [Hundhausen *et al.*, 1968]. Thus, observations of the solar wind elemental, isotopic, and ionic composition near earth can be used to deduce conditions deep within the corona and may contribute to a more complete understanding of how solar matter expands into interplanetary space. The reader is referred to recent papers of Geiss *et al.* [1970a], Nakada [1970], and Hundhausen [1970] and the references given by

these authors for discussions of mechanisms that may control differentiation of the solar material as it expands outward through the lower levels of the solar atmosphere. The review of Hundhausen [1970] also provides a discussion of composition and other solar wind properties and references to earlier solar wind reviews.

In this paper, observations of the solar wind composition made with artificial spacecraft are described. The paper is divided into three major parts; the first part is concerned with the ions of the two most abundant nuclides in the sun— $^1\text{H}^{+}$  and  $^4\text{He}^{+2}$ . The second part reviews reported abundances of the universe, solar system, photosphere, chromosphere, and solar cosmic rays; the expected ionization state of the solar wind is considered, and a predicted energy per charge spectrum is presented. The last part discusses spacecraft observations of  $^3\text{He}^{+2}$  and ions of the heavier elements  $^{14}\text{N}$ ,  $^{16}\text{O}$ ,  $^{28}\text{Si}$ , and  $^{56}\text{Fe}$ , and summarizes the present state of knowledge of the solar wind composition.

## $^1\text{H}^{+}$ AND $^4\text{He}^{+2}$

The sun is known to be composed chiefly of normal hydrogen and helium. Almost no helium is ionized at the photospheric temperature of  $6000^{\circ}\text{K}$ , so conventional spectroscopic determinations of the photospheric helium abundance are not possible. Helium is observed in prominences, but an unambiguous determination of the

---

*The author is at the University of California, Los Alamos Scientific Laboratory, Los Alamos, New Mexico.*

solar helium content cannot be made from such measurements [Unsöld, 1969].

Three indirect methods have been used to estimate the helium abundance:

1. Models of stellar interiors predict a mass-luminosity relation that depends on the helium content of the star. For the sun helium-hydrogen ratios (by number) have ranged between 0.077 and 0.095 and have an average close to 0.09 [Sears, 1964; Demarque and Percy, 1964; Weymann and Sears, 1965; and Morton, 1968]. These values pertain to the solar interior and need not be representative of the photosphere.
2. The abundance of helium relative to other nuclei found in the solar cosmic rays has been found to be relatively constant from one energetic particle event to the next [Gaustad, 1964; Biswas *et al.*, 1966]. A relative solar helium abundance of 0.09 has been found by comparing the cosmic ray abundances of helium, carbon, nitrogen, and oxygen with the spectroscopic values of the photospheric abundances of hydrogen, carbon, nitrogen, and oxygen. Later determinations of  $0.063 \pm 0.015$  have been made by Lambert [1967] and  $0.062 \pm 0.008$  by Durgaprasad *et al.* [1968]. This method assumes that helium and other ions are accelerated nonpreferentially in the solar cosmic ray energization process, and pertains to the lower solar atmosphere.
3. Iben [1969] has used the upper limit of the solar neutrino flux established by Davis *et al.* [1968] to infer an upper limit of 0.049 to 0.064 for the helium-hydrogen abundance ratio, but again, the result pertains to the solar interior.

Thus, although the helium abundance of the photosphere of the sun is not known accurately, values up to 0.10 might be expected. The remainder of solar material is mostly hydrogen, since the total abundances of all elements heavier than helium are only a few tenths of a percent at most.

#### Solar Wind Average Relative Abundance of $^4\text{He}$ and $^1\text{H}$

The detection of two groups of solar wind ions ascribed to  $^1\text{H}^+$  and  $^4\text{He}^{+2}$  has been reported by many observers, including Snyder and Neugebauer [1964], Wolfe and Silva [1965], Coon [1966], Lazarus *et al.* [1966], Neugebauer and Snyder [1966], Wolfe *et al.* [1966], Hundhausen *et al.* [1967], Ogilvie *et al.* [1968a], Ogilvie and Wilkerson [1969], Robbins *et al.* [1970], and Formisano *et al.* [1970]. The measured long-term average helium abundance is based on data from three spacecraft: Mariner 2, Vela 3, and Explorer 34. The results from these independent

sources, which agree reasonably well, show that the solar wind helium abundance may be significantly lower than the solar abundance estimates discussed earlier.

**Mariner 2 Observations.** The Mariner 2 positive-ion curved plate electrostatic analyzer [Snyder and Neugebauer, 1964; Neugebauer and Snyder, 1966] accepted particles in a  $6^\circ$  square angular window centered near the solar direction. The positive ion flux was measured in a series of logarithmically spaced energy per charge channels. Spectra with a large peak and a smaller secondary peak were often observed; an example is shown in figure 1. Because of the predominance of hydrogen and helium in the sun, these peaks were attributed to  $^1\text{H}^+$  and  $^4\text{He}^{+2}$  ions traveling at a common mean speed, so the helium ions have four times the energy of the hydrogen ions and twice the energy per charge  $E/Q$ . Ions of  $^4\text{He}^+$ , which would appear at four times the  $E/Q$  of  $^1\text{H}^+$ , were not observed. Because of the large gaps between energy windows of the analyzer, accurate determinations could not be made of the flux peak widths. Consequently, these data were analyzed under the assumption that the  $^4\text{He}^{+2}$  ions were four times as hot as the  $^1\text{H}^+$  ions; this assumption gave better fits to the data than the assumption of equal temperatures and is supported by the results of Robbins *et al.* [1970], which show that the helium-hydrogen temperature ratios measured by Vela 3 very rarely have values near 1 but are much more likely to have values near 2.5 to 4.5 and sometimes higher.

From a total of 14,147 spectra measured between August 29 and December 30, 1962, 1213 spectra could be used in an analysis that yielded an average helium-hydrogen number ratio of 0.046. Most of these spectra

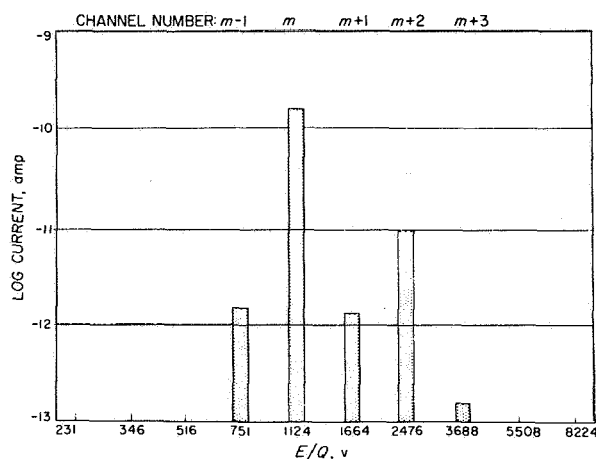
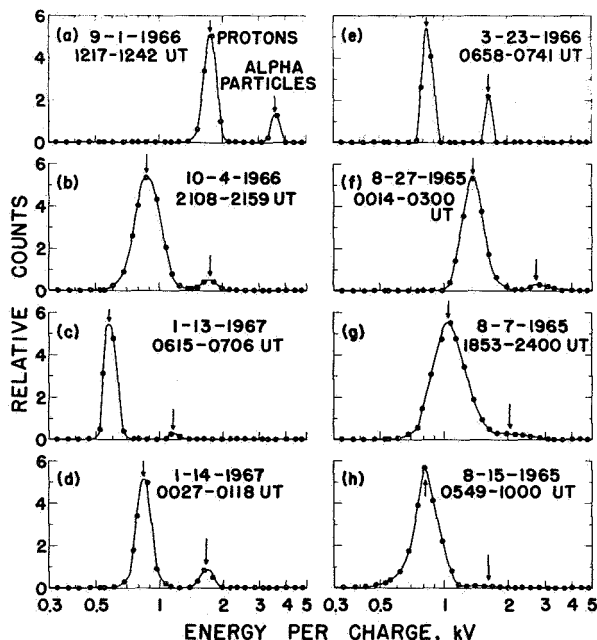


Figure 1. Sample solar wind spectrum obtained by the Mariner 2 ion analyzer showing two groups presumed to be  $^1\text{H}^+$  and  $^4\text{He}^{+2}$  [Neugebauer and Snyder, 1966].

were obtained when the solar wind speed was low, so there is some possibility of an observational bias in the derived ratio.

**Vela 3 Observations.** Hemispherical electrostatic analyzers using particle counting with electron multipliers [Bame et al., 1967; Gosling et al., 1967a; Hundhausen et al., 1967] measured the positive ion flux in fan-shaped angular windows at eight different orientations of the two spinning Vela 3 spacecraft. Figure 2 shows a variety of spectra obtained that show two flux peaks attributable to  $^1\text{H}^+$  and  $^4\text{He}^{+2}$ . This identification was strengthened by a pulse height analysis of the electron multiplier pulses in each peak (to be discussed later), which showed that the higher E/Q peaks are caused by ions of greater mass than those causing the lower peaks [Bame et al., 1968a]. The energy window spacing of the Vela 3 analyzers permitted more complete definitions of the spectral peaks; this greater resolution coupled with the directional information made it possible to determine helium-hydrogen ratios without assumptions about the ion temperatures.

An analysis of the 1964 Vela 3 energy-angle data matrices obtained between July 24 and August 29, 1965, gave an average helium-hydrogen ratio of 0.042 [Hundhausen et al., 1967]. More recently, Robbins et



**Figure 2.** Sample spectra from the Vela 3A and B analyzers. Two groups of ions, presumed to be  $^1\text{H}^+$  and  $^4\text{He}^{+2}$  are always observed in the solar wind. The second group was shown to have higher mass [Bame et al., 1968a].

al. [1970] reported a value of 0.037 obtained from the analysis of 10,214 measurements made between July 1965 and July 1967. This later analysis also showed that the flow speed of the  $^4\text{He}^{+2}$  ions is almost always the same as that of the  $^1\text{H}^+$  ions.

**Explorer 34 Observations.** Particles were accepted into the Explorer 34 plasma detector [Ogilvie et al., 1968b] in a fan-shaped angular window. Flux versus E/Q was measured in a single selected sector during a spacecraft rotation. In addition to the E/Q analysis, a crossed field velocity selector permitted a mass per charge separation of the ions with  $M/Q = 1(^1\text{H}^+)$  and  $M/Q = 2(^4\text{He}^{+2})$ .

Figure 3 shows typical solar wind E/Q spectra at the separate M/Qs corresponding to hydrogen and helium. The Explorer 34 experiment essentially confirms the conventional identification of the two peaks. However, some ambiguity remains due to the fact that other ions with  $M/Q = 2(^2\text{H}^+$  and fully ionized  $^{12}\text{C}$ ,  $^{14}\text{N}$ ,  $^{16}\text{O}$ , etc.) and the same mean speed would also fall into the second peak. However, very little deuterium is expected in the modern sun, and the heavier elements fully ionized have very low abundances compared to helium as will be seen in the next section. An additional confirmation of the presence of  $^4\text{He}$  is supplied by the mass spectrometer identification of  $^4\text{He}$  in the aluminum foils exposed on the lunar surface by the Apollo astronauts [Bühler et al., 1969; Geiss et al., 1970b]. Considering the exposure times of the foils, the amount of helium captured was consistent with the assumption

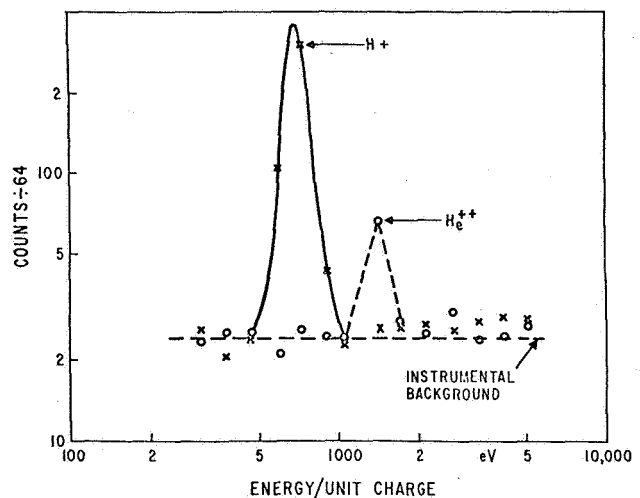


**Figure 3.** Sample spectra from the Explorer 34 ion analyzer. The spectrum shown by the crosses is for  $M/Q = 1$  ion ( $^1\text{H}^+$ ); the spectrum shown by circles is for  $M/Q = 2$  ions, presumed to be mainly  $^4\text{He}^{+2}$  [Ogilvie et al., 1968a].



that most of the second peak observed with spacecraft is  $^4\text{He}^{+2}$ .

Both the Vela 3 determination that the second group is higher mass and the Explorer 34 mass per charge separation eliminate the possibility that the peak ascribed to  $^4\text{He}^{+2}$  is in actuality a nonthermal tail on the  $^1\text{H}^+$  peak. The Explorer 34 channel spacing is similar to that in the Mariner 2 spectrum of figure 1, and an instrumental background produced by an on-board data processing system is present. Thus, under normal solar wind conditions, the observed  $^4\text{He}^{+2}$  peak shows counts above background in only one or two channels, and determination of the helium abundance requires an assumption relating the  $^4\text{He}^{+2}$  and  $^1\text{H}^+$  temperatures.

The analysis of Explorer 34 data obtained between May 30, 1967, and January 1, 1968, has been reported by *Ogilvie and Wilkerson* [1969]. Under solar wind conditions such that the proton density is  $> 10 \text{ cm}^{-3}$  and the  $^4\text{He}^{+2}$  temperature is high enough that a three-point helium peak is obtained (and no assumption about temperature is necessary), the average helium abundance was found to be 0.051, in good agreement with the Mariner 2 and Vela 3 values.

Table 1, taken from *Hundhausen* [1970], summarizes the observations from these three sources. The agreement between the average values is satisfactory, particularly in view of the fact that there may be a solar cycle variation in the average value as discussed below. Note that the Mariner 2 value was obtained during the declining part of the last solar cycle, but before minimum. The higher value reported from Explorer 34 comes from a period farther from solar minimum than the Vela 3 value, and would appear to agree well with an extrapolation of the Vela 3 time history given in figure 7. Although measurements throughout a solar cycle would be desirable, the density number ratio seems to be well established at near 0.045.

Nearly all of the previously discussed indirectly derived values of the solar helium abundance are larger

than the solar wind value of 0.045. As indicated earlier, some of the estimates are not necessarily representative of the outer layers of the sun. Possible effects of gravitational settling [*Parker*, 1963; *Geiss et al.*, 1970a; *Hundhausen*, 1970] also would permit differences in the solar photospheric and solar wind helium abundances.

#### Fluctuations in Solar Wind Helium Abundance

Substantial variations in the helium-hydrogen ratio have been reported by many observers, including *Coon* [1966], *Neugebauer and Snyder* [1966], *Hundhausen et al.* [1967], *Ogilvie et al.* [1968a], *Ogilvie and Wilkerson* [1969], and *Robbins et al.* [1970]. Figure 4 is the histogram from Explorer 34 presented by *Ogilvie and Wilkerson* [1969]. The histograms from Explorer 34 and Vela 3 are similar, and show a distinct skewing toward higher ratios. Values of the helium-hydrogen ratio have been observed with Vela 3 to range as low as 0.003 and

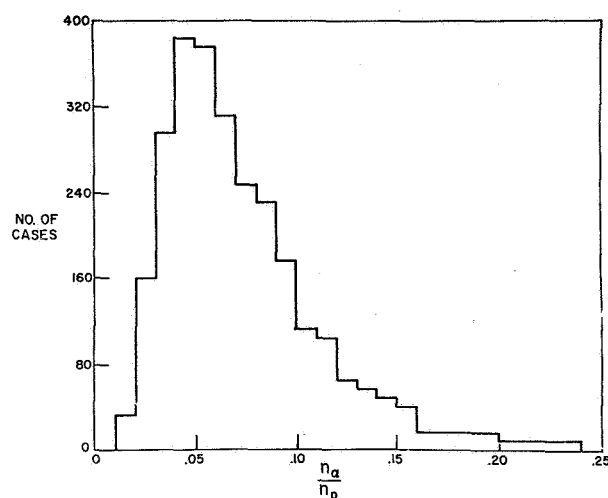


**Figure 4.** Helium to hydrogen density ratio distribution observed by Explorer 34 between May 30, 1967 and January 1, 1968 [*Ogilvie and Wilkerson*, 1969].

**Table 1** Observational determinations of the average relative abundance of helium and hydrogen in the solar wind

Source	Period	$\langle \text{He}/\text{H} \rangle$	Measurements	Comments
Mariner 2	Aug. 29 to Dec. 30, 1962	0.046	1,213	Energy-per-charge analysis only; assumptions about temperature; 10 percent of data included in analysis; sample favors low solar wind speeds
Vela 3	July 1965 to July 1967	0.037	10,314	Energy-per-charge analysis only; 60 percent of data included in analysis
Explorer 34	May 30, 1967 to Jan. 1, 1968	0.051	2,705	Energy-per-charge and mass analysis; 5 percent of data included in analysis; sample favors high solar wind density



as high as 0.25. Thus, the observations indicate that the helium abundance in the solar wind fluctuates over two orders of magnitude and that extremely high values are more common than would be expected if the abundances were distributed normally about the mean.

At times the helium abundance can remain at relatively high or low values for periods of many hours. An example from Vela 3 (fig. 5) shows that on September 3, 1966 the helium-hydrogen ratio remained above 7

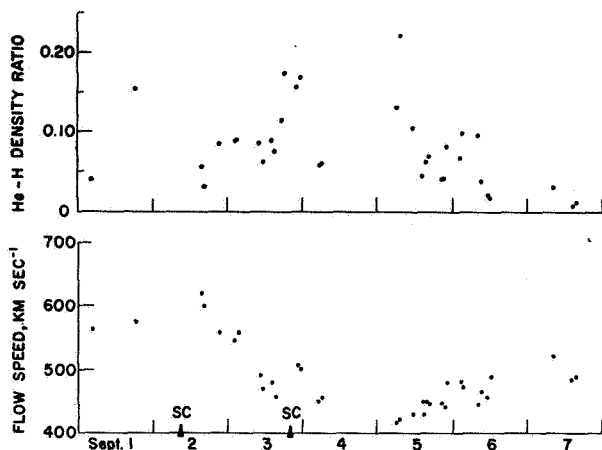


**Figure 5.** Time history of Vela 3 helium to hydrogen density ratios and solar wind flow speed showing higher than average values of the helium abundance persisting throughout September 3, 1966. This was a time of high solar activity. Gaps in the data are caused by orbital positions out of the solar wind and times of no data transmission.

percent most of the time over a period of a day. This was a time of considerable solar activity, which probably contributed to the high helium abundance, as discussed below.

An example of abnormally low abundance is given in figure 6. On December 10, 1965, the helium-hydrogen ratio remained in the 0.003-0.004 range for about 8 hr.

Further information about the helium abundance variations is gained by averaging the measurements over different time intervals. Figure 7 shows the helium-hydrogen number ratio, observed by Vela 3 satellites from July 1965, to June 28, 1967, averaged over both the 27-day solar rotation periods and over shorter 10-day periods. Averages over 27-day periods remove inhomogeneities that might exist in solar longitude and thus give the best spatial average over the entire solar corona that is possible with measurements made near the ecliptic plane. A small upward trend with time appears to be present in the 27-day averages. This trend appears

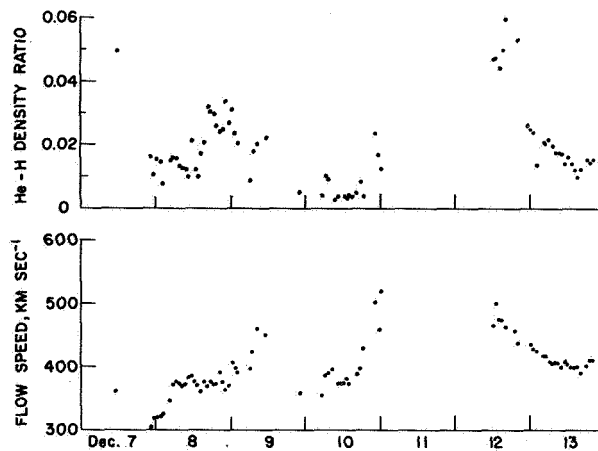


**Figure 6.** Time history of Vela 3 helium to hydrogen density ratios and solar wind flow speeds showing a time of unusually low helium abundance ( $\sim 0.003$ ) persisting for 8 hr.

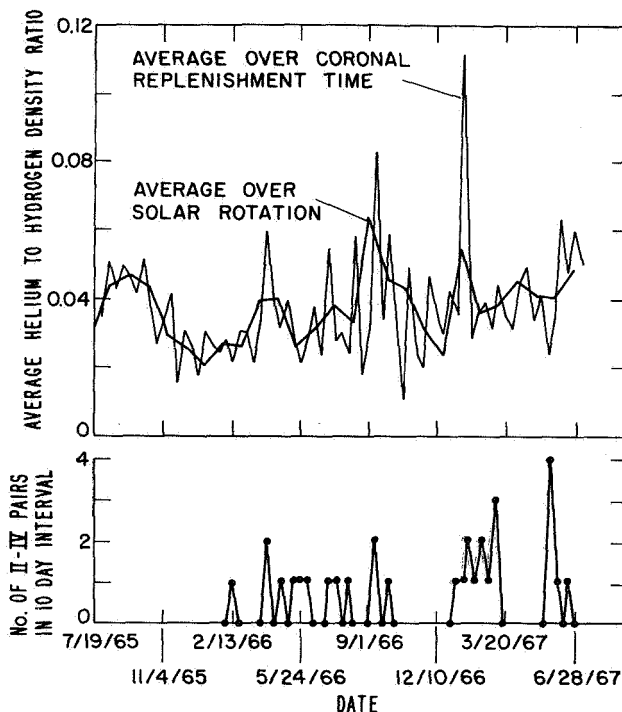


**Figure 7.** Time variation of the helium to hydrogen density ratio from Vela 3A and B averaged over solar rotations and 10-day intervals [Robbins et al., 1970]. Also shown are the number of type II and type IV radio bursts in the corresponding 10-day intervals.

to be real and is probably related to rising solar activity during this part of the solar cycle.

The 10-day averages show even larger fluctuations than the 27-day averages. Also plotted are the number of

pairs of type I and type IV radio noise bursts during the corresponding 10-day intervals. There appears to be a significant correlation between the occurrence of the radio noise bursts and peaks in the alpha abundance (Hundhausen, private communication). Such bursts are also known to be correlated with solar flares of large magnitude which often produce energetic particle events, interplanetary shock waves, and sudden commencements. Thus, again there seems to be a relationship between high helium content in the solar wind and solar activity.

#### Solar Wind Helium Abundance Enhancements

Evidence has been given suggesting that a high helium abundance in the solar wind seems to be directly related to solar flare activity. A number of observers have reported examples of a high helium content appearing 5 to 12 hr after an interplanetary shock or a geomagnetic sudden commencement. Table 2, taken from *Hirshberg et al.* [1970a], lists some of the reported events. For one of the events spectra obtained on January 13, 1967, before the interplanetary shock observation by Vela 3A and after the helium enhancement early on January 14, 1967, can be seen in figure 2. This helium enhancement apparently occurred at the time that the ATS 1 satellite observed a magnetopause crossing at  $6.6 R_E$  [Cumplings and Coleman, 1968]. The importance of the helium enhancement observed by Vela 3 [Bame et al., 1968b] in providing the solar wind pressure required to push back the magnetopause has been pointed out by Kavanagh et al. [1970].

Spectra measured by Vela 3A on February 15 and 16, 1967, which show the passage of an interplanetary shock

wave at 2345 UT on February 15 and the sudden helium enhancement on February 16, are shown in figure 8. The helium abundance was particularly low (0.01 to 0.02) both before and after the shock arrival. (No change is expected to occur in the helium abundance due to the passage of the shock, since the shock cannot change the composition of the ambient plasma through which it passes.) Nine hours after the shock passage the solar wind speed and density had increased beyond the postshock values, but the helium abundance was still low. The spacecraft was then engulfed in the magnetosheath by an outward movement of the bow shock and no further solar wind spectra were available until 0916 UT, after the bow shock had again moved behind the spacecraft. At this time a dramatic change had occurred in the helium abundance, but because of the wide spacing of energy channels available in the memory operating mode used at this time, exact values could not be determined. At 0940 UT a spectrum was obtained in the direct data transmission mode; in this mode many more energy channels are used and it is possible to compute a helium abundance of 0.22 for the 0940 UT spectrum. More complete descriptions of this event can be found in *Hirshberg et al.* [1970a] and *Hundhausen* [1970].

Further examples of helium enriched solar wind have been found in Vela 3 data obtained between July 1965 and July 1967 [Hirshberg et al., 1970b]. Most of the strongest enhancements ( $\text{He}/\text{H} > 15$  percent) followed major solar flares. During this period, 12 solar flares have been identified as probable sources of helium enrichment. An example is shown in figure 2(a), which shows a

**Table 2** Observations of helium-enriched interplanetary media discussed in the literature

Percent helium	Date	Reference	Comments*
10-15	April 17, 1965	<i>Gosling et al.</i> [1967b]	Helium appears about 12 hr after an interplanetary shock was detected
12	July 11, 1966	<i>Lazarus and Binsack</i> [1969]	Helium associated with high velocity ( $\approx 700$ km/sec) plasma
17	May 30, 1967	<i>Ogilvie et al.</i> [1968a]	Helium appears 5-1/2 hr after the sudden commencement of a geomagnetic storm; a class 3B flare occurred at $28^\circ\text{N}$ , $33^\circ\text{W}$ on May 28
18	January 14, 1967	<i>Bame et al.</i> [1968b]	Helium appears about 12 hr after an interplanetary shock was detected; a class 3B flare occurred on January 11, at $26^\circ\text{S}$ , $47^\circ\text{W}$
22	February 16, 1967	<i>Hirshberg et al.</i> [1970a]	Helium appears about 9 hr after an interplanetary shock was detected; a class 4B flare occurred on February 13 at $20^\circ\text{N}$ , $10^\circ\text{W}$

\*Evidence suggesting that the enrichment was associated with a solar flare event.

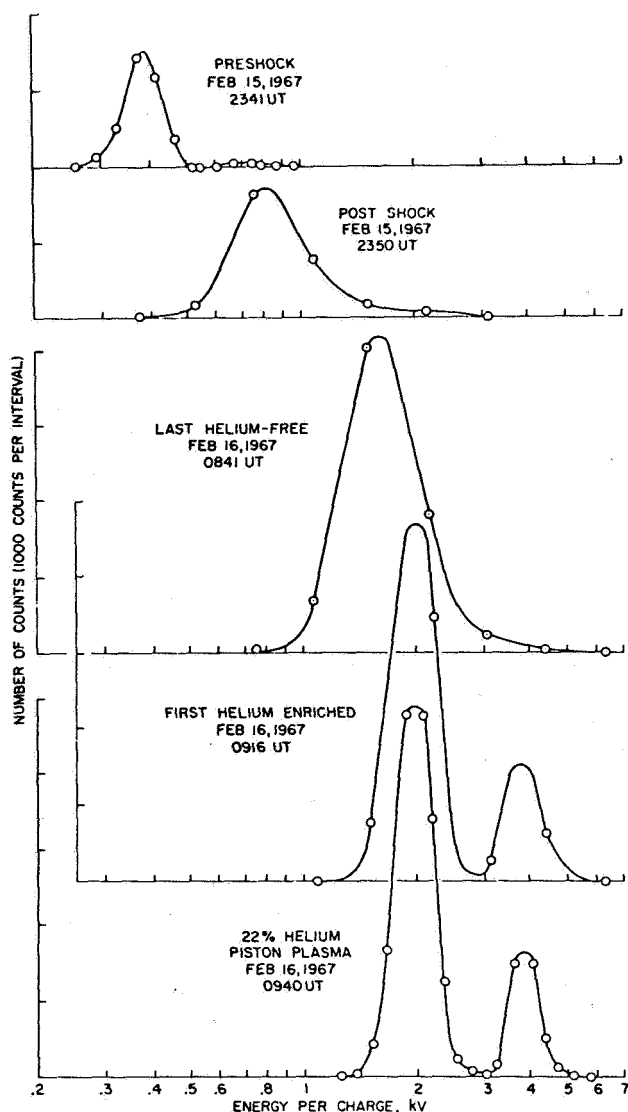


**Figure 8.** Solar wind spectra observed by Vela 3A during the solar wind disturbance of February 15-16, 1967 [Hirshberg *et al.*, 1970a].

spectrum obtained at a time following numerous flares in late August.

It has been suggested by Lazarus and Binsack [1969] that a solar wind density and velocity increase observed at Pioneer 6 on July 10, 1966, following an interplanetary shock on July 9, might represent the arrival of plasma from the flare region—that is, the “driver gas.” The events observed by Vela 3 and discussed previously seem to indicate that solar wind plasma with unusually high helium enrichment is ejected from flare regions lower in the solar atmosphere, where the coronal helium abundance is expected to be greater. Helium abundances near 0.20 are consistent with those predicted by the

model of Geiss *et al.* [1970a] for the lower corona. There seems little doubt that the appearance of an enhanced alpha abundance after a flare signals the arrival of the flare region plasma driving the interplanetary shock preceding the enhancement [Hirshberg *et al.*, 1970a; Bame *et al.*, 1968b].

Unusually high enhancements following flares often last for relatively short times. For example, the 0.22 helium abundance for the February 15-16, 1967, event lasted for about 30 min. However, higher than average abundances have been observed to persist for many hours (fig. 5), and such times of high abundance can usually be associated with solar activity. Another time of helium enhancement produced the spectrum seen in figure 2(e). This event has been discussed by Bame *et al.* [1968a], who showed that in addition to a helium enhancement, heavier ions were observable in the solar wind at this time. Hundhausen *et al.* [1968] and Hundhausen [1970] have shown that this solar wind stream can plausibly be associated with a single large plage area crossing the solar disk. The heavier ion abundances suggested that the stream began in a coronal region with temperatures higher than normal, as might be expected above a plage region.

Abrupt decreases, as well as increases, may be expected in the helium abundance, as the solar wind stream passing the earth changes from a coronal source region above an active area to a source region above a quiet area. An example of such an event is seen in figure 9. The upper spectrum contained a high helium abundance. This spectrum also contained observable amounts of  $^3\text{He}$  and  $^{16}\text{O}$  ions [Bame *et al.*, 1968a], which cannot be seen here because of the linear ordinate. Eight hours later another spectrum measurement showed that, although the solar wind speed and temperature were still about the same, the helium abundance had dropped from  $>0.10$  to about 0.005. Other sudden appearances of increased and decreased helium abundance, which show the stream-like character of the solar wind, can be found in figures 5 and 6.

#### ION SPECIES THAT MIGHT BE OBSERVABLE IN THE SOLAR WIND

Since the sun contains small quantities of elements and isotopes other than normal hydrogen and helium, it might be expected that other ions should be present in the solar wind. Indeed, the model of Geiss *et al.* [1970a] shows that if  $^4\text{He}^{+2}$  is observed in the solar wind, ions of other elements as heavy as iron should also be caught up by the expanding corona and carried along in the solar wind. In the preceding section, measurements showing that the solar wind always contains  $^4\text{He}^{+2}$  were reviewed, and it seems reasonable that other solar

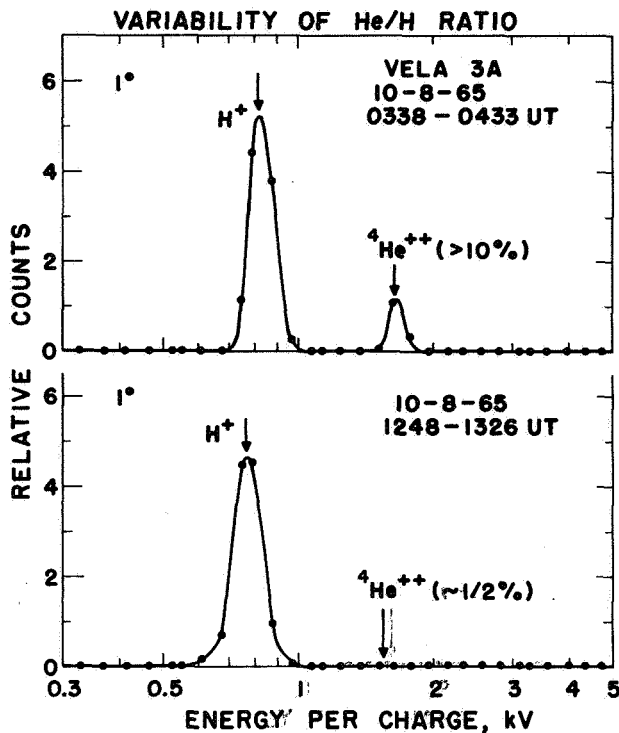


Figure 9. Solar wind spectra from Vela 3A showing a sudden decrease in the helium abundance.

materials should also be present, although probably in varying amounts compared to  $^1\text{H}^+$ .

#### Relative Abundances

Relative abundances of the more common nuclides normalized to oxygen are given in table 3. It might be argued that the abundances of the corona are most closely associated with the solar wind abundances, since

the solar wind is an extension of the corona into interplanetary space. Inspection of the table shows some striking differences in photospheric, coronal, and solar cosmic ray abundances, particularly for nuclides above  $^{20}\text{Ne}$  except for  $^{32}\text{S}$ .

Oxygen, carbon, and nitrogen are likely candidates for observation with a sufficiently sensitive and appropriately designed solar wind experiment. If the coronal abundances are most nearly related to solar wind abundances, the other elements listed in the coronal abundance column, with the possible exception of  $^{32}\text{S}$ , are also prime candidates for detection.

The possibility that solar wind abundances may be closely related to coronal abundances has been strengthened by the results of *Pecker and Pottasch* [1969]. These authors show that the chromospheric iron abundance is the same as the coronal iron abundance, and conclude that the coronal and chromospheric abundances are not significantly different. They also conclude that the differences between the chromospheric and photospheric abundances given by *Goldberg et al.* [1960] are significant, especially in the case of iron, and that the differences may be due to both departures in local thermodynamic equilibrium not taken into account, and the use of poorly determined  $f$  values to obtain the photospheric abundances. The abundances given by *Unsöld* [1969] and shown in table 3 also show large differences from those of the corona, especially in the case of  $^{56}\text{Fe}$ .

New calculations for the magnetic dipole transition probabilities of [Fe II] lines by *Nussbaumer and Swings* [1970] have led these authors to a redetermination of the photospheric iron abundance. They conclude that

Table 3 Relative abundances of the more common nuclides normalized to oxygen

Nuclide	Cosmic <i>Allen</i> [1963]	Solar system <i>Cameron</i> [1968]	Photosphere <i>Unsöld</i> [1969]	Corona (UV lines) <i>Pottasch</i> [1967]	Solar cosmic rays <i>Biswas et al.</i> [1966]
$^1\text{H}$	1480	1100	1700	--	varies
$^3\text{He}$	--	0.03	--	--	--
$^4\text{He}$	214	90	--	--	107
$^{12}\text{C}$	0.45	0.56	0.60	2.00	0.59
$^{14}\text{N}$	0.14	0.10	0.15	0.24	0.19
$^{16}\text{O}$	1.00	1.00	1.00	1.00	1.00
$^{20}\text{Ne}$	0.41	0.09	0.11	0.14	0.13
$^{24}\text{Mg}$	0.04	0.04	0.05	0.12	0.04
$^{28}\text{Si}$	0.04	0.04	0.05	0.20	0.03
$^{32}\text{S}$	0.03	0.02	0.03	0.08	--
$^{56}\text{Fe}$	0.01	0.04	0.006*	0.20	$\leq 0.02^*$

\*Newer values of these abundances are discussed in the text.

the iron abundance is in agreement with the abundance for the meteorites, corona, and chromosphere, as shown in table 4.

Much attention has been devoted to the coronal iron abundance. Measurements made by *Malville and Schmahl* [1968] during the eclipse of November 1966 have shown that the high abundance persists out to at least  $1.75 R_{\odot}$ . *Pottasch* [1964] analyzed the 1952 eclipse observations of *Fedoretz and Ezerskii* [1953], made out to  $2 R_{\odot}$ , and showed that the high iron abundance persisted to that height. Thus, iron seems likely to be present in the solar wind.

The attention devoted to the abundance of iron is partly due to the intensity and uniqueness of its optical spectrum from the corona. If equal attention were devoted to measurements of the photospheric and coronal lines of silicon, for example, it seems reasonable to suppose that some of the silicon abundance discrepancy seen in table 3 might be resolved also. Thus, at the present time it is not clear that there are any large differences in the abundances of the heavier elements in the photosphere, chromosphere, and corona.

The abundance of the iron-group nuclei relative to oxygen in the September 2, 1966, solar cosmic ray event has been reported as  $0.011 \pm 0.003$  by *Bertsch et al.* [1969], who believe that most of the measured nuclei were  $^{56}\text{Fe}$ . They conclude that the measured relative abundance is easily consistent with the lower values of the photospheric iron abundance discussed earlier in this section. If in fact the higher values given by *Nussbaumer and Swings* [1970] are more nearly correct, the result of *Bertsch et al.*, may imply a less efficient acceleration of the heavier nuclei in the solar cosmic rays. The

standard assumption that the photospheric and solar cosmic ray abundances of helium and heavier elements are the same would then be in doubt, and the photospheric helium abundance discussed earlier may actually be slightly smaller than the quoted values.

#### Ionization State of Solar Wind Constituents

It has been recognized for some years that the lower corona is very hot, having temperatures in the million-degree range. Hydrogen atoms coming from the photosphere are expected to become ionized as they expand into the corona. Helium is expected to become fully ionized; almost no  $^4\text{He}^+$  ions are expected to exist in the corona at a temperature of  $1 \times 10^6$  K [*Tucker and Gould*, 1966]. The existence of the two prominent ion species  $^1\text{H}^+$  and  $^4\text{He}^{+2}$  reviewed earlier confirm these expectations.

After hydrogen and helium, oxygen is one of the most abundant elements in the corona. In the corona the most abundant oxygen ions are expected to be  $^{16}\text{O}^{+6}$  and  $^{16}\text{O}^{+7}$  at temperatures between  $1 \times 10^6$  K and  $2 \times 10^6$  K [*Tucker and Gould*, 1966; *Allen and Dupree*, 1969; *C. Jordan*, 1969].

The ionization state of oxygen in the expanding corona has been considered by *Hundhausen et al.* [1968], for the ions  $^{16}\text{O}^{+5}$  to  $^{16}\text{O}^{+8}$ . Collisional ionization was taken to be the dominant process for raising the ionization level, while radiative and dielectronic recombination were taken to be the dominant processes for reducing the level. The ionization rates of *Tucker and Gould* [1966] were used in the coronal-solar wind model of *Whang and Chang* [1965]. It was shown

Table 4 Comparison of solar iron abundances

Solar layer	$\log N_{\text{Fe}}$ (where $\log N_{\text{H}} = 12.0$ )	Reference
Corona	from 7.3 to 7.7	<i>Jordan</i> [1966], <i>Pottasch</i> [1968], <i>Widing and Sandlin</i> [1968], <i>Nikolski</i> [1969]
Chromosphere	7.7	<i>Pecker and Pottasch</i> [1969]
Meteorites	7.5	<i>Urey</i> [1967]
Cosmic rays	7.0 to 7.2	<i>Bertsch et al.</i> [1969]
Photosphere	6.6 from Fe I and Fe II*	<i>Grevesse</i> [1969]
	7.5 from [Fe II]	<i>Grevesse and Swings</i> [1969]
	7.6 from Fe I and Fe II	<i>Garz et al.</i> [1969a,b], <i>Bascheck et al.</i> [1970]
	7.2 from Fe I	<i>Ross</i> [1970]
	7.5 from [Fe II] (magnetic dipole)	<i>Nussbaumer and Swings</i> [1970]

\*This value is a mean of all the usually admitted photospheric iron abundances from permitted lines obtained between 1960 and 1969, including the often-cited value 6.66 of *Goldberg et al.* [1960]. Not included were the more recent values of *Withbroe* [1969],  $\log N_{\text{Fe}} = 6.80$ ; and *Rogerson* [1969],  $\log N_{\text{Fe}} = 6.85$ .

that processes that change the ionization state become less probable as a parcel of coronal plasma expands away from the sun, due to the increase in the ionization and recombination times as the plasma becomes more tenuous. At the same time the expansion scale time decreases rapidly so that at relatively small heights above the solar surface, the ionization state is very nearly fixed, or "frozen-in." The results of this analysis for a base coronal temperature of  $1.58 \times 10^6$  °K are shown in figure 10 by the solid curves. The dashed curves show the state if the static solutions are assumed. The ionization state for the dynamic solution is frozen in at about  $1.5 R_{\odot}$  and should not change appreciably out to 1 AU. Thus, the ionization state observed near earth is representative of conditions deep within the corona.

The state of ionization of the solar wind oxygen as a function of temperature, derived from this analysis, is shown in figure 11. At temperatures between  $1 \times 10^6$  and  $2 \times 10^6$  °K,  $^{16}\text{O}^{+6}$  is the most abundant. Around  $2 \times 10^6$  °K,  $^{16}\text{O}^{+7}$  reaches a maximum abundance due to the decreasing  $^{16}\text{O}^{+6}$  and increasing  $^{16}\text{O}^{+8}$ . At  $3 \times 10^6$  °K, the major fraction of solar wind oxygen would be in  $^{16}\text{O}^{+8}$ , which has an  $M/Q$  value of about 2.0, so that it would fall in the same group with  $^4\text{He}^{+2}$  in an E/Q spectral analysis. Note that even at  $1 \times 10^6$  °K the abundance of  $^{16}\text{O}^{+5}$  is very low.

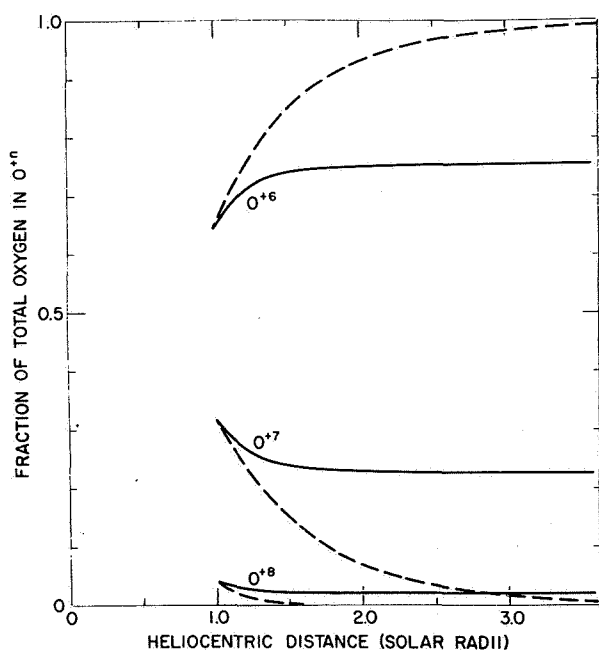


**Figure 10.** The oxygen ionization state in the expanding corona (solid lines) and in a static corona (dashed lines), for a base temperature of  $1.58 \times 10^6$  °K [Hundhausen et al., 1968].

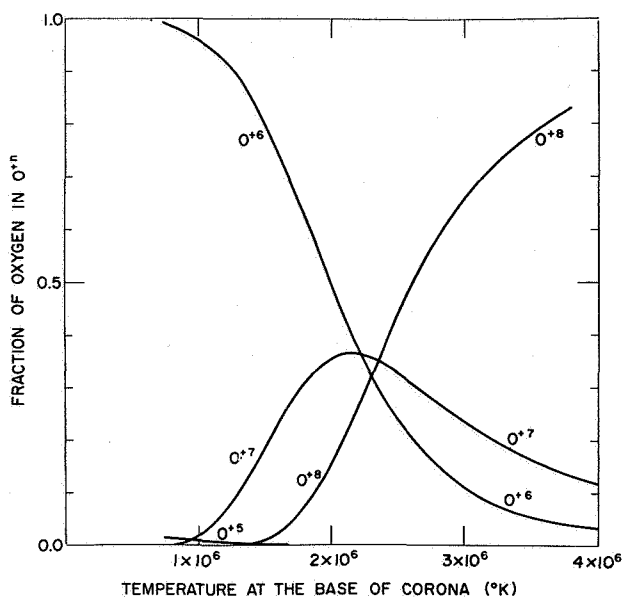


**Figure 11.** The oxygen ionization state at large heliocentric distances as a function of temperature at the base of the corona [Hundhausen et al., 1968].

Similar calculations have been carried out for  $^{12}\text{C}$  by Hundhausen et al. [1968]. For a coronal base temperature of  $1.58 \times 10^6$  °K, the frozen-in state has 96 percent of the carbon in the form of  $^{12}\text{C}^{+6}$ —that is, fully ionized—and the remaining 4 percent in the form of  $^{12}\text{C}^{+5}$ .

This ionization state analysis for an expanding corona has not been carried out for the heavier elements such as neon, magnesium, silicon and iron. Recent ionization equilibrium calculations of Cox and Tucker [1969], Jordan [1969], and Allen and Dupree [1969] can be used to estimate the ionization states of the elements as a function of the coronal temperatures where the states become frozen in the expanding plasma. To illustrate what may be expected for  $^{56}\text{Fe}$ , ionization state envelopes taken from Allen and Dupree for four temperatures are shown in figure 12. The distribution of iron ions is quite sensitive to temperature and presumably measurements of such distributions in the solar wind could provide coronal temperatures with some precision. However, the accuracy with which this technique might be used is partly limited by the accuracy of the ionization equilibrium calculations. Significant differences can be noted in the calculations made by various authors.

#### Predictions of the Solar Wind Composition and Ionization State

Several predictions of the E/Q spectrum of the solar wind have been published, using various values for the

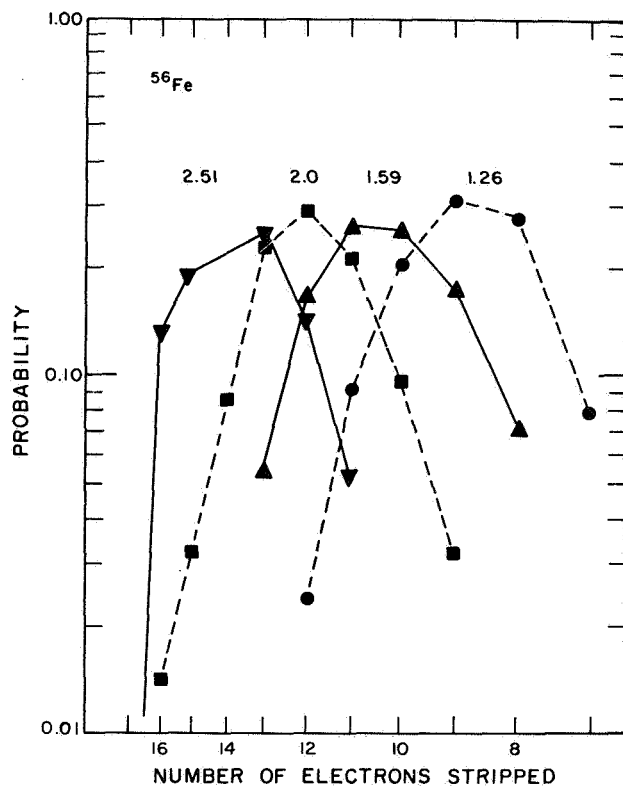


Figure 12. Ionization state envelopes of  $^{56}\text{Fe}$  for different coronal temperatures, in units of  $10^6$  °K, taken from the ionization equilibrium calculations of Allen and Dupree [1969].

composition and various ionization state determinations. The predictions have assumed that all ion species have the same mean velocity. This assumption has been proven valid experimentally as shown later. The model of Geiss *et al.* [1970a] also predicts the same velocities if the  $^1\text{H}^+$  and  $^4\text{He}^{+2}$  velocities are the same. Lange and Scherb [1970] have shown spectra calculated using the Cox and Tucker [1969] ionization state values for a static corona with  $T = 1.5 \times 10^6$  °K. Spectra for three assumed sets of oxygen, carbon, nitrogen, neon, magnesium, and silicon abundances relative to that of helium are given and compared with Vela 3 experimental determinations made by Bame *et al.* [1968a]. Lange and Scherb show that silicon ion species may produce resolvable peaks in a solar wind E/Q spectrum.

Similar predictions have been made by Holzer and Axford [1970a], who used the solar system abundances given by Cameron [1968] and shown in table 3, and the ionization equilibrium calculations of Jordan [1969] for  $T = 1.26 \times 10^6$  °K. The resulting spectra were again compared with the data from Vela 3. Holzer and Axford concluded that both silicon and iron ion species may produce resolvable peaks.

Another prediction has been given by Bame *et al.* [1970] and will be discussed here in some detail. The coronal abundances given by Pottasch [1967] were assumed to be the same for the solar wind for elements above helium. Table 5 gives the predicted solar wind ion

Table 5 Predicted solar wind ion species assuming Pottasch coronal abundances, a static corona ionization state for  $1.5 \times 10^6$  °K, and  $V = 440$  km sec $^{-1}$

Ion species	E/Q	Species fraction	Coronal abundance	Species abundance	Ion species	E/Q	Species fraction	Coronal abundance	Species abundance
$^1\text{H}^+$	1.00	1.00	--	--	$\text{Mg}^{+8}$	2.98	0.01	0.12	0.001
$^2\text{H}^+$	2.00	1.00	--	--	$\text{Mg}^{+9}$	2.64	0.15		0.02
$^3\text{H}^+$	3.00	1.00	--	--	$\text{Mg}^{+10}$	2.38	0.70		0.08
$^3\text{He}^{+2}$	1.50	1.00	--	--	$\text{Si}^{+7}$	3.97	0.11	0.20	0.02
$^4\text{He}^{+2}$	1.99	1.00	--	--	$\text{Si}^{+8}$	3.47	0.34		0.07
$\text{C}^{+5}$	2.38	0.15	2.00	0.30	$\text{Si}^{+9}$	3.08	0.36		0.07
$\text{C}^{+6}$	1.99	0.85		1.70	$\text{Si}^{+10}$	2.78	0.13	0.08	0.03
$\text{N}^{+5}$	2.78	0.20		0.05	$\text{S}^{+8}$	4.00	0.11		0.01
$\text{N}^{+6}$	2.32	0.60	0.24	0.14	$\text{S}^{+9}$	3.53	0.35	0.20	0.03
$\text{N}^{+7}$	1.99	0.20		0.05	$\text{S}^{+10}$	3.17	0.35		0.03
$\text{O}^{+6}$	2.65	0.83		0.83	$\text{Fe}^{+8}$	6.94	0.06	0.20	0.01
$\text{O}^{+7}$	2.27	0.17	1.00	0.17	$\text{Fe}^{+9}$	6.17	0.20		0.04
$\text{Ne}^{+8}$	2.48	0.98	0.14	0.14	$\text{Fe}^{+10}$	5.55	0.26		0.05
					$\text{Fe}^{+11}$	5.05	0.25		0.05
					$\text{Fe}^{+12}$	4.63	0.13		0.03
					$\text{Fe}^{+13}$	4.27	0.04		0.008

species abundances for a static corona ionization state at  $1.5 \times 10^6$  K. Included in the table are the energy per charge values at which the various ion species are expected if the  $^1\text{H}^+$  E/Q value is 1.00 and all species have the same velocity. For these assumptions, ion species positions should be  $M/M_p Q$ , where  $M$  is the ion mass,  $Q$  the ion charge, and  $M_p$  the proton mass. At proton energies other than 1.00, the same E/Q ratios are expected.

Ionization state calculations of *Cox and Tucker* [1969] were used for carbon, nitrogen and magnesium, those of *Allen and Dupree* [1969] for oxygen, neon, silicon, and iron, and those of *Jordan* [1969] for sulfur. The fractions of the various ion species expected, as shown in the table, were multiplied by the coronal abundances to obtain the species abundances.

Inspection of the table 5 species abundances and expected E/Q positions reveals a number of interesting features. The most abundant resolvable ions other than  $^1\text{H}^+$  and  $^4\text{He}^{+2}$  should be  $^{16}\text{O}^{+6}$  for a coronal temperature of  $1.5 \times 10^6$  K. Some species lie very close together such as  $^{12}\text{C}^{+5}$ ,  $^{14}\text{N}^{+6}$ ,  $^{16}\text{O}^{+7}$ , and  $^{24}\text{Mg}^{+10}$ , but of these the carbon and oxygen species are expected to be more abundant than the others. The ion species of  $^{24}\text{Mg}$  and  $^{32}\text{S}$  are not as abundant as those of  $^{28}\text{Si}$  and  $^{56}\text{Fe}$ . Some of the silicon and all of the iron ion species E/Q positions listed are well separated from the species of the lighter elements.

Using the results of table 5, a predicted spectrum was synthesized as follows. The  $^4\text{He}^{+2}$  peak from a particular solar wind spectrum measured on Vela 5A was used. Each of the ion species above  $^4\text{He}^{+2}$  was assumed to produce in the electrostatic analyzer 6 percent wide at half maximum gaussian peaks. The heights of the peaks are proportional to the ion species abundances. This synthesized spectrum was joined onto the helium high-energy tail in a special way, as described in the next section. The resulting spectrum is shown in figure 13. For simplicity, the hydrogen peak is omitted here. A second prediction using solar system abundances is also shown by the dashed groups which lie considerably lower. Use of the older photospheric abundance of iron given in table 3 would drop the iron lines off the graph.

Table 5 and figure 13 show that sulfur and magnesium lines are hidden below the more prominent lines. The  $^{16}\text{O}^{+7}$  line is hidden in the  $^4\text{He}^{+2}$  tail. A partly resolved line due to  $^{12}\text{C}^{+5}$  appears between  $^4\text{He}^{+2}$  and  $^{16}\text{O}^{+6}$ . Other lines below  $^{16}\text{O}^{+6}$ , such as  $^{20}\text{Ne}^{+8}$  and  $^{14}\text{N}^{+6}$ , are also hidden.

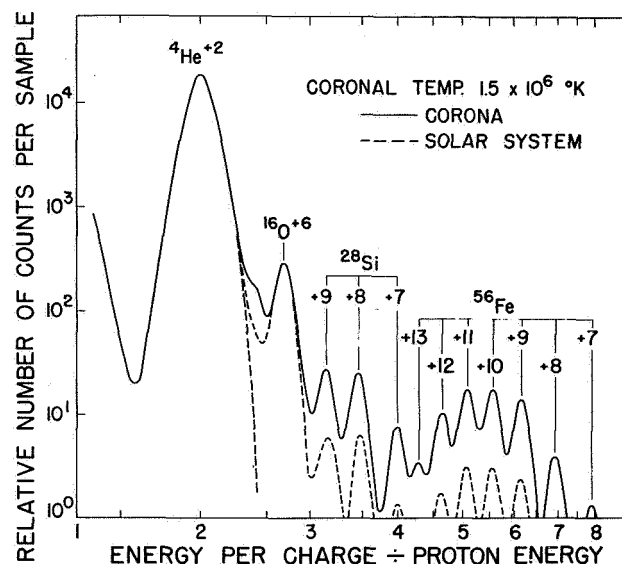


Figure 13. A predicted solar wind spectrum as it would be observed with a suitable electrostatic analyzer. The  $^1\text{H}^+$  peak is not shown. Relative peak heights of ion species above  $^4\text{He}^{+2}$  are taken from table 5.

#### SPACECRAFT OBSERVATIONS OF $^{16}\text{O}$ , $^3\text{He}$ , $^{28}\text{Si}$ , AND $^{56}\text{Fe}$ ION SPECIES

The first observations of ion species other than  $^1\text{H}^+$  and  $^4\text{He}^{+2}$  were made with electrostatic analyzers on the two Vela 3 spacecraft [Bame et al., 1968a]. Further observations are being made on the two pairs of earth-oriented satellites Vela 5A and B, and Vela 6A and B with improved instrumentation. A report of Vela 5A results has been given by Bame et al. [1970]. No other spacecraft instrument measurements of resolved ion species other than  $^1\text{H}^+$  and  $^4\text{He}^{+2}$  are known to the author. Measurements of some of the solar wind noble gas nuclides trapped in aluminum foils exposed on the lunar surface by the Apollo 11 and 12 astronauts have been reported by Böhler et al. [1969] and Geiss et al. [1970b].

#### Vela 3 Instrument Details

Each of the two spin-stabilized Vela 3 satellites carried a hemispherical electrostatic analyzer. Some general details of the instruments, orbits, and methods of analyzing the solar wind data have been given by Gosling et al. [1967a], Hundhausen et al. [1967], and Bame et al. [1967]. Additional details are needed for a discussion of the ion species measurements.

Special conditions are necessary for the ion species to be resolved. With Vela 3 analyzers the efficiency and cycle times require that the solar wind conditions remain rather constant for periods of around 20 to 30 min in order to collect sufficient numbers of counts to resolve



the ion species. The solar wind  $^1\text{H}^+$  and  $^4\text{He}^{+2}$  temperatures must be low, as well as those of other species, to permit resolution of the groups. The instrumental resolution must be high enough and E/Q level spacings close enough to resolve the closely spaced groups.

With Vela 3 these conditions are met part of the time, although it will be seen that the E/Q level spacings are marginal. The electrostatic analyzer intrinsic E/Q resolution is about 2.8 percent and level spacing is about 11 percent. Fixed voltage levels exercised in a 4 minute cycle are used on Vela 3A and B, so significant gaps exist between E/Q windows. Particles are accepted in a fan-shaped solid angle of approximately  $3^\circ$  in spacecraft longitude and  $100^\circ$  in latitude. The spin-stabilized spacecraft sweep the acceptance angle past the sun two times per second, while counting in intervals of 8 msec triggered by the sun in such a way that flux measurements are made in eight angular ranges. Five of these angular ranges are centered at angles of  $-11^\circ$ ,  $-5^\circ$ ,  $1^\circ$ ,  $7^\circ$ , and  $14^\circ$  from the solar direction. Usually the majority of counts from solar wind ions are observed in two or three angular ranges when temperatures are low enough for resolution of ion species.

Analyzed ions enter an electron multiplier and produce secondary electrons. The number of electrons produced is highly dependent on the ion mass for equal ion speeds. The electron multiplier pulses are amplified and counted above three charge threshold levels A, B, and C, which have relative sensitivities of 60, 6, and 1. Most of the ions are counted at level A, independent of their mass. Significant losses in counting protons and small losses for helium ions occur at level B. At level C, protons and helium ions are counted with much less efficiency than heavy ions. This feature helps in identifying heavy ions and in separating them from the high energy tail of the  $^4\text{He}^{+2}$  distribution.

At any given time, simultaneous counts from levels A and B or levels A and C are transmitted to the ground. The choice is made by command.

#### Vela 3 Solar Wind Heavy Ion Spectra

A spectrum demonstrating the presence of  $^{16}\text{O}^{+6}$  ions is given in figure 14. At this time the counts at levels A and B were transmitted. Counts measured at angles of  $-5^\circ$  and  $1^\circ$  in four data cycles between 1226 UT and 1243 UT were summed at each of the E/Q levels to form the spectra. The two peaks attributable to  $^1\text{H}^+$  and  $^4\text{He}^{+2}$ , always seen in Vela 3 spectra, are present. A third peak, present on the high energy  $^4\text{He}^{+2}$  tail, is caused by ions heavier than  $^4\text{He}^{+2}$ ; at level B, these ions are more efficiently counted than  $^4\text{He}^{+2}$ . Arrows are shown at positions where  $^{16}\text{O}^{+7}$  and  $^{16}\text{O}^{+6}$  ions would

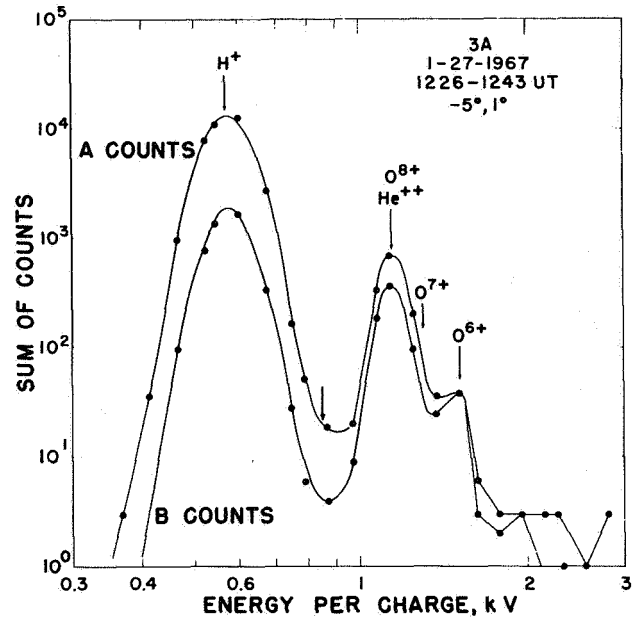


Figure 14. Solar wind spectra from Vela 3A obtained simultaneously at two different sensitivity levels. A third ion species attributed to  $^{16}\text{O}^{+6}$  is present, as well as other unresolved species.

be expected, based on the observed positions of the lighter ions. That  $^{16}\text{O}^{+6}$  ions are present in the spectrum is well established, but it is clear that other ion species such as  $^{16}\text{O}^{+7}$ ,  $^{12}\text{C}^{+5}$ ,  $^{14}\text{N}^{+7}$ , and  $^{20}\text{Ne}^{+8}$  could also be present but unresolved in this spectrum (compare the predicted spectrum of figure 13 and table 5). Counts at E/Q values above  $^{16}\text{O}^{+6}$  are partly background and partly unresolved heavier ions.

At the time that this spectrum was measured oxygen appears to have been particularly abundant. If allowance is made for other species, the He/O ratio is still rather small and may have a value near 30. The precision with which this ratio can be determined is not very great, of course. The ratio He/O as observed in a number of Vela 3 spectra is variable; the highest ratio measured is  $\sim 400$ .

One of the spectra published in Bame *et al.* [1968a] is shown in figure 15. The spacecraft was transmitting A and C level counts at this time. Counts from angles  $-5^\circ$  and  $1^\circ$  were summed for four data cycles between 0388 and 0355 UT. One count was added at each E/Q level to show level positions where the counts were zero. Based on the  $^1\text{H}^+$  and  $^4\text{He}^{+2}$  positions, arrows show where various ion species would be found if present. The arrows for oxygen ions at higher E/Q than  $^{16}\text{O}^{+5}$  are intended to give the E/Q scale and do not imply that those ions were present [Bame *et al.*, 1968a].

A peak at an E/Q position 1.5 times higher than  $^1\text{H}^+$

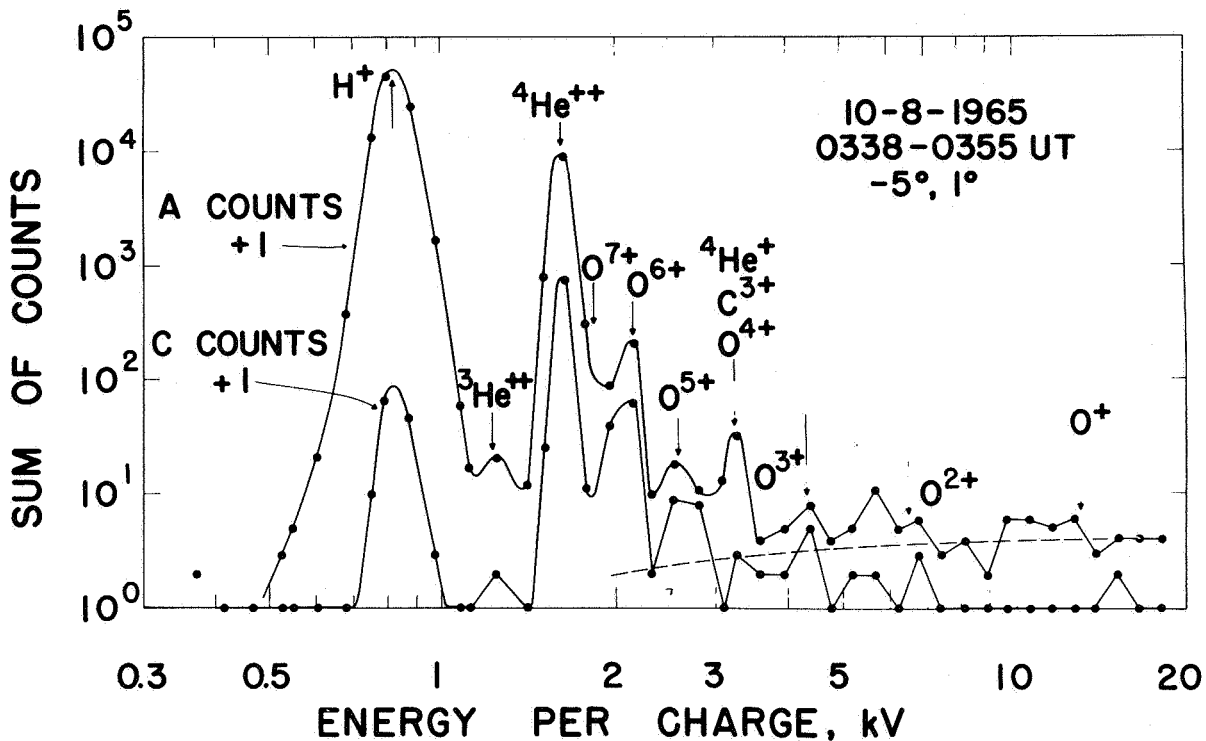


Figure 15. Solar wind spectra from Vela 3A obtained simultaneously at two different sensitivity levels. This spectrum was interpreted by Bame *et al.* [1968a] to show the presence of  ${}^3\text{He}^{+2}$ ,  ${}^{16}\text{O}^{+6}$ ,  ${}^{16}\text{O}^{+5}$ , and  ${}^4\text{He}^{+}$  ions, as well as other unresolved species. A new interpretation based on later Vela results eliminates the  ${}^{16}\text{O}^{+5}$  identification. (See fig. 19.)

appeared in this spectrum and a companion spectrum a little later. This can only correspond to  ${}^3\text{He}^{+2}$ , showing that  ${}^3\text{He}$  exists in the modern sun. The solar wind  ${}^3\text{He}$  abundance at this time was  $\sim 10^{-3}$  that of  ${}^4\text{He}$ . At another time when the ion temperatures were very low and  ${}^3\text{He}$  would have been resolved if sufficiently abundant, upper limits of  $2 \times 10^{-4}$  and  $4 \times 10^{-4}$  were set. In other examples the  ${}^3\text{He}/{}^4\text{He}$  ratio was higher than  $10^{-3}$  but the  ${}^1\text{H}^{+}$  and  ${}^4\text{He}^{+2}$  tails prevented accurate determinations. Thus, the spacecraft observations indicate a variable abundance of  ${}^3\text{He}$  relative to  ${}^4\text{He}$  in the solar wind. A similar conclusion has been reached by Geiss *et al.* [1970b] from the Apollo foil experiments.

Again, the  ${}^{16}\text{O}^{+6}$  group is quite prominent; the C-count spectrum shows  ${}^{16}\text{O}^{+7}$  to be less abundant. In some other examples, with the E/Q levels appropriately placed,  ${}^{16}\text{O}^{+7}$  can be more abundant, showing that the solar wind came from a hotter corona. Examples of this are shown in the original Vela 3 report [fig. 1 of Bame *et al.*, 1968a], and it has been argued by Hundhausen *et al.* [1968] that these particular examples are obtained in an solar wind stream coming from a single large plage region

on the sun [Hundhausen, 1970].

A prominent peak at an E/Q four times that of  ${}^1\text{H}^{+}$  in figure 15 has been attributed to  ${}^4\text{He}^{+}$ . As discussed earlier, almost no  ${}^4\text{He}^{+}$  is expected to survive in the corona and in the solar wind. However, because of the similar ratio of A/C counts in this peak compared to the  ${}^4\text{He}^{+2}$  peak, it is believed that significant amounts of  ${}^4\text{He}^{+}$  were present in the solar wind at this time. The ratio  ${}^4\text{He}^{+}/{}^4\text{He}^{+2}$  appeared to be about  $3 \times 10^{-3}$ . Most of the time a peak in this position is not found and upper limits as low as  $2 \times 10^{-4}$  have been set. Based on the identification of  ${}^4\text{He}^{+}$  in the solar wind, Hundhausen *et al.* [1968] suggested charge exchange of  ${}^4\text{He}^{+2}$  with interplanetary neutral hydrogen as a source. Holzer and Axford [1970b] have suggested the ions may result from photoionization of interstellar helium atoms which have penetrated interplanetary space. The infrequent appearance of the peak in the  ${}^4\text{He}^{+}$  position is not readily explained by either of these mechanisms, and as will be shown later, the  ${}^4\text{He}^{+}$  identification cannot be made with certainty at the present time.

The group at 2.5 kV was identified as  ${}^{16}\text{O}^{+5}$ . As

discussed earlier, very little of this species is expected to survive in the solar wind, and its presence was considered anomalous [Hundhausen *et al.*, 1968]. It has been suggested by Lange and Scherb [1970] and Holzer and Axford [1970a] that the counts in this group might be due to  $^{28}\text{Si}^{+9}$  and  $^{32}\text{S}^{+10}$ ; such identifications would avoid the difficulty with  $^{16}\text{O}^{+5}$ . As will be shown later this group is almost certain to consist mainly of  $^{28}\text{Si}^{+9}$  on the basis of Vela 5 measurements.

The counts in the *A* spectrum of figure 15 above 3.5 kV are very near to the instrumental background at level *A* (shown by the dashed curve). However, the instrumental background at level *C* is very low and it was felt that the *C* counts above 3.5 kV were caused by ions that could not be resolved because of the small numbers of counts and widely spaced levels. The significance of these counts can be judged by reference to table 3 of Holzer and Axford [1970a], which shows a matrix of *C* counts obtained shortly after the figure 15 data. Holzer and Axford correctly suggested iron ions caused these counts.

Inspection of spectra such as those in figure 15 and other Vela 3 spectra made it clear that the Vela 3 analyzer did not have sufficient efficiency, and that although the intrinsic analyzer efficiency might be adequate, the spacing of E/Q levels was marginal for resolving heavy ion species. A new instrument was designed to be carried on the Vela 5 and 6 satellites. This instrument and measurements from it [Bame *et al.*, 1970] are discussed below, followed by an interpretation of the spectrum of figure 15 in light of the newer measurements from Vela 5A.

#### Vela 5 and 6 Instrumentation

Each of the four Vela 5 and 6 earth-oriented satellites launched into circular orbits at  $20 R_E$  in May 1969 and April 1970 carries a pair of hemispherical electrostatic analyzers similar to analyzers carried on previous Vela satellites. Particles are analyzed with the sweeping voltage technique and counted in electron multipliers. Each satellite carries one analyzer for standard solar wind measurements, similar to the Vela 4 analyzers described in Montgomery *et al.* [1970]. The second instrument on each satellite has an aperture about three times larger than that of the first and is operated in two modes, which result in considerably higher efficiency for studies of low flux phenomena, including the heavy ion groups found with Vela 3 analyzers.

In the heavy ion operating mode, measurements are made in a total E/Q range from 8000 to 1000 V, which is divided into four separate ranges 1, 2, 3, and 4. Analyzed ions are counted with an electron multiplier and amplifier system having two discrimination levels *A*

and *B*; level *B* is 40 times less sensitive than *A*. As with Vela 3, all ions are counted with near 100 percent efficiency at level *A* and considerably less efficiently at *B* for lighter ions.

Spectra of *A* and *B* counts consisting of counts in 80 E/Q levels are measured in an 8.5-min cycle on the Vela 5 and 6 spacecraft, which rotate once every 64 sec. These data are obtained in one of the two operating modes, which can be changed from the ground. As a cycle begins, a sun sensor initiates a series of 25 energy sweeps in E/Q range 1. These sweeps continue over a 5-sec period ( $\sim 28^\circ$ ), which includes the solar direction in the center. Each sweep is divided into 20 contiguous counting intervals of 8 msec each. The 20 numbers obtained in a single sweep are retained in a memory, numbers from successive sweeps in a given counting interval are added throughout the 25 sweeps, and the totals are transmitted to the ground. In range 1, during the first rotation past the sun, *A* counts are measured. During the second rotation, *B* counts are measured, still in range 1. Range 2 is used, first for *A* counts and next for *B* counts, during the third and fourth revolutions, and so on throughout a complete cycle of eight revolutions.

A complete cycle produces *A*- and *B*-count spectra integrated over angle. Instrumental resolution varies depending on the orientation of the earth-oriented spacecraft. For measurements reported in Bame *et al.* [1970] and discussed here the resolution was  $\sim 4.5$  percent; the contiguous energy intervals are separated by 2.6 percent, so there are no energy gaps except for small gaps between the sweep ranges. The geometrical angular resolution, also a variable with spacecraft orientation, was  $\sim 5^\circ$ ; sweeps are separated by  $\sim 1.1^\circ$ , so there are no gaps in angle. Overall efficiency is increased by making a number of sweeps through the solar wind beam near the direction of peak flux intensity.

The number of usable sets of heavy ion data ultimately obtained from the Vela 5 and 6 heavy ion analyzers will be limited by a number of factors. Among these are the requirements for low ion temperatures, steady solar wind, absence of bow shock generated protons [Asbridge, *et al.*, 1968], proper orientation of the spacecraft roll axis, and that the spacecraft be in the solar wind, in the proper operating mode, and in the active transmitting mode. Vela satellites spend a large fraction of the time in a special memory mode, which does not have the capacity to store heavy ion data.

#### Vela 5A Heavy Ion Observations

On July 6, 1969, there were several periods of time when bow shock generated protons were not present at the spacecraft and heavy ion measurements could be

made. During these times a clearly delineated  $^{16}\text{O}^{+6}$  group was observed with a number of smaller peaks occurring at higher values of E/Q. Although the numbers of counts in the smaller peaks were low, the peaks were observed in successive sets of data. Examples are shown in figure 1 of *Bame et al.* [1970]. One of these examples of heavy ion data, combined with a solar wind spectrum integrated over angle, is shown in figure 16. Triangles represent the solar wind spectrum, which was somewhat similar in appearance to the Vela 3 spectrum in figure 14. The heavy ion spectrum (round points) was joined onto the solar wind spectrum by shifting it vertically to overlay the high-energy tail of the  $^4\text{He}^{+2}$  distribution present in both sets of data. Solar wind analyzer counts per sample are given by the left ordinate, and heavy ion counts on the right. The E/Q scale established by the  $^1\text{H}^{+}$  and  $^4\text{He}^{+2}$  peak positions is used to show the expected positions of other ion species; the points in these ion groups have been fitted with 6 percent FWHM gaussian curves, which provide a good fit to the data. Such a width is near enough to the experimental width to show that in this case, the actual

E/Q widths of the ion species were less than experimental and undeterminable. However, the  $^1\text{H}^{+}$  and  $^4\text{He}^{+2}$  widths were greater than experimental.

Lines of  $^{56}\text{Fe}^{+8}$  through  $^{56}\text{Fe}^{+12}$  are clearly present in this example ( $^{56}\text{Fe}^{+7}$  has been observed also). Three lines between  $^{16}\text{O}^{+6}$  and the iron lines could be silicon or sulfur ions within the accuracy of the measurement (table 5 and fig. 13). If the coronal abundances of table 3 are fairly accurate, most of these ions are  $^{28}\text{Si}^{+9}$ ,  $^{28}\text{Si}^{+8}$ , and  $^{28}\text{Si}^{+7}$ . Note that  $^{28}\text{Si}^{+7}$  occupies the expected position of  $^4\text{He}^{+}$ , but in this case the A/B counts ratio indicates ions heavier than  $^4\text{He}^{+}$ . The argument for the silicon identification of all three lines is strengthened later.

Comparison of figures 16 and 13 shows a remarkable resemblance between the measured and predicted spectra. Part of the resemblance is due to the choice of the  $^4\text{He}^{+2}$  experimental distribution for the prediction and the use of 6 percent line widths in the prediction. However, it is clear that the abundances in table 3 for the photosphere, solar system, and solar cosmic rays would not provide predictions nearly so close to the

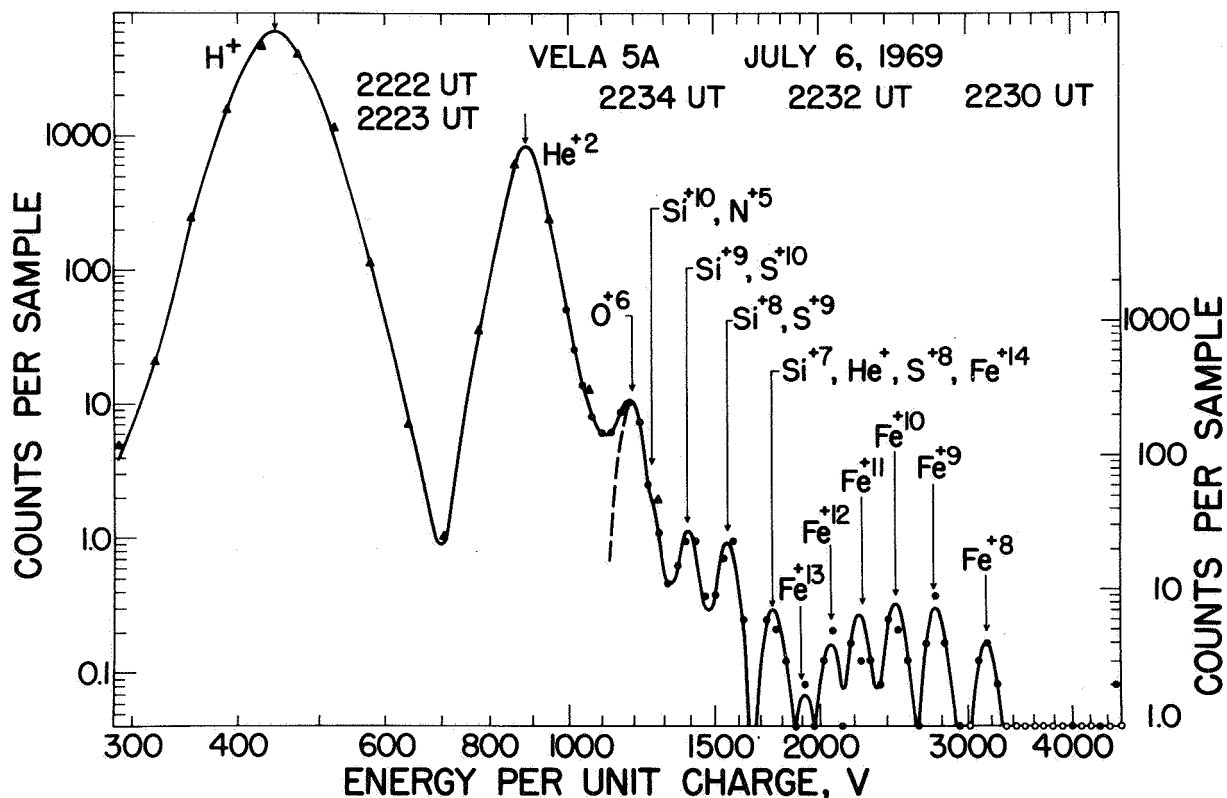


Figure 16. Combined spectra from the Vela 5A solar wind analyzer and heavy ion analyzer [Bame et al., 1970]. Arrows show the expected positions of various ion groups above  $^{16}\text{O}^{+6}$ . Iron lines are unambiguously resolved and various arguments allow the other three lines above  $^{16}\text{O}^{+6}$  to be identified as principally silicon ion species.

measured spectrum at this time. Producing a predicted spectrum in this manner provides insight into which ion species, such as those of sulfur and magnesium, can be expected to be hidden under the lines of the more abundant species; the extent to which these hidden lines contaminate the resolved lines can also be estimated.

One feature in the prediction not appearing in the data is the poorly resolved peak due to  $^{12}\text{C}^{+5}$ . The absence of this peak in the experimental data could be caused by a carbon coronal abundance determination that is too high, an unusually low abundance of carbon in this particular sample of solar wind, or an inaccurate ionization state prediction. If the *Hundhausen et al.* [1968] abundance of  $\sim 4$  percent  $^{12}\text{C}^{+5}$  and 96 percent  $^{12}\text{C}^{+6}$ , rather than the 15 percent  $^{12}\text{C}^{+5}$  value, were used in the prediction, most of the carbon peak would disappear.

*Ionization State Coronal Temperatures from Iron Ion Species Abundances.* As discussed earlier, solar wind relative abundances freeze in near the sun, and provide information on coronal temperatures. Three heavy ion spectra, including the one in figure 16, were combined to provide better statistics. Because the solar wind speed shifted from 296 to 285 km sec $^{-1}$  during the measurements, small shifts of the E/Q scales were necessary to obtain the best alinement of the groups. The summed spectrum is shown in figure 17. Because of a gap in E/Q coverage between adjacent sweeps, the line attributed to  $^{28}\text{Si}^{+7}$  in figure 16 was not covered in the succeeding two spectra, after the decrease in speed, so that line is missing in the summed spectrum.

The iron lines,  $^{56}\text{Fe}^{+8}$  through  $^{56}\text{Fe}^{+12}$ , are clearly resolved here. Because there are no gaps in energy-angle

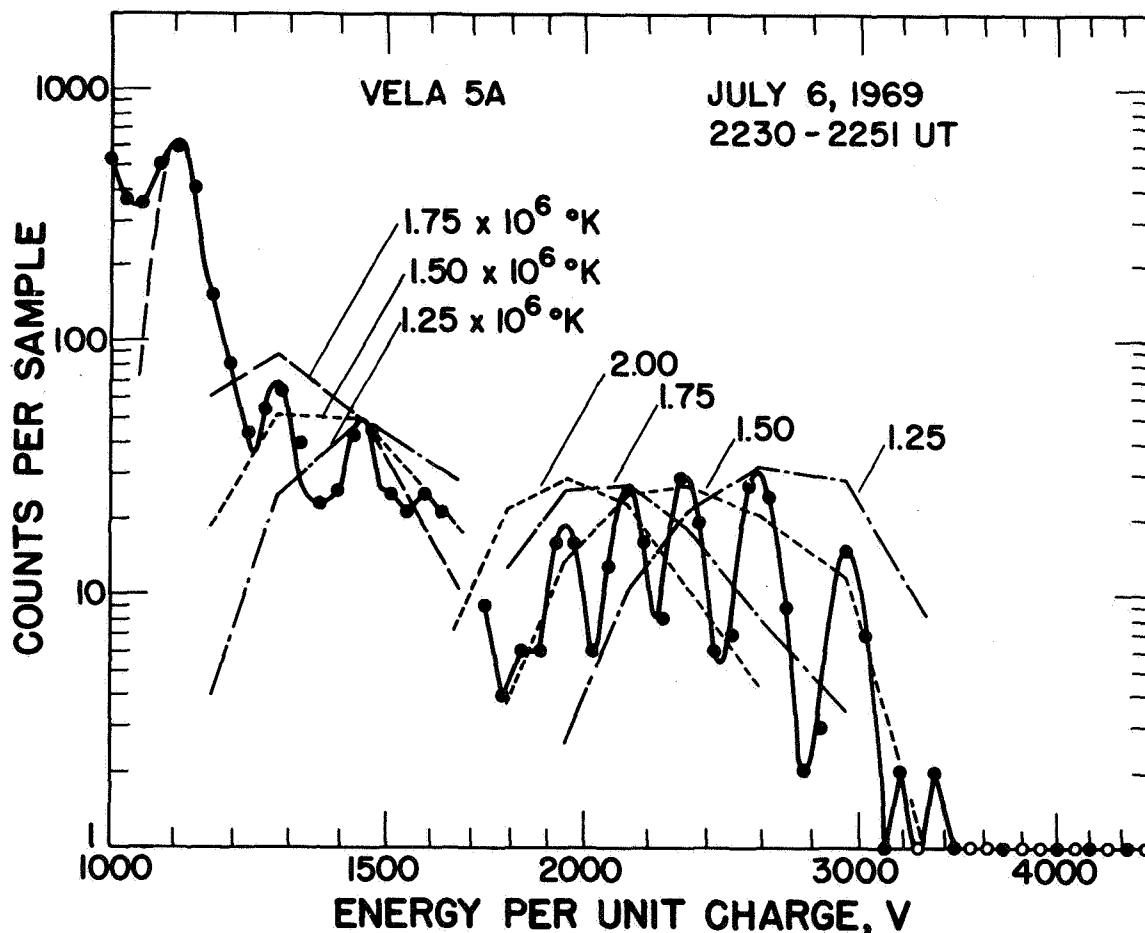


Figure 17. Vela 5A summed heavy ion spectra [Bame et al., 1970]. Ionization state envelopes from Allen and Dupree [1969] at various temperatures for  $^{56}\text{Fe}$  and  $^{28}\text{Si}$  are shown. The iron ion species abundance shows that the temperature of the corona in which this state was determined (frozen-in) was near  $1.5 \times 10^6 \text{ }^\circ\text{K}$ . A value  $0.25 \times 10^6 \text{ }^\circ\text{K}$  lower is obtained using the results of Jordan [1969].

coverage and the analyzer resolution is wider than the ion species widths, the peak heights in figure 17 can be used to judge the relative ion abundances for iron. Envelopes of the iron lines for various coronal temperatures, based on calculations by *Allen and Dupree* [1969] are shown. Similar envelopes are obtained with the calculations of *Jordan* [1969] for temperatures about  $0.25 \times 10^6$ °K lower. The iron envelope for  $1.5 \times 10^6$ °K (A and D) or  $1.25 \times 10^6$ °K (J) provides a good fit, but the experimental envelope is broader.

A broader experimental envelope is expected for the expanding corona because the ionization and recombination rates for the various ion species of an element are not the same, and abundance ratios of adjacent species freeze in at different altitudes in the corona. The negative radial temperature gradient in the corona causes the solar wind iron ionization state envelope to be broader than is predicted by the single temperature ionization equilibrium calculations.

Comparison of the ionization and recombination rates and the expansion scale time in the *Whang and Chang* [1965] model corona give about  $2 R_\odot$  as the heliocentric distance at which the  $^{56}\text{Fe}^{+12}/^{56}\text{Fe}^{+11}$  ratio freezes in and  $3 R_\odot$  for  $^{56}\text{Fe}^{+9}/^{56}\text{Fe}^{+8}$ . (These estimates are from A. J. Hundhausen.) From the data of figure 17, estimates of coronal temperatures for this sample of expanding corona are  $1.65 \times 10^6$ °K at  $2 R_\odot$  and  $1.50 \times 10^6$ °K at  $3 R_\odot$  (ionization state calculations of *Allen and Dupree* [1969]). Values about  $0.25 \times 10^6$ °K lower are obtained using the calculations of *Jordan* [1969]. Inspection of the numbers of counts in the iron lines shows that the precision of these temperature estimates is not great.

**Identification of Silicon Lines.** From table 5 E/Q values, it is apparent that the lines between those of iron and  $^{16}\text{O}^{+6}$  in figures 16 and 17 conceivably could be caused by either sulfur or silicon. There is no doubt that both elements are present in the solar wind. The lines are identified as principally silicon for the following reasons:

1.  $^{28}\text{Si}^{+9}$  and  $^{32}\text{S}^{+10}$  have the greatest separation. The E/Q positions determined in a number of examples, such as figure 18, favor silicon.
2. The measured abundance of iron, discussed later, is similar to the coronal abundance shown in table 3 [Pottasch, 1967]. The table shows silicon as almost three times more abundant than sulfur in the corona.
3. The figure 17 ratio of the lines identified as  $^{28}\text{Si}^{+9}$  and  $^{28}\text{Si}^{+8}$  gives a temperature of  $1.65 \times 10^6$ °K (A and D), which compares well with the determinations from the iron lines.
4. The calculations of *Jordan* [1969] include iron, silicon, and sulfur. Comparisons of the calculated and

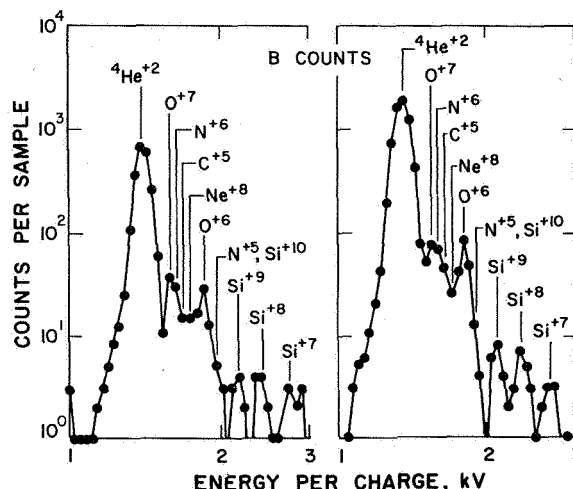


Figure 18. Two Vela 5A heavy ion spectra. In each, a peak attributed to  $^{16}\text{O}^{+7}$  and  $^{14}\text{N}^{+6}$  ions appears between the  $^4\text{He}^{+2}$  and  $^{16}\text{O}^{+6}$  peaks. Other ion species, such as  $^{12}\text{C}^{+5}$ ,  $^{20}\text{Ne}^{+8}$ ,  $^{14}\text{N}^{+5}$ , and  $^{28}\text{Si}^{+10}$  are also present but unresolved. The E/Q position of the peak identified as  $^{28}\text{Si}^{+9}$  favors that identification over  $^{32}\text{S}^{+10}$ .

experimental ionization states for  $T = 1.26 \times 10^6$ °K are shown in table 6. The experimental iron state comes from figure 17 and seems to agree adequately with the calculated state, showing that about the right temperature (for the calculations of *Jordan*) has been chosen. Ratios of the three lines in question in figures 16 and 17 are normalized at  $^{28}\text{Si}^{+8}$  and  $^{32}\text{S}^{+9}$  in the table to give the experimental states for

Table 6 Comparison of calculated and experimental ionization states of iron, silicon, and sulfur

	Calculated	Experimental
$\text{Fe}^{+7}$	0.01	--
$\text{Fe}^{+8}$	.08	0.12
$\text{Fe}^{+9}$	.23	.25
$\text{Fe}^{+10}$	.31	.24
$\text{Fe}^{+11}$	.23	.21
$\text{Fe}^{+12}$	.12	.14
$\text{Fe}^{+13}$	.02	--
$\text{Si}^{+7}$	.09	.11
$\text{Si}^{+8}$	.31	(.31)
$\text{Si}^{+9}$	.44	.41
$\text{Si}^{+10}$	.14	--
$\text{S}^{+8}$	.31	.14
$\text{S}^{+9}$	.43	(.43)
$\text{S}^{+10}$	.16	.55

silicon and sulfur. Comparison of these states with the calculated states clearly favors the silicon identification.

**Presence of  $^{16}\text{O}^{+7}$  and  $^{14}\text{N}^{+6}$  Ions.** Observations from Vela 3 have been interpreted in the past as showing cases when  $^{16}\text{O}^{+7}$  was more abundant than  $^{16}\text{O}^{+6}$ . Such an observation depended on chance alignment of levels near the expected ion species positions; inadequate numbers of levels prevented complete resolution of the experimental spectra. Vela 5 and 6 heavy ion measurements provide considerably better coverage, and in one case investigated thus far, the  $^4\text{He}^{+2}$  temperature was low enough to permit resolution of structure between  $^4\text{He}^{+2}$  and  $^{16}\text{O}^{+6}$ .

Vela 5A data taken June 22, 1969, at 2100 UT and June 23, 1969, at 0450 UT are shown in figure 18. Note that *B*-count spectra better separate heavier ions in the  $^4\text{He}^{+2}$  high-energy tail. Similar spectra were measured throughout the time span of these spectra. Lines show the expected positions (table 5) of various ion species based on the helium position. The presence of  $^{16}\text{O}^{+7}$  along with some  $^{14}\text{N}^{+6}$  in this solar wind sample seems well established. Smaller amounts of  $^{12}\text{C}^{+5}$  and  $^{20}\text{Ne}^{+8}$  are undoubtedly also present but not resolved.  $^{14}\text{N}^{+5}$  and  $^{28}\text{Si}^{+10}$  ions contribute to the high-energy tail of the  $^{16}\text{O}^{+6}$  peak, but are not resolved. The three prominent silicon lines indicate that this solar wind came from a corona at temperatures near  $1.5 \times 10^6 \text{ K}$ , or  $1.25 \times 10^6 \text{ K}$  depending on the choice of ionization state calculations. Relative abundances should not be estimated from these spectra because the *B*-counts response to various species is not known accurately. Relative abundance estimates of oxygen, silicon, and iron from this time, using the near 100 percent response of the *A*-count spectra, are about the same as those estimated from figures 16 and 17.

#### Reinterpretation of Vela 3 Spectra and the $^4\text{He}^{+}$ Problem

Spectra from Vela 3 can be reinterpreted on the basis of the more adequate sensitivity and *E/Q* coverage of the Vela 5A measurements. Figure 19 shows the Vela 3A spectrum given in figure 15; here the *A*-count points are fitted with a spectrum that draws on the Vela 5A results shown in figures 16, 17, and 18. The peak originally identified as  $^{16}\text{O}^{+5}$  can now be identified as  $^{28}\text{Si}^{+9}$ , eliminating the difficulties with the oxygen identification pointed out by *Hundhausen et al.* [1968], *Lange and Scherb* [1970], and *Holzer and Axford* [1970a]. The iron ion species peaks have no real significance other than to demonstrate the presence of iron ions above the background level; wide separations of the

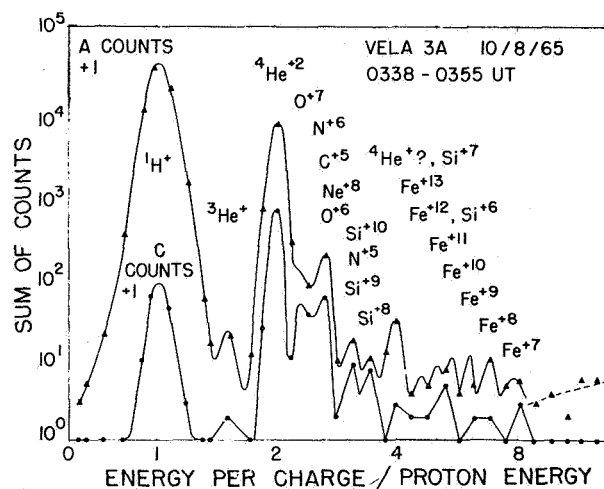


**Figure 19.** A Vela 3A spectrum (also shown in fig. 15) with identifications based on the more recent Vela 5A results. The multiple peaks drawn in the  $^{56}\text{Fe}$  ion positions are meant to show only that the experimental points are consistent with the presence of unresolved lines above background. The peak at 4.0 is anomalously high to be explained as due only to  $^{28}\text{Si}^{+7}$  ions.

Vela 3 *E/Q* levels and low sensitivity prevented resolution of individual lines.

In this case, *E/Q* levels fortunately fell near the silicon peak positions. It is difficult to reconcile the relative heights of the peaks to any reasonable ionization state of silicon. For this reason, there appears to be a significant excess of counts at the position of  $^{28}\text{Si}^{+7}$ , which is also the position of  $^4\text{He}^{+}$ . The *A/C* counts ratio at that position, although statistically not too accurate, suggests that helium-like ions might be present (compare *A/C* ratios at the  $^{28}\text{Si}^{+9}$  and  $^{28}\text{Si}^{+8}$  positions). Finally, the *Si/O* ratio from this spectrum would be high compared to Vela 5A results, if all the ions are taken to be  $^{28}\text{Si}^{+7}$  in the peak. If great differences occur in differentiation of elements in the corona, it is possible that this *E/Q* position at four times the  $^1\text{H}^{+}$  position might indicate an enhanced flux caused by  $^{28}\text{Si}^{+7}$ ,  $^{32}\text{S}^{+8}$ , and  $^{36}\text{Ar}^{+9}$  ions coming from a relatively cool location in the corona.

The identification of  $^4\text{He}^{+}$  in the solar wind [*Bame et al.*, 1968a] was based on three cases in which a peak occurred in the *E/Q* = 4.0 position. Figure 19 was one of the cases. Usually such peaks are absent in Vela 3 data. All three spectra with identifiable peaks are shown in figure 20, and in each example the prominent line at 4.0

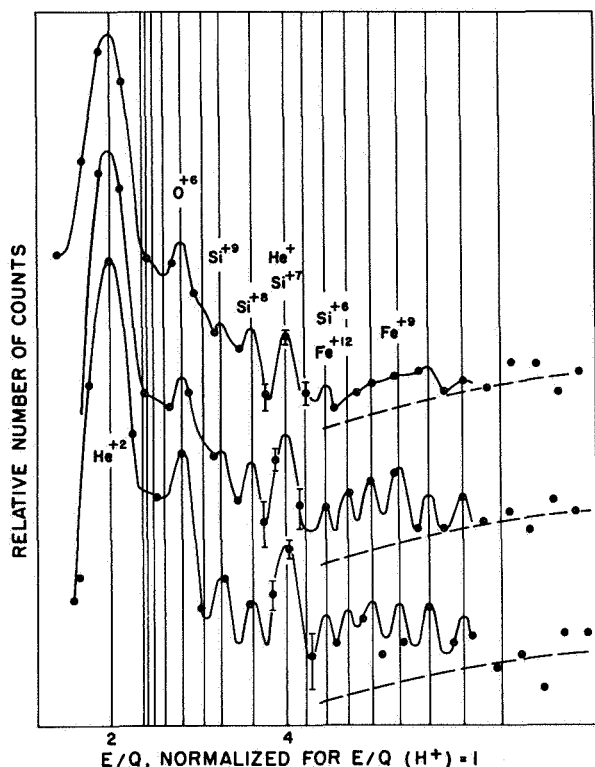


Figure 20. Three Vela 3 spectra with prominent peaks in the  $E/Q = 4.0$  positions. Vertical lines give the positions of various ion species which are expected to be present. Multiple peaks drawn through the points at the  $^{56}\text{Fe}$  species positions are symbolic only.

appears accentuated compared to the  $^{16}\text{O}^{+6}$  peaks of the Vela 5A data shown in figure 18. However, in two cases, points do not lie near the peaks of the  $^{16}\text{O}^{+6}$ ,  $^{28}\text{Si}^{+9}$ , and  $^{28}\text{Si}^{+8}$  positions, so the argument for  $^4\text{He}^{+}$  is not so strong as in the case shown in figure 19.

Whether or not  $^4\text{He}^{+}$  ions occasionally are present in the solar wind remains an open question. If they are, the higher sensitivity and better spectral resolution of the Vela 5 and 6 heavy ion analyzers should make possible a more definite identification, if  $^4\text{He}^{+}$  should appear during periods of measurements.

#### Solar Wind Composition

The Vela 5A spectra in figures 16 and 17 have been used to derive the abundances for the July 6, 1969, solar wind. For this sample, oxygen, silicon, and iron abundances are estimated from figure 17 data using relative peak heights. Hydrogen and helium abundances are estimated using the figure 16 data and taking into account the peak widths. It is assumed that peak heights are not seriously contaminated with unresolved species.

In the synthesized spectrum of figure 13, the maximum contamination in a resolved peak height was 20 percent for  $^{28}\text{Si}^{+9}$ . The  $^{16}\text{O}^{+6}$  peak height was contaminated by 10 percent. Oxygen is assumed to be 17 percent  $^{16}\text{O}^{+7}$  and 83 percent  $^{16}\text{O}^{+6}$ . Figure 16 is used to estimate  $^{28}\text{Si}^{+7}$  and the same amount of  $^{28}\text{Si}^{+10}$  is assumed. From these assumptions the relative abundances of hydrogen, helium, oxygen, silicon, and iron are found to be 5000, 150, 1.00, 0.21, and 0.17. The silicon and iron abundances relative to oxygen compare well with the table 3 coronal abundances. The uncertainty in these abundances is thought to be about  $\pm 30$  percent.

Table 7 summarizes the ion species identified in the solar wind. Whether or not  $^4\text{He}^{+}$  ever appears seems to be an open question. There seems to be no doubt that such species as  $^{12}\text{C}^{+5}$ ,  $^{20}\text{Ne}^{+8}$ ,  $^{24}\text{Mg}^{+10}$ ,  $^{14}\text{N}^{+5}$ ,  $^{32}\text{S}^{+9}$ , and  $^{32}\text{S}^{+10}$  are also carried in the solar wind. Ions of other less abundant coronal elements such as calcium and nickel must also be present, but may not be identified for some time to come.

Table 8 lists the elements and isotopes detected in the solar wind by means of spacecraft observations and the lunar collector foil technique used by Bühler *et al.* [1969] and Geiss *et al.* [1970b]. Again it should be pointed out that the elements and isotopes known to be present in the corona should also be present in the solar wind, but not all of them have yet been identified.

Table 9 summarizes relative abundances of heavier ions in the corona and solar wind. The values of Pottasch [1967] are used for the corona. Values of solar wind abundances for oxygen, silicon, and iron come from the Vela 5A data of July 6, 1969. A few other samples of Vela 5 data have shown similar O-Si-Fe ratios, but a greater sample of data must be studied before it is clear how constant these ratios may be. The abundances of the other common elements, such as carbon, nitrogen, and sulfur, in the solar wind remain to be determined since they are not sufficiently resolved in the Vela data. The abundance given for  $^{20}\text{Ne}$  has been estimated by Geiss *et al.* [1970b] on the basis of the Apollo foil experiments and the Vela 3 measurements of He/O ratios.

Estimates of He/O from Vela range from around 30 to over 400. There is no doubt about the variability of this ratio; the average may be near 100. The helium-hydrogen ratio is variable over a range of two orders of magnitude, and has a well established average near 0.045. The  $^3\text{He}/^4\text{He}$  ratio measured by Vela also is variable; an upper limit as low as  $2 \times 10^{-4}$  has been observed, while on other occasions the ratio exceeds  $10^{-3}$ . Geiss *et al.* [1970b] have observed  $^3\text{He}/^4\text{He}$  ratios



of  $5.4 \times 10^{-4}$  and  $4.1 \times 10^{-4}$  from the Apollo 11 and 12 solar wind experiments. These authors consider the variation to be real.

The temperatures of ion species above  $^4\text{He}^{+2}$  cannot be determined from the Vela 5 data given here, because of the narrow E/Q widths. It is clear that the tempera-

tures are lower than the ratios of masses of the heavier ions to hydrogen multiplied by the hydrogen temperature. In Vela 3 examples, directional distributions were also determined, from which transverse temperatures can be estimated. Again, heavier ions appear to generally have lower temperatures than the ratios of masses times the hydrogen temperature, but the accuracy of the result is limited by the fact that experimental widths are close to instrumental widths.

**Table 7** Ion species identified in solar wind

$^1\text{H}^+$	} Mariner 2, two groups in E/Q spectrum
$^4\text{He}^{+2}$	
	} Vela 3, second group higher mass
	} Explorer 34, M/Q analysis
$^3\text{He}^{+2}$	} Vela 3, E/Q spectrum
$^4\text{He}^+ ?$	
$^{14}\text{N}^{+6}$	Vela 5, E/Q spectrum
$^{16}\text{O}^{+6} - ^{16}\text{O}^{+7}$	Vela 3, E/Q spectrum
$^{28}\text{Si}^{+7} - ^{28}\text{Si}^{+9}$	} Vela 5, E/Q spectrum
$^{56}\text{Fe}^{+7} - ^{56}\text{Fe}^{+12}$	

**Table 8** Elements and isotopes identified in the solar wind

$^1\text{H}$	} Mariner 2, two groups in E/Q spectrum
$^4\text{He}$	
	} Vela 3, second group higher mass
	} Explorer 34, M/Q analysis
	} Apollo foil (mass spectrometer)
$^3\text{He}$	} Vela 3 E/Q spectrum, Apollo foil
$^{14}\text{N}$	
$^{16}\text{O}$	Vela 5 E/Q spectrum
$^{20}\text{Ne}$	} Vela 3 E/Q spectrum
$^{21}\text{Ne}$	
$^{22}\text{Ne}$	} Apollo foil, mass spectrometer
$^{28}\text{Si}$	
$^{56}\text{Fe}$	} Vela 5 E/Q spectrum

**Table 9** Corona and solar wind relative abundances

	Corona abundance	Solar wind abundance
$^{12}\text{C}$	2.00	--
$^{14}\text{N}$	.24	--
$^{16}\text{O}$	1.00	1.00
$^{20}\text{Ne}$	.14	.1
$^{24}\text{Mg}$	.12	--
$^{28}\text{Si}$	.20	.21
$^{32}\text{S}$	.08	--
$^{56}\text{Fe}$	.20	.17

## ACKNOWLEDGMENTS

The author wishes to thank Drs. J. R. Asbridge, A. J. Hundhausen, and M. D. Montgomery for discussions pertinent to this review. The assistance of Dr. P. D. Kearney of Colorado State University with some of the previously unpublished Vela data is gratefully acknowledged. The Vela portions of data presented here were obtained from the Vela nuclear test detection satellites that have been designed, developed and flown as a part of a joint program of the Advanced Research Projects Agency of the U.S. Department of Defense and the U.S. Atomic Energy Commission. The program is managed by the U.S. Air Force.

## REFERENCES

- Allen, C. W.: *Astrophysical Quantities 30-1*, Athlone Press, Univ. London, London, England, 1963.
- Allen, J. W.; and Dupree, A. K.: Calculations of Ionization Equilibria for Oxygen, Neon, Silicon, and Iron. *Astrophys. J.*, Vol. 155, 1969, p. 27.
- Asbridge, J. R.; Bame, S. J.; and Strong, I. B.: Outward Flow of Protons from the Earth's Bow Shock. *J. Geophys. Res.*, Vol. 73, 1968, p. 5777.
- Bame, S. J.; Asbridge, J. R.; Felthausen, H. E.; Hones, E. W.; and Strong, I. B.: Characteristics of the Plasma Sheet in the Earth's Magnetotail. *J. Geophys. Res.*, Vol. 72, 1967, p. 113.
- Bame, S. J.; Hundhausen, A. J.; Asbridge, J. R.; and Strong, I. B.: Solar Wind Ion Composition. *Phys. Rev. Lett.*, Vol. 20, 1968a, p. 393.
- Bame, S. J.; Asbridge, J. R.; Hundhausen, A. J.; and Strong, I. B.: Solar Wind and Magnetosheath Observations During the Jan. 13-14, 1967, Geomagnetic Storm. *J. Geophys. Res.*, Vol. 73, 1968b, p. 5761.
- Bame, S. J.; Asbridge, J. R.; Hundhausen, A. J.; and Montgomery, M. D.: Solar Wind Ions:  $^{56}\text{Fe}^{+8}$  to  $^{56}\text{Fe}^{+12}$ ,  $^{28}\text{Si}^{+7}$ ,  $^{28}\text{Si}^{+8}$ ,  $^{28}\text{Si}^{+9}$ , and  $^{16}\text{O}^{+6}$ . *J. Geophys. Res.*, Vol. 75, 1970, p. 6360.
- Baschek, B.; Garz, T.; Richter, J.; and Holweger, H.: Experimentelle Oszillatorenstärken von Fe II-Linien und die Solare Eisenhäufigkeit. *Astron. Astrophys.*, Vol. 4, 1970, p. 229.

- Bertsch, D. L.; Fichtel, C. E.; and Reames, D. V.: Relative Abundance of Iron-Group Nuclei in Solar Cosmic Rays. *Astrophys. J.*, Vol. 157, 1969, p. L53.
- Biswas, S.; Fichtel, C. E.; and Guss, D. E.: Solar Cosmic Ray Multiply Charged Nuclei and the July 18, 1961, Solar Event. *J. Geophys. Res.*, Vol. 71, 1966, p. 4071.
- Bühler, F.; Eberhardt, P.; Geiss, J.; and Meister, J.: Apollo 11 Solar Wind Composition Experiment: First Results. *Science*, Vol. 166, 1969, p. 1502.
- Cameron, A. G. W.: A New Table of Abundance of the Elements in the Solar System. *Origin and Distribution of the Elements*, edited by L. H. Ahrens, Pergamon Press, New York, 1968, pp. 125-143.
- Cummings, W. D.; and Coleman, P. J., Jr.: Magnetic Fields in the Magnetopause and Vicinity at Synchronous Altitude. *J. Geophys. Res.*, Vol. 73, 1968, p. 5699.
- Coon, J. H.: Vela Satellite Measurements of Particles in the Solar Wind and the Distant Geomagnetosphere. *Radiation Trapped in the Earth's Magnetic Field*, edited by B. M. McCormac, D. Reidel, New York, 1966, p. 231.
- Cox, D. P.; and Tucker, W. H.: Ionization Equilibrium and Radiative Cooling of a Low Density Plasma. *Astrophys. J.*, Vol. 157, 1969, p. 1157.
- Davis, R., Jr.; Harmer, D. S.; and Hoffman, K. C.: Search for Neutrinos From the Sun. *Phys. Rev. Lett.*, Vol. 20, 1968, p. 1205.
- Demarque, P. R.; and Percy, J. R.: A Series of Solar Models. *Astrophys. J.*, Vol. 140, 1964, p. 541.
- Durgaprasad, N.; Fichtel, C. E.; Guss, D. E.; and Reames, D. V.: Nuclear-Charge Spectra and Energy Spectra in the Sept. 2, 1966, Solar-Particle Event. *Astrophys. J.*, Vol. 154, 1968, p. 307.
- Fedoretz, V. A.; and Ezerskii, V. N.: *Circ. Kharkov. Obs.*, Vol. 18, 1953, p. 10.
- Formisano, V.; Palmiotto, F.; and Moreno, G.:  $\alpha$ -Particle Observations in the Solar Wind. *Solar Phys.*, Vol. 15, 1970, p. 479.
- Garz, T.; Holweger, H.; Kock, M.; and Richter, J.: Revision der solaren eisenhaufigkeit und ihre bedeutung das modell der sonnenphotosphäre. *Astron. Astrophys.*, Vol. 2, 1969a, p. 446.
- Garz, T.; Kock, M.; Richter, J.; Baschek, B.; Holweger, H.; and Unsöld, A.: Abundances of Iron and Some Other Elements in the Sun and in Meteorites. *Nature*, Vol. 223, 1969b, p. 1254.
- Gaustad, J. E.: The Solar Helium Abundance. *Astrophys. J.*, Vol. 139, 1964, p. 406.
- Geiss, J.; Hirt, P.; and Lentwyler, H.: On Acceleration and Motion of Ions in Corona and Solar Wind. *Solar Phys.*, Vol. 13, 1970a, p. 183.
- Geiss, J.; Eberhardt, P.; Bühler, F.; Meister, J.; and Signer, P.: Apollo 11 and 12 Solar Wind Composition Experiments: Fluxes of He and Ne Isotopes. *J. Geophys. Res.*, Vol. 75, 1970b, p. 5972.
- Goldberg, L.; Müller, E. A.; and Aller, L. H.: The Abundances of the Elements in the Solar Atmosphere. *Astrophys. J. Supp.*, Vol. 5, 1960, p. 1.
- Gosling, J. T.; Asbridge, J. R.; Bame, S. J.; and Strong, I. B.: Vela 2 Measurements of the Magnetopause and Bow Shock Positions. *J. Geophys. Res.*, Vol. 72, 1967a, p. 101.
- Gosling, J. T.; Asbridge, J. R.; Bame, S. J.; Hundhausen, A. J.; and Strong, I. B.: Measurements of the Interplanetary Solar Wind During the Large Geomagnetic Storm of April 17-18, 1965. *J. Geophys. Res.*, Vol. 72, 1967b, p. 1813.
- Grevesse, N.: Ph.D. Thesis, Liege, 1969.
- Grevesse, N.; and Swings, J. P.: Forbidden Lines of Fe II in the Solar Photospheric Spectrum. *Astron. Astrophys.*, Vol. 2, 1969, p. 28.
- Hirshberg, J.; Alksne, A.; Colburn, D. S.; Bame, S. J.; and Hundhausen, A. J.: Observation of a Solar-Flare-Induced Interplanetary Shock and Helium-Enriched Driver Gas. *J. Geophys. Res.*, Vol. 75, 1970a, p. 1.
- Hirshberg, J.; Bame, S. J.; and Robbins, D. E.: Helium Enriched Interplanetary Medium and Solar Flares. *Trans. Amer. Geophys. Union*, Vol. 51, 1970b, p. 818.
- Holzer, T. E.; and Axford, W. I.: Solar Wind Ion Composition. *J. Geophys. Res.*, Vol. 75, 1970a, p. 6354.
- Holzer, T. E.; and Axford, W. I.:  $\text{He}^+$  Ions in the Solar Wind. *Trans. Amer. Geophys. Union*, Vol. 51, 1970b, p. 411.
- Hundhausen, A. J.; Asbridge, J. R.; Bame, S. J.; Gilbert, H. E.; and Strong, I. B.: Vela 3 Satellite Observations of Solar Wind Ions: A Preliminary Report. *J. Geophys. Res.*, Vol. 72, 1967, p. 87.
- Hundhausen, A. J.; Gilbert, H. E.; and Bame, S. J.: Ionization State of the Interplanetary Plasma. *J. Geophys. Res.*, Vol. 73, 1968, p. 5485.
- Hundhausen, A. J.: Composition and Dynamics of the Solar Wind Plasma. *Rev. Geophys. Space Phys.*, Vol. 8, 1970, p. 729.
- Iben, Icko, Jr.: The  $\text{Cl}^{37}$  Solar Neutrino Experiment and the Solar Helium Abundance. *Ann. Phys.*, Vol. 54, 1969, p. 164.

- Jordan, C.: The Relative Abundance of Silicon, Iron, and Nickel in the Solar Corona. *Mon. Notic. Roy. Astron. Soc.*, Vol. 132, 1966, p. 463.
- Jordan, C.: The Ionization Equilibrium of Elements Between Carbon and Nickel. *Mon. Notic. Roy. Astron. Soc.*, Vol. 142, 1969, p. 501.
- Kavanagh, L. D., Jr.; Schardt, A. W.; and Roelof, E. C.: Solar Wind and Solar Energetic Particles: Properties and Interactions. *Rev. Geophys. Space Phys.*, Vol. 8, 1970, p. 389.
- Lambert, D. L.: Abundance of Helium in the Sun. *Nature*, Vol. 215, 1967, p. 43.
- Lange, J.; and Scherb, F.: Ion Abundances in the Solar Wind. *J. Geophys. Res.*, Vol. 75, 1970, p. 6350.
- Lazarus, A. J.; Bridge, H. S.; and Davis, J.: Preliminary Results from the Pioneer 6 MIT Plasma Experiment. *J. Geophys. Res.*, Vol. 71, 1966, p. 3787.
- Lazarus, A. J.; and Binsack, J. H.: Observations of the Interplanetary Plasma Subsequent to the July 7, 1966, Proton Flare. *Ann. IQSY*, Vol. 3, 1969, p. 378.
- Malville, J. M.; and Schmahl, E. J.: Photoelectric Measurements of the Green Coronal Line During the Eclipse of November 2, 1966. *Solar Phys.*, Vol. 4, 1968, p. 224.
- Montgomery, M. D.; Asbridge, J. R.; and Bame, S. J.: Vela 4 Plasma Observations Near the Earth's Bow Shock. *J. Geophys. Res.*, Vol. 75, 1970, p. 1217.
- Morton, D. C.: The Abundance of Helium in A- and B-Type Stars. *Astrophys. J.*, Vol. 151, 1968, p. 285.
- Nakada, M. P.: A Study of the Composition of the Solar Corona and Solar Wind. *Solar Phys.*, Vol. 14, 1970, p. 457.
- Neugebauer, M.; and Snyder, C. W.: Mariner 2 Observations of the Solar Wind, 1, Average Properties. *J. Geophys. Res.*, Vol. 71, 1966, p. 4469.
- Nikolski, G. M.: The Energy Distribution in the Solar EUV Spectrum and Abundance of Elements in the Solar Atmosphere. *Solar Phys.*, Vol. 6, 1969, p. 399.
- Nussbaumer, H.; and Swings, J. P.: [Fe II] Magnetic Dipole Transition Probabilities and the Problem of the Solar Iron Abundance. *Astron. Astrophys.*, Vol. 7, 1970, p. 455.
- Ogilvie, K. W.; Burlaga, L. F.; and Wilkerson, T. D.: Plasma Observations on Explorer 34. *J. Geophys. Res.*, Vol. 73, 1968a, p. 6809.
- Ogilvie, K. W.; McIlwraith, N.; and Wilkerson, T. D.: A Mass-Energy Analyzer for Space Plasmas. *Rev. Sci. Instrum.*, Vol. 39, 1968b, p. 441.
- Ogilvie, K. W.; and Wilkerson, T. D.: Helium Abundance in the Solar Wind. *Solar Phys.*, Vol. 8, 1969, p. 435.
- Parker, E. N.: Comments on Coronal Heating. *The Solar Corona*, edited by J. W. Evans, Academic Press, New York, 1963.
- Pecker, J. C.; and Pottasch, S. R.: On the Abundance Determination in the Solar Chromosphere. *Astron. Astrophys.*, Vol. 2, 1969, p. 81.
- Pottasch, S. R.: On the Chemical Composition of the Solar Corona. *Mon. Notic. Royal Astron. Soc.*, Vol. 128, 1964, p. 73.
- Pottasch, S. R.: The Inclusion of Dielectronic Recombination Processes in the Interpretation of the Solar Ultraviolet Spectrum. *Bull. Astron. Inst. Neth.*, Vol. 19, 1967, p. 113.
- Pottasch, S. R.: *Origin and Distribution of the Elements*, Edited by L. H. Ahrens, Pergamon Press, London, 1968.
- Robbins, D. E.; Hundhausen, A. J.; and Bame, S. J.: Helium in the Solar Wind. *J. Geophys. Res.*, Vol. 75, 1970, p. 1178.
- Rogerson, J. B.: On the Abundance of Iron in the Solar Photosphere. *Astrophys. J.*, Vol. 158, 1969, p. 797.
- Ross, J.: Abundance of Iron in the Solar Photosphere. *Nature*, Vol. 225, 1970, p. 610.
- Sears, R. L.: Helium content and Neutrino Fluxes in Solar Models. *Astrophys. J.*, Vol. 140, 1964, p. 477.
- Snyder, C. W.; and Neugebauer, M.: Interplanetary Solar Wind Measurements by Mariner 2. *Space Res.*, Vol. 4, 1964, p. 89.
- Tucker, W. H.; and Gould, R. J.: Radiation from a Low Density Plasma at  $10^6$ - $10^8$ °K. *Astrophys. J.*, Vol. 144, 1966, p. 244.
- Unsöld, A. O. J.: Stellar Abundances and Origin of Elements. *Science*, Vol. 163, 1969, p. 1015.
- Urey, H. C.: The Abundance of the Elements with Special Reference to the Problem of the Iron Abundance. *Quart. J. Roy. Astron. Soc.*, Vol. 8, 1967, p. 23.
- Weymann, R.; and Sears, R. L.: The Depth of the Convective Envelope on the Lower Main Sequence and the Depletion of Lithium. *Astrophys. J.*, Vol. 142, 1965, p. 174.
- Whang, Y. C.; and Chang, C. C.: An Inviscid Model of the Solar Wind. *J. Geophys. Res.*, Vol. 70, 1965, p. 4175.
- Widing, K. G.; and Sandlin, G. D.: Analysis of the Solar Spectrum in the Spectral Range 33-110 Å. *Astrophys. J.*, Vol. 152, 1968, p. 545.
- Withbroe, G. L.: The Photospheric Abundance of Iron. *Solar Phys.*, Vol. 9, 1969, p. 19.

- Wolfe, J. H.; and Silva, R. W.: Explorer 14 Plasma Probe Observations During the Oct. 7, 1962, Geomagnetic Disturbance. *J. Geophys. Res.*, Vol. 70, 1965, p. 3575.
- Wolfe, J. H.; Silva, R. W.; McKibbin, D. D.; and Mason, R. H.: The Compositional, Anisotropic, and Non-radial Flow Characteristics of the Solar Wind. *J. Geophys. Res.*, Vol. 71, 1966, p. 3329.

**DISCUSSION** *B. M. McCormac* To what extent did you consider autoionization in your predictions of the various species?

*S. J. Bame* I believe autoionization was considered by Allen, Dupree, and Jordan in their calculations. I have not made those calculations myself.

*B. M. McCormac* This should make a substantial difference, particularly in the nitrogen oxygen species.

*W. F. Feldman* You mentioned that there was one unimpeachable spectrum for helium plus and mentioned in your original paper a density of  $3 \times 10^{-3}$ . Could you quote an error bar?

*S. J. Bame* I wouldn't want to say it's unimpeachable.

*W. F. Feldman* Well, you said it couldn't be explained as silicon and it is anomalous.

*S. J. Bame* We can't explain it as silicon. It kept appearing in successive spectra, so it's very difficult to believe it wasn't there. With respect to the error, I think there was something on the order of about 50 counts in the peak of the sum spectra. So it's not of very high accuracy statistically.

*G. E. Thomas* Concerning the problem with presence of  $\text{He}^+$  in the solar wind, I understand from the publications concerning this that one of the explanations for it was  $\text{He}^{++}$  charge exchanging with neutral hydrogen.

*S. J. Bame* Yes.

*G. E. Thomas* Presumably the neutral hydrogen would come from the interstellar medium, and, as I understand, you noticed a flux of  $\sim 2 \times 10^6 \text{ cm}^{-2} \text{ sec}^{-1}$ . In our Lyman- $\alpha$  scattering measurements of neutral hydrogen it's difficult for us to understand such high fluxes, and we think probably a more realistic number would be 10 to  $10^2$  times less than that. I think the theoretical support is weak also.

*S. J. Bame* That is correct. There have been two suggestions as to possible causes of the  $\text{He}^+$  peak, one being charge exchange with interstellar hydrogen and the other charge exchange with interplanetary hydrogen. But one of the problems is that neither of these mechanisms, it seems to me, explains the fact that it is there sometimes and other times it is not.

*T. E. Holzer* We suggest a mechanism by which  $\text{He}^+$  from interstellar space is photoionized; I think that that will fit in with your Lyman- $\alpha$  observations.

*G. W. Simon* You showed a neon value. Is that from Geiss's work?

*S. J. Bame* Yes, that's Geiss's work. You may recall the last spectrum I showed (fig. 19) where we actually were able to see a little structure between the helium peak and the oxygen peak; the neon is in the valley between the group that we call  $\text{N}^{6+}$  and  $\text{O}^{7+}$ . We are just unable to resolve it so I would guess off-hand that the value of 0.1 that Geiss has given for its abundance relative to oxygen is probably reasonable.

*J. Geiss* When you have a high flux of helium, as in a driver gas, is the oxygen also enhanced relative to the hydrogen?

*S. J. Bame* I would guess that the answer to that question is yes, but it's a little questionable. Most of the times that we've been able to see the heavy ions have been times when the helium was particularly abundant. I don't think we have looked at many cases in which the helium is not very abundant as we cannot see the heavier ions at those times.

# ELEMENTAL AND ISOTOPIC ABUNDANCES IN THE SOLAR WIND *Johannes Geiss* An invited review

The use of collecting foils and lunar material to assay the isotopic composition of the solar wind is reviewed. Arguments are given to show that lunar surface correlated gases are likely to be most useful in studying the history of the solar wind, though the isotopic abundances are thought to give a good approximation to the solar wind composition. The results of the analysis of Surveyor material are also given. The conditions leading to a significant component of the interstellar gas entering the inner solar system are reviewed and suggestions made for experimental searches for this fraction. A critical discussion is given of the different ways in which the basic solar composition could be modified by fractionation taking place between the sun's surface and points of observation such as on the Moon or in interplanetary space. An extended review is made of the relation of isotopic and elemental composition of the interplanetary gas to the dynamic behavior of the solar corona, especially processes leading to fractionation. Lastly, connection is made between the subject of composition, nucleosynthesis and the convective zone of the sun, and processes leading to modification of initial accretion of certain gases on the Earth and Moon.

## ABSTRACT

## INTRODUCTION

During the last few years, the compositional aspect of the solar wind has been given increasing attention. While it had been established for quite some time [Snyder and Neugebauer, 1964; Wolfe *et al.*, 1966; Hundhausen *et al.*, 1967a; Ogilvie *et al.*, 1968] that a rather variable proportion of  $\text{He}^4$  is present in the solar wind, other ions have been found only recently. By means of high-resolution electrostatic analyzers, Bame *et al.* [1968] measured oxygen and also detected  $\text{He}^3$  during periods of low solar wind ion temperature, and Bame *et al.* [1970] showed that multiply charged Si and Fe are present during such periods. Geiss *et al.* [1970c] gave the abundances of the helium and neon isotopes during the Apollo 11 and 12 lunar landings, using a foil collection technique.

The He/H ratio in the solar wind is highly variable, values between 0.01 and 0.25 having been observed

[Hundhausen *et al.*, 1967a] with an average of about 0.04 [Neugebauer and Snyder, 1966; Ogilvie and Wilkerson, 1969; Robbins *et al.*, 1970]. Bame *et al.* [1968] reported variations in the O/Ne and  $\text{He}^4/\text{He}^3$  ratios, and Geiss *et al.* [1970c] in the  $\text{He}^4/\text{He}^3$  and  $\text{He}^4/\text{Ne}^{20}$  ratios, but there is yet very little statistical information for an assessment of the variability in the abundance of the rare ions.

The reasons for the generally observed variations of the He/H ratio in the solar wind are not clear. It is unknown so far whether heavier ions such as neon, argon, and iron show similar or even larger variations in their abundances or whether their abundances tend to be rather constant, relative to either hydrogen or helium. A comprehensive study of abundances and abundance variations in the solar wind that include several ion species should give much and unique information on processes taking place near the sun. The relative abundances of ions in the solar wind are not likely to be as much affected in interplanetary space as are other solar wind parameters such as the temperatures of ions and

---

*The author is at the Physikalisches Institut, University of Bern, Bern, Switzerland.*

electrons [Sturrock and Hartle, 1966; Forslund, 1970] and their anisotropy [Wolfe *et al.*, 1966; Hundhausen *et al.*, 1967b]. The abundances and abundance variations of a number of solar wind ions have to be measured if the mechanisms causing the variations are to be understood. The various mechanisms are expected to deplete or enrich different ion species in quite different ways. The charge/mass ratio of the ion ( $Z/A$ ) would enter into separation processes caused by quasistatic electromagnetic fields. Simple gravitational escape would depend primarily on the mass. Diffusion processes in the photosphere-corona boundary region depend strongly on the degree of ionization [Delache, 1965, 1967; Jokipii, 1965, 1966a; Nakada, 1969]. If dynamical friction is significant in the solar wind acceleration region, a factor similar to  $Z^2/A$  is important [Geiss *et al.*, 1970a]. Separation effects depending primarily on the ionization energy as suggested by Lehnert [1970] and Arrhenius and Alfvén [1971] should give large variations in element abundances, but would have relatively small effects on isotopic abundances. On the other hand, wave-particle interactions could lead to mass fractionation, including isotopic fractionation. Abundance correlation studies in the solar wind of the noble gas isotopes and of O, Si, and Fe with their wide range in  $Z$  and  $A$  should eventually enable us to distinguish between the various processes if these ions can be sampled often enough.

Only when the fractionation processes discussed above are sufficiently well understood can we begin to draw conclusions about solar abundances from solar wind abundance measurements. This is true not only for the relations between elements but also for isotopic ratios. A long time average of abundance ratios does not necessarily give the true solar abundance because the fractionation processes might well introduce a systematic bias.

## HELIUM AND NEON ISOTOPES

During the Apollo 11, 12, and 14 landings an aluminum foil was exposed at the lunar surface to collect solar wind particles for subsequent analysis in the laboratory. The concept of this Solar Wind Composition (SWC) experiment and experimental techniques were given by Signer *et al.* [1965], Bühler *et al.* [1966], Meister [1969], and Geiss *et al.* [1969]. For collection times of the order of a few days, the method is virtually restricted to noble gases, but it yields precise results not only for elemental abundances but also for isotopic compositions. Noble gas measurements in the solar wind are of particular importance because (1) their abundances in the sun are difficult to determine spectroscopically; (2) a contribution from infalling meteorites

can be definitely excluded; and (3) by comparative measurements in telluric and meteoritic matter the most interesting and puzzling isotope anomalies have been found in the noble gases.

Results on the fluxes of the He and Ne isotopes in the solar wind obtained from the Apollo 11 and Apollo 12 SWC experiments have been published by Bühler *et al.* [1969] and Geiss *et al.* [1970b, c]. They are summarized in table 1. Geiss *et al.* [1970c] have concluded that the relative abundances obtained from these experiments were not seriously affected by near-lunar perturbations, and that in particular the differences in the observed  $\text{He}^4/\text{He}^3$  and  $\text{He}^4/\text{Ne}^{20}$  ratios correspond to real variations in the abundances of the undisturbed solar wind. This conclusion was based on the observed distribution of the angles of incidence of  $\text{He}^4$  (fig. 1), the correlation between the  $\text{He}^4/\text{He}^3$  and  $\text{He}^4/\text{Ne}^{20}$  ratios [Geiss *et al.*, 1970c], and the undisturbed nature of the proton flow observed in near lunar space [Siscoe *et al.*, 1969; Freeman *et al.*, 1970; Clay *et al.*, 1971].

In table 1, the proton flux as observed by Bame and Hundhausen [1970] during the Apollo 12 foil exposure period is used to derive the He/H ratio. Note that the He/H ratio calculated from the results of these two different experiments is close to the established long-time average of about 0.04.

**Table 1.** Fluxes and ion abundance ratios determined for the Apollo 11 and Apollo 12 foil exposure periods (July 21, 1969, 03:35 – 04:52 GMT, and November 19, 1969, 12:35 GMT – Nov. 20, 1969, 07:17 GMT)

[The He/H ratio has been calculated by combining the Apollo 12 SWC He and the Vela proton data which were obtained simultaneously [Bame and Hundhausen, 1970]. Fluxes are given in  $\text{cm}^{-2} \text{sec}^{-1}$ .]

	Apollo 11	Apollo 12
	(Fluxes in $\text{cm}^{-2} \text{sec}^{-1}$ )	
$\text{He}^4$ – Flux	$(6.2 \pm 1.2) \times 10^6$	$(8.1 \pm 1.0) \times 10^6$
$\text{He}^3$ – Flux	$(3.3 \pm 0.7) \times 10^3$	$(3.3 \pm 0.4) \times 10^3$
$\text{Ne}^{20}$ – Flux	$(14 \pm 4) \times 10^3$	$(13 \pm 2) \times 10^3$
$\text{He}^4/\text{H}^1$	---	0.043
$\text{He}^4/\text{He}^3$	$1860 \pm 140$	$2450 \pm 100$
$\text{He}^4/\text{Ne}^{20}$	$430 \pm 90$	$620 \pm 70$
$\text{Be}^{20}/\text{Ne}^{22}$	$13.5 \pm 1.0$	$13.1 \pm 0.6$
$\text{Ne}^{22}/\text{Ne}^{21}$	---	$26 \pm 12$

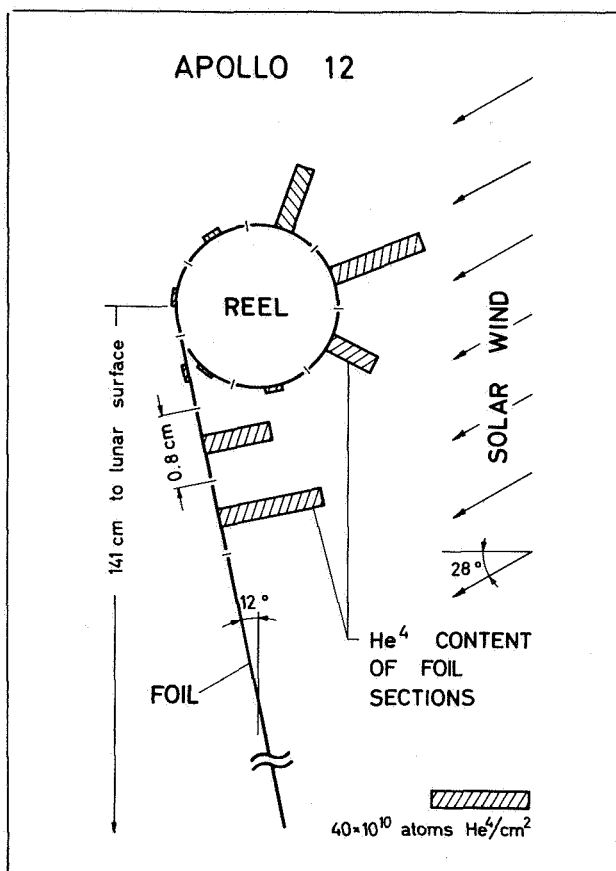


**Figure 1.** The upper part of the Apollo 12 SWC foil as it was exposed at the lunar surface. The uppermost part of the foil remained rolled around the reel, allowing a determination of the distribution of the angles of incidence of He<sup>4</sup>. The shaded bars represent the measured areal concentrations of He<sup>4</sup> in the foil pieces. The observed distribution corresponds to a distinctly directional flow and is compatible with a helium temperature below 10<sup>6</sup> °K. After Geiss et al., 1970b.

#### OXYGEN, SILICON, AND IRON

During periods of low solar wind ion temperature, O<sup>6+</sup> and O<sup>7+</sup>, Si<sup>7+</sup> to Si<sup>9+</sup>, and Fe<sup>8+</sup> to Fe<sup>12+</sup> have been identified by the Los Alamos group using the high-resolution solar wind energy/charge spectrometers on board the Vela satellites [Bame et al., 1968, 1970]. The abundances and abundance variations of these ions and their charge distributions are discussed and given in detail in the preceding paper. The elemental abundances

relative to oxygen derived by [Bame et al., 1968, 1970] are listed in table 2.

**Table 2.** He, O, Si, and Fe abundances in the solar wind obtained from the Vela 3 and 5 experiments [after Bame et al., 1968, 1970]

Spacecraft	Time	H	He	O	Si	Fe
Vela 3	Average of four spectra Oct. 8, 1965 to March 23, 1966	---	55	1	---	---
Vela 5	July 6, 1969 2222 - 2251 UT	5000	150	1	0.21	0.17

#### SOLAR WIND PARTICLES EMBEDDED IN FINE MATERIAL AT THE LUNAR SURFACE

There is very striking evidence that the fine material and many breccias found at the lunar surface are loaded with solar wind particles. In particular, the embedded hydrogen and noble gases can be recognized as being of solar origin because of their very low abundance in lunar surface rocks. From the low D/H ratios obtained, it can be concluded that most of the hydrogen found in the lunar fine material is in fact of solar wind origin [Epstein and Taylor, 1970; Friedman et al., 1970; Hintenberger et al., 1970]. The lowest D/H ratio reported so far is 9 times lower than the ratio in ocean water [Epstein and Taylor, 1970].

The relatively large amounts of noble gases found in breccias and lunar dust are concentrated in the outer layers of the individual grains. By means of etching experiments, Eberhardt et al. [1970] have shown that in the mineral ilmenite the noble gases from helium to xenon are essentially contained in the outermost 0.2 μ of the individual crystals (fig. 2). The range of solar wind particles in materials like ilmenite is estimated to be 0.03 to 0.15 μ.

The lunar dust contains solar wind particles down to a depth of at least 45 cm. As the lunar surface is gardened by impacts of all sizes and probably by other mechanisms, successive layers of grains come to the surface and are exposed to the solar wind.

Although there is a great quantity of solar wind matter at the lunar surface suitable for extensive studies, experimental data cannot easily be translated into solar wind abundances. From the observations it is obvious that the light noble gases have been depleted relative to the heavy ones by temperature diffusion and perhaps also by saturation effects (cf. table 8). Helium released

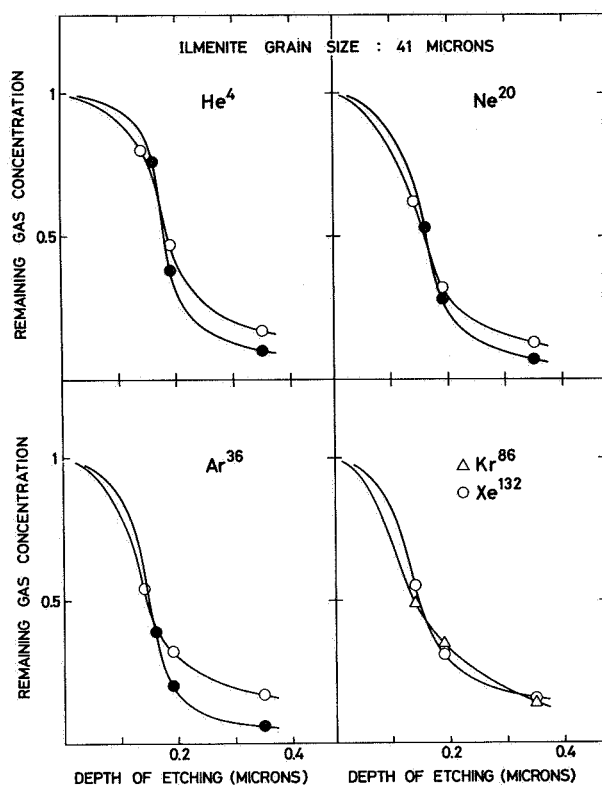


**Figure 2.** Noble gas concentrations (per gm) measured in a 41  $\mu$  ilmenite grain size fraction separated from Apollo 11 fine material (No. 10084) after removal of a thin surface layer by etching with HF. The horizontal axis is equivalent to the thickness of the layer removed from the surface of the individual grains. The vertical axis gives the concentration in the unetched ilmenite. The two curves for He<sup>4</sup>, Ne<sup>20</sup> and Ar<sup>36</sup> represent the two independent sets of etching experiments performed [after Eberhardt et al., 1970].

**Table 3.** Solar wind isotopic compositions inferred from trapped gases in lunar surface fine material

[For literature and origin of these data see text.]

He <sup>4</sup> /He <sup>3</sup>	2700±100
Ne <sup>20</sup> /Ne <sup>22</sup>	12.85±0.1
Ne <sup>20</sup> /Ne <sup>21</sup>	400±11
Ar <sup>36</sup> /Ar <sup>38</sup>	5.32±0.08
Ar <sup>40</sup> /Ar <sup>36</sup>	<0.15
Kr	Similar to terrestrial
Xe	See figure 4

to the lunar atmosphere will mostly escape before it becomes ionized. Heavier gases cannot escape gravitationally. They will be ionized within a few weeks and then accelerated by the electromagnetic field of the solar wind [Michel, 1964]. In this way, most of these gases escape, but a fraction is re-embedded in the lunar soil. The relatively high abundance of Ar<sup>40</sup> is thought to be the result of such re trapping [Heymann et al., 1970; Eberhardt et al., 1970; Heymann and Yaniv, 1970; Manka and Michel, 1970]. In a similar way other constituents of a steady-state or transient lunar atmosphere, such as old solar wind particles, products of outgassing of the lunar interior, or gases of cometary origin, may have been embedded in the surface layers of the grains of the lunar fine material. It would be difficult to distinguish them from the directly implanted solar wind particles. Such considerations have led Podosek et al. [1971] to speak of "surface-correlated" (SUCOR) rather than solar wind noble gases. Another possible source for surface correlated gases is the interstellar gas, which is discussed in a later section.

From all these arguments it is seen that the surface-correlated gases should not be considered as an *a priori* source of information on solar wind composition. In the long run, their value will probably lie in giving information on the history of the solar wind and its composition. Nevertheless, all evidence so far points to a solar wind origin of the bulk of the surface-correlated gases, and isotopic—not elemental—abundances are considered to give a good approximation to solar wind abundances.

Since the noble gases in the mineral ilmenite have apparently suffered least from diffusive losses, the isotopic ratios found for the surface-correlated gases in this mineral can be considered the best approximation to solar wind abundances. The results for the He and Ne isotopes and for Ar<sup>36</sup>/Ar<sup>38</sup> as obtained by Eberhardt et al. [1970] are given in table 3; these are discussed in a later section. Because of the re trapping of released lunar radiogenic Ar<sup>40</sup> mentioned above, one can give only an upper limit for the solar wind Ar<sup>40</sup>/Ar<sup>36</sup> ratio. The value obtained by Bloch et al. [1971] is given. The Kr isotopic composition found in the surface-correlated gas of lunar fine material is similar to that in terrestrial Kr [Eberhardt et al., 1970; Pepin et al., 1970; Hohenberg et al., 1970].

The isotopic composition of surface-correlated xenon is not easily assessed because for the lighter isotopes of this element there is a relatively high spallation component produced by cosmic rays and solar flare particles. However, a large difference from the isotopic composition of air xenon is well established [Hohenberg et al., 1970; Pepin et al., 1970; Marti et al., 1970; Eberhardt et



*al.*, 1970; Podosek *et al.*, 1971]. This is evident from the  $\text{Xe}^{128}/\text{Xe}^{130}$  versus  $\text{Xe}^{126}/\text{Xe}^{130}$  correlation diagram of figure 3, where data points represent measured isotopic ratios from samples of ilmenite of different grain size. If the measured gas samples are composed in

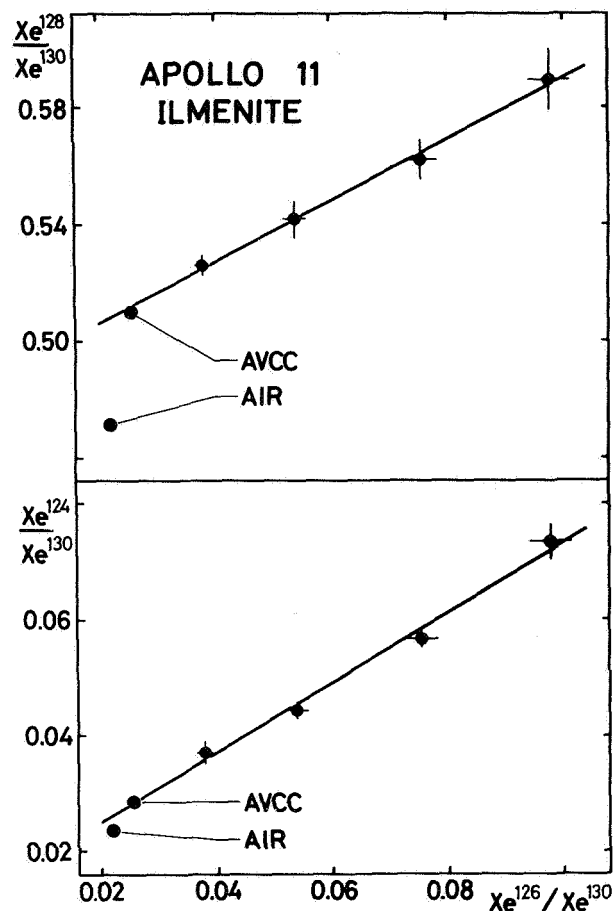


**Figure 3.** Xenon isotope diagram with isotopic ratios obtained in four grain size fractions of ilmenite (22, 41, 65 and 105 microns) separated from Apollo 11 fine material [Eberhardt *et al.*, 1970]. Xenon is a mixture of a spallation component produced in the lunar material by high energy particles, and a trapped component which is thought to be of solar wind origin. Since the latter component is surface correlated, its concentration per gram increases with decreasing grain size, while the spallation component is relatively independent of grain size. It is seen that the trapped xenon cannot have the isotopic composition of air xenon. The figure suggests that the relative abundances of  $\text{Xe}^{126}$ ,  $\text{Xe}^{128}$  and  $\text{Xe}^{130}$  are similar to those found in carbonaceous chondrites (AVCC = average in carbonaceous chondrites).

varying proportions of two isotopically different components, the data should fall on a straight line. It is seen that this is the case, but the straight line does not pass through the air xenon composition point. The surface-correlated xenon in the ilmenite therefore must be different from air xenon. Figure 3 shows that it can be—but does not have to be—identical to the xenon found in carbonaceous chondrites, a meteorite class thought to represent rather primitive solar system material. By making assumptions on the abundance of the spallation component, Eberhardt *et al.* [1970] and Podosek *et al.* [1971] have extrapolated their data to the isotopic composition of surface-correlated xenon in lunar fine material. The results of Podosek *et al.* [1971] are given in figure 4. The errors are an indication of the precision of the measurements and do not include the uncertainties inherent in the extrapolation process. Again a large and yet unexplained difference between surface-correlated and air xenon is obtained, whereas there appears to be agreement with carbonaceous chondrite xenon for the lighter isotopes. The difference in the heavy isotope abundances of AVCC xenon and surface-correlated xenon in lunar dust could be due to a fission component in the carbonaceous chondrites [Reynolds and Turner, 1964]. Dakowski [1969] and Anders and Heymann [1969] have suggested that the origin of this fission component could be due to spontaneous fission of extinct super heavy elements ( $Z \sim 112$ ). Recently, Alexander *et al.* [1971] have shown that the spontaneous fission of  $\text{Pu}^{244}$  gives quite a different xenon isotope spectrum, and therefore fission of a super heavy element seems to be the most likely source of this Xe component.

#### SOLAR WIND GASES TRAPPED IN SURVEYOR 3 MATERIAL

The Surveyor 3 material returned by the Apollo 12 astronauts had been exposed at the lunar surface from April 20, 1967, to November 20, 1969. Bühler *et al.* [1971] performed a preliminary investigation on a small piece of an aluminum tube that was brought back, and they observed the solar wind He and Ne isotopes trapped in this material. The results are shown in table 4. The He/Ne ratio is low in comparison with the Apollo 11 and 12 SWC results, and it is likely that some helium was lost as a result of the repeated severe heating during lunar noon. Also, the possibility that a residual dust contamination on the aluminum has somewhat affected the neon results cannot be excluded. Helium loss by temperature diffusion could also have changed the  $\text{He}^4/\text{He}^3$  isotopic ratio, but Bühler *et al.* [1971] estimate that such a change should not amount to more than 5 to 10 percent.

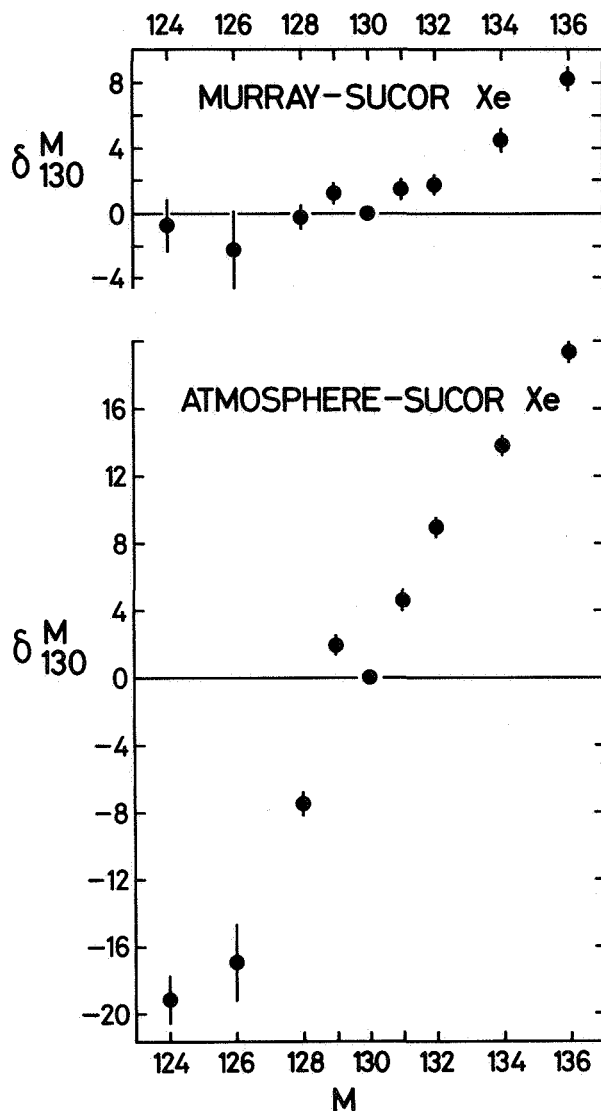


**Figure 4.** Comparison of isotopic composition of atmospheric xenon, xenon extracted from the carbonaceous chondrite "Murray" and surface correlated xenon "SUCOR" in lunar fine material [after Podosek et al., 1971]. The latter is interpreted as consisting essentially of trapped solar wind particles. The isotopic ratios are normalized to  $\text{Xe}^{130}$ . Plotted are the relative deviations in percent of atmospheric xenon and Murray xenon respectively from "SUCOR" xenon.

#### INTERSTELLAR GAS

If neutral, the interstellar gas surrounding the solar system can penetrate into the region of the inner planets. The dynamics has been studied in detail by Fahr [1969] and Blum and Fahr [1970]. These authors have published maps for the expected density of neutral

**Table 4.** Trapped solar wind He and Ne isotopes measured in returned Surveyor 3 aluminum tube [Bühler et al., 1971]

[The significance of these data and the limits of possible abundance falsifications are discussed in the text. The errors given are the analytical errors only.]

$\text{He}^4/\text{He}^3$	$2770 \pm 120$
$\text{He}^4/\text{Ne}^{20}$	$295 \pm 15$
$\text{Ne}^{20}/\text{Ne}^{22}$	$13.3 \pm 0.4$
$\text{Ne}^{22}/\text{Ne}^{21}$	$31 \pm 5$

hydrogen around the sun taking into account losses due to ionization by solar EUV and by the solar wind. Holzer and Axford [1970b] have evaluated and discussed the penetration of interstellar He into the solar system. Recently, Bertaux and Blamont [1971] and Thomas and Krassa [1971] have published contour maps of the observed Lyman- $\alpha$  background radiation. These authors conclude that the interstellar gas moves toward the solar system not from the direction of the solar apex, but from a direction close to the ecliptic plane at about  $270^\circ$  ecliptic longitude. The number density of interstellar hydrogen in the vicinity of the sun but outside its sphere of influence is estimated to be 0.05 to  $0.10 \text{ cm}^{-3}$  [Blamont, 1971]. We shall adopt here the value  $0.08 \text{ cm}^{-3}$ .

From the magnitude of the peculiar motion of the sun, the velocity of the gas  $v_O$  is assumed to be of the order of 20 km/sec. The flux of the interstellar gas is focused by the gravitational field of the sun to an extent determined by  $GM_\odot/v_O^2 r$ . For noble gases the radiation pressure effect ought to be small and therefore is not considered here. During the summer months, the earth is in the upstream position with respect to the interstellar gas flow, and it can readily be shown that in this case the flux is given by

$$F = n_O v_O \left\{ \frac{1}{2} \left[ 1 + \sqrt{1 + (V_\oplus/V_O)^2} \right] \right\}^2 S \quad (1)$$

where  $v_\oplus = 42.1 \text{ km/sec}$  is the escape velocity from the solar gravitational field at 1 AU. With  $v_O = 20 \text{ km/sec}$  we obtain  $F = 2.8 \times n_O v_O S$ .

The survival factor  $S$  takes into account the losses due to ionization by solar EUV and solar wind. Since the fluxes of these radiations are known to fall off with  $r^{-2}$ , the loss equation for particles directly approaching the sun can be integrated to give

$$S = \exp \left[ -2K \frac{r_{\oplus}}{v_{\oplus}} (\langle \sigma f_{\oplus} \rangle_{\text{EUV}} + \langle \sigma f_{\oplus} \rangle_{\text{SW}}) \right] \quad (2)$$

with

$$K = \sqrt{1 + (V_o/V_{\oplus})^2} - V_o/V_{\oplus}$$

For  $v_o = 20$  km/sec, one obtains  $K = 0.63$ . Terms of the form  $\langle \sigma f_{\oplus} \rangle$  are the loss rates due to EUV and solar wind at 1 AU. Numerical values are listed in table 5. The EUV flux and spectrum are taken from *Hinteregger et al.* [1965] and *Hall and Hinteregger* [1970] for wavelengths below and above 270 Å, respectively. The EUV ionization cross sections are given by *Lee and Weissler* [1955].  $\langle \sigma f_{\oplus} \rangle_{\text{SW}}$  has been calculated with the charge exchange and ionization cross sections for 800 eV protons given by *Green and McNeal* [1971], assuming a proton flux of  $2 \times 10^8 \text{ cm}^{-2} \text{ sec}^{-1}$  at 1 AU. We have adopted the abundances in gaseous nebulae [*Aller*, 1961] for the interstellar gas and obtain the neutral fluxes arriving in the upstream (southern) region of the earth orbit as given in table 5. The result for He compares well with the density given by *Holzer and Axford* [1970b], when scaled to the same interstellar density.

Most of these neutral atoms become ionized when further approaching the sun, and are swept back outward by the interplanetary magnetic field, leading to an ionized flux similar in magnitude to the incoming neutral flux. These ions are singly charged, and *Holzer and Axford* [1970a] have suggested that the  $\text{He}^+$  ions sometimes reported in the solar wind are of interstellar origin. *Geiss et al.* [1970a] have pointed out that these ions will have a smaller radial velocity than the solar wind ions and a non-radial velocity component. *Holzer and Axford* [1970b] have noted that  $\text{He}^+$  originating in this way has a very high apparent temperature. Since this  $\text{He}^+$  amounts to only about 1 percent of the solar wind  $\text{He}^{++}$  flux, it appears rather unlikely that it can actually be seen with an electrostatic analyzer unless, as *Holzer and Axford* [1970b] have postulated,  $\text{He}^+$  is sometimes

cooled by interactions with magnetic field irregularities.

A possible way of directly detecting neutral interstellar noble gas atoms at 1 AU is to capture them in a foil flown in near-earth orbit, as on a sky-lab or space station. When the earth is in the upstream position (summer months) the velocity of the incoming neutral atoms relative to a near earth satellite moving in the west-east direction is about 60 km/sec, corresponding to the kinetic energies given in the last column of table 5. At these energies, neon and argon can be captured in an aluminum foil [*Meister*, 1969], although only with relatively low efficiency. A surface composed of lighter elements, such as a beryllium foil, theoretically would give a higher capture probability. At an altitude of 400 to 500 km, absorption, ionization, and charge exchange with the atmosphere are small during the night—when the interstellar atoms should arrive. If the inclination of the satellite orbit is not too high, the flux of trapped or precipitating ions ought to be negligible under quiet conditions. With the flux given in table 5, enough neon for detection and isotopic analysis could be collected with foil exposure times of 1 to 2 months. The survival factor  $S$  for argon depends very strongly on the EUV flux, and to a lesser degree also on the solar wind velocity. Thus, during a quiet solar period  $S$  for argon may be appreciably larger than 14 percent so that argon could become detectable after 1 or 2 months of collection time.

If the interstellar gas in our vicinity has indeed a number density of only  $0.1 \text{ cm}^{-3}$ , the primary (neutral) and secondary (ionized) fluxes of interstellar gases are two orders of magnitude lower than the solar wind flux (*cf.* tables 1 and 5) and therefore should hardly affect the solar wind abundances obtained from the Vela and Apollo SWC experiments. However, number densities larger than  $1 \text{ cm}^{-3}$  occur in interstellar space, and therefore we cannot exclude the possibility that at certain times in the past the interstellar gas may have

**Table 5.** Estimated fluxes of interstellar neutral atoms at the orbit of the earth when the earth is in the upstream position (during summer)

[The  $\langle \sigma f_{\oplus} \rangle$  are the respective loss rates at 1 AU under relatively quiet solar conditions. Also given are impact energies of the atoms on an earth satellite.]

Element	Abundance relative to hydrogen	$\langle \sigma f_{\oplus} \rangle_{\text{EUV}}$ , $10^{-6} \text{ sec}^{-1}$	$\langle \sigma f_{\oplus} \rangle_{\text{SW}}$ , $10^{-6} \text{ sec}^{-1}$	Survival factor $S$ , percent	Flux at 1 AU (upstream), $\text{cm}^{-2} \text{ sec}^{-1}$	Impact energy on satellite, eV
He	0.19	0.048	0.003	81	$7 \times 10^4$	75
Ne	$1.1 \times 10^{-4}$	0.14	0.005	59	30	375
Ar	$8 \times 10^{-6}$	0.24	0.2	14	0.5	675

contributed appreciably to the influx of particles at the lunar surface. These interstellar gases might be detectable on the moon in certain layers of the fine material or in breccias.

### THEORETICAL TREATMENT OF ION MOTION IN CORONA AND SOLAR WIND

Here we review and discuss the question of solar wind abundances and their relationship to solar abundances from the theoretical point of view. *Delache* [1965, 1967], *Jokipii* [1965, 1966a], and more recently *Nakada* [1969] have applied the molecular diffusion equation as given by *Chapman and Cowling* [1958] to the motion of matter from the solar surface into the lower corona. For ions, the thermal diffusion factor  $\alpha_T$  is large and negative [*Chapman*, 1958] and therefore the authors find a tendency for strong enrichment of the heavier ions in the corona relative to the photosphere. However, this effect may be partially obliterated by turbulent mixing or inhibited by magnetic fields. *Nakada* [1969] has estimated the degree of mixing and has concluded that it should not be sufficient to extinguish completely the enrichments resulting from molecular diffusion.

The diffusion equation is not applicable in regions of strong acceleration and when the differences between bulk velocities of different ion species become large. Therefore, its validity is restricted to the lower corona. Other methods must be used in the actual acceleration region of the solar wind.

The general equation of motion derived from the Boltzmann equation has been applied to this problem by *Geiss et al.* [1970a]. They assumed a radial magnetic field direction and stationary, spherically symmetric radial motion. On the basis of *Parker's* [1958, 1963] polytropic expansion model *Geiss et al.* [1970a] discussed the general properties of the equation of motion of a rare ion species in a plasma essentially composed of protons and electrons, and gave numerical solutions.

*Nakada* [1970] has used a more general equation, not assuming  $n_I \ll n_p$ , and has treated the isothermal case. *Alloucherie* [1970] has numerically integrated the equation of ion motion for isothermal expansion and also on the basis of the *Sturrock and Hartle* [1966] two-fluid model for  $r \leq 7 R_\odot$ . With the density and temperature parameters chosen by *Sturrock and Hartle*, the solar wind reaches sonic velocity only at  $r \approx 9 R_\odot$ . Thus *Alloucherie's* [1970] results refer to the subsonic region only. In this region, his results are comparable to those of *Geiss et al.* [1970a] if an appropriate value for the polytropic index ( $\alpha \approx 1.2$ ) is chosen. To keep the problem tractable, all the authors assumed maxwellian velocity distributions. This latter assumption constitutes

the introduction of a hydrodynamic approximation. Such an approximation is applicable only if there are a sufficient number of collisions to maintain a semblance of an equilibrium.

In a proton-electron gas, the mean free path  $\lambda_p$  [*Spitzer*, 1962] for the protons is given by

$$\frac{\lambda_p}{R_\odot} = 0.11 \frac{T^2}{n_p} \quad (3)$$

where  $T$  is in  $10^6$  K,  $n_p$  is in  $10^6 \text{ cm}^{-3}$ , and  $R_\odot$  is the solar radius. If in the proton-electron gas there is a small population of heavier ions with charge  $Ze$  and mass  $Am_p$ , their mean free path  $\lambda(Z, A)$  is

$$\frac{\lambda(Z, A)}{R_\odot} = 0.09 \frac{T^2}{n_p} \frac{A^{1/2}}{Z^2} \quad (4)$$

Thus for  $^{20}\text{Ne}^{8+}$  the mean free path is 17 times smaller than for protons. The corresponding collision times,  $t_D$  are [*Spitzer*, 1962]

$$t_D(\text{Protons}) = 520 \frac{T^{3/2}}{n_p} \text{ sec} \quad (5)$$

and

$$t_D(Z, A) = 410 \frac{T^{3/2}}{n_p} \frac{A}{Z} \text{ sec} \quad (6)$$

( $T$  always in  $10^6$  K and  $n_p$  in  $10^6 \text{ cm}^{-3}$ ). The mean free paths and collision times given in table 6 are based on the densities and proton temperatures obtained from the two-fluid model of *Sturrock and Hartle* [1966]. In evaluating the importance of collisions, one must consider the distance that the ion travels with the local solar wind velocity between two collisions [*Hundhausen*, 1968]. Thus, the number of collisions occurring while the solar wind travels  $1 R_\odot$  is also given in table 6. Note that the number of collisions is four times larger for  $^{20}\text{Ne}^{8+}$  than for protons, and that collisions for neon are quite effective up to a solar distance of  $\sim 10 R_\odot$ —beyond the “sonic point” of the solar wind. Since in the model of *Geiss et al.* [1970a] the physically important region is  $\leq 10 R_\odot$ , the predictions obtained using that model should have physical significance.

#### Ion Acceleration by Coulomb Collisions

In discussing the ion motion in the corona and the solar wind, we follow essentially the treatment given by *Geiss et al.* [1970a] and use the same notation. However, we treat certain aspects more generally and add to the discussion of the physical significance and limits of the model. For treatment of the ion transport in the solar wind acceleration region the following approximations are made:

1. The bulk motions of electrons, protons, and heavier ions are radial and spherically symmetric.

2. Forces due to the magnetic field are neglected.
3. Compared to protons, all other ions have negligible abundances, specifically  $Z^2 n_I \ll n_p = n_e = n$ .
4. The velocity distribution of each particle species is Maxwellian around an individual bulk velocity.
5. The local temperatures of protons and electrons are equal  $T_p = T_e$ . As *Sturrock and Hartle* [1966] have shown, this assumption is probably invalid in the outer corona. However, the electron temperature does not affect the motion of heavier ions very strongly, since collisions with electrons are negligible. In fact,  $T_e$  enters into the equations of ion motion only through the electrical field term, and this term does not dominate the acceleration of heavier ions.

**Table 16.** Mean free paths and collision times. Solar wind parameters after *Sturrock and Hartle* [1966]

r	$\lambda (^{20}\text{Ne}^{8+})$	$t_D (^{20}\text{Ne}^{8+})$ , sec	Collisions while solar wind travels $1 R_\odot$	
			Protons	$^{20}\text{Ne}^{8+}$
$1 R_\odot$	$0.001 R_\odot$	12	---	---
$2 R_\odot$	$0.006 R_\odot$	130	45	180
$5 R_\odot$	$0.010 R_\odot$	320	6	24
$10 R_\odot$	$0.014 R_\odot$	750	1.5	6
$20 R_\odot$	$0.008 R_\odot$	720	1.5	6

In this approximation the equations for stationary motion of a particular ion species are

$$n_I V r^s = \text{const} \quad (7) \quad \text{with}$$

$$v \frac{dv}{dr} + \frac{1}{Am_p n_I} \frac{d}{dr} (n_I k T_I) + \frac{GM_\odot}{r^2} - \frac{ZeE}{Am_p} - C = 0 \quad (8)$$

with the collision term

$$C = \frac{4\pi e^4 \ln \Lambda}{m_p} \frac{n}{kT} \frac{Z^2 A + 1}{A A + \vartheta} G \left[ \left( \frac{A}{A + \vartheta} \frac{m_p}{2kT} \right)^{1/2} (V - v) \right] \quad (9)$$

and the expression for the electrical field

$$\frac{eE}{m_p} = \frac{1}{2} \left( \frac{GM_\odot}{r^2} + V \frac{dV}{dr} \right) \quad (10)$$

where  $v$  is the bulk velocity,  $n_I$  the number density,  $Am_p$  the mass,  $Ze$  the charge, and  $T_I$  the local

temperature of the ions; In  $\Lambda$  is approximately 22 [*Parker*, 1963];  $V$ ,  $n$ , and  $T$  are the corresponding values for the protons;  $T_I/T = \vartheta$  is assumed to be constant but is allowed to be different from unity. For radial flow  $s = 2$  while  $s > 2$  corresponds to a flow diverging more rapidly. *Spitzer* [1962] has tabulated  $G(x)$ , which is defined as

$$G(x) = [\phi(x) - x\phi'(x)] / 2x^2 \quad (11)$$

where  $\phi(x)$  is the error function. The asymptotic behavior

$$\left. \begin{aligned} G(x) &= 0.37x & \text{for } x \ll 1 \\ G(x) &= \frac{1}{2x^2} & \text{for } x \gg 1 \end{aligned} \right\} \quad (12)$$

shows that momentum transfer by collisions is strongly nonlinear. Another important feature of  $C$  is that it is approximately proportional to  $Z^2/A$ . This means that momentum transfer by collisions with protons is very effective for medium and heavy elements.

We complete the system of equations (7) through (10) by using *Parker's* [1963] polytropic expansion model:

$$\frac{dT_I}{T_I} = (\alpha - 1) \frac{dn_I}{n_I} \quad (13)$$

Now eliminate  $n$  and normalize the velocities, temperatures, and radius vector to the respective values at the critical ("sonic") point of the expanding proton-electron gas

$$\left. \begin{aligned} r &= r_c \xi \\ V(r) &= V_c W(\xi) \\ v(r) &= V_c w(\xi) \\ T(r) &= T_c \tau(\xi) \end{aligned} \right\} \quad (14)$$

$$\left. \begin{aligned} V_c &= \left( \frac{GM_\odot}{sr_c} \right)^{1/2} \\ T_c &= \frac{GM_\odot m_p}{2s\alpha k r_c} \end{aligned} \right\} \quad (15)$$

In terms of these dimensionless variables the equation of ion motion is written

$$\begin{aligned} \frac{dw}{d\xi} \left( 2w - \frac{\vartheta \tau}{\alpha A w} \right) &= \frac{\vartheta}{\alpha A} \left( \frac{s\tau}{\xi} - \frac{d\tau}{d\xi} \right) \\ &+ \frac{Z}{A} W \frac{dW}{d\xi} - \frac{2A - Z}{A} \frac{s}{\xi^2} \\ &+ \frac{Z^2}{A} \frac{A + 1}{A + \vartheta} \frac{f}{W \tau \xi^s} G(\Delta w) \end{aligned} \quad (16)$$

with

$$\Delta w = [\alpha A / (A + \vartheta) \tau]^{1/2} (W - w) \quad (17)$$

The dimensionless quantity  $f$  denotes the reduced flux

$$f = \frac{\phi_{\oplus}}{\phi_{\odot}} \alpha \left( \frac{s}{2} \right)^{5/2} \left( \frac{r_c}{r_{\oplus}} \right)^{7/2 - s} \quad (18)$$

with the flux unit [cf. *Geiss et al.*, 1970a]

$$\phi_{\odot} = 1.3 \times 10^5 \text{ cm}^{-2} \text{ sec}^{-1}$$

*Geiss et al.* [1970a] have given a general discussion of equation (16) for  $T_I = T$  and have shown that ions heavier than protons are accelerated to solar wind velocity only if two conditions are fulfilled:

1. The proton flux has to be above a certain critical value  $f_{\min}$ .
2. The effective polytropic index  $\alpha$  for the protons has to increase with solar distance and reach a value of at least 1.33. In the model of *Sturrock and Hartle* [1966],  $\alpha$  actually surpasses 1.33 at  $r = 10.7 R_{\odot}$ .

The magnitude of  $f_{\min}$  is model dependent and thus not easily specified. However, a simple relation between the critical proton fluxes for different ion species is approximately independent of the expansion model and is given by ( $T_I = T$ ):

$$f_{\min} \propto \Gamma^{(1)}(A, Z) \equiv \frac{2A - Z - 1}{Z^2} \quad (19)$$

If thermal diffusion due to nonmaxwellian velocity distributions is taken into account, equation (19) can be modified to give as an approximation

$$f_{\min} \propto \Gamma^{(2)}(A, Z) \equiv \frac{2A - Z - 1}{Z^2} + \frac{\alpha - 1}{\alpha} \frac{15}{8} \left( \frac{2A}{A + 1} \right)^{1/2} \left( 1 - \frac{1}{A} \right)$$

$$Z > 1$$

$$(20)$$

Minimum flux factors  $\Gamma^{(1)}$  and  $\Gamma^{(2)}$  for a number of ion species are listed in table 7. For the degree of ionization of O, Si, and Fe we take the most probable charges observed by *Bame et al.* [1970]. We have obtained the charges of Ne and Ar that correspond to the same ionization conditions from the ionization potentials given by *Lotz* [1967]. The striking result in table 7 is that the minimum proton flux for  ${}^4\text{He}^{2+}$  is higher than for all other ions listed. This means that in this idealized stationary model of the quiet solar wind heavier ions including  $\text{Fe}^{12+}$  are carried along in the solar wind as long as  ${}^4\text{He}^{2+}$  is.

**Table 7.** Minimum proton flux factors for different ion species

[The flux factors  $\Gamma$  are defined in equations (7.17), (7.18), and (7.19), and their significance is discussed in the text.]

	$\Gamma^{(1)}$	$\Gamma^{(3)}$	$\Gamma^{(2)}$
Ion	Without thermal diffusion		With thermal diffusion
	$T_I = T_p$	$T_I = \frac{1}{2}(A + 1)T_p$	$T_I = T_p$ $\alpha = 1.1$
${}^1\text{H}^+$	0	0	0
${}^3\text{He}^{2+}$	.75	.62	.89
${}^4\text{He}^{2+}$	1.25	1.14	1.41
${}^{16}\text{O}^{6+}$	.69	.70	.91
${}^{20}\text{Ne}^{8+}$	.48	.49	.70
${}^{22}\text{Ne}^{8+}$	.55	.56	.77
${}^{28}\text{Si}^{9+}$	.57	.59	.80
${}^{36}\text{Ar}^{8+}$	.98	1.05	1.22
${}^{56}\text{Fe}^{12+}$	.69	.74	.92

The existence of a minimum proton flux for an ion species is a result of the nonlinear behavior of the collision term  $C$  in equation (16). Figure 5 is a schematic picture of the solutions of the equations of ion motion (16). The eight figures represent the families of solutions for different proton fluxes  $f$ , with  $f$  rising from figure 5(a) to (h). Physically acceptable solutions have to agree with the boundary conditions (1) low velocity for small solar distance, and (2) vanishing particle pressure for solar distance  $\xi \rightarrow \infty$ . The latter condition is equivalent to  $v \neq 0$  for  $\xi \rightarrow \infty$  [cf. *Geiss et al.*, 1970a]. There is never more than one solution fulfilling these conditions, and this particular solution has to pass through the critical point for ions, one of the singular points of the differential equation (16). For small fluxes  $f$ , as in figure 5(a), the collision term has little influence and the ion velocity  $w$  remains much below the proton velocity  $W$ . With increasing flux two additional singular points appear (figs. 5(b) and (c)), but the physically acceptable solution still passes through the singularity with the highest  $\xi$ . When a certain flux value is reached (fig. 5(d)), there is a discontinuity in the physical solution  $w(\xi)$ , as the critical point switches from the singularity on the right to the one on the left. If the proton flux is increased further, the ion velocity  $w$  more and more approaches the proton velocity  $W$ , and the two singularities on the right begin to disappear.

The picture presented in figure 5 is borne out by the numerical solutions of equation (16). Figure 6 gives the position of the singular points as a function of the flux value  $f$  for  $\alpha = 1.4$ . Note that generally there is a range of

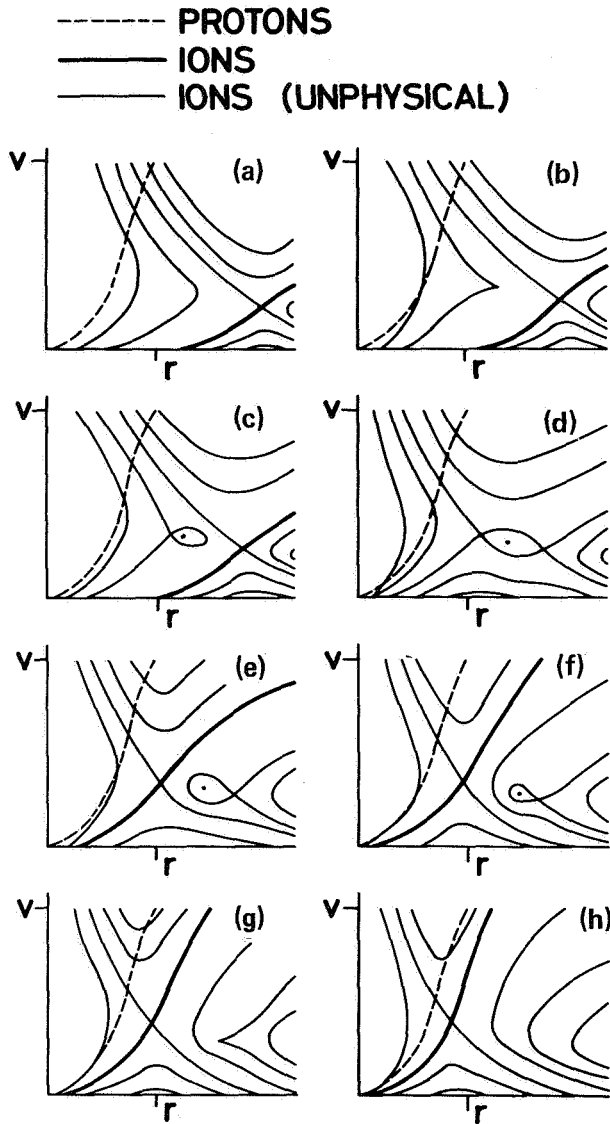


**Figure 5.** Schematic representation of the solutions (velocity versus solar distance) of the equation of ion motion (16). The eight figures represent the families of solutions for different proton fluxes  $f$ , with  $f$  rising from figures 5(a) to 5(h). The physically acceptable solution (heavy line) is determined by the boundary conditions.

flux values  $f$  with three singularities corresponding to the topologies shown in figure 5(c) through (f). The calculations show that only for lower  $\alpha$  and lower masses, such as  ${}^4\text{He}^{2+}$  for  $\alpha = 1.2$ , the three singular points do not develop. The numerical integrations show that the transition from topology 5(c) to (e) occurs for fluxes very near to the relative minimum in the  $f(\xi_c)$  plot. Thus, at a critical flux value  $f_{\min}$  we have for a small change in flux a very significant change in the physical situation of the heavier ions, which for  $\alpha = 1.4$  is

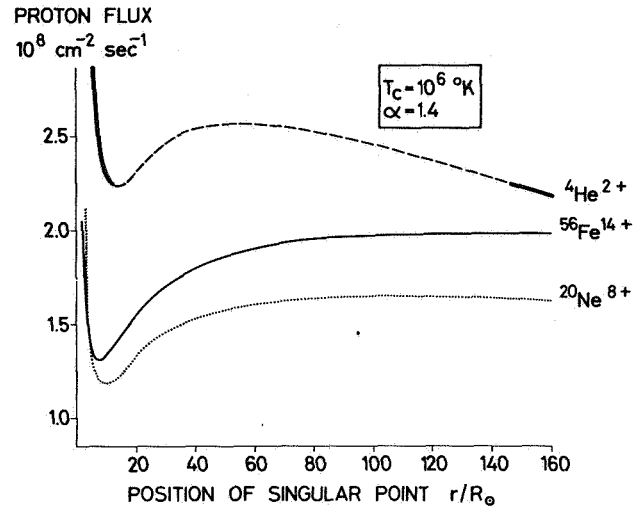


**Figure 6.** Position of the singular points of equation (16) (both sides in the equation vanish simultaneously) as a function of proton flux [after Geiss et al., 1970a]. A polytropic index  $\alpha = 1.4$ , and a temperature of  $10^6$  °K at the “sonic” point of the proton-electron gas are chosen. The dependence of the critical point for  ${}^4\text{He}^{2+}$  on the proton flux is shown by the heavy solid line. For low fluxes the critical point is far away from the sun. At a proton flux of about  $2.25 \times 10^8 \text{ cm}^{-2} \text{ sec}^{-1}$  the critical point jumps from about  $145 R_{\odot}$  to  $11 R_{\odot}$ , and with further increasing flux it moves continuously closer to the sun. For  ${}^{20}\text{Ne}^{8+}$  and  ${}^{56}\text{Fe}^{14+}$  this discontinuity in the position of the critical point is even more pronounced.

demonstrated in figure 7. We can describe this change as follows:

For  $f = 0$  the ion density distribution is similar to the one in the static atmosphere described by Parker [1961]. The scale height is somewhat larger in our case because of the  $V(dV/dr)$  term in the E-field equation (10), which does not exist in the static atmosphere. With increasing proton fluxes the scale height increases—that is, the ion atmosphere is lifted. Still there is no appreciable acceleration of the ions (cf. fig. 7). At some solar distance, equation (16) must become meaningless, since the forces included (gravitation,  $E$  field, and drag) fall off rapidly with increasing solar distance, and magnetic field disturbances and instabilities will become the dominating factors for maintaining a fluid-like behavior of the solar wind [Parker, 1958; Scarf, 1966]. At this distance the relative number density of the heavy ions has decreased to a very low value, and consequently their abundance in the solar wind will be low even if the disturbances mentioned can effectively carry them from here on out.

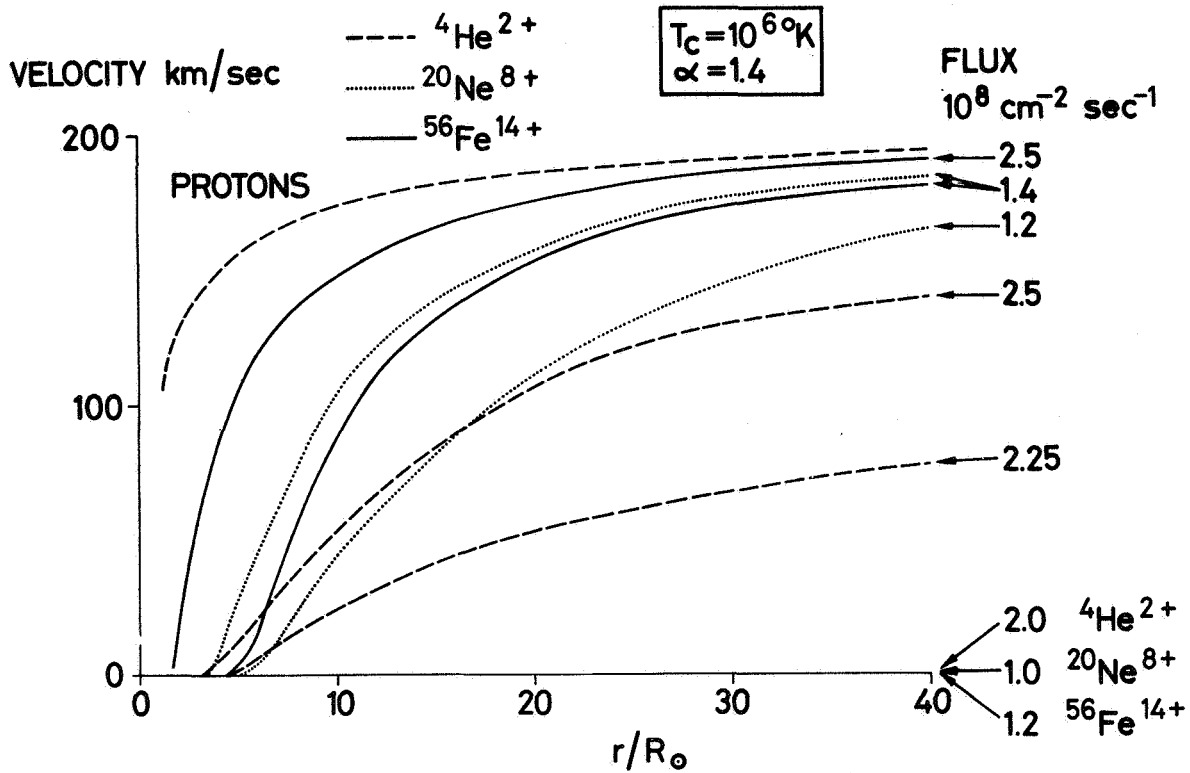


**Figure 7.** Ion velocities as a function of solar distance and proton flux, obtained by numerical integration of equation (16).  $T_I = T$ ,  $\alpha = 1.4$  and  $T_C = 10^6$  °K were chosen.  ${}^4\text{He}^{2+}$  and  ${}^{56}\text{Fe}^{14+}$  after Geiss et al. [1970a]. For  ${}^{20}\text{Ne}^{8+}$  and  ${}^{56}\text{Fe}^{14+}$  the locking-in of the ion velocity with the proton velocity at the minimum flux is clearly demonstrated. The minimum flux for  ${}^4\text{He}^{2+}$  is larger than for the other two ion species.

When  $f$  surpasses the critical value  $f_{\min}$ , the heavy ions are “locked-in” with the proton motion. In the example given in figure 7, this happens for  ${}^{56}\text{Fe}^{14+}$  at a 1 AU proton flux of about  $1.3 \times 10^8 \text{ cm}^{-2} \text{ sec}^{-1}$ , and for  ${}^{20}\text{Ne}^{8+}$  at about  $1.1 \times 10^8 \text{ cm}^{-2} \text{ sec}^{-1}$ . Since the masses and charges of helium and protons are not so very different, the “lock-in” effect for helium is not as marked. The critical proton flux  $f_{\min}$  for  ${}^4\text{He}^{2+}$  is around  $2.4 \times 10^8 \text{ cm}^{-2} \text{ sec}^{-1}$ . Thus the relation between the minimum fluxes of  ${}^4\text{He}^{2+}$ ,  ${}^{20}\text{Ne}^{8+}$  and  ${}^{56}\text{Fe}^{14+}$  approximately corresponds to the  $\Gamma^{(1)}$  values given in table 7, which were derived from an analytical approximation (eq. 16).

The existence of different proton minimum fluxes for different ion species has been demonstrated in figure 7 on the basis of the polytropic expansion model with  $\alpha = 1.4$ . Under quiet conditions such a high  $\alpha$  value is expected in the outer corona (cf.  $\alpha_p$  in the Sturrock and Hartle two-fluid model), which is the critical region for ion acceleration. However,  $\alpha = 1.4$  is unrealistic in the inner regions of the corona, and therefore leads to solar

wind velocities that are too low;  $\alpha = 1.1$  is probably a good approximation for the lower and middle corona. Numerical solutions are given in figure 8. Note that the heavier ions move more slowly in this region than the protons, and this leads to enhanced local abundances of the heavier ions. This will be further discussed in the next section.

So far, our discussion has been based on the assumption that  $T_I = T_p$ , or  $\vartheta = 1$  in the corona and solar wind acceleration region. Such an assumption appears to be justified since the energy equipartition times between protons and ions are similar to the mean collision times given in equation (6). However, it is possible that through heat dissipation by waves and turbulence the temperature of heavier ions is increased above the proton temperature. Ions might also get heated if their bulk velocity lags appreciably behind the proton bulk velocity. Since in the corona the measured electron and ion temperatures generally agree within a factor of about 2 [cf. Billings, 1966],  $T_I$  is not expected to be much larger than  $T$ , but we should discuss here the influence



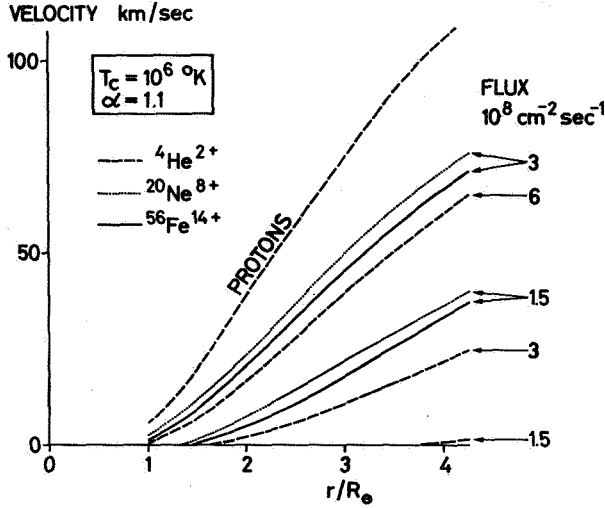


**Figure 8.** Ion velocities for different proton fluxes and  $T_I = T$ .  $\alpha = 1.1$  is a good approximation for solar distances of a few  $R_\odot$  [cf. Sturrock and Hartle, 1966]. It is seen that in this region ions move slower than protons. This leads to enhanced local ion abundances.

of a possible deviation of  $T_I$  from  $T$ . As can be seen from equation (16),  $\vartheta = T_I/T$  does not have a very strong influence on the collision term, and therefore one would not expect the minimum fluxes to change very much for  $\vartheta \neq 1$ . A minimum flux factor  $\Gamma^{(3)}$  can be derived from equation (16) that takes into account possible differences between the local ion and proton temperatures:

$$f_{\min} \propto \Gamma^{(3)} \equiv \frac{2A - Z - \vartheta}{Z^2} \frac{A + \vartheta}{A + 1} \quad (21)$$

This relation becomes unreliable for the limiting case  $T_I = AT$  ( $\vartheta = A$ ), where ions and protons have the same velocity dispersion. However, as mentioned before, such a high excess temperature of heavier ions is ruled out by observation. For  $\vartheta = (A+1)/2$ —that is,  $T_I = 1/2(A+1)T$ —equation (21) is still valid, and numbers for this case have been included in table 7. It is seen that the relation between the minimum fluxes of different ion species remains essentially unchanged, even for drastically increased ion temperatures in the solar wind acceleration region. In all three approximations  ${}^4\text{He}^{2+}$  needs a larger proton flux to be carried in the solar wind than all the other ions listed. This result implies that the largest abundance variability in the quiet, quasi-stationary solar wind should occur for  $\text{He}^4$ , if collisional momentum transfer is the dominant factor responsible for solar wind abundances and their variations.

### Ion Acceleration by Field Irregularities and Waves

We have seen that momentum transfer by Coulomb collisions appears to be a sufficient cause for accelerating heavier ions to solar wind velocities. Momentum transfer from waves or traveling magnetic irregularities will be in competition with Coulomb collisions as regards ion acceleration. The question is which of these processes is dominant at a certain time. In the absence of direct observational evidence on the degree of disorder of the magnetic field and on wave amplitudes in the solar wind acceleration region, this question can be answered best by investigating discrimination with respect to the mass and the charge of the ions.

Wave particle interactions have so far not been studied in the context of ion acceleration in the corona. In order to simplify the situation we shall assume here an average field  $B_0$  in the radial direction on which irregularities or waves are superimposed. It is assumed that the waves travel in the radial direction with a velocity  $V_w$ ;  $B_0$  and  $V_w$  are constants in space and time. Ions of mass  $A \cdot m_p$  and charge  $Ze$  are assumed to have initially a velocity distribution characterized by the temperature  $T_i$  centered around  $v = 0$ .

A longitudinal (ion-acoustic) wave can accelerate ions in the radial direction by way of Landau's [1946] trapping process [cf. Spitzer, 1962; Stix, 1962]. Ions to be trapped need a minimum radial velocity  $v_r$ , which is given by the relation [cf. Spitzer, 1962]

$$v_r > V_w - \left( \frac{2eU_0}{m_p} \frac{Z}{A} \right)^{1/2} \quad (22)$$

where  $U_0$  is the amplitude of the electric potential in the wave. If ion temperatures are essentially independent of mass, then the acceleration by trapping in longitudinal waves will strongly discriminate against (1) ions of large mass (small thermal velocity) and (2) ions with small  $Z/A$ .

Next we study the effects of magnetic disturbances traveling in the radial direction with a velocity  $V_w$ . We consider the problem in a frame of reference moving with the wave velocity  $V_w$ , which in our case is the Alfvén velocity. In this frame of reference we can consider the wave as a time-independent magnetic field variation. The ions to be accelerated initially have a thermal velocity distribution centered around a radial velocity  $-V_w$ . For heavier ions the average thermal velocity  $v_{th}$  will be much smaller than  $V_w$ —that is, the ions move backward with a narrow pitch angle distribution. Pitch angle scattering then results in an acceleration of the ions in the radial direction. The problem of pitch angle scattering by irregularities in a magnetic field has been treated by Jokipii [1966b], Hasselmann and

Wibberenz [1968], and others. Jokipii [1966a] has shown that pitch angle scattering is due to the transverse component of  $B$  having a frequency (as seen by the particle) near the gyrofrequency  $\omega_o$ . In our example, a particle in resonance with a circularly polarized wave will be accelerated according to

$$\frac{dv_{\perp}}{dt} = \omega_o V_w \frac{B_{\perp}}{B_o} \quad \omega_o = \frac{Z}{A} \frac{eB_o}{m_p} \quad (23)$$

With the assumption  $v_{\perp} \ll v_{\parallel} \approx V_w$ , it follows that

$$\frac{\langle (\Delta v_{\perp})^2 \rangle}{\Delta t} \propto \omega_o^2 V_w^2 \frac{B_{\perp}^2(\omega_o)}{B_o^2} \quad (24)$$

where  $B_{\perp}^2(\omega_o)$  is the square of the wave amplitude per unit frequency at the frequency  $\omega_o$ . Using conservation of energy, we obtain

$$\frac{dv_{\parallel}}{dt} = C_{\text{magn}} \propto \omega_o^2 V_w \frac{B_{\perp}^2(\omega_o)}{B_o^2} \quad (25)$$

Thus in this approximation the "magnetic collision term"  $C_{\text{magn}}$  is a function of  $\omega_o$ —that is, a function of  $Z/A$  alone. In analogy to observations in interplanetary space [Coleman, 1966; Sari and Ness, 1969; Coleman *et al.*, 1969], we may assume  $B_{\perp}^2 \propto \omega^{-\alpha}$ ,  $\alpha$  having values between 1 and 2. From (25) we obtain  $C_{\text{magn}} \propto Z/A$  for  $\alpha = 1$ .  $C_{\text{magn}}$  becomes independent of  $Z/A$  for  $\alpha = 2$ .

It is seen that accelerations from waves or field disturbances and from Coulomb collisions differ very much in their dependence on ion mass and charge. The former tend to discriminate against the heavy ions, whereas the latter favor them because of the  $Z^2/A$  factor in the collision term (eq. (9)).

#### Ion Separation by Diffusion in the Lower Corona

The diffusion equation can be derived from the momentum equation (8) by neglecting velocity terms of quadratic and higher order. Since thermal diffusion is an effect of nonmaxwellian velocity distributions and thus not contained in equations (8) and (9), the appropriate thermal diffusion term given by Chapman and Cowling [1958] has to be added. Assuming a radial magnetic field and radial motion, one obtains:

$$V - v = D \left[ \frac{d}{dr} \ln \left( \frac{n_I}{n} \right) + (2A - Z - 1) \frac{m_p G M_{\odot}}{2kTr^2} + \alpha_T \frac{d}{dr} \ln T \right] \quad (26)$$

with

$$D = \frac{3}{4} \frac{1}{\sqrt{2\pi}} \frac{(kT)^{5/2}}{e^4 m_p^{1/2} \ln \Lambda} \frac{1}{n} \left( \frac{A+1}{A} \right)^{1/2} \frac{1}{Z^2} \quad (27)$$

In first approximation,  $\alpha_T$  is given by [Chapman, 1958; Geiss *et al.*, 1970a]

$$\alpha_T = -\frac{15}{8} Z^2 \left( \frac{2A}{A+1} \right)^{1/2} \left( 1 - \frac{1}{A} \right) \quad Z > 1 \quad (28)$$

Equation (26) has been discussed and solved by Delache [1965, 1967], Jokipii [1965, 1966a], and Nakada [1969] for the photosphere-corona transition and the lower corona. These authors obtained large enrichments of ions heavier than protons in the corona.

We shall discuss equation (26) by assuming an initially homogenous composition—that is,  $d \ln(n_I/n)/dr = 0$ . In the lower corona  $d \ln T/dr$  is negative, and thus  $V > v$ . This velocity difference produces the *density* enhancement of heavy ions in the corona [Jokipii, 1965], which was discussed in connection with figure 8. Across the photosphere-corona boundary a *flux* enhancement of the positive ions relative to photospheric abundances is possible. Here the continuity equation is not applicable because the source reservoir is virtually unlimited. With a temperature gradient above the photosphere corresponding to  $d \ln T/dr \sim 10^{-4} \text{ km}^{-1}$  [cf. Billings, 1966], the thermal diffusion term can in fact be larger than the second term in equation (26) and lead to an enhanced flux of heavier ions. As stressed above and as we shall see in the next section, so far there is no observational evidence that would indicate that this flux enhancement is not virtually obliterated by mixing or impeded by a loop structure in the magnetic field.

#### DISCUSSION

In figure 9 we compare relative abundances of elements in different materials of solar origin. For hydrogen log  $N$  is normalized to 12.00.

Photospheric abundances for oxygen (log  $N = 8.8$ ) were taken from Müller *et al.* [1968] and Lambert [1968], and for silicon (7.55) from Lambert and Warner [1968]. In the past, the iron abundance in the photosphere has been subject to much discussion, since the reported Fe/Si ratio in the photosphere was much lower than Fe/Si in chondritic meteorites. Recently, Garz *et al.* [1969] and Baschek *et al.* [1970] have made new determinations of  $f$  values for Fe I and Fe II. These new determinations give good agreement for photospheric iron abundances derived from the Fe I and Fe II spectra (7.60 and 7.63, respectively). An average of log  $N = 7.62$  is adopted here.

The coronal abundances are taken from the work of Pottasch [1968]. They were derived from UV spectra obtained at the base of the corona, 10,000 to 30,000 km above the photosphere. Pottasch's [1968] analyses of the forbidden lines in the corona give comparable

results. These latter abundances refer to an altitude of about 75,000 km above the photosphere.

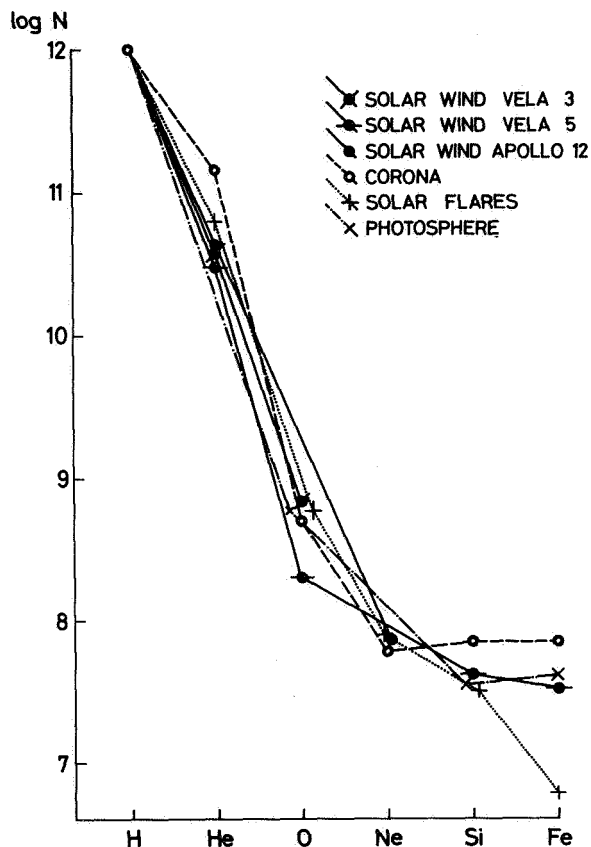


Figure 9. Abundances of elements in different materials of solar origin.

The solar flare particle abundances are taken from Fichtel's [1970] presentation. Since for these particles the abundance of hydrogen relative to the heavier ions cannot be determined with certainty, oxygen has been normalized to the photospheric value. Abundances of Si and Fe have been obtained after correcting for the less abundant elements in the elemental groups given by Fichtel [1970]. For the solar wind three sets of abundance data are presented in figure 9. The average He/O ratio obtained by Bame *et al.* [1968] from the Vela 3 data has been included by combining it with the average He/H ratio of 0.037 reported by Robbins *et al.* [1970]. The SWC Apollo 12 results [Geiss *et al.*, 1970c] have been chosen for helium and neon since they can be connected to hydrogen by simultaneous observations [Bame and Hundhausen, 1970]; compare table 1 of this paper.

If one considers the limitations of all these data, the general agreement is surprisingly good. The intrinsic

uncertainties in the photospheric and coronal abundances combined with the fact that solar wind and corona have only been sampled over limited periods lead us to conclude that the abundances of O, Ne, and Si relative to H agree within the limits of error in all these samples of solar matter. This means that normally the thermal diffusion enrichment process across the photosphere-corona boundary cannot be very effective and is largely obliterated by mixing or quenched by magnetic fields. The abundance enhancement of heavier ions in the corona as predicted from the calculations of Geiss *et al.* [1970a] and Alloucherie [1970] are not observed. This is not surprising since the corona data refer to  $r < 1.1 R_{\odot}$ . At these low altitudes, solar wind expansion models [cf. Sturrock and Hartle, 1966] give flow velocities below 10 km/sec, and thus effects arising from differences in flow velocities of a few km/sec can easily be annihilated by turbulent mixing. Thus, we expect that the local enrichment of heavier ions is real only at altitudes of a few hundred thousand km and more above the solar surface.

Figure 9 indicates a large deficit of the iron group in the solar flare particles. As Fichtel [1970] has pointed out the measurement by Bertsch *et al.* [1969] refers to relatively high energies ( $\geq 24.5$  MeV/nucleon), and no energy spectra are available. The mass/charge ratio for fully ionized iron is 2.15, slightly higher than the value of 2 for helium and medium nuclei. Bertsch *et al.* [1969] have estimated that this difference can lead to a low abundance of iron, but the effect should not be larger than 30 percent. A possible explanation would be that iron is not fully ionized during a substantial part of the acceleration process.

There are no direct measurements of the helium abundance in the photosphere. In prominences, Unsöld [1955] has derived a He/H ratio of 0.16, corresponding to  $\log N = 11.2$  for helium. This value is rather uncertain since theory concerning the helium lines in prominences is not completely clear [Unsöld, 1969]. Lambert [1967] and more recently Fichtel [1970] have combined the He/O ratio in solar flare particles with the H/O ratio in the photosphere and obtained  $\text{He}/\text{H} = 0.063 \pm 0.008$ . This ratio appears to be well founded, since the oxygen abundance in the photosphere is well determined and agreed on by several authors, and since fractionation between helium and oxygen in the solar flare particle population is excluded by substantial observational evidence [Fichtel, 1970]. All the helium abundances estimated for the photosphere and the corona are higher than the average solar wind abundance—that is, there is a strong indication that helium is systematically depleted in the solar wind. This

assertion is further supported by the fact that during one full solar rotation the He/H ratio in the solar wind was 0.064 [Robbins *et al.*, 1970]. Also the indicated correlation between general solar activity and He/H ratio [Robbins *et al.*, 1970; Hundhausen, 1970] points in this direction.

If He is indeed systematically suppressed in the solar wind by 30 to 50 percent, it is remarkable that the suppression is not progressively larger for the heavy elements O, Ne, Si, and Fe (fig. 9). This observation is readily explained, of course, if we assume that collisions are the main agent for acceleration of heavy ions during quiet solar conditions.

The time variations of the abundance in the solar wind and in particular the high He/H ratios observed to occur with a delay of the order to 10 hr after an interplanetary shock [Hirshberg *et al.*, 1970; Ogilvie and Wilkerson, 1969] are discussed in the preceding paper. Hirshberg *et al.* [1970] have suggested that these high helium contents may result from the sudden ejection of the helium-rich region in the corona which during the quiet preshock situation results from the retarded acceleration of helium (fig. 8).

The  $\text{He}^4/\text{He}^3$  ratios obtained from the SWC experiments appear to be systematically lower than the ratio found in the Surveyor 3 material (table 8). Bühler *et al.* [1971] have argued that a  $\text{He}^4$  excess of terrestrial origin in the magnetic tail of the earth could not account for this difference and that one might here observe a solar cycle effect. In fact, the Surveyor 3 exposure period coincides with the maximum of the solar cycle, and the average  $A_p$  number was  $25\gamma$ . During the Apollo 11 and 12 foil exposures the  $A_p$  numbers were approximately  $6\gamma$  and  $12\gamma$ , respectively. Again it is indicated that during solar maximum  $\text{He}^4$  is carried along in the solar wind more effectively than during the rest of the solar cycle.  $\text{He}^3$  would be less affected, in accordance with the theoretical considerations discussed in the preceding section.

During quiet and quasi-stationary conditions, one would expect on the basis of the Geiss *et al.* [1970a] model a positive correlation between solar wind proton flux and helium abundance. Such a correlation is not observed [Robbins *et al.*, 1970]. It could be that the flux at 1 AU is not a good measure of the flux in the source region. If the coronal structure is dominated by streamers, we have to consider  $s > 2$ . Variations in  $s$  strongly influence the minimum fluxes derived in the preceding section 7, if expressed in absolute fluxes at 1 AU (*cf.* equation (18)). On the other hand, it is possible that collisions often are not quite sufficient for

accelerating  $^4\text{He}^{2+}$ , and the  $^4\text{He}^{2+}$  abundance is strongly influenced by wave-particle interactions in the solar wind acceleration region, even under relatively quiet conditions. In this case, the heavy ions could still get their main acceleration from collisions. Argon has the highest flux factor  $\Gamma$  among those ions listed in table 7 that are heavier than helium. Therefore, larger abundance depletions and variations are expected for Ar than for O, Ne, Si, and Fe.

Ion separation effects in the boundary region between a plasma and a neutral gas [Lehnert, 1970] would depend on the first ionization energy. If such a process is operative at the base of the corona, then the abundances of He and Ne should be correlated, whereas O and Ar should be correlated to H.

As discussed earlier, the isotopic composition in the solar wind and in our atmosphere is nearly the same for Ar and Kr, and is quite different for Ne and Xe. The question is whether these differences are a result of isotopic fractionation or whether different nucleosynthetic sources have contributed to these noble gases. The difficulty with the first hypothesis is that the lightest gas (Ne) and the heaviest would have to be enriched, leaving the other two essentially unchanged. The second hypothesis has to explain the fact that differences of this kind in isotopic composition have not been observed for other elements.

The investigations on solar wind xenon trapped at the lunar surface have confirmed the suspicion derived from meteoritic data that solar Xe is very different from atmospheric Xe [Reynolds, 1963; Marti, 1969]. The nature of this difference has been discussed for many years, but so far it has been impossible to decide whether most of this difference is due to mass fractionation or whether we deal here with products of different nucleosynthetic origin.  $\text{Ne}^{20}/\text{Ne}^{22}$  ratios as low as and even lower than the atmospheric ratio have been found in the trapped neon of some meteorites [Pepin, 1967]. However, the difference between solar neon and atmospheric neon is probably due to mass fractionation in the earth atmosphere, since the variation in the  $\text{Ne}^{20}/\text{Ne}^{21}/\text{Ne}^{22}$  ratios is compatible with isotopic fractionation [Eberhardt *et al.*, 1970].

Table 8 gives a comparison of isotopic abundances of helium and neon in the solar wind, in lunar surface material, and in aubritic meteorites. Where necessary, the abundances have been corrected for the "nucleogenic component" (spallation, radioactive decay). The low  $\text{He}^4/\text{Ne}^{20}$  ratios in the lunar material clearly show gas losses by temperature diffusion and/or other processes. Also, in the Surveyor 3 material this ratio is

**Table 8.** Comparison of relative ion abundances from the Apollo SWC experiments with measured relative concentrations of solar wind particles implanted in lunar fine material, Surveyor 3 material and aubritic meteorites

	SWC Apollo 11 (a)	SWC Apollo 12 (a)	Surveyor 3 material (b)	Lunar dust (Apollo 11) bulk (c)	Lunar ilmenite (c)	Lunar breccia bulk (d)	Aubritic meteorites (e)	Earth's atmosphere
$\text{He}^4/\text{He}^3$	1860 $\pm 140$	2450 $\pm 100$	2770 $\pm 120$	2550 $\pm 250$	2720 $\pm 90$	2720 $\pm 100$	4000 $\pm 300$	---
$\text{He}^4/\text{Ne}^{20}$	430 $\pm 90$	620 $\pm 70$	295 $\pm 15$	90 $\pm 20$	217 $\pm 10$	55 $\pm 20$	380 $\pm 70$	---
$\text{Ne}^{20}/\text{Ne}^{22}$	13.5 $\pm 1.0$	13.1 $\pm 0.6$	13.3 $\pm 0.4$	12.65 $\pm 0.2$	12.85 $\pm 0.1$	12.6 $\pm 0.1$	12.2 $\pm 0.5$	9.8
$\text{Ne}^{22}/\text{Ne}^{21}$	---	26 $\pm 12$	31 $\pm 5$	31.0 $\pm 1.2$	31.1 $\pm 0.8$	---	---	34.5

<sup>a</sup>Geiss et al. [1970b]

<sup>b</sup>Bühler et al. [1971]

<sup>c</sup>Eberhardt et al. [1970]

<sup>d</sup>Hintenberger et al. [1970]; Pepin et al. [1970]

<sup>e</sup>Zähringer [1962a, 1962b]; Eberhardt et al. [1965a, 1966]; Marti [1969]

probably lowered. There is a large difference between the  $\text{He}^4/\text{He}^3$  ratios in aubritic meteorites and in the other sources. It should be mentioned that other meteorite classes, in particular many chondrites, have varying trapped  $\text{He}^4/\text{He}^3$  ratios, which can be as low as or even lower than those in the fine lunar material [Anders et al., 1970; Black, 1970]. We have chosen here the aubritic values, because it has been shown [Eberhardt et al., 1965a, b] that the trapped noble gases are contained at the surfaces of the individual grains of the meteorite, very similar to the solar wind gases in lunar fine material. Also the  $\text{He}/\text{Ne}$  ratio for this meteorite class is high, indicating that these meteorites have experienced relatively little diffusive losses.

There is an indication for a systematic variation in the  $\text{He}^4/\text{He}^3$  ratio, if one compares SWC and Surveyor 3 data with the helium embedded in lunar material. Judging from the cosmic ray exposure age, the solar wind particles found in the Apollo 11 lunar fine material were probably embedded during the last few hundred million years. The breccias have collected their solar wind particles before consolidating, i.e., probably earlier than the fine material. Thus there appears to be a correlation between observed  $\text{He}^4/\text{He}^3$  ratio and time.

However, more detailed investigations are necessary before we can eliminate the possibility that this apparent trend may be the result of secondary effects in the lunar material.

There are several possibilities to explain the differences in the  $\text{He}^4/\text{He}^3$  ratios:

1. The  $\text{He}^4/\text{He}^3$  ratio in the outer convective zone of the sun is constant at about 4000;  $\text{He}^4$  is systematically depressed in the solar wind relative to  $\text{He}^3$ . In an early phase, when the sun was more active, there was less discrimination in the solar wind and He trapped in aubrites represents this ancient solar wind.
2. There is a secular increase of the  $\text{He}^3$  content in the outer convective zone of the sun and as a consequence the  $\text{He}^4/\text{He}^3$  ratio in the solar wind has decreased from an early value of about 4000 to values below 3000 in recent times. Aubritic He would represent a solar wind sample from the early part of the solar history. The cause for such a secular increase in the  $\text{He}^3$  content of the outer convective zone could be due to either nuclear reactions at the solar surface or a small degree of mixing between the outer convective zone and the core of the sun, as was suggested by Schatzman [1970].

The number of  $\text{He}^3$  atoms produced per  $\text{cm}^2$  at the solar surface by nuclear reactions during the lifetime of the sun can be estimated from the following relation:

$$\text{He}^3 = \frac{1-\eta}{\eta} f_{\oplus} \left( \frac{r_{\oplus}}{R_{\odot}} \right)^2 \frac{n_{\text{He}}}{n_{\text{H}}} L \sigma T_s \quad (29)$$

where  $f_{\oplus}$  is the flux of solar protons at 1 AU. Multiplication by  $(r_{\oplus}/R_{\odot})^2$  gives the flux leaving the solar surface; this actually is an upper limit, since the diffusive character of the particle flow gives a radial decrease less than  $r^{-2}$ . The term  $\eta$  is the fraction of the accelerated particles leaving the sun,  $1-\eta$  the fraction returning into the sun.  $L$  is the range of the energetic protons in number of atoms/ $\text{cm}^2$ ,  $n_{\text{He}}/n_{\text{H}}$  the abundance ratio in the sun, and  $T_s$  the age of the sun. The flux of solar protons averaged over the last 1 million years is estimated at  $100 \text{ cm}^{-2} \text{ sec}^{-1}$  above 10 MeV [Finkel *et al.*, 1971]. This corresponds to a flux of about  $50 \text{ cm}^{-2} \text{ sec}^{-1}$  above 23 MeV, the threshold for  $\text{He}^3$  production in reactions of fast protons with  $\text{He}^4$ . The combined cross sections for all the  $p\text{--He}^4$  reactions leading to  $\text{He}^3$  or  $\text{H}^3$  for proton energies above 23 MeV is approximately 60 mb [cf. Audouze *et al.*, 1967]. With an estimated  $n_{\text{He}}/n_{\text{H}} = 0.1$ , we obtain

$$\text{He}^3 = \frac{1-\eta}{\eta} 10^{21} \text{ atoms/cm}^2$$

The production of  $\text{He}^3$  by fast  $\alpha$  particles on hydrogen can be neglected in this order of magnitude estimate.

The outer convective zone of the sun contains about  $10^{28} \text{ He}^3 \text{ atoms/cm}^2$ . Thus  $\eta$ , the fraction of the accelerated particles escaping from the sun, would have to be of the order of  $10^{-7}$ . Such a low value is contrary to present ideas about flares [cf. Lingenfelter and Ramaty, 1967], and is also in disagreement with the upper limits obtained from solar neutron fluxes [Daniel *et al.*, 1969]. A similar conclusion is reached by using the upper limit on the  $\text{He}^3$  abundance in flare particles given by Hsieh and Simpson [1970].

3. The  $\text{He}^4/\text{He}^3$  ratio in the solar nebula was  $\sim 4000$ . In the sun  $\text{He}^3$  was increased in the process of deuterium burning to give a lower  $\text{He}^4/\text{He}^3$  ratio [Ezer and Cameron, 1965]. This ratio was then essentially constant in the outer convective zone since the sun arrived on the main sequence. In this case the aubritic meteorites obtained their trapped helium from the solar nebula.

To distinguish between these possibilities, we need a better knowledge of the present day  $\text{He}^4/\text{He}^3$  average, we need to clarify through more observations and through theoretical work whether in the solar wind  $\text{He}^4$  is systematically depleted, and we need to establish the long-time change—if it exists—of the  $\text{He}^4/\text{He}^3$  ratio in the solar wind from detailed investigations of lunar surface material.

The  $\text{He}^4/\text{He}^3$  problem is just one question of fundamental astrophysical importance that has emerged from solar wind abundance studies. Progress during the last years has been rapid, and further studies in this general field should contribute to our understanding of solar and interplanetary physics and to our knowledge of the history of the solar system.

## ACKNOWLEDGMENTS

The author wishes to thank H. Leutwyler for valuable suggestions and discussions on the motion of neutral and ionized particles, and H. Chivers for critically reading the manuscript. He acknowledges discussions on various topics of this paper with J. Hirshberg, F. Bühler, H. Debrunner, P. Eberhardt, H. J. Fahr, and G. Wibberenz.

This work was supported in part by the Swiss National Science Foundation.

## REFERENCES

- Alexander, E. C.; Lewis, R. S.; Reynolds, J. H.; and Michel, M. C.: Plutonium-244: Confirmation as an Extinct Radioactivity. *Preprint*, 1971.
- Aller, L. H.: The Abundance of the Elements. *Inter-science*, 1961.
- Allouche, Y.: *J. Geophys. Res.*, Vol. 75, 1970, p. 6899.
- Anders, E.; and Heymann, D.: *Science*, Vol. 164, 1969, p. 821.
- Anders, E.; Heymann, D.; and Mazor, E.: *Geochim. Cosmochim. Acta*, Vol. 34, 1970, p. 127.
- Arrhenius, G.; and Alfvén, H.: *Earth Planet. Sci. Letters*, Vol. 10, 1971, p. 253.
- Audouze, J.; Ephre, M.; and Reeves, H.: High Energy Nuclear Reactions in Astrophysics, edited by B.S.P. Shen. W. A. Benjamin Inc., New York, 1967, p. 255.
- Bame, S. J.; Hundhausen, A. J.; Asbridge, J. R.; and Strong, I. B.: *Phys. Rev. Lett.*, Vol. 20, 1968, p. 393.
- Bame, S. J.; Asbridge, J. R.; Hundhausen, A. J.; and Montgomery, M. D.: *J. Geophys. Res.*, Vol. 75, 1970, p. 6360.
- Bame, S. J.; and Hundhausen, A. J.: Private Communication, 1970.

- Baschek, B.; Garz, T.; Holweger, H.; and Richter, J.: *Astron. Astrophys.*, Vol. 4, 1970, p. 229.
- Bertaux, J. L.; and Blamont, J. E.: *Astron. Astrophys.*, Vol. 11, 1971, p. 200.
- Bertsch, D. L.; Fichtel, C. E.; and Reames, D. V.: *Astrophys. J.*, Vol. 157, 1969, p. L53.
- Billings, D. E.: *A Guide to the Solar Corona*. Academic Press, New York, London, 1966.
- Black, D. C.: *Geochim. Cosmochim. Acta.*, Vol. 34, 1970, p. 132.
- Blamont, J. E.: Private Communication, 1971.
- Bloch, M.; Fechtig, H.; Funkhouser, J.; Gentner, W.; Jessberger, E.; Kirsten, T.; Müller, O.; Neukum, G.; Schneider, E.; Steinbruun, F.; Zähringer, J.: Location and Variation of Rare Gases in Apollo 12 Lunar Rocks. 2. *Apollo Lunar Sci. Conf.*, Houston, Jan. 1971.
- Blum, P. W.; and Fahr, H. J.: *Astron. Astrophys.*, Vol. 4, 1970, p. 280.
- Bühler, F.; Geiss, J.; Meister, J.; Eberhardt, P.; Huneke, J. C.; and Signer, P.: *Earth Planet. Sci. Letters*, Vol. 1, 1966, p. 249.
- Bühler, F.; Eberhardt, P.; Geiss, J.; Meister, J.; and Signer, P.: *Science*, Vol. 166, 1969, p. 1502.
- Bühler, F.; Eberhardt, P.; Geiss, J.; and Schwarzmüller, J.: *Earth Planet. Sci. Letters*, Vol. 10, 1971, p. 297.
- Chapman, S. C.: *Proc. Phys. Soc., London*, Vol. 72, 1958, p. 353.
- Chapman, S. C.; and Cowling, T. G.: *The Mathematical Theory of Non-Uniform Gases*. Cambridge University Press, Cambridge, 1958.
- Clay, D. R.; Neugebauer, M.; and Snyder, C. W.: Solar Wind Observations on the Lunar Surface with the Apollo 12 ALSEP. Preprint, 1971.
- Coleman, P. J.: *J. Geophys. Res.*, Vol. 71, 1966, p. 5509.
- Coleman, P. J.; Smith E. J. Jr.; Davis L. Jr.; and Jones, D. E.: *J. Geophys. Res.*, Vol. 74, 1969, p. 2826.
- Dakowski, M.: *Earth Planet. Sci. Letters*, Vol. 6, 1969, p. 152.
- Daniel, R. R.; Gokhale, G. S. Joseph, G.; Lavakare, P. J.; and Sekhon, B. S.: MO-39, *Proc. 11. Intern. Conf. Cosmic Rays*, Budapest, 1969.
- Delache, P.: *Comp. Rend. Acad. Sci. (France)*, Vol. 261, 1965, p. 643.
- Delache, P.: *Ann. Astron.*, Vol. 30, 1967, p. 827.
- Eberhardt, P.; Geiss, J.; and Grögler, N.: *Tschermak's Mineral. Petrogr. Mitt.*, Vol. 10, 1965a, p. 535.
- Eberhardt, P.; Geiss, J.; and Grögler, N.: *J. Geophys. Res.*, Vol. 70, 1965b, p. 4375.
- Eberhardt, P.; Geiss, J.; and Grögler, N.: *Earth Planet. Sci. Letters*, Vol. 1, 1966, p. 7.
- Eberhardt, P.; Geiss, J.; Graf, H.; Grögler, N.; Krähenbühl, U.; Schwaller, H.; Schwarzmüller, J.; and Stettler, A.: *Geochim. Cosmochim. Acta*, Suppl. 1, Vol. 2, 1970, p. 1037.
- Epstein, S.; and Taylor H. P. Jr.: *Geochim. Cosmochim. Acta*, Suppl. 1, Vol. 2, 1970, p. 1085.
- Ezer, D.; and Cameron, A. G. W.: *Can. J. Phys.*, Vol. 43, 1965, p. 1497.
- Fahr, H. J.: *Ann. Geophys.*, Vol. 25, 1969, p. 475.
- Fichtel, C. E.: Royal Society Meeting on Solar Studies with Special Reference to Space Observations. Preprint, April 1970.
- Finkel, R. C.; Arnold, J. R.; Reedy, R. C.; Fruchter, J. S.; Loosli, H. H.; Evans, J. C.; Shedlovsky, J. P.; Imamura, M.; and Delany, A. C.: Depth Variations of Cosmogenic Nuclides in a Lunar Surface Rock. 2. *Lunar Sci. Conf.*, Houston, 1971.
- Forslund, D. W.: *J. Geophys. Res.*, Vol. 75, 1970, p. 17.
- Freeman, J. W., Jr.; Fenner, M.; Hills, H. K.; and Balsiger, H.: *Trans. Amer. Geophys. Union*, Vol. 51(4), 1970, p. 407.
- Friedman, I.; Gleason, J. D.; and Hardcastle, K. G.: *Geochim. Cosmochim. Acta*, Suppl. 1, Vol. 2, 1970, p. 1103.
- Garz, T.; Holweger, H.; Kock, M.; and Richter, J.: *Astron. Astrophys.*, Vol. 2, 1969, p. 446.
- Geiss, J.; Eberhardt, P.; Signer, P.; Bühler, F.; and Meister, J.: Apollo 11 Preliminary Sci. Rep., NASA SP-214, 1969, p. 183.
- Geiss, J.; Hirt, P.; and Leutwyler, H.: *Solar Phys.*, Vol. 12, 1970a, p. 458.
- Geiss, J.; Eberhardt, P.; Signer, P.; Bühler, F.; and Meister, J.: Apollo 12 Preliminary Sci. Rept., NASA SP-235, 1970b, p. 99.
- Geiss, J.; Eberhardt, P.; Bühler, F.; Meister, J.; and Signer, P.: *J. Geophys. Res.*, Vol. 75, 1970c, p. 5972.
- Green, A. E. S.; and McNeal, R. J.: *J. Geophys. Res.*, Vol. 76, 1971, p. 133.
- Hall, L. A.; and Hinteregger, H. E.: *J. Geophys. Res.*, Vol. 75, 1970, p. 6959.
- Hasselmann, K.; and Wibberenz, G.: *Zh. Geophys.*, Vol. 34, 1968, p. 353.
- Heymann, D.; and Yaniv, A.: *Geochim. Cosmochim. Acta*, Suppl. 1, Vol. 2, 1970, p. 1261.
- Heymann, D.; Yaniv, A.; Adams, J. A. S.; and Fryer, G. E.: *Science*, Vol. 167, 1970, p. 555.
- Hintenberger, H.; Weber, H. W.; Voshage, H.; Wänke, H.; Begemann, F.; and Wlotzka, F.: *Geochim. Cosmochim. Acta*, Suppl. 1, Vol. 2, 1970, p. 1269.
- Hinteregger, J. E.; Hall, L. A.; and Schmidtke, G.: *Space Res.*, Vol. V, 1965, p. 1175.

- Hirshberg, J.; Alksne, A.; Colburn, D. S.; Bame, S. J.; and Hundhausen, A. J.: *J. Geophys. Res.*, Vol. 75, 1970, p. 1.
- Hohenberg, C. M.; Davis, P. K.; Kaiser, W. A.; Lewis, R. S.; and Reynolds, J. H.: *Geochim. Cosmochim. Acta*, Suppl. 1, Vol. 2, 1970, p. 1283.
- Holzer, T. E.; and Axford, W. I.: *Trans Amer. Geophys. Union*, Vol. 51, 1970a, p. 411.
- Holzer, T. E.; and Axford, W. I.: The Interaction Between Interstellar Helium and the Solar Wind, Preprint, 1970b.
- Hsieh, K. C.; and Simpson, J. A.: The Relative Abundances and Energy Spectra of  $\text{He}^3$  and  $\text{He}^4$  from Solar Flares, Preprint, 1970.
- Hundhausen, A. J.: *Space Sci. Rev.*, Vol. 8, 1968, p. 690.
- Hundhausen, A. J.; Asbridge, J. R.; Bame, S. J.; Gilbert, H. E.; and Strong, I. B.: *J. Geophys. Res.*, Vol. 72, 1967a, p. 87.
- Hundhausen, A. J.; Bame, S. J.; and Ness, N. F.: *J. Geophys. Res.*, Vol. 72, 1967b, p. 5265.
- Hundhausen, A. J.: Composition and Dynamics of the Solar Wind Plasma. Preprint, IUCSTP, *Symposium on Solar-Terrestrial Physics*, Leningrad, May 1970.
- Jokipii, J. R.: Thesis, California Institute of Technology, 1965.
- Jokipii, J. R.: *The Solar Wind*, Edited by R. J. Mackin and M. Neugebauer. Pergamon Press, New York, 1966a, p. 215.
- Jokipii, J. R.: *Astrophys. J.*, Vol. 146, 1966b, p. 480.
- Lambert, D. L.: *Nature*, Vol. 215, 1967, p. 43.
- Lambert, D. L.: *Mon. Notic. Roy. Astron. Soc.*, Vol. 138, 1968, p. 143.
- Lambert, D. L.; and Warner, B.: *Mon. Notic. Roy. Astron. Soc.*, Vol. 138, 1968, p. 181.
- Landau, L.: *J. Phys. (USSR)*, Vol. 10, 1946, p. 25.
- Lee, P.; and Weissler, G. L.: *Phys. Rev.*, Vol. 99, 1955, p. 540.
- Lehnert, B.: Minimum Temperature and Power Effect of Cosmical Plasmas Interacting with Neutral Gas. *Cosmic Electrodyn.*, Vol. 1, 1970, p. 397.
- Lingenfelter, R. E.; and Ramaty, R.: *High Energy Nuclear Reactions in Astrophysics*, Edited by B.S.P. Shen. W. A. Benjamin, Inc., New York, 1967, p. 99.
- Lotz, W.: *J. Opt. Soc. Amer.*, Vol. 57, 1967, p. 873.
- Manka, R. H.; and Michel, F. C.: *Science*, Vol. 169, 1970, p. 278.
- Marti, K.: *Science*, Vol. 166, 1969, p. 1263.
- Marti, K.; Lugmair, G. W.; and Urey, H. C.: *Geochim. Cosmochim. Acta*, Suppl. 1, Vol. 2, 1970, p. 1357.
- Meister, J.: Thesis, University of Bern, 1969.
- Michel, F. C.: *Planet. Space Sci.*, Vol. 12, 1964, p. 1075.
- Müller, E. A.; Baschek, B.; and Holweger, H.: *Solar Phys.* Vol. 3, 1968, p. 125.
- Nakada, M. P.: *Solar Phys.*, Vol. 7, 1969, p. 302.
- Nakada, M. P.: *Solar Phys.*, Vol. 14, 1970, p. 457.
- Neugebauer, M.; and Snyder, C. W.: *The Solar Wind*, edited by R. J. Mackin and M. Neugebauer. Pergamon Press, New York, 1966, p. 3.
- Ogilvie, K. W.; Burlaga, L. F.; and Wilkerson, T. D.: *J. Geophys. Res.*, Vol. 73, 1968, p. 6809.
- Ogilvie, K. W.; and Wilkerson, T. D.: *Solar Phys.*, Vol. 8, 1969, p. 435.
- Parker, E. N.: *Astrophys. J.*, Vol. 128, 1958, p. 664.
- Parker, E. N.: *J. Res. Nat. Bur. Standards*, Vol. 65, 1961, p. 537.
- Parker, E. N.: *Interplanetary Dynamical Processes*. Interscience, New York, London, 1963.
- Pepin, R. O.: *Earth Planet. Sci. Letters*, Vol. 2, 1967, p. 13.
- Pepin, R. O.; Nyquist, L. E.; Phinney, D.; and Black, D. C.: *Geochim. Cosmochim. Acta*, Suppl. 1, Vol. 2, 1970, p. 217.
- Podosek, F. A.; Huneke, J. C.; Burnett, D. S.; and Wasserburg, G. J.: *Earth Planet. Sci. Letters*, Vol. 10, 1971, p. 217.
- Pottasch, S. R.: *Origin and Distribution of the Elements*, edited by L. H. Ahrens. Pergamon, New York, 1968, p. 183.
- Reynolds, J. H.: *J. Geophys. Res.*, Vol. 68, 1963, p. 2939.
- Reynolds, J. H.; and Turner, G.: *J. Geophys. Res.*, Vol. 69, 1964, p. 3263.
- Robbins, D. E.; Hundhausen, A. J.; and Bame, S. J.: *J. Geophys. Res.*, Vol. 75, 1970, p. 1178.
- Sari, J. W.; and Ness, N. F.: *Solar Phys.*, Vol. 8, 1969, p. 155.
- Scarf, F. L.: *Raumfahrtforschung*, Vol. 3, 1966, p. 114.
- Schatzman, E.: Turbulent Diffusion in the Sun and Solar Neutrinos. *Cortina Conf. on Astrophys. Aspects of Weak Interactions*, Preprint, 1970.
- Signer, P.; Eberhardt, P. and Geiss, J.: *J. Geophys. Res.*, Vol. 70, 1965, p. 2243.
- Siscoe, G. L.; Lyon, E. F.; Binsack, J. H.; and Bridge, H. S.: *J. Geophys. Res.*, Vol. 74, 1969, p. 59.
- Snyder, C. W.; and Neugebauer, M.: *Proc. Intern. Space Sci. Symp.*, Vol. 4, 1964, p. 89.
- Spitzer, L.: *Physics of Fully Ionized Gases*, 2nd ed. Interscience, New York, London, 1962.
- Stix, T. H.: *The Theory of Plasma Waves*. McGraw-Hill, New York, 1962.
- Sturrock, P. A.; and Hartle, R. E.: *Phys. Rev. Letters*, Vol. 16, 1966, p. 628.



- Thomas, G. E.; and Krassa, R. F.: *Astron. Astrophys.*, Vol. 11, 1971, p. 218.
- Unsöld, A.: *Physik der Sternatmosphären*, Springer-Verlag, Berlin, 1955.
- Unsöld, A.: *Science*, Vol. 163, 1969, p. 1015.
- Wolfe, J. H.; Silva, R. W.; McKibbin, D. D.; and Matson, R. H.: *J. Geophys. Res.*, Vol. 71, 1966, p. 3329.
- Zähringer, J.: *Geochim. Cosmochim. Acta*, Vol. 26, 1962a, p. 665.
- Zähringer, J.: *Z. Naturforsch.*, Vol. 17a, 1962b, p. 460.

C. P. Sonett Could I ask you to comment further on the  $^4\text{He}/^3\text{He}$  where you showed the aubrites and the lunar case, i.e., Apollo 11 and 12. I think it is the 4000 ratio. I wonder if there is a possibility that instead of the 4000 for a fossil or primordial ratio, whether perhaps some different effect is taking place.

J. Geiss I should say first that there is other fossil helium in other meteorites, where ratios such as 2000, 3000, and 4000 exist. I selected these 4000 for the aubrites not only because it shows a difference but we have evidence of surface implantation. The aubrites are perhaps not as primordial as, for instance, the carbonaceous chondrites but I think, the matrix in the aubrites is rather original material, at least in terms of chemical composition. And one reason why I think this is an  $^4\text{He}/^3\text{He}$  ratio, which should be taken seriously, is that the He/Ne is so high. When the first data from the lunar surface became available, there was some evidence that the isotopic concentration of helium varied with successively older solar winds. In the consolidated dust, ratios such as 3400 were being obtained by the lunar receiving lab, but later others have measured the same stones and don't find these ratios. A year ago or so I was much more in favor of the idea that there is a gradual change in  $^4\text{He}/^3\text{He}$ . Now we just don't know and we have just this old—this 4000 ratio to worry about. We don't know enough about the modern  $^4\text{He}/^3\text{He}$  ratio yet, but by having a few more falls and by looking into the Surveyor material we should be able to establish some kind of average ratio. We have data on the Surveyor material and there the value is about 2700.

Unidentified Speaker Could you comment further about making the separations of  $^4\text{He}$  and H?

J. Geiss Well, there are two ways. I'm sure there are more ways, but I've tried to discuss two. One is that there is a separation between the photosphere and base of the corona by diffusion, as was first discussed by Jokipii and DeLache. There is, of course, an effect of thermal diffusion. Gravitational settling is offset by thermal diffusion because the temperature gradient is so high and the thermal diffusion for ions is very large; I think it was pointed out very early by Chapman and by Seaton that this might cause an enrichment of the corona by heavy elements. The argument was that the corona seemed to be more abundant; for instance, in iron, but this is now not so difficult to explain.

The other is that, as I have shown, if you have a very quiet situation and radial magnetic field, a certain flux is needed to drive the helium outward and this flux is higher than even for iron. There should then be correlation between flux and helium abundance, but this does not exist. It is possible, however, that such a correlation is obliterated, for instance, by the streamers, because we refer to the flux at 1 AU; and to extrapolate this backwards to the Sun very large errors may accrue if anything like streamers exist. Then we come to the very enhanced helium abundances. I want to mention that Hundhausen has suggested that once we had a source of enhanced helium abundance and other heavy

## DISCUSSION

---

NOTE: For the reader unacquainted with the terminology of meteoritics, the aubrites are a class of achondritic (stony and lacking chondrules) meteorites commonly called enstatite achondrites. Enstatite is a pyroxene mineral which is relatively iron-free. The name aubrite comes from the location of the first recorded fall of this class, Aubres. ED.

element abundance in the middle corona where the speeds of the heavier ions should be somewhat smaller than the speed of the protons (I think almost any model would suffice). If you suddenly drive out this gas, then you have enhanced abundance of the heavier ions. But this should also be then true for elements such as iron and oxygen.

*Unidentified Speaker* (Possibly Cowling): In the absence of Chapman perhaps I might make a comment about thermal diffusion. First of all, the thermal diffusion is affected very considerably by a magnetic field, but I don't think that is particularly important because one can rely fairly considerably on thermal diffusion along the magnetic field. On the other hand, one is inclined to overstress the importance of thermal diffusion. Thermal diffusion assists in separating out material to some extent, just because it is cut down less by the large size of the electrostatic forces than ordinary diffusion is, so that you would get a very considerable separation if you have no mixing. But the degree of upset by a moderate amount of mixing would be just as bad whether you have a large thermal diffusion or not.

*C. P. Sonett* Would you care at all to comment on where the deuterium and the  $^3\text{He}$  come from?

*J. Geiss* You mean, after God or after nuclear synthesis?

*C. P. Sonett* Isn't it correct that there is even a question involving nuclear synthesis?

*J. Geiss* The general idea always has been that something like spallation will contribute to the origin of these isotopes. Schatzman has worried very much about this. He has connected it with the lithium abundance and the three elements, lithium, beryllium, and boron. Now, if you make a detailed theory there are always some problems because we know too much about the exact isotopic composition of lithium (i.e., too many measured parameters). So one has to have many theoretical parameters. But it cannot be gotten out of stellar interiors and a high energy nonequilibrium mechanism. I should say that in the solar wind as we see it on the Moon we have no evidence for deuterium.

*C. P. Sonett* What about  $^3\text{He}$ ?

*J. Geiss*  $^3\text{He}$  is present as we see it in the foils, but  $^3\text{He}$  could be present on the solar surface because  $^3\text{He}$  does not burn in the outer convective zone, I am told; there, one is rather sure that deuterium burns and I think  $^6\text{Li}$  also burns in the outer convective zone. It may be that  $^3\text{He}$  is marginally stable in the outer convective zone.

*E. C. Roelof* With regard to the ratio of protons to helium in solar flares I would like to comment that recent observations at low energies, namely, about 1 MeV per nucleon, show that the ratio H/He is quite highly variable as opposed to the case of higher energy, perhaps two magnitudes higher in energy per nucleon, whereas one gets a ratio of something like 60 rather repeatedly at those energies. At low energies during an event the ratio can change by easily a factor of 3, and in quasi-stationary corotating events even the ratio is quite variable. The most interesting ordering aspects of this is that the ratio in the low energy seems to vary in accordance with the spectral steepness of the proton or helium spectrum is a way suggested by Professor Schatzman several years ago. So, in summary, the ratio is variable to low energies and it does seem to vary as the spectral steepness of the particle spectrum varies during an event and at almost any time one observes them.

*J. Geiss* Do you mean this whole effect is a result of the large difference in rigidity?

*E. C. Roelof* No, I don't believe that it's completely that, because one finds that the C and O to helium ratios at the same velocity and hence at the same rigidity, if they are fully ionized, will also vary during events. So there are a number of possible explanations, but the possible point is that no single number can be attached to the ratio C and O to helium, helium to proton, for solar flare at these low energies.

*D. Heymann* May I return for a moment to the question of the  $^1\text{H}/^2\text{H}$  ratio. The number is less than 50 parts in a million; but one can also look at it with some comfort because it's clear that if the spallation produced  $^3\text{He}$  and  $^{21}\text{Ne}$  is considered in these

samples, practically all the deuterium can be accounted for by spallation. Roughly, it depends on what is assumed for the relative yields for deuterium to the  $^3\text{He}$ . But it says that if the galactic cosmic ray flux relative to the solar wind had been ten times higher, a deuterium concentration similar to the one you can see on earth in these lunar samples would be present. This may not be the explanation for what exists on earth, but this number of about 50 parts in a million can be viewed in different ways. You can look at it with a long face and say it shouldn't be there. You can also say this is produced by galactic cosmic rays.

*J. Geiss* And solar flare particles?

*D. Heymann* And solar flare particles.

*Unidentified Speaker* I would like to point out that it is not impossible that you would get changes—and if it does decelerate you would expect the heavier matter to settle out. So the flare ejecta should be expected to have the heavier material in a thin shell on the outer face. Another point I would also like to make is I think a lot of the atmospheric escape evaporation work that has been done in the past should perhaps be taken with a large grain of salt, because you have assumed temperatures for the atmosphere which are very dubious, and if there are local hot spots in the atmosphere, as now seems to be possible according to some recent results, the escape base may be much faster than we have believed in the past; hence it is not possible that the neon isotopic ratios that you showed could be explained just on that basis alone.

*J. Geiss* I think that's quite right.

*D. Heymann* Of course it is true that one has to take the 4000 number for the  $^3\text{He}$  and aubrites seriously because you've shown that it is probably not affected by any fractionation since the helium to neon ratio is as high or similar to what you find in soils. If I adopt that argument, then I say you also have to take that ratio into combination with meteorites seriously because there, too, the ratio of 40:20 is quite high. You cannot reject one number on the basis of a certain argument and say the other one is valid.

*J. Geiss* I would say that is not valid, but that could be solar wind more recently.

*Unidentified Speaker* I can use that argument just as well to apply to a carbonaceous meteorite and say we have to accept these values.

*J. Geiss* Yes, but you can't say there was at one spot in the solar system a ratio of 4000, and the question is how important this was.

*M. Dryer* When particles strike the moon is it possible that some of them bounce off or perhaps knock other particles off?

*J. Geiss* Yes. The first slide I showed indicated the impacting of helium on the very well defined aluminum surface and even there the helium bounces off. Now, this very likely comes off as neutral, because there is enough time to attach all the electrons the nucleus requires for neutralization. On the lunar surface, there is a finite probability of a rapid escape at relatively high energy if the direction is right. The other possibility is that you have escape or release of these gases just by heating.

## SOLAR WIND HELIUM ENHANCEMENTS FOLLOWING MAJOR SOLAR FLARES *J. Hirshberg*

**ABSTRACT** The observations of solar wind helium enhancements following major solar flares are reviewed, and the hypothesis that helium enhancements often mark flare piston plasma is confirmed. Helium enhancements were observed during each of the three periods (March 1966, July 1966, August/September 1966) of major solar activity that occurred from October 1965 to October 1966. No enhancements were seen during the long quiet periods that occurred that year. During 1966-67,  $\text{He}/\text{H} \geq 10$  percent after 13 major flares, as listed. In 12 of the cases cited,  $\text{He}/\text{H} \geq 15$  percent in at least one plasma spectrum. Eight of the flares produced prompt solar cosmic ray protons. At 1 AU, the helium-enhanced plasma pistons had slowed so that the velocity was 80 percent of the mean transit velocity, in general agreement with theoretical models of the propagation of flare disturbances. A qualitative model, in which the piston plasma is accelerated from the flare site deep in the corona, is discussed briefly. If the model is valid in general outline, the piston plasmas provide samples of material from the lower levels of the corona.

### INTRODUCTION

The average relative helium abundance in the solar wind has been found to be of the order of 4 to 5 percent [Neugebauer and Snyder, 1966; Wolfe *et al.*, 1966; Robbins *et al.*, 1970; Ogilvie and Wilkerson, 1969; Formisano *et al.*, 1970]. However, individual spectra show  $\text{He}/\text{H}$  varying from less than 1 percent to greater than 25 percent. The causes of this variation are not yet understood. We have proposed that periods of enhanced helium abundance mark the piston plasmas accelerated into space by solar flares [Hirshberg *et al.*, 1970]. In this paper, we discuss evidence that supports our hypothesis and briefly consider a model that might produce a helium enhancement of the flare piston plasma.

### OBSERVATIONS

The propagation of flare plasma in space is shown schematically in figure 1. The shock due to the flare disturbance will be detected at earth several days after

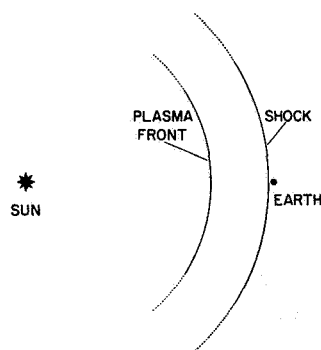


**Figure 1.** Schematic representation of the propagation of solar flare disturbances.

the flare. The velocity, temperature, density, and magnetic field intensity of the plasma will all increase discontinuously across the shock. However, the ratio of  $\text{He}/\text{H}$  will remain unchanged, since the region behind the shock simply consists of compressed ambient solar wind. The discontinuity between the compressed plasma and the flare piston itself, appears several hours after the shock has passed. If the helium enhancement marks the

---

*The author is at NASA-Ames Research Center, Moffett Field, California.*

plasma piston, it will occur behind the discontinuity between the piston and the ambient wind. The pattern we expect, then, is a flare, followed several days later by a shock with no change of helium, and then, some hours after that, a helium enhancement.

This expected pattern can be compared to the observations shown in figure 2 from *Hirshberg et al.* [1970]. A 3B flare had been observed on February 13, 1967, at 20°N, 10°W. No other major flares occurred within a week before this flare, or for 5 days afterward. A shock discontinuity was observed by Vela 3A in earth orbit at about midnight, February 15. The velocity, temperature, density, and magnetic field intensity all increased post-shock, while the relative helium abundance remained virtually unchanged. However, about 9 hr after the shock had passed, we see a marked increase in helium to an abundance of more than 20 percent. Similar patterns have been reported for the helium enhancements of 10 to 15 percent on April 17, 1968 [*Gosling et al.*, 1967], 12 percent on July 11, 1966 [*Lazarus and Binsack*, 1969], 17 percent on May 30, 1967 [*Ogilvie et al.*, 1968], and 18 percent on January 14, 1967 [*Bame et al.*, 1968], and for the series of flares of August/September 1966 [*Hirshberg et al.*, 1971].

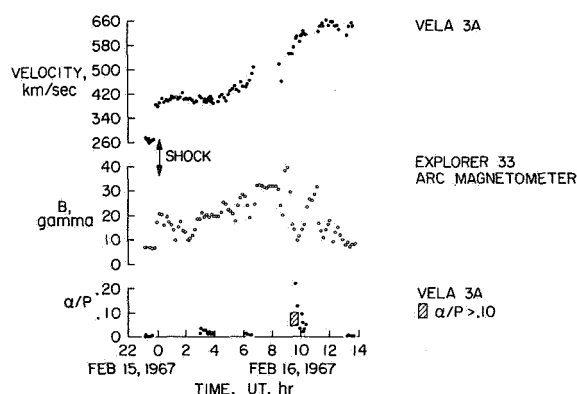


**Figure 2.** Interplanetary disturbance caused by the 3B flare, 13 Feb. 1966. Note shock discontinuity 2351, Feb. 15. The postshock He/H does not increase appreciably until 9 hr later, when He/H ~ 20 percent is detected. The helium enhancement marks the flare piston plasma [figure from *Hirshberg et al.*, 1970].

Although there are many examples of helium enhancements appearing at earth several days after major solar flares, the possibility that this apparent association between flares and helium enhancements is simply a

coincidence must be dealt with [*Ogilvie and Wilkerson*, 1969]. To do this we will discuss the observations made during the year from October 1965 to October 1966. During this period the interplanetary medium was observed by plasma probes on Vela 3A and 3B in earth orbit and by MIT's plasma probe on Pioneer 6, in solar orbit.

The solar cycle was very close to minimum in October 1965, but the sunspot number was increasing rapidly throughout the following year. Solar flare activity was characterized by long periods of quiet, interrupted by a few short periods of intense solar activity. The helium enhancements that occurred during the periods of intense flare activity are discussed below.

The first major period of solar activity of the new solar cycle occurred in March 1966. This activity has been preceded by a long quiet period. In the seven months before the March activity, only one flare (66-01-17, N19 E27) was listed as 3B by any observatories, and that flare was listed by only one observatory. Then, at the end of March, plage region 8207 became extremely active and produced five flares that were reported as 3B by at least one observatory, including the major proton flare of March 24.

The solar wind during this period was being monitored by Vela 3A and 3B, which collected data on the relative helium abundance during the 2 years from July 1965 to July 1967. During these two years, *Robbins et al.* [1970] reports that over 10,000 spectra were collected, 2 percent of which showed He/H > 10 percent. In their study, only 48 spectra show He/H ≥ 15 percent. Because of the rarity of such spectra, we will take He/H ≥ 15 percent as a criterion for saying that a helium enhancement has been observed by the Vela probes. With this criterion in mind, we note that the plasma probe collected 3,178 spectra during the quiet sun period between October 1965 and March 1966. There was not a single spectrum showing a helium abundance as large as 15 percent. Then, at the end of March, during the period of solar activity, six spectra showed He/H ≥ 15 percent. If we define an enhancement as a period during which at least one spectrum shows ≥ 15 percent helium, and no spectra show < 10 percent helium, we find three distinct periods of enhancement during the end of March. These enhancements contributed to the high average helium abundance of 6 percent during the period March 21 through 30, as discussed by *Hundhausen* [1970]. The three separate enhancements were attributed to the three major flares of March 20, 24, and 25 [*Hirshberg et al.*, 1971, in preparation]. The first helium enhancement could have been due to either the major flare of March 19 or March 20; however, the second was more likely.

There was no ambiguity in the assignment of the second and third enhancements to the proton flare of March 24, and the major flare of March 25, respectively.

The second period of major solar activity of the new solar cycle occurred during the first half of July, 1966. An intensive study of these events has been made [Annals of the IQSY, 1969]. There were three class 2B flares, on July 7, 8, and 9. The proton flare of July 7 was the largest of the three. The solar wind plasma was observed by Vela 3B in earth orbit, and Pioneer 6 in solar orbit 43.7° west of the earth. The flare of July 7 was a central meridian flare as seen from Pioneer. During the period when the flare plasma was expected both satellites detected plasma with velocities greater than 550 km/sec. Unfortunately, the Velas spent most of the period of interest (July 9-13) within the magnetosphere. Data were collected only during a 4½-hr period on July 10 and for less than an hour on July 11. The observed helium abundances were low (1-4 percent). However, helium enhancements typically pass the detector in a matter of a few hours. Thus a helium enhancement at earth could have easily been missed because of the poor data coverage. The observational situation at Pioneer 6 was more fortunate. On this vehicle, helium could be detected only when the proton component of the solar wind was relatively cold. On July 11, the temperature of the protons was low enough, and a relative abundance of helium of 12 percent was reported by Lazarus and Binsack [1969]. The enhancement was probably due to the July 9 flare. A helium enhancement, then, was seen at Pioneer 6 but not at earth. The failure to detect the enhancement at earth may well have been due to poor data coverage.

The third major period of solar activity occurred in August/September 1966. The activity has been described by Švestka and Simon [1969] who list two proton flares (August 28 and September 2) and several

additional class 2 flares (August 26, and August 31, and a limb flare on September 4). The plasma from the flares could be expected to arrive at earth between August 30 to September 9. This period has been discussed in detail elsewhere [Hirshberg *et al.*, 1971]. The plasma was observed by Vela, which had collected 1,231 spectra between the March 1966 events and these events of August/September. Having missed the July enhancement, Vela has not detected a single spectrum with He/H ≥ 15 percent during the 5-month period between March and August. In contrast, between August 30 and September 9, 1966, Vela collected 134 spectra, eleven of which (8.2 percent) showed He/H ≥ 15 percent while 28 (22 percent) showed abundances greater than 10 percent.

There were four distinct periods of helium enhancement. For the details of making specific flare-enhancement identifications, see Hirshberg *et al.* [1971]. The resulting identifications are shown in table 1. The two proton flares of August 28 and September 2 are both associated with helium enhancements, as is the major flare of August 31. The second enhancement listed in the table could not be reasonably associated with a flare major in H<sub>α</sub>. It is listed as due to a class 2 flare on August 30. The method of making that assignment will be discussed below. Returning to the major flares and their helium enhancements, the observed velocity of the helium enriched solar wind is given in the fourth column. The average transit velocity, calculated by assuming the plasma left the sun at the time of the beginning of the flare, is shown in the next column. We define a "slowing-ratio" as being the ratio of the observed velocity to the transit velocity. A slowing ratio of greater than 1 indicates that the plasma has speeded up on its way to the earth. The slowing ratios are shown in the final column of table 1. The helium enriched plasma due to the August 28 flare seems to have been

**Table 1.** Flares and associated solar wind helium enhancements, Aug./Sept. 1966 [adapted from Hirshberg *et al.*, 1971]

Flare	Class	Helium enhancement	Observed velocity, km/sec	Average transit velocity, km/sec	Slowing ratio
1966 Aug. 28	2B	Aug. 31	653	596	1.1
(Aug. 30)	(2)	Sept. 1	576		
Aug. 31	2N	Sept. 3	439	475	0.9
Sept. 2	3B	Sept. 5	424	580	0.7

speeded up, perhaps by the plasma from a later flare [Hirshberg *et al.*, 1971]. The slowing ratios for the last two events are more typical of other observed flare-helium events. Slowing ratios to be expected for solar flare shocks are estimated from theory to be of the order of 0.8 [Hundhausen and Gentry, 1969]. If we assume that slowing ratios of 0.8 are fairly typical for flare pistons, then we can hunt for a flare to assign to the second helium enhancement shown in table 1. The flare chosen was described as class 2 by Zirin and Lackner [1969].

Summing up, the year from October 1965 to October 1966 is characterized by long periods of quiet sun, broken by a few periods of intense solar activity. During the quiet time, the percentage of helium in the solar wind remained relatively low. Enhancements were detected following solar activity. Although one enhancement was tentatively attributed to a less important flare, all other enhancements during that year were associated with major  $H_{\alpha}$  flares.

After September 1966, solar activity increased to the point where there were no more long quiet periods. However, major flares were still fairly well isolated in time, and  $He/H \geq 15$  percent was not seen often. Other flare-enhancement associations have been reported for the period between October 1966 and May 1967 [Bame *et al.*, 1968; Hirshberg *et al.*, 1971, in preparation; Ogilvie *et al.*, 1968], but will not be reviewed in detail here.

In table 2 we have listed 13 flares that have been reliably associated with helium enhancements during the period from July 1965 to July 1967. The second column of the table shows the class of the flare. Most of the enhancements were due to the largest and brightest flares. A star indicates that solar protons were observed in space [Lin, 1970]. Every class 3 flare with prompt solar cosmic rays was followed by a helium enhancement. Column 3 shows the *maximum* percentage of helium observed during each enhancement. The *average* value of  $He/H$  during the enhancements seen by Vela was of the order of 15 percent. The final column shows the slowing ratio of the plasma pistons. The average slowing ratio is 0.8, in general agreement with theoretical calculations of the propagation of flare plasma [Hundhausen and Gentry, 1969].

## MODELS

One of the most interesting questions that these observations bring up is the problem of the cause of the flare helium enhancement. At the present state of observational and theoretical knowledge, we cannot come to any definitive conclusion on this question. However, we

**Table 2.** Flares and associated solar wind helium enhancements, July 1965-July 1967. See text for references.

Flare date	Class of flare	Maximum percent of He	Slowing ratio
66-03-20	3B	31	0.8
66-03-24	3B	26	0.7
66-03-25	3B	18	1.0
66-07-9	2B	12	0.8
66-08-28	2B	16	1.1
66-08-31	2N	17	0.9
66-09-2	3B	22	0.7
66-09-17	2B	17	0.7
66-10-14	2B	16	0.6
67-01-11	3B	29	0.7
67-02-13	3B	22	0.8
67-05-23	2B	16	0.8
67-05-28	3B	17	1.0

shall describe a qualitative model that appears reasonable and that may serve as a basis for further study.

The relationship between  $He/H$  observed at 1 AU and the relative helium abundance in the solar corona is not yet well understood. In addition, we do not know either the mean value of  $He/H$  in the corona or its distribution. It has long been recognized that the percentage of helium in the solar wind would be lower than that in the corona since helium is more difficult to accelerate into the wind than hydrogen [Brandt, 1966]. The distribution of helium in the corona and wind has been discussed in several recent theoretical papers. The basic approach is to consider diffusion in an atmosphere flowing away from the sun as a solar wind. The diffusion can be due to thermal or pressure gradients, electric fields and/or gravitation. It will lead to regions of the solar atmosphere that are relatively enhanced or depleted in helium. Since the heavy elements diffuse toward regions of high temperature, the lower corona will have  $He/H$  large relative to that of the cool chromosphere [Jokipii, 1966; Delache, 1967; Nakada, 1969]. There also will be a tendency for the helium to settle out of the upper corona, again producing a relative helium enrichment in the lower corona [Nakada, 1970; Yeh, 1970; Geiss *et al.*, 1970]. This tendency for solar atmospheric stratification will be opposed by mixing. However, unless the mixing is very strong, we may expect some enhancement in the relative abundance of helium at a few tenths of a solar radius above the

photosphere. In addition, the same mechanisms operating in the vicinity of an active region may cause local areas of enhanced helium abundance.

With these regions of probable coronal helium enhancement in mind, it is interesting to consider the model to produce flare piston plasma that has been suggested by Axford [1970]. Briefly, observations of solar flare disturbances in the interplanetary medium indicate that the flare piston plasma is ejected from sun with a sizable amount of its energy in the form of directed motion [Akasofu, 1966; Hirshberg, 1968]. Axford has proposed a mechanism for producing the directed motion. He suggests that the source of the flare piston plasma is in the lower corona. The flare heats a blob of plasma, which is then very buoyant and therefore rises rapidly through the corona. Magnetic fields confine the plasma within the blob. These same fields would also confine the helium so that it could not leak out and be left behind, as it would by a solar wind type of accelerating mechanism. If this model is valid in general outline, the flare pistons described in this paper are samples of plasma from the lower regions of the corona.

#### ACKNOWLEDGMENTS

This work was completed during tenure of a National Research Council Senior Postdoctoral Resident Research Associateship.

#### REFERENCES

- Akasofu, S. I.: Electrodynamics of the Magnetosphere. *Space Sci. Rev.*, Vol. 6, 1966, p. 21.
- Annals of the IQSY*, Volume 3, MIT Press, 1969.
- Axford, W. I.: A Survey of Interplanetary and Terrestrial Phenomena Associated with Solar Flares. *Intercorrelated Satellite Observations Related to Solar Events*, edited by V. Manno and D. E. Page. D. Reidel, Dordrecht, Holland, 1970.
- Bame, S. J.; Asbridge, J. R.; Hundhausen, A. J.; and Strong, I. B.: Solar Wind and Magnetosheath Observation During the Jan. 13-14, 1967 Geomagnetic Storm. *J. Geophys. Res., Space Phys.*, Vol. 73, 1968, p. 5761.
- Brandt, J. C.: Chemical Composition of the Photosphere and Corona as Influenced by the Solar Wind. *Astrophys. J.*, Vol. 143, 1966, p. 265.
- Delache, P.: Contribution à l'étude de la Zone de Transition Chromosphère-Couronne. *Ann. Astrophys.*, Vol. 30, 1967, p. 827.
- Formisano, V.; Palmiotto, F.; and Moreno, G.:  $\alpha$ -particle Observations in the Solar Wind. *Solar Phys.*, Vol. 15, 1970, p. 479.
- Geiss, J.; Hirt, P.; and Leetwyler, H.: On Acceleration and Motion of Ions in Corona and Solar Wind. *Solar Phys.*, Vol. 12, 1970, p. 458.
- Gosling, J. T.; Asbridge, J. R.; Bame, S. J.; Hundhausen, A. J.; and Strong, I. B.: Measurements of the Interplanetary Solar Wind During the Large Geomagnetic Storm of April 17-18, 1965. *J. Geophys. Res.*, Vol. 72, 1967, p. 1813.
- Hirshberg, J.: The Transport of Flare Plasma from the Sun to the Earth. *Planet. Space Sci.*, Vol. 16, 1968, pp. 3, 309.
- Hirshberg, J.; Alksne, A.; Colburn, D. S.; Bame, S. J.; and Hundhausen, A. J.: Observation of a Solar Flare Induced Interplanetary Shock and Helium Enriched Driver Gas. *J. Geophys. Res.*, Vol. 75, 1970, p. 1.
- Hirshberg, J.; Asbridge, J. R.; and Robbins, D. E.: The Helium-Enriched Interplanetary Plasma from the Proton Flares of August/September 1966. *Solar Phys.*, Vol. 18, 1971, p. 313.
- Hundhausen, S. J.; and Gentry, R. A.: Numerical Simulation of Flare-Generated Disturbances in the Solar Wind. *J. Geophys. Res.*, Vol. 74, 1969, p. 2908.
- Hundhausen, A. J.: Composition and Dynamics of Solar Wind Plasma. *Rev. Geophys. Space Phys.*, Vol. 8, 1970, p. 729.
- Jokipii, J. R.: Effects of Diffusion on the Composition of the Solar Corona and the Solar Wind. *The Solar Wind*, edited by R. J. Mackin, Jr., and M. Neugebauer. Pergamon Press, New York, 1966, p. 215.
- Lazarus, A. J.; and Binsack, J. H.: Observations of the Interplanetary Plasma Subsequent to the 7 July Proton Flare. *Ann. IQSY*, Vol. 3, 1969, p. 378.
- Lin, R. P.: The Emission and Propagation of 40 Kev Solar Flare Electrons I: The Relationship of 40 Kev Electron to Energetic Proton and Relativistic Electron Emission by the Sun. *Solar Phys.*, Vol. 12, 1970, p. 266.
- Nakada, M. P.: A Study of the Composition of the Lower Solar Corona. *Solar Phys.*, Vol. 7, 1969, p. 302.
- Nakada, M. P.: A Study of the Composition of the Solar Corona and Solar Wind. *Solar Phys.*, Vol. 14, 1970, p. 457.
- Neugebauer, M.; and Snyder, C. W.: Mariner 2 Measurements of the Solar Wind. *The Solar Wind*, edited by R. J. Mackin, and M. Neugebauer. Pergamon Press, New York, 1966, p. 3.
- Ogilvie, K. W.; Burlaga, L. F.; and Wilkerson, T. D.: Plasma Observations on Explorer 34. *J. Geophys. Res.*, Vol. 73, 1968, p. 6809.



- Ogilvie, K. W.; and Wilkerson, T. D.: Helium Abundance in the Solar Wind. *Solar Phys.*, Vol. 8, 1969, p. 435.
- Robbins, D. E.; Hundhausen, A. J.; and Bame, S. J.: Helium in the Solar Wind. *J. Geophys. Res., Space Phys.*, Vol. 75, 1970, p. 1178.
- Švestka, Z.; and Simon, P.: Proton Flare Project 1966, Summary of the August/September Particle Events in the McMath Region 8461. *Solar Phys.*, Vol. 10, 1969, p. 3.
- Wolfe, J. H.; Silva, R. W.; McKibbin, D. D.; and Mason, R. H.: The Compositional, Anisotropic and Nonradial Flow Characteristics of the Solar Wind. *J. Geophys. Res.*, Vol. 71, 1966, pp. 13, 3329.
- Yeh, T.: A Three-Fluid Model of Solar Winds. *Planet. Space Sci.*, Vol. 18, 1970, p. 199.
- Zirin, H.; and Russo Lackner, D.: The Solar Flares of August 28 and 30, 1966. *Solar Phys.*, Vol. 6, 1969, p. 86.

*E. C. Roelof* I hate to raise the spectre again of the corotating versus the radial shock, but three of the events that you have identified as having the helium driver gas following the shock are precisely the three events in 1967 which Lin and I did analyze and decided were corotating events. Those are the slides I did not show on Monday. Those were January 11, February 13, and May 28, 1967.

Now, there is obviously disagreement here. I would like to point out that there is the alternative explanation; the matter has to be settled somehow and if these are corotating events then simply what is happening is that you are not seeing a driver gas but merely a helium enriched stream from the region that produced the flare, which I feel is also quite a reasonable interpretation.

*J. Hirshberg* It seems to me that that picture would not give the slowing ratio which was shown in all those three events, that there is no particular reason to have that 0.8 slowing ratio. If you're dealing with solar wind, then it should be speeding up on the way out, not slowing down.

*J. Geiss* I wonder if I'm the only one that doesn't know what Axford's greasy balloon is.

*J. Hirshberg* Well, Axford has suggested that you suddenly heat up some material above the flare and then it pops out like a cork, and this he has referred to earlier in the conference as a greasy balloon. I am suggesting the balloon has a lot of helium in it.

*Unidentified Speaker* I think that we should not consider with a teaspoon in mind the large excess of Alpha particles which appear in solar flares. I think this is one of the major problems in plasma physics, to understand how it is possible to increase by such a large factor the concentration of Alpha particles in respect to protons.

*Dr. Dryer* I guess you know what I'm going to ask, Joan. Did you look at all of the—let me ask this question first, what was the time interval generally between the arrival of the shock and then the arrival of the piston, in hours?

*J. Hirshberg* Well, in many of these events, like the March events and August events, there were so many shocks and discontinuities that I couldn't assign a particular shock to a given helium enhancement. In the early events we seemed to get about 10 hours.

*Dr. Dryer* Yes. Did you ever make any effort to see if there might possibly be a reverse shock that might follow the piston?

*J. Hirshberg* No.

*Dr. Dryer* You didn't make the effort, or there were none?

*J. Hirshberg* I didn't make the effort.

*Dr. Dryer* Did you have magnetic field data?

*J. Hirshberg* No.

## DISCUSSION

## HEOS 1 HELIUM OBSERVATIONS IN THE SOLAR WIND

*D. Bollea, V. Formisano, P. C. Hedgecock,  
G. Moreno and F. Palmiotto*

**ABSTRACT** Results of  $\alpha$ -particle observations performed by the European satellite HEOS 1, in the period from December 9, 1968, to April 13, 1969, and from September 6, 1969, to April 15, 1970, are presented. The average bulk velocities of protons  $V_p$  and  $\alpha$ -particles  $V_\alpha$  appear to be equal; however, due to an instrumental bias, the possibility of  $V_\alpha$  being lower than  $V_p$  cannot be ruled out. Comparison with observations of Vela 3 and Explorer 34 satellites gives evidence of a dependence of helium abundance on the solar cycle. The problem of the stability of differences between the bulk velocities of protons and  $\alpha$ -particles is investigated. The behavior of  $\alpha$ -particles through interplanetary shock waves is illustrated in connection with magnetic field measurements.

### INTRODUCTION

Initial results on the observations of the helium component of the solar wind, performed by the ESRO satellite HEOS 1, are given by *Formisano et al.* [1970a] and *Formisano et al.* [1970b]. Here we summarize the results obtained during the period from December 9, 1968, to April 13, 1969, and from September 6, 1969, to April 15, 1970. Observations of three interplanetary shock waves are presented, using HEOS 1 plasma and magnetic field data. Details of the satellite orbit, the particle detector, and the measurement routine are given by *Bonetti et al.* [1969].

HEOS 1 was launched on December 5, 1968, on a highly eccentric orbit. The satellite is spin stabilized; the spin period is  $\sim 6$  sec, and the angle between spin axis and sun-satellite line is always in the range  $90^\circ \pm 20^\circ$ . The positive ion detector (consisting of a hemispherical

electrostatic deflector and a Faraday cup) points perpendicular to the spin axis. Each measurement consists essentially of the positive ion flux integrated over an angle of  $180^\circ$  centered about the sun-satellite direction. Flux measurements are performed in 28 adjacent energy channels according to a programmed sequence, covering the range of energy per unit charge from about 200 to about 16,000 eV/Z. A complete energy distribution is obtained every 6.4 min, which is the duration of a telemetry subframe. The particular time sequence chosen for the energy channels allows a discrete-step coverage of the whole energy range in four subcycles of 1.6-min duration. The sensitivity of the instrument is approximately  $10^7$  protons/cm<sup>2</sup>s or  $5 \times 10^6$   $\alpha$ -particles/cm<sup>2</sup>s.

The magnetic field experiment on board HEOS 1 has been described by *Hedgecock* [1970].

### AVERAGE PROPERTIES

During the time period considered,  $\alpha$ -particles were detected in 4,997 subframes, corresponding to a total observation time of  $\sim 20.8$  days. The method of analysis to obtain the parameters of interest ( $\alpha$ -particle number density  $N_\alpha$ , bulk velocity  $V_\alpha$ , most probable thermal speed  $W_\alpha$ ) has been described by *Bonetti et al.* [1969] and *Formisano et al.* [1970b].

---

*Drs. D. Bollea, V. Formisano, and F. Palmiotto are at the Laboratorio per lo Studio del Plasma nello Spazio del C.N.R., Roma, Istituto di Fisica dell'Università, Roma. Dr. P. C. Hedgecock is at the Department of Physics, Imperial College of Science and Technology, London. Dr. G. Moreno is at the Laboratorio per le Radiazioni Extraterrestri, C.N.R., Bologna-Firenze, Cattedra di Fisica dello Spazio, Università, Firenze.*

Figure 1 shows the frequency distribution of individual values of  $V_\alpha/V_p$  (ratio of  $\alpha$ -particle to proton bulk velocity). The average value of  $V_\alpha/V_p$  is 1.02, identical to the value obtained by Robbins *et al.* [1970] from Vela 3 observations. Though the deviation of this value

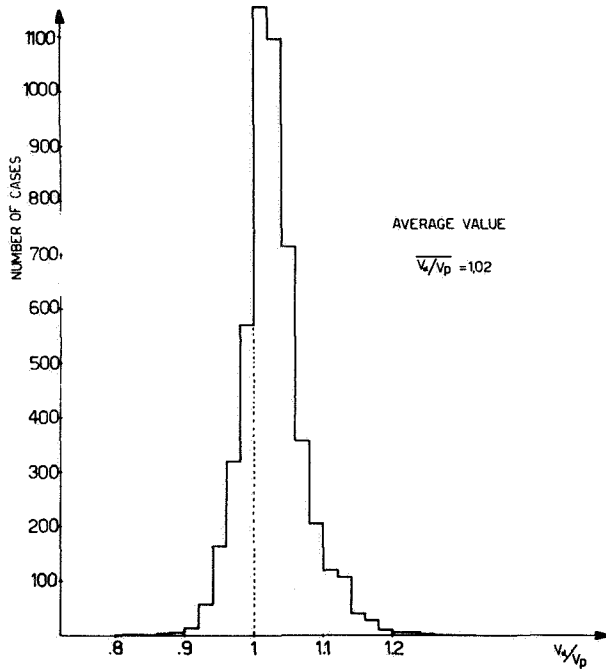


**Figure 1.** Frequency distribution of individual values of  $V_\alpha/V_p$ .

from 1 is relatively small, attention should be paid to the lack of symmetry of the histogram. In several cases  $V_\alpha$  is definitely larger than  $V_p$  (in more than 300 spectra the difference is greater than 10 percent), while only a few spectra give  $V_\alpha/V_p < 0.9$ . It is interesting to note that the frequency distribution of values of  $V_\alpha/V_p$  given by Robbins *et al.* [1970] exhibits the same asymmetry as the HEOS 1 histogram. On the other hand, theories of the solar corona expansion [Geiss *et al.*, 1970; Nakada, 1970] do not suggest any mechanism of preferential acceleration of helium relative to the hydrogen component of the solar wind (see also the discussion by Geiss, p. 566).

The only experimental bias that could affect both the Vela and the HEOS histogram seems to be that when  $V_\alpha < V_p$ , detection of  $\alpha$ -particles could sometimes be prevented by the higher proton fluxes; indeed, if  $V_\alpha = 0.7V_p$ , the  $\alpha$ -particle peak in the energy per unit charge spectrum becomes coincident with the proton

maximum and consequently cannot be observed. To evaluate the importance of the bias, we computed for each individual energy spectrum the lowest  $\alpha$ -particle bulk velocity  $V_{\alpha,min}$  that still could be resolved from the proton spectrum (that is, which would give an observable secondary peak) when no second peak for  $\alpha$ -particles was observed. Such computations were performed assuming  $W_\alpha = W_p$  and different values for the  $\alpha$ -particle abundance ( $N_\alpha/N_p$ ). Results are shown in figure 2 in the form of frequency distributions of values

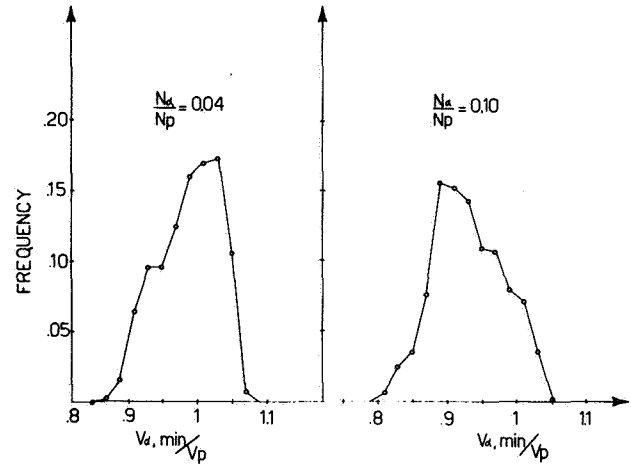


**Figure 2.** Frequency distributions of values of  $V_{\alpha,min}/V_p$  for two  $\alpha$ -particle abundances.  $V_{\alpha,min}$  is defined as the lowest  $\alpha$ -particle bulk velocity which still could be resolved from protons (i.e., which would give an observable secondary peak in the energy per unit charge spectrum).

of  $V_{\alpha,min}/V_p$  for two values of the ratio  $N_\alpha/N_p$ . As expected the bias decreases for high helium abundance, but it is certainly relevant for typical values of the ratio  $N_\alpha/N_p$  ( $\sim 0.05$ ). The behavior of the average values of  $V_\alpha$  and  $V_p$  versus  $N_\alpha$  (fig. 3) confirms this result; in fact for  $N_\alpha = 0.4 \text{ cm}^{-3}$ ,  $\bar{V}_\alpha$  reaches  $\bar{V}_p$ , becoming smaller than  $\bar{V}_p$  for higher helium densities. It should be noted, however, that only a few spectra give  $\bar{V}_\alpha < \bar{V}_p$ . In figure 3 only cases with  $|V_\alpha - V_p| > 20 \text{ km/sec}$  are considered consistent with detectability of a measurable difference between the two bulk velocities.

We can conclude that within the limitation of present experiments, no difference between the average bulk velocities of the two species is observed; however, an average  $\bar{V}_\alpha$  lower than  $\bar{V}_p$  would have not been observed. Deviations of the ratio  $V_\alpha/V_p$  from 1 appear to be present during particular time periods.

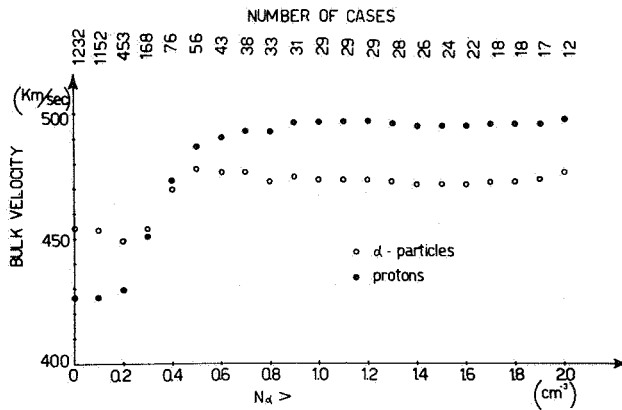


**Figure 3.** Average values of  $V_\alpha$  and  $V_p$  for  $N_\alpha$  larger than given values. Only cases with  $|V_\alpha - V_p| > 20$  km/sec have been considered.

The frequency distribution of the relative abundances of helium is given in figure 4. The average value of the ratio  $N_\alpha/N_p$  is 0.051. Figure 5 shows a time history of the helium abundance with the measured sunspot number taken as an index of solar activity. Values of  $N_\alpha/N_p$  obtained by Vela 3 [Robbins et al., 1970] and by Explorer 34 [Ogilvie and Wilkerson, 1969] are shown with HEOS 1 averages for comparison. Averages from HEOS 1 and Vela 3 satellites have been performed over

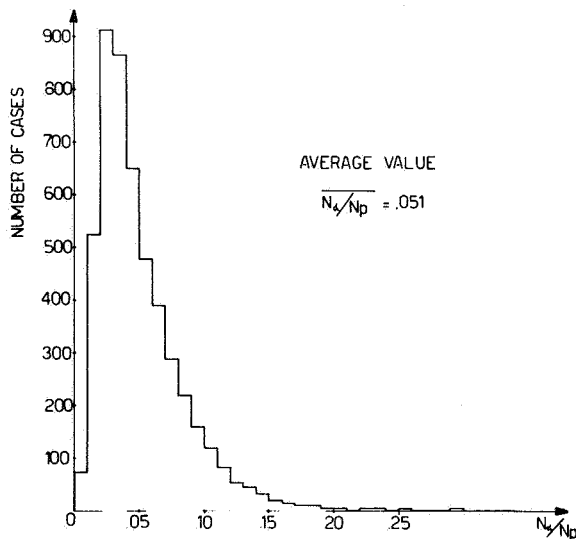


**Figure 4.** Frequency distribution of individual values of  $N_\alpha/N_p$ .

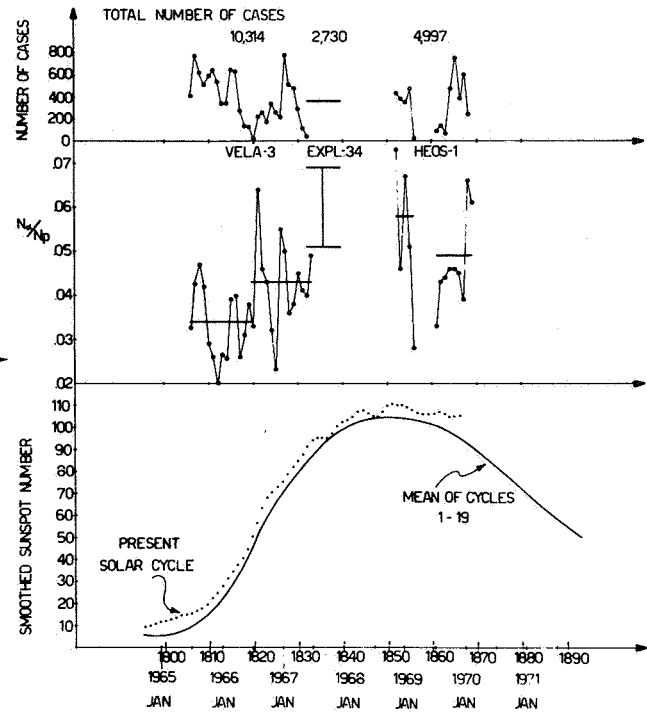


**Figure 5.** Time history of the ratio  $N_\alpha/N_p$ , according to observations performed by the satellites Vela 3, Explorer 34 and HEOS-1. Averages from HEOS-1 and Vela 3 [Robbins et al., 1970] have been performed over solar rotations (points) and over longer periods of time (bars). For Explorer 34 [Ogilvie and Wilkerson, 1969] only a total average is shown; the two values correspond to the average uncorrected for the instrumental bias (upper bar) and to the corrected average (lower bar). The number of cases over which the averages were performed is shown in the upper part of the figure. At the bottom, the measured sunspot number is given [Solar Geophysical Data, 1970].

solar rotations (points) and over longer periods of time (bars). For Explorer 34 only a total average was available; the two values given in the figure correspond to the average uncorrected value (lower bar). The general pattern of the ratio  $N_\alpha/N_p$  appears to confirm a dependence of helium abundance on the solar cycle.

The plasma bulk velocity appears correlated with the helium abundance. Figure 6 shows the average values of  $V_p$  and  $V_\alpha$  computed over the spectra with  $N_\alpha/N_p$  larger than 0.00, 0.01, 0.02, . . . . For the study of the steady-state condition of the solar wind, data referring to postshock periods (defined as 24 hr following a sudden

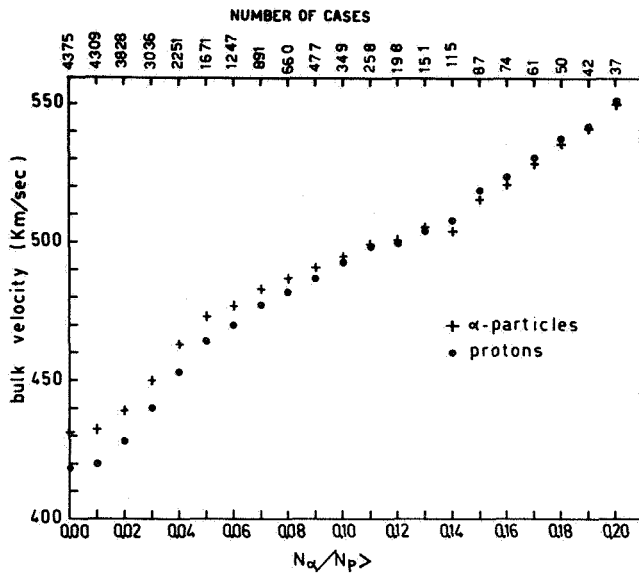


**Figure 6.** Average values of  $V_p$  and  $V_\alpha$  computed over the spectra with  $N_\alpha/N_p$  larger than given values. The number of cases, over which the averages were performed, is shown on the top.

commencement) have been removed from these averages. An increase of  $\sim 120$  km/sec is observed in the bulk velocity of both species when  $N_\alpha/N_p$  increases.

Figure 7 presents a comparison between the behavior of  $\bar{V}_\alpha$ ,  $\bar{V}_p$  versus  $N_\alpha$  and  $\bar{V}_p$  versus  $N_p$ . The  $\bar{V}_p$  versus  $N_p$  plot, which was made with all the proton data (fig. 7(b)), shows the well-known result that the proton flux  $N_p V_p$  is approximately constant, in contrast to the general pattern of the  $\bar{V}_\alpha$  versus  $N_\alpha$  plot (fig. 7(a)), which shows a tendency to an increase of  $\bar{V}_\alpha$  with  $N_\alpha$ . Again it should be noted that for high densities of  $\alpha$ -particles,  $\bar{V}_\alpha$  becomes lower than  $\bar{V}_p$ .

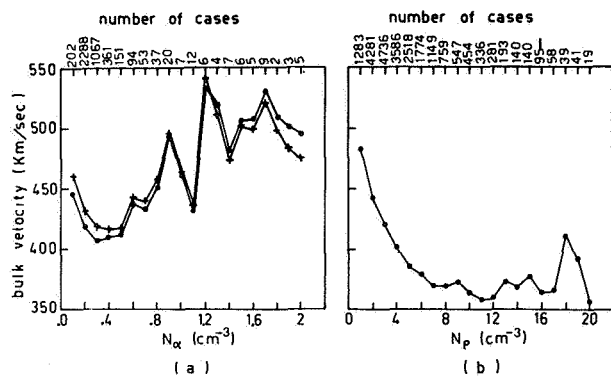


**Figure 7.** Average values of  $\bar{V}_\alpha$  and  $\bar{V}_p$  plotted versus  $N_\alpha$  (a) and of  $\bar{V}_p$  versus  $N_p$  (b). Number of cases is given on top. The  $\bar{V}_p$ - $N_p$  plot was made using all the available data.

The increase in helium abundance together with the increase in the bulk velocity is predicted by the diffusion models of the solar corona [Nakada, 1970]. An increase in the coronal temperature, indeed, should increase the solar wind bulk velocity following the magnetohydrodynamic models [Parker, 1963; Hartle and Sturrock, 1968] and should also decrease the diffusion time, increasing the helium abundance in the expanding corona.

## TWO-BEAM INSTABILITY

As shown in the previous section and by Formisano *et al.* [1970b] it is possible, occasionally, to observe different bulk velocities for protons and  $\alpha$ -particles. Theoretically, it has been predicted [Geiss *et al.*, 1970; Nakada, 1970; Yeh, 1970; Alloucherie, 1970] that the helium bulk velocity should be lower (about 20 percent or more) than the proton bulk velocity in the solar corona, while some instability of the two stream type should be operating in the solar wind to equalize  $V_p$  and  $V_\alpha$ . The problem has been studied with our data. The observations should reveal the quasi-steady state quickly reached by the solar wind at a few tenths of AU from the sun. Figure 8 shows the behavior of  $\bar{W}_p$ ,  $\bar{W}_\alpha$  versus  $V_\alpha/V_p$ . The protons and helium average most probable thermal speeds increase for values of  $V_\alpha$  and  $V_p$  different from 1. The observed variations of  $\bar{W}_\alpha$  and  $\bar{W}_p$  correspond to an increase of the proton and  $\alpha$ -particle temperature of a factor 2. This result was already shown by Formisano *et al.* [1970b]. Figure 8 refers to more data, and the result is confirmed.

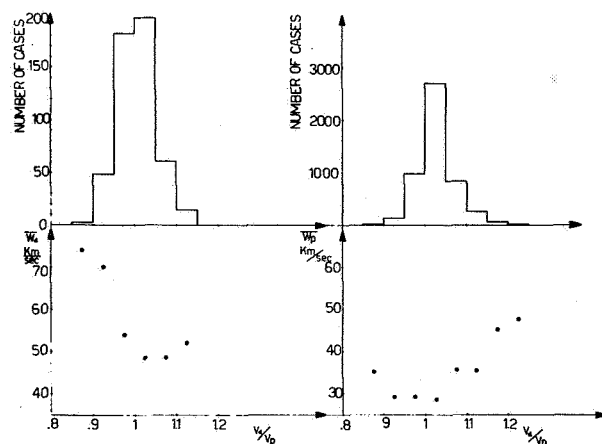


**Figure 8.** Average values of  $\bar{W}_\alpha$  and  $\bar{W}_p$  plotted versus  $V_\alpha/V_p$ . Averages have been performed on  $V_\alpha/V_p$  intervals of 0.05. In the upper part of the figure histograms of the total number of cases considered in the averages are given.

The two-stream instability predicts that the faster beam will be slowed down, giving energy to waves and increasing the thermal energy of the particles. If the faster beam is the major beam—that is, has higher density (protons in the solar wind)—the energy available for waves and thermalization is large, and therefore a more rapid increase of the temperature of the slower beam and a higher noise level of unstable waves is expected. If the faster beam is the minor one (lower density,  $\alpha$ -particles in the solar wind), a slower increase of the thermal energy of the slower beam is predicted. This behavior is shown in figure 8;  $\bar{W}_\alpha$  increases faster (for  $V_\alpha < V_p$ ) than  $\bar{W}_p$  (for  $V_\alpha > V_p$ ).

Figure 9 shows the actual solar wind points in relation to the two stream instability criterium of high frequency longitudinal waves for two maxwellian distributed beams [Taylor, 1970]. In a plane  $b, c$  [ $b = 4(W_p/W_\alpha)^2$ ,  $c = |V_\alpha - V_p|/W_p$ ] plasma will be stable or unstable depending on the quantity  $a = (N_\alpha/N_p)(W_p/W_\alpha)^3$ . The stable region is the one on the left of the line corresponding to the given value of the parameter  $a$ .

Figure 9 shows for each  $(b, c)$  pair the edge of the stable region. The "a" scale is given at the top of the figure. All the data plotted have  $|V_\alpha - V_p| > 10$  km/sec. All the points fall within the stable region, some just

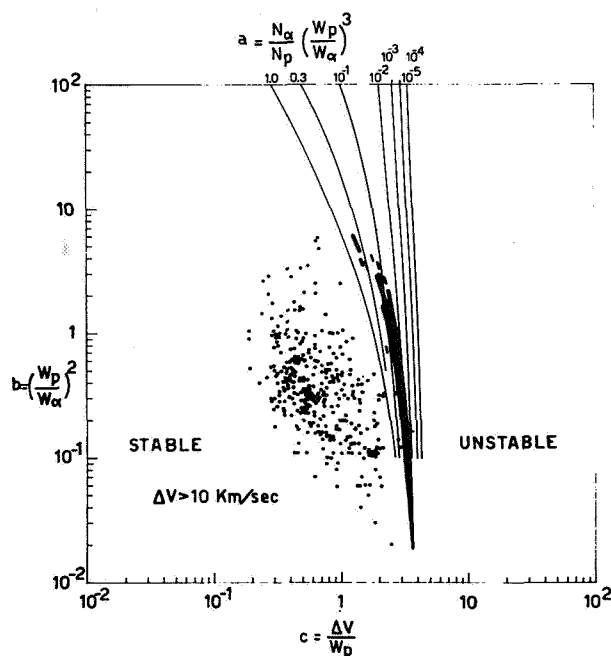


Figure 9. The scatter plot of  $b = (W_p/W_\alpha)^2$  and  $c = |V_\alpha - V_p|/W_p$ . The two-stream instability (for longitudinal waves) lines are shown for different values of the parameter  $a = N_\alpha/N_p (W_p/W_\alpha)^3$ . Black areas represent the edges of the stable region for each  $(b, c)$  pair.

behind the stability line, most well inside the stable region. Lower values of  $|V_\alpha - V_p|$  would give more points in the more highly stable region.

It should be remembered, however, that the two-streaming plasma is unstable with respect to both longitudinal and transverse waves. Parker [1961] has shown that Alfvén waves could be generated by a two-streaming plasma. Kennel and Petschek [1968] have related the firehose instability to the two-beam instability and the resulting instability criterium becomes

$$\beta \alpha_p \alpha_\alpha \left( \frac{V_\alpha - V_p}{W_p} \right)^2 + \Delta\beta \geq 2 \quad (1)$$

where

$$\beta = \sum_{p, e, \alpha} \frac{3}{4} \frac{mW^2}{B^2/8\pi}$$

is the ratio between the total particle pressure and the magnetic pressure,  $\alpha_p/\alpha_\alpha$  is the ratio between the proton ( $\alpha$ -particle) number density and the total ion number density;  $\Delta\beta = \beta_\parallel - \beta_\perp$ ;  $\beta_\parallel = 3\beta - 2\beta_\perp$ ; and  $\beta_\parallel/\beta_\perp = K$  is the anisotropy ratio. It is evident from equation (1) that the firehose instability is modified if  $\alpha$ -particles have  $V_\alpha \neq V_p$  and that the difference  $V_\alpha - V_p$  must be reduced by a firehose stable anisotropy in the three species. Figure 10 shows the stable region with respect to both firehose and two stream instability.

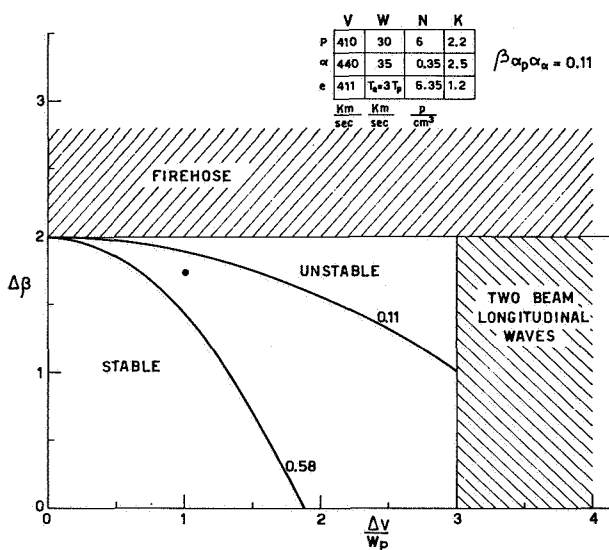


Figure 10. Stability region with respect to the firehose and two stream instability. Equation (1) has been plotted for  $\beta \alpha_p \alpha_\alpha = 0.11$  and  $0.58$ . The  $0.11$  value refers to the set of parameters given on the top of the figure (the corresponding position in the  $\Delta\beta, \Delta V/W_p$  plane is represented by the black point).

As an example, a possible set of parameters and the corresponding position in the  $\Delta\beta, \Delta V/W_p$  plane have been indicated.

It should also be noted that another instability, of the resonant type, has been found by *Barnes*, [1970] for bow shock reflected protons. It is not yet clear whether this instability can be important for the  $\alpha$ -particle and proton streams.

### SHOCK WAVE OBSERVATIONS

The behavior of  $\alpha$ -particles through two interplanetary shock waves (February 28 and March 19, 1969) has been studied by *Formisano et al.* [1970b] using the HEOS 1 plasma data. Here we present the  $\alpha$ -particle observations, together with interplanetary magnetic field measurements, during the two above-mentioned shocks and a third one, which occurred on March 25, 1969. This last event is discussed in detail by *Chao et al.* [1971].

Figure 11 shows the event, which occurred on February 28, 1969, detected at ground as a sudden commencement at UT 0425, by 19 stations. At UT 0422 a sudden increase of  $\alpha$ -particle density, bulk velocity, and thermal speed is observed;  $V_\alpha$  changes from 507 km/sec to 637 km/sec;  $N_\alpha$  from  $0.35 \text{ cm}^{-3}$  to  $0.80 \text{ cm}^{-3}$ ;  $W_\alpha$  from less than 57 km/sec to  $\sim 88 \text{ km/sec}$ .

The proton behavior is quite different: during about half an hour (from UT 0405 to UT 0431)  $V_p$  changes only  $\sim 50 \text{ km/sec}$ . The proton density, which has an increment of  $\sim 30$  percent at UT 0412, decreases to the previous value of  $5 \text{ cm}^{-3}$  when the  $\alpha$ -particle discontinuity is detected. A small gradual increase is observed for the proton thermal speed. The proton energy spectrum, which was previously maxwellian, exhibits a non-maxwellian high-energy tail after the  $\alpha$ -particle discontinuity, as had been shown by *Formisano et al.* [1970b]. The  $\alpha$ -particle parameters show the characteristic variations of a shock. The identification of the  $\alpha$ -particle discontinuity with a shock wave is confirmed by the magnetic field measurements. Indeed, simultaneously with the  $\alpha$ -particle discontinuity, the magnetic field intensity increases of a factor 2 (from  $\sim 6\gamma$  to  $\sim 12\gamma$ ).

Magnetic field oscillations are noted in the figure, before the sudden variation at UT 0422. They appear to be related to the earth's bow shock crossed by the satellite, moving outward from the earth, at UT 0120; during the 3-hr period from UT 0120 to UT 0422, these oscillations are permanently detected by HEOS 1, indicating the presence of waves associated with protons reflected from the earth's bow shock [*Asbridge et al.*, 1968].

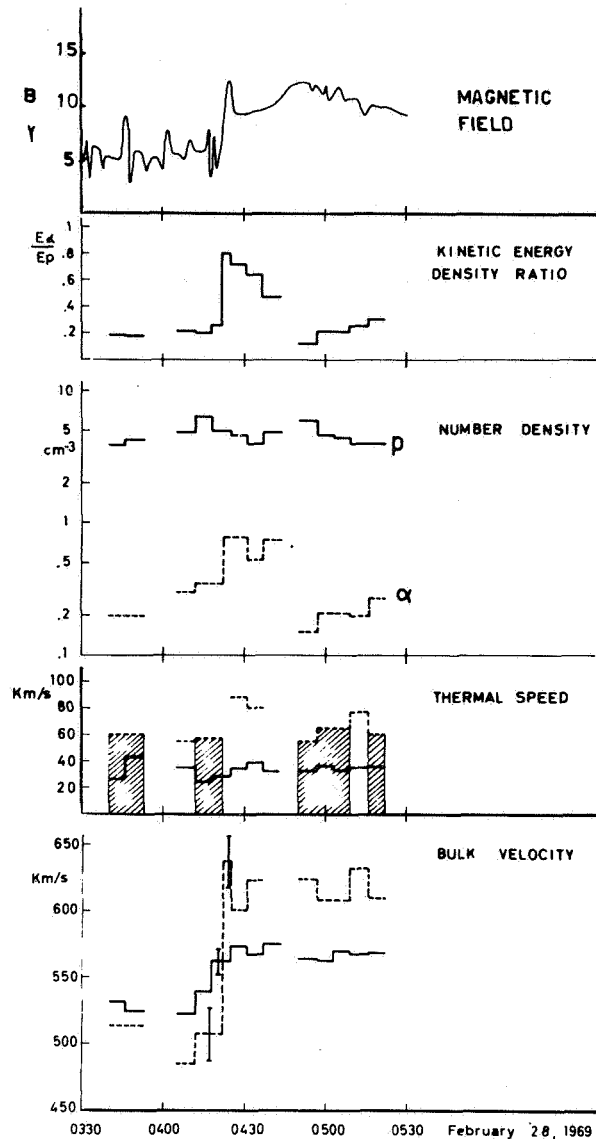


**Figure 11.** Positive ion parameters and magnetic field for the event of February 28, 1969. From the top are given: the magnetic field intensity, the  $\alpha$ -particle to proton kinetic energy density ratio; the  $\alpha$ -particle and proton number densities; the most probable thermal speeds of protons and  $\alpha$ -particles; the proton and  $\alpha$ -particle bulk velocities. Broken lines refer to  $\alpha$ -particles, continuous lines to protons.

Figure 12 illustrates the March 19 event observed at ground as a sudden commencement at UT 1959. Three minutes before (at UT 1956 with an error of  $\pm 0.8 \text{ min}$ ) the protons exhibit a velocity discontinuity of  $\sim 45 \text{ km/sec}$  (from  $396 \text{ km/sec}$  to  $439 \text{ km/sec}$ ) and a

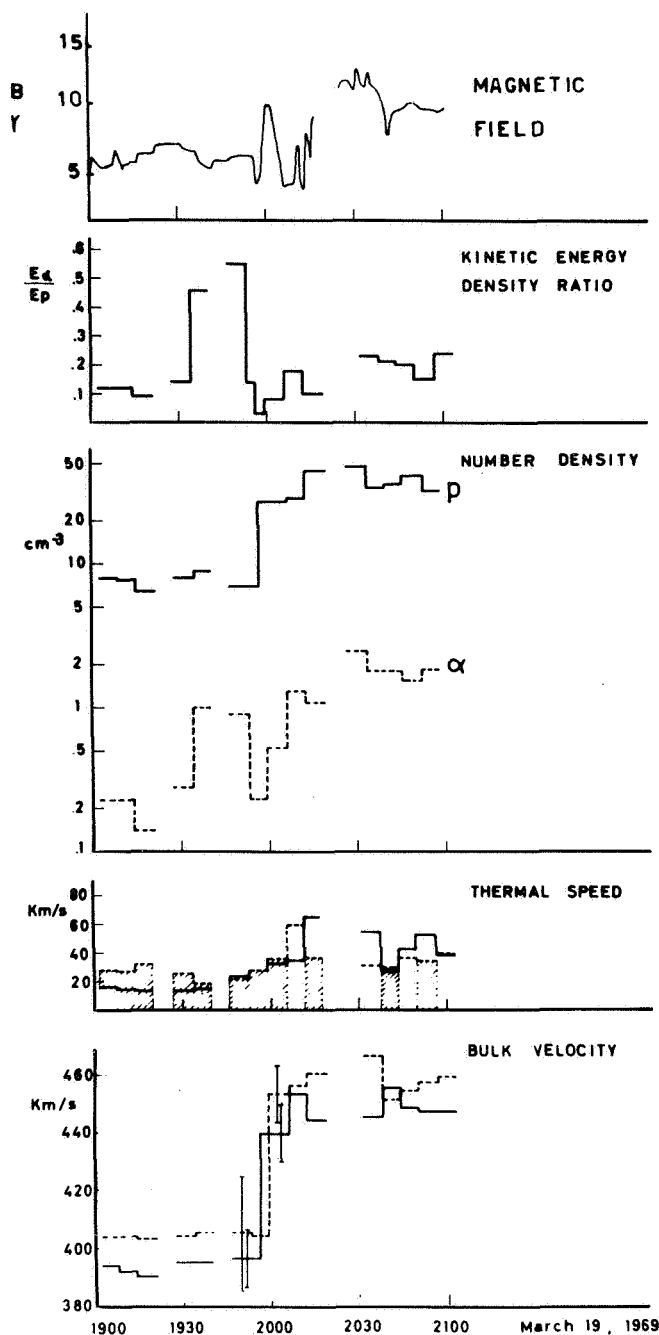


Figure 12. Positive ion parameters and magnetic field intensity for the event of March 19, 1969.

density increase by a factor of 4 (from 7 protons/cm<sup>3</sup> to 27 protons/cm<sup>3</sup>), while the thermal speed increases by only 10 km/sec. The  $\alpha$ -particle discontinuity ( $V_\alpha$  from 404 km/sec to 453 km/sec and  $N_\alpha$  from 0.2 cm<sup>-3</sup> to 0.5 cm<sup>-3</sup>) is observed with a time delay of  $\sim 3$  min

compared to the proton discontinuity [Formisano *et al.*, 1970b]. The magnetic field measurements show a sudden change of the field intensity (from  $\sim 5\gamma$  to  $\sim 10\gamma$ ) at 1956 UT, simultaneously to the proton discontinuity. Later on, the magnetic field undergoes strong fluctuations.

Figure 13 illustrates the third shock wave occurring on

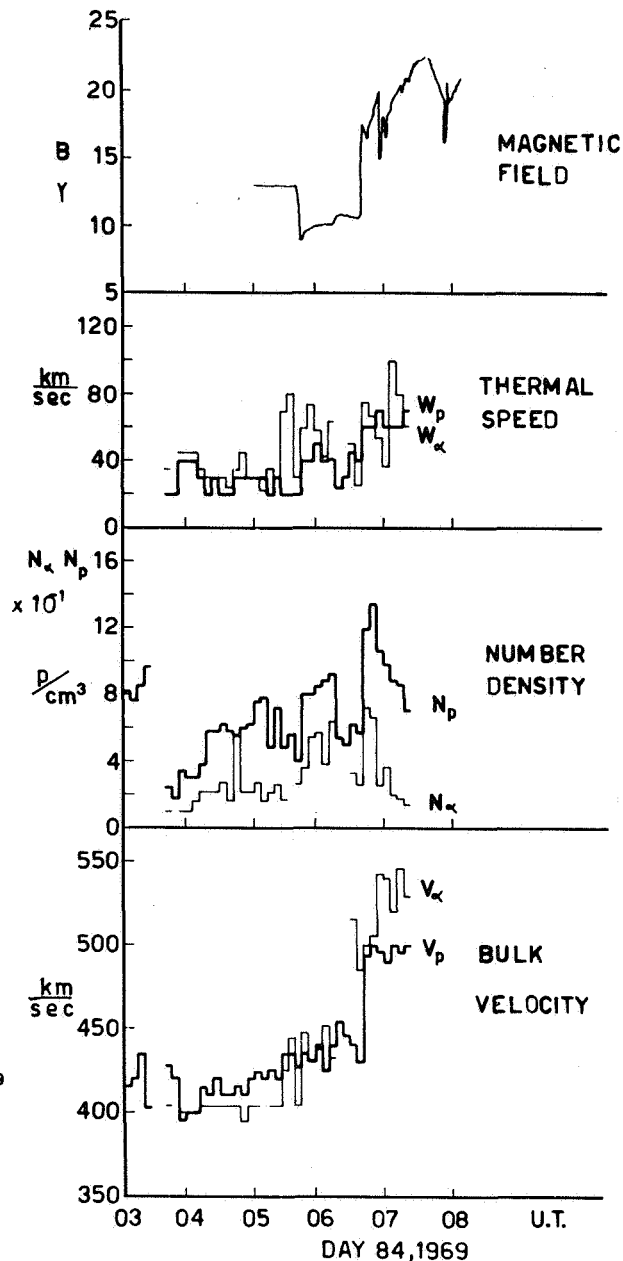


Figure 13. Positive ion parameters and magnetic field intensity for the event of March 25, 1969. In the number density plot the scale of  $N_\alpha$  should be multiplied by  $10^{-1}$ .



March 25. At UT 0646 a sudden variation of the proton parameters is observed ( $V_p$  from 435 km/sec to 490 km/sec;  $N_p$  from  $\sim 6 \text{ cm}^{-3}$  to  $10.4 \text{ cm}^{-3}$ ;  $W_p$  from 40 km/sec to 60 km/sec); at the same time, the magnetic field intensity increases from  $10\gamma$  to  $18\gamma$ . The  $\alpha$  particles exhibit a different behavior. No relevant change of  $V_\alpha$  is observed when the shock is detected, while a large discontinuity is observed a few minutes before the shock:  $V_\alpha$  goes from 430 km/sec at UT 0614 to 515 km/sec at UT 0633 (two measurements are missed between).

Due to the data gap, we have no information on  $N_\alpha$  at UT 0633, when the discontinuity of the  $\alpha$ -particle bulk velocity is observed; however, the fact that  $\alpha$  particles escape detection in the two subframes between UT 0614 and UT 0633 may suggest that  $N_\alpha$  was lower during that period. When the proton shock is detected, at UT 0646,  $N_\alpha$  increases from  $0.3 \text{ cm}^{-3}$  to  $0.7 \text{ cm}^{-3}$ .

The behavior of protons and  $\alpha$  particles through the shock is better illustrated in figure 14. Three energy per unit charge spectra are shown: subframe 25630 is observed before the  $V_\alpha$  change; subframe 25633 is observed just after the  $V_\alpha$  increase, but before the proton discontinuity; subframe 25635 is taken just behind the shock. A maxwellian distribution was fitted to the three highest fluxes for both protons and  $\alpha$ -particles; the obtained parameters are shown for both species. In all cases the maxwellian fits do not appear to be very good; in particular, a non-maxwellian high energy tail is clearly observed at UT 0633, when there was a large difference between proton and  $\alpha$ -particle bulk velocities.

## CONCLUSIONS

We can summarize our results as follows:

1. Within the limitations of present experiments, no difference between the average bulk velocities of protons and  $\alpha$ -particles is detected. However, due to an instrumental bias, the possibility of  $V_\alpha$  being lower than  $V_p$  cannot be ruled out.
2. Data from the satellites Vela 3, Explorer 34, and HEOS 1 give evidence of a dependence of helium abundance on the solar cycle.
3. On average, high helium abundances are observed together with high bulk velocities, in agreement with diffusion models of the solar corona.
4. When a definite difference between proton and  $\alpha$ -particle bulk velocity is observed, the stability with respect to high frequency longitudinal waves is ensured by higher thermal speeds. However, the problem of transverse wave instability, due to differences between  $V_\alpha$  and  $V_p$ , has not been investigated.

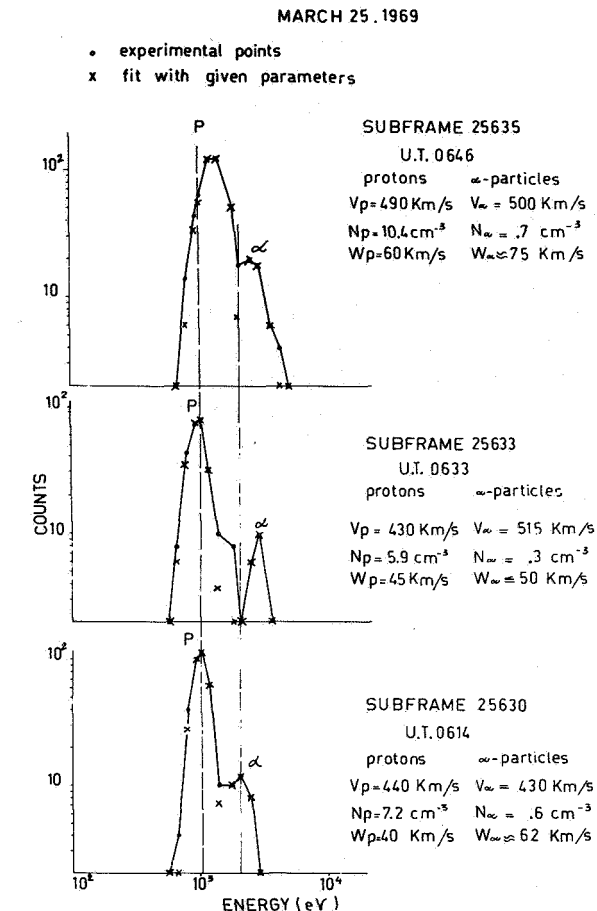


Figure 14. Positive ion energy spectra observed on March 25, 1969, at UT 0614, 0633 and 0646. Electrometer counts (black points) are plotted versus energy per unit charge. P indicates proton peaks;  $\alpha$  indicates  $\alpha$ -particle peaks. Crosses indicate the maxwellian fit of the observed spectra for the given values of proton and  $\alpha$ -particle parameters.

5. The behavior of  $\alpha$ -particles through interplanetary shock waves is not a simple one. Strong discontinuities may be observed in one species, without occurring in the other, or having different characteristics. In particular, the magnetic field observations confirm the interpretation of the  $\alpha$ -particle discontinuity, occurred on February 28, 1969, as a shock wave.
6. When a strong discontinuity is detected only for  $\alpha$ -particles, the proton distribution function shows a large non-maxwellian high-energy tail.

## ACKNOWLEDGMENTS

We are very grateful to Prof. A. Egidì for useful discussions. We are indebted to the other personnel of the

Laboratorio per il Plasma nello Spazio of Rome who have participated in the development of the solar wind experiment. This research has been supported by the Consiglio Nazionale delle Ricerche of Italy. The HEOS 1 magnetic field experiment was supported by the British Science Research Council.

## REFERENCES

- Alloucherie, Y.: Diffusion of Heavy Ions in the Solar Corona. *J. Geophys. Res.*, Vol. 75, 1970, p. 6899.
- Asbridge, J. R.; Bame, S. J.; and Strong, I. S.: Outward Flow of Protons from the Earth's Bow Shock. *J. Geophys. Res.*, Vol. 73, 1968, p. 5777.
- Barnes, A.: Theory of Generation of Bow Shock Associated Hydromagnetic Waves in the Upstream Interplanetary Medium. *Cosmic Electrodyn.*, Vol. 1, 1970, p. 90.
- Bonetti, A.; Moreno, G.; Cantarano, S.; Egidi, A.; Marconero, R.; Palutan, F.; and Pizzella, G.: Solar Wind Observations with the ESRO Satellite HEOS 1 in December 1968. *Nuovo Cimento B*, Vol. 64, 1969, p. 307.
- Chao, J. K.; Formisano, V.; and Hedgecock, P. C.: Shock Pair Observation in the Solar Wind. Preprint, 1971.
- Formisano, V.; Egidi, A.; and Moreno, G.: Observations of Solar Wind  $\alpha$ -Particles in the Magnetosheath. *Lettere Nuovo Cimento*, Vol. 3, 1970a, p. 209.
- Formisano, V.; Moreno, G.; and Palmiotto, F.:  $\alpha$ -Particle Observations in the Solar Wind. *Solar Phys.*, Vol. 15, 1970b, p. 479.
- Geiss, J.; Hirt, P.; and Leutwyler, H.: On Acceleration and Motion of Ions in Corona and Solar Wind. *Solar Phys.*, Vol. 12, 1970, p. 458.
- Hartle, R. E.; and Sturrock, P. A.: Two Fluid Model of the Solar Wind. *Astrophys. J.*, Vol. 151, 1968, p. 1155.
- Hedgecock, P. C.: The Solar Particle Event of February 25, 1969. *Intercorrelated Satellite Observations Related to Solar Events*, edited by V. Manno and D. E. Page. D. Reidel, Dordrecht-Holland, 1970, p. 419.
- Kennel, C. F.; and Petschek, H. E.: Magnetic Turbulence in Shocks. *Physics of the Magnetosphere*, edited by R. L. Carovillano, J. F. McClay, H. R. Radoski. D. Reidel, Dordrecht-Holland, 1968.
- Nakada, M. P.: A Study of the Composition of the Solar Corona and Solar Wind. *Solar Phys.*, Vol. 14, 1970, p. 457.
- Ogilvie, K. W.; and Wilkerson, J. D.: Helium Abundance in the Solar Wind. *Solar Phys.*, Vol. 8, 1969, p. 435.
- Parker, E. N.: A Quasi Linear Model of Plasma Shock Structure in a Longitudinal Magnetic Field. *J. Nucl. Energy C2*, 1961, p. 146.
- Parker, E. N.: *Interplanetary Dynamical Processes*. Interscience, New York, 1963.
- Robbins, D. E.; Hundhausen, A. J.; and Bame, S. J.: Helium in the Solar Wind. *J. Geophys. Res.*, Vol. 75, 1970, p. 1178.
- Solar Geophysical Data*, U.S. Department of Commerce, Washington, D.C., Sept., 1970.
- Taylor, I.: Penrose Criterion for Multistreaming Maxwellians, ESRIN Internal Note N.74, Feb. 1970.
- Yeh, T.: A Three Fluid Model of Solar Wind. *Planet. Space Sci.*, Vol. 18, 1970, p. 199.

## DISCUSSION

*J. Hirshberg* Remarking on the helium abundance increasing as the solar cycle goes on, I compared your data with the Vela data and it seems that in those two samples the most probable value remained stationary. What happened was that as the solar cycle progressed you obtained more high helium observations which would be consistent with the notion that enhanced helium was coming out of flares.

*G. Moreno* That's right, the modal value was the same in two cases, only the enhanced helium changed. I forgot to say that the correlation of the bulk velocity of both protons and  $\alpha$  particles bulk velocity with the helium abundance has been done only for quiet periods.

*M. Dryer* How many energy channels do you have in your analyzer?

*G. Moreno* Twenty-eight. Computation suggests that the velocity spread from one channel to the next error in velocity is perhaps less than 20 km; in many cases when  $\alpha$  particles are in three channels it becomes much less.

*D. Heymann* Several years ago, as you well know, it was suggested by Dr. Michel that a tenuous atmosphere on the moon is removed by the interaction of this atmosphere with the solar wind rather than by gravitational escape.  $^{40}\text{Ar}$  was not removed from the moon but was punched back into the lunar surface by essentially the same mechanism

that Michel proposed for the escape of neutral atoms, i.e., via ionization then acceleration in the interplanetary electric and magnetic field from the moon. The  $^{36}\text{A}$ , as he argued, varies quite a bit, but it varies because it is surface correlated. He argued and showed that all the  $^{36}\text{A}$  is essentially from the solar wind, and implanted in the surface of these particles. Now, the curious thing is that when we measured  $^{40}\text{A}$  in the same particles they correlate, I mean, they co-vary with  $^{36}\text{A}$ . And in fact  $^{40}\text{A}/^{36}\text{A}$  in these samples is about unity; that is a paradox because all theoreticians tell us that  $^{40}\text{A}/^{36}\text{A}$  in the sun ought to be much less than unity, in fact perhaps much lower than  $10^{-4}$ . So the question is where the  $^{40}\text{A}$  that we are seeing in the samples comes from. It cannot come from the solar wind proper. You may wonder and say perhaps this  $^{40}\text{A}$  has arisen from  $^{40}\text{K}$  decay in these samples and what we note is simply that these samples are low in  $^{40}\text{K}$  or have a young age or both, and that these samples have much potassium or have an old age or both. But that cannot be true because for any of these points if you calculate an honest  $^{40}\text{K}/^{40}\text{A}$  age you find that all the ages are greater than the accepted age of the moon and in fact calculate ages greater than  $7 \times 10^9$  yr. So the  $^{40}\text{A}$  has been produced from potassium not in these samples but somewhere else, has been separated, and then reimplanted into the lunar regolith. In other words, what we are looking at is Argon which was produced in the body of the moon, by potassium decay, was made available in the lunar atmosphere. You can, for example, envisage Argon just oozing out slowly. It might be that there were large impacts on the surface of the moon which threw out vast amounts of rock and that Argon was subsequently reimplanted—being coupled to the solar wind which is the driving agent of this reimplantation into the soil—and that is basically the reason we see the covariation of  $^{40}\text{A}$  and  $^{36}\text{A}$ .

## RADIO DETECTION OF SOLAR-WIND DISCONTINUITIES *Jeremy A. Landt*

**ABSTRACT** Geomagnetic field sudden increases or storm sudden commencements are compared with measurements of electron content of the solar wind. The latter data are obtained by a radio propagation experiment, which measures the electron content along a radio path between transmitters on the Stanford campus and several spacecraft in solar orbit. Measurements were examined during time periods that included 40 of the geomagnetic disturbances (gmd) reported between January 1, 1966, and June 30, 1969.

These studies indicate that some widely reported solar wind discontinuities have been detected by the radio propagation experiment. Eleven of the 40 gmd were classified as storm sudden commencements (ssc), which usually result when a shock in the solar wind strikes the magnetosphere. The relative timings of these 11 events are consistent with conclusions drawn from comparisons of experiment geometry to prevailing shock models. Compared to the nature of these 11 events, the characteristics of the solar-wind disturbances corresponding to the remaining 29 gmd were generally found to have been less favorable for detection by the radio propagation experiment, but sharp changes in the content were clearly evident at the time of several minor gmd.

### INTRODUCTION

Recent experimental and theoretical studies of blast waves in the solar wind have led to a general consensus about an average disturbance shape [Hirshberg, 1968; Taylor, 1969; DeYoung and Hundhausen, 1969]. The experimental studies have usually assumed a knowledge of the location of the disturbance near the sun (e.g., a solar flare site), and measurements were necessarily confined to the locale of spacecraft. This spatial limitation in the study of the structure of individual events can be partially overcome by combining such localized measurements with other measurements of the average density between the earth and a deep space probe. Spatially averaged electron number density data have been obtained since December 1965 by the radio propagation experiment using radio waves transmitted between powerful transmitters on the Stanford campus and several specially equipped spacecraft in orbit around the sun. These data have been determined from radio

delay measurements of electron content along the path connecting earth and the spacecraft. The trajectories of the spacecraft are shown in figure 1.

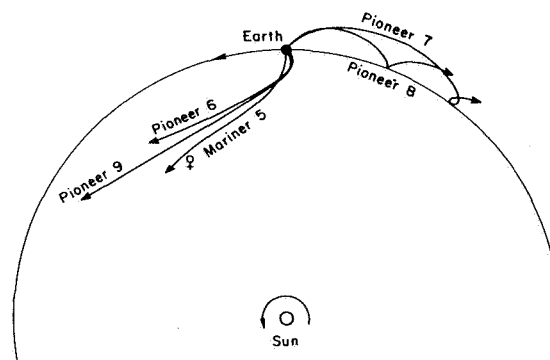


**Figure 1.** The paths of the five spacecraft used in this study, projected onto the ecliptic plane and shown in the frame that rotates with the earth.

*The author is at the Center for Radar Astronomy, Stanford University, Stanford, California.*

Records of the horizontal component of the earth's magnetic field provide one of the most complete data sets indicating solar-wind conditions near the earth. Some worldwide fluctuations in the earth's field are the result of compressions or expansions of the magnetosphere due to fluctuations in the streaming pressure of the solar wind. Before turning to individual events, we have attempted to determine whether solar wind discontinuities that cause sudden impulses (si) and storm sudden commencements (ssc) have been detected by the radio propagation experiment. This was done by comparing the timings of ssc and si to the times of sharp changes in the average electron density for the period from January 1, 1966, to June 30, 1969. During this period, 257 geomagnetic events were reported by ten or more stations and summarized in *Solar Geophysical Data*. We have also deduced the approximate orientations of some of these solar wind disturbances by comparing the relative timings of the events with the locations of the radio path.

#### THE EXPERIMENT

Coherent radio signals are sent from Stanford to receivers on several spacecraft in solar orbit. The differential group delay and phase advance of these signals are measured at the spacecraft and relayed to earth via the deep space network maintained by NASA. These measurements are related to the electron content between earth and the spacecraft. The content is the number of free electrons in a unit area column between the transmitter and receiver. The content can also be expressed as the product of the average electron number density along the path, and the length of the radio path.

Measurement of the content using phase advance data is quantized in steps of about  $0.04 \times 10^6$  electrons/m<sup>2</sup>, but this measurement contains an unknown additive constant, which is supplied by group delay data which has larger quantization increments. Here, we have relied mainly on the fine density versus time structure provided by the phase advance data.

The electron content from Stanford to the altitude of synchronous orbit is measured by monitoring the polarization plane of radio signals from geostationary satellites, mainly ATS 1. Using these measurements, the ionospheric contribution is calculated along the Pioneer line of sight and is subtracted from the total Pioneer measurement, yielding the interplanetary content. The error in this calculated ionospheric contribution is normally about  $\pm 4 \times 10^{16}$  electrons/m<sup>2</sup>, but can be larger when the radio path passes obliquely through the ionosphere during mid-day. Since the average density is found by dividing the interplanetary content by the distance to the spacecraft, the accuracy of the average

density improves as the spacecraft recedes from earth.

The experiment can be performed only while the desired spacecraft is visible from Stanford and within range of our transmitter. Thus, the maximum length of a single continuous data record is about 14 hr.

#### THE NATURE OF LARGE SOLAR-WIND DISCONTINUITIES

*Colburn and Sonett* [1966], *Spreiter et al.* [1968], and *Burlaga* [1970] have reviewed the five types of hydro-magnetic discontinuities that can occur in an isotropic plasma. In the comparisons of this paper, we have relied on the fact that the number density may change across four of these: The fast and slow shocks, contact surfaces, and tangential discontinuities. The density does not change across a rotational discontinuity.

The existence of hydromagnetic shock waves and tangential discontinuities in the solar wind has been inferred from direct solar-wind plasma observations. *Chapman and Ferraro* [1931] and *Gold* [1955] have suggested that ssc are the result of interplanetary shock waves propagating in the vicinity of the earth. *Burlaga and Ogilvie* [1969] have confirmed the correspondence between ssc and solar wind shocks for several events in 1967. They also found that some si have resulted from tangential discontinuities in the solar wind. Here, the term *geomagnetic disturbance* (gmd), refers to any geomagnetic event reported as an ssc or si. *Siscoe et al.* [1968] and *Ogilvie et al.* [1968] have found that the change in the horizontal component of the geomagnetic field varies as the change in the square root of the solar-wind streaming pressure  $[\alpha \rho v^2]$ , although the constant of proportionality was roughly half of that predicted by the magnetospheric model of *Mead* [1964]. The present knowledge of interactions between the geomagnetic field and solar-wind discontinuities has been reviewed recently by *Burlaga* [1970].

The propagation of shocks originating near the sun has been studied theoretically by *Parker* [1963], *Lee and Chen* [1968], and *Hundhausen and Gentry* [1969]; for a review, see *Hundhausen* [1970]. Heliocentric symmetry was assumed in these studies, but this assumption was relaxed by *DeYoung and Hundhausen* [1969], who predicted a roughly spherical shock shape with a radius of curvature of  $\sim 0.6$  AU by the time the shock reaches the earth's orbit (for a blast wave that initially subtended  $30^\circ$  in solar longitude at 0.1 AU). *Hirshberg* [1968] studied the strength of geomagnetic storms and found an average shock shape in the ecliptic plane. This shape agreed with the theoretical shape predicted later by *DeYoung and Hundhausen* [1969]. *Taylor* [1969] found similar shock orientations derived from measurements of the magnetic field in the solar wind near the

earth. In the direction normal to the ecliptic, the extent of the shocks may be more limited, resulting in a pancake-like shape [Hirshberg *et al.*, 1970; Greenstadt *et al.*, 1970], but this deduction from experimental observation has not yet been theoretically explained.

Tangential discontinuities and contact surfaces may be accompanied by abrupt changes in density. Burlaga [1969a, b] has found small changes in density at many tangential discontinuities and the radio propagation experiment is probably insensitive to these events. Discontinuities with large changes in density have been observed less often. It is thought that some tangential discontinuities or contact surfaces may separate the driver gas of a blast wave from the rest of the wind. The orientation of such a discontinuity may be similar to the orientation of the shock at the leading edge of the disturbance. It is also possible for a tangential discontinuity or contact surface to occur along the interaction surface between colliding solar wind streams, and these discontinuities are expected to be aligned roughly along an Archimedean spiral. Such orientations were found by Burlaga and Ness [1969].

#### DETECTION OF SOLAR-WIND DISCONTINUITIES IN ELECTRON CONTENT MEASUREMENTS

A worldwide geomagnetic event signals the arrival of a solar-wind disturbance at the earth. If a change in

density accompanies the disturbance, a change in the content must result, since the earth is at one end of the path along which the content is measured. Figure 2 shows results for a hypothetical disturbance corresponding to three different orientations of the radio path. In these examples, the disturbance is a heliocentric symmetric shell passing by the earth in 3 hr ( $\sim 0.03$  AU thick at 400 km/sec) with a density of  $20 \text{ cm}^{-3}$  in an ambient wind of  $10 \text{ cm}^{-3}$ . (Both densities are normalized to 1 AU and falling off as  $1/R^2$ .)

In these simple cases, each jump in the slope of the content versus time curve marks the time when a discontinuity first intersects the path, or when a discontinuity passes either end of the path. At the time a broad disturbance is tangent to the radio path, a large change in slope of the content versus time curve occurs. This orientation is the most favorable for detection of a discontinuity by the radio propagation experiment.

Changes in content corresponding to path A are likely to be overlooked because fluctuations in the ionospheric content tend to mask small interplanetary changes. Thus, some events may not be noticed even though the density changes by more than a factor of 2 at the discontinuity.

Commonly, increases in density of 1.5 to 3 times have been measured by other experimenters for shocks that are related to ssc [Ogilvie and Burlaga, 1969; Gosling *et*

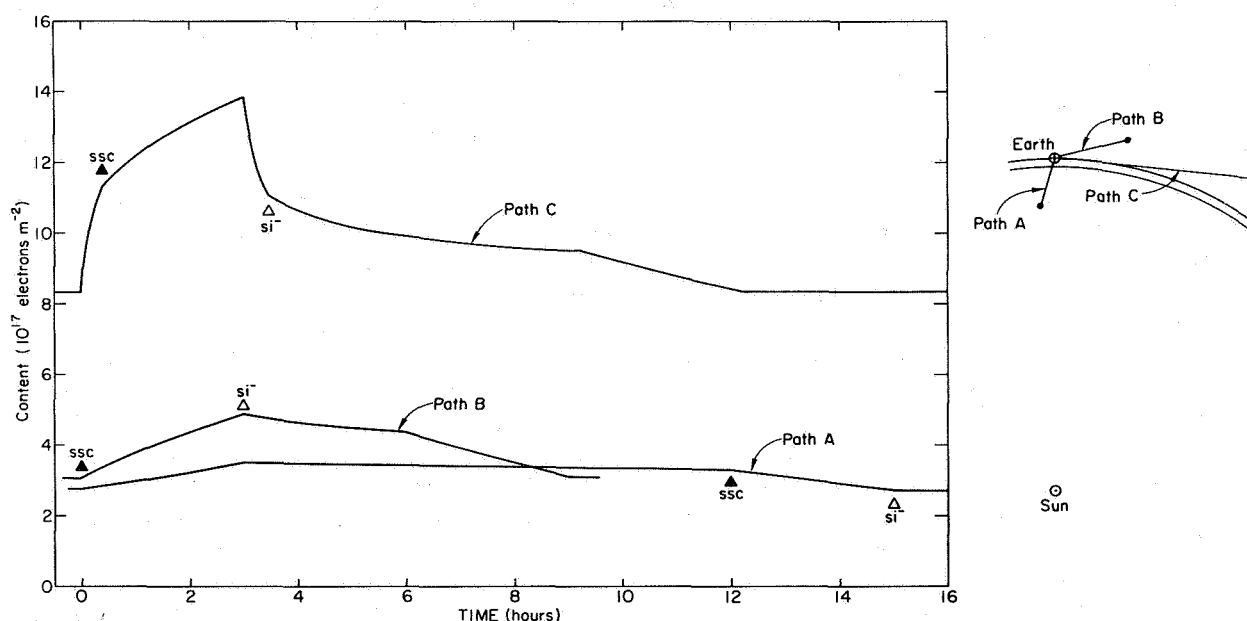


Figure 2. The electron content that results when a  $10 \text{ cm}^{-3}$  spherically symmetric pulse of electrons passes the earth in 3 hr, corresponding to the three orientations of the radio path shown. The solid triangle and ssc denote the time the shell reaches the earth. Hour 0 is the time the shell first intersects the radio path.

al., 1968]. Changes in content due to passages of weak shocks may go unnoticed, but the detection of some shock fronts in the solar wind is expected.

## OBSERVATIONS

Approximately 8000 hr of data were obtained between January 1, 1967, and June 30, 1969. Two lists were made for this interval. The first was a list of measurements that were abnormally high and contained fine scale fluctuations, or clearly indicated the passage of an unusual solar wind through the radio path. The decision to include or exclude some records from this list was subjective; to obtain unbiased statistics, this was done before comparison to the geomagnetic storm data. A clear onset of an event occurred in 22 percent of these records. The second list contained all coincidences between gmd and times when the radio propagation experiment was in operation. The 40 coincidences used in this study are summarized in tables 1, 2, and 3.

Tables 1 and 2 contain events for which the content measurements were "disturbed"; the remainder are in table 3. Some coincidences were not included in this study because of the poor quality of content data, or classification of the content event was not made because the gmd occurred near gaps in the content data.

The number of stations reporting a gmd is given in the tables, along with the date and time of the event and the variable  $A$ , which was introduced by Burlaga and Ogilvie [1969]:

$$A = \frac{N(\text{ssc}) - N(\text{si})}{N(\text{ssc}) + N(\text{si})}$$

where  $N(\text{ssc})$  is the number of stations that reported an ssc and  $N(\text{si})$  is the number that reported an si. Thus  $A = 1$  if all stations called the gmd and ssc, and  $-1$  if all called it an si. Burlaga and Ogilvie found that if  $A \gtrsim 0.8$ , the solar-wind discontinuity was usually a shock, and if  $A \lesssim -0.8$ , it was usually a tangential discontinuity.

Since the content is proportional to the length of the radio path, and since irregularities in the ionosphere tend to dominate our measurements at close ranges, the range to the spacecraft is given in the tables. An event that appeared to be undisturbed is not included in table 3 unless the range to the spacecraft was larger than 15 million km (0.1 AU). At this range, the content of the nighttime ionosphere is nearly that of the solar wind if it has a density of  $7 \text{ cm}^{-3}$ . For radio paths that pass through the daytime ionosphere, a 15-million km range may be insufficient to permit accurate measurement of the interplanetary content, but at this range, changes in the content of the solar wind should be evident. The decision to place a given record in table 3 was subjective.

Future careful examination may reveal that some of these records were slightly disturbed, but they did not contain any noticeable changes in content at the time of the gmd.

## CORRELATION BETWEEN GMD AND CONTENT EVENTS

It was calculated that if the 257 gmd were randomly distributed over the interval from January 1967 to June 1969, there should be about 67 coincidences of gmd with times when the radio propagation experiment was in operation; there were 69.

If gmd were not related to content events, then approximately 8 gmd should have randomly occurred during a content record that we previously had considered to be disturbed. In fact, 27 such occurrences took place. Consequently, it appears that at least some gmd and content disturbances were related, as expected.

There were 24 clear onsets of content events during the period of this study. Ten of these events are in table 1. Since the time intervals in which measurements can be made depend on the trajectories of the spacecraft, availability of spacecraft tracking for telemetry, and similar factors, and are unrelated to the solar wind, these 24 onsets should be good samples of this type of event. If gmd were not related to the onsets of content events, the calculated probability is 0.1 that a gmd would have randomly occurred within 15 minutes of an onset, but table 1 contains 6 such occurrences. The most plausible explanation is that solar-wind discontinuities corresponding to these six gmd intersected the radio path at the earth and were accompanied by appreciable changes in density.

## FEATURES OF DISCONTINUITIES CAUSED BY STRONG SSC EVENTS

Figures 3, 4, and 5 show data for selected strong ssc events ( $A \geq 0.8$ , with the number of stations reporting a gmd  $\geq 30$ ) of tables 1, 2, and 3, respectively. Four-minute averages of interplanetary average electron density are displayed along with the horizontal component of the earth's magnetic field recorded at San Juan, Puerto Rico. For each event, the geometry of the experiment is shown, and a circle of 1 AU radius is included for reference.

Four ssc occurred close to the time when a change in the average density was evident (events 1, 7, 8, and 10; call these events type A). Five of the ssc (events 6, 14, 15, 16, and 17; type B events) occurred several hours after the average density had become disturbed, and the two remaining ssc corresponded to low fluctuating average density levels (events 29 and 30; type C events).

**Table 1.** *Geomagnetic events that occurred within several hours of sharp changes in the electron content. In the spacecraft column, number 5 denotes Mariner 5, and numbers 6 through 9 denote Pioneers 6 through 9, respectively. These gmd's were found to occur within several minutes (a), before (b), or after (c) the first sharp change in content; or within several minutes of some other sharp change in content (d). The content corresponding to event 12 decreased, all others were increases.*

Geomagnetic event						Content event		
	Event	Date	Time, UT	Stations reporting a gmd	A	Spacecraft	Range, million km	Time of change, UT
(a)								
	1	10 Jun 68	2154	48	0.96	8	33.8	2200
	2	1 Jun 68	0109	13	0.54	8	31.0	0108
	3	22 Dec 66	0441	34	0.35	7	36.3	0442
	4	25 Jan 67	0001	10	0.20	7	54.3	0005
(b)								
	5*	19 Sep 66	0251	43	0.49	7	4.7	~0400
(c)								
	6	14 May 69	1929	68	0.97	9	119.3	1410
	7	4 Apr 67	0304	57	0.96	7	88.0	0230 to 0300
	8	7 May 68	0030	42	0.95	8	24.0	2320
	9	14 Jun 69	0422	8	0.00	8	84.4	0222
(d)								
	10	7 Jan 67	0800	51	0.88	7	45.1	0752
	11	16 Feb 67	0835	19	0.47	7	66.0	0823
	12	3 Nov 67	1338	9	-0.33	5	95.6	1342
	13	4 Aug 68	0252	24	-0.92	8	47.3	0100 to 0400

\*This event was noticed after comparison to the geomagnetic data. The timing is not accurate because of insufficient range to the spacecraft.

If the change in density was larger than  $\sim 10 \text{ cm}^{-3}$  at the shock fronts corresponding to the type B and C events, these shock fronts must have been oblique to the radio path at the earth. The shocks first encountered the radio path at the earth for type C events, but were oblique to the path so that the passage of the shocks were not apparent in the average density. The shocks corresponding to type A events intersected the radio path at or near the earth because of the agreement in timing of event onsets. These shocks were accompanied by changes in density of  $\sim 10 \text{ cm}^{-3}$  or larger, or the shock fronts were favorably oriented for detection (or both). The shocks of type B events intersected the radio path first, but at some distance from the earth. Since the average density was disturbed before the time of these ssc, it is thought that a limited radius of curvature for the shock fronts (less than 1 AU) would allow the shocks to be oblique to the radio path at the earth. This accounts for the lack of noticeable changes in the average density at the time of the ssc.

Hopefully, a better estimate of the size of individual shocks will emerge when details of the content data and local number density data are compared, but a spherical shock with a radius of curvature of  $\sim 0.6 \text{ AU}$  [DeYoung and Hundhausen, 1969] is consistent with these events.

## RESULTS

The number of gmd that occurred within minutes of sharp changes in the content was found to be far greater than the random prediction. This indicates that the two types of events are probably related. In turn, it is thought that these events were the result of disturbances in the solar wind. Some other gmd and disturbed content measurements were probably related, although exact coincidences in the timings of events were not apparent.

Several minor events were found to be associated with sharp changes in the content of the solar wind. Among the gmd reported by less than 30 stations with  $0 < A < 0.8$ , 50 percent coincided with sharp changes in



**Table 2.** *Geomagnetic events that did not coincide with sharp changes in the content, but during disturbed content measurements.*

Event	Geomagnetic event				Current event	
	Date	Time, UT	Stations reporting a gmd	A	Spacecraft	Range, million km
14*	10 Feb 69	2024	64	1.00	9	22.6
15	9 Jul 68	2155	46	1.00	8	41.6
16	12 Apr 69	2046	69	0.86	8	67.9
17	8 Jun 69	0509	64	0.81	8	82.7
18	27 Feb 69	0307	14	0.71	8	60.0
19	27 Apr 69	1831	39	0.69	9	100.3
20	28 Oct 67	1637	47	0.45	5	89.0
21	3 Nov 67	1628	10	-0.20	5	95.6
22	23 Mar 66	0012	29	-0.52	6	21.1
23*	13 Mar 67	0835	11	-0.64	7	78.1
24	31 Oct 67	1114	12	-0.67	5	92.4
25*	20 Sept 67	1736	18	-0.78	5	44.9
26	31 Oct 67	1449	33	-0.88	5	92.4
27	29 Oct 67	1324	12	-1.00	5	90.2

*\*These content events were small and went unnoticed until the content data were compared to the geomagnetic storm data.*

**Table 3.** *Geomagnetic events that occurred during content measurements that appeared to be undisturbed, where the range to the spacecraft is greater than 15 million km.*

Event	Geomagnetic event				Content event	
	Date	Time, UT	Stations reporting a gmd	A	Spacecraft	Range, million km
28	17 Oct 68	0031	6	1.00	8	56.8
29	2 Oct 68	0018	33	0.94	8	55.9
30	26 Feb 69	0158	68	0.92	8	60.0
31	2 May 69	1322	59	0.73	9	106.2
32	25 Jan 69	0036	13	0.69	8	57.6
33	6 Jan 67	0714	40	0.60	7	44.1
34	28 Feb 69	0423	68	0.44	8	60.2
35	27 Mar 66	1935	37	0.41	6	23.8
36	29 Aug 67	1738	32	0.19	5	26.6
37	7 Mar 69	2336	9	-0.33	8	61.2
38	2 Oct 68	0348	21	-0.52	8	55.9
39	19 May 66	2004	9	-0.56	6	65.7
40	2 May 69	1811	19	-0.90	9	106.2

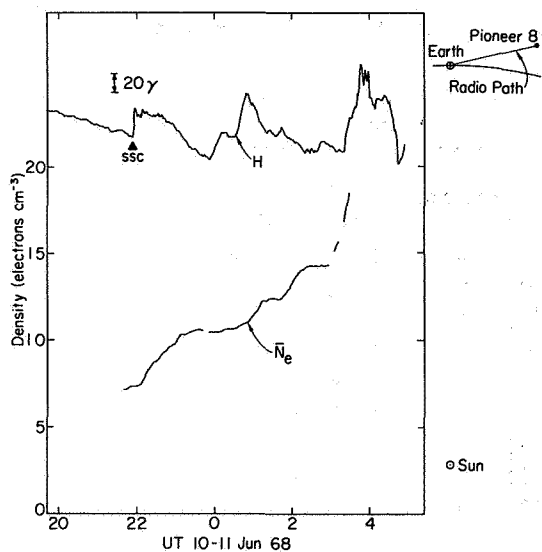


**Figure 3.** An example of near coincidence between a change in the average interplanetary electron density and a sudden change in the horizontal component of the earth's magnetic field recorded at San Juan. The location of the radio path is shown at the right in a frame of reference similar to that of figure 1. This is event 1 (type A) of table 1.

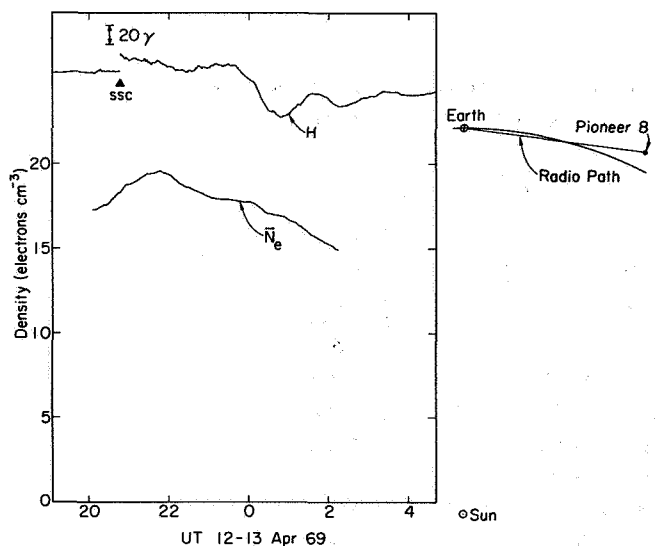


**Figure 4.** An example where the average interplanetary electron density is disturbed at the time of a sudden change in the horizontal component of the earth's magnetic field recorded at San Juan. This is an example of a type B event.

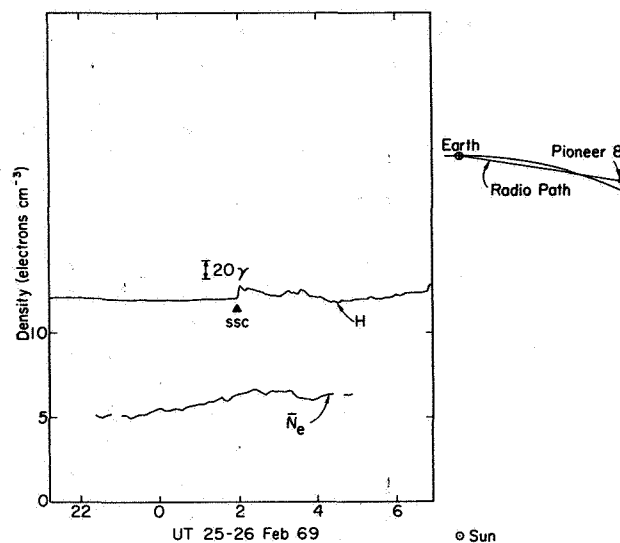


**Figure 5.** An example of a sudden change in the horizontal component of the earth's magnetic field recorded at San Juan with no corresponding event in the average interplanetary electron density. This is a type c event.

the content. Similar coincidences in timings of events occurred in 11 percent of the gmd with the same range of  $A$  reported by more than 30 stations, and in 36 percent of the strong ssc. These numbers may indicate that larger changes in solar-wind density have accompanied some of these less widely reported gmd than have accompanied the strong ssc.

For a blast wave with initial kinetic energy of  $2.8 \times 10^{30}$  ergs and initial velocity of 100 km/sec near the sun, DeYoung and Hundhausen [1969] predict a shock with a radius of curvature of about 0.6 AU and a change in density of about three times at the shock front when the shock reaches 1 AU. This model was found to be consistent with the relationships observed between ssc and sharp changes in electron content and the orientation of the radio path relative to the earth-sun line. However, this evidence is not so conclusive that we can rule out other models.

#### ACKNOWLEDGMENTS

The efforts of Professor Von R. Eshleman (principal investigator), and Mr. H. T. Howard (project manager), have been essential to the measurements presented here. The critical evaluation of the manuscript by Dr. Thomas A. Croft is greatly appreciated. The San Juan magnetograms were obtained from the World Data Center for Geomagnetism. This study was supported by NASA contract NAS-2-4672 and grant NGR-05-020-407.

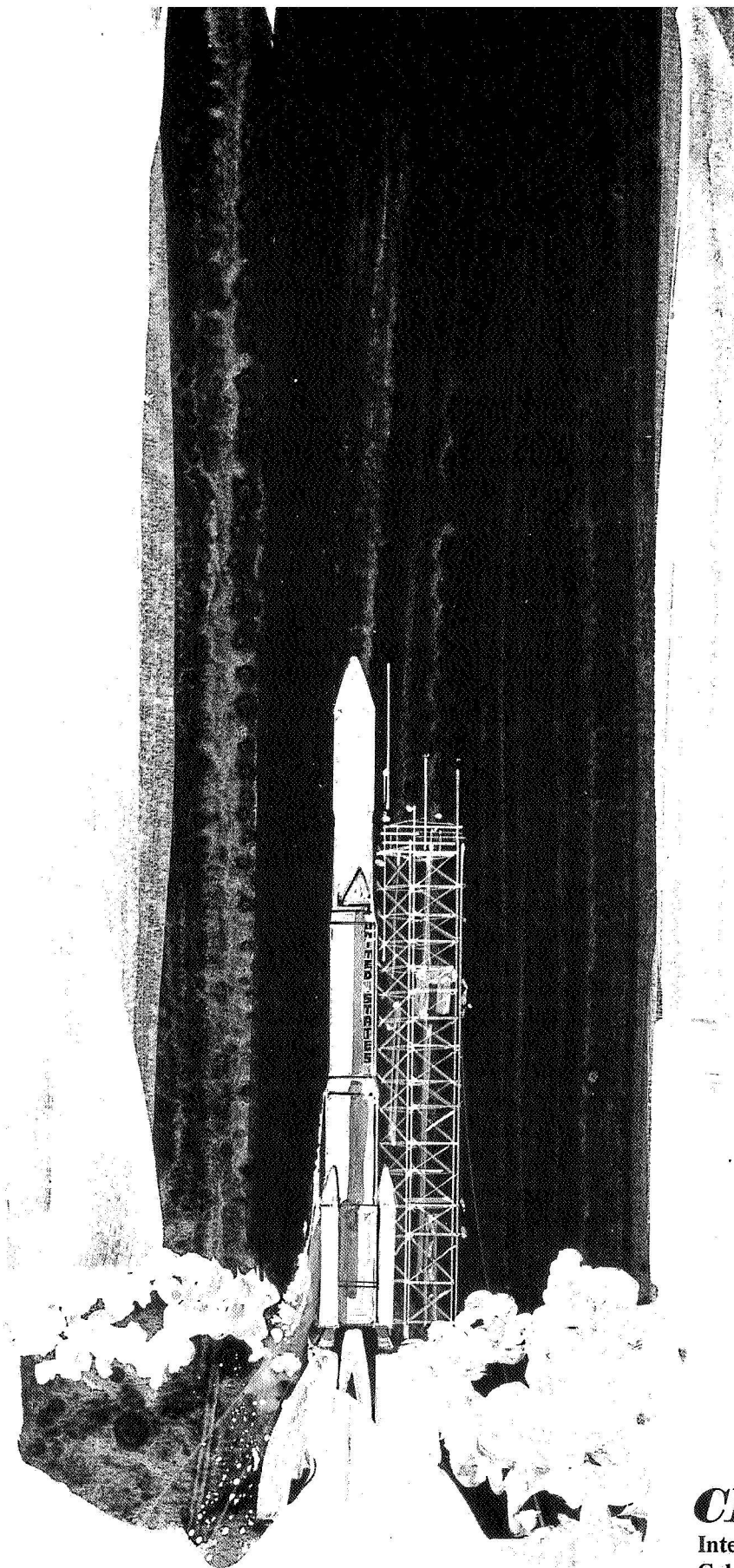
## REFERENCES

- Burlaga, L. F.: Directional Discontinuities in the Interplanetary Magnetic Field. *Solar Phys.*, Vol. 7, 1969a, p. 54.
- Burlaga, L. F.: Large Velocity Discontinuities in the Solar Wind. *Solar Phys.*, Vol. 7, 1969b, p. 72.
- Burlaga, L. F.: Discontinuities and Shock Waves in the Interplanetary Medium and Their Interaction with the Magnetosphere. Goddard Space Flight Center X-692-70-154, 1970.
- Burlaga, L. F.; and Ness, N. F.: Tangential Discontinuities in the Solar Wind. *Solar Phys.*, Vol. 9, 1969, p. 467.
- Burlaga, L. F.; and Oglivie, K. W.: Causes of Sudden Commencements and Sudden Impulses. *J. Geophys. Res.*, Vol. 74, 1969, p. 2815.
- Chapman, S.; and Ferraro, V. C. A.: A New Theory of Magnetic Storms. *Terr. Magn. Atmos. Elec.*, Vol. 36, 1931, p. 171.
- Colburn, D. S.; and Sonett, C. P.: Discontinuities in the Solar Wind. *Space Sci. Rev.*, Vol. 5, 1966, p. 439.
- DeYoung, D. S.; and Hundhausen, A. J.: Non-spherical Propagation of Flare-Associated Interplanetary Blast Wave (Abstract). *Tran. Amer. Geophys. Union*, Vol. 50, 1969, p. 668.
- Gold, T.: *Gas Dynamics of Cosmic Clouds*, Edited by H. C. van de Hulst and J. M. Burgers. North-Holland Publishing Co., Amsterdam, 1955, p. 103.
- Gosling, J. T.; Asbridge, J. R.; Bame, S. J.; Hundhausen, A. J.; and Strong, I. B.: Satellite Observations of Interplanetary Shock Waves. *J. Geophys. Res.*, Vol. 73, 1968, p. 43.
- Greenstadt, E. W.; Green, I. M.; Inouye, G. T.; and Sonett, C. P.: The Oblique Shock of the Proton Flare of 7 July 1966. *Planet. Space Sci.*, Vol. 18, 1970, p. 333.
- Hirshberg, J.: The Transport of Flare Plasma from the Sun to the Earth. *Planet. Space Sci.*, Vol. 16, 1968, p. 309.
- Hirshberg, J.; Alksne, A.; Colburn, D. S.; Bame, S. J.; and Hundhausen, A. J.: Observation of a Solar Flare Induced Interplanetary Shock and Helium-Enriched Driver Gas. *J. Geophys. Res.*, Vol. 75, 1970, p. 1.
- Hundhausen, A. J.: Composition and Dynamics of the Solar Wind Plasma. *Rev. Geophys. Space Sci.*, Vol. 8, 1970, p. 729.
- Hundhausen, A. J.; and Gentry, R. A.: Numerical Simulation of Flare-Generated Disturbances in the Solar Wind. *J. Geophys. Res.*, Vol. 74, 1969, p. 2908.
- Lee, T. S.; and Chen, T.: Hydromagnetic Interplanetary Shock Waves. *Planet. Space Sci.*, Vol. 16, 1968, pp. 1438, 1483.
- Mead, G. C.: Deformation of the Geomagnetic Field by the Solar Wind. *J. Geophys. Res.*, Vol. 69, 1964, p. 1181.
- Ogilvie, K. W.; and Burlaga, L. F.: Hydromagnetic Shocks in the Solar Wind. *Solar Phys.*, Vol. 8, 1969, p. 422.
- Ogilvie, K. W.; Burlaga, L. F.; and Wilkerson, T. D.: Plasma Observations on Explorer 34. *J. Geophys. Res.*, Vol. 73, 1968, p. 6809.
- Parker, E. N.: *Interplanetary Dynamical Processes*. Interscience, New York, 1963.
- Siscoe, G. L.; Formisano, V.; and Lazarus, A. J.: Relation between Geomagnetic Sudden Impulses and Solar Wind Pressure Changes—An Experimental Investigation. *J. Geophys. Res.*, Vol. 73, 1968, p. 4869.
- Spreiter, J. R.; Alksne, A. Y.; and Summers, A. L.: Plasma Flow Around the Magnetosphere. *Physics of the Magnetosphere*, edited by R. L. Carovillano, J. E. McClay and R. Radoski. D. Reidel, Dordrecht, Holland, 1968, p. 301.
- Taylor, H. E.: Sudden Commencement Associated Discontinuities in the Interplanetary Magnetic Field Observed by IMP 3. *Solar Phys.*, Vol. 6, 1969, p. 320.

A. Lazarus Just a very brief comment. It's going pretty far to say that each one of these ssc is due to a shock. Secondly, I think it's encouraging that you don't see a big change because you should be able to integrate out the small local changes that have been shown to cause these changes in magnetic field. There have been studies on how much the density should change for a given magnetic field change by Siscoe *et al.* And you should be able to integrate that out and see that it has very little effect on your measurements.

## DISCUSSION

*J. A. Landt* I've done a study like that. These events were classified, if you use the quantization of Burlaga and Ogilvie, larger than eight-tenths; because of the lack of time I did not include what you would expect in the content measurement from a given disturbance. Now you notice most of the shocks that have been displayed have an increase in density by a factor of at least two at the shock front, and this does make it very sensitive to the orientation of the shock front with respect to the orientation of the radio path. So I agree with you that we will not expect to see many coincidences unless the radio path is oriented just right with respect to the disturbance front and if the changes are large at the disturbance front.



## ***CHAPTER IX***

Interaction of the Heliosphere and the  
Galactic Medium: The Distant Solar Wind

Interaction of the solar wind with the local arm of the galaxy; the formation of a downward shock jump in the distant solar wind; general properties of the boundary; the diffusion of external neutral hydrogen into the solar system; observational evidence for a boundary, especially recent observation of L alpha parallax.

# THE INTERACTION OF THE SOLAR WIND WITH THE INTERSTELLAR MEDIUM

W. I. Axford

An invited review

## INTRODUCTION

The interaction between the solar wind and the interstellar medium has been a topic of interest for many years [Davis, 1955, 1962; Parker, 1961, 1963; Axford *et al.*, 1963], but progress has been rather slow largely because of the paucity of relevant observations. Recently, however, the situation has changed as a result of the clear evidence for the penetration of interstellar gas into the inner solar system obtained from OGO 5 [Thomas and Krassa, 1971; Bertaux and Blamont, 1971]. Furthermore, the prospect that there will be space probes traveling toward the outer regions of the solar system within a few years (see fig. 1) has created a need for a better understanding of the subject so that the most effective use can be made of the missions.

This review is a survey of the work, both published and unpublished, that has been carried out up to the time of writing. To the best of our knowledge, the bibliography is complete up to mid-1971. First, the expected characteristics of the solar wind, extrapolated from the vicinity of the earth are described, and several simple models are examined for the interaction of the solar wind with the interstellar plasma and magnetic field. The possibility that there is a substantial neutral component of the interstellar gas is ignored. In later sections, we consider various aspects of the penetration of neutral interstellar gas into the solar wind, and describe the dynamic effects of the neutral gas on the solar wind (to the extent that they are understood). Finally, we discuss problems associated with the interaction of cosmic rays with the solar wind.

We briefly summarize here the present status of knowledge concerning the properties of the interstellar medium in the vicinity of the solar system [see, e.g.,

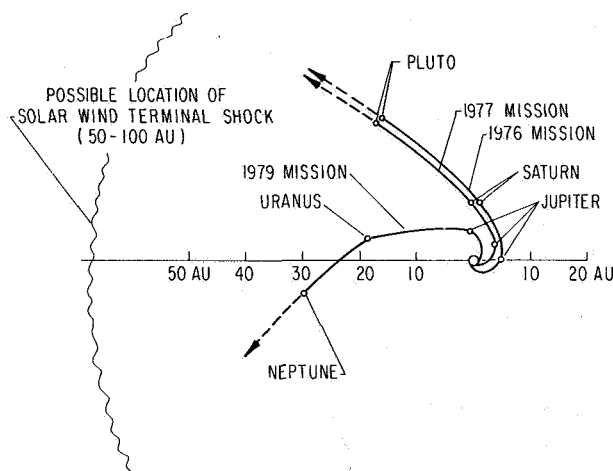


**Figure 1** Spacecraft trajectories for the proposed "Grand Tour" missions to Jupiter-Saturn-Pluto (1976-1977), and Jupiter-Uranus-Neptune (1979). The trajectories carry the spacecraft in the general direction of the projection of the solar apex into the ecliptic plane, the direction in which the distance to the solar wind termination is a minimum. The final portion of the trajectories (dashed) can be varied, since it depends on the last planetary encounter.

Allen, 1963]. The sun is located on the inner edge of the local (Orion) spiral arm at a distance of  $\sim 8$  parsec north of the plane of the galaxy. The solar motion relative to neighboring stars is  $20 \text{ km sec}^{-1}$  in the direction  $\alpha \approx 271^\circ$ ,  $\delta \approx +30^\circ$ , or  $l^{II} \approx 57^\circ$ ,  $b^{II} \approx +22^\circ$  (the "solar apex"). The nearest star is more than 1 parsec away, and the mean density of stars in the solar neighborhood is  $\sim 0.057$  solar masses per cubic parsec. Since the region containing the solar wind (the "heliosphere") has dimensions that are at most of the order of  $10^2$ - $10^3$  AU ( $< 10^{-2}$  parsec), and it seems reasonable to assume that stellar winds associated with nearby stars are not significantly more intense than the solar wind, we can be fairly

The author is with the Departments of Physics and Applied Physics and Information Science, University of California, San Diego, La Jolla, California.

sure that the solar wind interacts directly with the interstellar medium and that there is no overlapping of stellar winds in our vicinity. It should be noted that the sun appears to be on the fringes of the Gum nebula; however, according to *Brandt et al.* [1971] it lies some 60 parsecs outside and the local interstellar medium may not be directly affected by the presence of the nebula.

The mean interstellar electron density  $n_e$  in the disc of the galaxy can be determined in two ways: (1) by measurements of low frequency radio wave absorption [*Ellis and Hamilton*, 1966; *Smith*, 1965; *Bridle*, 1969; *Bridle and Venugopal*, 1969; *Alexander et al.*, 1969]; and (2) by measurements of the frequency dispersion of pulsar emissions [*Pilkington et al.*, 1968; *Lyne and Rickett*, 1968; *Habing and Pottasch*, 1968; *Davies*, 1969; *Prentice and Ter Haar*, 1969a,b; *Davidson and Terzian*, 1969; *Mills*, 1969; *Gould*, 1971; *Grewing and Walmsley*, 1971]. The first method yields the quantity  $\langle n_e^2 T_e^{-3/2} \rangle l$ , where  $l$  is the distance in the galaxy along the line of sight and  $T_e$  is the electron temperature; this tends to overemphasize the contributions from denser regions [*Gould*, 1971]. The second method yields  $\langle n_e \rangle l$  and thus permit. us to estimate  $\langle n_e \rangle$  directly if we know the distance to the pulsar by independent means (as in the case of the Vela and Crab pulsars), or if an estimate can be made of the neutral hydrogen content in the line of sight (e.g., from 21-cm absorption of the pulsar emission, as in the case of CP0329) so that a comparison can be made with 21-cm emission in the same direction. In fact, the interpretation of the observations is not easy because of the confusion introduced by dense HII regions, and the structure associated with the spiral arms of the galaxy. According to *Davidson and Terzian* [1969] the mean electron density in the disc of the galaxy is  $0.03\text{--}0.10\text{ cm}^{-3}$ . However, the result is model dependent, and according to *Gould* [1971], who notes that the path to the Crab pulsar crosses the interarm region where the density could be low, the local mean electron density in the galactic plane is  $\sim 0.12\text{ cm}^{-3}$ .

Evidence for the presence of a large-scale interstellar magnetic field arises from observations of (1) the polarization of starlight [*Davis and Greenstein*, 1951; *Mathewson*, 1968]; (2) the polarization of galactic non-thermal radio emission [*Mathewson and Milne*, 1965]; (3) the Zeeman effect at 21-cm wavelength [*Verschuur*, 1968; 1969a,b,c, 1970; *Davies et al.*, 1968]; (4) the Faraday rotation of polarized extragalactic radio sources [*Gardner and Whiteoak*, 1966; *Gardner and Davies*, 1966; *Gardner et al.*, 1967; *van de Hulst*, 1967; *Berge and Seielstad*, 1967; *Mathewson and Nicholls*, 1968]; and (5) the Faraday rotation of pulsar emissions [*Smith*, 1968a,b; *Radhakrishnan et al.*, 1969; *Ekers et al.*, 1969;

*Staelin and Reifenstein*, 1969; *Goldstein and Meisel*, 1969; *Hewish*, 1970], and of other polarized galactic sources [*Morris and Berge*, 1964; *Milne*, 1968]. Of these various types of observation, only the 21-cm Zeeman effect and the pulsar Faraday rotation measurements provide a value for the magnetic field strength, and these refer only to some weighted mean of the line-of-sight component. Magnetic fields of the order of  $10\text{ }\mu\text{G}$  have been found in some absorbing clouds; however, it seems likely that the field strength in such clouds is not typical of the interstellar magnetic field as a whole, and is in fact amplified as a result of the contraction of the clouds [*Verschuur*, 1969c]. The pulsar observations provide the most satisfactory results for our purposes since they refer to a region relatively close to the sun. If it is possible to obtain reasonably good values for the rotation measure ( $RM = 0.85 \int n_e \mathbf{B} \cdot d\mathbf{l}$ , with  $B$  in  $\mu\text{G}$  and  $l$  in parsecs) and the dispersion measure ( $DM = \int n_e dl$ ) from the ratio  $RM/DM$ , one can obtain a value of the mean line-of-sight component of  $\mathbf{B}$ , weighted with respect to the electron density. The measured values of  $B_{\parallel}$  range from  $0.7\text{ }\mu\text{G}$  to  $3\text{ }\mu\text{G}$ , and it seems reasonable therefore to assume that the largest value is representative of the interstellar magnetic field strength. This value is consistent with that found using the mean value of  $n_e$  obtained from pulsar measurements together with the rotation measures of extragalactic sources [*Davies*, 1969]. Furthermore, a magnetic field strength of this order is required to account for the nonthermal galactic radio emission [*Felten*, 1966; *Webber*, 1968; *Goldstein et al.*, 1970a], although there is some uncertainty concerning the unmodulated spectrum of cosmic ray electrons. These and other arguments concerning the interstellar magnetic field have been reviewed by *Burbidge* [1969].

Interstellar atomic hydrogen can be detected by observations of (1) the 21-cm line in emission and absorption [*Kerr and Westerhout*, 1965; *Kerr*, 1968, 1969], including absorption of pulsar emissions [*deJager et al.*, 1968; *Guelin et al.*, 1969; *Gordon et al.*, 1969; *Gordon and Gordon*, 1970; *Hewish*, 1970]; (2) Lyman  $\alpha$  absorption in the ultraviolet spectra of nearby early type stars [*Morton*, 1967; *Jenkins and Morton*, 1967; *Carruthers*, 1968, 1969, 1970a; *Morton et al.*, 1969; *Jenkins et al.*, 1969; *Smith*, 1969; *Wilson and Boksenberg*, 1969]; (3) the absorption of soft X rays from discrete sources [*Gorenstein et al.*, 1967; *Fritz et al.*, 1968; *Rappaport et al.*, 1969; *Grader et al.*, 1970]; and (4) the backscattering of solar Lyman  $\alpha$  [*Chambers et al.*, 1970; *Barth*, 1970a; *Thomas and Krassa*, 1971; *Bertaux and Blamont*, 1971]. Observations of 21-cm radio emission suggest that the mean



density of neutral hydrogen in the vicinity of the sun is  $\langle n_H \rangle \approx 0.7 \text{ cm}^{-3}$ . The 21-cm absorption measurements yield an estimate for  $\langle n_H \rangle l$  (where  $l$  is the distance to the source), provided one assumes a value for the spin temperature  $T_S$ ; it is generally assumed that  $T_S \approx 100^\circ \text{ K}$ . However, discrete sources such as pulsars do not show the absorption one would expect on the basis of measurements made using extended sources. This suggests that the interstellar medium may have a "raisin pudding" structure, with most of the 21-cm absorption occurring in small, dense clouds with low spin temperature [Clark, 1965; Kerr, 1969; Gordon and Gordon, 1970]. The ultraviolet absorption measurements show much the same effect; that is, the column density obtained from Lyman  $\alpha$  absorption lines in the spectra of early-type stars is usually, but not always, about one-tenth the value obtained from 21-cm emission measurements made in the same region of the sky [Carruthers, 1970a for a review of this topic]. Where Lyman  $\alpha$  and 21-cm absorption measurements have been made for essentially the same path (between the sun and the Orion nebula) the results suggest that  $T_S \approx 20^\circ$  [Carruthers, 1969].

There seems to be a discrepancy between the 21-cm emission and Lyman  $\alpha$  absorption measurements that needs to be resolved. Since the 21-cm measurement refers to the entire line of sight, it is possible that the answer is simply that there is a low density ( $n_H \approx 0.1 \text{ cm}^{-3}$ ) region near the sun, which affects the absorption measurements in at least some directions. In contrast, Jenkins *et al.* [1969] have reported values of  $\langle n_H \rangle$  from Lyman  $\alpha$  absorption measurements that exceed those obtained from 21-cm emission measurements. It is possible that the 21-cm emission process is not completely understood [Fischel and Stecher, 1967; Storer and Sciama, 1968]; however, more detailed comparisons are needed before we can be sure that a real discrepancy exists. The soft X-ray absorption measurements indicate that in the direction of the Crab nebula,  $\langle n_H \rangle \approx 0.3 \text{ cm}^{-3}$  [Rappaport *et al.*, 1969; Grader *et al.*, 1970], which is consistent with the 21-cm measurements. However, in the direction of ScoXR-1, where Jenkins *et al.* [1969] report  $\langle n_H \rangle \approx 1.4\text{--}3.0 \text{ cm}^{-3}$ , the soft X-ray absorption measurements are somewhat contradictory [Fritz *et al.*, 1968; Grader *et al.*, 1970]. As far as the region in the immediate vicinity of the sun is concerned, recent measurements of the intensity of backscattered solar Lyman  $\alpha$  can be interpreted as implying that  $\langle n_H \rangle \approx 0.03\text{--}0.12$ , depending on the model used [Blum and Fahr, 1970a; Thomas, 1971]. This is a relatively low value, but it is not inconsistent with other

observations (all of which refer to path lengths of the order of 100 parsecs or more), and indeed is quite consistent with most of the ultraviolet absorption measurements.

It has been conjectured that the interstellar gas might contain a significant fraction of molecular hydrogen [Gould and Salpeter, 1963; Gould *et al.*, 1963], and in cool, dense, dusty regions where the presence of a number of radicals has been detected from their radio emissions, this is to be expected [Hollenbach *et al.*, 1971]. Ultraviolet absorption measurements failed to show the presence of molecular hydrogen initially [Carruthers, 1967, 1970a]; however, recent measurements indicate that in some regions the concentrations of molecular and atomic hydrogen are comparable [Werner and Harwit, 1968; Carruthers, 1970b]. In the vicinity of the sun, however, where the atomic hydrogen density is quite low, and there is no evidence for dust, it is to be expected that molecular hydrogen is not an important constituent of the interstellar gas.

In HII regions, the temperature of the interstellar gas is usually  $5\text{--}10 \times 10^3 \text{ }^\circ \text{ K}$ , and is determined by a balance between heating due to photoelectrons, and cooling due to recombination, collisional excitation, and free-free transitions [Spitzer, 1968a,b]. In HI regions, the situation is more complex; taking into account the effect of heating by low-energy cosmic rays [Hayakawa *et al.*, 1961; Field, 1962; Spitzer and Tomasko, 1968; Pikel'ner, 1968] and cooling by collisional excitation it is found that two thermally stable states are possible, one with neutral hydrogen densities of the order of  $0.1 \text{ cm}^{-3}$ ,  $T \approx 10^4 \text{ }^\circ \text{ K}$ , and  $n_e/n_H \approx 0.1$ , and the other with neutral hydrogen densities of the order of  $10 \text{ cm}^{-3}$ ,  $T \lesssim 300^\circ \text{ K}$ , and  $n_e/n_H \approx 10^{-3}$  [Field *et al.*, 1969]. There are, however, some difficulties associated with cosmic ray heating [Werner *et al.*, 1970], especially in view of our lack of knowledge of the galactic cosmic ray spectrum at low energies [Goldstein *et al.*, 1970b; Gleeson and Urch, 1971a]. Limits placed on the low energy cosmic ray flux by indirect observations [Habing and Pottasch, 1967; Greenberg, 1969; Fowler *et al.*, 1970; Solomon and Werner, 1970] appear to make cosmic ray heating ineffective. It has been suggested that heating by soft X rays may be more important [Silk and Werner, 1969; Sunyaev, 1969; Werner *et al.*, 1970], and there are observational means of distinguishing between the two modes of heating [Silk and Brown, 1971; Bergeron and Souffrin, 1971; Habing and Goldsmith, 1971]. In any case, there is evidence from 21 cm and other observations in support of a two-component model of interstellar HI regions with properties as described above [Clark, 1965; Radhakrishnan and

Murray, 1969; Riegel and Jennings, 1969; Hjellming *et al.*, 1969; Rohlfs, 1971], and this would also be compatible with the Lyman  $\alpha$  absorption measurements [Jenkins, 1970].

It is to be expected that the interstellar gas has a velocity component of  $20 \text{ km sec}^{-1}$  from the direction of the solar apex. In addition, however, there is likely to be a component associated with a general streaming of the interstellar gas relative to the stellar population, perhaps associated with the "density wave" structure described by Lin *et al.* [1969] [see also Humphreys, 1971; and Burton, 1971], and a "turbulent" component that is evident from observations of interstellar absorption lines [Munch, 1968] and 21-cm observations [Kerr, 1968, 1969; Goldstein and MacDonald, 1969]. Since the "streaming" and "turbulent" components of the interstellar gas velocity can easily amount to  $10 \text{ km sec}^{-1}$  or more, we should not be surprised if the direction of relative motion between the sun and the gas differs substantially from the direction of the solar apex. Indeed the OGO 5 measurements of scattered solar Lyman  $\alpha$  suggest that the direction of relative motion lies close to the ecliptic plane [Thomas and Krassa, 1971; Bertaux and Blamont, 1971; Thomas, 1971], although as pointed out by Blum and Fahr [1971] this may result in part from the asymmetry of the solar Lyman  $\alpha$  emission.

A first estimate of the radius of the region in which the solar wind is supersonic can be obtained by equating the solar wind ram pressure to the pressure of the interstellar gas and magnetic field (see p. 616). On the basis of the observations described above, the radius is nominally of the order of 100 AU if the effects of neutral interstellar gas, the interplanetary magnetic field, and cosmic rays are neglected. This is well beyond the orbit of Pluto, the most distant of the known planets, and it is probably too far to be considered as a major objective of the proposed Outer Planet Grand Tour missions (fig. 1). However, according to the analyses presently available, all the effects that have been neglected in this estimate tend to reduce the distance by perhaps 10 to 15 percent, and hence together they could give rise to a significant and favorable change in our first estimate. In figure 1, therefore, we have shown the solar wind termination as occurring somewhere in the region 50 to 100 AU from the sun, with  $\sim 50$  AU being a not unrealistic possibility. It is recommended that a major effort be made to improve our understanding of this problem, and to provide better values for the various parameters involved.

## THE INTERPLANETARY MEDIUM BEYOND THE ORBIT OF EARTH

To date, *in situ* observations of the interplanetary medium have been carried out only in a very restricted region lying close to the ecliptic, between the orbits of Venus (0.7 AU heliocentric distance) and Mars (1.5 AU). Extensive reviews of these observations have been given by Hundhausen [1968a, 1970], Axford [1968], Ness [1967, 1968], Lüst [1967], Davis [1970], and Brandt [1970]. For information concerning other regions we have had to rely on inferences drawn from less direct observations, notably those involving comets, radio techniques, and cosmic rays [Axford, 1968]. Within the next decade we can reasonably hope for a considerable extension of the region of *in situ* observations as a result of the planned missions to the vicinity of Mercury, to Jupiter and the outer planets, and possibly out of the ecliptic following a Jupiter swingby. In this section we consider the extrapolation of theoretical models of the interplanetary medium into the unexplored regions at great distances from the sun, neglecting external influences (notably those due to the neutral interstellar gas).

From the theoretical point of view the solar wind is probably understood rather well in a qualitative sense, although the complexity of the phenomenon is such that we are unlikely ever to be able to produce a complete, quantitative model. Recent reviews of theoretical work have been given by Parker [1965a, 1969] and Holzer and Axford [1970a]. As a result of the lack of observations we must rely on theoretical models, even if they are oversimplified, to extrapolate our knowledge of the solar wind to heliocentric distances beyond the orbit of Mars, and to high heliolatitudes. The results of calculations based on one such model are shown in figures 2 and 3 [Leer and Axford, 1971]. In this model, it is assumed that the solar wind velocity is radial everywhere, and that the protons are heated by hydromagnetic waves emitted by the sun in a region with a characteristic radius of  $5 R_{\odot}$  [Barnes, 1968, 1969]. Otherwise, it is assumed that the interplanetary magnetic field does not affect the dynamics apart from its effects on the electron thermal conductivity and on the proton temperature anisotropy. Whatever assumptions are made concerning the processes that take place near the sun (in  $r \lesssim 0.5 \text{ AU}$ ), it is to be expected that at large distances from the sun ( $r \gtrsim 1 \text{ AU}$ ), the predictions of any steady flow model are essentially as shown in figure 2 provided the effects of the interstellar medium are not taken into account. In particular the solar wind speed is very nearly constant and the number density varies inversely as  $r^2$  beyond  $r \approx 1 \text{ AU}$ .

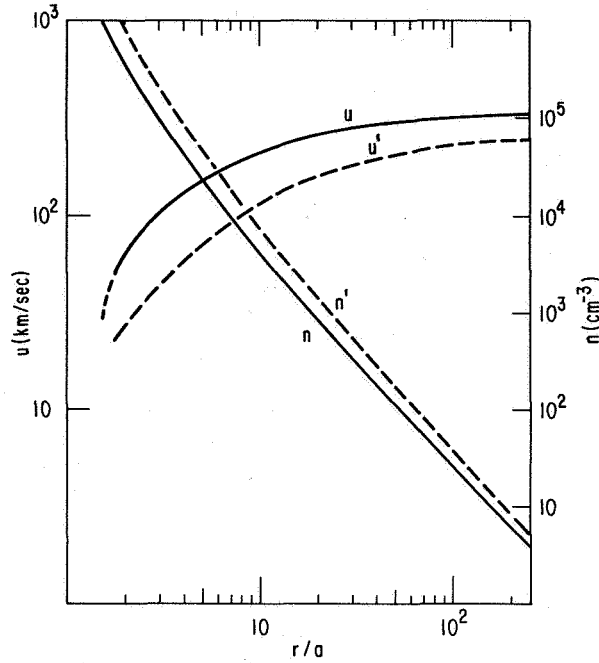


**Figure 2** Variation of the solar wind number density  $n$  and radial velocity  $u$  with radial distance from the sun in units of solar radii  $a$ , according to the model of Leer and Axford [1971]. The dashed lines refer to the case in which there is no heat input [Hartle and Sturrock, 1968].

The interplanetary magnetic field, which is controlled by the solar wind, by the rotation of the sun, and by conditions in the solar photosphere, should be such that at large distances the field lines form conical Archimedean spirals in the manner described by Parker [1958, 1963]; the spirals are determined by the intersection of the surfaces

$$r = \frac{u}{\Omega} (\phi - \phi_0) \quad \theta = \theta_0 \quad (1)$$

where  $u$  is the solar wind speed,  $\Omega$  is the angular velocity of the sun, and  $(r, \theta, \phi)$  are spherical polar coordinates. The angle made by the spiral relative to the radial direction (the "garden hose" angle) is given by

$$\psi = \tan^{-1} \left( \frac{r\Omega \sin \theta}{u} \right) \quad (2)$$

The garden hose angle is shown as a function of radial distance and heliolatitude in figure 3(a). The components of the magnetic field can be written

$$(B_r, B_\theta, B_\phi) = \left( \frac{B_0 a^2}{r^2}, 0, \frac{B_0 a^2 \Omega \sin \theta}{ru} \right) \quad (3)$$

where  $B_0$  is the field strength at the corresponding point at the surface of the sun ( $r = a$ ). The magnetic field strength is also shown as a function of radial distance

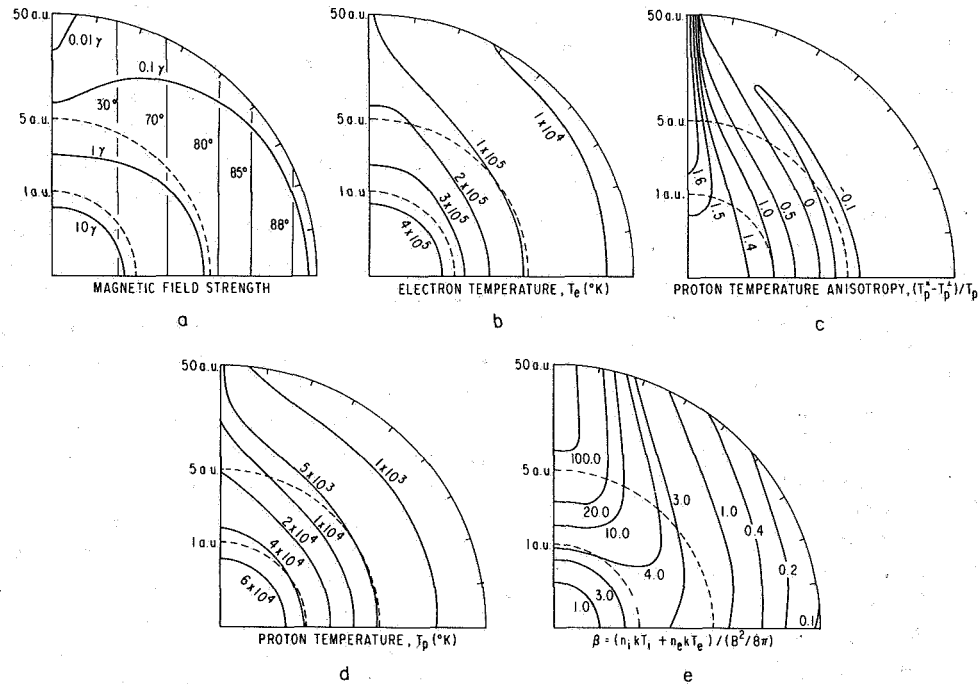


**Figure 3** Contours of various quantities in the interplanetary medium in a polar plot in which the abscissa lies in the ecliptic plane and the ordinate coincides with the axis of rotation of the sun, according to the model of Leer and Axford [1971].

and heliolatitude in figure 3(a). It should be noted that in the ecliptic plane ( $\theta = \pi/2$ ) the direction of the magnetic field becomes essentially azimuthal at large distances from the sun (i.e.,  $\psi > 80^\circ$  for  $r > 5$  AU), and the field strength varies as  $1/r$ . In contrast, in the polar regions ( $\theta = 0, \pi$ ) the magnetic field lines are radial and the field strength varies as  $1/r^2$ . As a result of this behavior the ratio of solar wind dynamic pressure to the magnetic field pressure

$$\beta_v = \frac{8\pi n \bar{m} u^2}{B^2} \quad (4)$$

tends to a constant value ( $\beta_v \approx 500$ ) at large values of  $r$  near the ecliptic plane, but increases as  $r^2$  at high heliolatitudes. Here and elsewhere, we have taken the mean mass of the solar wind ions  $\bar{m}$  to be  $2 \times 10^{-24}$  gm to allow for the presence of helium and heavier elements.

Wherever the garden hose angle is small the electron temperature is dominated by heat conduction; hence

$$T_e \approx T_{e0} \left( \frac{r}{r_0} \right)^{-2/7} \quad (5)$$

where  $T_{e0}$  is the electron temperature at some reference level  $r = r_0$ . As the direction of the magnetic field becomes more azimuthal however, the effects of adiabatic expansion become more important, and ultimately  $T_e \propto r^{-4/3}$ . The electron temperature is shown as a function of heliocentric distance and heliolatitude in figure 3(b). As shown in figure 4, the electron collision frequency is everywhere comparable with, or greater than, the characteristic expansion rate ( $v_{\text{exp}} = -(u/n)(dn/dr)$ ), and hence we do not expect that the electron temperature should be anisotropic anywhere under normal conditions. In contrast the proton collision frequency may be less than  $v_{\text{exp}}$  beyond a few solar radii and remain so until the magnetic field direction becomes essentially azimuthal. Thus, we can expect the proton temperature to be anisotropic, since when it approaches a constant speed the expansion of the solar wind takes place anisotropically (the radial dimension of an element of fluid remains unchanged, while the transverse dimensions expand in proportion to  $r$ ). In regions where the magnetic field direction is essentially radial we should find  $T_p^{\parallel} > T_p^{\perp}$ , while in regions where the field is essentially azimuthal we should find that  $T_p^{\parallel} \propto 1/r^2$ ,  $T_p^{\perp} \propto 1/r$  so that eventually  $T_p^{\perp} > T_p^{\parallel}$ . However, in the latter case the mean temperature  $T_p = (T_p^{\parallel} + 2T_p^{\perp})/3$  may decrease sufficiently rapidly for the proton collision frequency to become comparable to the expansion rate

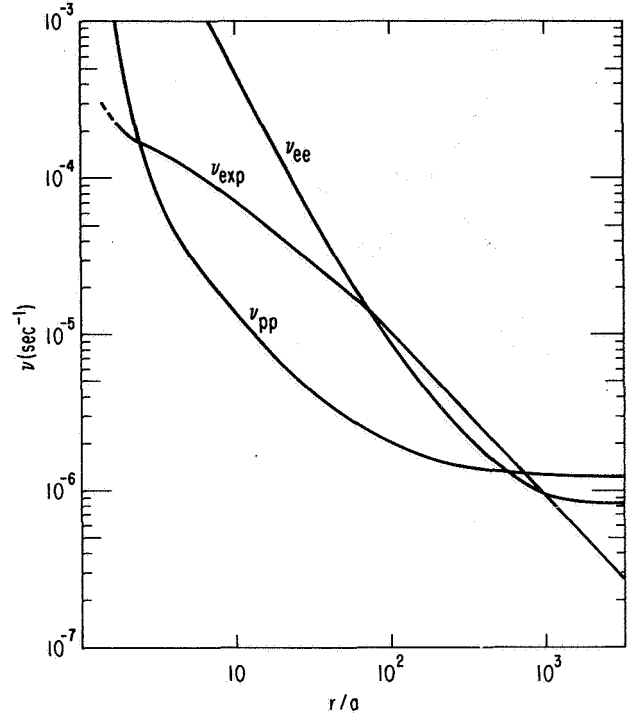


**Figure 4** The characteristic expansion rate ( $v_{\text{exp}}$ ), the electron collision frequency ( $v_{ee}$ ), and the proton collision frequency ( $v_{pp}$ ) in the ecliptic plane as functions of distance from the sun in units of solar radii, according to the model of Leer and Axford [1971].

once more, so that collisions suppress the anisotropy and  $T_p \propto r^{-4/3}$ . These effects are all evident in figures 3(c) and 3(d), which show the proton temperature anisotropy and the mean proton temperature, respectively, as functions of heliocentric distance and heliolatitude.

The model from which the above description of the behavior of the solar wind is drawn involves several assumptions that are not strictly valid. The most important of these is that the flow is assumed to be steady and (near the sun) spherically symmetric. Unsteady flow may affect the behavior of the solar wind at great heliocentric distances since the interaction of fast and slow streams beyond the orbit of the earth can result in a mean flow that is considerably hotter than suggested in figure 3(d), with correspondingly smaller proton collision frequencies and hence a larger temperature anisotropy than suggested in figure 3(c). Departures from spherical symmetry that do not involve unsteady effects must occur since at any given time solar active regions tend to be concentrated in latitude; however, apart from producing a variation with heliolatitude of the asymptotic solar wind speed and perhaps slightly changing the temperature contours in figures 3(b), (c), and (d), it is

unlikely that qualitatively significant effects can arise in this way.

The effects on the solar wind of the interplanetary magnetic field and of the rotation of the sun have been neglected in the model calculation apart from the control exerted by the field on the electron thermal conductivity and on the proton temperature anisotropy. Close to the sun, however, where the solar wind speed is comparable with or less than the Alfvén speed, the magnetic field is capable of inducing significant nonradial motions of the plasma [Weber and Davis, 1967]. Indeed, it seems likely that the solar wind has almost the full angular velocity of the sun out to perhaps  $20 R_{\odot}$ . This rotational component of the solar wind velocity should decay inversely with heliocentric distance and become negligible at the orbit of earth and beyond. A meridional component of the solar wind velocity should be induced near the sun, causing the magnetic field to bend toward the solar equatorial plane as suggested by observations of radio sources near the sun [Hewish and Wyndham, 1963; Slee, 1966]. Accordingly, the solar wind in the polar regions must expand more rapidly than spherical geometry would suggest, and hence it can reach a higher velocity at a given heliocentric distance than it would achieve at the same distance in the solar equatorial plane. It seems possible that the observations of Dennison and Hewish [1967], which suggest that the solar wind speed increases at high heliolatitudes, could be explained in this way. It is unlikely, however, that any of these effects lead to substantial departures from the description given in figures 2 and 3 of the behavior of the solar wind at large distances from the sun.

It has been assumed in the previous discussion that the solar wind can be considered to be a perfect electrical conductor, and hence the magnetic field behaves as if it were frozen into the plasma. Field lines cannot reconnect in these circumstances, and hence adjacent regions of inward- and outward-directed fields are separated by neutral sheets that spiral away from the sun indefinitely in the same manner as the field lines themselves. These neutral sheets can be identified with "sector boundaries" [Wilcox and Ness, 1965; Wilcox, 1968], and their observed persistence can be taken to indicate that the configuration is stable against reconnection in the sense that this would not lead to a state of lower energy [Axford, 1967]. As shown in figure 3(e), the parameter  $\beta$ , defined as

$$\beta = \frac{8\pi nk(T_p + T_e)}{B^2} \quad (6)$$

is an increasing function of heliocentric distance in regions where the magnetic field lines are almost radial (i.e.,  $\beta \propto r^{12/7}$ ) and a decreasing function of heliocentric distance in regions where the field lines are almost azimuthal and the plasma is cooling adiabatically ( $\beta \propto r^{-4/3}$ ). If the stability of neutral sheets against reconnection is determined by  $\beta$ , it seems possible that the sector boundaries may begin to break up somewhere beyond the orbit of earth where  $\beta$  is small [cf. Davis, 1970]. This process may be aided by the divergence of the flow, which causes elements of plasma in the neutral sheet to drift apart where the magnetic field is azimuthal; in contrast, near the sun where the field is nearly radial, the separation between elements of plasma in the neutral sheet stays almost constant. It is emphasized that if such an instability should occur it is likely to be of a macroscopic rather than a microscopic nature, since it has been shown that quasilinear diffusion can easily stabilize a neutral sheet against microscopic tearing instabilities [Biskamp et al., 1970].

We have neglected the possible effects of plasma instabilities associated with anisotropies of the velocity distributions of solar wind particles. Perhaps the most important of these is the instability resulting from the asymmetry of the electron distribution function associated with heat conduction [Forslund, 1970]; this can reduce the effective electron thermal conductivity and also alter its dependence on temperature, so that the distribution of electron temperature could be significantly different from that shown in figure 3(b). Other instabilities may be associated with anisotropy of the proton temperature [Parker, 1963; Kennel and Scarf, 1968; Hollweg and Volk, 1970]; however, the anisotropy is not observed to be large [Hundhausen et al., 1967; Eviatar and Schulz, 1970] nor is it expected to be so (see, e.g., fig. 3(c)). Thus any instabilities that may result from this source might be expected to produce only a rather low level of plasma turbulence. On the other hand, there is at least indirect evidence for important instabilities involving the protons and other ions, in that the heavier ions usually appear to have the same bulk speed, but a higher temperature than the protons [Snyder and Neugebauer, 1964; Robbins et al., 1970; Bame et al., 1970; Egidi et al., 1970]. Furthermore, it is possible that the solar wind ions are heated via the electrons, rather than directly as we have assumed, in which case some form of plasma turbulence must be generated to provide sufficiently high electron-proton energy exchange rates and to reduce the proton temperature anisotropy to the observed low values [Nishida, 1969; Toichi, 1971]. As far as the solar wind at great distances is concerned, plasma turbulence may play an important

role in providing an effective interaction with ions of interstellar origin [Holzer and Axford, 1971].

As a first approximation, the composition of the solar wind might be expected to be that of material having something like the cosmic abundance of elements in ionization equilibrium at the temperatures of  $1-2 \times 10^6$  °K that exist in the solar corona [cf. Holzer and Axford, 1970b]. The observed variability of the helium abundance in the solar wind [Robbins et al., 1970; Hundhausen, 1970] and some theoretical work [Jokipii, 1966a; Geiss et al., 1970a] suggest that the approximation might not be wholly adequate, although there is no indication that it is seriously wrong [Bame et al., 1970; Geiss et al., 1970b]. As pointed out by Hundhausen et al. [1968], the ionization state of the solar wind plasma is essentially "frozen" at a heliocentric distance of at most a few solar radii, where the electron temperature is not substantially less than it is in the lower corona. At great distances from the sun, radiative recombination times are very long indeed and one cannot expect this process to play an important role in determining the dynamics of the solar wind. For example, for an ion with charge  $Ze$  in the region beyond  $r = 1$  AU where  $T_e \propto r^{-4/3}$ , the radiative recombination time  $\tau_{\text{rec}}$  [Allen, 1963] is such that

$$\tau_{\text{rec}} \nu_{\text{exp}} \approx \frac{3 \times 10^9 T_e^{3/4} u |dn/dr|}{Z^2 n^2} \approx \frac{2 \times 10^7}{Z^2} \quad (7)$$

which is a large number even for the more highly ionized constituents ( $Z \approx 15$ ). In high latitude regions where  $T_e \propto r^{-2/7}$ ,  $\tau_{\text{rec}} \nu_{\text{exp}}$  is larger and increases with increasing  $r$ . Nevertheless, changes in the state of ionization may occur as a result of neutralization of solar wind ions on interplanetary dust grains [Bandermann and Singer, 1965; Banks, 1971], evaporation of the dust grains themselves followed by photoionization [Banks, private communication, 1971], evaporation of material from comets and planets, and most importantly the penetration of interstellar gas into the inner solar system, as discussed in a later section (p. 623). The suggestion that the solar wind should contain a substantial (solar) neutral component [Akasofu, 1964; Wax et al., 1970] encounters difficulties [Brandt and Hunten, 1966; Cloutier, 1966; Axford, 1969], and would lead to a much larger flux of  $\text{He}^+$  ions than is observed.

#### INTERACTION OF THE SOLAR WIND WITH IONIZED INTERSTELLAR GAS AND MAGNETIC FIELD

Here we consider the nature of the interaction between the solar wind and the local interstellar medium for the case where the latter is part of an HII region containing

only a negligible neutral component. Many of the essential features of this interaction were discussed by Davis [1955, 1962] in his work concerning the effect of the solar wind cavity on cosmic rays. A more detailed analysis was carried out by Parker [1961], with the assumption that the effects of the interplanetary (solar) magnetic field can be neglected. This discussion is based largely on Parker's work [1963].

It was pointed out by Clauser [1960] and Weymann [1960] that the solar wind should undergo a shock transition so that it can come into equilibrium with the interstellar medium [McCrea, 1956; Holzer and Axford, 1970a]. The situation is closely analogous to the discharge from a Laval nozzle into the atmosphere [Liepmann and Roshko, 1957], and to the flow of water over a dinner plate (see appendix). In the absence of a neutral component of the interstellar gas, a shock must always exist if the pressure exerted by the interstellar medium is finite. The suggestion made by Faus [1966] that the solar wind might terminate as a "free expansion" is incorrect; indeed, the solar wind itself can be regarded as a free expansion within the shock transition.

If the effects of the interplanetary magnetic field are neglected, and the solar wind is assumed to behave as a perfect fluid with specific heat ratio  $\gamma = 5/3$ , then since the Mach number ( $M$ ) of the supersonic solar wind is very large at the expected position of the shock transition, the shock is "strong." In this case the Rankine-Hugoniot relations yield

$$u_{n2} \approx \frac{\gamma-1}{\gamma+1} u_{n1}, \quad \rho_2 \approx \frac{\gamma+1}{\gamma-1} \rho_1, \quad p_2 \approx \frac{2}{\gamma+1} \rho_1 u_{n1}^2 \quad (8)$$

and

$$M_{n2}^2 = \frac{(\gamma-1)M_{n1}^2 + 2}{2\gamma M_{n1}^2 - (\gamma-1)} \approx \frac{\gamma-1}{2\gamma} \quad (9)$$

Here subscripts 1 and 2 denote conditions on the upstream (supersonic) and downstream (subsonic) sides of the shock, respectively, and the subscript  $n$  indicates that the component of velocity normal to the shock is involved;  $p$  is the total pressure, and  $\rho = n\bar{m}$  is the mass density of the gas. In the subsonic region beyond the shock, the Bernoulli equation holds along each streamline:

$$\frac{1}{2} u^2 + \frac{\gamma}{\gamma-1} \frac{p}{\rho} = \frac{\gamma}{\gamma-1} \frac{p_s}{\rho_s} \quad (10)$$

together with

$$\frac{p}{\rho^\gamma} = \frac{p_s}{\rho_s^\gamma} \quad (11)$$

where the subscript  $s$  denotes the stagnation value ( $u = 0$ ). On combining equations (10) and (11) and using the definition  $M^2 = u^2/c^2 = \rho u^2/\gamma p$ , the following equations can be obtained for  $p$ ,  $\rho$ ,  $c^2$ , and  $T$ :

$$\frac{c^2}{c_s^2} = \frac{T}{T_s} = \left(1 + \frac{\gamma-1}{2} M^2\right)^{-1} \quad (12)$$

$$\frac{\rho}{\rho_s} = \left(1 + \frac{\gamma-1}{2} M^2\right)^{-1/(\gamma-1)} \quad (13)$$

$$\frac{p}{p_s} = \left(1 + \frac{\gamma-1}{2} M^2\right)^{-\gamma/(\gamma-1)} \quad (14)$$

It is evident from (9) that  $M^2$  is small on the subsonic side of the shock transition, and if it remains small it is permissible to neglect terms  $O(M^4)$ , so that (10) reduces to

$$\frac{1}{2} \rho_s u^2 + p = p_s \quad (15)$$

Also from (13) we see that  $\rho = \rho_s + O(M^2)$ , so that if  $M^2 \ll 1$  the flow can be considered as being incompressible.

In general the shock is not spherical, and hence the flow in the subsonic region contains vorticity, and the stagnation pressure is not the same along all streamlines. However, for streamlines that lead to stagnation points at the interface between the solar plasma and the interstellar medium, the conditions for equilibrium require that  $p_s = p_o$ , where  $p_o$  is the local pressure of the interstellar gas and magnetic field. In the simple configurations of interest, these streamlines are normal to the shock and hence  $u_{n1} = u_1$  (the solar wind speed on the supersonic side of the shock). For these streamlines it can be deduced from equations (8), (9), and (10) that

$$\rho_1 u_1^2 = n_1 \bar{m} u_1^2 = \frac{\gamma+1}{2} \left[ \frac{4\gamma}{(\gamma+1)^2} \right]^{\gamma/(\gamma-1)} p_o = K p_o \quad (16)$$

where, for  $\gamma = 5/3$ ,  $K \approx 1.13$ . Since  $n_1 = n_e r_s^2$ , where  $r_s$  is the radial distance to the shock and the subscript  $e$  denotes quantities evaluated at the orbit of earth ( $r_e = 1$  AU), this equation can be used to determine  $r_s$ . Note that this should be expected to be the minimum distance to the shock, and that  $r_s$  may be substantially different on other streamlines.

Let us consider the case in which the interstellar gas is at rest with respect to the sun and there is no interstellar magnetic field. The configuration is spherically symmetric, and hence (16) must apply to all streamlines if we interpret  $p_o$  as the pressure of the interstellar medium (and therefore of the solar wind) at infinity. Since the Mach number in the subsonic region can only decrease with heliocentric distance ( $M^2 < M_2^2 \approx 0.2$ ), the approximation of incompressibility must be quite accurate. Hence, from mass conservation we obtain

$$u = u_2 \left( \frac{r_s}{r} \right)^2 \quad r > r_s \quad (17)$$

and thus at large distances the sun would appear to be a point source of incompressible fluid.

Next let us consider the case in which there is an interstellar magnetic field which is uniform and has strength  $B_o$  at great distances from the sun. We generalize Parker's [1963] treatment of this problem by the inclusion of static interstellar gas, which exerts a uniform pressure  $p_g$ , and also by allowing for the effects of compressibility in the region of subsonic solar wind flow. It is assumed that the magnetic scalar potential in the external region (fig. 5) is given approximately by

$$\Psi_m = -[(1/2)l^3/r^2 + r] B_o \cos \theta \quad (18)$$

where  $(r, \theta, \phi)$  are spherical polar coordinates with  $\theta = 0$  the axis of symmetry, and  $l$  is the radius of the diamagnetic sphere that would produce the same external field. The magnetic field lines are given by

$$\left[ \left( \frac{r}{b} \right)^3 - \left( \frac{l}{b} \right)^3 \right] \sin^2 \theta = \left[ 1 - \left( \frac{l}{b} \right)^3 \right] \left( \frac{r}{b} \right) \quad (19)$$

where  $r = b$  is the radial distance to the point where the field line intersects the plane  $\theta = \pi/2$ . If the interface between the interstellar medium and the solar wind is determined by (19) with  $b = b_o$ , then at large distances from the sun ( $z = r \cos \theta$  large) the distance of the interface from the axis of symmetry is given by

$$c_o = b_o \left[ 1 - \left( \frac{l}{b_o} \right)^3 \right]^{1/2} \quad (20)$$

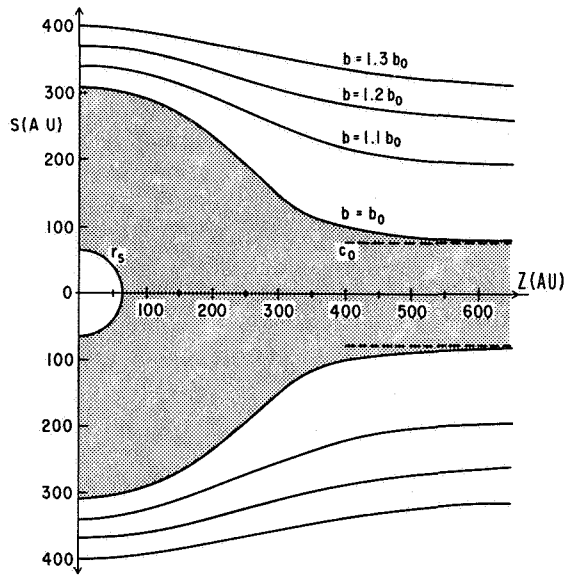


**Figure 5** Calculated shape of the region of subsonic solar wind flow (shaded), for the case when the solar wind plasma is entirely confined by a uniform interstellar magnetic field. The solar wind is supersonic in  $r < r_s$ , and exits in the  $\pm z$  directions to infinity. The configuration of the interstellar magnetic field is indicated by some sample field lines in the outer region. The parameters used in this example are as follows:  $B_g = 6 \mu G$ ,  $n_s = 0.05 \text{ cm}^{-3}$ ,  $T_g = 10^4 \text{ }^\circ K$ , with  $B_e = 3 \times 10^{-5} G$ ,  $\rho_e = 10^{-23} \text{ gm cm}^{-3}$ ,  $u_e = 400 \text{ km sec}^{-1}$ .

The condition of pressure balance at the stagnation line  $r = b$ ,  $\theta = \pi/2$ , yields

$$p_s = \frac{B_o^2}{8\pi} \left[ 1 + \left( \frac{1}{2} \right) \left( \frac{l}{b_o} \right)^3 \right]^2 + p_g = \frac{\rho_1 u_1^2}{K} \quad (21)$$

Similarly, along the interface of the exit channels, where  $M^2 \rightarrow M_\infty^2$  as  $z \rightarrow \infty$ , we require for pressure equilibrium that

$$p_s \left( 1 + \frac{\gamma-1}{2} M_\infty^2 \right)^{-\gamma/(\gamma-1)} = \frac{B_o^2}{8\pi} + p_g \quad (22)$$

Finally, from mass conservation, and assuming that the flow in the exit channels becomes uniform as  $z \rightarrow \infty$ ,

$$2\pi c_o^2 (\gamma p_s \rho_s)^{1/2} M_\infty \left( 1 + \frac{\gamma-1}{2} M_\infty^2 \right)^{-1/2(\gamma+1)/(\gamma-1)} = Q \quad (23)$$

where  $Q$  is the total solar wind mass flux. Given  $B_o$ ,  $p_g$ ,  $M_\infty$ , and the parameters characterizing the supersonic solar wind, we can solve equations (20) through (23) for  $c_o$ ,  $b_o$ ,  $r_s$ , and  $l$ . As in the analogous problem of the flow due to a point source in a rotating fluid [Barua, 1955], it is necessary to specify the exit conditions to obtain a unique solution. In the case of the solar wind, the appropriate condition would seem to be that the fluid should escape freely to infinity, and hence we have taken  $M_\infty^2 = 1$  together with reasonable values of  $B_o$  and  $p_g$  to obtain the solution shown in figure 5.

The above solutions are likely to be inadequate as representations of the actual interaction between the solar wind and the interstellar medium, since any relative motion between the sun and the interstellar gas must cause the solar wind plasma in the subsonic region to be blown away. This effect is illustrated in the third problem treated by Parker [1961]: the case in which there is no interstellar magnetic field but a steady interstellar wind having a small Mach number relative to the sun. The solution to this problem is obtained easily if it is assumed that the solar wind can be replaced by a point source of incompressible fluid, and that the interstellar gas can also be considered as being incompressible. On combining the scalar velocity potentials for a source and a uniform flow, the streamlines of the resulting flow are found to be given by

$$\frac{z}{(z^2 + s^2)^{1/2}} = \frac{s^2}{2r_o^2} + C \quad (24)$$

in terms of cylindrical polar coordinates  $(s, \phi, z)$ , where  $C$  is a constant on each streamline, and  $r_o = r_s (\rho_2 u_2^2 / \rho_g V^2)^{1/4}$ . The streamline defining the interface between the solar wind and the interstellar gas is given by  $C = -1$  if the interstellar wind flows in the positive  $z$  direction. The stagnation point occurs at  $s = 0$ ,  $z = -r_o$ , and for  $z \gg r_o$ , the solar wind is confined to a circular cylinder of radius  $2r_o$ , as shown in figure 6(a).

The major defects of this model, as far as the solar wind is concerned, are (1) the assumption that the interstellar gas behaves as an incompressible fluid, and (2) the implicit assumption that  $r_s^2 \ll r_o^2$ ; that is,  $u_2/V \gg (\rho_g/\rho_2)^{1/2}$ . Although it is not easy to satisfy these requirements with acceptable values for the various quantities involved, we expect that the general nature of the flow remains more or less the same, as indicated in figure 6(a), even for the extreme case of a hypersonic interstellar wind. Thus, the value of  $r_s$  can still be calculated from (16), provided  $p_o$  is taken to be the stagnation pressure of the interstellar wind ( $p_o = p_g + \rho_g V^2$ ).



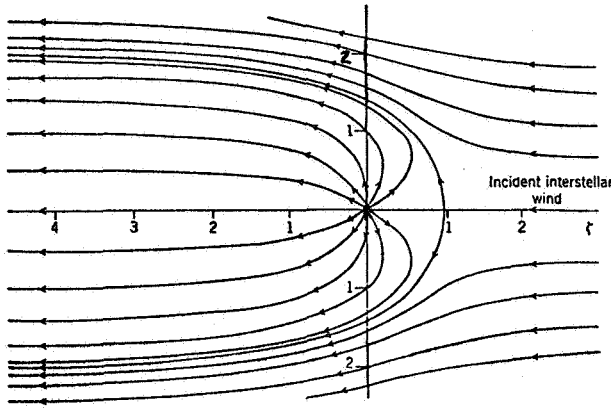


**Figure 6(a)** Streamlines in a model of the interaction between the solar wind and the interstellar wind in which both fluids are treated as being incompressible [Parker, 1961, 1963].

This will represent only the minimum value of  $r_s$ , however, since the cavity within which the solar wind is supersonic must become progressively more asymmetric as the Mach number of the interstellar wind increases.

Provided we restrict our attention to the flow in the vicinity of the axis of symmetry in the upstream direction, it should be possible to obtain estimates for the radius of curvature of the solar wind shock and for the positions of the interface and of a possible shock in the interstellar medium, using the approximate theory for a hypersonic shock standoff region due to Lighthill [Hayes and Probstein, 1966; pp. 232-254]. If the radius of curvature of the solar wind shock exceeds  $r_s$  on the axis of symmetry as indicated in figure 6(b), the shock is not normal to the flow everywhere, and the vorticity induced in the subsonic region can play an important role in turning the flow into the wake.

An alternative procedure using Busemann's method [Hayes and Probstein, 1966; pp. 78, 156] has been adopted by Baranov *et al.* [1970], who treat the subsonic region as a thin layer separating two hypersonic streams. In this case the details of the region of subsonic flow are ignored and one simply writes equations representing conservation of mass and momentum for the layer as a whole, which can be represented as a curve of the form  $r = r_s \xi(\theta)$ . Thus, the mass flow is

$$\Phi = \pi r^2 \rho_g V^2 + 2\pi r^2 (1 - \cos \theta) \rho_2 u_2 \quad (25)$$

at a point  $(r, \theta)$  in the layer. The momentum equations are

$$\rho_g V_n^2 = \rho_2 u_{2n}^2 + \frac{\Phi v}{2\pi r R \sin \theta} \quad (26)$$

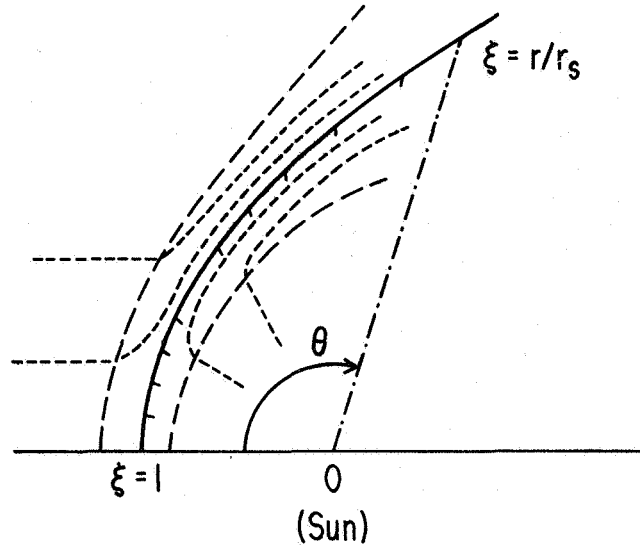


**Figure 6(b)** Calculated shape of the interaction region of the solar and interstellar winds assuming hypersonic flow [Baranov *et al.*, 1970]. The shape of the streamlines, and the positions of shock fronts are indicated by the (sketched) dashed lines.

$$\frac{d}{ds} (\Phi v) = 2\pi r \sin \theta (\rho_g V_n V_t + \rho_2 u_{2n} u_{2t}) \quad (27)$$

where subscripts  $n, t$  indicate normal and tangential components, respectively,  $v$  is the mean speed of the compressed gas in the layer,  $s$  is the distance measured along the layer from the stagnation point at  $\theta = 0$ , and

$$R = \frac{(r^2 + r'^2)^{3/2}}{r^2 + 2r'^2 - rr''}$$

is its radius of curvature. Note that the equation for momentum conservation in the direction of the normal contains a term representing the centrifugal force acting on the plasma in the layer, but this does not affect the distance to the stagnation point ( $r = r_s$ ) since  $\Phi v = 0$  at  $\theta = 0$ . With some manipulation  $v$  and  $\Phi$  can be eliminated from these equations, leaving a third-order, nonlinear differential equation for  $\xi(\theta)$  that must be solved numerically (see fig. 6(b)). The thickness of the layer, which can be obtained using the Lighthill method, would be expected to be of the order of 30 percent of the radius of curvature of the layer at the stagnation point ( $R = 5r_s/3$ ).

The closely analogous problem of the interaction between the solar wind and the ionized head of a comet has been treated as being equivalent to a source of incompressible fluid in a supersonic flow by Ioffe

[1966a,b; 1968]. Other aspects of the case in which the interstellar wind is supersonic have been considered by Dokuchaev [1964], Brengauz [1969], and Sakashita [1970], who note that the shock waves produced by randomly moving stars surrounded by extensive stellar wind regions could be a significant source of energy for the interstellar gas. It should be noted, however, that provided the stellar winds are supersonic near the stars, there can be no drag whatsoever on the stars themselves. The momentum imparted to the interstellar gas is taken up by the outer subsonic part of the stellar wind region as it is turned to form a comet-like wake behind the star. In fact, this must be essentially correct even if the stellar wind is subsonic everywhere, provided the dimensions of the star are small compared with those of the associated stellar wind region.

Although we have not been able to construct a completely satisfactory model of the interaction between the solar wind and an ionized interstellar medium, three significant results have been established: (1) in the presence of an interstellar wind the region of subsonic solar wind flow should form a comet-like tail in the wake of the sun; (2) the cavity within which the solar wind is supersonic can be expected to be asymmetric; (3) the minimum radius of the cavity is determined by the maximum pressure exerted by the interstellar gas and magnetic field, since the point of maximum external pressure must be a stagnation point of the (subsonic) interior flow. Thus, we can calculate the minimum radius of the solar wind shock transition from equation (16) by taking  $p_o$  to be the maximum external pressure:

$$n_e \bar{m} u_1^2 \left( \frac{r_e}{r_s} \right)^2 = K \left[ \alpha \frac{B_o^2}{8\pi} + n_g (2kT_g + \bar{m} V^2) \right] \quad (28)$$

where  $\alpha$  is a factor that allows for the enhancement of the interstellar magnetic field due to the presence of the solar wind (cf. eq. (21)). The minimum  $r_s$  according to (28), for a range of possible values of  $B_o$  and  $n_g$ , and fixed values of the remaining parameters, can be read directly from figure 7. It should be noted that in the absence of any ionized interstellar gas,  $r_s \approx 140$  AU if we assume that  $B_o \approx 3 \times 10^{-6}$  gauss as suggested by the observations described earlier. If we assume that  $n_g \approx 0.05 \text{ cm}^{-3}$  then with  $V \approx 20 \text{ km sec}^{-1}$  our estimate for  $r_s$  is reduced to 100 AU. For the transition to occur in the vicinity of the orbit of Jupiter as suggested by Lanzerotti and Schulz [1969], or even closer to the sun as suggested by Brandt and Michie [1962], quite

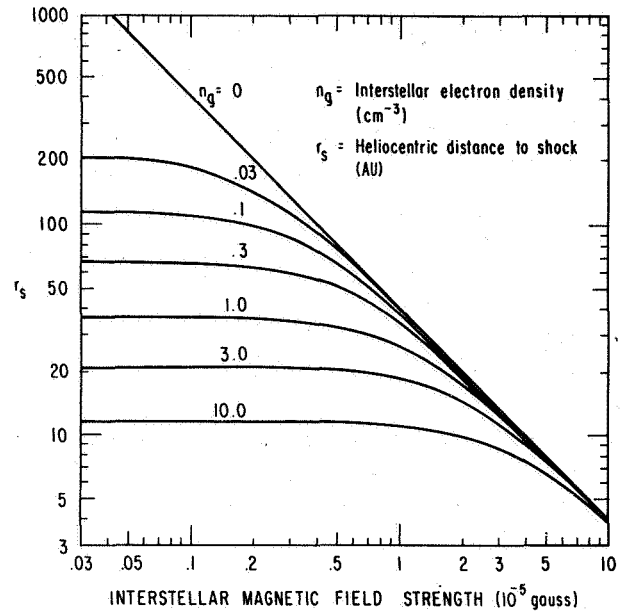


Figure 7 Minimum distance to the solar wind shock transition ( $r_s$ ), as a function of interstellar magnetic field strength for various values of the interstellar electron density. The curves have been calculated from equation (28) assuming  $\alpha = 2.25$ ,  $T_g = 10^4$  °K, and  $V = 20 \text{ km sec}^{-1}$ .

implausible values of the parameters involved in equation (28) are required, or else an entirely different model should be considered, as discussed later (p. 623).

In the previous discussion we have ignored the effects of the interplanetary magnetic field on the flow of the solar wind. This is a reasonable procedure in the supersonic region in the absence of effects associated with neutral interstellar gas, since  $\beta_p \gtrsim 500$ , and in any case the Maxwell stresses are very nearly in self equilibrium. However, in the subsonic region it is easily seen that inconsistencies arise if the effects of the magnetic field are neglected and the flow is treated as if it were incompressible. For example, if we assume that the flow is spherically symmetric and radial, and that the magnetic field is azimuthal, then since

$$ruB = \text{constant} \quad (29)$$

we see that with  $u \propto r^{-2}$  (eq. (17)),  $B \propto r$  and hence the magnetic field strength increases indefinitely. Although the flow is likely to be nonradial and the dimensions of the subsonic region are restricted as indicated in figures 6(a) and (b), the tendency for the magnetic field strength to increase is unavoidable. Indeed, a very similar situation is found in the earth's magnetosheath where

the interplanetary magnetic field strength near the solar wind stagnation point is often found to be comparable to that of the geomagnetic field just within the magnetopause [Cahill and Amazeen, 1963].

The manner in which the magnetic field can be enhanced in the subsonic region, so that it ultimately dominates the plasma behavior, is demonstrated rather well by the case of steady, radial flow with spherical divergence, in the presence of a purely azimuthal magnetic field [Cranfill, 1971]. Let us assume that the region of subsonic flow begins at a shock transition occurring at  $r = r_s$ : the Rankine-Hugoniot equations can be written in normalized form

$$\bar{\rho}_2 \bar{u}_2 = 1 \quad (30)$$

$$\bar{p}_2 + \bar{\rho}_2 \bar{u}_2^2 + \frac{\bar{B}_2^2}{\beta_v} = 1 + \frac{1}{\beta_v} \quad (31)$$

$$\frac{1}{2} \bar{u}_2^2 + \left( \frac{\gamma}{\gamma-1} \right) \frac{\bar{p}_2}{\bar{\rho}_2} + \left( \frac{2}{\beta_v} \right) \frac{\bar{B}_2^2}{\bar{\rho}_2} = \frac{1}{2} + \frac{2}{\beta_v} \quad (32)$$

$$\bar{B}_2 \bar{u}_2 = 1 \quad (33)$$

where  $\bar{\rho} = \rho/\rho_1$ ,  $\bar{u} = u/u_1$ ,  $\bar{B} = B/B_1$ ,  $\bar{p} = p/\rho_1 u_1^2$ , and subscripts 1,2 denote upstream and downstream conditions, respectively. The equations of motion in the subsonic region can be integrated to yield

$$\bar{\rho} \bar{u} \bar{r}^2 = 1 \quad (34)$$

$$\frac{1}{2} \bar{u}^2 + \left( \frac{\gamma}{\gamma-1} \right) \frac{\bar{p}}{\bar{\rho}} + \frac{2\bar{B}^2}{\beta_v} = \frac{1}{2} + \frac{2}{\beta_v} \quad (35)$$

$$\frac{\bar{p}}{\bar{\rho}^\gamma} = \frac{\bar{p}_2}{\bar{\rho}_2^\gamma} \quad (36)$$

$$\bar{r} \bar{u} \bar{B} = 1 \quad (37)$$

where  $\bar{r} = r/r_s$ . For a given value of  $\beta_v$ , equations (30) through (33) can be solved for  $\bar{p}_2$  and  $\bar{\rho}_2$ , and equations (34) through (37) can in turn be solved for  $\bar{u}$ ,  $\bar{B}$ ,  $\bar{\rho}$ , and  $\bar{p}$  as functions of  $\bar{r}$ . It should be noted that the normalization results in the elimination of  $r_s$  from the equations, leaving  $\beta_v$  as the only parameter. The solution for a value of  $\beta_v$  appropriate to the ecliptic plane is shown in figure 8. It is evident that  $\bar{r}$  must be large to

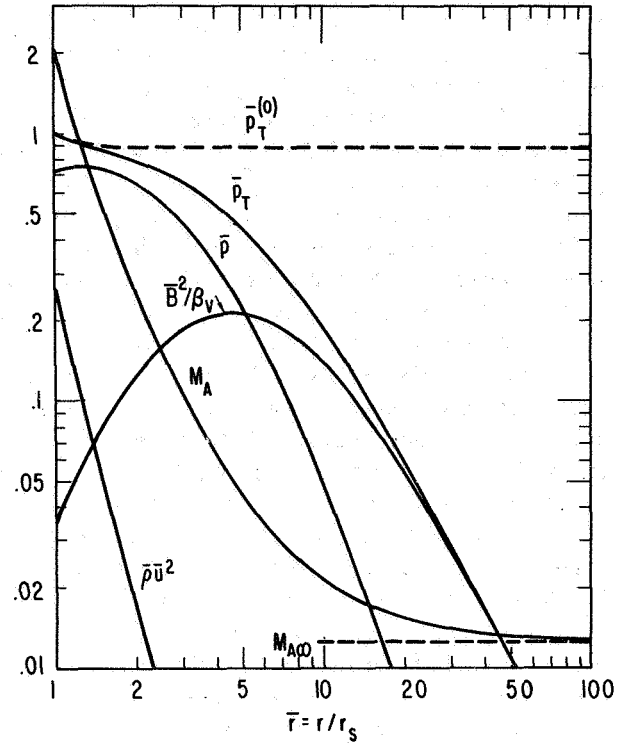


**Figure 8** Solution of equations (34)-(37) with initial conditions determined by equations (30)-(33) and with  $\beta_v = 500$ . Note that the presence of the magnetic field has caused the total pressure  $\bar{p}_T$  to decrease to zero as  $\bar{r} \rightarrow \infty$ , rather than remaining constant ( $\bar{p}_T^{(0)}$ ) as it does in the field-free case [from Cranfill, 1971].

make a substantial change in the total pressure  $\bar{p}_T = \bar{p} + \bar{\rho} \bar{u}^2 + \bar{B}^2/\beta_v$ , although the changes are not insignificant for moderate values of  $\bar{r}$ . At  $\bar{r} = 2$  for example,  $\bar{p}_T$  is reduced by about 12 percent from the value  $\bar{p}_T^{(0)}$  obtained in the absence of magnetic field.

In a more realistic model with nonradial flow it should be expected that the effectiveness of the magnetic field in reducing the total pressure beyond the shock transition is more marked than in the model with strictly radial flow. Lateral flow along the magnetic field lines permits the gas pressure to decrease and be compensated by a corresponding increase in the pressure of the magnetic field. It is easily shown that the reduction in total pressure  $\Delta p$  across a layer of thickness  $d$  and radius of curvature  $R$  is given approximately by

$$\Delta p \approx \frac{\langle B^2 \rangle}{8\pi} \left( \frac{2d}{R} \right) \quad (38)$$

where  $\langle B^2 \rangle$  is the mean square magnetic field strength in the layer. This result applies equally well to the earth's

magnetosheath, and one might expect the values of  $\Delta p/p_s$  to be comparable in the two cases. Observations made in the magnetosheath suggest that  $\Delta p/p_s$  could easily be 0.1–0.2, and hence we can reduce the minimum distance to the solar wind shock transition from our previous estimate of 100 AU to perhaps 80 to 90 AU.

We have assumed that the interplanetary magnetic field can be considered as being frozen into the solar wind plasma in the above discussion. However, magnetic field directional discontinuities must exist within the solar wind plasma (sector boundaries), and at the interface with the region of interstellar plasma and magnetic field. Throughout most of the region of subsonic solar wind flow, it might be expected that sector boundaries are stable against reconnection since  $\beta$  tends to be  $O(1)$  or greater. However, there is no obvious reason why the interface with the interstellar region should be stable against reconnection, and hence we can expect that the interstellar and interplanetary (solar) magnetic fields are connected in much the same manner as the interplanetary magnetic field connects with the geomagnetic field [Dungey, 1961; Levy *et al.*, 1964].

It would be of great interest if the shell of hot plasma

formed by the region of subsonic solar wind flow could be observed from a distance; however, this does not appear to be feasible. The suggestion that free-free transitions in this region might produce a detectable flux of soft X rays with a roughly isotropic distribution was originally made by Reiffel [1960]. The spectrum of the observed isotropic X-ray background is shown in figure 9, together with calculated spectra based on the (favorable) assumptions that the electron and proton temperatures are equal in the shell of hot solar wind plasma, and that the thickness of the shell is  $4r_s$ . The contribution from free-bound transitions associated with the ultimate recombination of all stellar wind plasma originating from stars within 330 parsecs of the sun is also shown. It is evident that neither the solar wind nor stellar winds in general can be considered to be likely sources for the observed X-ray flux [Bowyer and Field, 1969; Cranfill, 1971].

The shock transition that terminates the supersonic solar wind may be collision free, in which case its thickness is no more than a few proton gyroradii (about  $10^{10}$  cm for  $\theta = \pi/2$ ,  $r_s \approx 100$  AU). However, it is also possible that the transition is as wide as the system will

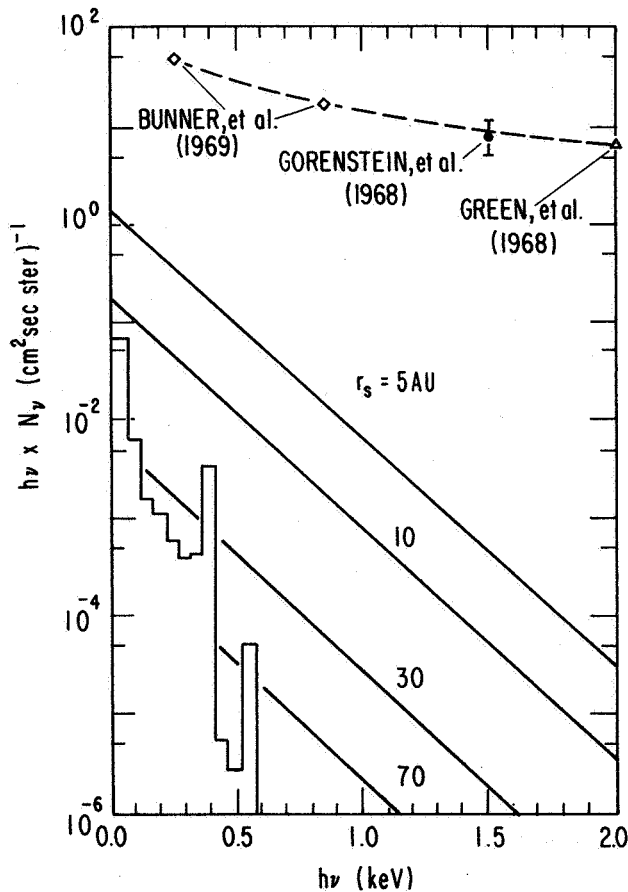


**Figure 9** A comparison of observations of the diffuse soft X-ray flux (dashed line), with estimates of the X-ray flux resulting from (a) free-free emission from the region of subsonic solar wind flow (straight solid lines), and (b) recombinations of stellar wind ions (bar graph). The thickness of the region of subsonic solar wind flow is taken to be  $4r_s$ , with  $T_e = 184$  eV, and  $n = 4n_e r_e^2 / r_s^2$  with  $n_e = 5 \text{ cm}^{-3}$ . Even though we have assumed a rather large thickness for the subsonic region, it is evident that for reasonable values of  $r_s$  (i.e.,  $r_s \gtrsim 50$  AU) the free-free emission fails to account for the observed flux by a factor of the order of  $10^3$ . The bar graph represents 0.05 keV averages of the free-bound emission resulting from the recombination of heavy ions that have been injected into the interstellar medium by stellar winds. It is assumed that a steady state has been reached with the recombination rate equal to the injection rate, and that all stars within 330 parsecs of the sun contribute. The star density is taken to be  $0.08 \text{ parsec}^{-3}$ , and all stellar winds are assumed to be similar to the solar wind in composition and total flux. Ground state recombinations of all appropriate ion states of He, C, N, O, Ne, Mg, Si, and Fe have been included. It is evident that the recombination radiation is also insufficient to account for the observed soft X-ray flux [Cranfill, 1971].

permit [Schindler, private communication], in which case the shock structure would be determined by proton-proton collisions. The thickness of such a shock is presumably of the order of  $\lambda \cos^2 \psi \approx \lambda(u/r\Omega \sin \theta)^2$  where  $\lambda$  is the mean free path. Since at large distances  $\lambda/u < 1/v_{\text{exp}} \approx r/2u$  (fig. 4), it is evident that the thickness must be less than  $1/(2r_s \sin^2 \theta)$  AU. Thus, in the ecliptic plane ( $\theta = \pi/2$ ), we expect that the shock thickness is less than  $10^{11}$  cm, even if the shock is collision dominated.

### NEUTRAL INTERSTELLAR GAS IN THE VICINITY OF THE SUN

If there were no relative motion between the sun and the surrounding interstellar gas, and if the complications introduced by the solar wind could be ignored, the sun could produce a quite substantial HII region if the density of the ionized gas is not too large [Newkirk *et al.* 1960; Brandt, 1964a; Lenckek, 1964; Williams, 1965]. However, if there is relative motion, the situation is drastically altered, and even with quite modest speeds of the order of  $20 \text{ km sec}^{-1}$  it can be shown that the neutral interstellar gas can penetrate almost unattenuated into the inner solar system within the orbit of Jupiter [Blum and Fahr, 1969, 1970a; Holzer, 1970; Holzer and Axford, 1971; Semar, 1970]. In this section, we assume that the interstellar medium in the vicinity of the solar system is part of an HI region, and examine the manner in which the neutral gas is affected by the solar wind and by ionizing radiation from the sun.

Let us consider first the very simple model in which the nearby interstellar gas is stationary with respect to the sun, with the solar HII region assumed to be fully ionized and having the same pressure as the surrounding HI region. On equating the flux of ionizing photons emitted by the sun  $Q$  to the total recombination rate we find that the radius of the HII region  $r_{II}$  is given by Stromgren's result:

$$r_{II} = \left( \frac{3Q}{4\pi\alpha n_{II}^2} \right)^{1/3} \quad (39)$$

where  $\alpha \approx 3 \times 10^{-10} T_{II}^{3/4}$  is the coefficient for recombination to all levels [Allen, 1963, p. 90]. The condition of pressure equilibrium yields

$$2n_{II}T_{II} = n_I T_I \quad (40)$$

Figure 10 gives these relationships for various values of  $T_I$  and  $T_{II}$  for the case  $n_I = 0.2 \text{ cm}^{-3}$ , with

$Q = 4 \times 10^{37} \text{ sec}^{-1}$ ; the points of intersection of the two sets of lines give the values of  $r_{II}$  for the various combinations of values of  $T_I$  and  $T_{II}$ . The thickness of the ionization front separating the HI and HII regions is of the order of  $\Delta = 1/\sigma_L n_I$ , where  $\sigma_L \approx 6.3 \times 10^{-18} \text{ cm}^2$  is the photoionization cross section for hydrogen atoms at the Lyman limit. In cases where  $r_{II} \leq \Delta \approx 5 \times 10^4 \text{ AU}$  our assumption that the HII region is well defined is invalid and a more detailed analysis must be carried out [Gould *et al.*, 1963; Lenckek, 1964; Williams, 1965]. The thickness of the ionization front is somewhat greater than  $\Delta$  since the absorption coefficient decreases approximately as  $\nu^{-3}$  beyond the Lyman limit, and consequently the radiation reaching the outer part of the HII region is such that the effective absorption coefficient is much less than  $\sigma_L$ . Nevertheless, the value of  $r_{II}$  calculated from equation (39) has some significance as a "characteristic" dimension, even in circumstances where the HII region is not sharply bounded.

In principle, the solar HII region could contribute to the low frequency cutoff in the spectrum of galactic nonthermal radio noise, as suggested by Lenckek [1964]. However, the density required to produce significant absorption at frequencies of the order of 1 MHz is quite large ( $n_{II} \approx 10 \text{ cm}^{-3}$ ) even if the electron temperature is as low as  $10^3 \text{ }^\circ\text{K}$ .

In the absence of any interstellar magnetic field, there would be little point in considering a static HII region of the type described above, since the solar wind would push the interstellar gas to such a great distance that ultimately the HII region would either overlap those of other stars or be limited by recombination of the solar wind plasma. In the latter case, the solar wind would terminate at a recombination front [Newman and Axford, 1968]. The interstellar magnetic field should not be expected to have any important direct effect on a static, approximately spherical solar HII region; however, it would effectively shield the HII region from the solar wind, which would be channeled harmlessly away in the manner indicated in figure 4.

The chief defect of these models of a solar HII region is the requirement that there be no relative velocity between the sun and the local interstellar gas, when in fact a relative speed of the order of  $20 \text{ km sec}^{-1}$  might be considered more appropriate. An atom of interstellar gas, approaching the sun with speed  $V = 20 \text{ km sec}^{-1}$ , has a mean free path against loss by ionization given by

$$\lambda_i = \frac{V}{\beta} = \frac{V}{\sum_j \beta_j} \quad (41)$$

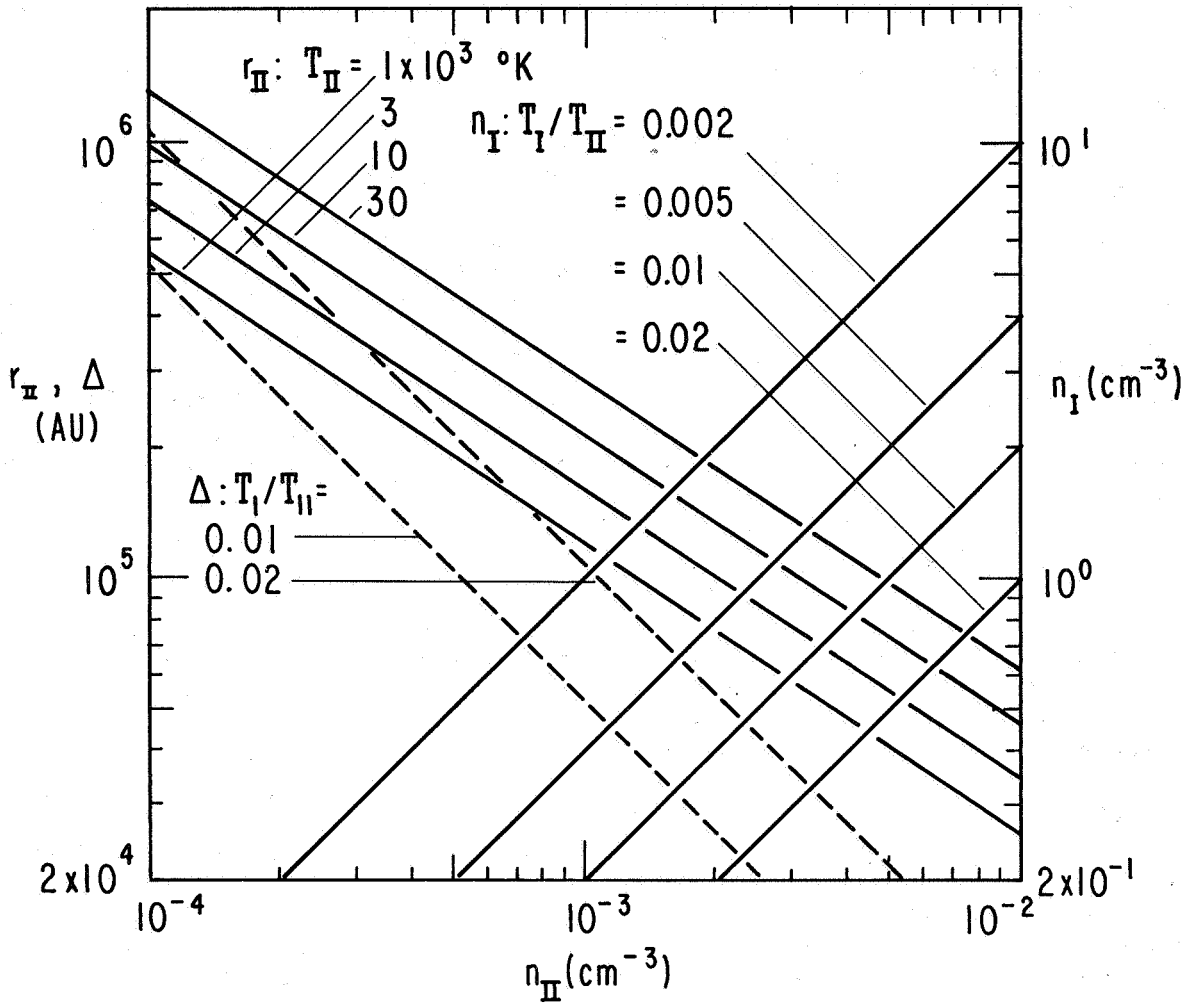


**Figure 10** The values of  $r_{II}$  and  $n_I$  (solid lines) are plotted for various values of  $T_{II}$  and  $T_I/T_{II}$  according to equations (39) and (40). The intersection of these lines defines representative allowed sets of parameters describing model solar HII regions. The ionization front thickness  $\Delta$  is shown for two values of  $T_I/T_{II}$  (dashed lines). As an example, for  $T_{II} = 3 \times 10^3$  °K, and  $T_I = 30$  °K, we see that  $r_{II} \approx 7 \times 10^4$  AU, and  $\Delta \approx 10^4$  AU.

where the  $\beta_j$  are rate coefficients for all possible ionization processes (table 1). In general,  $\beta = \beta_0(r_e^2/r^2)$ , where  $\beta_0$  is a constant for each atomic species. It is to be expected therefore that a substantial fraction of interstellar atoms approaching the sun can penetrate to within a heliocentric distance of the order of  $r_i = (\beta_0 r_e^2/V)$ . From table 1 we see that interstellar hydrogen atoms can easily penetrate to within the orbit of Jupiter, while interstellar helium atoms can penetrate to the orbit of earth. Clearly then, we must expect to be involved in quite a different situation than that of a static, spherical HII region that effectively excludes neutral interstellar gas from the region occupied by the solar wind.

The flow of neutral interstellar gas past the sun has been studied by *Fahr* [1968a], *Blum and Fahr* [1969, 1970a], *Holzer* [1970], *Holzer and Axford* [1971], *Tinsley* [1971], and *Semar* [1970]. The following discussion is based on *Holzer's* treatment of the problem (essentially the same as that of *Blum and Fahr*), with a slight generalization to allow for solar radiation pressure. As a first approximation, solar radiation pressure can be assumed to produce a radial outward force that varies inversely with the square of the distance from the sun. Thus it can be taken into account by introducing an "effective" gravitational constant  $(1-\mu)G$ , where  $\mu$  is the ratio of the force on an atom resulting from radiation pressure to the force of gravity. For hydrogen, the large

**Table 1** Loss coefficients at  $r=r_e(\beta=\beta_0)$ , and penetration distances for  $V=20 \text{ km sec}^{-1}$  ( $r_i$ ). The solar ultraviolet flux has been taken from Hinteregger [1970]

Species	Reaction	$\sigma(\text{cm})^2$	Reference	Rate ( $10^{-7} \text{ s}^{-1}$ )	$r_i(\text{AU})$
H	$\text{H} + h\nu \rightarrow \text{H}^+ + e$		Banks and Kockarts [1972]	1.5	
	$\text{H} + \text{H}^+ \rightarrow \text{H}^+ + \text{H}$	$2 \times 10^{-15}$	Fite <i>et al.</i> [1962]	4	4
	$\text{H} + \text{He}^{+2} \rightarrow \text{H}^+ + \text{He}^+$	$4 \times 10^{-16}$	Fite <i>et al.</i> [1962]	0.036	
	$\text{He} + h\nu \rightarrow \text{He}^+ + e$		Lowry <i>et al.</i> [1965]; Cairns and Samson [1965]	0.62	
He	$\text{He} + \text{H}^+ \rightarrow \text{He}^+ + \text{H}$	$1.5 \times 10^{-17}$	Afrosimov <i>et al.</i> [1969]	0.03	0.5
	$\text{He} + \text{He}^{++} \rightarrow 2\text{He}^+$	$2 \times 10^{-17}$	Hertel and Koski [1964]	0.0018	
C	$\text{C} + h\nu \rightarrow \text{C}^+ + e$		McGuire [1968]	40	30
N	$\text{N} + h\nu \rightarrow \text{N}^+ + e$		Henry [1968]	1.7	
	$\text{N} + \text{H}^+ \rightarrow \text{N}^+ + \text{H}$	$1.8 \times 10^{-15}$	Stebbins <i>et al.</i> [1960]	3.6	4
O	$\text{O} + h\nu \rightarrow \text{O}^+ + e$		Huffman [1969]	2.4	
	$\text{O} + \text{H}^+ \rightarrow \text{O}^+ + \text{H}$	$8 \times 10^{-16}$	Fite <i>et al.</i> [1962]	1.6	3
Ne	$\text{Ne} + h\nu \rightarrow \text{Ne}^+ + e$		Ederer and Tomboulou [1964], Samson [1965]	1.9	
	$\text{Ne} + \text{H}^+ \rightarrow \text{Ne}^+ + \text{H}$	$10^{-16}$	Afrosimov <i>et al.</i> [1969]	0.2	1.6
Si	$\text{Si} + h\nu \rightarrow \text{Si}^+ + e$		McGuire [1968]	60	45
Ar	$\text{Ar} + h\nu \rightarrow \text{Ar}^+ + e$		Cairns and Samson [1965]; Rustgi [1964]; Madden <i>et al.</i> [1969]	2.8	
	$\text{Ar} + \text{H}^+ \rightarrow \text{Ar}^+ + \text{H}$	$10^{-15}$	Koopman [1967]	2	3.6
Fe	$\text{Fe} + h\nu \rightarrow \text{Fe}^+ + e$		McGuire [1968]	2.4	
	$\text{Fe} + \text{H}^+ \rightarrow \text{Fe}^+ + \text{H}$	$< 10^{-16}$	Lee and Hasted [1965]		1.8

solar Lyman  $\alpha$  flux results in  $\mu$  being of order unity, and hence the effects of radiation pressure are very important [Wilson, 1960; Brandt, 1961; Tinsley, 1971], which is contrary to the conclusion of Fahr [1968a]. However, for other species  $\mu \ll 1$ , and hence solar gravity determines their dynamic behavior. In a more accurate treatment it would be necessary to take into account the variation of  $\mu$  with position resulting from Doppler shifts and the reduction in the intensity of the solar radiation resulting from scattering. It should also be noted that the solar Lyman  $\alpha$  flux varies with solar activity especially at the center of the line where 100 percent variations can occur [Blamont and Madjar, 1971].

If we neglect the thermal velocities of interstellar atoms ( $\leq 1 \text{ km sec}^{-1}$  if  $T_I \approx 100^\circ \text{ K}$ ) in comparison with the bulk velocity of the gas relative to the sun ( $V \approx 20 \text{ km sec}^{-1}$ ), then the trajectory of every atom lies in the plane determined by its velocity vector at infinity and the sun. Since the mean free path for atom-atom collisions is very large ( $\sim 10^{16}$ – $10^{17} \text{ cm}$ ), and the most

important collisions with solar wind particles are ionizing, it is appropriate to make use of a free particle treatment allowing for losses associated with ionization, with loss coefficients as given in table 1. Taking polar coordinates ( $r, \theta'$ ) in any such plane, it can readily be shown that the trajectories are hyperbolae with the sun as focus, given by

$$\frac{A}{r} = 1 + B \sin(\theta' + \alpha) \quad (42)$$

with

$$u_r = \pm \left[ V^2 + \frac{2(1-\mu)GM}{r} - \frac{p^2}{r^2} \right]^{1/2} \quad (43)$$

$$u_\theta = \frac{p}{r} \quad (44)$$

where  $\theta' = 0$  is antiparallel to the incident flow velocity  $V$ ,  $p$  is the angular momentum of the atom about the sun,  $u_r, u_\theta$  are velocity components in the  $r, \theta'$  directions,  $M$  is the mass of the sun, and

$$A = \frac{p^2}{(1-\mu)GM} \quad (45)$$

$$B = \left(1 + \frac{V^2 A^2}{p^2}\right)^{1/2} \quad (46)$$

$$\sin \alpha = -\frac{1}{B} \quad (47)$$

In general, any point in the plane  $(r, \theta')$  is a point of intersection of two trajectories having angular momenta given by

$$p_1, p_2 = \frac{1}{2} V \left\{ r \sin \theta' \pm \left[ r^2 \sin^2 \theta' + \frac{4r(1 - \cos \theta')}{C} \right]^{1/2} \right\} \quad (48)$$

where  $C = V^2/(1 - \mu)GM$ , and the plus sign is associated with  $p_1$  and the minus sign with  $p_2$ . As indicated in figure 11,  $p_1 > 0, p_2 < 0$  if  $\mu < 1$ , and  $p_1 > 0, p_2 > 0$  if  $\mu > 1$ . In the case  $\mu < 1$ , some particles may be lost by striking the sun. In the case  $\mu > 1$ , the stream of particles cannot enter the region defined by

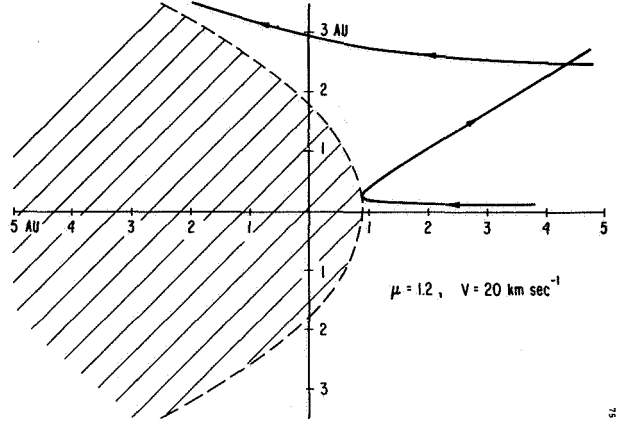


**Figure 11(b)** Same as (a), but with the effects of radiation pressure exceeding gravity. A parabolic forbidden region (hatched) is produced with the sun at the focus.

$$r(1 + \cos \theta') \leq \left(\frac{4GM}{V^2}\right) (\mu - 1) \quad (49)$$

since the angular momenta given by equation (48) become imaginary. In the case  $\mu = 1$ , the trajectories are straight lines parallel to  $\theta' = 0$  and  $p_2 = 0$ .

The number density  $n$  of a particular species in interplanetary space can be calculated from the equation of continuity, with the trajectories (42) being treated as streamlines. We use an orthogonal coordinate system  $(\xi, \Psi, \phi)$  such that  $\hat{e}_\xi = \mathbf{u}/u$ , and  $\phi$  is the azimuthal coordinate relative to the axis  $\theta' = 0$ . Thus

$$\text{div}(n\mathbf{u}) = \frac{1}{h_\xi h_\Psi h_\phi} \frac{\partial}{\partial \xi} (n u h_\Psi h_\phi) = -\beta n \quad (50)$$

with  $\beta$  as given in table 1, and

$$\int_{-\infty}^{\xi} d [\ln(n u h_\Psi h_\phi)] = - \int_{-\infty}^{\xi} \left(\frac{\beta}{u}\right) h_\xi d\xi \quad (51)$$

If we take  $\Psi = p/V$ , then it can be shown that

$$h_\Psi = \frac{|2\Psi - r \sin \theta'|}{|\Psi|(1 + 2/rC)^{1/2}} = \frac{[r^2 \sin^2 \theta' + 4r(1 - \cos \theta')/C]^{1/2}}{|\Psi|(1 + 2/rC)^{1/2}} \quad (52)$$

Also, since the displacement  $d\xi$  is along a trajectory

$$h_\xi d\xi = \frac{ur d\theta'}{u\theta} \quad (53)$$

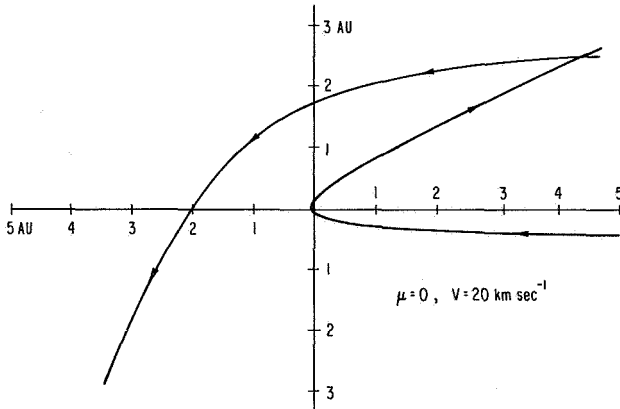


**Figure 11(a)** Examples of intersecting particle trajectories for a case of a cold interstellar wind approaching the sun (at the origin) from the right of the diagram at  $20 \text{ km sec}^{-1}$ , and with radiation pressure absent ( $\mu = 0$ ). Note that all trajectories cross the axis of symmetry on the downwind side of the sun.



Hence on putting  $h_\phi = r|\sin \theta'|$ , and taking  $\beta = \beta_0 r e^2 / r^2$ , we obtain from (51)

$$n(r, \theta) = \sum_j \frac{N p_j^2 \exp(-\beta_0 r e^2 \theta_j / |p_j|)}{V^2 r \sin \theta [r^2 \sin^2 \theta + 4r(1 - \cos \theta)/C]^{1/2}} \quad (54)$$

where  $\theta$  is the polar angle from the axis of symmetry ( $0 \leq \theta \leq \pi$  and  $|\sin \theta'| = \sin \theta$ ),  $N$  is the number density of the incident stream at infinity, and  $\theta_j = \theta$  if  $p_j > 0$ ,  $\theta_j = (2\pi - \theta)$  if  $p_j < 0$ . If either of the trajectories that

intersect at  $(r, \theta')$  strikes the sun before reaching the point, its contribution to  $n$  must be discounted. Note that if  $\mu \rightarrow 1$ ,  $C \rightarrow \infty$ , then  $u = V$ ,  $b_1 = Vr \sin \theta'$ ,  $p_2 = 0$ , and (54) reduces to the simple result

$$n(r, \theta) = N \exp\left(\frac{-\beta_0 r e^2 \theta}{Vr \sin \theta}\right) \quad (55)$$

Equal number density contours for hydrogen and helium have been calculated with  $\mu = 0, 0.8, 1.0$ , and  $1.2$  for the case of hydrogen (figs. 12(a)–(d)) and with  $\mu = 0$

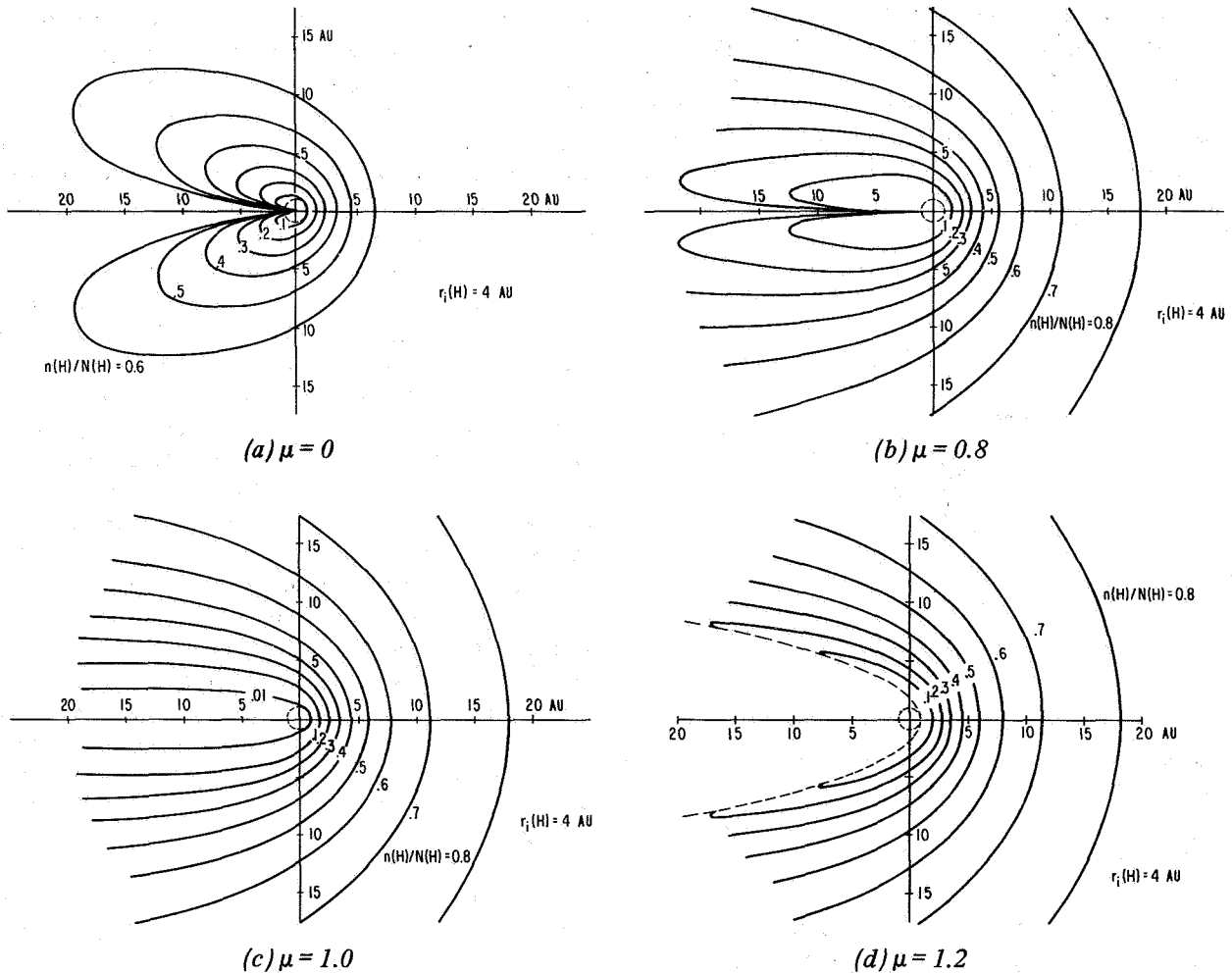


**Figure 12** Contours of equal density of neutral interstellar hydrogen. The sun is at the center of each diagram and the orbit of earth is shown as a dashed line. The plane of the diagram is the plane containing the velocity vector of the interstellar wind and the sun. The three-dimensional contours are of course axisymmetric. Note the high density on the axis of symmetry ( $\theta = \pi$ ) for  $\mu < 1$ , and the paraboloidal void which appears when  $\mu$  exceeds 1.

for helium (fig. 13). Note that  $n(r, \theta)$  is finite on  $\theta = 0$  in each case, but if  $\mu < 1$ ,  $n(r, \theta) \rightarrow \infty$  as  $\theta \rightarrow \pi$  as shown in a slightly different context by *Danby and Camm* [1957]. This singularity disappears if one relaxes the assumption that the incident stream of atoms has no thermal velocities [*Danby and Bray*, 1967]. For  $\mu \geq 1$ ,  $n(r, \pi) = 0$ , and for  $\mu > 1$  an empty region develops in the wake of the sun. In the upstream direction the interstellar neutral gas penetrates to a heliocentric distance of order  $r_i = \beta_0 r_e^2 / V$ , as argued previously, and hence there are likely to be observable effects that permit us to determine  $N(H)$ ,  $N(He)$ , and  $V$ .

*Fahr* [1968a,b; 1969] has examined the possibility that the local fluxes of neutral interstellar gas and of neutral hydrogen produced in the solar wind by charge exchange should be sufficient to cause changes in the structure of the upper atmosphere. However, on taking reasonable values for the various parameters concerned, one finds that it is unlikely that observable effects can be produced. *Holzer and Axford* [1971] have argued that accretion of interstellar gas could be an important

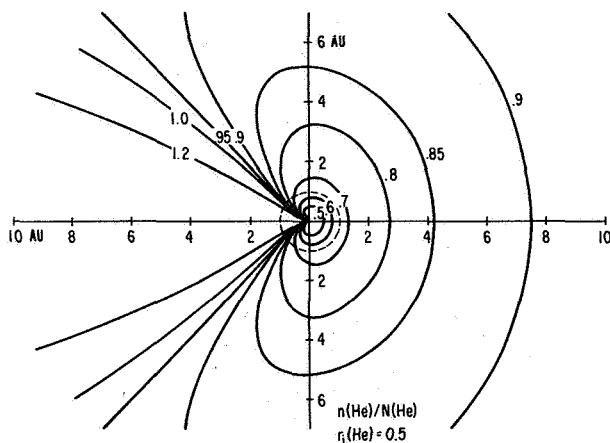


**Figure 13** Contours of equal number density of interstellar helium in the plane containing the sun and the velocity vector of the interstellar gas. The orbit of the earth is shown as a dashed line.

item in the terrestrial budget of  $^3\text{He}$  but not of other gases unless conditions were vastly different in the past. It is evident from the calculations described above that the number density of neutral helium near the earth is only slightly less ( $\sim 25$  percent) than it is in the interstellar gas. If we assume that  $[^4\text{He}]:[^3\text{He}] \approx 3000:1$  [*Cameron*, 1968], it is estimated that the average flux of interstellar  $^3\text{He}$  atoms accreted by the earth is approximately  $50 N(H)$  atoms  $\text{cm}^{-2} \text{sec}^{-1}$ . According to

*Johnson and Axford* [1969], the average rate of loss of atmospheric  $^3\text{He}$  by evaporation is approximately  $7 \text{ atoms cm}^{-2} \text{sec}^{-1}$ ; hence, allowing for contributions from other sources, we find that  $N(H) \approx 0.05\text{--}0.1 \text{ cm}^{-3}$ . At certain times of the year, the relative velocity between the earth and the interstellar gas can be as high as  $80 \text{ km sec}^{-1}$ . This is sufficient for heavier atoms to be trapped in a target foil, thus raising the possibility that the isotopic composition of the interstellar gas (especially neon and argon) might be measured directly [*Geiss*, private communication].

It might also be possible to estimate the density of the neutral interstellar gas in the vicinity of the solar system from observations of the state of ionization of the solar wind. For example, charge exchange between solar wind protons and interstellar hydrogen atoms produces a neutral hydrogen component of the solar wind; similarly, photoionization of interstellar helium atoms, together with other less important processes, results in the appearance of  $\text{He}^+$  ions in the solar wind (fig. 14). The hydrogen flux in the solar wind is estimated to be less than  $10^{-4}$  of the proton flux if  $N(H) = 0.1 \text{ cm}^{-3}$ , and is probably too small to be easily measured. The expected flux of  $\text{He}^+$  ions in the solar wind is shown in figure 14(d) for the case  $N(H) = 1 \text{ cm}^{-3}$ . There have been reports of a singly ionized helium component of the solar wind [*Bame et al.*, 1968; *Wolfe et al.*, 1966], with a flux of the order of  $10^{-3}$  times that of  $\text{He}^{+2}$  ions. On the basis of these results, *Holzer and Axford* [1971] have estimated that  $N(H) \approx 0.1 \text{ cm}^{-3}$ , which is consistent with the estimate based on the terrestrial  $^3\text{He}$  budget. More recent observations by *Bame et al.* [1970] showed no evidence for the presence of  $^4\text{He}^+$  ions in the solar wind possibly because they were masked by other ions with the same charge-mass ratio ( $\text{Si}^{+7}$ ,  $\text{S}^{+8}$ ,  $\text{A}^{+9}$ ,  $\text{Fe}^{+14}$ ) or because they had a bulk flow velocity and temperature significantly different from those of other ions and could not be easily identified in an energy-per-unit-charge spectrum. There is clearly a need for further observations using a detector which can identify  $^4\text{He}^+$  ions unambiguously [*Ogilvie et al.*, 1968; *Ogilvie and Wilkerson*, 1969].

The interstellar gas can be detected directly by observations of resonant scattering of solar photons, notably Lyman  $\alpha$  ( $\lambda 1216 \text{ H I}$ ) and  $\lambda 584 \text{ He I}$  [*Morton and Purcell*, 1962; *Kurt*, 1965, 1967; *Kurt and Dostovalov*, 1968; *Kurt and Syunyaev*, 1968; *Young et al.*, 1968; *Chambers et al.*, 1970; *Mange and Meier*, 1970; *Thomas and Krassa*, 1971; *Bertaux and Blamont*, 1971; *Wallace*, 1969; *Tinsley*, 1969; *Reay and Ring*, 1969; *Barth*, 1970a,b; *Barth et al.*, 1967, 1968; *Metzger and Clark*, 1970; *Byram et al.*, 1961; *Bowyer et al.*, 1968; *Johnson*

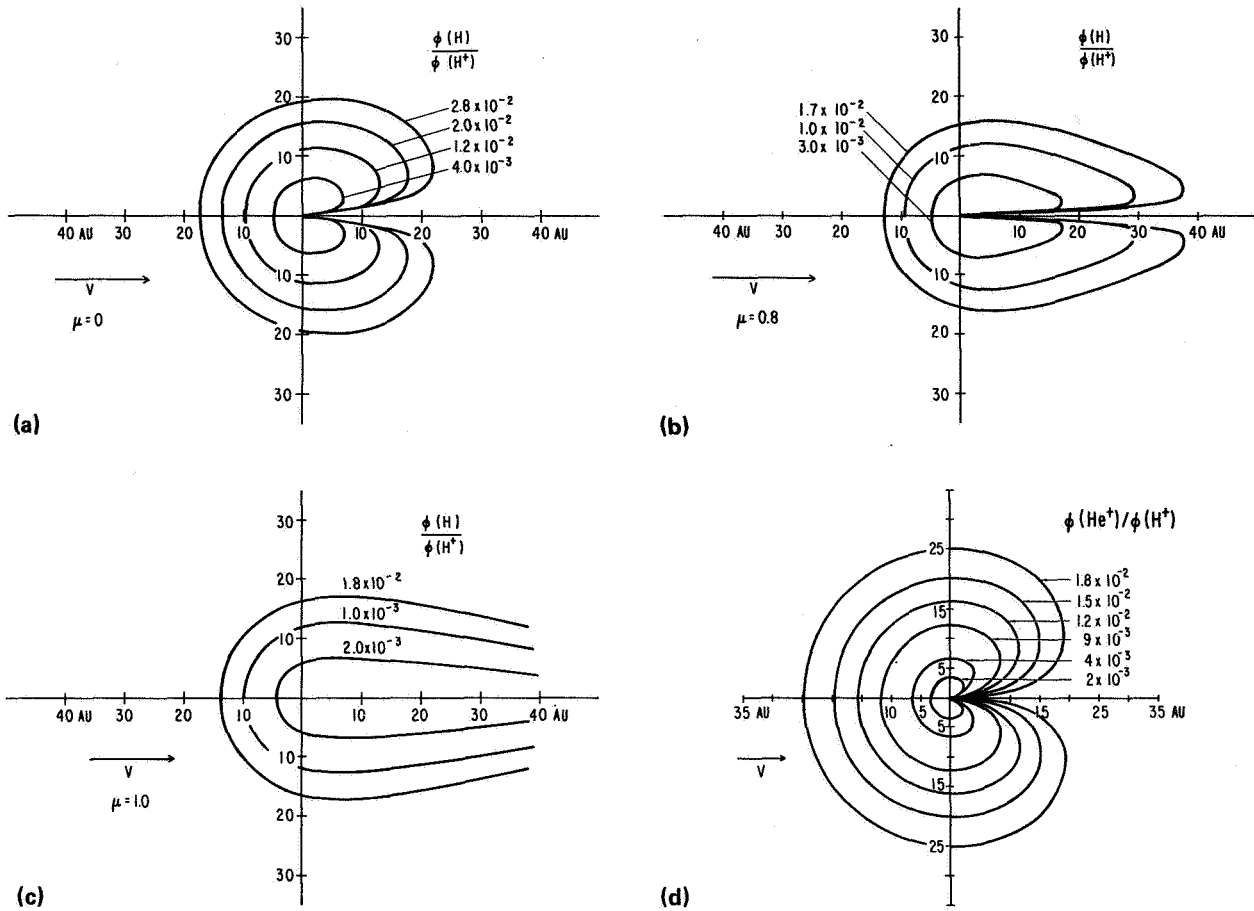


**Figure 14** Contours of equal flux of hydrogen in the solar wind resulting from charge exchange with interstellar hydrogen, relative to the solar wind proton flux (assumed to be  $2 \times 10^8 \text{ cm}^{-2} \text{ sec}^{-1}$  at 1 AU). The plane of the diagram is defined by the velocity vector of the interstellar gas and the sun. There is an enhancement of solar wind hydrogen along the downwind axis of symmetry in (a) and (b) where  $\mu = 0.0$  and  $0.8$ , respectively, but not in (c) where  $\mu = 1$ .

The flux of  $\text{He}^+$  ions in the solar wind resulting from ionization of the interstellar gas, relative to the solar wind proton flux, is shown in (d). The interstellar gas density has been assumed to be  $1 \text{ cm}^{-3}$  in these calculations, with  $N(\text{H}) = 0.92 \text{ cm}^{-3}$ , and  $N(\text{He}) = 0.08 \text{ cm}^{-3}$ . For other values of  $N(\text{H})$  and  $N(\text{He})$  the figures should be rescaled appropriately.

*et al.*, 1971; Ogawa and Tohmatsu, 1971]. From such observations, we can in principle deduce the composition and density of neutral interstellar gas flowing past the solar system, the velocity vector, and also the temperature. Accordingly, they are of great significance for our understanding of the behavior of the solar wind at great distances from the sun. Interpretations of these observations in terms of various models of the interaction between the solar wind and the interstellar medium have been given by Patterson *et al.* [1963], Brandt [1964b, 1970], Hundhausen [1968b], Kurt and

Germogenova [1967], Blum and Fahr [1969, 1970b,c, 1971], Tohmatsu [1970], Bowers [1970], Tinsley [1971], Holzer [1971], Thomas [1971], and Wallis [1971].

Let us consider a simple model for the scattering of solar radiation by neutral atoms in the interplanetary medium. The flux  $J(r, \theta, \nu)$  of solar photons in the frequency range  $(\nu, \nu + d\nu)$  satisfies the equation

$$\frac{1}{r^2} \frac{\partial}{\partial r} (r^2 J) = -\alpha n J \quad (56)$$

where  $\alpha(r, \theta; \nu)$  is the absorption coefficient, and we have neglected multiply scattered photons. If  $\mathbf{r}, \mathbf{r}'$  are the position vectors of a point in space relative to the sun and earth, respectively, then the intensity of singly scattered photons in a fixed direction  $\hat{\mathbf{r}}'$  is given by

$$J'(\nu) = \frac{1}{4\pi} \int_0^\infty \alpha(\mathbf{r}; \nu) n(\mathbf{r}) J(\mathbf{r}; \nu) dr' \quad (57)$$

where the integration is carried out along the line of sight from the earth,  $\nu$  refers to the frequency before scattering takes place, and absorption of the scattered photons is neglected. The total intensity of singly scattered photons from a given solar emission line is therefore

$$I = 4\pi \times 10^6 \int_{-\infty}^{\infty} J'(\nu) d\nu \quad (\text{Rayleighs}) \quad (58)$$

It does not matter that the frequency of the scattered photons need not be the same as that of the absorbed photons (in the observer's frame) since observations are usually carried out with broadband detectors. However it might be important in some cases to allow for Doppler shifts in calculating the absorption coefficient if the solar emission line is not broad and featureless. In the case of Lyman  $\alpha$  for example (see fig. 15), the intensity

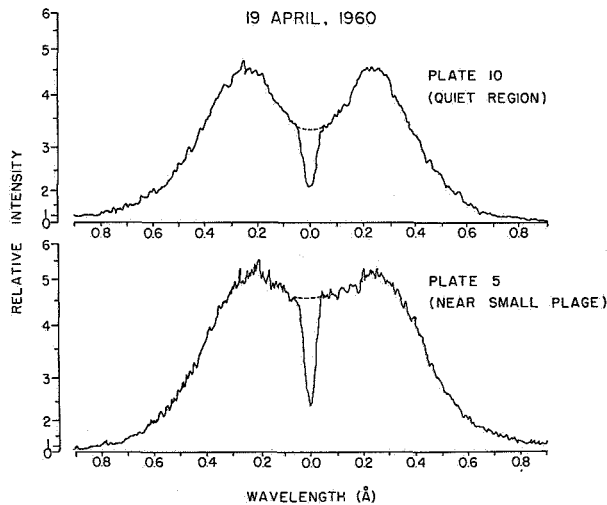


**Figure 15** Solar Lyman  $\alpha$  profiles for two regions on the sun obtained by Meier and Prinz [1970]. The central core is produced by the earth's hydrogen corona, and the dashed line indicates the expected unattenuated intensity.

at the center of the line is only 70 percent of the maximum intensity in quiet solar conditions, and the maxima occur at  $\pm 0.25 \text{ \AA}$  from the center (corresponding to Doppler shifts such that  $|u_r| \approx 60 \text{ km sec}^{-1}$ ). If it is considered that the above analysis is unnecessarily complicated in view of the fact that the solar emission line is quite variable, and that multiple scattering has been neglected, a simplification can be achieved by assuming that the medium is optically thin. In this case the right hand side of equation (56) is equated to zero, so that instead of

$$J(\mathbf{r}; \nu) = \frac{r_e^2}{r^2} J(r_e; \nu) \exp \left[ - \int_{r_e}^r \alpha(\mathbf{r}; \nu) n(\mathbf{r}) dr \right] \quad (59)$$

with the integration being carried out along the radius vector from the sun, we neglect the exponential term and simply use

$$J(\mathbf{r}; \nu) = \frac{r_e^2}{r^2} J(r_e; \nu) \quad (60)$$

in (57). In any case, these calculations will usually tend to overestimate the intensity of the scattered light for given  $N$ , as a result of the neglect of multiple scattering.

Examples of calculated total intensity profiles of scattered solar radiation from neutral hydrogen ( $\lambda 1216 \text{ H I}$ ) are shown in figures 16(a) and (b) and from neutral helium ( $\lambda 584 \text{ He I}$ ) in figures 16(c) and (d). In figures 16(a) and (c) the earth is shown situated on the upstream axis of symmetry ( $\alpha_e = 0$ ), and in figures 16(b) and (d) it is shown situated at  $90^\circ$  from the axis of symmetry ( $\alpha_e = 90^\circ, 270^\circ$ ). We have not attempted to obtain an exact fit between the models and the observations (fig. 17), but instead have simply taken  $N(\text{H}) = 0.1 \text{ cm}^{-3}$ ,  $N(\text{He}) = 0.008 \text{ cm}^{-3}$ , and  $V = 20 \text{ km sec}^{-1}$ , with the interstellar wind vector in the plane of the ecliptic; this choice provides a reasonable match to the observations if  $\mu \approx 1$ . The direction of the interstellar wind is determined by the direction of maximum Lyman  $\alpha$  intensity, although as pointed out by Blum and Fahr [1971], some distortion may be produced as a result of asymmetries in the solar Lyman  $\alpha$  emission. The velocity of the interstellar wind is determined by the parallax effect shown in figure 16(b) (see also figs. 17(a)–(c)). The value of  $N(\text{H})$  is determined from the maximum intensity of scattered Lyman  $\alpha$ , although it should be noted that there is some ambiguity since it is also necessary to account for the observed minimum intensity of  $\sim 250 R$  [Thomas, 1971]. Note that for small values of  $\mu$  the peak Lyman  $\alpha$  emission

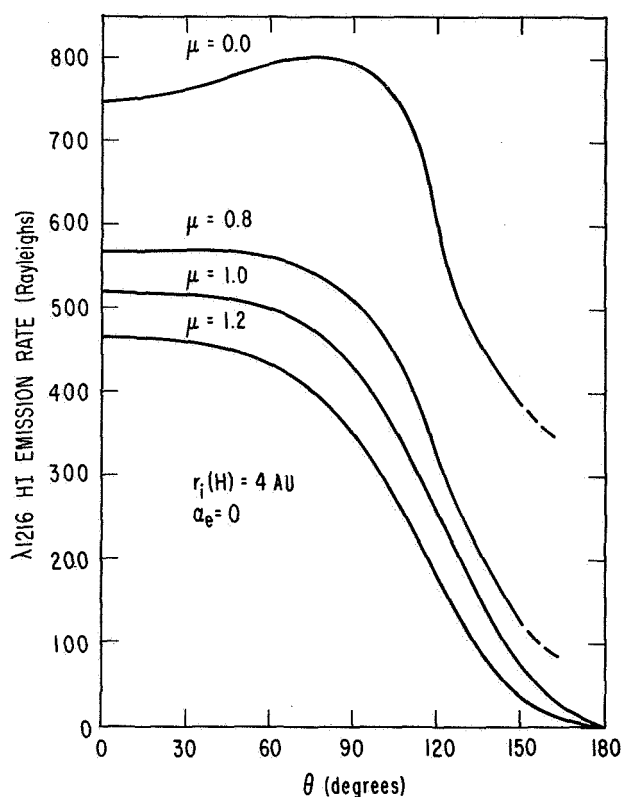


**Figure 16(a)** Calculated scattered intensity of Lyman  $\alpha$  ( $\lambda 1216$  HI) corresponding to the results shown in figure 12 for various values of  $\mu$ , with  $N(\text{H}) = 0.1 \text{ cm}^{-3}$  and  $V = 20 \text{ km sec}^{-1}$ . The earth is on the axis of symmetry on the upstream side of the sun ( $\alpha_e = 0$ ). For  $\mu < 1.0$  there is a singularity at  $\theta = 180^\circ$  corresponding to the singularities on the axis of symmetry shown in figures 12(a) and (b).

occurs at  $\theta \approx 90^\circ$ , and there would not be a single maximum as observed (fig. 17). If  $\mu \geq 1$ , the minimum intensity is zero according to our calculations, which are based on the assumption that  $T_I = 0$ .

The observed minimum intensity of  $\sim 250 R$  can be accounted for in any of three ways: (1) the effect of radiation pressure is such that  $\mu < 1$ ; (2) there may be a uniform galactic background of Lyman  $\alpha$  [Kurt and Syunyaev, 1968; Tinsley, 1969, 1971; Adams, 1971]; or (3) the interstellar hydrogen has a relatively high temperature ( $T_I \approx 10^4 \text{ }^\circ\text{K}$ ) as discussed earlier [Thomas, 1971]. If  $T_I$  is small and the effects of radiation pressure do not exceed those of gravity ( $\mu \approx 0.7$ ), then a small bright patch should occur near the center of the region of low intensity as a result of the high neutral hydrogen density in the vicinity of the axis of symmetry [Blum and Fahr, 1970b]. However, the bright patch may not

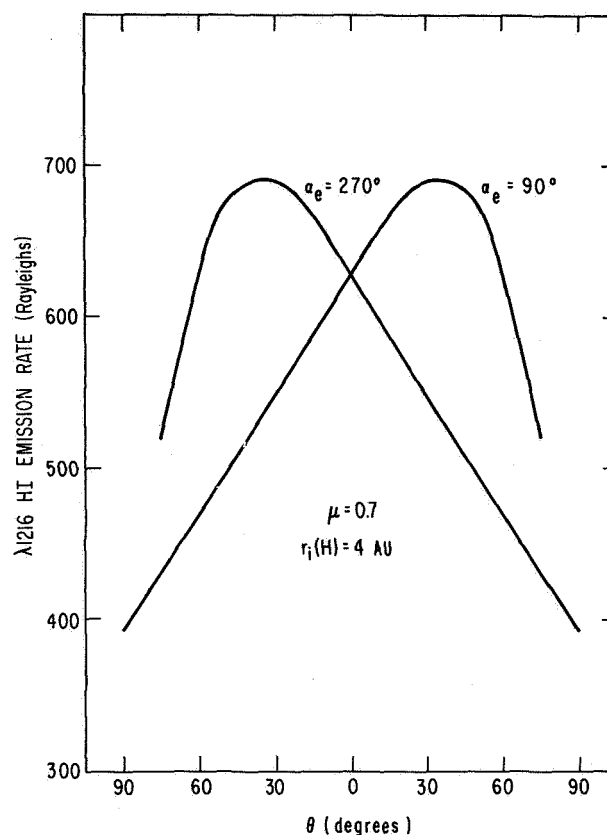


**Figure 16(b)** The same as (a) but with the earth at  $\pm 90^\circ$  from the axis of symmetry (i.e.,  $\alpha_e = 90^\circ, 270^\circ$ ) showing the effect of parallax. With  $\mu = 0.7$ , and the same values assumed for the various parameters involved, the direction of the region of maximum emission intensity can vary by about  $60^\circ$  throughout the year.

be very prominent unless observations are made exactly along the axis of symmetry ( $\alpha_e = \theta = 180^\circ$ ). Preliminary calculations indicate that for  $\alpha_e \neq 180^\circ$  the secondary intensity maximum is not at all pronounced and could be easily missed by observations made with wide-angle detectors [Johnson, 1971]. If the minimum intensity represents galactic Lyman  $\alpha$ , then this should be distinguishable from the scattered solar Lyman  $\alpha$  since the line width is expected to be considerably greater. Furthermore, as pointed out by Blum and Fahr [1970c], galactic and local components of the diffuse Lyman  $\alpha$  radiation can be distinguished by the fact that the former must be constant in time, while the latter must reflect changes in the solar Lyman  $\alpha$  flux, especially the 27-day variations [Meier, 1969]. Observations of such time variations could remove these uncertainties, as could observations made at greater distances from the sun (beyond the orbit of Jupiter) where the galactic

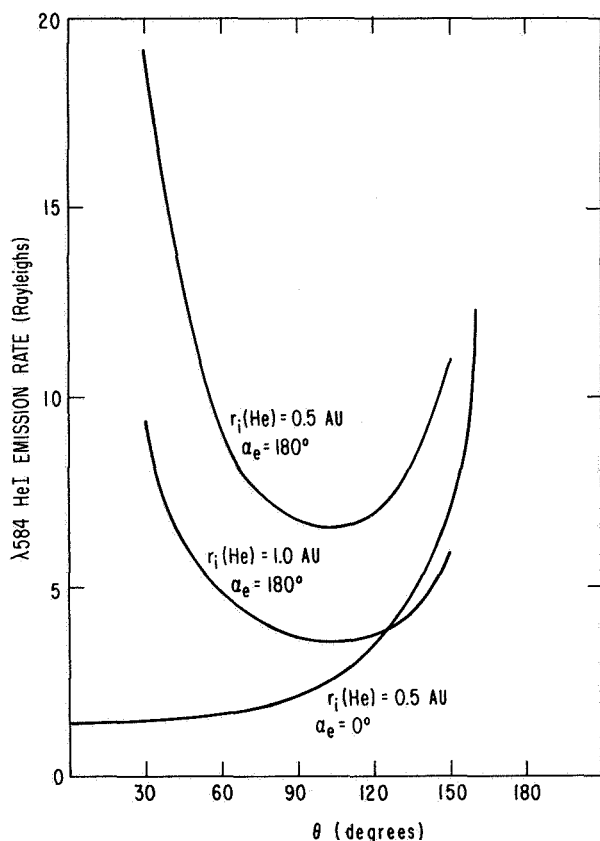


**Figure 16(c)** Intensity of scattered  $\lambda 584$  HeI; we have used the same parameters as in (a) and (b), and assumed that the interstellar gas contains 8 percent He. Note that there is a maximum in the direction of the sun as well as in the direction of the downstream axis of symmetry. The former maximum occurs in the case of helium but not hydrogen because the helium is easily able to penetrate to within the orbit of earth. The effect of varying  $r_i(\text{He})$  from 0.5 to 1.0 is shown for the case  $\alpha_e = 180^\circ$ . The solar line width is assumed to be  $0.023 \text{ \AA}$  [e.g., Donahue and Kumer, 1971] which is probably too small, however the scattered intensity varies approximately inversely with the line width, and for other values the scattered intensity can be obtained by simply rescaling this diagram.

component should be dominant. The suggestion by Thomas [1971] that  $T_I$  is relatively large is consistent with theoretical work on the intercloud component of a neutral interstellar gas. This is certainly a possibility if the background soft X-ray flux is sufficient to heat the interstellar gas [Silk and Werner, 1969; Werner *et al.*, 1970], but probably not if it is necessary to rely on heating by low-energy cosmic rays. There are at least

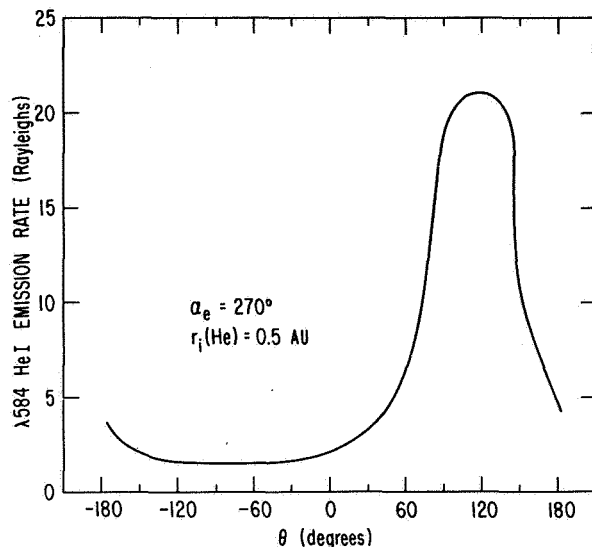


**Figure 16(d)** The same as (c), but with  $\alpha_e = 270^\circ$ , showing the displacement of region of maximum intensity.

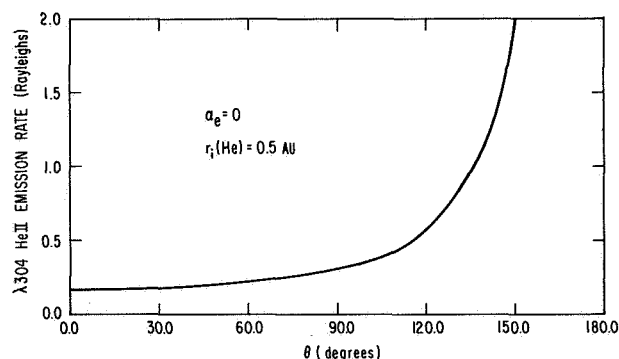


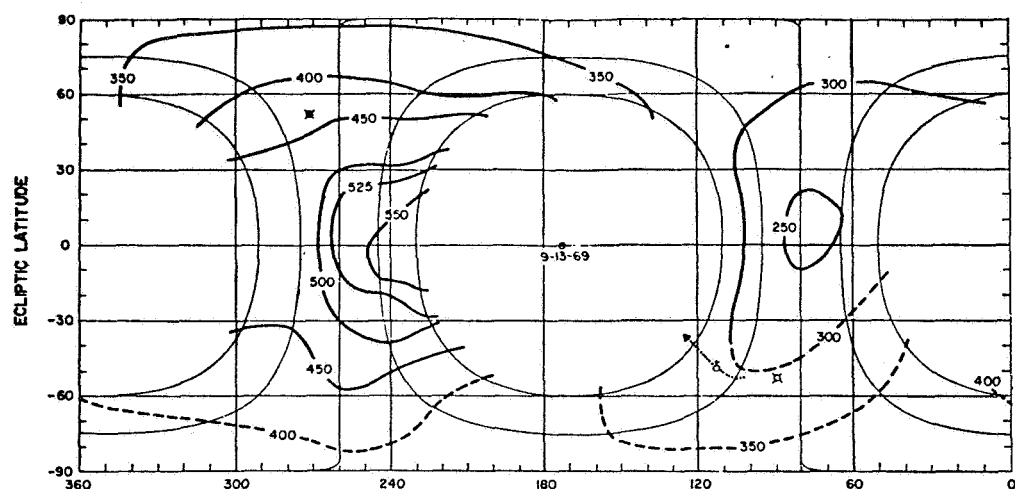
**Figure 16(e)** Intensity of scattered  $\lambda 304$  HeII resulting from the presence of singly ionized helium in the solar wind for  $\alpha_e = 0^\circ$ , and  $r_i(\text{He}) = 0.5$ . Most of the scattered light comes from the direction of the sun. The scattered intensity is approximately inversely proportional to the assumed solar line width, which in this case has been taken to be  $0.06 \text{ \AA}$ .

two ways of determining whether or not the temperature of the interstellar gas is large: (1) from measurements of the intensity of scattered  $\lambda 584$  HeI, which should show a very pronounced maximum in the direction of the axis of symmetry  $\alpha_e = 180^\circ$ , and to some extent for other values of  $\alpha_e$  if  $T_I$  is small (figs. 16(c) and (d)); and (2) from measurements of the width of the scattered solar Lyman  $\alpha$  line, made when  $\alpha_e = 90^\circ, 270^\circ$ , and away from the sun ( $\theta = 90^\circ, 270^\circ$ ), where scattering

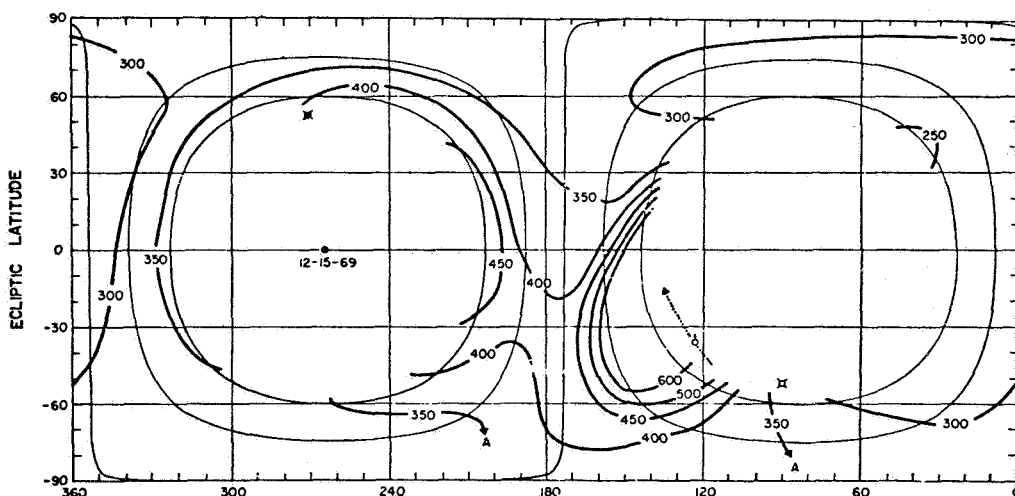
should take place in the line center if  $T_I$  is small. In this case, a hydrogen absorption cell should have a pronounced effect on the observed radiation unless there is a substantial galactic component [Blamont, private communication, 1971].

The resonantly scattered helium radiation ( $\lambda 584$  HeI) is of particular interest since helium atoms penetrate easily to within the orbit of earth, and hence there is always a maximum in the direction of the sun. The

intensity minimum occurs in the direction away from the sun except when  $\alpha_e \approx 180^\circ$  (figs. 16(c) and (d)). These effects could also be found in the case of Lyman  $\alpha$  for observations made in the region  $r \geq 5$  AU. In our calculations we have adopted a solar line width of  $0.023\text{\AA}$  [Donahue and Kumer, 1971]; this line width may be too small, in which case the expected scattered intensity should be reduced proportionately downward from the values shown in figures 16(c) and (d). There



(a) SU 1 on 13 September 1969



(b) SU 2 on 15 December 1969

**Figure 17** Contour maps of the solar Lyman  $\alpha$  background in ecliptic coordinates for the three spinups (SU's) of OGO 5: (a) SU 1 on 13 September 1969; (b) SU 2 on 15 December 1969; and (c) SU 3 on 1 April 1970. These figures have been taken from Thomas and Krassa [1971]. Similar diagrams have been given by Bertaux and Blamont [1971]. (d) Contour map of scattered  $\lambda 304$  HeII radiation based on the observations of Johnson et al. [1971], and taken from Ogawa and Tohmatsu [1971].

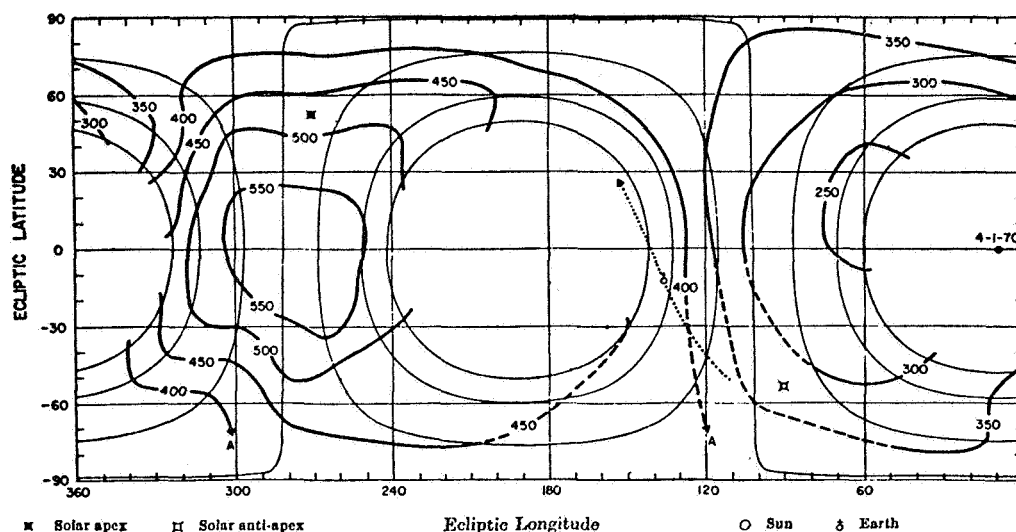


Figure 17 Continued.

have been only a few observations of the diffuse helium radiation to date; these indicate an upper limit of  $\sim 2 R$  for the intensity of the diffuse  $584\text{\AA}$  radiation from extraterrestrial neutral helium in a direction away from the sun [Young *et al.*, 1968; Johnson *et al.*, 1971; Ogawa and Tohmatsu, 1971]. We suggest that these observations be pursued for various combinations of values of  $\alpha_e$  and  $\theta$ , and also outside the influence of the neutral helium envelope of the earth.

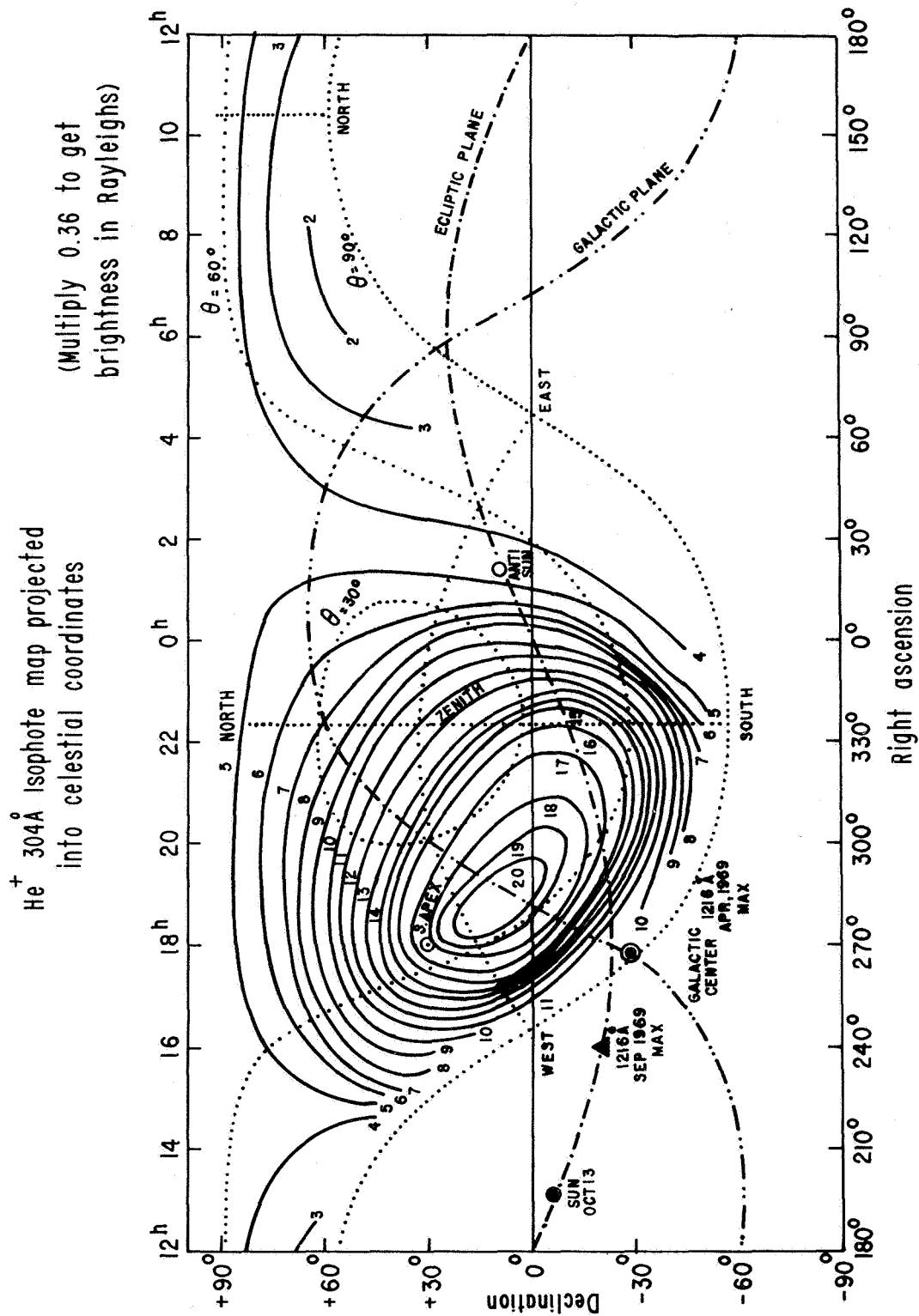
There must be diffuse Lyman  $\alpha$  and  $\lambda 304$  HeII radiation resulting from the presence of neutral hydrogen and singly ionized helium in the solar wind as indicated in figure 14. The Lyman  $\alpha$  produced in this way can be distinguished from that described above since it should be red-shifted by about  $1.5\text{\AA}$  from the center of the solar line. However, calculations by Gregory [1971] indicate that for  $\mu = 0.8$ ,  $N(\text{H}) = 0.1 \text{ cm}^{-3}$ , and  $\alpha_e = 0$ , the intensity of the scattered Lyman  $\alpha$  from this source is only  $\sim 3.5 R$  in the direction  $\theta = 0$ , which is probably too small to be distinguished from the galactic background. The intensity of scattered  $304\text{\AA}$  radiation is shown in figure 16(e) for the case  $\alpha_e = 0$ ; as in the case of radiation scattered by neutral helium, maximum emission occurs in the direction of the sun. For  $\theta \approx 120^\circ$  to  $150^\circ$ , the intensity of the scattered radiation is  $\sim 1 R$ , which is consistent with an observation of  $1.0 \pm 0.2 R$  reported by Ogawa and Tohmatsu [1971].

Another possible source of diffuse Lyman  $\alpha$  radiation is scattering from fast hydrogen atoms produced by charge exchange in the region of subsonic solar wind flow beyond the shock transition. In this case the emission should be centered at  $\sim 0.3\text{\AA}$  to the red side of the

center of the solar line, and have a half width of about  $1\text{\AA}$  as a result of the random velocities of the hydrogen atoms produced in this region. This emission has been considered by Patterson *et al.* [1963] and Hundhausen [1968b] in an attempt to account for an observation of  $\sim 540 R$  of Doppler-broadened Lyman  $\alpha$  reported by Morton and Purcell [1962]. However, this observation showed only that there is more or less isotropic emission outside  $\pm 0.04\text{\AA}$  from the center of the line, which is easily accounted for by scattering from interstellar hydrogen, since it is moving at velocities exceeding  $20 \text{ km sec}^{-1}$ , and will in general produce Lyman  $\alpha$  emission displaced about  $0.1\text{\AA}$  from the line center. The calculations of Patterson *et al.* [1963] and Hundhausen [1968b] indicate that the isotropically moving hydrogen atoms must be produced in the region  $r = 10$  to  $20 \text{ AU}$  to explain the observed emission intensity. However, since it seems likely that as noted, the transition to subsonic flow does not occur within  $50 \text{ AU}$ , this should not be an important source of diffuse Lyman  $\alpha$ .

It would be of interest to extend the calculations described in this section to include other emissions. Undoubtedly other hydrogen and helium lines are present in the diffuse radiation with intensities proportional to those of the  $\lambda 1216 \text{ HI}$  and  $\lambda 584 \text{ HeI}$  emissions [Reay and Ring, 1969; Tohmatsu, 1970]. Furthermore, the possibility of scattering by other species is also of interest, and on the basis of table 1 it would appear that neon in particular might produce a detectable emission, since  $r_i(\text{Ne})$  is small and neon is a relatively abundant element.





(d) Contour map of scattered  $\lambda 304$  He II radiation based on the observations of Johnson et al. [1971], and taken from Ogawa and Tohmatsu [1971].

Figure 17 Concluded.

## INTERACTION OF THE SOLAR WIND WITH NEUTRAL INTERSTELLAR GAS

In this section we consider the effect on the solar wind of the neutral component of the interstellar gas. Various aspects of this interaction have been considered by several authors [Axford *et al.*, 1963; Patterson *et al.*, 1963; Axford and Newman, 1965; Dessler, 1967; Kern and Semar, 1968; Hundhausen, 1968a; Fahr, 1968a,b, 1969, 1970; Blum and Fahr, 1969, 1970a,b; Semar, 1970; Holzer, 1970, 1971; Holzer and Axford, 1971; Wallis, 1971; Bhatnagar and Fahr, 1971]. In this discussion of the problem, we shall follow the treatment given by Holzer [1971], which is similar to the work of Wallis [1971] but somewhat more detailed.

It has been shown that the interstellar neutral gas penetrates to within a few astronomical units of the sun before becoming significantly affected by losses due to photoionization and charge exchange. Since the solar wind is expected to extend to a heliocentric distance of the order of 100 AU in the absence of any interaction with neutral interstellar gas, it is evident that as a first approximation we can treat the solar wind as if it were flowing through a uniform background of neutral gas with density  $N$ , temperature  $T_n$ , and velocity  $\mathbf{V}$  relative to the sun. Even with this assumption, the problem is very difficult since there must be nonradial flow in the region of supersonic solar wind flow as well as in the subsonic region; furthermore, the effects of the interplanetary magnetic field should not be ignored. However, a simplification can be achieved if we consider only the directions parallel and antiparallel to the velocity vector of the interstellar gas, since the flow can then be treated as being approximately radial. In this case, as noted earlier, the azimuthal component of the interplanetary magnetic field is dominant in  $r \gtrsim 5$  AU and accordingly we may assume that  $B_r \approx 0$  and  $B \approx B_\phi \propto (ur)^{-1}$ .

If we represent the solar wind as a steady, radial, spherically symmetric flow of a proton-electron plasma through an atomic hydrogen gas, then neglecting viscosity and heat conduction, the equations of motion can be formulated as follows:

$$\frac{1}{r^2} \frac{d}{dr} (nur^2) = q_p \quad (61)$$

$$\begin{aligned} \frac{1}{r^2} \frac{d}{dr} (nu^2 r^2) = & -\frac{1}{\gamma} \frac{d}{dr} (nc_s^2) - \frac{G\mathcal{H}}{r^2} n \\ & + \frac{1}{mc} (\mathbf{j} \times \mathbf{B})_r + Q_p^m + Q_c^m \end{aligned} \quad (62)$$

$$\frac{1}{r^2} \frac{d}{dr} \left[ nur^2 \left( \frac{1}{2} u^2 + \frac{1}{\gamma-1} c_s^2 \right) \right] = -\frac{G\mathcal{H}}{r^2} nu + \frac{\mathbf{j} \cdot \mathbf{E}}{m} + Q_p^e + Q_c^e \quad (63)$$

Here  $c_s (= \sqrt{\gamma p / \rho})$  is the plasma sound speed,  $m$  is the proton mass, and  $c$  is the speed of light. The rates of mass, momentum, and energy production are represented by  $q$ ,  $Q^m$ , and  $Q^e$ , per proton mass per unit volume, respectively, with the subscripts  $p$  and  $c$  referring to the processes of photoionization and charge exchange. Thus

$$q_p = q_0 N \left( \frac{r_0}{r} \right)^2 \exp \left( -\sigma_p \int_{r_0}^r N dr' \right) \quad (64)$$

$$Q_p^m = q_p V \quad (65)$$

$$Q_p^e = q_p \left( \frac{1}{2} V^2 + \frac{3}{2} \frac{kT_n}{m} + \frac{\mathcal{E}}{m} \right) \quad (66)$$

$$Q_c^m = v n (V - u) \quad (67)$$

$$Q_c^e = v n \left( \frac{1}{2} V^2 + \frac{3}{2} \frac{kT_n}{m} - \frac{1}{2} u^2 - \frac{\alpha}{\gamma-1} \frac{kT}{m} \right) \quad (68)$$

$$v = \sigma_c N \left[ \frac{128k}{9\pi m} (\alpha T + T_n) + (u - V)^2 \right]^{1/2} \quad (69)$$

where  $\sigma_p$  is a mean photoionization cross section,  $\mathcal{E}$  is the average energy of a photoelectron produced in the photoionization process,  $T (= T_e + T_p)$  is the plasma temperature,  $\alpha T$  is the proton temperature, and  $\sigma_c$  is the resonant charge exchange cross section. The velocity of the interstellar neutral gas ( $\mathbf{V}$ ) is taken to be radial.

The electric field ( $\mathbf{E}$ ), the current ( $\mathbf{j}$ ), and the magnetic field satisfy the equations

$$\nabla \times \mathbf{B} = \frac{4\pi}{c} \mathbf{j} \quad (70)$$

$$\mathbf{E} = -\frac{1}{c} \mathbf{u} \times \mathbf{B} \quad (71)$$

Thus, with the assumption that the magnetic field is azimuthal, we find that

$$\frac{1}{c} (\mathbf{j} \times \mathbf{B})_r = -\frac{d}{dr} \left( \frac{B^2}{8\pi} \right) - \frac{B^2}{4\pi r} \quad (72)$$

and

$$\mathbf{j} \cdot \mathbf{E} = -u \frac{d}{dr} \left( \frac{B^2}{8\pi} \right) - u \frac{B^2}{4\pi r} \quad (73)$$

We can now write the equations of motion in the form

$$\frac{1}{u} \frac{du}{dr} (u^2 - c_s^2 - c_A^2) = \frac{2}{r} c_s^2 - \frac{G\mathcal{M}}{r^2} + \mathfrak{Q}_1 \quad (74)$$

$$\frac{dc_s^2}{dr} = (\gamma - 1) \left( -\frac{2}{r} c_s^2 - \frac{c_s^2}{u} \frac{du}{dr} + \mathfrak{Q}_2 \right) \quad (75)$$

with the following definitions:

$$\mathfrak{Q}_1 = -\left( \frac{q_p}{\mathcal{F}} + \frac{v}{u} \right) \left[ \frac{1}{2} u^2 + \frac{\gamma}{2} (u - V)^2 - \frac{1}{2} V^2 + \frac{3}{2} (\gamma - 1) \frac{kT_n}{m} \right] + \frac{v}{u} \frac{\alpha}{\gamma} c_s^2 - \frac{q_p}{\mathcal{F}} (\gamma - 1) \frac{\mathfrak{E}}{m} \quad (76)$$

$$\mathfrak{Q}_2 = \gamma \left( \frac{q_p}{\mathcal{F}} + \frac{v}{u} \right) \left[ \frac{1}{2} (u - V)^2 + \frac{3}{2} \frac{kT_n}{m} - \frac{\alpha}{\gamma(\gamma - 1)} c_s^2 \right] + \frac{q_p}{\mathcal{F}} \left( \frac{\alpha - 1}{\gamma - 1} c_s^2 + \frac{\gamma \mathfrak{E}}{m} \right) \quad (77)$$

$$\mathcal{F} = nu = \frac{1}{r^2} \left( n_o u_o r_o^2 + \int_{r_o}^r r'^2 q_p dr' \right) \quad (78)$$

$$c_A^2 = \frac{B^2}{4\pi nm} = \frac{B_o^2 u_o^2 r_o^2}{4\pi m \mathcal{F} r^2 u} \quad (79)$$

where the subscript  $o$  denotes quantities evaluated at a point  $r = r_o$  close to the sun.

In the special case where  $B = G = V = T_n = \mathfrak{E} = 0$ , equations (74) and (75) reduce to a single first-order differential equation in terms of the Mach number  $M = u/c_s$ :

$$\frac{1}{M} \frac{dM}{dr} (M^2 - 1) = \frac{\gamma + 1}{r} + \frac{\gamma - 1}{r} (M^2 - 1)$$

$$-\frac{q_p}{\mathcal{F}} \left( \frac{\gamma^2 - \gamma}{4} M^4 + \frac{3\gamma - 1}{4} M^2 + \frac{1}{2} \right)$$

$$-\frac{v}{u} \left( \frac{\gamma^2 - \gamma}{4} M^4 + \frac{3\gamma - 2\alpha + 1}{4} M^2 - \frac{\alpha}{2\gamma} \right) \quad (80)$$

Note that  $v/u$  is a function only of  $M$ , since in this special case (69) reduces to

$$v = \sigma_c Nu \left( 1 + \frac{128\alpha}{9\pi\gamma} \frac{1}{M^2} \right)^{1/2} \quad (81)$$

Many features of the solutions of the more general equations (74) and (75) can be understood from an examination of the solutions of (80). In effect, this is the problem considered by Semar [1970], who carried out a numerical integration of the equations of motion (61), (62), and (63), for this case taking  $\gamma = 2$ ,  $\alpha = 1$ , and omitting the term enclosed in the bracket in (81). Unfortunately, the existence of a singular point at  $M = 1$  was overlooked in Semar's analysis, which consequently implies that a shock-free ("transonic") transition to subsonic flow will always occur. In fact, as pointed out by Wallis [1971] and Holzer [1971], this is not necessarily the case.

Equation (80) has a singular point at which  $(M^2 - 1)$  and the right-hand side of (80) vanish simultaneously. If this point is defined to be at  $r = r_c$ , then

$$r_c = \frac{1}{4f_c} \left\{ 3 - \gamma - 2Rf_c + [4R^2 f_c^2 + (20 + 4\gamma)Rf_c + (\gamma - 3)^2]^{1/2} \right\} \quad (82)$$

where, using (64) and (69), and assuming that the neutral gas is optically thin in the region  $r_o < r < r_c$ , we have

$$\frac{q_p}{\mathcal{F}} = \frac{1}{R + r} \quad (83)$$

$$R = \frac{n_0 u_0}{q_0 N} - r_0 \quad (84)$$

$$f_c = \left( \frac{\gamma+1}{2} - \frac{\alpha}{\gamma} \right) \sigma_c N \left( \frac{128\alpha}{9\pi\gamma} + 1 \right)^{1/2} \quad (85)$$

Note that under typical solar wind conditions and with  $0.05 \leq N \leq 1.0 \text{ cm}^{-3}$ ,  $r_c \propto 1/N$ .

The form of the characteristics passing through the singular point can be determined by expanding (80) about  $M = 1$ ,  $r = r_c$ . Defining  $\lambda = M - 1$  and  $\xi = (r/r_c) - 1$ , we obtain to first order in  $\lambda$  and  $\xi$

$$\frac{d\lambda}{d\xi} = a \frac{\xi}{\lambda} + b \quad (86)$$

where

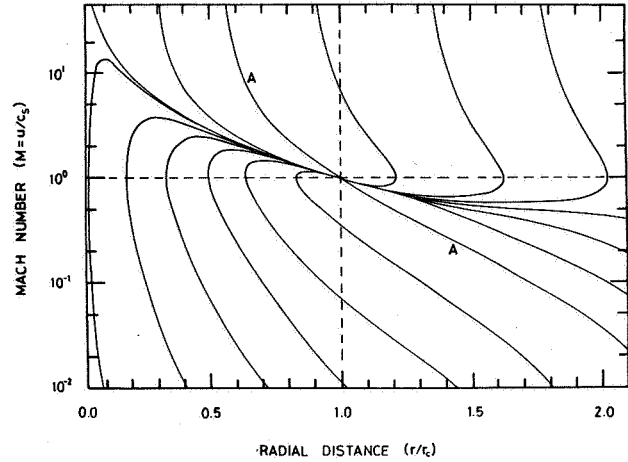
$$a = \frac{(\gamma+1)^2}{8} \left( \frac{r_c}{R+r_c} \right)^2 - \frac{\gamma+1}{2} \quad (87)$$

$$b = \gamma - 1 - \frac{(2\gamma-1)(\gamma+1)}{4} \frac{r_c}{r_c + R} - \frac{\gamma+1}{4} r_c f_c \cdot \left[ - \left( \frac{128\alpha}{9\pi\gamma} \right) \left( \frac{128\alpha}{9\pi\gamma} + 1 \right)^{-1} + \frac{4\gamma^2 - 2\gamma + \frac{4\gamma}{\gamma+1}(1-\alpha)}{\gamma^2 + \gamma - 2\alpha} \right] \quad (88)$$

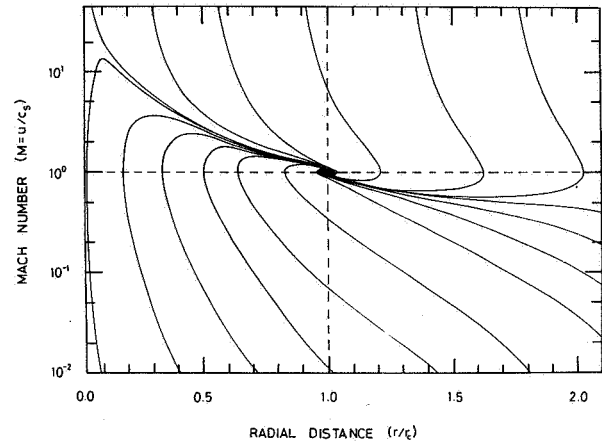
A characteristic passing through the singular point has a slope at the singular point given by  $S = \lim_{\xi \rightarrow 0} (\lambda/\xi)$ . Hence  $S$  can take one of the two values

$$S_{\pm} = \frac{1}{2} \left( b \pm \sqrt{b^2 + 4a} \right) \quad (89)$$

If  $b^2 + 4a > 0$ , the characteristics passing through the singular point can have slopes  $S_+$  or  $S_-$ . If  $b^2 + 4a = 0$ , all characteristics passing through the singular point have slope  $S_+ = S_- = b/2$ . If  $b^2 + 4a < 0$ , the characteristics in the vicinity of the singular point are spirals and the corresponding solutions are multivalued in  $M$ . A family of solutions of (80) for which  $b^2 + 4a > 0$  is shown in figure 18(a) and a family for which  $b^2 + 4a < 0$  is shown in figure 18(b).



(a)  $b^2 + 4a > 0$



(b)  $b^2 + 4a < 0$

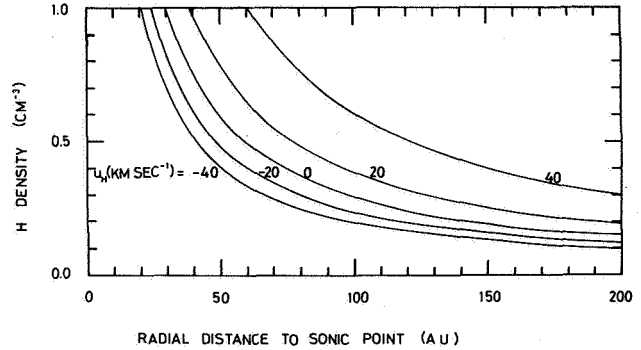
**Figure 18** Characteristics of equation (58) [from Holzer, 1971]. Note that a transonic solution is possible in (a) but not in (b) where the singular point is a focus.

On examination of the possible solutions displayed in figures 18(a) and (b) one finds that only one characteristic leads to infinity in each case, and that these are such that the pressure  $p \rightarrow 0$  as  $r \rightarrow \infty$ ; there are no solutions that yield a finite pressure at infinity. For the case of moderate and low interstellar densities, the characteristics are as shown in figure 18(a), and it is always possible to find a solution starting with suitable conditions at  $r = 5 \text{ AU}$ , say, which contains a smooth transition to subsonic flow and eventually has vanishing pressure at infinity. For somewhat higher interstellar densities ( $N \gtrsim 10 \text{ cm}^{-3}$ , depending on the value chosen for other parameters), the characteristics are likely to be as shown in figure 18(b); in this case, again it is possible

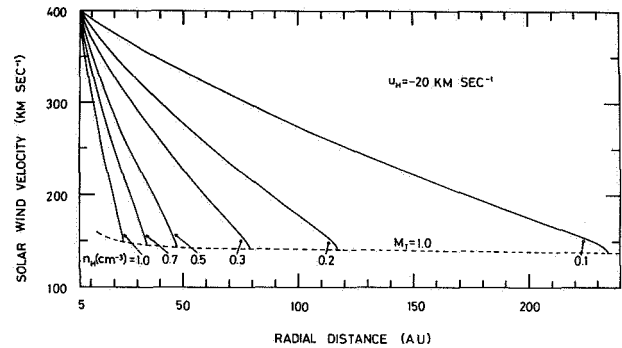
to find a solution starting with suitable conditions at  $r = 5$  AU, and with vanishing pressure at infinity, but it is necessary to insert a shock at a correctly determined location near the singular point to make the solution single valued. In the numerical treatment carried out by Semar [1970] these complexities have passed unnoticed, although the results obtained are probably a fairly good representation of the solution except in the vicinity of the singular point. It should be noted, however, that the form for the collision frequency  $\nu$  used by Semar is inadequate if the Mach number is not large, and the former has an important effect on the properties of the characteristics in the subsonic region.

The solutions of equation (80) are useful in that they suggest what we can expect in the more general case involving a pair of differential equations — namely, (74) and (75) — that must be solved simultaneously for two unknowns  $u$  and  $c_s$ . Holzer [1971] has treated this problem by a straightforward integration of (74) and (75), having assigned values for  $u$ ,  $\rho$ ,  $T$ , and  $B$  at a point relatively close to the sun ( $r = 5$  AU) where the solar wind can be expected to be essentially unaffected by the presence of neutral interstellar gas. The integration proceeds in the direction of increasing  $r$ , until the Mach number  $M_T = u/(c_s^2 + c_A^2)^{1/2}$  decreases to unity, or (if a shock transition is inserted) until the solutions approach some asymptotic form that can be recognized. In this procedure, there is some danger that singular points might be missed and that the solutions might be unstable; however, the results obtained appear to be satisfactory. Examples of solutions of equations (74) and (75) obtained in this manner are shown in figures 19(a) and (b) and 20(a)–(c). The initial conditions have been taken to be  $u_0 = 400$  km sec $^{-1}$ ,  $n_0 = 0.2$  cm $^{-3}$ ,  $c_{s0} = 15$  km sec $^{-1}$ ,  $B_0 = 0.7 \times 10^{-5}$  gauss at  $r = r_0 = 5$  AU, together with a range of values for the density ( $N$ ) and velocity ( $V$ ) of the interstellar neutral gas.

The location of the sonic point ( $M = 1$ ;  $r = r_c$ ) is shown in figure 19(a) for a range of values of  $N$  and  $V$ ; this yields an outer limit for the position of any possible shock transition in the flow. Note that the location of the sonic point is quite sensitive to the density of the neutral interstellar gas, varying roughly as  $N^{-1}$ . Furthermore, there is a substantial difference between the values of  $r_c$  on the upwind ( $V < 0$ ) and downwind ( $V > 0$ ) sides of the sun, which should produce a distinct asymmetry in the region of supersonic solar wind flow — for example, for  $N = 0.1$  cm $^{-3}$  and  $V = 20, -20$  km sec $^{-1}$ ,  $r_c = 250$  AU, 400 AU, respectively. The variation of solar wind speed with distance is shown in figure 19(b) for  $V = -20$  km sec $^{-1}$  and various values of  $N$ . If we



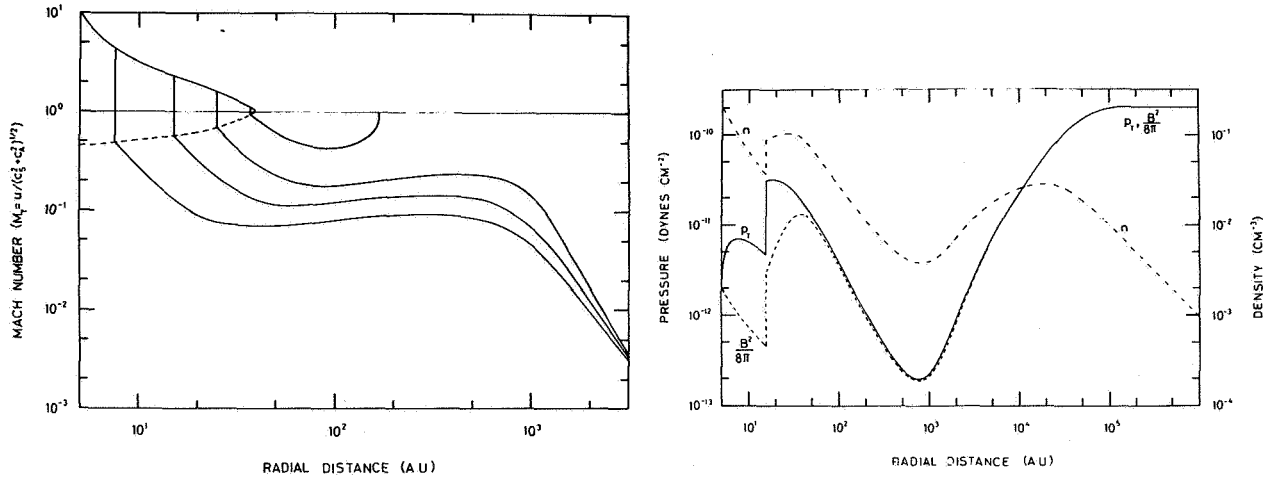
(a) Radial distance to the sonic point (see figs. 16(a), (b)) for various assumed values of the relative velocity of the interstellar gas, and interstellar hydrogen densities in the range 0.0 to 1.0 cm $^{-3}$ .



(b) Solar wind velocity as a function of radial distance from the sun for the case in which the interstellar gas has a velocity of 20 km sec $^{-1}$  towards the sun, and for various assumed values of the interstellar hydrogen density. Note that for the preferred value (0.1 cm $^{-3}$ ) the solar wind velocity is reduced to  $< 300$  km sec $^{-1}$  at a distance of 100 AU where the shock transition might be expected to occur (see fig. 7).

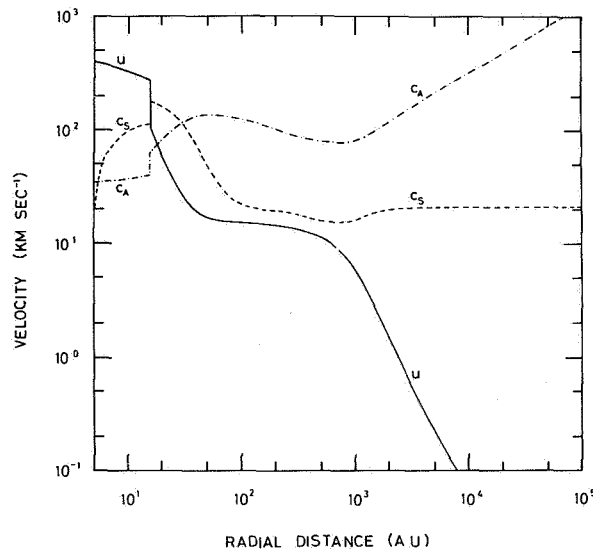
Figure 19 Effect of interstellar neutral gas hydrogen on the solar wind [from Holzer, 1971].

assume that  $N = 0.1$  cm $^{-3}$  and  $V = -20$  km sec $^{-1}$ , as suggested by the observations described in the preceding section, it can be seen that the solar wind speed is reduced from 400 km sec $^{-1}$  at 5 AU, to about 270 km sec $^{-1}$  at 100 AU, which we have estimated to be the likely position of the shock transition. Since photoionization is a relatively unimportant process the mass flux in the solar wind is essentially unaffected by the deceleration and hence the momentum flux (or ram pressure) is reduced in proportion to the velocity. This result can also be deduced easily by noting that the



(a) Variation of the Mach number with radial distance for various assumed positions of the shock transition. Note that the solutions terminate at a finite distance from the sun if the shock is inserted too close to the critical point.

(b) Variation of the plasma density  $n$ , total pressure  $p_T$ , and magnetic field pressure  $B^2/8\pi$ , as a function of radial distance for the case where the shock is inserted at 15 AU.



(c) Variation of the solar wind speed  $u$ , the sound speed  $c_s$ , and the Alfvén speed  $c_A$ , with radial distance for the case in which the shock transition is inserted at 15 AU.

**Figure 20** Variation of solar wind parameters with distance for the case  $V = 20 \text{ km/sec}^{-1}$ , and  $N = 1.0 \text{ cm}^{-3}$  [from Holzer, 1971]. Note that the solutions are somewhat similar to those shown in figure 7 for distances less than a few hundred AU. At very large radial distances the solutions may not be at all realistic; however, it is interesting that the asymptotic forms create a balance between the stresses associated with the magnetic field and the frictional interaction between the plasma and the neutral interstellar wind.

mean free path of solar wind protons against charge exchange is approximately 300 AU if  $N = 0.1 \text{ cm}^{-3}$ , and hence on reaching a heliocentric distance of 100 AU, the plasma must lose  $(1 - e^{-1/3}) \approx 1/3$  of its momentum per unit mass. Formally, this is equivalent to making the approximation  $M_T^2 \gg 1$  in (74) and putting  $\mathcal{Q}_1 = -[(\gamma + 1)/2]v$ . Thus we see that loss of momentum due to charge exchange within the region of supersonic solar wind is likely to have a significant effect on the location of the shock transition (in the sense that  $r_s$  might be reduced by 10 to 15 percent from the value estimated previously).

Solutions of equations (74) and (75) for the postshock flow have also been considered by *Holzer* [1971], again with the assumption that the flow is strictly radial; an example with  $V = 20 \text{ km sec}^{-1}$  and  $N = 1 \text{ cm}^{-3}$  is shown in figures 20(a)–(c). There appear to be no solutions that extend to infinity in the upwind direction ( $V < 0$ ); in the downwind direction ( $V > 0$ ), however, such solutions exist, provided the transition to subsonic flow takes place within a certain critical radius ( $r = r_1$ ). The Mach number is shown as a function of radial distance in figure 20(a). Note that if the shock location is such that  $r_s > r_1$ , the solution in the subsonic region bends upward, intersecting the line  $M_T = 1$  with infinite slope, and does not extend to  $r \rightarrow \infty$ . In cases where  $r_s < r_1$  the solutions in the subsonic region asymptotically approach the same curve, which is of the form  $M_T r^{3/2} = \text{constant}$ . The behavior of the other dependent variables for the case  $r_s = 15 \text{ AU} < r_1$  is shown in figures 20(b) and (c). The flow in the subsonic region can be divided into three parts: (1) in  $15 \text{ AU} < r < 50 \text{ AU}$ , the plasma is hot but is rapidly cooled as a result of charge exchange, thus causing the velocity to decrease and the magnetic field strength to increase; (2) in  $50 \text{ AU} < r < 10^3 \text{ AU}$ , the magnetic field dominates the total pressure, but the velocity is controlled by photoionization and charge exchange and is approximately equal to  $V$ ; (3) in  $r > 10^3 \text{ AU}$ , the magnetic field strength increases and the velocity decreases so that the asymptotic state is controlled by a balance between the tension stresses of the magnetic field and the frictional drag due to photoionization and charge exchange.

It is evident from the scales involved that we do not have to take these last results too seriously. Nevertheless, they do demonstrate rather clearly the complexity of the interaction that can be expected in more realistic situations when nonradial flow is important. We see, for example, that in the subsonic region on the upwind side of the heliosphere the most important effect of charge

exchange is to cool the plasma, thus permitting the magnetic field strength to grow more rapidly than it would otherwise (fig. 8). Charge exchange should not be important in the upwind subsonic region as far as the pressure/momentum balance is concerned since the streaming velocities are low. However, the increase of magnetic field strength enhances the inward force due to the tension stress associated with the field, and as noted earlier, this could produce a small but significant radial pressure gradient in the subsonic region. This effect, together with the loss of solar wind momentum due to charge exchange, could easily render our previous estimate of  $r_s = 100 \text{ AU}$  for the location of the shock transition too large by perhaps 20 to 30 percent [*Kern and Semar*, 1968]. However, a better self-consistent treatment is required before we can be sure that this is the case.

On the downwind side of the sun (in the “tail” of the heliosphere) we can expect the solar wind in the supersonic region to lose momentum due to charge exchange, so that the shock transition (if any) is not as far from the sun as it would be otherwise. In the subsonic region, the plasma should at first be cooled by charge exchange until  $\beta$  drops to such low values that the magnetic field has an important influence in controlling the flow. Momentum exchange due to photoionization and charge exchange will maintain the velocity of the flow at approximately that of the interstellar neutral gas. Similarly, the temperature of the plasma should ultimately be controlled by the input from photoelectrons and by the temperature of the interstellar gas. There is no strong reason for believing that the magnetic field will eventually increase as indicated in figure 20(b) since at the radial distances involved ( $r > 10^3 \text{ AU}$ ) in the actual heliosphere the magnetic field will certainly not be azimuthal as assumed in the calculations. Indeed, it should be expected that at distances of the order of a few hundred astronomical units the tail of the heliosphere should gradually deflate and collapse as the thermal pressure is removed from the plasma as a result of charge exchange. As the  $\beta$  of the plasma decreases to small values the magnetic structure of the tail should disintegrate due to field line reconnection at any surviving neutral sheets. Eventually, the field must become completely connected to the interstellar magnetic field and the plasma will disperse into the interstellar medium along the field lines. Thus we do not expect the tail of the heliosphere to be very long; indeed, after the first few hundred astronomical units, the term “wake” would be more appropriate. Finally, it should be noted that as a result of the very low densities involved, the plasma in the tail and wake is unlikely to be rapidly neutralized by

recombination unless the temperature of the interstellar neutral gas is relatively low ( $T_I \approx 10^2$  °K).

### THE INTERACTION BETWEEN GALACTIC COSMIC RAYS AND THE SOLAR WIND

Although galactic cosmic rays must pass through the outer regions of the heliosphere to reach the earth, they do not appear to carry much information about these regions. Nevertheless, it is useful to consider various aspects of the behavior of galactic cosmic rays within the heliosphere, especially as it is likely that the situation will change when observations from deep space probes become available.

At very high particle energies ( $\gtrsim 200$  GeV), it is found that the solar wind and the interplanetary magnetic field have no effect on the mean cosmic ray intensity observed at the earth in the sense that there is no solar cycle modulation or evidence for Forbush decreases. It might be expected, therefore, that if the cosmic ray "gas," including these particles, has a velocity  $V_{cr}$  relative to the solar system, then this should be detectable as a sidereal diurnal variation of the intensity. That is, the differential intensity in the kinetic energy range ( $T, T + dT$ ) should have the form

$$j(T, t) = j_0(T) [1 + \xi(T) \cos \phi(t)] \quad (90)$$

where  $t$  is the time,  $\phi(t)$  is the angle between the detector acceptance direction and  $V_{cr}$ , and  $\xi(T)$  is the anisotropy given by

$$\xi(T) = \frac{3CV_{cr}}{\nu} \quad (91)$$

where  $\nu$  is the particle speed corresponding to kinetic energy  $T$ , and  $C$  is the Compton-Getting factor:

$$C(T) = 1 - \frac{1}{3U} \frac{\partial}{\partial T} (\alpha TU) \quad (92)$$

where  $\alpha = (T + 2E_0)/(T + E_0)$ ,  $E_0$  is the particle rest energy, and  $U(T) = 4\pi j(T)/\nu$  is the differential number density in ( $T, T + dT$ ) [Gleeson and Axford, 1968a; Forman, 1970]. At high energies ( $T \gg E_0$ ), it is a good approximation to take  $\alpha = 1$ ,  $\nu = c$ , and  $j(T) \propto T^{-\mu}$  where  $\mu \approx 2.5$ . Thus  $C \approx (2 + \mu)/3 \approx 1.5$ , and if  $V_{cr} \approx V \approx 20$  km sec $^{-1}$ , we should expect that  $\xi \approx 0.03$  percent, in principle an observable value.

Unfortunately, the situation is not as simple as this analysis suggests, since although the irregular component

of the interplanetary magnetic field does not significantly affect particles with energies of the order of 100 GeV and higher, the regular (Archimedes spiral) field can bend the particle trajectories so that any anisotropy becomes obscured. This is evident in figure (21), which also shows contours on which particles have gyroradii in the local mean interplanetary magnetic field equal to the scale length of the field ( $B/\nabla B$ ). Within each contour, the trajectories of particles with energies less than the designated energy can be completely turned by the magnetic field. McCracken [unpublished, but see

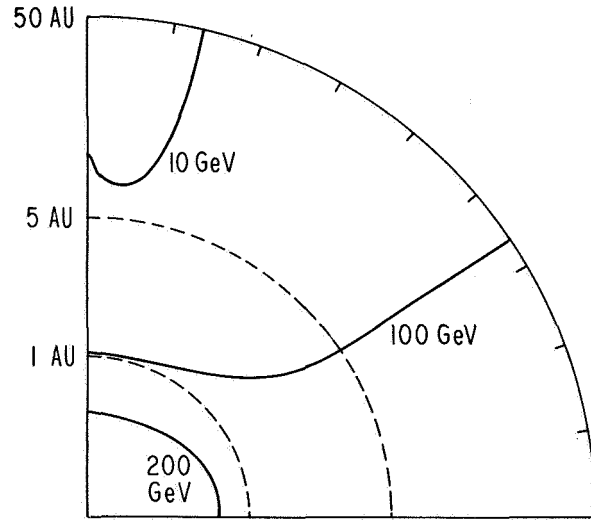


**Figure 21** Contour diagrams similar to those shown in figure 3 indicating regions of the interplanetary medium in which cosmic rays of a given energy have a gyroradius in the local magnetic field which is less than the characteristic scale of the field ( $B/\nabla B$ ). The diagram is somewhat misleading in the low latitude region beyond the few astronomical units since it does not take into account the sector structure of the interplanetary magnetic field. Since the sectors have a characteristic scale of only a few astronomical units, the trajectories of particles with gyroradii much larger than this will be essentially unaffected by the field.

Antonucci et al., 1970] has examined the nature of the sidereal variations to be expected in the energy range 50–500 GeV (the range appropriate to underground muon detectors). He has shown that diurnal and semi-diurnal intensity variations are to be expected, with the diurnal variation varying in amplitude throughout the year in such a manner that sidebands in the modulation should occur at 364 and 368 cycles/yr.



There is some evidence for the existence of a sidereal anisotropy obtained from detectors at 60 to 80 m.w.e. [Elliot *et al.*, 1970; Antonucci *et al.*, 1970]; however, it is not wholly convincing. For example, underground muon detectors at depths less than about 165 m.w.e. are sensitive to particles having energies less than 100 GeV [Ahluwalia, 1971], and the solar diurnal modulation (to which such particles are clearly subject) can produce pseudosidereal effects that can contaminate any genuine sidereal variation [Swinson, 1971]. It is probably necessary to make use of extensive air shower observations to obtain a good value for the cosmic ray anisotropy, since the particles involved have energies in excess of  $10^{12}$  eV and should not be noticeably affected by the interplanetary magnetic field or solar modulation. Unfortunately, the intensity of cosmic rays with energies  $\gtrsim 10^{12}$  eV is low, and so far it has been possible only to place an upper limit of about 0.1 percent on the anisotropy.

At energies less than 100 GeV, galactic cosmic rays are modulated in intensity in a variety of ways by their interaction with the solar wind and interplanetary magnetic field; Jokipii [1971] has reviewed the theory of some of these effects. In particular, the cosmic rays undergo a solar cycle modulation that appears to be the result of a reduction of intensity in the inner solar system due to outward transport of the particles by the solar wind with associated energy changes [Parker, 1963, 1965b; Gleeson and Axford, 1967; Gleeson, 1969; Jokipii and Parker, 1970]. The equations describing the behavior of the differential number density  $U$  and current density  $S$ , assuming that the solar wind is steady and radial, and taking only radial diffusion into account, are

$$\frac{1}{r^2} \frac{\partial}{\partial r} (r^2 S) = -\frac{1}{3} u \frac{\partial^2}{\partial r \partial T} (\alpha T U) \quad (93)$$

$$S = CuU - \kappa \frac{\partial U}{\partial r} \quad (94)$$

where  $u$  is the solar wind speed and  $\kappa(r, T)$  the effective radial diffusion coefficient for cosmic rays in the (irregular) interplanetary magnetic field.

It is rather difficult to obtain solutions of equations (93) and (94) with the boundary conditions appropriate to the modulation problem ( $U \rightarrow U_\infty(T)$  as  $r \rightarrow \infty$ ,  $r^2 S \rightarrow 0$  as  $r \rightarrow 0$ ), although classes of exact solutions exist if it is assumed that  $\alpha$  can be treated as a constant [Fisk and Axford, 1969]. Purely numerical treatments of the problem such as those of Fisk [1971a], Gleeson and Urch [1971b], Lezniak and Webber, [1971], and

Urch [1971] have been helpful; however, for many purposes it is more convenient to use various approximate forms of equations (93) and (94) such as those of Fisk and Axford [1969] and Gleeson *et al.*, [1971] that yield asymptotically valid solutions. Gleeson and Axford [1967, 1968b] and Fisk and Axford [1969] have shown that an adequate approximation for  $T \gtrsim 200$  MeV/nucleon at the earth can be achieved by neglecting the term  $S$  on the left of equation (94); the resulting equation

$$CuU = \kappa \frac{\partial U}{\partial r} \quad (95)$$

is termed the *force-field* equation.

If  $\kappa(r, T)$  is a separable function of  $r$  and  $T$  — that is,  $\kappa(r, T) = \kappa_1(r)\kappa_2(T)$  — this equation can be integrated to yield a result similar to Liouville's theorem:

$$\frac{j(r, E)}{E^2 - E_0^2} = \frac{j(\infty, E + \Phi)}{(E + \Phi)^2 - E_0^2} \quad (96)$$

where  $E = T + E_0$  is the total energy of the particles, and  $\Phi$  can be regarded as a “potential” associated with the (apparent) force exerted on the cosmic ray distribution. In particular, for the case in which  $\kappa_2 \propto Pv/c = \alpha Tv/c$ , which appears to be a reasonable choice in the vicinity of the earth for rigidities  $P \gtrsim 1$  Gv [Jokipii and Coleman, 1968],  $\Phi = |Ze| \phi(r)$ , where

$$\phi(r) = \frac{1}{3} \int_r^\infty \frac{u(r')}{\kappa_1(r')} dr' \quad (97)$$

It is found that equations (96) and (97) provide a very good description of the (11-yr) solar modulation of protons,  $\alpha$  particles, and heavier nuclei for energies greater than 100–200 MeV/nucleon. The “potential difference” between the earth and infinity is typically found to be in the range 150–500 MV, and the modulation shows the predicted  $Z$  dependence [Gleeson and Axford, 1968b; Lezniak and Webber, 1971]. Goldstein *et al.* [1970b] and Gleeson and Urch [1971a] have found from numerical solutions of the full equations (93) and (94) that galactic cosmic rays with initial energies less than 100–200 MeV/nucleon are effectively excluded from the interplanetary medium at the earth's orbit (fig. 22), which is consistent with the idea that the modulation can be described in terms of a force field. Clearly it should be considered a prime task of any deep space mission to measure the spectra of various species

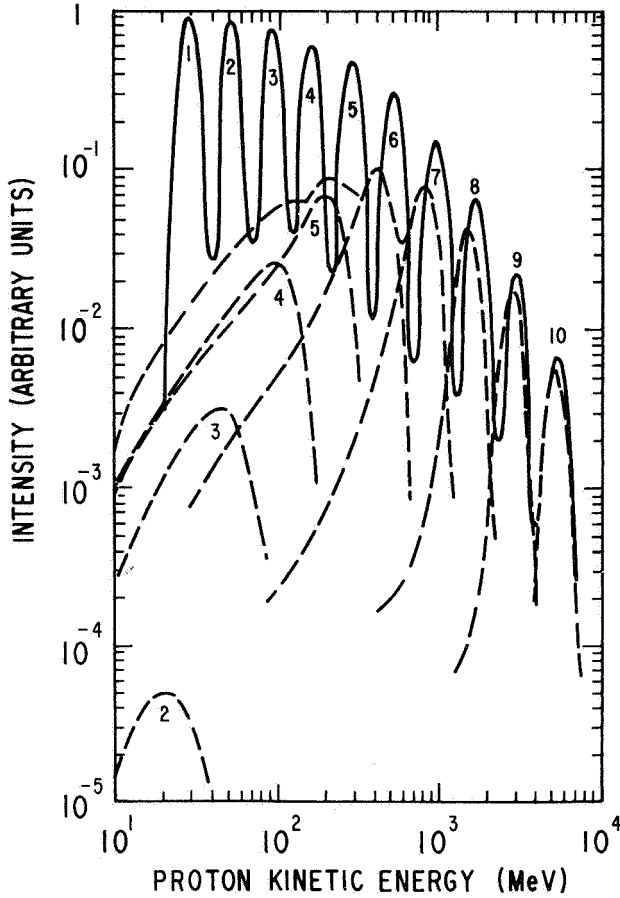


**Figure 22** A series of essentially monoenergetic proton spectra in interstellar space (solid line) and the corresponding modulated spectra at earth (dashed lines) obtained from numerical solutions of equations (93) and (94) [from Goldstein et al., 1970b]. The “force-field” solution (eq. (96)) provides a very good fit to the envelope of the modulated spectra for energies above about  $10^2$  MeV. It is important to note that particles with energies  $\lesssim 200$  MeV in interstellar space (i.e., unmodulated peaks 1-3) make a negligible contribution to the spectrum at earth, where this energy range is dominated by particles having higher energies in interstellar space (i.e., unmodulated peaks 4-6) and which have lost energy as a result of the modulating process. In effect, galactic cosmic rays with energies less than 100 MeV are unobservable at earth.

of cosmic rays as a function of radial distance from the sun as a basis for determining the unmodulated spectra and the variation of the diffusion coefficient with distance.

The radial gradient of the cosmic ray density or intensity at energies greater than  $\sim 200$  MeV/nucleon is given

directly by (97) as

$$\frac{1}{U} \frac{\partial U}{\partial r} = \frac{1}{j} \frac{\partial j}{\partial r} = \frac{Cu}{\kappa} \quad (98)$$

On taking a value for the diffusion coefficient consistent with that obtained by Jokipii and Coleman [1968], one finds that the gradient is of the order of 20–30 percent/AU for 1 GeV protons, and decreases at somewhat higher energies approximately as  $1/P$ . There is some evidence that gradients of this general magnitude exist, at least for  $P \gtrsim 1$  GV, from spacecraft observations [O’Gallagher and Simpson, 1967; O’Gallagher, 1967], measurements of radio activity in meteorites [Forman et al., 1971], and observations of the associated cosmic ray anisotropy perpendicular to the ecliptic [Yoshida et al., 1971].

If such gradients were to exist throughout the region in which the solar wind is supersonic (say,  $r \lesssim 50$  AU) then the total energy density of galactic cosmic rays outside the heliosphere would be enormously larger than that observed at the earth. In fact, it seems unlikely that the unmodulated spectrum for  $T \gtrsim 1$  GeV has a steeper slope than a spectrum with  $j(T) \propto T^{-\mu}$  with  $\mu \approx 2.5$ . This spectrum matches the (apparently unmodulated) observed spectrum in  $T \gtrsim 10^2$  GeV. It would require that the energy density of galactic cosmic rays be greater by only a factor of 2 or 3 outside the heliosphere than near the earth for  $T \gtrsim 1$  GeV, and hence that the radial gradient cannot be maintained at the value quoted above for more than a few AU from the sun. This argument is essentially the same as that of Gleeson and Axford [1968b], who for convenience assumed that  $\kappa_1(r) \propto e^{r/r_0}$  in (97), and found that if the “potential difference” between the earth and infinity is 100–200 MV, then  $r_0$  must be of the order of 1 AU.

Additional confirmation that the modulation of galactic cosmic rays with  $T \gtrsim 1$  GeV occurs in a region that is effectively contained within a few AU of the sun arises from comparisons of the solar cycle variation of the cosmic ray intensity (measured by neutron monitors, for example) and various indices of solar activity [Simpson, 1962; Simpson and Wang, 1967, 1970; Hatton et al., 1968; Guschina et al., 1970; Kolomeets et al., 1970; Wang, 1970]. It is argued that the lag obtained from a cross correlation analysis involving these quantities should provide a rough estimate of the time required for the solar wind to traverse the modulating region. A cross correlation between cosmic ray intensity and the geomagnetic activity index  $K_p$  yields a lag of the order of 6 to 12 months, which suggests that the radius of the modulating region might be as large as

50 to 80 AU [Dorman and Dorman, 1966]. However, it has been found that if a cross correlation is made between the coronal green line ( $\lambda$  Fe XIV 5303), the lag is only of the order of 1 month, which yields a radius of  $\sim 7$  AU for the modulating region of particles detected by neutron monitors [Simpson and Wang, 1967; Barker and Hatton, 1970; Kolomeets et al., 1970].

It is not possible to draw similar conclusions for the low energy end of the galactic cosmic ray spectrum, simply because the degree of modulation at low energies is expected to be so large that we are completely ignorant of the form of the unmodulated spectrum (fig. 21). Furthermore, at the lowest energies, the spectrum observed near the earth appears to consist mostly of particles of solar origin [Axford, 1970]. The effects of adiabatic deceleration associated with the expansion of the solar wind dominate the behavior of these particles.

It seems likely that galactic cosmic ray protons and heavier nuclei with energies of the order of 1–10 MeV/nucleon are to a large extent excluded from the region of supersonic solar wind flow, although they may penetrate the region of subsonic flow more easily since the effects of convection in this region are less important. At the shock transition separating these regions it is possible for significant acceleration of low-energy particles to occur, thus producing, in a sense, a local “source” of cosmic rays [Jokipii, 1968]. This effect can be demonstrated by means of appropriate solutions of equations (93) and (94). Let us suppose that the effective radial diffusion coefficient is small ( $\kappa \ll ur_s$ ) and that the solar wind convects energetic particles of solar origin toward the shock in such a manner that  $U(r, T) \rightarrow U_0(T) = AT^{-\mu}$  for  $(r_s - r)u/\kappa \rightarrow \infty$ . In these circumstances, the effects of spherical divergence can be neglected in  $r < r_s$ , and we find that equations (93) and (94) can be replaced by

$$S = u_1 U_0 - \frac{1}{3} u_1 \frac{\partial}{\partial T} (\alpha T U) \quad (99)$$

$$u_1 (U - U_0) = \kappa_1 \frac{\partial U}{\partial r} \quad (100)$$

having put  $u = u_1$  and  $(\partial/\partial r)(r^2 S) \approx r^2 (\partial S/\partial r)$ , and integrating (93). Thus we find that if  $\kappa = \kappa_1$  is assumed to be independent of  $r$  and  $T$ , and  $\alpha$  is taken to be constant, then

$$U = \left\{ A + B \exp \left[ \frac{u_1}{\kappa_1} (r - r_s) \right] \right\} T^{-\mu} \quad (101)$$

$$S = u_1 \left\{ \left[ 1 + \frac{1}{3} \alpha (\mu - 1) \right] A + \frac{1}{3} \alpha (\mu - 1) B \exp \left[ \frac{u_1}{\kappa_1} (r - r_s) \right] \right\} T^{-\mu} \quad (102)$$

where  $B$  is a constant obtained in the integration of (100), and it is assumed that  $U \propto T^{-\mu}$  everywhere. Beyond the shock transition (in  $r > r_s$ ), we can treat the flow as if it were incompressible to a first approximation, so that  $u = (1/4)u_1(r_s/r)^2$ ; hence, equations (93) and (94) become

$$S = \frac{1}{4} u_1 \left[ C(T) - \frac{1}{3} \frac{\partial}{\partial T} (\alpha T U) \right] \left( \frac{r_s}{r} \right)^2 \quad (103)$$

$$\frac{1}{4} u_1 [U - C(T)] \left( \frac{r_s}{r} \right)^2 = \kappa_2 \frac{\partial U}{\partial r} \quad (104)$$

where  $C(T) = CT^{-\mu}$  arises from the integration of (93). The appropriate solutions of these equations are such that  $U, S \rightarrow 0$  as  $r \rightarrow \infty$ :

$$U = CT^{-\mu} \left[ 1 - \exp \left( \frac{-4\kappa_2}{u_1 r} \right) \right] \approx \frac{4\kappa_2 CT^{-\mu}}{u_1 r} \quad (105)$$

$$S \approx \frac{1}{4} u_1 CT^{-\mu} \left( \frac{r_s}{r} \right)^2 + O \left( \frac{\kappa_2}{u_1 r_s} \right) \quad (106)$$

Provided there is no source of particles within the shock itself, both  $U$  and  $S$  must be continuous at the shock [Gleeson and Axford, 1967], and hence the constants  $B$  and  $C$  can be determined:

$$B \approx \frac{3A [1 - (\alpha/3)(\mu - 1)]}{\alpha(\mu - 1)} \quad C \approx \frac{3u_1 r_s A}{4\kappa_2 \alpha(\mu - 1)} \quad (107)$$

Note that the enhancement of the cosmic ray density resulting from the presence of the shock ( $C/A$ ) depends on the value of the diffusion coefficient in the subsonic region, and may be very large if  $\kappa_2/u_1 r_s \ll 1$ . The cosmic ray intensity near the earth is not significantly affected by the presence of this enhancement since if  $\kappa \ll ur$  the particles are convection dominated and downstream boundary conditions have little influence. It is possible to solve equations (93) and (94) exactly with the solar wind distribution assumed in the above analysis, provided  $\alpha$  is taken to be constant,  $\kappa$  is independent

of  $T$ , and  $U \propto T^{-1/2}$  [Fisk, 1969]. The solutions are consistent with those obtained here in the limit  $ur_s/\kappa \gg 1$ ; they also show that it is possible to produce an enhancement of the intensity of galactic cosmic rays in the vicinity of the shock transition under suitable conditions. On this basis, therefore, it should be expected that a low-energy cosmic ray enhancement similar to those associated with propagating shocks [Fisk, 1971b] is associated with the shock transition terminating the supersonic solar wind, and this may provide useful confirmation of the presence of the transition.

The possibility that the solar wind itself might be significantly affected by cosmic rays has been considered by several authors [Axford, 1965; Axford and Newman, 1965; Dorman and Dorman, 1968; Modisette and Snyder, 1968; Sousk and Lenchek, 1969; Wallis, 1971]. In the early analyses it was assumed that there is no exchange of energy between the solar wind and the cosmic rays, and that the cosmic ray pressure  $\pi$  satisfies the convection-diffusion equation

$$K \frac{d\pi}{dr} = u\pi \quad (108)$$

where  $K(r)$  is the "effective" diffusion coefficient and

$$\pi = \frac{1}{3} \int_0^\infty \alpha T U dT \quad (109)$$

In more recent treatments [Sousk and Lenchek, 1969; Wallis, 1971], which take the energy exchange into account, equation (108) is used together with the following equations for the conservation of mass, momentum and energy of the solar wind plasma:

$$\frac{d}{dr} (\rho u r^2) = 0 \quad (110)$$

$$\rho u \frac{du}{dr} = -\frac{dp}{dr} - \frac{G\lambda\rho}{r^2} - \frac{d\pi}{dr} \quad (111)$$

$$\frac{1}{r^2} \frac{d}{dr} \left[ \rho u r^2 \left( \frac{1}{2} u^2 + \frac{\gamma}{\gamma+1} \frac{p}{\rho} + \frac{G\lambda}{r} \right) \right] = u \frac{d\pi}{dr} \quad (112)$$

On combining equations (110)–(112), we can show that  $p/\rho^\gamma = \text{constant}$ . The right-hand side of equation (112) is easily shown from (93) to be given by

$$\frac{1}{r^2} \frac{d}{dr} \left( r^2 \int_0^\infty ST dT \right) = u \frac{d\pi}{dr} \quad (113)$$

where  $\int_0^\infty ST dT$  is the net radial flux of energy in cosmic rays; since  $u d\pi/dr > 0$ , it is evident that there is a net transfer of energy from the solar wind to the cosmic rays [cf. Jokipii and Parker, 1967].

In the treatment of the problem by Axford and Newman [1965] and others, the right-hand side of (112) was omitted; since this term represents an effective heat sink for the solar wind, the results obtained by these authors are such that the Mach number decreases toward unity too rapidly with increasing radial distance. Wallis [1971] has pointed out that when equations (109)–(112) are reduced to a single equation for the Mach number in terms of radial distance, the characteristics of the equation have properties similar to those described in the preceding section for the case of interaction with interstellar neutral gas. In particular, there is a singular point at a large radial distance, the nature of which depends on the values assumed for the various parameters involved. It is found, however, that if the interaction is sufficiently strong that a significant effect is produced on the solar wind, then the cosmic ray pressure required in the interstellar medium is unacceptably high (more than 10 times the value observed at the position of the earth). An example of a solution obtained by Sousk and Lenchek [1969] for the case where  $K$  is independent of  $r$  is shown in figure 23; it is evident that quite unreasonable cosmic ray pressures are necessary in this case to reduce the solar wind speed by as much as 25 percent. As a corollary to calculations of this sort, it is found that the cosmic ray pressure cannot be prevented from becoming excessive unless the net diffusion coefficient  $K$  increases more strongly than linear with radial distance. This is consistent with the conclusion of Simpson and Wang [1967] and others that the dimensions of the modulating region must be relatively small ( $\sim 7$  AU).

Cosmic rays are affected by the regular component of the interplanetary magnetic field as well as by irregularities, and as a consequence they tend to rotate with the magnetic field about the sun. The resulting anisotropy is observed at the earth as a solar diurnal variation of the cosmic ray intensity, which is of the order of 0.3 to 0.4 percent, given approximately by

$$\xi_\phi(T) = \frac{C(T)\Omega r \sin \theta}{v} \quad (114)$$

where  $\Omega$  is the angular velocity of the sun [Ahluwalia and Dessler, 1962; Parker, 1964; Axford, 1965]. This anisotropy has yet to be detected at low energies ( $T \lesssim 2$  GeV) from spacecraft; it is possible that it is absent at energies less than about 200 MeV/nucleon

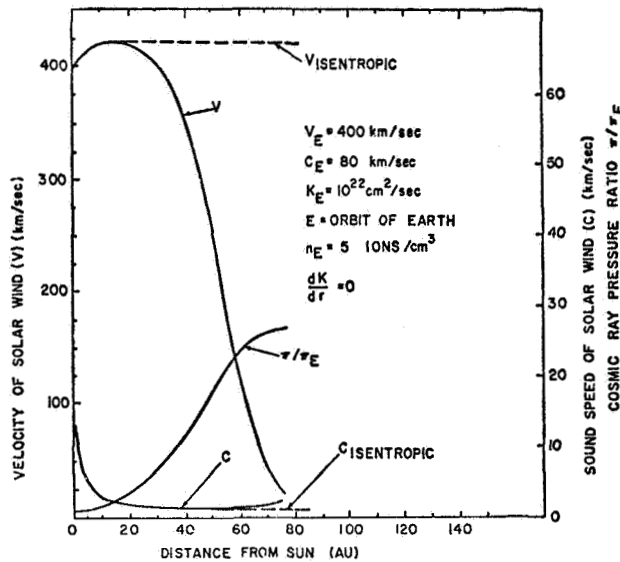


**Figure 23** Variation of the solar wind speed  $V$ , sound speed  $C$ , and cosmic ray pressure  $\pi$ , with distance from the sun for the case in which the effective diffusion coefficient  $K$  is constant [from Sousk and Lenchek, 1969]. It should be noted that in order for the solar wind speed to drop to  $300 \text{ km sec}^{-1}$ , the cosmic ray pressure must rise by a factor of 10 over its value at the orbit of earth, which seems unacceptably large. The solutions have not been carried through the singular point of the equations where the solar wind and the sound speed are equal [cf. Wallis, 1971].

where  $\chi(T) \approx 0$  [Gleeson and Axford, 1968a]. It is difficult to escape the conclusion that this anisotropy must increase with increasing heliocentric distance, and become very large indeed at distances of the order of 50 AU. However, the anisotropy can be suppressed in two ways: by (1) a gradient of the intensity perpendicular to the ecliptic, and (2) isotropy of the diffusion tensor. The enormous intensity gradients necessary for any significant effect in this respect are difficult to accept, but the second possibility may well be important. A more accurate form of equation (114) is

$$\xi_{\phi}(T) = \frac{3C\Omega r \sin \theta}{\nu} \frac{\kappa_{\parallel} - \kappa_{\perp}}{\kappa_{\parallel} + \kappa_{\perp} \tan^2 \phi} \quad (115)$$

where  $\kappa_{\parallel}$  and  $\kappa_{\perp}$  are the diffusion coefficients parallel and perpendicular to the mean magnetic field direction, respectively. It has been pointed out by Jokipii [1966b, 1971] and Jokipii and Parker [1969] that as a result of the wandering of magnetic field lines with respect to the direction of the mean field it is possible for  $\kappa_{\perp} \rightarrow \kappa_{\parallel}$ , in

which case the anisotropy given by (115) must disappear. This effect is probably not as pronounced at the orbit of earth as suggested by Jokipii and Parker [1969] [Subramanian, 1971]; however, it is expected to increase in importance with increasing heliocentric distance and ultimately may be capable of keeping  $\xi_{\phi}$  within reasonable limits. A breakup of the interplanetary magnetic field sector structure as described earlier would serve the same purpose. It should be noted that in the presence of a large value of  $\xi_{\phi}$ , the medium comprising the solar wind plasma and the cosmic ray gas would be liable to streaming instabilities [Wentzel, 1969], which in turn would tend to reduce both  $\kappa_{\parallel}$  and  $\kappa_{\perp}$  and thus increase the overall modulation.

The problem of how cosmic rays penetrate the region occupied by the solar wind and interplanetary magnetic field is of some interest. In the absence of direct connection between the interplanetary and interstellar magnetic fields it is difficult to understand how low-energy electrons, for example, could enter the interplanetary region with any reasonable efficiency. Parker [1968] has suggested that the effect of field line wandering described above might be adequate to bring any given field line sufficiently close to the interface between the solar plasma and interstellar region to allow it to receive its full quota of cosmic rays, regardless of where the field line intersects the surface of the sun. Alternatively, we would argue that the access of cosmic rays can take place most easily if the interplanetary field is connected directly to the interstellar medium. There is little reason for believing that this is not so, and in the case of the interplanetary magnetic field and the geomagnetic field, for example, the evidence for interconnection is very compelling [Akasofu and Axford, 1971].

Schatten and Wilcox [1969, 1970] have suggested that interconnection of the interplanetary and interstellar magnetic fields could explain the 20-year cycle of the diurnal variation of the cosmic ray intensity at the earth reported by Forbush [1967, 1969]. It is argued that the effect is related to the 20-year solar magnetic cycle, and that the access of cosmic rays is controlled to some extent according to whether or not the solar magnetic field is favorably directed so that cosmic rays have easy access to the heliosphere. In fact, the situation is quite complex, and it is not obvious that this is the correct explanation. However, it should be noted that a similar situation exists in the case of access of anisotropic fluxes of solar energetic particles into the earth's magnetosphere, where the direction of the interplanetary magnetic field can lead to a pronounced asymmetry in the particle fluxes observed at low altitudes in the polar magnetosphere [Reid and Sauer,

1967; Engelman *et al.*, 1971; Van Allen *et al.*, 1971]. The possibility that interconnection of the interplanetary and interstellar magnetic fields might affect the intensity of low-energy cosmic ray electrons has been discussed by Fisk and Van Hollebeke [1971] in an attempt to explain the "quiettime increases" of these particles [Simnett *et al.*, 1971]. Kovar and Dessler [1967] have suggested that the sidereal anisotropy of galactic cosmic rays might be related to the asymmetry of the outer heliosphere. As noted previously, however, the particles that can be expected to show a sidereal anisotropy must have such high energies that they pass unaffected through the complex field structure of the outer heliosphere. As a result of the configuration of the interplanetary magnetic field, any effect associated with the asymmetry of the heliosphere will lead to spatial variations of the mean intensity of cosmic rays rather than a sidereal anisotropy.

#### APPENDIX: A HYDRAULIC ANALOGY TO THE SOLAR WIND

Consider the flow resulting from a jet of liquid incident on a horizontally held dinner plate. Under steady conditions, the total mass flux

$$\rho Q = 2\pi r h u \quad (\text{A1})$$

is constant, where  $\rho$  is the density of the liquid,  $r$  is the radial distance from the center of the plate,  $h(r)$  is the depth, and  $u(r)$  the mean radial velocity of the liquid. It can be shown that the flow pattern divides in general into a supercritical region ( $r < r_j$ ) and a subcritical region ( $r_j < r < R = \text{radius of the plate}$ ), in which the Froude number  $F = u/(gh)^{1/2}$  is greater than or less than unity, respectively.

Conservation of radial momentum requires that

$$\left(u^2 + \frac{1}{2}gh\right)h = \text{constant} = \frac{1}{2}gH^2 \quad (\text{A2})$$

where  $H$  is the "total head." Accordingly, if  $F \gg 1$ ,  $u$  is approximately constant and  $h(r) \propto 1/r$ ; if  $F \ll 1$ ,  $h$  is approximately constant and  $u \propto 1/r$ . In the case of the solar wind, where the Mach number plays the same role as the Froude number, these results are analogous to the constancy of  $u$  when  $M \gg 1$ , and of  $p$  when  $M \ll 1$ .

The regions of supercritical and subcritical flow are separated by a hydraulic jump at  $r = r_j$ , across which conservation of mass and momentum require that

$$h_1 u_1 = h_2 u_2 = \frac{Q}{2\pi r_j} \quad (\text{A3})$$

$$\left(u_1^2 + \frac{1}{2}gh_1\right)h_1 = \left(u_2^2 + \frac{1}{2}gh_2\right)h_2 = \frac{1}{2}gH^2 \quad (\text{A4})$$

where subscripts 1 and 2 refer to upstream and downstream conditions, respectively. For given values of  $Q$  and  $H$ , these equations are sufficient to determine  $u(r)$ ,  $h(r)$ , and  $r_j$ , provided we also specify conditions at  $r = R$ .

#### ACKNOWLEDGEMENTS

The author wishes to thank P. M. Banks, C. A. Barth, J. E. Blamont, W. H. Chambers, C. W. Cranfill, C. T. Gregory, T. E. Holzer, H. E. Johnson, T. N. L. Patterson, B. J. Rickett, F. Scherb, G. E. Thomas, B. A. Tinsley, M. P. Ulmer, and M. Wallis for their assistance in preparing this review.

This work was supported by the National Aeronautics and Space Administration under Contract NGR-05-009-081.

#### REFERENCES

- Adams, T. F.: On Lyman-Alpha Emission From the Galaxy. *Astron. Astrophys.*, Vol. 12, 1971, p. 280.
- Afrosimov, V. V.; Mamaev, Yu. A.; Panov, M. N.; and Fedorenko, N. V.: Coincidence Method for Studying Charge-Exchange in Proton-Inert Gas Interactions. *Sov. Phys. - Tech. Phys.*, Vol. 14, 1969, p. 109.
- Ahluwalia, H. S.: Median Primary Energy of Response of a Cosmic Ray Telescope Underground. *J. Geophys. Res.*, Vol. 76, 1971, p. 5358.
- Ahluwalia, H. S.; and Dessler, A. J.: Diurnal Variation of Cosmic Radiation Intensity Produced by a Solar Wind. *Planet. Space Sci.*, Vol. 9, 1962, p. 195.
- Akasofu, S.-I.: The Neutral Hydrogen Flux in the Solar Plasma Flow-I. *Planet. Space Sci.*, Vol. 12, 1964, p. 905.
- Akasofu, S.-I.; and Axford, W. I.: Magnetospheric Substorms: A Review. In preparation, 1971.
- Alexander, J. K.; Brown, L. W.; Clark, T. A.; Stone, R. G.; and Weber, R. R.: The Spectrum of the Cosmic Radio Background Between 0.4 and 6.5 MHz. *Astrophys. J.*, Vol. 157, 1969, p. L163.
- Allen, C. W.: *Astrophysical Quantities*. Athlone Press, London, 1963.
- Antonucci, E.; Castagnoli, G. C.; and Doderio, M. A.: On the Diurnal Variations of the Cosmic Ray Intensity Observed 70 m.w.e. Underground. *Proc. 11th Int. Conf. on Cosmic Rays*, Budapest, 1970, p. 157.
- Axford, W. I.: Anisotropic Diffusion of Solar Cosmic Rays. *Planet. Space Sci.*, Vol. 13, 1965, p. 1301.
- Axford, W. I.: The Interaction Between the Solar Wind and the Magnetosphere. *Aurora and Airglow*, B. M. McCormac, ed., Reinhold Publishing Co., New York, 1967, p. 409.
- Axford, W. I.: Observations of the Interplanetary Plasma. *Space Sci. Rev.*, Vol. 8, 1968, p. 331.

- Axford, W. I.: Helium in the Atmosphere, Aurora and Solar Wind. *Atmospheric Emissions*. B. M. McCormac and Anders Omholt, eds., Reinhold Publishing Co., New York, 1969, p. 317.
- Axford, W. I.: A Review of Theoretical Work on the Effects of Solar Wind Transport on Energetic Solar Particles. Presented at USSR Academy of Sciences Seminar on Cosmic Ray Generation on the Sun, Leningrad, 1970 (to be published).
- Axford, W. I.; Dessler, A. J.; and Gottlieb, B.: Termination of Solar Wind and Solar Magnetic Field. *Astrophys. J.*, Vol. 137, 1963, p. 1268.
- Axford, W. I.; and Newman, R. C.: The Effect of Cosmic Ray Friction on the Solar Wind. *Proc. 9th Int. Conf. Cosmic Rays, Phys. Soc.*, London, 1965, p. 173.
- Bame, S. J.; Hundhausen, A. J.; Asbridge, J. R.; and Strong, I. B.: Solar Wind Ion Composition. *Phys. Rev. Letters*, Vol. 20, 1968, p. 393.
- Bame, S. J.; Asbridge, J. R.; Hundhausen, A. J.; and Montgomery, M. D.: Solar Wind Ions:  $^{56}\text{Fe}^{+8}$  to  $^{56}\text{Fe}^{+12}$ ,  $^{28}\text{Si}^{+7}$ ,  $^{28}\text{Si}^{+8}$ ,  $^{28}\text{Si}^{+9}$ , and  $^{16}\text{C}^{+6}$ . *J. Geophys. Res.*, Vol. 75, 1970, p. 6360.
- Bandermann, L. W.; and Singer, S. F.: Neutral Hydrogen in Interplanetary Gas. *Trans. Amer. Geophys. Union*, Vol. 46, 1965, p. 133.
- Banks, P. M.: Interplanetary Hydrogen and Helium From Cosmic Dust and the Solar Wind. *J. Geophys. Res.*, Vol. 76, 1971, p. 4341.
- Banks, P. M.; and Kockarts, G.: *Aeronomy*, Academic Press, to be published, 1972.
- Baranov, V. B.; Krasnobayev, K. V.; and Kulikovskiy, A. G.: A Model of the Interaction Between the Solar Wind and an Interstellar Medium. GSFC Tech. Trans. of "Model vzaimodeystviya solnechnogo vetra s mezhzvezdnoy sredoy," *Dokl. Akad. Nauk SSSR*, Vol. 194, 1970, p. 41.
- Barker, M. C.; and Hatton, C. J.: The Yearly Variation of the Cosmic Ray Intensity From 1963-67 and Its Relation to the Observed Variation of Solar Activity With Heliolatitude and Time. *Proc. 11th Int. Conf. Cosmic Rays*, Budapest, 1970, p. 177.
- Barnes, A.: Collisionless Heating of the Solar-Wind Plasma, 1. Theory of the Heating of Collisionless Plasma by Hydromagnetic Waves. *Astrophys. J.*, Vol. 154, 1968, p. 751.
- Barnes, A.: Collisionless Heating of the Solar Wind Plasma, 2. Application of the Theory of Plasma Heating by Hydromagnetic Waves. *Astrophys. J.*, Vol. 155, 1969, p. 311.
- Barth, C. A.: Mariner 6 Measurements of the Lyman  $\alpha$  Sky Background. *Astrophys. J.*, Vol. 161, 1970a, p. L181.
- Barth, C. A.: Mariner 5 Measurements of Ultraviolet Emission From the Galaxy. *Ultraviolet Stellar Spectra and Ground-Based Observations*. I.A.U. Symp. No. 36, L. Houziaux and H. E. Butler, eds., Reidel Pub. Co., Dordrecht, 1970b, p. 28.
- Barth, C. A.; Pearce, J. B.; Kelly, K. K.; Wallace, L.; and Fastie, W. G.: Ultraviolet Emissions Observed Near Venus From Mariner 5. *Science*, Vol. 158, 1967, p. 1675.
- Barth, C. A.; Wallace, L.; and Pearce, J. B.: Mariner 5 Measurement of Lyman-Alpha Radiation Near Venus. *J. Geophys. Res.*, Vol. 73, 1968, p. 2541.
- Barua, S. N.: A Source in a Rotating Fluid. *Quart. J. Mech. Appl. Math.*, Vol. VIII, Pt. 1, 1955, p. 22.
- Berge, G. L.; and Seielstad, G. A.: New Determinations of the Faraday Rotation for Extragalactic Radio Sources. *Astrophys. J.*, Vol. 148, 1967, p. 367.
- Bergeron, J.; and Souffrin, S.: Heating of HI Regions by Hard UV Radiation: Physical State of the Interstellar Matter. *Astron. Astrophys.*, Vol. 11, 1971, p. 40.
- Bertaux, J. L.; and Blamont, J. E.: Evidence for a Source of an Extraterrestrial Hydrogen Lyman-Alpha Emission: The Interstellar Wind. *Astron. Astrophys.*, Vol. 11, 1971, p. 200.
- Bhatnagar, V. P.; and Fahr, H. J.: Solar Wind Expansion Beyond the Heliosphere. Preprint, 1971.
- Biskamp, D.; Sagdeev, R. Z.; and Schindler, K.: Non-linear Evolution of the Tearing Instability in the Geomagnetic Tail. *Cosmic Electrodyn.*, Vol. 1, 1970, p. 297.
- Blamont, J. E.; and Madjar, A. V.: Monitoring of the Lyman-Alpha Emission Line of the Sun During the Year 1969. *J. Geophys. Res.*, Vol. 76, 1971, p. 4311.
- Blum, P. W.; and Fahr, H. J.: Solar Wind Tail and the Anisotropic Production of Fast Hydrogen Atoms. *Nature*, Vol. 223, 1969, p. 936.
- Blum, P. W.; and Fahr, H. J.: Interaction Between Interstellar Hydrogen and the Solar Wind. *Astron. Astrophys.*, Vol. 4, 1970a, p. 280.
- Blum, P. W.; and Fahr, H. J.: The Distribution of Interplanetary Hydrogen. *Astrophys. Letters*, Vol. 5, 1970b, p. 127.
- Blum, P. W.; and Fahr, H. J.: Lyman- $\alpha$  Scattering During the Solar Rotation Period. *Astron. Astrophys.*, Vol. 8, 1970c, p. 236.
- Blum, P. W.; and Fahr, H. J.: Interpretation of Extraterrestrial Lyman-Alpha Observations. *Nature*, Vol. 231, 1971, p. 171.
- Bowers, B.: Galactic Lyman-Alpha and the Interstellar Shock Wave. *Nature*, Vol. 228, 1970, p. 1182.

- Bowyer, C. S.; and Field, G. B.: The Intensity of the Soft X-ray Background Flux. *Nature*, Vol. 223, 1969, p. 573.
- Bowyer, C. S.; Livingston, P. M.; and Price, R. D.: Upper Limits to the 304- and 584-A Night Helium Glow. *J. Geophys. Res.*, Vol. 73, 1968, p. 1107.
- Brandt, J. C.: Interplanetary Gas, IV. Neutral Hydrogen in a Model Solar Corona. *Astrophys. J.*, Vol. 133, 1961, p. 688.
- Brandt, J. C.: Interplanetary Gas, IX. Effects on the Local Interstellar Medium. *Icarus*, Vol. 3, 1964a, p. 253.
- Brandt, J. C.: On Diffuse Galactic Lyman  $\alpha$  in the Night Sky. *Planet. Space Sci.*, Vol. 12, 1964b, p. 650.
- Brandt, J. C.: *Introduction to the Solar Wind*. G. Burbidge and M. Burbidge, eds., W. H. Freeman and Co., San Francisco, Calif., 1970.
- Brandt, J. C.; and Michie, R. W.: Semiempirical Model of the Interplanetary Medium. *Phys. Rev. Letters*, Vol. 8, 1962, p. 195.
- Brandt, J. C.; and Hunten, D. M.: On Ejection of Neutral Hydrogen From the Sun and the Terrestrial Consequences. *Planet. Space Sci.*, Vol. 14, 1966, p. 95.
- Brandt, J. C.; Stecher, T. P.; Crawford, D. L.; and Maran, S. P.: The Gum Nebula: Fossil Strömgren Sphere of the Vela X Supernova. *Astrophys. J.*, Vol. 163, 1971, p. L99.
- Brengauz, V. D.: Radiation by Magnetosonic Waves Generated in a Stellar Wind. *Soviet Astron.-AJ*, Vol. 13, 1969, p. 37.
- Bridle, A. H.: Spectra of Extended Extragalactic Radio Sources. *Nature*, Vol. 224, 1969, p. 889.
- Bridle, A. H.; and Venugopal, V. R.: Distribution and Temperature of Interstellar Electron Gas. *Nature*, Vol. 224, 1969, p. 545.
- Bunner, A. N.; Coleman, P. C.; Kraushaar, W. L.; McCammon, D.; Palmieri, T. M.; Shilepsky, A.; and Ulmer, M.: Soft X-ray Background Flux. *Nature*, Vol. 223, 1969, p. 1222.
- Burbidge, G. R.: The Galactic Magnetic Field. *Comments Astrophys. Space Phys.*, Vol. 1, 1969, p. 25.
- Burton, W. B.: Galactic Structure Derived From Neutral Hydrogen Observations Using Kinematic Models Based on the Density Wave Theory. *Astron. Astrophys.*, Vol. 10, 1971, p. 76.
- Byram, E. T.; Chubb, T. A.; and Friedman, H.: Attempt to Measure Night Helium Glow – Evidence for Metastable Molecules in the Night Ionosphere. *J. Geophys. Res.*, Vol. 66, 1961, p. 2095.
- Cahill, L. J.; and Amazeen, P. G.: The Boundary of the Geomagnetic Field. *J. Geophys. Res.*, Vol. 68, 1963, p. 1835.
- Cairns, R. B.; and Samson, J. A. R.: Absorption and Photoionization Cross Sections of  $\text{CO}_2$ , CO, Ar, and He at Intense Solar Emission Lines. *J. Geophys. Res.*, Vol. 70, 1965, p. 99.
- Cameron, A. G. W.: A New Table of Abundances of the Elements in the Solar System, in *Origin and Distribution of the Elements*. L. H. Ahrens, ed., Pergamon Press, New York, 1968, p. 125.
- Carruthers, G. R.: An Upper Limit on the Concentration of Molecular Hydrogen in Interstellar Space. *Astrophys. J.*, Vol. 148, 1967, p. L141.
- Carruthers, G. R.: Far-Ultraviolet Spectroscopy and Photometry of Some Early-Type Stars. *Astrophys. J.*, Vol. 151, 1968, p. 269.
- Carruthers, G. R.: Observation of the Lyman-Alpha Interstellar Absorption Line in Theta Orionis. *Astrophys. J.*, Vol. 156, 1969, p. L97.
- Carruthers, G. R.: Atomic and Molecular Hydrogen in Interstellar Space. *Space Sci. Rev.*, Vol. 10, 1970a, p. 459.
- Carruthers, G. R.: Rocket Observation of Interstellar Molecular Hydrogen. *Astrophys. J.*, Vol. 161, 1970b, p. L81.
- Chambers, W. H.; Fehlan, P. E.; Fuller, J. C.; and Kunz, W. E.: Anisotropic Atomic Hydrogen Distribution in Interplanetary Space. *Nature*, Vol. 225, 1970, p. 713.
- Clark, B. G.: An Interferometer Investigation of the 21-centimeter Hydrogen-Line Absorption. *Astrophys. J.*, Vol. 142, 1965, p. 1398.
- Clauser, F.: Johns Hopkins Univ. Lab. Rep. AFOSRTN 60-1386, 1960.
- Cloutier, P. A.: A Comment on 'The Neutral Hydrogen Flux in the Solar Plasma Flow' by S.-I. Akasofu. *Planet. Space Sci.*, Vol. 14, 1966, p. 809.
- Cranfill, C.: Ph.D. Dissertation, Univ. of Calif., San Diego, 1971.
- Danby, J. M. A.; and Camm, G. L.: Statistical Dynamics and Accretion. *M.N.R.A.S.*, Vol. 117, 1957, p. 50.
- Danby, J. M. A.; and Bray, T. A.: Density of Interstellar Matter Near a Star. *Astron. J.*, Vol. 72, 1967, p. 219.
- Davidson, K.; and Terzian, Y.: Dispersion Measures of Pulsars. *Astron. J.*, Vol. 74, 1969, p. 849.
- Davies, R. D.: Distance of Pulsars and the Interstellar Electron Gas. *Nature*, Vol. 223, 1969, p. 355.
- Davies, J. G.; Horton, P. W.; Lyne, A. G.; Rickett, B. J.; and Smith, F. G.: Pulsating Radio Source at  $\alpha = 19^{\text{h}}19^{\text{m}}$ ,  $\delta = +22^\circ$ . *Nature*, Vol. 217, 1968, p. 910.
- Davis, L., Jr.: Interplanetary Magnetic Fields and Cosmic Rays. *Phys. Rev.*, Vol. 100, 1955, p. 1440.



- Davis, L., Jr.: The Effect of Solar Disturbances and the Galactic Magnetic Field on the Interplanetary Gas. *J. Phys. Soc., Japan*, Vol. 17, A-II, 1962, p. 543.
- Davis, L., Jr.: The Configuration of the Interplanetary Magnetic Field. Leningrad STP Symp. Paper No. II-2, 1970.
- Davis, L., Jr.; and Greenstein, J. L.: The Polarization of Starlight by Aligned Dust Grains. *Astrophys. J.*, Vol. 114, 1951, p. 206.
- de Jager, G.; Lyne, A. G.; Pointon, L.; and Ponsonby, J. E. B.: Measurement of the Distance of Pulsar CP 0328. *Nature*, Vol. 220, 1968, p. 128.
- Dennison, P. A.; and Hewish, A.: The Solar Wind Outside the Plane of the Ecliptic. *Nature*, Vol. 213, 1967, p. 343.
- Dessler, A. J.: Solar Wind and Interplanetary Magnetic Field. *Rev. Geophys.*, Vol. 5, 1967, p. 1.
- Dokuchaev, V. P.: Mission of Magnetoacoustic Waves in the Motion of Stars and Cosmic Space. *Sov. Astron.-AJ*, Vol. 8, 1964, p. 23.
- Donahue, T. M.; and Kumer, J. B.: An Observation of the Helium I 548-Å Day-Glow Radiation Between 400 and 1000 km. *J. Geophys. Res.*, Vol. 76, 1971, p. 145.
- Dorman, I. V.; and Dorman, L. I.: The Importance of the Solar System Geometry in the Cosmic Ray Variations Observed on the Earth. *Geomagn. Aeron. (USSR)*, Vol. 6, 1966, p. 231.
- Dorman, I. V.; and Dorman, L. I.: Cosmic Rays and the Dynamics of Solar Wind, 1. *Geomagn. Aeron. (USSR)*, Vol. 8, 1968, p. 652.
- Dungey, J. W.: Interplanetary Magnetic Field and the Auroral Zones. *Phys. Rev. Letters*, Vol. 6, 1961, p. 407.
- Ederer, D. L.; and Tomboulion, D. H.: Photoionization Cross Section of Neon in the 80 to 600 Å Region. *Phys. Rev.*, Vol. 133, 1964, p. A1525.
- Egidi, A.; Formisano, V.; Palmiotto, F.; Saraceno, P.; and Moreno, G.: Solar Wind and Location of Shock Front and Magnetopause at the 1969 Solar Maximum. *J. Geophys. Res.*, Vol. 75, 1970, p. 6999.
- Ekers, R. D.; Lequeux, J.; Moffet, A. T.; and Seielstad, G. A.: A Measurement of the Galactic Magnetic Field Using the Pulsating Radio Source PSR 0833-45. *Astrophys. J.*, Vol. 156, 1969, p. L21.
- Elliot, H.; Thambyahpillai, T.; and Peacock, D. S.: Search for a Sidereal Anisotropy at 60 m.w.e. Depth. *Acta Phys. Acad. Sci. Hungar.*, Vol. 29, Suppl. 1, 1970, p. 491.
- Ellis, G. R. A.; and Hamilton, P. A.: Ionized Hydrogen in the Plane of the Galaxy. *Astrophys. J.*, Vol. 146, 1966, p. 78.
- Engelmann, J.; Hynds, R. J.; Morfill, G.; Axisa, F.; Bewick, A.; Durney, A. C.; and Koch, L.: Penetration of Solar Protons Over the Polar Cap During the February 25, 1969 Event. *J. Geophys. Res.*, Vol. 76, 1971, p. 4245.
- Eviatar, A.; and Schulz, M.: Ion-Temperature Anisotropies and the Structure of the Solar Wind. *Planet. Space Sci.*, Vol. 18, 1970, p. 321.
- Fahr, H. J.: On the Influence of Neutral Interstellar Matter on the Upper Atmosphere. *Astrophys. Space Sci.*, Vol. 2, 1968a, p. 474.
- Fahr, H. J.: Neutral Corpuscular Energy Flux by Charge-Transfer Collisions in the Vicinity of the Sun. *Astrophys. Space Sci.*, Vol. 2, 1968b, p. 496.
- Fahr, H. J.: Influence of Interstellar Matter on the Density of Atmospheric Hydrogen. *Ann. Geophys.*, Vol. 25, 1969, p. 475.
- Fahr, H. J.: Interstellar Hydrogen Densities in the Surroundings of the Solar System. *Nature*, Vol. 226, 1970, p. 435.
- Faus, A. A.: Solar Wind Beyond the Earth's Orbit. The Transition Zone. *Planet. Space Sci.*, Vol. 14, 1966, p. 143.
- Felton, J. E.: Radio Electrons and Magnetic Fields in the Galactic Halo. *Astrophys. J.*, Vol. 145, 1966, p. 589.
- Field, G. B.: Thermal Instabilities in the Interstellar Medium. *Interstellar Matter in Galaxies*, L. Woltjer, ed., W. A. Benjamin, Inc., New York, 1962, p. 183.
- Field, G. B.; Goldsmith, D. W.; and Habing, H. J.: Cosmic-Ray Heating of the Interstellar Gas. *Astrophys. J.*, Vol. 155, 1969, p. L149.
- Fischel, D.; and Stecher, T. P.: On the Interstellar Hydrogen Density. *Astrophys. J.*, Vol. 150, 1967, p. L51.
- Fisk, L. A.: Ph.D. Dissertation, Univ. Calif., San Diego, 1969.
- Fisk, L. A.: Solar Modulation of Galactic Cosmic Rays, 2. *J. Geophys. Res.*, Vol. 76, 1971a, p. 221.
- Fisk, L. A.: Increases in the Low-Energy Cosmic Ray Intensity at the Front of Propagating Interplanetary Shock Waves. *J. Geophys. Res.*, Vol. 76, 1971b, p. 1662.
- Fisk, L. A.; and Axford, W. I.: Solar Modulation of Galactic Cosmic Rays, 1. *J. Geophys. Res.*, Vol. 74, 1969, p. 4973.
- Fisk, L. A.; and Van Hollebeke, M.: Quiet-Time Electron Increases, A Measure of Conditions in the Outer Solar System. Submitted to *J. Geophys. Res.*, 1971.
- Fite, W. L.; Smith, A. C. H.; and Stebbings, R. F.: Charge Transfer in Collisions Involving Symmetric and Asymmetric Resonance. *Proc. Roy. Soc. (London)*, Vol. A-268, 1962, p. 527.

- Forbush, S. E.: A Variation, With a Period of Two Solar Cycles, in the Cosmic-Ray Diurnal Anisotropy. *J. Geophys. Res.*, Vol. 72, 1967, p. 4937.
- Forbush, S. E.: Variation With a Period of Two Solar Cycles in the Cosmic-Ray Diurnal Anisotropy and the Superposed Variations Correlated With Magnetic Activity. *J. Geophys. Res.*, Vol. 74, 1969, p. 3451.
- Forman, M. A.: The Compton-Getting Effect for Cosmic-Ray Particles and Photons and the Lorentz-Invariance of Distribution Functions. *Planet. Space Sci.*, Vol. 18, 1970, p. 25.
- Forman, M. A.; Stoenner, R. W.; and Davis, R., Jr.: Cosmic Ray Gradient Measured by the Argon-37/Argon-39 Ratio in the Lost City Meteorite. *J. Geophys. Res.*, Vol. 76, 1971, p. 4109.
- Forslund, D. W.: Instabilities Associated With Heat Conduction in the Solar Wind and Their Consequences. *J. Geophys. Res.*, Vol. 75, 1970, p. 17.
- Fowler, W. A.; Reeves, H.; and Silk, J.: Spallation Limits on Interstellar Fluxes of Low-Energy Cosmic Rays and Nuclear Gamma Rays. *Astrophys. J.*, Vol. 162, 1970, p. 49.
- Fritz, G.; Meekins, J. F.; Henry, R. C.; Byram, E. T.; and Friedman, H.: Soft X-rays From Scorpius XR-1. *Astrophys. J.*, Vol. 153, 1968, p. L199.
- Gardner, F. F.; and Davies, R. D.: Faraday Rotation of the Emission From Linearly Polarized Radio Sources. *Austral. J. Phys.*, Vol. 19, 1966, p. 129.
- Gardner, F. F.; and Whiteoak, J. B.: The Polarization of Cosmic Radio Waves. *Ann. Rev. Astron. Astrophys.*, Vol. 4, 1966, p. 245.
- Gardner, F. F.; Whiteoak, J. B.; and Morris, D.: Evidence for an Association Between Magnetic Field and Gas Outflow From a Spiral Arm. *Nature*, Vol. 214, 1967, p. 371.
- Geiss, J.; Hirt, P.; and Lentwyler, H.: On Acceleration and Motion of Ions in Corona and Solar Wind. *Solar Phys.*, Vol. 13, 1970a, p. 183.
- Geiss, J.; Eberhardt, P.; Bühler, F.; Meister, J.; and Signer, P.: Apollo 11 and 12 Solar Wind Composition Experiments: Fluxes of He and Ne Isotopes. *J. Geophys. Res.*, Vol. 75, 1970b, p. 5972.
- Gleeson, L. J.: The Equations Describing the Cosmic-Ray Gas in the Interplanetary Region. *Planet. Space Sci.*, Vol. 17, 1969, p. 31.
- Gleeson, L. J.; and Axford, W. I.: Cosmic Rays in the Interplanetary Medium. *Astrophys. J.*, Vol. 149, 1967, p. L115.
- Gleeson, L. J.; and Axford, W. I.: The Compton-Getting Effect. *Astrophys. Space Sci.*, Vol. 2, 1968a, p. 431.
- Gleeson, L. J.; and Axford, W. I.: Solar Modulation of Galactic Cosmic Rays. *Astrophys. J.*, Vol. 154, 1968b, p. 1011.
- Gleeson, L. J.; and Urch, I. H.: Energy Losses and Modulation of Galactic Cosmic Rays. *Astrophys. Space Sci.*, Vol. 11, 1971a, p. 288.
- Gleeson, L. J.; and Urch, I. H.: Solar Sources and the Cosmic Ray Transport Equation. *J. Geophys. Res.*, Vol. 76, 1971b, p. 2510.
- Gleeson, L. J.; Krimigis, S. M.; and Axford, W. I.: Low-Energy Cosmic Rays Near Earth. *J. Geophys. Res.*, Vol. 76, 1971, p. 2228.
- Goldstein, S. J., Jr.; and MacDonald, D. D.: Observations of the 21-cm Hydrogen Line Toward High-Latitude Stars. *Astrophys. J.*, Vol. 157, 1969, p. 1101.
- Goldstein, S. J.; and Meisel, D. D.: Frequency Dependence of Polarization of Pulsar CP0328. *Science*, Vol. 163, 1969, p. 810.
- Goldstein, M. L.; Ramaty, R.; and Fisk, L. A.: Interstellar Cosmic Ray Spectra From the Nonthermal Radio Background From 0.4 to 400 Mhz. *Phys. Rev. Letters*, Vol. 24, 1970a, p. 1193.
- Goldstein, M. L.; Fisk, L. A.; and Ramaty, R.: Energy Loss of Cosmic Rays in the Interplanetary Medium. *Phys. Rev. Letters*, Vol. 25, 1970b, p. 832.
- Gordon, C. P.; Gordon, K. J.; and Shalloway, A. M.: Estimates of Pulsar Distances From Neutral Hydrogen Absorption. *Nature*, Vol. 222, 1969, p. 129.
- Gordon, K. J.; and Gordon, C. P.: Measurements of Neutral-Hydrogen Absorption in the Spectra of Four Pulsars. *Astrophys. J.*, Vol. 5, 1970, p. L153.
- Gorenstein, P.; Giacconi, R.; and Gursky, H.: The Spectra of Several X-ray Sources in Cygnus and Scorpio. *Astrophys. J.*, Vol. 150, 1967, p. L85.
- Gorenstein, P.; Kellogg, E. M.; and Gursky, H.: The Spectrum of Diffuse Cosmic X-rays, 1-13 keV. *Astrophys. J.*, Vol. 156, 1968, p. 315.
- Gould, R. J.: Pulsar Dispersion Measures and the Mean and Mean-Squared Interstellar Electron Density. *Astrophys. Space Sci.*, Vol. 10, 1971, p. 265.
- Gould, R. J.; and Salpeter, E. E.: The Interstellar Abundance of the Hydrogen Molecule, I. *Astrophys. J.*, Vol. 138, 1963, p. 393.
- Gould, R. J.; Gold, T.; and Salpeter, E. E.: The Interstellar Abundance of the Hydrogen Molecule, II. Galactic Abundance and Distribution. *Astrophys. J.*, Vol. 138, 1963, p. 408.
- Grader, R. J.; Hill, R. W.; Seward, F. D.; and Hiltner, W. A.: The Soft X-ray Spectra of Three Cosmic Sources and Simultaneous Optical Observations of SCO XR-1. *Astrophys. J.*, Vol. 159, 1970, p. 201.

- Green, D. W.; Wilson, B. G.; and Baxter, A. J.: A Spectral Measurement of the Cosmic X-ray Background Down to 2 keV. in *Space Research IX*. K. S. W. Champion, P. A. Smith, and R. L. Rose-Smith, eds., North-Holland Pub. Co., Amsterdam, 1968, p. 222.
- Greenberg, D. W.: A Radio Observational Test for Low-Energy Cosmic Rays in the Galaxy. *Astrophys. J.*, Vol. 155, 1969, p. L51.
- Gregory, C. T.: Ph.D. Dissertation, Univ. Calif., San Diego, 1971.
- Grewing, M.; and Walmsley, M.: On the Interpretation of the Pulsar Dispersion Measure. *Astron. Astrophys.*, Vol. 11, 1971, p. 65.
- Guelin, M.; Guibert, J.; Huchtmeier, W.; and Weliachew, L.: Measurement of Pulsar Distances by Galactic Hydrogen Absorption. *Nature*, Vol. 221, 1969, p. 249.
- Guschina, R. T.; Dorman, I. V.; Dorman, L. I.; and Pimenov, I. A.: Correlation of Solar Activity With Cosmic Ray Intensity and Solar Wind Properties. *Acta Phys. Acad. Sci. Hungar.*, Vol. 29, Suppl. 2, 1970, p. 219.
- Habing, H. J.; and Goldsmith, D. W.: Heating of the Interstellar Medium by X-rays and by Cosmic Rays. *Astrophys. J.*, Vol. 166, 1971, p. 525.
- Habing, H. J.; and Pottasch, S. R.: Low-Energy Cosmic Rays and the Electron Density in  $H_I$  Regions. *Astrophys. J.*, Vol. 149, 1967, p. L119.
- Habing, H. J.; and Pottasch, S. R.: Distances to the Pulsating Radio Sources. *Nature*, Vol. 219, 1968, p. 1137.
- Hartle, R. E.; and Sturrock, P. A.: Two-Fluid Model of the Solar Wind. *Astrophys. J.*, Vol. 151, 1968, p. 1155.
- Hatton, C. J.; Marsden, P. L.; and Willetts, A. C.: Rigidity Dependence and the Correlation With Solar Activity of the 11-Year Variation. *Can. J. Phys.*, Vol. 46, 1968, p. S915.
- Hayakawa, S.; Nishimura, S.; and Takayanagi, K.: Radiation From the Interstellar Hydrogen Atoms. *Publ. Astron. Soc. Jap.*, Vol. 13, 1961, p. 184.
- Hayes, W. D.; and Probstein, R. F.: *Hypersonic Flow Theory*. Academic Press, New York, 1966.
- Henry, R. J. W.: Photoionization Cross Sections for N and O. *J. Chem. Phys.*, Vol. 48, 1968, p. 3635.
- Hertel, G. R.; and Koski, W. S.: Cross Sections for the Single Charge Transfer of Doubly-Charged Rare-Gas Ions in Their Own Gases. *J. Chem. Phys.*, Vol. 40, 1964, p. 3452.
- Hewish, A.: Pulsars. *Ann. Rev. Astron. Astrophys.*, Vol. 8, 1970, p. 265.
- Hewish, A.; and Wyndham, J. D.: The Solar Corona in Interplanetary Space. *Mon. Not. Roy. Astron. Soc.*, Vol. 126, 1963, p. 469.
- Hinteregger, H. E.: Extreme Ultraviolet Solar Spectrum and Its Variation During a Solar Cycle. *Ann. Geophys.*, Vol. 26, 1970, p. 547.
- Hjellming, R. M.; Gordon, C. P.; and Gordon, K. J.: Properties of Interstellar Clouds and the Inter-Cloud Medium. *Astron. Astrophys.*, Vol. 2, 1969, p. 202.
- Hollenbach, D. J.; Werner, M. W.; and Salpeter, E. E.: Molecular Hydrogen in  $H_I$  Regions. *Astrophys. J.*, Vol. 163, 1971, p. 165.
- Hollweg, J. V.; and Völk, H. J.: New Plasma Instabilities in the Solar Wind. *J. Geophys. Res.*, Vol. 75, 1970, p. 5297.
- Holzer, T. E.: Stellar Winds and Related Flows. Ph.D. Thesis, Univ. Calif., San Diego, 1970.
- Holzer, T. E.: In preparation, 1971.
- Holzer, T. E.; and Axford, W. I.: The Theory of Stellar Winds and Related Flows. *Ann. Rev. Astron. Astrophys.*, Vol. 8 1970a, p. 31.
- Holzer, T. E.; and Axford, W. I.: Solar Wind Ion Composition. *J. Geophys. Res.*, Vol. 75, 1970b, p. 6354.
- Holzer, T. E.; and Axford, W. I.: The Interaction Between Interstellar Helium and the Solar Wind. To appear in *J. Geophys. Res.*, 1971.
- Huffman, R. E.: Absorption Cross-Sections of Atmospheric Gases for Use in Aeronomy. *Can. J. Chem.*, Vol. 47, 1969, p. 1823.
- Humphreys, R. M.: Streaming Motions in the Carina-Centaurus Region. *Astrophys. J.*, Vol. 163, 1971, p. L111.
- Hundhausen, A. J.: Direct Observations of Solar-Wind Particles. *Space Sci. Rev.*, Vol. 8, 1968a, p. 690.
- Hundhausen, A. J.: Interplanetary Neutral Hydrogen and the Radius of the Heliosphere. *Planet. Space Sci.*, Vol. 16, 1968b, p. 783.
- Hundhausen, A. J.: Composition and Dynamics of the Solar Wind Plasma. *Rev. Geophys. Space Phys.*, Vol. 8, 1970, p. 729.
- Hundhausen, A. J.; Bame, S. J.; and Ness, N. F.: Solar Wind Thermal Anisotropies: Vela 3 and IMP 3. *J. Geophys. Res.*, Vol. 72, 1967, p. 5265.
- Hundhausen, A. J.; Gilbert, H. E.; and Bame, S. J.: Ionization State of the Interplanetary Plasma. *J. Geophys. Res.*, Vol. 73, 1968, p. 5485.
- Ioffe, Z. M.: Comets in the Solar Wind. *Soviet Astron.-AJ*, Vol. 10, 1966a, p. 138.
- Ioffe, Z. M.: Comets in the Solar Wind, 2. *Soviet Astron.-AJ*, Vol. 10, 1966b, p. 517.
- Ioffe, Z. M.: Some Magnetohydrodynamic Effects in Comets. *Soviet Astron.-AJ*, Vol. 11, 1968, p. 1044.

- Jenkins, E. B.: Observations of Interstellar Lyman- $\alpha$  Absorption, in *Ultraviolet Stellar Spectra and Ground-Based Observations*. I.A.U. Symp. No. 36, L. Houziaux and H. E. Butler, eds., D. Reidel Pub. Co., Dordrecht, 1970.
- Jenkins, E. B.; and Morton, D. C.: Far Ultra-Violet Spectra of Orion Stars. *Nature*, Vol. 215, 1967, p. 1257.
- Jenkins, E. B.; Morton, D. C.; and Matilsky, T. A.: Interstellar  $\text{Ly}\alpha$  Absorption in  $\beta^1$ ,  $\delta$ , and  $\pi$  Scorpii. *Astrophys. J.*, Vol. 158, 1969, p. 473.
- Johnson, C. Y.; Young, J. M.; and Holmes, J. C.: Magnetoglow, A New Geophysical Resource. *Science*, Vol. 171, 1971, p. 379.
- Johnson, H. E.: Ph.D. Thesis, Univ. Calif., San Diego, 1971.
- Johnson, H. E.; and Axford, W. I.: Production and Loss of  $\text{He}^3$  in the Earth's Atmosphere. *J. Geophys. Res.*, Vol. 74, 1969, p. 2433.
- Jokipii, J. R.: Effects of Diffusion on the Composition of the Solar Corona and the Solar Wind, in *The Solar Wind*. R. J. Mackin, Jr., and M. Neugebauer, eds., Pergamon Press, New York, 1966a, p. 215.
- Jokipii, J. R.: Cosmic-Ray Propagation, I. Charged Particles in a Random Magnetic Field. *Astrophys. J.*, Vol. 146, 1966b, p. 480.
- Jokipii, J. R.: Acceleration of Cosmic Rays at the Solar-Wind Boundary. *Astrophys. J.*, Vol. 152, 1968, p. 799.
- Jokipii, J. R.: Propagation of Cosmic Rays in the Solar Wind. *Rev. Geophys. Space Phys.*, Vol. 9, 1971, p. 27.
- Jokipii, J. R.; and Coleman, P. J., Jr.: Cosmic-Ray Diffusion Tensor and Its Variation Observed With Mariner 4. *J. Geophys. Res.*, Vol. 73, 1968, p. 5495.
- Jokipii, J. R.; and Parker, E. N.: Energy Changes of Cosmic Rays in the Solar System. *Planet. Space Sci.*, Vol. 15, 1967, p. 1375.
- Jokipii, J. R.; and Parker, E. N.: Stochastic Aspects of Magnetic Lines of Force With Application to Cosmic-Ray Propagation. *Astrophys. J.*, Vol. 155, 1969, p. 777.
- Jokipii, J. R.; and Parker, E. N.: On the Convection, Diffusion, and Adiabatic Deceleration of Cosmic Rays in the Solar Wind. *Astrophys. J.*, Vol. 160, 1970, p. 735.
- Kennel, C. F.; and Scarf, F. L.: Thermal Anisotropies and Electromagnetic Instabilities in the Solar Wind. *J. Geophys. Res.*, Vol. 73, 1968, p. 6149.
- Kern, J. W.; and Semar, C. L.: Solar-Wind Termination and the Interstellar Medium. *Trans. Amer. Geophys. Union*, Vol. 49, 1968, p. 203.
- Kerr, F. J.: Radio-Line Emission and Absorption by the Interstellar Gas. *Nebulae and Interstellar Matter*. B. M. Middlehurst and L. H. Aller, eds., Univ. Chicago Press, 1968, p. 575.
- Kerr, F. J.: The Large-Scale Distribution of Hydrogen in the Galaxy. *Ann. Rev. Astron. Astrophys.*, Vol. 7, 1969, p. 39.
- Kerr, F. J.; and Westerhout, G.: Distribution of Interstellar Hydrogen. *Stars Stellar Sys.*, Vol. V, 1965, p. 167.
- Kolomeets, E. V.; Shakhova, Y. A.; and Zusmanovich, A. J.: Solar Activity and Dimension of Modulation Region. *Acta Phys. Acad. Sci. Hungar.*, Vol. 29, Suppl. 2, 1970, p. 305.
- Koopman, D. W.: Charge Exchange of  $\text{H}^+$  and  $\text{H}_2^+$  in Atmospheric Constituents. *Fifth Intern. Conf. Phys. Electron. Atomic Collisions*, I. P. Flaks, ed., Nauka, Leningrad, 1967, p. 410.
- Kovar, R. P.; and Dessler, A. J.: On the Anisotropy of Galactic Cosmic Rays. *Astrophys. Letters*, Vol. 1, 1967, p. 15.
- Kurt, V. G.: Measurement of Scattered  $\text{Ly}\alpha$ -Radiation in the Vicinity of the Earth and in Interplanetary Space. *Trans. All Union Conf. Space Phys., NASA-TTF*, Vol. 389, 1965, p. 769.
- Kurt, V. G.: Observations of Scattered Lyman- $\alpha$  Radiation in the Earth's Neighborhood. *Cosmic Res.*, Vol. 5, 1967, p. 770.
- Kurt, V. G.; and Germogenova, T. A.: Scattering of Solar Lyman- $\alpha$  Radiation by Galactic Hydrogen. *Soviet Astron.*, Vol. 11, 1967, p. 278.
- Kurt, V. G.; and Dostovalov, S. B.: For Ultraviolet Radiation From the Milky Way. *Nature*, Vol. 218, 1968, p. 258.
- Kurt, V. G.; and Syunyaev, R. A.: Observations and Interpretation of the Ultraviolet Radiation of the Galaxy. *Soviet Astron.*, Vol. 11, 1968, p. 928.
- Lanzerotti, L. J.; and Schulz, M.: Interaction Between the Boundary of the Heliosphere and the Magnetosphere of Jupiter. *Nature*, Vol. 222, 1969, p. 1054.
- Lee, A. R.; and Hasted, J. B.: Calculations of Atomic Asymmetric Charge Transfer. *Proc. Phys. Soc. (London)*, Vol. 85, 1965, p. 673.
- Leer, A.; and Axford, W. I.: A Two-Fluid Solar Wind Model with Anisotropic Proton Temperature. To be submitted to *Solar Phys.*, 1971.
- Lenchek, A. M.: The Solar HII Region and the Radio Spectrum of the Non-Thermal Radiation of the Galaxy. *Ann. Astrophys.*, Vol. 27, 1964, p. 219.
- Levy, R. H.; Petschek, H. E.; and Siscoe, G. L.: Aerodynamic Aspects of the Magnetospheric Flow. *AIAA J.*, Vol. 2, 1964, p. 2065.

- Lezniak, J. A.; and Webber, W. R.: Solar Modulation of Cosmic Ray Protons, Helium Nuclei, and Electrons. *J. Geophys. Res.*, Vol. 76, 1971, p. 1605.
- Liepmann, H. W.; and Roshko, A.: *Elements of Gas-dynamics*. John Wiley and Sons, Inc., New York, 1957.
- Lin, C. C.; Yuau, C.; and Shu, F. H.: On the Spiral Structure of Disk Galaxies, III. Comparison With Observations. *Astrophys. J.*, Vol. 155, 1969, p. 721.
- Lowry, J. F.; Tomboulain, D. H.; and Ederer, D. L.: Photoionization Cross Section of Helium in the 100- to 250-Å Region. *Phys. Rev.*, Vol. 137, 1965, No. 54, A1057.
- Lüst, R.: The Properties of Interplanetary Space, in *Solar Terrestrial Physics*, J. W. King and W. S. Newman, eds., Academic Press, London, 1967, p. 1.
- Lyne, A. G.; and Rickett, B. J.: Measurements of the Pulse Shape and Spectrum of the Pulsating Radio Sources. *Nature*, Vol. 218, 1968, p. 326.
- McCrea, W. H.: Shock Waves in Steady Radial Motion Under Gravity. *Astrophys. J.*, Vol. 124, 1956, p. 461.
- McGuire, E. J.: Photoionization Cross Sections of the Elements Helium to Xenon. *Phys. Rev.*, Vol. 175, 1968, p. 20.
- Madden, R. P.; Ederer, D. L.; and Codling, K.: Resonances in the Photo-Ionization Continuum of Ar I (20–150eV). *Phys. Rev.*, Vol. 177, 1969, p. 136.
- Mange, P.; and Meier, R. R.: Ogo 3 Observations of the Lyman-Alpha Intensity and the Hydrogen Concentration Beyond 5 R<sub>E</sub>. *J. Geophys. Res.*, Vol. 75, 1970, p. 1837.
- Mathewson, D. S.: The Local Galactic Magnetic Field and the Nature of the Radio Spurs. *Astrophys. J.*, Vol. 153, 1968, p. L47.
- Mathewson, D. S.; and Milne, D. K.: A Linear Polarization Survey of the Southern Sky at 408 Mc/s. *Austral. J. Phys.*, Vol. 18, 1965, p. 635.
- Mathewson, D. S.; and Nicholls, D. C.: The Local Spiral-Arm Magnetic Field. *Astrophys. J.*, Vol. 154, 1968, p. L11.
- Meier, R. R.: Temporal Variations of Solar Lyman Alpha. *J. Geophys. Res.*, Vol. 74, 1969, p. 6487.
- Meier, R. R.; and Prinz, D. K.: Absorption of the Solar Lyman Alpha Line by Geocoronal Atomic Hydrogen. *J. Geophys. Res.*, Vol. 75, 1970, p. 6969.
- Metzger, P. H.; and Clark, M. A.: On the Diurnal Variation of the Exospheric Neutral Hydrogen Temperature. *J. Geophys. Res.*, Vol. 75, 1970, p. 5587.
- Mills, B. Y.: Pulsar Distances, Spiral Structure and the Interstellar Medium. *Nature*, Vol. 224, 1969, p. 504.
- Milne, D. K.: Radio Emission From the Supernova Remnant Vela-X. *Austral. J. Phys.*, Vol. 21, 1968, p. 201.
- Modisette, J. L.; and Snyder, J. W.: Interaction of the Solar Wind With the Interstellar Medium (Abstract). *Trans. Amer. Geophys. Union*, Vol. 49, 1968, p. 263.
- Morris, D.; and Berge, G. L.: Direction of the Galactic Magnetic Field in the Vicinity of the Sun. *Astrophys. J.*, Vol. 139, 1964, p. 1388.
- Morton, D. C.: The Far-Ultraviolet Spectra of Six Stars in Orion. *Astrophys. J.*, Vol. 147, 1967, p. 1017.
- Morton, D. C.; and Purcell, J. D.: Observations of the Extreme Ultraviolet Radiation in the Night Sky Using an Atomic Hydrogen Filter. *Planet. Space Sci.*, Vol. 9, 1962, p. 455.
- Morton, D. C.; Jenkins, E. B.; and Brooks, N. H.: Far-Ultraviolet Spectra of Zeta Puppis and  $\gamma^2$  Velorum. *Astrophys. J.*, Vol. 155, 1969, p. 875.
- Munch, G.: Interstellar Absorption Lines, in *Nebulae and Interstellar Matter*. B. M. Middlehurst and L. H. Aller, eds., Univ. Chicago Press, 1968, p. 365.
- Ness, N. F.: Observations of the Interaction of the Solar Wind With the Geomagnetic Field During Quiet Conditions, in *Solar Terrestrial Physics*. J. W. King and W. S. Newman, eds., Academic Press, London, 1967, p. 57.
- Ness, N. F.: Observed Properties of the Interplanetary Plasma. *Ann. Rev. Astron. Astrophys.*, Vol. 6, 1968, p. 79.
- Newkirk, G. A.; Warwick, J. W.; and Zirin, H.: Backscatter of Cosmic Rays by the Sun's HII Sphere. *J. Geophys. Res.*, Vol. 65, 1960, p. 2540.
- Newman, R. C.; and Axford, W. I.: Recombination Fronts in Stellar-Wind Flows. *Astrophys. J.*, Vol. 151, 1968, p. 1145.
- Nishida, A.: Thermal State and Effective Collision Frequency in the Solar Wind Plasma. *J. Geophys. Res.*, Vol. 74, 1969, p. 5155.
- O'Gallagher, J. J.: Cosmic-Ray Radial Density Gradient and Its Rigidity Dependence Observed at Solar Minimum on Mariner IV. *Astrophys. J.*, Vol. 150, 1967, p. 675.
- O'Gallagher, J. J.; and Simpson, J. A.: The Heliocentric Intensity Gradients of Cosmic-Ray Protons and Helium During Minimum Solar Modulation. *Astrophys. J.*, Vol. 147, 1967, p. 819.
- Ogawa, T.; and Tohmatsu, T.: Sounding Rocket Observation of Helium 304Å and 584Å Glow. To appear in *J. Geophys. Res.*, 1971.
- Ogilvie, K. W.; Burlaga, L. F.; and Wilkerson, T. D.: Plasma Observations on Explorer 34. *J. Geophys. Res.*, Vol. 73, 1968, p. 6809.

- Ogilvie, K. W.; and Wilkerson, T. D.: Helium Abundance on the Solar Wind. *Solar Phys.*, Vol. 8, 1969, p. 435.
- Parker, E. N.: Dynamics of the Interplanetary Gas and Magnetic Fields. *Astrophys. J.*, Vol. 128, 1958, p. 664.
- Parker, E. N.: The Stellar-Wind Regions. *Astrophys. J.*, Vol. 134, 1961, p. 20.
- Parker, E. N.: *Interplanetary Dynamical Processes*. Interscience, New York, 1963.
- Parker, E. N.: Theory of Streaming of Cosmic Rays and the Diurnal Variation. *Planet. Space Sci.*, Vol. 12, 1964, p. 735.
- Parker, E. N.: Dynamical Theory of the Solar Wind. *Space Sci. Rev.*, Vol. 4, 1965a, p. 666.
- Parker, E. N.: The Passage of Energetic Charged Particles Through Interplanetary Space. *Planet. Space Sci.*, Vol. 13, 1965b, p. 9.
- Parker, E. N.: The Role of Stochastic Fields in Admitting Low-Energy Galactic Cosmic Rays to the Solar System. *J. Geophys. Res.*, Vol. 73, 1968, p. 6842.
- Parker, E. N.: Theoretical Studies of the Solar Wind Phenomenon. *Space Sci. Rev.*, Vol. 9, 1969, p. 325.
- Patterson, T. N. L.; Johnson, F. S.; and Hanson, W. B.: The Distribution of Interplanetary Hydrogen. *Planet. Space Sci.*, Vol. 11, 1963, p. 767.
- Pikel'ner, S. B.: Ionization and Heating of the Interstellar Gas by Subcosmic Rays, and the Formation of Clouds. *Soviet Astron.*, Vol. 11, 1968, p. 737.
- Pilkington, J. D. H.; Hewish, A.; Bell, S. J.; and Cole, T. W.: Observations of Some Further Pulsed Radio Sources. *Nature*, Vol. 218, 1968, p. 126.
- Prentice, A. J. R.; and Ter Haar, D.: HII Regions and the Distances to Pulsars. *Nature*, Vol. 222, 1969a, p. 964.
- Prentice, A. J. R.; and Ter Haar, D.: On HII Regions and Pulsar Distances. *M.N.R.A.S.*, Vol. 146, 1969b, p. 423.
- Radhakrishnan, V.; and Murray, J. D.: The Spin Temperature of Interstellar Neutral Hydrogen. *Proc. Astron. Soc. Austral.*, Vol. 1, 1969, p. 215.
- Radhakrishnan, V.; Cooke, D. J.; Komesaroff, M. M.; and Morris, D.: Evidence in Support of a Rotational Model for the Pulsar PSR 0833-45. *Nature*, Vol. 221, 1969, p. 443.
- Rappaport, S.; Bradt, H. V.; and Mayer, W.: Interstellar Absorption of 10-Å X-rays. *Astrophys. J.*, Vol. 157, 1969, p. L21.
- Reay, N. K.; and Ring, J.: Radial Velocity and Intensity Measurements of the Night Sky H $\beta$  Emission Line. *Planet. Space Sci.*, Vol. 17, 1969, p. 561.
- Reid, G. C.; and Sauer, H. H.: Evidence for Nonuniformity of Solar-Proton Precipitation Over the Polar Caps. *J. Geophys. Res.*, Vol. 72, 1967, p. 4383.
- Reiffel, L.: Low-Energy X-rays From Interplanetary Space. *Nature*, Vol. 185, 1960, p. 229.
- Riegel, K. W.; and Jennings, M. C.: Observations of an Unusual Cold Cloud in the Galaxy. *Astrophys. J.*, Vol. 157, 1969, p. 563.
- Robbins, D. E.; Hundhausen, A. J.; and Bame, S. J.: Helium in the Solar Wind. *J. Geophys. Res.*, Vol. 75, 1970, p. 1178.
- Rohlf, K.: On the Structure of Interstellar Matter, I. Kinematics of the Interstellar Gas and the Brightness Temperature of the 21 cm Line Emission. *Astron. Astrophys.*, Vol. 12, 1971, p. 43.
- Rustgi, O. P.: Absorption Cross Sections of Argon and Methane Between 600 and 170Å. *J. Opt. Soc. Amer.*, Vol. 54, 1964, p. 464.
- Sakashita, S.: Interaction of Stars and Interstellar Gas. Preprint, 1970.
- Samson, J. A. R.: Photoionization Cross Sections of Neon From Threshold to 200Å. *J. Opt. Soc. Amer.*, Vol. 55, 1965, p. 935.
- Schatten, K. H.; and Wilcox, J. M.: Direction of the Nearby Galactic Magnetic Field Inferred From a Cosmic-Ray Diurnal Anisotropy. *J. Geophys. Res.*, Vol. 74, 1969, p. 4157.
- Schatten, K. H.; and Wilcox, J. M.: Solar Modulation of Galactic Cosmic Rays With a Twenty-Year Period: Interpretation and Inferences. *Acta Phys. Acad. Sci. Hungar.*, Vol. 29, Suppl. 2, 1970, p. 279.
- Semar, C. L.: Effect of Interstellar Neutral Hydrogen on the Termination of the Solar Wind. *J. Geophys. Res.*, Vol. 75, 1970, p. 6892.
- Silk, J.; and Werner, M. W.: Heating of H $\text{I}$  Regions by Soft X-rays. *Astrophys. J.*, Vol. 158, 1969, p. 185.
- Silk, J.; and Brown, R. L.: On the Ultraviolet Absorption-Line Spectra Produced by H $\text{I}$  Regions. *Astrophys. J.*, Vol. 163, 1971, p. 495.
- Simnett, G. M.; Cline, T. L.; and McDonald, F. B.: The Multifarious Temporal Variations of Low Energy, Relativistic Cosmic Ray Electrons. Submitted to *J. Geophys. Res.*, 1971.
- Simpson, J. A.: Recent Investigations of the Low Energy Cosmic and Solar Particle Radiations, *Semaine d'Étude sur le Problème du Rayonnement Cosmique dans L'Espace Interplanétaire*, Pontifical Acad. Sci., Vatican City, Vol. 281, 1962, p. 323.
- Simpson, J. A.; and Wang, J. R.: Dimension of the Cosmic Ray Modulation Region. *Astrophys. J.*, Vol. 149, 1967, p. L73.

- Simpson, J. A.; and Wang, J. R.: The Eleven-Year and Residual Solar Modulation of Cosmic Rays (1952–1969). *Astrophys. J.*, Vol. 161, 1970, p. 265.
- Slee, O. B.: The Outer Solar Corona During the Declining Portion of the Solar Activity Cycle. *Planet. Space Sci.*, Vol. 14, 1966, p. 255.
- Smith, A. M.: Rocket Spectrographic Observations of  $\alpha$  Virginis. *Astrophys. J.*, Vol. 156, 1969, p. 93.
- Smith, F. G.: Cosmic Radio Noise as Measured in the Satellite Ariel II. Pt. II, Analysis of the Observed Sky Brightness. *Mon. Notic. Roy. Astron. Soc.*, Vol. 131, 1965, p. 145.
- Smith, F. G.: Measurement of the Interstellar Magnetic Field. *Nature*, Vol. 218, 1968a, p. 325.
- Smith, F. G.: Faraday Rotation of Radio Waves From the Pulsars. *Nature*, Vol. 220, 1968b, p. 891.
- Snyder, C. W.; and Neugebauer, M.: Interplanetary Solar-Wind Measurements by Mariner II. *Space Res.*, Vol. 4, 1964, p. 89.
- Solomon, P. M.: and Werner, M. W.: In preparation, 1970.
- Sousk, S. F.; and Lenchek, A. M.: The Effect of Galactic Cosmic Rays Upon the Dynamics of the Solar Wind. *Astrophys. J.*, Vol. 158, 1969, p. 781.
- Spitzer, L., Jr.: Dynamics of Interstellar Matter and the Formation of Stars. *Nebulae and Interstellar Matter*. B. M. Middlehurst and L. H. Aller, eds., Univ. Chicago Press, 1968a, p. 1.
- Spitzer, L., Jr.: *Diffuse Matter in Space*. Interscience, New York, 1968b.
- Spitzer, L., Jr., and Tomasko, M. G.: Heating of H<sub>I</sub> Regions by Energetic Particles. *Astrophys. J.*, Vol. 152, 1968, p. 971.
- Staelin, D. H.; and Riefenstein, E. C., III: Faraday Rotation in Pulsars. *Astrophys. J.*, Vol. 156, 1969, p. L121.
- Stebbins, R. F.; Fite, W. L.; and Hummer, D. G.: Charge Transfer Between Atomic Hydrogen and N<sup>+</sup> and O<sup>+</sup>. *J. Chem. Phys.*, Vol. 33, 1960, p. 1226.
- Storer, S. H.; and Sciamia, D. W.: Is Interstellar Hydrogen Capable of Maser Action at 21 Centimeters? *Nature*, Vol. 217, 1968, p. 1237.
- Subramanian, G.: Amplitude of Diurnal Anisotropy of Cosmic Ray Intensity. *J. Geophys. Res.*, Vol. 76, 1971, p. 1093.
- Sunyaev, R. A.: Interaction of the Ionizing Background Radiation With Galaxies, and Limits on the Inter-galactic Gas Density. *Astron. Zh.*, Vol. 46, 1969, p. 929.
- Swinson, D. B.: Solar Modulation Origin of 'Sidereal' Cosmic Ray Anisotropies. *J. Geophys. Res.*, Vol. 76, 1971, p. 4217.
- Thomas, G. E.: Properties of Nearby Interstellar Hydrogen Deduced From Lyman Alpha Sky Background Measurements. Presented at the Solar Wind Conf., Asilomar, Pacific Grove, Calif., March 21–26, 1971.
- Thomas, G. E.; and Krassa, R. F.: OGO 5 Measurements of the Lyman Alpha Sky Background. *Astron. Astrophys.*, Vol. 11, 1971, p. 218.
- Tinsley, B. A.: Anisotropic Galactic Emissions at Lyman Alpha and Nearby Wavelengths. *J. Geophys. Res.*, Vol. 9, 1969, p. 2327.
- Tinsley, B. A.: Extraterrestrial Lyman Alpha. *Rev. Geophys. Space Phys.*, Vol. 9, 1971, p. 89.
- Tohmatsu, T.: The Hydrogen and Helium Ultraviolet Glow, Its Origins and Aeronomical Significance. *Space Res.*, Vol. 10, 1970, p. 608.
- Toichi, T.: Thermal Properties of the Solar Wind Plasma. To be published in *Solar Phys.*, Vol. 15, 1971.
- Urch, I. H.: Ph.D. Dissertation, Univ. Adelaide, Australia, 1971.
- Van Allen, J. A.; Fennell, J. F.; and Ness, N. F.: Asymmetric Access of Energetic Solar Protons to the Earth's North and South Polar Caps. *J. Geophys. Res.*, Vol. 76, 1971, p. 4262.
- van de Hulst, H. C.: Observing the Galactic Magnetic Field. *Ann. Rev. Astron. Astrophys.*, 1967, p. 167.
- Verschuur, G. L.: Positive Determination of an Interstellar Magnetic Field by Measurement of the Zeeman Splitting of the 21 cm Hydrogen Line. *Phys. Rev. Letters*, Vol. 21, 1968, p. 775.
- Verschuur, G. L.: Measurements of Magnetic Fields in Interstellar Clouds of Neutral Hydrogen. *Astrophys. J.*, Vol. 156, 1969a, p. 861.
- Verschuur, G. L.: Further Measurements of Magnetic Fields in Interstellar Clouds of Neutral Hydrogen. *Nature*, Vol. 223, 1969b, p. 140.
- Verschuur, G. L.: Magnetic Fields in Interstellar Neutral-Hydrogen Clouds. *Astrophys. J.*, Vol. 155, 1969c, p. L149.
- Verschuur, G. L.: Further Measurements of the Zeeman Effect at 21 Centimeters and Their Limitations. *Astrophys. J.*, Vol. 161, 1970, p. 867.
- Wallace, L.: Analysis of the Lyman-Alpha Observations of Venus Made From Mariner 5. *J. Geophys. Res.*, Vol. 74, 1969, p. 115.
- Wallis, M.: Transonic Deceleration of the Solar Wind Via Planetary, Cometary or Interstellar Gas. Preprint, 1971.
- Wang, J. R.: Dynamics of the Eleven-Year Modulation of Galactic Cosmic Rays. *Astrophys. J.*, Vol. 160, 1970, p. 261.

- Wax, R. L.; Simpson, W. R.; and Bernstein, W.: Large Fluxes of 1-keV Atomic Hydrogen at 800 km. *J. Geophys. Res.*, Vol. 75, 1970, p. 6390.
- Webber, W. R.: On the Relationship Between Recent Measurements of Cosmic Ray Electrons, Nonthermal Radio Emission From the Galaxy, and the Solar Modulation of Cosmic Rays. *Austral. J. Phys.*, Vol. 21, 1968, p. 845.
- Weber, E. J.; and Davis, L., Jr.: The Angular Momentum of the Solar Wind. *Astrophys. J.*, Vol. 148, 1967, p. 217.
- Wentzel, D. G.: The Propagation and Anisotropy of Cosmic Rays, 1. Theory for Steady Streaming. *Astrophys. J.*, Vol. 156, 1969, p. 303.
- Werner, M. W.; and Harwit, M.: Observational Evidence for the Existence of Dense Clouds of Interstellar Molecular Hydrogen. *Astrophys. J.*, Vol. 154, 1968, p. 881.
- Werner, M. W.; Silk, J., and Rees, M. J.: Heating of H<sub>I</sub> Regions by Soft X-rays, II. The Effect of Galactic Soft X-ray Sources. *Astrophys. J.*, Vol. 161, 1970, p. 965.
- Weymann, R.: Coronal Evaporation as a Possible Mechanism for Mass Loss in Red Giants. *Astrophys. J.*, Vol. 132, 1960, p. 380.
- Wilcox, J. M.: The Interplanetary Magnetic Field, Solar Origin and Terrestrial Effects. *Space Sci. Rev.*, Vol. 8, 1968, p. 258.
- Wilcox, J. M.; and Ness, N. F.: Quasi-Stationary Corotating Structure in the Interplanetary Medium. *J. Geophys. Res.*, Vol. 70, 1965, p. 5793.
- Williams, R. E.: The Size of a Solar HII Region. *Astrophys. J.*, Vol. 142, 1965, p. 314.
- Wilson, O. C.: A Suggested Mechanism for the Ejection of Matter From M-Type Stars. *Astrophys. J.*, Vol. 131, 1960, p. 75.
- Wilson, R.; and Boksenberg, A.: Ultraviolet Astronomy. *Ann. Rev. Astron. Astrophys.*, Vol. 7, 1969, p. 421.
- Wolfe, J. H.; Silva, R. W.; and Myers, M. A.: Observations of the Solar Wind During the Flight of Imp 1. *J. Geophys. Res.*, Vol. 71, 1966, p. 1319.
- Yoshida, S.; Ogita, N.; and Akasofu, S.-I.: Cosmic Ray Variation and the Interplanetary Sector Structures. Submitted to *J. Geophys. Res.*, 1971.
- Young, J. M.; Carruthers, G. R.; Holmes, J. C.; Johnson, C. Y.; and Patterson, N. P.: Detection of Lyman- $\beta$  and Helium Resonance Radiation in the Night Sky. *Science*, Vol. 160, 1968, p. 990.

## DISCUSSION

*C. P. Sonett* For the distant solar wind the energy density decreases as  $1/r^2$  at least. At great distance, say a hundred astronomical units, a simple calculation suggests that the galactic cosmic ray energy density exceeds that of the solar wind. The cosmic ray gas is, of course, an extremely hot gas and it is hard to visualize a supersonic flow in such a gas. Now, for the mixture of these two gases (solar wind and cosmic rays) is it still likely that one can talk about some kind of shock transition?

*W. I. Axford* I think it is quite reasonable to treat the two gases separately at least as a first approximation, since the coupling is not very strong. One sees plenty of shock waves in the interplanetary medium moving through the cosmic ray gas. A strong shock does affect the cosmic rays noticeably, but I do not think the shock wave itself is much affected. I described these effects briefly at the end of my talk: as the termination of the supersonic solar wind flow is approached we expect that the intensity of cosmic rays will gradually increase to the interstellar level and then remain roughly constant in the subsonic region. There may be some acceleration of low energy cosmic rays at the shock as discussed by Jokipii [*Astrophys. J.*, 152, 799, 1968], but the more energetic cosmic rays do not seem to be noticeably affected. If this acceleration of low energy particles is significant and the unmodulated energy density of low energy cosmic rays is much larger than observed near the earth (which is possible) then one definitely would have to take into account the effect of the cosmic rays on the shock wave. Nevertheless there should still be a shock wave of sorts even if it is somewhat smeared out.

*C. P. Sonett* It's true from a structural standpoint, since the gyroradii are larger than the solar system, but there are still  $\mathbf{J} \times \mathbf{B}$  forces so I'm not sure that one can completely ignore the fact that the cosmic ray gas has an enormous temperature.

Another question is in relation to Geiss' comment regarding the ratio  $^4\text{He}/^3\text{He}$ . The values that he showed for the Apollo samples were 1860–2720, while the value for



certain classes of meteorites was about 4000. I wonder, in view of what you said this morning, whether the  $^3\text{He}$  gradient might be such that the density is higher farther out. This class of meteorites have spent most of their lives outside 1 AU and perhaps that would account for the concentration.

*W. I. Axford* I think that the  $^3\text{He}$  concentration in meteorites could be expected to differ from that found in the lunar samples, since the latter are saturated with solar wind gases, whereas meteorites have the outer layers (which should also contain solar wind material) ablated away. Presumably the  $^3\text{He}$  concentration in meteorites is affected by cosmic ray implantation and spallation, and any other  $^3\text{He}$  deep within the meteorites must be primordial in some sense. There is a radial gradient in the density of interstellar  $^3\text{He}$ , but the density within 10 AU is less than that of the solar wind, and of course the particle energy is very much less. I doubt that interstellar  $^3\text{He}$  could be important as far as the interior of meteorites is concerned, and it seems unlikely that it could have much effect on the concentrations in lunar dust.

*C. P. Sonett* Also, there's the component from charge exchange.

*W. I. Axford* With the presently accepted values for the density of interstellar gas near the sun, I doubt that this could double the  $^3\text{He}$  content anywhere in the solar wind within 100 AU from the sun.

*J. R. Jokipii* I would like to comment on Dr. Sonett's point and then ask a question. It seems to me that if there are regions where the pressure of the cosmic rays is great enough, then the cosmic rays will indeed affect the supersonic or the subsonic nature of the gas. I'm not sure whether this will ever happen or not.

*W. I. Axford* Yes, it can in principle (see p. 645), but the answer depends upon how well the cosmic ray gas is coupled to the solar wind gas, and we have no way of determining this without actually exploring the termination region.

*J. R. Jokipii* Then one must consider the effect of sound waves actually being propagated through the cosmic ray gas. The sound speed is essentially the total pressure divided by the density, provided only that the wavelengths are long enough that the cosmic rays and plasma are coupled. We're talking about 0.01 to 0.1 AU, which is the cyclotron radius of a typical cosmic ray and this is small on this scale. Anyway, that's just the comment. The question I have concerns the interstellar density of hydrogen. Presumably your value is not intended to be an average for the interstellar density of hydrogen. It seems to me from some work of Parker and perhaps previous work of others that there is trouble with the virial theorem if the density of matter is too low.

*W. I. Axford* That is a problem and, of course, people have been searching for the extra mass for many years. But the mass of neutral hydrogen would not be enough even if the number density was as much as  $1\text{ cm}^{-3}$ . My assumed value of  $0.1\text{ cm}^{-3}$  is not necessarily the general density, but it appears to be very close to the local value (within  $\sim 100\text{ pc}$ ). As far as the "missing mass" is concerned, there simply is not enough atomic hydrogen in the galaxy to matter, and there are observations which suggest that the total amount of molecular hydrogen is also not significant in this respect. The only suggestion that seems to work is that the missing mass is in the form of black holes — which has the nice feature of being almost impossible to reject on observational grounds. As far as the confinement of cosmic rays within the galaxy is concerned, I think we must begin to revise our models for the behavior of cosmic rays, perhaps by considering "galactic wind" type models in which there is more emphasis on "flow" rather than "leakage" of the cosmic ray gas out of the galaxy.

*J. C. Brandt* About the mass of the galaxy, that has been missing for decades, I don't think that it's time to get too worried about it. But there are large areas in the galaxy where the number density is apparently  $0.1/\text{cm}^3$  and I think we just have to live with that.

*M. Dryer* I have a question about the term "shock wave." Whenever we hear the term we think of Rankine-Hugoniot conditions, and we happily make comparisons between these conditions, including magnetic effects, and observations. Are we still talking about the same kind of thin layer in this context, that is, need we worry about these things on this scale, or will the meaning of the word "shock wave" be less well-specified in this context?

*W. I. Axford* I don't see why there should be any problem at all. The scale of the system is very large — 100 AU. As long as there is some mechanism which will make the shock look "thin" on this scale the Rankine-Hugoniot conditions must be satisfied. Since these represent conservation of mass, momentum and energy, there can hardly be much wrong with them. However, one might worry about the effective value of the ratio of specific heats, which appears prominently in the Rankine-Hugoniot relations. I doubt that the number of degrees of freedom can differ significantly from 3 per particle, but electron heat conduction could have a noticeable effect on the transition, as it presumably does in the case of shocks observed in the vicinity of the earth.

*C. P. Sonett* Would you care to comment on the time-dependent problem, for example, the time-dependent problem that would arise because of the motion of the heliosphere through the local arm. This part of the galaxy is very spotty with clouds and as the solar system moves through it, the background density varies, the field direction changes, and so on. Specifically, how does the information on a change in boundary then propagate back into the solar system or heliosphere?

*W. I. Axford* The "relaxation" time for the system to reach equilibrium is of the order of the time the solar wind takes to get to the terminating shock wave. Since the solar wind travels an astronomical unit every 4 days, the time scale for the system to reach equilibrium is about a year. This is short compared with any possible time scale for changes occurring outside the solar system. At a number density of  $0.1 \text{ cm}^{-3}$ , the mean free path is about  $10^{17} \text{ cm}$ . At 20 km/sec, which is roughly the velocity of the interstellar gas past the sun, an interval of  $5 \cdot 10^{10} \text{ sec}$  is required for a "cloud" with a scale size equal to one mean free path to go past the solar system. So a cloud which is only one mean free path across takes about 2000 years to go past the sun at this speed. If you take 1000 mean free paths for the size of an interstellar cloud, one sees that the heliosphere should be stationary over time scales of a million years.

*C. P. Sonett* Is that true also for the wave field? Supposing there were a wave field on the outside, as we suspect there probably is.

*W. I. Axford* Well, the waves that I would imagine to be important are Alfvén waves. The Alfvén speed is also quite small, something like 30 km/sec, so the time scale is still going to be of the order of  $10^6$  years if the wavelengths are comparable to cloud dimensions.

## OBSERVATION OF LYMAN- $\alpha$ EMISSION IN INTERPLANETARY SPACE

J. L. Bertaux and J. E. Blamont

The extraterrestrial Lyman- $\alpha$  emission was mapped by the OGO 5 satellite, when it was outside the geocorona. Three maps, obtained at different periods of the year, are presented and analyzed. ABSTRACT

The results suggest that at least half of the emission takes place in the solar system, and give strong support to the theory that in its motion towards the apex, the sun crosses neutral atomic hydrogen of interstellar origin, giving rise to an apparent interstellar wind.

### INTRODUCTION

At our request, OGO 5 was temporarily placed in a special spinning mode on three occasions: 12–14 September 1969, 15–17 December 1969, and 1–3 April 1970. These spinup operations, referred to as SU 1, SU 2, and SU 3, respectively, took place when OGO 5 was well outside the geocorona (above 90,000 km altitude).

Two different experiments on board OGO 5 were able to map the Lyman- $\alpha$  background from these maneuvers. One was the two-channel photometer of C. Barth and G. Thomas, from the Laboratory for Atmospheric and Space Physics, University of Colorado, which will be referred to as the LASP instrument [Thomas and Krassa, 1971]. The other was a monochromatic photometer built at the Service d'Aéronomie du Centre National de la Recherche Scientifique, referred to as the Paris instrument [Bertaux and Blamont, 1970].

Although based on different principles and independently operated, both instruments provided the same results. Data were analyzed independently and compared after completion of the analysis. We use the Paris data here since their agreement with LASP data is excellent, but for a difference in calibration of about 25 percent, and they give essentially the same information.

### DESCRIPTION OF THE DATA

The extraterrestrial Lyman- $\alpha$  emission could be provided by the free atoms of hydrogen in *interstellar space*, which are excited by light emission of the stars at the wavelength of Lyman- $\alpha$ . Then it is expected that they would absorb and re-emit Lyman- $\alpha$  photons. This emission could have two possible angular distributions:

1. The emission could come directly from the distant parts of the galaxy. Because of Doppler shifting, the emission would not be completely absorbed by the interstellar hydrogen. Then a map of this Lyman- $\alpha$  ( $\pm 40\text{\AA}$ ) hydrogen emission would coincide with a map of the galaxy. This is the interpretation of the observations of Mariner and Venera given by Barth, [1970] and Kurt and Dostovalov [1968], and it can be termed the *anisotropic galactic distribution*.
2. The emission of the distant parts of the galaxy could be completely absorbed and re-emitted far away from the solar system and the anisotropy of the source would be completely obliterated; around the solar system the interstellar hydrogen would scatter the remnants of this Lyman- $\alpha$  emission, resulting in an *isotropic distribution* of Lyman- $\alpha$  at the solar system.

The first distribution must be rejected on the basis of our data, but the second distribution, corresponding to a maximum intensity of 200  $R$ , cannot be completely ruled out. Superimposed on this emission, a strong emission due to scattering of the solar Lyman- $\alpha$  radiation by the hydrogen of the interplanetary space is to be expected.

---

The authors are at Centre National de la Recherche Scientifique Service D'Aéronomie, 91-Verrières-Le-Buisson, Paris, France.

## SU 1 RESULTS

When plotted in celestial coordinates in which  $\alpha$  is the right ascension and  $\delta$  is the declination (fig. 1), the emission shows the following features.

1. There are no small-scale emission features apparent except a diffuse glow covering the whole celestial sphere with an intensity varying slowly with the direction of observation.
2. There is no apparent symmetry to the galactic plane.
3. A maximum of intensity of 500  $R$  originates from the region  $230^\circ < \alpha < 250^\circ$ ,  $0^\circ > \delta > -40^\circ$ . The center of this maximum is not far away from the plane of the ecliptic.
4. A deep minimum of 200  $R$  is located in the region  $0^\circ < \alpha < 80^\circ$ ,  $40^\circ > \delta > 0^\circ$ . The center of this minimum is not far from the plane of the ecliptic, and is located in the region  $40^\circ < \alpha < 60^\circ$ ,  $20^\circ < \delta < 40^\circ$ .

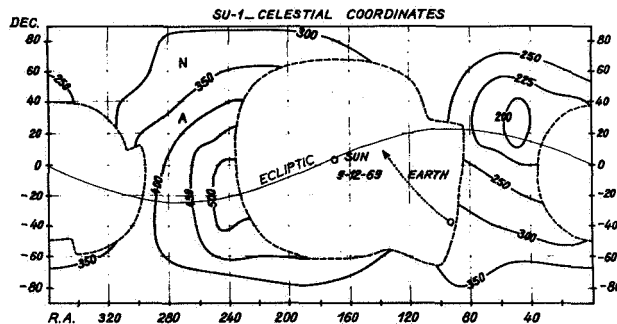


**Figure 1** Contour map of the Lyman- $\alpha$  intensity in celestial coordinates for SU 1. Contour curves are graduated every 50  $R$ . The dotted line represents the movement of the earth as seen from OGO 5. The dashed line is the limit of the area covered on the sky during SU 1, after removal of geocoronal measurements. The letter A indicates the position of the apex; the letter N indicates the position of the ecliptic north pole.

When the signal is plotted in galactic coordinates (fig. 2), it becomes even more obvious that the galactic plane is not a privileged emission area, since the minimum already described extends over the galactic equator between the galactic longitudes of  $130^\circ$  to  $180^\circ$ , and the maximum located in longitude near the galactic center is displaced toward  $20^\circ$  N of galactic latitude. Then the galactic origin of the Lyman- $\alpha$  emission observed by the Venera and Mariner spacecraft becomes extremely doubtful.

### The Emission Minimum

Figure 2 shows no obvious anisotropic emission that could be directly attributed to a distant part of the

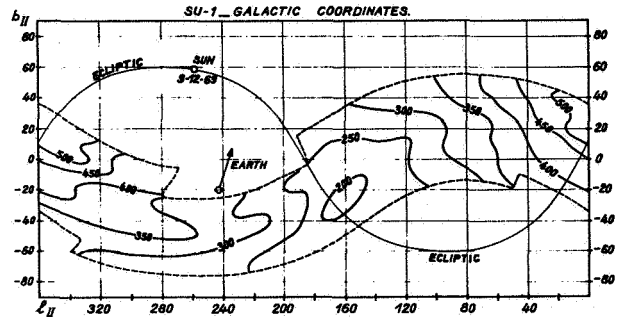


**Figure 2** Contour map of Lyman- $\alpha$  intensity in galactic coordinates for SU 1;  $l_{II}$  is the galactic longitude measured from the direction of the galactic center;  $b_{II}$  is the galactic latitude. The dotted line represents the movement of the earth as seen from OGO 5. There is no evident correlation between intensity and regions of low galactic latitude.

galaxy; thus, the 200  $R$  observed at the minimum must have another origin — a source inside or near the solar system. Since the direction from which the minimum is observed is not *a priori* privileged, an intensity of at least 200  $R$  must be available in all directions arising from a relatively local source and if there is any distant galactic source, it will have to be superimposed on these 200  $R$ .

### The Emission Maximum

This feature, which coincides both in intensity and situation with the emission observed by Barth, Kurt, and others, originates from a region that is: (1) broadly centered around the constellation of Sagittarius, (2) broadly centered around the ecliptic plane, and (3) distant by  $50^\circ$  from the direction of the solar apex.

### Interpretation

Two explanations can be given for the experimental results of SU 1: (1) There is a local background of about 200 to 250  $R$  and an emission originating from the direction of Sagittarius with an intensity of no more than 50 to 100  $R$  corresponding to the enhancement measured in this region; or (2) there is no galactic emission observed but a local (interplanetary or near the solar system) emission with a symmetry more or less related to the ecliptic plane where both the maximum and the minimum are situated, with the maximum lying  $50^\circ$  away from the apex.

## SU 2 RESULTS

The data obtained during SU 2 provide information on the part of the celestial sphere that could not be observed during SU 1 (fig. 3). The SU 2 data essentially

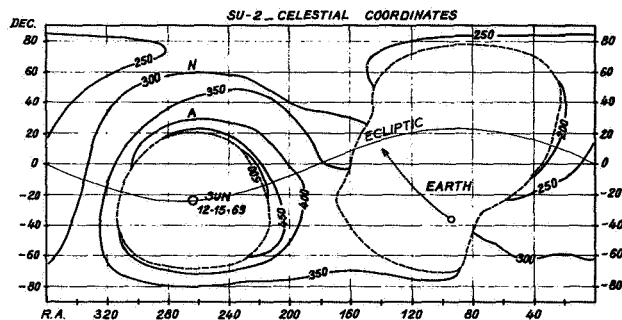


Figure 3 Contour map of the Lyman- $\alpha$  intensity in the celestial coordinates for SU 2.

confirm the results obtained with SU 1; no small-scale emission features appear; there is no privileged situation near the galactic equator.

No noticeable new features appear from these data. The center of both the maximum and the minimum discovered during SU 1 is situated in the part of the sky not observable with the spacecraft configuration and maneuvers during December 1969; however, the SU 2 observations cover regions of strong and weak intensities that continue the regions of the maximum and minimum of SU 1.

The large intensity regions (500 to 400 R) appear near the sun ( $\alpha \sim 220^\circ$ ,  $+10^\circ > \delta > -20^\circ$ ) and extend over a part of the sky not observed before ( $\alpha > 180^\circ$ ,  $-10^\circ > \delta > -50^\circ$ ). The weak-intensity region continues the weak region of SU 1 around  $\delta = +30^\circ$ ,  $-40^\circ > \alpha > 0^\circ$  with the absolute minimum of less than 200 R at  $30^\circ > \alpha > 20^\circ$ ,  $50^\circ > \delta > 0^\circ$ .

SU 2 did not produce startling new results, essentially because the position of the sun near the maximum of emission was not very favorable; however, it was essential to confirm the situation described by the SU 1 data and complete the sky mapping.

### SU 3 RESULTS

The SU 3 data provide essentially the same map as SU 1 and confirm the earlier findings as described above (fig. 4): the absence of small-scale features, absence of galactic predominance over the distribution of the emission, presence of a maximum of emission of 450 R and of a minimum of emission around 200 R.

However, a new fact of prime importance emerges from the SU 3 data. The maximum and the minimum were not situated in the same direction as they were during SU 1. The coordinates of the maximum are now  $\alpha = 290^\circ \pm 5^\circ$ ,  $+15^\circ > \delta > -15^\circ$ . From SU 1 to SU 3, the direction of the center of the maximum region changed from  $\alpha = 240^\circ$ ,  $\delta = -20^\circ$  to  $\alpha = 290^\circ$ ,  $\delta = -10^\circ$ , representing

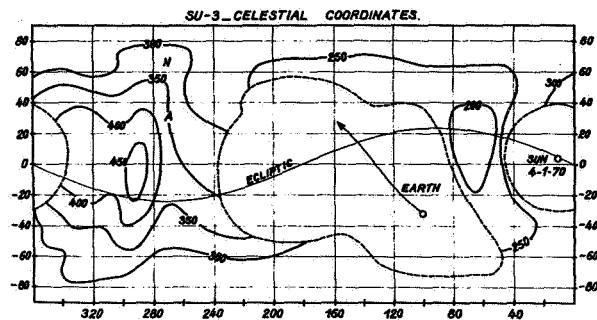


Figure 4 Contour map of the Lyman- $\alpha$  intensity in the celestial coordinates for SU 3.

a displacement of  $50^\circ$  on the celestial sphere; the direction of the center of the minimum region changed from  $\alpha = 50^\circ$ ,  $\delta = 30^\circ$  to  $\alpha = 60^\circ$ ,  $\delta = 20^\circ$ , representing a displacement of only  $\sim 10^\circ$ .

The difference between the two sets of measurements is the position of the earth in its orbit, and the displacement of the maximum could be very well interpreted as a parallax effect when the earth moved by 2 AU between SU 1 and SU 3. In this case, the distance to the sun of the region where the maximum of Lyman- $\alpha$  emission appears would be of the order of 2.5 AU. The direction of this region, as seen from the sun, would be  $\alpha = 265^\circ$ ,  $\delta = -15^\circ$ . From this parallax effect we would expect a displacement of the minimum from SU 1 to SU 3 in the opposite direction that the one which was measured ( $\sim 10^\circ$ ). However, the direction of such a small displacement should not be considered very significant, for it is difficult to accurately draw isophotes in a region where the gradient of emission is very low. What is more significant is that the displacement of the minimum, if any, is small ( $< 10^\circ$ ), indicating that the zone of emission in the direction of the minimum is at least at 15 AU.

### COMPARISON OF SU 1, SU 2, AND SU 3 DATA ORIGINATING FROM ONE REGION

The Paris instrument observed a region clear of parasitic sources during all three maneuvers, the region of the north ecliptic pole, indicated by the letter N on the celestial maps. The emission of the south pole was contaminated by geocoronal emission. The intensity originating from the north ecliptic pole during each maneuver was for SU 1, 320 R; SU 2, 280 R; and SU 3, 330 R. The relevant fact is the lower intensity at SU 2. The geometry of the situation is given by figure 5 where the intensity of Lyman- $\alpha$  in the region of the maximum has been represented over a celestial sphere. If this intensity originated from a distant isotropic source, the direction of observation of the north ecliptic pole would be

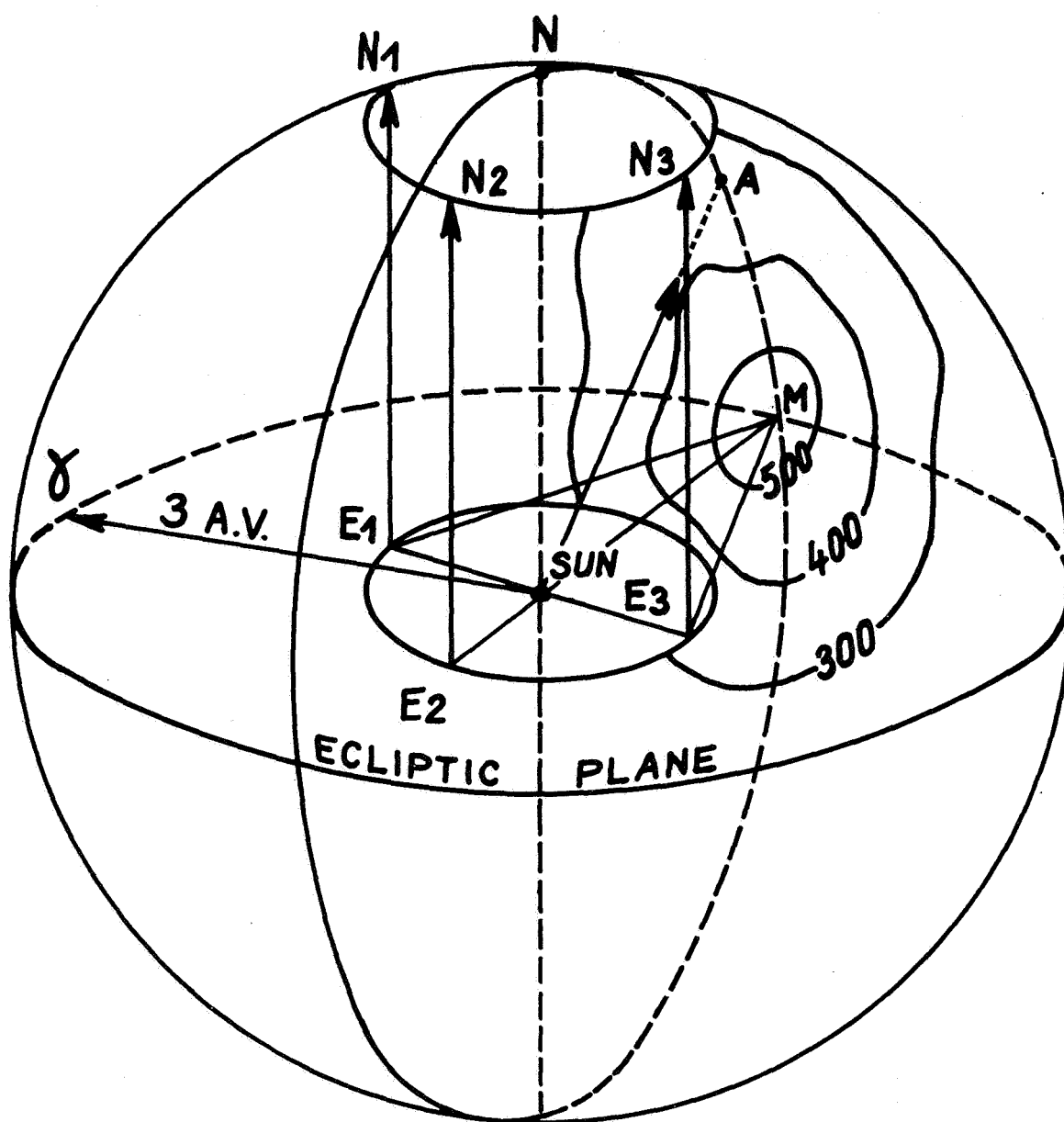


**Figure 5**  $E_1$ ,  $E_2$ , and  $E_3$  are the positions of the earth on its orbit around the sun, respectively, for SU 1, SU 2, and SU 3. Contour map of the maximum region is projected on the inside surface of a sphere of 3 AU of radius. The direction of first point of Aries is  $\gamma$ ;  $M$  is the approximate location of the center of the maximum region;  $A$  is the direction of apex;  $N$  is the direction of north ecliptic pole. The intersections  $N_1$ ,  $N_2$ , and  $N_3$  are with the sphere of lines of sight in the direction of north ecliptic pole when the earth was in  $E_1$ ,  $E_2$ , and  $E_3$ , respectively.  $N_2$  is farther away from  $M$  than  $N_1$  and  $N_3$ .

equal for the three observations. On the other hand, should the source be near the orbit of the earth, for instance localized on a sphere of radius 3 AU, the north pole direction of observation at SU 2 would correspond

to an intersection with this sphere farther from the position of the maximum than at SU 1 and SU 3, and they would correspond to a weaker intensity, as is found experimentally. This comparison directly confirms the

proximity of the emission maximum, which is independent of the first evidence related only to SU 1 and SU 3 observations.

## DISCUSSION

The heliosphere — the region of undisturbed solar wind extension — moves toward the direction of the apex  $\alpha = 270^\circ$ ,  $\delta = +30^\circ$  with a velocity of 20 km/sec, through the interstellar medium, which contains a certain number of hydrogen atoms/cc and possibly protons if the solar system is embedded in a *HII* region.

A shock front [Axford *et al.*, 1963] is produced at the boundary in the forward direction of the heliosphere due to the reaction of the solar wind against the galactic magnetic field and charge-exchange collisions with the interstellar neutral hydrogen. The distance of the outer part of the shock front to the sun is not well known, but could be anywhere from 20 to 80 AU.

The interstellar ("cold") hydrogen and part of the hydrogen created from the solar wind protons by charge exchange ("hot" component) penetrate into the heliosphere from the boundary that constitutes a source, which has been considered among others by Patterson *et al.* [1963], Dessler [1967], Hundhausen [1968], and Blum and Fahr [1970].

Blum and Fahr have shown that the major part of the hydrogen penetrating inside the solar system must be assigned to the cold component, which then defines an interstellar wind characterized by the macroscopic motion of the interstellar medium relative to the sun in the vicinity of the heliosphere — that is, a direction, a hydrodynamic velocity, and a hydrogen number density. When moving toward the sun, the number density of hydrogen atoms decreases because of photoionization by the EUV solar radiation and charge exchange with solar wind components. Blum and Fahr [1970] have computed the hydrogen density distribution as a function of the distance to the sun, taking into account the focusing effect of the solar gravitational field but not the Lyman- $\alpha$  radiation pressure, which is nearly equal to the gravitation, or might even compensate for it. This is a point that must be corrected.

Then using this distribution of hydrogen, Fahr has computed the Lyman- $\alpha$  emission to be observed. The Lyman- $\alpha$  measurements provide information only on the interstellar wind and not on the hot component; not only does the hot component correspond to a small number density compared to the density of the cold hydrogen, but it has a velocity of the order of 300 km sec<sup>-1</sup>, producing Doppler shifts up to 1.2 Å (depending on the direction of travel), to be compared with the half width of the exciting solar line of 0.5 Å. It

must also be remarked that one should be careful when deriving densities of neutral hydrogen from extraterrestrial Lyman- $\alpha$  observations. When doing the calculations, it is generally admitted that the solar Lyman- $\alpha$  profile is flat. However, according to the measurements of Bruner and Parker [1969], the solar Lyman- $\alpha$  line is deeply self reversed. The Doppler effect of cold atoms moving with a speed of 20 to 30 km/sec relative to the sun will shift the resonance wavelength by 0.12 Å, from the bottom of the reversal to one side of the reversal, increasing the useful resonant flux by at least 20 percent. Notwithstanding, by normalizing the Blum and Fahr [1970] theoretical results with the 160 R of Lyman- $\alpha$  emission measured by Chambers *et al.* [1970] in the apex direction from the Vela 4 spacecraft at 110,000 km of altitude in 1967, Fahr obtained a density of 0.06 cm<sup>-3</sup> for the interstellar wind. This wind penetrates deeply because the loss mechanism is not very strong. Blum and Fahr find a penetration distance, depending on the density of the interstellar wind, of the intensity of the solar EUV radiation and of the intensity of the solar proton flux, which varies from 1 AU at low solar activity to 7 AU for large solar activity.

In this model, the Lyman- $\alpha$  emission due to this interstellar wind would present a maximum in the direction of the velocity of the solar system relative to the surrounding medium, because it is in this direction that a maximum of density of interplanetary hydrogen would arise; a minimum would arise in the opposite direction where the interstellar hydrogen has been swept by the passage of the sun and consequently the hydrogen density reduced to a low value, in such a way that the cavity extends farther in the aft region of the heliosphere than in the forward direction (possibly to 60 AU) if solar radiation pressure is taken into account.

Then it is obvious that this model of Lyman- $\alpha$  emission is compatible with the data which are characterized by the existence of a broad maximum and a broad minimum, and by a position of the maximum at a distance from the sun not greater than 2 to 4 AU when the solar activity is on the high side.

It is interesting to note [Tinsley, 1971] that the emission rate per unit volume in the apex direction can be written as

$$S = g_{12} n_O (r_E/r)^2 \exp(-r_O/r)$$

where

$n_O \exp(-r_O/r)$  is the radial distribution of density in the apex direction if  $n_O$  is the density at infinity and the penetration distance  $r_O = 4$  AU according to Blum and Fahr [1970].

$g_{12}$  is the number of Lyman photons scattered per atom per sec for hydrogen at 1 AU.

$(r_E/r)^2$  is the inverse square decrease of solar Lyman- $\alpha$  intensity normalized at the earth.

Then  $S_{max}$  is obtained for  $dS/dr = 0$  or  $r = r_0/2 = 2$  AU. This agreement is surprisingly good. However, the direction of the maximum does not coincide with the solar apex, as would be expected from this model, but rather coincides with the projection of the apex direction on the ecliptic plane and is a vector located at the intersection of the ecliptic plane and of the galactic plane — that is, a vector contained in both these planes. We are therefore left with two possible explanations:

First, the direction of the maximum coincides with the direction of the velocity of the solar system relative to the ambient. Then, since the direction of the motion of the solar system is well known, the medium surrounding the heliosphere must move at an angle of  $50^\circ$  to the apex direction as seen from the sun. This displacement of the interstellar hydrogen around the heliosphere takes place in the galactic plane in the sense inverse to the displacement of the heliosphere. There is nothing wrong with this explanation, but the coincidence of the direction of the interstellar wind vector with the ecliptic plane is surprising. If this explanation proved to be correct, it might have some implications for the origin of the solar system.

Second, the direction of the maximum is not directly related to the direction of the interstellar wind but to the real maximum of the distribution of interplanetary hydrogen (in contrast to the Blum and Fahr model). The density, for some reason yet unknown, would present a symmetry to the ecliptic plane with a maximum in this plane. Note that a shift of the maximum from the apex would be caused by the interplanetary magnetic field since the interstellar wind would be more attenuated in the direction of field lines if they channel a flow of solar wind plasma [Parker, 1963]. Our observation of the maximum could be explained by the interaction of the interstellar wind coming from the apex with a preferential flow of solar wind plasma created by a symmetry of the interplanetary magnetic field to the ecliptic plane far from the sun. We would then only observe secondary properties of the interstellar wind — that is, properties of the interstellar wind after its interaction with this anisotropic component. However, it would be difficult to explain the direction of the minimum near the ecliptic plane, and the first hypothesis consequently appears more plausible.

## CONCLUSION

The data presented in this paper can be described as follows:

1. The Lyman- $\alpha$  hydrogen emission observed from outside the geocorona shows no enhancement or diminution in the galactic plane.
2. The emission has a smooth variation from a maximum region of  $500 R$  to a minimum region of  $200 R$ .
3. The direction of the maximum changes by  $50^\circ$  between September and March; then the region where the maximum originates is situated near the earth at about 2 AU.
4. The direction of the maximum coincides with the intersection of the galactic plane and the ecliptic plane.
5. The region where the minimum originates is situated at 15 AU at least.
6. The direction of the minimum is roughly opposite to the direction of the maximum.

These data are consistent with the following alternate interpretations:

1. The galactic component has an intensity less than  $50 R$ ; then all the emission observed is due to hydrogen present in the solar system (varying from 500 to  $200 R$ ).
2. The galactic component has an intensity up to  $200 R$  and is isotropic; then the interplanetary component varies from 300 to  $50 R$  or less.

Whatever the value attributed to the galactic component, the interplanetary component can be interpreted as due to: (1) an interstellar wind with a velocity vector located in the ecliptic and in the galactic plane and not in the apex direction; or (2) an interstellar wind in the apex direction interacting with a solar wind whose symmetry is not radial but ecliptic.

## REFERENCES

- Axford, W. I.; Dessler, A. J.; and Gottlieb, B.: Termination of Solar Wind and Solar Magnetic Field. *Ap. J.*, Vol. 137, 1963, p. 1268.
- Barth, C. A.: Mariner 6 Measurements of the Lyman-Alpha Sky Background. *Ap. J. (Letters)*, Vol. 161, 1970, p. L181.
- Bertaux, J. L.; and Blamont, J. E.: OGO-5 Measurements of Lyman-Alpha Intensity Distribution and Line-width up to 6 Earth Radii. *Space Res.*, Vol. 10, 1970, p. 591.
- Blum, P. W.; and Fahr, H. J.: Interaction Between Interstellar Hydrogen and the Solar Wind. *Astr. Astrophys.*, Vol. 4, 1970, p. 280.



- Brumer, E. C.; and Parker, P. W.: Hydrogen Geocorona and Solar Lyman-Alpha Line. *J. Geophys. Res.*, Vol. 74, 1969, p. 107.
- Chambers, W. F.; Fehlan, D. E.; Fuller, J. C.; and Kruuz, W. E.: Anisotropic Atomic Hydrogen Distribution in Interplanetary Space. *Nature*, Vol. 225, 1970, p. 713.
- Dessler, A. J.: Solar Wind and Interplanetary Magnetic Field. *Rev. Geophys.*, Vol. 5, 1967, p. 1.
- Hundhausen, A. J.: Interplanetary Neutral Hydrogen and the Radius of the Heliosphere. *Planet. Space Sci.*, Vol. 16, 1968, p. 783.
- Kurt, V. G.; and Dostovalov, J. B.: Far Ultraviolet Radiation From the Milky Way. *Nature*, Vol. 218, 1968, p. 258.
- Patterson, T. N. L.; Johnson, F. S.; and Hanson, W. B.: The Distribution of Interplanetary Hydrogen. *Planet. Sp. Sci.*, Vol. 11, 1963, p. 767.
- Parker, E. N.: *Interplanetary Dynamical Processes*. Interscience Publishers, New York, 1963.
- Thomas, G. E.; and Krassa, R. F.: OGO-5 Measurements of the Lyman-Alpha Sky Background. *Astr. Astrophys.*, Vol. 11, 1971.
- Tinsley, B. A.: Extraterrestrial Lyman-Alpha. *Rev. Geophys. Sp. Phys.*, Vol. 9, 1971, p. 89.

# PROPERTIES OF NEARBY INTERSTELLAR HYDROGEN DEDUCED FROM LYMAN $\alpha$ SKY BACKGROUND MEASUREMENTS

G. E. Thomas

**ABSTRACT** For a sufficiently rapid relative motion of the solar system and the nearby interstellar gas, neutral atoms may be expected to penetrate the heliosphere before becoming ionized. Recent satellite measurements of the Lyman  $\alpha$  emission above the geocorona indicate such an "interstellar wind" of neutral hydrogen emerging from the direction of Sagittarius and reaching to within a few astronomical units of the sun. We present here a detailed model of the scattering of solar Lyman  $\alpha$  from the spatial distribution of neutral hydrogen in interplanetary space. This asymmetric distribution is established by solar wind and solar ultraviolet ionization processes along the trajectories of the incoming hydrogen atoms. The values of the interstellar density, the relative velocity, and the gas temperature are adjusted to agree with the Lyman  $\alpha$  measurements. The results may be interpreted in terms of two models, the "cold" model and the "hot" model of the interstellar gas, depending on whether galactic Lyman  $\alpha$  emission is present at its maximum allowable value or negligibly small. The cold model predicts densities between 0.03 and 0.06  $\text{cm}^{-3}$ , temperatures below a few hundred degrees K, and a wind velocity of about 10 km/sec. The hot model predicts densities between 0.09 and 0.12  $\text{cm}^{-3}$ , temperatures in the range  $10^3$  to  $10^4$  °K, and a wind velocity of about 6 km/sec. Since it is unlikely that any appreciable galactic emission is present, the results suggest that the solar system is within a large turbulent cell of hot tenuous gas, the so-called intercloud medium.

## INTRODUCTION

We are concerned with the small part of the energy emitted from the quiet sun that is dissipated in the local interstellar medium. This energy is mainly in the form of extreme ultraviolet radiation (EUV) below the Lyman continuum ( $\lambda < 911 \text{ \AA}$ ) and the fast-moving protons in the solar wind. The deposition of both types of energy results in ionization of the local medium. The interstellar neutral hydrogen, whose abundance is of the order of 90 percent, undergoes photoionization and charge exchange with solar wind protons. The spatial distribution of the resulting ionization about the sun is a sensitive function of the relative velocity of the sun and the local gas. For the special case of zero relative motion, an

extensive *HII* region will be formed similar to the classical Stromgren sphere. The radius of this region depends on the interstellar hydrogen density  $n_{\text{H}}$  and has been calculated by Williams [1965] to be  $\sim 1500 n_{\text{H}}^{-2/3}$  in AU. A balance between ionizations and recombinations is established on a time scale of the order of  $10^6$  years [Brandt, 1964].

For such a large time scale, it is a simple matter to show that a relative velocity of as little as 500 cm/sec can destroy this equilibrium state. For a relative velocity of the order of 1 km/sec or greater, the distribution of ionization may be described by a dynamic equilibrium [Blum and Fahr, 1970a]. The basis of this description is the probability of ionization  $P(\mathbf{r})$  of an interstellar hydrogen atom at the distance  $\mathbf{r}$  from the sun and is given by

$$P(\mathbf{r}) = \exp \left[ - \int_{\mathbf{r}}^{\infty} ds J(\mathbf{r}') / V_r(\mathbf{r}') \right] \quad (1)$$

---

The author is at the Department of Astro-Geophysics and the Laboratory for Atmospheric and Space Physics, University of Colorado, Boulder, Colorado.

where  $J(r')$  and  $V_r(r')$  are the total ionization rate and the relative velocity at the point  $r'$ . The integration is performed over the particle trajectory to the point  $r$ . The neutral density is calculated by adding up the contributions from all trajectories passing through the point. Detailed calculations have been performed by *Blum and Fahr* [1970a], hereafter referred to as BF, who show that for a relative velocity of 20 km/sec an asymmetrical ionization cavity is formed. The small dimension of the cavity lies in the forward direction of flow and is of the order of 1 to 5 AU, depending on solar activity.

The BF theory does not include the effects of the bow-shock termination of the solar wind, which probably occurs well outside the effective boundary of the ionization cavity [*Axford et al.*, 1963; *Hundhausen*, 1968; *Blum and Fahr*, 1969]. Blum and Fahr show that neutral hydrogen flows through this region with negligible interaction. The countereffect of the ionization cavity on the location of the shock front has been recently studied by *Semar* [1970]. His results suggest that this interaction is not likely to be important for the range of interstellar densities determined in this paper ( $0.03\text{--}0.12\text{ cm}^{-3}$ ). Accordingly, these regions may be considered as separate and independent and we will refer hereafter only to the ionization cavity.

How can such an ionization cavity be observed? It was first suggested by *Kurt* [1967] that the Lyman  $\alpha$  sky background emission represents the scattering of solar Lyman  $\alpha$  from beyond the cavity. *Kurt and Germogenova* [1967] calculated the diffuse radiation field within a spherical cavity surrounding the sun as a function of the cavity radius. Using the measured intensity of Lyman  $\alpha$  emission from the Venus probe Zond 1 of 75  $R$  ( $1R = 10^6/4\pi\text{ photons cm}^{-2}\text{-sec}^{-1}$ ) they obtained a value of 3500 AU.

The more recent Lyman  $\alpha$  measurements of *Chambers et al.* [1970] have been cited as evidence by *Blum and Fahr* [1970b] for their model of a cavity of much smaller dimensions. These measurements showed a smoothly varying Lyman  $\alpha$  emission with a maximum in the direction nearest the apex of the solar motion. (Hereafter we refer to this direction as simply the apex.) It is located at the coordinates  $RA = 270^\circ$ ,  $\delta = 30^\circ$  [*Allen*, 1964]. A minimum was observed at a direction about  $180^\circ$  from the maximum. As pointed out by Blum and Fahr this is the variation of scattered solar Lyman  $\alpha$  expected from hydrogen outside a cavity elongated in the direction of the apex. The inflowing hydrogen atoms would approach most closely in the direction of motion. They would be most likely to be ionized in the opposite (downwind) direction.

We have recently reported extensive Lyman  $\alpha$  background measurements taken from a spinning OGO satellite [*Thomas and Krassa*, 1971; *Bertaux and Blamont*, 1971]. Our intensity amps clearly show that the Lyman  $\alpha$  intensity reaches its greatest value in the direction  $RA \cong 263^\circ$ ,  $\delta = -22^\circ$ . (It is now clear that the measurements of *Chambers et al.* [1970] could not define its precise location but only a meridian of maximum brightness, since all their scans were made over a single great circle in the sky.) This suggests that the nearby hydrogen possesses its own peculiar velocity, which combined with the solar system apex motion produces the observed direction of the "interstellar wind."

When we compared two sets of measurements separated by an interval of 7 months, we discovered a parallax effect in the intensity distribution (recently confirmed from a preliminary examination of recent OGO data taken in September 1970). This finding is the most direct evidence of a nearby source of scattering and makes it possible to triangulate to determine the effective distance of the scattering region.

We will describe a theory of the distribution of hydrogen in the solar system, similar to that of Blum and Fahr, but including two important effects neglected by them. The first of these is the outward solar Lyman  $\alpha$  radiation pressure force, which nearly balances the inward gravitational force [*Wilson*, 1960; *Brandt*, 1961], causing the inflowing hydrogen atoms to pass the solar vicinity in straight-line trajectories. Furthermore, the velocities of the hydrogen atoms at all solar distances are unvarying and equal to the relative velocity of approach at infinity. This results in a considerable mathematical simplification of the theory. It also disposes of the necessity to account for the absence in all the measurements of a cusp-like feature predicted by BF as a result of gravitational focusing in the downwind direction.

The second effect we consider is that of a random (thermal) component of velocity in the interstellar medium. In the absence of gravitational focusing, the OGO measurements demand a considerable "filling-in" of the downwind direction. If this is not provided by an external source of diffuse emission from the galaxy, then a rather high temperature (up to  $10^4\text{ }^\circ\text{K}$ ) of the nearby medium is needed. As discussed in the final section, such a high temperature is in agreement with 21-cm measurements of the temperature of the low-density intercloud medium.

#### THE OGO DATA AND THE INFERRED MOTION OF THE LOCAL HYDROGEN

Figures 1 and 2 are maps of Lyman  $\alpha$  isointensity contours for the periods September 12-13, 1969 (SU 1) and

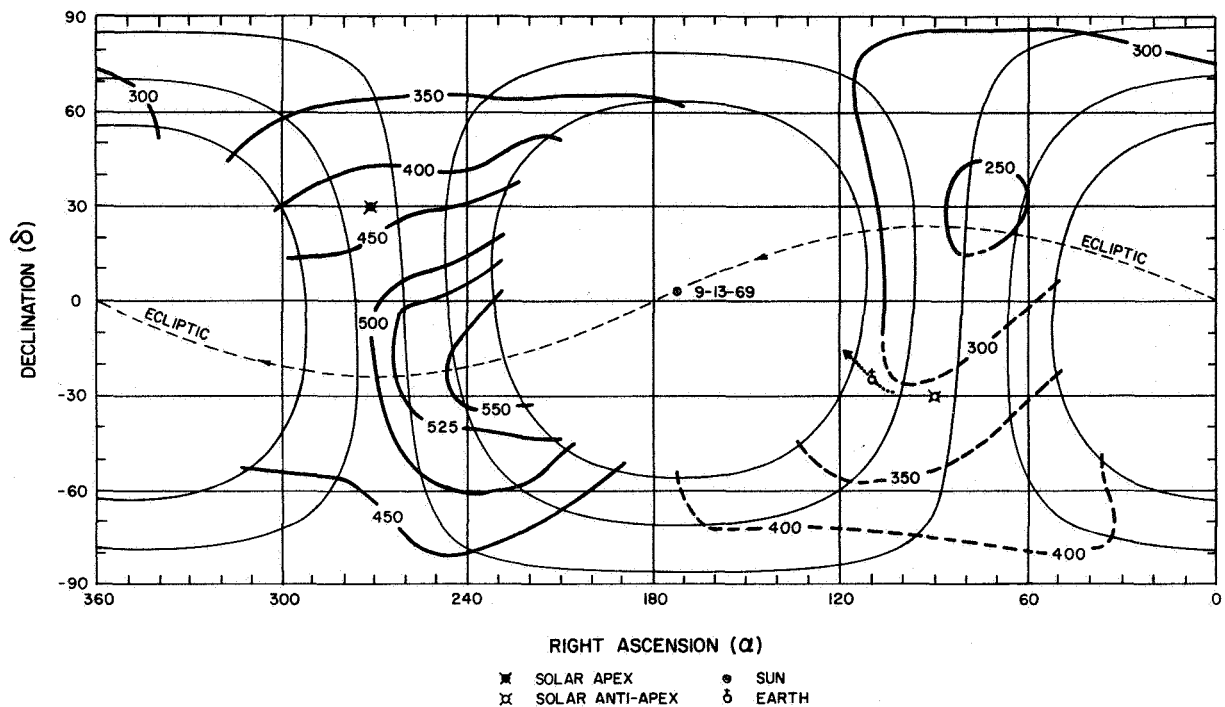


**Figure 1** LASP contour map of the  $L\alpha$  sky background in celestial coordinates for SU 1. The units labelling the contour lines are Rayleighs. The light curves indicate the paths of the field of view. The path of the earth between 2000 GMT, 12 September 1969, and 1000 GMT, 13 September 1969, as seen from the satellite is shown as a dotted line. The data used for constructing the map were all taken in this period. The dashed lines are the contour lines which have been interpolated beneath the geocorona.

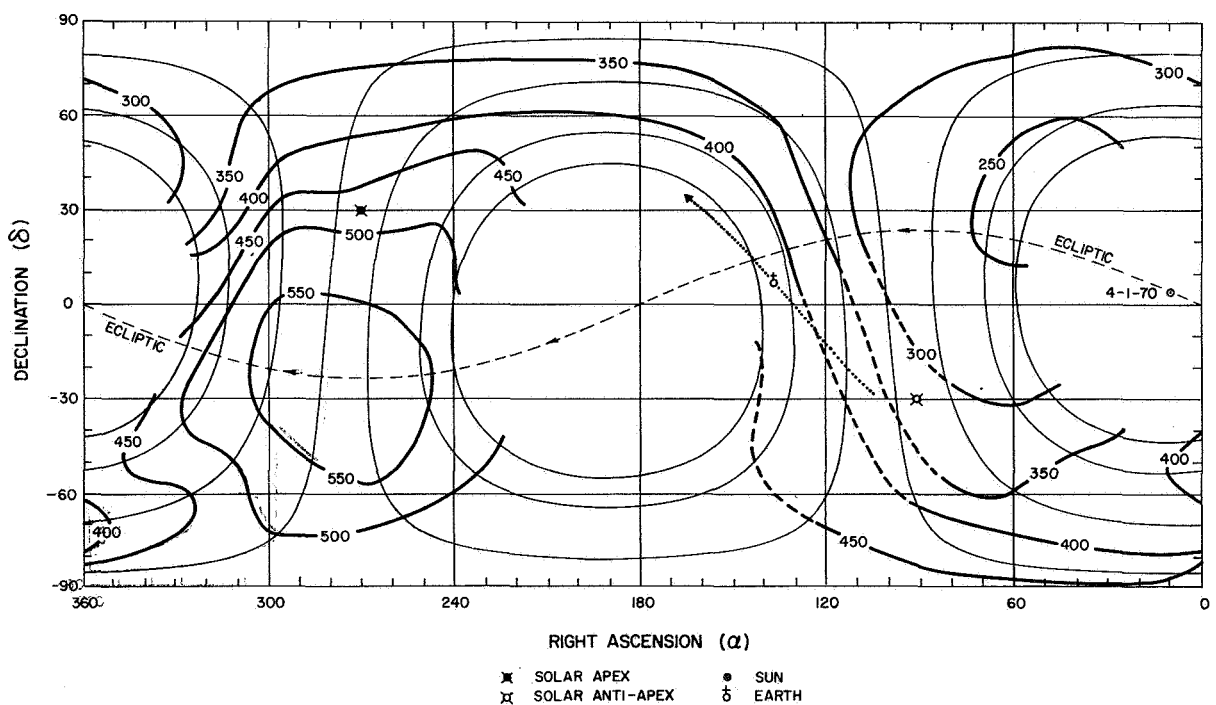


**Figure 2** Contour map of the  $L\alpha$  sky background in celestial coordinates for SU 3. The path of the earth is shown between 0600 GMT, 1 April 1970, to 2200 GMT, 2 April 1970.

April 1-2, 1970 (SU 3). These data were taken by the Laboratory for Atmospheric and Space Physics at the University of Colorado (LASP). The Paris maps [Bertaux and Blamont, 1971] are very similar. Figure 3 is a comparison of the two sets of data plotted along the ecliptic

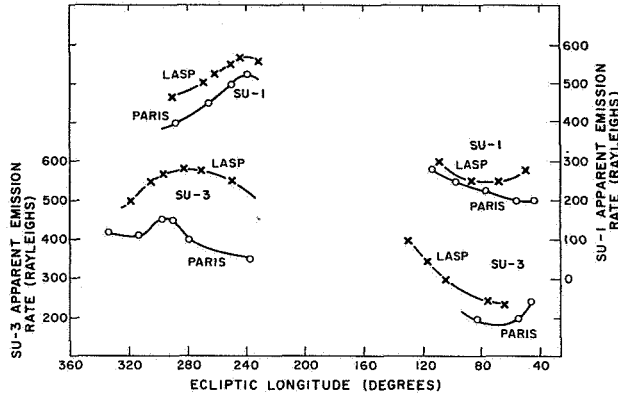


**Figure 3** The LASP and Paris Lyman  $\alpha$  data plotted along the ecliptic equator for the two spin-up periods SU 1 and SU 3.

equator. This plane passes very nearly through the points of maximum and minimum Lyman  $\alpha$  intensity and is a convenient coordinate plane for displaying the important spatial variations. We do not consider the overall disagreement of about 30 percent significant in view of absolute calibration difficulties in the ultraviolet. The discrepancies in the location and shape of the maximum and minimum are probably a result of minor problems in the removal of unresolved stars from the background in the LASP data, and in the removal of effects of charged particles and statistical noise in the Paris data.

The important features of the data for this discussion are the shifts along the ecliptic in the positions of the maximum and the minimum that occurred between the two dates. For the LASP data these displacements amount to  $37^\circ$  and  $20^\circ$ , implying effective distances of 3 AU and 6 AU for the source regions of the maximum and minimum, respectively. The Paris data show a larger displacement of the maximum ( $50^\circ$ ) but indicate a motion of only  $10^\circ$  for the minimum that is opposite to that expected for a parallax motion. Because of the greater difficulty of accurately locating the position of the minimum, it is possible that this effect is not real. Indeed, there is a  $13^\circ$  discrepancy between the two sets of data for the SU 3 period in locating the maximum. This suggests that errors of at least this magnitude must be present in the low brightness regions of the maps.

Accordingly, we will place more emphasis on the parallax motion of the maximum.

The mean position of the Lyman  $\alpha$  maximum is located at  $RA = 263^\circ$ . This is assumed to be the true direction of the "interstellar wind"  $V_r$ , which is the result of two velocities  $V_H$  and  $-V_\odot$  shown in figure 4;  $V_H$  is the velocity of the interstellar gas and  $V_\odot$  is the velocity of the solar system (20 km/sec), both relative to the local standard of rest (LSR). The wind speed  $V_H$  and the angular separation  $\xi$  of the vectors  $V_r$  and  $V_H$  are given by

$$V_H^2 = V_\odot^2 + V_r^2 - 2V_r V_\odot \cos \xi \quad (2)$$

$$\cos \xi = \frac{V_r - V_\odot \cos \xi}{V_H} \quad (3)$$

$\xi$  is the angle ( $53^\circ$ ) between the mean position of the Lyman  $\alpha$  maxima and the apex. In a later section we

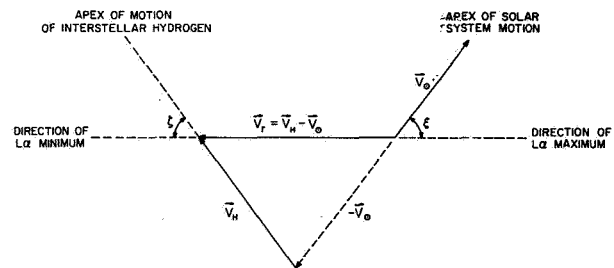


**Figure 4** The geometry of the interstellar wind. The relative velocity  $V_r$  is the difference between the hydrogen velocity  $V_H$  and the solar system velocity  $V_\odot$ . The ecliptic plane passes through and is perpendicular (within  $10^\circ$ ) to the line connecting the Lyman  $\alpha$  maximum and minimum (the direction of  $V_r$ ).

show that  $V_r$  is of the order of 5 to 10 km/sec. From equation (2) the value of  $V_H$  is calculated to be about 19 km/sec for both values of  $V_r$ , with corresponding values for  $\xi$  of  $111^\circ$  and  $96^\circ$ . This indicates that the "true" velocity of the interstellar hydrogen is directed from the vicinity of the constellation Triangulum Australe, making an angle of about  $30^\circ$  with the galactic plane.

At first sight this conclusion appears to contradict the findings of *Venugopal and Shuter* [1967] and previous radio investigations. On the basis of 21-cm line shifts from nearby hydrogen they found no systematic differential motion between neutral hydrogen and the LSR. However, the average distance of the observed hydrogen emission can be estimated to be  $\sim 100$  parsecs from the galactic latitude of their measurements ( $\pm 20$  to  $\pm 45^\circ$ ). Even though small on a galactic scale this distance ( $\sim 10^7$  AU) is still enormous compared with the size of the region ( $\sim 10$  AU) probed by solar Lyman  $\alpha$  scattering. It is possible that 21-cm measurements represent an average over a large number of irregularities in the velocity field.

### THE DISTRIBUTION OF INTERPLANETARY HYDROGEN

We will refer to as “interplanetary” those nearby interstellar hydrogen atoms that have survived ionization and make an appreciable contribution to the scattering of solar Lyman  $\alpha$  in the vicinity of the earth. The Lyman  $\alpha$  scattering plays two roles: it renders the neutral hydrogen visible to ultraviolet photometers and it produces a force that effectively balances the gravitational force. To demonstrate the latter role, we note that the average force on a hydrogen atom is the product of the photon momentum  $h\nu/c$  and the number of photons scattered per second. The latter quantity is known as the  $g$  factor and is useful in expressions relating an airglow intensity to the column density of scattering atoms along the line of sight [*Chamberlain*, 1961]. *Barth* [1969] calculates this value to be  $2.1 \times 10^{-3} \text{ sec}^{-1}$ . We have used the high-resolution solar Lyman  $\alpha$  measurements of *Bruner and Rense* [1969] and the photon flux reported by *Hinteregger* [1970] to calculate a slightly larger value  $g = 2.3 \times 10^{-3} \text{ sec}^{-1}$ . For the latter value, the outward radiation force and the gravitational force differ by only 2 percent.

#### The “Cold” Model of Interstellar Hydrogen

We first consider the case of a unidirectional streaming velocity, the “cold” model. With no gravitational bending of the trajectories, the continuity equation for the density of neutral hydrogen  $n_H$  is

$$\frac{d}{dx} n_H = -\frac{(\sigma\Phi + J)n_H}{V_r} \quad (4)$$

where  $x$  is the coordinate measured along the streaming axis (fig. 5),  $\sigma$  is the charge exchange cross section, and  $\Phi$  is the solar proton flux. The quantity  $J$  is the photoionization rate per atom and is given by

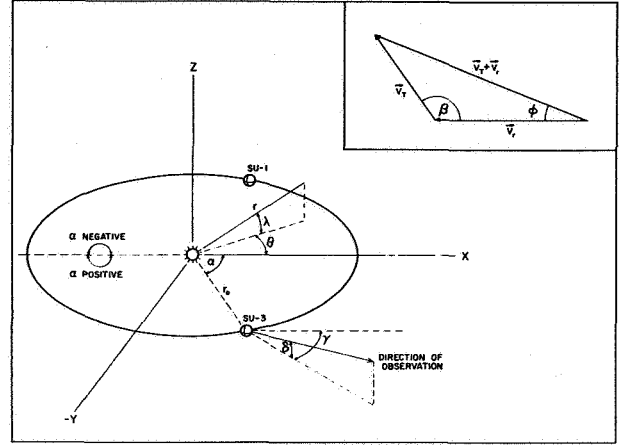


**Figure 5** The coordinate system for describing the interplanetary distribution of hydrogen. The  $X$   $Y$  plane is the ecliptic plane. The earth's positions at the two spin-up periods  $SU1$  and  $SU3$  are shown. The inset shows the addition of the thermal velocity  $V_T$  to the relative velocity of flow (i.e., the mean flow)  $V_r$ .

$$J = \int k_\lambda F_\lambda d\lambda \quad (5)$$

$k_\lambda$  is the ionization cross section of atomic hydrogen and  $F_\lambda$  is the solar photon flux. In equation (4) a term of order  $V_r/V_{sw}$  is ignored. Here  $V_{sw}$  is the (constant) solar wind velocity ( $\sim 300$  km/sec). As we will show  $V_r < 30$  km/sec and hence the ignored term is  $< 10$  percent.

Assuming that  $\Phi$  and  $F_\lambda$  vary as  $r^{-2}$  over the region of interest, equation (4) may be integrated along the streaming direction from  $+\infty$  to the point  $r(r, \theta, \lambda)$ . The result is

$$n_H(r) = n_H(\infty) \exp \left\{ -\frac{r_c X}{r} \left[ \frac{\pi}{2} - \tan^{-1}(X \cos \lambda \cos \theta) \right] \right\} \quad (6)$$

where

$$r_c = \frac{r_e^2 (\sigma\Phi_e + J)}{V_r} \quad (7)$$

$$X = (\cos^2 \lambda \sin^2 \theta + \sin^2 \lambda)^{1/2} \quad (8)$$

$\Phi_e$  and  $J_e$  are, respectively, the solar wind flux and photoionization rate at  $r_e = 1$  AU;  $n_H(\infty)$  is the interstellar hydrogen density;  $r$ ,  $\theta$ , and  $\lambda$  are the sun-centered coordinates of the point  $r$  shown in figure 5. Since the measured positions of the maximum and minimum are nearly in the ecliptic plane we will identify  $\gamma$  with the ecliptic longitude measured from the meridian passing through the  $+X$  axis (ecliptic longitude,  $263^\circ$ ). Similarly,

the angle  $\delta$  shown in figure 5 is the ecliptic latitude measured from the earth. For points in the ecliptic (XY) plane ( $\delta = 0$ ), equation (6) reduces to expressions given by *Semar* [1970] and *Tinsley* [1971].

$$n_H = n_H^{(\infty)} \exp \left[ -\frac{r_c f(\theta)}{r} \right] \quad (9)$$

where

$$\begin{aligned} f(\theta) &= \frac{\theta}{\sin \theta} & (0 \leq \theta \leq \pi/2) \\ &= \frac{\pi}{2} + \frac{\theta - \pi/2}{\sin \theta} & (\pi/2 \leq \theta \leq \pi) \end{aligned} \quad (10)$$

The quantity  $r_c$  is the "effective cavity radius" in the forward direction (+X) of streaming. It depends on the wind velocity and the total loss rate but is independent of  $n_H^{(\infty)}$ .

#### The "Hot" Model of Interstellar Hydrogen

We now include in the theory the possibility of a random component of velocity superimposed on the streaming velocity. It is sufficient to assume that in the moving frame a single velocity  $V_T$  is distributed isotropically. Since the mean free path of hydrogen is  $\sim 10^3$  AU the atoms will describe collisionless trajectories. For simplicity the equations will apply to points in the XY plane. The generalization to three dimensions is straightforward. The density at any point is due to contributions from atoms whose velocities lie within a cone of half-angle  $\phi$ , where

$$\tan \phi = -\frac{(V_T/V_r) \sin \beta}{1 - (V_T/V_r) \cos \beta} \quad (11)$$

where  $\beta$  is the angle between the velocities  $V_r$  and  $V_T$  shown in figure 5. The resulting  $V_r + V_T$  has a component along the streaming direction of

$$V_x = (V_r^2 - 2V_r V_T \cos \beta + V_T^2)^{1/2} \quad (12)$$

Since the random velocity  $V_T$  is distributed isotropically each stream (defined by  $\phi$ ) is weighted only by its probability of ionization. The total is therefore a sum over all angles  $\beta$ , that is

$$n_H = \frac{n_H^{(\infty)}}{2\pi} \int_{-\pi}^{\pi} d\beta \exp \left\{ \frac{-r_c V_r f[\theta - \phi(\beta)]}{r V_x(\beta)} \right\} \quad (13)$$

#### Scattering of Solar Lyman $\alpha$ by Interplanetary Hydrogen

Given the distribution of hydrogen  $n_H$ , the single-scattered Lyman  $\alpha$  intensity is calculated from

$$4\pi I = g_e \int_0^{\infty} ds n_H r_e^2 / r^2 \quad (14)$$

where  $ds$  is an element of length along the direction in which the intensity is to be calculated, and  $g_e$  is the  $g$  factor at the radial distance  $r_e$  (1 AU). For the direction outward from the sun ( $\gamma = \alpha$ ,  $\delta = 0$ ) the integration over  $s$  may be performed analytically for both models:

##### "Cold" model

$$4\pi I(r_o) = \frac{g_e r_e^2 n_H^{(\infty)}}{r_c f(\theta)} \left\{ 1 - \exp \left[ \frac{-r_c f(\theta)}{r_o} \right] \right\} \quad (15)$$

##### "Hot" model

$$4\pi I(r_o) = \frac{g_e r_e^2 n_H^{(\infty)}}{2\pi r_c} \int_{-\pi}^{\pi} d\beta \frac{1 - \exp[-r_c A(\beta)/r_o]}{A(\beta)} \quad (16)$$

where

$$A(\beta) = \frac{V_r f[\theta - \phi(\beta)]}{V_x} \quad (17)$$

For more general directions of viewing, it is necessary to perform a numerical integration of equation (14).

#### COMPARISON WITH OGO LYMAN $\alpha$ MEASUREMENTS

The adjustable parameters of the theory are  $n_H^{(\infty)}$ ,  $V_T/V_r$ , and  $r_c$ . The important observational quantities are the values of the Lyman  $\alpha$  intensity, the ratio of the maximum and minimum intensities, and the parallactic displacements of the maximum derived from measurements taken at different periods. The uncertainties attached to each of these quantities (insofar as the LASP data are concerned) are estimated to be: (1) *intensity* — a factor of 2 is not unlikely in the laboratory calibration [Pearce et al., 1971]; (2) *maximum/minimum ratio* — estimated to be accurate to within 5 percent, this ratio involves the relative accuracies, together with the small degree to which the effect of stars influences the determination of the sky background; and (3) *parallactic displacement* — a maximum or a minimum is defined by a

smooth curve through at least three points on three different circular scans of the sky (as in fig. 3). The maximum error in this quantity is of the order  $\pm 5^\circ$ , causing the error in the parallax measurement to be about  $\pm 7^\circ$ . If similar errors are present in the Paris data, it is clear the discrepancies of figure 3 are not unexpected. Rather than carry the estimated formal uncertainties through each of the derived quantities of the theory, we prefer to be conservative and assume that these quantities will lie somewhere in the range defined by the LASP and Paris data.

The procedure in fitting the cold model to the OGO measurements is to vary the parameter  $r_c$  in the intensity calculations that apply to the periods SU 1 and SU 3. The ecliptic longitude of the earth on those dates was  $351^\circ$  and  $191^\circ$ , respectively, corresponding to values of  $\alpha$  (see fig. 5) of  $-88^\circ$  and  $+72^\circ$ . From the intensities calculated on the two dates, the angular separation of the intensity maxima is obtained and is plotted in

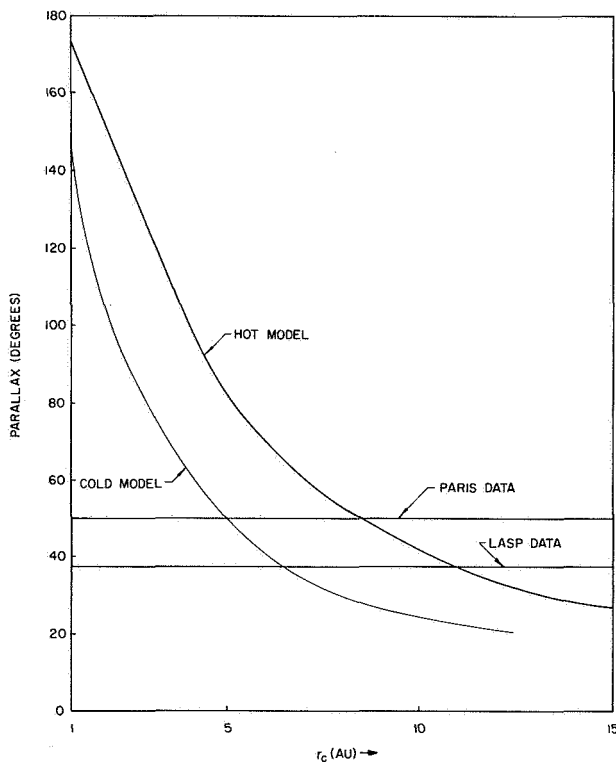


**Figure 6** The separation in degrees along the ecliptic of the Lyman  $\alpha$  maxima for the periods SU 1 and SU 3, denoted by "parallax" versus the parameter  $r_c$ , the "effective cavity radius." The horizontal lines show the measured values of the separation for the two OGO experiments.

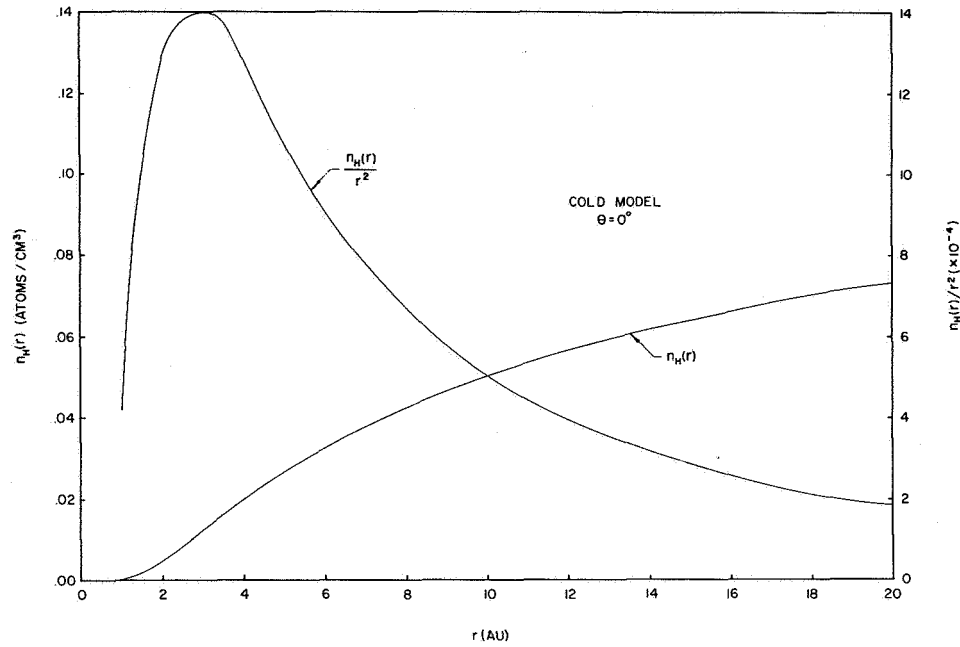
figure 6 as a function of  $r_c$ . The value implied for the LASP data is  $r_c = 6.4 \pm 1.0$  AU, and for the Paris data,  $r_c = 5.1$  AU, with a similar uncertainty.

Figure 7 is a plot of the density for the cold model in the  $\theta = 0^\circ$  direction as a function of  $r$ . This also shows the "source function"  $n_H(r)/r^2$ , which is the integrand in equation (14) for the direction  $\alpha = 0^\circ$ ,  $\gamma = 0^\circ$ . This illustrates that the effective distance of the emitting direction is about 3 AU, the value obtained from a simple geometrical parallax calculation.

For the direction  $\alpha = 180^\circ$ ,  $\gamma = 180^\circ$ , the intensity calculated from the cold model should be zero, a consequence of complete ionization for this direction. This can be seen in equation (9), since  $f(\theta) \rightarrow \infty$  as  $\theta \rightarrow \pi$ . For the actual positions of the earth (and the OGO satellite) the predicted intensity is finite but extremely small for this general "downwind" direction. To account for the measurement of 240 R in this direction, it is necessary to invoke an outside Lyman  $\alpha$  source. The most likely candidate is the diffuse Lyman  $\alpha$  radiation from the galaxy. Adams [1971] has considered the detailed history of Lyman  $\alpha$  photons originating in recombination in HII regions with subsequent scattering in HI regions and the possibility of absorption on interstellar dust grains. His upper limit of a few hundred Rayleigh for the diffuse sky background corresponds to the case of no dust absorption. Therefore, although it is unlikely, we cannot absolutely exclude 240 R of isotropic galactic Lyman  $\alpha$  as a possible contribution to the OGO measurements. When this value is added to the prediction of the cold model and the total normalized to the LASP measurement at the maximum, the value for  $n_H(\infty)$  is  $0.061 \text{ cm}^{-3}$ .

For the hot model, the intensity in the downwind direction is provided by scattering from neutrals that enter the "shadow" region by virtue of their inclined trajectories. For  $V_T > V_r$ , a wind from all directions occurs. For this case, neutral atoms may approach the solar system from the opposite direction of the flow. For  $V_T \gg V_r$ , the wind flux and thus the scattered intensity is nearly isotropic. The observed maximum/minimum ratio of 2.38 (for the LASP data) is achieved with a thermal velocity equal to 1.44 times the wind velocity. With the quantity  $V_T/V_r$  known, the parallax may now be calculated from equations (13) and (14) as a function of  $r_c$ . The results are shown in figure 6, from which the values of  $r_c$  may be deduced as before. Finally, the parameter  $n_H(\infty)$  is adjusted until the maximum intensity is matched. The interplanetary density for the hot model is plotted in figure 8 for both the upwind ( $\theta = 0^\circ$ ) and downwind ( $\theta = 180^\circ$ ) directions,





**Figure 7** The distribution of neutral hydrogen  $n_H(r)$  and the source function for Lyman  $\alpha$  scattering,  $n_H(r)/r^2$ , plotted against radial distance from the sun for the direction of maximum Lyman  $\alpha$  scattering.

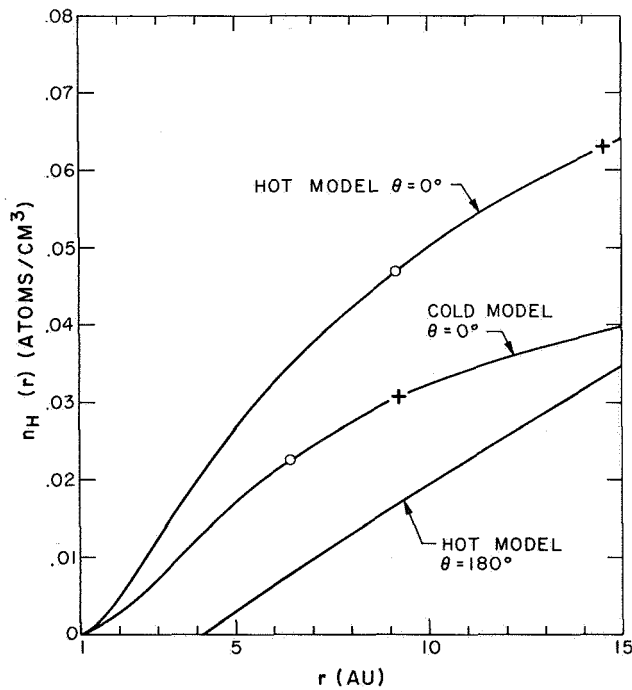


**Figure 8** The distribution of neutral hydrogen for the "cold" and "hot" models as a function of radial distance from the sun. The symbols + and o indicate positions where the interstellar density is reduced by the amounts 50 percent and  $(1/e)$ , respectively.

and is compared with that of the cold model. Figure 9 is a comparison of the LASP measurements and the theory for both models.

With the knowledge of the ionization rates  $\sigma\Phi$  and  $J$ , and the quantity  $r_c$ , we can determine the wind speed  $V_r$  from equation (7). Furthermore if  $V_r$  is known, the random velocity  $V_T$  may be determined from the ratio  $V_T/V_r$ . Using the data of *Hinteregger* [1970] for the ionizing flux  $F_\lambda$  between 911Å and 280Å, and the cross section  $k_\lambda$  given by *Allen* [1964], the value of  $J_e$  is calculated to be  $6.89 \times 10^{-8} \text{ sec}^{-1}$ , corresponding to a 10.7 cm solar radio flux of 144 (in units of  $10^{-22} \text{ watts m}^{-2} \text{ Hz}^{-1}$ ). The average value for  $F_{10.7}$  for the 6 months preceding each of the two spinup periods was 148 [*Solar-Geophysical Data*, 1970]; thus, no scaling to a different radio flux is needed. (A 6-month average was selected since the interplanetary atoms will move through about 2 AU during that time, the approximate width of the source function region shown in figure 7.)

Typical quiet-time solar wind fluxes of  $1.6 \times 10^8 \text{ cm}^{-2} \text{ sec}^{-1}$  are reported by *Hundhausen* [1970]. Increases in flux as large as  $6 \times 10^8 \text{ cm}^{-2} \text{ sec}^{-1}$  can occur during the passage of a disturbed magnetic sector region [*Neugebauer and Snyder*, 1966]. However, these transient effects are expected to exert very little influence on the average ionization rate. The charge-exchange

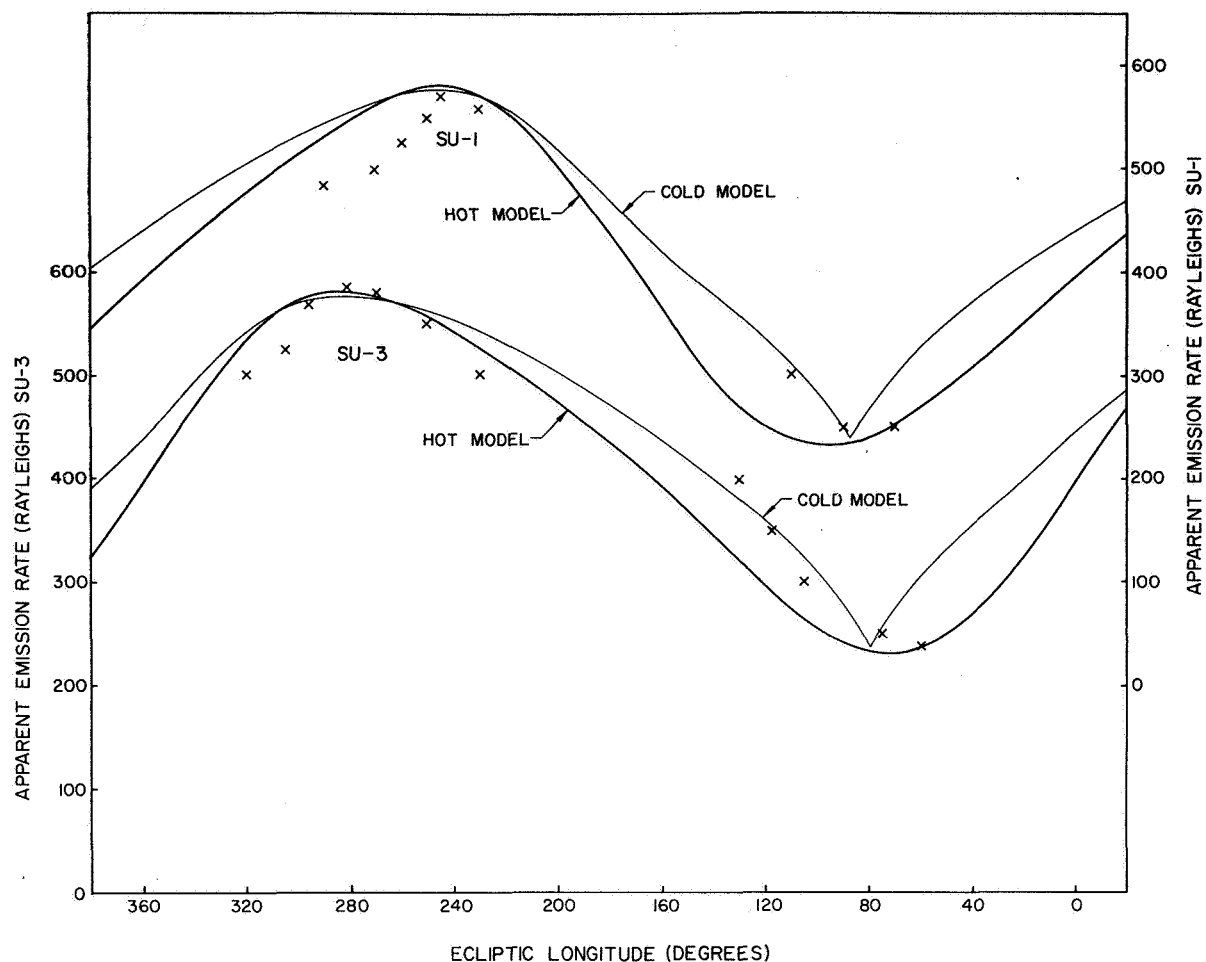


**Figure 9** The comparison with the LASP data of the theoretical Lyman  $\alpha$  scattering intensity for the "cold" and "hot" models of the interstellar gas. The cold model contains an isotropic intensity of 240 R.

cross section is about  $2 \times 10^{-15} \text{ cm}^2$  [Fite *et al.*, 1962]. Table 1 is a summary of the final results using  $\sigma\Phi = 3.2 \times 10^{-7} \text{ sec}^{-1}$ . The temperatures for both sets of data are derived from the relative flow velocities  $V_r$  and the ratio  $V_T/V_r = 1.44$ , using the formula  $m_H V_T^2 = 2kT$ ;  $m_H$  is the mass of the hydrogen atom and  $k$  is Boltzmann's constant. The reader may scale these results according to any total ionization rate he chooses.

#### ADDITIONAL EFFECTS NOT CONSIDERED IN PRESENT ANALYSIS

##### Temporal Effects

A perfect balance of radiation pressure and gravitation is not expected. Furthermore the net force will vary during the solar rotation period in response to 27-day changes in the line-center region of solar Lyman  $\alpha$  [Meier,

**Table 1** Basic heliosphere parameters for "hot" and "cold" models.

Experiment	Deduced quantity	Cold model	Hot model
LASP	$r_c$ (AU)	6.4	10.9
	$V_r$ (km/sec)	9.1	5.3
	$T$ ( $^\circ\text{K}$ )	0.0	$3.56 \times 10^3$
	$n_H$ ( $\text{cm}^{-3}$ )	0.061	0.12
Paris	$r_c$ (AU)	5.0	8.5
	$V_r$ (km/sec)	11.6	6.9
	$T$ ( $^\circ\text{K}$ )	0.0	$5.87 \times 10^3$
	$n_H$ ( $\text{cm}^{-3}$ )	0.030	0.090

1969]. The net force may also vary appreciably along the trajectory due to a Doppler shift of the resonant frequency within the self-reversed solar Lyman  $\alpha$  line profile. The use of a constant net radial force (assumed here to be zero) and constant values of the EUV and solar wind fluxes are justified because of the small distances covered by the interstellar hydrogen atoms (0.1-0.2 AU) during one solar rotation period. This produces a strong averaging effect on the photoionization as discussed by *Blum and Fahr* [1970c].

### Secondary Ionization

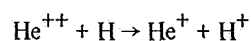
In addition to the loss processes considered here, neutral hydrogen will be lost by impact ionization from fast protons and neutrals (the latter created by charge exchange). The measured value of the relevant cross section for 9 keV hydrogen atoms is  $6 \times 10^{-17} \text{ cm}^2$  [*Allison*, 1958], only 3 percent of the charge-exchange cross section. This process is therefore of negligible importance.

### Doppler Shifts

For relative velocities ranging from 5 to 10 km/sec, the center of the absorption profile will be shifted by as much as 0.02 to 0.04 Å, respectively. (The earth's orbital velocity of 30 km/sec can add up to  $\pm 0.12$  Å to the measured line shift.) The high-resolution solar Lyman  $\alpha$  line profile of *Bruner and Rense* [1969] shows that such shifts can increase the resonance  $g$  factor over its line-center value by only a small amount. This could cause a slight sharpening of the intensity maximum predicted for a constant  $g$  factor, a desirable gain for the theory in view of the measured sharpness shown in figure 9. However, it would also lead to a broadening of the minimum, probably to a greater extent than the data indicate, although more measurements are needed in this portion of the sky before this can be stated with certainty. Such modifications would be most important for the cold model and for the higher values of  $V_r$ .

### Additional Solar Wind Loss Processes

*Hundhausen et al.* [1968] have suggested that the asymmetrical charge-exchange process



can modify the ionization state of the solar wind by conversion of outflowing  $\text{He}^{++}$  to  $\text{He}^+$ . The measured cross section for this process is  $\sim 3 \times 10^{-16} \text{ cm}^2$  [*Fite et al.*, 1962]. Even with the admixture of as much as 15 percent  $\text{He}^{++}$  in the solar wind [*Hundhausen et al.*,

1967], the loss rate of neutral hydrogen by this mechanism would not exceed 3 percent of the charge-exchange loss.

*Hundhausen* and his coworkers also suggested that the anomalously high concentration of  $\text{He}^+$  measured in the solar wind could be explained by this process if the incoming neutral hydrogen flux were  $\sim 2 \times 10^6 \text{ cm}^{-2} \text{ sec}^{-1}$ . However, none of our models gives fluxes greater than  $1 \times 10^5 \text{ cm}^{-2} \text{ sec}^{-1}$  even at large distances from the sun.

### Photoionization of $\text{H}_2$ , OH, and $\text{H}_2\text{O}$ in the Interstellar Medium

Although the concentrations of these molecules are expected to be very small in the interstellar medium, it is of some interest to estimate the effects of the breakup of these molecules in the inflowing gas. Consider first the effects of EUV and solar wind on an  $\text{H}_2$  molecule. Since charge exchange occurs readily and photoionization is more likely than photodissociation, an  $\text{H}_2$  molecule will be converted mainly into an  $\text{H}_2^+$  ion rather than into two hydrogen atoms. These ions will be accelerated very quickly by the  $\nu \times \mathbf{B}$  electric field and swept away by the solar wind. Thus  $\text{H}_2$  would probably not contribute to the interplanetary hydrogen atom population, unless it has a much greater abundance than H in the nearby interstellar medium.

The  $\text{H}_2\text{O}$  molecule is readily dissociated in the solar ultraviolet with a photodissociation rate of about  $10^{-5} \text{ sec}^{-1}$  [*Anderson*, 1971]. Thus, the breakup of water molecules occurs at distances ten times greater than hydrogen atom ionization. The interplanetary distribution of H atoms would be nearly the same as if the interstellar medium were originally composed of H atoms and OH radicals.

The ultraviolet absorption cross sections of the OH molecule have not been measured. However, if the interplanetary hydrogen were primarily a dissociation product of OH (or equivalently of  $\text{H}_2\text{O}$ ), interplanetary O atoms would be present in comparable numbers to H atoms. This possibility could be tested by searching for the 1304 Å sky background emission. Unfortunately, the  $g$  factor is only  $1.5 \times 10^{-6}$  [*Barth*, 1969] due to a very faint solar 1304 Å line. The long-wavelength channel of the LASP ultraviolet photometer [*Thomas and Krassa*, 1971] could have detected an intensity greater than 20  $R$ . This imposes only the weak restriction that the interplanetary atomic oxygen is less than about  $1 \text{ cm}^{-3}$ .

The above discussion is intended only to show that the measurements themselves do not necessarily exclude photodissociation of interstellar molecules as the origin

of the observed interplanetary hydrogen. To definitely rule out such possibilities it is necessary to calculate a detailed spatial distribution of the "hot atoms" produced by photodissociation and the Lyman  $\alpha$  scattering expected from such a distribution. This would permit the assignment of upper limits to the abundances of hydrogen-bearing molecules in the nearby gas.

### Solar Lyman $\alpha$ Attenuation

At a sufficiently great radial distance, the solar Lyman  $\alpha$  will be appreciably depleted in parts of the line so that solar radiation pressure no longer plays an important role. Therefore, the incoming atoms will initially be accelerated. This acceleration continues until the atom approaches sufficiently close so that the attenuation is no longer effective, or until its Doppler shift causes the resonance wavelength to move into a spectral region where attenuation is unimportant. The resulting distribution of velocities with distance will cause an originally cold gas to scatter the solar line as if it were at a finite "effective temperature"  $T_e$ . The value of  $T_e$  may be estimated by first calculating the distance  $R_1$  at which the line-center optical depth is unity for a variety of gas temperatures. The distance  $R_1(T)$  ranges from 8 AU at  $T = 10^2$  °K to 20 AU at  $T = 10^4$  °K. We next assume that the incoming atoms are accelerated by solar gravitation beyond  $R_1$  (and maintain a constant speed and direction for  $r < R_1$ ). The velocity increments  $\Delta V(R_1)$  are then computed from  $(V_r^2 + 2M_\odot G/R_1)^{1/2} - V_r$ , where  $V_r$  is the initial relative velocity,  $M_\odot$  is the solar mass, and  $G$  is the gravitational constant. The velocity increment  $\Delta V$  may be converted to an effective temperature  $T_e = m_H \Delta V^2 / 2k$  as a function of  $R_1$ . At the point where  $T_e(R_1) = T(R_1)$ , we obtain the velocity increment and effective temperature that is reached by the accelerating gas before it becomes balanced by solar radiation pressure. For an initial velocity of 10 km/sec (see table 1),  $\Delta V$  is calculated to be  $\sim 3$  km/sec, and  $T_e \sim 600^\circ$  K. For an initially finite gas temperature the effect is to add  $\Delta V$  to the thermal velocity. This argument is valid for the  $\theta = 0^\circ$  direction only. For  $\theta \neq 0^\circ$ , the velocity increment along the radial direction and hence  $T_e$  will be somewhat less.

The major conclusion that was drawn from the cold model was that the unidirectional streaming velocity could not fill in the downwind direction with neutral atoms. This is not quite true with the above modifications, since those trajectories for  $\theta \neq 0^\circ$  will be slightly bent toward the sun and will produce a nonzero population along the  $\theta = 180^\circ$  axis. However, our calculations show that unless  $V_T > V_r$  ( $T > 5 \times 10^3$  °K for  $V_r = 10$  km/sec) the effect of filling in the shadow is

very small as far as the Lyman  $\alpha$  scattering intensity is concerned.

### Multiple Scattering of Lyman $\alpha$ Photons

Since the mean free path for scattering of Lyman  $\alpha$  (8–20 AU) is not much greater than the effective dimension of the source region (fig. 7), the effects of multiple scattering may not be negligible. A rule of thumb for estimating its importance at a distance  $r$  is to compare the number of solar photons  $N_s$  available for scattering to the number  $N_g$  available for rescattering from the surrounding gas. If  $N_s \gg N_g$ , multiple scattering may be ignored. At 1 AU,  $N_s = 1 - 4 \times 10^{10}$  photons  $\text{cm}^{-2} \text{sec}^{-1}$  and the value of the mean scattered intensity  $N_g \approx 4.5 \times 10^8$  photons  $\text{cm}^{-2} \text{sec}^{-1}$ ;  $N_s$  decreases as  $r^{-2}$  out to the attenuation distance  $R_1$  and then rapidly falls to zero. According to equation (15) or (16) the outward first-order scattered intensity initially falls rapidly with  $r$ , and then approaches a variation of  $r^{-1}$ . However, we may estimate the average (over all solid angles) falls off approximately as  $r^{-1}$  at all distances. The value of  $r$  for which  $N_s = 10N_g$  is therefore about 4 AU. When  $N_s = 2N_g$ ,  $r \approx 20$  AU. Thus, in the source region of the Lyman  $\alpha$  scattering (1–8 AU), second-order scattering is likely to be only 10 to 20 percent of the primary scattering. At greater distances, the effect becomes more important, but the number of photons available for scattering is very small. Thus we do not consider this effect a serious one in our analysis.

### DISCUSSION

If the galactic Lyman  $\alpha$  emission is as high as 200 to 240  $R$ , the interstellar hydrogen density is between 0.03 and 0.06  $\text{cm}^{-3}$ . In this model, the interstellar gas temperature is low ( $\sim 10^2$  °K) and the interplanetary hydrogen is completely ionized in the downwind direction. On the other hand, if the galactic contribution is negligible, the gas temperature must be high (up to  $10^4$  °K) to fill in the downwind region with neutral hydrogen. An intermediate value of the galactic emission leads to a "warm" model of the gas with  $0.03 < n_H < 0.12 \text{ cm}^{-3}$ . Knowledge of the galactic emission is not very important in determining the interstellar density; however, it is critical in determining the gas temperature. Adams [1971] has suggested a means of differentiating the galactic and local components by measuring the line width of the Lyman  $\alpha$  sky background. The galactic component will be broad (1 to 3 Å). The present analysis predicts a width of the interplanetary component to be of the order of 0.05 Å. Its Doppler shift (up to 0.12 Å) depends on the direction of viewing and the season of observation.

Previous determinations of the interstellar HI density from radio measurements give average values of 0.4 to  $0.7 \text{ cm}^{-3}$  [see *Brandt et al.*, 1971 for a recent discussion of these measurements]. *Jenkins* [1970] has calculated an upper limit of  $0.04 \text{ cm}^{-3}$  for the average hydrogen density along the 100-pc distance to  $\alpha$  Vir from rocket measurements of the Lyman  $\alpha$  interstellar absorption by A. Smith. A rocket-borne spectrometer measurement of an enhancement of 1216Å emission from  $\alpha$  Bootes (Arcturus) has been recently reported by *Rottman et al.* [1971]. Assuming the emission line width of Lyman  $\alpha$  is comparable to that of the sun ( $\sim 1\text{\AA}$ ), we can calculate the column density of hydrogen that would barely extinguish the emission line. Over the 11-pc distance, the average hydrogen density would be no larger than  $0.05 \text{ cm}^{-3}$ . For distances of a few hundred pc where a number of bright ultraviolet stars are available for Lyman  $\alpha$  absorption measurements, the average densities are on the order of  $0.1 \text{ cm}^{-3}$  [*Jenkins*, 1970]. The well-publicized discrepancy between the 21-cm results and the Lyman  $\alpha$  absorption results has apparently not yet been resolved. Our results lend support to the Lyman  $\alpha$  absorption measurements; however, it should be emphasized that our value refers to a very much smaller distance scale than either of the above techniques. Small-scale irregularities in density could easily account for the discrepancy between our result and the radio measurements. Irregularities are apparently incapable of resolving the problem of the 21-cm versus the Lyman  $\alpha$  absorption measurements [*Jenkins*, 1970].

The 21-cm observational evidence for the thermal state of the intercloud medium indicates temperatures between  $1 \times 10^3$  and  $5 \times 10^3 \text{ }^\circ\text{K}$  [*Rohlfs et al.*, 1969].

A current theory of the heat balance of HI regions predicts two stable phases of the neutral gas existing in pressure equilibrium [*Spitzer*, 1968; *Field et al.*, 1969]. These ideas can account for the known existence of dense, cold clouds ( $n_{\text{H}} \sim 10 \text{ cm}^{-3}$ ,  $T \sim 10^2 \text{ }^\circ\text{K}$ ) and a tenuous, hot intercloud medium ( $n_{\text{H}} \sim 0.1 \text{ cm}^{-3}$ ,  $T \sim 10^3\text{--}10^4 \text{ }^\circ\text{K}$ ) if the medium is postulated to be heated by a large subcosmic ray flux. Another theory favors the mechanism of heating by soft X rays [*Werner et al.*, 1970]. A time-dependent model involving the possible contributions from supernova outbursts has been advanced by *Bottcher et al.* [1970].

Since the hydrogen clouds occupy only 10 percent of the galactic volume, we would expect from pure chance that the solar system is contained within the intercloud medium. Our results for the density of the nearby gas clearly indicate that this is the case. Our results are also consistent with the intercloud gas temperatures deduced

from radio measurements, provided the galactic Lyman  $\alpha$  contribution is not too large.

## SUMMARY

Our recent Lyman  $\alpha$  sky background measurements have provided much new information on the nature and location of the scattering sources. They indicate that most if not all the emission is interplanetary in origin, and place the effective scattering distance within about 3 AU of the sun. Through the use of a simple model of the distribution of the neutral interplanetary hydrogen we have shown that the OGO data are consistent with an interstellar hydrogen density between  $0.03$  and  $0.12 \text{ cm}^{-3}$ , an interstellar gas temperature as high as  $10^4 \text{ }^\circ\text{K}$ , and an interstellar wind velocity between 5 and 10 km/sec. The interstellar hydrogen velocity relative to the local standard of rest is calculated to be about 19 km/sec, directed from the southern hemisphere at an angle of about  $30^\circ$  with the galactic plane.

The deduced motion of the nearby gas may be a manifestation of a turbulent motion on a scale that is probably much greater than a mean free path ( $10^3$  AU) but much smaller than the thickness of the galactic plane ( $10^7$  AU). The gas temperature required of the "hot" model is consistent with 21-cm evidence of the high temperature of the galactic intercloud medium. However the measurements are also consistent with a cold model of the gas, provided about 200 R of galactic emission is present in the sky background. Removal of this uncertainty will require high spectral resolution measurements above the geocorona, or measurements made from spacecraft traveling to the outer boundaries of the solar system.

## ACKNOWLEDGMENTS

I acknowledge with appreciation the helpful comments of C. Barth, R. Bohlin, C. Lillie, and R. F. Krassa. This work was supported under NASA Contract Number NAS 5-9327 and NASA Grant Number NGR 06-003-052.

## REFERENCES

- Adams, T. F.: On Lyman-Alpha Emission From the Galaxy. Submitted to *Astron. Astrophys.*, 1971.
- Allen, C. W.: *Astrophysical Quantities*. Athlone Press, Univ. of London, 1964.
- Allison, S. K.: Experimental Results on Charge-Changing Collisions of Hydrogen and Helium Atoms and Ions at Kinetic Energies Above 0.2 keV. *Rev. Mod. Phys.*, Vol. 30, 1958, p. 1137.

- Anderson, J. G.: Rocket Borne Ultraviolet Spectrometer Measurement of OH Resonance Fluorescence With a Diffusive Transport Model for Mesospheric Photochemistry. *J. Geophys. Res.*, Vol. 76, 1971, p. 4634.
- Axford, W. I.; Dessler, A. J.; and Gottlieb, B.: Termination of Solar Wind and Solar Magnetic Field. *Astrophys. J.*, Vol. 137, 1963, p. 1268.
- Barth, C. A.: Planetary Ultraviolet Spectroscopy. *Appl. Opt.*, Vol. 8, 1969, p. 1295.
- Bertaux, J. L.; and Blamont, J. E.: Evidence for a Source of an Extraterrestrial Hydrogen Lyman-Alpha Emission: the Interstellar Wind. *Astron. Astrophys.*, Vol. 11, 1971, p. 200.
- Blum, P. W.; and Fahr, H. J.: Solar Wind Tail and the Anisotropic Production of Fast Hydrogen Atoms. *Nature*, Vol. 223, 1969, p. 936.
- Blum, P. W.; and Fahr, H. J.: Interaction Between Interstellar Hydrogen and the Solar Wind. *Astron. Astrophys.*, Vol. 4, 1970a, p. 280.
- Blum, P. W.; and Fahr, H. J.: The Distribution of Interplanetary Hydrogen. *Astrophys. Letters*, Vol. 5, 1970b, p. 127.
- Blum, P. W.; and Fahr, H. J.: Lyman- $\alpha$  Scattering During the Solar Rotation Period. *Astron. Astrophys.*, Vol. 8, 1970c, p. 226.
- Bottcher, C.; McCray, R. A.; Jura, M.; and Dalgarno, A.: Time Dependent Model of the Interstellar Medium. *Astrophys. Letters*, Vol. 6, 1970, p. 237.
- Brandt, J. C.: Interplanetary Gas, IV. Neutral Hydrogen in a Model Solar Corona. *Astrophys. J.*, Vol. 133, 1961, p. 688.
- Brandt, J. C.: Interplanetary Gas, IX. Effects on the Local Interstellar Medium. *Icarus*, Vol. 3, 1964, p. 253.
- Brandt, J. C.; Stecher, T. P.; Crawford, D. L.; and Maran, S. P.: The Gum Nebula: Fossil Stromgren Sphere of the Vela X Supernova. *Astrophys. J.*, Vol. 163, 1971, p. L99.
- Bruner, E. C.; and Rense, W. A.: Rocket Observations of Profiles of Solar Ultraviolet Emission Lines. *Astrophys. J.*, Vol. 157, 1969, p. 417.
- Chamberlain, J. W.: *Physics of the Aurora and Airglow*. Academic Press, Inc., New York, 1961.
- Chambers, W. H.; Fehla, P. E.; Fuller, J. C.; and Kunz, W. E.: Anisotropic Atomic Hydrogen Distribution in Interplanetary Space. *Nature*, Vol. 225, 1970, p. 713.
- Field, G. B.; Goldsmith, D. W.; and Habing, H. J.: Cosmic-Ray Heating of the Interstellar Gas. *Astrophys. J.*, Vol. 155, 1969, p. L149.
- Fite, W. L.; Smith, A. C. H.; and Stebbings, R. F.: Charge Transfer in Collisions Involving Symmetric and Asymmetric Resonance. *Proc. Roy. Soc. London A*, Vol. 268, 1962, p. 527.
- Hinteregger, H. E.: The Extreme Ultraviolet Solar Spectrum and Its Variation During a Solar Cycle. *Ann. Geophys.*, Vol. 26, 1970, p. 547.
- Hundhausen, A. J.; Asbridge, J. R.; Bame, S. J.; Gilbert, H. E.; and Strong, I. B.: Vela Satellite Observations of Solar Wind Ions. *J. Geophys. Res.*, Vol. 72, 1967, p. 1979.
- Hundhausen, A. J.: Interplanetary Neutral Hydrogen and the Radius of the Heliosphere. *Planet. Space Sci.*, Vol. 16, 1968, p. 783.
- Hundhausen, A. J.; Gilbert, H. E.; and Bame, S. J.: Ionization State of the Interplanetary Plasma. *J. Geophys. Res.*, Vol. 73, 1968, p. 5485.
- Hundhausen, A. J.: Solar Wind Properties and the State of the Magnetosphere. *Ann. Geophys.*, Vol. 26, 1970, p. 427.
- Jenkins, E. B.: Observations of Interstellar Lyman- $\alpha$  Absorption, in *Ultraviolet Stellar Spectra and Ground-Based Observations*. I.A.U. Symp. No. 36, L. Houziaux and H. E. Butler, eds., D. Reidel Pub. Co., Dordrecht, 1970.
- Kurt, V. G.: Observations and Interpretation of Ultraviolet Emission From the Galaxy. *Astron. Zh.*, Vol. 44, 1967, p. 1157.
- Kurt, V. G.; and Germogenova, T. A.: Scattering of Solar Lyman- $\alpha$  Radiation by Galactic Hydrogen. *Astron. Zh.*, Vol. 44, 1967, p. 352; *Soviet Astron.-AJ*, Vol. 11, 1967, p. 278.
- Meier, R. R.: Temporal Variations of Solar Lyman- $\alpha$ . *J. Geophys. Res.*, Vol. 74, 1969, p. 6787.
- Neugebauer, M.; and Snyder, C. W.: Mariner 2 Observations of the Solar Wind, 1. Average Properties. *J. Geophys. Res.*, Vol. 71, 1966, p. 4469.
- Pearce, J. B.; Barth, C. A.; Headley, R. P.; Kelly, K. K.; Mackie, E. F.; and Thomas, G. E.: OGO-5 Ultraviolet Photometer Experiment. To be submitted to *Appl. Opt.*, 1971.
- Rohlfs, K.; Mebold, U.; and Grewing, M.: Interstellar Electron Temperatures From Pulse Delay Measurements and Hydrogen Line Spectra. *Astron. Astrophys.*, Vol. 3, 1969, p. 347.
- Rottman, G. J.; Moos, H. W.; Berry, J. R.; and Henry, R. C.: Lyman- $\alpha$  Emission From Arcturus. Johns Hopkins Univ. Rep., 1971.
- Semar, C. L.: Effect of Interstellar Neutral Hydrogen on the Termination of the Solar Wind. *J. Geophys. Res.*, Vol. 75, 1970, p. 6892.

- Spitzer, L. J.: Dynamics of Interstellar Matter and the Formation of Stars, in *Nebulae and Interstellar Matter*. B. M. Middlehurst and L. H. Aller, eds., Univ. of Chicago Press, Chicago, 1968, p. 1.
- Thomas, G. E.; and Krassa, R. F.: OGO-5 Measurements of the Lyman-Alpha Sky Background. *Astron. Astrophys.*, Vol. 11, 1971, p. 218.
- Tinsley, B. A.: Extraterrestrial Lyman-Alpha. *Rev. Geophys. Space Sci.*, Vol. 9, 1971, p. 89.
- Venugopal, V. R.; and Shuter, W. L. H.: Solar Motion Determined From 21-cm Line Observations. *Astron. J.*, Vol. 72, 1967, p. 534.
- Werner, M. W.; Silk, J.; and Rees, M. J.: Heating of HI Regions by Soft X-rays, II. The Effect of Galactic Soft X-ray Sources. *Astrophys. J.*, Vol. 161, 1970, p. 965.
- Williams, P. E.: The Size of the Solar HII Region. *Astrophys. J.*, Vol. 142, 1965, p. 314.
- Wilson, O. C.: A Suggested Mechanism for the Ejection of Matter From M-Type Stars. *Astrophys. J.*, Vol. 131, 1960, p. 75.

**T. E. Holzer** I have two comments. The first is with regard to the Lyman  $\alpha$  that you observed in the tail or null region. For a cold gas coming in at  $100^\circ$  or something like that, you find that the absorption cross section at the center of the line is approximately 100 times larger than the average absorption cross section calculated in the optically thin approximation. In general this makes a very small difference in all calculations with regard to Lyman  $\alpha$  and so the optically thin approximation is very good. But this difference has two effects. The first is that it can produce a variable addition to the gravitational field from the sun so that the field may change from inward at larger distances to an outward field at smaller distances. This would effectively give a large temperature effect and throw some particles into the null region and thus give you a small Lyman  $\alpha$  flux there. I don't know the magnitude of this effect, so I don't know whether it's enough to account for the observations. But from the calculations I made with regard to something else I think it may be.

## DISCUSSION

My second point is also with regard to the optically thin approximation for the absorption at the center of the line. Even though the gas is generally optically thin, this absorption will tend to increase the density that you would predict. At  $0.1 \text{ particle/cm}^3$  the increase can be as much as a factor of 2. Consequently, instead of from  $0.03$  to  $0.12 \text{ cm}^{-3}$ , your density might be from  $0.06$  to  $0.24 \text{ cm}^{-3}$ . As you may have noted, this difference makes a considerable difference in the effect of the interstellar gas on the solar wind.

**G. E. Thomas** In regard to the first point concerning the effect of absorption on the solar Lyman  $\alpha$  as it progresses outward, I would point out that this absorption is due to a scattering by hydrogen atoms so that eventually the center of the line is eaten out by neutral hydrogen. But, as I recall, the mean free path for Lyman  $\alpha$  proton with these sorts of densities is of the order of 10 AU or so. I can't remember exactly. We decided that such an effect was really unimportant, that is, out to about 5 AU or so. Such things might happen beyond 5 AU, but they would not strongly affect the Lyman  $\alpha$  scattering measurements.

Now let me comment on the second point concerning the importance of multiple scattering. If you again take the mean free path to be about 10 AU, it turns out that multiple scattering effects produce an intensity that is small compared to the singly scattered intensity we calculated. If you turn the argument around and suppose there's a lot of multiple scattering, then you quickly come to the conclusion that you shouldn't get the large asymmetries that are observed. As you see the ratio between the maximum and the minimum is better than 2/1. If multiple scattering were dominant, it would tend to wipe out that difference between the maximum and the minimum.

**T. E. Holzer** I was talking about absorption near the center of the line with regard to the second point as well as the first. With regard to the second point, it does make a factor of 2 difference. With regard to the first point, it may or may not be significant; it's

hard to say.

*G. E. Thomas* Those are difficult calculations.

*J. C. Brandt* What is the absorption cross section in the center of the line?

*T. E. Holzer* I can't give you a number, but if you assume that the Lyman  $\alpha$  line has a flat topped peak 1 Å wide and then you assume the temperature of the neutral gas to be 100° you can calculate the cross section of the center of the line and you can calculate a mean cross section for the whole line. The cross section of the center of the line is a factor of 100 larger than the mean cross section. Actually, it's a factor of 300 larger for a temperature of 100° and the other assumptions.

*J. C. Brandt* Take it at the center line, and you'll get the maximum value.

*T. E. Holzer* Right. But the point is that there is a factor of 100 or 300 between the average cross section and the central cross section, because in taking the mean cross section one tends to neglect the effects of any absorption of the line. In any case, I wanted to suggest that the actual absorption effects are somewhat important because, although they don't change Dr. Thomas' results basically, they can increase the density by a factor of 2.

*G. E. Thomas* I think the importance of multiple scattering depends very much on the temperature. For the hot model, the cross section at the center of the line is much smaller than in the cold model, and mean free paths are larger so the net effect is to reduce the importance of multiple scattering. For reasons I have already given, I tend to believe the hot model.

*F. Scherb* I would like to mention a likely perturbation on the picture that you presented. As I understand it, the axis along which the flow is directed lies nearly in the ecliptic plane. If I have done the arithmetic correctly, about a year from now Jupiter will cross this axis at 5 AU; thus, Jupiter, a source at 3 AU, and the sun will lie on a line, and the gravitational perturbations by Jupiter might be observable if one were observing the Lyman  $\alpha$  distribution in this region of the sky. The perturbations might not be entirely negligible in view of the fact that the sun's gravity appears to be virtually absent as far as the hydrogen is concerned.

*G. E. Thomas* Well, it might be interesting to look for a bright spot and I agree, the bright spot might be there, but I'm not sure what we would learn by it.

*J. C. Brandt* Jupiter's shadow also might be quite long. I'm sure it couldn't be done with the wide-resolution instruments on OGO 5. Instruments with better spatial resolution might see the shadow. I'm sure it's quite long, approximately 1 AU.

*C. P. Sonett* Just one very short note, which I think bears on this. There is a considerable body of work now indicating that the temperature of some interstellar clouds is quite high, perhaps due to heating by low-energy cosmic rays.

*J. C. Brandt* You can get a good argument on that particular point with any group of astronomers containing two or more people. Some of us have been discussing a process of heating the interstellar medium with 304 Å (HeII) photons from a supernova event. The calculations indicate that the process contributes. However, in all of the colloquia and discussions I've heard on this subject recently, people just throw up their hands at the end. Ultimately, this will be sorted out, but I don't think there's any agreement at the present time.

*W. I. Axford* Could I ask if anyone knows what is the status of observations of the temperature of the neutral hydrogen, apart from the 21-cm measurements? Is there anything based on the width of absorption lines that suggests there might be a high temperature somewhere?

*J. C. Brandt* If you look, for example, at the spectra, of the kind that Münch takes, or used to take, the lines are very narrow and very closely spaced and in fact very hard to tell apart. The gas appears to be cool.



*E. N. Parker* The only comment I could add is that if one sees a broad absorption line, he attributes it to turbulence rather than to the high temperature of the neutral hydrogen. So I don't know that one can unravel it by standard observations apart from those of the 21-cm lines.

*J. C. Brandt* Yes, there is the random component of 10 or 20 km/sec.

*W. C. Feldman* Concerning what you would learn by looking at Jupiter when it comes around, I would like to point out that you have the same sort of gravitational focusing effect as was shown by Axford, and the only thing that limits the cusp is temperature. By looking at the size and brightness of the spot you might get an indication of the temperature of the gas.

*F. Scherb* With regard to the temperature of the neutral gas there is a program under way now at Wisconsin to measure Balmer emission lines from the neutral gas due to recombination of ionized hydrogen. By making measurements of  $H_{\alpha}$  and  $H_{\beta}$  you can in fact infer the temperature of the gas because the probability of emission of an  $H_{\beta}$  photon is virtually independent of the temperature at which the recombination occurs, whereas this is not true for  $H_{\alpha}$ . This effect is most useful for temperatures below  $1000^{\circ}$  K. Above  $1000^{\circ}$  one just measures the line profile. So it should be possible, with the proper sensitivity and spectral resolution, to infer the temperatures by studying the  $H_{\alpha}$  and  $H_{\beta}$  emission from the clouds.

*J. C. Brandt* Where in the galaxy do you expect to get sufficient brightness to be able to observe this?

*F. Scherb* This has already been observed by looking just off the Crab, far enough so that the Crab itself was not in the field of view. The  $H_{\beta}$  emission was detected. The program will be continued, with better equipment, at the Goddard Space Flight Center over the next 2 years.

*W. I. Axford* One way of getting an answer to this question of the temperature would be to look at the scattered radiation from helium atoms at 584A. Helium atoms are not affected by radiation pressure and their thermal speed is half that of hydrogen atoms. Therefore, if the gas is relatively cold, the focusing effect will be quite pronounced. Although one expects that the general intensity from the helium will only be perhaps 1 to 10  $R$  depending on the width of the solar line, the bright spot associated with the helium cusp could be very much more intense if the gas is cold. It might well be 100  $R$  or so in a small area, and I believe that this could be detected quite easily.

## INTERSTELLAR HELIUM IN INTERPLANETARY SPACE

William C. Feldman, J. J. Lange, and F. Scherb

**ABSTRACT** The velocity distribution function of  $\text{He}^+$  in the solar wind at 1 AU is calculated with the assumption that the source is photoionization of a cold ( $T = 100^\circ \text{K}$ ), neutral interstellar wind. If the spiral magnetic field is noise free, the velocity distribution is diffuse and would not produce a peak at  $4(E/Q)_H$  in an  $E/Q$  particle spectrum. If the velocity of the interstellar wind with respect to the sun lies in the ecliptic, a large variation of the  $\text{He}^+$  number density with respect to ecliptic longitude is expected.

### INTRODUCTION

A peak appearing at four times the energy/charge ( $E/Q$ ) location of the hydrogen peak in two Vela 3 electrostatic analyzer spectra of solar wind ions was interpreted as being mostly due to  $\text{He}^+$  [Bame *et al.*, 1968]. The  $\text{He}^+$  abundance relative to  $\text{He}^{++}$  was measured to be  $3 \times 10^{-3} \pm 50$  percent (Bame, p. 548). Two other spectra published by Bame *et al.* [1968] yielded only an upper limit of  $10^{-3}$  for  $n_{\text{He}^+}(r_e)/n_{\text{He}^{++}}(r_e)$ , the ratio of number densities at  $r = r_e = 1 \text{ AU}$ . A more recent attempt [Bame *et al.*, 1970] to determine the mass and charge composition in the solar wind attributed a peak located at four times the  $E/Q$  location of  $\text{H}^+$  as probably due to  $\text{Si}^{7+}$  instead of  $\text{He}^+$ .

The Vela 3 observation cannot be explained simply since  $n_{\text{He}^+}(r_e)/n_{\text{He}^{++}}(r_e)$  is expected to be of the order of  $3 \times 10^{-6}$  for a  $10^6^\circ \text{K}$  corona [Tucker and Gould, 1966]. Hundhausen *et al.* [1968] attempted an explanation in terms of a model proposed earlier by Patterson *et al.* [1963]. This model considers the solar wind protons converted by charge exchange with galactic hydrogen into hot, isotropic neutral hydrogen atoms at an assumed spherical shock boundary surrounding the heliosphere. These fast neutrals flow in toward the sun where a small fraction charge exchange with the solar wind  $\text{He}^{++}$  to produce the  $\text{He}^+$ . They find that if 1 percent of the solar wind protons find their way back

and interact within 1 AU, enough  $\text{He}^+$  could be produced to explain the Vela 3 data. Holzer and Axford [1970] tried to explain the ratio of  $3 \times 10^{-3}$  by assuming that the solar system is moving through an interstellar gas cloud. Neutral He would be gravitationally focused by the sun, photoionized, and then incorporated into the solar wind as  $\text{He}^+$ .

Rocket observations of diffuse extreme ultraviolet radiation (EUV) [Young *et al.*, 1968, Johnson *et al.*, 1971a] from the night sky yielded an upper limit of 2  $R$  of 584Å radiation [Johnson *et al.*, 1971b]. If all diffuse 584Å radiation were to be interpreted as due to the solar 584Å line backscattered by neutral He in interplanetary space, then 2  $R$  corresponds to  $n_{\text{He}}(\infty) \approx 3 \times 10^{-2} \text{ cm}^{-3}$ . This is not a restriction to the Holzer and Axford [1970] interpretation of the Vela 3 measurements.

In this paper we consider the orbits of interstellar  $\text{He}^+$  ions injected into an ideal (noise-free) Archimedean spiral magnetic field. The  $\text{He}^+$  ions originate from infalling interstellar wind neutral He atoms that are ionized in the interplanetary medium. We thus determine the velocity distribution function of  $\text{He}^+$  expected at 1 AU as a function of azimuthal position  $\phi$  in the ecliptic for different interstellar wind parameters. This study also gives orbits of atoms or molecules that escape from solar system bodies and are ionized in interplanetary space. An example of such a source could be neutral hydrogen ionized beyond the disturbed interface between the Venusian ionosphere and the solar wind. Detection and identification of such particles could yield information concerning atmospheric abundances and thermalization processes in the solar wind. Finally, we

W. C. Feldman, Los Alamos Scientific Laboratory, Los Alamos, New Mexico; J. J. Lange, Wright Patterson Air Force Base, Ohio; F. Scherb, University of Wisconsin, Madison, Wisconsin.

compare the various interpretations of infalling neutral He within the interplanetary medium.

### PITCH ANGLE SCATTERING BY MAGNETIC IRREGULARITIES IN THE SOLAR WIND

Before proceeding to a discussion of the orbits of very low-energy charged particles injected into the solar wind, we consider the magnitude of the perturbation caused by cyclotron-resonant pitch-angle scattering from magnetic irregularities convected by the solar wind. The problem with relevance to the low-energy particles of interest here has been treated theoretically by *Sturrock* [1966] and *Hall and Sturrock* [1967], and applied by *Barnes* [1970] to fast particles accelerated at the earth's bow shock and moving upstream in the solar wind. Assuming the dominant scattering process is pure magnetic cyclotron-resonant pitch-angle scattering, the particle velocity pitch-angle distribution function  $F$  is well approximated by a diffusion equation of the form

$$\frac{DF}{Dt} = \left( \frac{\partial}{\partial t} + V_{\parallel} \frac{\partial}{\partial Z} \right) F \cong \frac{1}{\sin \theta} \frac{\partial}{\partial \theta} \left[ \sin \theta G(V_{\parallel}) \frac{\partial F}{\partial \theta} \right]$$

where  $V_{\parallel}$  is the particle's velocity component parallel to the unperturbed magnetic field  $B_0$ , and

$$G(V_{\parallel}) = \frac{\pi^2 \nu^2}{B_0^2} P(\nu')$$

where  $\nu = eB_0/2\pi mc$  is the cyclotron frequency, and  $P(\nu')$  is the power density spectrum of the transverse magnetic field fluctuations evaluated at the frequency  $\nu'$ , which is Doppler shifted into the cyclotron frequency in the rest frame of the particle. To obtain an order of magnitude of the time scale  $\tau$  for the disruption of a beam of  $\text{He}^+$  particles moving relative to the solar wind, we approximate  $G$  as a constant and set  $x = \cos \theta$  so that

$$\frac{DF}{Dt} = G \frac{d}{dx} \left[ (1-x^2) \frac{dF}{dx} \right]$$

In the frame of reference moving with the particle beam

$$F(x, t) = \sum_{l=0}^{\infty} \exp[-l(l+1)Gt] P_l(x)$$

where the  $P_l(x)$  are  $l$ th-order Legendre polynomials. Thus the decay time  $\tau_l$  is given by

$$\tau_l = \frac{1}{l(l+1)G}$$

Power spectra of the interplanetary magnetic field have been reported by *Coleman* [1966] for the Mariner 2 magnetometer, by *Siscoe et al.* [1968] for the Mariner 4 magnetometer, and by *Sari and Ness* [1969] for the Pioneer 6 magnetometer. Comparison of these results indicates that the power level at a given frequency can vary significantly depending on solar activity. Since the  $\text{He}^+$  particles to be discussed later are for the most part moving away from the sun, a conservative choice of frequency for evaluating the power spectrum is the cyclotron frequency which for  $\text{He}^+$  in a  $6\gamma$  magnetic field (at 1 AU) is  $2.3 \times 10^{-2}$  Hz. Choosing  $P(2 \times 10^{-2} \text{ Hz}) = 3 \times 10^{-1} \gamma^2/\text{Hz}$  from Mariner 4 data for quiet periods yields

$$2G = 2 \times 10^{-6} \text{ sec}^{-1}$$

and consequently  $\tau_1 = 5 \times 10^5$  sec. But  $5 \times 10^5$  sec is about equal to the expected ion transit times from  $r = 0.1$  AU to 1 AU if the He radial velocity at the point of ionization is away from the sun.

This estimate for  $\tau$  is probably uncertain by at least two orders of magnitude due primarily to the approximate nature of the diffusion equation, the evaluation of  $P$  at 1 AU and the choice of  $l = 1$ . Of course, more peaked pitch-angle distribution functions are characterized by higher  $l$  values and so are damped more quickly. Most important, because it is unknown experimentally, is the radial dependence of the power spectrum evaluated at the Doppler shifted gyrofrequency. Evidence from Mariner 4 magnetic field data [*Coleman et al.*, 1969] indicates that the power density for a given frequency generally decreases roughly as  $r^{-2}$  for  $1 \text{ AU} < r < 1.43 \text{ AU}$  where  $r$  is the heliocentric distance. but as  $r$  increases,  $B$  decreases and so does the gyrofrequency. The radial dependence relevant to our problem is that of the power density spectrum evaluated at the Doppler shifted gyrofrequency. From figure 14 of *Coleman et al.* [1969] it is seen that this is almost independent of  $r$  for  $1 \text{ AU} < r < 1.43 \text{ AU}$ . In any case, it is expected to be less dependent upon  $r$  than the power density spectrum evaluated at a fixed frequency.

Considering these uncertainties coupled with the measured variability of the solar wind, one can conclude neither that significant pitch-angle scattering occurs in transit to 1 AU nor that the  $\text{He}^+$  orbits remain unperturbed by magnetic field fluctuations. Furthermore, as pointed out by *Barnes* [1970],  $\tau_1$  refers only to the disruption of the beam by hydromagnetic waves but not to thermalization. The time scale for thermalization is expected to be longer.

It is thus useful to determine the unperturbed orbits in an ideal spiral magnetic field as a function of injection

position and velocity. It is expected that particles injected at small  $r$  will undergo some degree of pitch-angle scattering, whereas those injected around 1 AU will follow unperturbed orbits. One can then compare future measurements of the  $\text{He}^+$  velocity distribution function with both the thermalized and unperturbed limits to obtain information concerning interstellar wind parameters as well as wave-particle interactions in the solar wind.

### UNPERTURBED ORBITS OF A TEST PARTICLE INJECTED INTO THE SOLAR WIND

The coordinate system relevant to this discussion is shown in figure 1. The sun is assumed to move with velocity  $\langle V_\infty \rangle$  relative to a cold ( $T = 100^\circ \text{ K}$ ) interstellar cloud such that in the frame of reference with the sun at rest at the origin, neutral He atoms appear to be moving parallel to the YZ plane at an angle  $\Theta$  with respect to the Z axis. The positive Z axis is oriented northward perpendicular to the ecliptic. The XY plane is coincident with the ecliptic. Infalling He atoms follow hyperbolic trajectories before being ionized by solar EUV. After ionization they are accelerated by a radially convected spiral magnetic field. Although the spiral magnetic field pattern is cylindrically symmetric, the subsequent charged particle trajectories are not, due to the asymmetric initial injection velocities.

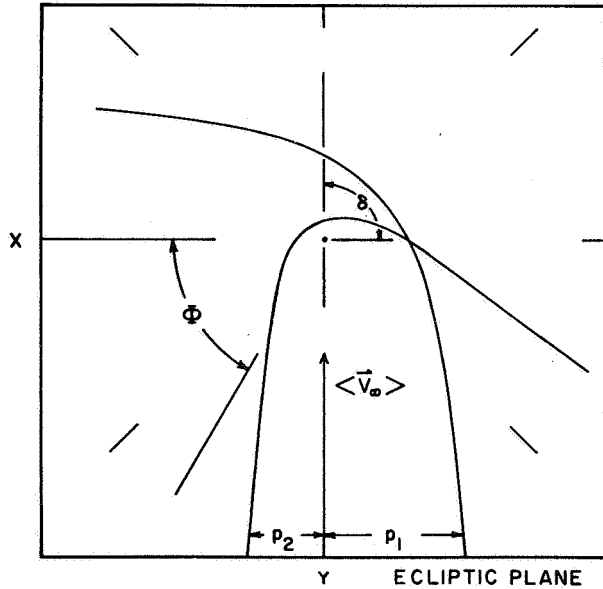


Figure 1 Interstellar infall coordinate system with  $\langle V_\infty \rangle$  in the ecliptic.

Each He atom hyperbolic orbit is planar. Every point in the orbit plane can be specified equivalently by  $r$ , the radial distance from the sun, and  $\delta$ , the angle between  $r$  and  $\langle V_\infty \rangle$ , or by two impact parameters  $p_1$  and  $p_2$  identifying both a direct and indirect orbit, respectively, which pass through that point. Fahr [1968] obtained an expression for the neutral number density  $n_{\text{He}}^0(r)$  at any point for  $T = 0^\circ \text{ K}$  using the continuity equation. Rewriting his results we obtain

$$n_{\text{He}}^0(r) = n_1 \exp \left[ \frac{-r_e^2 P(r_e)(\pi - \delta)}{\langle V_\infty \rangle p_1} \right] + n_2 \exp \left[ \frac{-r_e^2 P(r_e)(\pi + \delta)}{\langle V_\infty \rangle p_2} \right] \quad (1)$$

where

$$n_1 = \left( \frac{p_1^2}{p_1^2 - p_2^2} \right) n_{\text{He}}(\infty)$$

$$n_2 = n_1 - n_{\text{He}}(\infty)$$

$$p_1 = \frac{r \sin \delta}{2} + \left[ \left( \frac{r \sin \delta}{2} \right)^2 + rb(1 + \cos \delta) \right]^{1/2}$$

$$p_2 = p_1 - r \sin \delta$$

$$b = \frac{GM}{\langle V_\infty \rangle^2}$$

and  $n_{\text{He}}(\infty)$  is the number density of neutral He at  $r = \infty$ ,  $P(r_e)$  is the probability per sec for ionization at  $r_e = 1 \text{ AU}$ ,  $G$  is the gravitational constant, and  $M$  is the solar mass;  $P(r_e)$  is variable, but is chosen here as

$$P(r_e) = 6.8 \times 10^{-8} \text{ sec}^{-1}$$

In figures 2 and 3, we plot two cuts through the normalized neutral He number density distribution  $n_{\text{He}}^0(r)/n_{\text{He}}(\infty)$ . The radial dependence of  $n_{\text{He}}^0(r)/n_{\text{He}}(\infty)$  for  $\langle V_\infty \rangle = 20 \text{ km/sec}$  oriented in the ecliptic ( $\Theta = 90^\circ$ ) is plotted in figure 2 for ecliptic positions oriented at right angles to  $\langle V_\infty \rangle$ . One sees that, beyond 1 AU,  $n_{\text{He}}^0(r)/n_{\text{He}}(\infty)$  is essentially constant. On the other hand, the azimuthal dependence is dominated by a dense tail in the antiapex direction. This feature is characteristic of the gravitational focusing problem; it is real and limited only by the temperature of the infalling

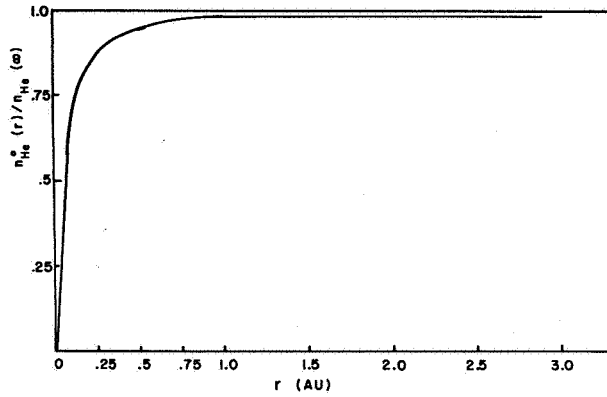


**Figure 2** Normalized neutral He number density as a function of heliocentric distance:  $\langle V_\infty \rangle = 20$  km/sec,  $\Theta = 90^\circ$ ,  $\phi = 0^\circ$  or  $180^\circ$ .

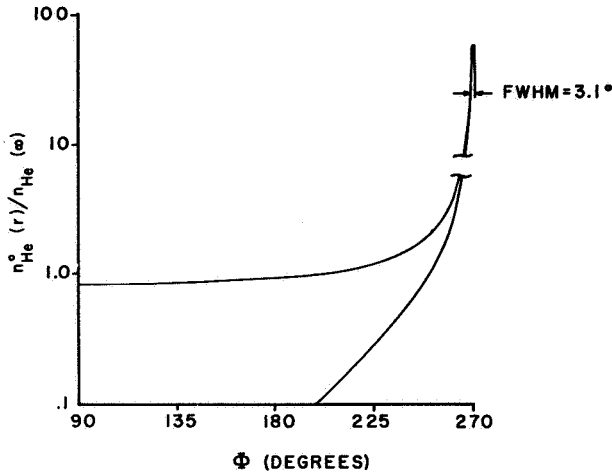


**Figure 3** Normalized neutral He number density as a function of azimuth:  $\langle V_\infty \rangle = 20$  km/sec,  $T = 100^\circ$  K,  $r = 0.5$  AU. The He density plotted in the neighborhood of  $\phi = 270^\circ$  is the sum of contributions from both direct and indirect orbits.

gas. For  $\delta = 0$  and  $T = 0^\circ$  K,  $p_1 = p_2$ ; hence, both  $n_1$  and  $n_2 = \infty$ . For  $T$  different from zero but such that  $m\langle V_\infty \rangle^2 / 2kT \gg 1$ , we can obtain an analytic expression for  $n_1$  and  $n_2$  at  $\delta = 0$  by integrating  $n_{\text{He}}^0(r)$  weighted by an isotropic maxwellian velocity distribution over  $V_\infty$ . The velocity-space coordinate system for this calculation is outlined in figure 4.

For  $\delta \ll 1$ , we can write a maxwellian distribution in the form

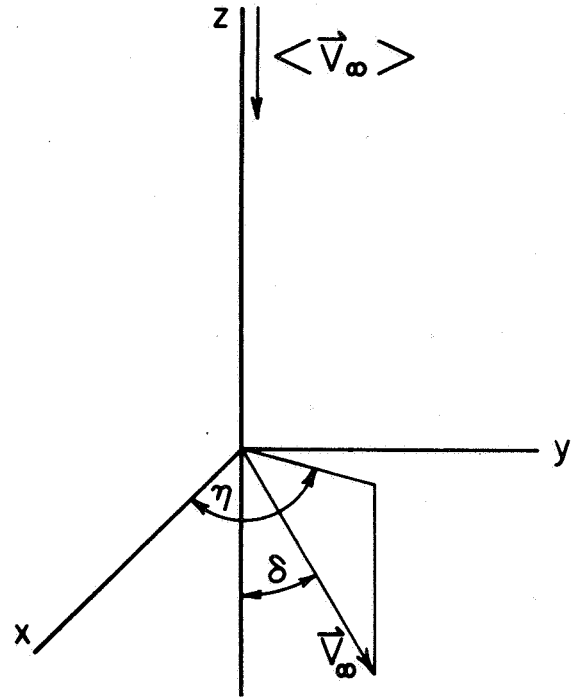


**Figure 4** Velocity space coordinate system relevant to calculation of the neutral He number density for  $\delta = 0$ .

$$F(V_\infty) d^3 V_\infty = \left( \frac{m}{2\pi kT} \right)^{3/2} \exp \left[ \frac{-m(V_\infty - \langle V_\infty \rangle)^2}{2kT} \right] \exp \left[ \frac{-mV_\infty \langle V_\infty \rangle \delta^2}{2kT} \right] d^3 V_\infty$$

Then,

$$n_{\text{He}}^0(r, \delta) = \int_0^\infty \int_0^\pi \int_0^{2\pi} n_{\text{He}}^0(r, \delta) F(V_\infty) V_\infty^2 dV_\infty \sin \delta d\delta d\eta$$

To find  $n_{\text{He}}^0(r, \delta)$ , note that

$$\lim_{\delta \rightarrow 0} p_1 = (2br)^{1/2} \quad \lim_{\delta \rightarrow 0} (p_1 - p_2) = r\delta$$

hence

$$n_{\text{He}}^0(r, \delta) = \frac{1}{\delta} n_{\text{He}}^0(\infty) \left( \frac{2b}{r} \right)^{1/2} \exp \left[ \frac{-\pi r_e^2 P(r_e)}{(2br)^{1/2} \langle V_\infty \rangle} \right]$$

and

$$n_{\text{He}}(r, \phi)$$

$$= 2\pi n_{\text{He}}^{(\infty)} \left( \frac{m}{2\pi kT} \right)^{3/2} \left( \frac{2b}{r} \right)^{1/2} \exp \left[ \frac{-\pi r e^2 P(r_e)}{(2br)^{1/2} \langle V_{\infty} \rangle} \right] \times$$

$$\int_0^{\infty} \frac{\langle V_{\infty} \rangle}{V_{\infty}} \exp \left[ \frac{(V_{\infty} - \langle V_{\infty} \rangle)^2}{2kT} \right] V_{\infty}^2 dV_{\infty} \times$$

$$\int_0^{\infty} \exp \left[ \frac{-m V_{\infty} \langle V_{\infty} \rangle \delta^2}{2kT} \right] d\delta$$

Here we have extended the limits of integration for  $\delta$  to  $+\infty$  since  $m V_{\infty} \langle V_{\infty} \rangle / 2kT \gg 1$  and the exponential will cut off the integral. The  $\delta$  integral can then be evaluated exactly. Integration over  $V_{\infty}$  is straightforward. The result is

$$n_{\text{He}}(r, \phi) = n_{\text{He}}^{(\infty)} \left( \frac{\pi G M m}{r k T} \right)^{1/2} \exp \left[ \frac{-\pi r e^2 P(r_e)}{(2 G M r)^{1/2}} \right]$$

Off-axis values of  $n_{\text{He}}(r, \delta)$  were constructed using the parabolic-interpolation formula

$$n_{\text{He}}(r, \delta) = n_{\text{He}}(r, \phi) (1 - D \delta^2)$$

where  $D$  is determined by the imposed constraint

$$n_{\text{He}}(r, \phi) (1 - D \delta_c^2) = \frac{1}{\delta_c} n_{\text{He}}^{(\infty)} \left( \frac{2b}{r} \right)^{1/2} \times \exp \left[ \frac{-\pi r e^2 P(r_e)}{(2 G M r)^{1/2}} \right]$$

at some angle  $\delta_c$ . This yields

$$\delta_c = \frac{3}{2} \left( \frac{\pi m \langle V_{\infty} \rangle^2}{2kT} \right)^{-1/2}$$

and

$$D = \frac{2\pi m \langle V_{\infty} \rangle^2}{27kT}$$

The neutral He-normalized number density distribution is plotted in figure 3 as a function of ecliptic azimuth  $\phi$  for  $\langle V_{\infty} \rangle = 20$  km/sec,  $T = 100^\circ$  K, and  $r = 0.5$  AU. The upper curve refers to direct orbits (characterized by impact parameter  $p_1$ ), and the lower curve refers to indirect orbits (characterized by impact parameter  $p_2$ ). The He density plotted in the neighborhood of  $\phi = 270^\circ$  is the sum of contributions from both direct and indirect orbits. Two important characteristics of the curves should be noted. First, in the forward hemisphere direct orbit densities dominate indirect orbit densities due to the much longer angular distance traveled by the latter. Second, there is a marked anisotropy (here 67:1) of number density in backward and forward directions resulting from an enhanced tail with FWHM =  $3.1^\circ$  for  $T = 100^\circ$  K.

We now specify the ion position in the usual ecliptic polar coordinates  $r, \theta, \phi$  where  $r$  is the radial distance from the sun,  $\theta$  is the polar angle with respect to the north ecliptic, and  $\phi$  is the azimuthal angle with respect to the  $x$  axis. We further define  $\chi$  as the angle between  $\mathbf{r}$  and the magnetic field  $\mathbf{B}$ . Then the Archimedean spiral magnetic field is given by

$$\left. \begin{aligned} B_r &= B_a \left( \frac{a}{r} \right)^2 \\ B_\theta &= 0 \\ B_\phi &= -B_a \left( \frac{a}{r} \right)^2 \tan \chi \\ B &= B_a \left( \frac{a}{r} \right)^2 / \cos \chi \end{aligned} \right\} \quad (2)$$

where  $\cos \chi = [1 + (r \omega \sin \theta / V_{sw})^2]^{-1/2}$ , the angular speed of the sun  $\omega = 2.9 \times 10^{-6}$  rad/sec,  $B_a$  is the radial component of the magnetic field at some reference radius  $a$ , and  $V_{sw}$  is the radial solar wind velocity.

The equations governing the motion of a charged test particle in a slowly varying electric and magnetic field in the guiding center approximation were developed by Northrop [1963]. The motion can be separated into three components: (1) the superposition  $V_D$  of various drift velocities perpendicular to the magnetic field, (2) a circulating velocity  $V_\perp$  about the magnetic field, (3) a velocity  $V_\parallel$  parallel to the magnetic field. We now treat each of these components in turn specializing to the

above radially convected spiral magnetic field pattern.

The only perpendicular drift velocity of consequence is that due to the appearance of an electric field in the frame of reference at rest with respect to the sun. Here  $V_D = V_{sw} \sin \chi$  with direction perpendicular to  $\mathbf{B}$  but confined to the cone specified by  $\theta = \text{constant}$ .

The component of motion circulating about  $\mathbf{B}$  is determined in the adiabatic limit (which fits our problem) by the conservation of the magnetic moment  $\mu$ , given by

$$\mu = \frac{mV_{\perp}^2}{2B} \quad (3)$$

The equation governing the motion parallel to the field direction given by *Northrup* [1963] is

$$\begin{aligned} \frac{m dV_{\parallel}}{dt} = mg_{\parallel} + qE_{\parallel} - \mu \frac{\partial B}{\partial s} + mV_D \\ \cdot \left[ \frac{\partial \mathbf{e}_{\parallel}}{\partial t} + V_{\parallel} \frac{\partial \mathbf{e}_{\parallel}}{\partial s} + (\mathbf{V}_D \cdot \nabla) \mathbf{e}_{\parallel} \right] \end{aligned} \quad (4)$$

where  $m$  is the mass of the particle, the magnetic field direction is specified by the unit vector  $\mathbf{e}_{\parallel}$ ,  $g_{\parallel}$  is the component of the sun's gravitational acceleration along  $\mathbf{e}_{\parallel}$ ,  $q$  is the particle charge,  $E_{\parallel}$  is the component of electric field parallel to  $\mathbf{e}_{\parallel}$ , and  $s$  is arc length along  $\mathbf{e}_{\parallel}$ . In our problem  $E_{\parallel} = 0$  and  $\partial \mathbf{e}_{\parallel} / \partial t = 0$ . Setting  $\partial / \partial s = \mathbf{e}_{\parallel} \cdot \nabla$  in equation (4) and carrying through the algebra, we obtain

$$\begin{aligned} \frac{dV_{\parallel}}{dt} = \frac{\mu}{m} \frac{B \cos \chi}{r} (1 + \cos^2 \chi) - \frac{GM \cos \chi}{r^2} \\ + \frac{V_{sw} \sin^2 \chi}{r} [V_{sw} \cos^3 \chi - V_{\parallel} (1 + \cos^2 \chi)] \end{aligned} \quad (5)$$

The total noncirculating velocity is then given by

$$\mathbf{V} = V_{\parallel} \mathbf{e}_{\parallel} + \mathbf{V}_D$$

yielding

$$\frac{dr}{dt} = V_{\parallel} \cos \chi + V_{sw} \sin^2 \chi \quad (6)$$

Combining equations (5) and (6) to eliminate the time, we obtain (after some algebra) an equation for  $V_{\parallel}$  in terms of  $r$  alone:

$$\begin{aligned} d \left( \frac{V_{\parallel}^2}{2} + V_{\parallel} \frac{V_{sw} \sin^2 \chi}{\cos \chi} \right) \\ = dr \left[ \frac{\mu}{m} \frac{B(r)}{r} (1 + \cos^2 \chi) - \frac{GM}{r^2} + (V_{sw}^2) \frac{\sin^2 \chi \cos^2 \chi}{r} \right] \end{aligned} \quad (7)$$

Equation (5) can be integrated to yield

$$V_r = (V_{\parallel} \cos \chi + V_{sw} \sin^2 \chi) = \pm \frac{V_{sw} f(\xi)}{(1 + \xi^2)^{1/2}} \quad (8)$$

$$\begin{aligned} V_{\phi} = (-V_{\parallel} \sin \chi + V_{sw} \sin \chi \cos \chi) \\ = \frac{\xi V_{sw}}{(1 + \xi^2)^{1/2}} [(1 + \xi^2)^{1/2} \mp f(\xi)] \end{aligned} \quad (9)$$

where

$$\begin{aligned} f(\xi) = \left\{ (\xi^2 - \xi_0^2) - \left( \frac{V_{\perp 0}}{V_{sw}} \right)^2 \left[ \frac{(1 + \xi^2)^{1/2} \xi_0^2}{(1 + \xi_0^2)^{1/2} \xi^2} - 1 \right] \right. \\ \left. + \left( \frac{2GM \omega \sin \theta}{V_{sw}^3} \right) \left( \frac{1}{\xi} - \frac{1}{\xi_0} \right) \right. \\ \left. + \left[ \frac{V_{\parallel 0}}{V_{sw}} + \frac{\xi_0^2}{(1 + \xi_0^2)^{1/2}} \right]^2 \right\}^{1/2} \end{aligned} \quad (10)$$

Here  $\xi = \omega r \sin \theta / V_{sw}$  is a dimensionless radial distance, and all quantities appearing with a subscript zero refer to the initial conditions. The equation for the trajectory can be written in dimensionless form as

$$\frac{d\xi}{d\phi} = \frac{\xi \sin \theta V_r}{V_{\phi}} = \pm \frac{\sin \theta f(\xi)}{[(1 + \xi^2)^{1/2} \mp f(\xi)]} \quad (11)$$

where the minus and plus signs refer to motion in, toward or away from the sun, respectively.

To complete the problem the initial velocity conditions at the point of injection need be specified. We

consider first the trajectories resulting from a zero initial velocity and then proceed to the interstellar wind problem.

#### Zero-Velocity Initial Conditions

Here  $V_{||0} = 0$  and  $V_{\perp 0} = V_D = V_{sw} \sin \chi_0$  since the orbits are initially cycloidal. Equation (11) was solved on the University of Wisconsin's Univac 1108 computer with a "Math-Pack" subroutine utilizing Hamming's method of solving ordinary first-order differential equations. The initial noncirculating velocity is perpendicular to  $B$  but away from the sun. Since  $B$  decreases as  $r$  increases, the conservation of the magnetic moment converts part of the circulating velocity into the parallel component. Specializing to the problem of injection into the unperturbed solar wind at Venus, the azimuthal angle as a function of radius characterizing the trajectory is plotted in figure 5. Components of the velocity as a function of  $r$  are plotted in figure 6. Again,  $V_{sw} = 400$  km/sec. Since both the spiral field pattern and the initial injection conditions are azimuthally symmetric about the sun, there is no focusing of the particle beam in the ecliptic. Thus its observed angular diameter should remain constant. Any deviation would then be due to interaction with magnetic irregularities convected by the wind.

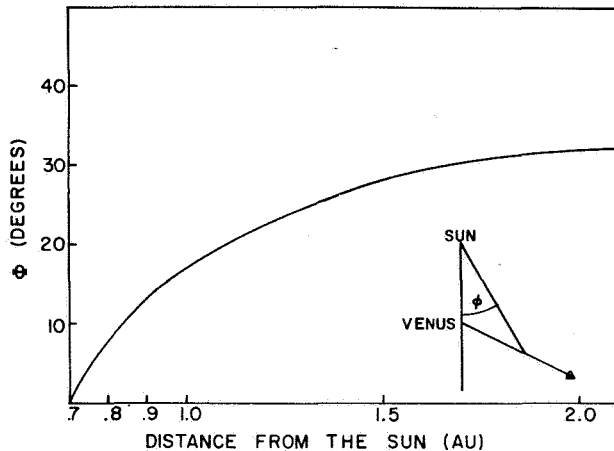


Figure 5 Azimuthal position of a charged particle relative to the azimuthal position of injection into the solar wind at Venus.

#### Interstellar Infall Initial Conditions

The neutral particle velocity at the point of ionization is determined by conservation of energy and angular momentum. For the indirect orbits  $V_r = V_{\infty} [1 + 2b/r_0 - (p_1/r_0)^2]^{1/2}$  and  $V_{\gamma} = -V_{\infty} p_1/r_0$ , where  $b = GM/V_{\infty}^2$ . For the direct orbits

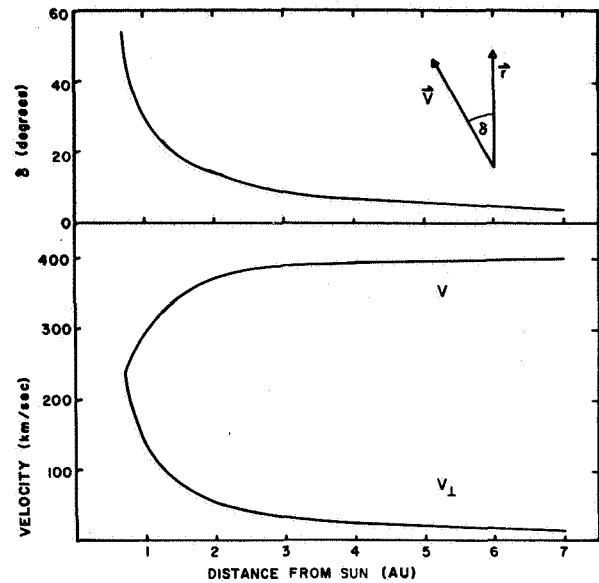


Figure 6 Components of the velocity of a charged particle injected into the solar wind at Venus as a function of heliocentric distance.

$V_r = \pm V_{\infty} [1 + 2b/r - (p_1/r)^2]^{1/2}$  where the  $\pm$  refers to  $\gamma \gtrless \gamma_{\min} = \tan^{-1}(-p_1/b)$  and  $V_{\gamma} = V_{\infty} p_1/r_0$ . The initial neutral velocity is  $V_N = V_r e_r + V_{\gamma} e_{\gamma}$  yielding  $(V_{||})_{\infty} = V_N \cdot e_{||}$  and  $(V_{\perp})_{\infty} = V_N - V_N \cdot e_{||} = V_D$ . The effect of the asymmetry of these initial conditions with respect to azimuthal injection angle  $\phi_0$  on the subsequent trajectories is greater as  $r_0$  decreases. This asymmetry is illustrated in figures 7 and 8 for injection from direct and indirect neutral orbits, respectively, at  $r_0 = 0.15$  AU with  $V_{\infty}$  and  $r_0$  in the ecliptic. The effect is most noticeable for the direct orbits characterized by  $90^\circ \leq \phi_0 \leq 270^\circ$ . As  $\phi_0$  increases from  $90^\circ$ , the magnetic moment decreases due to a cancellation effect reducing the magnetic mirror repulsion of the diverging field lines. Consequently, there is a region of impact angles around  $\phi_0 = 180^\circ$  for which ionized He atoms have access to the photosphere. This assumes a noise-free Archimedean spiral model extending all the way in to the photosphere which is not the case in reality. Proceeding further around in azimuthal angle,  $V_r$  decreases to zero as well, yielding trajectories that circulate about the sun through large angles before making their way out to large  $r$ . One such trajectory not plotted in figure 7 circled about the sun three times before reaching large  $r$ . Of course, such an orbit is unphysical due to interaction with magnetic irregularities but it illustrates the azimuthal focusing characteristics of the problem. The indirect orbits are illustrated in figure 8. These are much more regular but still demonstrate a degree of azimuthal



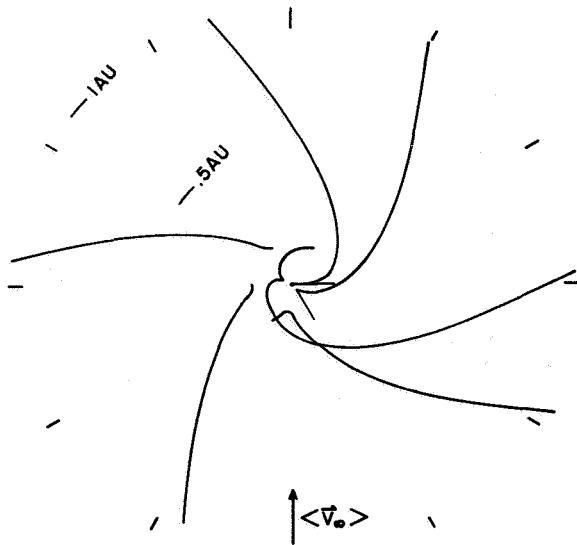


Figure 7  $\text{He}^+$  orbits in an ideal spiral magnetic field following injection from direct neutral helium orbits:  $\langle V_\infty \rangle = 20$  km/sec,  $\Theta = 90^\circ$ ,  $V_{sw} = 400$  km/sec, and  $r_0 = 0.15$  AU.



Figure 8  $\text{He}^+$  orbits in an ideal spiral magnetic field following injection from indirect neutral helium orbits:  $\langle V_\infty \rangle = 20$  km/sec,  $\Theta = 90^\circ$ ,  $V_{sw} = 400$  km/sec, and  $r_0 = 0.15$  AU.

focusing. The effects of the asymmetric initial conditions on the trajectories become less pronounced as the injection radius increases since the infall velocity becomes small compared to the drift velocity  $V_D = V_{sw} \sin \chi$ .

We are interested in calculating the  $\text{He}^+$  velocity distribution function, which would be measured by a spacecraft observing at 1 AU in the ecliptic. Toward this end we need to know the locus of all source points for particle trajectories intersecting a given angular sector at 1 AU. This was accomplished numerically for  $20^\circ$  wide angular sectors centered on  $\phi = 0^\circ, 90^\circ, 180^\circ$ , and  $270^\circ$ , for  $\langle V_\infty \rangle = 10, 20$ , and  $40$  km/sec, and for angles of incidence  $\Theta$  with respect to the north ecliptic of  $0^\circ, 45^\circ$ , and  $90^\circ$ . All orbits penetrating to  $r_0$  less than  $0.05$  AU were excluded from consideration. Typical configurations are illustrated for direct and indirect orbits in figures 9 and 10 for  $\langle V_\infty \rangle = 20$  km/sec and  $\Theta = 45^\circ$ . As

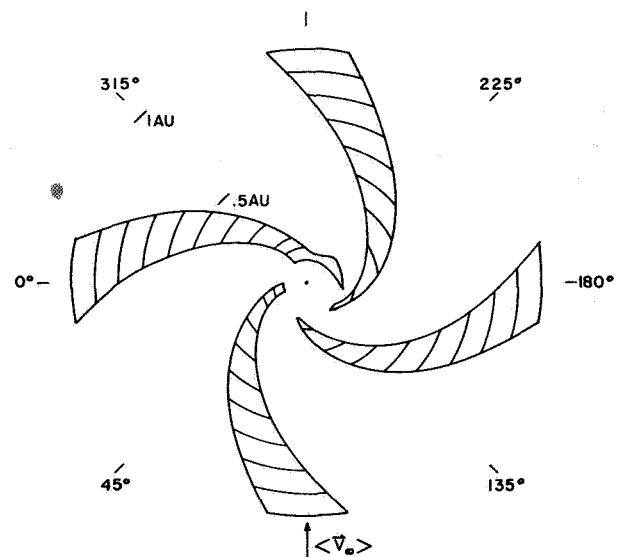
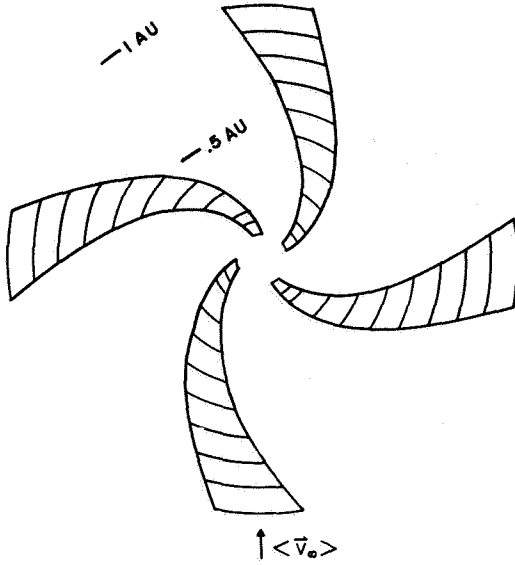


Figure 9 Locus of source points of  $\text{He}^+$  for detection at 1 AU following injection from direct neutral helium orbits:  $\langle V_\infty \rangle = 20$  km/sec,  $\Theta = 45^\circ$ ,  $V_{sw} = 400$  km/sec.

can be seen, the focusing effect of the interplanetary fields becomes more prominent at small injection radii. For example, the locus of points intersecting the  $\phi = 0^\circ$  sector from  $r_0 = 0.15$  AU splits into two angular sectors at  $0.15$  AU due to the partial cancellation of the magnetic moment coupled with the changing sign (from minus to plus as  $\phi_0$  increases past the angle of perihelion) of the initial radial velocity.

To construct the  $\text{He}^+$  velocity distribution function we must sum separately the contributions enclosed within each sectorized locus diagram for both direct and indirect orbits. Denoting direct neutral orbit initial conditions by  $J = 1$  and indirect neutral orbits by  $J = 2$ , we



**Figure 10** Locus of source points of  $\text{He}^+$  for detection at 1 AU following injection from indirect neutral helium orbits:  $\langle V_\infty \rangle = 20$  km/sec,  $\Theta = 45^\circ$ ,  $V_{sw} = 400$  km/sec.

obtain from flux conservation

$$n_{\text{He}^+}^{(J)}(r_e, \phi_e) = \int_0^{r_e} \frac{dN^+}{dr_o} dr_o \quad (12)$$

where

$$\frac{dN^+}{dr_o} = \frac{n_{\text{He}}^{(J)}(r_o, \phi_o) P(r_e)}{V_r^{(J)}(r_e, \phi_e; r_o, \phi_o)} \left( \frac{d\phi_o}{d\phi_e} \right) \quad (13)$$

and  $n_{\text{He}^+}^{(J)}(r_e, \phi_e)$  is the  $\text{He}^+$  number density at the point  $(r_e, \phi_e)$ ;  $n_{\text{He}}^{(J)}(r_o, \phi_o)$  is the neutral He number density at the point  $(r_o, \phi_o)$ ;  $V_r^{(J)}(r_e, \phi_e; r_o, \phi_o)$  is the radial component of  $\text{He}^+$  velocity at  $(r_e, \phi_e)$  for those particles originating at  $(r_o, \phi_o)$ ; and  $d\phi_o/d\phi_e$  denotes the ratio of the azimuthal angular sector  $d\phi_o$  at  $(r_o, \phi_o)$  to the given sector  $d\phi_e$  at  $(r_e, \phi_e)$  into which  $d\phi_o$  is mapped. The integral is evaluated along the locus sector.

The integrand of equation (12) is plotted as a function of  $r_o$  and  $\phi_e$  in figures 11 through 14 for  $\langle V_\infty \rangle = 10, 20$ , and  $40$  km/sec and  $\Theta = 45^\circ$  and  $0^\circ$ . No plots for  $\Theta = 90^\circ$  are given due to the extreme anisotropy resulting from the presence of the dense, well-defined neutral-particle tail mentioned earlier. The definition of this tail depends strongly on the neutral gas temperature.

For  $T = 100^\circ$  K its contribution to  $n_{\text{He}^+}^{(J)}(r_e, \phi_e)$  depends critically on  $\Theta$  since the FWHM of the tail is about  $3^\circ$ .

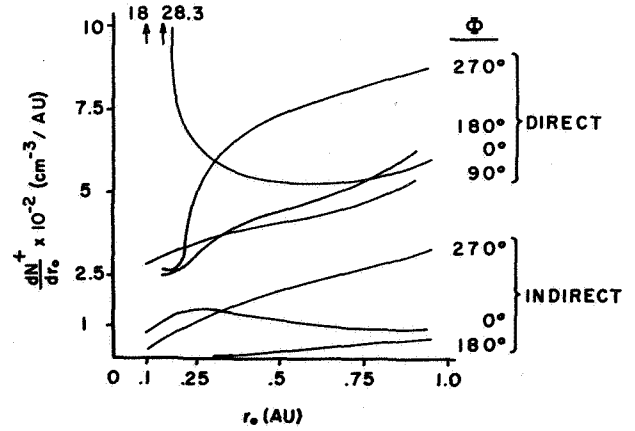


**Figure 11** Differential  $\text{He}^+$  number density at 1 AU as a function of injection radius:  $\langle V_\infty \rangle = 10$  km/sec,  $\Theta = 45^\circ$ ;  $\phi_e$  denotes the azimuthal position of observation in the ecliptic.

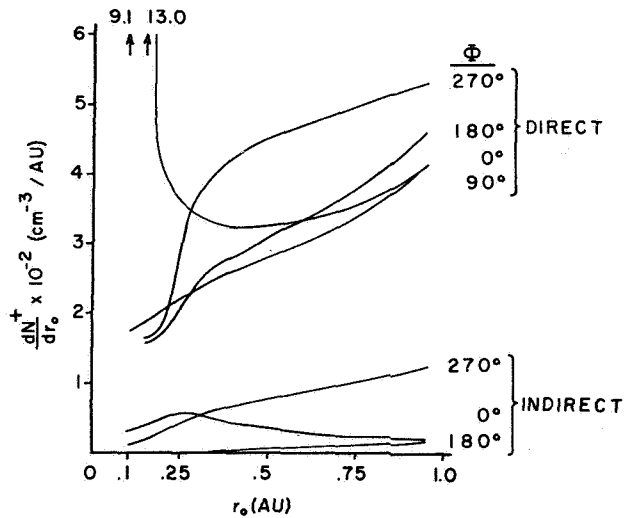


**Figure 12** Differential  $\text{He}^+$  number density at 1 AU as a function of injection radius:  $\langle V_\infty \rangle = 20$  km/sec,  $\Theta = 45^\circ$ ;  $\phi_e$  denotes the azimuthal position of observation in the ecliptic.

Furthermore, a crude (for  $3^\circ$  FWHM variation)  $15^\circ$  grid was used in our numerical analysis to calculate  $n_{\text{He}^+}^{(J)}(r_e, \phi_e)$  and thus is not suited for calculation in this case.

For  $\Theta = 90^\circ$  and  $T = 100^\circ$  K, one might expect to observe anisotropies in  $n_{\text{He}^+}^{(J)}(r_e, \phi_e)$  of the order of 50 (fig. 3).

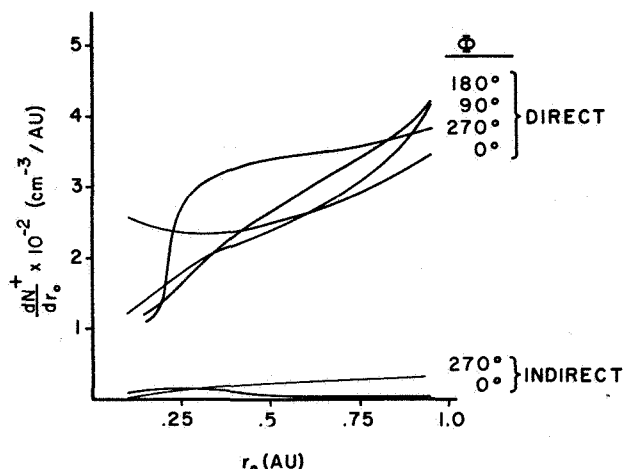


Figure 13 Differential  $\text{He}^+$  number density at 1 AU as a function of injection radius:  $\langle V_\infty \rangle = 40$  km/sec,  $\Theta = 45^\circ$ ;  $\phi_e$  denotes the azimuthal position of observation in the ecliptic.

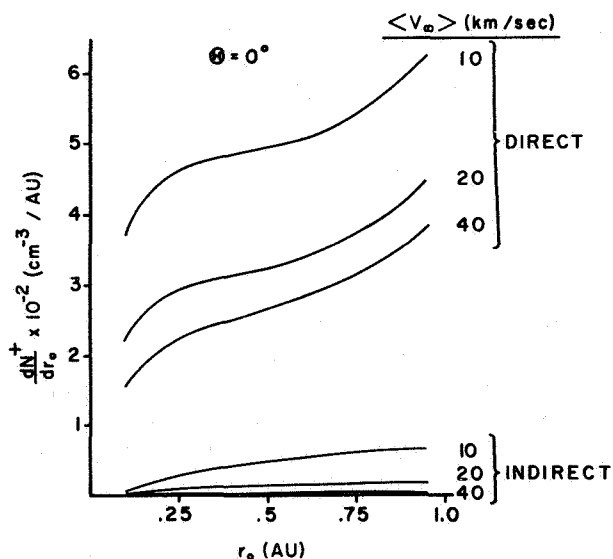


Figure 14 Differential  $\text{He}^+$  number density at 1 AU as a function of injection radius for  $\Theta = 0^\circ$ .

The  $\text{He}^+$  number density at 1 AU integrated over velocity space and normalized to  $n_{\text{He}(\infty)}$  is summarized in table 1 for  $\Theta = 45^\circ$  and  $0^\circ$  and  $\langle V_\infty \rangle = 10, 20$ , and 40 km/sec. It can be seen that  $n_{\text{He}^+}^{(J)}(r_e, \phi_e)$  increases with decreasing  $\langle V_\infty \rangle$  and that the anisotropy with respect to azimuthal phase  $\phi_e$  at 1 AU increases with

Table 1 Integrated normalized  $\text{He}^+$  number density  $n_{\text{He}^+}(r_e, \phi_e)/n_{\text{He}(\infty)}$  at 1 AU

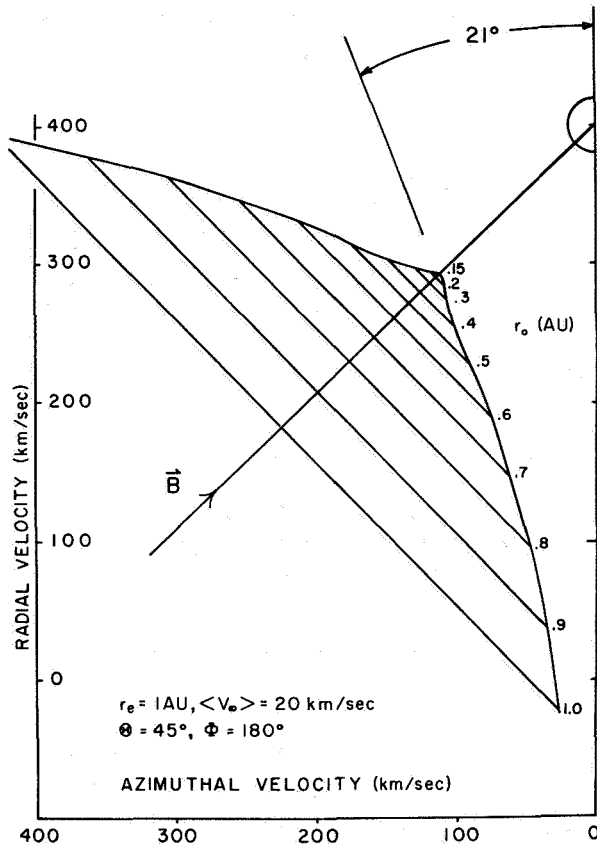
$\Theta = 45^\circ$				
$\langle V_\infty \rangle$ (km/sec)	$n_{\text{He}^+}(r_e, \phi_e)/n_{\text{He}(\infty)}$			
	$\phi_e = 90^\circ$	$\phi_e = 180^\circ$	$\phi_e = 270^\circ$	$\phi_e = 360^\circ$
10	$3.8 \times 10^{-2}$	$4.2 \times 10^{-2}$	$7.9 \times 10^{-2}$	$7.5 \times 10^{-2}$
20	$2.7 \times 10^{-2}$	$2.8 \times 10^{-2}$	$4.4 \times 10^{-2}$	$4.1 \times 10^{-2}$
40	$2.4 \times 10^{-2}$	$2.4 \times 10^{-2}$	$3.0 \times 10^{-2}$	$2.5 \times 10^{-2}$

$\Theta = 0^\circ$	
$\langle V_\infty \rangle$ (km/sec)	$n_{\text{He}^+}(r_e)/n_{\text{He}(\infty)}$
10	$5.0 \times 10^{-2}$
20	$3.2 \times 10^{-2}$
40	$2.5 \times 10^{-2}$

increasing  $\Theta$  as well as decreasing  $\langle V_\infty \rangle$ . These effects primarily reflect the behavior of the neutral He number density in interplanetary space, but are also affected somewhat by the greater anisotropy of initial velocity conditions as  $\Theta$  increases to  $90^\circ$ .

From equations (3), (8), and (9), we know the velocity of particles at 1 AU as a function of their injection position. Combining this information with  $dN^+/dr_0$  from equation (13) we can construct the unperturbed velocity distribution function. Figure 15 shows a projection into the ecliptic of the position in velocity space occupied by ions with injection radii ranging between  $r_0 = 0.15$  AU and 1.0 AU. The actual positions in velocity space are circles about B with diameters indicated in the figure. A spherical velocity contour of 20 km/sec about the solar wind velocity  $V_{\text{sw}} = 400$  km/sec is sketched in for reference purposes. The minimum velocity angle with respect to the radial direction is  $21^\circ$  for the conditions  $\langle V_\infty \rangle = 20$  km/sec,  $\Theta = 45^\circ$ , and  $\phi_e = 180^\circ$ . This minimum velocity angle for different sun-cloud configurations is tabulated in table 2. It is seen that this angle varies only slightly for markedly different incident conditions. The cone of occupation can change shape by at most 15 percent to 20 percent for the different incident conditions considered here. But since the distribution function is so diffuse to begin with, this is not a major effect.



**Figure 15** Projection of the  $\text{He}^+$  velocity distribution function into the ecliptic. Each line drawn perpendicular to  $\mathbf{B}$  represents the diameter of a circle about  $\mathbf{B}$  corresponding to  $\text{He}^+$  ions injected into the solar wind at  $r = r_0$ . The circle about a radial velocity of 400 km/sec represents the projection of a sphere with 20 km/sec radius.

## DISCUSSION

We proceed now to the question of whether the model of cold interstellar He infalling into interplanetary space is consistent with the Vela 3 observations of  $\text{He}^+$ . The two relevant Vela 3 observational results are: (1) Most of the time, the ratio  $n_{\text{He}^+}(r_e)/n_{\text{He}^{++}}(r_e)$  is less than  $10^{-3}$ ; and (2) on rare occasions,  $n_{\text{He}^+}(r_e)/n_{\text{He}^{++}}(r_e)$  is observed to be  $3 \times 10^{-3} \pm 50$  percent [Bame et al., 1968].

Furthermore, we require that the model be consistent with recent observations of extraterrestrial diffuse Lyman  $\alpha$  radiation observed with instruments on OGO 5 [Thomas and Krassa, 1971; Bertaux and Blamont, 1971]. To interpret these observations, Thomas [1971] considered two models of interstellar neutral hydrogen streaming relative to the sun. His first model

**Table 2** Minimum velocity angle  $\beta$  of the  $\text{He}^+$  velocity distribution function with respect to the radial direction

$\Theta = 45^\circ$				
$\langle V_\infty \rangle$ (km/sec)	$\beta$ (deg)			
	$\phi_e = 90^\circ$	$\phi_e = 180^\circ$	$\phi_e = 270^\circ$	$\phi_e = 360^\circ$
10	20.0	21.0	22.1	19.9
20	19.8	20.8	22.1	19.7
40	19.4	20.7	22.0	19.3

$\Theta = 0^\circ$		
$\langle V_\infty \rangle$ (km/sec)	$\beta$ (deg)	
10	21.2	
20	21.1	
40	20.9	

required a cold ( $T = 100^\circ \text{ K}$ ) streaming flow with  $n_{\text{H}}(\infty) = 0.06 \text{ cm}^{-3}$ ;  $\langle V_\infty \rangle \approx 10 \text{ km/sec}$  oriented in the ecliptic, and an isotropic galactic Lyman  $\alpha$  background of about 200 R. This was considered unlikely since current theories of the interstellar medium usually associate high temperatures ( $T \approx 10^4 \text{ K}$ ) with a hydrogen number density as low as  $0.06 \text{ cm}^{-3}$ . Furthermore, a calculation by Adams [1971] of the galactic Lyman  $\alpha$  background radiation yielded an upper limit of 200 R without including the effects of Lyman  $\alpha$  absorption due to interstellar dust grains. Thomas' second model requires a hot ( $T \approx 5 \times 10^3 \text{ K}$ ) flow with  $n_{\text{H}}(\infty) \approx 0.12 \text{ cm}^{-3}$ ,  $\langle V_\infty \rangle \approx 6 \text{ km/sec}$  oriented approximately in the ecliptic, and no galactic Lyman  $\alpha$  background. (The upper limit of 2 R of 584 Å radiation set by Johnson et al. [1971b] does not contradict the presence of neutral He consistent with the above models.)

The model of infalling interstellar gas considered in the present paper is valid for a finite gas temperature  $T$  at  $r = \infty$  as long as  $m\langle V_\infty \rangle^2/2kT \gg 1$ . For the cold model,  $m\langle V_\infty \rangle^2/2kT = 243 \gg 1$ , and our results are applicable. But, for the hot model ( $V_\infty = 6 \text{ km/sec}$ ,  $T = 5000^\circ \text{ K}$ ),  $m\langle V_\infty \rangle^2/2kT = 1.72$  and our expressions for the neutral He number density in the antiapex region break down. In the following discussion we therefore concentrate on the cold interstellar gas model; the hot model will be discussed in a later paper.

As mentioned earlier, placement of  $\langle V_\infty \rangle$  in the ecliptic results in large variations in  $n_{\text{He}^+}(r_e, \phi_e)$ . Figure 9 shows that enhanced fluxes are expected for

$270^\circ \lesssim \phi_e \lesssim 360^\circ$ .

In the neighborhood of  $\phi_e = 270^\circ$  the major contribution comes from neutral He atoms ionized in the dense tail close to 1 AU (see figs. 3 and 9). These ions occupy the region at the base of the triangular cross section of the velocity distribution as indicated in figure 15. Since these ions travel a relatively small distance in the interplanetary field before reaching 1 AU, one does not expect much pitch angle scattering. Hence these ions would probably not contribute to a peak in an  $E/Q$  particle spectrum at  $4(E/Q)_H$ .

In the neighborhood of  $\phi_e = 0^\circ$ , the major contribution comes from neutral He atoms ionized in the dense tail close to the sun. These ions normally occupy the region of velocity space at the apex of the triangular distribution which is closest to the solar wind velocity. In view of the evidence for enhanced noise in the solar wind near the sun, a high  $l$  value characterizing the initial pitch angle distribution of  $\text{He}^+$  ions, and the long travel times to 1 AU, it is expected that a good fraction of these ions could be incorporated into the solar wind to contribute to a peak at  $E/Q = 4(E/Q)_H$ .

One might also expect a contribution to a peak at  $4(E/Q)_H$  for azimuths in the range  $100^\circ \lesssim \phi_e \lesssim 240^\circ$  (for radial ionization distances  $0 < r_o \lesssim 0.2$  AU). Here the magnetic moment is small so that  $\text{He}^+$  ions penetrate deeply into the corona (see fig. 7). Such ions would be expected to be thermalized and therefore incorporated into the solar wind.

Last, a thermalized  $\text{He}^+$  contribution is expected at  $\phi_e = 270^\circ$  due to neutral He in the tail ionized at  $r_o \lesssim 0.1$  AU. This  $\text{He}^+$  number density is given by

$$n_{\text{He}^+}(r_e, 270^\circ) = \int_0^{0.1 \text{ AU}} n_{\text{He}}(r_o, 270^\circ) \frac{P(r_e)}{V_{sw}} dr_o$$

so that we obtain

$$\frac{n_{\text{He}^+}(r_e, 270^\circ)}{n_{\text{He}^{++}}(r_e)} \sim 5 \times 10^{-4}$$

for  $n_{\text{He}(\infty)} = 3 \times 10^{-3} \text{ cm}^{-3}$ ,  $\langle V_\infty \rangle = 10 \text{ km/sec}$ ,  $T = 100^\circ \text{K}$ ,  $n_{\text{He}^{++}}(r_e) = 0.25 \text{ cm}^{-3}$ ,  $V_{sw} = 400 \text{ km/sec}$  and  $P(r_e) = 6.8 \times 10^{-8} \text{ sec}^{-1}$ . This ratio is not inconsistent with the Vela 3 result, but Vela 3 was at  $\phi_e = 210^\circ$  when the  $\text{He}^+$  was observed.

One further comment with respect to the above calculations is in order.  $P(r_e) = 6.8 \times 10^{-8} \text{ sec}^{-1}$  was chosen

on the basis of the solar EUV data of *Watanabe and Hinteregger* [1962]. A more recent measurement by *Hall and Hinteregger* [1970] revealed that the original measurements were systematically high. Use of the new data would decrease  $P(r_e)$  and hence increase the neutral He density close to the sun. This would tend to make the  $\text{He}^+$  density at 1 AU larger than the values calculated above. On the other hand, we did not include collisional ionization in calculating  $P(r_e)$ . This becomes important close to the sun which would tend to decrease  $n_{\text{He}^+}(r_e, 270^\circ)$ .

*Hundhausen et al.* [1968] proposed, as an explanation of the Vela 3 measurements, that backstreaming hot neutral hydrogen atoms produced by charge exchange of solar wind protons with interstellar hydrogen at the heliosphere boundary could charge exchange with solar wind  $\text{He}^{++}$ , producing  $\text{He}^+$ . This mechanism requires the flux of incoming hot ( $\langle V_\infty \rangle \sim 400 \text{ km/sec}$ ) neutrals at 1 AU (which become ionized before leaving 1 AU out the reverse side) to be 1 percent of the solar wind flux of  $\text{H}^+$ . This fraction  $F(r_e)$  can be estimated if we assume that all solar wind protons are converted to an isotropic flux of hot neutrals at the heliosphere boundary. Then if  $f(\text{H}^+)$  is the flux density of solar wind protons at 1 AU, the total flux of fast H atoms backstreaming through any radius is  $4\pi r_e^2 f$ . The fast H atoms move along nearly rectilinear paths. Specifying the impact parameter of a backstreaming H atom by  $p$  and defining  $\delta$  as previously, the probability  $\alpha$  of an interaction within 1 AU is

$$\alpha = \exp \left[ \frac{-r_e^2 P(r_e)(\pi - \delta)}{V_o p} \right] \left\{ 1 - \exp \left[ \frac{-r_e^2 P(r_e)(\pi + \delta)}{V_o p} \right] \right\}$$

Then

$$F(r_e) = \int_0^{r_e} \left( \frac{\alpha}{4\pi R^2} \right) 2\pi p dp$$

where  $R$  is the radius of the heliosphere. Integrating numerically, we obtain

$$F(r_e) = 0.088 \left( \frac{r_e}{R} \right)^2$$

But  $R$  is expected to be at least 10 AU so that we obtain  $F(r_e) \lesssim 10^{-3}$ . This is an order of magnitude smaller than required by *Hundhausen et al.* [1968] to account for the Vela 3 measurement.

## CONCLUSIONS

We conclude that although the possibility exists that  $n_{\text{He}^+}(r_e, \phi_e)/n_{\text{He}^{++}}(r_e)$  in the solar wind is substantially higher than predicted from ionization equilibrium in a  $10^6$  °K expanding corona, it could be highly variable and depend strongly on  $\phi_e$ , the azimuthal position of observation about the sun. We have shown that if the spiral magnetic field is noise free, the velocity distribution of  $\text{He}^+$  at 1 AU is diffuse. Such a spectrum would not produce a peak at  $4(E/Q)_H$  in an  $E/Q$  spectrum. If  $\langle V_\infty \rangle$  is in the ecliptic, large variations in  $n_{\text{He}^+}(r_e, \phi_e)$  with respect to  $\phi_e$  are expected. Since solar wind magnetic irregularities are expected to be enhanced close to the sun, certain  $\phi_e$  values will be more favorable than others for observing  $\text{He}^+$  in a peak at  $4(E/Q)_H$  in an  $E/Q$  spectrum. For example, azimuthal positions in the neighborhood of  $100^\circ \lesssim \phi_e < 240^\circ$  corresponding to injection radii  $0 < r_0 \lesssim 0.2$  AU receive contributions due to a cancellation of the initial magnetic moment, resulting in deeply penetrating  $\text{He}^+$  orbits. This may result in effective thermalization. Another likely range of locations for observing thermalized  $\text{He}^+$  ions is  $270^\circ \lesssim \phi_e \lesssim 360^\circ$ .

A value of  $n_{\text{He}^+}(r_e)/n_{\text{He}^{++}}(r_e)$  in the solar wind of  $\approx 5 \times 10^{-4}$  can be predicted by the presence of a dense neutral tail due to interstellar infall. More  $\text{He}^+$  is available from the interstellar infall, but a calculation of its relative magnitude appearing in a spectral peak requires a knowledge of the radial dependence of the power density spectrum of magnetic irregularities in the solar wind at times just preceding the observation.

It is interesting to note that the Vela 3 spectra with the anomalous peak attributed to  $\text{He}^+$  were obtained on October 8. October 8 corresponds to  $\phi_e = 210^\circ$  for the earth. This is in the neighborhood where magnetic moment cancellation is expected to produce deep radial penetration and hence thermalization. Of course, deep penetration could also result in a second ionization yielding  $\text{He}^{++}$ . We feel that one should not place too much emphasis on a comparison of a single measurement with the ideas presented above.

## ACKNOWLEDGMENTS

We are grateful for helpful conversations with A. Barnes and E. Roelof concerning pitch angle scattering and thermalization of charged particles in the solar wind. This work was supported under NASA Research Grants NGL 50-002-044 and NGR 50-002-162.

## REFERENCES

- Adams, T. F.: On Lyman-Alpha Emission From the Galaxy. *Astron. Astrophys.*, Vol. 12, 1971, p. 200.
- Bame, S. J.; Asbridge, J. R.; Hundhausen, A. J.; and Montgomery, M. D.: Solar Wind Ions:  $^{56}\text{Fe}^{+8}$  to  $^{56}\text{Fe}^{+12}$ ,  $^{28}\text{Si}^{+7}$ ,  $^{28}\text{Si}^{+8}$ ,  $^{28}\text{Si}^{+9}$ , and  $^{16}\text{O}^{+6}$ . *J. Geophys. Res.*, Vol. 75, 1970, p. 6360.
- Bame, S. J.; Hundhausen, A. J.; Asbridge, J. R.; and Strong, I. B.: Solar Wind Ion Composition. *Phys. Rev. Letters*, Vol. 20, 1968, p. 393.
- Barnes, A.: Theory of Generation of Bow-Shock-Associated Hydromagnetic Waves in the Upstream Interplanetary Medium. *Cosmic Electrodyn.*, Vol. 1, 1970, p. 90.
- Bertaux, J. L.; and Blamont, J. E.: Evidence for a Source of an Extraterrestrial Hydrogen Lyman-Alpha Emission: the Interstellar Wind. *Astron. Astrophys.*, Vol. 11, 1971, p. 200.
- Coleman, P. J., Jr.: Variation in the Interplanetary Magnetic Field: Mariner 2, 1. Observed Properties. *J. Geophys. Res.*, Vol. 71, 1966, p. 5509.
- Coleman, P. J., Jr.; Smith, E. J.; Davis, L., Jr.; and Jones, D. E.: The Radial Dependence of the Interplanetary Magnetic Field: 1.0–1.5 AU. *J. Geophys. Res.*, Vol. 74, 1969, p. 2826.
- Fahr, H. J.: On the Influence of Neutral Interstellar Matter on the Upper Atmosphere. *Astrophys. Space Sci.*, Vol. 2, 1968, p. 474.
- Hall, L. A.; and Hinteregger, H. E.: Solar Radiation in the Extreme Ultraviolet and Its Variations With Solar Rotation. *J. Geophys. Res.*, Vol. 75, 1970, p. 6959.
- Hall, D. E.; and Sturrock, P. A.: Diffusion, Scattering, and Acceleration of Particles by Stochastic Electromagnetic Fields. *Phys. Fluids*, Vol. 10, 1967, p. 2620.
- Holzer, T. E.; and Axford, W. I.:  $\text{He}^+$  Ions in the Solar Wind. EOS, *Trans. Amer. Geophys. Union*, Vol. 51, 1970, p. 411.
- Hundhausen, A. J.; Gilbert, G. E.; and Bame, S. J.: Ionization State of the Interplanetary Plasma. *J. Geophys. Res.*, Vol. 73, 1968, p. 5485.
- Johnson, C. Y.; Young, J. M.; and Holmes, J. C.: Magnetoglow, a New Geophysical Resource. *Science*, Vol. 171, 1971a, p. 379.
- Johnson, C. Y.; Young, J. M.; and Holmes, J. C.: To be published in *J. Geophys. Res.*, 1971b.
- Northrup, T. G.: *The Adiabatic Motion of Charged Particles*. Interscience Pub., New York, 1963.

- Patterson, T. N. L.; Johnson, F. S.; and Hanson, W. B.: The Distribution of Interplanetary Hydrogen. *Planet. Space Sci.*, Vol. 11, 1963, p. 767.
- Sari, J. W.; and Ness, N. F.: Power Spectra of the Interplanetary Magnetic Field. *Solar Phys.*, Vol. 8, 1969, p. 155.
- Siscoe, G. L.; Davis, L., Jr.; Coleman, P. J., Jr.; Smith, E. J.; and Jones, D. E.: Power Spectra and Discontinuities of the Interplanetary Magnetic Field: Mariner 4. *J. Geophys. Res.*, Vol. 73, 1968, p. 61.
- Sturrock, P. A.: Stochastic Acceleration. *Phys. Rev.*, Vol. 141, 1966, p. 141.
- Thomas, G. E.: Properties of Nearby Interstellar Hydrogen Deduced From Lyman-Alpha Sky Background Measurements. Preprint, 1971.
- Thomas, G. E.; and Krassa, R. F.: OGO-5 Measurements of the Lyman-Alpha Sky Background. *Astron. Astrophys.*, Vol. 11, 1971, p. 218.
- Tucker, W. H.; and Gould, R. J.: Radiation From a Low Density Plasma at  $10^6$ – $10^8$  °K. *Astrophys. J.*, Vol. 144, 1966, p. 244.
- Watanabe, K.; and Hinteregger, H. E.: Photoionization Rate in E and F Regions. *J. Geophys. Res.*, Vol. 67, 1962, p. 999.
- Young, J. M.; Carruthers, G. R.; Holmes, J. C.; Johnson, C. Y.; and Patterson, N. P.: Detection of Lyman-Beta and Helium Resonance Radiation in the Night Sky. *Science*, Vol. 160, 1968, p. 990.

## EFFECTS OF INTERSTELLAR PARTICLES UPON THE INTERPLANETARY MAGNETIC FIELD

Paul J. Coleman, Jr., and Edwin M. Winter

**ABSTRACT** The flow of interstellar neutral particles into the interplanetary medium and their subsequent ionization in the presence of the electromagnetic field of the solar wind can cause a loss of field angular momentum by the solar wind. One effect of this loss of field angular momentum is a significant unwinding of the spiral field. This effect is evaluated using simple models for neutral density and ion production. For a free-stream interstellar medium with a neutral hydrogen density of  $1 \text{ cm}^{-3}$  and a velocity relative to the sun of  $10$  to  $20 \text{ km-sec}^{-1}$ , the spiral angle at the orbit of Jupiter will be less than its nominal value of  $45^\circ$  at the orbit of the earth.

### INTRODUCTION

Recent Lyman  $\alpha$  measurements with instruments on board Vela 4 [Chambers *et al.*, 1970] and OGO 5 [Thomas and Krassa, 1970] satellites indicate that neutral interstellar matter penetrates interplanetary space to within a few AU of the sun. Each of these instruments detected a definite maximum in the scattered Lyman  $\alpha$  intensity. In each case the minimum was  $180^\circ$  from the maximum. The OGO 5 investigation reported a parallax effect over a 6-month period of observations of the position of these features. This was interpreted by Thomas and Krassa as showing that the distance of the interstellar hydrogen is comparable to the diameter of the earth orbit.

The Vela 4 and OGO 5 results place the maximum at different positions. The former show the maximum in the direction of the solar apex motion, which is approximately  $50^\circ$  from the ecliptic. The latter show this enhancement to be at the same galactic longitude but near the ecliptic in the direction of Scorpio-Sagittarius.

Blum and Fahr [1969; 1970a,b] considered the behavior of a neutral interstellar medium moving relative to the solar system. As a result of this relative motion ( $\sim 10$ - $20 \text{ km/sec}$ ), some neutral hydrogen moves into

interplanetary space. The lifetime of these neutrals, which are exposed to solar energetic ultraviolet radiation, is determined by the appropriate ionization time. The neutral penetration distance is then determined by the relative velocity. If the interstellar medium is at rest in the galactic frame, it will be seen to approach the solar system from the direction of solar apex motion. Motion of the interstellar gas relative to the galactic frame can alter the speed and direction of approach of the neutrals. For velocities comparable to the solar apex velocity, the theory of Blum and Fahr predicts penetration to within several AU of the earth's orbit.

Apparently, then, the region of solar wind flow several AU outside the orbit of the earth consists of flowing solar wind plasma moving relative to the neutral interstellar medium. This neutral hydrogen is continuously exposed to ionizing radiation and, when ionized, is accelerated by the solar wind electromagnetic field. The effect of this volume mass source on the mechanical variables of the solar wind flow was considered for a gas dynamic case by Semar [1970], although details such as the mechanism for accelerating the particles were not discussed.

In this note we show that one important effect of these ionized interstellar particles is to unwind the spiral of the interplanetary magnetic field. Thus, at any point, the deviation of the mean spiral angle from its predicted value may be a sensitive indicator of the density of these particles.

---

The authors are at the Department of Planetary and Space Science and Institute of Geophysics and Planetary Physics, University of California, Los Angeles, California.



## ANGULAR MOMENTUM

A neutral atom, when ionized in an electric and magnetic field, will be accelerated in the  $\mathbf{E} \times \mathbf{B}$  direction. If  $\mathbf{E}$  is produced by a plasma moving with velocity  $\mathbf{V}_p$  so that  $\mathbf{E} = -(1/c)(\mathbf{V}_p \times \mathbf{B})$ . The force on a charged particle moving with an arbitrary velocity  $\mathbf{V}$  in a plasma moving at velocity  $\mathbf{V}_p$  is given by  $\mathbf{F} = e(\mathbf{E} + \mathbf{V} \times \mathbf{B})/c$ . Using the above electric field, this becomes [cf. Winge and Coleman, 1968].

$$\mathbf{F} = e(\mathbf{V} - \mathbf{V}_p) \times \frac{\mathbf{B}}{c} \quad (1)$$

Thus, for the case where  $\mathbf{V} \times \mathbf{B} = \mathbf{V}_p \times \mathbf{B}$ , the particle will experience no force.

Particles ionized in the moving plasma will experience no force after the acceleration to the  $\mathbf{E} \times \mathbf{B}$  velocity. Unless the magnetic field is perpendicular to  $\mathbf{V}_p$ , this acceleration will have a component transverse to  $\mathbf{V}_p$ .

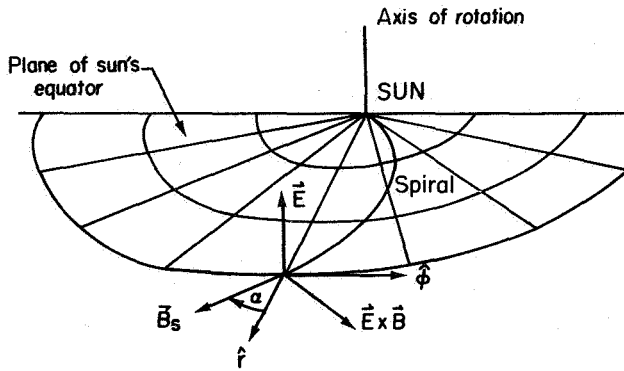


Figure 1  $\mathbf{E} \times \mathbf{B}$  drift direction in the solar wind.

In the solar wind the situation is as shown in figure 1. Thus, the solar wind electromagnetic field will lose angular momentum to interstellar particles that are moving directly toward the sun at the time they are ionized. This loss of angular momentum to these particles is then

$$\frac{dL_m}{dt} = -A_p V_D \times \mathbf{r} \quad (2)$$

where  $A_p$  = rate of mass addition per unit volume,  $\mathbf{V}_D = (1/B^2)\mathbf{E} \times \mathbf{B}$  is the drift velocity so that  $V_{D\phi}$  is the  $\phi$  component of the drift velocity, that is,

$$V_{D\phi} = \frac{c(\mathbf{E} \times \mathbf{B})_\phi}{B^2} = \frac{[-(\mathbf{V} \times \mathbf{B}) \times \mathbf{B}]_\phi}{B^2}$$

$$= \frac{V_\phi - V_r B_\phi^2}{B^2} - \frac{V_r B_r B_\phi}{B^2} \quad (3)$$

and  $\mathbf{V}$  is the solar wind velocity. We have neglected the time required to accelerate the newly ionized particles to the drift velocity.

The solar wind electromagnetic angular momentum flow is given by equation (4)

$$\frac{dL_m}{dt} = -\mathbf{r} \times (\mathbf{J} \times \mathbf{B}) = -\frac{\mathbf{r} \times [(\nabla \times \mathbf{B}) \times \mathbf{B}]}{4\pi} \quad (4)$$

which can be expressed for a spherically symmetric solar wind as

$$\frac{dL_m}{dt} = -\frac{B_r(d/dr)rB_\phi}{4\pi} \quad (5)$$

the torque associated with magnetic stress per unit volume [cf. Weber and Davis, 1967]. Equating (5) and (2):

$$B_r \frac{d}{dr} (rB_\phi) = 4\pi A_p r V_\phi \left( \frac{1 - B_\phi^2}{B^2} - \frac{4\pi A_p r V_r B_r B_\phi}{B^2} \right) \quad (6)$$

In the case where

$$V_r \gg \frac{V_\phi(B_r^2 + B_\phi^2)}{B_\phi B_r}$$

or

$$V_r \gg \frac{V_\phi B_r}{B_\phi}$$

the first term on the right side of equation (6) can be neglected. Typical values at 1 AU are

$$|B_r| \approx |B_\phi| = 3.0 \gamma$$

$$V_r = 400 \text{ km/sec}$$

$$V_\phi = 5 \text{ km/sec}$$

Models of the solar wind flow in the outer solar system [Weber and Davis, 1967; Weber and Davis, 1970] do not show any increase in  $V_\phi$ . Furthermore,  $B_r/B_\phi$  decreases as  $1/r$ . Equation (6) can therefore be written as

$$\frac{d}{dr} (B_\phi r) = \frac{4\pi(B_\phi r)A_p V_r}{B_\phi^2 + B_r^2} \quad (7)$$

or on integration

$$B_{\phi}r = B_{\phi 0}r_0 \exp \left( - \int_{r_0}^r \frac{4\pi A_p V_r dr}{B_{\phi}^2 + B_r^2} \right) \quad (8)$$

Even in the case of mechanical interactions, the solar wind velocity  $V_r$  remains essentially constant to a distance at which mass loading affects the momentum in the radial direction. *Semar* [1970] determined this distance to be considerably beyond 5 AU. The quantity  $A_p$  in equation (8) is the rate of plasma mass addition per unit volume, and it may be approximated by

$$A_p = \frac{q_p \rho_n r_0^2}{r^2} + \frac{q_c \rho_n r_0^2}{r^2}$$

where  $q_p$  is the photoionization rate,  $q_c$  is the charge exchange rate, and  $\rho_n$  is the neutral density. The rate of charge exchange reactions in the solar wind is the subject of some debate. Various proposed rates and cross sections are given in table 1. The rate of photoionization, however, is more accurately known [*Hinteregger*, 1960;

**Table 1.** Comparison of published charge exchange rates.

Charge-exchange cross section in solar wind	Charge-exchange ionization rate
$3 \times 10^{-16} \text{ cm}^2$	$7.5 \times 10^{-8} \text{ sec}^{-1}$ [Walker <i>et al.</i> , 1970]
$3 \times 10^{-15} \text{ cm}^2$	$6 \times 10^{-7} \text{ sec}^{-1}$ [Semar, 1970]
$10^{-15} \text{ cm}^2$	$1.5 \times 10^{-7} \text{ sec}^{-1}$ [Blum and Fahr, 1970a]

*Walker et al.*, 1970; *Semar*, 1970]. In this paper, we assume  $q_p = 4.5 \times 10^{-7} \text{ sec}^{-1}$  in agreement with the above authors. This is the value for photoionization of atomic hydrogen at 1 AU for a fairly active sun. This value will also serve as the total ionization rate, keeping in mind a possible error of a factor of 2 due to the additional contribution of charge exchange. For the neutral density in interplanetary space  $\rho_n$ , we will use the densities introduced by *Blum and Fahr* [1969, 1970a,b]. If the gravitational effects of the sun are neglected, the density of neutrals at a distance  $r$  measured from the sun in the direction of the incoming interstellar particles is given by

$$\rho_n = \rho_{n0} e^{-(qr_0^2/V_H r^2)}$$

where

- $\rho_{n0}$  the interstellar density external to the solar system
- $q$  photoionization rate at 1 AU
- $r$  distance from the sun
- $V_H$  velocity of the interstellar medium relative to the sun
- $r_0$  radius of the earth's orbit

A net effect of gravity over light pressure (as was assumed in *Blum and Fahr* [1970a]) will result in greater densities in the inner solar system. For a relative interstellar velocity of 20 km/sec, the neutral density will be  $1/e$  times its density outside the solar system at approximately 3.5 AU.

Equation (8) can be integrated numerically by iterative methods and behavior of  $B_{\phi}$  compared with that predicted by the spiral angle model. However, it is immediately apparent that for the limiting case in which there is no relative motion between the interstellar medium and the solar wind, the usual spiral field, with  $B_{\phi}$  varying inversely with  $r$ , results.

## RESULTS AND DISCUSSION

The results of this integration for  $rB_{\phi}$  are plotted in figures 2 and 3. We assumed that, at  $r = 0.1$  AU,

$$B_{\phi 1} = 30 \gamma \quad B_{r1} = 300 \gamma \quad V_r = 400 \text{ km/sec}$$

The values of the magnetic field vector components were chosen to yield  $B_{\phi} = B_r = 3\gamma$  at 1 AU for the spiral model in which there is no interaction of the solar wind with interstellar matter.

The radial magnetic field is also plotted. For all positions where  $B_{\phi}r$  is greater than  $B_r r$ , the spiral angle will

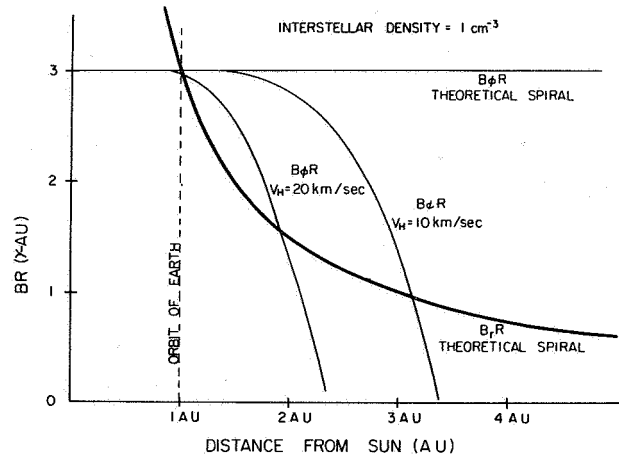


**Figure 2** Magnetic field strength for interstellar density  $\rho_0 = 1 \text{ cm}^{-3}$ .

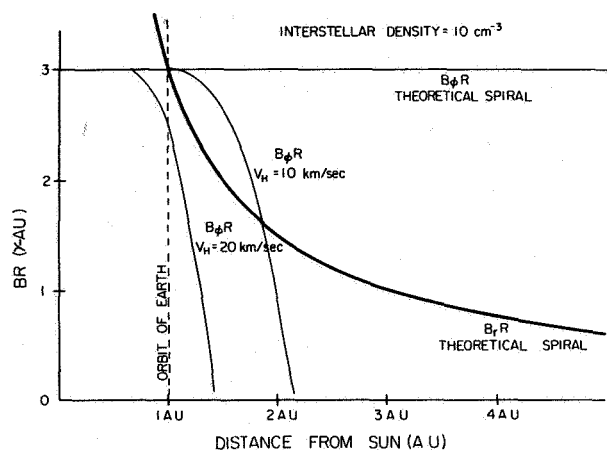


**Figure 3** Magnetic field strength for interstellar density  $\rho_0 = 10 \text{ cm}^{-3}$ .

be greater than  $45^\circ$ . Thus, for the case in figure 2 with  $V_H$ , the free-stream velocity of the interstellar neutrals relative to the sun equal to 10 km/sec and radially inward in the solar equatorial plane, the spiral angle will increase through  $45^\circ$  at the orbit of the earth increasing with distance from the sun. Because of loss of angular momentum to the interstellar hydrogen, the spiral angle will again decrease to  $45^\circ$  near 3 AU. The unwinding of the spiralled interplanetary field in the direction of interstellar inflow can be seen from the following argument considering currents.

One can describe the effect on  $B_\phi$  in another way. A current density  $\mathbf{J} = J_\theta \hat{\theta}$  is associated with the acceleration of the interstellar particles in the direction of  $\mathbf{E} \times \mathbf{B}$ . For  $B_r$  outward from the sun,  $J_\theta$  is northward. Since  $\nabla \times \mathbf{B} = 4\pi \mathbf{J}/c$

$$\frac{d|rB_\phi|}{dr} = -\frac{4\pi J_\theta r}{c}$$

Thus, there is a negative gradient of  $|rB_\phi|$  with  $r$ , the distance from the sun.

## CONCLUSION

The effect of ionization of interstellar particles on the electromagnetic angular momentum of the solar wind has been examined. For models that predict penetration of significant densities into the solar system, a significant departure from spiral angle (unwinding) is indicated. The

effect will be a maximum in the direction of the approach of interstellar gas.

## ACKNOWLEDGMENTS

We wish to thank C. R. Winge, Jr., for helpful discussions. The computer calculations were funded by the Regents of the University of California. One of us (EMW) was supported by a traineeship from the National Science Foundation. The work was also supported in part by the National Aeronautics and Space Administration under research grant NGL 05-007-004.

## REFERENCES

- Blum, P. W.; and Fahr, H. J.: Solar Wind Tail and the Anisotropic Production of Fast Hydrogen Atoms. *Nature*, Vol. 223, 1969, p. 936.
- Blum, P. W.; and Fahr, H. J.: Interaction Between Interstellar Hydrogen and the Solar Wind. *Astron. Astrophys.*, Vol. 4, 1970a, p. 280.
- Blum, P. W.; and Fahr, H. J.: The Distribution of Interplanetary Hydrogen. *Astrophys. Letters*, Vol. 5, 1970b, p. 127.
- Chambers, W. H.; Fehla, P. E.; Fuller, J. C.; and Kunz, W. E.: Anisotropic Atomic Hydrogen Distribution in Interplanetary Space. *Nature*, Vol. 225, 1970, p. 713.
- Hinteregger, H. E.: Interplanetary Ionization by Solar Extreme Ultraviolet. *Astrophys. J.*, Vol. 132, 1960, p. 801.
- Semar, C. L.: Effect of Interstellar Neutral Hydrogen on the Termination of the Solar Wind. *J. Geophys. Res.*, Vol. 75, 1970, p. 6892.
- Thomas, G. E.; and Krassa, R. F.: OGO 5 Measurements of the Lyman  $\alpha$  Sky Background. Preprint, Department of Astro-geophysics, University of Colorado, Boulder, 1970.
- Walker, J. C. G.; Turekian, K. K.; and Hunten, D. M.: An Estimate of the Present-Day Deep-Mantle Degassing Rate From Data on the Atmosphere of Venus. *J. Geophys. Res.*, Vol. 75, 1970, p. 3558.
- Weber, E. J.; and Davis, L., Jr.: The Angular Momentum of the Solar Wind. *Astrophys. J.*, Vol. 148, 1967, p. 217.
- Weber, E. J.; and Davis, L., Jr.: The Effect of Viscosity and Anisotropy in the Pressure on the Azimuthal Motion of the Solar Wind. *J. Geophys. Res.*, Vol. 75, 1970, p. 2419.
- Winge, C. R.; and Coleman, P. J., Jr.: The Motion of Charged Particles in a Spiral Field. *J. Geophys. Res.*, Vol. 73, 1968, p. 165.

## DISCUSSION

*J. C. Brandt* What would be the effect, if the density at infinity were in fact one-tenth, which seems more probable at the present time.

*P. J. Coleman* It's directly proportional to the momentum. If the velocity were 20 km/sec, it would be slightly less than I showed for the curve of 1 and 5 km/sec. I think one can look at this as the interaction of an electromagnetic wave with these newly ionized particles, the absorption of the wave by the freshly charged particles. The momentum components that are of interest here are the radial and azimuthal ones, at least insofar as this unwinding of the spiral is concerned.

*T. G. Cowling* Would it be correct to say that, in effect, we have a reduced conductivity so that the freezing-in condition is being violated?

*P. J. Coleman* I prefer to look at it as the results of polarizing the particles as they become ionized. I think the net effect is the same, that is, there is a current flow and the spiral field straightens out. The results may be the same either way except perhaps that this process may not involve any dissipation that changes the temperatures of the freshly ionized interstellar particles. Instead all the energy may go into directed flow.

*T. G. Cowling* Yes, but you are in fact dissipating energy. You have energy continually transmitted between the neutrals and the charged particles because they are trying to move with different velocities, one frozen-in and the other not.

*P. J. Coleman* It is true that they have different velocities, but we have neglected particle-particle interactions altogether. So in this simple model the transformation of electromagnetic energy into mechanical energy is such that all of the former goes into directed flow energy rather than thermal energy.

*L. Davis, Jr.* There are many alternative ways of looking at this, all of which, if done carefully, lead to the same result. The way that seems convenient to me is to regard the incoming neutrals as flowing through the other medium. When they first become ionized they still have the same velocity, with components parallel and perpendicular to the magnetic field. The parallel component merely continues as a guiding center drift until some instability or irregularity causes the particles to be swept up by the wind. The perpendicular component becomes thermalized and the particles immediately become hot. They will be very hot because they get a thermal velocity roughly corresponding to the solar wind speed. The average velocity normal to the field in this thermal motion will be zero. In other words, to give them this average velocity requires a transfer of momentum to them which will come out of the momentum for the whole ensemble of gas and magnetic field and will lead to the change of the spiral angle, as Paul described.

*P. J. Coleman* I would just like to add one thing. Your mention of instabilities to me implies a process that is effectively dissipative and I don't think dissipation is required. This is the simplest case in which the particles are cold and they get ionized in the presence of the solar wind electromagnetic field.

*W. I. Axford* I don't understand this result at all! The essential effect is that you are adding new particles to the solar wind and that these are given a component of velocity in the sense of corotation with the sun and also the radially outward component. The momentum change appears to me to be such that the spiral must become tighter rather than open up.

*P. J. Coleman* What you're talking about is the situation in which the mechanical component of the momentum is conserved. But in the model I have described, we consider the solar wind momentum in two parts, electromagnetic and mechanical, and simply treat the transformation of the electromagnetic part into mechanical momentum in the newly ionized particles. You could almost consider that the motion of the solar wind particles is unaffected by this loss of the electromagnetic component of the momentum.

*W. I. Axford* You must conserve total momentum and satisfy the equations of motion. I don't think you split the momentum up as easily as that.

*P. J. Coleman* I'm conserving total momentum. Perhaps you could look at it this way. If we neglect the solar wind flow, which we can't do, and let these newly ionized particles interact with a pure electromagnetic wave, the wave would give them a kick such as this.

*T. E. Holzer* The thing that seems peculiar to me is that you are imparting momentum to the particles in the direction in which you must impart momentum to the field in order to unspiral the field and you are claiming that the field becomes unspiraled, or unwound. It seems to me that instead of subtracting two momenta and coming out with zero net change you are adding the two. Do you see what I mean?

*P. J. Coleman* No. The solar wind has electromagnetic momentum in the positive  $\phi$  direction.

*T. E. Holzer* And you want to reduce that.

*P. J. Coleman* Yes. Suppose we think about the interstellar matter coming in along the direction of relative motion. Then it has no angular momentum relative to the sun to start with and if we look right along that line those particles will be kicked so that they have positive azimuthal or  $\phi$  momentum. I say that this momentum is just the part that was originally electromagnetic.

*T. E. Holzer* What if you had a circular field? How much angular momentum would the field be able to impart to the particles?

*P. J. Coleman* A circular magnetic field?

*T. E. Holzer* Yes.

*P. J. Coleman* If there is no electrical field around, none.

*T. E. Holzer* Isn't that the condition toward which you are going if you reduce the angular momentum? You reduce the capability of the field to give angular momentum to the particles. If you straighten the field out you're going to be exerting more angular momentum than ever. Are you not?

*P. J. Coleman* It's true that I would be if I were transferring mechanical momentum from one species to another. Perhaps we should talk about this in private.

*L. Davis, Jr.* I have a lot of sympathy for everyone involved in this discussion. I have some advantage over many of you because I heard this from Paul a couple of days ago. My first reaction was that if you transfer momentum in the plus  $\phi$  direction to the gas as it is ionized, it obviously flattens the spiral out rather than steepens it. After thinking about it overnight I'm about 95 percent convinced that Paul is right and I have the usual 5 percent residual doubt. Until I have really seen all the mathematics I won't fully understand it, but I think the argument goes like this. Imagine you've made a solution for this whole angular momentum problem, the kind that Weber did, but now you put in this transfer of angular momentum to the infalling material. So you've got your integral for the constant total angular momentum of the electromagnetic field plus particles. This solution, of course, has the characteristic that at least some of the constants are determined by the requirement that the solution pass through the critical point. The solution on both sides of the critical point is partly determined by this requirement; it isn't completely determined by local effects. Next, consider what you see as you go out from a region into which no infalling neutral gas penetrates to one in which neutrals are being ionized and added to the solar wind. In the latter region you see the infalling material being added to the angular momentum budget. Thus, just as Paul says, to keep the total angular momentum constant, the field has to carry less angular momentum here than it did in the inner region and it is more nearly radial where infalling gas is being ionized than it is farther in.

## NEW EVIDENCE FOR SOLAR CYCLE VARIATIONS AT GREAT DISTANCES

*D. Venkatesan and V. K. Balasubrahmanyam*

**ABSTRACT** Recent studies of solar planetary relationships are directed toward exploring how far out from the sun one could observe solar cycle variations. A positive solar Jovian relationship is suggested from a Chree superposed epoch study of the intensity of the great red spot of Jupiter over a period of about six solar cycles. The characteristic double maxima observed in the solar cycle variation is common to other observations of solar events in the photosphere, chromosphere, and corona; radio and corpuscular emissions from the sun; cosmic ray intensity and geomagnetic activity. The same method of analysis adopted for the study of luminosity changes of the planets Jupiter, Saturn, Uranus, and Neptune indicates that the fluctuations of luminosity follow the single maximum solar cycle represented by sunspot numbers. In conjunction with changes of upper atmospheric density and temperature, it is suggested that the extreme ultraviolet (EUV) emission from the sun may be connected with luminosity changes. Further, in principle, we have a method of distinguishing between phenomena related to solar wind and those related to solar EUV. The study concludes that there is evidence that the 11-year solar cycle variation is observed up to  $\sim 30$  AU.

Long-term studies of aurorae, geomagnetic storms, various types of cosmic ray intensity variations, changes in the trapped particle population in the geomagnetic field, and other areas exhibiting solar-terrestrial relationship have all been undertaken with a view to establish the nature of solar modulation. From observations on the earth and in the immediate geophysical environment, there is general agreement about the existence of an 11-year solar cycle dependence.

In the past, investigators have generally used  $R$ , the Zurich relative sunspot number, as the parameter for solar activity. The 11-year solar cycle, as revealed by  $R$ , shows a fast rise to a maximum and a slower fall to the minimum. But recent studies have focused attention on the difference between the sunspot cycle with a single maximum and the 11-year cycle of many phenomena

exhibiting a characteristic double maxima. The existence of a double maxima in the 11-year solar cycle of activity has been pointed out by *Gnevyshev* [1963, 1967], *Antalova and Gnevyshev* [1965] and by *Gentili di Giuseppe et al.* [1966] who in particular observe this feature in the intensity of the coronal green line 5303 Å. These studies reveal that this characteristic feature is substantiated by events at various levels on the sun: photosphere, chromosphere, and corona, as well as by radio and particle emission from the sun. This feature of double maxima during the solar cycle relates to occurrences of polar cap absorption events [*Gnevyshev*, 1967]; cosmic ray flares of MeV and BeV ranges [*Sakurai*, 1967]; solar type IV bursts [*Krivsky and Kruger*, 1966] and proton flares, occurrence of large sunspots [*Sakurai*, 1967] and microwave impulsive bursts [*Fokker*, 1963]. The studies of the amplitude of the quasiperiodic 27-day variation in cosmic ray intensity [*Venkatesan*, 1958] and of the mean cosmic-ray intensity and geomagnetic activity [*Balasubrahmanyam*, 1968; *Balasubrahmanyam and Venkatesan*, 1970a] also reveal the characteristic double maxima. Some of these

---

*Dr. Venkatesan is at the Physics Department, University of Calgary, Calgary, Alberta, Canada, and Dr. Balasubrahmanyam is at NASA/Goddard Space Flight Center, Greenbelt, Maryland.*

are shown in figure 1 [from *Balasubrahmanyam and Venkatesan, 1970b*].

There are indications that the separation between the two maxima may vary from one cycle to another and the possibility of not being able to distinguish between the two peaks in any particular cycle cannot be ruled out either. Thus there is general agreement that in all these, the single maximum solar cycle variation represented by the sunspot numbers is not a very appropriate measure of solar variability.

The next question is, irrespective of the type of 11-year variation, be it one maximum or two maxima, how far from the sun can one detect this variation? This would give some indication of the extent of solar influence of physical phenomena. The investigations of *Dessler [1967]*, *Simpson and Wang [1967]*, and *Hundhausen [1968]* estimate that the boundary of the region of cosmic ray modulation may extend from 5 AU to 50 AU. Another useful approach would be to explore whether any recorded data of planetary activity over long periods of time could give some indication of an existence or otherwise of a solar cycle variation. Of course it should be realized from the start that a completely satisfactory set of data is hard to come by in this

area. Gaps are bound to exist in any such data and hence one can only hope to arrive at tentative conclusions, if any. Nevertheless, it was thought that the approach would be useful.

The great red spot of Jupiter is a predominant feature on the Jovian surface and has been observed continuously since 1891. The British amateur astronomer *Peek [1958]* has collated all the observations for the period 1892-1947. He assigns numbers to represent the intensity or darkness of the red spot, as described by observers at each apparition. Peek comments that some arbitrariness is unavoidable in assigning these numbers to the estimates of observers, but indicates that every care has been taken to avoid any serious distortion of facts. Thus annual means are published by him for the entire period, the numbers ranging as follows: 0 = invisible, 1 = visible but very faint, 2 = very difficult to see early in the apparition, later plain and distinct, 3 = fairly well defined, 4 = well defined, 5 = easy to see, 6 = easy to see and fairly conspicuous, 8 = very dark and conspicuous, 7 does not figure on the scale.

In view of the subjective nature of the evaluation, we have restricted ourselves to the use of only the data carefully collated by a single person, although some data are available for the period 1948-1967 [*Reese as reported in Solberg and Chapman, 1969*]. Visible changes of the red spot are observed even within a year [*Vsekjsvyatskii, 1969*]. We have no means of knowing how many observations are averaged over each year, as Peek does not give any indication. Hence we doubt very much whether we could meaningfully intercompare annual values from one year to another, but believe it is appropriate to study the average behavior over a number of solar cycles.

The superposition method similar to the Chree method [*Chree, 1913; Chree and Stagg, 1928*] was adopted for the analyses of the annual means of the Zurich relative sunspot number and Peek's darkness parameter for the Jovian red spot for the period 1892-1947. The zero epoch for both analyses corresponded to the years of solar maxima as determined from sunspot numbers — namely, 1893, 1905, 1917, 1928, 1937, and 1947. The values for 4 years preceding and 7 years following the years of maxima were used for superposition. The results are shown in figure 2 [from *Balasubrahmanyam and Venkatesan, 1970b*]. The double maxima in the average 11-year variation, in the case of the intensity of the Jovian parameter, are seen, consistent with other studies referred to earlier. It is relevant to refer to the study of *Newton and Milsom [1954]* of 420 non-sc geomagnetic storms during the period 1878-1879 to 1952-1955, which is comparable to our

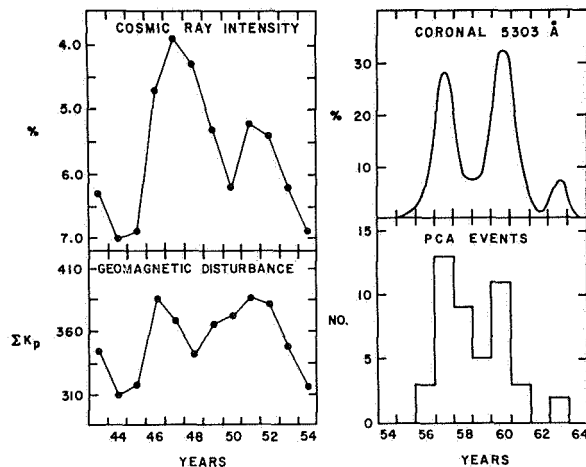


**Figure 1** Examples of phenomena exhibiting double maxima during solar cycles 18 and 19; cosmic ray intensity refers to annual mean values at Cheltenham (Fredericksburg), in units of 0.1 percent from fiducial value; geomagnetic disturbance refers to the sum of daily values of  $K_p$ , the planetary geomagnetic index, for the 60 most disturbed days for the year (five values for each month); coronal 5303 Å refers to the intensity of the coronal line at 5303 Å averaged around the limb; PCA events refer to the annual number of polar cap absorption events. The last two curves have been taken from *Gnevyshev [1967]*.

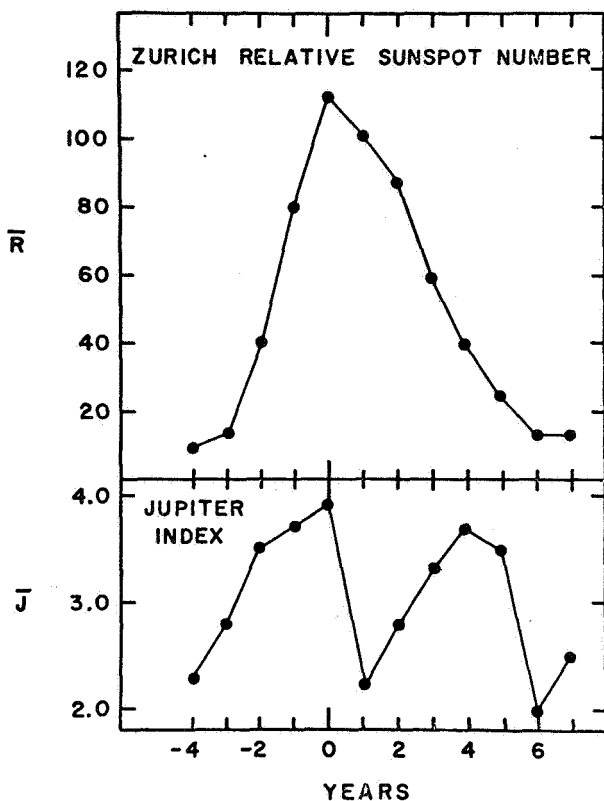


Figure 2 Chree type analysis; average over six solar rotations, zero epoch years correspond to years of maximum solar activity as chosen from annual means of sunspot numbers. Jupiter index refers to the darkness parameter of the great red spot of Jupiter [Peek, 1958].

period of study of Jupiter. They find that the frequency distribution exhibits double maxima with a 4-year separation between the peaks. We do not claim that these two have the same cause. Our desire is merely to point out the existence of a similar feature in another study over a comparable period. Hence we believe we have evidence of the observation of an 11-year solar cycle variation, as far as 5 AU from the sun. Note that it is premature at the present time to speculate on exactly how the intensity changes of the Jovian red spot are related to solar activity.

Our next attempt was to look at the available data of the luminosity of the planets Jupiter, Saturn, Uranus, and Neptune collected and reduced to the standard Harvard visual system by Becker [1933, 1949]. He has given details about the original sources of observations and corrections. Data for Jupiter, Saturn, Uranus, and Neptune correspond to 1846-1923, 1858-1948, 1864-1944, and 1878-1932, respectively, with unfortunate gaps in data due to lack of observation.

Becker concluded that there was no central cause for luminosity fluctuations.

However, in this context it is relevant to point out that Shapiro [1953] has shown that the variations of Jupiter's disc brightness follows the variation of sunspot numbers for the period 1926-1950. Johnson and Iriarte [1959] have pointed out that the blue magnitude change of Uranus and Neptune increases over 1952-1958, a period of increasing sunspot numbers.

It is unfortunate that the gaps in the observational data compiled by Becker preclude any detailed determination of the periodicity of the luminosity variation. However, we believe that the Chree method of superposition can be effectively used, at least to detect a possible solar cycle dependence. We have chosen for the zero epochs the years of solar maxima and minima of the sunspot cycle [Waldmeier, 1961]. The results of the Chree analyses are given for Jupiter and Saturn in figure 3 [from Balasubrahmanyam and Venkatesan, 1970c]. A solar cycle change of ~20 percent in the luminosity can be observed, with maximum planetary luminosity during solar maximum. Results of the analyses for Uranus and Neptune given in figure 4 [from Balasubrahmanyam and Venkatesan, 1970c] show a similar trend, although the limitations of observations are more severe for these than for Jupiter and Saturn. We conclude that all the four planets seem to exhibit similar behavior with regard to their luminosities around solar minima and maxima. The results of Shapiro [1953] for Jupiter and Johnson and Iriarte [1959] for Uranus and Neptune for short periods are qualitatively consistent with our results.

The density, atmosphere, composition, albedo, etc., are similar for the four planets [Allen, 1963]. The albedos range from ~0.41 to 0.56 in comparison with the value of 0.34 for earth. The planets have optically thick atmospheres and their solid surfaces are not visible. The compositions of their atmospheres are comparable [Urey, 1959] and hence it is reasonable to expect similar interactions with solar activity and also similar types of radiative transfer within the planetary atmospheres. Thus we believe we have evidence of a solar cycle variation up to ~30 AU from the sun. The importance of careful observations of planetary luminosities even in terms of solar activity and solar planetary relationships is clearly seen.

It is appropriate to conclude this article with some general comments on solar cycle variation. The 11-year cycle of solar activity seems to have two distinct features; that of the solar wind consisting of corpuscular radiation and that of the solar extreme ultraviolet



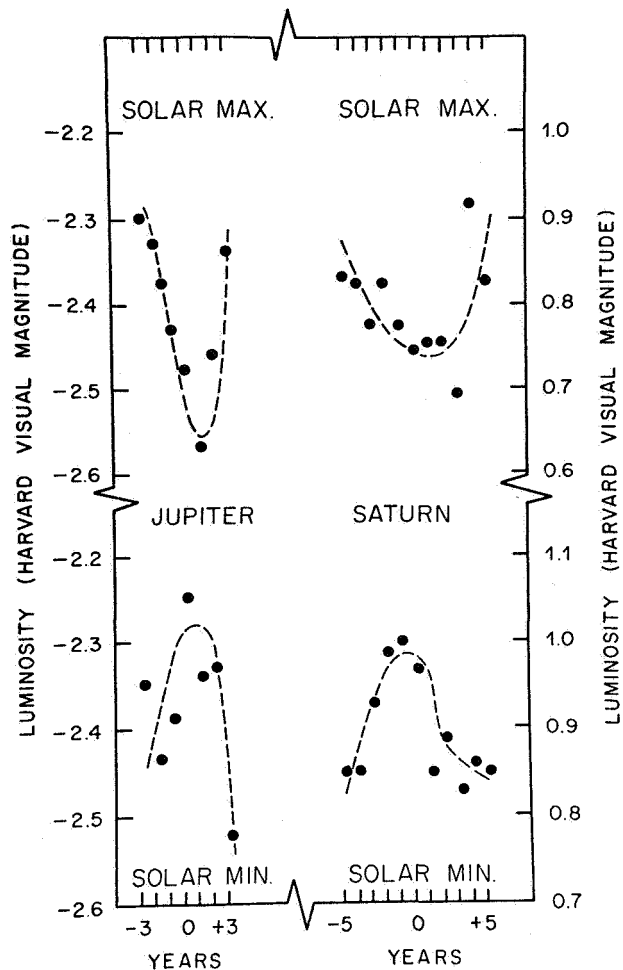


**Figure 3** The luminosity variation of Jupiter and Saturn, according to Chree superposition analysis. Note that for Saturn the luminosity magnitude is a positive number while for Jupiter it is a negative number.

emission. The investigations of *Bordeau et al.* [1964], *Nicolet* [1963], and *Jacchia and Slowey* [1964] show that the variations of density and temperature of the terrestrial atmosphere are due to the solar extreme ultra-violet radiation. While contribution due to corpuscular heating during short periods of enhanced activity has also been detected, the major effect, however, is attributed to the solar EUV.

The analyses of the planetary luminosity data are certainly not detailed enough to show whether the solar plasma or EUV is the primary cause for the observed

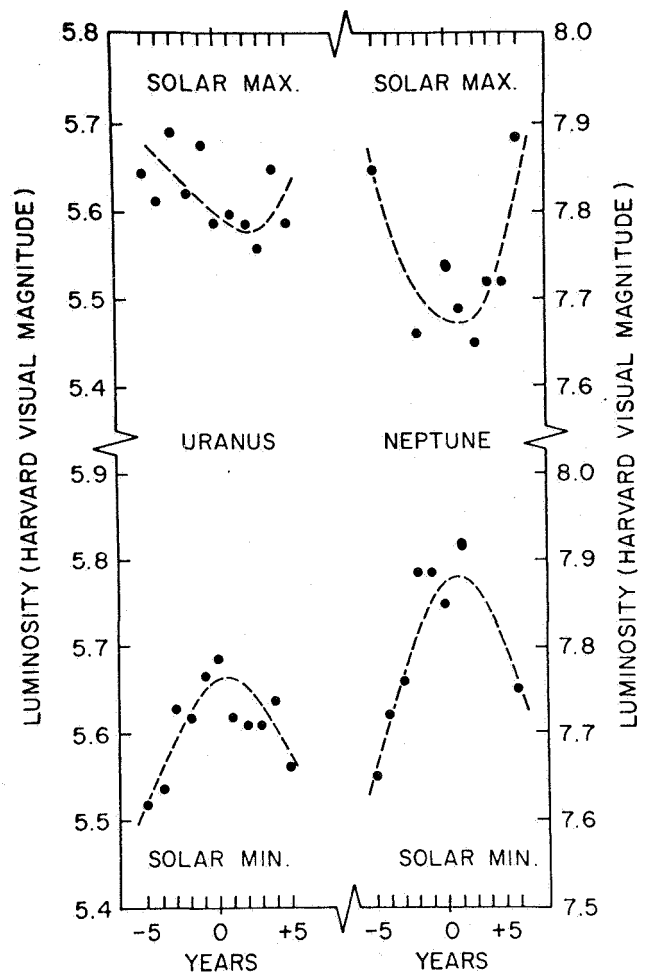


**Figure 4** The luminosity variation of Uranus and Neptune according to Chree superposition analysis.

changes. But we feel that the double maxima solar cycle variation, in principle, could be used to distinguish between the phenomena related to solar wind and EUV. The former exhibit the characteristic double hump structure in its 11-year variation, as conclusively indicated by the many geophysical, interplanetary, geomagnetic and cosmic-ray studies. The latter follows the Zurich relative sunspot numbers and the 2800 MHz flux with a single maximum in solar cycle. If, for example, the planetary atmospheres respond to the EUV just like the terrestrial atmosphere and expand during solar maxima, the increased luminosity of the planets is understandable in terms of the larger effective scattering region.

## REFERENCES

- Allen, C. W.: *Astrophysical Quantities*. University of London, The Althone Press, Second ed., 1963, p. 145.
- Antalova, A.; and Gnevyshev, M. N.: Principal Characteristics of the 11-Year Solar Activity Cycle. *Soviet Astronomy-AJ*, Vol. 9, 1965, p. 198.
- Balasubrahmanyam, V. K.: Solar Activity and the 11-Year Modulation of Cosmic Rays. *Solar Phys.*, Vol. 7, 1968, p. 39.
- Balasubrahmanyam, V. K.; and Venkatesan, D.: Solar Activity, 27-Day Variation and Long Term Modulation of Cosmic Ray Intensity. *Solar Phys.*, Vol. 11, 1970a, p. 151.
- Balasubrahmanyam, V. K.; and Venkatesan, D.: Solar Activity and the Great Red Spot of Jupiter. *Astrophys. Letters*, Vol. 6, 1970b, pp. 123-126.
- Balasubrahmanyam, V. K.; and Venkatesan, D.: Solar Activity and Planetary Luminosity. Accepted for publication, *Solar Phys.* 1970c. (NASA-Goddard preprint X-661-70-380).
- Becker, W.: Über Helligkeitsschwankungen der Planeten Mars, Jupiter, Saturn, Uranus, Neptune und Damit Zusammenhängende Erscheinungen. *Sitzungs Preuss-Akad (Phys-Maths)*, Vol. 28, 1933, p. 839.
- Becker, W.: Der Physiche Lichtwechsel der Planeten Saturn und Uranus. *Astron. Nachrichten*, Vol. 277, 1949, p. 65.
- Bordeau, R. E.; Chandra, S.; and Neupert, W. M.: Time Correlation of Extreme Ultraviolet Radiation and Thermospheric Temperature. *J. Geophys. Res.*, Vol. 69, 1964, p. 4531.
- Chree, C.: Some Phenomena of Sunspots and of Terrestrial Magnetism at Kew Observatory. *Phil. Trans. A.*, Vol. 212, 1913, p. 76.
- Chree, C.; and Stagg, I. M.: Recurrence Phenomena in Terrestrial Magnetism. *Phil. Trans. A.*, Vol. 227, 1928, p. 21.
- Dessler, A. J.: Solar Wind and the Interplanetary Magnetic Field. *Revs. Geophys.*, Vol. 5, 1967, p. 1.
- Fokker, A. D.: Solar Microwave Bursts and Centres of Activity. *B.A.N.*, Vol. 17, 1963, p. 84.
- Gentili di Guiseppe, M.; Hugon, M.; Leroy, J. L.; Rosch, J.; and Trellis, M.: Evolution de l'Intensite des Raies Coronales 5303A et 6374A au Cours des Deux Derniers Cycles Solaires (1944-1964). *Ann. D'Astrophys.*, Vol. 29, 1966, p. 43.
- Gnevyshev, M. N.: The Corona and 11-Year Cycle of Solar Activity. *Soviet Astron.-AJ*, Vol. 7, 1963, p. 311.
- Gnevyshev, M. N.: On the 11-Year Cycle of Solar Activity. *Solar Phys.*, Vol. 1, 1967, p. 107.
- Hundhausen, A. J.: Interplanetary Neutral Hydrogen and the Radius of the Heliosphere. *Planet. Space Sci.*, Vol. 16, 1968, p. 783.
- Jacchia, L. G.; and Slowey, J.: Temperature Variation in the Upper Atmosphere During Geomagnetically Quiet Intervals. *J. Geophys. Res.*, Vol. 69, 1964, p. 4145.
- Johnson, H. L.; and Iriarte, B.: The Sun as a Variable Star. *Lowell Obs. Bull.*, Vol. 4, 1959, p. 96.
- Krivsky, L.; and Kruger, A.: Flares With IV-Type Bursts and the Corona in the 11-Year Cycle. *Bull. Astron. Inst. Czech.*, Vol. 17, 1966, p. 243.
- Newton, H. W.; and Milsom, A. S.: The Distribution of Great and Small Geomagnetic Storms in the Sunspot Cycle. *J. Geophys. Res.*, Vol. 59, 1954, p. 203.
- Nicolet, M.: Solar Radio Flux and Temperature of the Upper Atmosphere. *J. Geophys. Res.*, Vol. 68, 1963, p. 6121.
- Peek, B. M.: *The Planet Jupiter*. London, Faber, and Faber, 1958, pp. 239-240.
- Sakurai, K.: Comments on the Indices of Solar Activity and Its Eleven-Year Cycle Variation. *Special Contributions, Geophys. Inst., Kyoto Univ.*, Vol. 7, 1967, p. 1.
- Shapiro, R.: A Planetary-Atmospheric Response to Solar Activity. *J. Meteorology*, Vol. 10, 1953, p. 350.
- Simpson, J. A.; and Wang, J. R.: Dimension of the Cosmic Ray Modulation Region. *Astrophys. J.*, Vol. 149, 1967, p. L73.
- Solberg, H. G.; and Chapman, C. R.: Correlation Between Zurich Sunspot Number and Prominence of Jupiter's Red Spot. *Nature*, Vol. 221, 1969, p. 352.
- Urey, H. C.: The Atmosphere of the Planets. *Handbuk der Physik*, Springer-Verlag, Berlin, Vol. 52, 1959, p. 393.
- Venkatesan, D.: Changes in Amplitude of the 27-Day Variation During a Cycle of Solar Activity. *Tellus*, Vol. 10, 1958, p. 117.
- Vsekhsvyatskii, S. K.: *The Planet Jupiter*. Edited by V. A. Bronshten, Akademiya Nauk, USSR. NASA TTF-563-30, 1969.
- Waldmeier, M.: *The Sunspot Activity in the Years 1610-1960*. Schultess and Co., Zurich, 1961, p. 18.

## CONFERENCE ATTENDEES

*Dr. Michel P. Aubry*  
Space Science Center  
Institute of Geophysics and Planetary Physics  
University of California  
Los Angeles, California 90024

*Professor W. Ian Axford*  
Department of Applied Physics and Information  
Science  
University of California — San Diego  
La Jolla, California 92037

*Dr. F. Axisa*  
Observatoire de Meudon  
Meudon 78, France

*Professor Jae R. Ballif*  
Department of Physics and Astronomy  
Brigham Young University  
Provo, Utah 84601

*Dr. S. J. Bame*  
Los Alamos Scientific Laboratory  
University of California  
P. O. Box 1663  
Los Alamos, New Mexico 87544

*Professor Peter M. Banks*  
Department of Applied Physics  
University of California — San Diego  
La Jolla, California 92037

*Dr. Aaron Barnes*  
Theoretical Studies Branch — N-245-3  
NASA Ames Research Center  
Moffett Field, California 94035

*Professor David B. Beard*  
Chairman, Department of Physics and  
Astronomy  
The University of Kansas  
Lawrence, Kansas 66044

*Dr. J. M. Beckers*  
Sacramento Peak Observatory  
Headquarters Air Force Cambridge Research  
Laboratories (OAR)  
Department of the Air Force  
Sunspot, New Mexico 88349

*Dr. John Belcher*  
George W. Downs Laboratory of Physics  
California Institute of Technology  
Pasadena, California 91109

*Dr. Joseph H. Binsack*  
Center for Space Research  
Massachusetts Institute of Technology  
(N51-330)  
Cambridge, Massachusetts 02139

*Dr. J. E. Blamont*  
University of Paris  
Service d'Aeronomie du Centre National de  
la Recherche Scientifique  
du Verrieres le Guisson  
Paris, France

*Dr. John C. Brandt, Head*  
Solar Physics Branch  
NASA Goddard Space Flight Center  
Greenbelt, Maryland 20771

*Professor H. Bridge*  
Department of Physics  
Massachusetts Institute of Technology  
Cambridge, Massachusetts 02139

*Dr. V. Bumba*  
Astronomical Institute of the  
Czechoslovakia Academy of Science  
Observatory Ondrejov  
Ondrejov, Czechoslovakia

*Dr. Leonard F. Burlaga*  
Space Plasma Physics Branch  
NASA Goddard Space Flight Center  
Greenbelt, Maryland 20771

*Dr. Wallace H. Campbell*  
Environmental Research Laboratory  
NOAA  
Boulder, Colorado 80302

*Mr. A. R. Cannon*  
Space Sciences Laboratory  
University of California — Berkeley  
Berkeley, California 94720

*Dr. Robert L. Carovillano*  
Chairman, Department of Physics  
Boston College  
Chestnut Hill, Massachusetts 02167

*Dr. Patrick M. Cassen*  
Theoretical Studies Branch – N-245-3  
NASA Ames Research Center  
Moffett Field, California 94035

*Dr. D. D. Childers*  
Space Science Center  
Institute of Geophysics and Planetary Physics  
Los Angeles, California 90024

*Dr. Paul A. Cloutier*  
Space Science Department  
Rice University  
Houston, Texas 77001

*Dr. P. J. Coleman, Jr.*  
Institute for Geophysics and Planetary Science  
University of California – Los Angeles  
Los Angeles, California 90024

*Dr. W. A. Coles*  
Department of Applied Physics and Information  
Science  
University of Southern California  
Los Angeles, California 90007

*Professor T. G. Cowling*  
Department of Applied Mathematics  
The University  
Leeds 2, England

*Dr. Thomas A. Croft*  
Center for Radar Astronomy  
Stanford Electronics Laboratory  
Stanford, California 94305

*Dr. Willard M. Cronyn*  
Space Disturbances Laboratory  
NOAA – Environmental Research  
Laboratories  
Boulder, Colorado 80302

*Dr. W. D. Cummings, Chairman*  
Department of Physics  
Grambling College  
Grambling, Louisiana 71245

*Dr. Sami Cuperman*  
Department of Physics and Astronomy  
Tel-Aviv University  
Ramat-Aviv  
Israel

*Professor L. Davis, Jr.*  
Department of Physics  
California Institute of Technology  
1201 East California Street  
Pasadena, California 91102

*Dr. A. J. Dessler*  
Department of Space Science  
Rice University  
Houston, Texas 77001

*Dr. David S. DeYoung*  
National Radio Astronomy Observatory  
Charlottesville, Virginia 22203

*Dr. R. H. Dicke*  
Department of Physics  
Joseph Henry Laboratories  
Princeton University  
P. O. Box 708  
Princeton, New Jersey 08540

*Mr. Robert Doeker*  
Space Disturbance Forecast Center  
NOAA – Environmental Research  
Laboratories  
Boulder, Colorado 80302

*Dr. Murray Dryer*  
Space Disturbance Forecast Center  
NOAA – Environmental Research  
Laboratories  
Boulder, Colorado 80302

*Dr. B. Durney*  
National Center for Atmospheric Research  
P. O. Box 1470  
Boulder, Colorado 80302

*Dr. Carl-Gunne Fälthammar*  
Division of Plasma Physics  
The Royal Institute of Technology  
Stockholm 70, Sweden

*Professor C. Y. Fan*  
Department of Physics  
University of Arizona  
Tucson, Arizona 85721

*Dr. William C. Feldman*  
Los Alamos Scientific Laboratory  
University of California  
P. O. Box 1663  
Los Alamos, New Mexico 87544

*Dr. John W. Firor*, Director  
National Center for Atmospheric Research  
P. O. Box 1470  
Boulder, Colorado 80302

*Dr. Vitorio Formisano*  
Istituto Di Fisica "Guglielmo Marconi"  
Pizzale delle Science 5  
Rome, Italy

*Dr. David W. Forslund*  
Los Alamos Scientific Laboratory  
University of California  
P. O. Box 1663  
Los Alamos, New Mexico 87544

*Dr. Robert W. Fredricks*  
Space Physics Analysis Department  
TRW Systems Group, Inc.  
One Space Park  
Redondo Beach, California 90278

*Professor J. Geiss*  
Physikalisches Institut  
Sidlerstrasse 5  
3000 Bern, Switzerland

*Dr. George Gloeckler*  
College of Arts and Sciences  
Department of Physics and Astronomy  
University of Maryland  
College Park, Maryland 20742

*Dr. Walter Gonzales*  
Space Sciences Laboratory  
University of California – Berkeley  
Berkeley, California 94720

*Dr. J. T. Gosling*  
High Altitude Observatory  
Boulder, Colorado 80303

*Dr. Susan Gussenhoven*  
Department of Physics  
Boston College  
Chestnut Hill, Massachusetts 02167

*Dr. F. P. Haddock*  
Astronomy Department  
University of Michigan  
Ann Arbor, Michigan 48104

*Dr. R. E. Hartle*  
Thermosphere and Exosphere Branch  
Code 615  
NASA Goddard Space Flight Center  
Greenbelt, Maryland 20771

*Miss Ruth Hedeman*  
McMath-Hulbert Observatory  
895 Lake Angelus Road – N.  
Pontiac, Michigan 48055

*Dr. Peter Hedgecock*  
Imperial College of Science and Technology  
Prince Consort Road  
South Kensington  
London, S. W. 7, England

*Commander George Heffernan*  
Chief of Naval Research – Code 422  
Department of Navy  
800 N. Quincey Street  
Arlington, Virginia 22217

*Dr. A. Hewish*  
Cavendish Laboratory  
Free School Lane  
Cambridge, England

*Dr. Deiter Heymann*  
Department of Space Science  
Rice University  
Houston, Texas 77001

*Dr. Joan Hirshberg*  
Theoretical Studies Branch – N-245-3  
NASA Ames Research Center  
Moffett Field, California 94035

*Dr. Joseph V. Hollweg*  
George W. Downs Laboratory of Physics  
California Institute of Technology  
Pasadena, California 91109

*Dr. Thomas E. Holzer*  
Department of Physics  
Imperial College of Science and Technology  
Prince Consort Road  
London, S. W. 7, England

*Dr. H. T. Howard*  
Center for Radar Astronomy  
Stanford Electronics Laboratories  
Stanford, California 94305

*Dr. Robert Howard*  
Hale Observatories  
813 Santa Barbara Street  
Pasadena, California 91106

*Dr. K. C. Hsieh*  
Department of Physics  
The University of Arizona  
Tucson, Arizona 85721

*Dr. A. J. Hundhausen*  
National Center for Atmospheric Research  
P. O. Box 1470  
Boulder, Colorado 80302

*Dr. J. Huneke*  
Division of Geological Sciences  
California Institute of Technology  
Pasadena, California 91109

*Dr. R. J. Hynds*  
Department of Physics  
Imperial College  
London, S. W. 7, England

*Professor Andrew Ingersoll*  
Division of Geological Sciences  
California Institute of Technology  
Pasadena, California 91109

*Dr. Devrie S. Intrilligator*  
George W. Downs Laboratory of Physics  
California Institute of Technology  
Pasadena, California 91109

*Dr. J. R. Jokipii*  
George W. Downs Laboratory of Physics  
California Institute of Technology  
Pasadena, California 91109

*Dr. Douglas E. Jones*  
Department of Physics and Astronomy  
Brigham Young University  
Provo, Utah 84601

*Professor Darrell Judge*  
Department of Physics  
University of Southern California  
Los Angeles, California 90007

*Dr. Sharad R. Kane*  
Space Sciences Laboratory  
University of California – Berkeley  
Berkeley, California 94720

*Dr. R. A. Kopp*  
High Altitude Observatory  
Boulder, Colorado 80301

*Dr. R. P. Kraft*  
University of California – Santa Cruz  
Santa Cruz, California 95060

*Dr. Jeremy A. Landt*  
Center for Radar Astronomy  
Stanford Electronics Laboratories  
Stanford, California 94305

*Professor David Layzer*  
Harvard College Observatory  
60 Garden Street  
Cambridge, Massachusetts 02138

*Dr. Alan J. Lazarus*  
Center for Space Research  
Massachusetts Institute of Technology  
Cambridge, Massachusetts 02139

*Professor T. S. Lee*  
Department of Electrical Engineering  
University of Minnesota  
Minneapolis, Minnesota 55455

*Professor R. B. Leighton*  
George W. Downs Laboratory of Physics  
California Institute of Technology  
Pasadena, California 91109

*Dr. Harold Leinbach*  
Space Disturbance Laboratory  
NOAA – Environmental Research  
Laboratories  
Boulder, Colorado 80302

*Dr. Ronald P. Lepping*  
Code 692  
NASA Goddard Space Flight Center  
Greenbelt, Maryland 20771

*Dr. Robert P. Lin*  
Space Sciences Laboratory  
University of California – Berkeley  
Berkeley, California 94720

*Dr. William C. Livingston*  
Solar Division  
Kitt Peak National Observatory  
950 North Cherry Avenue  
P. O. Box 4130  
Tucson, Arizona 85717

*Mr. Charles Lombard*  
Department of Applied Mechanics  
Stanford University  
Stanford, California 94305

*Dr. R. Lüst*  
Institute for Extraterrestrial Physics  
Max-Planck Institute for Physics and Astronomy  
8046 Garching Bei  
Munich 23, Germany

*Dr. Hans Mark*  
Director  
NASA Ames Research Center  
Moffett Field, California 94035

*Dr. Franco Mariani*  
Istituto Di Fisica  
Citta Universitaria  
Rome, Italy

*Dr. Billy McCormac*  
Lockheed Palo Research Laboratory  
Department 52-14  
3251 Hanover Street  
Palo Alto, California 94304

*Dr. Patrick McIntosh*  
Space Disturbances Laboratory  
NOAA – Environmental Research  
Laboratories  
Boulder, Colorado 80302

*Dr. James F. McKenzie*  
ESRIN  
Frascati  
Rome, Italy

*Dr. John McKinnon*  
Space Disturbances Laboratory  
NOAA – Environmental Research  
Laboratories  
Boulder, Colorado 80302

*Dr. Ching -I. Meng*  
Space Sciences Laboratory  
University of California – Berkeley  
Berkeley, California 94720

*Dr. L. Mestel*  
Department of Astronomy  
The University of Manchester  
Manchester 13, England

*Dr. F. C. Michel*  
Space Science Department  
Rice University  
Houston, Texas 77001

*Dr. J. Modisette*  
Houston Baptist College  
7502 Fondren Road  
Houston, Texas 77036

*Dr. Michael D. Montgomery*  
Los Alamos Scientific Laboratory  
University of California  
P. O. Box 1663  
Los Alamos, New Mexico 87544

*Dr. Giovanni Moreno*  
C/O Officine Galileo  
Via Carlo Bini 44  
Firenze 50134  
Italy

*Dr. Norman F. Ness, Chief*  
Laboratory for Extraterrestrial Physics  
Code 692  
NASA Goddard Space Flight Center  
Greenbelt, Maryland 20771

*Dr. Fritz Neubauer*  
Mendelssohnstre 1  
Braunschweig 33  
Germany

*Dr. Marcia Neugebauer*  
Jet Propulsion Laboratory  
California Institute of Technology  
4800 Oak Grove Drive  
Pasadena, California 91103

*Dr. Gordon Newkirk, Jr.*  
Director  
High Altitude Observatory  
Boulder, Colorado 80302

*Dr. G. K. Oertel*  
Chief, Solar Physics – Code SG  
Physics and Astronomy Programs  
National Aeronautics and Space Administration  
Washington, D. C. 20546

*Dr. Keith W. Ogilvie*, Head  
Space Plasma Physics Branch – Code 692  
NASA Goddard Space Flight Center  
Greenbelt, Maryland 20771

*Dr. S. Olbert*  
Department of Physics  
Massachusetts Institute of Technology  
Cambridge, Massachusetts 02139

*Dr. Dimitri A. Papanastassiou*  
Arms (170-25)  
California Institute of Technology  
Pasadena, California 91109

*Dr. Francis W. Perkins*  
Plasma Physics Laboratory  
James Forrestal Campus  
Princeton University  
P. O. Box 451  
Princeton, New Jersey 08540

*Dr. M. Pick*  
Solar Department  
Meudon Observatory  
Meudon (92)  
France

*Dr. George F. Pieper*  
Director of Space Sciences – Code 600  
NASA Goddard Space Flight Center  
Greenbelt, Maryland 20771

*Dr. G. W. Pneuman*  
High Altitude Observatory  
Boulder, Colorado 80302

*Dr. F. Podosek*  
Division of Geological Sciences  
California Institute of Technology  
Pasadena, California 91109

*Dr. Barnaby Rickett*  
Department of Applied Physics and  
Information Science  
University of California – San Diego  
La Jolla, California 92037

*Mr. Art Rizzi*  
Department of Applied Mechanics  
Stanford University  
Stanford, California 94305

*Dr. Edmond C. Roelof*  
Space Science Center  
DeMeritt Hall  
University of New Hampshire  
Durham, New Hampshire 03824

*Dr. R. Rosenbauer*  
Institut for Extraterrestrial Physics  
Max-Planck Institute for Physics and  
Astronomy  
8046 Garching Bei  
Munich, Germany

*Dr. Victor H. Rumsey*  
Department of Applied Physics and  
Information Science  
University of California – San Diego  
La Jolla, California 92037

*Dr. Christopher Russell*  
Space Science Center  
Institute of Geophysics and Planetary Physics  
University of California – Los Angeles  
Los Angeles, California 90024



*Dr. Frederick L. Scarf*, Manager  
Space Physics Analysis Department  
TRW Systems Group, Inc.  
Bldg. R-1, Rm. 1070  
One Space Park  
Redondo Beach, California 90278

*Dr. Jeff Scargle*  
Lick Observatory  
University of California – Santa Cruz  
Santa Cruz, California 95060

*Dr. Alois W. Schardt*  
Deputy Director of Physics and Astronomy  
Programs – Code SG  
National Aeronautics and Space Administration  
Washington, D. C. 20546

*Dr. Kenneth H. Schatten*  
Space Plasma Physics Branch – Code 692  
NASA Goddard Space Flight Center  
Greenbelt, Maryland 20771

*Dr. Dennis Schatz*  
Space Sciences Laboratory  
University of California – Berkeley  
Berkeley, California 94720

*Dr. E. Schatzman*  
98 Bis Boulevard Arozo  
F75 Paris 14  
France

*Dr. Frank Scherb*  
Department of Physics  
The University of Wisconsin  
475 North Charter Street  
Madison, Wisconsin 53706

*Dr. Philip H. Scherrer*  
Space Sciences Laboratory  
University of California – Berkeley  
Berkeley, California 94720

*Dr. Karl Schindler*  
ERSIN  
via Frascati  
Rome, Italy

*Dr. E. R. Schmerling*  
Acting Chief, Magnetospheric Physics  
Code SG  
National Aeronautics and Space Administration  
Washington, D. C. 20546

*Dr. Herman Schmidt*  
Max-Planck-Institute for Physics and  
Astrophysics  
Fohringer Ring 6  
Munich 23, Germany

*Dr. Gerald Schubert*  
Department of Planetary and Space Sciences  
University of California – Los Angeles  
Los Angeles, California 90024

*Dr. Michael Schulz*  
Space Physics Laboratory  
Aerospace Corporation  
El Segundo, California 90045

*Dr. Ken Schwartz*  
American Nucleonics Corporation  
6036 Variel Avenue  
Woodland Hills, California 91364

*Dr. Jack D. Scudder*  
Code 962  
NASA Goddard Space Flight Center  
Greenbelt, Maryland 20771

*Dr. N. R. Sheeley, Jr.*  
Solar Division  
Kitt Peak National Observatory  
950 North Cherry Avenue  
P. O. Box 4130  
Tucson, Arizona 85717

*Dr. George W. Simon*  
Sacramento Peak Observatory  
Sunspot, New Mexico 88349

*Dr. George L. Siscoe*  
Department of Meteorology  
University of California – Los Angeles  
Los Angeles, California 90024

*Dr. Bruce F. Smith*

Special Projects Office – N-245-2  
NASA Ames Research Center  
Moffett Field, California 94035

*Dr. Edward J. Smith*

Jet Propulsion Laboratory  
California Institute of Technology  
4800 Oak Grove Drive  
Pasadena, California 91103

*Dr. Henry J. Smith*

Code SS  
National Aeronautics and Space Administration  
Washington, D. C. 20546

*Dr. Sheldon M. Smith*

Physics Branch – N-230-1  
NASA Ames Research Center  
Moffett Field, California 94035

*Dr. C. P. Sonett*

Deputy Director of Astronautics  
NASA Ames Research Center  
Moffett Field, California 94035

*Dr. David Southwood*

Institute of Geophysics and Planetary Physics  
University of California – Los Angeles  
Los Angeles, California 90024

*Dr. John R. Spreiter*

Department of Applied Mechanics  
Stanford University  
Stanford, California 94305

*Dr. Jan Olof Stenflo*

High Altitude Observatory  
Boulder, Colorado 80302

*Dr. Ian B. Strong*

Los Alamos Scientific Laboratory  
University of California  
P. O. Box 1663  
Los Alamos, New Mexico 87544

*Dr. Peter A. Sturrock*

Institute for Plasma Research  
Stanford University  
Stanford, California 94305

*Dr. Steven Suess*

Space Disturbances Laboratory  
NOAA – Environmental Research  
Laboratories  
Boulder, Colorado 80302

*Dr. Graham Suffolk*

Physikalisches Institut  
University of Bern  
Sidlerstrasse 5  
3012 Bern, Switzerland

*Dr. Andrew S. Tanenbaum*

Space Sciences Laboratory  
University of California – Berkeley  
Berkeley, California 94720

*Dr. Gary E. Thomas*

4741 Chatham Street  
Boulder, Colorado 80302

*Dr. Richard M. Thorne*

Department of Meteorology  
University of California – Los Angeles  
Los Angeles, California 90024

*Dr. Eigil Ungstrup*

Danish Space Research Institute  
Lundtoftevej Space 7  
2800 Lyngby  
Denmark

*Dr. D. Venkatesan*

Department of Physics  
University of Calgary  
Calgary 44, Alberta, Canada

*Dr. H. Volk*

Max-Planck-Institut für Physik und Astrophysik  
Fohringer Ring 6  
Munich 23, Germany

*Dr. Edmund J. Weber*

Solar Division  
Kitt Peak National Observatory  
950 North Cherry Avenue  
P. O. Box 4130  
Tucson, Arizona 85717

*Professor Y. C. Whang*  
Department of Space Science and Applied  
Physics  
The Catholic University of America  
Washington, D. C. 20017

*Professor John Wilcox*  
Institute of Plasma Physics  
Stanford Electronics Laboratory  
Via Crespi  
Stanford University  
Stanford, California 94305

*Dr. T. Wilkerson*  
Institute for Fluid Dynamics and Applied  
Mathematics  
University of Maryland  
College Park, Maryland 20742

*Dr. Olin C. Wilson*  
Hale Observatories  
813 Santa Barbara Street  
Pasadena, California 91106

*Dr. C. R. Winge*  
Institute of Geophysics and Planetary Physics  
University of California — Los Angeles  
Los Angeles, California 90024

*Dr. John H. Wolfe*  
Special Projects Office — N-245-2  
NASA Ames Research Center  
Moffett Field, California 94035